USGS
science for a changing world

Ground-Water Resources Program
National Research Program

Ground-Water Recharge in the Arid and Semiarid Southwestern United States

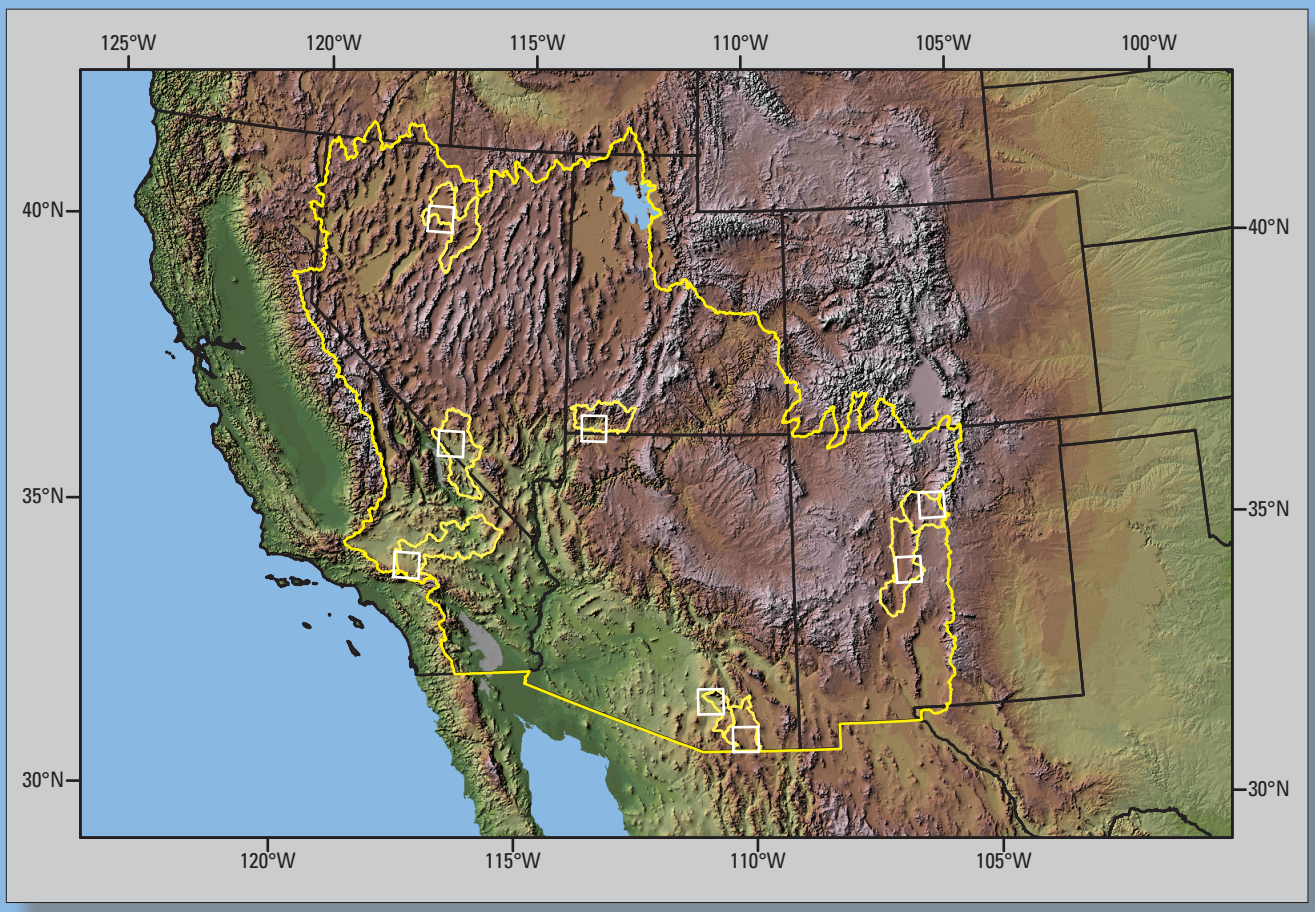

Professional Paper 1703

U.S. Department of the Interior
U.S. Geological Survey

Ground-Water Recharge in the Arid and Semiarid Southwestern United States

Edited by David A. Stonestrom, Jim Constantz, Ty P.A. Ferré[1], and Stanley A. Leake

With contributions by Jared D. Abraham, Kelsey S. Adams, Brian J. Andraski, Matthew A. Bailey, Andrew M. Binley[2], Kyle W. Blasch, James B. Callegary, Alissa L. Coes, Jim Constantz, Steven M. Crawford, Ty P.A. Ferré, James B. Fink[3], Alan L. Flint, Lorraine E. Flint, Philip M. Gardner, Patrick A. Glancy, James R. Harrill, Victor M. Heilweil, John P. Hoffmann, John A. Izbicki, Russell U. Johnson, Justin Kulongoski, Marc T. Levitt[3], Randell J. Laczniak, Stephanie J. Moore, Richard G. Niswonger, Donald R. Pool, Steven Predmore, David E. Prudic, Bridget R. Scanlon[4], D. Kip Solomon[5], Amy E. Stewart-Deaker, David A. Stonestrom, Michelle A. Walvoord, and James L. Wood

[1]University of Arizona; [2]Lancaster University; [3]Hydrogeophysics, Inc.; [4]University of Texas at Austin; [5]University of Utah

Volume comprises chapters A, B, C, D, E, F, G, H, I, J, K, and appendicies 1 and 2

Professional Paper 1703

U.S. Department of the Interior
U.S. Geological Survey

U.S. Department of the Interior
DIRK KEMPTHORNE, Secretary

U.S. Geological Survey
Mark D. Myers, Director

U.S. Geological Survey, Reston, Virginia: 2007

This report and any updates to it are available online at:
http://pubs.usgs.gov/pp/pp1703/

For product and ordering information:
World Wide Web: http://www.usgs.gov/pubprod
Telephone: 1-888-ASK-USGS (1-888-275-8747)

For more information on the USGS—the Federal source for science about the Earth,
its natural and living resources, natural hazards, and the environment:
World Wide Web: http://www.usgs.gov
Telephone: 1-888-ASK-USGS (1-888-275-8747)

Any use of trade, product, or firm names is for descriptive purposes only and does not imply
endorsement by the U.S. Government.

Although this report is in the public domain, permission must be secured from the individual copyright owners to
reproduce any copyrighted material contained within this report.

Suggested citation:
Stonestrom, D.A., Constantz, J., Ferré, T.P.A., and Leake, S.A., eds., 2007, Ground-water recharge in the arid and semi-arid southwestern United States: U.S. Geological Survey Professional Paper 1703, 414 p.

Cataloging-in-publication data are on file with the Library of Congress (http://www.loc.gov/).

Produced in the Western Region, Menlo Park, California
Manuscript approved for publication, July 24, 2007
Text edited by Tracey L. Suzuki
Layout by Judy Weathers

FRONT COVER. Digital elevation map of the southwestern United States showing the boundary of the regional-analysis area (large yellow outline) and site-specific study areas (small yellow outlines and white squares). Base map, extracted from the USGS National Atlas product "Shaded Relief of North America," shows elevations from below sea level (gray) to greater than 3,000 meters (white). The caption of figure 1 in chapter C provides additional details.

Foreword

The population of the arid and semiarid southwestern United States is growing at a rate roughly three times that of the Nation as a whole. With limited rainfall and surface-water resources, the area relies heavily on ground water for beneficial uses. The sustainability of ground-water resources, including the life-supporting springs, wetlands, and streams that are fed by natural ground-water discharge, depends on the often sensitive balance of replenishment and depletion.

Recharge is the input to ground-water systems, yet determining recharge has long remained one of the most difficult challenges in hydrologic science. Ground-water systems are seldom at steady state, particularly in dry regions where precipitation and temperature are highly variable. Water-resources planning in such regions relies not only on identifying the timing, locations, and amounts of recharge but also on understanding the interacting processes that modulate recharge. An improved understanding of recharge dynamics can enhance our ability to assess and potentially mitigate the susceptibility of ground-water resources to natural and anthropogenic climatic and vegetational shifts.

As part of the U.S. Geological Survey mission to provide reliable information for resource management, this volume represents a systematic attempt to improve understanding of ground-water recharge in the arid and semiarid southwestern United States. The studies contained herein represent a major step toward characterizing recharge processes and rates throughout this part of the Nation and toward advancing methods for conducting recharge assessments and related scientific research in similar regions around the world.

Robert M. Hirsch

Associate Director for Water

Acknowledgments

The U.S. Geological Survey's (USGS) Office of Ground Water provided guidance and funding for the studies summarized herein. Support was also provided by the USGS National Research Program, National Water Quality Assessment Program, and Toxic Substances Hydrology Program. Additional support came from the Arizona Department of Water Resources (Rillito Creek study); the Mojave Water Agency, Victor Valley Water District, Joshua Basin Water District, and United States Marine Corps (Mojave Desert study); the Upper San Pedro Partnership and U.S. Bureau of Land Management (San Pedro tributaries study); and the Nevada Department of Conservation and Natural Resources (Trout Creek study).

Professor Andrew M. Binley's borehole geophysics study (reported in appendix 2) was funded by the United Kingdom's Natural Environment Research Council under grant GR3/11500.

Many employees helped in the execution of studies and with report preparation and review. In accordance with USGS practice, these employees are not acknowledged by name. Nevertheless, their efforts were essential to the field, modeling, and laboratory aspects of this research and resulted in an improved final document. In addition to the efforts of the internal reviewers, Professor Ty P.A. Ferré (University of Arizona), James R. Harrill (USGS-retired), and Professor Kamini Singha (Pennsylvania State University) provided helpful suggestions and comments on individual sections of the document.

Volume Contents

Foreword iii
Acknowledgments iv

Chapters:

A. Ground-Water Recharge in the Arid and Semiarid Southwestern United States — Climatic and Geologic Framework 1
By David A. Stonestrom and James R. Harrill

B. Regional Analysis of Ground-Water Recharge 29
By Lorraine E. Flint and Alan L. Flint

C. Overview of Ground-Water Recharge Study Sites 61
By Jim Constantz, Kelsey S. Adams, and David A. Stonestrom

D. Streamflow, Infiltration, and Ground-Water Recharge at Abo Arroyo, New Mexico 83
By Amy E. Stewart-Deaker, David A. Stonestrom, and Stephanie J. Moore

E. Focused Ground-Water Recharge in the Amargosa Desert Basin 107
By David A. Stonestrom, David E. Prudic, Michelle A. Walvoord, Jared D. Abraham, Amy E. Stewart, Patrick A. Glancy, Jim Constantz, Randell J. Laczniak, and Brian J. Andraski

F. Streamflow, Infiltration, and Recharge in Arroyo Hondo, New Mexico 137
By Stephanie J. Moore

G. Ground-Water Recharge From Small Intermittent Streams in the Western Mojave Desert, California 157
By John A. Izbicki, Russell U. Johnson, Justin Kulongoski, and Steven Predmore

H. Focused Infiltration, Percolation, and Recharge at the Rillito Creek Investigation Site, Southeastern Arizona 185
By John P. Hoffmann, Kyle W. Blasch, Donald R. Pool, Matthew A. Bailey, and James B. Callegary

I. Infiltration and Recharge at Sand Hollow, an Upland Bedrock Basin in Southwestern Utah 221
By Victor M. Heilweil, D. Kip Solomon, Philip M. Gardner

J. Ephemeral-Stream Channel and Basin-Floor Infiltration and Recharge in the Sierra Vista Subwatershed of the Upper San Pedro Basin, Southeastern Arizona 253
By Alissa L. Coes and Donald R. Pool

K. Streambed Infiltration and Ground-Water Recharge From the Trout Creek Drainage, an Intermittent Tributary to the Humboldt River, North-Central Nevada 313
By David E. Prudic, Richard G. Niswonger, James R. Harrill, and James L. Wood

Appendicies:

1. Thermal Methods for Investigating Ground-Water Recharge 353
By Kyle W. Blasch, Jim Constantz, and David A. Stonestrom

2. Geophysical Methods for Investigating Ground-Water Recharge 377
By Ty P.A. Ferré, Andrew M. Binley, Kyle W. Blasch, James B. Callegary, Steven M. Crawford, James B. Fink, Alan L. Flint, Lorraine E. Flint, John P. Hoffmann, John A. Izbicki, Marc T. Levitt, Donald R. Pool, and Bridget R. Scanlon

Conversion Factors and Datums

Multiply	By	To obtain
	Length	
millimeter (mm)	3.93701	hundreth of an inch (1/100 in)
centimeter (cm)	0.393701	inch (in)
meter (m)	39.3701	inch (in)
meter (m)	3.28084	foot (ft)
kilometer (km)	0.621371	mile (mi)
	Area	
square meter (m^2)	10.76391	square foot (ft^2)
hectare (ha)	2.47104	acre (acre)
square kilometer (km^2)	247.104	acre (acre)
square kilometer (km^2)	0.386102	square mile (mi^2)
	Volume	
cubic centimeter (cm^3)	0.0610237	cubic inch (in^3)
liter (L)	0.264172	gallon (gal)
cubic meter (m^3)	264.172	gallon (gal)
cubic hectometer (hm^3)	810.710	acre foot (acre-ft)
million cubic meters (Mm^3)	810.710	acre foot (acre-ft)
	Mass	
milligram (mg)	0.0154327	grain, avoirdupois (gr)
gram (g)	0.0352740	ounce, avoirdupois (oz)
kilogram (kg)	2.20462	pound, avoirdupois (lb)
	Density	
gram per cubic centimeter (g/cm^3)	0.578037	ounce per cubic inch (oz/in^3)
megagram per cubic meter (Mg/m^3)	62.4280	pound per cubic foot (lb/ft^3)
	Rate or flux density	
millimeter per second (mm/s)	0.0393701	inch per second (in/s)
millimeter per year (mm/yr)	0.0393701	inch per year (in/yr)
meter per hour (m/hr)	3.28084	foot per hour (ft/hr)
meter per hour (m/hr)	78.7402	foot per day (ft/day)
meter per day (m/d)	3.28084	foot per day (ft/d)
meter per year (m/yr)	3.28084	foot per year (ft/yr)
liter per second (L/s)	15.8503	gallon per minute (gal/min)
cubic meter per second (m^3/s)	35.3147	cubic foot per second (ft^3/s)
cubic meter per minute (m^3/min)	0.588578	cubic foot per second (ft^3/s)
cubic meter per day (m^3/d)	35.3147	cubic foot per day (ft^3/d)
cubic meter per day (m^3/d)	264.1721	gallon per day (gal/d)
cubic hectometer per year (hm^3/yr)	810.710	acre foot per year (acre-ft/yr)
million cubic meters per year (Mm^3/yr)	810.710	acre foot per year (acre-ft/yr)
	Hydraulic conductivity	
meter per day (m/d)	3.28084	foot per day (ft/d)
	Pressure	
kilopascal (kPa)	0.145038	pound per square inch (psi)
megapascal (MPa)	9.86923	atmosphere (atm)

Conversion Factors and Datums—Continued

Multiply	By	To obtain
	Heat	
joule (J)	0.23885	calorie, international (cal)
	Volumetric heat capacity	
joule per cubic meter per degree Celsius (J/m^{3}ºC)	0.0037575	calorie per cubic foot per degree Fahrenheit (cal/ft^{3}ºF)
	Thermal conductivity	
watt per meter per degree Celsius (W/mºC)	0.040445	calorie per second per foot per degree Fahrenheit (cal/s ft^{3}ºF)
	Radioactivity	
becquerel per liter (Bq/L)	27.027	picocurie per liter (pCi/L)

Except as noted, horizontal coordinates refer to the North American Datum of 1927 (NAD 27).

Vertical coordinates refer to the North American Vertical Datum of 1988 (NAVD 88).

"Altitude" in this report refers to the vertical distance above the vertical datum.

Temperature in degrees Celsius (°C) can be converted to degrees Fahrenheit (°F) as follows:

$$°F = (1.8 \times °C) + 32$$

Concentration units for chemical constituents in water are milligrams of solute per liter of solution (mg/L), or micrograms of solute per liter of solution (µg/L).

Specific-conductance units are microsiemens per centimeter at 25 degrees Celsius (µS/cm at 25 °C).

Ground-Water Recharge in the Arid and Semiarid Southwestern United States — Climatic and Geologic Framework

By David A. Stonestrom and James R. Harrill

Abstract

Ground-water recharge in the arid and semiarid southwestern United States results from the complex interplay of climate, geology, and vegetation across widely ranging spatial and temporal scales. Present-day recharge tends to be narrowly focused in time and space. Widespread water-table declines accompanied agricultural development during the twentieth century, demonstrating that sustainable ground-water supplies are not guaranteed when part of the extracted resource represents paleorecharge. Climatic controls on ground-water recharge range from seasonal cycles of summer monsoonal and winter frontal storms to multimillennial cycles of glacial and interglacial periods. Precipitation patterns reflect global-scale interactions among the oceans, atmosphere, and continents. Large-scale climatic influences associated with El Niño and Pacific Decadal Oscillations strongly but irregularly control weather in the study area, so that year-to-year variations in precipitation and ground-water recharge are large and difficult to predict. Proxy data indicate geologically recent periods of multidecadal droughts unlike any in the modern instrumental record. Anthropogenically induced climate change likely will reduce ground-water recharge through diminished snowpack at higher elevations, and perhaps through increased drought. Future changes in El Niño and monsoonal patterns, both crucial to precipitation in the study area, are highly uncertain in current models. Land-use modifications influence ground-water recharge directly through vegetation, irrigation, and impermeable area, and indirectly through climate change. High ranges bounding the study area—the San Bernadino Mountains and Sierra Nevada to the west, and the Wasatch and southern Colorado Rocky Mountains to the east—provide external geologic controls on ground-water recharge. Internal geologic controls stem from tectonic processes that led to numerous, variably connected alluvial-filled basins, exposure of extensive Paleozoic aquifers in mountainous recharge areas, and distinct modes of recharge in the Colorado Plateau and Basin and Range subregions.

Introduction

The arid and semiarid southwestern United States is among the fastest growing regions in the country. Because surface-water supplies are limited, exploitation of ground water played an important part in the development of agricultural and urban areas during the twentieth century. Ground-water pumpage in large areas grew to exceed rates of natural recharge starting in the midcentury, revealing effects of overexploitation. These effects included land subsidence, loss of springs and riparian habitat, and declining levels and quality of ground water (Alley and others, 1999; Galloway and others, 1999; Leake and others, 2000).

The current study area comprises about a million square kilometers of Arizona, California, Nevada, New Mexico, Utah, and small parts of Colorado, Idaho, and Oregon (fig. 1). The region is arid to semiarid, except for localized wetter areas in the mountains, and it is bounded on the west by the Sierra Nevada and San Bernadino Mountains, on the east by the Wasatch and southern Rocky Mountains, on the north by the south rim of the upper Snake River drainage, and on the south by the international boundary with Mexico. Hyperarid conditions occur in Imperial Valley and Death Valley of California, and in the Yuma Basin of southwestern Arizona. Relatively wet conditions on the east and west bound the relatively dry region comprising the study area.

Population and total water use have trended upward since the southwestern states were opened for development. Somewhat surprisingly, the fraction of water derived from aquifers started declining in the 1970s (Konieczki and Heilman, 2004). A review of water-use trends between 1950 and 2000 shows that, while agriculture still consumed the largest portion of ground water in study-area states, the fraction of ground-water withdrawals for agriculture declined from 94 percent in 1950 to 80 percent in 2000.

Census data show continuing population growth throughout the study area. During the most recent period for which county-level estimates are available—April 1, 2000, to July1, 2005—the total population in the study area grew 16.5 percent, equivalent to an annual growth rate of 3.0 percent. This rate exceeds the growth rate of the overall U.S. population by a factor of three (fig. 2). Counties with the highest rates of growth during the five-year period include Lyon County, Nevada (greater Reno-Carson City area, 38 percent), Washington County, Utah (Saint George area, 32 percent), Pinal County, Arizona (greater Phoenix area, 28 percent), Riverside

County, California (interior southern California, 26 percent), Clark County, Nevada (Las Vegas area, 24 percent), and Sandoval County, New Mexico (greater Albuquerque area, 19 percent; U.S. Census Bureau, 2006). Historical declines in ground-water levels largely mirror these centers of population and agricultural growth (fig. 3).

Purpose and Scope

Subsequent chapters in this professional paper present (first) a regional analysis of ground-water recharge across the entire study area (chapter B) followed by individual case studies representing different subareas of the geographically diverse region (chapters C–K). The regional analysis includes detailed hydrologic modeling within the framework of a high-resolution geographic-information system. Results from the regional analysis are used to explore both the distribution of ground-water recharge for mean climatic conditions as well as the influence of two climatic patterns—the El Niño-Southern Oscillation and Pacific Decadal Oscillation—that impart a high degree of variability to the hydrologic cycle. Individual case studies in chapters C–K employ a variety of geophysical and geochemical techniques to investigate recharge processes in different geographic subareas, and to relate these processes to local geologic and climatic conditions. All of the case studies made use of naturally occurring tracers to quantify recharge.

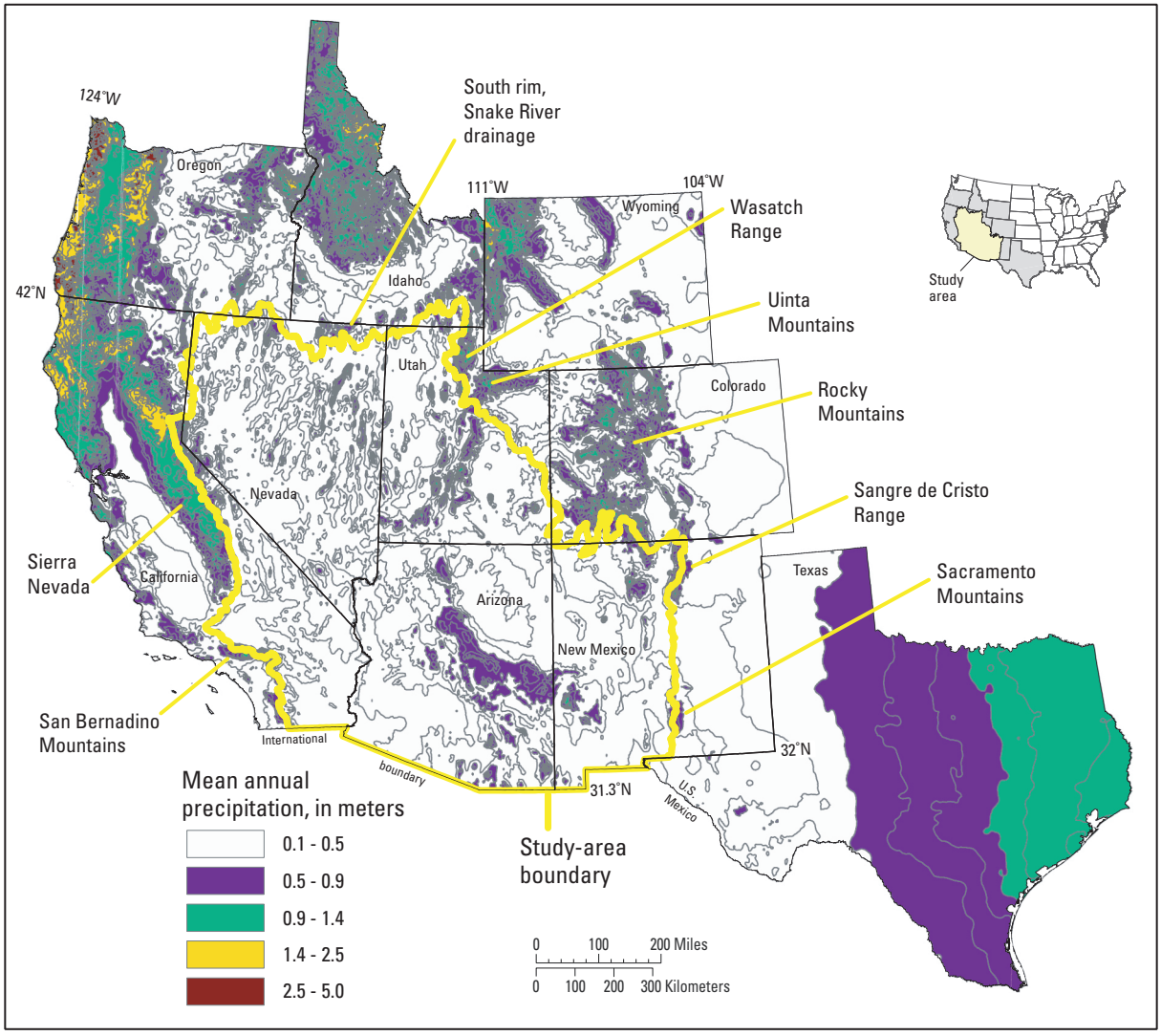

Figure 1. The arid and semiarid southwestern U.S. study area is an interior continental region characterized by generally low precipitation. Mean annual precipitation estimates in the figure were generated with the PRISM (precipitation-elevation regressions on independent slopes) model (Daly and others, 1994) on the basis of 1961–1990 monthly means at NOAA Cooperative Weather Station sites, USDA SNOTEL sites, and selected state stations. Data-poor regions were supplemented by stations with at least 20 years of record. The PRISM model accounts for orographic position, including aspect. From http://www.ocs.orst.edu/prism/state_products/ maps.phtml (last accessed May 25, 2006).

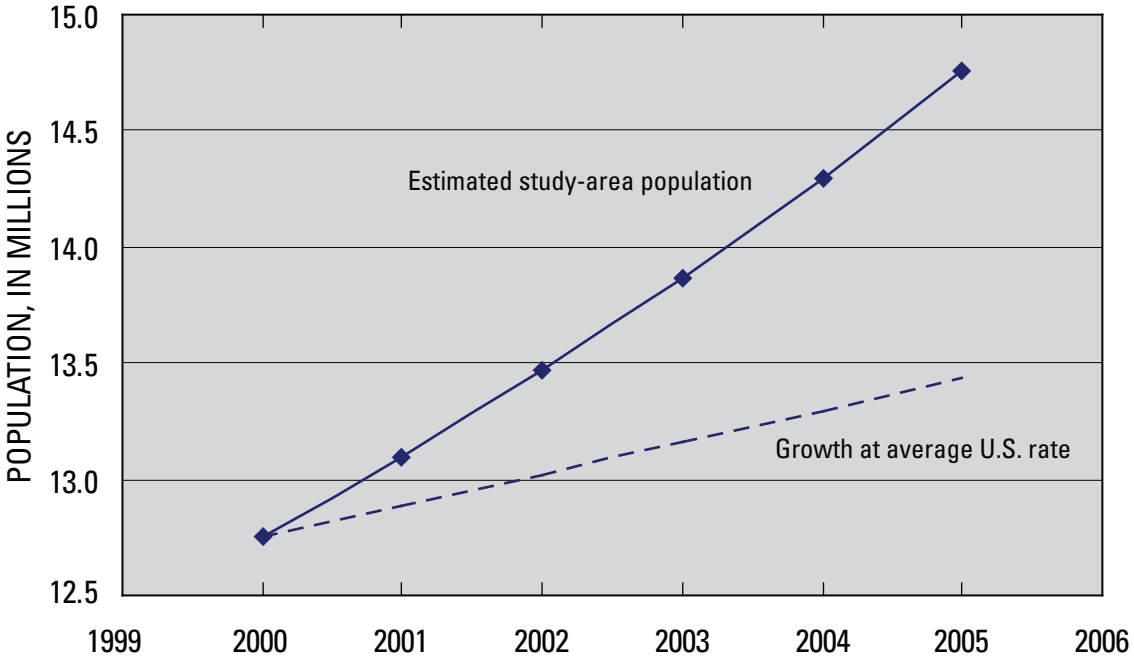

Figure 2. Estimated population of the arid and semiarid southwestern U.S., 2000–2005. Compiled from county-level estimates (U.S. Census Bureau, 2006). Points represent the sum of population estimates for counties having at least half their acerage within the study-area boundary. Dashed line shows theoretical growth at the average rate for the entire United States during the same time period.

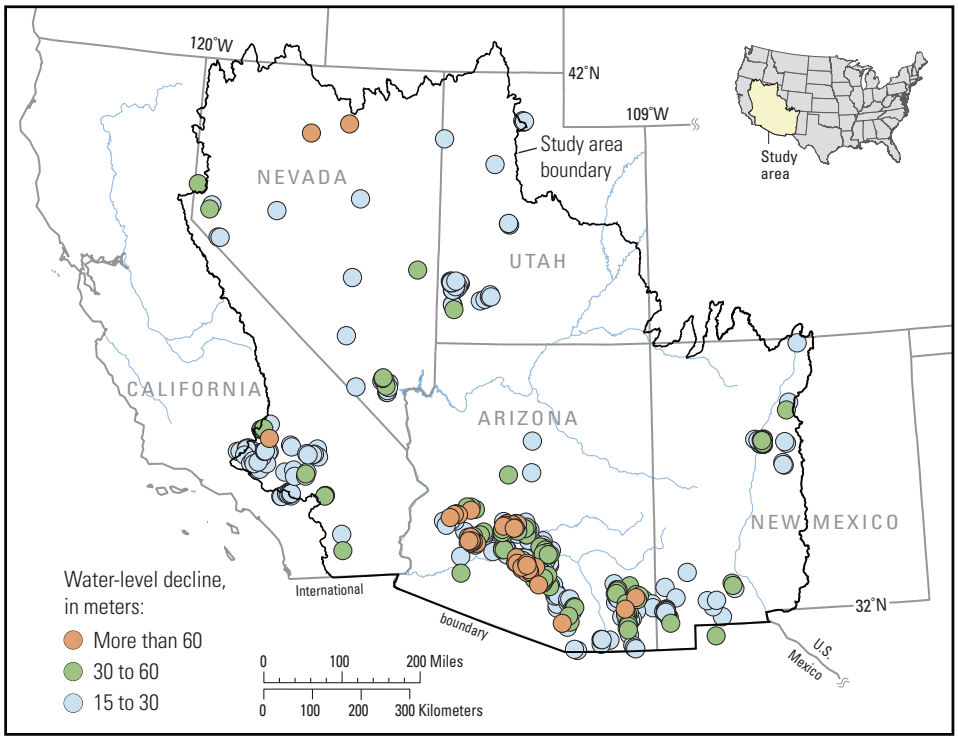

Figure 3. Historic water-level declines in producing aquifers of the arid and semiarid southwestern United States. Water levels have recovered in some areas in response to reduced pumping, optimization, and other management measures. Modified from Leake and others (2000) and Bartolino (2003).

Thermal and geophysical techniques that were developed in the course of the studies are presented in the appendices.

The purpose of this chapter is to provide an overview of climatic and geologic controls on ground-water recharge in the study area. Vegetative and land-use controls also are discussed. Controls on recharge involve a wide range of time scales, from seasonal fluctuations to multimillennial cycles of glaciation and deglaciation. The pluvial periods responsible for much of the ground-water resource in parts of the study area are associated with the growth of massive ice sheets north of the study area. Rates of ground-water recharge during pluvial periods were as much as an order of magnitude higher than at present.

Climatic Framework of Ground-Water Recharge

Mean Circulation, Storms, and Seasonality

The characteristic aridity of the study area results primarily from global circulation patterns and topographic effects. Average atmospheric circulation is roughly aligned with latitude, as manifested most clearly in the tropics (Peixoto and Oort, 1992). Preferential solar heating of equatorial regions with planetary rotation gives rise to Hadley cells, which straddle the intertropical convergence zone (ITCZ). Surface air in the Hadley cells moves obliquely toward the ITCZ, picking up moisture from tropical oceans before rising aloft. Rising air cools by expansion, creating copious "signature" clouds, before diverging poleward. Moisture-depleted air returns earthward at about 30° north and south latitude. Subsiding air warms by compression, reducing relative humidity. Earth's nonpolar deserts, including the study area, are located within zones of descending dry air at the poleward limits of Hadley cells.

The transport of heat, momentum, and water vapor in the midlatitudes is largely through the emergent action of cyclones, fronts, meandering jets, and planetary waves (Martin, 2006). Nevertheless, winds in the extratropics tend to be westerly. Storms in the study area usually arrive from the Pacific Ocean—particularly in winter, when the area receives most of its precipitation from large-scale frontal systems. In summer, the westerlies weaken. Summer storms form mostly in response to thermally and topographically driven breezes fed by tropical and subtropical moisture entering the region in brief bursts. This general picture of moisture transport is irregularly but recurrently disrupted by storm-track shifts and tropical feeds associated with El Niño-Southern Oscillations and other large-scale interactions between the oceans and atmosphere (Liu and Alexander, 2007).

Moving inland, air masses pass over mountain ranges, losing moisture from orographic lifting. With respect to prevailing storm tracks, the study area is in the rain shadow of its bounding ranges.

Topographic feedback can induce and amplify instabilities. The interaction of prevailing westerlies with the crest of the Sierra Nevada generates cyclones that, given sufficient humidity, bring modest but ecologically critical quantities of rain to the eastern Great Basin in spring and fall (Houghton, 1969).

Large-scale horizontal atmospheric transport is unstable. Storms form at the boundaries of contrasting air masses, which reorganize the air masses to steepen frontal boundaries. The broad band of westerly winds in the midlatitudes, especially over the North Pacific, steers atmospheric disturbances into or around the study area. In summer, an area of persistent high pressure forms west of the study area, at about 30–40° north latitude and 140–150° west longitude. Clockwise rotation around this high-pressure area deflects eastward-moving storms north of the study area. In winter, the high-pressure area weakens and shifts southward. While most storms still miss the study area, their trajectories dip southward, imparting a strong winter-precipitation signal to regional climate. Storms originating in the north Pacific increase in frequency and intensity, as a persistent area of low-pressure near the Aleutian Islands deepens in winter (Houghton, 1969).

Combined with planetary rotation and redistribution of heat, long-range momentum transport gives rise to jet streams in the lower stratosphere (Baldwin and others, 2007). Recent work has focused on a different set of jet streams that form in the lower troposphere, about 0.5 to 2 km above sea level (Ralph and others, 2006). These low-level jets feed narrow plumes of tropical and subtropical moisture to winter storms affecting the study area. These "atmospheric rivers" provide the bulk of precipitation to many of the wettest storms (Kerr, 2006).

Preferential heating of the continent relative to the ocean in summer induces onshore shifts in low-altitude winds. This summer monsoon feeds tropical moisture to convective afternoon thunderstorms formed by thermal updrafts over topographic highs. Monsoonal precipitation often dominates in the southern and eastern portions of the study area.

The Arizona monsoon that affects the study area represents the highly variable northernmost fringe of the much larger, North American Monsoon, centered in northern Mexico (Douglas and others, 1993). Most of the monsoonal moisture reaching the study area comes from the tropical Pacific, although the Gulf of Mexico contributes as well (Hales, 1973; Michaud and others, 1995; Diem and Brown, 2006). The Gulf of California forms a topographic corridor that channels monsoonal "surges" across the southwestern boundary of the study area (Hales, 1972; Brenner, 1974). Monsoonal transport is characterized by gentle breezes in the lower troposphere (Bordoni and others, 2004). Occasionally the transport gains upper-level support, resulting in rapid movement of large quantities of moisture into the study area. Figure 4 shows a monsoonal event that delivered torrential rain to the southeastern part of the study area in 2006 (Magirl and others, 2007). Monsoonal events can deliver precipitation farther west or north than in the selected example, or to nearly the entire study area at once.

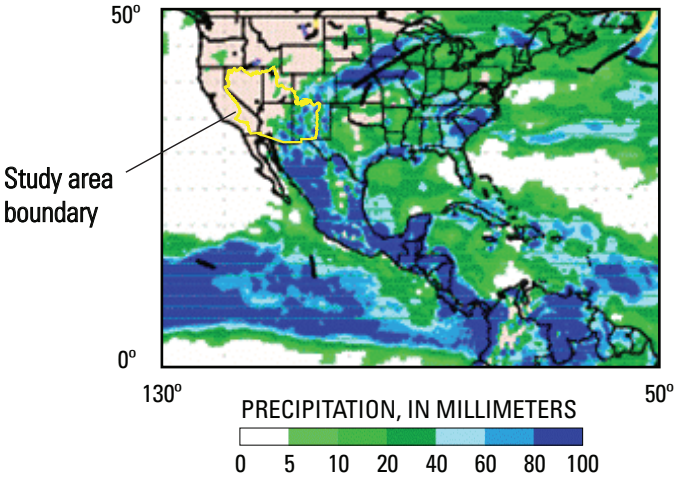

Figure 4. Monsoonal conditions bring rain to the arid and semiarid southwestern U.S. in summer. Example shows total rainfall during August 1–10, 2006, a period of exceptionally heavy monsoonal storm activity. Image derived from National Weather Service, Climate Prediction Center, storm track assessment for August 2006 (http://www.cpc.ncep.noaa.gov/products/precip/CWlink/stormtracks/NHA_200608_full.gif, last accessed October 24, 2006).

The main sources of atmospheric moisture reaching the study area are the tropical and subtropical oceans in summer and the tropical through North Pacific Ocean in winter. Although oceans provide the primary reservoir for atmospheric water vapor, soil moisture represents a secondary reservoir that can add persistence to wet periods by supplying water through evapotranspiration (Entekhabi and others, 1996). Work in the Sahel, the southern border of the Sahara Desert, suggests that soil-moisture and evapotranspiration gradients actively modify surface winds in monsoonally affected arid and semi-arid regions (Taylor and others, 2007).

Walker Circulation, El Niño-Southern Oscillation, and Pacific Decadal Oscillation

Superimposed on seasonal changes in precipitation are longer-acting processes that strongly affect the study area. Free oscillations of the coupled ocean-atmosphere system, known as El Niño-Southern Oscillation (ENSO), produce irregular three-to-seven year cycles in the location of warm Pacific surface waters, polarity of atmospheric-pressure anomalies, and strength and direction of equatorial trade winds (Bjerknes, 1969; Philander, 1990; McPhaden and others, 2006). Under normal conditions, easterly trade winds push warm surface water to the western side of the tropical Pacific. Cool replacement water rising from the depths of the eastern Pacific diminishes the supply of atmospheric moisture to the Americas. Pooling warm water in the western equatorial Pacific is the locus of upwelling moist air, which—after cooling and losing moisture—diverges eastward in the upper troposphere before subsiding downward over the Americas to close the loop (Walker, 1924). The Walker circulation is embedded in and interrupts the Hadley-cell circulation.

The normal mode of Walker circulation results from positive feedback between ocean and atmosphere. Trade winds push warm water to the western Pacific, where rising hot air sustains the trade-wind circulation (Philander, 1990). During the El Niño (or positive) phase of the ENSO cycle, the feedback becomes negative—the trade winds weaken, the pool of warm water migrates east, and the study area becomes wetter (fig. 5). El Niño conditions bring southward adjustments of winter tracks, leading to wetter conditions—particularly in the Great Basin and Mojave Deserts (Menking and Anderson, 2003).

Enhanced precipitation during the positive phase of ENSO cycles forms part of a precipitation dipole, that is, increases in the study area are offset by decreases in the Pacific Northwest (Dettinger and others, 1998). The strength of the ENSO-induced dipole becomes weaker or stronger according to a longer-period fluctuation in the ocean-atmospheric system, the Pacific Decadal Oscillation (PDO; Mantua and others, 1997). The PDO results from multiyear persistence in North Pacific sea-surface temperatures, perhaps from large-scale circulations of surface water (Mantua and Hare, 2002). The PDO imparts decadal-scale variability to

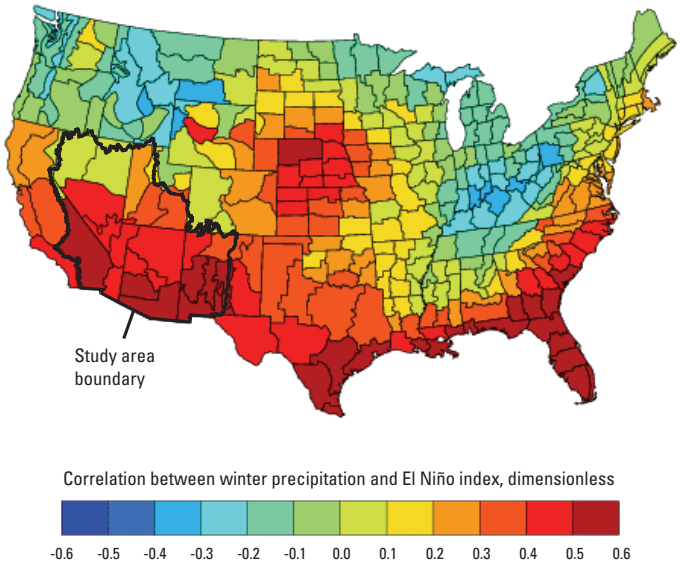

Figure 5. Correlation of the El Niño 3.4 index (positive during El Niño phases of El Niño-southern oscillation cycles) with precipitation from December through March for the period of record (1949–2006). The index is the average anomaly (departure from mean) of equatorial Pacific surface-water temperatures within a region bounded by +5 to -5 degrees latitude and -120 to -170 degrees longitude (Curtis and Adler, 2000). Data from the NOAA Climate Diagnostics Center, http://precip.gsfc.nasa.gov (last accessed December 7, 2006).

North American climatic patterns (Cayan and others, 1998; McCabe and Dettinger, 2002).

Interacting ENSO and PDO processes modulate precipitation and ground-water recharge in the study area (Flint and others, 2004; chapter B, this volume). Ground-water levels near areas of active recharge respond, in a damped fashion, to produce an integrated climatic signal (Dickinson and others, 2004). Ground-water recharge near Tucson, Ariz., during 1977–1998—a period of frequent El Niños and high values of the PDO index—was three times higher than during 1941–1957—a period of more-normal ENSO and PDO index values (Pool, 2005). Spectral analysis shows that ENSO, PDO, and the North American monsoon index modulate ground-water recharge in basins all across the study area (Hanson and others, 2006).

Natural Variability—Pleistocene Pluvials to Holocene Droughts

Glacial-Interglacial Cycles

Variability in the climate system is considerable. The largest variations relevant to ground-water recharge relate to the expansion of continental ice during glacial periods, when the interior southwestern United States became cooler and wetter than it is today (Grayson, 1993). Persistent pluvial conditions caused lakes to form and grow in inland basins. Closed-basin lakes overtopped their divides, coalescing into massive fresh-water seas that covered large parts of the study area (Feth, 1961; Benson, 2004).

The isotopic composition of ground water indicates that much of it represents paleorecharge that occurred prior to the Holocene in drier parts of the study area (Winograd and Thordarson, 1975; Benson and Klieforth, 1988; Eastoe and others, 2004; Izbicki and Michel, 2004; Plummer and others, 2004; Stonestrom and others, 2004). Numerical models of ground-water flow indicate that recharge rates were more than an order of magnitude higher during the last glacial maximum in New Mexico and likely elsewhere in the study area (Sanford and others, 2004). Midlatitude deserts elsewhere contain paleorecharge, although the timing of pluvials was not entirely synchronous on all continents (Edmunds, 1998; Scanlon and others, 2006).

Ice ages almost certainly involve orbital forcing, although changes in atmospheric carbon-dioxide levels, vegetation, and oceanic-atmospheric circulation patterns form a complex web of feedbacks that control the balance of continental ice (Gildor, 2003; Ji and others, 2006; Paillard, 2006; Roe, 2006; Montanez and others, 2007). The initiation of glacial-interglacial cycles three million years ago corresponded to the replacement of persistent El Niño conditions in the tropical Pacific by a modern ENSO mechanism—about the time the Panamanian isthmus formed an eastern limit to tropical Pacific circulation (Ravelo and others, 2006). About four-hundred thousand years ago, the cycle of glaciations and deglaciations changed from a roughly one-hundred thousand year period to a forty-thousand year period. During the last four-hundred thousand years, atmospheric levels of carbon dioxide have fluctuated between 180 and 300 parts per million, in virtual lockstep with global temperatures (Fedorov and others, 2006).

Present circulation patterns tend to steer frontal systems north of the study area, as previously discussed. Paleoclimate models and proxy data indicate that the Laurentide ice sheet split the northern hemisphere jet stream into a polar jet and a low-latitude jet, bringing abundant precipitation to the study area (Antevs, 1948; Kutzbach and Wright, 1985; COHMAP, 1988; Webb and Bartlein, 1992). In addition to storm-track modification, lower temperatures would reduce evapotranspiration rates, further increasing ground-water recharge during glacial periods.

During interglacial periods, ecological succession established xerophytes that were highly adapted for scavenging soil moisture (Walvoord and others, 2002; Walvoord and others, 2004). Vegetation is decisive in determining the near-surface water balance under conditions of high aridity (Gee and others, 1994). The presence and amount of ground-water recharge in most parts of the study area is strongly controlled by plants (Phillips and others, 2004; Scanlon, Levitt, and others, 2005; Seyfried and others, 2005; Sandvig and Phillips, 2006).

Holocene Droughts and Holocene Pluvials

Severe drought gripped the study area during 1999–2004 (chapter C). This drought was the most severe in the United States since the late 1930s and early 1940s (Phillips and Thomas, 2005; Andreadis and others, 2005). Warm, dry conditions extended far beyond the study area. The spatial extent and magnitude of temperature anomalies exceeded those during the Medieval Warm Period (roughly 800–1300 AD), which affected major parts of the Northern Hemisphere (Osborn and Briffa, 2006).

Compared with present-day conditions, large parts of the study area during the past millennium have been characterized by extended, severe droughts with minimal ground-water recharge. Occasional wetter periods with elevated recharge—though shorter and less frequent— also have occurred. Indicators of preinstrumental climate change include plant remains in packrat middens (Betancourt and others, 2000), isotopic variations in lake sediments (Benson and others, 2002), landforms in intermittently deflationary basins (Menking and Anderson, 2003), and annual growth rings in trees and speleothems (Cook and others, 2004; Rasmussen and others, 2006; Leavitt, 2007).

The frequency of drought during the twentieth century is strongly linked to oceanic-atmospheric feedbacks embodied in the Pacific Decadal Oscillation and Atlantic Multidecadal Oscillation (McCabe and others, 2004; Benson and others, 2006). Paleoclimate reconstructions based on tree-ring data for the last 1,200 years indicate that extended droughts occurred repeatedly from 900 to 1300 (Cook and others, 2004; Meko and others, 2007). This 400-year period of chronic drought

generally had negative PDO index values, and it coincided with the collapse of major agricultural societies within the study area (MacDonald and Case, 2005; Benson and others, 2007).

Though less well resolved, the middle Holocene was also characterized by prolonged drought. Severe drought from 6.5 to 3.8 thousand years before present is evident in the sediments of dry lakes in the western Great Basin (Benson and others, 2002). Desiccation arrived earlier in the Estancia Basin of New Mexico, where blowouts and eolian landforms indicate that ground-water levels started dropping markedly nine thousand years ago (Menking and Anderson, 2003).

Tree-ring data for the past 1,200 years indicate the presence of several pluvial periods during the last 1,200 years. The best characterized of these is a 13-year period of wet conditions that affected the southwestern United States from 1905 to 1917 (Woodhouse and others, 2005). Also, the general climate of the study area was significantly wetter during the early to mid twentieth century than during the earlier part of the record. This trend reversed in the second half of the twentieth century when, despite moderate increases in precipitation, sharply rising temperatures contributed to increasing drought severity across the interior southwest (Andreadis and others, 2005; Andreadis and Lettenmaier, 2006).

Anthropogenic and Land-Cover Controls on Recharge

Global warming of the last few decades is projected to continue (Houghton and others, 2001, 2004; Stainforth and others, 2005; IPCC, 2007; Rahmstorf and others, 2007; Raupach and others, 2007). As currently implemented, global circulation models of climate may underpredict warming due to feedbacks produced by global carbon pools (Scheffer and others, 2006; Torn and Harte, 2006; Zimov and others, 2006; Matthews and Keith, 2007), increasing humidity in the upper troposphere (Soden and others, 2005), and model bias (Shukla and others, 2006). An expected effect of warming is intensification of the hydrologic cycle, reflecting increased heat storage and thermal gradients (Pierrehumbert, 2000; Huang, 2006). Consensus estimates from global circulation models suggest that the intensity of storms in the study area will increase, if not necessarily the total amount of precipitation, as will the frequency and severity of heat waves and droughts (Tebaldi and others, 2006; Hoerling and Eischeid, 2007; Seager and others, 2007). The recent drought, which affected southwest Asia and southern Europe in addition to the study area, corresponded to unprecedented warmth in the western Pacific in 1998-2002 (Hoerling and Kumar, 2003).

Global circulation models that successfully simulate the Aleutian low and north Pacific storm tracks, among other features, suggest that North American storm tracks could shift poleward under a wide range of projected climates (Yin, 2005; Salathé, 2006). Hadley cell enlargement is expected to cause poleward expansion of dry subtropical zones (Lu and others, 2007). However, such shifts in zonal averages produce only small changes in precipitation at mid-latitudes, where agreements between model predictions and measurements are poor (Zhang and others, 2007). The response of El Niño-Southern Oscillation to warming is far more relevant to the study area, if less clear. Models and data suggest that the Walker circulation may weaken with warming (Vecchi and others, 2006). Persistent El-Niño conditions have been predicted under several emissions scenarios (Meehl and others, 2006). The significance of these results is unclear, as close inspection shows that current models have difficulty matching historic ENSO patterns (Lin, 2007). Models of monsoonal precipitation response are likewise uncertain (Webster and others, 1998; Mo and others, 2005).

Climate change is predicted to have a large effect on water resources east of the study area (Small, 2005; Scibek and Allen, 2006; Baettig and others, 2007). The most likely change expected in the study area is a marked shift in precipitation to less snow and smaller snowpack accumulation. The effects of warmer temperatures on snowpack are already evident in earlier runoff generation (Service, 2004; Dettinger, 2005). Snowmelt is highly efficient at generating ground-water recharge, so that a shift from snow to rain will decrease recharge even if total precipitation remains the same (Earman and others, 2006).

Large-scale replacement of native vegetation by urban, suburban, and agricultural land use may have impacted ground-water recharge more than recent changes in climate (Foley and others, 2005). Construction of impermeable areas alters rainfall-runoff relations and location of infiltration (Filippone and Leake, 2005). Irrigation induces ground-water recharge (Stonestrom and others, 2004) and produces evaporative cooling over large regions (Kueppers and others, 2007). Because native vegetation is highly adapted to extracting soil moisture, its replacement by agricultural crops can reverse the direction of water flow in the unsaturated zone, inducing ground-water recharge even in regions of dryland farming (Scanlon, Reedy, and others, 2005).

Considering future climates, anthropogenic emissions may have precluded an imminent return to glacial-pluvial conditions (Crucifix and Berger, 2006; Ruddiman, 2006). Carbon-dioxide levels during the Pliocene suggest that a level of about 400 parts per million will prevent the formation of continental ice sheets in the Northern hemisphere (Sternberg, 2006). Levels of 400 parts per million are expected within ten years under all emissions scenarios (Sarmiento and Gruber, 2002).

Geologic Framework of Ground-Water Recharge

The study area has been subdivided into six geologic subregions to facilitate description of the wide range of conditions present. The areas are the Eastern Great Basin, Western Great Basin, Mojave-Colorado Desert Area, Arizona Sonoran Desert-Mexican Highland Area, Rio Grande Rift-Southwest-

ern New Mexico, and the South-Central Colorado Plateau Area (fig. 6). These areas have been further subdivided into hydrologic units used by the U.S. Geological Survey. The 195 hydrologic units present are shown on figure 6. These units consist of one or more structural basins that have been grouped together for study and accounting purposes. The principal characteristics of the geologic regions are summarized in table 1.

The Eastern Great Basin is an area of internal drainage that receives most of its water supply from precipitation that falls along the Wasatch Front on the eastern side of the subregion. Winter snowfall accumulates in the higher mountains, and much of the annual recharge is derived from spring snowmelt. Mountains along the western and northern borders also provide additional moisture. The central part of the subregion is occupied by several large desert basins, the Great Salt Lake, the Salt Lake Desert, Sevier Desert, and the Escalante Desert. Carbonate rocks are present in much of the Eastern Great Basin, where they form mountains and underlie basin-fill sediments. The carbonate rocks generally are permeable, and relatively high rates of recharge occur in mountains where they are exposed. In some areas, this causes the recharge process to be dominated by in-place recharge in the mountains. Multibasin ground-water flow systems exist where there is a regional ground-water gradient and hydraulic continuity between basins is provided by carbonate rocks.

The Western Great Basin in many ways mirrors the Eastern Great Basin, where much of the water supply comes from precipitation that falls on the Sierra Nevada. Additional moisture is provided by several high mountain ranges along the northeastern and eastern boundaries of the subregion. As with the Eastern Great Basin, most of the annual recharge occurs during the spring snowmelt. A significant difference between the two subregions is the rain shadow that exists along the eastern margin of the Sierra Nevada. Although the eastern margin receives significant runoff from the mountains, local precipitation is much less than it would be without

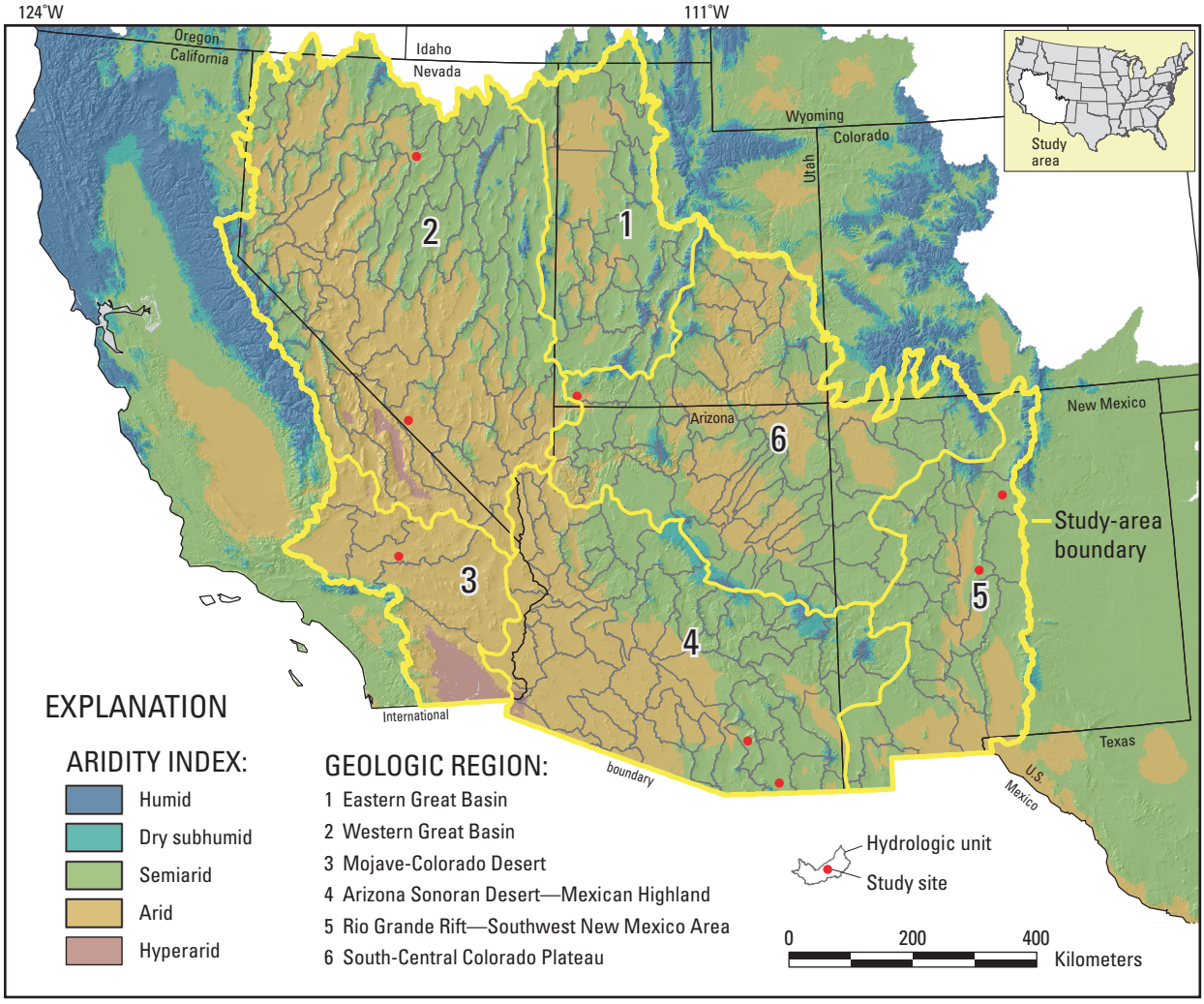

Figure 6. Geologic regions, hydrologic areas, and aridity classification for the southwestern U.S. study area. The aridity index is the ratio of mean annual precipitation to mean annual potential evapotranspiration. Index values ranging from 0 to 0.05 denote hyperarid conditions. Ranges of 0.05–0.2, 0.2–0.5, 0.5–0.65, and greater than 0.65 denote arid, semiarid, dry subhumid, and humid conditions, respectively (UNESCO, 1979).

Table 1. Principal characteristics of geologic subregions.

	Eastern Great Basin	Western Great Basin	Mojave-Colorado Desert	Arizona Sonoran Desert-Mexican Highland	Rio Grande Rift-Southwestern New Mexico	South Central Colorado Plateau
Area, in thousands of square kilometers	106	315	71	204	114	233
Climate classification and number of hydrologic units						
Hyperarid	0	1	1	0	0	0
Arid	7	25	5	24	10	19
Semiarid	12	27	0	27	10	27
Dry subhumid	0	0	0	0	0	0
Humid	0	0	0	0	0	0
Total	19	53	6	51	20	46
Drainage type and principal rivers						
Drainage type	Internal	Internal[1]	Internal	Mostly external, to Colorado River[2]	Mostly external, to Rio Grande[3]	External, to Colorado River
Principal rivers	Jordan R.[4] Logan R.[4] Sevier R.[4] Weber R.[4]	Carson R.[4] Humboldt R.[4] Owens R.[4] Truckee R.[4] Walker R.[4] Colorado R. Muddy R. Virgin R.	Mojave R.[4]	Gila R. Colorado R. Little Colorado R. Salt R.	Rio Grande	Green R. Colorado R.
Location and altitude of highest and lowest points						
Highest point and altitude, in meters	Delano Peak 3,697	Mount Whitney 4,418	San Gorgonio Mountain 3,501	Humphreys Peak 3,682	Wheeler Peak 4,011	Windom Peak 4,295
Lowest point and altitude, in meters	Great Salt Lake 1,281	Death Valley -86	Salton Sea -72	Colorado R. at the Southerly International Boundary 30	Rio Grande near El Paso, Texas 1,140	Colorado R. at Grand Canyon NP[5] 366

[1]Most areas have internal drainage; however, several areas drain to Colorado River.

[2]Most areas drain to Colorado River; however, several areas have internal drainage.

[3]Areas east of continental divide drain to Rio Grande.

[4]River flows to terminal basin.

[5]Colorado River at west boundary of Grand Canyon National Park (NP).

the rain shadow. Carbonate rocks are present in much of the eastern and southeastern part of the subregion. The western and west-central parts of the subregion are underlain mostly by volcanic, intrusive, and metamorphic rocks. Carbonate rocks are present in localized areas. The subregion has been, and still is, undergoing structural extension. This extension has resulted in a basin-and-range topography where generally north-south trending mountain ranges are separated by intervening valleys. The valleys are structural depressions that are partly filled by materials derived from the adjacent mountains. A pronounced regional topographic gradient exists in the southern part of this subregion. The valley floors in the east-central part of the subregion have altitudes of slightly more than 1,830 m. These altitudes decrease to the south and southwest to a low of 86 m below sea level on the Death Valley playa. This gradient exists in an area that is mostly underlain by carbonate rocks and has interbasin ground-water flow. Some of these areas of carbonate rock are highly permeable and readily allow recharge to occur. In these areas the recharge occurs mostly in the mountains.

The Mojave-Colorado Desert subregion occupies southern California south of Panamint and southern Owens Valleys. It is bordered on the west by the southern Sierra Nevada, the western San Bernadino Mountains, and several costal basins. Snowmelt creates substantial amounts of runoff from the two major mountain ranges. Snowmelt runoff in the remainder of the area is minor. The Mexican border, a political division, forms the southern boundary of the current study area, even though the Mojave-Colorado physiographic region extends about 80 km farther south. The western boundary of the Colorado River drainage forms the eastern boundary. The most significant mountain ranges are the southern Sierra Nevada and the San Bernadino Mountains. The Mojave River originates on the northern flank of the San Bernadino Mountains and flows to the north where it terminates at the Soda Lake Playa near the northern boundary of the subregion. Mountain ranges in the rest of the area are relatively small and have little local relief. This area is underlain mostly by intrusive, volcanic, and metamorphic rocks that do not transmit water readily. The structural basins are filled with materials derived from the nearby mountains. Consequently most recharge and ground-water flow occurs in basin-fill deposits.

The Arizona Sonoran Desert-Mexican Highlands subregion occupies the southwestern half of Arizona and includes small areas of southwestern New Mexico and southeastern California. The subregion is bordered on the north by the Colorado Plateau, on the west by the drainage divide of the Colorado River and the Mojave-Colorado Desert Area, on the south by Mexico and on the east by basins of the Rio Grande Rift-Southwestern New Mexico subregion. The subregion contains basin and range structures similar to those in the Eastern and Western Great Basins; however, their orientation differs slightly, and major basin subsidence ended 6–10 million years ago (Anderson and others, 1992, p 13). Extension remains active in the Eastern and Western Great Basins. Consequently, the basin and range topography in the Arizona Sonoran Desert-Mexican Highlands subregion is more mature than in the Eastern and Western Great Basin subregions. The structural basins are more completely filled and, overall, the local relief between valley floors and mountain crests is less. This suggests that the orographic effect that causes much of the precipitation in the higher mountains of the Eastern and Western Great Basin is less of a factor in this subregion. However, monsoonal summer rains are significant in the Arizona Sonoran Desert-Mexican Highlands subregion. These rains are triggered primarily by convective heating and are not as dependent on local relief and the orographic effect as the winter precipitation and snowmelt runoff, which provides most of the water supply in the Eastern and Western Great Basins. The Arizona Sonoran Desert-Mexican Highlands subregion is underlain mostly by intrusive, volcanic, and metamorphic rocks that do not transmit water readily. Consequently, most recharge and ground-water flow occurs in basin-fill deposits.

The Rio Grande Rift-Southwestern New Mexico subregion is along the southeastern boundary of the study area in Central New Mexico. It is bounded on the west by the South-Central Colorado Plateau subregion and the Arizona Sonoran Desert-Mexican Highlands subregion (the western boundary also corresponds roughly with the continental divide), on the south by Mexico, on the east by the Great Plains physiographic province, and on the north by the San Luis Valley. This subregion is traversed by the Rio Grande River, which flows through the down-dropped graben associated with the rift structure. Some of the hydrologic areas drain directly to the Rio Grande River, others are isolated basins. The basin fill is recharged by infiltration of runoff at or near the mountain front and by some direct infiltration of precipitation and snowmelt. Monsoonal summer rains are common in this subregion, and they supply a significant part of the annual recharge. Areas along the Rio Grande can receive recharge from or discharge water to the river depending on the relation between the water table and river stage.

The South-Central Colorado Plateau subregion includes the southwestern part of Utah, most of northern and northeastern Arizona, and the northwestern part of New Mexico. The hydrologic areas are drained externally and are part of the Colorado River drainage. This subregion differs from the others in that its most significant characteristic is a large area of relatively uniform uplift. The uplifted area has been eroded to form the canyon-plateau topography that typifies the subregion. This subregion does not contain the extensive basin-fill deposits characteristic of the other subregions. Alluvium is present as flood-plain deposits, and in some cases as valley floor deposits, but these deposits formed in a canyon or valley that is primarily an erosional feature. Recharge occurs as direct infiltration of precipitation and snowmelt, or as seepage of streamflow into joints, fractures, and pore spaces of consolidated and semiconsolidated rocks.

Evolution of the Geologic Framework

The geologic history and evolution of the arid southwest has produced a framework of igneous and metamorphic rocks,

sedimentary rocks and deposits, structures, topography, and landforms that exert strong controls on the occurrence and distribution of recharge. The six subregions that comprise the study area vary in their history and in the way that the geologic framework effects the occurrence and distribution of recharge. Discussion of the evolution of the geologic framework begins in Proterozoic time when basement-rock aquitards were formed beneath most of the study area. This initial event was followed by a series of successive geologic events and processes that extend to the present. The more significant of these events are listed in table 2 (adapted from Chuang and others, 2003). Table 2 also lists the hydrogeologic consequences of the events for each of the six subregions. For any given event, the hydrogeologic consequences sometimes vary between the subregions. Major events in the evolution of the geologic framework affecting the present-day occurrence and distribution of recharge are listed below in chronological order.

Paleozoic Era

During the Paleozoic Era, spatially extensive carbonate units formed in the Eastern and Western Great Basins, and smaller carbonate units formed in the Mojave-Colorado Desert and Arizona Sonoran Desert-Mexican Highland subregions. Today these carbonates constitute regional and locally important aquifers. Extensive exposures of permeable carbonates crop out in the mountains of both Eastern and Western Great Basin subregions. Rainfall and snowmelt in the mountainous areas provides the dominant component of recharge to the carbonate aquifers in these areas.

Mesozoic Era

During the Mesozoic Era, continental sediments and sandstone aquifer units formed in the Colorado Plateau subregion. Most of the present-day recharge in the subregion occurs in the areally extensive eolian sandstone that formed during this time.

Tertiary Period

Onset of extensional faulting began in early Tertiary time in all areas except the Colorado Plateau. The extensional faulting has resulted in the basin and range topography characteristic of most of the study area. The basins have partially filled with alluvial and colluvial deposits that form the basin-fill aquifers. Most of the present-day recharge occurs to aquifers that started forming in the early-to-mid Tertiary. Recharge to the extensive Paleozoic carbonate aquifers is often through basin fill in the Eastern Great Basin. Mountain ranges that formed during Tertiary extension receive more precipitation (in the form of rain and snow) than the intervening valleys. This orographically produced precipitation produces most of the present-day recharge. Active extension continues at present in the Eastern and Western Great Basins.

Pliocene Epoch to Quaternary Period

The regional uplift and desiccation of the Colorado Plateau and integration of drainages included the formation of the Colorado, Gila, and Salt Rivers and formation of the present-day topography. There was also a period of Pleistocene pluvial conditions when lakes were formed throughout the study area, and most drainages supported perennial streams and rivers. The pluvial period ended during the Holocene Epoch, when there was widespread aridification. Playas dried and flow in streams and rivers was reduced or, in some cases, dried up. Ground-water recharge and discharge were reduced in accordance with the degree of aridification. Currently, recharge in the study area appears to be approximately in balance with the natural ground-water discharge. There is little change in ground-water storage except for the depletion caused by pumping.

Hydrogeologic Units

During the evolution of the geologic framework, a series of sedimentary, volcanic, intrusive, and metamorphic rocks was formed throughout the study area. For purposes of this study, these units have been grouped into categories with similar hydrologic properties. The five groups are (1) basin-fill/alluvium, (2) noncarbonate sedimentary rocks, (3) carbonate sedimentary rocks, (4) volcanic rocks, and (5) intrusive and metamorphic rocks. The distribution of these rocks is shown in figure 7, and their characteristics are described in table 3.

Major Aquifers

Throughout the arid and semiarid Southwest, ground water provides a substantial part of the water supply—in some places providing the sole source of water. The U.S. Geological Survey National Atlas delineates five major aquifers in the study area (fig. 8): (1) basin-fill, (2) carbonate-rock, and (3) volcanic-rock aquifers in the Great Basin subregions, (4) Colorado Plateau aquifers in the South-Central Colorado Plateau subregion, and (5) the aquifer system of the Rio Grande Rift-Southwestern New Mexico subregion (comprising mostly basin-fill aquifers).

Basin-fill aquifers are capable of storing large amounts of water that is readily supplied to wells. Basin-fill aquifers are the most common aquifers in the study area and are the dominant aquifer type in all subregions except the Colorado Plateau. Most of the pumpage in the study area is from basin-fill aquifers, and recharge occurs mainly at or near the surrounding mountain fronts. Recharge also occurs where streams flow across alluvial fans and where streams or rivers flow through valley lowlands. During sustained precipitation events, there can also be direct recharge from precipitation.

Basin and range carbonate-rock aquifers occur in the mountains and underlie basin-fill deposits in large parts of the Eastern and Western Great Basin subregions. Where carbonate rocks are present, significant recharge commonly occurs in

Table 2. Hydrogeologic framework of the arid and semiarid southwestern United States

[Adapted from Chuang and others (2003). Dashes denote regional absence or indirect manifestation only though inheritance. Bold italics indicate formation and recharge of current aquifers]

Eon, era, period, or epoch	Geologic process	Hydrologic consequence, by region					
		Eastern Great Basin	Western Great Basin	Mojave-Colorado Desert	Arizona Sonoran Desert-Mexican Highland	Rio Grande Rift-Southwestern New Mexico	South-Central Colorado Plateau
Proterozoic	Continental basement rocks created	Aquitards form	Aquitards form	Aquitards form	Aquitards form	Aquitards form.	Aquitards form
	Local rift basins open	—	Local ***carbonate aquifers*** form	Local ***carbonate aquifers*** form	Local ***carbonate aquifers*** form	—	Local siliclastic units form
	Continental rifting and truncation	—	Most older basement rocks obliterated	—	—	—	—
Paleozoic	Continental slope and oceanic basin deposition	—	Locally ***thick carbonate aquifers*** form	—	—	—	—
	Passive margin marine shelf deposition	***Thick carbonate aquifers*** form	Locally ***thick carbonate aquifers*** form	—	—	—	—
	Continental and shallow marine deposition	—	—	Thin ***carbonate aquifers*** form	Thin ***carbonate aquifers*** form	Thin ***carbonate aquifers*** form.	Thin ***eolian sand*** and ***carbonate aquifers*** form
	Orogenesis, chiefly contractual	—	—	—	—	—	—
	Overthrusting	Carbonate aquifers disrupted	Carbonate aquifers locally concealed	—	—	—	—
	Deposition of foreland basin wedges	Carbonate aquifers disrupted or concealed	Carbonate aquifers disrupted or concealed	—	—	—	—
	Late Paleozoic uplift, basin formation, regional desiccation	Local evaporites form	—	Local evaporites form	Local evaporites form	—	Highlands erode, basins fill with clastics; local evaporites form
Mesozoic to early Cenozoic	Contractional orogenesis	—	—	—	—	—	—
	Regional uplift, emergence, and erosion in most areas	—	—	—	—	—	—
	Overthrusting	Carbonate aquifer disrupted	Carbonate aquifer disrupted	—	—	—	—
	Arc magmatism and metamorphism	Local plutonic basement forms	Metavolcanic and plutonic basement forms	Plutonic basement forms	Volcanic and plutonic basement forms	—	—
	Orogenisis; sedimentation in foreland basins	Marine clastics deposited	Marine clastics locally deposited	Marine clastics deposited	Marine clastics deposited	—	Marine and non-marine clastics deposited
	Deposition of windblown sand sheets	Local ***sandstone aquifers*** form	—	Quartzites form	Quartzites form		Local ***sandstone aquifers*** form
	Monclinal and block uplift	Local evaporites form	—	—	—	—	Horizontal aquifers disrupted
Tertiary	Activation of transform continental margin	Sinistral faulting	Walker Lane faulting; ***basin-fill aquifers*** form	E. Calif. shear faulting; ***basin-fill aquifers*** form	—	—	Colorado Plateau rotates clockwise
	Eocene extension and calcic-alkaline magmatism	Broad alluvial basin conglomerates, lake-bed sediments, lavas, and welded tuffs form	—	—	—	—	—

Table 2. Hydrogeologic framework of the arid and semiarid southwestern United States.—Continued

Era, period, or epoch	Geologic process	Hydrologic consequence, by region					
		Eastern Great Basin	Western Great Basin	Mojave-Colorado Desert	Arizona Sonoran Desert-Mexican Highland	Rio Grande Rift-Southwestern New Mexico	South-Central Colorado Plateau
Tertiary—Continued	Oligocene-Miocene extensional faulting	Basins form; basement aquitards lifted up in core complexes; structures greatly disrupted in highly extended areas				Basins form; structures disrupted.	—
	Oligocene-Miocene nonmarine horst-and-graben faulting; basin infilling	Fanglomerates and fine-grained axial valley clastics deposited; lakebed sediments, ***landslide-breccia,*** and ***fluvial sand and gravel aquifers*** deposited. ***Bouse and Imperial aquifer***s form in Mojave and Colorado Deserts; ***Bouse aquifer*** forms in the Arizona Sonoran Desert.				Same as Great Basin; ***breccia*** and ***fluvial aquifers*** deposited	—
	Oligocene-Pliocene (chiefly Miocene) hyperextension and core complex formation	Structures broadly disrupted; crystalline rocks lifted up	Structures locally disrupted; crystalline rocks lifted up	Structures broadly disrupted; crystalline rocks lifted up	Structures broadly disrupted; crystalline rocks lifted up	—	—
	Oligocene-Miocene isolation of Colorado Plateau highland	Evaporites and ***carbonate aquifers*** form downgradient from margin	—	—	Evaporites and ***carbonate aquifers*** form down gradient from margin	—	—
	Oligocene-Miocene calcic-alkaline magmatism	Calderas form, ash deposited; ***lava and tuff aquifers*** form locally	***Lava and tuff aquifers*** form locally	—	—	—	—
	Miocene-Quaternary bimodal volcanism	***Welded tuff and basalt aquifers*** form locally	Calderas form; ***welded-tuff, ash, and basalt aquifers*** form	***Basalt aquifers*** form locally	***Basalt aquifers*** form locally	***Welded-tuff, ash, and basalt aquifers*** form	***Basalt aquifers*** form
	Miocene-Quaternary Yellowstone hot-spot and northern Nevada Rift activation	Widespread ash units form	Snake River flood basalts form	—	—	—	—
Pliocene to Quaternary	Tectonic extension and faulting	Lake deposits, ***fanglomerate and fluvial aquifers*** form		Salton Trough created; lake deposits and ***alluvial aquifers*** form	—	—	—
	Continued basin-fill deposition	Playa deposits, ***fanglomerate and fluvial aquifers*** form		Playa deposits, ***fanglomerate and fluvial aquifers*** form		Same as Great Basin; ***alluvial aquifers*** form	—
	Drainage integration and regional dissection	Colorado R. and upper Humboldt R. drainages dissected	Humboldt River form by lake overflows; ***alluvial aquifers*** form	Mojave and Owens Rivers form; ***alluvial aquifers*** form	***Aquifers*** form along Colorado, Gila, Salt, San Pedro, and Bill Williams Rivers	***Productive aquifer clastics*** deposited by Rio Grande	Colorado River drainage dissected
	Uplift of Sierra Nevada and Transverse Ranges	Rain shadow forms; aridity increases	Rain shadow forms; aridity increases	Rain shadow forms; aridity increases	Rain shadow forms; aridity increases	—	—
	Pleistocene pluvial conditions	***Aquifers recharged***; pluvial lakes form; littoral deposits form	***Aquifers recharged***; pluvial lakes form; littoral deposits form	***Aquifers recharged***; playas inundated	***Aquifers recharged***; local dunes form	***Aquifers recharged***; glaciers form	***Aquifers recharged***; local dunes form
	Holocene aridification	Playas desiccated; salt pans and local dunes form	Playas desiccated; local dunes form	Playas desiccated; salt pans and local dunes form	Local dunes form	—	Local dunes form

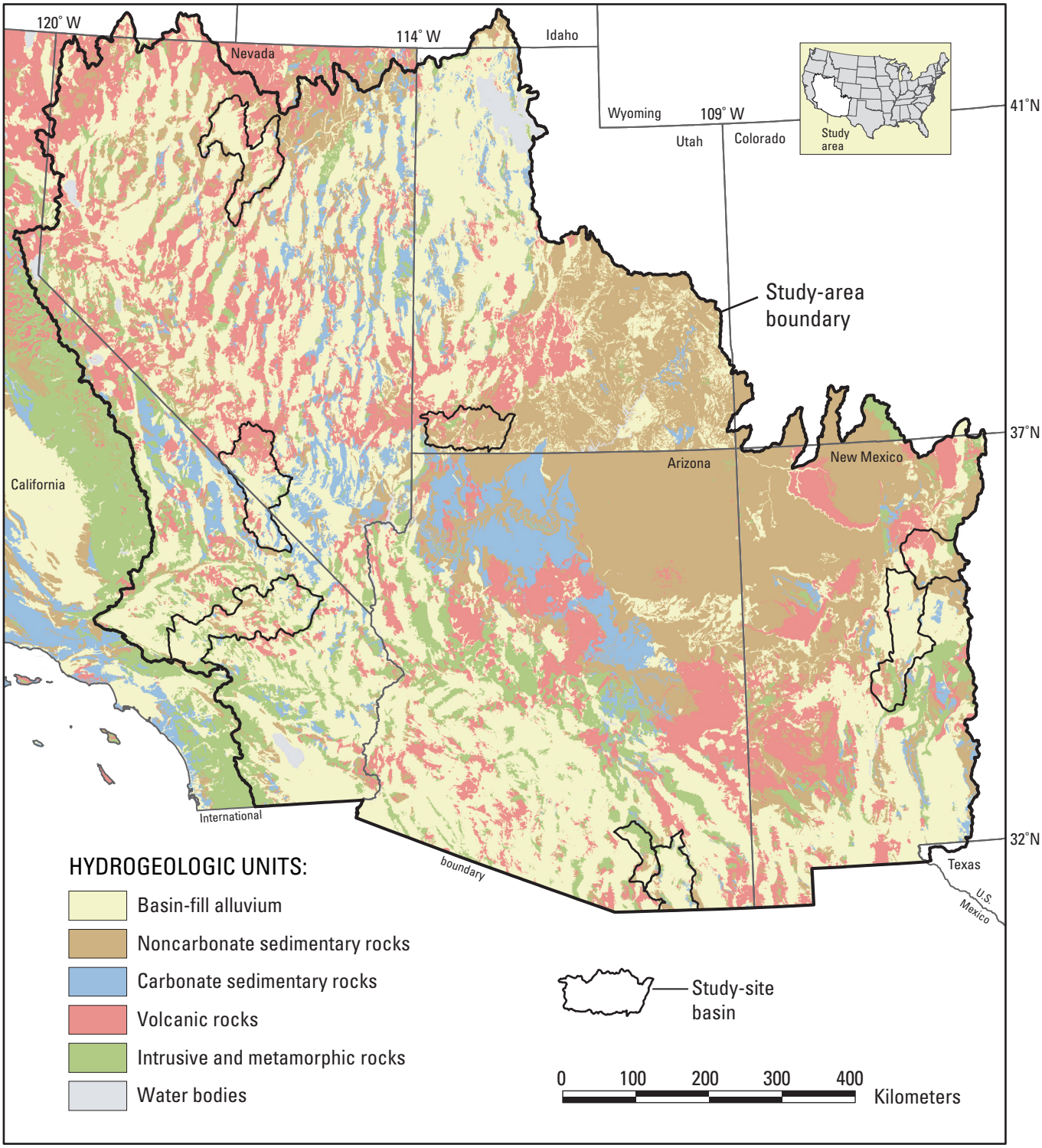

Figure 7. Hydrogeologic units, for the study area, arid and semiarid southweastern United States (from U.S. Geological Survey National Atlas digital data; http://nationalatlas.gov/).

Table 3. Hydrogeologic units in the arid and semiarid southwestern United States.

[Adapted from Harrill and Prudic, 1998]

Hydrogeologic unit	Generalized geology	Water-bearing characteristics
Basin-fill alluvium	Younger basin-fill deposits consist of unconsolidated to semi-consolidated alluvial fans and pediments (unsorted to poorly sorted silt, sand, gravel, and boulders) in valley lowlands and playas (moderately sorted to well sorted clay, silt, sand, and gravel), and in stream flood plains (moderately sorted to well sorted beds of silt and clay or sand and gravel). Older basin-fill deposits consist of semiconsolidated to consolidated fanglomerate, sandstone, siltstone, mudstone, limestone, and interbedded volcanic rocks.	Younger and older basin-fill deposits form aquifers that yield much of the ground water used in the study area. Excluding flood plain deposits, hydraulic conductivities range approximately from 0.0007 to 43 meters per day (m/d) and average 24 m/d. Conductivities of flood-plain deposits range approximately from 5 to 335 m/d and average 40 m/d. Regional-scale basin-fill aquifers include those in the Basin and Range and Rio Grande aquifer system (fig. 8).
Volcanic rock	Subunit of sedimentary and igneous rocks of late Precambrian to Quaternary age. Flows and flow breccias that range in composition from basalt to rhyolite and silicic welded tuffs. Where these rocks are highly fractured, they form aquifers instead of confining units.	Localized conditions of high permeability characterize this unit. Basalt aquifers occur as individual units and interbedded with basin-fill deposits. Lava flows and welded tuffs at the Nevada Test Site in south-central Nevada are the largest area of volcanic rock aquifers shown on figure 8.
Clastic sedimentary rock	Contains clastic sedimentary rocks of late Precambrain to Quaternary age. Includes siltstone, shale, sandstone, and conglomerate.	Fine-grained clastics (siltstone and shale) form confining units unless highly fractured. Sandstone and conglomerates have permeability from primary porosity and sometimes fractures. An extensive area of clastic sedimentary rocks in the Colorado Plateau (fig. 7) contains sandstone units of the Colorado Plateau aquifers (fig. 8).
Carbonate sedimentary rock	Contains carbonate (and some interbedded clastic) sedimentary rocks of Middle Cambrian to Cretaceous age. Includes interbedded limestone, dolomite, sandstone, and shale. Locally contains some beds of conglomerate and gypsum.	Carbonate-rock units form aquifers in the eastern Great Basin and eastern and south-central parts of the western Great Basin. Ground water flows mostly along joints and fractures. Hydraulic conductivity can be very high in areas that are faulted and fractured.
Igneous and metamorphic rock	Contains sedimentary and igneous rocks of late Precambrian to Quaternary age. Includes fine-grained sedimentary rocks, most volcanic rocks, intrusive rocks, metamorphic rocks, and older crystalline basement.	This unit forms a poorly permeable barrier to ground-water flow. It inhibits flow between hydrographic basins and does not readily yield water to wells. Its occurrence generally corresponds to areas of non-aquifer rocks shown on figure 8.

the mountains but runoff to the adjacent valleys is minor. If a regional hydraulic gradient is present, carbonate-rock aquifers can transmit significant interbasin flow. These aquifers have not been stressed extensively by pumping, however, discharge from large springs supported by these aquifers is almost all allocated for agricultural, municipal, and environmental purposes.

Basin and range volcanic-rock aquifers occur in localized parts of the study area. Not all volcanic rocks function as aquifers, so the area of aquifers shown in figure 8 is smaller than the area of volcanic rock shown in figure 7. The largest area of volcanic-rock aquifer shown in figure 8 is an area of highly fractured welded tuff in south-central Nevada. Basalt flows also form productive volcanic-rock aquifers at several locations, but the size of these aquifers is too small to be shown on figure 8. Volcanic rocks also yield small to moderate amounts of water to a number of domestic wells throughout the study area. Although the amounts of water are generally too small to be considered as part of a major aquifer, the supply is significant to a number of individual users. Most recharge to the volcanic-rock aquifers is from direct infiltration of precipitation or snowmelt in the mountains, or from infiltration of streamflow in the mountains. The recharge occurs through secondary openings, such as joints

or fractures. In addition, basalt aquifers often are interbedded with basin-fill alluvium, allowing recharge to the basalt aquifer through the adjoining alluvium.

The Colorado Plateau aquifers occur in southeastern Utah, Northeastern Arizona, and northwestern New Mexico (fig. 8). These aquifers are composed primarily of sandstones of Mesozoic age that transmit water primarily through interconnected joints and fractures. Recharge is primarily by direct infiltration of precipitation and streamflow. The aquifers have not been heavily developed, but some of the water is used for municipal, domestic, and agricultural purposes.

The Rio Grande Rift-Southwestern New Mexico Area aquifer system consists primarily of basin-fill aquifers, but also includes some areas of volcanic rock. Most recharge is supplied by monsoonal storm and snowmelt runoff that infiltrates alluvial materials near the edges of the rift basin. Pumpage from this area is mostly for urban and industrial uses.

Geologic Controls on Recharge Processes

The geologic framework influences the recharge process in three general ways. First, the topography, relief, and orientation of mountain ranges modify the flow of moist air as it moves across mountains and valleys. This modification of airflow influences the occurrence and distribution of precipitation. Second, once the precipitation has fallen, topographic factors such as slope, exposure, and shading determine if the water will tend to remain where it has fallen or move, and if it will be subject to high or low evaporation losses. Third, the permeability of surface and near-surface materials determines

Figure 8. Major aquifers in the arid and semiarid southwestern U.S. study area (from data compiled for the U.S. Geological Survey Ground-Water Atlas of the United States—Whitehead, 1994; Planert and Williams, 1995; Robson and Banta, 1995).

how readily water will infiltrate the land surface and percolate down to the water table.

Topographic factors that influence recharge (fig. 9) include:

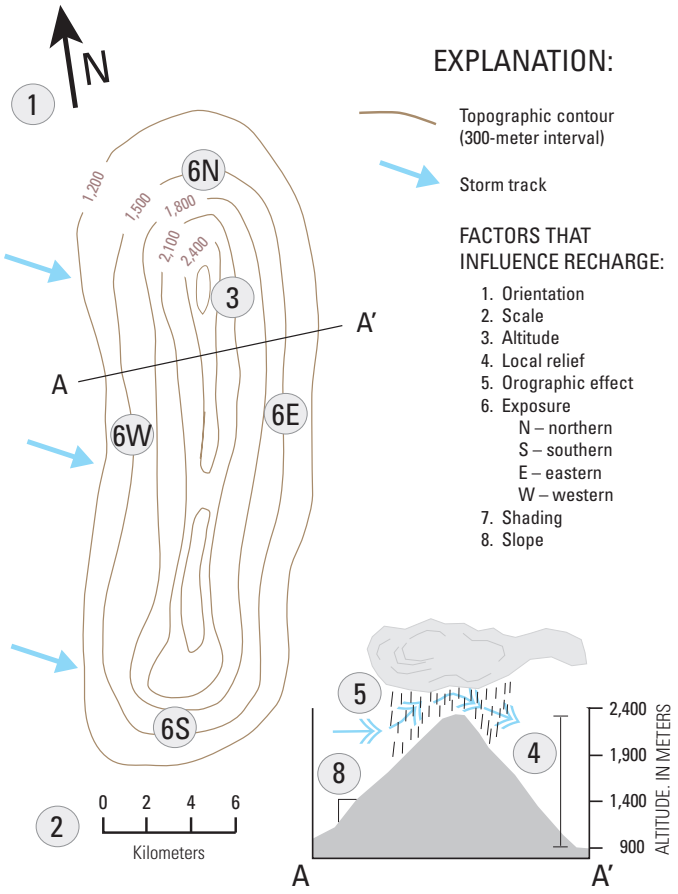

Figure 9. Topographic factors that influence recharge in the arid and semiarid southwestern U.S. study area. Example typifies the Basin and Range subregion.

Orientation

Mountain ranges that are oriented perpendicular to prevailing storm tracks will receive more precipitation than ranges that have a parallel orientation because they present a larger area to the moving moist air masses and are less likely to be bypassed. In addition, when a mountain range is oriented perpendicular to the storm track, the flank of the mountain facing the storm track will receive more precipitation than the leeward side of the mountain, which is in a local rain shadow.

Scale

A large mountain mass will disrupt the flow of a body of moist air more than a small mountain mass will. Therefore, higher rates and larger volumes of precipitation tend to be associated with the larger mountain ranges.

Altitude

The altitude of the crest of a mountain range influences the amount and character of precipitation. Observations throughout the study area indicate that areas of higher altitude receive more precipitation than do areas of lower altitude. The temperature is cooler at higher altitudes; consequently, most high altitude winter precipitation occurs as snow. This snow accumulates during winter and provides snowmelt for spring runoff, which in most areas is the major recharge event of the year.

Local Relief

Local relief, as used in this report, is the difference in altitude between the crest of a mountain range and the adjacent valley floor. This relief is proportional to the vertical distance that air will be forced to rise as it moves across the area. This rise is a key factor in triggering precipitation.

Orographic Effects

The orographic effect happens as air moves across the basin and range topography and rises when crossing mountain ranges. The temperature drops in response to adiabatic cooling that occurs as the air rises. If the air is carrying significant moisture, this drop in temperature will be sufficient to trigger precipitation. Local relief is usually the most significant factor that drives the orographic effect, but other factors, such as altitude, scale, and orientation, also affect the process.

Exposure

Most commonly, exposure is related to the amount of solar radiation that will be retained. A northern exposure (fig. 9, factor 6N) generally retains the lowest amount of solar radiation of all the exposures discussed. In addition, in winter months, when the sun is low in the sky, not only will the incident angle of sunshine on the land surface be lowest, but portions of the exposure also may be shaded for parts of the day, resulting in a lower rate of evapotranspiration. Snow tends to accumulate on northern exposures, and these areas do not dry out as readily as other exposures. Other topographic factors being equal, there will be more water available on the northern exposures to supply recharge.

Southern exposures retain more solar radiation than other exposures, resulting in high amounts of evapotranspiration. Snow melts quickly on the southern exposures, and these areas dry out relatively fast, resulting in less water available for recharge.

East-facing and west-facing exposures retain more solar radiation than the north-facing exposures and less than the south-facing exposures. The solar input varies throughout the day. East-facing exposures retain more solar radiation in the morning than in the afternoon and conversely west-facing exposures retain more solar radiation in the afternoon

than in the morning. Evapotranspiration in these areas is not extremely high or low, and the amount of water available to support recharge is about average.

Shading

Shading occurs where the crests of mountain ranges or high peaks cast a shadow on a portion of the mountain. The area that is shaded varies throughout the day as the sun moves across the sky and varies from a minimum at the summer solstice to a maximum at the winter solstice. Consequently, a specific location for factor 7 is not shown on figure 9. Shading also can occur along reaches of deeply incised stream channels, near cliffs, and in areas of steep slope, depending on local conditions. Areas that experience a high incidence of shading have lower rates of evapotranspiration and are more likely to have some water available to generate recharge.

Slope

Slope is a factor that determines if precipitation will remain in place where it falls or will become runoff. The effect of slope on recharge depends on interactions with other factors. For example, if the slope is relatively flat and surface material is permeable, precipitation will mostly remain in place, and water not consumed by evapotranspiration will infiltrate to become recharge. However, if the slope if relatively flat and the surface material is poorly permeable, precipitation will tend to stay in place, but most will be taken up by evapotranspiration and little will infiltrate to become recharge. If the slope is steep and the surface material is permeable, precipitation will be split between recharge occurring in place and runoff. Areas with sufficiently high subsurface permeability, such as carbonate terrains in eastern Nevada, produce little or no runoff even on the steepest slopes. If the slope is steep and the surface material is poorly permeable, most of the excess precipitation will become runoff. Eventually, the runoff will either be taken up by evapotranspiration or generate recharge, depending on the conditions downslope.

For purposes of discussion, the preceding discussion isolated each of the eight topographic factors that influence recharge at the scale of hill slopes to mountain ranges. Under field conditions, the interactions of these factors determine how much water, if any, will be available to supply recharge.

The composition and character of surface and near-surface materials determines if water will infiltrate and percolate to the water table. This discussion will describe conditions at the scale of outcrops. The main factors considered in this report are whether or not there are openings at the land surface capable of accepting infiltration and, where these openings exist, whether or not they are sufficiently interconnected to provide a pathway capable of transporting water from the land surface to the water table.

Consolidated rock openings are mostly formed by joints and fractures (fig. 10*A*). In some rocks, such as limestone, these openings can be enlarged by solution (fig. 10*B*). Hydraulic continuity is created when several sets of fractures intersect and form a network of openings. These features form after the rock has formed so the fracture permeability is a secondary feature. Some rocks have primary permeability that is created when the rock is formed. An example is sandstone in which the grains of sand have been cemented enough to form a consolidated rock, that still has enough open interstices to provide

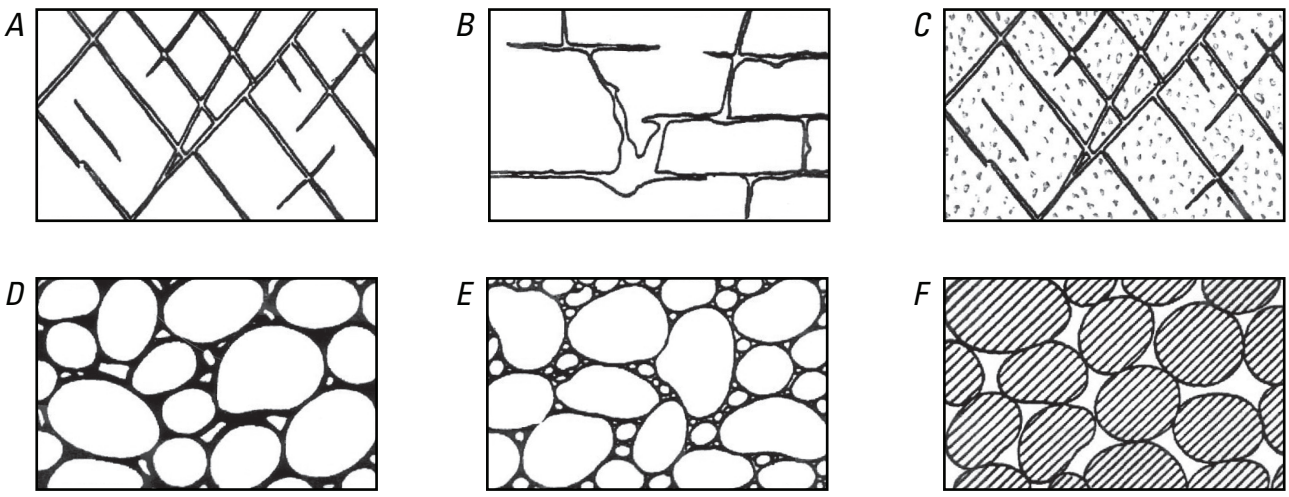

Figure 10. Surface openings that influence infiltration. *A*, rock rendered porous by fracturing; *B*, rock rendered porous by solution; *C*, fractured sandstone that exhibits dual porosity and permeability; *D*, well-sorted sedimentary deposit whose porosity has been diminished by the deposition of mineral matter in the interstices; *E*, poorly sorted sedimentary deposit having low porosity; *F*, well-sorted sedimentary deposit having high porosity (after Meinzer, 1923).

primary permeability (fig. 10*C*). Some of the sandstone aquifers of the Colorado Plateau have both primary and secondary permeability (fig. 10*D*).

Unconsolidated basin-fill deposits are porous media that may differ in composition, grain size, sorting, and cementation. The most permeable basin-fill deposits are well-sorted coarse-grained materials (fig. 10*F*). Permeability decreases with grain size. Well-sorted fine sand can still transmit a significant amount of water, but finer materials, such as silt and clay, generally act as confining units. Lack of sorting also reduces permeability. Poorly sorted sediments (fig. 10*E*) tend to have permeability representative of the finer-grained materials present. As illustrated for the previously discussed case of sandstone, cementation decreases interstitial space, reducing both porosity and permeability (fig. 10*D*). A type of cementation common in the arid southwest is the formation of caliche that develops because of repeated wetting and drying of the soil. The infiltration from sparse precipitation is often insufficient to support percolation below shallow depths, and the water evaporates as the soil dries. A thin layer of minerals is deposited as evaporation occurs. Each cycle of drying increases the thickness of the mineral deposits and reduces interstitial space. In time, thick layers of impermeable caliche can develop and provide local controls on the occurrence of recharge.

The preceding discussion described examples of the most common types of openings on rock surfaces. A comprehensive discussion of primary and secondary permeability is beyond the scope of this chapter (but see, for example, Watson and Burnett, 1993; Lichtner, 1996; Worthington and others, 2000; Ismat and Mitra, 2001; and Gluyas, 2005). The main point of this general discussion is that all of the various rock-surface openings are components of the hydrogeologic framework and, collectively, they exert strong controls on the recharge process.

The permeability of bedrock also has a major effect on the occurrence and distribution of recharge at a basin-size scale. Figure 11 shows sketches of three topographically similar basins that have different combinations of bedrock permeability and climate.

Figure 11*A* shows an arid basin that has permeable bedrock. Most recharge occurs in the mountains and there is meager runoff onto the alluvial fan. Water percolates deeply in the mountains and moves to the basin fill as subsurface flow. The area of ground-water recharge is separated from the area of ground-water discharge by a zone of lateral ground-water flow.

Figure 11*B* shows an arid basin with poorly permeable bedrock. Recharge in the mountains is small and ground-water flow is limited to a shallow zone of weathered rock. Most of the excess water leaves the mountain as streamflow. Most of the recharge occurs on the alluvial fan, and most of the ground-water flow occurs in the basin fill. The zone of recharge is separate from the zone of ground-water discharge, as before, but the zone of lateral ground-water flow is now smaller.

Figure 11*C* shows a semiarid basin with poorly permeable bedrock. There is more precipitation on the mountain, however, recharge on the mountain remains low (similar to that shown in figure 11*B*) because the recharge is limited by the poor permeability of the bedrock. The excess precipitation leaves the mountain as streamflow and flows across the alluvial fan to the valley lowland. The zone of recharge extends to the valley floor and overlaps the zone of ground-water discharge. There is still a zone of predominantly lateral ground-water flow, but it is smaller than shown in figures 11*A* and 11*B*, and there is recharge and discharge at the upper surfaces of the zone.

The above examples illustrate how a single component of the hydrogeologic framework can exert significant control on the hydrologic regimen of a basin.

The factors that control recharge processes in the Colorado Plateau subregion are the same as those for the rest of the study area; however, the geologic history and the topographic setting differ. The Colorado Plateau has not been subjected to the strong extension and structural deformation that has occurred throughout the rest of the study area. The Colorado Plateau has experienced regional uplift and subsequent downcutting of streams and rivers, which has resulted in a plateau-and-canyon topography where the sedimentary units that underlie the Plateau are mostly flat lying. The geohydrology of part of this subregion was evaluated by Freethy and Cordy (1991), who noted that most of the recharge originates from (1) infiltration of precipitation (including snowmelt) through the unsaturated zone to the water table (fig. 12*A*) and (2) infiltration of streamflow from stream channels into the zone of saturation (fig. 12*B*).

Summary

Aridity in the study area results from the combination of descending dry air at the boundary of the Hadley cell and orographic drying of air masses crossing the bordering mountains. Rainfall in the study area is strongly seasonal, with frontal cyclonic storms mostly occurring in winter and convective and monsoonal rains mostly occurring in summer. The Pacific Ocean is the primary source of moisture to the study area, although the Gulf of Mexico contributes moisture, mostly to the southeastern portion of the study area, during the summer monsoonal season. Precipitation and associated ground-water recharge in the northwestern part of the study area have a significant winter component, whereas the southeastern part of the study area has a strong monsoonal component.

Climatic controls on ground-water recharge are complex and exhibit a large degree of natural variability. Droughts more severe than any in the modern instrumental record are evident in tree-rings and other proxy indicators. Pluvial periods that accompanied recent ice ages produced ground-water recharge rates an order of magnitude higher than present rates in parts of the study area. Isotopic

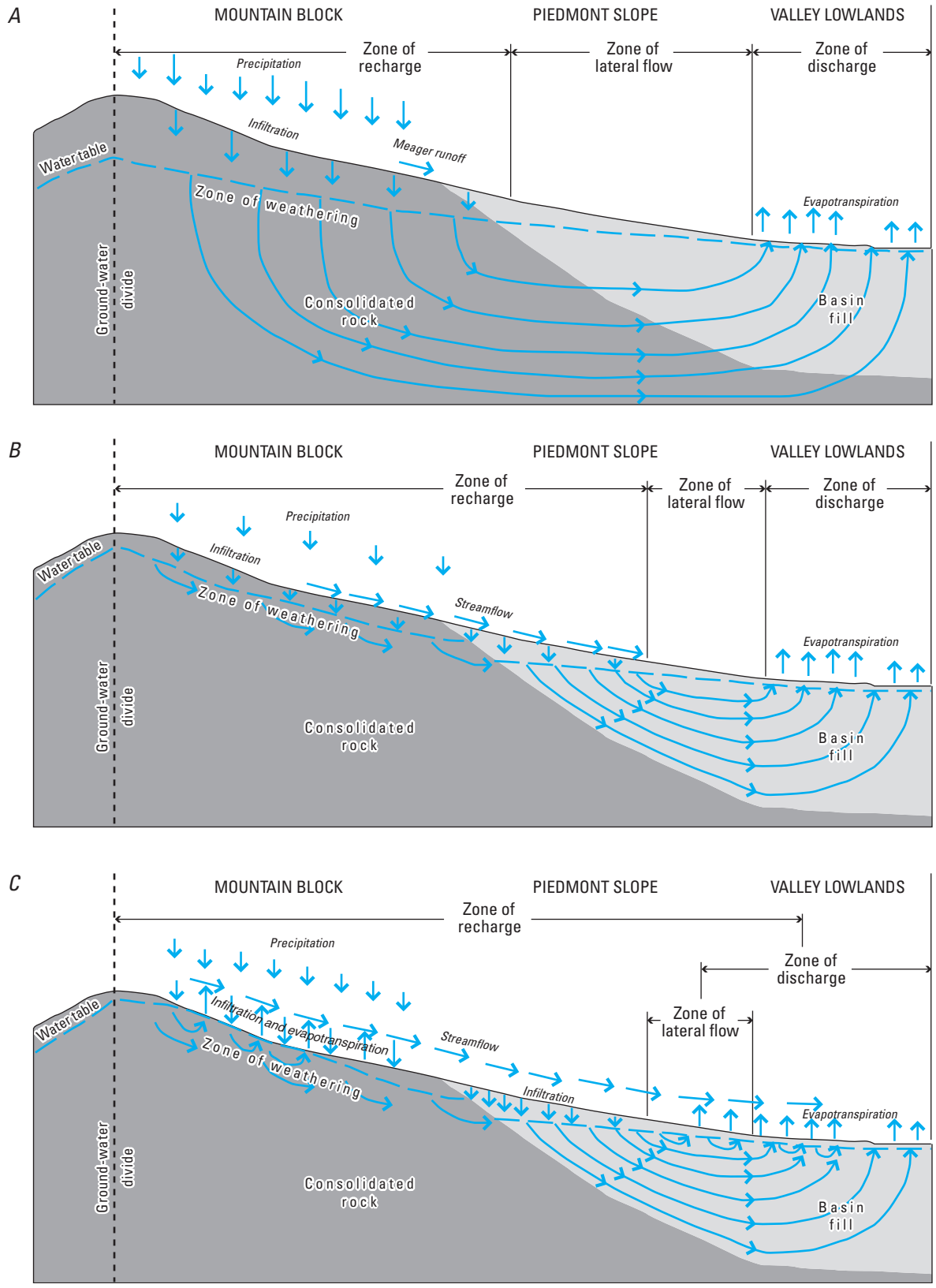

Figure 11. Cross-sections of typical basins showing controls on recharge due to variations in bedrock permeability. *A*, Arid basin having permeable bedrock; *B*, arid basin having poorly permeable bedrock; *C*, semiarid basin having poorly permeable bedrock (from Berger, 2000).

evidence shows that much of the ground-water resource in these areas was recharged during previous geological epochs that were wetter and cooler than today.

Anthropogenic effects are superimposed on natural variability. Projected climate change will likely reduce ground-water recharge through reduced snowpack and perhaps through increased severity of drought. These factors reflect rising temperatures and the possible northward shifting of storm tracks.

Geologic controls on recharge in the study area include the formation of the Sierra Nevada and San Bernadino Mountains that bound the Mojave Desert and Basin and Range to the west and the southern Rocky Mountain Cordillera to the east. Extensional tectonism produced internally drained, alluvial-filled basins and exposed Paleozoic aquifers in mountainous recharge areas in most of the study area. Extensional tectonism did not affect the southern Colorado Plateau; however, it did create differences in predominant modes of recharge. In addition, geologic controls on permeability (through infiltration and subsequent percolation) and topography (through microclimate) provide important controls on ground-water recharge at smaller scales.

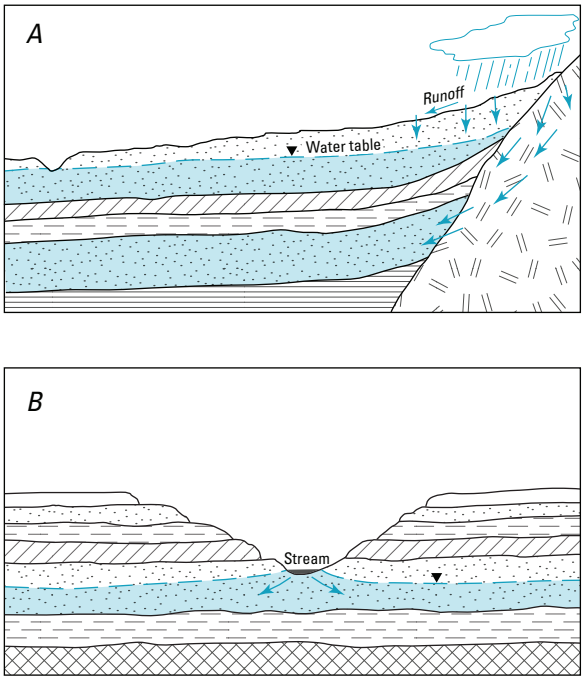

Figure 12. Typical modes of recharge in the Colorado Plateau subregion (adapted from Freethy and Cordy, 1991). *A*, Direct infiltration of precipitation; *B*, seepage from losing reach of stream.

References Cited

Alley, W.M., Reilly, T.E., and Franke, O.L., 1999, Sustainability of ground-water resources: U.S. Geological Survey Circular 1186, 79 p.

Anderson, T.W., Freethey, G.W., and Tucci, P., 1992, Geohydrology and water resources of alluvial basins in south-central Arizona and parts of adjacent states: U.S. Geological Survey Professional Paper 1406-B, 67 p.

Andreadis, K.M., Clark, E.A., Wood, A.W., Hamlet, A.F., and Lettenmaier, D.P., 2005, Twentieth-century drought in the conterminous United States: Journal of Hydrometeorology, v. 6, no. 6, p. 985–1001, doi:10.1175/JHM450.1.

Andreadis, K.M., and Lettenmaier, D.P., 2006, Trends in 20th century drought over the continental United States: Geophysical Research Letters, v. 33, doi:10.1029/2006GL025711.

Antevs, E.V., 1948, The Great Basin, with emphasis on glacial and postglacial times, III, Climatic changes and pre-white man: Bulletin of the University of Utah, v. 38, no. 20, p. 168–191.

Baettig, M.B., Wild, M., and Imboden, D.M., 2007, A climate change index—Where climate change may be most prominent in the 21st century: Geophysical Research Letters, v. 34, doi:10.1029/2006GL028159.

Baldwin, M.P., Rhines, P.B., Huang, H.-P., and McIntyre, M.E., 2007, The jet-stream conundrum: Science, v. 315, no. 5811, p. 467–468, doi:10.1126/science.1131375.

Bartolino, J.R., 2003, Ground-water depletion across the Nation: U.S. Geological Survey Fact Sheet 103-03, 4 p.

Benson, Larry, 2004, Western lakes, *in* Gillespie, A.R., Porter, S.C., and Atwater, B.F., eds., The Quaternary Period in the United States: Developments in Quaternary science, v. 1: New York, Elsevier, p. 185–204.

Benson, Larry, Petersen, K., and Stein, J., 2006, Anasazi (Pre-Columbian Native-American) migrations during the middle-12th and late-13th Centuries—Were they drought induced?: Climatic Change, published online March 28, 2006, 27 p., doi:10.1007/s10584-006-9065-y.

Benson, L.V., Berry, M.S., Jolie, E.A., Spangler, J.D., Stahle, D.W., and Hattori, E.M., 2007, Possible impacts of early-11th-, middle-12th-, and late-13th-century droughts on western Native Americans and the Mississippian Cahokians: Quaternary Science Reviews, v. 26, no. 3–4, p. 336–350, doi:10.1016/j.quascirev.2006.08.001.

Benson, L., Kashgarian, M., Rye, R., Lund, S., Paillet, F., Smoot, J., Kester, C., Mensing, S., Meko, D., and Lindstrom, S., 2002, Holocene multidecadal and multicentennial droughts affecting Northern California and Nevada: Quaternary Science Reviews, v. 21, no. 4-6, p. 659–682, doi:10.1016/S0277-3791(01)00048-8.

Benson, L.V., and Klieforth, H., 1989, Stable isotopes in precipitation and ground water in the Yucca Mountain region, southern Nevada; paleoclimatic implications, *in* Peterson, D.H., ed., Aspects of climate variability in the Pacific and the western Americas: American Geophysical Union, Geophysical Monograph, v. 55, p. 41–59.

Berger, D.L., 2000, Water budget estimates for the 14 hydrographic areas in the middle Humboldt River basin, north-central Nevada: U.S. Geological Survey Water Resources Investigations Report 00–4168, 55 p.

Betancourt, J.L., van Devender, T.R., and Martin, P.S., eds., 2000, Packrat middens—The last 40,000 years of biotic change: Tucson, University of Arizona Press, 467 p.

Bjerknes, Jacob, 1969, Atmospheric teleconnections from the equatorial Pacific: Monthly Weather Review, v. 97, no. 3, p. 163–172.

Bordoni, Simona, Ciesielski, P.E., Johnson, R.H., McNoldy, B.D., and Stevens, B., 2004, The low-level circulation of the North American Monsoon as revealed by QuikSCAT: Geophysical Research Letters, v. 31, doi:10.1029/2004GL020009.

Brenner, I.S., 1974, A surge of maritime tropical air—Gulf of California to the southwestern United States: Monthly Weather Review, v. 102, no. 5, p. 375–389.

Cayan, D.R., Dettinger, M.D., Diaz, H.F., and Graham, N.E., 1998, Decadal variability of precipitation over Western North America: Journal of Climate, v. 11, p. 3148–3166.

Chuang, F.C., McKee, E.H., and Howard, K.A., 2003, Hydrogeologic factors that influence ground water movement in the desert southwest United States: U.S. Geological Survey Open-File Report 2003–294, 39 p.

COHMAP [Cooperative Holocene Mapping Project] Members, 1988, Climatic changes of the last 18,000 years—Observations and model simulations: Science, v. 241, no. 4869, p. 1043–1052, doi:10.1126/science.241.4869.1043.

Cook, E.R., Woodhouse, C., Eakin, C.M., Meko, D.M., and Stahle, D.W., 2004, Long-term aridity changes in the western United States: Science, doi:10.1126/science.1102586.

Crucifix, Michel, and Berger, A., 2006, How long will our interglacial be?: Eos (American Geophysical Union Transactions), v. 87, no. 35, p. 352–353.

Curtis, Scott, and Adler, R., 2000, ENSO indices based on patterns of satellite-derived precipitation: Journal of Climate, v. 13, no. 15, p. 2786.

Daly, Christopher, Neilson, R.P., and Phillips, D.L., 1994, A statistical-topographic model for mapping climatological precipitation over mountainous terrain: Journal of Applied Meteorology, v. 33, no. 2, p. 140–158.

Dettinger, M.D., 2005, Changes in streamflow timing in the western United States in recent decades: U.S. Geological Survey Fact Sheet 2005–3018, 4 p.

Dettinger, M.D., Cayan, D.R., Diaz, H.F., and M., M.D., 1998, North-south precipitation patterns in western North America on interannual-to-decadal timescales: Journal of Climate, v. 11, no. 12, p. 3095–3111.

Dickinson, J.E., Hanson, R. T., Ferré, T. P. A., and Leake, S. A., 2004, Inferring time-varying recharge from inverse analysis of long-term water levels: Water Resources Research, v. 40, doi:10.1029/2003WR002650.

Diem, J.E., and Brown, D.P., 2006, Tropospheric moisture and monsoonal rainfall over the southwestern United States: Journal of Geophysical Research, v. 111, no. D16, [np], doi:10.1029/2005JD006836.

Douglas, M.W., Maddox, R.A., Howard, K., and Reyes, S., 1993, The Mexican monsoon: Journal of Climate, v. 6, no. 8, p. 1665–1677.

Earman, S., Campbell, A.R., Phillips, F.M., and Newman, B.D., 2006, Isotopic exchange between snow and atmospheric water vapor—Estimation of the snowmelt component of groundwater recharge in the southwestern United States: Journal of Geophysical Research, v. 111, doi:10.1029/2005JD006470.

Eastoe, C.J., Gu, A., and Long, A., 2004, The origins, ages and flow paths of groundwater in Tucson Basin—Results of a study of multiple isotope systems, *in* Hogan, J.F., Phillips, F.M., and Scanlon, B.R., eds., Groundwater recharge in a desert environment—The Southwestern United States: American Geophysical Union, Water Science and Applications Series, v. 9, p. 217–234, doi:10.1029/0009WSA03.

Edmunds, W.M., 1998, Recharge to groundwater in arid and semi-arid regions from the Holocene to the present, *in* Alsharhan, A.S., Glennie, K.W., Whittle, G.L., and Kendall, C.G.S.C., eds., Quaternary deserts and climatic change: Rotterdam, A. A. Balkema, p. 419–431.

Entekhabi, Dara, Rodriguez-Iturbe, I., and Castelli, F., 1996, Mutual interaction of soil moisture state and atmospheric processes: Journal of Hydrology, v. 184, no. 1–2, p. 3–17, doi:10.1016/0022-1694(95)02965-6.

Fedorov, A.V., Dekens, P.S., McCarthy, M., Ravelo, A.C., deMenocal, P.B., Barreiro, M., Pacanowski, R.C., and Philander, S.G., 2006, The Pliocene paradox (mechanisms for a permanent El Niño): Science, v. 312, no. 5779, p. 1485–1489, doi:10.1126/science.1122666.

Feth, J.H., 1961, A new map of western conterminous United States showing the maximum known or inferred extent of Pleistocene lakes, short papers in the geologic and hydrologic sciences: U.S. Geological Survey Professional Paper 424-B, p. 110–112.

Filippone, C., and Leake, S.A., 2005, Time scales in the sustainable management of water resources: Southwest Hydrology, v. 4, no. 1, p. 16–17, 26.

Flint, A.L., Flint, L.E., Hevesi, J.A., and Blainey, J.B., 2004, Fundamental concepts of recharge in the desert southwest—A regional modeling perspective, *in* Hogan, J.F., Phillips, F.M., and Scanlon, B.R., eds., Groundwater recharge in a desert environment—The Southwestern United States: American Geophysical Union, Water Science and Applications Series, v. 9, p. 159–184, doi:10.1029/0009WSA10.

Foley, J.A., DeFries, R., Asner, G.P., Barford, C., Bonan, G., Carpenter, S.R., Chapin, F.S., Coe, M.T., Daily, G.C., Gibbs, H.K., Helkowski, J.H., Holloway, T., Howard, E.A., Kucharik, C.J., Monfreda, C., Patz, J.A., Prentice, I.C., Ramankutty, N., and Snyder, P.K., 2005, Global consequences of land use: Science, v. 309, no. 5734, p. 570–574, doi:10.1126/science.1111772.

Freethey, G.W., and Cordy, G.E., 1991, Geohydrology of Mesozoic rocks in the upper Colorado River Basin in Arizona, Colorado, New Mexico, Utah, and Wyoming, excluding the San Juan Basin: U.S. Geological Survey Professional Paper 1411-C, 118 p.

Galloway, D.L., Jones, D.R., and Ingebritsen, S.E., 1999, Land subsidence in the United States: U.S. Geological Survey Circular 1182, 175 p.

Gee, G.W., Wierenga, P.J., Andraski, B.J., Young, M.H., Fayer, M.J., and Rockhold, M.L., 1994, Variations in water balance and recharge potential at three western desert sites: Soil Science Society of America Journal, v. 58, no. 1, p. 63–72.

Gildor, Hezi, 2003, When Earth's freezer door is left ajar: Eos (American Geophysical Union Transactions), v. 84, no. 23, p. 215.

Gluyas, J., 2005, Sedimentary rocks; sandstones, diagenesis and porosity evolution, *in* Selley, R.C., Cocks, L., Robin, M., and Plimer, I.R., eds., Encyclopedia of Geology: Oxford, England, Elsevier Academic Press, v. 5, p. 141–151.

Grayson, D.F., 1993, The Desert's Past: A natural prehistory of the Great Basin: Washington, D.C., Smithsonian Institution Press, 356 p.

Hales, J.E., Jr., 1972, Surges of maritime tropical air northward over the Gulf of California: Monthly Weather Review, v. 100, no. 4, p. 298–306.

Hales, J.E., Jr., 1973, Southwestern United States summer monsoon—Gulf of Mexico or Pacific Ocean?: NOAA Technical Memo NWSWR-84, 26 p.

Hanson, R.T., Dettinger, M.D., and Newhouse, M.W., 2006, Relations between climatic variability and hydrologic time series from four alluvial basins across the southwestern United States: Hydrogeology Journal, v. 14, no. 7, p. 1122–1146, doi:10.1007/s10040-006-0067-7.

Harrill, J.R., and Prudic, D.E., 1998, Aquifer systems in the Great Basin region of Nevada, Utah, and adjacent states—Summary report: U.S. Geological Survey Professional Paper 1409-A, 66 p.

Hoerling, M.P., and Eischeid, J., 2007, Past peak water in the southwest: Southwest Hydrology, v. 6, no. 1, p. 18–19, 35.

Hoerling, Martin, and Kumar, A., 2003, The perfect ocean for drought: Science, v. 299, no. 5607, p. 691–694, doi:10.1126/science.1079053.

Houghton, J.G., 1969, Characteristics of rainfall in the Great Basin: Reno, Desert Research Institute, University of Nevada, 205 p.

Houghton, J.T., 2004, Global warming—The complete briefing (3rd ed.): Cambridge, UK, Cambridge University Press, 351 p.

Houghton, J.T., Ding, Y., Griggs, D.J., Noguer, M., van der Linden, P.J., and Xiaosu, D., eds., 2001, Climate change 2001—The scientific basis—Contribution of Working Group I to the Third Assessment Report of the Intergovernmental Panel on Climate Change (IPCC): Cambridge, UK, Cambridge University Press, 944 p.

Huang, Shaopeng, 2006, 1851–2004 annual heat budget of the continental landmasses: Geophysical Research Letters, v. 33, doi:10.1029/2005GL025300.

IPCC (Intergovernmental Panel on Climate Change) Working Group I, 2007, Climate change 2007—The physical science basis: Cambridge, UK, Cambridge University Press, 1,056 p.

Ismat, Z., and Mitra, G., 2001, Evolution of fracture porosity and permeability during folding by cataclastic flow; implications for syntectonic dilational pumping [abs.], *in* Earth system processes, Edinburgh, UK, June 24-28, 2001: Boulder, Colo., Geological Society of America and Geological Society of London, p. 52.

Izbicki, J.A., and Michel, R.L., 2004, Movement and age of ground water in the western part of the Mojave Desert, southern California, USA: U.S. Geological Survey Water-Resources Investigations Report 03–4314, 35 p.

Ji, Junfeng, Balsam, W., Chen, X., Chen, J., Chen, Y., and Wang, H., 2006, Rate of solar insolation change and the glacial/interglacial transition: Geophysical Research Letters, v. 33, doi:10.1029/2005GL025401.

Kerr, R.A., 2006, Rivers in the sky are flooding the world with tropical waters: Science, v. 313, no. 5786, p. 435, doi:10.1126/science.313.5786.435.

Konieczki, A.D., and Heilman, J.A., 2004, Water-use trends in the desert southwest—1950–2000: U.S. Geological Survey Scientific Investigations Report 2004–5148, 32 p.

Kueppers, L.M., Snyder, M.A., and Sloan, L.C., 2007, Irrigation cooling effect—Regional climate forcing by land-use change: Geophysical Research Letters, v. 34, doi:10.1029/2006GL028679.

Kutzbach, J.E., and Wright, H.E.J., 1985, Simulation of the climate of 18,000 years BP—Results for the North American/North Atlantic/European sector and comparison with the geologic record of North America: Quaternary Science Reviews, v. 4, no. 3, p. 147–187.

Leake, S.A., Konieczki, A.D., and Rees, J.A.H., 2000, Desert basins of the southwest: U.S. Geological Survey Fact Sheet 2000–86, 4 p.

Leavitt, S.W., 2007, Southwestern U.S. drought maps from pinyon tree-ring carbon isotopes: Eos (American Geophysical Union Transactions), v. 88, no. 4, p. 39–40.

Lichtner, P.C., 1996, Continuum formulation of multiphase multicomponent reactive transport, *in* Lichtner, P.C., Steefel, C.I., and Oelkers, E.H., eds., Reactive transport in porous media: Reviews in Mineralogy, v. 34, p. 1–81.

Lin, J.-L., 2007, Interdecadal variability of ENSO in 21 IPCC AR4 coupled GCMs: Geophysical Research Letters, v. 34, doi:10.1029/2006GL028937.

Liu, Z., and Alexander, M., 2007, Atmospheric bridge, oceanic tunnel, and global climatic teleconnections: Reviews of Geophysics, v. 45, doi:10.1029/2005RG000172.

Lu, J., Vecchi, G.A., and Reichler, T., 2007, Expansion of the Hadley cell under global warming: Geophysical Research Letters, v. 34, doi:10.1029/2006GL028443.

MacDonald, G.M., and Case, R. A., 2005, Variations in the Pacific decadal oscillation over the past millennium: Geophysical Research Letters, v. 32.

Magirl, C.S., Shoemaker, C., Webb, R.H., Schaffner, M., Griffiths, P.G., and Pytlak, E., 2007, Debris flows and record floods from extreme mesoscale convective thunderstorms over the Santa Catalina Mountains, Arizona: U.S. Geological Survey Open-File Report 2007–1108.

Mantua, N.J., and Hare, S.R., 2002, The Pacific Decadal Oscillation: Journal of Oceanography, v. 58, p. 35–44.

Mantua, N.J., Hare, S.R., Zhang, Y., Wallace, J.M., and Francis, R.C., 1997, A Pacific interdecadal climate oscillation with impacts on salmon production: Bulletin of the American Meteorological Society, v. 78, no. 6, p. 1069–1079.

Martin, J.E., 2006, Mid-latitude atmospheric dynamics—A first course: Chichester, England, John Wiley and Sons, 336 p.

Matthews, H.D., and Keith, D.W., 2007, Carbon-cycle feedbacks increase the likelihood of a warmer future: Geophysical Research Letters, v. 34, doi:10.1029/2006GL028685.

McCabe, G.J., and Dettinger, M.D., 2002, Primary modes and predictability of year-to-year snowpack variations in the western United States from teleconnections with Pacific Ocean climate: Journal of Hydrometeorology, v. 3, no. 1, p. 13–25, doi:10.1175/1525-7541(2002)003<0013:PMAPOY>2.0.CO;2.

McCabe, G.J., Palecki, M.A., and Betancourt, J.L., 2004, Pacific and Atlantic Ocean influences on multidecadal drought frequency in the United States: Proceedings of the National Academy of Sciences of the United States of America, v. 101, no. 12, p. 4136–4141, doi:10.1073/pnas.0306738101.

McPhaden, M.J., Zebiak, S.E., and Glantz, M.H., 2006, ENSO as an integrating concept in Earth science: Science, v. 314, no. 5806, p. 1740-1745, doi:10.1126/science.1132588.

Meehl, G.A., Washington, W.M., Santer, B.D., Collins, W.D., Arblaster, J.M., Hu, A., Lawrence, D.M., Teng, H., Buja, L.E., and Strand, W.G., 2006, Climate change projections for the twenty-first century and climate change commitment in the CCSM3: Journal of Climate, v. 19, no. 11, p. 2597–2616, doi:10.1175/JCLI3746.1.

Meinzer, O.E., 1923, The occurrence of ground water in the United States, with a discussion of principles: Geological Survey Water-Supply Paper 489, U.S. Geological Survey, 321 p.

Meko, D.M., Woodhouse, C.A., Baisan, C.A., Knight, T., Lukas, J.J., Hughes, M.K., and Salzer, M.W., 2007, Medieval drought in the upper Colorado River Basin: Geophysical Research Letters, v. 34, doi:10.1029/2007GL029988.

Menking, K.M., and Anderson, R.Y., 2003, Contributions of La Niña and El Niño to middle Holocene drought and late Holocene moisture in the American southwest: Geology, v. 31, no. 11, p. 937–940, doi:10.1130/G19807.1.

Michaud, J.D., Auvine, B.A., and Penalba, O.C., 1995, Spatial and elevational variations of summer rainfall in the southwestern United States: Journal of Applied Meteorology, v. 34, no. 12, p. 2689–2703.

Mo, K.C., Schemm, J.-K., Juang, H.M.H., Higgins, R.W., and Song, Y., 2005, Impact of model resolution on the prediction of summer precipitation over the United States and Mexico: Journal of Climate, v. 18, no. 18, p. 3910–3927, doi:10.1175/JCLI3513.1.

Montanez, I.P., Tabor, N.J., Niemeier, D., DiMichele, W.A., Frank, T.D., Fielding, C.R., Isbell, J.L., Birgenheier, L.P., and Rygel, M.C., 2007, CO_2-forced climate and vegetation instability during late Paleozoic deglaciation: Science, v. 315, no. 5808, p. 87–91, doi:10.1126/science.1134207.

Osborn, T.J., and Briffa, K.R., 2006, The spatial extent of 20th-century warmth in the context of the past 1200 years: Science, v. 311, no. 5762, p. 841–844, doi:10.1126/science.1120514.

Paillard, Didier, 2006, What drives the ice age cycle?: Science, v. 313, no. 5786, p. 455-456, doi:10.1126/science.1131297.

Peixoto, J.P., and Oort, A.H., 1992, Physics of climate: New York, American Institute of Physics, 520 p.

Philander, S.G.H., 1990, El Niño, La Niña, and the Southern Oscillation: International Geophysics Series, v. 46: San Diego,Calif., Academic Press, 293 p.

Phillips, F.M., Walvoord, M.A., and Small, E.E., 2004, Effects of environmental change on groundwater recharge in the desert southwest, *in* Hogan, J.F., Phillips, F.M., and Scanlon, B.R., eds., Groundwater recharge in a desert environment—The Southwestern United States: American Geophysical Union, Water Science and Applications Series, v. 9, p. 273–294, doi:10.1029/0009WSA15.

Phillips, J.V., and Thomas, B.E., 2005, Hydrologic conditions in Arizona during 1999–2004—A historical perspective: U.S. Geological Survey Fact Sheet 2005-3081, 4 p.

Pierrehumbert, R.T., 2000, Climate change and the tropical Pacific—The sleeping dragon wakes: Proceedings of the National Academy of Sciences of the United States of America, v. 97, no. 4, p. 1355–1358, doi:10.1073/pnas.97.4.1355.

Planert, M., and Williams, J.S., 1995, Ground water atlas of the United States—California, Nevada: U.S. Geological Survey Hydrologic Investigations Atlas HA 730-B, 28 p.

Plummer, L.N., Bexfield, L.M., Anderholm, S.K., Sanford, W.E., and Busenberg, E., 2004, Geochemical characterization of ground-water flow in the Santa Fe Group aquifer system, middle Rio Grande Basin, New Mexico: U.S. Geological Survey Water-Resources Investigations Report 03–4131, 395 p.

Pool, D.R., 2005, Variations in climate and ephemeral channel recharge in southeastern Arizona, United States: Water Resources Research, v. 41, doi:10.1029/2004WR003255.

Rahmstorf, Stefan, Cazenave, A., Church, J.A., Hansen, J.E., Keeling, R.F., Parker, D.E., and Somerville, R.C.J., 2007, Recent climate observations compared to projections: Science, 2007, v. 316, no. 5825, p. 709, doi:10.1126/science.1136843.

Ralph, F.M., Neiman, P.J., Wick, G.A., Gutman, S.I., Dettinger, M.D., Cayan, D.R., and White, A.B., 2006, Flooding on California's Russian River—Role of atmospheric rivers: Geophysical Research Letters, v. 33, doi:10.1029/2006GL026689.

Rasmussen, J.B.T., Polyak, V.J., and Asmerom, Y., 2006, Evidence for Pacific-modulated precipitation variability during the late Holocene from the southwestern USA: Geophysical Research Letters, v. 33, doi:10.1029/2006GL025714.

Raupach, M.R., Marland, G., Ciais, P., Le Quere, C., Canadell, J.G., Klepper, G., and Field, C.B., 2007, Global and regional drivers of accelerating CO2 emissions: Proceedings of the National Academy of Sciences of the United States of America, v. 104. p. 10,288–10,293 doi:10.1073/pnas.0700609104.

Ravelo, A.C., Dekens, P.S., and McCarthy, M., 2006, Evidence for El Niño-like conditions during the Pliocene: GSA Today, v. 16, no. 3, p. 4–11, doi:10.1130/1052-5173(2006)016<4:EFENLC>2.0.CO;2.

Robson, S.G., and Banta, E.R., 1995, Ground water atlas of the United States—Arizona, Colorado, New Mexico, Utah: U.S. Geological Survey Hydrologic Investigations Atlas HA 730-C, 32 p.

Roe, Gerard, 2006, In defense of Milankovitch: Geophysical Research Letters, v. 33, doi:10.1029/2006GL027817.

Ruddiman, W.F., 2006, On "The Holocene CO_2 rise—Anthropogenic or natural?": Eos (American Geophysical Union Transactions), v. 87, no. 35, p. 352–353.

Salathé, E.P., Jr., 2006, Influences of a shift in North Pacific storm tracks on western North American precipitation under global warming: Geophysical Research Letters, v. 33, doi:10.1029/2006GL026882.

Sandvig, R.M., and Phillips, F.M., 2006, Ecohydrological controls on soil moisture fluxes in arid to semiarid vadose zones: Water Resources Research, v. 42, doi:10.1029/2005WR004644.

Sanford, W.E., Plummer, L.N., McAda, D.P., Bexfield, L.M., and Anderholm, S.K., 2004, Hydrochemical tracers in the Middle Rio Grande basin, USA—2. Calibration of a ground-water flow model: Hydrogeology Journal, v. 12, p. 389–407, doi:10.1007/s10040-004-0326-4.

Sarmiento, J.L., and Gruber, N., 2002, Sinks for anthropogenic carbon: Physics Today, v. 55, no. 8, p. 30–36.

Scanlon, B.R., Keese, K.E., Flint, A.L., Flint, L.E., Gaye, C.B., Edmunds, W.M., and Simmers, I., 2006, Global synthesis of groundwater recharge in semiarid and arid regions: Hydrological Processes, v. 20, no. 15, p. 3335–3370, doi:10.1002/hyp.6335.

Scanlon, B.R., Levitt, D.G., Reedy, R.C., Keese, K.E., and Sully, M.J., 2005, Ecological controls on water-cycle response to climate variability in deserts: Proceedings of the National Academy of Sciences of the United States of America, v. 102, no. 17, p. 6033–6038, doi:10.1073/pnas.0408571102.

Scanlon, B.R., Reedy, R.C., Stonestrom, D.A., Prudic, D.E., and Dennehy, K.F., 2005, Impact of land use and land cover change on groundwater recharge and quality in the southwestern US: Global Change Biology, v. 11, no. 10, p. 1577–1593, doi:10.1111/j.1365-2486.2005.01026.x.

Scheffer, Marten, Brovkin, V., and Cox, P.M., 2006, Positive feedback between global warming and atmospheric CO_2 concentration inferred from past climate change: Geophysical Research Letters, v. 33, doi:10.1029/2005GL025044.

Scibek, Jacek, and Allen, D.M., 2006, Modeled impacts of predicted climate change on recharge and groundwater levels: Water Resources Research, v. 42, doi:10.1029/2005WR004742.

Seager, R., Ting, M., Held, I., Kushnir, Y., Lu, J., Vecchi, G., Huang, H.-P., Harnik, N., Leetmaa, A., Lau, N.-C., Li, C., Velez, J., and Naik, N., 2007, Model projections of an imminent transition to a more arid climate in southwestern North America: Science, v. 316, p. 1181–1184, doi:10.1126/science.1139601.

Service, R.F., 2004, As the west goes dry: Science, v. 303, no. 5661, p. 1124–1127, doi:10.1126/science.303.5661.1124.

Seyfried, M.S., Schwinning, S., Walvoord, M.A., Pockman, W.T., Newman, B.D., Jackson, R.B., and Phillips, F.M., 2005, Ecohydrological control of deep drainage in arid and semiarid regions: Ecology, v. 86, no. 2, p. 277–287.

Shukla, Jagadish, DelSole, T., Fennessy, M., Kinter, J., and Paolino, D., 2006, Climate model fidelity and projections of climate change: Geophysical Research Letters, v. 33, doi:10.1029/2005GL025579.

Small, E.E., 2005, Climatic controls on diffuse groundwater recharge in semiarid environments of the southwestern United States: Water Resources Research, v. 41, doi:10.1029/2004WR003193.

Soden, B.J., Jackson, D.L., Ramaswamy, V., Schwarzkopf, M.D., and Huang, X., 2005, The radiative signature of upper tropospheric moistening: Science, v. 310, no. 5749, p. 841–844, doi:10.1126/science.1115602.

Stainforth, D.A., Aina, T., Christensen, C., Collins, M., Faull, N., Frame, D.J., Kettleborough, J.A., Knight, S., Martin, A., Murphy, J.M., Piani, C., Sexton, D., Smith, L.A., Spicer, R.A., Thorpe, A.J., and Allen, M.R., 2005, Uncertainty in predictions of the climate response to rising levels of greenhouse gases: Nature, v. 433, no. 7024, p. 403–406, doi:10.1038/nature03301.

Sternberg, Joseph, 2006, Preventing another ice age: Eos (American Geophysical Union Transactions), v. 87, no. 48, p. 39 and 42.

Stonestrom, D.A., Prudic, D.E., Laczniak, R.J., and Akstin, K.C., 2004, Tectonic, climatic, and land-use controls on ground-water recharge in an arid alluvial basin: Amargosa Desert, U.S.A., *in* Hogan, J.F., Phillips, F.M., and Scanlon, B.R., eds., Groundwater recharge in a desert environment—The Southwestern United States: American Geophysical Union, Water Science and Applications Series, v. 9, p. 29–47, doi:10.1029/0009WSA03.

Taylor, C.M., Parker, D.J., and Harris, P.P., 2007, An observational case study of mesoscale atmospheric circulations induced by soil moisture: Geophysical Research Letters, v. 34, doi:10.1029/2007GL030572.

Tebaldi, Claudia, Hayhoe, K., Arblaster, J.M., and Meehl, G.A., 2006, Going to the extremes—An intercomparison of model-simulated historical and future changes in extreme events: Climatic Change, v. 79, no. 3-4, p. 185–211.

Torn, M.S., and Harte, J., 2006, Missing feedbacks, asymmetric uncertainties, and the underestimation of future warming: Geophysical Research Letters, v. 33, doi:10.1029/2005GL025540.

UNESCO, 1977, Map of the world distribution of arid regions, explanatory note: Paris, France, MAB Technical Note 7, 54 p.

U.S. Census Bureau, 2006, Annual estimates of the population for counties of Arizona (California, Colorado, Idaho, Nevada, New Mexico, Utah): April 1, 2000 to July 1, 2005, CO-EST2005-01-04 (-06, -08, -16, -32, -35, -49), release date March 16, 2006 [http://www.census.gov/popest/counties/tables, last accessed January 23, 2007].

Vecchi, G.A., Soden, B.J., Wittenberg, A.T., Held, I.M., Leetmaa, A., and Harrison, M.J., 2006, Weakening of tropical Pacific atmospheric circulation due to anthropogenic forcing: Nature, v. 441, no. 7089, p. 73–76, doi:10.1038/nature 04744.

Walker, G.T., 1924, Correlation in seasonal variations of weather, IX—A further study of world weather: Indian Meteorological Memoirs, v. 24, p. 275–332.

Walvoord, M.A., Plummer, M.A., Phillips, F.M., and Wolfsberg, A.V., 2002, Deep arid system hydrodynamics 1—Equilibrium states and response times in thick desert vadose zones: Water Resources Research, v. 38, no. 12, p. 44–1 to 44–15, doi:10.1029/2001WR000824.

Walvoord, M.A., Stonestrom, D.A., Andraski, B.J., and Striegl, R.G., 2004, Constraining the inferred paleohydrologic evolution of a deep unsaturated zone in the Amargosa Desert: Vadose Zone Journal, v. 3, no. 2, p. 502–512.

Watson, I., and Burnett, A.D., 1993, Hydrology, an environmental approach—Theory and applications of ground water and surface water for engineers and scientists: Boca Raton, Lewis Publishers [CRC Press], 702 p.

Webb, Thompson, III, and Bartlein, P.J., 1992, Global changes during the last 3 million years—Climatic controls and biotic responses: Annual Review of Ecology and Systematics, v. 23, p. 141–173.

Webster, P.J., Magaña, V.O., Palmer, T.N., Shukla, J., Thomas, R.A., Yanai, M., and Yasunari, T., 1998, Monsoons—Processes, predictability, and the prospects for prediction: Journal of Geophys. Res., v. 103, no. C7, p. 14,451–14,510.

Whitehead, R.L., 1994, Ground water atlas of the United States—Idaho, Oregon, Washington: U.S. Geological Survey Hydrologic Investigations Atlas HA 730-H, 31 p.

Winograd, I.J., and Thordarson, W., 1975, Hydrogeologic and hydrochemical framework, South-Central Great Basin, Nevada-California, with special reference to the Nevada Test Site: U.S. Geological Survey Professional Paper 712-C, 126 p.

Woodhouse, C.A., Kunkel, K.E., Easterling, D.R., and Cook, E.R., 2005, The twentieth-century pluvial in the western United States: Geophysical Research Letters, v. 32, doi:10.1029/2005GL022413.

Worthington, S.R.H., Ford, D.C., and Beddows, P.A., 2000, Porosity and permeability enhancement in unconfined carbonate aquifers as a result of solution, *in* Klimchouk, A.B., Ford, D.C., Palmer, A.N., and Dreybrodt, W., eds., Speleogenesis evolution of karst aquifers: Huntsville, Ala., National Speleological Society, p. 463–472.

Yin, J.H., 2005, A consistent poleward shift of the storm tracks in simulations of 21 century climate: Geophysical Research Letters, v. 33, doi:10.1029/2005GL023684.

Zhang, X., Zwiers, F.W., Hegerl, G.C., Lambert, F.H., Gillett, N.P., Solomon, S., Stott, P.A., and Nozawa, T., 2007, Detection of human influence on twentieth-century precipitation trends: Nature, v. 448, no. 7152, p. 461–465, doi:10.1038/nature06025.

Zimov, S.A., Davydov, S.P., Zimova, G.M., Davydova, A.I., Schuur, E.A.G., Dutta, K., and Chapin, F.S., III, 2006, Permafrost carbon—Stock and decomposability of a globally significant carbon pool: Geophysical Research Letters, v. 33, doi:10.1029/2006GL027484.

Regional Analysis of Ground-Water Recharge

By Lorraine E. Flint and Alan L. Flint

Abstract

A modeling analysis of runoff and ground-water recharge for the arid and semiarid southwestern United States was performed to investigate the interactions of climate and other controlling factors and to place the eight study-site investigations into a regional context. A distributed-parameter water-balance model (the Basin Characterization Model, or BCM) was used in the analysis. Data requirements of the BCM included digital representations of topography, soils, geology, and vegetation, together with monthly time-series of precipitation and air-temperature data. Time-series of potential evapotranspiration were generated by using a submodel for solar radiation, taking into account topographic shading, cloudiness, and vegetation density. Snowpack accumulation and melting were modeled using precipitation and air-temperature data. Amounts of water available for runoff and ground-water recharge were calculated on the basis of water-budget considerations by using measured- and generated-meteorologic time series together with estimates of soil-water storage and saturated hydraulic conductivity of subsoil geologic units. Calculations were made on a computational grid with a horizontal resolution of about 270 meters for the entire 1,033,840 square-kilometer study area. The modeling analysis was composed of 194 basins, including the eight basins containing ground-water recharge-site investigations. For each grid cell, the BCM computed monthly values of potential evapotranspiration, soil-water storage, in-place ground-water recharge, and runoff (potential stream flow). A fixed percentage of runoff was assumed to become recharge beneath channels operating at a finer resolution than the computational grid of the BCM. Monthly precipitation and temperature data from 1941 to 2004 were used to explore climatic variability in runoff and ground-water recharge.

The selected approach provided a framework for classifying study-site basins with respect to climate and dominant recharge processes. The average climate for all 194 basins ranged from hyperarid to humid, with arid and semiarid basins predominating (fig. 6, chapter A, this volume). Four of the 194 basins had an aridity index of dry subhumid; two of the basins were humid. Of the eight recharge-study sites, six were in semiarid basins, and two were in arid basins. Average-annual potential evapotranspiration showed a regional gradient from less than 1 m/yr in the northeastern part of the study area to more than 2 m/yr in the southwestern part of the study area. Average-annual precipitation was lowest in the two arid-site basins and highest in the two study-site basins in southern Arizona. The relative amount of runoff to in-place recharge varied throughout the study area, reflecting differences primarily in soil water-holding capacity, saturated hydraulic conductivity of subsoil materials, and snowpack dynamics. Climatic forcing expressed in El Niño and Pacific Decadal Oscillation indices strongly influenced the generation of precipitation throughout the study area. Positive values of both indices correlated with the highest amounts of runoff and ground-water recharge.

Introduction

A regional analysis was performed to assess the processes, properties, and climatic factors that affect recharge and runoff variability in the arid and semiarid southwestern United States. The regional analysis was part of a larger study designed to improve understanding of ground-water–surface-water interactions and their effects on the availability and sustainability of ground-water supplies within the study area. The study area includes aquifer systems in Arizona and parts of California, Nevada, New Mexico, and Utah (chapter A, this volume; fig. 1), most of the Basin and Range physiographic province in Arizona, California, Nevada, New Mexico, and Utah, and a large portion of the Colorado Plateau in Arizona, New Mexico, and Utah (Fenneman, 1931). The regional analysis complemented the site-specific ground-water recharge studies, which examined frequency and distribution of stream-flow losses and attendant recharge for typical streams and subbasins across the study area. Results from the recharge study-site investigations are described in chapters D–K.

Without a regional framework, results from individual study sites would be difficult to assess given that sites are widely separated, and that climate, soils, and geology differ among the sites. A regional framework increases the extrapolative value of subbasin-scale studies by systematically quantifying the interactions among processes, properties, and climatic factors producing runoff and ground-water recharge. The objective of the analysis was to provide a regionally consistent framework that could be used to characterize basins throughout the entire study area. The distributed-parameter, water-balance model known as the Basin Characterization Model (BCM; Flint and others, 2004; Flint and Flint, 2007) was applied to evaluate regional climatic factors and physical properties that produce runoff and ground-water recharge. The analysis model employs a deterministic mathematical approach that accounts for the temporal and spatial distribu-

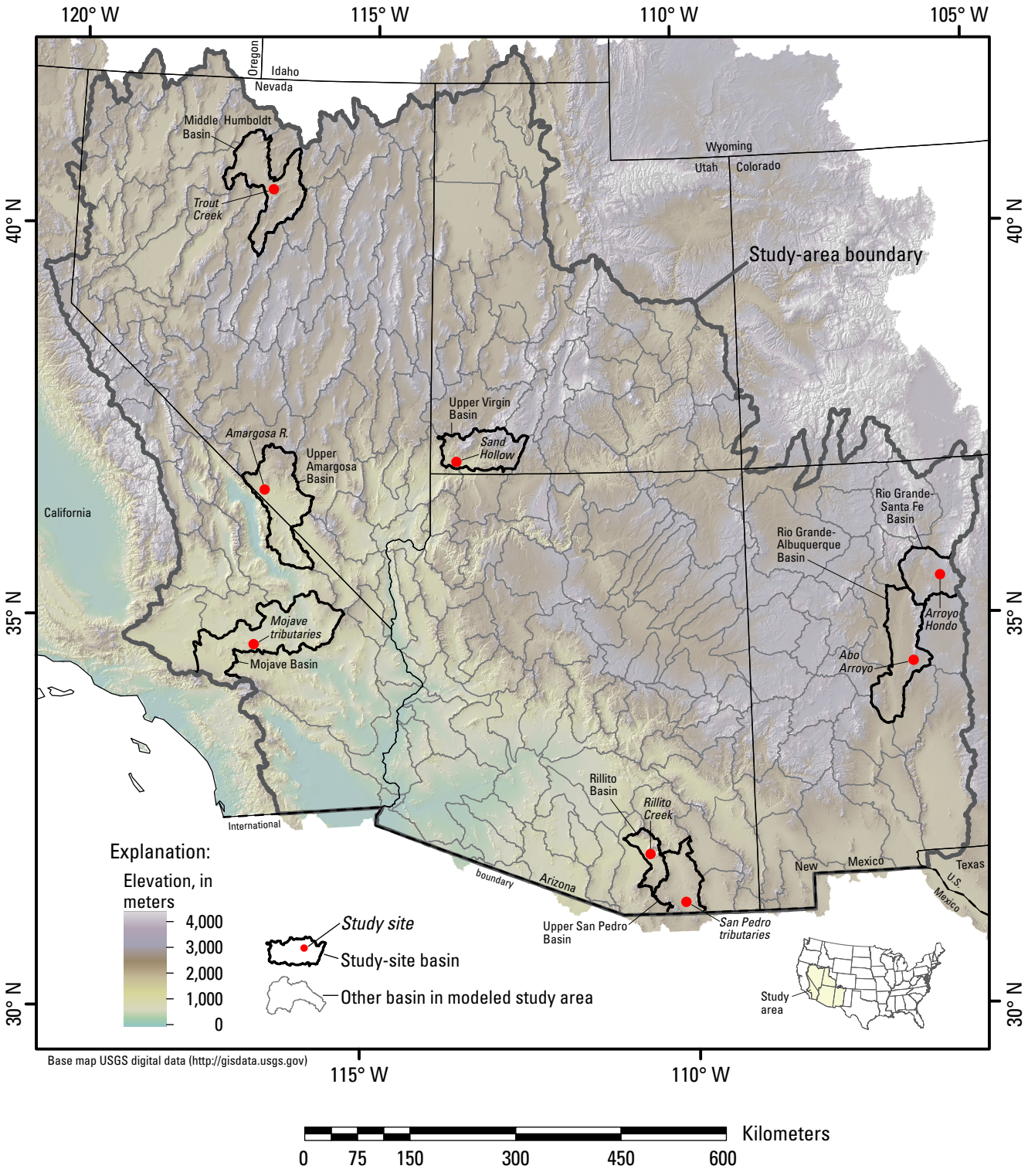

Figure 1. Digital elevation map showing locations of the 194 basins within the modeled arid and semiarid southwestern United States study area. Red dots indicate ground-water recharge study sites (chapters D–K, this volume). Basin outlines are drainage areas of USGS 1:250,000 hydrologic accounting units, each of which is identified by an eight-digit hydrologic accounting code (8-digit HUC in table 1) (Seaber and others, 1987).

tion of precipitation (including the accumulation and melting of snow) together with the spatial distribution of soils, vegetation, and hydraulic conductivity of underlying materials; the model also estimates potential evapotranspiration and accounts for changing quantities water stored in the soil (Flint and others, 2004). Available geographic-information-system data (digital GIS coverages), including topography, vegetation, soils, geology, and average monthly precipitation and air temperature were used for the analysis. Estimates of slope and aspect were generated within the model on the basis of digital topographic data.

The BCM was used to estimate quantities of water available for generating runoff (potential streamflow) and in-place (subsoil) recharge within the 194 basins that make up the study area (fig. 1). The 194 basins were defined by using the drainage areas of the U.S. Geological Survey's 1:250,000-scale hydrologic units (Seaber and others, 1987; http://water.usgs.gov/GIS/metadata/usgswrd/XML/huc250k.xml). The analysis allowed the basins containing the eight recharge-study sites to be compared to one another, as well as to other basins in the study area. Figure 1 shows the location of each study site. The eight study sites occupied a relatively small portion of the basins for which in-place recharge and runoff were estimated by using the BCM. Comparison of study-site basins with other basins provides a basis for assessing representativeness within the context of the entire region, and for interpreting differences in precipitation, snowpack dynamics, and in-place recharge or runoff within the context of geologic, vegetational, and soil differences. The analysis included climatic conditions from 1996–2002 for interpretations relevant to the recharge study-site investigations and climatic conditions from 1941–2004 for evaluation of longer-term climate cycles.

Conceptual Framework

A Classification of Basins by Water-Balance Considerations

Basins were classified on the basis of their climate, runoff, and in-place recharge. Spatially distributed estimates of in-place recharge and runoff provided a means to explore fundamental concepts and evaluate mechanisms that control ground-water recharge in all basins of the study area relative to the basins of the eight ground-water recharge-study sites. The effects of precipitation, snowpack accumulation and melting, soil properties including thickness, and hydraulic conductivity of underlying geologic materials were evaluated by using the BCM model. Basins were characterized as being dominated by runoff or by in-place recharge.

The basins of the study area typically consist of three principal geomorphic features—mountains, piedmont slopes consisting of coalescing alluvial fans or a piedmont alluvial plain, and lower valley floors (Thornbury, 1969, p. 271). Piedmont slopes are transition areas between the higher mountains and valley floors. Precipitation generally is higher in the mountains and lower on valley floors, whereas temperature generally is warmer on valley floors and cooler in the mountains (Houghton and others, 1975). Consequently, snow accumulation typically is greater and potential evapotranspiration is less in the mountains than on the piedmont slopes and valley floors.

Ground-water recharge in the mountains occurs from infiltration of precipitation and snowmelt; infiltration of runoff in perennial, intermittent, and ephemeral streams; and from infiltration beneath wetlands and lakes. Direct infiltration into bedrock can occur without runoff in mountainous areas where bedrock is sufficiently permeable, such as areas in eastern Nevada and western Utah underlain by thick sequences of permeable carbonates (Mifflin and Hess, 1979; Harrill and Prudic, 1998; Flint and Flint, 2007). Ground-water recharge on piedmont slopes commonly is limited to infiltration losses along intermittent or ephemeral streams that cross generally coarse-grained basin-fill deposits (chapters D–K). Ground-water recharge on the valley floors can occur from infiltration losses from regional rivers, such as the Colorado, Rio Grande, and Humboldt. Ground-water recharge on valley floors also can occur beneath intermittent and ephemeral streams, playas, lakes, and reservoirs, and—at higher elevations—from direct infiltration during years with extensive snowmelt. Most runoff is generated in the mountains where there is more precipitation and accumulation of winter snow (Eakin and others, 1976; Prudic and others, 1995). A fraction of runoff from the mountains becomes ground-water recharge from infiltration losses along streams that cross piedmont slopes or valley floors.

Conceptually, these processes can be considered "mountain-block recharge" where the water recharges directly into bedrock; "mountain-front recharge" where runoff from the mountain block reaches the piedmont slopes and infiltrates; "diffuse recharge" on the valley floor, and "recharge from stream flow" (Stephens, 1995). The simplified approach used by the BCM calculates mountain-block and diffuse recharge as potential in-place recharge. The recharge is considered potential because the BCM does not keep track of whether or not the water returns to the surface as spring flow from a perched water table before reaching the regional aquifer. Neither runoff nor ground water is routed within the model; rather, the amounts of runoff and in-place recharge are treated as basin characteristics. Some runoff subsequently becomes ground-water recharge. The percentage of runoff that becomes ground-water recharge is variable, depending on the hydraulic properties of soils, geologic units, and streambeds, as well as the hydraulic gradient between ground water and surface water. Estimates of recharge and runoff were made for twelve basins of the Basin and Range carbonate-aquifer system (Flint and Flint, 2007). Results indicated that about 15 percent of runoff typically becomes recharge on the basis of ground-water discharge estimates and estimates of interbasin flow (Laczniak and others, 2007; Lundmark and others, 2007). Stonestrom and others (2004) calculated that 12–15 percent of ephemeral runoff became recharge in the Amargosa River in southern

Nevada. A calibrated model of unsaturated-zone heat and water flow combined with evapotranspiration measurements, chloride-mass balance estimates, and microgravity measurements at the Walnut Gulch watershed in southeastern Arizona indicated that recharge from ephemeral-stream flow constituted 15–40 percent of total flow during a high runoff year (Goodrich and others, 2004). Studies in the southern Mojave Desert indicated that about 10 percent of ephemeral-stream flow became recharge (Izbicki, 2002). A distributed-parameter rainfall-runoff-recharge model, calibrated to (1) stream discharge and (2) a calibrated ground-water model for the Death Valley regional flow system, resulted in approximately 10 percent of runoff becoming recharge (Hevesi and others, 2003). Prudic and others (chapter K, this volume) and Ronan and others (1998) found that as much as 90 percent of runoff became recharge in the Trout Creek area of the Middle Humboldt Basin and in the Carson River drainage near Carson City, Nevada, respectively. These sites are characterized by high precipitation, snowpack, and runoff compared to most other basins in the study area. The resulting unsaturated zone is thin, optimizing the connection between surface water and ground water while enhancing stream flow recharge. The percentage of runoff that becomes recharge is spatially and temporally variable and difficult to quantify. For the purposes of initial comparisons, the present BCM analysis assumed that 15 percent of runoff subsequently became ground-water recharge.

Methods of Estimating Ground-Water Recharge

Flint and others (2002) and Scanlon and others (2002) reviewed methods that have been used to estimate ground-water recharge in the study area. Among methods most commonly used are calculations based on Darcy's law, calculations based on repeated measurements of water-content profiles, inverse calculations based on deviations of measured temperature profiles from heat-conduction-only profiles, chloride-mass balance calculations, calculations based on the decay of atmospherically deposited radionuclides, empirical-transfer methods relating precipitation to ground-water discharge, and distributed-parameter water-balance modeling. Of these methods, only the distributed-parameter water-balance modeling and empirical transfer methods provide spatially distributed estimates throughout a selected region. Maxey and Eakin (1949) developed an empirical method to estimate average annual ground-water recharge in 13 basins in eastern Nevada by using annual precipitation maps delineated by isohyetal contours (Hardman, 1936; 1965). Ground-water recharge was estimated as a percentage of mean-annual precipitation for five distinct ranges of precipitation. Recharge estimates did not address where recharge occurs within a basin. The method was evaluated by Watson and others (1976), who found it useful for providing initial approximations. Estimates of recharge for 12 basins in eastern Nevada produced with the BCM were somewhat higher but relatively close to the estimates of Maxey and Eakin (Flint and Flint, 2007).

Estimating Runoff and In-Place Recharge With a Distributed-Parameter Water-Balance Model

The BCM was used to identify locations and climatic conditions that allow for excess water to become potential runoff or potential in-place recharge, and to estimate the amount of each. Runoff is the volume of water for a given time frame that becomes stream flow and either infiltrates down slope or exits the basin as stream flow. As shown in subsequent chapters, much of the down-slope infiltration exits the basin as evapotranspiration. In-place recharge is calculated as the volume of water for a given time frame that can drain from the soil zone directly into consolidated bedrock or unconsolidated deposits. Ground-water recharge is the combination of in-place recharge and 15 percent of runoff.

A water-balance equation for each 270-meter grid cell was developed by using monthly estimates of precipitation, maximum and minimum air temperature, and potential evapotranspiration. Composite values were used to calculate the monthly volume of runoff and in-place recharge for each basin. The volume of water potentially available for runoff and in-place recharge (*AW*) per unit area of each cell was estimated monthly on the basis of the following equation:

$$AW = P + S_m - PET - S_a + S_s, \qquad (1)$$

where P is the estimated precipitation for the grid cell, S_m is the estimated snowmelt, PET is the potential evapotranspiration, S_a is the estimated snow accumulation, and S_s is the soil-water storage from the previous month. Snow accumulation that does not melt during the month is carried over into the following month. All volumes per grid-cell area are in units of millimeters per month.

Runoff is generated from water in excess of the total soil-water storage capacity (soil porosity multiplied by soil depth). In-place recharge is generated from soil water in excess of the field capacity of the soil (the water content at which drainage becomes negligible), and occurs at a rate determined by the hydraulic conductivity of the underlying materials.

Potential evapotranspiration is modeled on a daily basis from solar radiation that is modeled by using topographic shading and a correction for cloudiness (Flint and Flint, 2008), and is partitioned on the basis of vegetation cover to represent bare-soil evaporation and evapotranspiration due to vegetation. These results are averaged into monthly values for use in equation 1. Depending on the soil-water storage and hydraulic conductivity of the underlying consolidated rocks and basin-fill deposits, excess water is partitioned as either in-place recharge or runoff that potentially can become ground-water recharge from infiltration losses further downstream in the mountains, piedmont slopes or valley floors.

Excess water, calculated as the summed values of average monthly precipitation minus average monthly potential

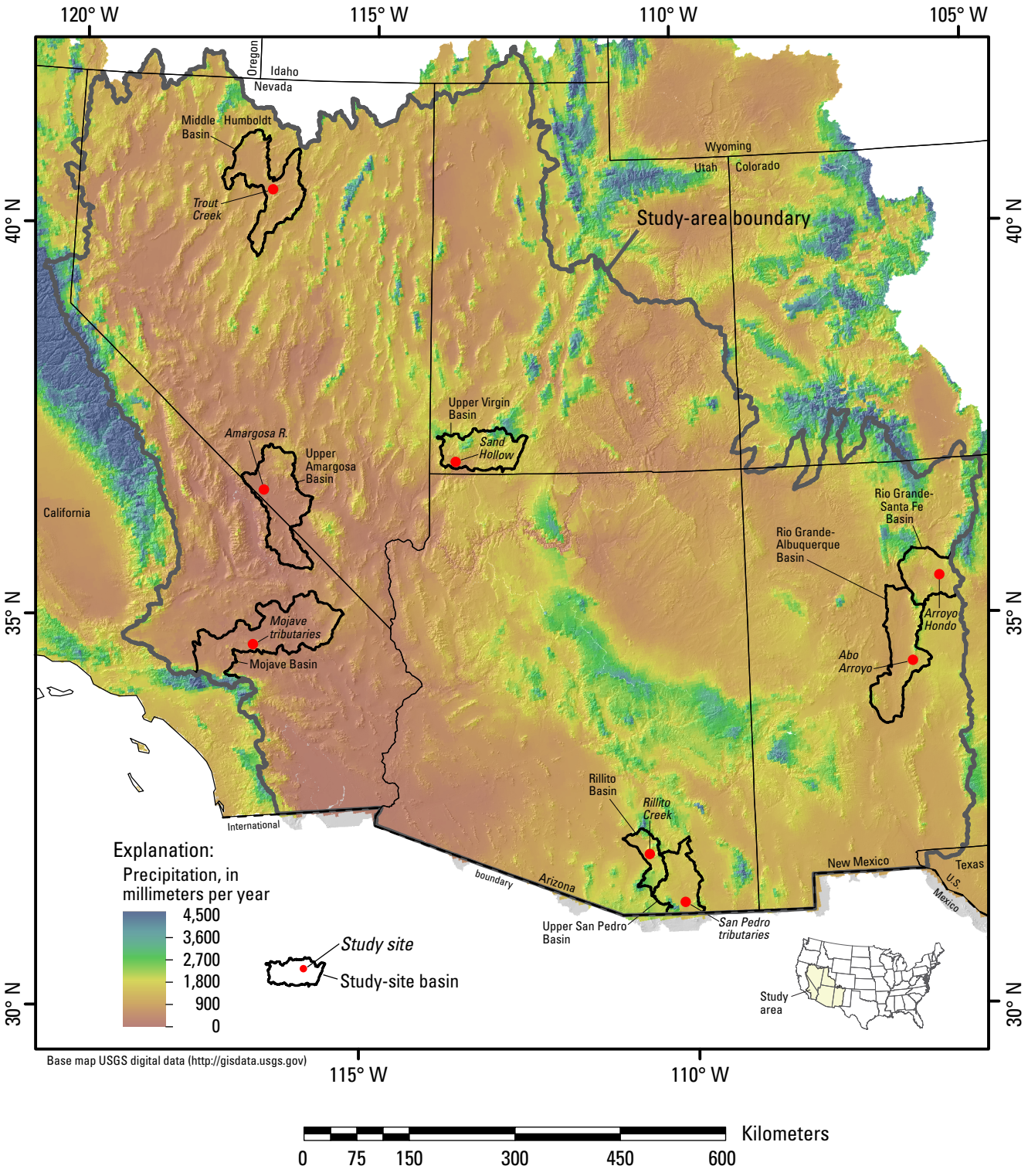

Figure 2. Average annual precipitation for 1971–2000 within the modeled arid and semiarid southwestern United States study area, calculated from monthly Precipitation-elevation Regression on Independent Slopes Method (PRISM) data (Daly and others, 2004).

evapotranspiration, is illustrated in figure 3. The excess water is the amount of water that remains in the system, assuming evapotranspiration consumes the maximum possible amount of water. This excess water is the amount available to replenish soil-water storage and generate runoff and in-place recharge. Although recharge can occur in areas with no excess water, the monthly time step limits the ability of the model to resolve short-term dynamics. Figure 3 illustrates this simple water balance concept—no excess water is calculated by using a monthly time step in most of the low-lying desert areas in southern Arizona, southeastern California, southern Nevada, and southern New Mexico. Most of the excess water is in the higher-elevation mountains and plateaus.

Maximum in-place recharge is limited by the assumed hydraulic conductivity of consolidated rocks in the mountains, or basin-fill deposits on the piedmont slopes and valley floors. The volumetric rate is expressed in millimeters per month. When soil-water storage is at total capacity, in-place recharge is set equal to the hydraulic conductivity of the underlying consolidated rocks in the mountains, or basin-fill deposits in the piedmont slopes and valley floors; drainage will continue until the soil-water storage is at field capacity. Any remaining water in the soil zone above field capacity at the end of the month is added to soil-water storage (S_s) at the beginning of the next month. Additionally, any remaining snow accumulation and soil-water storage from the end of a month is added to the beginning of the next month. This becomes important when temperatures are cold enough for precipitation to arrive as snow. Because snow may persist for several months before melting, large volumes of water can be made available for runoff and in-place recharge in a single monthly time step.

The model does not distinguish where runoff may infiltrate through the streambed and become ground-water recharge, nor does it explicitly define the percentage of runoff that becomes ground-water recharge. Because there is insufficient information to partition excess water into runoff and in-place recharge accurately without further refinements to the BCM and additional calibration of parameters, average annual estimates and distribution of runoff, in-place recharge, and ground-water recharge in each basin should be treated as general approximations.

An additional limitation to the BCM is that the calculation of ground-water recharge assumes that water draining past the root zone becomes recharge within that monthly time step, without consideration of the potential for extended periods of ground-water travel time through the unsaturated zone. In the more arid portions of the study area, the unsaturated zone may exceed 100 meters (m) in thickness across broad areas. Calculations of ground-water travel time in the southern Great Basin area have exceeded 10,000 years (Flint and others, 2000) due to variation in net infiltration rates and the thickness of the unsaturated zone, which is commonly 10–100 m thick, but can exceed 2,000 m. However, some locations in mountainous areas have shallow unsaturated zones and may recharge to local ground-water within the monthly time step.

Despite the simplifications of the model, the consistent application of the parameters controlling runoff and in-place recharge provides a means for regional analysis of these mechanisms during the 1996–2002 time frame of the eight ground-water recharge-site investigations. In addition, the BCM allows for the evaluation of runoff and in-place recharge during past wetter and drier climates and the role of decadal-scale climate cycles (El Niño/La Niña and the Pacific Decadal Oscillation).

Precipitation, snowmelt, and overland runoff from upslope areas provide the source of water that infiltrates into the soil zone. Thickness of the soil zone, porosity, and drainage characteristics determine how much water is stored in the soil zone. Rooting depth, type of vegetation, percentage of bare-soil surfaces, and the energy balance control the rate of potential evapotranspiration. Evapotranspiration is highest during the warm summer months, which decreases the amount of water stored in the soil zone, and lowest during the cool winter months, which allows for increased soil-water storage from precipitation, snowmelt, and run-on events. The topography and atmospheric conditions control much of the energy available for potential evapotranspiration. Drainage below the root zone occurs when sufficient water is available to exceed the water-storage capacity of the soil (or rock), only then does "net infiltration" have the potential to become ground-water recharge.

Generally, the hydraulic conductivity of consolidated rocks in the mountains or basin-fill deposits on piedmont slopes and valley floors, soil-water storage capacity, and potential evapotranspiration are the factors that determine the rate of drainage from the soil zone. In locations with thin soils, soil thickness becomes the most important factor affecting soil-water storage capacity. The soil-water storage in thin soils underlain by fractured bedrock will approach capacity (saturation) because the water-entry potential of the fracture network must be exceeded before significant drainage into the underlying bedrock can occur. If the soil is thin and the hydraulic conductivity of the underlying consolidated rocks or basin-fill deposits is low, then evapotranspiration has more time to remove stored water between periods of precipitation, snowmelt, and run-on from upslope areas. If the hydraulic conductivity of the underlying consolidated rock or basin-fill deposits is high, evapotranspiration has less time to remove stored water between infiltration events.

In locations with thick soil, a greater volume of water is needed, compared with thin soil locations, to exceed the soil-water storage capacity of the root zone. If the soil-water storage capacity is high and the hydraulic conductivity of the soil zone is low (for example, fine-grained silt and clay), then drainage through the root zone occurs slowly, and evapotranspiration has more time to remove stored water between periods of precipitation, snowmelt, and run-on from upslope areas. If the soil-water storage capacity is low and the hydraulic conductivity of the soil zone is high (coarse sand and gravel), then drainage through the root zone occurs rapidly, and evapotranspiration has less time to remove stored water.

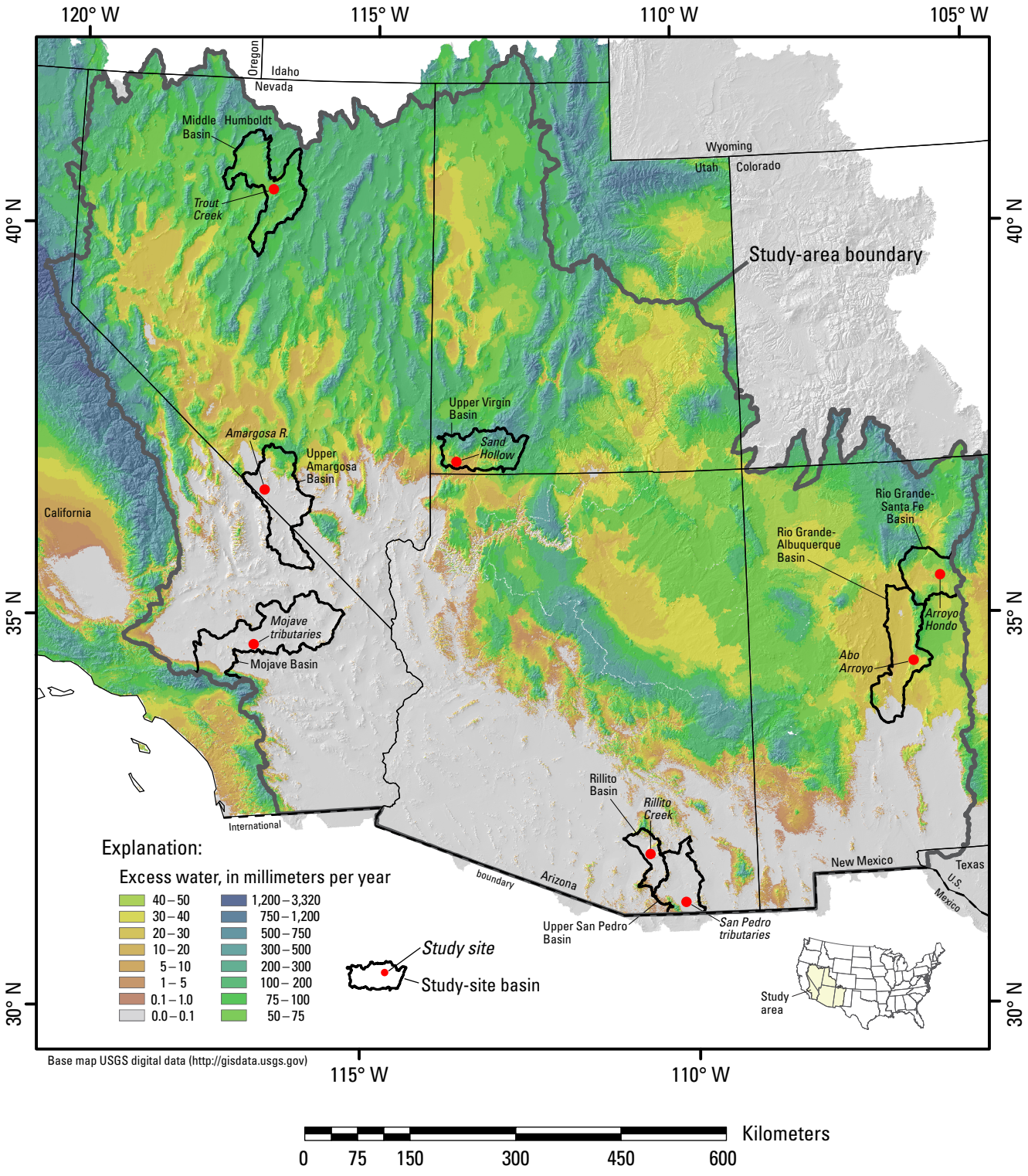

Figure 3. Estimates of annual excess water within the modeled arid and semiarid southwestern United States study area, calculated as the summed values of average monthly precipitation minus average monthly potential evapotranspiration. Texas, Wyoming, and portions of Colorado outside the study area were not included in the analysis.

The mechanisms controlling drainage from the soil zone influence where drainage will occur in a given basin. The location of in-place recharge is important, particularly if one intends to quantify or analyze it by means of field measurements. Limiting measurements to locations where streams cross onto basin fill excludes consideration of in-place recharge higher in the mountains that might contribute sizeable amounts of subsurface flow to aquifers underlying piedmont slopes and valley floors. At the same time, applying simplified distributed-parameter water-balance models without sufficient information about controlling parameters also can result in large errors in estimated recharge and runoff. An advantage of using a distributed-parameter water-balance model to complement site-specific studies is that probable locations for runoff and in-place recharge can be identified reasonably well because the distribution of precipitation, snowmelt, evapotranspiration, soil-water storage capacity, and hydraulic conductivity are mapped at moderately high resolution for the various types of soils, consolidated rocks and basin-fill deposits within the study area.

Input Parameters Used in the Water-Balance Model

Spatially Distributed Properties of Soils and Geologic Units

Soil-water storage capacity (fig. 4) was estimated by using soil-texture estimates from STATSGO (State Soil Geographic Database), a geospatial database of soil properties that generally are consistent across state boundaries (USDA-SCS, 1991; http://www.ncgc.nrcs.usda.gov/products/dataset/statsgo/). Uncertainties in soil properties are discussed by Hevesi and others (2003) and Gutmann and Small (2007). Soil thickness was estimated from STATSGO data for all locations, except those where Quaternary basin fill (alluvium) was mapped (fig. 5). In locations with alluvium, a depth of 6 m was chosen on the basis of field observations made in the Mojave Desert of desert plant root penetration into alluvium and bedrock. Thus, the BCM assumes that all processes controlling net infiltration occur within the top 6 m of surface materials. This assumption is supported by data from Yucca Mountain in the southern Great Basin (Flint and Flint, 1995). Relatively large soil-water storage capacities were estimated for the areas of Quaternary basin fill in the Basin and Range Province of Arizona, Nevada, southern California, New Mexico, and western Utah (fig. 4), whereas smaller capacities were estimated for much of the Colorado Plateau in northern and eastern Arizona, southern Utah, and northern and western New Mexico.

The surficial geology was classified broadly for the purpose of assigning saturated hydraulic conductivity values to sub-soil consolidated and unconsolidated materials throughout the region. Geologic units were obtained from geologic maps (Arizona: Hirschberg and Pitts, 2000; California: Jennings, 1977; Colorado: Green, 1992; Idaho: Johnson and Raines, 1996; Nevada: Stewart and others, 2003; Oregon: Walker and McLeod, 1991; Utah: Hintz and others, 2000). The principal geologic units include Quaternary to Tertiary unconsolidated to indurated alluvial, eolian, playa, and lacustrine deposits and volcanic rocks; Mesozoic granitic and other intrusive rocks, sandstone, limestone, and other sedimentary, metavolcanic, and metamorphic rocks; Paleozoic carbonate and clastic rocks (quartzite, argillite, shale); and Precambrian igneous, metamorphic, and clastic sedimentary rocks. The units are mapped on the basis of hydrologic character, rather than geologic age (fig. 5). The saturated hydraulic conductivity (fig. 6) was estimated for each surficial bedrock or unconsolidated surficial unit listed in figure 5. Saturated hydraulic conductivities were estimated from literature values, aquifer-test results, and surface-based infiltration experiments. The hydraulic properties of macropores and fractures are incorporated in the bulk estimates of hydraulic conductivity. Hydraulic conductivity estimates of bedrock are relatively uncertain because of the unknown hydraulic properties and spatial distributions of fractures, faults, fault gouge, and shallow infilling materials associated with different bedrock types.

Quaternary basin-fill deposits have the highest saturated hydraulic conductivity in the study area, particularly the eolian deposits and sand and gravel units, whereas finer-grained flood-plain deposits, clay-rich lacustrine deposits, and playa deposits have the lowest values of the basin-fill deposits (fig. 6). Saturated hydraulic conductivity of surficial bedrock usually differs from underlying transmissivity per unit thickness due to surface weathering and infilling of fractures and faults from soils and calcium-carbonate development. However, relative estimates for various rock types can be derived on the basis of ground-water assessments. Carbonates and sandstones are generally the most permeable of the consolidated rocks (Bedinger and others, 1989). Where fractured and porous, carbonates and sandstones have hydraulic conductivities similar to those of sand and gravel aquifers in the basin fill (Winograd and Thordarson, 1975; Dettinger and others, 2000). Granitic rocks, metamorphic rocks (slates, argillites, marbles, and quartzites), and fine-grained sedimentary rocks (siltstones, and shales) typically have very low saturated hydraulic conductivities and porosities (Davis and DeWiest, 1966; Freeze and Cherry, 1979). Volcanic rocks consist of a variety of rocks associated with volcanic activity. Basalt flows and welded tuffs can be highly permeable and have sufficient porosity to store and transmit large quantities of water (Glancy, 1986; Winograd and Thordarson, 1975). Typically, volcanic rocks in the study area are far less porous and permeable than the sand and gravel of the basin fill or the carbonate rocks (fig. 6).

Temporally and Spatially Distributed Parameters of Climate

Spatially distributed monthly estimates of precipitation, minimum and maximum air temperature, and potential

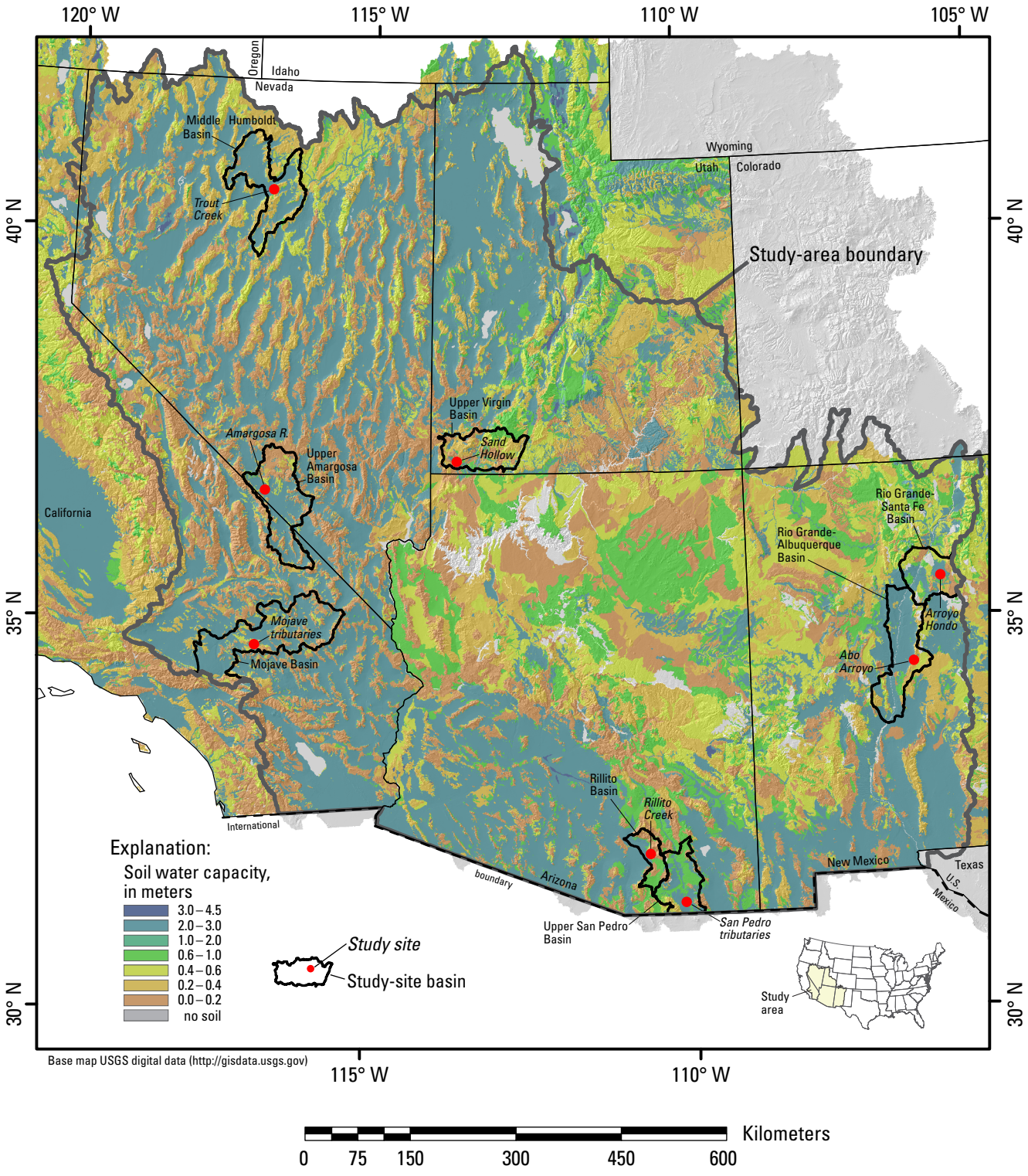

Figure 4. Total soil-water storage capacity for the modeled arid and semiarid southwestern United States study area. Gray areas within the study boundary indicate soil-free bedrock or surface water.

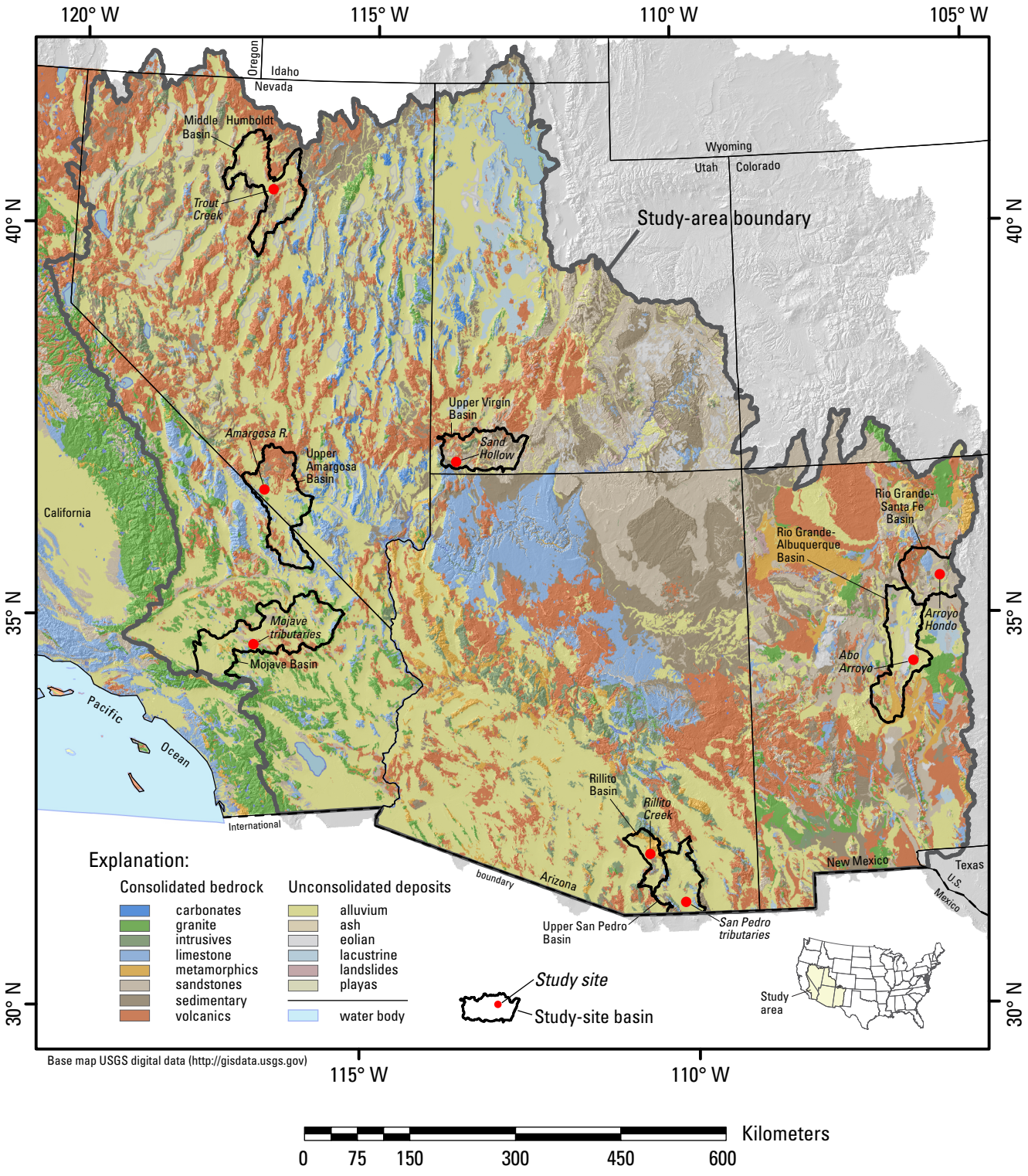

Figure 5. Surficial geology of the modeled arid and semiarid southwestern United States study area. Compiled from: (Arizona) Hirschberg and Pitts, 2000; (California) Jennings, 1977; (Colorado) Green, 1992; (Idaho) Johnson and Raines, 1995; (Nevada) Stewart and others, 2003; and (Utah) Hintz and others, 2000.

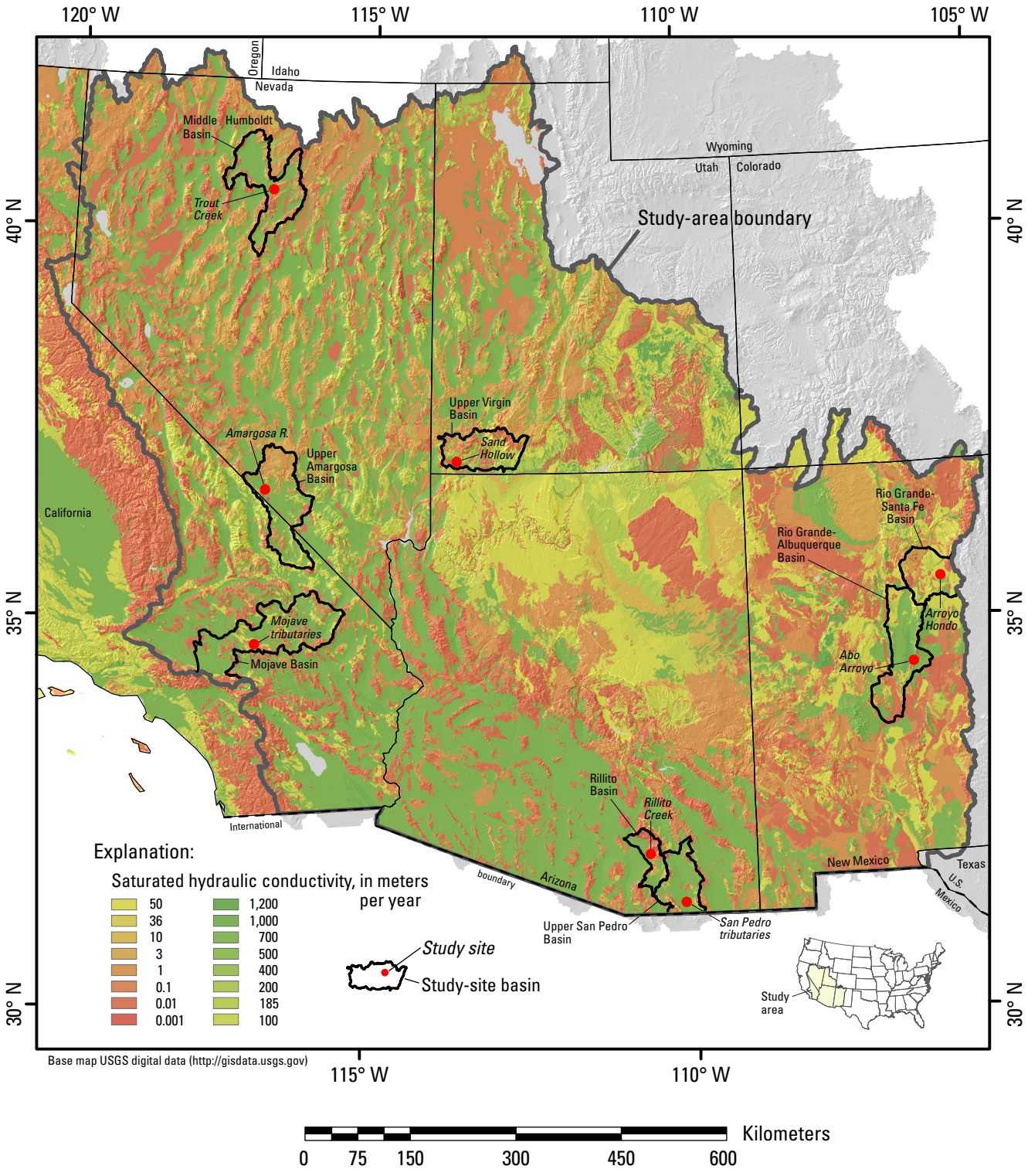

Figure 6. Estimated saturated hydraulic conductivity of surficial geologic units in the modeled arid and semiarid southwestern United States study area. Input to the Basin Characterization Model assumed 16 discrete values of conductivities as shown. Data for water bodies and portions of states outside the study area are not depicted.

evapotranspiration were used to calculate quantities of water available for runoff and in-place recharge by consideration of soil-water storage capacity and hydraulic conductivity of underlying bedrock or unconsolidated materials. Areas of excess water were estimated on a monthly basis.

Precipitation and maximum and minimum air temperatures were derived from a climatic database covering 1941–2004 on a 4,000-m grid (Daly and others, 2004). Centroids of the grid cells were used in downscaling the data to the 270-m BCM grid by applying a multiple-regression method that evaluates spatial gradients by using inverse-distance squared weighting (GIDS) along northing, easting, and elevation dimensions (Nalder and Wein, 1998; Flint and Flint, 2008). The 1941–2004 record was used in a transient analysis to evaluate the effects of antecedent soil-moisture and impacts of recent climatic trends on hydrologic responses, and to provide climatic context for individual study sites. Average monthly values of precipitation and air temperature were also estimated for the period 1971–2000, corresponding to 30-year climatic "normals" (Doggett and others, 2004).

Potential evapotranspiration was estimated by using a computer program modified from Flint and Childs (1987) that calculates solar radiation for the latitude and longitude of each grid cell on the basis of percent of sky viewed due to topographic shading. Computed solar radiation, combined with air temperature, is converted to net radiation and soil-heat flux (Shuttleworth, 1993). The result was used with the Priestley–Taylor equation (Priestley and Taylor, 1972) to estimate potential evapotranspiration (fig. 7), taking into account vegetated and bare-soil areas by using estimates of vegetation cover (fig. 8; National Gap Analysis Program; http://gapanalysis.nbii.gov).

The regional-scale approach of the BCM used computed potential evapotranspiration during monthly time periods in making estimates of ground-water recharge for evaluating mechanisms and differences among basins. Potential evapotranspiration was compared to reference-crop evapotranspiration, ET_o, measured on well-irrigated plots at evapotranspiration stations in Arizona (http://ag.arizona.edu/azmet/) and California (http://www.cimis.water.ca.gov/cimis/). Monthly potential evapotranspiration simulated by the BCM compared well to measured ET_o values, with BCM values overestimated by approximately 10 percent for June, July, and August (fig. 9).

An energy- and mass-balance model for computing snow accumulation and ablation (sublimation plus snowmelt) was adapted from the Snow-17 operational model of the National Weather Service as described by Anderson (1976) and Shamir and Georgakakos (2005). Potential snowmelt was calculated from air temperature and an empirical snowmelt factor that varied by day of year (Lundquist and Flint, 2006). Snow depth was calculated for areas where precipitation occurred with air temperatures at or below 1.5 degrees Celsius. Sublimation was estimated as a percentage of evapotranspiration. Snowmelt was predicted from snowpack energy-balance considerations when air temperatures were above freezing. Empirical snow-accumulation and snowmelt factors were adjusted to match the predicted areal extent of snowpack to satellite data measured with the Moderate-Resolution Imaging Spectroradiometer (MODIS; http://edcdaac.usgs.gov/modis/dataproducts.asp mod43) and fine tuned by varying the temperature threshold at which snowmelt begins (Lundquist and Flint, 2006). Examples of simulated snow cover compared to MODIS-derived snow cover are shown in figure 10 for February 2001, when snowpack was at a maximum, and April 2001, when ablation processes were at a maximum. Although modeled snow distributions differed from observations in detail, the overall snowpack dynamics were represented reasonably well, especially during periods of accumulation and runoff generation.

The results of the BCM were not calibrated to any measured runoff or recharge data. The runoff and recharge estimates produced by the model can thus be viewed as hypothetical values that are perhaps most useful for exploring the relative differences among basins. The BCM did not route water from cell to cell. For simplicity, the percentage of runoff that became recharge was uniformly estimated to be 15 percent. Two submodels of the BCM, one for solar radiation and potential evapotranspiration and one for snow-cover dynamics, were calibrated to measured values. This implies that the water-balance calculations of the BCM have somewhat larger uncertainties in relation to soil properties and precipitation estimates. The partitioning of excess water into runoff and recharge presents the largest uncertainty, as it relies on the estimation of saturated hydraulic conductivity of near-surface materials.

Application to Study-Area Basins

The BCM was applied to the 64-year time series from water year 1941–2004 to evaluate the impact of antecedent hydrologic conditions, and to evaluate recharge mechanisms and amounts under wetter and drier climatic conditions. This period extends through a complete cycle of the negative and positive Pacific Decadal Oscillation. Subsets of this time series were used to provide context for the eight recharge-site investigations. A 30-year record, 1971–2000, was used to compute "normal" monthly conditions for the study area. The 30-year average does not take into account antecedent hydrologic conditions that cause persistence. The nonlinear response of recharge to precipitation tends to underestimate recharge for average monthly conditions because wetter-than-average conditions produce nonlinearly greater amounts of recharge (Flint and others, 2004; Flint and Flint, 2007)

Estimates of annual ground-water recharge for average conditions (calculated as in-place recharge plus 15 percent of runoff) were compiled for all 194 basins in the study area (fig. 11). The results shown indicate that most of the recharge occurs in the mountains of each basin. This was an expected result because the mountains typically have higher precipitation, lower air temperatures, and thinner soils relative to piedmont slopes and valley floors of each basin. Large areas of basin floors with excess water did not produce ground-water recharge because soil-water storage was sufficiently

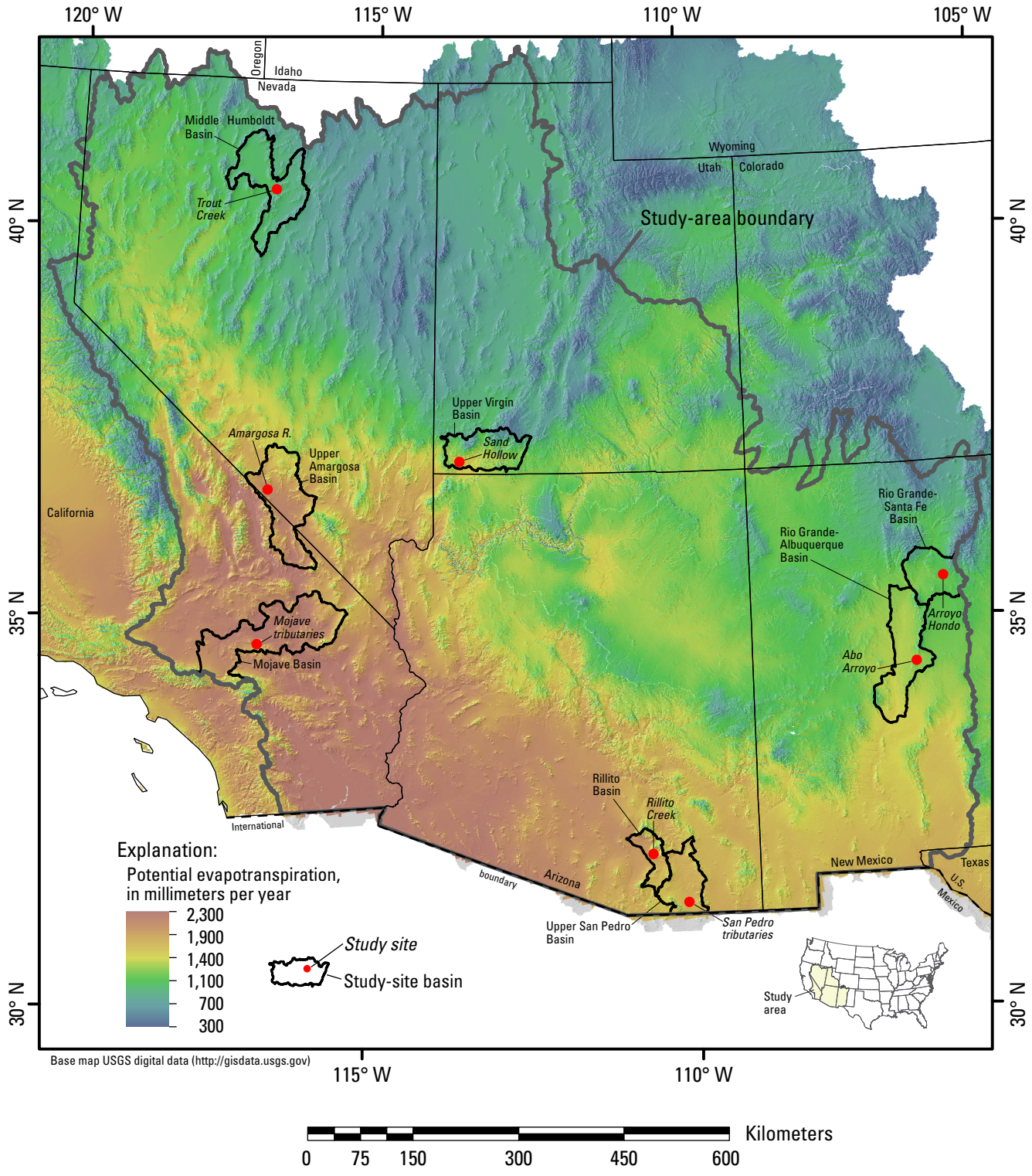

Figure 7. Average annual potential evapotranspiration in the modeled arid and semiarid southwestern United States.

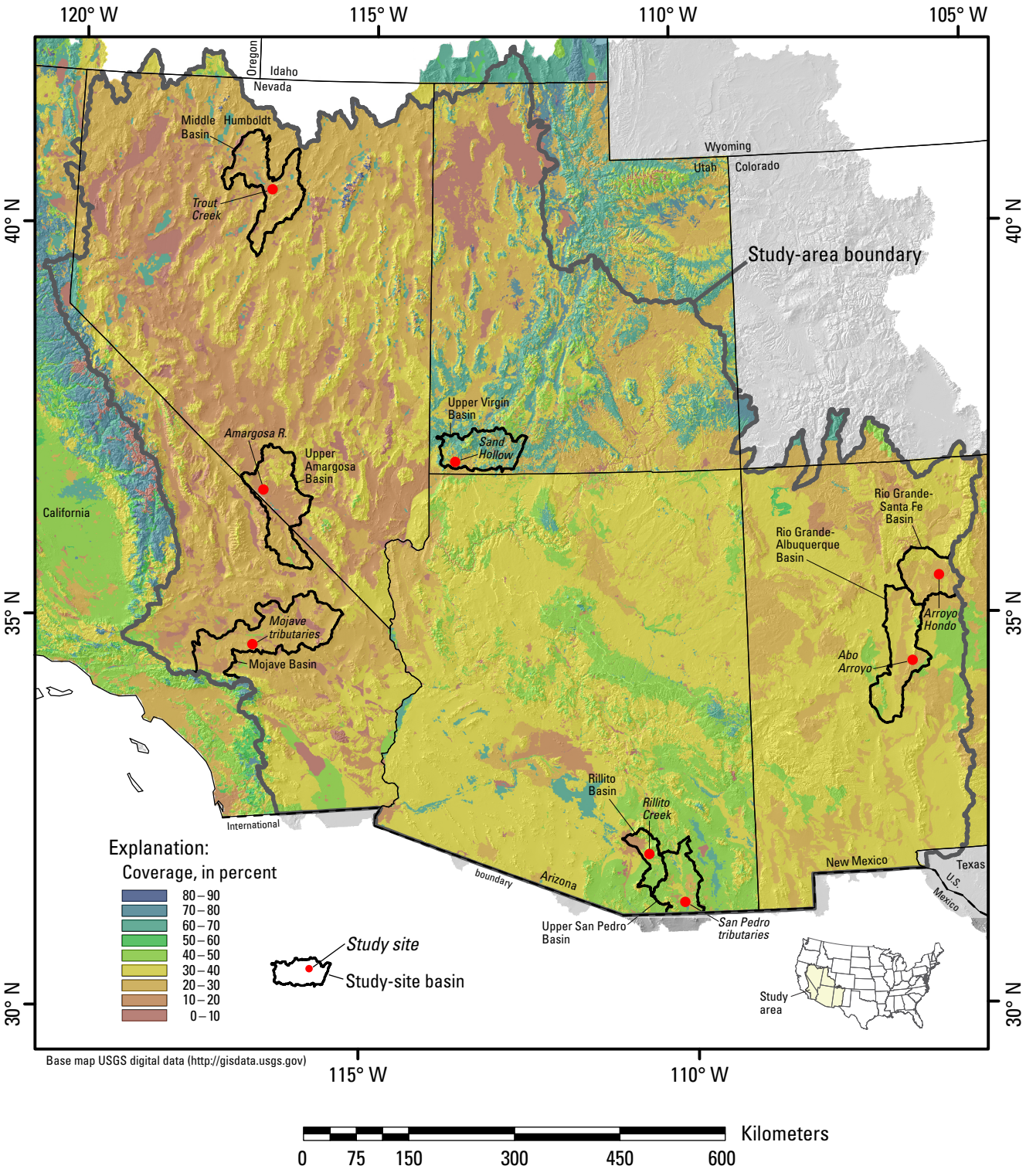

Figure 8. Percentage of area covered by vegetation in the modeled arid and semiarid southwestern United States.

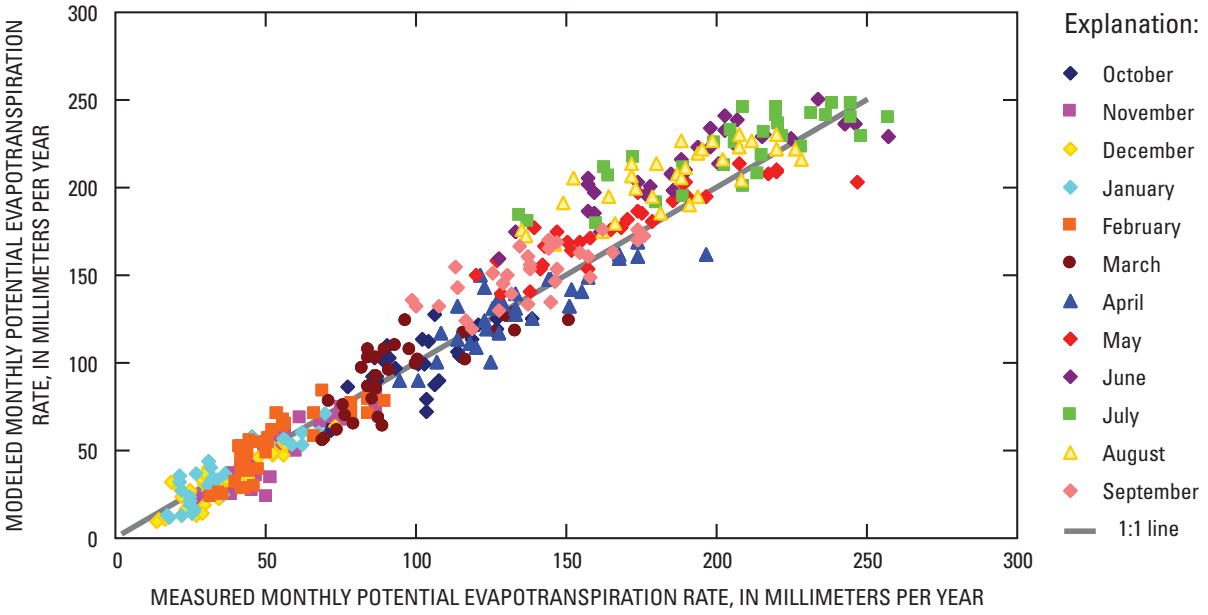

Figure 9. Submodel calibration for potential evapotranspiration (ETo) using values calculated with data from stations in California and Arizona.

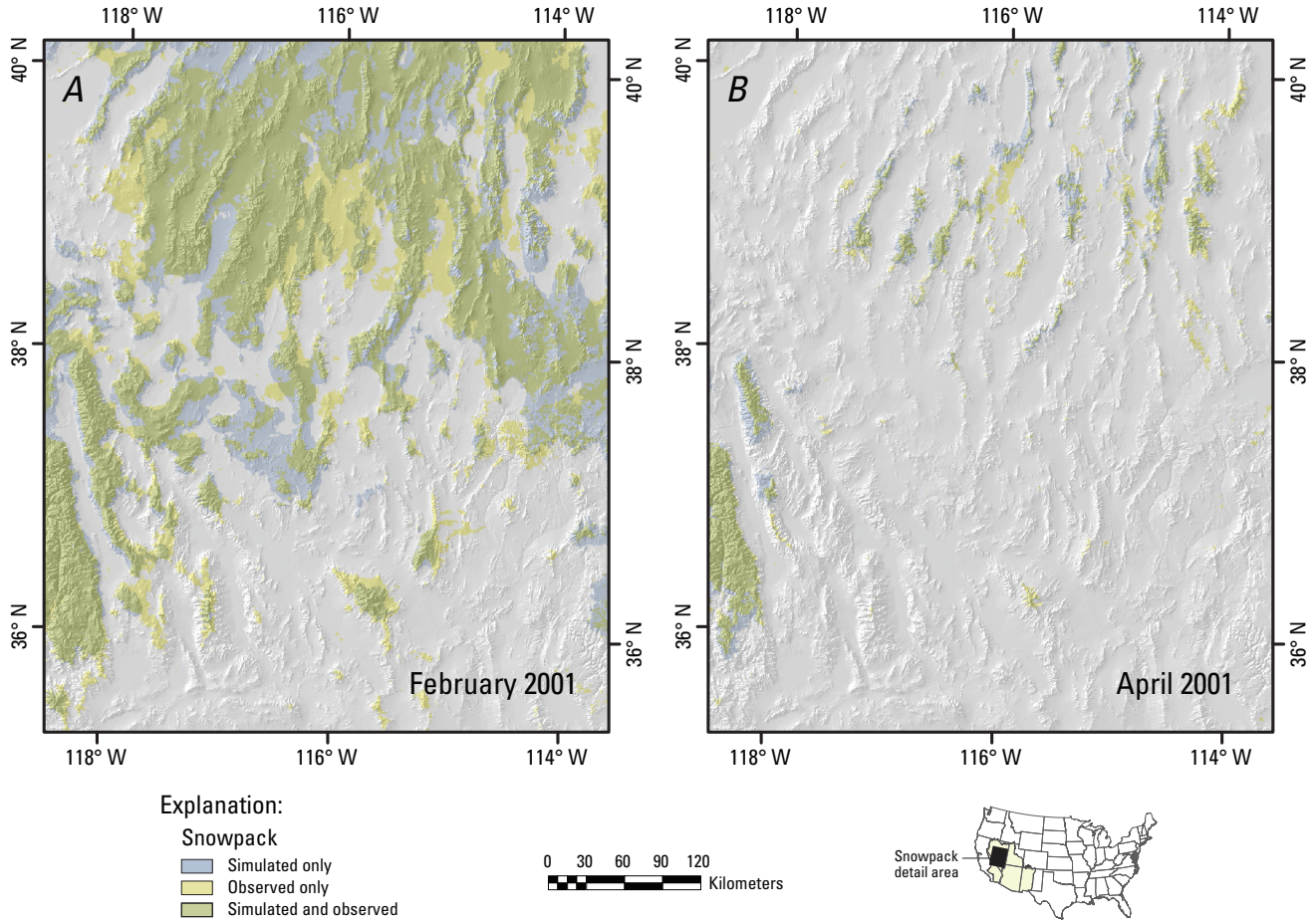

Figure 10. Distribution of model-simulated snowpack compared with measured snowpack in *A*, February 2001, and *B*, April 2001. Blue indicates greater than 30 millimeters of accumulated snowpack calculated by the Basin Characterization Model (BCM). Yellow indicates snowpack measured by MODIS, the Moderate Resolution Imaging Spectroradiometer aboard Terra and Aqua Earth-observing satellites (http://modis.gsfc.nasa.gov/). Where the image appears green, simulated snowpack is co-located with observed snowpack.

high that the excess water generated during winter months was removed by evapotranspiration during spring and summer months. The eight recharge study-site basins generally represented larger and drier basins, with the exception of the Upper Virgin Basin in Utah.

Estimates of ground-water recharge produced by the BCM for basins in Nevada and western Utah were compared by Flint and others (2004) to chloride-mass balance estimates for 14 basins (Dettinger, 1989; Harrill and Prudic, 1998) and to discharge estimates for 15 basins (Nichols, 2000). Flint and others (2004) also compared BCM estimates with estimates from a similar model employing a daily time step (Hevesi and others, 2002; 2003). The version of the BCM used in that analysis used an earlier version of the potential evapotranspiration model. The BCM estimates compared well with recharge estimates from the other approaches (Flint and others, 2004).

Physical characteristics of the basins that include the eight ground-water recharge-study sites are listed in table 1. The northern-most basin is the Middle Humboldt in north central Nevada, the southern-most basin is the Upper San Pedro in southern Arizona, the eastern-most basin is the Rio Grande-Sante Fe in central New Mexico, and the western-most basin is the Mojave in southern California. Drainage areas range from 2,410 km^2 for the Rillito Basin in southern Arizona to 12,084 km^2 for the Mojave Basin in southern California. Average elevations range from 838 m in the Mojave Basin to 1,998 m in the Rio Grande-Santa Fe Basin. The dominant bedrock in the study-sites basins range from relatively impermeable granitic and metamorphic rocks (Rillito Creek) to permeable sandstone (Sand Hollow); however, the dominant geologic rocks in the higher reaches of the basins, where runoff is generated, tend to be less-permeable volcanic, granitic, and metamorphic rocks. The southern-most basin in New Mexico, Rio Grande-Albuquerque, is dominated by relatively permeable Mesozoic sandstone. Total annual soil-water storage ranges from 97 mm for the Upper Amargosa Basin to 421 mm for the Middle Humboldt Basin.

Average annual (1971–2000) climatic conditions, in-place recharge, runoff, and ground-water recharge estimated by the BCM are listed in table 2. Average annual precipitation ranged from a low of 152 mm in the Upper Amargosa Basin to 463 mm for the Rillito Basin. The percentage of precipitation that fell as snow was lowest (2 percent) for the Mojave Basin, 3 and 5 percent for southern Arizona basins (Upper San Pedro and Rillito, respectively), 26 percent for the Middle Humboldt Basin, and highest (32 percent) for the Upper Virgin Basin. Average annual ground-water recharge (calculated as in-place recharge plus 15 percent of runoff) ranged from less than 1 mm for the central New Mexico and Upper San Pedro Basins to 24 mm for the Upper Virgin Basin. Average annual runoff was highest for the Upper Virgin and Mojave Basins relative to the other six study-site basins. The ratio of in-place recharge to runoff indicates which process is dominant in each basin. While all basins corresponding to the eight ground-water recharge-study sites are dominated by runoff, ratios ranged from 0–0.1 for the Rio Grande-Santa Fe, Mojave, and Rillito Basins to 0.8–0.9 for the Rio Grande-Albuquerque and Upper San Pedro Basins.

Effects of Climate Variability

Snow accumulation is the dominant factor in converting excess water into runoff and in-place ground-water recharge. Accumulation of snow delays delivery of liquid water to the land surface, thus increasing the possibility that subsequent combinations of precipitation and snowmelt in ensuing months will exceed soil-water storage capacity and result in drainage past the base of the root zone and, possibly, also in runoff. Therefore, computing ground-water recharge for an *N*-year period by using *N* x 12 monthly calculations results in a more realistic, somewhat higher value of total recharge than would be obtained by using 12 calculations with average monthly values and multiplying the 12-month total by *N* (Flint and others, 2004). BCM results computed by using average monthly values are shown in table 2.

The long-term ocean temperature fluctuation of the Pacific Ocean, called the Pacific Decadal Oscillation (PDO), involves an approximately periodic cycle lasting 50–70 years (Mantua and Hare, 2002) The 64-year time series used in this analysis, 1941–2004, includes one complete PDO cycle. The warm phase, or positive PDO, impacted the study area with below-average rainfall and above-average temperatures. Superimposed on the PDO and acting at shorter time scales of less than 10 years, the El Niño/Southern Oscillation (ENSO) provides an even more important source of climate variability (see chapter A, this volume; Cayan and others, 1998). Negative values of the index represent the cold ENSO phase (La Niña), while positive values represent the warm phase (El Niño). El Niño cycles within positive PDO cycles result in the strongest impacts to the study area, producing above-average rainfall and temperatures (McCabe and Dettinger, 2002).

Annual-precipitation data and ground-water-recharge estimates from 1941 to 2004 for study-site basins are shown in figure 12, along with indications of the PDO climate cycle and the time interval of the investigations. The relation of precipitation to ground-water recharge differs among the eight basins. The Mojave Basin has next to the lowest average-annual precipitation, but has relatively high average annual ground-water recharge, whereas the Rillito and Upper San Pedro Basins have relatively high average-annual precipitation but relatively low-average annual ground-water recharge (table 2, fig. 12). The Rillito and Upper San Pedro Basins have little precipitation that falls as snow, and more rainfall that falls during summer monsoons when evapotranspiration is high. Droughts during the 1950s through 1970s caused a reduction in annual runoff and ground-water recharge in most of the basins, whereas droughts during 1990s and early 2000s were more pronounced in the Mojave Basin in southern California, the Upper Amargosa Basin in southern Nevada, and in the Upper San Pedro and Rillito Basins in southern Arizona.

Annual precipitation and estimated annual ground-water recharge data averaged for different climate patterns are shown in table 3 for each of the basins containing ground-water recharge-study sites. Average-annual precipitation amounts typically were highest in the Rillito and Upper

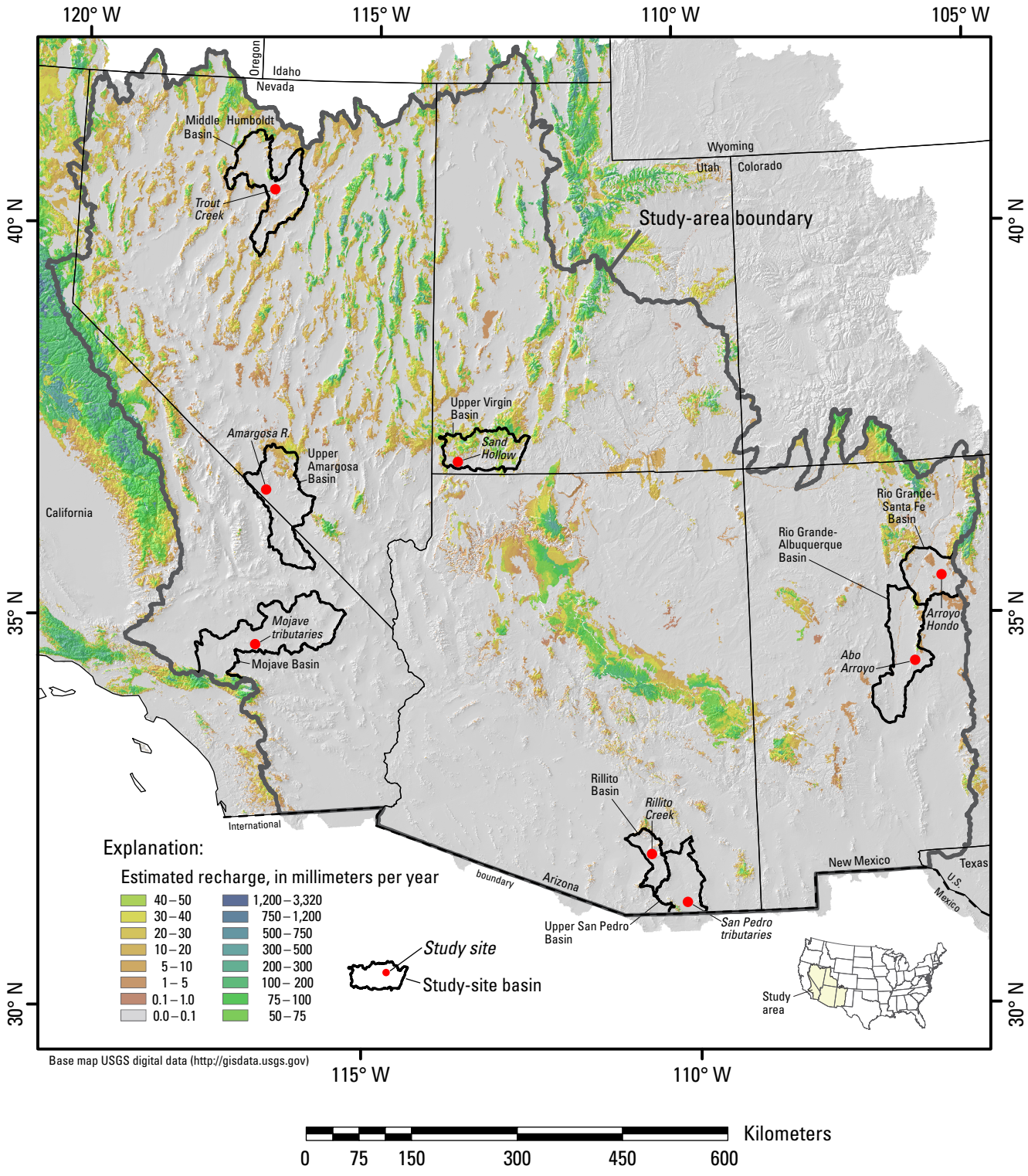

Figure 11. Average annual ground-water recharge within the modeled arid and semiarid southwestern United States study area, calculated with the Basin Characterization Model as in-place recharge plus 15 percent of runoff. Calculations used 30 years of average monthly precipitation and other dynamic input data from 1971–2000. Portions of Colorado outside the study area, Texas, and Wyoming were not modeled.

Table 1. Physical characteristics of the eight recharge study sites, and parameters used in the Basin Characterization Model.

Study site	Basin name	USGS basin identification number (8-digit HUC[1])	Basin area, in square kilometers	Average basin elevation, in meters	Dominant bedrock type	Dominant bedrock type in runoff area	Average bedrock conductivity in runoff area, in meters per year	Average annual soil-water storage in runoff area, in meters
Abo Arroyo	Rio Grande-Albuquerque	13020203	8,169	1,717	Granitic and sedimentary	Sandstone	50.	1.7
Amargosa River	Upper Amargosa	18090202	8,764	1,084	Ash-flow tuffs	Ash-flow and rhyolitic tuffs	2.0	1.3
Arroyo Hondo	Rio Grande-Santa Fe	13020201	4,748	1,998	Granitic and sedimentary	Sandstone	50.	1.1
Mojave tributaries	Mojave	18090208	12,084	838	Granite	Granite	0.01	1.4
Rillito Creek	Rillito	15050302	2,410	1,285	Igneous, metamorphic, and sedimentary	Granite and metamorphics	0.01	0.9
San Pedro tributaries	Upper San Pedro	15050202	4,635	1,419	Igneous, metamorphic, and sedimentary	Granite and volcanics	0.10	1.3
Sand Hollow	Upper Virgin	15010008	5,609	1,735	Navajo sandstone	Granite	0.01	0.7
Trout Creek	Middle Humboldt	16040105	8,318	1,623	Chert and volcanics	Volcanics and sedimentary	1.0	1.6

[1]Hydrologic unit code (HUC).

Table 2. Average annual (1971–2000) conditions determined by using the Basin Characterization Model for the eight ground-water recharge study sites.

[Ground-water recharge is equal to in-place recharge plus 15 percent of runoff]

Study site	Basin name	Precipitation, in millimeters	Potential evapotranspiration, in millimeters	Maximum air temperature, in degrees Celsius	Minimum air temperature, in degrees Celsius	Precipitation that falls as snow, in percent	In-place recharge, in millimeters	Runoff, in millimeters	Ground-water recharge, in millimeters	Ratio of in-place recharge to runoff
Abo Arroyo	Rio Grande-Albuquerque	307	1,163	21.2	2.9	10.3	0.8	0.1	0.9	0.83
Amargosa River	Upper Amargosa	152	1,472	23.5	3.5	16.8	1.2	1.9	1.4	0.57
Arroyo Hondo	Rio Grande-Santa Fe	381	1,075	18.6	4.9	10.5	0.3	1.6	0.5	0.04
Mojave tributaries	Mojave	185	1,664	24.5	7.5	1.9	1.8	12.8	3.7	0.13
Rillito Creek	Rillito	463	1,470	25.2	6.9	4.8	0.3	4.9	1.1	0.07
Sand Hollow	Upper Virgin	418	1,011	18.8	0.0	32.1	19.4	29.3	23.8	0.66
San Pedro tributaries	Upper San Pedro	415	1,462	24.7	7.2	3.4	0.7	0.7	0.8	0.86
Trout Creek	Middle Humboldt	264	990	17.4	1.6	26.5	2.5	5.2	3.3	0.44

Virgin Basins and lowest in the Upper Amargosa and Mojave Basins, whereas average-annual ground-water recharge was highest in the Upper Virgin Basin and lowest in the Rio Grande-Albuquerque and San Pedro Basins—even though annual precipitation levels exceeded those in the Upper Amargosa and Mojave Basins. The difference between high precipitation values and low potential ground-water recharge in the basins in southern Arizona and central New Mexico also is apparent because much of the precipitation falls during the summer months when potential evapotranspiration vales are highest. The Middle Humboldt Basin has the lowest sensitivity to climate cycles, whereas the southern Arizona and Upper Amargosa Basins have the highest sensitivities to climate cycles (table 3).

Annual precipitation during water year 2000 was below average for all basins in the study area, except in the Middle Humboldt Basin (tables 2 and 4). These below-average precipitation values resulted in estimates of potential ground-water recharge in the northern and western basins that were near the 64-year minimums (fig. 12), while the central New Mexico and southern Arizona basins had increased recharge, likely due to the timing of the precipitation. Thus, data collection for the eight site investigations generally did not coincide with average annual conditions.

Areas Dominated by Processes Contributing to In-Place Recharge and Runoff

Estimates of the ratio of in-place recharge to runoff (fig. 13) provide an indication of the mechanisms that likely are dominant in controlling ground-water recharge for a given basin. This analysis provides the distribution of the dominant mechanisms within basins. A ratio of 0.5 or less indicates that more than twice as much water has the potential to become runoff than to become in-place recharge. A ratio of 2.0 or greater indicates that water has at least twice as much potential to become in-place recharge than to become runoff. Little if any recharge or runoff occurs within the areas covered by basin fill or other unconsolidated Quaternary deposits (fig. 11); in most of these locations, neither recharge nor is dominant. In areas of consolidated bedrock, geology—through the associated saturated hydraulic conductivity—largely controls the dominant process (fig. 13). In-place recharge dominates (ratio greater than 2.0) in the mountains of the Great Basin carbonate-rock province, where thick sections of Paleozoic carbonate rock crop out (Mifflin and Hess, 1979; Prudic and others, 1995), and in the upland areas of the Kaibab section of the Colorado Plateau, where thick sections of Mesozoic sandstone crop out (figs. 5 and 6). The importance of geology in determining recharge

Table 3. Average annual precipitation (in millimeters) and ground-water recharge (in millimeters, calculated as in-place recharge plus 15 percent of runoff) for selected climate patterns (1941–2004) in basins conta ining the eight recharge-study sites.

[Pacific Decadal Oscillation (PDO) time periods are identified on figure 12. Positive El Niño-Southern Oscillation (ENSO) conditions correspond to El Niños; negative ENSO conditions correspond to La Niñas]

		Positive PDO, neutral ENSO		Negative PDO, neutral ENSO		All PDO, positive ENSO		All PDO, negative ENSO		Positive PDO, positive ENSO	
Study site	Basin name	Precipitation	Recharge	Precipitation	Recharge	Precipitation	Recharge	Precipitation	Recharge	Precipitation	Recharge
Abo Arroyo	Rio Grande-Albuquerque	318	4	259	2	294	4	254	2	301	5
Amargosa River	Upper Amargosa	400	5	327	3	370	6	326	3	380	7
Arroyo Hondo	Rio Grande-Santa Fe	171	7	125	3	183	9	107	2	196	11
Mojave tributaries	Mojave	207	13	150	8	229	14	125	4	254	18
Rillito Creek	Rillito	513	16	422	7	502	15	387	4	512	19
Sand Hollow	Upper Virgin	458	61	365	34	472	74	335	22	494	83
San Pedro tributaries	Upper San Pedro	424	5	370	2	417	5	347	1	416	6
Trout Creek	Middle Humboldt	279	8	243	6	268	7	263	7	282	8

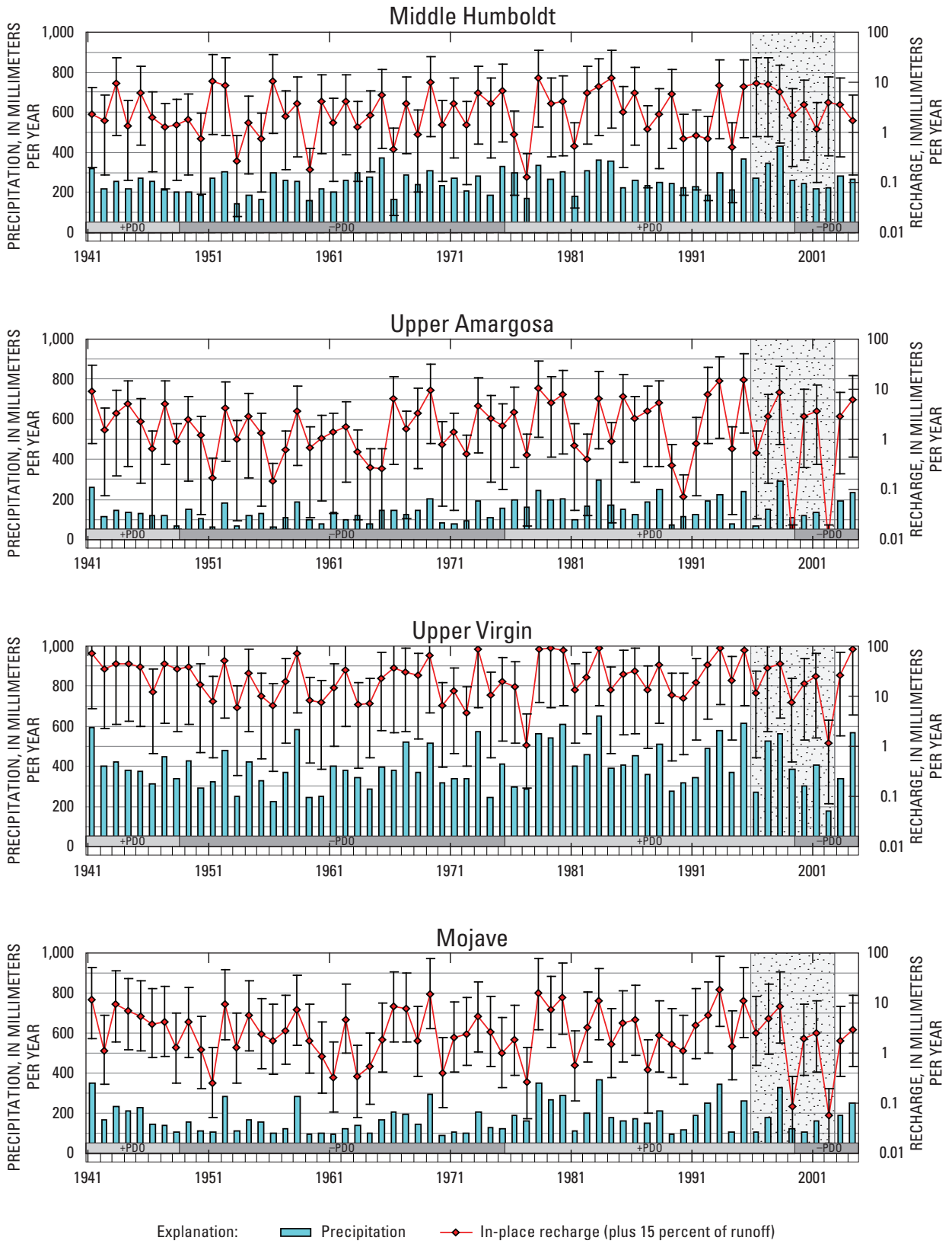

Figure 12. Annual precipitation and ground-water recharge in the basins corresponding to the eight recharge study sites from 1941-2004 in relation to positive and negative Pacific Decadal Oscillations (+PDO and –PDO, respectively). Stippling indicates the nominal period of study-site investigations. Error bars indicate recharge calculated by using 10 and 90 percent of runoff.

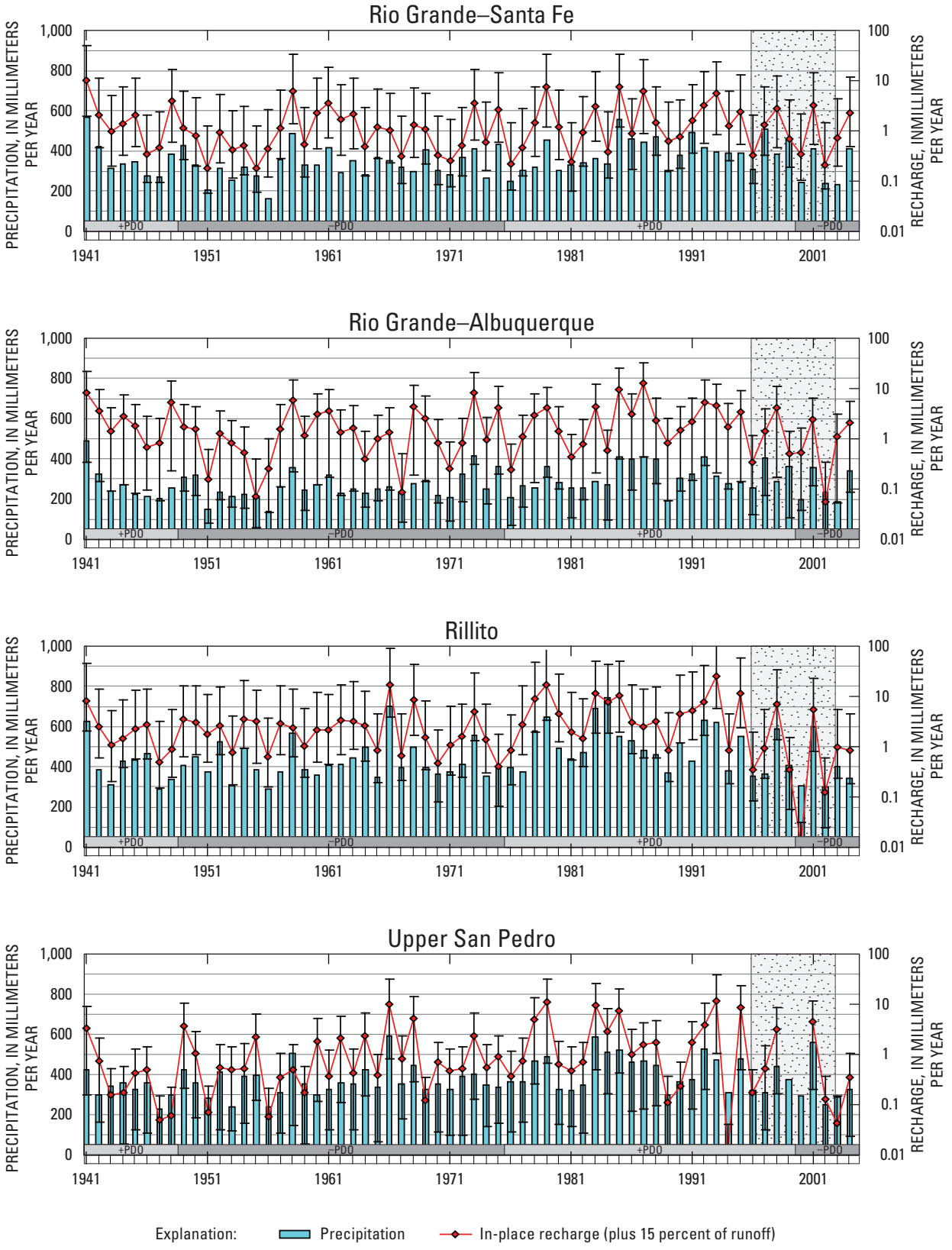

Figure 12.—Continued.

Table 4. Hydrologic conditions for water year 2000 determined by using the Basin Characterization Model for basins corresponding to the eight recharge-study sites.

Study site	Basin name	Water year 2000					
		Precipitation, in millimeters	Potential evapotranspiration, in millimeters	In-place recharge, in millimeters	Runoff, in millimeters	Ground-water recharge, in millimeters	Ratio of in-place recharge to runoff
Abo Arroyo	Rio Grande-Albuquerque	195	1,163	1.7	1.8	2.0	0.95
Amargosa River	Upper Amargosa	121	1,472	0.6	1.9	0.9	0.32
Arroyo Hondo	Rio Grande-Santa Fe	243	1,075	0.6	6.9	1.7	0.09
Mojave tributaries	Mojave	106	1,664	0.9	7.0	1.9	0.12
Rillito Creek	Rillito	303	1,470	2.7	11.2	4.4	0.24
Sand Hollow	Upper Virgin	303	1,011	13.	28.2	17.3	0.46
San Pedro tributaries	Upper San Pedro	294	1,462	3.4	3.2	3.9	1.06
Trout Creek	Middle Humboldt	246	990	2.7	5.6	3.6	0.49

mechanisms was similarly revealed by a detailed water-balance model for the Death Valley region, which indicated higher recharge in mountains dominated by carbonate-rock outcrops and lower recharge in mountains dominated by thick soils and volcanic rock outcrops (Hevesi and others, 2002). Most study-site basins are dominated by runoff in the mountains at their peripheries (fig. 13), as indicated by the basin-wide calculation of the ratio of in-place recharge to runoff (tables 2 and 4). The exception is the Rio Grande-Albuquerque Basin, which has very low ground-water recharge. The ratio of in-place recharge to runoff changed for several of the basins during water year 2000 in response to climatic conditions. The Upper Amargosa, New Mexico, and Upper Virgin Basins all had more runoff in comparison to recharge, whereas the southern Arizona Basins had more recharge in comparison to runoff compared to average annual conditions (tables 2 and 4).

Runoff and In-Place Recharge in Basins Containing the Ground-Water Recharge-Study Sites

With the exception of the Upper Virgin River sandstone basin, the ground-water recharge-study sites were selected in areas where runoff from the mountains routinely discharges onto the piedmont slopes and valley floors due to the importance of estimating the quantity of runoff becoming ground-water recharge in these transitional topographic locations. Runoff and in-place recharge estimates for water year 2000 in the eight basins containing study sites are shown in figure 14. During this relatively dry year, all basins in the study area, with the exception of the Upper San Pedro Basin, were dominated by runoff.

Runoff and in-place recharge for each of the eight basins are different and range from very little recharge and runoff in the Upper Amargosa Basin to large amounts of runoff in the mountain ranges bounding the southwestern edge of the Mojave Basin to diffuse runoff and in-place recharge throughout the Upper Virgin Basin. Most of the estimated runoff and in-place recharge in the Upper Amargosa Basin is in the northwestern part of the basin. The Middle Humboldt Basin, having a large perimeter-to-area ratio due to its compound shape, generates runoff and ground-water recharge in the many mountain ranges defining the basin. Several basins are notable in their spatial variability of runoff or in-place recharge, especially the Mojave Basin, which receives nearly all of its runoff and in-place recharge from the mountains that border its southwestern edge. Similarly, for the Rio Grande Basins, the majority of runoff and in-place recharge is estimated to occur in the highest mountains of each basin.

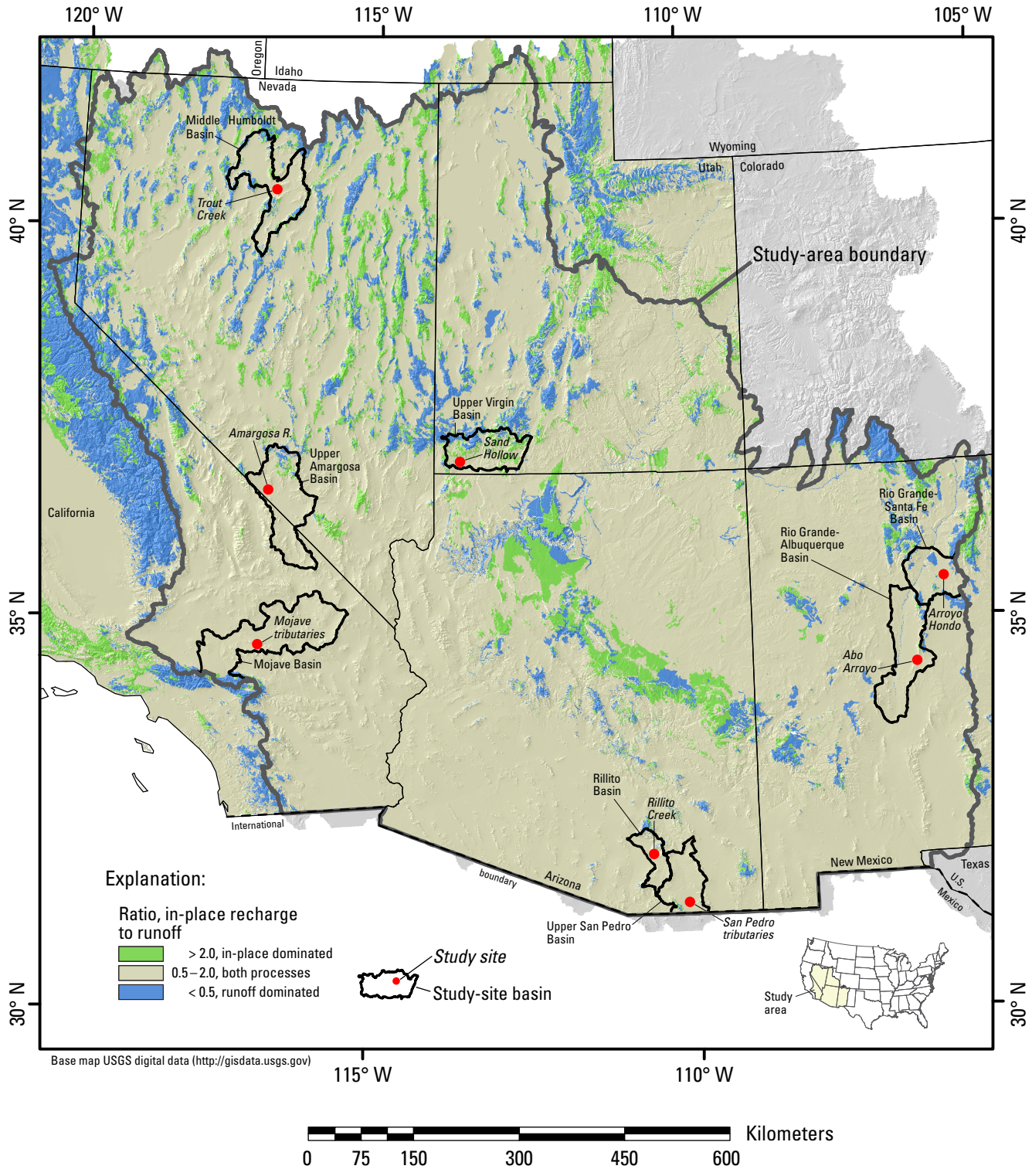

Figure 13. Areas within the modeled arid and semiarid southwestern U.S. study area, where runoff or in-place recharge is dominant, or where runoff and in-place recharge are nearly equal.

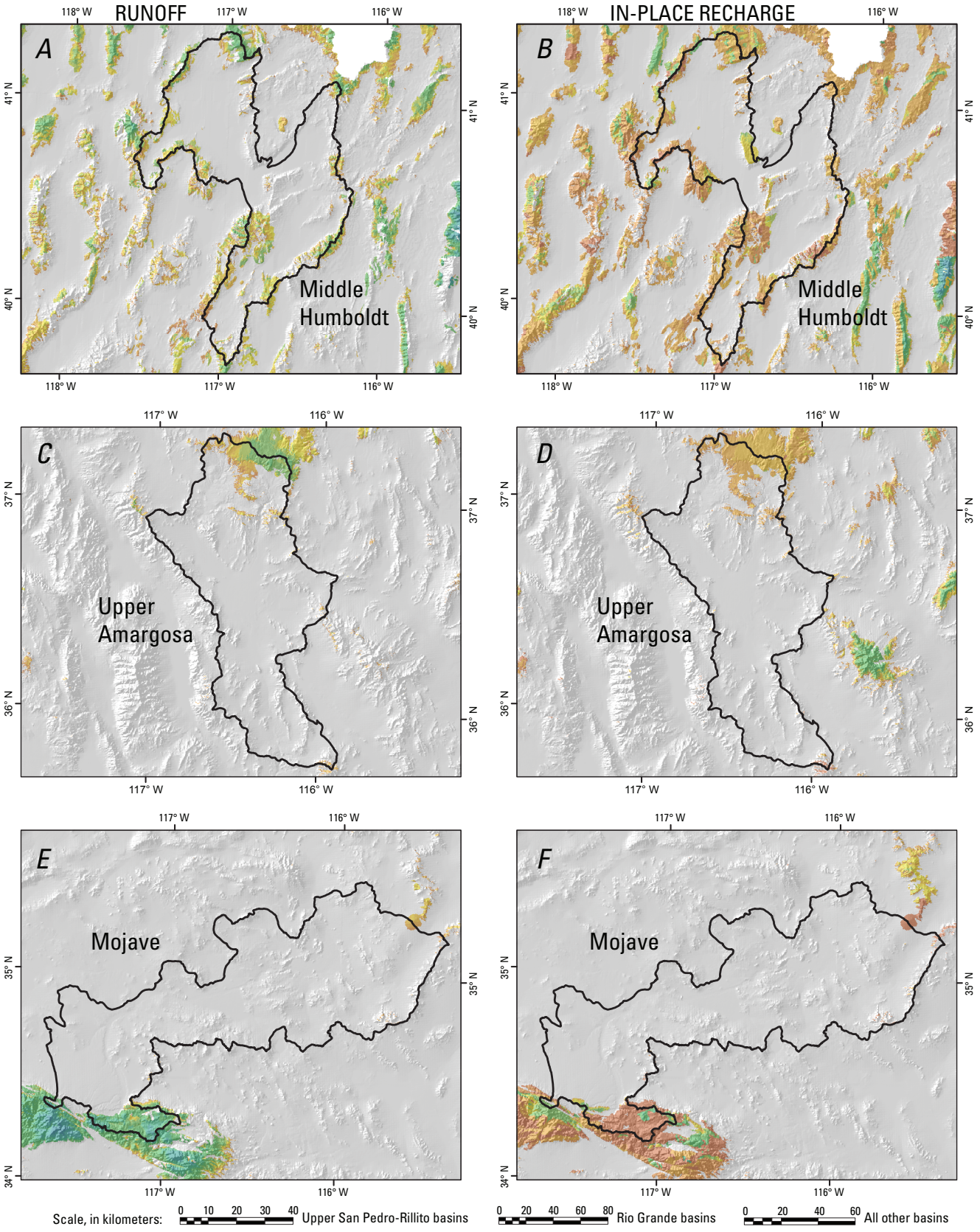

Figure 14. Runoff and in-place recharge for water year 2000 in basins that correspond to the eight study sites. Runoff and in-place recharge in the: *A, B,* Middle Humboldt; *C, D,* Upper Amargosa; *E, F,* Mojave; *G, H,* Upper Virgin; *I, J,* Rio Grande-Santa Fe/Rio Grande-Albuquerque; and *K, L,* Rillito/Upper San Pedro Basins. Scale varies as shown.

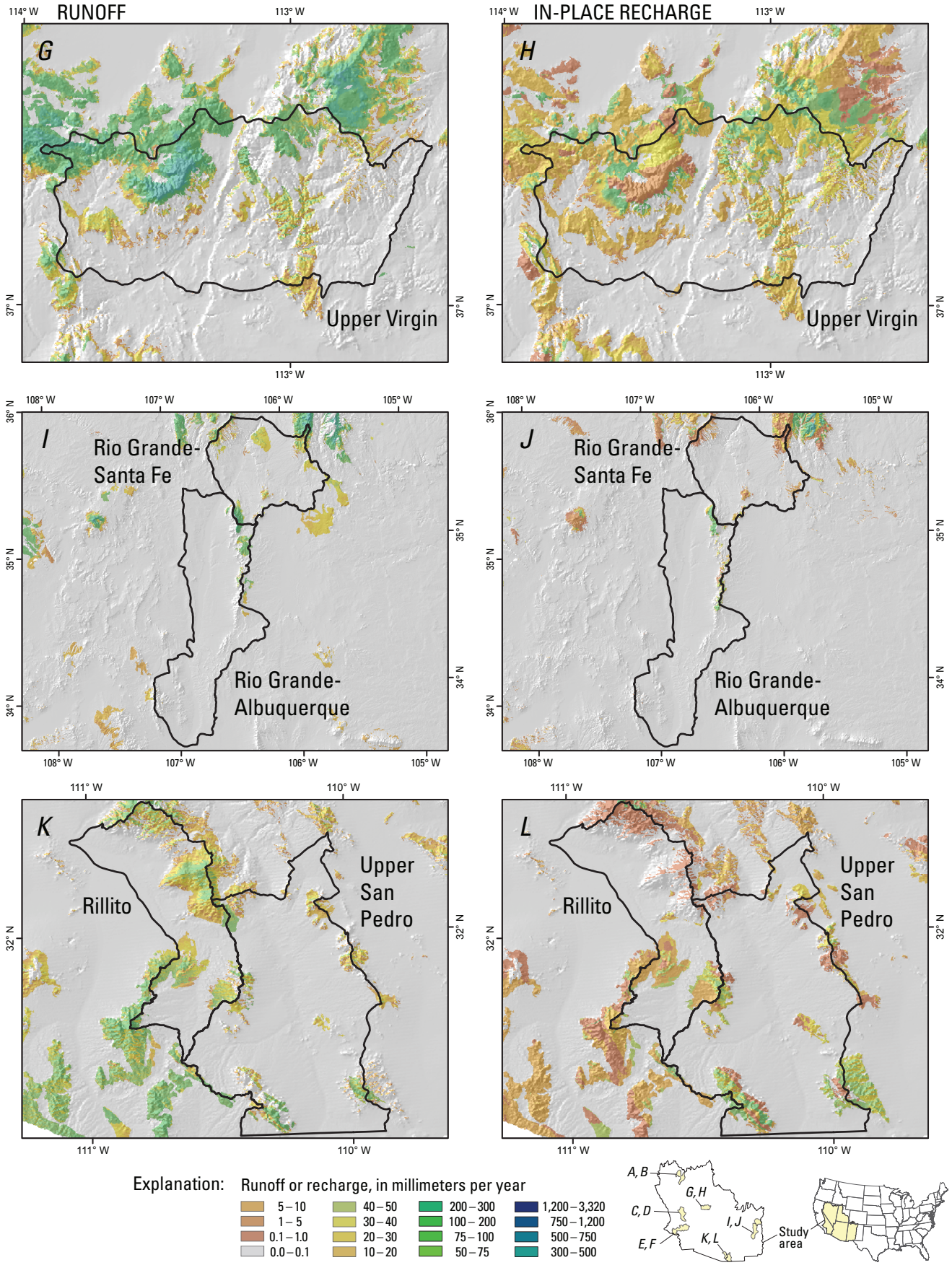

Figure 14. —Continued.

The sensitivity of ground-water recharge to changes in precipitation, for distinct groupings of climatic conditions that occurred during 1941–2004, is shown for the recharge study-site basins (fig. 15). The response generally is nonlinear, such that the change in ground-water recharge is nearly twice the change in precipitation. The nonlinearity reflects the fact that changes in evapotranspiration and soil-water storage are not proportional to changes in precipitation. During years of low precipitation, a greater fraction of precipitation is lost to evapotranspiration and soil-moisture replenishment. During years of high precipitation, a smaller fraction of precipitation is lost to evapotranspiration and soil-moisture replenishment. Soil-water storage typically is not close to capacity and evapotranspiration rates not at potential, except for localized areas at high elevations. An example is Lamoille Canyon in the Ruby Mountains, where runoff is roughly linearly related to precipitation, and about 70 percent of annual precipitation becomes runoff (Prudic and others, 2006). In general, however, evapotranspiration and soil-moisture replenishment account for most incoming water, thus preventing conditions that lead to runoff and ground-water recharge.

General trends in the data indicate that the Rillito and Upper San Pedro Basins have a greater sensitivity of ground-water recharge to changes in precipitation, whereas the Middle Humboldt, Mojave, and Upper Amargosa Basins have a smaller sensitivity. This likely is due to the timing of precipitation in the southern Arizona Basins, which experience monsoonal conditions that often deliver large quantities of precipitation in short periods of time, overwhelming soil-water storage and resulting in increased recharge and runoff, even though on an annual basis the total volume of precipitation does not increase correspondingly.

The ratio of ground-water recharge to precipitation was less than 2 percent for all climatic conditions in the Upper San Pedro Basin in Arizona and the two Rio Grande Basins in New Mexico (fig. 16). However, the ratio increased slightly from years of La Niña and negative PDO to years of El Niño and positive PDO. The highest ratio of ground-water recharge to precipitation was in the Upper Virgin Basin, which also had the largest sensitivity to different climatic conditions. The ratio of ground-water recharge to precipitation increased from about 7 percent for La Niña years to about 17 percent for El Niño years with a positive PDO (fig. 16). The ratio of ground-water recharge to precipitation was least affected by the different climate patterns in the Middle Humboldt Basin.

Relation of Selected Characteristics Among All Basins in the Study Area

Selected characteristics for all basins within the study area are summarized in figure 17. Basins are ranked from low to high for each characteristic. Thus, the order of basins generally changes from plot to plot. For example, the Upper Amargosa Basin ranks 11th with respect to aridity, but ranks 155th with respect to potential evapotranspiration. Aridity indices were determined as the ratio of average annual precipitation divided by potential evapotranspiration (fig. 6, chapter A). Hyperarid conditions denote ratios of 0–0.05, arid conditions denote ratios of 0.05–0.2, semiarid conditions denote ratios of 0.2–0.5, dry subhumid conditions denote ratios of 0.5–0.65, and humid conditions denote ratios of greater than 0.65 (UNESCO, 1979). Basins corresponding to the eight ground-water recharge-study sites are highlighted in each ranking.

Of the basins that correspond to the recharge-study sites, the Upper Amargosa and Mojave Basins are classified as arid, whereas the other six basins are classified as semiarid. The Upper Virgin Basin is the least arid. The Middle Humboldt and Upper Virgin Basins have the lowest values of potential evapotranspiration, whereas the Mojave Basin has the highest value of potential evapotranspiration. The eight recharge study-site basins generally are well distributed among all the basins for precipitation, although about ten percent of the study-area basins have higher average annual precipitation. The eight basins also are generally well distributed with respect to runoff and in-place recharge. All of the eight basins have more estimated runoff than in-place recharge, whereas

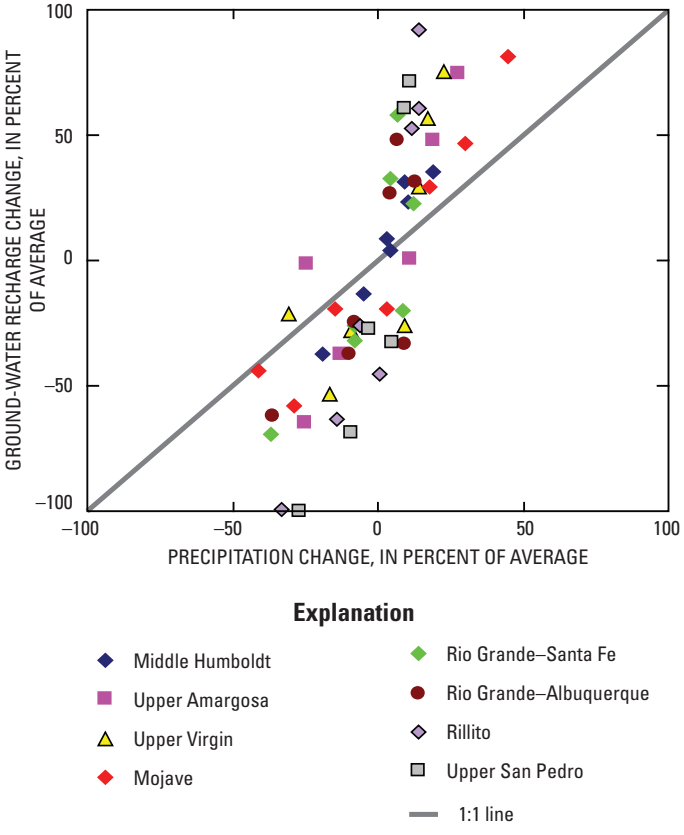

Figure 15. Change in ground-water recharge with change in precipitation, relative to respective 1971–2000 averages, for the eight basins containing recharge study sites. Different points for each basin represent varying combinations of climatic conditions as manifested in the El Niño-Southern Oscillation and Pacific Decadal Oscillation indices during 1941–2004. Ground-water recharge is estimated by using the Basin Characterization Model and assumes in-place recharge plus 15 percent of runoff.

about 30 percent of all basins in the study area have more estimated in-place recharge than runoff. This analysis does not take into account the dominant process contributing to ground-water recharge in a basin—in other words, whether it is a result of in-place recharge or infiltration from runoff—just the physical and hydrologic characteristics of basins that lead to the potential for either runoff or in-place recharge.

The model used to estimate runoff and in-place recharge was not calibrated extensively, and represents basin averages that may not reflect results from the individual study sites. Instead, the model provides general information about the dominant processes within each basin. As previously noted, error produced by assuming a constant percentage of runoff that becomes recharge, here 15 percent throughout the entire study area, may be relatively large in the Middle Humboldt Basin. A further uncertainty lies in the estimates of saturated hydraulic conductivity of subsoil materials. Future studies done by using the BCM will attempt to refine these estimates of runoff and in-place recharge by using measured runoff in basins with predominantly one rock type. Sensitivity analyses indicate that increasing the saturated hydraulic conductivity of the bedrock by one order of magnitude switches the Middle Humboldt from a basin dominated by runoff to a basin dominated by in-place recharge, in agreement with the results of the recharge study-site investigation (Prudic and others, chapter K, this volume). Although it is possible that basins other than the Middle Humboldt have greater runoff than in-place recharge, sufficient data are not available to evaluate this possibility.

The results of the analysis presented herein indicate that the eight ground-water recharge-study sites represent a reasonable distribution of the hydrologic conditions throughout the study area, which includes different timing of precipitation and snowfall, different influences from summer monsoons, and varying bedrock types and soil depths. The main similarity of the eight recharge-study sites is that runoff is an important hydrologic component. On the basis of site-specific analysis alone, however, important mechanisms that contribute to runoff and in-place recharge in a given basin may be overlooked without consideration of the spatially distributed hydrologic-framework analysis.

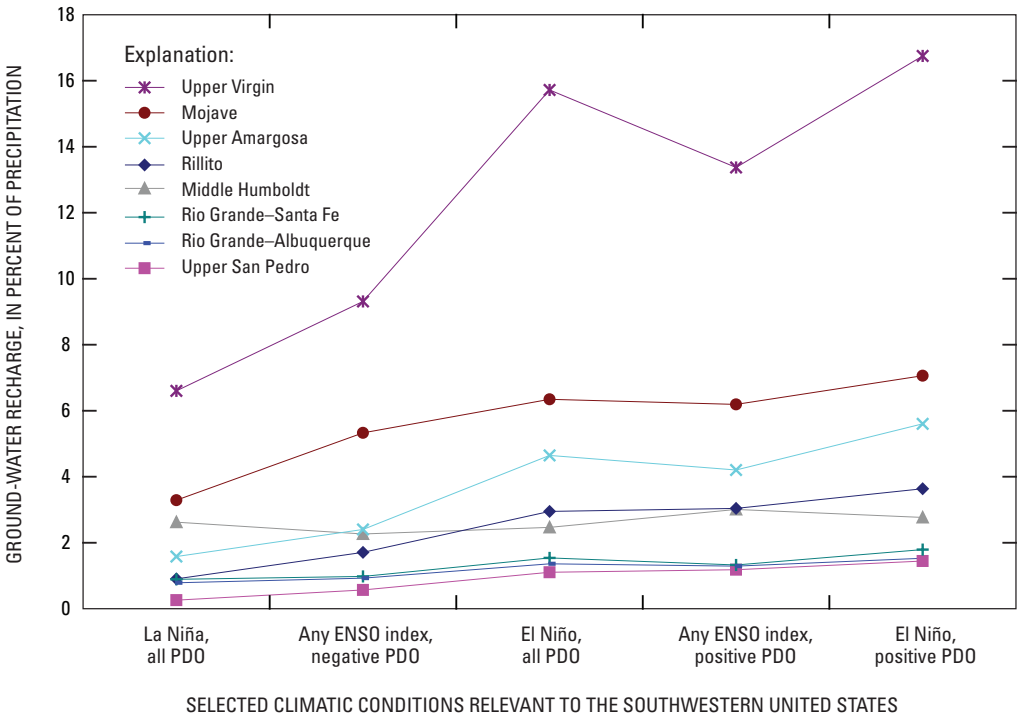

Figure 16. Ground-water recharge as a percentage of precipitation for different climatic conditions 1941–2004 for the eight basins containing the ground-water recharge study sites. The El Niño-Southern Oscillation (ENSO) index indicates shifting of warm Pacific equatorial surface water either toward (positive ENSO index; El Niño conditions) or away from (negative ENSO index; La Niña conditions) the Americas. On a longer (decadal) time scale, the Pacific Decadal Oscillation (PDO) index indicates warm (positive PDO index) or cool (negative PDO index) surface water in the eastern Pacific Ocean north of 20º north latitude. Ground-water recharge as estimated with the Basin Characterization Model assumes in-place recharge plus 15 percent of runoff.

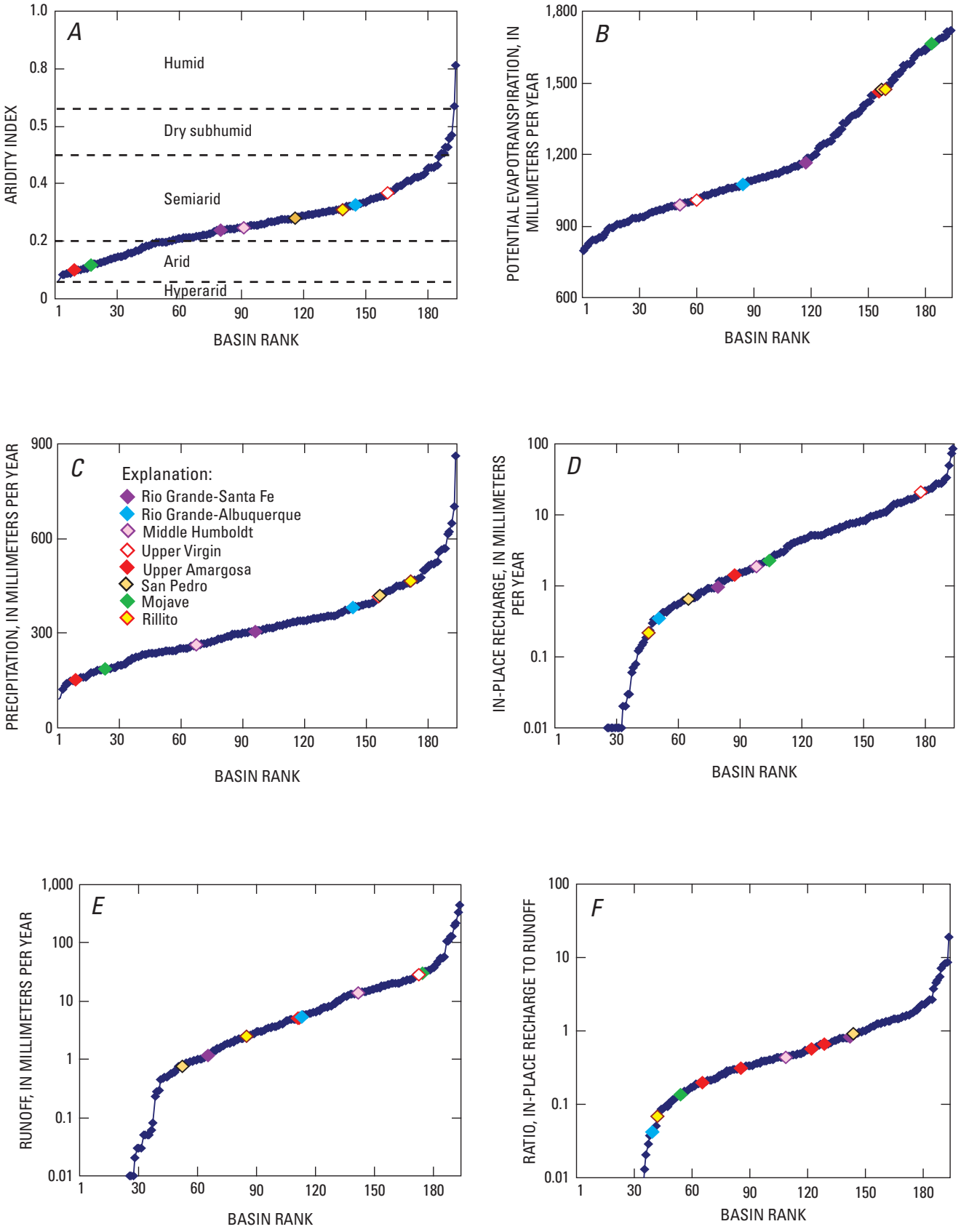

Figure 17. The eight study-site basins ranked among all basins in the study area assuming average annual conditions (1971–2000) for: *A*, aridity; B, potential evapotranspiration; *C*, precipitation; *D*, runoff; *E*, in-place recharge; and *F*, ratio of in-place recharge to runoff.

Summary and Conclusions

Average annual runoff and in-place recharge were estimated by using a spatially distributed water-balance model called the Basin Characterization Model (BCM). Estimates were used to compare similarities and differences among the eight ground-water recharge-study sites and among all basins within the study area. A total of 194 basins were modeled covering 1,033,840 square kilometers. Basins were defined by the drainage areas of the U.S. Geological Survey's 1:250,000-scale hydrologic units. Basin areas ranged from 2,410 to 12,084 km^2. The eight recharge-study sites generally were representative of the basins in the study area. Runoff exceeded in-place recharge in all study-site basins, but runoff exceeded in-place recharge in only three quarters of total basins. Among the basins corresponding to the eight study sites, average annual precipitation ranged from 152 mm for the Upper Amargosa Basin in southern Nevada to 463 mm for the Rillito Basin in southern Arizona. Average annual runoff ranged from 0.1 mm for the Rio Grande-Albuquerque Basin in central New Mexico to 29 mm for the Upper Virgin Basin in southern Utah. Average annual in-place recharge ranged from 0.3 mm in the Rio Grande-Santa Fe Basin in central New Mexico and the Rillito Basin in southern Arizona to about 19 mm for the Upper Virgin Basin. The ratio of average annual ground-water recharge—computed as the sum of in-place recharge plus 15 percent of runoff—to average annual precipitation ranged from less than 0.3 percent in the southern Arizona and central New Mexico Basins to about 6 percent in the Upper Virgin Basin in southern Utah. In-place recharge and runoff in the study area indicated significant sensitivity to variations in climate. The climatic variability was a function of sea-surface temperatures manifested in the Pacific Decadal Oscillation (PDO) and El Niño-La Niña cycles. El Niño years with positive PDO typically produced the largest amounts of precipitation, runoff, and in-place recharge. El Niño years, regardless of whether the PDO was positive (warmer) or negative (cooler), also generally produced greater than average amounts of precipitation, runoff, and in-place recharge. Conversely, La Niña years typically produced below-average precipitation, runoff, and in-place recharge. Basins in the southern part of the study area were more sensitive to the different climate conditions than were basins in the northern part, exemplified by the two basins in southern Arizona compared with the Middle Humboldt Basin in north-central Nevada.

Results from the spatially distributed water-balance model show that runoff is an important component (in addition to in-place recharge) to the available ground-water supply in the basins corresponding to the eight recharge-study sites. The individual site investigations thus provide a detailed understanding of when and where runoff from mountains in the study area becomes ground-water recharge on piedmont slopes and valley floors. The combination of regional modeling and site-specific investigations provides a synergistic understanding of recharge to ground-water systems in the arid and semi-arid southwestern United States.

References Cited

Anderson, E.A., 1976, A point energy and mass balance model of a snow cover: Silver Spring, Md., U.S. National Oceanographic and Atmospheric Administration (NOAA), Technical Report NWS 19, 150 p.

Bedinger, M.S., Langer, W.H., and Reed, J.E., 1989, Ground-water hydrology, *in* Bedinger, M.S., Sargent, K.A., and Langer, W.H., eds., Studies of geology and hydrology in the Basin and Range Province, Southwestern United States, for isolation of high-level radioactive waste—Characterization of the Death Valley region, Nevada and California: U.S. Geological Survey Professional Paper 1370-F, p. 28–35.

Cayan, D.R., Dettinger, M.D., Diaz, H.F., and Graham, N.E., 1998, Decadal variability of precipitation over western North America: Journal of Climate, v. 11, p. 3148–3166.

Daly, C., Gibson, W.P., Doggett, M., Smith, J., and Taylor, G., 2004, Up-to-date monthly climate maps for the conterminous United States, *in* 14th Conference on Applied Climatology, 84th American Meteorological Society Annual Meeting [January 13–16, 2004], Combined preprints: Seattle, Wash., Paper 5.1, CD-ROM.

Davis, S.N., and DeWiest, R.J.M., 1966, Hydrogeology: New York, John Wiley, 463 p.

Dettinger, M.D., 1989, Reconnaissance estimates of natural recharge to desert basins in Nevada, U.S.A., by using chloride-balance calculations: Journal of Hydrology, v. 106, p. 55–78.

Dettinger, M.D., Cayan, D.R., McCabe, G.J., and Marengo, J.A., 2000, Multiscale streamflow variability associated with El Niño/Southern Oscillation, *in* Diaz, H.F. and Markgraf, V., eds., El Niño and the Southern Oscillation, multiscale variability and global and regional impacts: Cambridge, U.K., Cambridge University Press, p. 113–147.

Doggett, M., Daly, C., Smith, J., Gibson, W., Taylor, G., Johnson, G., and Pasteris, P., 2004, High-resolution 1971–2000 mean monthly temperature maps for the western United States, *in* 14th Conference on Applied Climatology, 84th American Meteorological Society Annual Meeting [January 13–16, 2004], Combined preprints: Seattle, Wash., Paper 4.3, CD-ROM.

Eakin, T.E., Price D., and Harrill, J.R., 1976, Summary appraisals of the Nation's ground-water resources, Great Basin region: U.S. Geological Survey Professional Paper 813–G, 36 p.

Fenneman, N.M., 1931, Physiography of Western United States: New York, McGraw-Hill, 534 p.

Flint, A.L., and Childs, S.W., 1987, Calculation of solar radiation in mountainous terrain: Journal of Agricultural and Forest Meteorology, v. 40, p. 233–249.

Flint, A.L., and Flint, L.E., 2007, Application of the basin characterization model to estimate in-place recharge and runoff potential in the Basin and Range carbonate-rock aquifer system, White Pine County, Nevada, and adjacent areas in Nevada and Utah: U.S. Geological Survey Scientific Investigations Report 2007–5099, 20 p.

Flint, A.L., Flint, L.E., Hevesi, J.A., and Blainey, J.M., 2004, Fundamental concepts of recharge in the Desert Southwest, a regional modeling perspective, *in* Hogan, J.F., Phillips, F.M., and Scanlon, B.R., eds., Groundwater recharge in a desert environment, the Southwestern United States: American Geophysical Union, Water Science and Applications Series, v. 9, p. 159–184.

Flint, A.L., Flint, L.E., Hevesi, J.A., D'Agnese, F.A., and Faunt, C.C., 2000, Estimation of regional recharge and travel time through the unsaturated zone in arid climates, *in* Faybishenko, B., Witherspoon, P., and Benson, S., eds., Dynamics of fluids in fractured rock: American Geophysical Union, Geophysical Monograph, v. 122, p. 115–128.

Flint, A.L., Flint, L.E., Kwicklis, E.M., Fabryka-Martin, J.T., and Bodvarsson, G.S., 2002, Estimating recharge at Yucca Mountain, Nevada, USA, comparison of methods: Hydrogeology Journal, v. 10, p. 180–204.

Flint, L.E., and Flint, A.L., 1995, Shallow infiltration processes at Yucca Mountain—Neutron logging data 1984–93: U.S. Geological Survey Water-Resources Investigations Report 95–4035, 46 p.

Flint, L.E. and Flint, A.L., 2008, A basin-scale approach to estimating stream temperatures of tributaries to the Lower Klamath River, California: Journal of Environmental Quality, v. 37, p. 57–68.

Freeze, R.A., and Cherry, J.A., 1979, Groundwater: Englewood Cliffs, New Jersey, Prentice-Hall, 604 p.

Glancy, P.A., 1986, Geohydrology of the basalt and unconsolidated sedimentary aquifers in the Fallon area, Churchill County, Nevada: U.S. Geological Survey Water Supply Paper 2263, 62 p.

Goodrich, D.C., Williams, D.G., Unkrich, C.L., Hogan, J.F., Scott, R.L., Hultine, K.R., Pool, D., Coes, A.L., and Miller, S., 2004, Comparison of methods to estimate ephemeral channel recharge, Walnut Gulch, San Pedro River Basin, Arizona, *in* Hogan, J.F., Phillips, F.M., and Scanlon, B.R., eds., Groundwater recharge in a desert environment, the Southwestern United States: American Geophysical Union, Water Science and Applications Series, v. 9, p. 77–99.

Green, G.N., 1992, The digital geologic map of Colorado in ARC/INFO format: U.S. Geological Survey Open-File Report 92-507 [http://geo-nsdi.er.usgs.gov/metadata/open-file/92-507/metadata.faq.html, accessed Jan. 31, 2001].

Gutmann, E.D., and Small, E.E., 2007, A comparison of land surface model soil hydraulic properties estimated by inverse modeling and pedotransfer functions: Water Resources Research, v. 43, doi:10.1029/2006WR005135.

Hardman, G., 1936. Nevada precipitation and acreage's of land by rainfall zones: University of Nevada, Reno, Agricultural Experimental Station Report and Map, 10 p.

Hardman, G., 1965. Nevada precipitation map, adapted from map prepared by George Hardman and others, 1936: University of Nevada, Reno, Agricultural Experimental Station Bulletin 185, 27 p.

Harrill, J.R., and Prudic, D.E., 1998, Aquifer systems in the Great Basin region of Nevada, Utah and adjacent states—Summary report: U.S. Geological Survey Professional Paper 1409, 66 p.

Hevesi, J.A., Flint, A.L., and Flint, L.E., 2002, Preliminary estimates of spatially distributed net infiltration and recharge for the Death Valley region, Nevada-California: U.S. Geological Survey Water Resources Investigations Report 02–4010, 36 p.

Hevesi, J.A., Flint, A.L., and Flint, L.E., 2003, Simulation of net infiltration using a distributed parameter watershed model for the Death Valley regional flow system, Nevada and California: U.S. Geological Survey Water Resources Investigation Report 03–4090, 104 p.

Hintze, L.F., Willis, G.C., Laes, D., Sprinkel, D.A., and Brown, K.D., 2000, Digital geologic map of Utah: Utah Geological Survey Map 179DM, scale 1:500,000.

Hirschberg, D.M., and Pitts, G.S., 2000, Digital geologic map of Arizona, a digital database derived from the 1983 printing of the Wilson, Moore, and Cooper 1:500,000-scale map: U.S. Geological Survey Open-File Report 00–409 [version 1.0], 67 p.

Houghton, J.G., Sakamoto, C.M., and Gifford, R.O., 1975, Nevada's weather and climate: Nevada Bureau of Mines and Geology Special Publication 2, 78 p.

Izbicki, J.A., 2002, Geologic and hydrologic controls on the movement of water through a thick, heterogeneous unsaturated zone underlying an intermittent stream in the western Mojave Desert, southern California: Water Resources Research, v. 38, p. 1–14.

Jennings, C. W., 1977, Geologic map of California: California Division of Mines and Geology Geologic Data Map Number 2, scale 1:750,000.

Johnson, B.R., and Raines, G.L., 1996, Digital representation of the Idaho state geologic map, a contribution to the Interior Columbia Basin Ecosystem Management Project: U.S. Geological Survey Open-File Report 95–690, 24 p.

Laczniak, R.J., Flint, A.L., Moreo, M.T., Kochenmus, L.A., Lundmark, K.W., Pohll, Greg, Carroll, R.W.H., Smith. J.L., Welbron, T.L., Heilweil, V.M., and Pavelko, M.T., 2007, Ground-water budgets, *in* Welch, A.H., and Bright, D.J., eds., Water resources of the Basin and Range carbonate-rock aquifer system in White Pine County, Nevada, and adjacent areas in Nevada and Utah—draft report: U.S. Geological Survey Open-File Report 2007–1156, p. 49–89.

Lundmark, K.W., Pohll, G.M., and Carroll, R.W.H., 2007, A steady-state water budget accounting model for the carbonate aquifer system in White Pine County, Nevada, and adjacent areas in Nevada and Utah: DHS [Division of Hydrologic Sciences] publication number 41235: Reno, Nev., Desert Research Institute, Nevada System of Higher Education, 56 p.

Lundquist, J.D., and Flint, A.L., 2006, 2004 onset of snowmelt and streamflow, how shading and the solar equinox may affect spring runoff timing in a warmer world: Journal of Hydroclimatology, v. 7, p. 1199–1217.

Mantua, N.J., and Hare, S.R., 2002, The Pacific decadal oscillation: Journal of Oceanography, v. 58, p. 35–44.

Maxey, G.B., and Eakin, T.E., 1949, Ground water in White River Valley, White Pine, Nye, and Lincoln Counties, Nevada: Nevada State Engineer, Water Resources Bulletin 8, 59 p.

McCabe, G.J., and Dettinger, M.D., 2002, Primary modes and predictability of year-to-year snowpack variations in the western United States from teleconnections with Pacific Ocean climate: Journal of Hydrometeorology, v. 3, p. 13–25.

Mifflin, M.D., and Hess, J.W., 1979, Regional carbonate flow systems in Nevada: Journal of Hydrology, v. 43, p. 217–237.

Nalder, I.A., and Wein, R.W., 1998, Spatial interpolation of climatic normals, test of a new method in the Canadian boreal forest: Agricultural and Forest Meteorology, v. 92, p. 211– 225.

Nichols, W.D., 2000, Regional ground-water evapotranspiration and ground-water budgets, Great Basin, Nevada: U.S. Geological Survey Professional Paper 1628, 82 p.

Priestley, C.H.B., and Taylor, R.J., 1972, On the assessment of surface heat flux and evaporation using large-scale parameters: Monthly Weather Review, v. 100, p. 81–92.

Prudic, D.E., Harrill, J.R., and Burbey, T.J, 1995, Conceptual evaluation of regional ground-water flow in the carbonate-rock province of the Great Basin, Nevada, Utah, and adjacent states: U.S. Geological Survey Professional Paper 1409-D, 102 p.

Prudic, D.E., Niswonger, R.G., and Plume, R.W., 2006, Trends in streamflow on the Humboldt River between Elko and Imlay, Nevada, 1950-99: U.S. Geological Survey Scientific Investigations Report 2005–5199, 58 p.

Ronan, A.D., Prudic, D.E., Thodal, C.E., and Constantz, J., 1998, Field study and simulation of diurnal temperature effects on infiltration and variably saturated flow beneath an ephemeral stream: Water Resources Research, v. 34, no. 9, p. 2137–2153, doi:10.1029/98WR01572.

Seaber, P.R., Kapinos, F.P., and Knapp, G.L., 1987, Hydrologic unit maps: U.S. Geological Survey Water-Supply Paper 2294, 63 p.

Shamir, E., and Georgakakos, K.P., 2005, Distributed snow accumulation and ablation modeling in the American River Basin: Advances in Water Resources, v. 29, p. 558–570.

Scanlon, B.R., Healy, R., and Cook, P.G., 2002, Choosing appropriate techniques for quantifying groundwater recharge: Hydrogeology Journal, v. 10, p. 18–39.

Shuttleworth, W.J., 1993, Evaporation, *in* Maidment, D.R. ed., Handbook of hydrology: New York, McGraw-Hill, 53 p. [chapter 4]

Stephens, D.B., 1995, Vadose zone hydrology: Boca Raton, Fla., CRC Press, 347 p.

Stewart, J.H., Carlson, J.E., Raines, G.L., Connors, K.A., Moyer, L.A., and Miller, R.J., 2003, Spatial digital database for the geologic map of Nevada: U.S. Geological Survey Open-File Report 03–66, version 3.0, 32 p. [accessed May 17, 2007, at http://pubs.usgs.gov/of/2003/of03-66/].

Stonestrom, D.A., Prudic, D.E., Laczniak, R.J., and Akstin, K.C., 2004, Tectonic, climatic, and land-use controls on ground-water recharge in an arid alluvial basin: Amargosa Desert, U.S.A., *in* Hogan, J.F., Phillips, F.M., and Scanlon, B.R., eds., Groundwater recharge in a desert environment, the Southwestern United States: American Geophysical Union, Water Science and Applications Series, v. 9, p. 29–47.

Thornbury, W.D., 1969, Principles of geomorphology (2d ed.): New York: John Wiley and Sons, Inc., 594 p.

UNESCO [United Nations Educational, Scientific and Cultural Organization], 1979, Map of the world distribution of arid regions, accompanied by explanatory note: Paris, France, MAB [Programme on Man and the Biosphere] Technical Note number 7, 54 p.

USDA-SCS [U.S. Department of Agriculture-Soil Conservation Service], 1991, State soil geographic data base (STATSGO), data users guide: Washington, D.C., Miscellaneous Publication 1492, 88 p.

Walker, G.W., and McLeod, N.S., 1991, Geologic map of Oregon: U.S. Geological Survey, scale 1: 500,000 [2 sheets, digital version available at http://geology.wr.usgs.gov/docs/geologic/or/oregon.html, accessed June 28, 2007].

Watson, P., Sinclair, P., and Waggoner, R. 1976, Quantitative evaluation of a method for estimating recharge to the desert basins of Nevada: Journal of Hydrology, v. 31, p. 335–357.

Winograd, I.J., and Thordarson, W., 1975, Hydrogeologic and hydrochemical framework, south-central Great Basin, Nevada-California, with special reference to the Nevada Test Site: U.S. Geological Survey Professional Paper 712–C, 126 p.

Overview of Ground-Water Recharge Study Sites

By Jim Constantz, Kelsey S. Adams[1] , and David A. Stonestrom

Abstract

Multiyear studies were done to examine meteorologic and hydrogeologic controls on ephemeral streamflow and focused ground-water recharge at eight sites across the arid and semiarid southwestern United States. Campaigns of intensive data collection were conducted in the Great Basin, Mojave Desert, Sonoran Desert, Rio Grande Rift, and Colorado Plateau physiographic areas. During the study period (1997 to 2002), the southwestern region went from wetter than normal conditions associated with a strong El Niño climatic pattern (1997–1998) to drier than normal conditions associated with a La Niña climatic pattern marked by unprecedented warmth in the western tropical Pacific and Indian Oceans (1998–2002). The strong El Niño conditions roughly doubled precipitation at the Great Basin, Mojave Desert, and Colorado Plateau study sites. Precipitation at all sites trended generally lower, producing moderate- to severe-drought conditions by the end of the study. Streamflow in regional rivers indicated diminishing ground-water recharge conditions, with annual-flow volumes declining to 10–46 percent of their respective long-term averages by 2002. Local streamflows showed higher variability, reflecting smaller scales of integration (in time and space) of the study-site watersheds. By the end of the study, extended periods (9–15 months) of zero or negligible flow were observed at half the sites. Summer monsoonal rains generated the majority of streamflow and associated recharge in the Sonoran Desert sites and the more southerly Rio Grande Rift site, whereas winter storms and spring snowmelt dominated the northern and westernmost sites. Proximity to moisture sources (primarily the Pacific Ocean and Gulf of California) and meteorologic fluctuations, in concert with orography, largely control the generation of focused ground-water recharge from ephemeral streamflow, although other factors (geology, soil, and vegetation) also are important. Watershed area correlated weakly with focused infiltration volumes, the latter providing an upper bound on associated ground-water recharge. Estimates of annual focused infiltration for the research sites ranged from about 10^5 to 10^7 cubic meters from contributing areas that ranged from 26 to 2,260 square kilometers.

[1] Now with Engeo Incorporated, San Ramon, California (kadams@engeo.com).

Introduction and Scope

The Colorado River, Rio Grande, and other regional drainages dominate the hydrographic landscape of the arid and semiarid southwestern United States (chapter A, this volume). These perennial rivers, together with their major tributaries, comprise a natural network distributing recent precipitation from mountain highlands to distant locations. The shear number of minor tributaries and isolated channels in which flow is ephemeral warrants investigation for generating potentially important amounts of infiltration and ground-water recharge. Process-based understanding of ephemeral flow, infiltration, and associated recharge is needed to quantify where, when, and how much these events contribute to ground-water resources.

Investigations at eight study sites across the arid and semiarid southwestern United States ("Southwest" hereafter) examined streamflow, infiltration, and ground-water recharge during a multiyear campaign (nominally 1997–2002). Study sites were in Arizona (two Sonoran Desert sites), California (one Mojave Desert site), New Mexico (two Rio Grande Rift sites), Nevada (one Mojave Desert and one Great Basin site), and Utah (one Colorado Plateau site; fig. 1; for desert boundaries see fig. 6, chapter A, this volume). Satellite images show each tributary (or basin) in relation to the regional drainage (fig. 2). In addition to the primary characteristic of ephemeral flow, each study site had regionally specific characteristics, resulting in observations of recharge-producing conditions over a range of hydrogeologic settings.

This chapter briefly reviews the literature on focused ground-water recharge from ephemeral infiltration and introduces the study sites, providing context for the chapters that follow. A synopsis of climatic conditions that were observed during the study indicates that streamflow and recharge in dry environments are sensitive to climatic fluctuations, and it demonstrates the value of multiyear data.

Previous Work

Since antiquity, irrigators of arid lands have realized that seepage losses occur when water is routed through unlined channels to distant fields (Gulhati and Smith, 1967). A scientific approach to the sequential processes of infiltration, percola-

tion, and ground-water recharge began with the pioneering work of Henry Darcy in the mid 1800s (Darcy, 1856). Following the dawn of quantitative hydrology, engineers and scientists studied these processes under a variety of rubrics, including consumptive use, transmission losses, and surface-water—ground-water interactions. Interest in recent years has included the deliberate enhancement of ground-water recharge by capturing ephemeral flow with engineered structures and by introducing reclaimed or imported water into channels that would otherwise be dry (Colby and Jacobs, 2006).

During the past quarter century, studies around the world have contributed greatly to the understanding of ground-water recharge in arid regions (Scanlon and others, 2006). Examples include studies in Africa (Crerar and others, 1988), Australia (Allison and Hughes, 1978), Chile (Houston, 2002), Mexico (Ponce and others, 1999), the Middle East (Levin and others, 1980), and India (Rangarajan and Athavale, 2000), in addition to the Southwest (Hogan and others, 2004). Yet few studies address the challenge of quantifying recharge from channels in which a perennial trickle of water is suddenly interrupted by a once-in-a-decade flash flood.

Early studies of focused infiltration in the Southwest were performed at budding population centers including Albuquerque, New Mex., Las Vegas, Nev., and Tucson, Ariz. As these centers grew, in part due to favorable water-resource availability, many formerly remote stream channels from upland basins became concrete-lined flood-control structures draining suburban communities. Early work partitioned streamflow losses into evapotranspiration (ET) and ground-water recharge (Troxell, 1936). Such studies are of value today as much for their historical information on changing land-use patterns as for their insights on recharge processes.

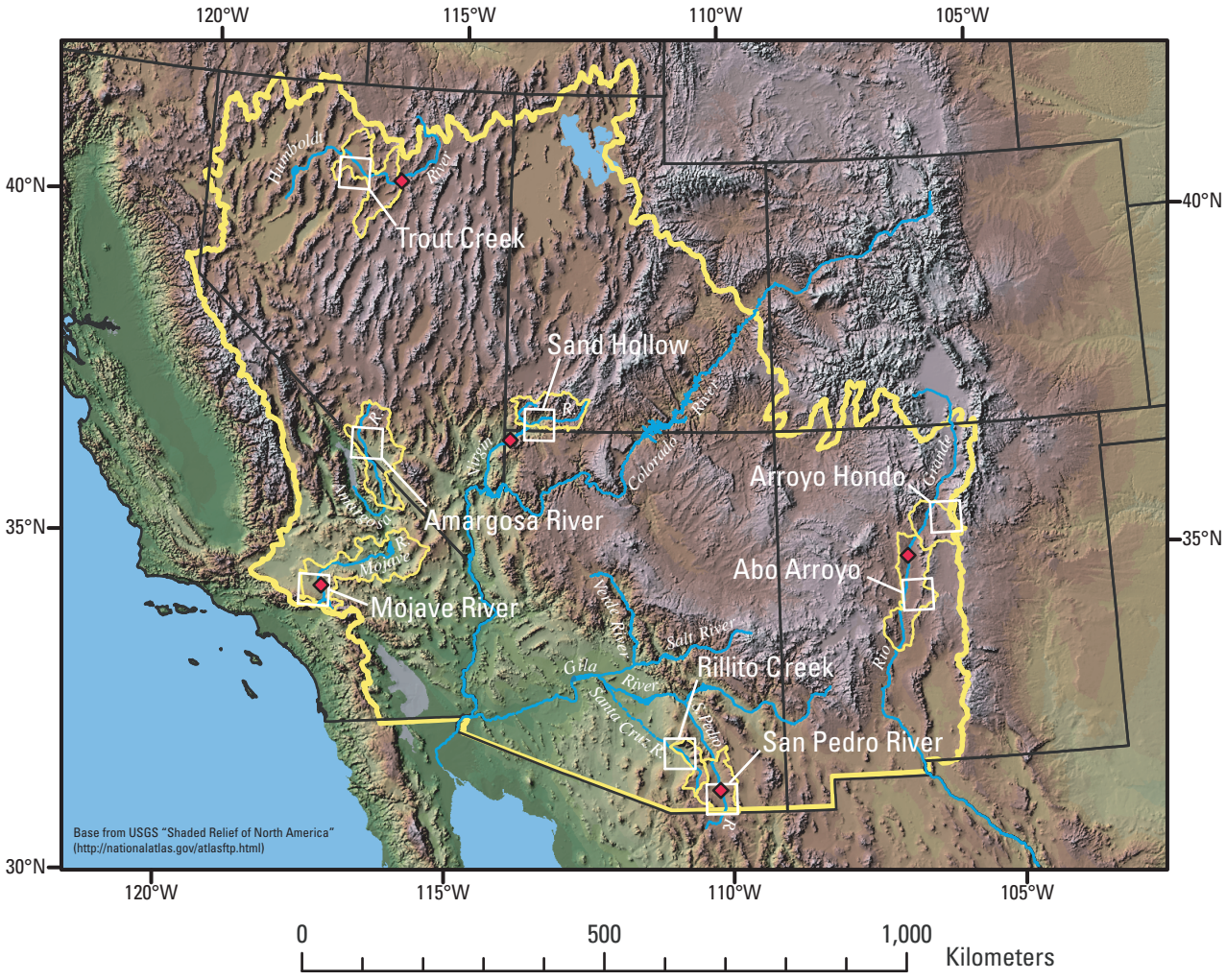

Figure 1. General locations of the focused ground-water-recharge study sites (white squares) are indicated within the overall arid and semiarid southwestern United States study area (thick yellow outline). Squares, labeled by the study-site names, indicate locations of the satellite images shown on figure 2. The thin yellow outlines indicate locations of the corresponding hydrologic basins that were simulated by using the basin-scale recharge model (chapter B, this volume). Red diamonds indicate locations of the streamflow-gaging stations for which multidecadal data were used in analyzing regional trends (see fig. 9 and table 2)

Early work examined hydrodynamic processes, such as the role of sediment transport in ephemeral-streamflow hydraulics (Leopold and Miller, 1961), in addition to the influence of geology and topography in generating ephemeral flow (Hely and Peck, 1964). Quantifying the amount of ground-water recharge from ephemeral mountain runoff proved to be an important but difficult task (Crippen, 1965).

There are few multiyear studies. Exceptions include long-term studies at the U.S. Department of Agriculture (USDA) Walnut Gulch catchment in southeastern Arizona (Renard 1970, Renard and others, 1993). Studies initiated in 1953 to quantify watershed processes in arid regions continue today (Goodrich and others, 2004). These studies showed that ephemeral-flow events, though brief, can be effective in producing ground-water recharge. A long-term study by the U.S. Geological Survey over three decades showed that roughly 70 percent of ephemeral streamflow was lost to infiltration before leaving the Tucson Basin in south-central Arizona (Burkham, 1970). More recently, multiyear investigations at the Nevada Test Site in southern Nev., have showed that runoff and infiltration events can produce deep percolation beneath small washes that rarely flow (LeCain and others, 2002). This latter study used heat as an indicator of deep percolation, an approach applied at six of the study sites.

Naturally occurring hydrologic tracers such as chloride, heat, and isotopes have been used to quantify ground-water recharge by examining ground-water chemistry at the basin scale (Dettinger, 1989; Anderholm, 2000) and by examining focused recharge at smaller scales (Stonestrom and others, 2003). Due to advances in computational analysis, field measurements are increasingly complemented by numerical modeling of watershed-runoff (Maurer, 2002) and unsaturated-zone heat, fluid, and solute transport (Walvoord and others, 2004). This latter study used modeling and observations to show that climate and vegetational changes that occur on multimillennial time scales can determine the presence or absence of ground-water recharge.

Obtaining accurate observations of hydrological processes in arid regions is inhibited by the high-energy nature of ephemeral channels, the long time scales of climatic fluctuations, and the difficulty of methodological research and development in remote areas. Such challenges contribute to a general lack of information on focused infiltration and associated ground-water recharge in arid regions throughout the world.

Although sufficiently accurate streamflow data can provide information on streamflow losses, measurement error generally is larger in dry-region streams than in their humid-region counterparts due to the flashy nature of streamflow and unstable geometry of alluvial channels. Direct determinations of channel losses during ephemeral flow often are impractical due to unstable channel conditions. Considerable effort in the present study concerned the development of thermal methods for estimating losses in channels with ephemeral flow (Constantz and others, 2001; Constantz and others, 2002; Blasch and others, 2004; Niswonger and others, 2005). Geophysical and environmental-tracer methods, which provide time-integrated indications of deep percolation and ground-water recharge, also were advanced (Parker and Pool, 1998; Izbicki and others, 2002; Hoffmann and others, 2003; Stonestrom and others, 2003; Heilweil and others, 2006).

In subhumid and humid regions, watershed size and geology correlate closely with mean annual runoff and base flow, both of which provide indicators of recharge when used in regression models (Nolan and others, 2007). Such relations are more elusive in arid regions. Correlations between watershed area and streamflow for short periods of record are little better than what would occur by chance, as shown by watersheds in the Mojave Desert (fig. 3*A*). Factors including mountain-block permeability, topographic aspect with respect to prevailing storm tracks, vegetational dynamics, and meteorologic granularity (spottiness) become increasingly important with increasing aridity. The relatively high levels of climatic variability in the Southwest, including multiyear droughts, can bias all but the longest records. This is evident in the Mojave Desert example, where restricting analysis to basins with at least 20 years of record improves the correlation considerably (fig. 3*B*).

Infiltration and recharge are less uniformly distributed in arid regions than in humid regions. Arid-region recharge tends to be more concentrated in space—in permeable mountain terrains, beneath losing stream channels, and at contacts between impermeable bedrock and alluvium. Figure 4 shows a conceptual diagram contrasting distributed recharge in humid regions with the focused recharge in arid regions. The volume of infiltration (water entering the subsurface, given by the area under the green infiltration-rate curve) is greater than the volume of percolation beneath the root zone (the area under the dotted black line) due to evapotranspiration, which returns a higher fraction of infiltrating water to the atmosphere in arid regions than in humid regions. Large plants in arid regions can concentrate water around their stems, creating focused infiltration (fig. 4*B*). Ground-water recharge (solid orange line), refers to flow across the water table, into the saturated zone.

Percolating water from line sources (stream channels) spreads laterally as it moves downwards toward the water table, but the rate of horizontal spreading diminishes quickly if infiltration proceeds in sufficiently homogeneous, deep unsaturated zones (Philip, 1983). Once the wetting front connects to the water table, creating mounded conditions, lateral flow becomes dominant once again. Impermeable horizons, such as buried clay and caliche-rich layers, can cause lateral spreading at intermediate depths (Nimmo and others, 2002).

Together with mountain-block infiltration (chapter B, this volume), stream-channel infiltration at the mountain front and downstream in alluvial-filled basins is hypothesized to be the dominant process of ground-water recharge in most of the study area. Geochemical and isotopic studies show that recharge from ephemeral streamflow is focused beneath large channels (Claassen, 1985; Woocay and Walton, 2004). Distributed recharge has been documented, nevertheless, beneath woody vegetation receiving high amounts of precipitation—ponderosa-pine associations on the upper west flank of the

Trout Creek, Nevada

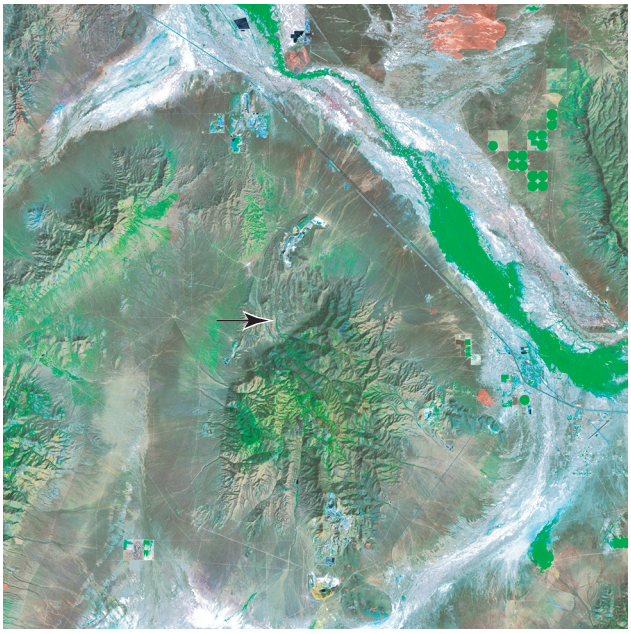

Sand Hollow, Utah

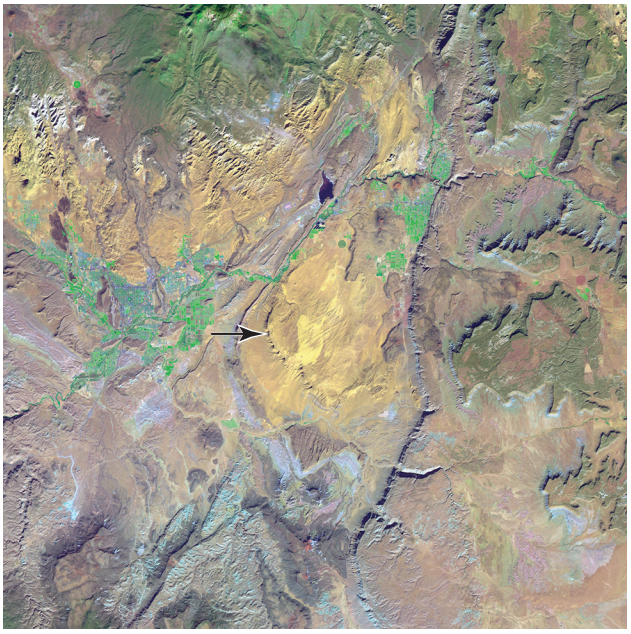

Mojave River, California

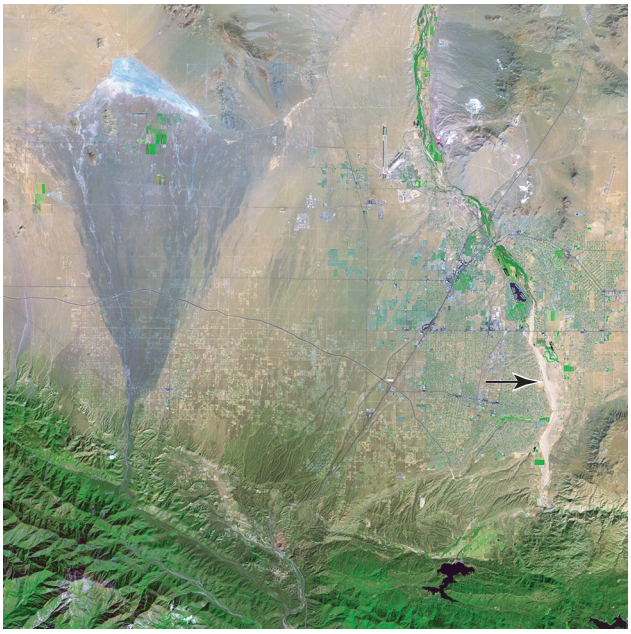

Amargosa River, Nevada

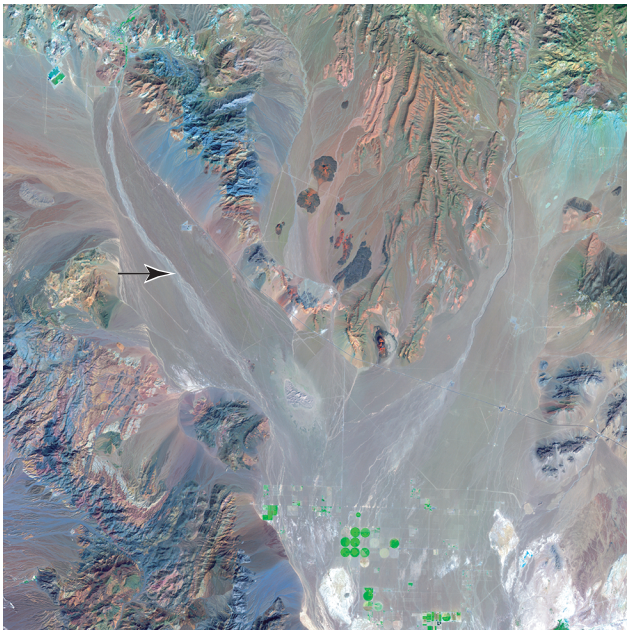

Figure 2. Satellite images of the study sites. The images are 50 kilometers on a side and were acquired by the Landsat 7 Enhanced Thematic Mapper Plus (http://landsat.usgs.gov); spectral bands 7, 4, and 1 are shown as red, green, and blue, respectively. Active vegetation is green; sandstone at Sand Hollow Basin is yellow. In each image, the geographical feature indicated by the arrow and acquisition date are as follows: Abo Arroyo, Sept. 28, 1999; Amargosa River, Sept. 29, 1999 and Oct. 15, 1999 (two images, stitched together); Arroyo Hondo, Oct. 14, 2000; Mojave River, Sept. 9, 2000 and Oct. 4, 2001 (two images, stitched together); Rillito River, Oct. 19, 1999; San Pedro River, Nov. 13, 1999; Sand Hollow, Nov. 2, 1999; and Trout Creek, Sept. 4, 1999. Trout Creek flows north from Battle Mountain (center of image) to the Humboldt River (broad green swath). Arroyo Hondo merges with the Santa Fe River before entering the Middle Rio Grande Basin (at left side of image) through Santa Fe Canyon. See figure 1 for image locations.

Rillito Creek, Arizona

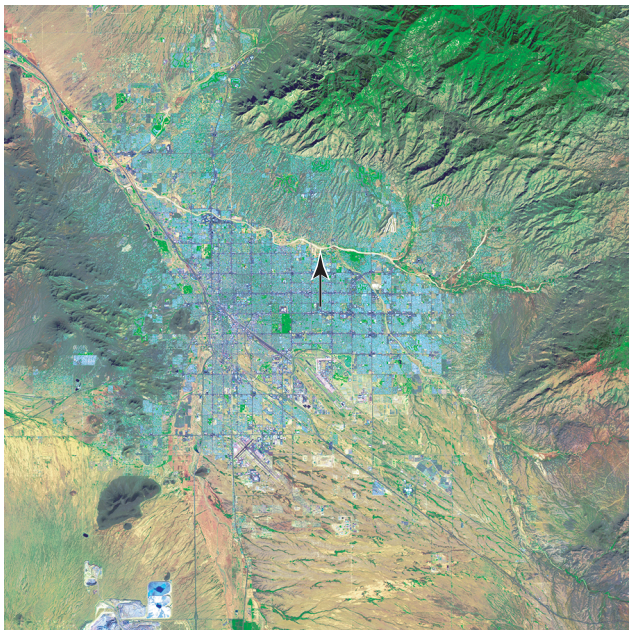

Arroyo Hondo, New Mexico

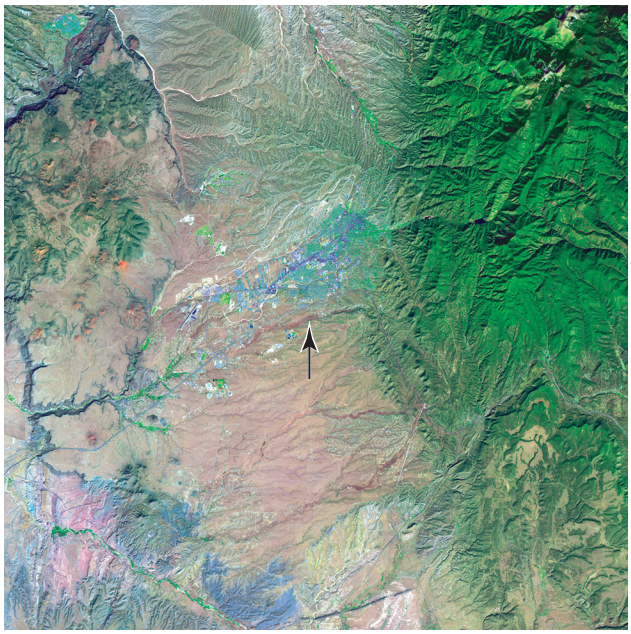

San Pedro River, Arizona

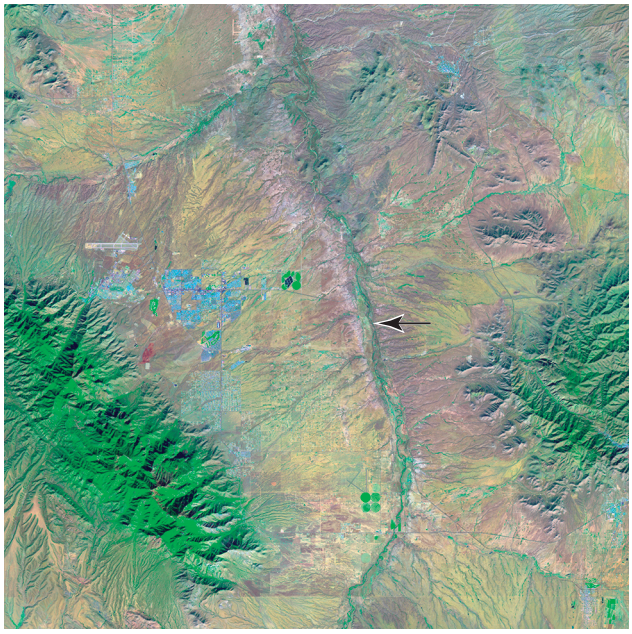

Abo Arroyo, New Mexico

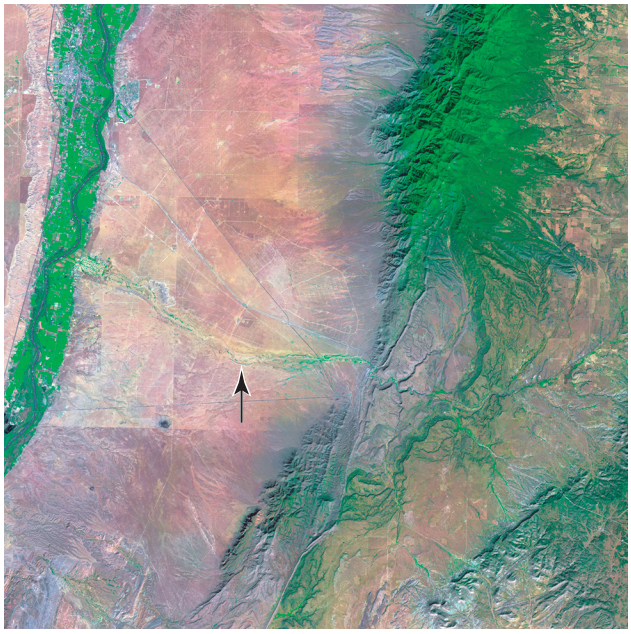

Figure 2.—Continued.

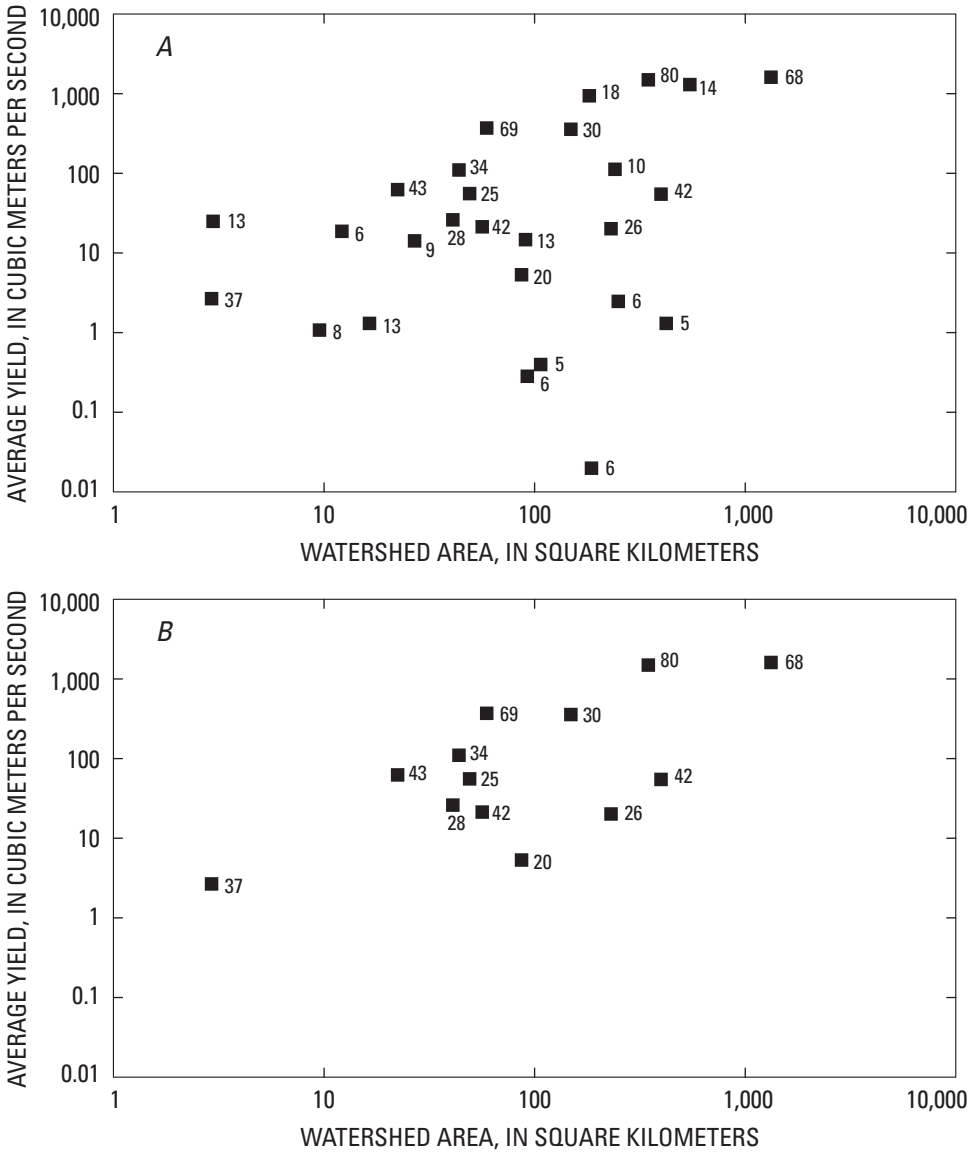

Figure 3. Plot of basin yield (average streamflow exiting watershed) versus watershed area. Numbers to the right of each symbol indicate number of years of record *A*, data for all watersheds; and *B*, data from watersheds that have at least 20 years of record. Data from Lines (1996).

Rio Grande Rift (Sandvig and Phillips, 2006) and juniper associations in westernmost Texas, southeast of the study area (Walvoord and Phillips, 2004). But across vast areas, potential evapotranspiration so greatly exceeds precipitation as to largely prevent direct recharge from rain infiltration in vegetated portions of alluvial basin floors under current climatic conditions (Phillips, 1994).

Site Selection

The approach of the current study was to measure streamflow together with hydrologic, thermal, and chemical parameters at selected sites throughout the Southwest. Seven sites included channels representative of ephemeral flow into either a regional river system (the Rio Grande or Humboldt River, for example) or a regional terminal basin (Death Valley). The eighth site was selected to investigate potential focused recharge on the Colorado Plateau (table 1). All sites are sufficiently isolated from ocean bodies by intervening ranges that their non-mountain portions are arid to semiarid. Sites with ephemeral streamflow relied on streambed temperature analysis to determine infiltration timing and associated percolation.

Sites were selected along transitional reaches of Trout Creek (northern Basin and Range, Nev.), the Amargosa River (southern Basin and Range–Mojave Desert, Nev.), Rillito Creek (Sonoran Desert, south central Ariz.), Abo Arroyo (Rio Grande Rift, central N. Mex.), and Arroyo Hondo (Rio Grande

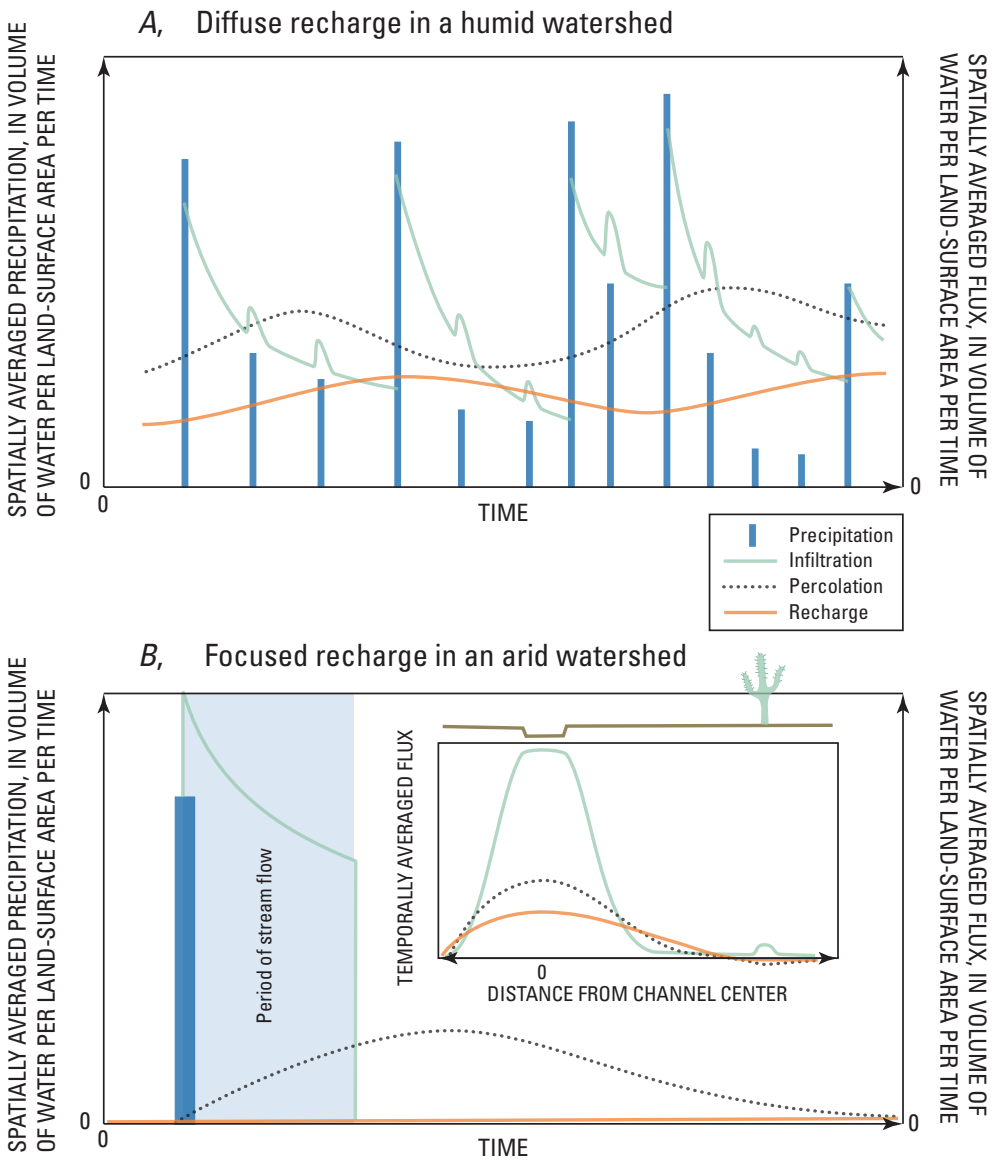

Figure 4. Conceptual diagram of *A*, diffuse ground-water recharge in humid regions—distributed due to diffuse infiltration and percolation—versus *B*, focusedrecharge in arid regions—concentrated due to focused infiltration and percolation. The insert in the lower graphic portrays time-averaged infiltration, percolation, and recharge as a function of distance from the arid channel. Infiltration is downward water flow across the land surface; percolation is flow within the unsaturated zone; and recharge is flow across the water table. Infiltration and subsurface fluxes in *A* and *B* are at different scales, with arid fluxes being relatively small. See text for additional explanation.

Rift, north-central N. Mex.). Transitional reaches included the crossover between streamflow generation in an upland catchment and recharge generation in a downstream alluvial basin. Sites were selected that had an existing or planned streamflow-gaging station ("gage" hereafter) near the crossover point, which typically corresponded to basin-bounding faults. Research followed similar protocols in hydraulic and thermal instrumentation to monitor streamflow and streamflow losses downstream of the gage; however, studies ranged from intensive investigations of limited duration and scope to large multidisciplinary studies that included geophysical, chemical, and modeling components. Spatial scales of contributing catchments varied from several tens of square kilometers to more than two thousand square kilometers (table 1). Temporal scales also varied, although data collection spanned multiple years at most sites (fig. 5). In addition, five tributaries of the Mojave River Basin (Mojave Desert, central southern California) were studied together—Big Rock Creek, Sheep Creek Wash, Oro Grande Wash, Yucca Wash, and Quail Springs Wash. Only Big Rock Creek was instrumented with gages, but data are presented for all tributaries (chapter G, this volume). Similarly, five tributaries of the San Pedro River Basin (Sonoran Desert, southeastern Arizona) were studied, including the gaged channel of Walnut Gulch (chapter J, this volume). Sand Hollow (Colorado Plateau, southwestern Utah), a sandstone basin near the Virgin River, provided information on infiltration in a bedrock basin on the Colorado Plateau (chapter I, this volume).

Physiographic Setting

Brief summaries of the hydrogeologic setting for each site appear below, followed by an overview of climatic

Table 1. Characteristics of focused ground-water recharge study sites, southwestern United States.

[Gage, streamflow-gaging station]

Site (gage identification number)	Regional drain	Average temperature at gage[1], in degrees Celsius	Average annual precipitation at gage[1], in meters	Altitude of gage[2], in meters	Maximum catchment altitude[2], in meters	Contributing area at gage, in square kilometers	Distinguishing characteristics
Abo Arroyo (08331660)	Rio Grande	11.2	0.30	1,667	3,048	650	Moderate monsoon influence; snowmelt affected
Amargosa River (10251217)	Death Valley	14.8	0.15	1,003	2,210	1,200	Strong El Niño influence; arid end member
Arroyo Hondo (08317050)	Rio Grande	9.7	0.36	2,180	2,700	26	Strongly snowmelt affected; some monsoon influence
Mojave River tributaries[3] (10263500)	Mojave River	15.3	0.16	1,234	2,850	75	Strong Pacific Ocean influence; weak snowmelt influence
Rillito Creek (09485700)	Santa Cruz River	19.8	0.32	710	2,780	2,256	Strong monsoon influence; some snowmelt influence
Sand Hollow[4]	Virgin River	16.7	0.21	903	1,300	50	Fractured sandstone basin; strong El Niño influence
San Pedro tributaries[5] (09471200)	San Pedro River	17.8	0.36	1,222	1,540	149	Strong monsoon influence
Trout Creek (3GT[6])	Humboldt River	9.4	0.32	1,600	2,570	48	Strongly snowmelt affected; strong El Niño influence

[1]Interpolated on the basis of elevation from 30-year (1971–2000) normals at nearby climate stations (http://lwf.ncdc.noaa.gov/oa/climate/normals/usnormals.html, accessed March 31, 2007).

[2]National Geodetic Vertical Datum of 1929.

[3]Tabulated values are for Big Rock Creek (downstream portion called Big Rock Wash).

[4]No gage at this site. "Gage" values are for well 27, near the center of catchment (see chapter I, this volume).

[5]Tabulated values are for Walnut Gulch.

[6]Temporary gage for this study (see chapter K, this volume).

conditions and streamflow during the study period. Detailed descriptions are in individual study-site chapters.

Hydrogeologic Framework

Except for the Colorado Plateau study site, stream channels emerge from mountain-block catchments by crossing a fault (or fault zone) associated with sharp increases in sediment thickness. Often the fault is concealed, but the inflection point where the thickness of alluvial fill increases sharply marks the mountain front and provides hydraulic conditions conducive to recharge. Basin-fill alluvium generally is coarsest near mountain fronts, leading to high hydraulic conductivities and rapid streamflow losses. Sediments fine downstream, leading to lower conductivities and streamflow losses away from the mountain front. This pattern occurs throughout the Southwest, and provides the geologic framework for streambed infiltration and ground-water recharge from ephemeral flow (chapter A, this volume). Sand Hollow is a Colorado Plateau sandstone basin that slopes towards a regional drainage, the Virgin River. The basin has sufficient bedrock permeability (largely through fractures intersecting the surface) and soil-moisture storage that little streamflow is generated.
Table 1 compares precipitation, catchment areas, and other attributes of the eight study areas. Brief descriptions of distinguishing features in each of the study sites follow.

Abo Arroyo Study Site

Abo Arroyo divides the northern tip of the Los Piños Mountains (maximum elevation 2,347 m) from the southern portion of the Manzano Mountains in central New Mexico. The study reach begins near the mountain front, where it has a contributing area of 650 square kilometers (km^2; table 1;

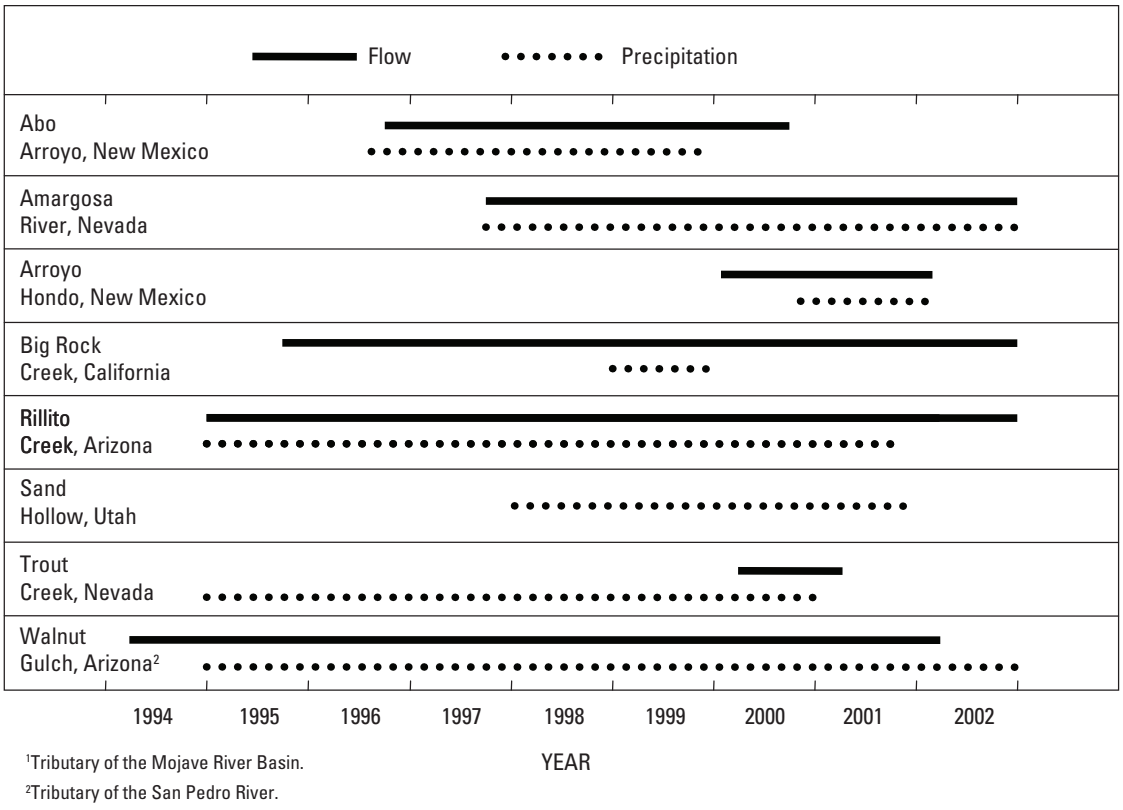

Figure 5. Streamflow and precipitation record for each study site investigated during a multiyear investigation of ground-water recharge, southwestern United States. (Figure by Stanley A. Leake.)

chapter D, this volume). The arroyo enters the Middle Rio Grande Basin, cutting deeply into a bajada (piedmont alluvial plain) formed by the coalescence of many individual alluvial fans. Approximately 12 km from the mountain front, the piedmont terminates, and Abo Arroyo cuts into a stepped sequence of ancestral fluvial terraces of the Rio Grande. The study reach terminates at the confluence of Abo Arroyo and the Rio Grande floodplain (fig. 2). Abo Arroyo is the largest catchment on the eastern side of the Middle Rio Grande Basin.

Amargosa River Study Site

For this study, the selected reach of the Amargosa River is in the Amargosa Desert, a southeast-trending valley where the southern Great Basin overlaps the northern Mojave Desert. The Amargosa River Basin is bounded by block-faulted mountains composed primarily of lower-Paleozoic sedimentary rocks and Tertiary volcanic rocks, and was formed by detachment and normal faulting (chapter E, this volume). The channel enters the Amargosa Desert downstream of Beatty, Nev. The watershed above the entry point has an area of approximately 1,200 km^2 (table 1). Downstream of the entry point, basin-fill alluvium thickens rapidly from less than one meter to several hundred meters. The Amargosa River terminates in Death Valley, Calif. The Amargosa Desert area is among the most arid regions in the United States.

Arroyo Hondo Study Site

Arroyo Hondo is a small mountain-front stream in the southeastern Española Basin, north-central New Mexico (chapter F, this volume). Arroyo Hondo is typical of mountain-front streams draining the western slopes of the Sangre de Cristo Mountains. The mountain front is a sharply defined contact between granitic bedrock and basin-fill alluvium forming the Tesuque aquifer, approximately 2 km below the reach of perennial flow. Arroyo Hondo joins the Santa Fe River before dropping into the Middle Rio Grande Basin (fig. 2). The area of the Arroyo Hondo watershed at the bottom of the instrumented reach is approximately 156 km^2, with 26 km^2 (17 percent) upstream of the mountain front (table 1). The Arroyo Hondo study reach had the highest elevations of the eight research sites.

Tributaries of the Mojave River Basin Study Site

The study area in the western Mojave Desert is northeast of the Los Angeles Basin, along the northern slope of the San Bernardino and San Gabriel mountains (chapter G, this volume). The San Bernardino Mountains are composed largely of granitic rock. The San Gabriel Mountains are composed of granitic and metamorphic rock. Ephemeral flow and associated recharge were examined in five tributaries flowing into the Mojave River Basin. Headwater areas are modified by

active tectonism. One of the tributaries, Oro Grande Wash, no longer has contact with the mountain front due to strike-slip movement along the bounding San Andreas Fault.

Rillito Creek Study Site

Rillito Creek is an ephemeral tributary of the Santa Cruz River in south-central Arizona. Surrounding mountains consist of block-faulted granitic, metamorphic, volcanic, and consolidated sedimentary rocks (chapter H, this volume). Basin-fill ranges from gravel to clay-rich and anhydrous playal deposits. Coarse sediments along the basin margins grade to fine-grained and evaporitic sequences in the central parts of the basins. Alluvial thicknesses range from a few meters along mountain fronts to more 3,000 m in the center of the basin. Rillito Creek had the largest contributing area of the study sites (table 1).

Sand Hollow Study Site

Sand Hollow (southwestern Utah) is a bowl-like feature on the Colorado Plateau created by synclinal (concave upward) warpage of Navajo Sandstone, which crops out to form the rim of the basin (fig. 2). The sandstone consists of well-sorted, wind-deposited fine-to-medium sand (primarily quartz) cemented by calcite (chapter I, this volume). The thickness of the sandstone bedrock reaches 350 m. Cross-bedding structures impart small-scale anisotropy to permeability. Fracture zones impart a main control on ground-water recharge. Fractures zones are up to tens of meters wide, separated by wider zones without much fracturing. Lower parts of the basin are covered with up to three meters of soil. Soils range from coarse-grained sand adjacent to bedrock at higher elevations to loamy sands and sandy loams at lower elevations. Evapotranspiration returns most precipitation to the atmosphere (chapter I, this volume). Thin layers of calcrete (less than 1-m thick) commonly form at the contact between soils—particularly fine-grained soils—and underlying sandstone. The sandstone basin lacked a stream connection to the regional drain.

Tributaries of the San Pedro River Study Site

The San Pedro River (southeastern Arizona) runs northward through basin-fill alluvium separating mountain blocks of relatively subdued topography (table 1; fig. 2). A mixture of rock types similar to those in the Rillito Creek study area form the mountain blocks. Basin soils are dominated by lithic, loamy, and fine-grained paleosoils near the mountains, and clayey and calcium-carbonate rich soils along the lower reaches of tributary watersheds (chapter J, this volume). Loamy soils form narrow corridors along the tributary channels, separated by large expanses of less-permeable soils. Calcium-carbonate soils dominate the eastern part of the basin, and the southwestern part of the basin is dominated by sandy soils. The study characterized 27 tributaries on the basis of geomorphology, vegetation, and soils. Ephemeral flow and associated ground-water recharge were detailed for five streams—Banning Creek, Greenbush Draw, Miller Canyon Wash, Willow Creek, and Walnut Gulch.

Trout Creek Study Site

Trout Creek drains a mountain-block watershed in the northern part of the Great Basin, Nevada. A normal fault separates the upper-mountain reach from the middle-mountain reach (chapter K, this volume). The distribution of bedrock influences runoff generation and associated ground-water recharge from rainfall and snowmelt. The highest reaches of the watershed are underlain by folded and faulted Paleozoic sedimentary rocks of low permeability. Downstream of the fault, the channel crosses Tertiary volcanics overlain by poorly sorted Pleistocene alluvium. The channel continues on recent alluvium deposited by streams that began cutting downward into older gravel fans in the late Pleistocene. Once on the Humboldt River plain, the channel continues on Holocene alluvium incised into older alluvium. Trout Creek is a mountain tributary that receives most of its runoff from snowmelt.

Precipitation During the Study Period

Winter rain and spring snowmelt generally are more effective at producing ground-water recharge than is an equal amount of summer precipitation, due to lower evapotranspiration losses associated with lower temperatures and dormant vegetation (chapter B, this volume). Antecedent conditions control the initial water content of channel sediments, which regardless of season can determine whether a given volume of streamflow generates recharge after entering a basin. Because of antecedent conditions, the timing of precipitation can have as much importance as the total amount.

Precipitation during the study period exhibited regionally dependent seasonal and inter-annual patterns. These patterns reflected proximity to moisture sources (primarily the Pacific Ocean and Gulf of California), annual shifts in storm tracks and monsoonal circulation, and global-scale, multiyear fluctuations (chapter A, this volume). Winter and spring precipitation dominated the western and northern sites (Amargosa, Mojave, and Trout Creek; blue sections, fig. 6, and summer and fall precipitation dominated the southern (San Pedro and Rillito) and eastern (Abo Arroyo and Arroyo Hondo) sites (orange and yellow sections, fig. 6). Precipitation at the Sand Hollow site, near the center of the study area, had the most balanced seasonal pattern. While sampling periods varied, observed patterns were consistent with regional expectations (chapter A, this volume). The Amargosa Desert had the lowest daily frequency of precipitation, at eight percent, while Arroyo Hondo had the highest daily frequency of precipitation, at 23 percent.

The climatic pattern during the study period (1997–2002) was one of generally wetter-than-normal conditions near the beginning followed by a shift to gen-

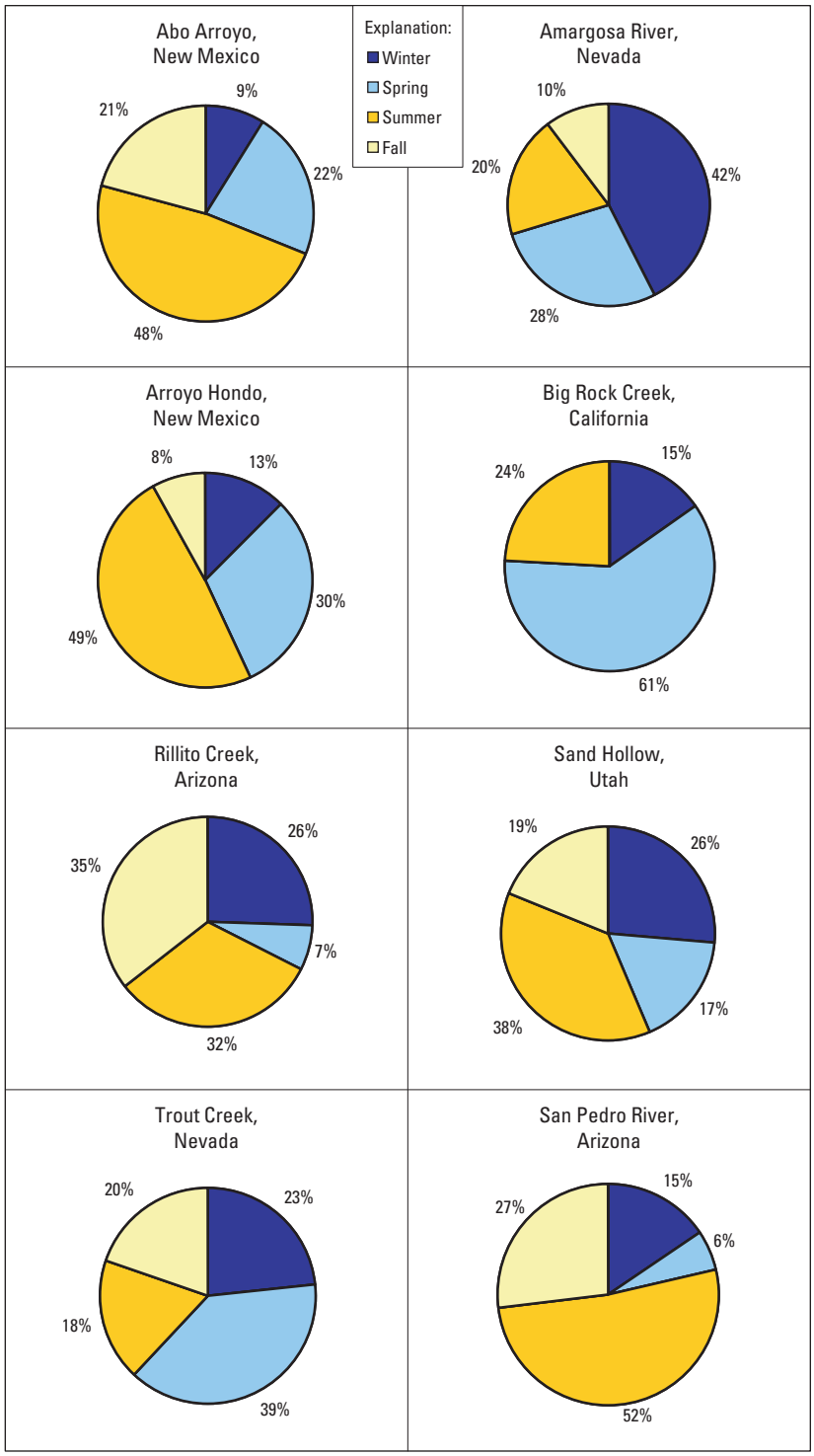

Figure 6. Seasonal distribution of precipitation at the eight study sites during the investigation. Numbers indicate the percentage of annual precipitation during the indicated season. Winter (December, January, and February) is dark blue; spring (March, April, and May) is light blue; summer (June, July, and August) is orange; and fall (Sepember, October, and November) is yellow.

erally drier-than-normal conditions (figs. 7–8). Figure 7 shows regional precipitation and a drought-severity index at two-year intervals. By the end of the study, moderate to severe drought affected nearly all western and midwestern states (fig. 7). Initial wetter-than-normal conditions included development of an El-Niño pattern that brought warm water to the eastern tropical Pacific and shifted North American winter storms southward into the study area (chapter A, this volume). The 1997–98 El Niño was the strongest on record, as determined by satellite-measured sea-surface temperatures (Curtis and Adler, 2000). The subsequent drought was associated with La Niña conditions that included unprecedented warmth in the tropical western Pacific and Indian oceans (Hoerling and Kumar, 2003).

Figure 8 shows trends in annual precipitation for each of the study sites as percentages of mean conditions. The estimates of mean conditions were derived from the global synthesis of meteorologic data archived by the National Oceanic and Atmospheric Administration (Kalnay and others, 1996). Plotted values are estimates for each two-degree by two-degree cell containing a study site (about 220 km north-south by 180 km east-west). These estimates provide an internally consistent comparison of regional variations throughout the study period.

Study sites fall into three groups with respect to regional climatic influences. Sites to the north and west (fig. 8*A*) were more strongly affected by El-Niño conditions than were the sites to the east and south (fig. 8*B*). Sites to the east and south, in turn, were more strongly affected by the weakening of monsoonal conditions. Sand Hollow, near the center of the study area, was affected by both El-Niño and monsoonal conditions, and it showed large relative changes during the study period.

Streamflow During the Study Period

Surface water and ground water are interlinked systems (Alley and others, 2002). Ground-water discharge provides base flow to gaining portions of streams; conversely, enhanced streamflow in response to storms and snowmelt produces ground-water recharge beneath losing portions of streams. Even though lags are introduced by storage changes together with variable-frequency travel times through channel networks, unsaturated zones, and ground-water systems, stream flows are roughly correlated with ground-water recharge. Streamflow records thus provide indirect, but readily accessible information on seasonal and year-to-year trends in ground-water recharge.

The shift to drought conditions during the study period reduced streamflow—and associated ground-water recharge—across the range of drainage-integration areas. To demonstrate these changes at a regional scale, figure 9 compares mean daily streamflows in 1998 and 2002 with long-term average mean daily streamflows for selected regional rivers in the study area—the Rio Grande in central New Mexico (USGS streamflow-gaging station 08330000), the Humboldt River in north-central Nevada (10322500), the Virgin River in northern Arizona (09415000), the Mojave River in central southern California (10261500), and the San Pedro River in southeastern Arizona (09471000). Diamonds in figure 1 show the locations of the gages, which were selected for having continuous records dating back at least to mid century. While all streamflows are impacted by human activities to some degree, rivers and stations were selected for having relatively small anthropogenic effects.

Average mean-daily streamflow for the period 1945–2002 (thick colored lines, fig. 9) show patterns consistent with regional climatic trends. For example, flows in the Humboldt River increase after the arrival of winter storms and peak in early June, due to the dominant influence of spring snowmelt. Flows in the Mojave River peak soon after the arrival of winter storms (January–February), but lack a strong snowmelt signature. The Rio Grande shows a broad peak in flows, from April through June, due to sustained snowmelt from the southern Colorado Rockies. Rio Grande flows rise again to a secondary peak in early November, after the growing season. A similar feature in the Humboldt record (barely apparent at the plotted scale) is explained by the seasonal slowdown of evapotranspiration (Prudic and others, 2006). The July and August peak in San Pedro flows marks the arrival of the summer-monsoon season.

With the exception of the San Pedro River, flow volumes in regional rivers were higher than normal in 1998 (fig. 9). Compared to their respective long-term (1945–2002) averages, annual flow volumes ranged from 101–180 percent of normal in the Rio Grande, Humboldt, Virgin, and Mojave Rivers (table 2). By 2002, annual flow volumes had declined to 10–46 percent of average, revealing the effects of severe drought. In 1998, annual total flow in the San Pedro River was only 31 percent of the 1945–2002 average, and it decreased further to 21 percent by 2002. San Pedro River annual flow volumes, while highly variable, have decreased 66 percent from 1913 to 2002 due to factors other than a shift in climate (Thomas and Pool, 2006).

Discussions of streamflow at individual study sites are presented in subsequent chapters. Streamflow-gaging stations for each site are shown in figure 10. Figure 10 also shows a general view of Sand Hollow, where no stream was present. The bedrock channel at the Big Rock Creek gage (Mojave River Basin) minimized shifts from deposition, scour, and vegetation. The channel at the Walnut Gulch gage (San Pedro River Basin) was a concrete weir designed to accurately measure a wide range of flow rates. The channel at the Abo Arroyo gage was floored by bedrock, but walled by semi-consolidated alluvium, whereas the gage at Rillito Creek was walled by soil cement, but floored by unconsolidated sediment. Statistically fitted curves relating streamflow to stage (water depth) had correlation coefficients whose squares ranged from 0.97 for Big Rock Creek to 0.54 for Arroyo Hondo, which had the smallest catchment (table 1) and largest influences from changing vegetation and shifting sediments.

Figure 11 compares streamflow records for the seven gaged sites, although, records at Arroyo Hondo and Trout Creek were of limited duration. Gages integrated runoff from catchments over a wide range of sizes (table 1) and were sensitively expressive of exact position with respect to the crossover

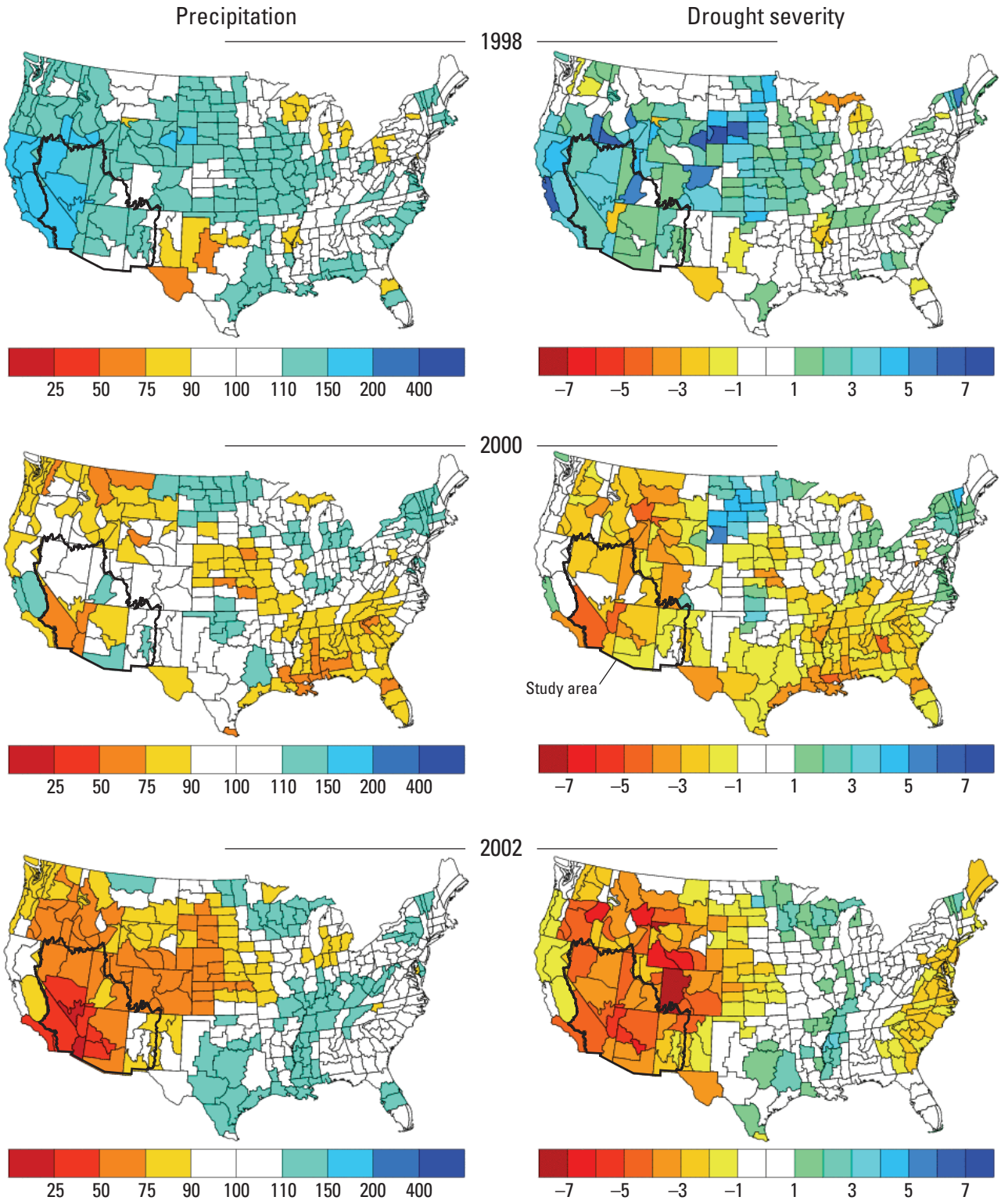

Figure 7. Development of drought conditions in the United States during the study period. Figures at left show annual precipitation in 1998, 2000, and 2002 as a percentage of a long-term (46-year) average (1950–1995). Figures at right show a version of the Palmer drought severity index, which takes into account cumulative soil-moisture deficit and heat stress (Heim, 2002). Negative values indicate drier than normal conditions, with –3 indicating the onset of severe drought. Data by climate division, from the National Oceanic and Atmospheric Administration (http://www.cdc.noaa.gov/USclimate, accessed December 7, 2006).

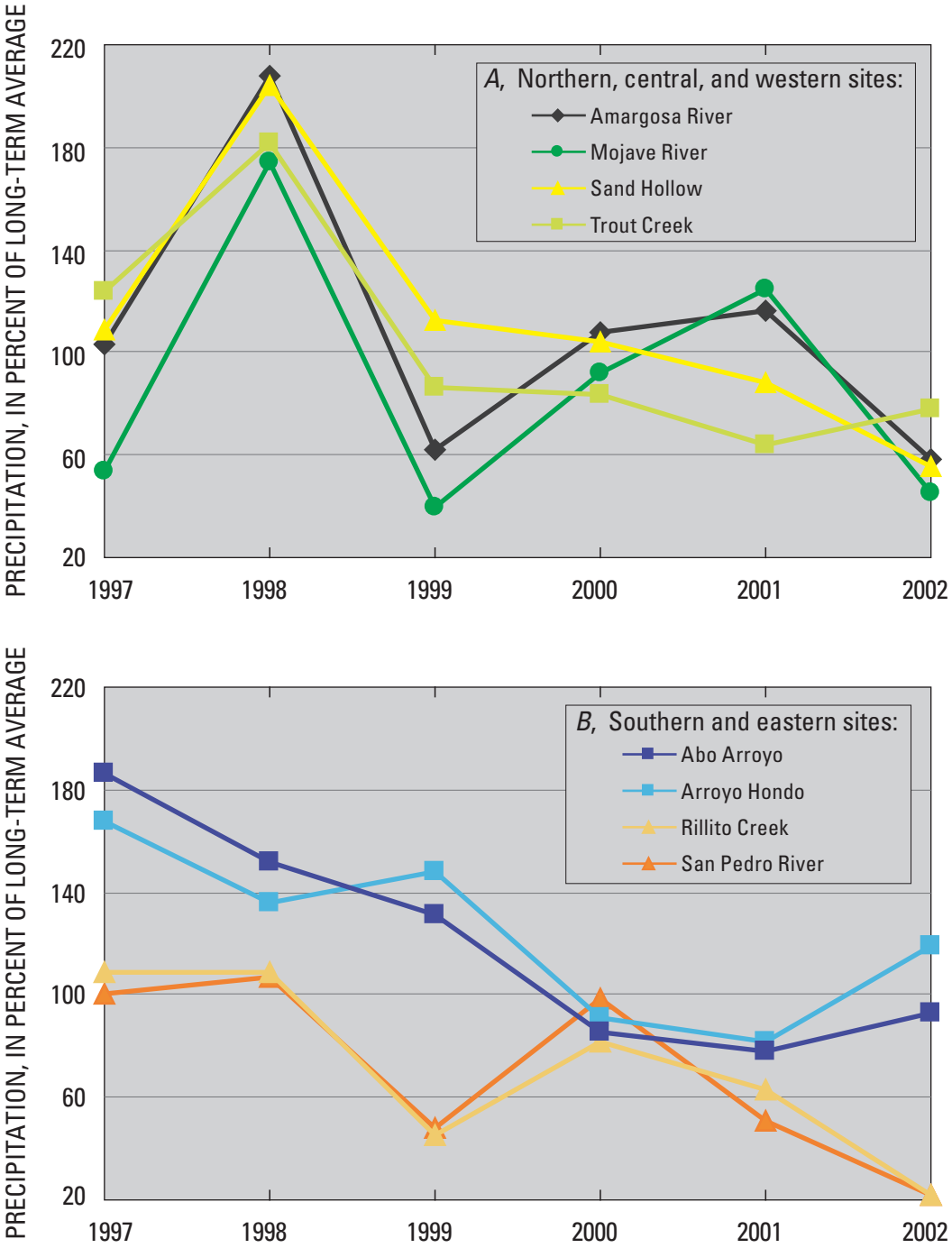

Figure 8. Precipitation as a percentage of long-term (1948–2005) average precipitation for *A*, northern, central, and western study sites and *B*, southern and eastern study sites. Data for each two-degree by two-degree latitude-longitude cell from http://www.cdc.noaa.gov/Timeseries, accessed December 5, 2006.

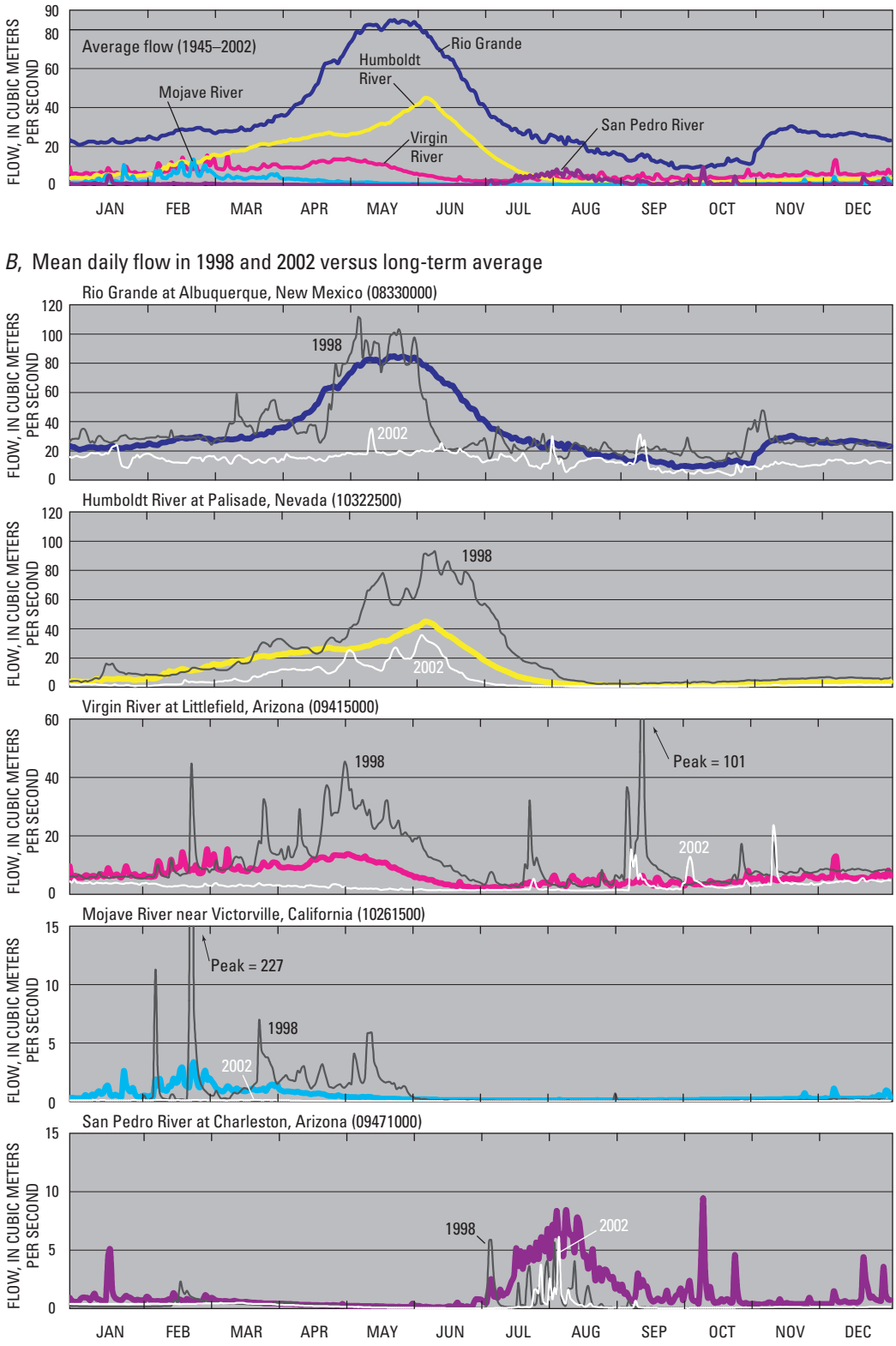

Figure 9. Hydrographs of regional rivers, comparing *A*, long-term average daily mean streamflow (thick colored lines) with *B*, daily mean streamflow for 1998 (black lines) and 2002 (white lines). Values in parentheses are USGS streamflow-gaging station identifiers; figure 1 shows the streamflow-gaging station locations. Data from http://waterdata.usgs.gov/nwis (accessed March 28, 2007).

Table 2. Annual flow volumes in regional rivers, compared to long-term averages, southwestern United States.

[Volumes computed from mean daily flows obtained from http://waterdata.usgs.gov/nwis, accessed April 24, 2007; numbers in parentheses are USGS streamflow-gaging station identifiers. Colors indicate highest—blue and lowest—red annual flow volume for each river]

Period	Rio Grande, New Mexico (08330000)	Humboldt River, Nevada (10322500)	Virgin River, Utah (09415000)	Mojave River, California (10261500)	San Pedro River, Arizona (09471000)
Average annual flow volume, in cubic meters					
1945–2002	$1.05\ 10^{9}$	$3.78\ 10^{8}$	$2.05\ 10^{8}$	$5.75\ 10^{7}$	$4.01\ 10^{7}$
Annual flow volume, in percent of 1945–2002 average					
1997	**141**	168	93	19	40
1998	101	**176**	**172**	**180**	31
1999	113	101	71	18	68
2000	66	55	67	14	**224**
2001	69	**27**	62	11	57
2002	**41**	46	**46**	**10**	**21**

between streamflow generation and streamflow loss. Even so, the effects of climatic variability on streamflow at the ground-water recharge study sites were readily apparent. Summer monsoonal precipitation produced substantial flow at Rillito Creek throughout the developing drought. Gages at Walnut Gulch (a tributary of the San Pedro River) and sites beyond the influence of monsoonal storms (Trout Creek and Big Rock Creek, for example) recorded extended periods of negligible flow (fig. 11). Four of the study sites had extended periods of zero or negligible flow that lasted about 9–15 months. The higher variability of study-site streamflow relative to regional streamflow reflects smaller scales of integration in time and space of the study-site watersheds.

Annual focused infiltration volumes at the study sites ranged from less than 0.1 to about 10 million cubic meters per year (Mm^3/yr) (chapters D–K, this volume). Environmental tracers indicated that Sand Hollow produced recharge directly through the bedrock, controlled largely by fracturing. For the other sites, comparison of estimated average annual infiltration volumes with corresponding catchment areas suggests an upper limit on associated recharge for sites with focused infiltration from streamflow (fig. 12). The low correlation between focused infiltration rates and watershed size is consistent with results shown in figure 3, partly reflecting short records but also indicating differences in orography and other factors.

The Amargosa River produced comparatively little focused infiltration for its basin size relative to the Mojave tributaries. Despite having similar precipitation at their respective gages, the Mojave tributaries collect runoff from higher elevations located near the leading edge of Pacific storms (table 1). Trout Creek and Arroyo Hondo were sampled only during drier-than-normal conditions and, therefore, would be expected to have higher average annual focused-infiltration volumes for a longer period of record. Substantial volumes of focused infiltration were estimated for Rillito Creek, Abo Arroyo, and San Pedro tributaries, resulting primarily from summer monsoonal precipitation. In contrast, for Trout Creek, the Amargosa River, and the Mojave River Basin tributaries, focused infiltration was largely from winter precipitation (and subsequent snowmelt at Trout Creek).

Conclusions

Large variations in seasonal patterns of precipitation affected regional streamflows, focused infiltration, and associated ground-water recharge during the study period (1997–2002). The timing of precipitation and snowmelt controlled the timing of streamflow. Strong El Niño conditions in 1997–1998 roughly doubled the annual precipitation (in 1998)

Abo Arroyo (Rio Grande Rift, central New Mexico)

Jim Constantz

Amargosa River (southern Basin and Range, Nevada)

Amy E. Stewart-Deaker

Arroyo Hondo (Rio Grande Rift, north-central New Mexico)

Jim Constantz

Big Rock Creek (Mojave River Basin, California)

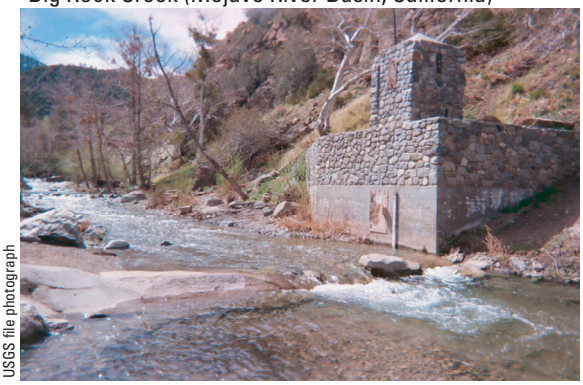

USGS file photograph

Rillito Creek (Santa Cruz River Basin, Arizona)

Jim Constantz

Sand Hollow (southwestern Colorado Plateau, Utah)

Victor C. Heilweil

Trout Creek (northern Basin and Range, Nevada)

James L. Wood

Walnut Gulch (San Pedro River Basin, Arizona)

USDA file photograph

Figure 10. Streamflow-gaging stations listed in table 1 for seven of the study sites, plus a general view of Sand Hollow, where no stream was present. Figure 1 shows study-site locations.

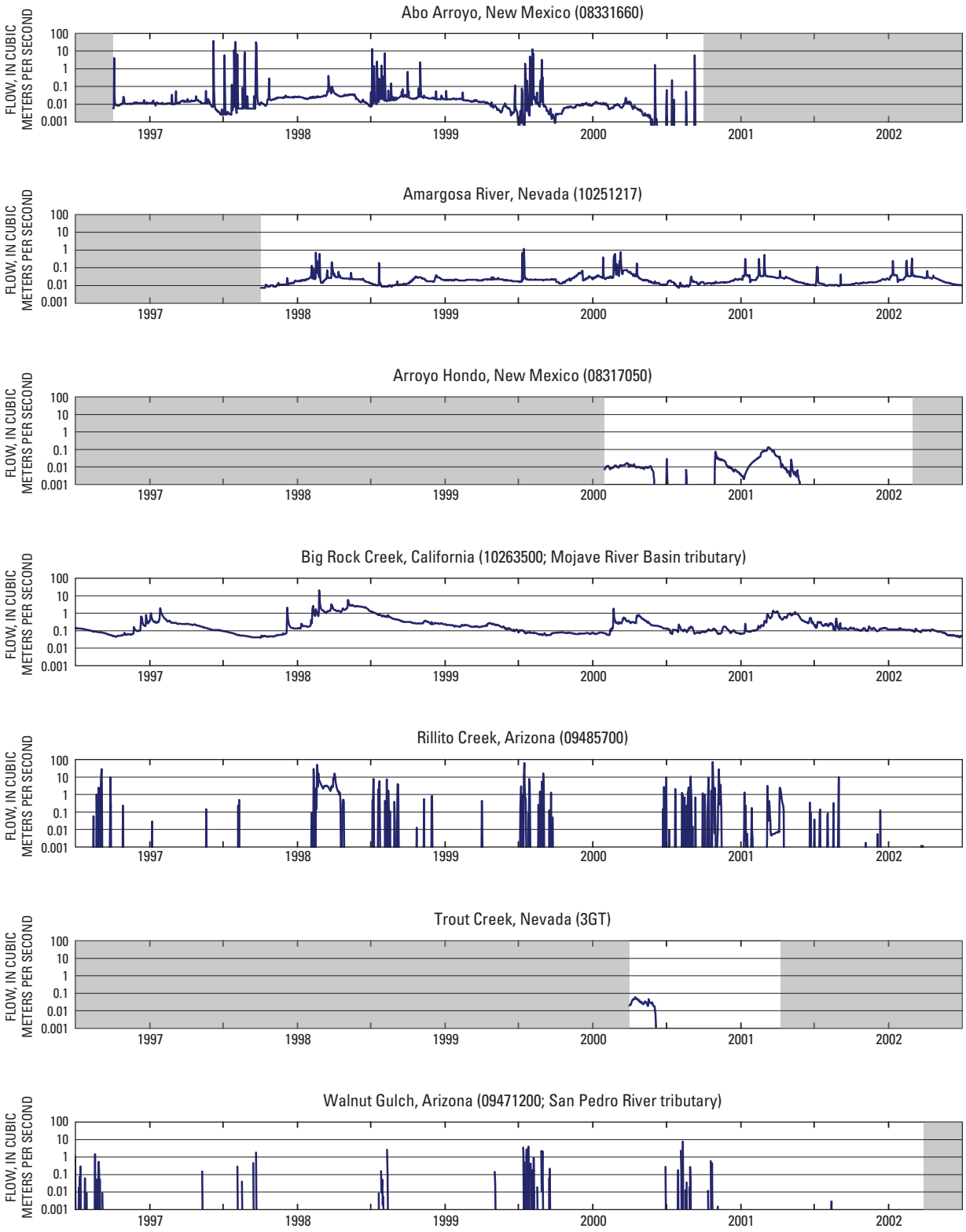

Figure 11. Hydrographs showing streamflow data from July 1, 1996 to July 1, 2002, for the seven study sites with streams, southwestern United States. Gray areas indicate periods without streamflow data. Station identifiers are given in parentheses (see table 1 for explanations).

at the northern, western, and central sites. Subsequent development of severe drought affected streamflow in regional rivers, as well as at the study sites. Overall, summer monsoonal rainfall was the main contributor to runoff and associated recharge at the southern sites, while winter precipitation (and associated snowmelt, where present) was the main contributor at the northern and western sites.

Most of the study sites feature one or more stream channels that originate in contributing upland watersheds dominated by bedrock and cross mountain-front faults into adjoining alluvial basins. Abrupt increases in the thickness of coarse sediments downstream of the mountain front are associated with rapid streamflow losses and focused ground-water recharge. The prolonged drought during the study reduced streamflows crossing the mountain fronts, thereby reducing the potential for focused infiltration and ground-water recharge during this phase of the climatic cycle. Intra- and inter-annual variations in precipitation control streamflow generation and associated ground-water recharge. A main conclusion of the study is the degree to which interpretations of infiltration and ground-water-recharge estimates require knowledge of the meteorologic and climatic conditions to which they correspond.

Ephemeral streamflow produced volumes of focused infiltration in the study area that scaled roughly with catchment area, placing an upper limit on ground-water recharge from transmission losses. The timing of focused infiltration in the Southwest is highly variable and sensitive to climatic fluctuations, such as El Niño cycles and drought. Drought impacted regional flows, as well as focused infiltration volumes throughout the study area, reducing contributions of focused infiltration to basin recharge. Measurements made at the study sites indicate that focused infiltration can become negligible during extended periods of severe drought; however, sites receiving summer monsoonal rains can continue to generate focused recharge even during droughts.

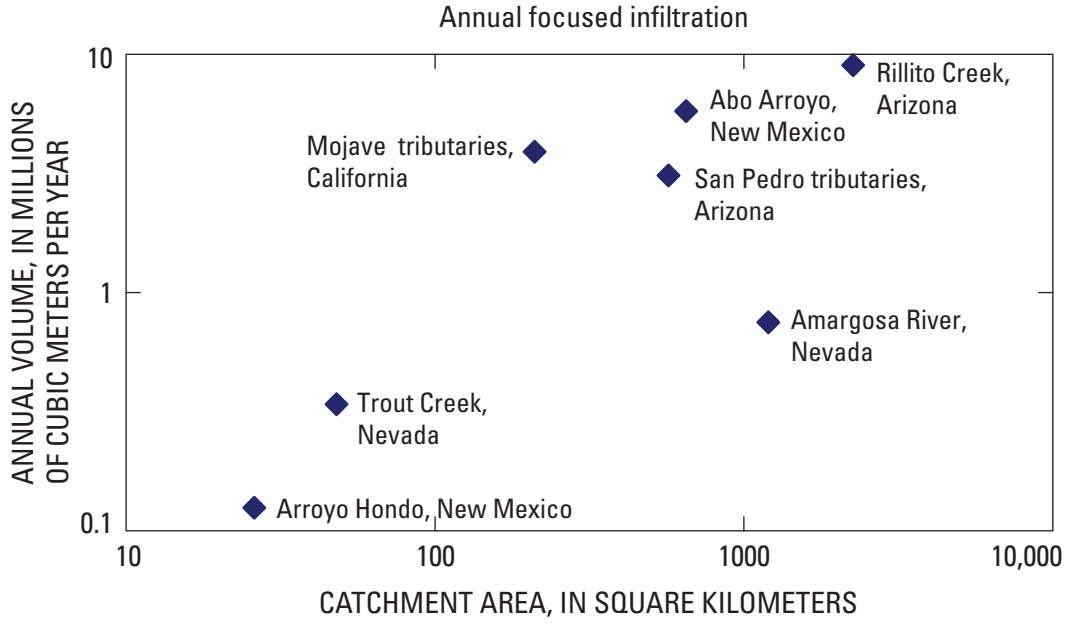

Figure 12. Estimated annual focused-infiltration volumes versus catchment areas (aggregated in the case of the Mojave River Basin tributaries and San Pedro River tributaries).

References Cited

Alley, W.M., Healy, R.W., LaBaugh, J.W., and Reilly, T.E., 2002, Flow and storage in groundwater systems: Science, v. 296, p. 1985–1990.

Allison, G.B., and Hughes, M.W., 1978, The use of environmental chloride and tritium to estimate total recharge to an unconfined aquifer: Australian Journal of Soil Research, v. 16, p. 181–195.

Anderholm, S.K., 2000, Mountain-front recharge along the eastern side of the Middle Rio-Grande Basin, central New Mexico: U.S. Geological Survey Water-Resources Investigations Report 00–4010, 36 p.

Blasch, K.W., Ferré, T.P.A., and Hoffmann, J.P., 2004, A statistical technique for interpreting streamflow timing using streambed sediment thermographs: Vadose Zone Journal, v. 3, p. 936–946.

Burkham, D.E., 1970, Depletion of streamflow by infiltration in the main channels of the Tucson Basin, southeastern Arizona: U.S. Geological Survey Water-Supply Paper 1939-B, 36 p.

Claassen, H.C., 1985, Sources and mechanisms of recharge for ground water in the west-central Amargosa Desert, Nevada—A geochemical interpretation: U.S. Geological Survey Professional Paper 712-F, 31 p.

Colby, B.G., and Jacobs, K.L., eds., 2006, Arizona Water Policy—Management innovations in an urbanizing, arid region: Washington, D.C., Resources for the Future Press, 247 p.

Constantz, J.E., Stonestrom, D.A., Stewart, A.E., Niswonger, R.G., and Smith, T.R., 2001, Analysis of streambed temperatures in ephemeral channels to determine streamflow frequency and duration: Water Resources Research, v. 37, no. 2, p. 317–328.

Constantz, J.E., Stewart, A.E., Niswonger, R.G., and Sarma, L., 2002, Analysis of temperature profiles for estimating stream loss beneath ephemeral channels: Water Resources Research, v. 38, no. 12, p. 52–1 to 52–13, doi: 10.1029/2001WR001221.

Crerar, S., Fry, R.G., Slater, P.M., van Langehove, G., and Wheeler, D., 1988, An unexpected factor affecting recharge from ephemeral river flows in SWA/Namibia, *in* Simmers, ed., Estimation of natural groundwater recharge: Dordrecht, Holland, D. Reidel Publishing Company, p.11–28.

Crippen, J. R., 1965, Natural water loss and recoverable water in mountain basins of Southern California: U.S. Geological Survey Professional Paper 417-E, 24 p.

Curtis, S., and Adler, R., 2000, ENSO indices based on patterns of satellite-derived precipitation: Journal of Climate, v. 13, no. 15, p. 2786.

Darcy, Henry, 1856, Les fontaines publiques de la Ville de Dijon: Paris, Victor Dalmont, 647 p.

Dettinger, M.D., 1989, Reconnaissance estimates of natural recharge to desert basins in Nevada, U.S.A., by using chloride-balance calculations: Journal of Hydrology, v. 106, no. 1-2, p. 55–78.

Goodrich, D.C., Williams, D.G., Unkrich, C.L., Hogan, J.F., Scott, R.L., Hultine, K.R., Pool, D., Coes, A., and Miller, S., 2004, Comparison of methods to estimate ephemeral channel recharge, Walnut Gulch, San Pedro River Basin, Arizona, *in* Hogan, J.F., Phillips, F.M., and Scanlon, B.R., eds., Groundwater recharge in a desert environment—The southwestern United States: American Geophysical Union, Water Science and Applications Series, v. 9, p. 77–99, doi:10.1029/0009WSA10.

Gulhati, N.D., and Smith, W.C., 1967, Irrigated agriculture—An historical review, *in* Hagan, R.M., Haise, H.R., and Edminster, T.W., eds., Irrigation of agricultural lands: Madison, American Society of Agronomy, p. 3–11.

Heilweil, V.M., Solomon, D.K., and Gardner, P.M., 2006, Borehole environmental tracers for evaluating net infiltration and recharge through desert bedrock: Vadose Zone Journal, v. 5, no. 1, p. 98–120, doi:10.2136/vzj2005.0002.

Heim, R.R., Jr., 2002, A review of twentieth-century drought indices used in the United States: Bulletin of the American Meteorological Society, v. 83, no. 8, p. 1149–1165.

Hely, A.G., and E.L. Peck, 1964, Precipitation, runoff and water loss in the lower Colorado River—Salton Sea area: U.S. Geological Survey Professional Paper 486-B, 16 p.

Hoerling, M., and Kumar, A., 2003, The perfect ocean for drought: Science, v. 299, no. 5607, p. 691–694, doi:10.1126/science.1079053.

Hoffmann, J.P., Blasch, K.W., and Ferré, T.P.A., 2003, Combined use of heat and soil-water content to determine stream/ground-water exchanges, Rillito Creek, Tucson, Arizona, *in* Stonestrom, D.A., and Constantz, J., eds., Heat as a tool for studying the movement of ground water near streams: U.S. Geological Survey Circular 1260, p. 47–55.

Hogan, J.F., Phillips, F.M., and Scanlon, B.R., eds., 2004, Groundwater recharge in a desert environment—The southwestern United States: American Geophysical Union, Water Science and Applications Series, v. 9, 294 p.

Houston, J., 2002, Groundwater recharge through an alluvial fan in the Atacama Desert, northern Chile—Mechanisms, magnitudes and causes: Hydrologic Processes, v. 16, no. 15, p. 3019–3025.

Izbicki, J.A., Radyk, J., and Michel, R.L., 2002, Movement of water through the thick unsaturated zone underlying Oro Grande and Sheep Creek Washes in the western Mojave Desert, USA: Hydrogeology Journal, v. 10, p. 409–427.

Kalnay, E., Kanamitsu, M., Kistler, R., Collins, W., Deaven, D., Gandin, L., Iredell, M., Saha, S., White, G., Woollen, J., Zhu, Y., Leetmaa, A., Reynolds, B., Chelliah, M., Ebisuzaki, W., Higgins, W., Janowiak, J., Mo, K.C., Ropelewski, C., Wang, J., Jenne, R., and Joseph, D., 1996, The NCEP/NCAR reanalysis project: Bulletin of the American Meteorological Society, v. 77, no. 3, p. 437–471.

LeCain, G.D., Lu, N., and Kurzmack, M., 2002, Use of temperature, pressure, and water potential data to estimate infiltration and monitor percolation in Pagany Wash associated with the winter of 1997–98 El Niño precipitation, Yucca Mountain, Nevada: U.S. Geological Survey Water-Resources Investigations Report 02–4035, 25 p.

Leopold, L.B., and J.P. Miller, 1961, Ephemeral streams—Hydraulic factors and their relation to the drainage net: U.S. Geological Survey Professional Paper 282-A, 38 p.

Levin, M., Gat, J.R., and Issar, A., 1980, Precipitation, flood, and groundwaters of the Negev Highlands—An isotopic study of desert hydrology, *in* Fontes, J., ed., Arid zone hydrology—Investigations with isotope techniques: Vienna, International Atomic Energy Agency, p. 3–22.

Lines, G.C., 1996, Ground-water and surface-water relations along the Mojave River, southern California: U.S. Geological Survey Water-Resources Investigation Report 95–4189, 43 p.

Maurer, D., 2002, Ground-water flow and numerical simulation of recharge from streamflow infiltration near Pine Nut Creek, Douglas County, Nevada: U.S Geological Survey Water-Resources Investigations Report 02–4145, 37 p.

Nimmo, J.R., Deason, J.A., Izbicki, J.A., and Martin, P., 2002, Evaluation of unsaturated zone water fluxes in heterogeneous alluvium at a Mojave Basin site: Water Resources Research, v. 38, no. 10, p. 33–1 to 33–13.

Niswonger, R.G., Prudic, D.E., Pohll, G., and Constantz, J., 2005, Incorporating seepage losses into the unsteady streamflow equations for simulating intermittent flow along mountain front streams: Water Resources Research, v. 41, doi:10.1029/2004WR003677.

Nolan, B.T., Healy, R.W., Taber, P.E., Perkins, K.S., Hitt, K.J., and Wolock, D.M., 2007, Factors influencing ground-water recharge in the eastern United States: Journal of Hydrology, v. 332, p. 187–205.

Parker, J.T.C., and Pool, D.R., 1998, Use of microgravity to assess the effects of El Niño on ground-water storage in southern Arizona: U.S. Geological Survey Fact Sheet 060–98, 2 p.

Philip, J.R., 1983, Infiltration in one, two, and three dimensions, *in* Slack, D.C., ed., Advances in infiltration: St. Joseph, Michigan, American Society of Agricultural Engineers, p. 1–13.

Phillips, F.M., 1994, Environmental tracers for water movement in desert soils of the American Southwest: Soil Science Society of America Journal, v. 58, no. 1, p. 15–24.

Ponce, V.M., Pandey, R.P., and Kumar, S., 1999, Groundwater recharge by channel infiltration in El Barbon Basin, Baja California, Mexico: Journal of Hydrology, v. 214, n. 1-4, p. 1–7.

Prudic, D.E., Niswonger, R.G., and Plume, R.W., 2006, Trends in streamflow on the Humboldt River between Elko and Imlay, Nevada, 1950–99: U.S. Geological Survey Scientific Investigations Report 2005–5199, 58 p.

Rangarajan, R., and Athavale, R.N., 2000, Annual replenishable ground water potential of India, an estimate based on injected tritium studies: Journal of Hydrology, v. 234, no.1-2, p. 38–53.

Renard, K.G., 1970, The hydrology of semiarid rangeland watersheds: Washington, D.C., U.S. Department of Agriculture, Agricultural Research Service Report ARS 41-162, 26 p.

Renard, K.G., Lane, L.J., Simanton, J.R., Emmerich, W.E., Stone, J.J., Weltz, M.A., Goodrich, D.C., and Yakowitz, D.S., 1993, Agricultural impacts in an arid environment—Walnut Gulch case study: Hydrological Science and Technology, v. 9, n. 1-4, p. 145–190.

Sandvig, R.M., and Phillips, F.M., 2006, Ecohydrological controls on soil moisture fluxes in arid to semiarid vadose zones: Water Resources Research, v. 42, doi:10.1029/2005WR004644.

Scanlon, B.R., Keese, K.E., Flint, A.L., Flint, L.E., Gaye, C.B., Edmunds, W.M., and Simmers, I., 2006, Global synthesis of groundwater recharge in semiarid and arid regions: Hydrological Processes, v. 20, no. 15, p. 3335–3370, doi:10.1002/hyp.6335.

Stonestrom, D.A., Abraham, J.D., Lucius, J.E., and Prudic, D.E., 2003, Focused subsurface flow in the Amargosa Desert characterized by direct-current resistivity profiling [abs.]: Eos, Transactions, American Geophysical Union Fall Meeting Supplement, v. 84, no. 46, p. F660.

Stonestrom, D.A., Prudic, D.E., Laczniak, R.J., Akstin, K.C., Boyd, R.A., and Henkelman, K.K., 2003, Estimates of deep percolation beneath irrigated fields, native vegetation, and the Amargosa River channel, Amargosa Desert, Nye County, Nevada: U.S. Geological Survey Open-File Report 03–104, 83 p.

Thomas, B.E., and Pool, D.R., 2006, Trends in streamflow of the San Pedro River, southeastern Arizona, and regional trends in precipitation and streamflow in southeastern Arizona and southwestern New Mexico: U.S. Geological Survey Professional Paper 1712, 79 p.

Troxell, H. C., 1936, The diurnal fluctuation in ground water and flow of the Santa Ana River and its meaning: Eos, Transactions, American Geophysical Union, v. 17, p. 496–507.

Walvoord, M.A., and Phillips, F.M., 2004, Identifying areas of basin-floor recharge in the Trans-Pecos region and the link to vegetation: Journal of Hydrology, v. 292, no. (1-4), p. 59–74, doi:10.1016/j.jhydrol.2003.12.029.

Walvoord, M.A., Stonestrom, D.A., Andraski, B.J., and Striegl, R.G., 2004, Constraining the inferred paleohydrologic evolution of a deep unsaturated zone in the Amargosa Desert: Vadose Zone Journal, v. 3, no. 2, p. 502–512.

Woocay, A., and Walton, J.C., 2004, Multivariate analysis of Amargosa Desert, NV groundwater chemistry [abs]: Eos, Transactions, American Geophysical Union, Fall Meeting Supplement, v. 85, no. 47, p. F862.

USGS Professional Paper 1703—Ground-Water Recharge in the Arid and Semiarid Southwestern United States—Chapter D

Streamflow, Infiltration, and Ground-Water Recharge at Abo Arroyo, New Mexico

By Amy E. Stewart-Deaker[1], David A. Stonestrom, and Stephanie J. Moore[2]

Abstract

Abo Arroyo, an ephemeral tributary to the Rio Grande, rises in the largest upland catchment on the eastern side of the Middle Rio Grande Basin (MRGB). The 30-kilometer reach of channel between the mountain front and its confluence with the Rio Grande is incised into basin-fill sediments and separated from the regional water table by an unsaturated zone that reaches 120 meters thick. The MRGB portion of the arroyo is dry except for brief flows generated by runoff from the upland catchment. Though brief, ephemeral flows provide a substantial fraction of ground-water recharge in the southeastern portion of the MRGB. Previous estimates of average annual recharge from Abo Arroyo range from 1.3 to 21 million cubic meters. The current study examined the timing, location, and amount of channel infiltration using streamflow data and environmental tracers during a four-year period (water years 1997–2000). A streamflow-gaging station ("gage") was installed in a bedrock-controlled reach near the catchment outlet to provide high-frequency data on runoff entering the basin. Streamflow at the gage, an approximate bound on potential tributary recharge to the basin, ranged from 0.8 to 15 million cubic meters per year. Storm-generated runoff produced about 98 percent of the flow in the wettest year and 80 percent of the flow in the driest year. Nearly all flows that enter the MRGB arise from monsoonal storms in July through October. A newly developed streambed temperature method indicated the presence and duration of ephemeral flows downstream of the gage. During the monsoon season, abrupt downward shifts in streambed temperatures and suppressed diurnal ranges provided generally clear indications of flow. Streambed temperatures during winter showed that snowmelt is also effective in generating channel infiltration. Controlled infiltration experiments in dry arroyo sediments indicated that most ephemeral flow is lost to seepage before reaching the Rio Grande. Streambed temperature records confirmed this, providing evidence of only two flows reaching the Rio Grande during a three-year period (water years 1998–2000). Sub-channel chloride concentrations indicate that approximately half of the seepage loss eventually becomes ground-water recharge. Vertical profiles of pore-water chloride in transects adjacent to the channel indicate that basin-floor recharge outside the arroyo is negligible under current climatic conditions.

Introduction

Abo Arroyo is an impressive example of the ephemeral streams linking lateral upland catchments to the Rio Grande, the regional axial drainage of the extensional Rio Grande Rift. The arroyo's headwaters spread over a large, elevated catchment separated from the Middle Rio Grande Basin (MRGB) by the Manzano and Los Piños Mountains (fig. 1). The exposed Precambrian bedrock of these ranges forms the southeastern border, or mountain front, of the basin. Upstream of the mountain front, Abo Arroyo comprises a dendritic system of meandering canyons cut into Paleozoic sedimentary rocks. Base flow is small and restricted to a bedrock-controlled reach near the mountain front. Downstream of the mountain front, where it lacks substantial tributaries, the normally dry arroyo cuts into unconsolidated Cenozoic sands and gravels. Abo Arroyo crosses several distinct geomorphologic settings between the upland catchment and the Rio Grande. The exposed bedrock of the upland catchment and alluvial cliffs and terraces along the arroyo reflect millions of years of landscape evolution under hydraulic conditions often different from those today.

Sparse vegetation lines the arroyo banks within the MRGB. The channel floor, free of vegetation but strewn with boulders, evinces sporadic interruption of no-flow conditions by flash flood events. Understanding present-day ground-water recharge requires information about the spatial and temporal patterns of ephemeral flows, associated streambed infiltration, and subsequent losses of infiltrated water to evapotranspiration. Because bedrock at the mountain front is largely impermeable (Anderholm, 2000), recharge to MRGB ground water from the upland catchment is primarily restricted to infiltration from flows crossing into the basin. Water that enters the basin as sub-channel seepage from the small but persistent base flow just upstream of the mountain front may also be important.

[1] Present address Berkeley, California (amystew@gmail.com).

[2] Present address D.B. Stephens and Associates, Albuquerque, New Mexico (smoore@dbstephens.com).

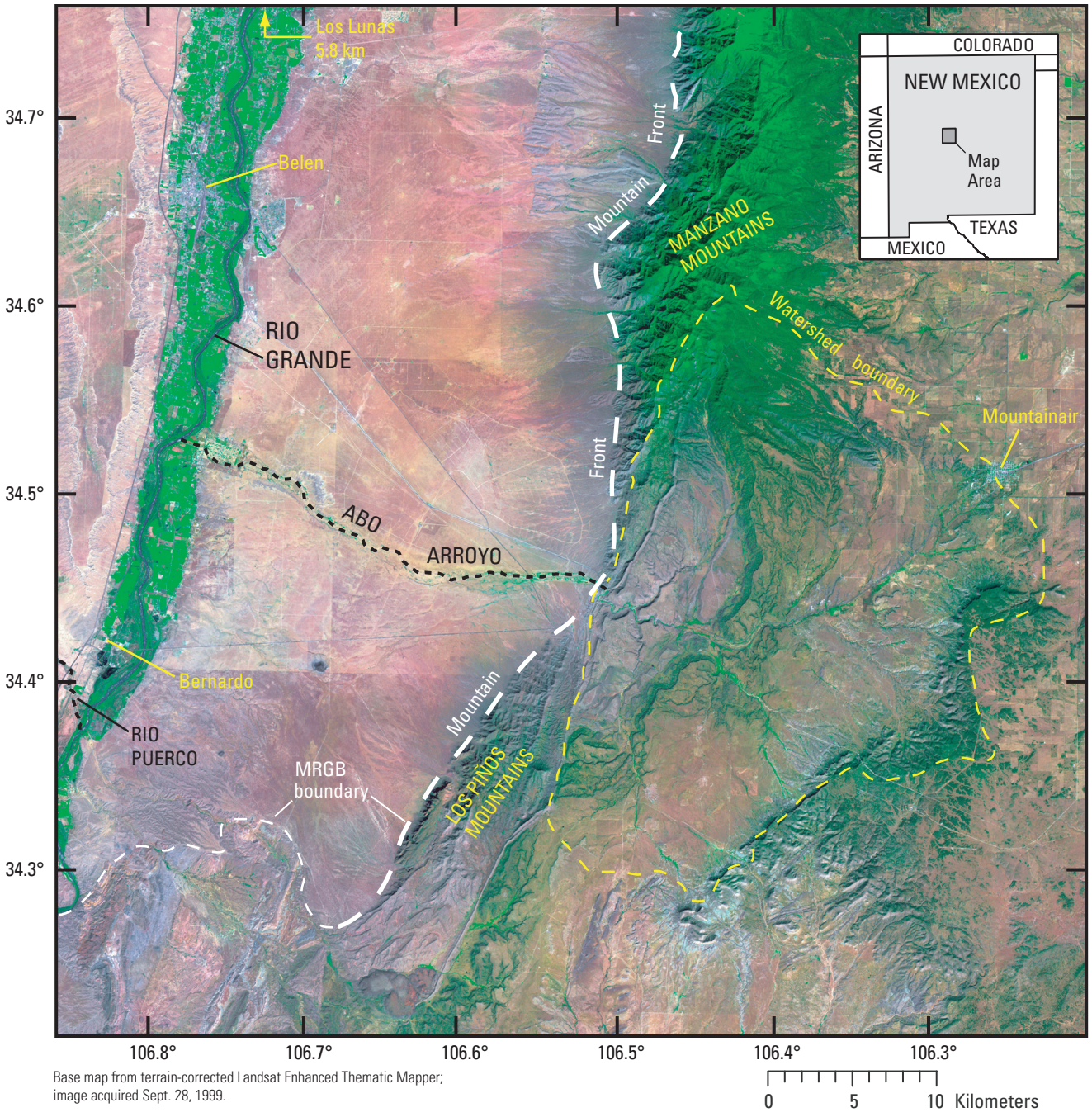

Figure 1. Abo Arroyo in the southeastern Middle Rio Grande Basin (MRGB) with its contributing watershed (upland catchment). False-color satellite image shows active vegetation as bright green, basin-fill and ancestral Rio Grande floodplain deposits as shades of pink, Paleozoic sedimentary rocks of Abo Canyon (east of the mountain front) as brown to purplish gray, basalt flows (most prominently at the south end of the Los Piños Mountains) as dark gray with red, and urban areas as speckled gray.

Traditional methods for gaging streams are ill suited to normally dry alluvial channels with infrequent, high-energy flows. Moving bedload is destructive and changes channel geometry. As a result, ephemeral streamflow data are scarce.

As a prominent example of an ungaged and undeveloped basin in the semiarid southwest, Abo Arroyo presented the opportunity to develop needed techniques for determining focused recharge from ephemeral flows. At the same time, the remoteness of Abo Arroyo presented challenges to instrument development and hydrologic conceptualization. The primary approach was to develop unattended temperature-based methods as a simple means for determining ephemeral streamflow and associated infiltration-induced recharge. Thermal techniques used at the other southwest ground water recharge sites trace their origins to this work. Abo Arroyo proved valuable for developing hydrologic concepts as well. The juxtaposition of hydraulic settings and their seasonal interactions provided a natural laboratory for studying a system dominated by ephemeral flow.

High frequency monitoring of streambed temperatures downstream of the mountain front, together with flow monitoring in the upland catchment, allowed detailed characterization of streamflow and recharge in time and space. The protocol for temperature-based determination of streamflow in arid environments evolved during the course of the study by model-guided trial and error. In addition to temperature-based monitoring, infiltration tests in dry arroyo sediments provided information on potential losses during flow events. Profiles of chloride and bromide in unsaturated-zone pore water provided supporting information on the amount of infiltrated channel water becoming ground-water recharge and on potential recharge from infiltrating precipitation adjacent to the channel. This latter work water indicated focusing of recharge beneath the active channel and long times of accumulation, or time since recharge last occurred, on terraces adjacent to the channel.

Hydrogeologic Setting

Abo Arroyo joins the Rio Grande about 65 km south of Albuquerque, between the towns of Belen and Bernardo (fig. 1). The altitude of the confluence is about 1,450 m. The 30-km study reach flows east to west, entering the MRGB through a narrow canyon separating the northern tip of the Los Piños Mountains from the southern tip of the Manzano Mountains. Maximum altitudes in these ranges reach 2,347 and 3,048 m, respectively. The arroyo crosses the mountain front at an altitude of 1,651 m. The watershed supplying the arroyo upstream of the mountain front has an area of about 650 km^2 (Anderholm, 2000).

The study reach begins near the mountain front (fig. 2). Once inside the MRGB, the arroyo cuts into the piedmont formed by coalescing alluvial fans issuing from the mountains (Hawley and others, 1982). The piedmont pinches out 5-10 km downstream of the mountain front, where Abo Arroyo cuts into a stepped sequence of abandoned fluvial terraces of the ancestral Rio Grande (Titus, 1963). The study reach terminates at its intersection with the active floodplain of the modern Rio Grande.

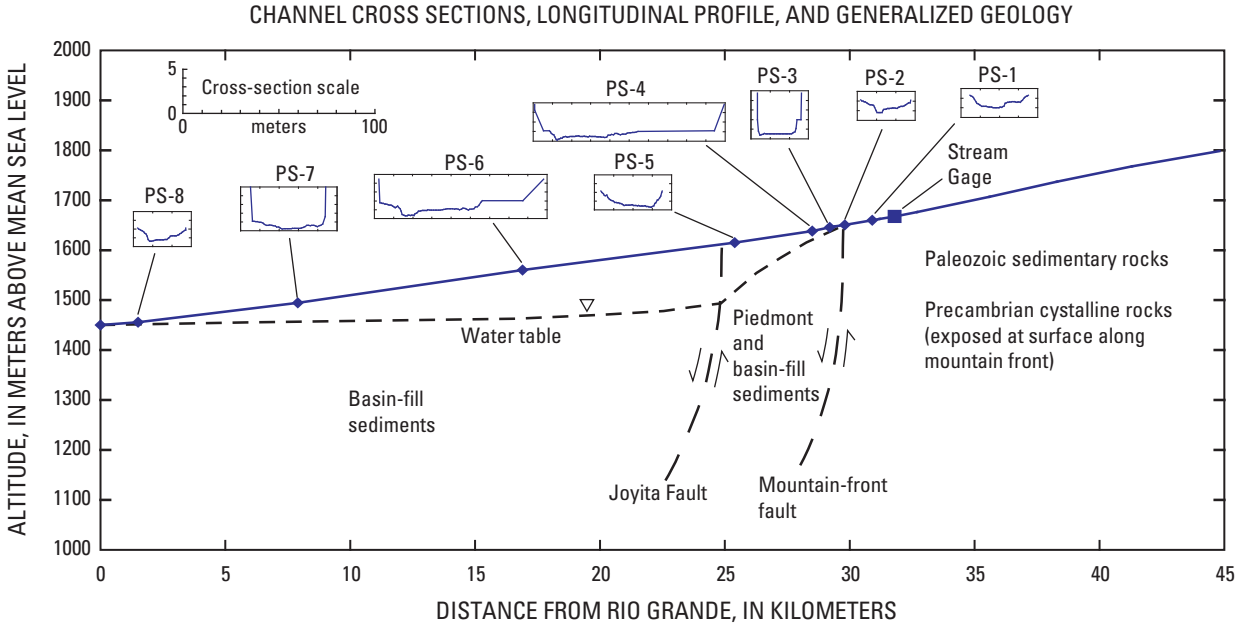

Figure 2. Longitudinal profile, and generalized geology of Abo Arroyo from its confluence with the the Rio Grande (altitude 1,450 meters) to an altitude of 1,800 meters, with channel cross-sections at probe-site (temperature monitoring) locations PS-1 to PS-8. Vertical exaggerations of the longitudinal profile and channel cross sections are 1:20 and 1:4, respectively. Longitudinal profile runs roughly west (left) to east (right). Channel cross-sections run north (left) to south (right). Water-table profile is from contour map of predevelopment levels (Bexfield and Anderholm, 2000). Locations of the Joyita and unnamed mountain-front faults are from figure 4 of Kernodle, McAda, and Thorn (1995).

Base flow is usually perennial just upstream of the mountain front, where the alluvium is thin. As the channel crosses onto the thick alluvium of the MRGB, base flow becomes nonexistent and flows are limited to short events caused by storm runoff from the upland catchment. Tributary inflows are negligible downstream of the mountain front. The unsaturated zone beneath the channel ranges from 30 to 120-m thick near the mountain front to 5 to 30-m thick near the Rio Grande (Titus, 1963; Bexfield and Anderholm, 2000).

Sediments transported into the arroyo derive primarily from Paleozoic sedimentary rocks in the upland catchment (fig. 1). The dominant source rocks are Pennsylvanian limestones and shales in the lower elevations near the mountain front, and Permian arkosic redbeds (mostly sandstones) in the higher elevations away from the mountain front (Spiegel, 1955; Dane and Bachman, 1965; Scholle, 2003). Contacts and bedding dip eastward in opposition to the channel gradient, impeding flow toward the MRGB. Within the basin, channel sediments range from boulders to fine sand near the mountain front to fine to medium sands near the Rio Grande (fig. 3). The downstream fining indicates a loss of transport power associated with high rates of channel infiltration. In the lower half of the study reach, at PS-6 and 7, the channel surface tended to crust when dry due to recessional deposition of small amounts of fines (fig. 2). Little crusting was observed upstream, where sediments were coarser.

The channel bottom supports little vegetation beyond scattered individuals of fast-growing species—mostly grasses—indicating frequent scour. Mixed vegetation lines the channel banks, with salt cedars (*Tamarix*) dominating the active floodplain upstream of the mountain front (fig. 3*A*) and near the floodplain of the Rio Grande (fig. 3*D*). Grasses, cacti, and shrubs form sparse cover on the elevated terrace adjacent to the channel (figs. 3*B*,*C*). Grasses are the most abundant plant adjacent to the channel, with shorter species near the mountain front giving way to taller species at lower elevations in the MRGB. Unexposed slopes in the upland catchment support piñon pines and junipers (figs. 3*A*,*B*)

Unconsolidated terrace sediments form dark red cliffs along the arroyo. In the middle of the study reach, the arroyo opens up to widths around 100 meters where channel banks have collapsed. The channel slope is relatively steep throughout the study reach, varying from 11 m/km near the mountain front to 6 m/km near the Rio Grande (fig. 2).

The primary land use within the Abo Arroyo section of the MRGB is rangeland. Irrigated crops grow at the downstream end of the study reach, forming a rectangular projection from the cultivated Rio Grande corridor. The upland catchment is almost entirely undeveloped (fig. 1).

Precipitation within the MRGB generally averages less than 300 mm/yr (Thorn and others, 1993). Precipitation increases in the bordering highlands due to orographic effects, reaching an estimated annual average of 760 mm along the crest of the Manzano Mountains (Anderholm, 2000). The largest amount of precipitation falls during the summer monsoon, with July, August, and September accounting for half the annual total (fig. 4). Winter precipitation at higher elevations consists primarily of snowfall, leading to occasional periods of snowmelt-supplied streamflow. Annual precipitation shows large year-to-year and sub-decadal fluctuations (fig. 5). Precipitation at Bernardo was 329 mm during the first year of the study, 54 percent above average, and 161 mm during the final year of the study, 25 percent below average. Even during the wettest years, potential evaporation (1,700 mm/yr) far exceeded precipitation (Stephens and Knowlton, 1986).

Previous Work

The desire to sustainably develop ground water has prompted repeated efforts to quantify recharge in the MRGB. Due to its large contributing area, the potential importance of Abo Arroyo was recognized by early ground-water modelers. Methods of estimating recharge, and estimates themselves, varied widely (fig. 6). The earliest estimate, a water-balance calculation by J. Dewey (reported by Kernodle and Scott, 1986), was about 19 million cubic meters per year (Mm^3 yr^{-1}). Subsequent estimates, based on outflow from the upland catchment ("basin yield"), ranged from 5 to 21 Mm^3 yr^{-1} (fig. 6). These estimates were based on nonlinear relationships—among precipitation, catchment area, and basin yield—that were developed with data from similar, gaged catchments. Basin-yield estimates assume that all streamflow exiting the upland catchment becomes ground-water recharge.

Anderholm (2000) derived an estimate of 1.6 Mm^3 yr^{-1} on the basis of an assumed steady-state mass-balance between meteoric chloride entering the catchment (in precipitation and dry deposition) and chloride leaving the catchment (in recharge to the basin aquifer). This approach used ground water near the mountain front to approximate the chloride concentration of recharge. Nimmo and others (2001) derived a nearly identical estimate by sampling the unsaturated hydraulic conductivity beneath the channel, applying Darcy's law, and distributing the calculated recharging fluxes on the basis of broad geomorphic setting (Rio Grande floodplain, ancestral fluvial terrace, and piedmont slope).

Sanford and others (2004) matched water levels, ages, and solute compositions in a numerical model of the MRGB aquifer by adjusting hydraulic properties and recharge rates. This work, which drew on extensive geochemical characterization of Plummer and others (2004), successfully simulated the shape of the MRGB water table, including a prominent trough-like feature that had not previously been explained. Simulated recharge rates for the last glacial maximum were higher than today's rates by ten to twenty times. The boundary of the numerical model was midway between the mountain front and the Rio Grande. Estimated current recharge in the modeled portion of the arroyo was 1.3 Mm^3 yr^{-1}.

Hydrochemical zonation of ground water clearly shows the imprint of Abo Arroyo recharge. Figure 7, adapted from Plummer and others (2004), synthesizes data in the southeastern MRGB. A region of relatively cool ground water lies

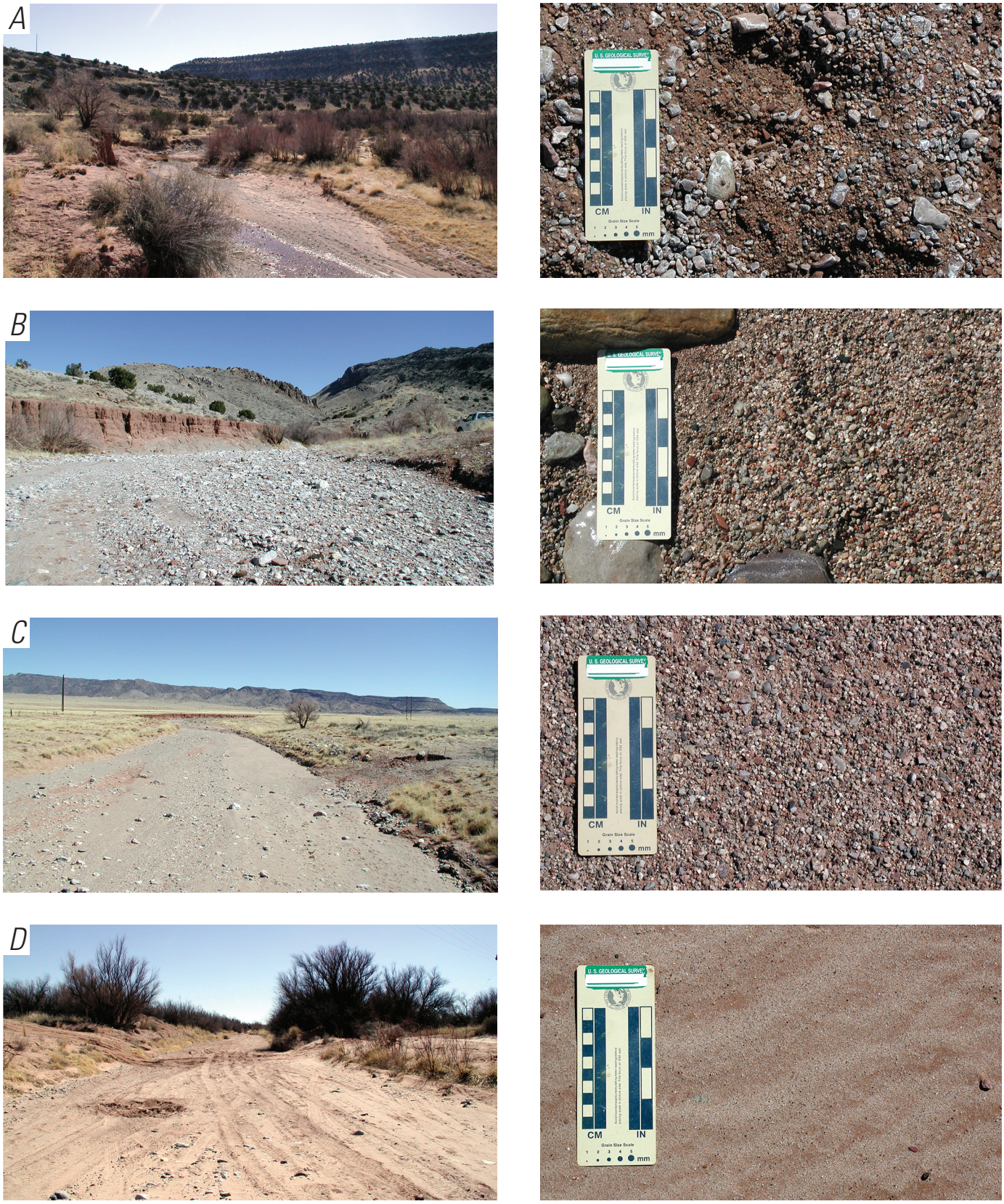

Figure 3. Photographs of Abo Arroyo sediments fining in the downstream direction, March 2003. *A,* Near site PS-1, 1.4 km upstream of the mountain front. *B,* At PS-4, 1.3 km downstream of the front. *C,* PS-6, 12.9 km downstream of the front. *D,* PS-8, 28.3 km downstream of the front. Photo *A* looks downstream (west); *B-D* look upstream (east). Figure 2 shows locations. Figure by J. Constantz and K.S. Adams.

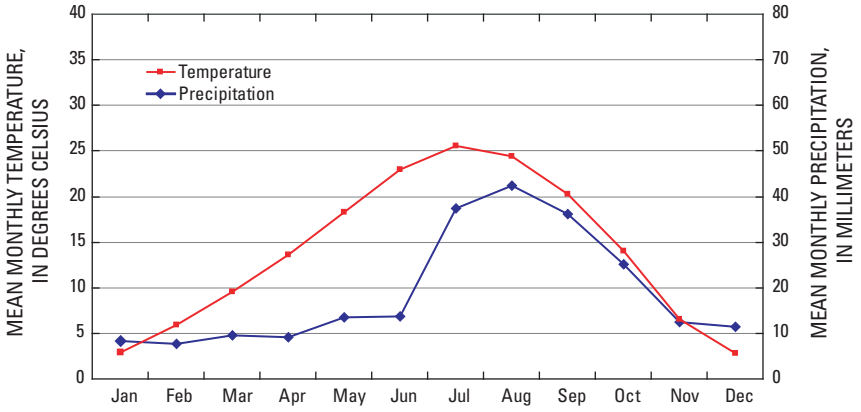

Figure 4. Mean monthly temperature and precipitation at National Weather Service station Bernardo (co-op station number 290915) for 1971 through 2000. Data from http://www.wrcc.dri.edu/Climsum.html, accessed October 30, 2006. See figure 1 for location.

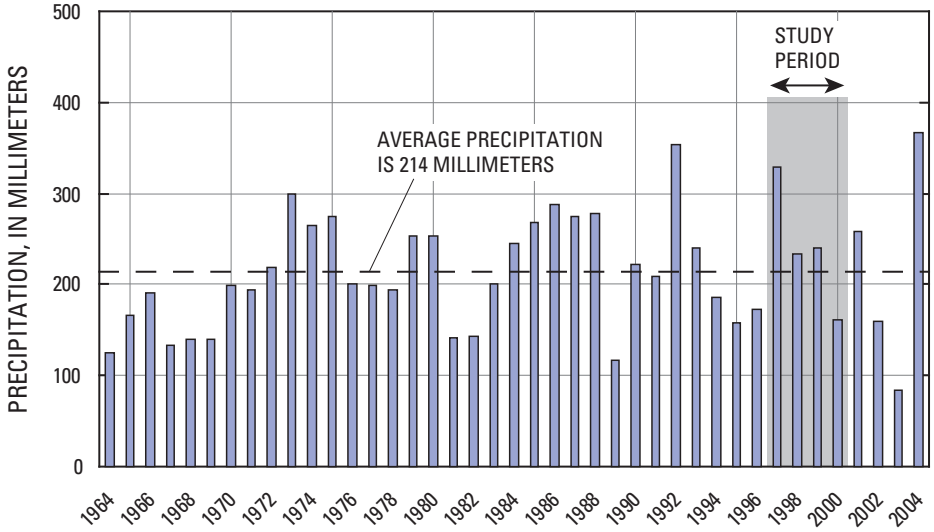

Figure 5. Total annual precipitation at Bernardo (National Weather Service cooperative station 290915) for water years 1964 through 2004. Based on monthly values obtained from http://cdo.ncdc.noaa.gov/ancsum/ACS, accessed October 30, 2006. Values for missing and incomplete months were estimated from precipitation at Los Lunas (station 295150). The Bernardo and Los Lunas stations bracket the confluence of Abo Arroyo with the Rio Grande (fig. 1).

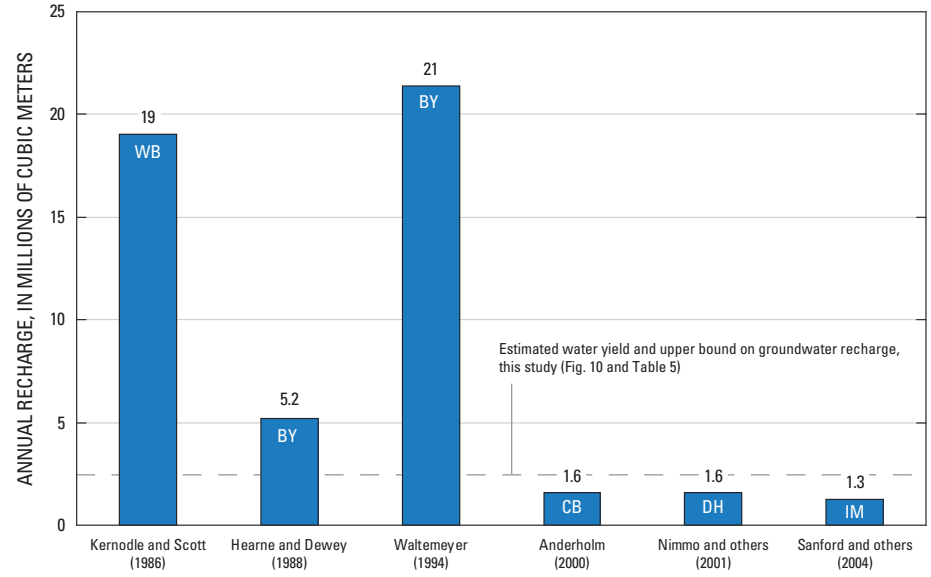

Figure 6. Previous estimates of ground-water recharge from Abo Arroyo to the Middle Rio Grande Basin. Methods included water balance (WB), basin yield (BY), chloride mass balance (CB), Darcy based hydraulic measurements (DH), and inverse modeling (IM) of ground-water heads and chemical composition. Anderholm (2000) developed the chloride mass-balance estimate and compared it to estimates he obtained with the basin-yield relations of Hearne and Dewey (1988) and Waltemeyer (1994); McAda and Barroll (2002) corrected the latter estimate to the value shown here.

beneath middle to upper reaches of the arroyo (fig. 7*A*). Sulfate-to-chloride ratios (fig. 7*B*) carry the chemical signature of the upland catchment, where Paleozoic sediments contain gypsum-bearing units. Ground-water ages become progressively older longitudinally down the channel and laterally away from the channel, with youngest ground water closest to the mountain front (fig. 7*C*).

While recent studies add greatly to the understanding of recharge within the MRGB, the wide range of estimates for Abo Arroyo highlight the uncertainties of surface-water–ground-water exchanges in strongly ephemeral systems. The timing and duration of recharge-producing streamflow and infiltration are largely unknown. The current study addressed this gap. The objectives of the study were to (1) develop thermal techniques for determining the timing and distribution of ephemeral streamflow, (2) measure actual yields of the contributing catchment during a four-year period, (3) establish the relative potential contributions of base flow and storm flow, (4) evaluate the variation of infiltration capacity along the channel, and (5) estimate the proportion of infiltration that becomes recharge, both beneath the channel and on adjacent terrace surfaces. The remainder of this report summarizes the main results.

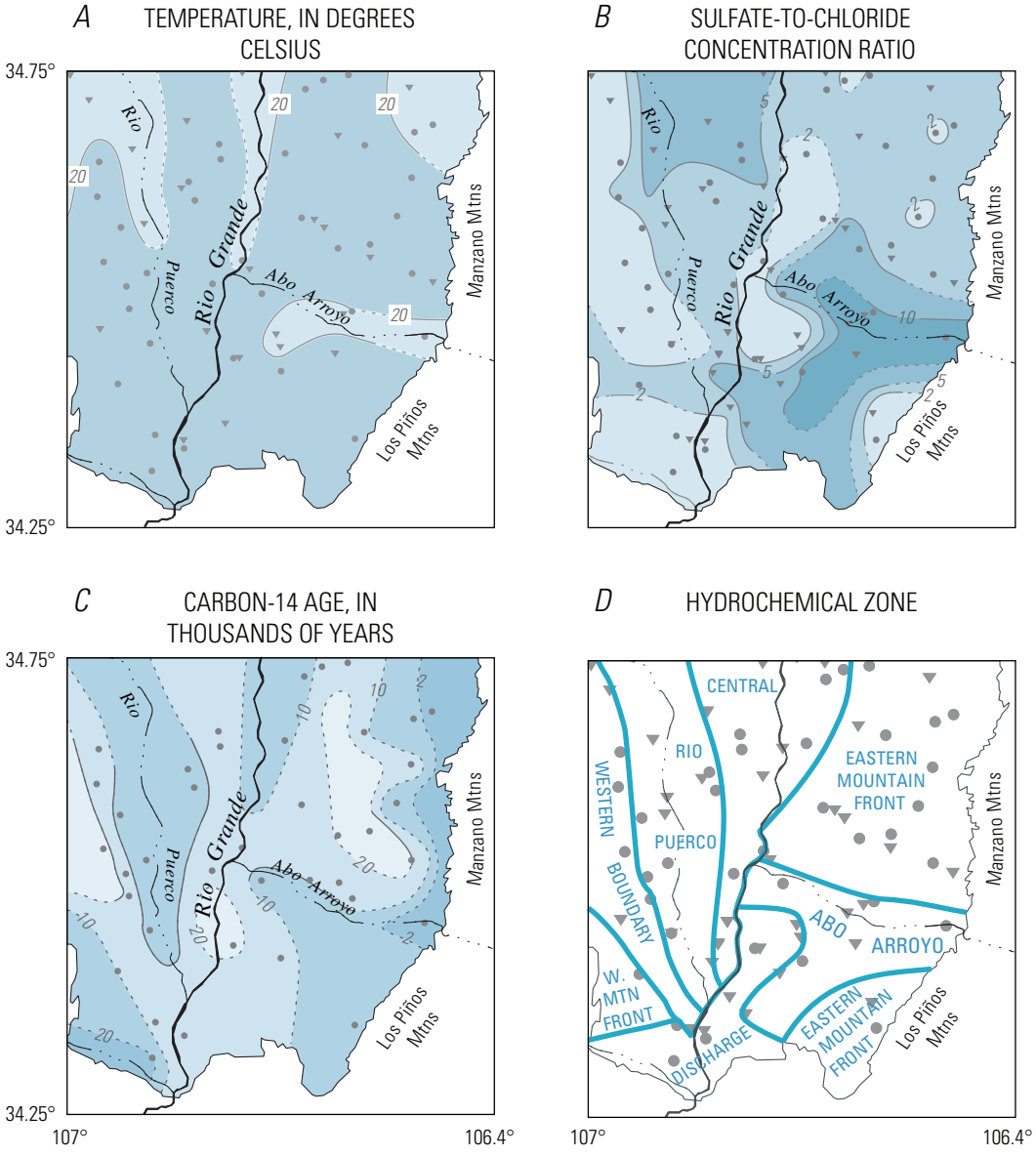

Figure 7. Physical and chemical characteristics of ground water in the vicinity of the Middle Rio Grande Basin affected by recharge from Abo Arroyo. Modified from figures 30, 35, 78, and 100 of Plummer and others (2004). *A*, Temperature. *B*, Sulfate-to-chloride concentration ratio. *C*, Carbon-14 age. *D*, Hydrochemical zone. Triangles and circles, respectively, show locations of archived (USGS National Water Information System) and newly acquired (Plummer and others, 2004) data. Contours dashed where less certain.

Methods

The present study combined long established with newly developed techniques to characterize streamflow, infiltration, and recharge within the Abo Arroyo watershed. This section provides a brief summary of instrumentation and data analysis.

Streamflow

Establishing streamflow characteristics for Abo Arroyo was a priority of the current study. Prior data were limited to annual peak-flow estimates for two tributaries high in the upland catchment—Canada Montoso, a tributary draining less than 15 percent of the upland catchment, and an unnamed tributary draining less than 1 percent of the upland catchment. An automated streamflow-gaging station was established in August 1996 as close as possible to the mountain front following procedures described in Carter and Davidian (1968). The station (USGS 08331660, Abo Arroyo near Blue Springs) monitored streamflow from August 14, 1996 through September 30, 2000 by measuring stream stage at 15-minute intervals. A pressure transducer attached to a nitrogen bubbler measured stage. The measurement point was located in a straight reach of channel two km from the mountain front containing an elevated terrace for housing the pressure transducer, gas controls, and recording equipment. The channel at the gage cut into underlying bedrock, providing stability for the rating curve and a robust anchor for the bubbler outlet. Between the gage and mountain front, the channel receives additional runoff from two tributaries that in aggregate drain almost one percent of the upland catchment. Thus, streamflow at the gage underestimates basin yield by roughly the same proportion. The larger of the two tributaries, Sand Canyon, is a large ravine that has lost most of its contributing area to stream capture by lower-order tributaries feeding Priest Canyon, which joins Abo Arroyo upstream of the gage.

Streambed Temperature

Streambed-temperature anomalies were used to infer ephemeral flow downstream of the gage, as described in Constantz and others (2001) and Stewart (2003). Attempts to detect streamflow with thermocouples (Constantz and Thomas, 1997) failed when flash floods repeatedly disrupted connections to data loggers during the first year of the study. Thereafter, self-contained data loggers (probes) recorded channel temperatures at the locations listed in table 1. Probes resolved temperature to ± 0.16 degrees Celsius (°C) within a nominal range of –5 to 37°C. Temperatures outside this range were truncated (that is, recorded as being at the respective limit). Starting in October 1997, probes were shielded in 15-cm lengths of 1.5-inch diameter schedule-40 polyvinylchloride pipe, which was tethered by aircraft cable to steel pipes driven into the channel below the depth of maximum scour. Starting in February 1998, additional probes were installed outside the channel to serve as controls for distinguishing flow-induced anomalies from anomalies caused by cloud-cast shadows, non-ponding precipitation, and other spurious signals. Initial deployments were on the channel surface to maximize sensitivity to flow. Somewhat serendipitously, sediment movement during larger flows buried several probes to various depths. Inspection of data from buried probes revealed that shallow burial filtered out most non-flow anomalies. Modeling the transport of heat and water for hypothetical test cases indicated that the optimal depth for the thermal detection of flow was approximately 0.2 m (Constantz and others, 2001). During subsequent stages of the study, the redeployment depth of all probes (test and control) was standardized at 0.2 m.

Due to the thick, permeable unsaturated zone downstream of the mountain front, high rates of infiltration accompanied ephemeral flows. Infiltrating water increases the heat capacity and thermal conductivity of channel sediments. The increase in moisture content alone would produce an anomalous temperature response to diurnal, seasonal and other perturbations. The even larger response of streambed temperatures to streamflow events (fig. 8) reflects the rapid advection of heat by infiltrating water (Constantz and others, 2001; Stonestrom and Constantz, 2004). Continuously varying convective and radiative heat exchanges between the dry channel surface and the air and sky cause temperature gradients to be a permanent dynamic of shallow sediments. The temperature of ephemeral flow usually differs from the temperature of the channel sediments prior to flow. Chemical and isotopic data show that storm flow in perennially flowing streams (such as Abo Arroyo near outlet of the upland catchment) is largely released from ground-water storage (Genereux and Hooper, 1998). Ground water has a temperature buffered toward the annual mean. During the summer monsoonal period, storm flow can be many degrees cooler than the ambient surface temperature.

Cessation of flow is less pronounced in temperature records than initiation of flow. Upon cessation, infiltration gives way to the slow process of drainage-limited redistribution. The subsurface flow rate drops sharply, and conduction replaces advection as the dominant heat-transporting process. In contrast to the abrupt change in sediment temperature associated with infiltration, the cessation of flow is marked by a gradual, conduction-dominated recovery to preflowing conditions. Consequently, the response at the end of flow is not symmetric with the response at the beginning. Nevertheless, the cessation of flow is often apparent (fig. 8).

Analysis of thermal records relied on visual inspection. Automated procedures such as the moving standard deviation method (Blasch and others, 2004) proved unreliable for detecting streamflow from Abo Arroyo thermographs due to inconsistent burial depths (Stewart, 2003).

Channel Infiltration

Infiltration measurements in dry arroyo sediments allowed evaluation of potential channel losses during ephem-

Table 1. Locations of stream-gage and channel temperature-measurement sites.

Site	Latitude[1], in degrees	Longitude[1], in degrees	Elevation[2], in meters	Distance to Rio Grande, in kilometers	Distance from mountain front[3], in kilometers
Gage	34.4469	106.4966	1667	31.8	-2.0
PS-1	34.4517	106.5006	1660	30.9	-1.1
PS-2	34.4571	106.5039	1651	29.8	0.0
PS-3	34.4590	106.5106	1646	29.2	0.6
PS-4	34.4622	106.5163	1638	28.5	1.3
PS-5	34.4592	106.5493	1615	25.4	4.4
PS-6	34.4662	106.6297	1560	16.9	12.9
PS-7	34.5075	106.7028	1495	7.9	21.9
PS-8	34.5253	106.7632	1456	1.5	28.3

[1]North American Datum of 1927.

[2]National Geodetic Vertical Datum of 1929.

[3]Channel distance. Negative value is distance upstream; positive value is downstream.

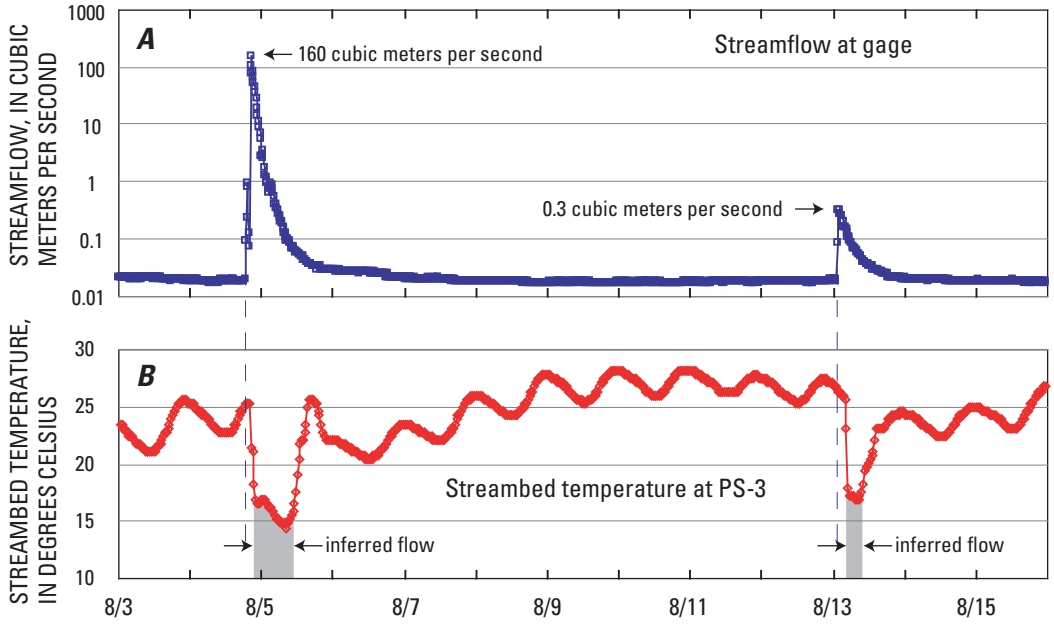

Figure 8. *A*, Streamflow at Abo Arroyo (USGS gage 08331660) and *B*, streambed temperature at probe site PS-3, 2.6 kilometer downstream (and 0.6 kilometer downstream from the mountain front), Aug. 3-16, 1998. The temperature probe was about 0.2 meters below the channel surface when recovered. Shaded areas on the thermograph indicate periods of inferred flow.

eral flow events. Preliminary measurements took place in October 1998 at PS-3, PS-6, and PS-8, 0.6, 13, and 28 km from the mountain front (fig. 2). Measurements at each site were made at three locations in the channel. Additional measurements in June 1999 revisited earlier sites as well as PS-5 and PS-7, 4.4 and 22 km from the mountain front. Measurements followed standard procedures (Bouwer, 1986); however, the rocky nature of the arroyo, especially near the mountain front, prevented hammering conventional steel rings into the ground to obtain a watertight seal.

In October 1998, single-use infiltrometers were fabricated from pairs of sheet metal strips that were formed into concentric rings and emplaced into the channel bed (fig. 9). Concrete poured into the annular space between the rings created a seal with channel sediments. Drums trucked into the arroyo supplied the infiltrometers with water. A float valve maintained a constant head of about 0.05 m while infiltration rates were measured. Infiltration runs lasted 0.5 to 2 hours, with infiltration rates usually stabilizing after 10 to 30 minutes. The circular infiltrometers had an area of 0.3 m^2. Sheet metal forms were supplanted in June 1999 with reusable wooden frames that created square infiltration basins having an inside area of approximately 0.8 m^2. The wooden forms were sturdier than the sheet metal forms and had a larger annular opening for concrete, improving the seal between the infiltrometer and the sediments. In addition to providing a better seal, the larger area of the square infiltrometers reduced effects of lateral divergence beneath the infiltrometer.

Unsaturated-Zone Solutes

Atmospherically derived solutes also served as tracers of infiltration and recharge. Unsaturated-zone chloride and bromide profiles from beneath the channel and from transects adjacent to the channel were collected in late spring and summer of 1996 and 1997, prior to the start of monsoonal storms. Channel profiles were sampled 1.2 km upstream from the mountain front and 0.3, 0.4, 2.4, 4.1, and 28.2 km downstream from the mountain front. Transect profiles were sampled on terrace surfaces adjacent to Abo Arroyo 1.4 km upstream from the mountain front and 0.4 and 4.4 km downstream from the mountain front.

Continuous cores were obtained with a hydraulically driven sampler to depths of 5–6 m on terrace transects and as deep as possible within the channel. After drying samples to determine water content, soluble salts were extracted by using methods described in Stone (1984). Chloride and bromide concentrations were determined by using single-column ion chromatography with silica-bonded ion exchangers. Analytical uncertainty was about five percent. Pore water concentrations of chloride ranged from 3 to 5,100 milligrams per liter (mg/L). Pore water concentrations of bromide ranged from less than 0.02 to 62 mg/L.

A chloride mass-balance approach was used to infer recharge rates in areas of active recharge (Edmunds and others, 1988; Allison and others, 1994) and accumulation times in areas of negligible recharge (Tyler and others, 1996). A value of 0.29 grams of chloride per cubic meter of precipitation was used to calculate atmospheric chloride deposition on the basis of atmospheric deposition collected near Santa Fe, N. Mex. (Anderholm, 1994).

Profiles of unsaturated-zone pore water beneath the channel and in transects adjacent to the channel were analyzed to evaluate the proportion of infiltrating water that becomes deep percolation and ground-water recharge from evapoconcentration of shallow pore water. Concentrations of conservative solutes beneath the depth of evapotranspirative extraction indicate the fraction of infiltrating water percolating toward the water table. This approach assumes steady-state conditions exist between the time-averaged mass flux of solute at the land surface and at the sampling depth (Edmunds and others, 1988). Alternatively, where steady conditions do not exist, the mass of accumulating solute from the imbalance between infiltration and deep drainage indicates the time since recharging conditions last prevailed (Tyler and others, 1996).

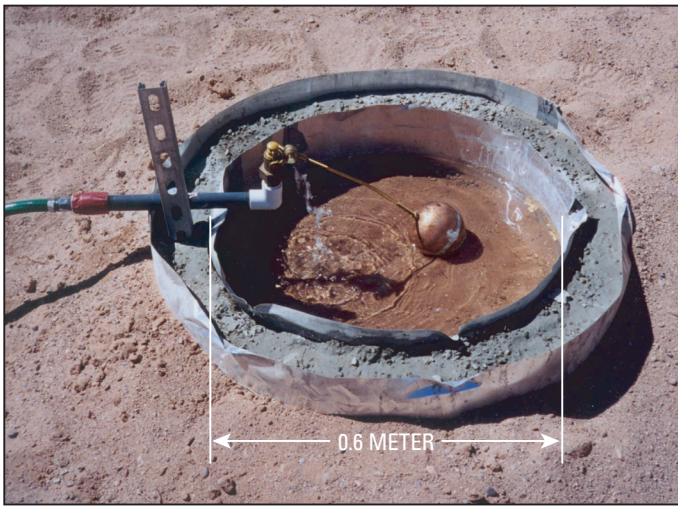

Figure 9. Single-use infiltration ring showing concrete seal and flow-regulating valve that maintains constant depth of ponding during measurements.

Results and Discussion

Streamflow Characteristics

Streamflow in Abo Arroyo reflects the interaction of monsoon-dominated precipitation with the relatively large proportion of exposed bedrock comprising the upland watershed. Streamflow responds quickly to storms. Base flow (perennial flow between storms) is minimal in volume and extent. Only at the gage does base flow persist. Except for possible snowpack, the storage capacity of the upland catchment would seem limited by the relatively impermeable bedrock. Even so, only a small fraction of precipitation becomes streamflow.

Annual streamflow increases non-linearly with annual precipitation (fig. 10). Orographically weighted average precipitation in the upland catchment about 368 mm per year (Anderholm, 2000), 1.7 times higher than the average at Bernardo (214 mm, water years 1964–2004). Adjusting measured precipitation amounts at Bernardo (altitude 1443 m above sea level) by a factor of 1.7 yields the estimated precipitation for the upland catchment (1660–3048 m above sea level) for each year of the study. Multiplying these values by the area of the upland catchment (650 km^2) approximates the yearly volumes of precipitation contributing to streamflow at the gage. The total streamflow in WY 2000, the driest year, represented about 1 percent of the estimated precipitation volume. The total streamflow in WY 1997, the wettest year, represented about 9 percent of the precipitation volume. Streamflow volumes in water years 1998 and 1999 each represented about 3 percent of estimated precipitation. As annual precipitation increases, runoff volumes rise disproportionately (Langbein, 1949). The upward curvature of the relation between annual streamflow and precipitation (fig. 10) reflects the decreasing relative importance of evapotranspiration, sublimation, and depression-storage losses as precipitation increases in the watershed.

Total annual streamflow during the study period ranged from 0.8 to 15.3 million cubic meters (Mm^3), a factor of 19. In contrast, precipitation at the Bernardo weather station during the same time varied between 161 and 329 mm, a factor of 2, (fig. 10). Annual streamflow was largest during WY-1997, when annual precipitation at Bernardo (329 mm) was 154 percent of the 41-year average. Water year 1997 was the third wettest year on record. Annual streamflow was smallest in WY 2000, when annual precipitation at Bernardo (161 mm) was 75 percent of the 41-year average. The total annual streamflow corresponding to the long-term average annual precipitation, which approximates the average annual basin yield, is about 2.0 Mm^3. This is less than one tenth of the largest previous estimated basin yield (fig. 6).

Records of daily mean and peak instantaneous streamflows illustrate the ephemeral, flashy nature of Abo Arroyo discharge. Daily mean streamflows (the average of all 15-minute instantaneous streamflows on a given day) varied from zero to 37.7 m^3/s during the four-year study period (fig. 11). The four-year median value of 0.012 m^3/s was less than 1/3000 of the maximum. Annual median values varied from 0.006 m^3/s in WY 2000 to 0.025 m^3/s in WY 1998 (table 2). Daily mean streamflow was 37.7 m^3/s on June 6, 1997 during a monsoonal flow that lasted eight hours at the gage. Maximum instantaneous streamflow on that day was 195.5 m^3/s.

The highest instantaneous streamflow during the study period, 227 m^3/s, occurred on July 31, 1997, during the second of two flash floods arriving roughly eleven hours apart. Each event lasted about four hours. Daily mean streamflow was 32.6 m^3/s on that day.

Flow at the gage is bimodal, with brief storm flows interrupting long periods of minimal base flow. Ninety-five percent of daily average values (average flows on 1386 days) were less than 0.058 m^3/s (inset, fig. 11).

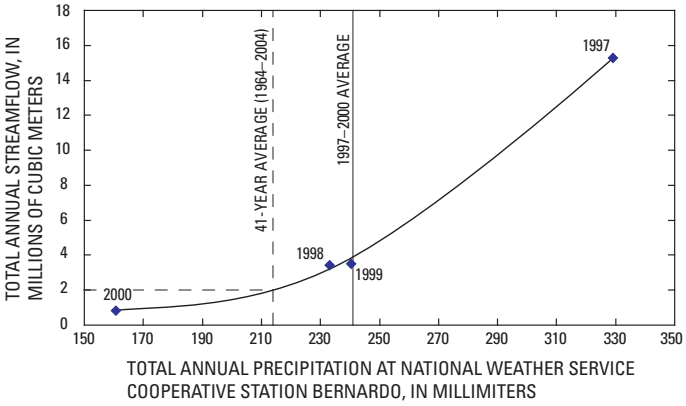

Figure 10. Relationship between annual streamflow at the Abo Arroyo gage (USGS 08331660) and annual precipitation at Bernardo (National Weather Service cooperative station 290915) for water years 1997–2000.

Base flow is critical for sustaining the riparian ecosystem near the mountain front. In terms of duration, base flow dominates the four-year record. In terms of volume, however, storm flow accounts for nearly all water passing though the gage. Ranked average daily streamflows show a sharp inflection at the 95-percentile level (inset, fig. 11). Defining the corresponding flow rate, 0.058 m^3/s, as the threshold between base flow and storm flow, 80 percent of the total flow in WY 2000, the driest year, was storm flow (table 2). The channel was dry for periods up to 29 days at the gage in that year (fig. 11). In WY 1997, the wettest year, storm flow accounted for 98 percent of total flow at the gage, even though the channel flowed throughout the year. While brief even in aggregate, monsoonal storm flows dominate the discharge from the upland catchment. Basin recharge from streambed infiltration is almost entirely from storms associated with summer monsoons.

Temperature-Based Indications of Flow

The channel at the mountain front was seasonally persistent, as documented by site visits (fig. 12). Streambed temperatures exhibited three distinct patterns—two when flowing and one when dry. During water years 1998 and 1999, which had typical precipitation, diurnal temperature amplitudes dropped sharply for 10–14 weeks following the onset of monsoonal storms. The pattern was already in effect at the beginning of the thermograph record, following monsoonal storms in 1997. Diurnal amplitudes generally remained below 2–3°C; daily averages remained relatively constant and close to the average annual temperature (in the range of 15–20°C). The channel was flowing when visited during these periods. In WY 1997 and 1998, starting in October or November, these relatively constant periods were followed by 7–8-month periods of intermediate diurnal amplitudes (typically 5–10°C) that tracked the seasonally varying temperature. The channel was also flowing when visited during these periods. The intermediate periods

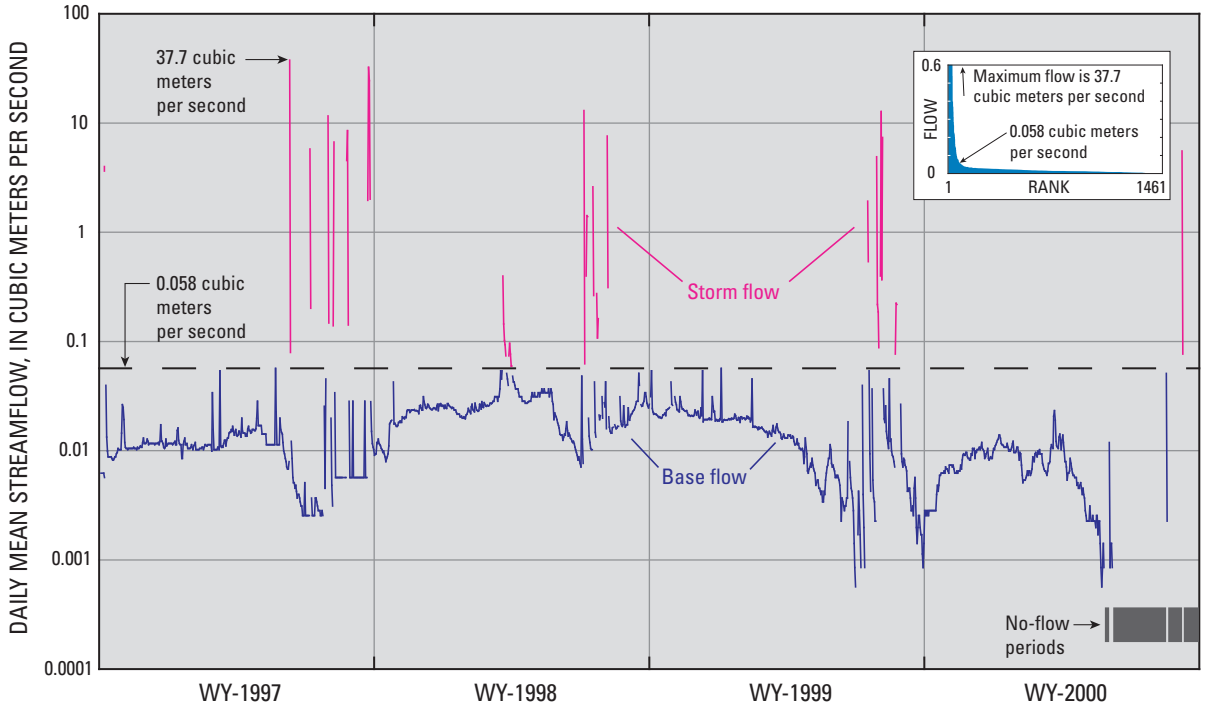

Figure 11. Daily mean streamflow at Abo Arroyo (USGS gage 08331660) during water years 1997-2000. Inset shows ranked values on a linear scale truncated at 0.6 cubic meters per second to display low flows. The dashed line on the main plot is the level below which 95 percent of daily mean streamflows occurred. This threshold operationally divides storm-generated runoff from base flow. Of the 75 values greater than the threshold, 88 percent (66) occurred within one day, all but one within three days, and none more than four days of a storm-induced runoff event. The total number of daily values is 1461.

Table 2. Stream flow at Abo Arroyo (USGS gage 08331660) for water years 1997-2000. Summary daily statistics and total storm-flow versus base-flow volumes.

[Derived from daily means data obtained at http://waterdata.usgs.gov/nwis; accessed September 25, 2006]

Water year[1]	Median daily average flow, in cubic meters per second	Maximum daily average flow, in cubic meters per second	Minimum daily average flow, in cubic meters per second	Total volume[2], in millions of cubic meters	Storm-flow volume[2], in millions of cubic meters	Base-flow volume[2], in millions of cubic meters	Storm-flow proportion of total volume, in percent
1997	0.011	37.7	0.003	15.3	14.9	0.3	98
1998	0.025	13.0	0.007	3.4	2.8	0.7	80
1999	0.015	12.7	0.000[3]	3.5	3.1	0.4	88
2000	0.006	5.6	0.000[4]	0.8	0.7	0.2	80
Four-year study period							
1997–2000	0.012	37.7	0.000[5]	23.1	21.4	1.6	93

[1]Water year is October 1 through September 30 and denoted by calendar year in which it ends.

[2]Values rounded for reporting purposes. Calculations used unrounded numbers, causing apparent discrepancies in least significant digit.

[3]Channel was dry for periods of 1–2 days (4 days total during water year).

[4]Channel was dry for periods of 4–29 days (112 days total during water year).

[5]Channel was dry for a total of 116 days during the four-year study period.

were followed by abrupt transitions to high diurnal amplitudes, often exceeding 15°C, which also tracked the seasonal temperature. The channel was dry when visited during these periods (fig. 12).

The response of sediment temperatures to diurnal forcing from the atmosphere reflects not only the presence or absence of flowing water, but also the direction of water exchange between the stream and underlying sediments. Gaining streams show smaller diurnal temperature variations than losing streams because ground water is buffered from fluctuations at the land surface (Constantz and Stonestrom, 2003). Thus, periods of relatively constant temperatures suggest gaining conditions. The mountain-front thermograph shows seasonal cycles of monsoonally driven gaining conditions followed (in water years 1997 and 1998) by losing conditions followed (in all water years) by dry conditions. The period of channel loss in WY 1999 was too short to resolve as drought set in at the end of the study.

Figure 13 illustrates streamflow at the gage together with temperatures in the channel and adjacent to the channel for August 1999, which was an active monsoonal period. This period included eleven flows with peaks that ranged from less than 1 m^3/s to 155 m^3/s. Shading on the streambed thermographs indicates periods of inferred flow. Despite variations among records reflecting differences in burial depths, the utility of streambed thermographs for inferring ephemeral flow downstream of the gage is readily apparent.

Analysis of thermographs provides information about the timing and duration of ephemeral flows within the basin. The majority of flows extending into the basin occurred in July through September. Comparison of thermographs with

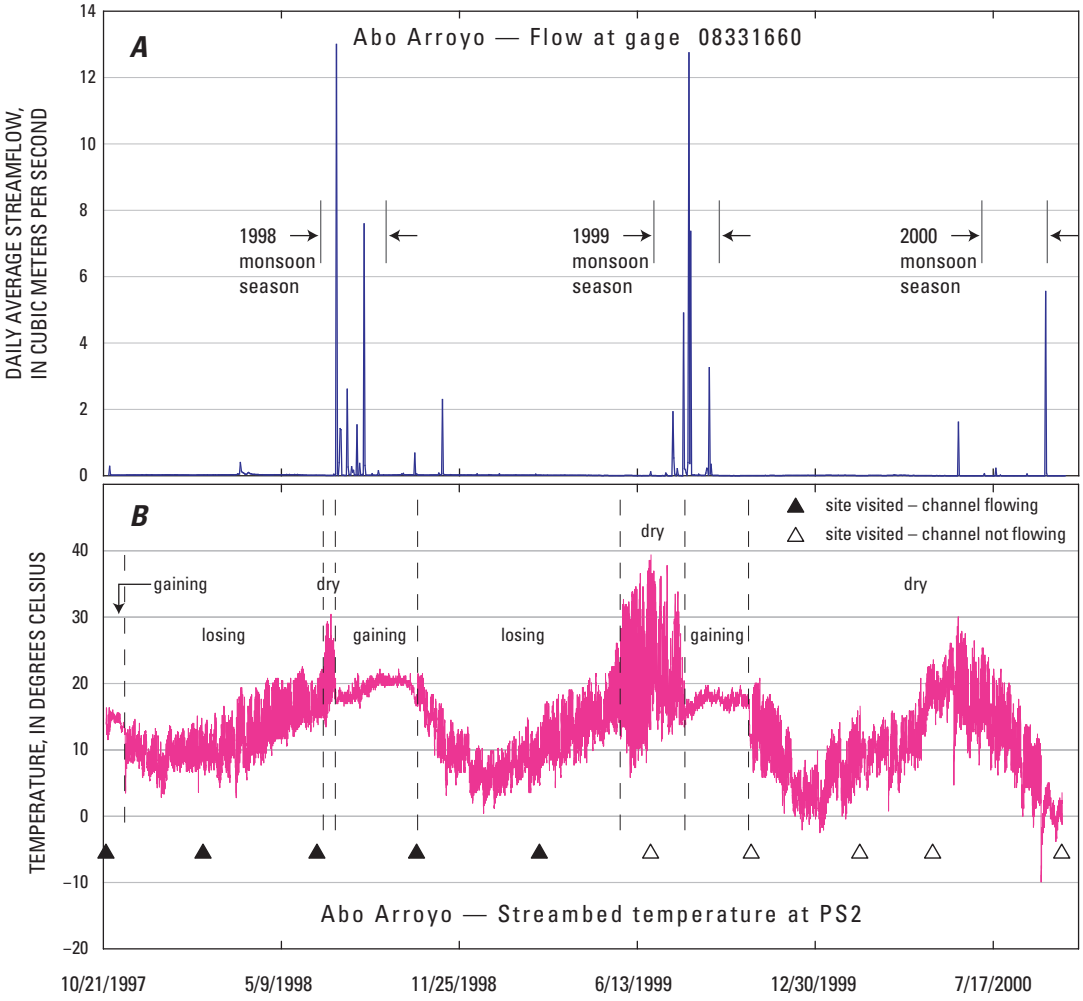

Figure 12. Relation between streamflow and mountain-front channel temperatures for the period of record at the mountain-front temperature logger (probe site PS-2, two kilometers downstream from the gage). *A*, Monsoonally driven streamflow at the Abo Arroyo gage (USGS 08331660). *B*, Mountain-front streambed thermograph and interpretation of temperature patterns as seasonally driven transitions from a monsoonally induced gaining state (ground water entering the reach) to a post-monsoonal losing state (stream water leaving the reach) to a dry state. The preceding water year (1997) had 154 percent of normal precipitation; water years 1998-2000 ranged from 112 to 75 percent of normal. Filled and hollow triangles indicate channel state during site visits.

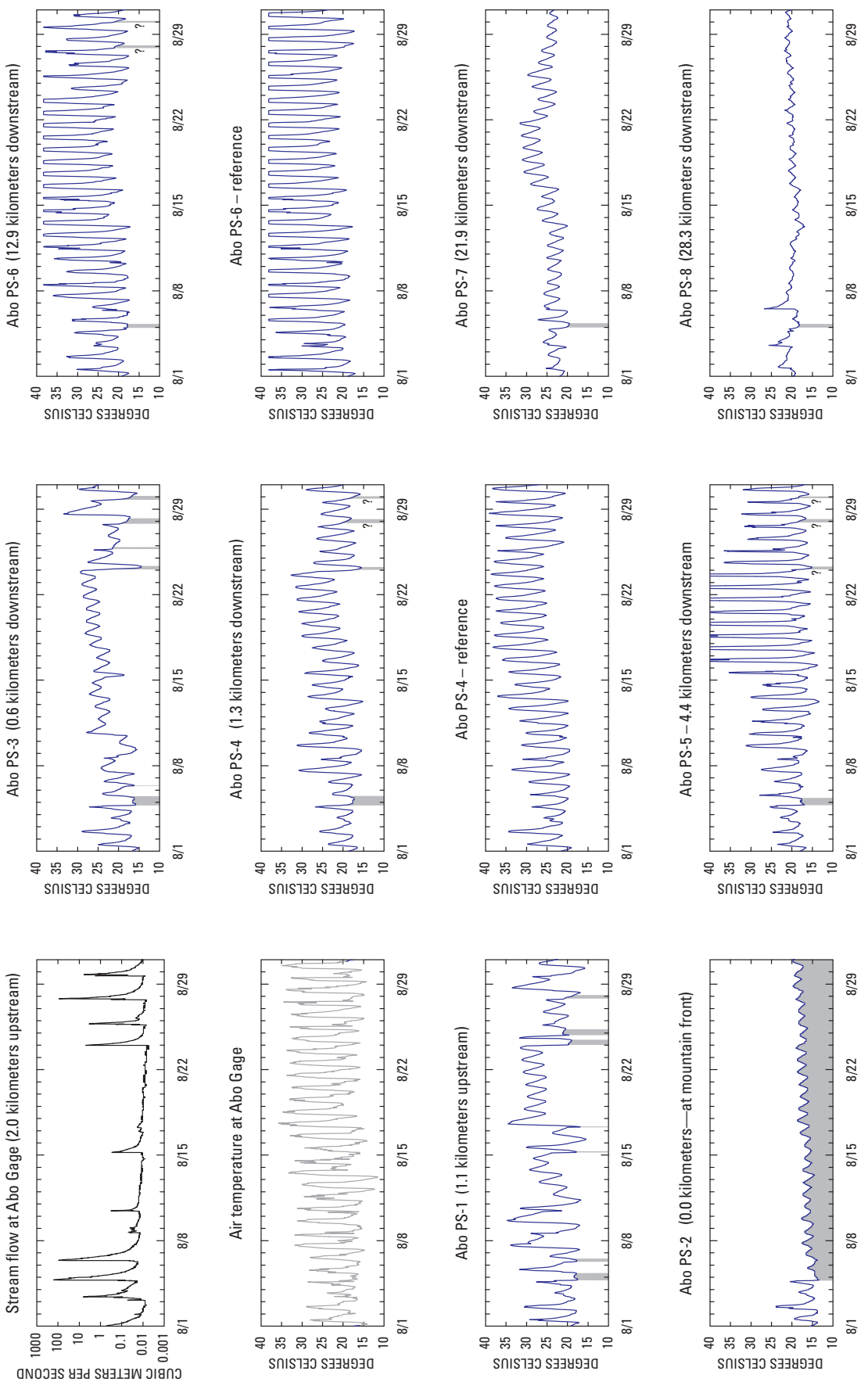

Figure 13. Streamflow at gage (measured) and downstream (shaded areas, as inferred from channel and reference temperatures), Abo Arroyo, New Mex. August 1999.

streamflow at the gage provided information on the general relationship of catchment flow and ephemeral flow downstream of the gage. Infiltration losses during ephemeral flows are high, with only the largest flows reaching the Rio Grande. Flows were classified according to how far into the basin they extended (table 3). Class I flows extended all the way the Rio Grande floodplain. Class II flows extended at least a kilometer into the basin, as detected by PS-4 (1.3 km from the mountain front), but did not reach the Rio Grande. Class III flows infiltrated into the coarse sediments near the mountain-front, upstream of PS-4. Storm hydrographs exhibited a high degree of self-similarity, with roughly similar shapes regardless of magnitude (fig. 8). The duration of classified flows varied from 3.0 to 6.5 hours, with a median duration of 5.0 hours (table 3).

Stewart (2003) presents the complete set of thermographs for Abo Arroyo. The record includes a number of gaps and is of a shorter duration than the streamflow record. Therefore, the relationship between flow in the MRGB inferred from available thermal data and flow at the gage was applied to the entire streamflow record to provide statistics for the four-year study period. Inspection of the thermographs indicated that runoff events with peak flow rates greater than about 150 m^3/s extended all the way to the Rio Grande floodplain. Similarly, those with peak flow rates exceeding a value of about 12 m^3/s extended past PS-4. In general, those with peak flows smaller than 12 m^3/s did not reach PS-4 (table 3).

Applying these thresholds to the stream flow record, there were five class I flows during the four-year period (two each in WY 1997 and 1998, one in WY 1999, and none in WY 2000), or on average about one per year. There were 17 class II flows during the four-year period, or about four per year. Nearly all of the class I and class II flows (18 in total) occurred in the months of July, August, and September. Four class II flows occurred in June and October (two in each month). Including snowmelt-generated events, there were 84 class III flows during the four-year period, or about 21 per year.

Snowmelt events were type III, with one exception. In December 1997, an unusually large amount of snow fell throughout the area, accumulating on the higher mountains. National Weather Service cooperative weather stations at Bernardo (altitude 1443 m), Los Lunas (1475 m), and Mountainair (1987 m) recorded greater than 0.20, 0.28, and 0.53 m of snowfall for the month, with the heaviest snowfall at Bernardo falling on December 20. At higher altitudes (2,600-2,900 m), three SNOTEL stations within a radius of 173 kilometers from PS-2 (stations 06p01s, 05p04s, and 07s04s, with azimuths from north relative to PS-2 of 3, 24, and 225°) recorded regional snowstorms on December 1-3, 6-8, 10, and 20-27 (USDA-NRCS, 2006). The cooperative weather station at the

Table 3. Classification of ephemeral flows by thermally determined downstream distance.

Class[1]	Time of peak flow[2]	Peak flow value, in cubic meters per second	Event flow volume, in millions of cubic meters	Event flow duration[3], in hours
I	1998/07/04 16:30	181.7	22.17	5.0
I	1999/08/04 18:45	154.9	25.41	5.7
II	1999/08/06 09:15	91.2	16.12	6.5
II	1999/08/27 19:15	86.5	3.28	3.0
II	1998/07/16 21:15	43.9	3.77	4.0
II	1998/07/08 17:45	37.6	2.28	5.3
II	1998/07/27 16:15	37.6	1.66	3.2
III	1998/07/07 18:15	11.1	0.49	3.8
III	1998/07/30 17:15	8.3	0.47	4.0
III	1998/07/21 22:00	6.6	0.66	5.8
III	1999/08/03 09:30	6.3	0.65	5.5
II	1999/08/23 23:45	4.7	0.47	5.0
III	1999/08/25 17:45	3.3	0.34	4.7

[1]Class I flows extended to the Rio Grande floodplain. Class II flows extended past probe site PS-4, 1.3 kilometers from the mountain front. Class III flows dissipated prior to reaching PS-4.

[2]Mountain standard time.

[3]Cutoff for event duration was 2.5 percent of the respective peak flow value.

Albuquerque airport, which records detailed hourly weather conditions, recorded snow on December 3 and 10–11, followed by alternating periods of snow and light rain December 20–25.

The Abo gage recorded only minor increases in stream flow above base-flow levels (fig. 11). In contrast, streambed thermographs indicated extended periods of snowmelt-fed infiltration throughout the channel, starting on December 20 (fig. 14). At PS-3, 0.6 km from the mountain front, infiltration continued until January 3, 1998. At PS-8, 28 km from the mountain front, the infiltration period was shorter, lasting only 1–2 days. Nearly constant, slightly positive streambed temperatures indicated the presence of liquid water in sufficiently close proximity to melting snow and ice to regulate the temperature. Once proximal snow and ice had melted, removing the source of infiltrating water as well as the regulation of temperature by the latent heat of fusion, streambed temperatures again followed air temperatures (fig. 14).

These results show that snowmelt can lead to extended periods of infiltration. The rate of melt-water generation, as indicated by the stream gage, in this case was low. The rate of infiltration was presumably similarly limited by the rate of melt-water generation (supply controlled). While not observed during the four-year study period, the potential exists for considerably larger flows generated by rain from a slowly moving frontal system melting heavy snowpack.

Stream-Channel Infiltration

Infiltration measurements along the dry arroyo allowed evaluation of potential seepage variations during ephemeral-flow events. The first measurements, with the 0.3 m^2 infiltrometer (see methods) were in June 1998 after the channel had been dry for eight months. Subsequent measurements, with the 0.8 m^2 infiltrometer, were in October 1998 and June 1999. The channel had been dry for two and five months, respectively, prior to the latter measurements.

The first set of measurements suggested that potential infiltration rates decreased down channel toward the Rio Grande (fig. 15). Point-to-point variability was large, especially near the mountain front (28 km from the Rio Grande). This was consistent with expectations, as sediment size decreased while sorting increased down channel. However, the smallest value was obtained near the mountain front, in a fine-invaded low-flow channel. Leakage was often difficult to eliminate, especially with the sheet-metal forms in the coarsest sediments. The larger wooden forms of the square infiltrometers created better concrete seals. Subsequent measurements with the large infiltrometers suggested less dependence on location (square symbols, fig. 15).

Quasi-steady rates from the large infiltrometers averaged 5.5×10^{-5} m/s with a standard error of 1.2×10^{-5} m/s (fig. 15). Early time infiltration rates ranged from 0.3 to 2 mm/s. The product of the infiltration rate and the wetted area of the channel gives a lower bound on instantaneous loss rate during early flow. The channel at PS-4, 1.3 km downstream of the mountain front, is about 90 m wide (fig. 2). Assuming an infiltration rate of one mm/s, the corresponding loss rate at PS-4 would be about 0.3 Mm^3 per kilometer of channel per hour. This rate can account for the observed flow loss in most cases, and underestimates losses due to seepage into channel banks and due to higher hydraulic-pressure gradients during streamflow than during infiltrometer measurements. Thermographs show that infiltration losses consume most flows in transit. Computational methods for estimating seepage losses from a transient pulse of water moving down an initially dry, permeable channel are currently under development (Niswonger and others, 2006). Flood-pulse velocities in such situations can be an order of magnitude slower than predicted by standard equations for the propagation of kinematic waves.

Environmental Tracers

Profiles of pore-water chloride and bromide indicate focused recharge beneath the active channel of Abo Arroyo and no recharge currently on the adjacent terrace. Figure 16 shows water content and solute profiles near PS-1. Bromide concentrations mimic those of chloride, supporting assumptions of conservative behavior and meteoric origin. Chloride and bromide concentrations beneath the channel are uniformly low, indicating continued removal of infiltrating solutes by deep percolation and recharge. In contrast, profiles beneath the adjacent terrace surfaces show large accumulations of chloride and bromide between depths of 0.1–0.5 m—the approximate bottom of the root zone—and 5 m. Solute profiles near PS-1 (fig. 16) were intermediate between those near PS-3, closer to the mountain front, and PS-5, farther from the mountain front. Channel profiles varied little throughout the reach.

Anderholm (1994) determined the amount of chloride in wet fall and dryfall near Santa Fe in the Española Basin, an upland catchment draining into the northeast portion of the MRGB. Assuming the same effective concentration in precipitation at Abo Arroyo as that measured near Santa Fe (0.3 grams of chloride per cubic meter of precipitation) and an average precipitation rate of 0.3 m/yr at the mountain front, the meteoric deposition rate is 0.09 gram of chloride per square meter of land surface per year. Assuming the chloride deposition rate has remained relatively constant, the time required to accumulate a given mass of chloride is the profile inventory divided by the deposition rate (both expressed per area of land surface).

Figure 17 and table 4 summarize the chloride inventories for transects near PS-1, PS-3, and PS-5. Figure 17 shows the inventories in integral form (cumulative mass of solute per cumulative volume of water, starting at land surface). The slope of each curve indicates the pore-water concentration. Curves representing the channel profiles are approximately linear with low slopes, indicating low concentrations, consistent with steady movement of chloride through the profile by recharging water. Curves representing profiles away from the channel and mountain front are non-linear, with higher slopes near the land surface, at the origin of each plot. These

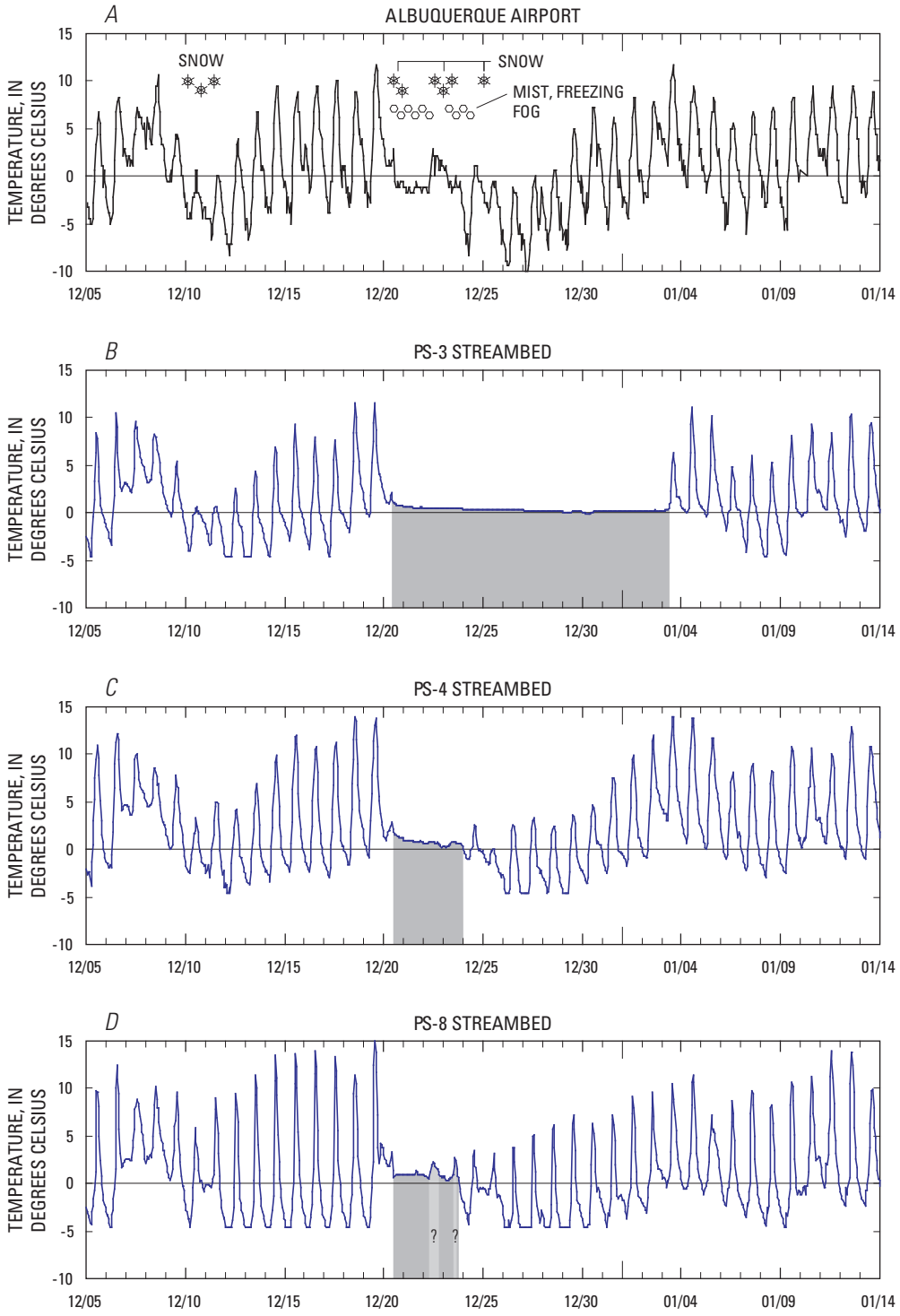

Figure 14. Weather conditions and channel-surface temperatures for Abo Arroyo downstream from the mountain front for period marked by snow accumulation, followed by extended period of snowmelt infiltration. *A*, Air temperature and logged weather conditions at Albuquerque airport (National Weather Service cooperative station 290234, about 63 kilometers north of PS-4, elevation 1617 meters; data from http://cdo.ncdc.noaa.gov/ulcd/ULCD, accessed Nov. 3, 2006). *B–D*, Streambed thermographs at PS-3, PS-4, and PS-8, respectively, 0.6, 1.3, and 28.3 kilometers downstream from the mountain front. Shading indicates intervals of inferred snowmelt infiltration. Graphs show data from December 5, 1997 to January 14, 1998.

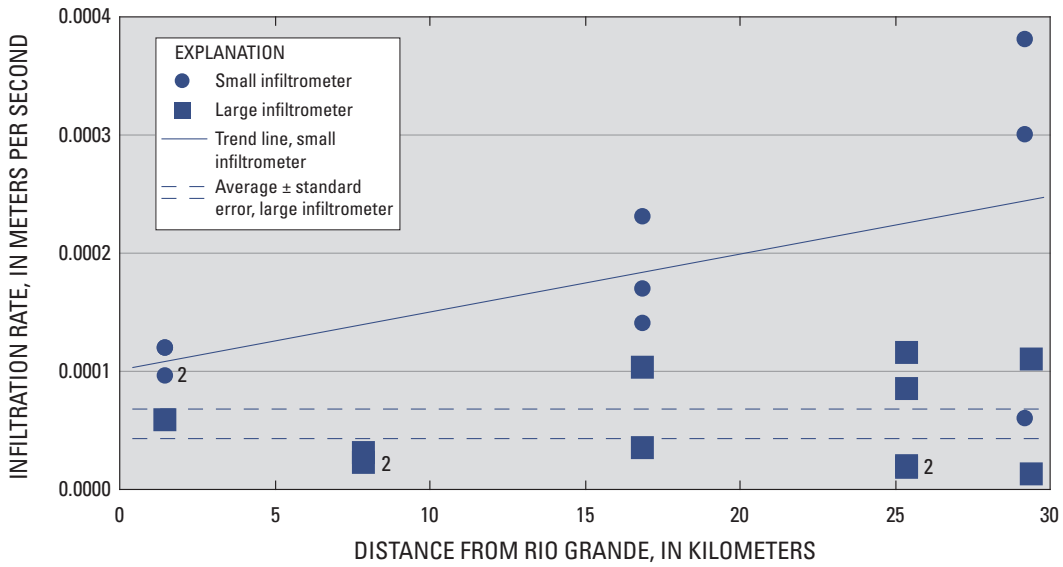

Figure 15. Late-time (quasi-steady) infiltration rates in the dry streambed of Abo Arroyo at five locations between the mountain front and the Rio Grande. Preliminary measurements with the small infiltrometer were in June 1998. Subsequent measurements with the large infiltrometer were in October of 1998 and June of 1999. Numbers next to data symbols indicate number of overlapping points.

high slopes correspond to the sub-root bulges of figure 16 and indicate net accumulation of incoming solutes under current climatic conditions.

Chloride inventories beneath the terrace are large, reaching 1.3 kg/m^2 in the top 8.5 m of unsaturated zone 0.5 km from the channel near PS-5, 4.4 km from the mountain front (table 4). This amount of chloride represents 15 thousand years of accumulation at current rates of deposition. Chloride inventories in terrace profiles near PS-3, close to the mountain front, represent six to seven hundred years of accumulation in the sampled interval (uppermost 4–5 m). Integral solute profiles are straighter closer to the mountain front (fig. 17). These locations were evidently flushed more recently, perhaps by snowmelt from the adjacent mountains during a cooler climatic period.

All transect profiles indicate negligible recharge through terrace surfaces and focused recharge beneath the channel. Conventional chloride mass-balance calculations assume steady state conditions, which do not apply to the terraces at present. Such calculations, however, provide an upper limit on recharging fluxes. This upper bound for terrace profiles varied from 0.04 mm/year (near PS-5) to 0.9 mm/year (near PS-3). Current recharge rates are lower, and may be negative. Studies in arid and semiarid basins suggest that under current climatic conditions there may be small amounts upward flow across the water table in much of the MRGB (Scanlon and others, 2006). Even a positive recharge rate of 1 mm/yr for the entire Abo recharge zone (fig. 7) would provide less than 0.3 Mm^3 per year of total recharge. Direct recharge through extra-arroyo surfaces is clearly minimal.

The concentration of chloride in pore-water becomes higher than that of infiltrating streamflow due to evaporative losses of water during dry periods between flows. The ratio of concentrations in infiltrating water and in pore water below the depth of evaporative removal indicates the fraction of infiltration that percolates toward the water table, eventually becoming recharge. Base flow provides a robust upper bound on the concentration of chloride in infiltrating streamflow. A lower bound is harder to identify, but can reasonably be approximated by the concentration of chloride in pure mountain-front recharge as determined by Plummer and others (2003).

Calculations based on these end-member estimates of chloride concentration indicate that much of the water that infiltrates into the channel eventually becomes recharge (table 5). Pore water from the shallower intervals (1.8–3.5 m) indicates that recharge is between 14 and 100 percent of channel infiltration. Pore water from the two deepest intervals (4.3–4.9 and 4.3–6.7 m) indicates that 43 to 100 percent of infiltration becomes recharge. While the uncertainty is large, as a first approximation it appears that roughly half of infiltrating water recharges the underlying aquifer based on meteoric chloride. From the relation between annual streamflow and precipitation (fig. 10), the long-term estimate of average annual streamflow is 2.0 Mm^3 , on the basis of 41 years of precipitation. During the four-year study period, flows reached the Rio Grande only during wetter than average years. If all streamflow becomes infiltration before reaching the Rio Grande, the long-term average annual recharge rate is about 1.0 Mm^3. This is in agreement with recent estimates and as much as twenty times less than prior estimates (fig. 6).

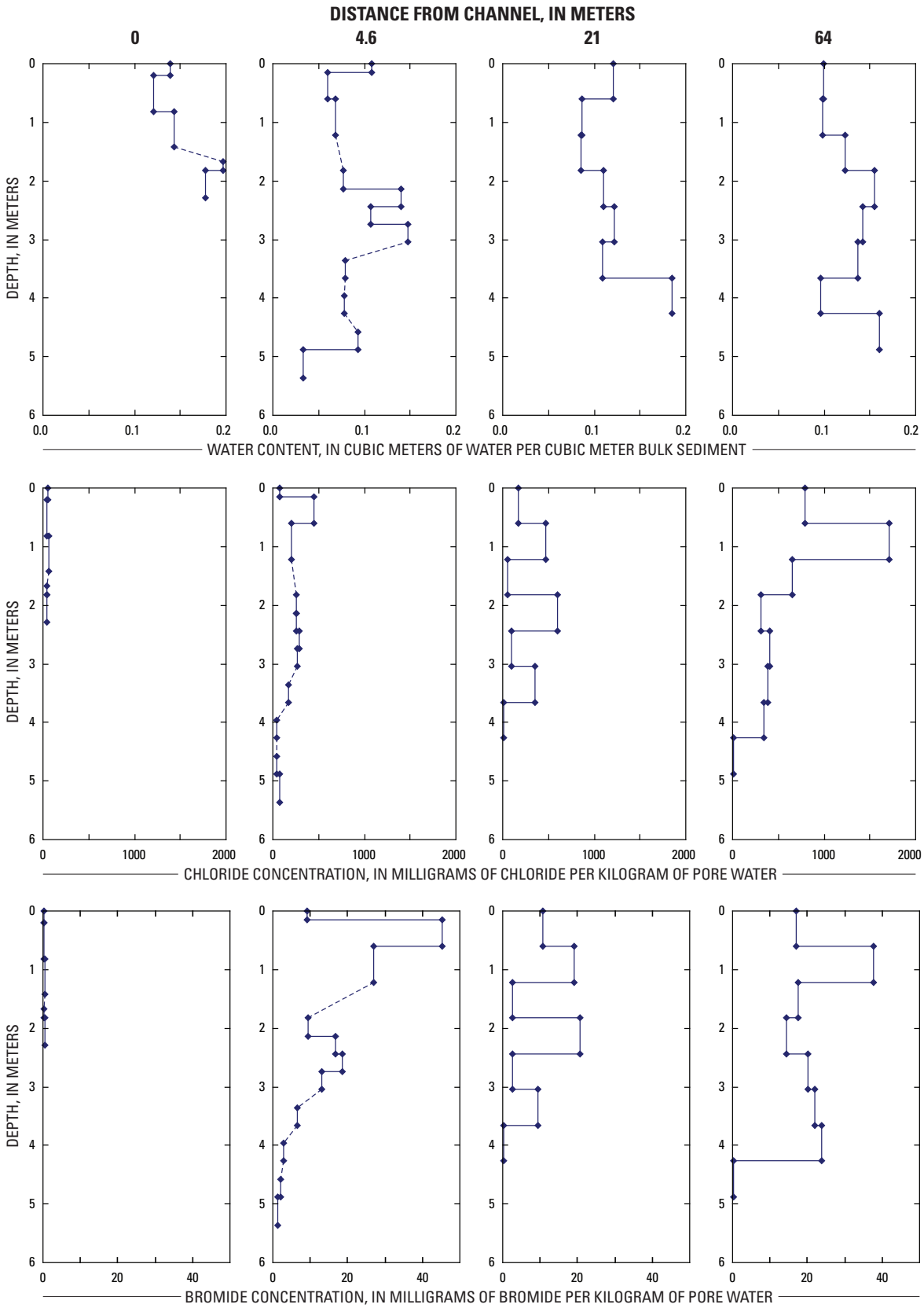

Figure 16. Unsaturated-zone profiles of water content and pore-water concentrations of chloride and bromide along a transect perpendicular to Abo Arroyo, 1.4 kilometers upstream from the mountain front (between gage and PS-1; table 1).

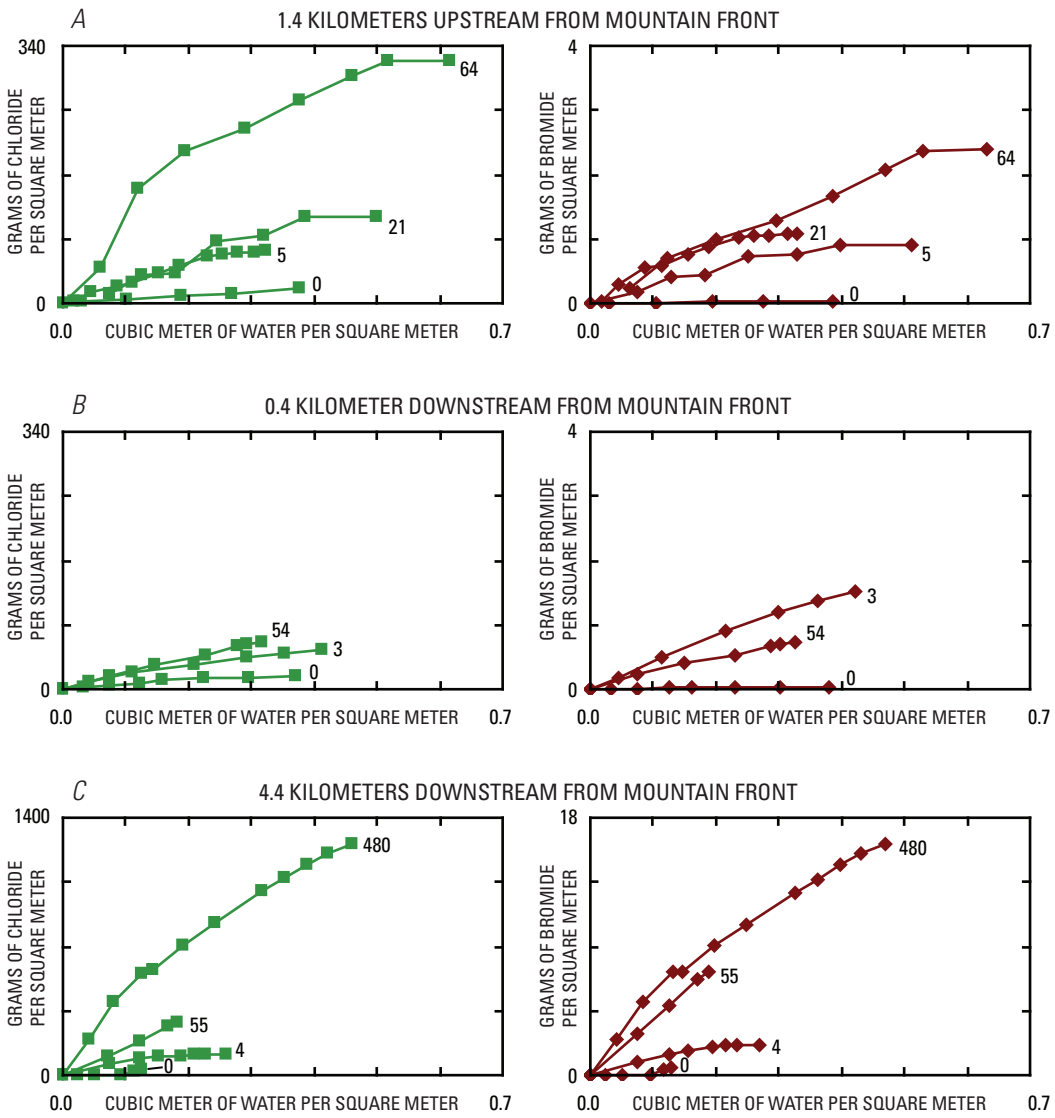

Figure 17. Relationship between cumulative chloride (bromide) and cumulative water along transects starting from Abo Arroyo onto the adjacent terrace. Plotted quantities are per square meter of land surface. Integration is from land surface downward into the unsaturated zone. Numbers next to the plotted data series indicate distance from the corresponding profile to the channel, in meters. *A,* Transect located 1.4 kilometers upstream from the mountain front, near PS-1. *B,* Transect located 0.4 kilometer downstream from the mountain front, near PS-3. *C,* Transect located 4.4 kilometers downstream of the mountain front, near PS-5.

Table 4. Chloride inventories and accumulation times from unsaturated-zone profiles sampled on transects normal to Abo Arroyo, New Mexico.

Distance from channel[1], in meters	Sampled depth, in meters	Chloride inventory[2], in grams	Accumulation time[3], in years
Near PS-1, 1.4 kilometers upstream from mountain front			
5	5.4	69	770
21	4.3	114	1300
64	4.9	320	3600
Near PS-3, 0.4 kilometers downstream from mountain front			
3	4.9	53	590
54	4.3	62	690
Near PS-5, 4.4 kilometers downstream from mountain front			
4	6.1	118	1300
55	3.0	297	3300
480	8.5	1319	15000

[1]Measured from closest channel bank.

[2]Mass of chloride in pore water, per square meter of land surface, between land surface and bottom of sampled profile.

[3]Assuming a deposition rate of 0.09 gram of chloride per square meter per year.

Table 5. Chloride concentrations in streambed pore water and inferred bounds on deep percolation, Abo Arroyo, New Mexico.

Distance from mountain front[1], in kilometers	Top of interval, in meters	Bottom of interval, in meters	Chloride concentration, in grams per kilogram of pore water	Lower bound on percolation[2], as a percentage of infiltration	Upper bound on percolation[3], as a percentage of infiltration
-1.2	1.8	3.5	33	20	100
0.3	1.8	3.5	17	39	100
0.4	4.3	4.9	15	43	100
2.4	1.8	2.4	46	14	100
4.1	1.8	2.4	41	16	100
28.2	4.3	6.7	10	63	100

[1]Distance upstream is negative; downstream is positive.

[2]Based on infiltration having the end-member composition of eastern mountain-front recharge (Plummer and others, 2003).

[3] Based on infiltration having the composition of base flow at the Abo gage (see text). Values greater than 100% reported as 100%.

Conclusions

This chapter presents an overview of a four-year study of streamflow, infiltration, and associated ground-water recharge at Abo Arroyo in south-central New Mexico. The study provided the foundation for using heat as a tracer of streamflow in strongly ephemeral systems.

A stream gage installed for the duration of the study collected high frequency measurements in the upland catchment near a gap in the mountain front through which the arroyo enters the Middle Rio Grande Basin (MRGB). Total annual streamflow at the Abo Arroyo gage ranged from 15.3 million cubic meters (Mm^3) in water year (WY) 1997, the first and wettest year of the study, to 0.8 Mm^3 in the last and driest year (WY-2000). A wide range of precipitation conditions prevailed during the course of the study, with annual precipitation ranging between 75 and 154 percent of average. Total annual streamflow increased nonlinearly with total annual precipitation, indicating that storage and evapotranspiration losses in the upland catchment become increasingly important with increasing aridity.

Summer monsoonal runoff dominated streamflow volume during all four years. Base flow at the gage accounted for only 20 percentage total runoff during the driest year and 2 percent during the wettest year. Daily mean streamflow varied from zero (dry channel) to 37.7 m^3/s. Nearly all flows that reached the basin represented discrete pulses of runoff from brief monsoonal storms. The maximum peak streamflow was 227 m^3/s during the study period. The duration of runoff pulses at the gage varied little, with an average duration of about five hours.

Streambed temperatures at eight locations in the MRGB indicated the timing and extent of streamflow. Much of the study involved development and improvement of the thermal detection technique. Shallow burial of temperature probes (at 0.2 m) and deployment of controls facilitated the determination of flow.

Streambed temperatures indicated that most runoff entering the basin becomes infiltration prior to reaching the Rio Grande. Only the largest flows reached the Rio Grande, during the monsoon season. A classification of flows based on the thermal detection of travel distance indicated that five flows reached the Rio Grande during the four-year study period. Flows were minimal during non-monsoonal months. Streambed temperatures in December 1997 indicated a period of snowmelt-fed infiltration that extended throughout the reach. Snowmelt infiltration lasted two weeks near the mountain front; however, data at the gage indicated that flow rates were small.

Chloride mass-balance calculations provided estimates of the proportion of infiltration that becomes deep percolation and eventual recharge. Chloride in unsaturated-zone pore water beneath the channel suggests that approximately half of infiltrating streamflow becomes recharge, although the range of estimates is large (14–100 percent). Analysis of unsaturated-zone chloride and bromide profiles from transects adjacent to Abo Arroyo showed that direct recharge through terrace surfaces is negligible under current climatic conditions. Analysis of streamflow and streambed temperature records, combined with recharge information from environmental tracers, indicates that the long-term average recharge in the study reach is about 1.0 million cubic meters per year.

References Cited

Allison, G.B., Gee, G.W., and Tyler, S.W., 1994, Vadose zone techniques for estimating groundwater recharge in arid and semiarid regions: Soil Science Society of America Journal, v. 58, p. 6–14.

Anderholm, S.K., 1994, Ground-water recharge near Santa Fe, north-central New Mexico: U.S. Geological Survey Water-Resources Investigations Report 94-4078, 68 p.

Anderholm, S.K., 2000, Mountain-front recharge along the eastern side of the Middle Rio-Grande Basin, central New Mexico: U.S. Geological Survey Water-Resources Investigations Report 00-4010, 36 p.

Bexfield, L.M., and Anderholm, S.K., 2000, Predevelopment water-level map of the Santa Fe Group aquifer system in the Middle Rio Grande Basin between Cochiti Lake and San Acacia, New Mexico: U.S. Geological Survey Water-Resources Investigation Report 2000-4249 [1 sheet].

Blasch, K.W., Ferre, T.P.A., and Hoffman, J.P., 2004, A statistical technique for interpreting streamflow timing using streambed sediment thermographs: Vadose Zone J., v. 3, p. 936–946.

Bouwer, Herman, 1986, Intake rate: cylinder infiltrometer, *in* Klute, A., ed., Methods of Soil Analysis, Part 1, Physical and Mineralogical Methods (2nd edition): Madison, Wisconsin, American Society of Agronomy, p. 825–844.

Carter, R.W., and Davidian, J., 1968, General procedure for gaging streams: U.S. Geological Survey Techniques for Water-Resources Investigations, book 3, chapter A6, 13 p.

Constantz, Jim, Stonestrom, D.A., Stewart, A.E., Niswonger, R.G., and Smith, T.R., 2001, Analysis of streambed temperatures in ephemeral channels to determine streamflow frequency and duration: Water Resources Research, v. 37, no. 2, p. 317–328.

Constantz, Jim, and Stonestrom, D.A., 2003, Heat as a tracer of water movement near streams, *in* Stonestrom, D.A., and Constantz, J., eds., Heat as a tool for studying the movement of ground water near streams: U.S. Geological Survey Circular 1260, p. 1–6.

Constantz, Jim, and Thomas, C.L., 1997, Stream bed temperature profiles as indicators of percolation characteristics beneath arroyos in the Middle Rio Grande Basin, USA: Hydrological Processes, v. 11, no. 12, p. 1621–1634.

Dane, C.H., and Bachman, G.O., comps., 1965, Geologic Map of New Mexico: U.S. Geological Survey, scale 1:500,000 [2 sheets].

Edmunds, W.M., Darling, W.G., and Kinniburgh, D.G., 1988, Solute profile techniques for recharge estimation in semi-arid and arid terrain, *in* Summers, I., ed., Estimation of Natural Groundwater Recharge: Norwell, Mass., D. Reidel, p. 139–157.

Genereux, D.P., and Hooper, R.P., 1998, Oxygen and hydrogen isotopes in rainfall-runoff studies, *in* Kendall, C., and McDonnell, J.J., eds., Isotope Tracers in Catchment Hydrology: Amsterdam, Elsevier Science B.V., p. 319–346.

Hawley, J.W., Love, D.W., and Lambert, P.W., 1982, Roadlog segment I-C, Abo Canyon-Blue Springs area to Albuquerque via Belen and Los Lunas, *in* Grambling, J.A., and Wells, S.G., eds., Albuquerque Country II, New Mexico Geological Society Thirty-third Annual Field Conference, November 4–6, 1982: Socorro, New Mexico Geological Society, p. 1–27.

Hearne, G.A., and Dewey, J.D., 1988, Hydrologic analysis of the Rio Grande Basin north of Embudo, New Mexico; Colorado and New Mexico: U.S. Geological Survey, Water-Resources Investigations Report 86-4113, 244 p.

Kernodle, J.M., and Scott, W.B., 1986, Three-dimensional model simulation of steady-state ground-water flow in the Albuquerque-Belen Basin, New Mexico: U.S. Geological Survey, Water-Resources Investigations Report 84-4353, 58 p.

Kernodle, J.M., McAda, D.P., and Thorn, C.R., 1995, Simulation of ground-water flow in the Albuquerque Basin, central New Mexico, 1901–1994, with projections to 2020: U.S. Geological Survey, Water-Resources Investigations Report 94-4251, 114 p.

Langbein, W.B., 1949, Annual runoff in the United States: U.S. Geological Survey Circular 52, 14 p.

McAda, D.P., and Barroll, P., 2002, Simulation of groundwater flow in the Middle Rio Grande Basin between Cochiti and San Acacia, New Mexico: U.S. Geological Survey Water-Resources Investigations Report 02-4200, 81 p.

Nimmo, J.R., Lewis, A.M., and Winfield, K.A., 2001, Discernable large- and small-scale features affecting recharge in Abo Arroyo and similar basins, *in* Cole, J.C., ed., U. S. Geological Survey Middle Rio Grande Basin study; proceedings of the fourth annual workshop, Albuquerque, New Mexico, February 15–16, 2000: U.S. Geological Survey Open-File Report 00-488, p. 41–43.

Niswonger, Richard, Prudic, D.E., Stonestrom, D.A., and Fogg, G.E., 2006, Flow in an initially dry stream channel [abs.]: Eos, Transactions, American Geophysical Union, Fall Meeting Supplement, v. 87, no. 52, p. F950.

Plummer, L.N., Bexfield, L.M., Anderholm, S.K., Sanford, W.E., and Busenberg, E., 2004, Geochemical characterization of ground-water flow in the Santa Fe Group aquifer system, Middle Rio Grande Basin, New Mexico: U.S. Geological Survey Water-Resources Investigations Report 03-4131, 395 p.

Sanford, W.E., Plummer, L. N., McAda, D. P., Bexfield, L. M., and, and Anderholm, S.K., 2004, Hydrochemical tracers in the Middle Rio Grande Basin, USA: 2. Calibration of a ground-water flow model: Hydrogeology Journal, v. 12, p. 389–407, doi:10.1007/s10040-004-0326-4.

Scanlon, B.R., Keese, K.E., Flint, A.L., Flint, L.E., Gaye, C.B., Edmunds, W.M., and Simmers, I., 2006, Global synthesis of groundwater recharge in semiarid and arid regions: Hydrological Processes, v. 20, no. 15, p. 3335–3370, doi:10.1002/hyp.6335.

Scholle, P.A., comp., 2003, Geologic Map of New Mexico: Socorro, New Mexico Bureau of Geology and Mineral Resources, scale 1:500,000 [2 sheets].

Spiegel, Zane, 1955, Geology and ground-water resources of northeastern Socorro County, New Mexico: Socorro, New Mexico State Bureau of Mines and Mineral Resources Ground-Water Report No. 4, 99 p.

Stephens, D.B., and Knowlton, R., Jr., 1986, Soil water movement and recharge through sand at a semiarid site in New Mexico: Water Resources Research, v. 22, no. 6, p. 881–889.

Stewart, A.E., 2003, Temperature based estimates of streamflow patterns and seepage losses in ephemeral channels: Stanford, Calif., Stanford University, Ph.D. dissertation, 248 p.

Stone, W.J., 1984, Recharge in the Salt Lake coal field based on chloride in the unsaturated zone: Socorro, New Mexico State Bureau of Mines and Mineral Resources Open-File Report No. 214: 64 p.

Stonestrom, D.A., and Constantz, J., 2004, Using temperature to study stream-ground water exchanges: U.S. Geological Survey Fact Sheet 2004-3010, 4 p.

Thorn, C.R., McAda, D.P., and Kernodle, J.M., 1993, Geohydrologic framework and hydrologic conditions in the Albuquerque Basin, central New Mexico: U.S. Geological Survey Water-Resources Investigations Report 93-4149, 106 p.

Titus, F.B., 1963, Geology and ground-water conditions in eastern Valencia County, New Mexico: Socorro, New Mexico State Bureau of Mines and Mineral Resources Ground-Water Report No. 7, 113 p.

Tyler, S.W., Chapman, J.B., Conrad, S.H., Hammermeister, D.P., Blout, D.O., Miller, J.J., Sully, M.J., and Ginanni, J.M., 1996, Soil-water flux in the southern Great Basin, United States: Temporal and spatial variations over the last 120,000 years: Water Resources Research, v. 32, no. 6, p. 1481–1499.

USDA-NRCS (U.S. Department of Agriculture, National Resources Conservation Service), 2006, SNOTEL data and products, http://www.wcc.nrcs.usda.gov/snotel, accessed 2006/11/07.

Waltemeyer, S.D., 1994, Methods for estimating streamflow at mountain fronts in southern New Mexico: U.S. Geological Survey Water-Resources Investigations Report 93-4213, 17 p.

Focused Ground-Water Recharge in the Amargosa Desert Basin

By David A. Stonestrom, David E. Prudic, Michelle A. Walvoord, Jared D. Abraham, Amy E. Stewart-Deaker[1], Patrick A. Glancy, Jim Constantz, Randell J. Laczniak, and Brian J. Andraski

Abstract

The Amargosa River is an approximately 300-kilometer-long regional drainage connecting the northern highlands on the Nevada Test Site in Nye County, Nev., to the floor of Death Valley in Inyo County, Calif. Streamflow analysis indicates that the Amargosa Desert portion of the river is dry more than 98 percent of the time. Infiltration losses during ephemeral flows of the Amargosa River and Fortymile Wash provide the main sources of ground-water recharge on the desert-basin floor. The primary use of ground water is for irrigated agriculture. The current study examined ground-water recharge from ephemeral flows in the Amargosa River by using streamflow data and environmental tracers. The USGS streamflow-gaging station at Beatty, Nev., provided high-frequency data on base flow and storm runoff entering the basin during water years 1998–2001. Discharge into the basin during the four-year period totaled 3.03 million cubic meters, three quarters of which was base flow. Streambed temperature anomalies indicated the distribution of ephemeral flows and infiltration losses within the basin. Major storms that produced regional flow during the four-year period occurred in February 1998, during a strong El Niño that more than doubled annual precipitation, and in July 1999. The study also quantified recharge beneath undisturbed native vegetation and irrigation return flow beneath irrigated fields. Vertical profiles of water potential and environmental tracers in the unsaturated zone provided estimates of recharge beneath the river channel (0.04–0.09 meter per year) and irrigated fields (0.1–0.5 meter per year). Chloride mass-balance estimates indicate that 12–15 percent of channel infiltration becomes ground-water recharge, together with 9–22 percent of infiltrated irrigation. Profiles of potential and chloride beneath the dominant desert-shrub vegetation suggest that ground-water recharge has been negligible throughout most of the basin since at least the early Holocene. Surface-based electrical-resistivity imaging provided areal extension of borehole information from sampled profiles. These images indicate narrowly focused recharge beneath the Amargosa River channel, flanked by large tracts of recharge-free basin floor.

Introduction and Setting

The Amargosa Desert Basin contains a large quantity of high quality ground water (Walker and Eakin, 1963; Claassen, 1985; Kilroy, 1991). Beneficial uses of ground water include sustenance of wildlife at discharge points within Ash Meadows National Wildlife Refuge and support of irrigated agriculture within the Amargosa Farms area (fig. 1). Recharge of ground water is a relatively uncharacterized component of the hydrologic budget. The basin is part of the larger Death Valley regional ground-water flow system. While numerous studies have examined the Death Valley system at a regional scale (Winograd and Thordarson, 1975; Harrill and others, 1988; D'Agnese and others, 1999; Tiedeman and others, 2004), the sparsely populated Amargosa Desert Basin—especially its upper reaches—has received relatively little study. Considerable uncertainties remain in subsurface residence times and fluxes under current climatic and land-use conditions. Appraisal of ground-water resources and management of competing demands from developing land-use patterns requires an improved understanding of ground-water recharge in this desert environment.

Population, Land Use, and Water Withdrawals

The Amargosa Desert Basin is sparsely populated and relatively undeveloped. The average population density is less than one person per square kilometer. Primary land uses are farming and recreation. The town of Beatty straddles the Amargosa River just upstream of its entry into the basin (fig. 1). The estimated population of Beatty in 2000 was 1,085 (U.S. Census Bureau, 2003). The Amargosa Farms area spreads across the outlet of the basin. The census division that includes the farms area, Amargosa Valley, had an estimated population in 2000 of 1,142.

In view of rapid population growth in nearby areas, the Amargosa Desert Basin has substantial potential for growth. Population estimates at the county level extend back to 1870. The early population of the county jumped roughly six-fold after prospectors found gold near Beatty in 1904, and rose again in the 1950s and 1960s during expansion of irrigated agriculture and defense activities at the Nevada Test Site (fig. 2). Even so, total county population remained below 10,000 before 1981.

[1] Present address Berkeley, California (amystew@gmail.com).

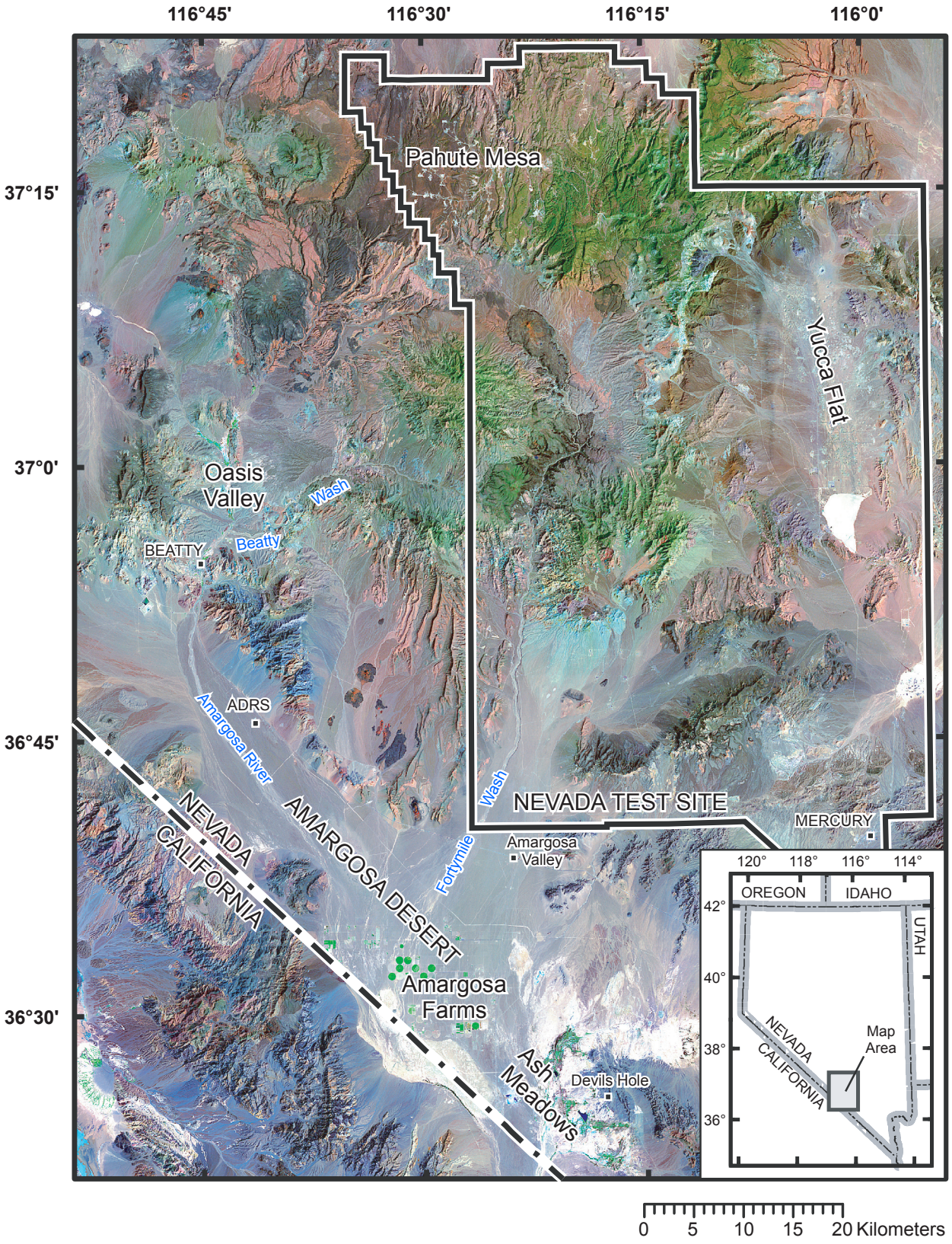

Figure 1. Physiographic and cultural features in the Amargosa Desert study area and vicinity, Nye County, Nev., and Inyo County, Calif. During the study, an active streamflow-gaging station was located in Beatty, Nev. Weather stations were located at Beatty, Nev., Amargosa Valley, Nev., Amargosa Farms, Nev., and at the ADRS (Amargosa Desert Research Site; Andraski and Stonestrom, 1999). Figure 9 shows channel- and borehole-sampling locations.

The county grew substantially starting in the late 1970s due to migration into Pahrump Valley, an adjacent basin southeast of Ash Meadows.

The primary use of ground water in the Amargosa Desert Basin is for irrigation. Irrigation began around 1917 and continued on a modest scale until 1954. Between 1954 and 1965, the number of wells grew by about 150 to support agricultural production. Irrigation withdrawals have fluctuated since 1965, but maximum withdrawals about 20 million cubic meters per year ($Mm^3\ yr^{-1}$) rival the natural discharge of ground water at Ash Meadows (about 22–26 $Mm^3\ yr^{-1}$; Laczniak and others, 1999; Stonestrom, Prudic, and others, 2003).

Hydrogeologic Setting

The Amargosa Desert Basin is bounded by large mountain blocks comprised of rocks ranging from Precambrian through Tertiary. Dominant rock types include Precambrian to Cambrian quartzite, Precambrian to Devonian massive dolomite and limestone, Carboniferous interbedded limestone and shale, and Tertiary rhyolites and basalts. Late Tertiary to Quaternary sediments form poorly indurated to unconsolidated basin-floor deposits (Winograd and Thordarson, 1975; Nichols, 1987; Sweetkind and others, 2001; Workman and others, 2002).

The present basin configuration resulted from distinct episodes and styles of tectonic deformation (Carr and Yount, 1984; Hamilton, 1987; Glazner and others, 2002; Park and Wernicke, 2003). Cretaceous folding and thrusting imparted an east-to-northeasterly grain to the Paleozoic bedrock. Tear faulting of low-angle overthrusted slabs followed, ending in mid-Tertiary (Carr and Yount, 1984). Tear faulting impacted the entire area, creating northwesterly striking offsets (tears) in bedrock units of tens of kilometers. A northeasterly trending corridor of folding and faulting divides the Amargosa Desert Basin into upper and lower regions. This corridor, marked by the lower reaches of Fortymile Wash, appears to have formed by the early Tertiary (Carr and Yount, 1984). Low-angle detachment faulting starting in mid Tertiary accompanied subcontinental extension, producing the horst and graben topography characteristic of the southern Great Basin (Hamilton, 1987). Horst and graben-style faulting associated with large-scale detachments locally activated preexisting northeasterly and northwesterly trending structures, forming deep basins that filled with alluvium. Widespread volcanism accompanied extension (Workman and others, 2002). Active deformation of 9 mm yr^{-1} north-northwesterly trending right-lateral shear continues to shape the region (Park and Wernicke, 2003). Small blocks of bedrock crop out through basin-floor alluvium along a northwesterly trending line through the Amargosa Desert Research Site (Stonestrom and others, 2004). Tectonic subsidence in the central part of the Amargosa Farms area is roughly matched by alluvial deposition from the Amargosa River and Fortymile Wash (Stonestrom, Prudic, and others, 2003).

As part of the Mojave Desert ecosystem, the Amargosa Desert Basin is one of the driest areas in the United States.

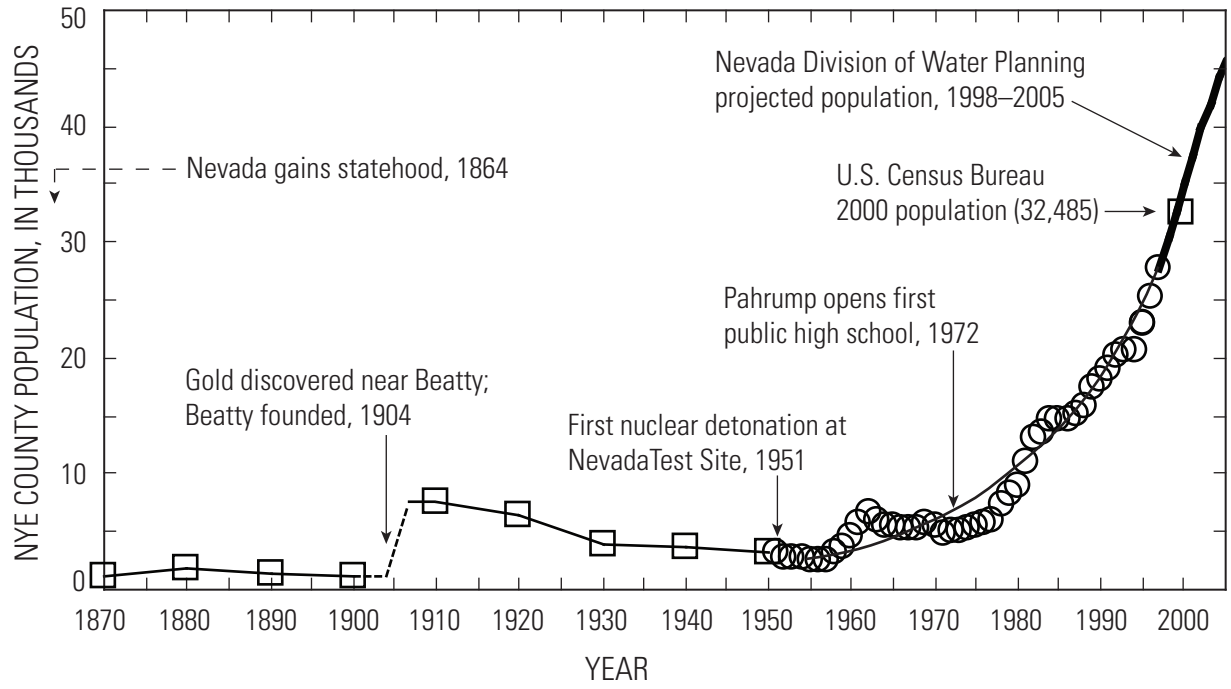

Figure 2. The population of Nye County, Nev., increased exponentially from the mid 1950s through mid 1990s, at about six percent per year (thin curved line). Early data (squares) are from the University of Virginia's Fisher Library (http://fisher.lib.virginia.edu/census, last accessed June 10, 2003). Later estimates (circles, 1950–1997) and forecasts (thick line, 1998–2005) are from the Nevada Division of Water Planning (http://www.water.nv.gov/water%20planning/plan-app/ny-tab01.pdf; last accessed March 1, 2005).

The present climate is arid-thermic, with moderate seasonality with respect to precipitation and strong seasonality with respect to temperature (Bull, 1991). Daily average temperatures range from 33 degrees Celsius (ºC) in August to 3ºC in December (fig. 3). Precipitation on the basin floor averages about a tenth of a meter per year based on long-term records at Amargosa Farms (1971–2000; 99.6 mm yr^{-1}; NOAA, 2002) and at the Amargosa Desert Research Site (1981–2005; 112 mm yr^{-1}; Johnson and others, 2007). About 60 percent of annual precipitation arrives in frontal systems during the months of December through March, with enhanced amounts during moderate to strong El Niño events (fig. 4).

Ground-water discharge maintains perennial flow in the Amargosa River at Beatty, near the entrance to the basin. Base flow dissipates within a few kilometers downstream. Speculation that no modern-day flows were capable of completely traversing the Amargosa Desert Basin was falsified by field reconnaissance following storms in March 1995 that produced continuous flow from the Nevada Test Site to Death Valley (Beck and Glancy, 1995).

Except for storm-generated runoff, the Amargosa River is usually dry downstream of Beatty. Storm flows are brief—despite an upstream drainage area of about 1,200 square kilometers—as shown by 15-minute discharge data at Beatty during the study period (fig. 5). Ephemeral flow is generated primarily by runoff from the mountains surrounding Oasis Valley, but runoff from Bare Mountain (which forms the northeastern side of the basin), the Bullfrog Hills (northern side), the Funeral Mountains (southwestern side), as well as runoff from the basin floor itself can contribute flow in unnamed tributaries. Ephemeral flows exhibit extreme variability in magnitude, as shown by annual peak flows at the basin inlet (fig. 6).

The dominant plant in the Mojave Desert is creosote bush (*Larrea tridentata*; Smith, Monson, and others, 1997), which covers nearly the entire Amargosa Desert Basin floor. Saltbush (*Atriplex*) co-dominates, becoming dominant beside channel reaches that were scoured by major flooding in the past. The active channel is largely vegetation free. On surfaces more than a few meters away from the channel, the native vegetation has likely been undisturbed for many centuries. Creosote and saltbush plants are perennial, with several meters typically separating the above-ground portions of adjacent plants. Typical mature heights are 0.5 m (saltbush) to 1–2 m (creosote bush).

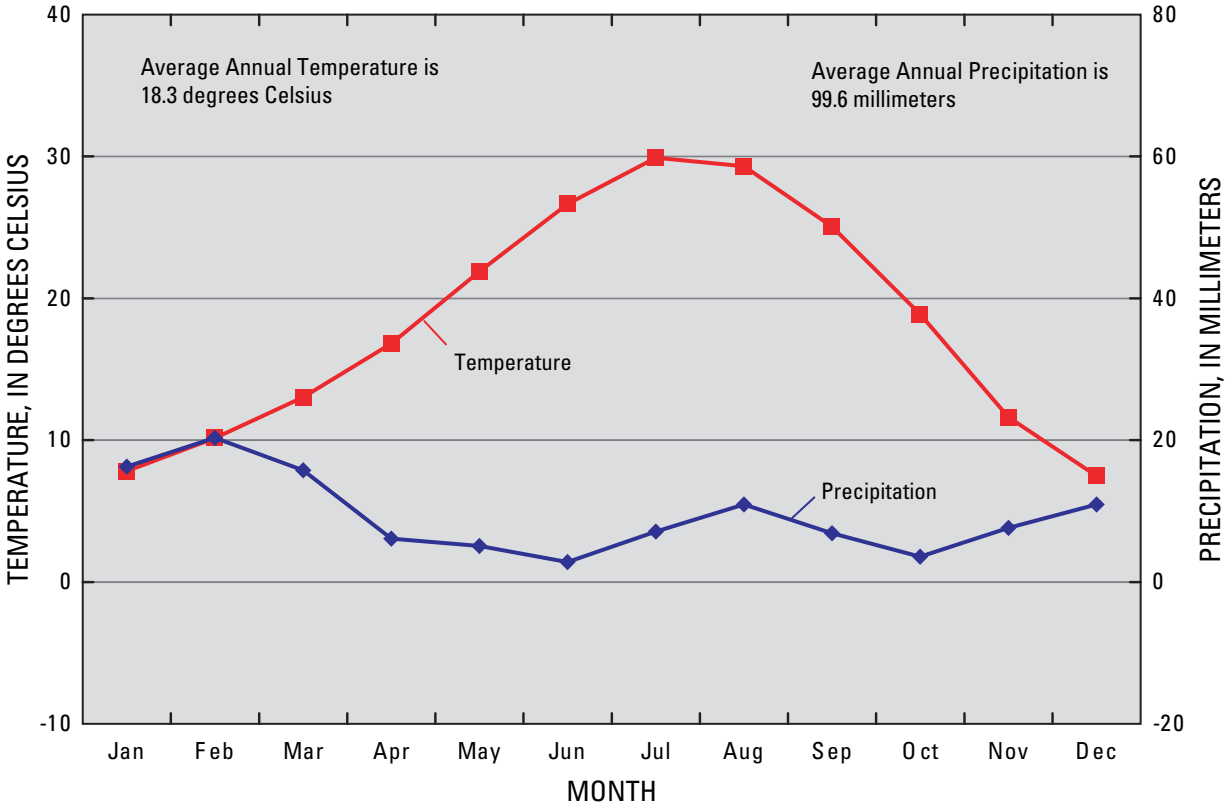

Figure 3. Mean monthly temperature and precipitation for 1965–2000 at Amargosa Farms, Nev. (National Weather Service cooperative station 260150). Altitude of station is 747 meters above sea level (National Geodetic Vertical Datum of 1929).

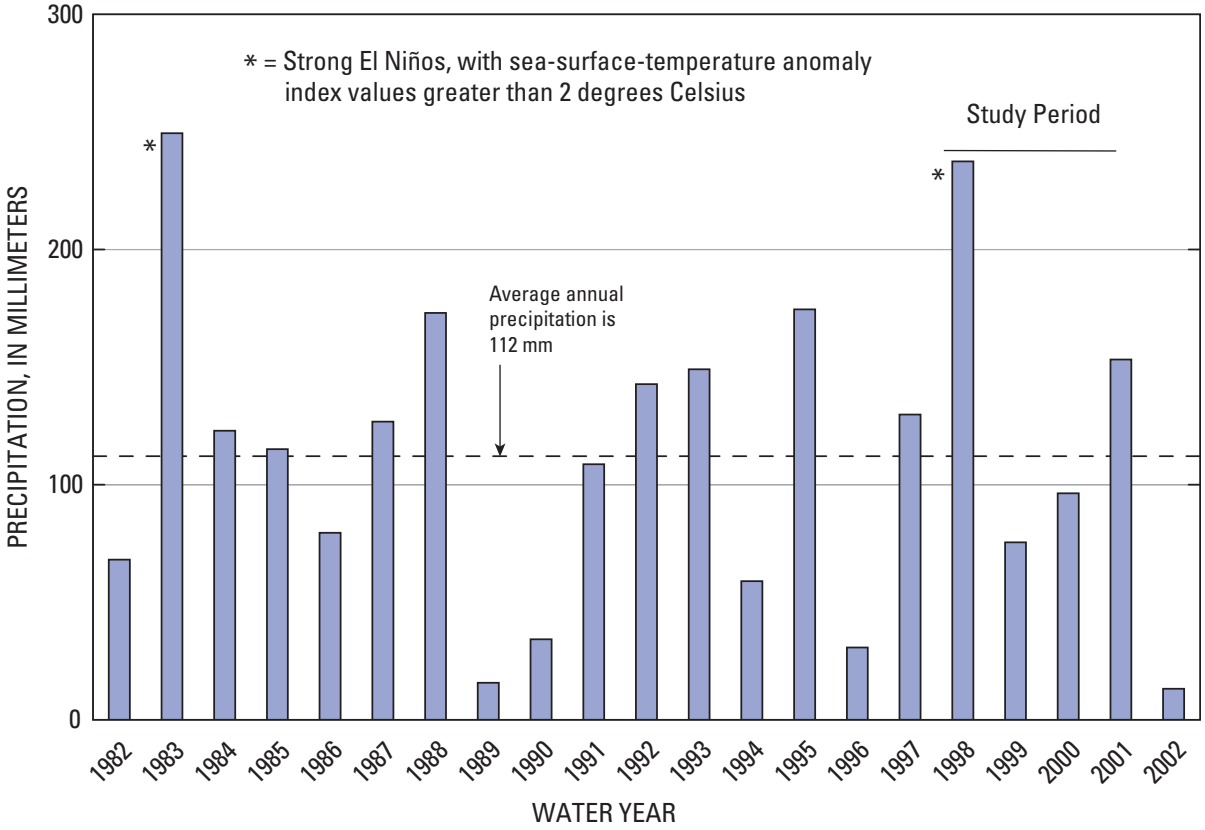

Figure 4. Annual precipitation at the Amargosa Desert Research Site (ADRS) for water years 1982–2002 (Johnson and others, 2007). El Niño index is from McPhaden and others (2006). Water year runs from October 1 to September 30 and is denoted by the calendar year in which it ends. Figure 1 shows the location of the Amargosa Desert Research Site.

In addition to these large perennials, a variety of small annuals quickly fill the intervening gaps after accumulation of more than a few millimeters of precipitation when conditions are favorable. At the entrance to the basin, perennial flow supports a salt-cedar–willow community along the Amargosa River.

Potential evapotranspiration in the Amargosa Desert Basin greatly exceeds precipitation on an annual basis. Nichols (1987) estimated potential evaporation to be 2.5 m yr^{-1}, exceeding average annual precipitation by a factor of 23. Daily accounting of actual evaporation in conjunction with a water-balance model showed that deep percolation (precipitation in excess of evaporation and soil-moisture replenishment) might have occurred beneath non-vegetated surfaces on three separate occasions during 1961-1976, in amounts ranging from 5 to 26 mm (Nichols, 1987).

Micrometeorological and soil data from the Amargosa Desert Research Site clearly show the decisive role of desert vegetation in controlling the near-surface water balance. Early work indicated that removal of vegetation for five years (1987–1992) reversed the potential gradient for water movement, from upward to downward, in a gradually deepening layer (Andraski, 1997). Measured evapotranspiration from native vegetation (48 mm) exceeded total precipitation (3.5 mm) by a factor of 13.7 in 2002 (Johnson and others, 2007). A net decrease in soil moisture during 2002 made up the difference. Precipitation data at Beatty show that 2002 was the driest year in 64 years of record. Lysimeter data for the same plant association on the Nevada Test Site showed that complex feedbacks between native vegetation and available moisture maintained upward gradients for water movement from 1994 through 2001 (Scanlon and others, 2005). Due to increased plant vigor, upward gradients strengthened rather than weakened in response to the period of El Niño enhanced precipitation during 1997–1998.

Previous Work and Scope

Relatively few studies have examined ground-water recharge in the Amargosa Desert Basin. Walker and Eakin (1963) provided an early reconnaissance estimate based on earlier work in east-central Nevada, where recharge (assumed to be equal to ground-water discharge through springs and evapotranspiration) in 13 closed basins was correlated with precipitation (Maxey and Eakin, 1949; Eakin and Maxey, 1951; Avon and Durbin, 1994). Walker and Eakin divided the greater Amargosa area into precipitation zones. The current study area is entirely in the driest precipitation zone (less than 200 mm), in which recharge was estimated to be zero.

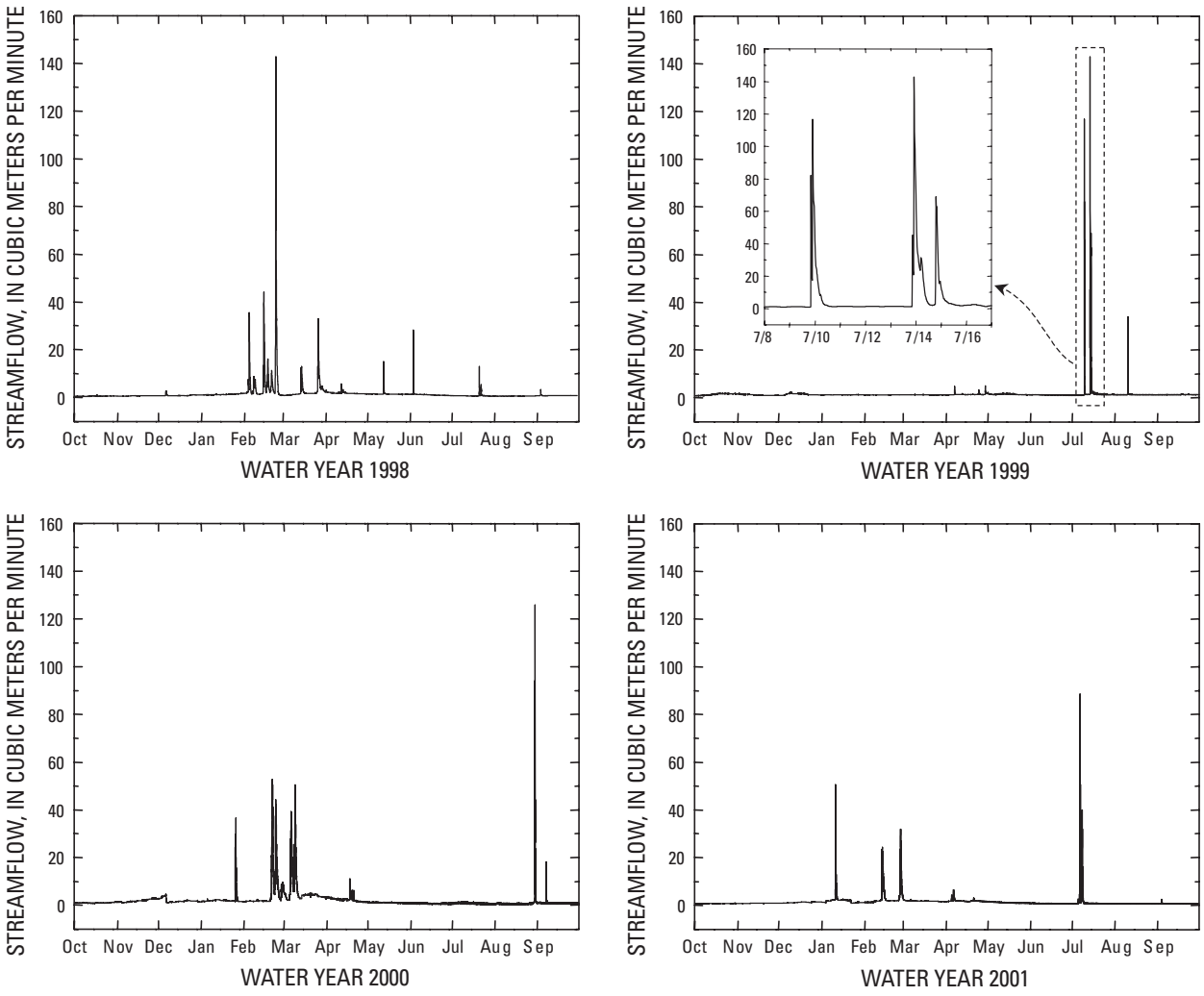

Figure 5. Discharge of the Amargosa River at Beatty, Nev., for water years 1998–2001 (USGS streamflow-gaging station 10251217). Inset shows detailed record for three stormflow events in July 1999. Under typical (non-storm) conditions, all base flow is lost to infiltration and evaporation within a few kilometers of the gage.

Claassen (1985) examined the geochemical composition of ground water in the west-central part of the basin and concluded that recharge was primarily from direct infiltration of overland flow in or near present day stream channels, rather than from subsurface inflows from the surrounding mountains. Depletion of stable isotopes oxygen-18 and deuterium in water indicate that most of the recharge originated as snowmelt. Carbon-14 dates indicate that most of the sampled ground water recharged during late Wisconsin to early Holocene time, with unadjusted ages ranging from 9 to 17 thousand years before present.

Osterkamp and others (1994) used a distributed-parameter water-balance approach to estimate recharge arising from contemporary streambed infiltration. This approach classified the Amargosa River into geomorphically similar reaches and assumed that all infiltration became recharge. Between the basin entrance near Beatty and outlet near Amargosa Farms, channel losses produced a total estimated annual recharge of 0.5 million cubic meters per year ($Mm^3\ yr^{-1}$).

The geographic focus of the current study is the portion of the basin through which the Amargosa River flows. In addition, Beatty Wash—the largest tributary upstream of the Amargosa Desert—was instrumented near its confluence with the Amargosa River, in Oasis Valley (fig. 1). The study also considered recharge from irrigation return in the Amargosa Farms area near the downstream end of the study reach. The primary data for the study are from water-years 1998 through 2001, which spanned a range of wet to dry conditions (fig. 4). In addition to developing recharge estimates, the goal of the study was to gain understanding of recharge processes and controls, with particular regard to the timing and extent of recharge-producing events.

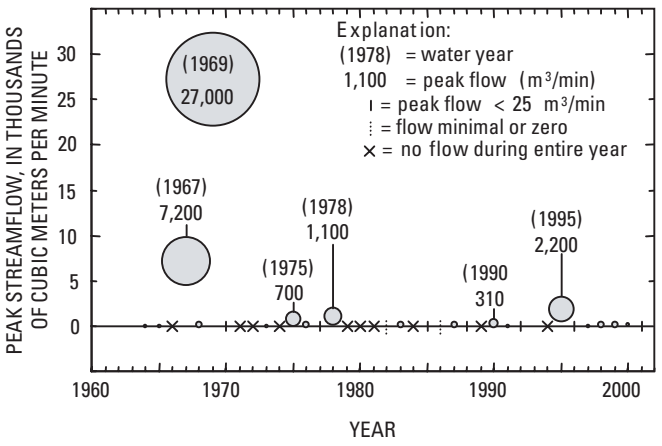

Figure 6. Annual peak flows, Amargosa River near Beatty, Nev., for October 1963 through September 2001. Data for water years 1964–1968 and 1991–1995 are from USGS streamflow-gaging station 10251218, 3.7 km downstream of station 10251217 (Amargosa River at Beatty, Nev.; temperature station PS-1). Data for water years 1969–1990 are from crest-stage partial-record station 10251220 (at PS-2), 5.4 km downstream of the Beatty gage. Data for water years 1996–2002 are from the Beatty gage. No gages were active in water years 1982 and 1986; however, flows were zero or small. The channel downstream of 10251220 is dry more than 98 percent of the time. The 1969 flood was the largest on record, producing a peak flow that exceeded the median annual peak flow by more than two orders of magnitude. From Stonestrom, Prudic, and others (2004).

Methods

This study combined thermal flow detection with analyses of vertical profiles of water potential and naturally occurring environmental tracers to characterize infiltration and recharge within the Amargosa Desert Basin. Sampling locations included sites within the channel, irrigated fields, and beneath undisturbed native vegetation on the basin floor. Direct-current (DC) resistivity imaging, a surface geophysical technique, allowed generalization of results obtained at the limited number of sampled sites to areas of the basin with similar geomorphology and vegetation. This section briefly describes instrumentation, sampling, and data analysis. Detailed descriptions appear in cited references.

Streambed-temperature anomalies indicated ephemeral flow at instrumented locations (Constantz and others, 2001; Stewart, 2003; table 1). Measurement techniques included deployment of single-channel temperature loggers at a nominal depth of 0.1 m in channel sediment, nested thermocouples near the inlet to the basin and at the Amargosa Desert Research Site, and borehole-temperature loggers at two locations in the channel (Stonestrom and Blasch, 2003). Streambed-temperature measurements were supplemented by peak-flow estimates by using slope-conveyance and slope-area techniques (Benson and Dalrymple, 1967; Dalrymple and Benson, 1968).

Sediment samples were obtained from boreholes within the channel (sites C1 and C2), beneath native vegetation near the Amargosa Desert Research Site (ADRS) and Amargosa Farms area (sites ADRS and AFNV), and beneath irrigated fields (sites AF-A1–AF-C2; table 2; fig. 7). Water potentials for each sample were determined with a water-activity meter (Gee and others, 1992). Gravimetric water contents were determined by oven drying at 105° C (Gardner, 1986). Pore-water chemistry was characterized by using methods in Page and others (1982) and Sparks (1996). Each oven-dried sample was mixed with an equal mass of deionized water and shaken periodically for 24 hours. Supernatant liquid was filtered and analyzed for chloride and nitrate by using ion chromatography. Supernatant concentrations were converted to pore-water concentrations by dividing by gravimetric water contents and multiplying by the pore-water density (assumed to be 1.00×10^6 gram m^{-3}). Volumetric water contents were obtained by multiplying gravimetric water content by bulk densities estimated on the basis of lithologic description. Unsaturated-zone chloride-mass-balance and tracer-velocity techniques provided estimates of deep percolation and recharge (Stonestrom, Prudic, and others, 2003). Water for stable isotopic analysis was extracted by complete-recovery cryodistillation (Prudic and others, 1997).

Surface-based DC-resistivity measurements were made in May of 2003 along transects normal to the sedimentary depositional fabric in three distinct geomorphologic settings; one where the Amargosa channel is incised into the adjacent terrace sediments (near PS-4), one where the channel forms an actively migrating distributory network (near PS-6E), and one on the alluvial surface adjacent to the ADRS. Water years 2002 and 2003 were dry, producing no flows that extended more than a few kilometers into the basin. At each resistivity transect, linear arrays of 32 to 80 electrodes were deployed with a uniform 2 to 5-m spacing between adjacent electrodes. A multiplexing 8-channel resistivity instrument was used to make automated resistivity measurements along the line, combining sounding and profiling for vertical and horizontal resolution (fig. 8; Stonestrom, Abraham, and others, 2003; Abraham and Lucius, 2004). Each measurement used four electrodes at a time, with geometry varying between inverse-Schlumberger and inverse-Wenner configurations (Telford and others, 1990). Sodium-chloride solution was used to improve electrical contact between electrodes and the extremely dry surface soil. Imposed currents ranged from 250 to 400 milliamps. The line was shifted incrementally until composite transects consisted of 168 to 232 electrode positions. Each transect produced vertical arrays of 3,000 to 4,000 apparent resistivity soundings.

Apparent resistivity soundings were used in a constrained inversion scheme, generating a model distribution of subsurface DC resistivities based on the difference between measured and predicted apparent resistivities. The inversion

Table 1. Locations of streamflow-gaging station and peak-flow- and temperature-measurement sites, Amargosa Desert study area.

Description	Code	Latitude[1], in degrees	Longitude[1], in degrees	Altitude[2], in meters	Distance from basin inlet[3], in kilometers
Beatty Wash	BW	36.9434	116.7190	1049	-8.3
Amargosa River at Beatty (station 10251217)	GAGE	36.9106	116.7564	1003	-3.0
Amargosa River near highway 95 bridge	PS-1	36.8802	116.7525	966	0.8
Amargosa River near airport road	PS-2	36.8678	116.7595	954	2.4
Amargosa River near highway 95 bend	PS-3	36.8595	116.7570	942	3.4
Amargosa River near beacon road	PS-4	36.7979	116.7555	888	10.6
Unnamed tributary near beacon road	PS-4T	36.7932	116.7647	887	NA[4]
Amargosa River west of ADRS[5]	PS-5	36.7658	116.7323	859	14.9
Amargosa River near Ashton site, east channel	PS-6E	36.7111	116.6772	807	22.9
Amargosa River near Ashton site, west channel	PS-6W	36.7066	116.6805	805	22.9
Unnamed tributary near Ashton site	PS-6T	36.6887	116.6880	799	NA
Amargosa River near Big Dune	PS-7	36.6324	116.6111	749	33.7

[1]North latitude and west longitude; North American Datum of 1927.

[2]Land surface altitude, National Geodetic Vertical Datum of 1929.

[3]Measured from gap in bedrock at entrance to basin, 3.0 km downstream of USGS streamflow-gaging station 10251217 (Amargosa River at Beatty, Nev.). Negative value is distance upstream; positive is distance downstream.

[4]NA—not applicable.

[5]ADRS is the Amargosa Desert Research Site (Andraski and Stonestrom, 1999; http://nevada.usgs.gov/adrs/).

Table 2. Locations of sampled boreholes within the Amargosa Desert study area.

Description	Code	Latitude[1], in degrees	Longitude[1], in degrees	Altitude[2], in meters	Borehole depth, in meters
Amargosa channel site 1, at PS-4	C1	36.7981	116.7525	889	14
Amargosa channel site 2, at PS-6E	C2	36.7131	116.6764	808	14
ADRS[3], native vegetation	ADRS	36.7656	116.6936	847	48
Amargosa farms, native vegetation	AFNV	36.5656	116.5261	724	15
Amargosa farms, field 1, hole A	AF-1A	36.5647	116.5261	723	12
Amargosa farms, field 1, hole B	AF-1B	36.5622	116.5275	722	15
Amargosa farms, field 2, hole A	AF-2A	36.5536	116.5264	719	10
Amargosa farms, field 2, hole B	AF-2B	36.5497	116.5325	717	10
Amargosa farms, field 3, hole A	AF-3A	36.5461	116.4897	717	15
Amargosa farms, field 3, hole B	AF-3B	36.5442	116.4917	718	16

[1]North latitude and west longitude; North American Datum of 1927.

[2]Land surface altitude, National Geodetic Vertical Datum of 1929.

[3]Composited data from boreholes at the Amargosa Desert Research Site (see Stonestrom, Prudic, and others, 2004).

A. Native Vegetation

B. Amargosa River Channel

C. Irrigated Field

D. Core Sample of Sediments

Figure 7. Photographs of unsaturated-zone sediment sampling in the Amargosa Desert study area. *A*, Native vegetation, Amargosa Farms; *B*, Amargosa River channel; *C*, irrigated field; *D*, sediment core from channel.

assumed an exponential distribution of data errors, minimizing an L1-norm of combined data misfits and model stabilization constraints (Abraham and Lucius, 2004). Figure 9 shows the locations of resistivity transects, unsaturated-zone sampling boreholes, and temperature measurement sites.

Results and Discussion

Streamflow Characteristics

The volume of water passing the USGS streamflow-gaging station at Beatty, Nev. (10251217; "Beatty gage" hereafter) during the four-year study period was 3.03 million cubic meters (Mm^3), averaging 0.76 Mm^3 per year (table 3; fig. 5). Even though precipitation during the study period was greater than the long-term average—25 percent greater at the ADRS, for example—the streamflow represents only a small fraction (less than 4 percent on an average annual basis) of historic maximum ground-water withdrawals in the Amargosa Farms area. Ranking the daily average flows, a sharp inflection point separates base flow from storm runoff at about 2.5 cubic meters per minute ($m^3\ min^{-1}$). Base flow dominates the record in terms of duration and volume. About 95 percent (1389 of 1461) of daily average flows were less than 2.5 $m^3\ min^{-1}$. From a volume standpoint, roughly three quarters of the discharge at the Beatty gage during the four-year period—2.26 Mm^3 of 3.03 Mm^3—was base flow. The dominance of base flow into the Amargosa Desert Basin contrasts sharply with the dominance of storm flow in the Abo Arroyo portion of the middle Rio Grande Basin (chapter D, this volume), reflecting weaker monsoonal influences, higher aridity, and the relatively permeable rocks and sediments of the Amargosa headwaters compared to the Abo Arroyo headwaters.

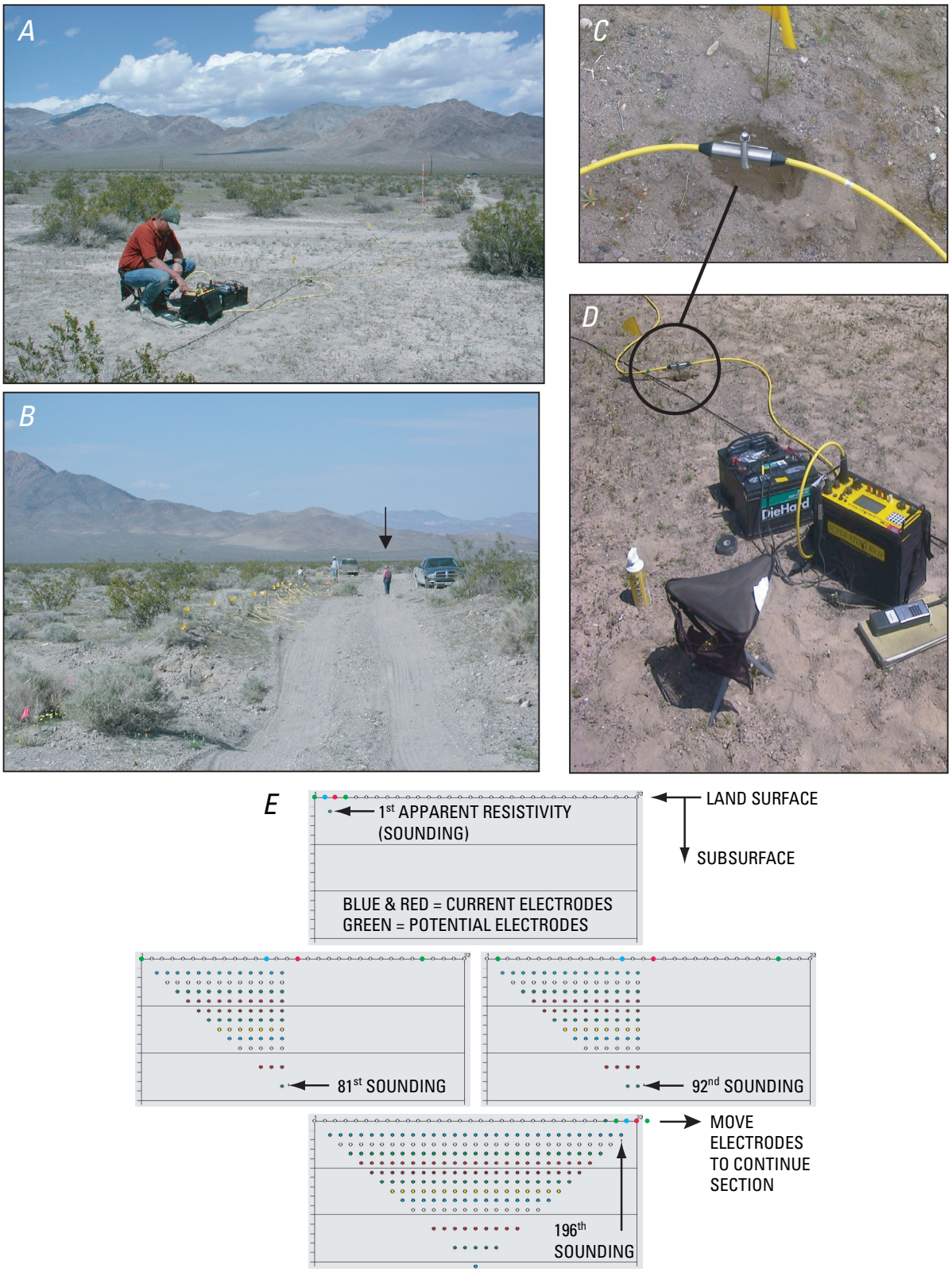

Figure 8. Direct-current resistivity imaging in the Amargosa Desert study area. *A,* Transect near Amargosa Desert Research Site (ADRS; Andraski and Stonestrom, 1999); *B,* transect across Amargosa River channel (arrow points to person in channel); *C*, electrode (stainless steel stake); with wetted sediment around electrode to decrease contact resistance; *D*, multiplexing resistivity meter; *E,* sequence of measurements.

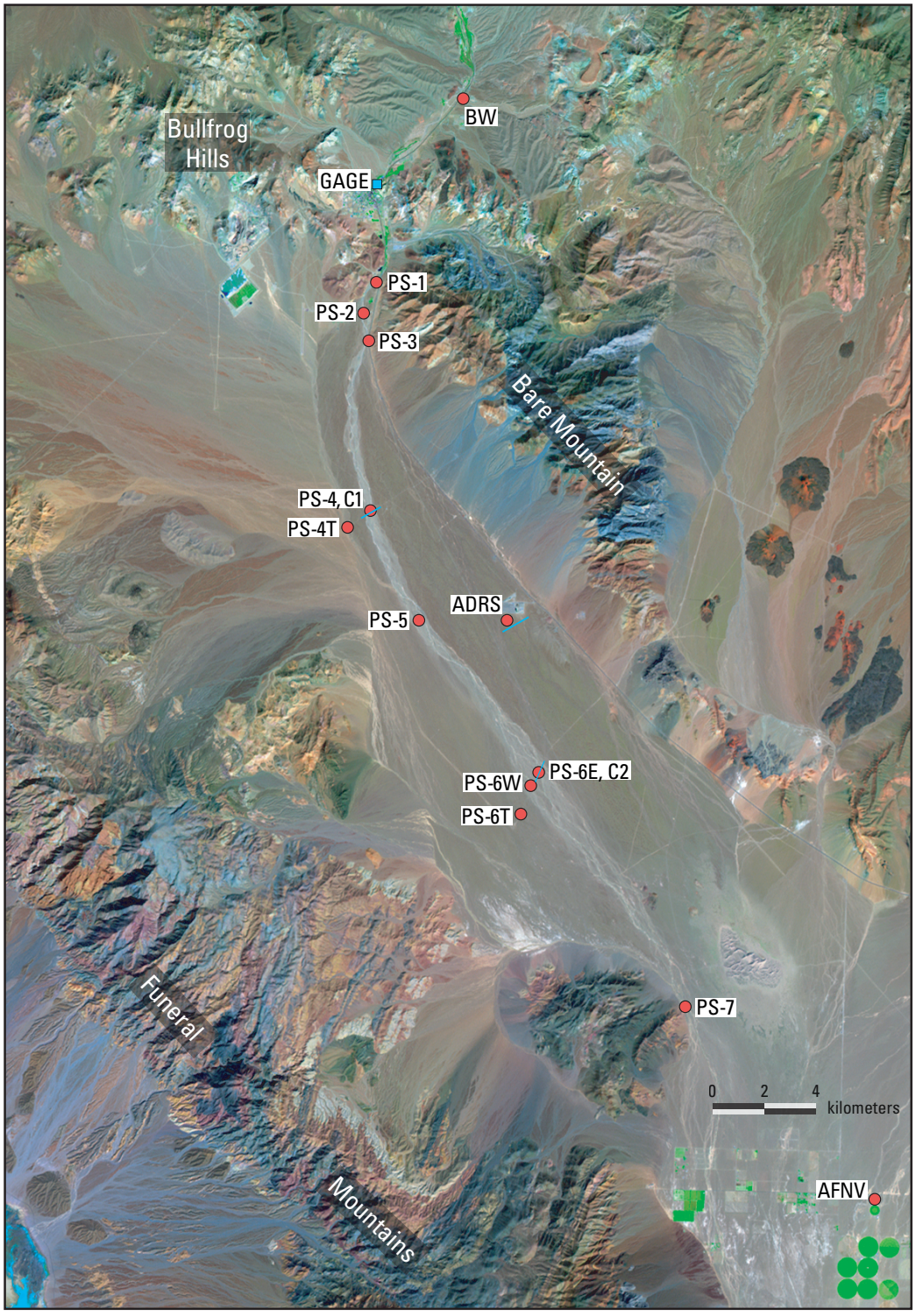

Figure 9. Detailed locations of temperature sites, resistivity transects, and unsaturated-zone boreholes in the Amargosa Desert study area. Temperature-measurement sites are denoted by PS-number (table 1). ADRS and AFNV denote boreholes in undisturbed native vegetation at the Amargosa Desert Research Site and in the Amargosa Farms area (table 2). Additional boreholes in irrigated fields south and southeast of AFNV (not shown) are listed in table 2. Resistivity transects are denoted by blue lines near probe sites PS-4, PS-6, and borehole ADRS. Blue square (GAGE) denotes the USGS streamflow-gaging station at Beatty, Nev. (10251217). Figure 1 shows the study-area location with latitudes and longitudes.

Table 3. Amargosa River flow at Beatty, Nev. (USGS streamflow-gaging station 10251217) for water years 1998–2001. Summary daily statistics and total storm-flow versus base-flow volumes.

Water year[1]	Median daily average flow, in cubic meters per minute	Maximum daily average flow, in cubic meters per minute	Minimum daily average flow, in cubic meters per minute	Total volume[2], in millions of cubic meters	Storm-flow volume[2], in millions of cubic meters	Base-flow volume[2], in millions of cubic meters	Base-flow volume, in percentage of total volume
1998[3]	1.1	37	0.42	0.88	0.36	0.52	59
1999[3]	1.2	19	0.41	0.69	0.08	0.61	89
2000[3]	1.0	13	0.46	0.73	0.17	0.56	77
2001[4]	0.9	20	0.55	0.74	0.17	0.56	77
Four-year study period							
1998–2001	1.1	37	0.41	3.0	0.78	2.3	74

[1]Water year is October 1 through September 30 and denoted by calendar year in which it ends.

[2]Values rounded for reporting purposes. Calculations used unrounded numbers.

[3]Water-year statistics derived from daily means obtained at http://waterdata.usgs.gov/nwis; accessed January 3, 2007.

[4]Statistics derived from daily means of 15-minute data.

The strongest El Niño of the modern instrumental record (post 1981) produced increased precipitation during the first year of the study period (Curtis and Adler, 2000; Vecchi and others, 2006). Rainfall at the ADRS in water year 1998 was 238 mm, more than twice the long-term average (Johnson and others, 2002). February was the wettest month, accounting for about 42 percent of annual precipitation. Frontal systems moving through the region resulted in several flows into the Amargosa Desert Basin, with peak flows at the Beatty gage larger than 20 m^3 min^{-1} on two occasions by mid month, February 4, 1998 (36 m^3 min^{-1}) and February 15, 1998 (44 m^3 min^{-1}). These storms were followed by a large, slow-moving system that produced widespread flooding on February 23–24. The largest flow of the study period, about 150 m^3 min^{-1}, occurred on February 23 (fig. 5).

Other large runoff events occurred in July 1999, August 2000, and July 2001 (fig. 5). Of these, only the July 1999 flows traversed more than a few kilometers into the Amargosa Desert Basin. The July 1999 flows stemmed from a stationary region of high-pressure that started building over the four-corners region early in the month. Associated anticylonic circulation transported subtropical moisture from the Gulf of California into the Amargosa area. Flashy runoff from convective storms was recorded by the Beatty gage on July 9, 13, and 14 (fig. 5).

Site visits following large storms established the extent and peak rates of flow. Table 4 shows estimated peak flows for storms during the study period that produced peak flows at the Beatty gage exceeding 80 m^3 min^{-1}. Peak-flow estimates were made by using the slope-area method, where the energy gradient was determined by detailed surveying of high-water marks, and the slope-conveyance method, where the gradient is approximated by the channel slope. Whereas slope-area estimates are more accurate, they too are uncertain (Jarrett, 1987). In both cases the largest errors are systematic, making relative changes instructive.

An actively used road to a mining operation crosses the channel near PS-2, 2.4 kilometers from the entrance to the basin (fig. 9). The unpaved road lacked culverts and was regraded following flow events that extended into the basin past the road. The February 1998 flows readily breached a low roadbed, judging from high-water marks upstream and downstream of the road. The first of the July 1999 flows breached a higher roadbed, which acted as a temporary dam. Thus, peak flows of the July 1999 event downstream of PS-1 were artificially increased by the sudden release of ponded water.

Streamflow passing through the Beatty gage is generally lost to seepage within a few kilometers of entering the Amargosa Desert Basin. The storm-generated flow of February 23-24, 1998 passed through the entire basin, extending from the Nevada Test Site to Death Valley (Tanko and Glancy, 2001). The peak flow rate was estimated to be 156 m^3 min^{-1} at Beatty (90 cubic feet per second) and 36 m^3 min^{-1} at Big Dune (20 cubic feet per second). These estimates indicate that 120 m^3 min^{-1} of flow were lost along the reach, if lateral inflows were negligible. Assuming a uniform loss rate, the average loss rate was about 3.4 m^3 min^{-1} per kilometer. This suggests that a flow event with a peak rate of at least 44 m^3 min^{-1} at the Beatty gage would reach channel site C1, the instrumented borehole at PS-4, and similarly 85 m^3 min^{-1} would reach channel site C2, the instrumented borehole at PS-6E. Site C1 and C2, respectively, are 13.6 and 25.9 km downstream of the Beatty gage.

Table 4. Estimates of peak flow in the Amargosa River and its main tributaries in the Amargosa Desert study area for major runoff events during water years 1998–2001.

[<, less than; ~, approximately]

Brief description and site code[1]	February 23–24, 1998	July 13, 1999	August 30, 2000	July 7, 2001
	Estimated peak streamflow, in cubic meters per minute[2]			
Beatty Wash (BW)	39 (51)	0	0	204
Beatty gage (GAGE[2])	143 (153)	143	126	88
Highway 95 bridge (PS-1)	117	51	minor	3
Airport road (PS-2)	65	204	~0[3]	<0.2
Bend (PS-3)	56	119	~0[3]	—[4]
Beacon road (C1)	39	76	0	—[4]
Beacon tributary (PS-4T)	0	~0[3]	~0[3]	—[4]
West of ADRS (PS-5)	53	51	~0[3]	—[4]
Ashton east branch (C2)	39	8	~0[3]	0
Ashton weat branch (PS-6W)	24	17	~0[3]	0
Ashton tributary (PS-6T)	0	0	0	0
Big Dune (PS-7)	16 (34)	2	0	0

[1]Tables 1 and 2 give site locations.

[2]Sites not at USGS streamflow-gaging station 10251217—Amargosa River at Beatty, Nev. (GAGE) were estimated by slope-conveyance method. Slope-area estimates, where available, are in parentheses.

[3]Peak flow too small to measure (approximately zero)—evidence of sheet flow or segmented flow and local ponding only.

[4]Site not visited, but presumed to have had no flow.

To characterize the frequency of flows capable of reaching C1 and C2, data from stream-gaging stations at Beatty (including historic partial-record crest-stage stations listed in the caption to fig. 6) were compiled for the 37-year period of record. Flow events with a peak discharge greater than 44 $m^3\ min^{-1}$ occurred on at least 26 occasions (Stonestrom, Prudic, and others, 2003). Flows with peaks greater than 85 $m^3\ min^{-1}$ occurred on at least 16 occasions. Not all flows were documented, as only annual peak discharges were recorded in most years. The largest flow on record occurred on February 24, 1969 (fig. 6). This flood peaked at about 27,000 $m^3\ min^{-1}$, surpassing other flows by a factor of 3.8 (Moosburner, 1978).

Flow durations were characterized with data from the Beatty gage, where stage was recorded every 15 minutes from August 1993 to April 1995 and from January 1996 to October 2001. Flow was divided into 4 categories: 0 to 6 $m^3\ min^{-1}$, greater than 6 to 44 $m^3\ min^{-1}$, greater than 44 to 85 $m^3\ min^{-1}$, and greater than 85 $m^3\ min^{-1}$. Flow at the Beatty gage was less than 6 $m^3\ min^{-1}$ about 99 percent of the time. Flows greater than 44 $m^3\ min^{-1}$ occurred only about 0.13 percent of the time. Flows greater than 85 $m^3\ min^{-1}$ occurred only about 0.04 percent of the time. Assuming no lateral inflow from tributary channels, and a uniform loss rate, the estimated total duration of flow at C1 is about 11 hr yr^{-1} at C1 and 3.5 hr yr^{-1} at C2. Average seepage losses during flow events, assuming an average channel width of three meters, is about 1.1 millimeters per minute, or 68 millimeters per hour. Multiplying this rate by 11 hours yields an annual infiltration rate of about 0.75 m yr^{-1} at C1. Similarly, multiplying by 3.5 hr yields an annual infiltration rate of about 0.24 m yr^{-1} at C2 (table 5). These estimates are approximate and do not consider possible additions from tributaries or direct runoff from the basin floor. They also do not consider antecedent conditions and variations in channel width. Nevertheless, the data indicate that seepage losses occur throughout the study reach.

Thermal Detection of Streamflow and Infiltration

Streambed thermal anomalies provided detailed information on the extent and duration of flows. Figure 10 shows precipitation, streamflow, and example thermographs for the

Table 5. Infiltration- and recharge-flux densities as estimated from pore-water concentrations of chloride and nitrate in contrasting hydrologic settings, Amargosa Desert study area.

[m/yr, cubic meters of water per square meter of land surface per year; g/m^2 yr, grams per square meter of land surface per year; g/m^3, grams per cubic meter of pore water; m^3/m^3, cubic meter of pore water per cubic meter of bulk sediment]

Borehole code[1]	Infiltration-flux density[2], in m/yr	Chloride-mass flux across land surface[2], in g/m^2 yr	Interval used for calculation, in meters	Recharge, in percentage of infiltration	Chloride concentration in interval, in g/m^3	Recharge-flux density from chloride mass-balance, in m/yr	Average water content in interval, in m^3/m^3	Estimated time to reach water table[3], in years	Recharge-flux density from tracer-velocity[2], in m/yr
Amargosa River channel (ephemeral flow, normally dry)									
C1	0.75	11	1.1–14.4	12	121	0.09	0.21	225	NA[4]
C2	0.24	4	1.6–9.5	15	97	0.04	0.18	470	0.07
Undisturbed native vegetation (interfluvial surfaces)									
ADRS	0.11	0.06	—[5]	—	—	—	—	—	—
AFNV	0.11	0.06	—	—	—	—	—	—	—
Field 1 (7.7–year old irrigated field, used continuously)									
AF-1A	2.1	14	1.5–5.9	6	116	0.12	0.21	60	0.19[6]
AF-1B	2.1	14	1.2–14.0	10	69	0.21	0.20	34	0.30[6]
Field 2 (irrigated field, used intermittently since the 1960s)									
AF-2A	2.1	14	0.8–9.8	22	30	0.47	0.16	12	0.17[7]
AF-2B	2.1	14	1.2–9.7	9	71	0.20	0.16	30	0.13[7]
Field 3 (irrigated field, used continuously since the 1960s)									
AF-3A	2.8	19	0.8–9.9	14	48	0.44	0.17	14	NA[4]
AF-3B	2.8	19	0.8–16.0	17	42	0.50	0.22	15	NA[4]

[1]See table 2 and figure 9 for locations.

[2]Surface fluxes and chloride concentrations from Stonestrom, Prudic, and others (2003).

[3]Water table is about 35 meters deep beneath the Amargosa farms (AF) sites and 100 meters deep beneath the Amargosa River channel (C1 and C2) sites. Travel times assume one-dimensional vertical flow.

[4]NA, not available.

[5]—, not applicable.

[6]From velocity of chloride peak.

[7]From velocity of nitrate peak.

February 23–24, 1998 flow event. Comparisons of the channel thermographs with control thermographs outside the active channel at PS-1, PS-5, and PS-6E allowed non-flow events to be differentiated from flow events, even for low-flow conditions (fig. 11; Constantz and others, 2001).

Figures 12 and 13 show typical thermographs for dry-channel and flowing conditions, repectively. In Beatty Wash, just upstream of its confluence with the Amargosa River, flow began at about 10:00 a.m. on February 23 and ended 17 hours later. The duration was extended by snowmelt from higher elevations (Tanko and Glancy, 1999). The initiation of flow is indicated by the change from a diurnally varying temperature to a nearly constant temperature. The cessation of flow is indicated by reappearance of the diurnal signal. Flow exhumed the temperature logger, increasing the diurnal range. Twelve hours after arriving at Beatty Wash, flow arrived at the PS-1 site, 9.1 kilometers downstream. Flow at PS-1 lasted about 8 hours. Flow arrived at PS-6E at about 3:00 a.m. on February 24, 31.2 kilometers downstream from Beatty Wash, and lasted about 3 hours.

Flows in February 1998 occurred during long periods of overcast skies, reducing the magnitude of thermal signals. Summer flows were marked by larger signals. Figure 14 shows thermographs indicating the July 1999 flows. The contrast between ambient streambed temperatures and ephemeral streamflow averages about 10°C. Flows are more easily identified in summer than in winter, because of greater contrasts between the temperature of streamflow and channel sediments prior to flow.

Brief periods of flow near the basin inlet also were indicated by thermocouple-nest data corresponding to the January-February 2001 flow events. Times of peak flows as recorded by the Beatty gage (fig. 5) are indicated by arrows (fig. 15). Downward advection of heat by infiltrating water compressed the ambient range in temperatures and carried diurnal fluctuations deep into the profile. The thermal anomalies from brief periods of ephemeral flow appear as perturbations on the seasonal turnover of the temperature gradient (fig. 15).

Nearly all of the thermal records are for dry-channel conditions, but even these show systematic variations consistent with the relative frequency of flow. Average channel temperatures increased with distance from the basin inlet. The increase is greater than the 0.0098°C per meter of altitude decrease expected on the basis of weather-station data, suggesting cooling from greater quantities of infiltration and evaporation closer to the basin inlet. Deep temperature profiles support this suggestion. Annual temperature envelopes at the two channel locations (C1 and C2) and at the ADRS (between C1 and C2) show that the highest temperatures are outside the channel, where deep percolation and evaporated streamflow amounts are negligible. The coolest conditions are at the upstream channel location, where streamflow is most frequent and deep percolation amounts highest (fig. 16). The temperature difference between upstream and downstream locations is about 20 percent greater than can be accounted by the difference in elevation. The difference between the warmest temperatures, at the ADRS, and coolest temperatures, at the downstream channel site, is opposite that expected from altitude.

The difference in annual volume of infiltrated water between upstream and downstream channel locations is about 1.5 m^3 per meter of channel length. Assuming reasonable values for sediment density (2.0×10^6 gram m^{-3}) and heat capacity (2.2×10^6 joule m^{-3} $°C^{-1}$) at ambient water content, and given the large latent heat of evaporation (2.27×10^9 joule m^{-3}), the cooling power of infiltrated water is more than sufficient to account for the difference in temperatures. If half of the infiltrated volume later evaporated, channel sediment 3 meters wide (the width of the active channel) by 20 meters deep would cool about 13°C per year if all heat came from cooling of the sediment. Depth and degrees of cooling are inversely proportional. The actual cooling is far less than this because of heat exchange with surrounding sediments. Nevertheless, average temperatures reflect differences consistent with infiltration and recharge regimes.

Recharge Estimates from Potential and Environmental-Tracer Profiles

Profiles of water potential, water content, and solute concentrations beneath irrigated fields, undisturbed native vegetation, and the normally dry channel of the Amargosa River also reflect the contrast in recharge regimes. Examples of water-potential profiles beneath the channel, native vegetation, and irrigated fields are shown in figure 17. Water potentials generally are low beneath native vegetation, with potentials lower (more negative) than –5 megapascals (MPa) in most of the profile. The profile beneath native vegetation in the Amargosa Farms area is similar to the profile beneath native vegetation at the ADRS, where calculated deep-percolation fluxes are zero to slightly upward (Walvoord and others, 2004). Gradients of temperature, water potential, and stable isotopes beneath undisturbed native vegetation at the ADRS indicate a net upward flow of heat and water throughout the profile (Stonestrom and others, 1999). Models of heat and water movement indicate that these profiles are not in equilibrium with current climatic conditions—instead, they are slowly drying in response to the change from pluvial to arid conditions that occurred in the late Pleistocene (Walvoord and others, 2004).

In contrast, to the profiles beneath native vegetation, water potentials beneath irrigated fields and the Amargosa River channel indicate net downward movement of water, with potentials close to zero in most of the profile (fig. 17). Water potentials are more variable beneath a more recently converted field than beneath fields converted in the 1960s, reflecting the shorter duration of irrigation return flow. High, nearly uniform water potentials beneath the older fields and channel sites indicate long-established deep percolation in which the sediments have water potentials associated with approximately steady-state downward flow (Stonestrom, Prudic, and others, 2003).

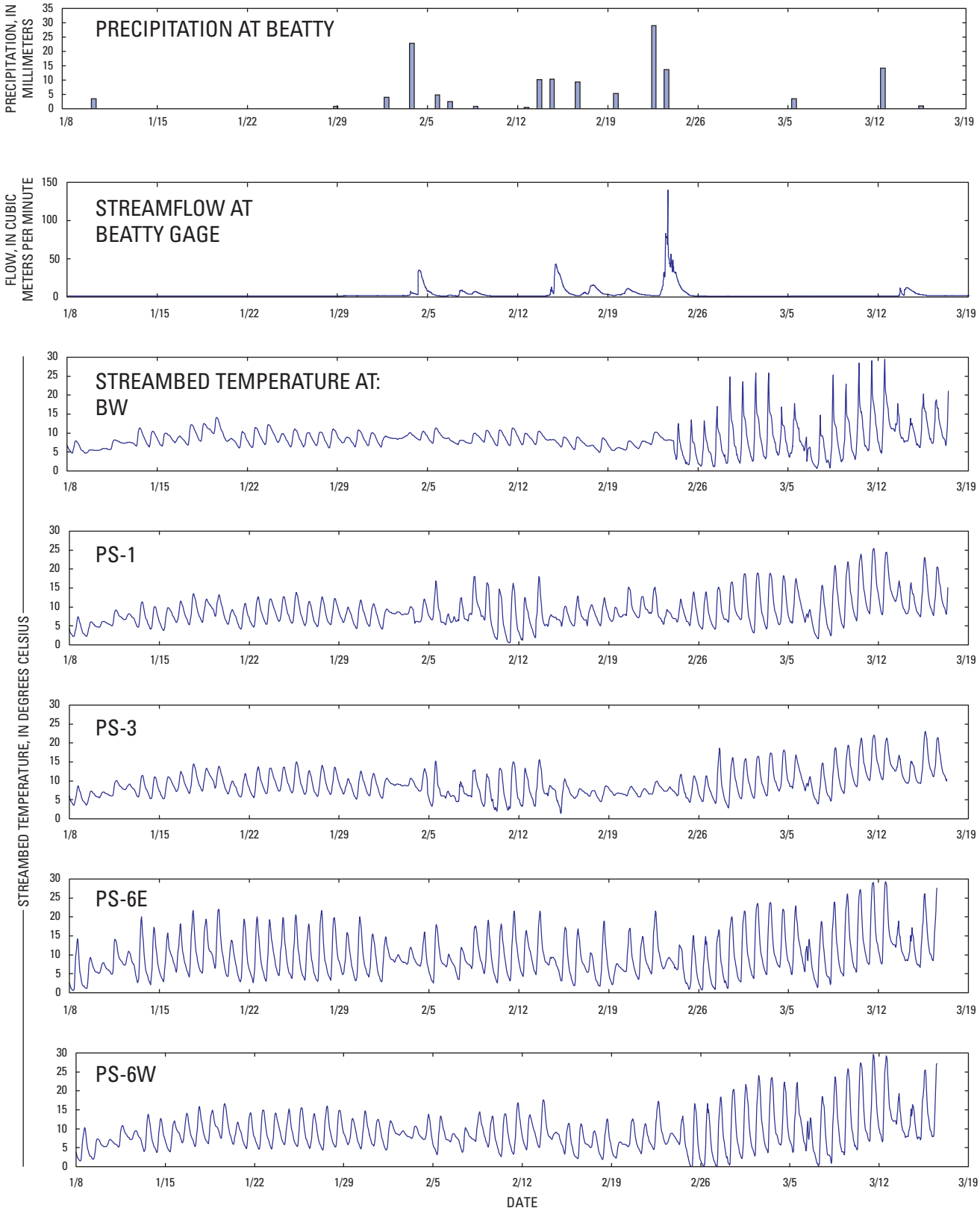

Figure 10. Precipitation and streamflow at Beatty, Nev., and streambed temperatures at selected sites in Beatty Wash (BW) and the Amargosa River channel, January 8 through March 17, 1998. Site locations are shown on figure 9.

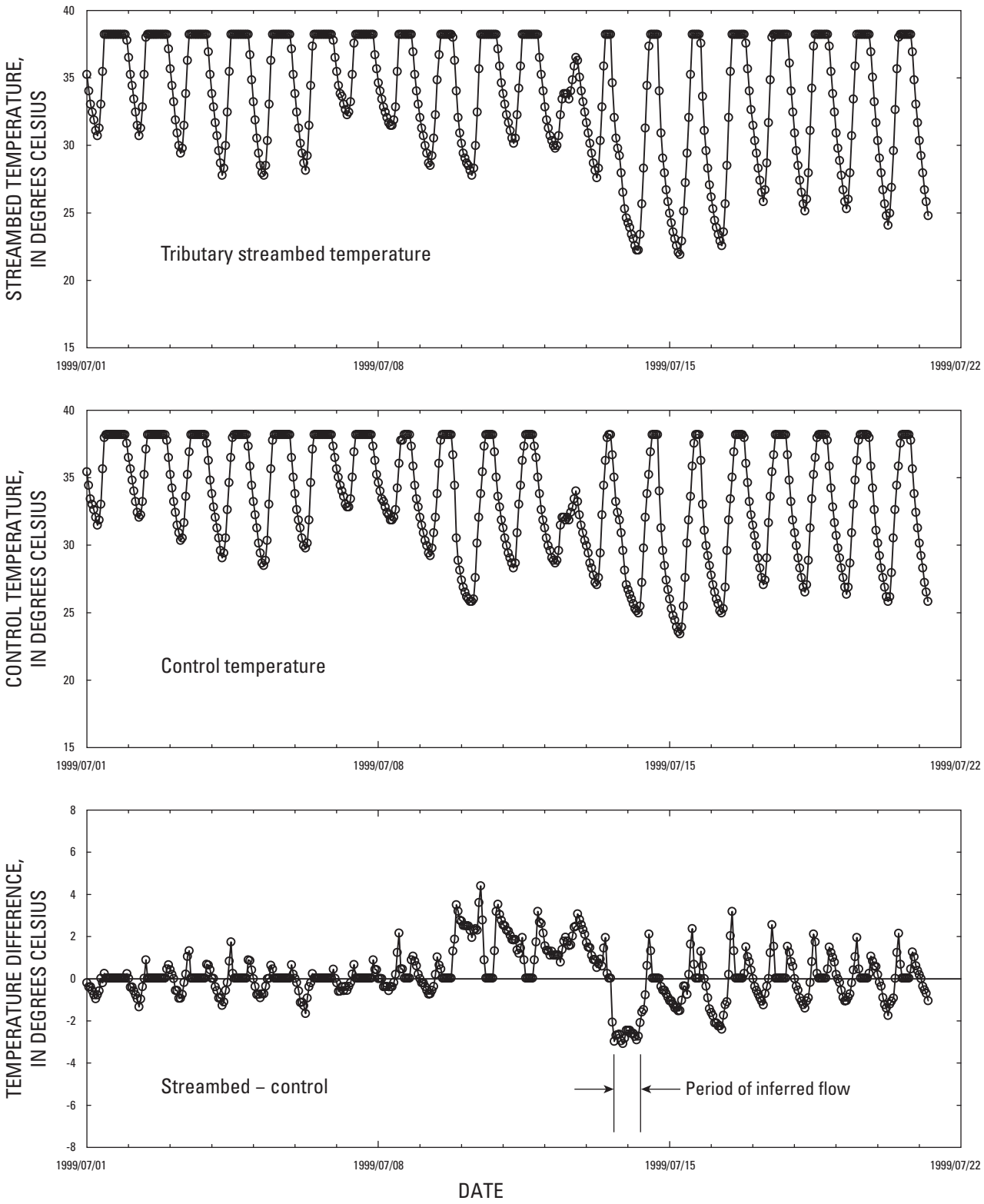

Figure 11. Timing of sheet flow in an unnamed minor tributary to the Amargosa River (site PS-6T, figure 9) is indicated by a drop in the streambed temperature as compared to the control temperature. Temperatures higher than the upper limit of the temperature logger are truncated at 38ºC.

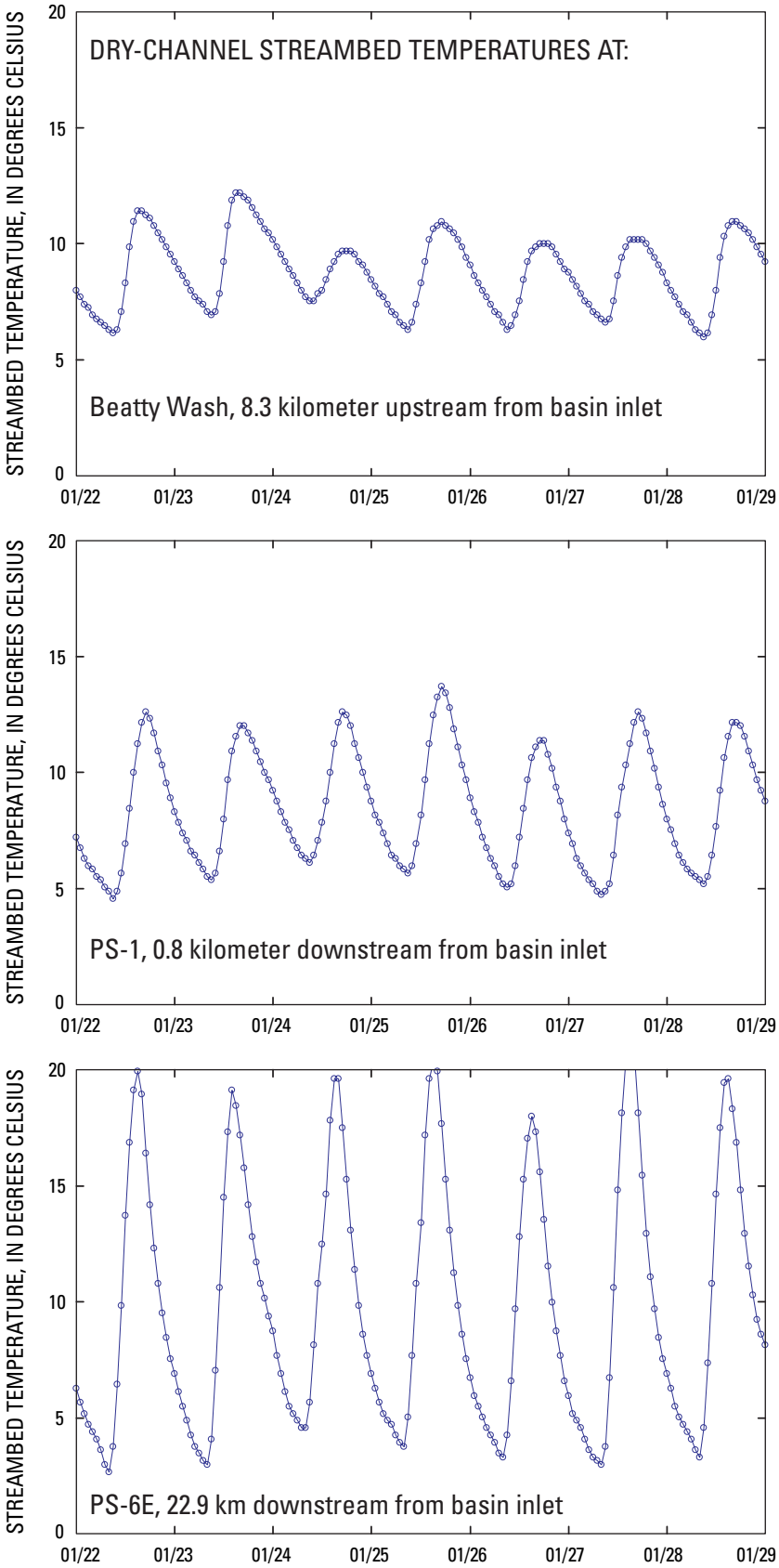

Figure 12. Example streambed temperatures during dry conditions, Amargosa Desert study area, January 22 through 28, 1998. Site locations are shown on figure 9.

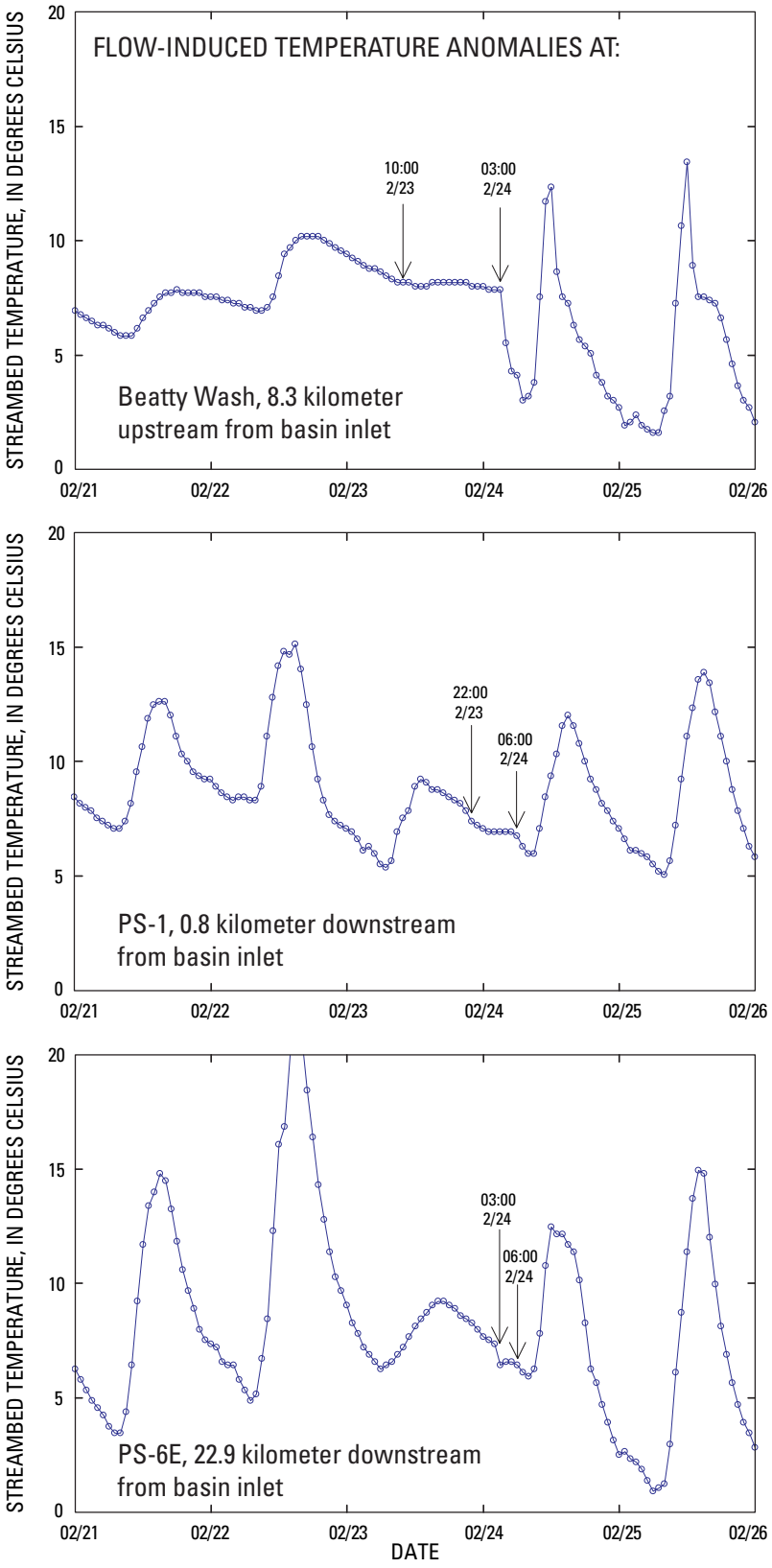

Figure 13. Example streambed temperatures during period with ephemeral flow, Amargosa Desert study area, February 21 through 25, 1998. Arrows indicate thermal anomalies interpreted as initiation and cessation of flow. Site locations are shown on figure 9.

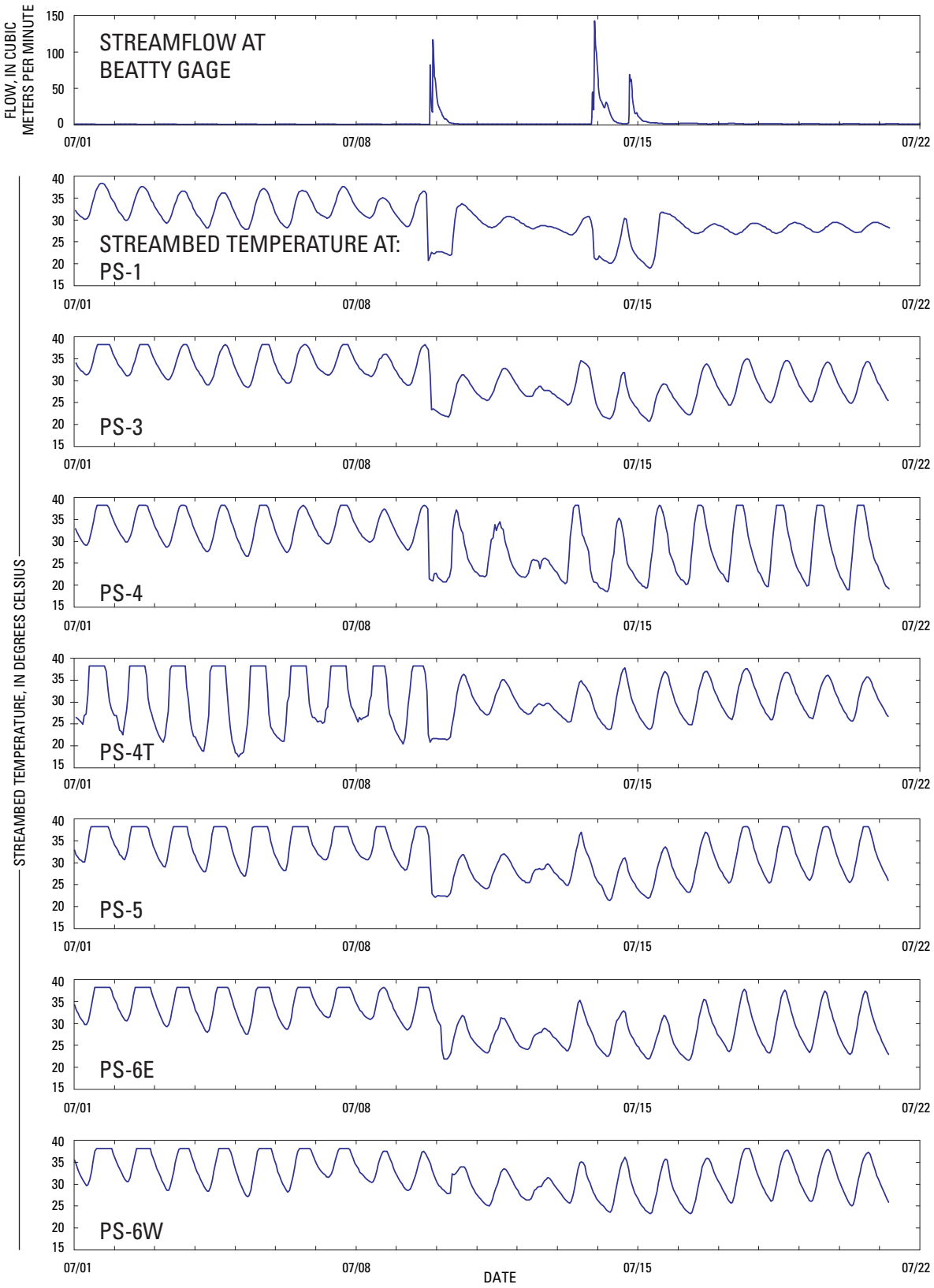

Figure 14. Amargosa River streamflow at Beatty, Nev., and streambed temperatures downstream, July 1 through 21, 1999. Temperatures higher than the upper limit of the temperature logger are truncated at 38ºC. Figure 9 shows site locations.

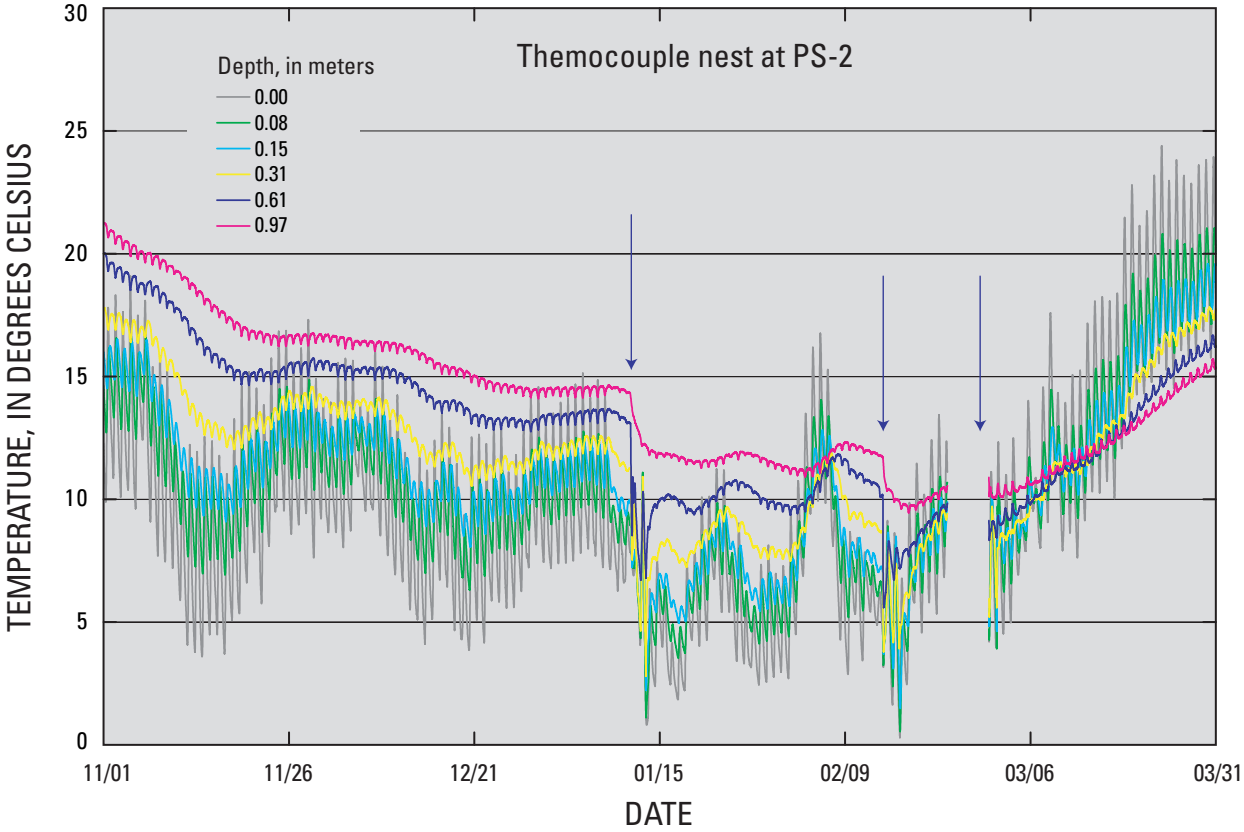

Figure 15. Channel temperatures at six depths near PS-2, 2.4 kilometers from the basin inlet, Amargosa Desert study area, November 2000 through March 2001. Arrows show times of peak flow at Beatty (fig. 5). Gap in record is due to loss of power to data logger.

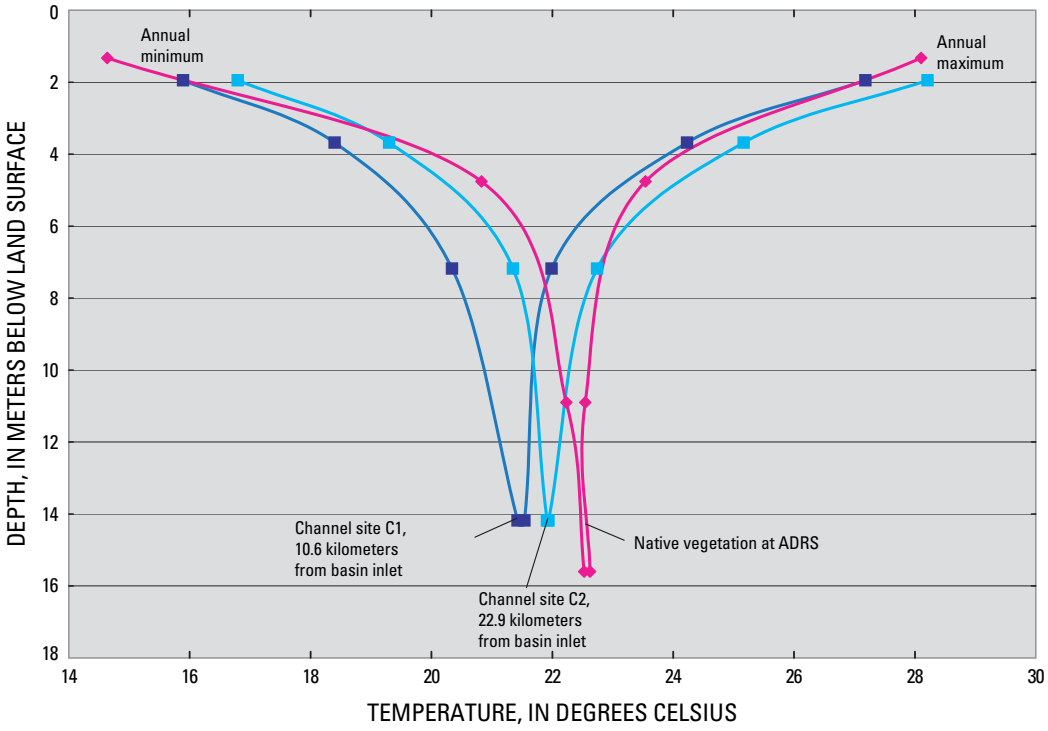

Figure 16. Annual temperature envelopes beneath channel site C1 and C2, 10.6 and 22.9 km downstream from the Amargosa Desert Basin inlet, and beneath native vegetation at the Amargosa Desert Research Site (ADRS), halfway between C1 and C2. Figure 9 shows site locations.

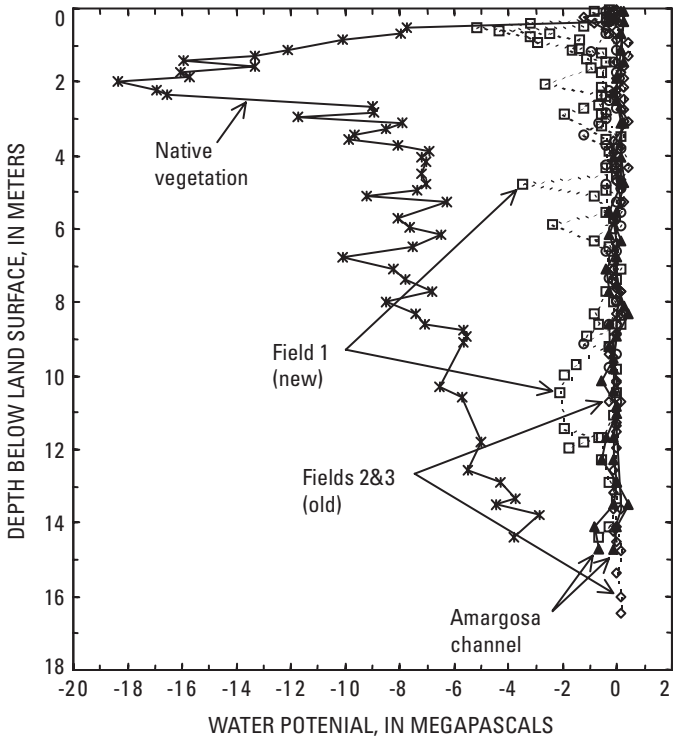

Figure 17. Unsaturated-zone water potential profiles beneath native vegetation and irrigated fields in the Amargosa Farms area, and the normally dry Amargosa River channel. Storms wetted surface sediments prior to sampling in February 2001, producing near-zero water potentials at shallow depths at all sites. Water potentials beneath the Amargosa River channel (C1 and C1, triangles) and older fields (2 and 3, circles and diamonds) are close to zero throughout the profile. Water potentials beneath the new field (open squares) are near zero but more variable than beneath the older field. From Stonestrom and others (2004).

Chloride and nitrate profiles at all undisturbed native-vegetation sites are similar, with large increases in concentration (bulges) just below the root zone (fig. 18). Bulges in the concentrations of atmospherically derived salts are common beneath desert plants (Phillips, 1994; Tyler and others, 1996; Hartsough and others, 2001). Initiation of chloride accumulation dates back to the major change in climate from the cool and wet (pluvial) conditions prevailing during the late Pleistocene to the arid-thermic conditions prevailing today (Walvoord and others, 2004). Increasing aridity led to the succession of xerophytes efficient at scavenging moisture, resulting in accumulation of atmospherically deposited salts just beneath the root zone (Walvoord, Plummer, and others, 2002; Walvoord, Phillips, and others, 2002). The change from pluvial to dry conditions in the Amargosa Desert Basin may have started as early as 20,000 years ago on the basis of vegetation changes in the area (Spaulding, 1985), paleoclimate modeling (Spaulding and Graumlich, 1986), and an abrupt decline in ground-water level recorded at Devils Hole (fig. 1; Szabo et al., 1994).

Assuming that the profiles beneath field 1 were initially like those beneath undisturbed native vegetation, chloride peaks at depths of about 9 and 13 m demonstrate that deep percolation from irrigation return flow is moving previously accumulated chloride downward from just below the root zone (fig. 18*A*). Eight years of irrigation is insufficient to flush accumulated salts from the sampled profile completely. Sub-root-zone nitrate profiles are similar to the chloride profiles, reinforcing this conclusion (fig. 18*B*).

Chloride concentrations beneath the root zone of field 2 are uniformly low, indicating that deeply percolating irrigation water has flushed the presumed preexisting bulge completely from the measured profile (fig. 18*A*). Sub-root-zone nitrate concentrations are much lower than chloride concentrations at most depths, except for one interval in each profile where nitrate concentrations are consistently at least twice the chloride concentrations. These well-defined nitrate peaks occur in the 6.9–8.3-m interval at one borehole and in the 8.3–9.8-m interval at the other (fig. 18*B*). The peaks most likely represent heavy application of liquid fertilizer in 1992, when the field was returned to production.

Profiles of chloride and nitrate beneath the Amargosa River channel are similar to those beneath the irrigated fields in that they lack salt accumulations near land surface (fig 18). Chloride and nitrate concentrations at the upstream site are low throughout the profile at all depths greater than 1 m. Concentrations at the downstream site rise sharply in the 10 to 14-m depth interval. This abrupt rise suggests downward displacement of a previously formed salt bulge, similar to the downward-advected bulge at field 1.

The active channel at C2 appears to have moved to its current position during the record flood of 1969 (fig. 6). Aerial photographs taken before 1969 show the channel at C2 about 0.5 kilometer east of its present location and the channel at C1 in its present location. Photos taken after 1969 show the channel in its present location at both sites. As at field 1, the duration of deep percolation at C2 has been insufficient to move previously accumulated salts completely from the sampled profile.

General Patterns of Deep Percolation and Ground-Water Recharge

The slope of the relation between cumulative chloride and cumulative water represents a depth-integrated pore-water chloride concentration. A linear relation that passes through the origin is consistent with the hypothesis that chloride fluxes at depth are in approximate equilibrium with time-averaged fluxes across the land surface, in accordance with the assumptions of the chloride mass-balance method (Stonestrom, Prudic and others, 2003).

Almost all of the profiles beneath the irrigated fields and channel sites show evidence of approximately steady-state

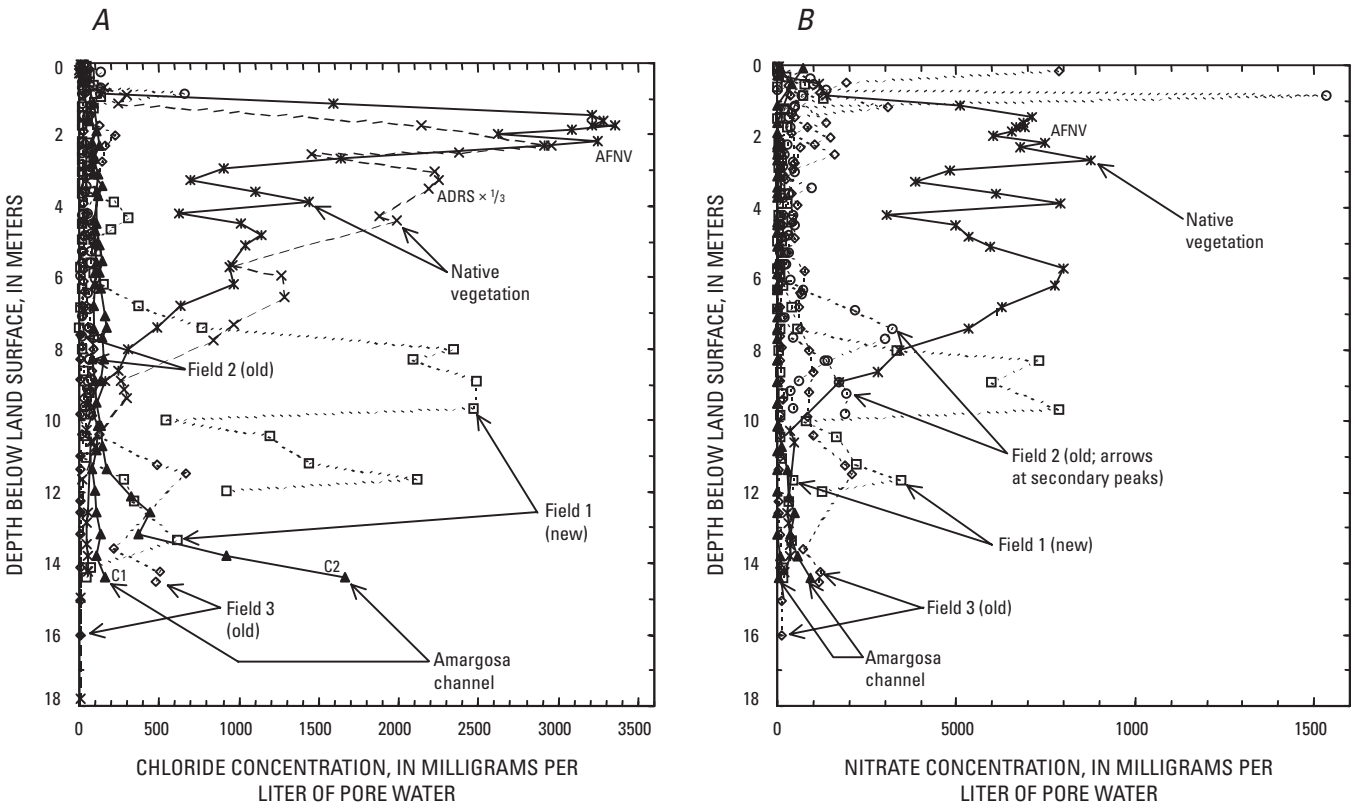

Figure 18. Profiles of anion concentrations in pore water beneath native vegetation, irrigated fields, and the Amargosa River channel, in the Amargosa Desert study area. *A,* chloride-concentration profiles; *B*, nitrate-concentration profiles. The ADRS is the Amargosa Desert Research Site (fig. 9). From Stonestrom and others (2004).

deep percolation, that is, simple linear relations that extrapolate towards the origin (fig. 19). Deviations in slope near the origin reflect the effects of unfiltered variations in surface forcing from meteorological conditions in the immediate past. The new field and the downstream channel site show concave upward departures from linearity at depth. As already discussed, these reflect previously formed shallow salt accumulations moving downward through the profile due to the recent onset of deep percolation.

In contrast to the sites indicating steady deep percolation, relations between cumulative chloride and cumulative water content beneath native vegetation are characterized by steep segments at shallow depths (close to the origin) that do not extrapolate through the origin, followed by sharp inflections to relatively low slopes beneath the root zone (far from the origin; fig. 19). These patterns indicate a lack of chloride throughput due to lack of water movement between the bottom of the root zone and the water table. The non-linear relations show that chloride fluxes at depth are not in equilibrium with fluxes across the land surface, violating a key assumption of the chloride mass-balance approach (Scanlon, 2000).

Multiyear observations at the ADRS indicate that precipitation on areas of undisturbed native vegetation penetrates to depths of less than one meter before returning to the atmosphere (Fischer, 1992; Andraski, 1997). Isotopic data from the ADRS (Stonestrom and others, 1999) and the Nevada Test Site (Tyler and others, 1996) support the conclusion of negligible recharging fluxes under current climatic conditions and rule out dilution of deep pore water by preferential flow of recent infiltration. Instead, low chloride concentrations in pore water beneath shallow chloride and nitrate bulges represent relict recharge from pluvial periods. Modeling studies of coupled heat and water movement indicate that the net movement of water (liquid plus vapor) is upwards in an increasingly deep region beneath the root zone under current climatic conditions (Walvoord and others, 2004).

Estimates of Recharging Fluxes Beneath Irrigated Fields

Table 5 shows chloride mass-balance estimates of recharging fluxes beneath irrigated fields. The table includes the depth intervals and average pore-water chloride concentrations corresponding to the linear portions of the cumulative-water versus cumulative-chloride curve for which the chloride mass-balance method applies (fig. 19).

The chloride-mass balance estimates of deep percolation for field 1 are 0.12 and 0.21 m yr^{-1}. Downward displacement of the salt bulge following onset of irrigation in field 1

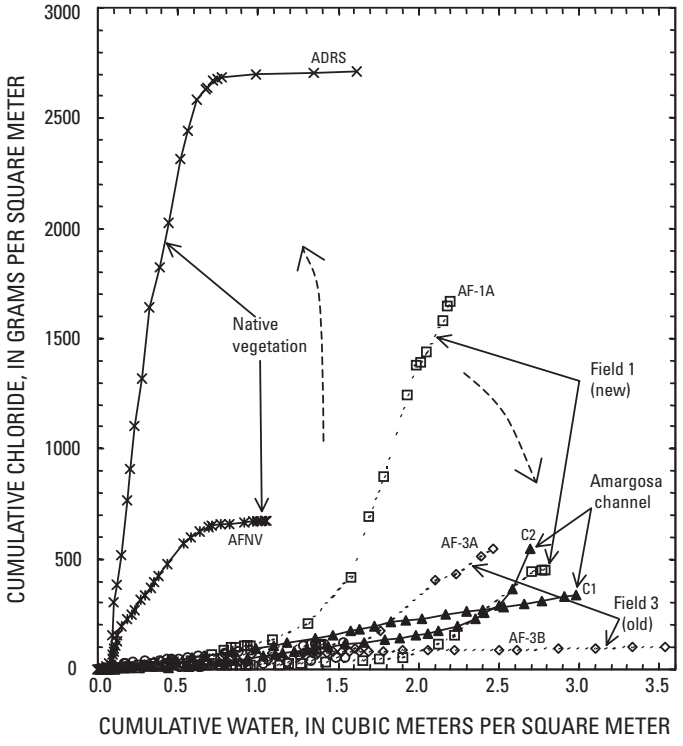

Figure 19. Cumulative mass of chloride versus cumulative volume of water beneath undisturbed native vegetation, irrigated fields, and the Amargosa River channel, in the Amargosa Desert study area. Slopes of the curves represent pore-water concentrations of chloride, which are inversely proportional to recharge rates for steady-state conditions (linear relations). AF-3B is in the interior of the field; 3A is on the perimeter. Dashed arrows indicate time trajectories of profile evolution under current climatic and land-use conditions. The ADRS is the Amargosa Desert Research Site (fig. 9). From Stonestrom and others (2004).

provides a largely independent estimate of deep percolation. Assuming that the center of mass of the chloride moved from about 1.8 m (the observed depth under native vegetation) to 8.9 and 13 m in 7.7 years, the macroscopic velocities of the bulge are 0.9 and 1.5 m yr^{-1}, respectively. Multiplying by the average water content gives deep-percolation estimates of 0.19 and 0.30 m yr^{-1} (table 5). These rates are about 50 percent higher than the chloride mass-balance estimates, reflecting the uncertainty of the estimates (Stonestrom, Prudic and others, 2003). Similar variations in deep-percolation rates characterized a sandy agricultural field in a semiarid region in the western Murray Basin, South Australia (Cook and others, 1989).

The chloride mass-balance estimates of deep percolation for field 2 are 0.20 and 0.47 m yr^{-1}. Travel-time estimates based on the nitrate peak are 0.13 and 0.17 m yr^{-1} (table 5). These estimates are based on the assumption that the deep nitrate peaks represent surface application of liquid fertilizer in 1992, when field 2 went back into production after being fallow for nine years. The lower nitrate-based values suggest retardation of nitrate relative to chloride in the root zone (Smith, Doyle, and others, 1997). Chloride mass-balance estimates of deep percolation beneath field 3 are 0.44 and 0.50 m yr^{-1} (table 5). The percentage of irrigation water returning to the water table is simply the ratio of chloride concentration in irrigation water to that in deep pore water. The average estimated percentage of return flow is 8 percent for field 1, 15 percent for field 2, and 16 percent for field 3. Differences correlated with cultivation histories. Field 3 had the highest rates of irrigation and the highest percentage of return flow.

The depth to ground water beneath the irrigated fields is about 35 m (Kilroy, 1991). Assuming vertical, one-dimensional flow, the estimated time for irrigation return flow to reach the water table is 12–30 years beneath fields 2 and 3, and 34–60 years beneath field 1 (table 5). This pattern is consistent with asymptotically decreasing divergence of infiltrating water through time following the onset of irrigation in an initially dry profile (Philip, 1983).

Estimates of Recharging Fluxes Beneath the Amargosa River Channel

Chloride mass-balance estimates of deep percolation for the upstream-channel site (C1) used the entire profile below 1.1 m, the depth below which the cumulative chloride-cumulative pore water relationship indicated approximately steady conditions (table 5). Estimates for the downstream site excluded concentrations deeper than 9.5 m. Elevated chloride beneath this depth evidently represents a near-surface accumulation that began moving downward when the active channel shifted to its current location, as indicated by aerial photographs. Chloride mass-balance deep-percolation rates were 0.09 m yr^{-1} at the upstream site and 0.04 m yr^{-1} at the downstream site. These rates exceed estimated sub-root zone liquid and vapor fluxes at the ADRS by several orders of magnitude (Walvoord and others, 2004). Thus, virtually all deep percolation beneath the channel becomes ground-water recharge.

Assuming that the chloride bulge at C2 moved downward from 1.8 to 14.4 m in the 32 years between the flood of 1969 and sampling in 2001, the macroscopic velocity is 0.39 m yr^{-1}. The travel-time estimate of deep percolation is the product of the macroscopic velocity times the volumetric water content of 0.18, or 0.07 m yr^{-1} (table 5). This value is in approximate agreement with the chloride mass-balance rate of 0.04 m yr^{-1}.

The percentage of channel infiltration that becomes deep percolation is about 12 percent for the upstream site and about 15 percent for the downstream site (table 5). Multiplying by the average annual streamflow volume of 3.0 Mm^3 yr^{-1} (table 3), the amount of ground-water recharge from channel infiltration is about 0.4 Mm^3 yr^{-1}.

Depth to ground water beneath the Amargosa River west of the ADRS was 103 m in 1985 (W.D. Nichols, USGS,

Carson City, Nev., unpub. data, 1985). Assuming the water table is about 100 m below the riverbed, channel infiltration takes approximately 225 years to reach the aquifer at C1 and 470 years at C2. These estimates are minimum times because the effects of lateral flow are not taken into account. While uncertainties in estimated recharge rates are considerable, the approximate agreement between travel-velocity estimates and chloride mass-balance estimates supports the general magnitude of the results.

Areal Generalization by Direct-Current Resistivity Imaging

The unsaturated-zone profiles considered above indicate that ground-water recharge is localized beneath the main channel of the Amargosa River and beneath irrigated fields, with little present-day recharge beneath native vegetation. These borehole-based results can be regionalized by remote sensing by using geomorphologic, pedologic, and vegetational mapping. To bridge the scales between remote sensing and borehole-profile analysis, the current study employed DC-resistivity imaging.

Numerical inversions of automated Schlumberger-array soundings assumed lateral homogeneity normal to the vertical slices being imaged, producing solution sets of resistivity values at several thousand points within each modeled cross section. Imaged sections were about 30 to 80 m deep and 1 kilometer wide. Root-mean square errors between apparent resistivities in the model inversions and field-measured apparent resistivities were about 10 percent (Stonestrom, Abraham, and others, 2003; Abraham and Lucius, 2004).

On the basis of core data from cased boreholes, inverted resistivity (Ω) values denoted three categories of alluvium: (1) low water-content coarse gravel and highly desiccated surface material, with ρ greater than 200 Ohm-meters (Ω-m), (2) vertical regions of moist alluvium in areas of active recharge, with ρ less than 20 Ω-m, and (3) other low to low-medium water-content alluvium in areas without active recharge, with intermediate values of ρ (fig. 20). The cross section beneath native vegetation near the ADRS reveals laterally extensive gravel layers that provide preferential pathways for gas transport but that are impeding layers for downward movement of water through the unsaturated zone (Mayers and others, 2005).

The DC-resistivity images indicate focusing of active recharge beneath the Amargosa River channel. At the incised channel location upstream (C1), vertically elongated, low-resistivity regions indicating relatively moist sediments span the half-kilometer width of the channel (fig. 20*A*). A finger of low-resistivity sediment lies beneath the present low-flow channel. Pronounced low-resistivity regions are also found beneath the migrating reaches of the channel at the downstream site (C2; fig. 20*B*). The ADRS transect and extra-channel portions of channel transects (fig. 20*C*) suggest that little recharge occurs throughout most of the basin floor.

Summary and Conclusions

The current study characterized streamflow and ground-water recharge in the sparsely populated Amargosa Desert Basin of Nye County, Nev. High frequency streamflow and channel-temperature data indicated patterns of ephemeral streamflow during a 4-year period (water years 1998 through 2001). The period included the largest El Niño of the modern instrumental period, which enhanced precipitation, and two years of below-average precipitation.

The channel of the Amargosa River is dry more than 98 percent of the time beyond a few kilometers downstream from the basin inlet, where perennial flow supports riparian vegetation. Base flow accounted for about three quarters of the 3.0 million cubic meters (Mm^3) of discharge at the Beatty gage during the 4-year study period. The average annual flow, 0.76 M m^3 per year, was small relative to historic ground-water withdrawals for irrigation.

Streambed temperature anomalies indicated the duration and extent of storm-generated ephemeral flow into the basin. Only two flows traversed the entire reach of the Amargosa River during the 4-year study period. Durations and amount of flow declined rapidly down channel due to infiltration losses. Channel temperatures increased as infiltration and evaporation amounts decreased. Temperatures were warmest at the ADRS site, which received no flow, and lowest at the upstream channel site that received the most flow.

Unsaturated-zone profiles of water potential and environmental tracers indicate sharply contrasting recharge regimes beneath native vegetation, irrigated fields, and the normally dry channel of the Amargosa River. Recharge is negligible beneath undisturbed native vegetation covering most of the Amargosa Desert floor, where water-potential profiles indicate upward flow and atmospherically deposited salts have been accumulating more or less continuously since the end of the Pleistocene. Accumulation of salts has formed pronounced bulges just below the root zone.

Near-zero water potentials and low salt concentrations beneath irrigated fields and the Amargosa River channel indicate active deep percolation and ground-water recharge. Transit times of recharge beneath the channel are on the order of centuries. Transit times of irrigation-return flow are on the order of decades. Velocities of displaced chloride and nitrate bulges beneath a migrated channel and a newly irrigated agricultural field provide largely independent estimates of recharging fluxes that are in approximate agreement with chloride mass-balance estimates.

Chloride mass-balance calculations indicate that 12 to 15 percent of infiltrated channel water becomes recharge. The bulk of infiltrated water returns to the atmosphere. The associated evaporation cools the channel and reduces the amount of water available for ground-water recharge. The estimated amount of ground-water recharge from channel infiltration is about 0.4 $Mm^3\ yr^{-1}$.

DC-resistivity imaging proved useful for extrapolating borehole-based values of ground-water recharge. Resistivity

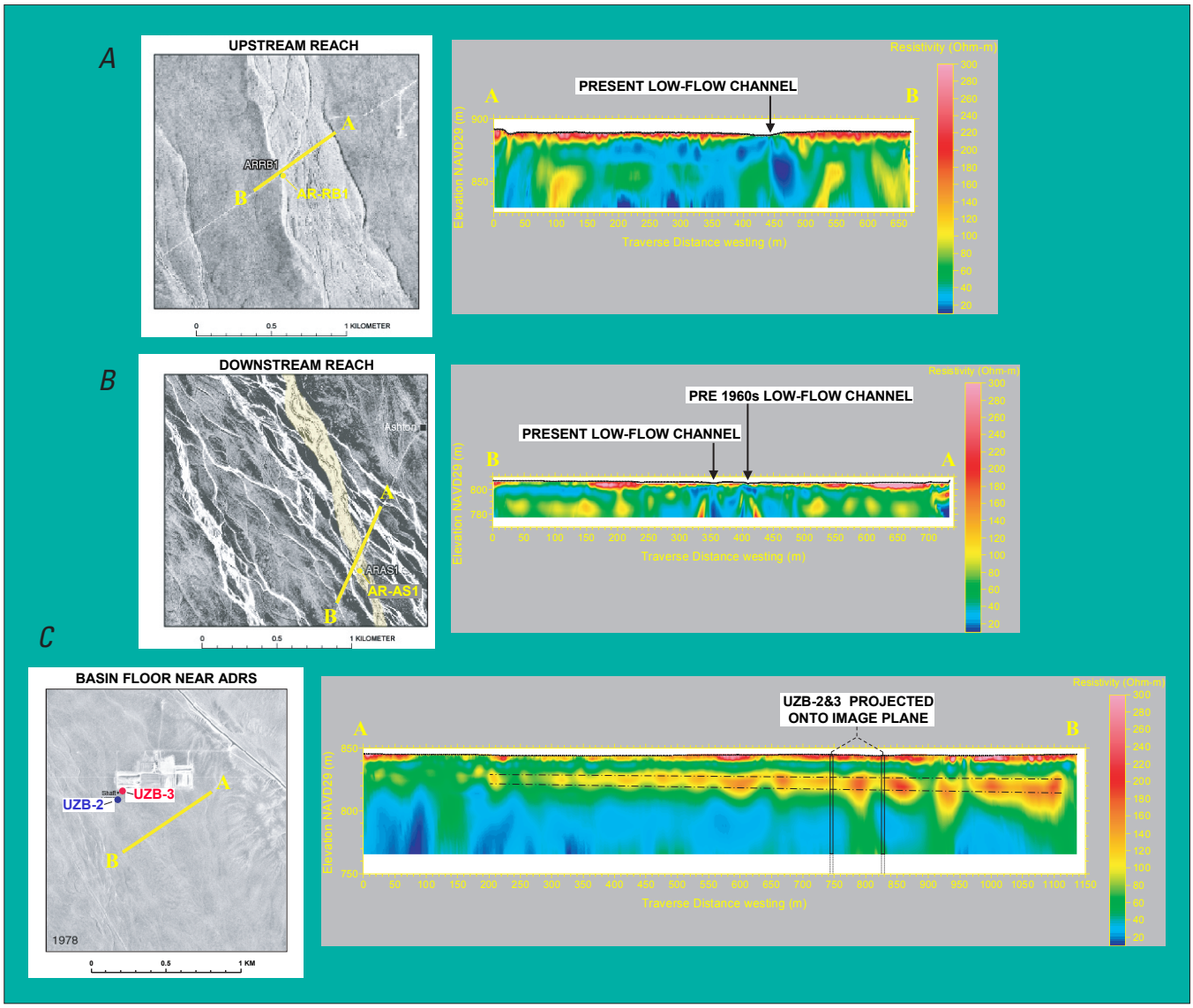

Figure 20. Direct-current resistivity transects in the Amargosa Desert study area. *A*, transect across the Amargosa River channel at site C1, 10.6 km from the basin inlet; *B*, transect across the Amargosa River channel at site C2, 22.9 km from the basin inlet, and; *C*, transect at the Amargosa Desert Research Site (ADRS). Figure 9 shows site locations.

images of unsaturated-zone sediment clearly show focusing of recharge beneath the normally dry Amargosa River channel. Low-resistivities correspond to high water contents associated with active recharge from ephemeral streamflow. High-resistivities indicate coarse gravel layers and low water potentials, corresponding to regions without active ground-water recharge under current climatic conditions. Infiltration losses from the Amargosa River channel produce small amounts of recharge along the basin floor of the Amargosa Desert.

References Cited

Abraham, J.D., and Lucius, J.E., 2004, Direct current resistivity profiling to study distribution of water in the unsaturated zone near the Amargosa Desert Research Site, Nevada: U.S. Geological Survey Open-File Report 2004–1319, 16 p.

Andraski, B.J., 1997, Soil-water movement under natural-site and waste-site conditions—A multiple-year field study in the Mojave Desert, Nevada: Water Resources Research, v. 33, no. 9, p. 1901–1916.

Andraski, B.J., and Stonestrom, D.A., 1999, Overview of research on water, gas, and radionuclide transport at the Amargosa Desert Research Site, Nevada, *in* Morganwalp, D.W., and Buxton, H.T., eds., U.S. Geological Survey Toxic Substances Hydrology Program—Proceedings of the Technical Meeting, Charleston, South Carolina, March 8–12, 1999—Volume 3—Subsurface Contamination from Point Sources: U.S. Geological Survey Water Resources Investigations Report 99–4018C, p. 459–465.

Avon, Lizanne, and Durbin, T.J., 1994, Evaluation of the Maxey-Eakin method for estimating recharge to groundwater basins in Nevada: Water Resources Bulletin, v. 30, no. 1, p. 99–111.

Beck, D.A., and Glancy, P.A., 1995, Overview of runoff of March 11, 1995, in Fortymile Wash and Amargosa River, Southern Nevada: U.S. Geological Survey Fact Sheet FS–210–95, 4 p.

Benson, M.A., and Dalrymple, T., 1967, General field and office procedures for indirect discharge measurements: U.S. Geological Survey Techniques of Water-Resource Investigations, Book 3 Chapter A1, 30 p.

Bull, W.B., 1991, Geomorphic responses to climatic change: New York, Oxford University Press, 326 p.

Carr, M.D., and Yount, J.C., eds., 1988, Geologic and Hydrologic Investigations of a Potential Nuclear Waste Disposal Site at Yucca Mountain, Southern Nevada: U.S. Geological Survey Bulletin 1790: Washington, D.C., 152 p.

Claassen, H.C., 1985, Sources and mechanisms of recharge for ground water in the west-central Amargosa Desert—A geochemical interpretation: U.S. Geological Survey Professional Paper 712–, 31 p.

Constantz, Jim, Stonestrom, D.A., Stewart, A.E., Niswonger, R.G., and Smith, T.R., 2001, Analysis of streambed temperatures in ephemeral channels to determine streamflow frequency and duration: Water Resources Research, v. 37, no. 2, p. 317–328.

Constantz, Jim, and Stonestrom, D.A., 2003, Heat as a tracer of water movement near streams, *in* Stonestrom, D.A., and Constantz, J., eds., Heat as a tool for studying the movement of ground water near streams: U.S. Geological Survey Circular 1260, p. 1–6.

Cook, P.G., Walker, G.R., and Jolly, I.D., 1989, Spatial variability of groundwater recharge in a semiarid region: Journal of Hydrology, v. 111, no. 1-4, p. 195–212.

Curtis, Scott, and Adler, R., 2000, ENSO indices based on patterns of satellite-derived precipitation: Journal of Climate, v. 13, no. 15, p. 2786.

Dalrymple, Tate, and Benson, M.A., 1968, Measurement of peak discharge by the slope-area method: U.S. Geological Survey Techniques of Water-Resource Investigations, Book 3 Chapter A3, 12 p.

D'Agnese, F.A., Faunt, C.C., Hill, M.C., and Turner, A.K., 1999, Death Valley regional ground-water flow model calibration using optimal parameter estimation methods and geoscientific information systems: Advances in Water Resources, v. 22, no. 8, p. 777–790.

Eakin, T.E., and Maxey, G.B., 1951, Ground water in Ruby Valley, Elko and White Pine counties, Nevada, *in* Contributions to the hydrology of eastern Nevada: Nevada State Engineer's Office, Water Resources Bulletin, v. 12, p. 64–93.

Edmunds, W.M., Darling, W.G., and Kinniburgh, D.G., 1988, Solute profile techniques for recharge estimation in semiarid and arid terrain, *in* Summers, I., ed., Estimation of ntural goundwater rcharge: Norwell, Mass., D. Reidel, p. 139–157.

Fischer, J.M., 1992, Sediment properties and water movement through shallow unsaturated alluvium at an arid site for disposal of low-level radioactive waste near Beatty, Nye County, Nevada: U.S. Geological Survey Water-Resources Investigations Report 92–032, 63 p.

Gardner, W.H., 1986, Water content, *in* Klute, A., ed., Methods of soil analysis, part 1—Physical and mineralogical methods: Madison, Wisc., American Society of Agronomy, p. 493–544.

Gee, G.W., Campbell, M.D., Campbell, G.S., and Campbell, J.H., 1992, Rapid measurement of low soil water potentials using a water activity meter: Soil Science Society of America Journal, v. 56, no. 4, p. 1068–1070.

Glazner, A.F., Walker, D., and Bartley, J., eds., 2002, Geologic evolution of the Mojave Desert and southwestern Basin and Range: Boulder, Colorado, Geological Society of America, 314 p.

Hamilton, W.B., 1987, Crustal extension in the Basin and Range Province, southwestern United States, *in* Coward, M.P., Dewey, J.F., and Hancock, P.L., eds., Continental extensional tectonics: Geological Society of America Special Publication 28, p. 155–176.

Harrill, J.R., Gates, J.S., and Thomas, J.M., 1988, Major ground-water flow systems in the Great Basin region of Nevada, Utah, and adjacent states: U.S. Geological Survey Hydrologic Investigations Atlas HA–694–C, scale 1:1,000,000.

Hartsough, Peter, Tyler, S.W., Sterling, J., and Walvoord, M.A., 2001, A 14.6 kyr record of nitrogen flux from desert soil profiles as inferred from vadose zone pore waters: Geophysical Research Letters, v. 28, no. 15, p. 2955–2958.

Jarrett, R.D., 1987, Errors in slope-area computations of peak discharge in mountain streams: Journal of Hydrology, v. 96, no. 1-4, p. 53–67.

Johnson, M.J., Mayers, C.J., and Andraski, B.J., 2002, Selected micrometeorological and soil-moisture data at Amargosa Desert Research Site in Nye County near Beatty, Nevada, 1998–2000: U.S. Geological Survey Open-File Report 02–348, 21 p.

Johnson, M.J., Mayers, C.J., Garcia, C.A., and Andraski, B.J., 2007, Selected micrometeorological, soil-moisture, and evapotranspiration data at Amargosa Desert Research Site in Nye County near Beatty, Nevada, 2001–2005: U.S. Geological Survey Digital Data Series 284, 52 p.

Kilroy, K.C., 1991, Ground-water conditions in the Amargosa Desert, Nevada-California, 1952–87: U.S. Geological Survey Water-Resources Investigations Report 89–4101, 91 p.

Laczniak, R.J., DeMeo, G.A., Reiner, S.R., Smith, J.L., and Nylund, W.E., 1999, Estimates of ground-water discharge as determined from measurements of evapotranspiration, Ash Meadows area, Nye County, Nevada: U.S. Geological Survey Water-Resources Investigations Report 99–4079, 70 p.

Maxey, G.B., and Eakin, T.E., 1949, Ground water in White River Valley, White Pine, Nye, and Lincoln Counties, Nevada, Nevada State Engineer's Office, Water Resources Bulletin, v. 8, 59 p.

Mayers, C.J., Andraski, B.J., Cooper, C.A., Wheatcraft, S.W., Stonestrom, D.A., and Michel, R.L., 2005, Modeling tritium transport through a deep unsaturated zone in an arid environment: Vadose Zone J., v. 4, no. 4, p. 967–976, doi:10.2136/vzj2004.0179.

McPhaden, M.J., Zebiak, S.E., and Glantz, M.H., 2006, ENSO as an integrating concept in Earth science: Science, v. 314, no. 5806, p. 1740–1745, doi:10.1126/science.1132588.

Moosburner, Otto, 1978, Flood investigations in Nevada through 1977 water year: U.S. Geological Survey Open-File Report 78–610, 94 p.

Nichols, W.D., 1987, Geohydrology of the unsaturated zone at the burial site for low-level radioactive waste near Beatty, Nye County, Nevada: U.S. Geological Survey Water-Supply Paper 2312, 57 p.

NOAA (National Oceanic and Atmospheric Administration), 2002, Monthly station normals of temperature, precipitation, and heating and cooling degree days, 1971–2000; 26, Nevada; Climatography of the United States No. 81: Ashville, National Climatic Data Center, 26 p.

Osterkamp, W.R., Lane, L.J., and Savard, C.S., 1994, Recharge estimates using a geomorphic/distributed-parameter simulation approach, Amargosa River Basin: Water Resources Bulletin, v. 30, no. 3, p. 493–507.

Page, A.L., Miller, R.H., and Keeney, D.R., eds., 1982, Methods of Soil Analysis, Part 2, Chemical and Microbiological Properties (2nd ed.): Madison, American Society of Agronomy, Inc., 1188 p.

Park, S.K., and Wernicke, B., 2003, Electrical conductivity images of Quaternary faults and Tertiary detachments in the California Basin and Range: Tectonics, v. 22, no. 4, p. 4–1 to 4–17, doi:10.1029/2001TC001324.

Philip, J.R., 1983, Infiltration in one, two, and three dimensions, *in* Slack, D.C., ed., Advances in infiltration: St. Joseph, Michigan, American Society of Agricultural Engineers, p. 1–13.

Phillips, F.M., 1994, Environmental tracers for water movement in desert soils of the American Southwest: Soil Science Society of America Journal, v. 58, no. 1, p. 15–24.

Prudic, D.E., Stonestrom, D.A., and Striegl, R.G., 1997, Tritium, deuterium, and oxygen-18 in water collected from unsaturated sediments near a low-level radioactive-waste burial site south of Beatty, Nevada: U.S. Geological Survey Water-Resources Investigations Report 97–4062, 23 p.

Scanlon, B.R., 2000, Uncertainties in estimating water fluxes and residence times using environmental tracers in an unsaturated zone: Water Resources Research, v. 36, no. 2, p. 395–409.

Scanlon, B.R., Levitt, D.G., Reedy, R.C., Keese, K.E., and Sully, M.J., 2005, Ecological controls on water-cycle response to climate variability in deserts: Proceedings of the National Academy of Sciences of the United States of America, v. 102, no. 17, p. 6033–6038.

Smith, R.V., Doyle, R.M., Burns, L.C., and Stevens, R.J., 1997, A model for nitrite accumulation in soils: Soil Biology and Biochemistry, v. 29, no. 8, p. 1241–1247.

Smith, S.D., Monson, R.K., and Anderson, J.E., 1997, Physiological Ecology of North American Desert Plants: Berlin, Springer-Verlag, 286 p.

Spaulding, W.G., 1985, Vegetation and climates of the last 45,000 years in the vicinity of the Nevada Test Site, south-central Nevada: U.S. Geological Survey Professional Paper 1329, 83 p.

Spaulding, W.G., and Graumlich, L.J., 1986, The last pluvial climatic episodes in the deserts of southwestern North America: Nature, v. 320, p. 441–444.

Sparks, D.L., ed., 1996, Methods of Soil Analysis, Part 3, Chemical Methods: Madison, Wisc., American Society of Agronomy, 1390 p.

Stewart, A.E., 2003, Temperature based estimates of streamflow patterns and seepage losses in ephemeral channels: Stanford, Calif., Stanford University, Ph.D. dissertation, 248 p.

Stonestrom, D.A., Abraham, J.D., Lucius, J.E., and Prudic, D.E., 2003, Focused subsurface flow in the Amargosa Desert characterized by direct-current resistivity profiling [abs.]: Eos (American Geophysical Union Transactions), Fall Meeting Supplement, v. 84, no. 46, p. F660.

Stonestrom, D.A., and Blasch, K.W., 2003, Determining temperature and thermal properties for heat-based studies of surface-water ground-water interactions, *in* Stonestrom, D.A., and Constantz, J., eds., Heat as a tool for studying the movement of ground water near streams: U.S. Geological Survey Circular 1260, p. 73–80.

Stonestrom, D.A., Prudic, D.E., Laczniak, R.J., Akstin, K.C., Boyd, R.A., and Henkelman, K.K., 2003, Estimates of deep percolation beneath irrigated fields, native vegetation, and the Amargosa River channel, Amargosa Desert, Nye County, Nevada: U.S. Geological Survey Open-File Report 03–104, 83 p.

Stonestrom, D.A., Prudic, D.E., Laczniak, R.J., and Akstin, K.C., 2004, Tectonic, climatic, and land-use controls on ground-water recharge in an arid alluvial basin: Amargosa Desert, U.S.A., *in* Hogan, J.F., Phillips, F.M., and Scanlon, B.R., eds., Groundwater recharge in a desert environment—The southwestern United States: American Geophysical Union, Water Science and Applications Series, v. 9, p. 29–47, doi:10.1029/0009WSA03.

Stonestrom, D.A., Prudic, D.E., and Striegl, R.G., 1999, Isotopic composition of water in a deep unsaturated zone beside a radioactive-waste disposal area near Beatty, Nevada, *in* Morganwalp, D.W., and Buxton, H.T., eds., U.S. Geological Survey Toxic Substances Hydrology Program—Proceedings of the Technical Meeting, Charleston, South Carolina, March 8–12, 1999—Volume 3—Subsurface Contamination from Point Sources: U.S. Geological Survey Water Resources Investigations Report 99–4018C, p. 467–473.

Sweetkind, D.S., Dickerson, R.P., Blakely, R.J., and Denning, P.D., 2001, Interpretive Geologic Cross Sections for the Death Valley Regional Flow System and Surrounding Areas, Nevada and California: U.S. Geological Survey Miscellaneous Field Studies Map MF–2370, scale 1:750,000.

Szabo, B.J., Kolesar, P.T., Riggs, A.C., Winograd, I.J., and Ludwig, K.R., 1994, Paleoclimatic inferences from a 120,000-yr old calcite record of water-table fluctuation in Browns Room of Devils Hole, Nevada: Quaternary Research, v. 41, p. 59–69.

Tanko, D.J., and Glancy, P.A., 1999, Flooding in the Amargosa River Basin, February 23–24, southern Nevada and eastern California, including the Nevada Test Site: U.S. Geological Survey Fact Sheet FS–036-01, 4 p.

Telford, W.M., Geldart, L.P., and Sheriff, R.E., 1990, Applied geophysics (2nd ed.): New York, Cambridge University Press, 770 p.

Tiedeman, C.R., D. M. Ely, M. C. Hill, and G. M. O'Brien, 2004, A method for evaluating the importance of system state observations to model predictions, with application to the Death Valley regional groundwater flow system: Water Resources Research., v. 40, no. 12, p. 1–14, doi:10.1029/2004WR003313.

Tyler, S.W., Chapman, J.B., Conrad, S.H., Hammermeister, D.P., Blout, D.O., Miller, J.J., Sully, M.J., and Ginanni, J.M., 1996, Soil-water flux in the southern Great Basin, United States—Temporal and spatial variations over the last 120,000 years: Water Resources Research, v. 32, no. 6, p. 1481–1499.

U.S. Census Bureau, 2003, Nevada 2000 Summary Social, Economic, and Housing Characteristics, 2000 Census of Population and Housing, Publication PHC-2-30: Washington, D.C., 162 p.

Vecchi, G.A., Wittenberg, A.T., and Rosati, A., 2006, Reassessing the role of stochastic forcing in the 1997–1998 El Niño: Geophysical Research Letters, v. 33, doi:10.1029/2005GL024738.

Walker, G.E., and Eakin, T.E., 1963, Geology and ground water of Amargosa Desert, Nevada-California: Nevada Department of Conservation and Natural Resources, Ground-Water Resources Reconnaissance Series Report 14, 45 p.

Walvoord, M.A., Phillips, F.M., Tyler, S.W., and Hartsough, P.C., 2002, Deep arid system hydrodynamics 2. Application to paleohydrologic reconstruction using vadose zone profiles from the northern Mojave Desert: Water Resources Research, v. 38, no. 12, p. 27–1 to 27–12.

Walvoord, M.A., Plummer, M.A., Phillips, F.M., and Wolfsberg, A.V., 2002, Deep arid system hydrodynamics 1. Equilibrium states and response times in thick desert vadose zones: Water Resources Research, v. 38, no. 12, p. 44–1 to 44–15, doi:10.1029/2001WR000824.

Walvoord, M.A., Stonestrom, D.A., Andraski, B.J., and Striegl, R.G., 2004, Constraining the inferred paleohydrologic evolution of a deep unsaturated zone in the Amargosa Desert: Vadose Zone Journal, v. 3, no. 2, p. 502–512.

Winograd, I.J., and Thordarson, W., 1975, Hydrogeologic and hydrochemical framework, South-Central Great Basin, Nevada-California, with special reference to the Nevada Test Site: U.S. Geological Survey Professional Paper 712–C, 126 p.

Workman, J.B., Menges, C.M., Page, W.R., Taylor, E.M., Ekren, E.B., Rowley, P.D., Dixon, G.L., Thompson, R.A., and Wright, L.A., 2002, Geologic map of the Death Valley ground-water model area, Nevada and California: U.S. Geological Survey Miscellaneous Field Studies Map MF–2381–A, 46 p., 2 sheets.

Streamflow, Infiltration, and Recharge in Arroyo Hondo, New Mexico

By Stephanie J. Moore[1]

Abstract

Infiltration events in channels that flow only sporadically produce focused recharge to the Tesuque aquifer in the Española Basin. The current study examined the quantity and timing of streamflow and associated infiltration in Arroyo Hondo, an unregulated mountain-front stream that enters the basin from the western slope of the Sangre de Cristo Mountains. Traditional methods of stream gaging were combined with environmental-tracer based methods to provide the estimates. The study was conducted during a three-year period, October 1999–October 2002. The period was characterized by generally low precipitation and runoff. Summer monsoonal rains produced four brief periods of streamflow in water year 2000, only three of which extended beyond the mountain front, and negligible runoff in subsequent years. The largest peak flow during summer monsoon events was 0.59 cubic meters per second. Snowmelt was the main contributor to annual streamflow. Snowmelt produced more cumulative flow downstream from the mountain front during the study period than summer monsoonal rains.

The presence or absence of streamflow downstream of the mountain front was determined by interpretation of streambed thermographs. Infiltration rates were estimated by numerical modeling of transient vertical streambed temperature profiles. Snowmelt extended throughout the instrumented reach during the spring of 2001. Flow was recorded at a station two kilometers downstream from the mountain front for six consecutive days in March. Inverse modeling of this event indicated an average infiltration rate of 1.4 meters per day at this location. For the entire study reach, the estimated total annual volume of infiltration ranged from 17,100 to 246,000 m^3 during water years 2000 and 2001. During water year 2002, due to severe drought, streamflow and streambed infiltration in the study reach were both zero.

Introduction

In the semiarid climate of the Española Basin, a rapidly growing population relies on scarce ground-water and surface-water resources. The Tesuque aquifer, which provides a significant portion of drinking-water supplies to cities and rural residences, is recharged by several processes, including (1) direct recharge, (2) subsurface inflow from adjacent aquifers, and (3) focused recharge. Focused recharge results from streambed infiltration through the unsaturated zone to the underlying aquifer.

Focused recharge along ephemeral streams may provide a substantial source of recharge to the alluvial aquifer of the Española Basin, which is referred to as the Tesuque aquifer (Spiegel and Baldwin, 1963; McAda and Wasiolek, 1988; Duke Engineering and Services, 2001). However, the sporadic nature of streamflow of ephemeral streams in the Española Basin, as well as throughout the Southwest, has resulted in poor documentation of streamflow and streambed infiltration of ephemeral streams. Consequently, focused recharge is one of the most uncertain components of regional water budgets (Duke Engineering and Services, 2001). Information on the quantity and timing of streamflow and streambed infiltration in ephemeral streams would allow for improved estimates of the focused-recharge component of water budgets.

Purpose and Scope

This chapter presents the results of a three-year study of streamflow, infiltration, and recharge in Arroyo Hondo, New Mexico. Data were collected from October 1, 1999 through September 30, 2002 (water years 2000–02). Traditional and experimental methods were used to characterize streamflow in Arroyo Hondo. Traditional methods were used to characterize streamflow at a continuous-record streamflow-gaging station (stream gage). Experimental temperature-based methods were used to estimate the presence and duration of streamflow at selected sites along Arroyo Hondo. In addition, precipitation and soil-water content were collected at selected locations throughout the watershed. Streambed infiltration rates were estimated through use of an inverse modeling technique that fits simulated to measured subsurface temperatures. Cumulative streambed infiltration rates were estimated from streambed infiltration rates, channel widths, and the downstream extent and duration of streamflow. Environmental tracers (chloride and bromide) were used to investigate the presence of recharge at selected sites.

[1] Present address D.B. Stephens and Associates, Albuquerque, New Mexico (smoore@dbstephens.com).

Previous Investigations

Ground-water recharge is an important process in the Española Basin (Spiegel and Baldwin, 1963; Anderholm, 1994; Duke Engineering and Services, 2001). Many studies have been conducted on the various recharge processes in the Tesuque aquifer.

Direct recharge (also known as diffuse or areal recharge) occurs by infiltration of precipitation through the unsaturated zone to the saturated zone. Thick unsaturated zones and high evapotranspiration rates, both of which are common in the Española Basin, preclude large amounts of direct recharge. Previous investigators have attempted to quantify direct recharge in the Española Basin. Spiegel and Baldwin (1963, p. 192) estimated direct recharge to be 1.3 centimeters per year (cm/yr) in the Arroyo Hondo area. Lee Wilson and Associates (1978, p. 1–62) estimated direct recharge to be 0.7 cm/yr in the Santa Fe area. McAda and Wasiolek (1988, p. 30) estimated direct recharge to be 1.3 cm/yr in the Arroyo Hondo area. Duke Engineering and Services (2001, p. 131) assumed a direct recharge rate of zero.

Spiegel and Baldwin conducted a comprehensive study of geology and water resources in the Santa Fe area. They reported the average annual yield of surface-water runoff from the upper 17.35 square kilometers (km^2) of the Arroyo Hondo watershed to be 660,000 cubic meters (m^3; Spiegel and Baldwin, 1963, p. 188); this estimate was determined from crest-stage data collected from 1913 to 1922. They also reported (p. 188) that most streamflow in Arroyo Hondo recharges the regional ground-water aquifer (the Tesuque aquifer).

McAda and Wasiolek simulated ground-water flow in the Tesuque aquifer. They estimated 625,000 m^3 per year of recharge to the Tesuque aquifer from streambed infiltration in Arroyo Hondo (McAda and Wasiolek, 1988, p. 29–31). This value, which represented a long-term average, was initially based on that reported by Spiegel and Baldwin (1963), and was subsequently constrained during model calibration. McAda and Wasiolek applied streambed infiltration at a constant rate of 1,712 m^3/day throughout the year.

Anderholm applied the chloride mass-balance method to estimate mountain-front recharge (which includes subsurface inflow from the mountain block and focused recharge from streambed infiltration) in the Santa Fe area. He estimated 1,020,000 m^3 per year of mountain-front recharge in Arroyo Hondo (Anderholm, 1994, p. 37).

Hydrogeologic Setting

Arroyo Hondo is a small mountain-front stream located in the southeastern part of the Española Basin, in central New Mexico (fig. 1). Arroyo Hondo is typical of many mountain-front streams draining the western slopes of the Sangre de Cristo Mountains in that it is a gaining stream in its upper reaches and a losing stream in its lower reaches. Streamflow is generally perennial upstream and ephemeral downstream from the mountain front. The mountain front is defined as the contact between the mountain block (bedrock) aquifer and the alluvial aquifer system (the Tesuque aquifer) and is located approximately 2.1 km below streamflow-gaging station Arroyo Hondo near Santa Fe, N. Mex. (08317050; fig. 2). The Arroyo Hondo watershed comprises 156 km^2 upstream from its confluence with Cienega Creek; 17 percent (26 km^2) of its drainage area is located upstream from the mountain front. Elevations in the watershed vary from about 1,800 to 2,700 m above sea level (fig. 1).

The climate of the Española Basin and the Arroyo Hondo watershed is semiarid (fig. 3). At higher elevations, most precipitation falls as snow during winter months, whereas at lower elevations most precipitation falls as rain during the late summer and early fall (July through October) monsoon season. Normal precipitation in the Santa Fe area is 363 mm (fig. 4; Western Regional Climate Center, 2002); for purposes of this report, "normal" precipitation is defined as mean annual precipitation for 1972–2001 at the National Weather Service Cooperative Santa Fe 2 Station.

Arroyo Hondo can be divided into two reaches on the basis of the location of the mountain front (fig. 2). Upstream from the mountain front, the stream channel is well defined, narrow, and bedrock controlled. Precambrian gneiss and granite underlie most of the watershed and scattered areas of terrace deposits of Quaternary age flank the arroyo (Spiegel and Baldwin, 1963). A series of sedimentary and volcanic rocks of Tertiary age are exposed just upstream from the mountain front, including the reddish sandstone, conglomerate and mudstone of the Galisteo Formation, and latitic to andesitic volcanic flows and breccias (Spiegel and Baldwin, 1963). A perennial spring (fig. 2) discharges from the Galisteo Formation.

Downstream from the mountain front, the arroyo channel and arroyo valley widen as they cross the alluvial fan deposits of the Española Basin (Spiegel and Baldwin, 1963). The alluvial fan deposits are part of the Santa Fe Group, which includes the Tesuque Formation of Tertiary age and the Ancha Formation of Tertiary age. The older and thicker Tesuque Formation, which consists primarily of pinkish-tan, silty to conglomeratic sand and sandstone, is exposed along the 1.6-km reach of the arroyo immediately downstream from the mountain front. The younger Ancha Formation, which consists of silt, sand, and gravel, overlies the remainder of the watershed. The Arroyo Hondo streambed is composed of recent alluvium, which generally thickens in the downstream direction. The alluvium includes a mixture of silt, sand, and gravel; some large cobbles are present in the upper reaches, where gradients are steeper.

Perennial flow generally extends from the headwaters of the arroyo to the mountain front (Spiegel and Baldwin, 1963; McAda and Wasiolek, 1988) and is partially sustained by the spring discharging from the Galisteo Formation. However, during years of below normal precipitation, the arroyo may be dry between the stream gage and the mountain front except for that portion of the arroyo fed by discharge from

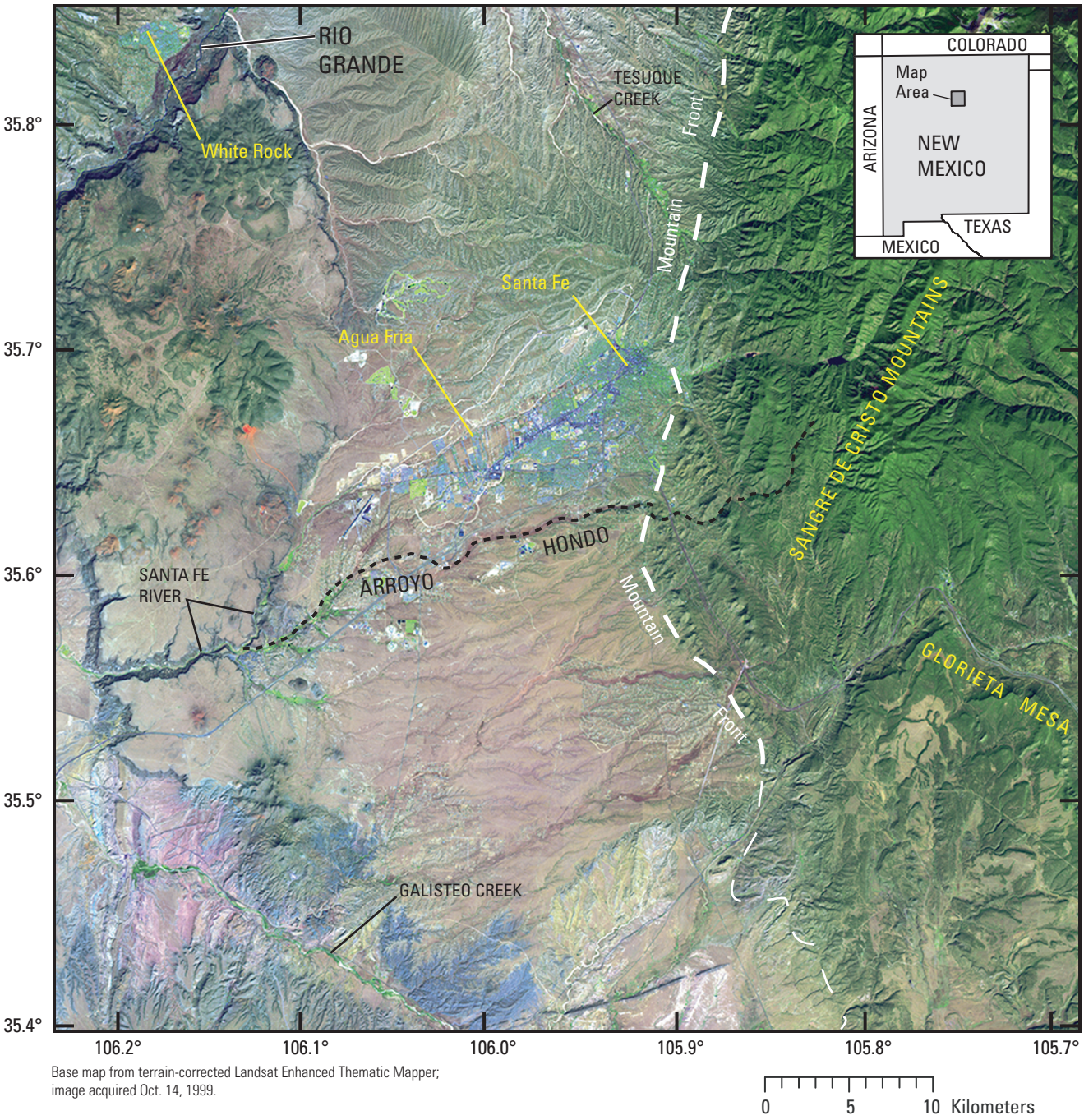

Figure 1. Arroyo Hondo, New Mexico, on the northeast rim of the Middle Rio Grande Basin. False-color satellite image shows active vegetation as deep shades of green (as in the volcanic highlands south of White Rock and in the crystalline Sangre de Cristo Mountains); sedimentary rocks as pastel shades of brown and green (younger and older Santa Fe clastics, respectively); pink (shale) and blue (volcaniclastics), near Galisteo Creek; and extrusive volcanics as dark gray with red (as in mounds north and south of junction of Arroyo Hondo with the Santa Fe River). The Middle Rio Grande Basin is at the base of cliffs dissected by the Santa Fe River, along the lower left edge of the image.

the spring. Downstream from the mountain front, the stream is ephemeral and flows only in response to runoff from snowmelt and intense summer thunderstorms (monsoons).

Depth to water varies spatially throughout the Arroyo Hondo watershed. A generalized longitudinal hydrogeologic section of part of the Arroyo Hondo watershed is shown in figure 5. Upstream from the mountain front, the water table is generally less than 50 m below land surface. Depth to the water table may exceed 90 m immediately downstream from the mountain front and generally decreases to the west.

Methods

Thermal and tracer-based methods were used to investigate streamflow, infiltration, and recharge in the Arroyo Hondo watershed. Instrumentation and data collection are discussed in this section. Methods of interpretation are discussed in subsequent sections of this chapter.

Study design was guided by general knowledge of streamflow in Arroyo Hondo (based on a literature review and initial reconnaissance of the study area) and of focused recharge processes in alluvial basins. Observations of channel morphology indicate that (1) streamflow is relatively frequent in the upper ephemeral reaches of Arroyo Hondo (in the 2.6 km immediately downstream from the mountain front; fig. 2) and (2) streamflow seldom extends continuously from the mountain front to its confluence with Cienega Creek (fig. 1). The thick, coarse-grained alluvium and frequent streamflows in the 2.6-km reach immediately downstream from the mountain front create ideal conditions for focused recharge.

Streamflow

Traditional and experimental methods were used to characterize streamflow in Arroyo Hondo. A continuous-record stream gage, Arroyo Hondo near Santa Fe, New Mexico (08317050), was installed in January 2000 to quantify streamflow in the perennial reach of the arroyo just upstream from the mountain front (fig. 2).

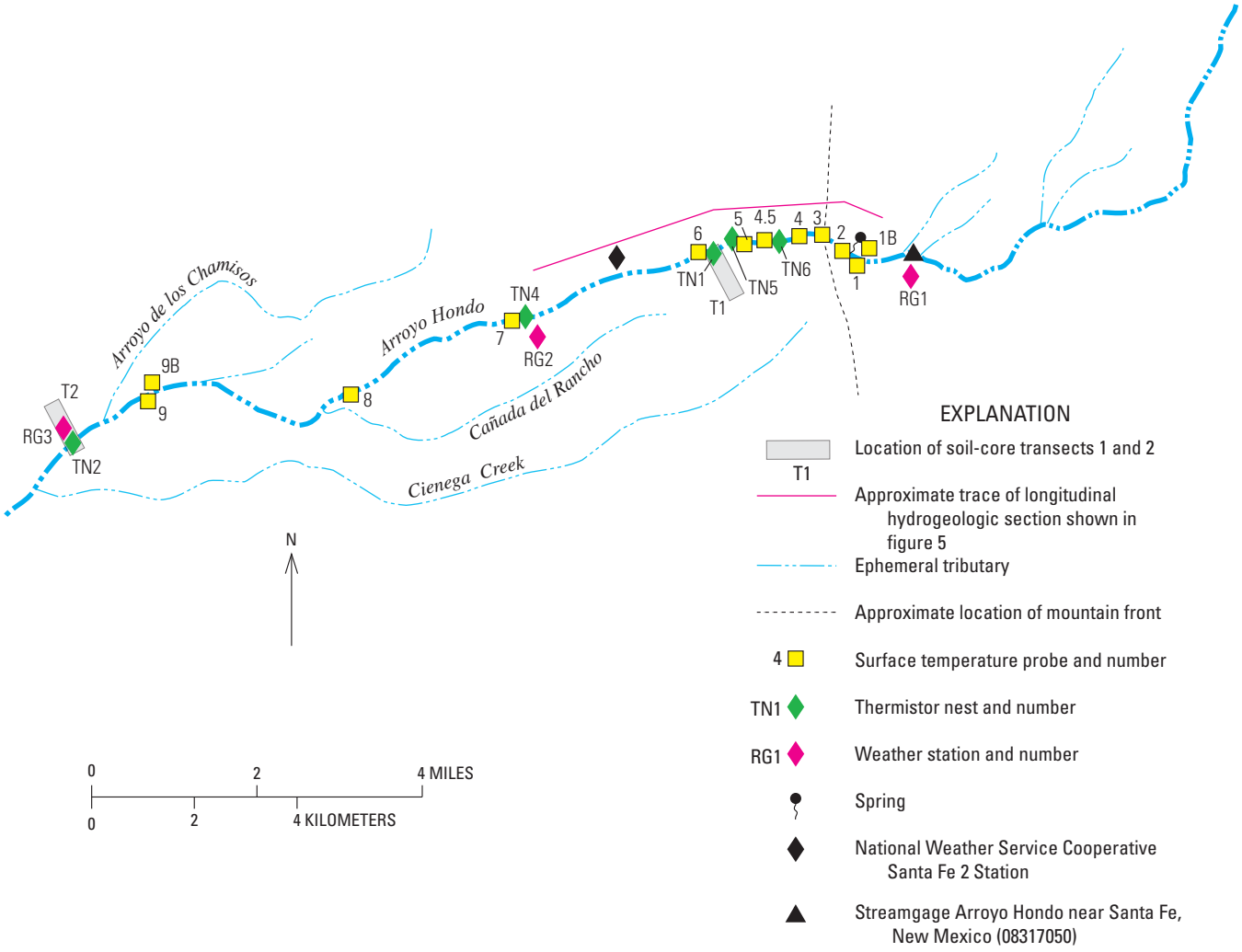

Figure 2. Schematic of the Arroyo Hondo, New Mexico study area.

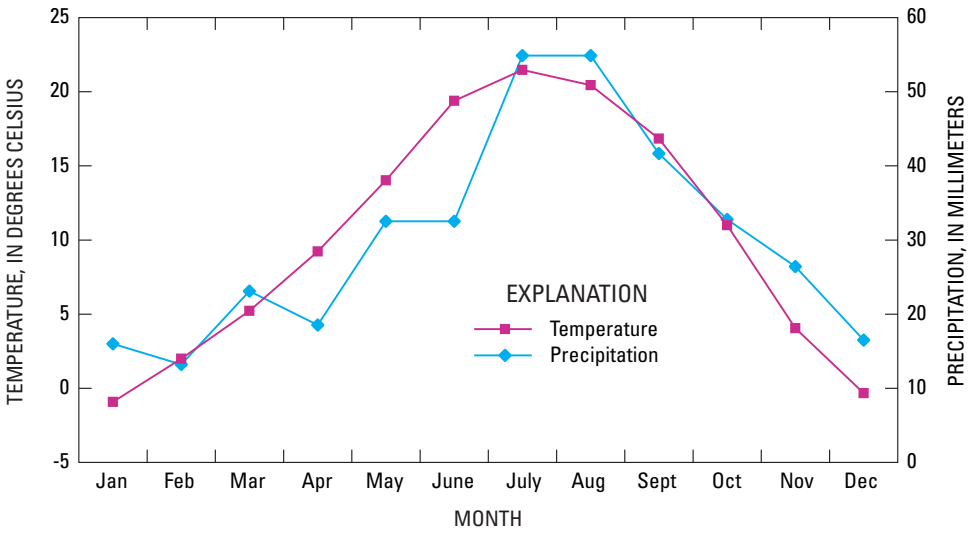

Figure 3. Mean monthly temperature and precipitation for the Arroyo Hondo, New Mexico study area. Data are from the National Weather Service Cooperative Santa Fe 2 station for 1972–2001. The location of the weather station is shown on figure 2.

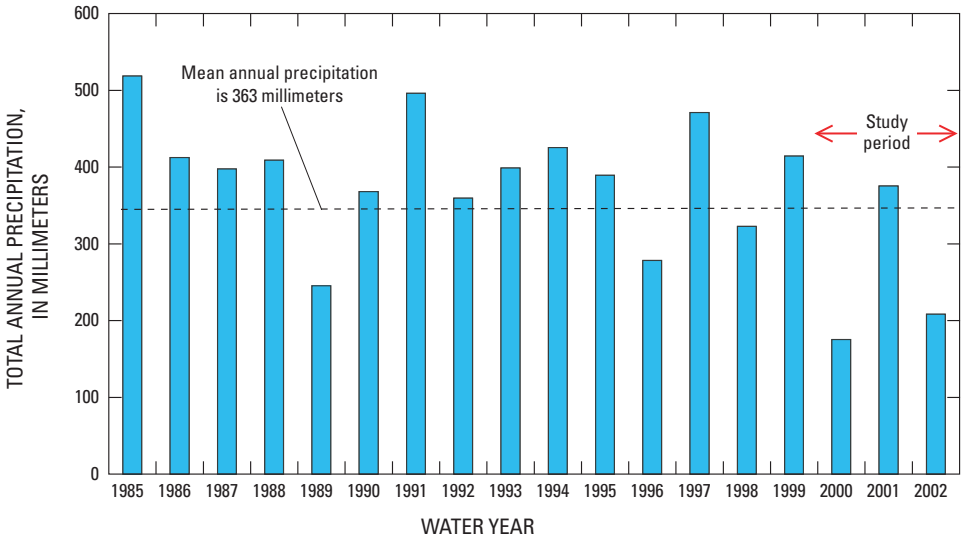

Figure 4. Total annual precipitation for the Arroyo Hondo, New Mexico study area. Data are from the National Weather Service Cooperative Santa Fe 2 station for water years 1985–2002. The location of the weather station is shown on figure 2.

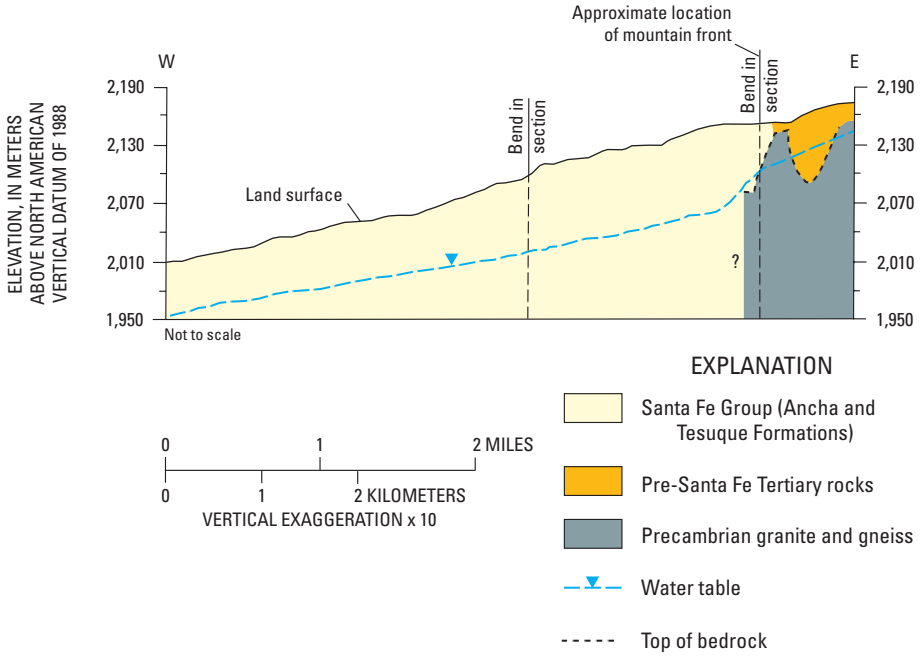

Figure 5. Generalized longitudinal hydrogeologic cross-section of Arroyo Hondo, New Mexico, modified from Spiegel and Baldwin (1963). The trace of the section is shown in figure 2.

Experimental temperature-based methods were used to determine the downstream extent and duration of streamflow (Constantz and others, 2002; Stewart, 2003). Twelve surface-temperature probes, which consist of a thermistor with a self-contained, single-channel data logger, were installed at selected locations in and near the arroyo channel. Each probe recorded temperature at 30-minute intervals; these data were used to construct a continuous thermograph for each location. Variations in the diurnal temperature signal were interpreted to determine if streamflow was present at a particular location in the arroyo, thus providing a continuous record of the downstream extent and duration of streamflow (Constantz and others, 2002; Stewart, 2003). During October 1999, nine surface-temperature probes (sites 1–9) were installed in the arroyo channel and two surface-temperature probes (sites 1B and 9B) were installed outside the active channel as benchmarks. Data from benchmark temperature probes helped to distinguish meteorological events (such as cold fronts and precipitation) from streamflow events. For surface-temperature sites in the perennial reach of the arroyo (sites 1–3), probes were placed on the channel surface and covered with large rocks to hold them in place. For those sites in the ephemeral reach of the arroyo (sites 4–9) and for benchmark sites adjacent to the arroyo channel (1B and 9B), probes were buried at depths ranging from 0.06 to 0.2 m. One additional surface temperature probe (site 4.5) was installed between sites 4 and 5 during March 2000 to gain additional streamflow information.

Three tipping-bucket rain gages with data loggers were installed in July 2000 along the arroyo (RG1–3; fig. 2) to measure spatial and temporal variations in precipitation. In addition to the general value gained from knowledge of spatial and temporal variations in precipitation, the data help to distinguish precipitation events from streamflow events (on the basis of temperature data).

Streambed Infiltration

Vertical sediment-temperature profiles have been used to estimate streambed infiltration rates (Lapham, 1987; Constantz and Thomas, 1996; Constantz and others, 2002; Constantz and others, 2003; Stewart, 2003). Thermistor nests, consisting of a self-contained data logger and four thermistors located at multiple depths in a vertical profile, were installed at selected locations in the ephemeral reach of the active channel (fig. 2). Temperature was recorded at 30-minute intervals. Thermographs constructed from data collected at each thermistor nest were used to indirectly estimate instantaneous infiltration rates during streamflow events. Thermistor nests TN1 and TN2 (fig. 2) were installed by using a truck-mounted, direct-push drill rig in October 2000. Thermistor nests TN4, TN5, and TN6 were manually installed in July 2002. At each nest, one thermistor was placed on the streambed surface and the other three thermistors were buried below the streambed surface at approximate depths of 0.3 m, 1.0 m, and 2.0 m.

Recharge

Environmental tracers (chloride and bromide) were used to investigate the presence or absence of recharge at selected sites. Soil cores were collected along transects T1 and T2 of Arroyo Hondo (fig. 2). At each transect, three soil cores were collected: one in the active channel (T1a and T2a), one 45–50 m from the active channel (T1b and T2b), and one 80–90 m from the active channel (T1c and T2c). Transect T1 is located 2.6 km downstream from the mountain front; soil cores T1a, T1b, and T1c were collected at 0, 45, and 80 m from the active channel. Transect T2 is located approximately 12 km downstream from the mountain front; soil cores T2a, T2b, and T2c were collected at 0, 50, and 90 m from the active channel. A truck-mounted, direct-push drill rig was used to collect 2.54-cm-diameter soil cores in October 2000. Each soil core extended from land surface to a depth of 5 to 7 m and was subsampled at intervals ranging from 0.15 to 0.91 m. Each subsample was analyzed for water content and chloride and bromide concentrations.

Streamflow

The magnitude, duration, and downstream extent of streamflow directly affect the quantity, duration, and distribution of streambed infiltration; that is, streambed infiltration is limited by the amount of streamflow in a particular stream, and the area over which streambed infiltration occurs is restricted to the portion of the stream where streamflow is present. Therefore, a detailed characterization of streamflow is necessary to improve understanding of streambed infiltration.

Temporal variations in streamflow are largely due to temporal variations in precipitation; therefore, variations in precipitation provide insight to variations in streamflow. Although the exact relation varies from one watershed to another, streamflow generally increases with increasing precipitation. To make reasonable comparisons between measured (or estimated) streamflow for different time periods, variations in precipitation for those same time periods need to be considered.

Precipitation during the study period was below normal for two of three years (Western Regional Climate Center, 2002; fig. 4). The normal streamflow (or a long-term average streamflow) is unknown for the stream gage at Arroyo Hondo because data were collected for only a three-year period during this study and no previous streamflow data exist.

The relation between streamflow and precipitation is demonstrated by streamflow records for two nearby stream gages located above diversions and (or) reservoirs on small, mountain-front streams in the Española Basin (table 1 and fig. 6) and referenced in the following discussions. These data show that streamflow is positively correlated with precipitation at all three stream gages (fig. 6).

Table 1. Annual streamflow and precipitation data in the Santa Fe area.

[NA, no data available]

Water year[1]	Total annual precipitation[2], in millimeters	Annual mean discharge[3], in cubic meters per minute			Total annual discharge[4], in millions of cubic meters		
		Tesuque Creek[5]	Arroyo Hondo[6]	Santa Fe River[7]	Tesuque Creek[5]	Arroyo Hondo[6]	Santa Fe River[7]
1937	NA	6.4	NA	NA	3.3	0.3	98
1938	NA	3.3	NA	NA	1.8	0.7	80
1939	NA	5.0	NA	NA	2.6	0.4	88
1940	NA	5.1	NA	NA	2.7	NA	NA
1941	NA	13.8	NA	NA	7.3	NA	NA
1942	NA	13.3	NA	NA	7.0	NA	NA
1943	NA	3.2	NA	NA	1.7	NA	NA
1944	NA	5.6	NA	NA	3.0	NA	NA
1945	356	6.8	NA	NA	3.6	NA	NA
1946	330	2.6	NA	NA	1.4	NA	NA
1947	262	3.3	NA	NA	1.7	NA	NA
1948	335	4.7	NA	NA	2.5	NA	NA
1949	425	6.0	NA	NA	3.2	NA	NA
1950	267	1.3	NA	NA	0.66	NA	NA
1951	211	1.3	NA	NA	0.69	NA	NA
1998	323	5.0	NA	NA	2.6	NA	NA
1999	414	5.0	NA	10.9	2.6	NA	5.7
2000	175	2.4	NA	3.6	1.3	NA	1.9
2001	375	5.3	0.9	11.4	2.8	0.47	6.0
2002	208	0.8	0.0	1.6	0.43	0.00	0.82

[1]Twelve-month period ending September 30th of designated year.

[2]Data prior to 1972 from the "Santa Fe" station; data from 1972 to present from the "Santa Fe 2" station (Western Region Climate Center, 2003).

[3]From U.S. Geological Survey digital data; also published in USGS Annual Data Reports (1937-2002).

[4]Calcuated as annual mean daily discharge times 365 days.

[5]U.S. Geological Survey streamflow-gaging station 08302500 (Tesuque Creek above diversions near Santa Fe, N. Mex.).

[6]U.S. Geological Survey streamflow-gaging station 08317050 (Arroyo Hondo near Santa Fe, N. Mex.).

[7]U.S. Geological Survey streamflow-gaging stations 08316000 (Santa Fe River near Santa Fe, N. Mex.; 1937–1951 data) and 08315480 (Santa Fe River above McClure Reservoir near Santa Fe, N. Mex.; 1998–2002 data).

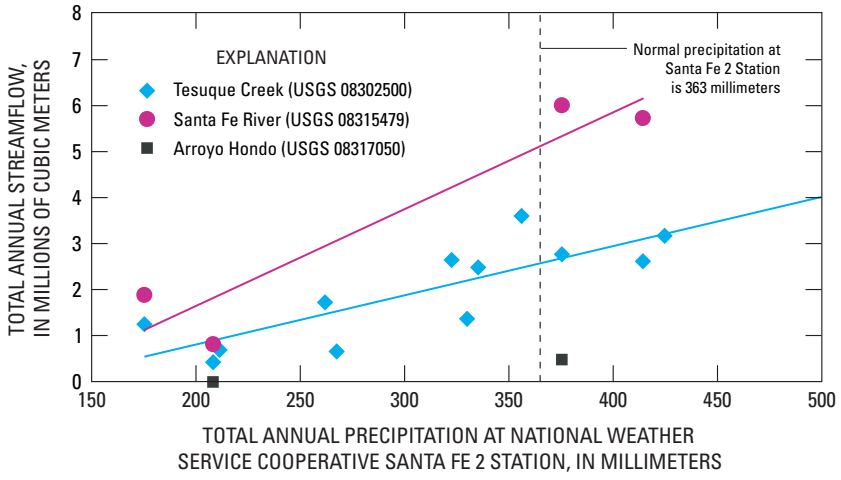

Figure 6. Relation between total annual streamflow and total annual precipitation at three USGS streamflow gaging stations in the Arroyo Hondo, New Mexico, study area. See figure 1 for stream locations.

Measured Streamflow

When the study began in October 1999, base flow in Arroyo Hondo was estimated to be less than 0.01 m^3/s at the stream gage. Streamflow at the gage ceased in May 2000, and the stream remained dry through the remainder of the water year (June through September) except for a few days of monsoon-induced streamflow events (monsoon events). Streamflow at the gage began again in late October 2000 and peaked in mid-March 2001 as a result of snowmelt. Streamflow at the gage ceased in June 2001. The stream remained dry throughout the remainder of the study period (fig. 7).

Total annual streamflow in Arroyo Hondo ranged from zero to 474,000 m^3 during the study period (water years 2000–02; fig. 7). Annual streamflow was largest (474,000 m^3) in WY 2001 when annual precipitation (375 mm) at the Santa Fe 2 weather station was 103 percent of normal. Annual streamflow was smallest in WY 2002 (zero m^3) when annual precipitation (208 mm) at Santa Fe 2 was 57 percent of normal. Below-normal precipitation in the Santa Fe area during WY 2002 resulted in the smallest streamflows on record at stream gages Tesuque Creek above diversions, near Santa Fe, N. Mex., and Santa Fe River above McClure Reservoir near Santa Fe, N. Mex. (fig. 6).

Daily mean streamflow (the mean of the computed streamflow for a particular day) at the Arroyo Hondo stream gage ranged from zero to 0.13 m^3/s during the study period (fig. 7). Daily mean streamflow was largest on March 10, 2001, during a snowmelt-induced streamflow event (snowmelt event). Streamflow on March 10 was steady throughout the day.

Instantaneous streamflow ranged from zero to approximately 0.59 m^3/s during the study period. The largest instantaneous streamflow occurred on July 1, 2000, during a monsoon event. Daily mean streamflow on July 1 was 0.03 m^3/s.

The previous two examples highlight important differences that are characteristic of snowmelt- and monsoon-induced streamflow events in Arroyo Hondo. Snowmelt events typically have relatively steady flows that often result in the largest daily mean streamflow for a particular year. Additionally, snowmelt events last longer and, therefore, result in larger total streamflow for a particular time period. Monsoon events may produce the highest peak streamflow for a particular year. However, streamflow during monsoon events is typically unsteady and of short duration (often lasting less than 24 hours), which results in a smaller total streamflow for a particular time period. Because snowmelt events result in a larger total streamflow than monsoon events, they likely result in a larger volume of streambed infiltration.

Use of Heat to Determine the Presence of Streamflow

Streambed infiltration can occur only in areas of a stream where streamflow is present. Therefore, knowledge of the distribution and timing of streamflow will improve understanding of streambed infiltration. Temperature variations in streambed sediments were used to determine the presence of streamflow (Constantz and others, 2002; Stewart, 2003).

The use of two different installation methods for temperature probes complicated the interpretation of streambed temperatures. Upstream from the mountain front, temperature probes were placed on the streambed of the active arroyo channel. At these sites, streamflow dampened the amplitude of the diurnal temperature signal because water buffered the temperature probe from the extremes of air temperature (fig. 8). Downstream from the mountain front, temperature probes were buried below the streambed at depths of 0.2 – 0.6 m. At these sites, infiltration of streamflow increased the amplitude of the diurnal temperature signal because advection (the dominant heat-transport mechanism during infiltration) transfers heat into the streambed more efficiently than conduc-

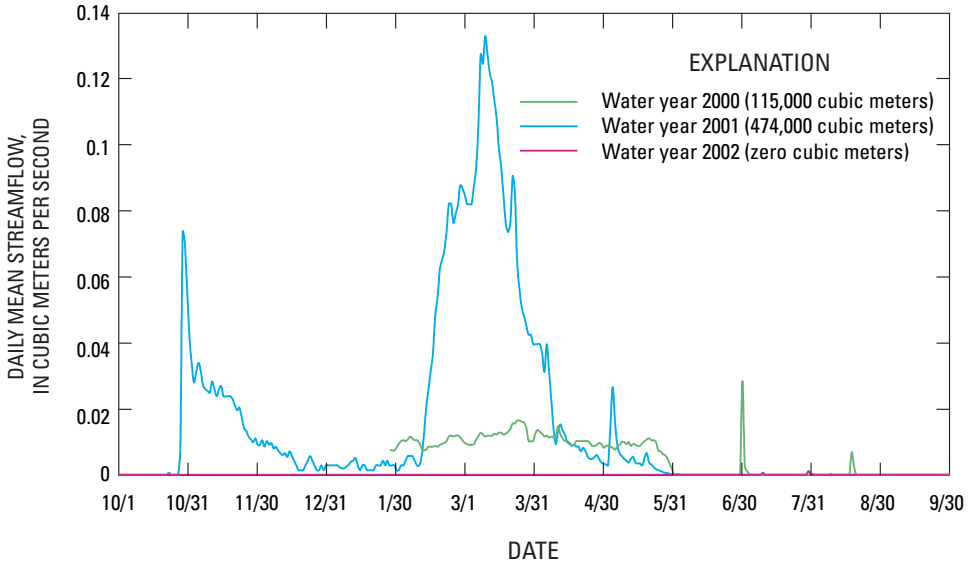

Figure 7. Daily mean discharge at streamflow-gaging station 08317050, Arroyo Hondo near Santa Fe, New Mexico, for water years 2000-02. The volume of total annual streamflow is shown in parentheses. The stream-gage location is shown on figure 2.

tion (the dominant heat-transport mechanism in dry sediments; fig. 9). For temperature probes buried at depths less than 0.2 m, changes in the amplitude of the diurnal temperature signal caused by the presence of streamflow are less obvious. Additionally, the duration of monsoon events may be far less than 24 hours, in which case the diurnal temperature signal would be only briefly interrupted and the amplitude may not be significantly affected. Theoretically, some form of automated time-series analysis could be used to interpret results; however, because of complications described above, visual inspection was primarily used to interpret thermographs for each temperature probe.

Downstream Extent and Duration of Streamflow

The presence or absence of streamflow was determined through inspection of each thermograph. The presence or absence of streamflow was used to ascertain the minimum downstream extent of continuous streamflow for every day in the study period, as described in Constantz and others (2002) and Stewart (2003). The minimum downstream extent of streamflow and its relation to daily mean streamflow at the stream gage are shown for the two most active periods of streamflow during this study (figs. 10–11).

Monsoon rains resulted in four short periods of streamflow during WY 2000, three of which caused streamflow to extend beyond the mountain front (fig. 10). The largest monsoon event occurred in early July when instantaneous streamflow at the stream gage reached 0.59 m^3/s (not shown in fig. 10), daily mean streamflow reached 0.03 m^3/s, and the distal end of streamflow extended at least 3.8 km downstream from the stream gage.

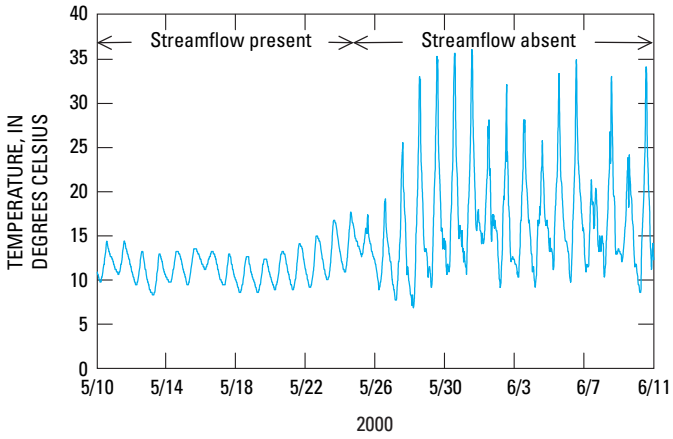

Figure 8. Streambed temperatures at a probe on the surface of the streambed, Arroyo Hondo study area, New Mexico.

Two monsoon events in early August 2000 produced streamflow at and downstream from the mountain front despite a daily mean streamflow of less than 0.01 m^3/s at the stream gage (fig. 10). In other words, streamflow was virtually absent at the gage but present downstream. This situation is likely due to the spatial distribution of the relatively spotty monsoon rains during the early August 2000 events. Precipitation may fall on only a portion of the watershed during a given storm. If the portion of the watershed receiving precipitation is located downstream from the stream gage, any streamflow resulting from that precipitation will not flow past the stream gage.

Arroyo Hondo was dry between the stream gage and the mountain front at the beginning of WY 2001 (October 1, 2000; fig. 11). Because of increasing precipitation, the distal end of streamflow reached the mountain front by late October

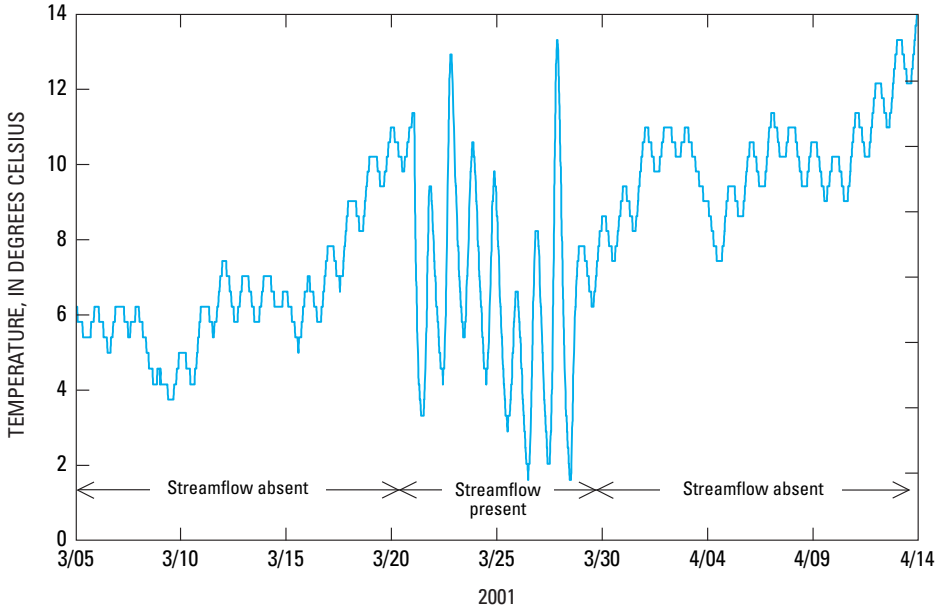

Figure 9. Streambed temperatures at a probe buried approximately 0.3 meter below the streambed, Arroyo Hondo study area, New Mexico.

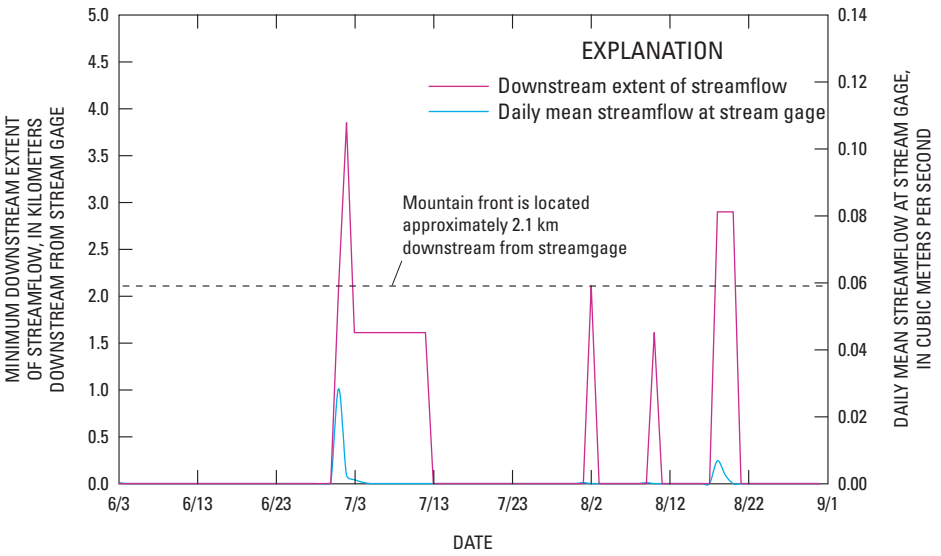

Figure 10. Minimum downstream extent and magnitude of flow at streamflow-gaging station 08317050, Arroyo Hondo near Santa Fe, N. Mex., during summer of 2000.

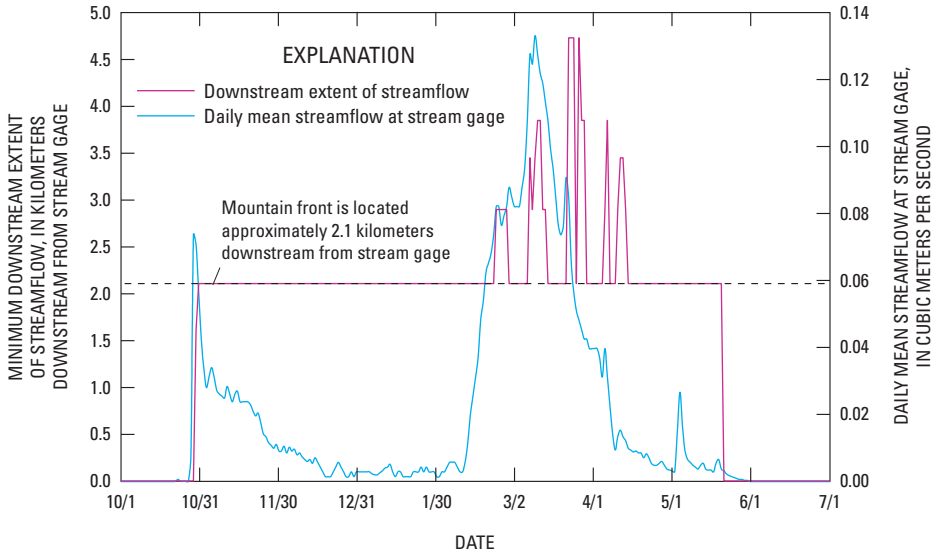

Figure 11. Minimum downstream extent and magnitude of flow at streamflow-gaging station 08317050, Arroyo Hondo near Santa Fe, N. Mex., October 2000 to June 2001.

2000 and persisted through the beginning of snowmelt in February 2001 (fig. 11). Rapid increases in daily mean streamflow resulted in the distal end of streamflow advancing further downstream (fig. 11). The distal end of streamflow reached its maximum downstream extent (at least 4.73 km below the stream gage) in late March, several days after the maximum daily mean streamflow of 0.13 m^3/s at the stream gage. The delay between the maximum downstream extent of streamflow and the maximum daily mean streamflow may be attributed to depleted soil moisture conditions (resulting from below-normal precipitation during WY 2000) that were likely present throughout the arroyo. The distal end of streamflow retreated upstream as daily mean streamflow steadily decreased.

For a given daily mean streamflow, monsoon events extend a greater distance downstream than snowmelt events (figs. 10–11). However, the duration of streamflow below the mountain front is greater for snowmelt events than for monsoon events, regardless of the magnitude of daily mean streamflow. Throughout the study period, snowmelt events produced more streamflow downstream from the mountain front than monsoon events; the increased extent of streamflow may be due to higher residual moisture contents in streambed

sediments during spring than during summer months. Snowmelt events are more likely than monsoon events to result in streambed infiltration because (1) streamflow is of longer duration below the mountain front, (2) the total volume of streamflow is larger below the mountain front, (3) almost all streamflow is lost to infiltration, and (4) evapotranspiration rates are smaller during spring than summer and fall months.

Streambed Infiltration

Streambed infiltration rates were estimated through use of an inverse modeling technique that fits simulated to measured temperatures (Niswonger and Prudic, 2003). A variably saturated, two-dimensional, heat transport model (VS2DI) was used to simulate streambed infiltration during streamflow events (Hsieh and others, 2000). The model, which includes a graphical-user interface that runs the simulation model VS2DH (Healy and Ronan, 1996), has been successful in simulating heat and ground-water transport below streams (Ronan and others, 1998; Thomas and others, 2000).

Simulation of complex processes (such as streambed infiltration into unsaturated, layered sediments) is possible by using many simplifying assumptions. Further discussion of these assumptions and their consequences are available in Healy and Ronan (1996), Ronan and others (1998), Constantz and others (2002), and Niswonger and Prudic (2003). The manual trial-and-error calibration method was used for this study and the best fit (model solution) of simulated to measured temperatures was identified through visual inspection (Constantz and others, 2002; Niswonger and Prudic, 2003).

The best fit may not be unique because of the possibility that a suitable solution may be obtained by a variety of logical model configurations. While the model configuration and assumed properties of the best fit (described in the following sections) are reasonable, it is not suggested that this configuration is an accurate representation of actual conditions. Therefore, it is recognized that the best fit does not represent a unique solution and does not validate the assumed configuration and properties. Despite these limitations, model results are presented to provide an estimate of streambed infiltration and to provide insight into possible streambed infiltration processes.

Although data were collected at five thermistor nests, only one streamflow event was recorded because of below-normal precipitation conditions that persisted throughout the study period. During the spring snowmelt in 2001, the distal end of streamflow extended at least 4.73 km downstream from the stream gage. Thermistor nest TN1 (fig. 2) recorded streambed-sediment temperatures at the streambed surface, and at depths of 0.30, 0.94, and 2.1 m below land surface. The onset of streamflow, around midday on March 20, can be identified by the abrupt change in amplitude of the diurnal temperature signals (fig. 12); streamflow was present at this site for about 6 days. Streambed infiltration at TN1 was simulated by using VS2DI for this time period.

Model Configuration

The model configuration must be defined for the numerical simulation of streambed infiltration. Aspects of the model configuration include the geometry of the model domain, the hydraulic and transport properties of the streambed sedi-

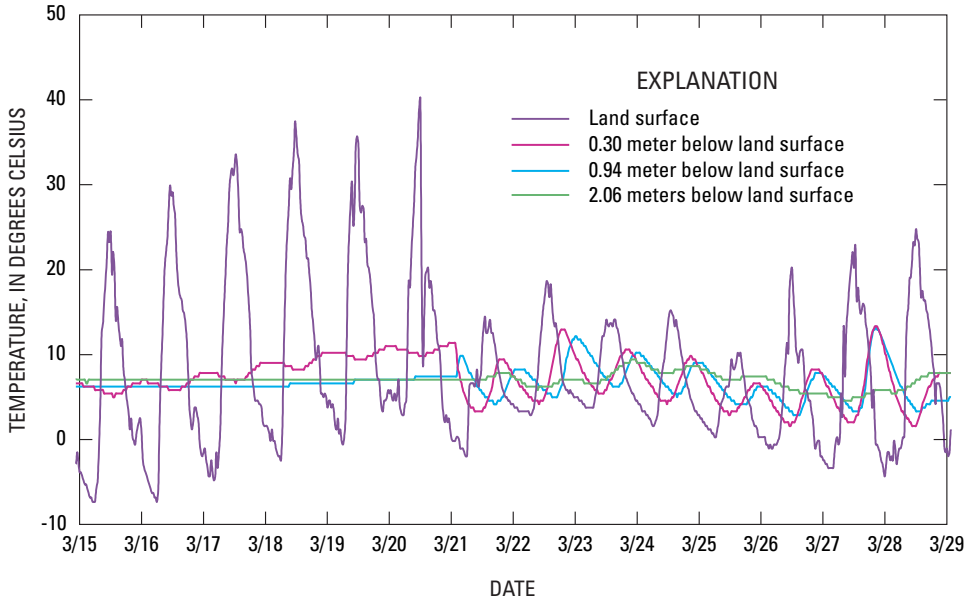

Figure 12. Temperatures at thermistor nest 1 (TN1) during March 2001, Arroyo Hondo study area, New Mexico. Streamflow began around midday on March 20, 2001. The location of TN1 is shown on figure 2.

ments, and the boundary and initial conditions. The model configuration is defined according to the conceptual framework of the system to be modeled; further details of model configuration are available in Hsieh and others (2000), and Niswonger and Prudic (2003).

This section describes the model configuration that resulted in the best fit of simulated to measured temperatures. Many aspects of the best-fit configuration were determined during the calibration process, as described in the next section.

The two-dimensional model domain is a longitudinal cross section of the streambed sediments (fig. 13). The model domain extends vertically from the streambed surface to the water table, which is located at 22 m below land surface for modeling purposes. The model domain is 30 m wide, with the streambed surface extending horizontally along the entire 30 m of the upper layer. Three observation points are centered horizontally in the model domain at depths corresponding to the locations of thermistors (0.30, 0.94, and 2.1 m below land surface). Grid spacing varies from 0.27 to 0.55 m in the horizontal direction and from 0.08 to 0.26 m in the vertical direction; the smallest cells are located near the observation points at the top and center of the model domain.

Boundary conditions (for temperature and pressure) were assigned for all boundaries of the model domain. The uppermost layer of cells in the model domain represents the stream and was defined by (1) a constant pressure head boundary and a (2) time-varying temperature boundary; temperatures at this boundary were varied according to those measured at the streambed surface at TN1. The water table was represented by the lowermost layer of cells in the model domain and was assigned a constant pressure head of zero meters and a constant temperature of 7°C. The two lateral boundaries of the model domain were designated as no-flow boundaries.

Initial hydraulic conditions were defined by an equilibrium profile (pressure head equals the negative elevation head above the water table), in which pressure head varied linearly with depth from zero m at the water table to –23 m at land surface. Initial temperatures in the model domain were specified at the observation points to be equal to measured temperatures at TN1. In the upper 2 m of the model domain, initial temperatures were assumed to be constant in the horizontal direction and to vary linearly with depth; below 2 m, initial temperatures were assumed to remain constant with depth.

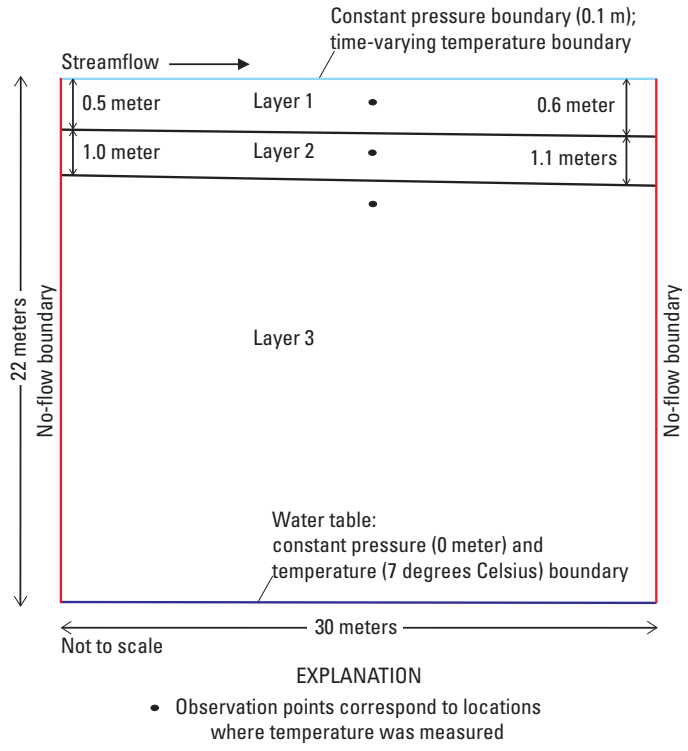

Figure 13. Schematic showing the best-fit model configuration, Arroyo Hondo study area, New Mexico.

Model Calibration

Model calibration was achieved through use of the manual trial and error approach (Constantz and others, 2002; Niswonger and Prudic, 2003). The objective of calibration is to obtain the best fit by minimizing the difference between simulated and measured temperatures. The best fit is identified through visual inspection of simulated and measured temperatures at the various observation points (fig. 13). The model (and, thus, the simulated streambed infiltration rate) is sensitive to particular hydraulic and transport properties. These properties, which include saturated hydraulic conductivity, anisotropy ratio, and longitudinal and transverse dispersivities, are varied during calibration in an attempt to minimize the difference between simulated and measured temperatures. Further details of the calibration process are available in Niswonger and Prudic (2003).

For this study, the model configuration progressed from simple to more complex during the calibration procedure. Initially, the two-dimensional model domain was defined as a perpendicular cross section of the stream channel (streamflow perpendicular to the model domain). The model domain consisted of a single layer (that is, hydraulic and transport properties were consistent for every point in the model domain).

The best fit was achieved by using a longitudinal cross section of the stream channel (streamflow parallel to the model domain) that consisted of three layers of varying hydraulic and transport properties (fig. 13). The geometry of the layers was not based on actual physical conditions of the streambed sediments; however, the configuration used for these simulations seems reasonable given that alluvial sediments are deposited in a layered fashion. The longitudinal cross section of the stream channel likely resulted in an improved fit because of the anisotropic nature typical of streambed sediments that results in a small component of horizontal flow (Niswonger and Prudic, 2003).

Sensitivity Analyses

Sensitivity analyses were performed to ensure that two simplifying assumptions (discussed below) used to assign boundary and initial conditions did not affect the estimated average infiltration rate. One assumption involves initial hydraulic condition for the model domain, which was defined as an equilibrium profile with the water table located 22 m below land surface. The water table is probably deeper than 22 m (fig. 5), but the exact location of the water table is not known. To investigate how the exact position of the water table (and associated changes in the equilibrium profile) affects infiltration rates, the depth of the water table was varied from 22 to 55 m. Results of these simulations indicate that the average infiltration rate was insensitive to the exact location of the water table.

The second assumption involves boundary conditions for the upper surface of the model domain. Boundary conditions for the upper surface were defined as a constant pressure head of 0.1 m because attempts to measure and record stream stage at TN1 were unsuccessful and the actual time-varying pressure head was unknown. Sensitivity analysis showed that the average infiltration rate was not affected by varying pressure head over its probable range of 0.05 to 0.2 m, which was determined through site inspection of high-water marks following the streamflow event.

Simulated Infiltration Rates

The best fit of simulated and measured temperatures (fig. 14) resulted in an effective saturated hydraulic conductivity of approximately 3 m/d and an estimated average infiltration rate of 1.4 m/d. The model domain required to achieve this fit consisted of three layers (fig. 13) and varying hydraulic and transport properties (table 2).

The estimated average infiltration rate (1.4 m/d) seems reasonable when compared with rates reported for the Santa Fe River (shown in fig. 1). Constantz and others (2002, p. 52–7) reported an initial streambed infiltration rate of 2.0 m/d, followed by a steady streambed infiltration rate of 0.1 m/d; both rates were determined by using VS2DI inverse-modeling techniques. Constantz and others (2002, p. 52–8) also reported an initial streambed channel loss of 1.0 m/d at the same location on the Santa Fe River, followed by a steady loss of 0.4 m/d; these rates were estimated by using more traditional surface-water techniques.

Cumulative Streambed Infiltration

The estimated average streambed infiltration rate was used in conjunction with the downstream extent of streamflow to estimate cumulative streambed infiltration along Arroyo Hondo. The following simplifying assumptions were used: (1) the average streambed infiltration rate for the 2.6-km reach immediately downstream from the mountain front is 1.4 m/d and (2) the wetted area of the active channel for any given day can be estimated from the minimum downstream extent of streamflow. For every day during the study period, the wetted area of the active channel can be estimated from channel widths measured at each surface temperature probe site and channel lengths. Because the actual downstream extent of streamflow is not known, minimum and maximum wetted channel areas were estimated.

The minimum wetted area for a given day was estimated as the sum of (1) the wetted channel area between the mountain front and the most downstream probe site with streamflow present, and (2) 5 percent of the wetted channel area of the next downstream segment (a segment is the reach of the channel between any two probe sites). The additional 5 percent of the wetted channel area was included because it is unlikely that streamflow ceased immediately downstream from a particular probe location. The maximum wetted channel area was estimated as the sum of (1) the wetted channel area between the mountain front and the farthest downstream probe site with streamflow present, and (2) 95 percent of the wetted channel area of the next downstream segment.

Minimum and maximum cumulative daily streambed infiltration values were calculated for every day in the study period. Minimum and maximum cumulative annual streambed infiltration values were estimated as the sum of all daily values for a particular water year.

Cumulative streambed infiltration was estimated to range from 17,100 m^3 to 230,000 m^3 during WY 2000 and from 58,500 m^3 to 246,000 m^3 during WY 2001. During WY 2002, cumulative streambed infiltration was zero. For purposes of comparison, estimates of cumulative streambed infiltration are shown in figure 15 along with streamflow measured during the study period, previous estimates of streamflow (Spiegel and Baldwin, 1963), and previous estimates of streambed infiltration (McAda and Wasiolek, 1988).

Estimates of cumulative streambed infiltration do not equal measured streamflow, except during WY 2002 (fig. 15). The differences are likely due to the simplifying assumptions used to estimate cumulative infiltration. For example, the streambed infiltration rate is unlikely to be constant throughout the upper ephemeral reach of Arroyo Hondo because infiltration rates are strongly influenced by the hydraulic conductivity of streambed sediments. Therefore, any variations in the hydraulic conductivity of streambed sediments, including variations in grain size and layering of sediments, would result in variations in the streambed infiltration rate. Additionally, estimates of wetted channel width (and thus wetted channel area) were assumed to remain constant from one streamflow event to another, although the active channel width probably varied from one streamflow event to another.

For every year of the study period, estimates of cumulative streambed infiltration are lower than previous estimates of streamflow and streambed infiltration (fig. 15). McAda and Wasiolek (1988) reported 625,000 m^3 per year of recharge from streambed infiltration; this value represents an aver-

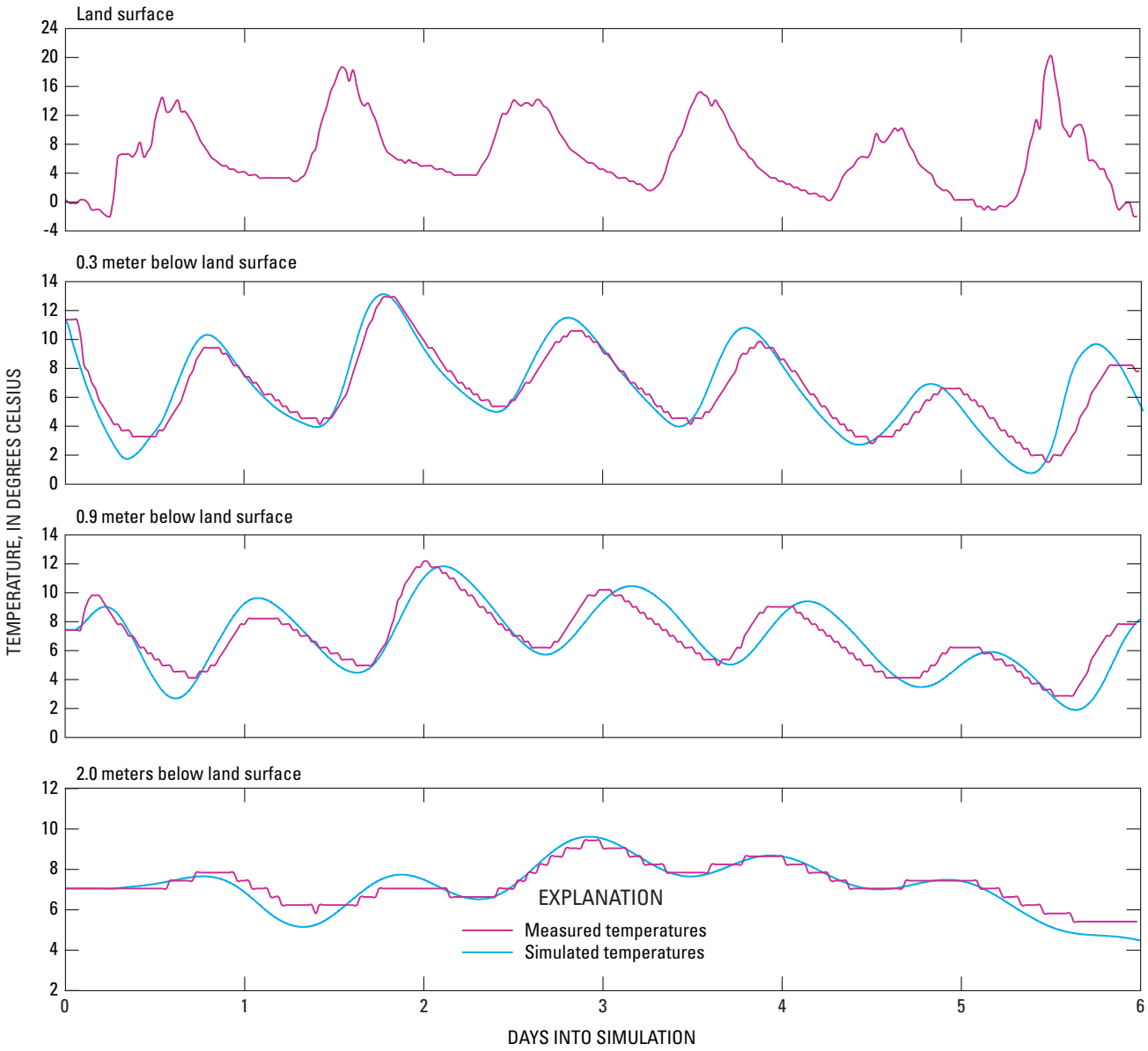

Figure 14. Measured and simulated temperatures at thermistor nest 1 (TN1) during March 2001 streamflow event, Arroyo Hondo study area, New Mexico. The location of TN1 is shown on figure 2.

Table 2. Selected hydraulic and transport properties used to simulate streambed infiltration.

Property (symbol)	Unit	Layer 1	Layer 2	Layer 3
Saturated hydraulic conductivity (K_{hh})	Meters per second	2.4×10^{-5}	3.5×10^{-5}	7.0×10^{-3}
Anisotropy ratio (K_{zz}/K_{hh})	Dimensionless	0.60	0.60	0.40
Porosity (η)	Dimensionless	0.38	0.38	0.38
Longitudinal dispersivity (α_L)	Meters	0.10	0.03	0.01
Transverse dispersivity (α_T)	Meters	0.10	0.03	0.01

age recharge rate. Normal precipitation, which represents a 30-year average value, for the Santa Fe area is 363 mm, which is 43 percent higher than mean annual precipitation (253 mm) measured during this study period. The annual water yield reported by Spiegel and Baldwin (660,000 m^3; 1963) was based on crest-stage gage data collected from 1913 to 1922. Based on long- term precipitation records for the Santa Fe 2 and Santa Fe weather stations, mean annual precipitation from 1913 to 1921 was approximately 379 mm per year (Western Regional Climate Center, 2002), which is about 50 percent higher than mean annual precipitation during the study period. Lower precipitation rates during this study may account for the smaller measured streamflow and, in part, for smaller estimates of cumulative streambed infiltration.

Recharge

Environmental tracers (chloride and bromide) were used to investigate the presence (or absence) of long-term recharge at selected locations in the Arroyo Hondo watershed. The basic principles of the chloride-mass balance method were applied to interpret environmental tracer data collected from soil cores in Arroyo Hondo.

Because chloride is water soluble, it moves through the unsaturated zone with infiltrating water. Therefore, large amounts of chloride in the unsaturated zone indicate that recharge is not occurring, and small amounts of chloride in the unsaturated zone indicate that recharge is occurring (Anderholm, 1994, p. 21–28; Izbicki and others, 2000, p. 206). Results of the chloride mass-balance method are valid only if the underlying assumptions are met (Scanlon, 2000).

Interpretation of Environmental Tracers

Variations in water content and chloride concentrations are shown in figure 16, in addition to variations in bromide concentrations. Chloride and bromide concentrations have similarly shaped profiles in each soil core (fig. 16). Chloride-bromide ratios varied from zero to 100. Discussion in this section is restricted to chloride concentrations; however, bromide concentrations are presented for comparison.

Volumetric water contents along transect 1 varied from 1 to 25 percent (fig. 16). Water contents were generally less than 10 percent in the upper 3 m of cores T1a and T1c; the largest water contents were about 5 m below land surface. The largest water content in core T1b occurred 1 m below land surface; water contents decreased to less than 10 percent

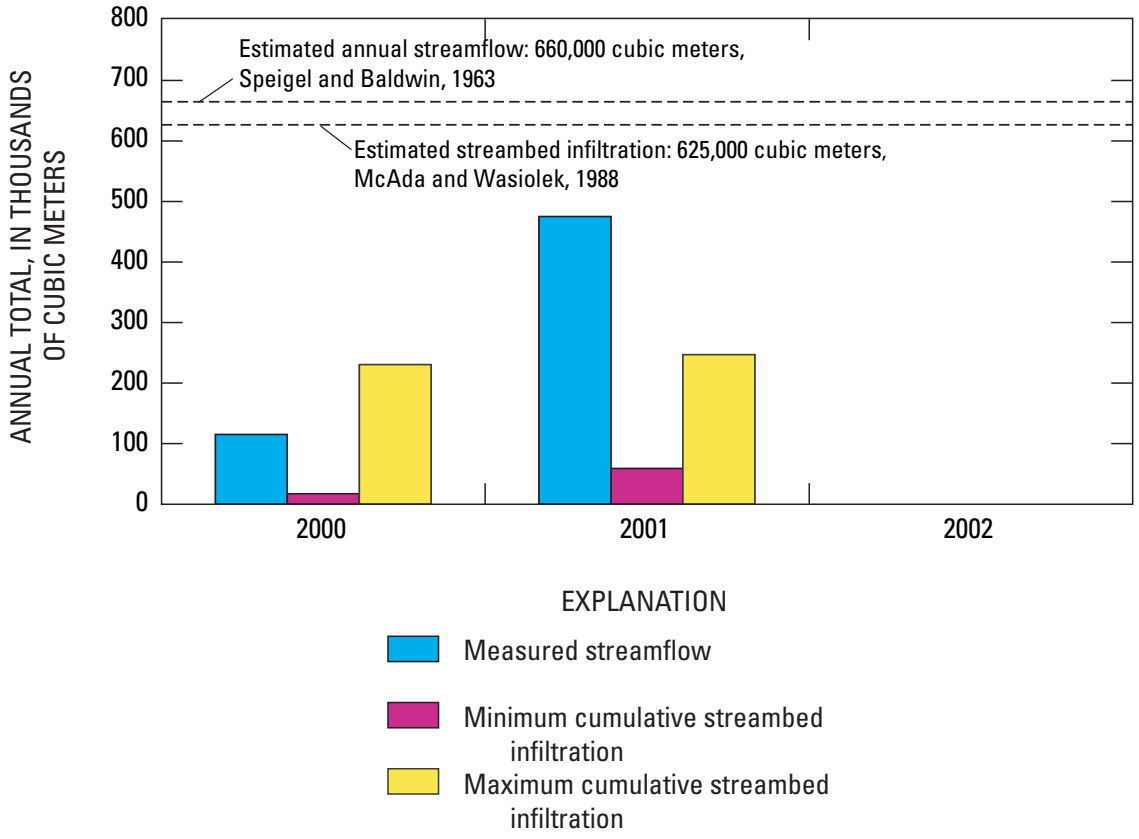

Figure 15. Measured streamflow, estimates of cumulative streambed infiltration, and previous estimates of streamflow and streambed infiltration, Arroyo Hondo study area, New Mexico.

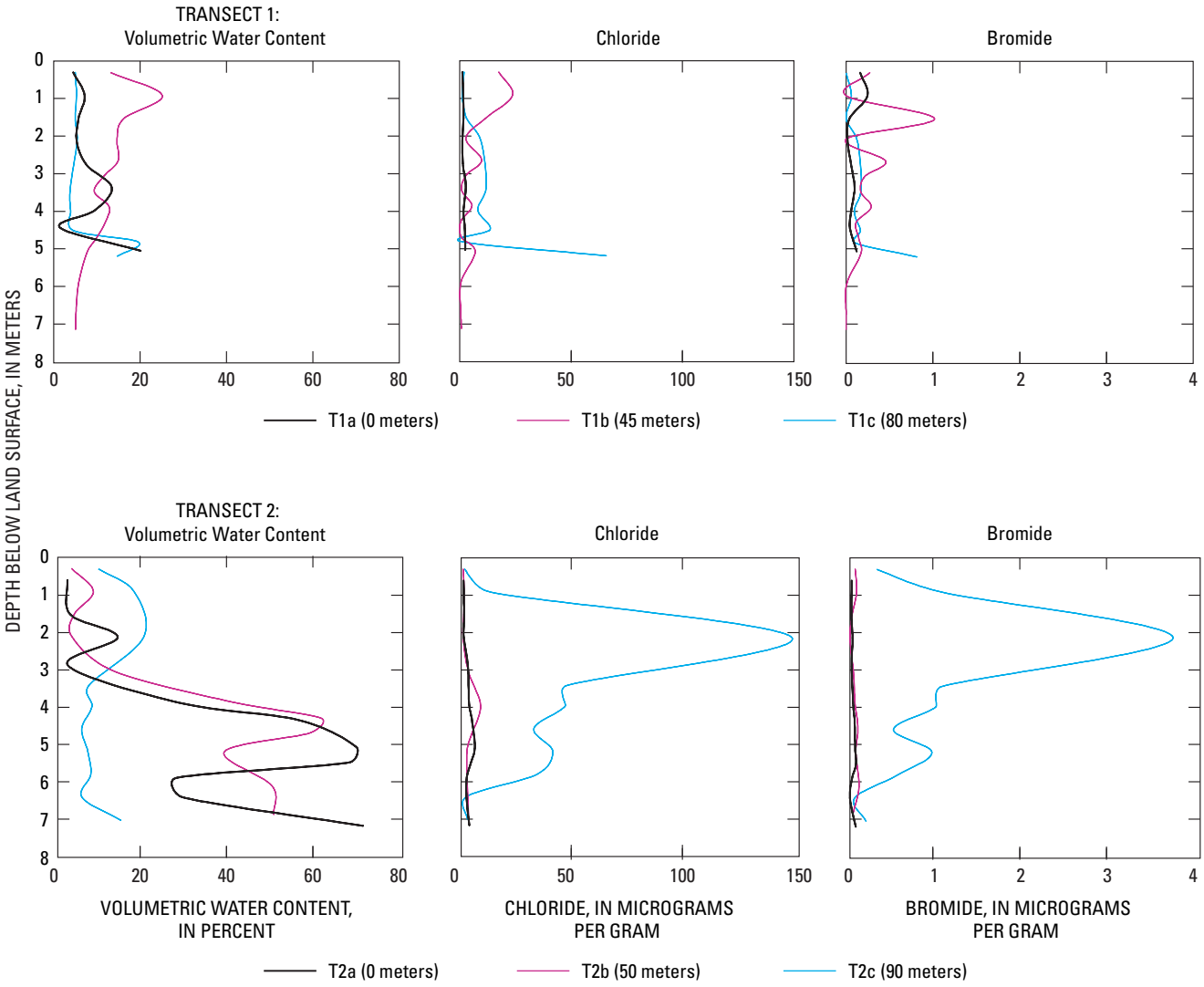

Figure 16. Volumetric water content and chloride and bromide concentration profiles for soil cores collected along transects 1 and 2 of the Arroyo Hondo study area, New Mexico. Distance from the arroyo channel is shown in parentheses. The locations of the transects are shown on figure 2.

at 7 m below land surface. Along transect 2, water contents varied from 2 to 70 percent. Water contents were less than 20 percent in the upper 3 m of cores T2a and T2b and increased to a maximum of 70 percent below 4 m. A thin layer (less than 0.3 m thick) of saturated, coarse-grained sand was penetrated between 5 and 6 m in cores T2a and T2b; a thin layer of silt was immediately below this layer. This layering may account for the unusually large volumetric water contents below 4 m in cores T2a and T2b. In core T2c, water contents were largest (about 20 percent) in the upper 3 m and smallest (less than 10 percent) in the lower 4 m.

Chloride concentrations ranged from less than 0.1 to 65 µg/g along transect 1 and from less than 0.1 to 147 µg/g along transect 2 (fig. 16). Core T1a, located in the active channel of the upper ephemeral reach, had the smallest chloride concentrations. Core T2c, located 90 m from the active channel in the lower ephemeral reach, had the largest chloride concentrations.

Chloride concentrations in core T2c (fig. 16) form a distinctive bulge-shaped profile that is typical of desert soils and indicate that direct recharge does not occur at that particular location. Chloride concentrations increase from 1.5 µg/g near land surface to a maximum of 147 µg/g at about 2 m below land surface, and then gradually decrease with depth to approximately 2 µg/g at about 7 m below land surface. Anderholm (1994, p. 21–23) reported similarly shaped profiles at three locations (“mesa sites”) within the Española Basin. Previous investigators have reported similar profiles in various arid regions including South Australia (Allison and others, 1985), western Texas (Scanlon, 1991), and the Mojave Desert (Izbicki and others, 2000; Stonestrom and others, 2003). The mass of chloride stored in the upper 7 meters of core T2c is 609.24 g/m2. Given a mean annual chloride deposition rate of 0.105 g/m2 (Anderholm, 1994, p. 18), this amount of chloride would take an estimated 5,800 years to accumulate (table 3). This

Table 3. Results of environmental tracer applications at selected locations in the Arroyo Hondo watershed.

Core identification	Transect location	Distance from active channel, in meters	Accumulation time[1], in years	Recharge[2]
T1a[3]	Upper ephemeral reach[4]	0	170	Yes
T1b	Upper ephemeral reach[4]	45	800	Possible low rate
T1c	Upper ephemeral reach[4]	80	1,300	Possible low rate
T2a[3]	Lower ephemeral reach[5]	0	350	Yes
T2b	Lower ephemeral reach[5]	50	350	Yes
T2c	Lower ephemeral reach[5]	90	5,800	Negligible

[1]The time required for the mass of chloride stored in the core to accumulate, as calculated from application of the chloride mass-balance method.

[2]Environmental tracers indicate only the presence or absence of recharge. The type of recharge (direct or focused) cannot be determined by using this method.

[3]Located in the active ephemeral channel.

[4]Transect T1 is located appoximately 2.6 kilometers downstream from the mountain front.

[5]Transect T2 is located approximately 12 kilometers downstream from the mountain front.

indicates that recharge is not presently occurring at the valley margin in the lower reaches of Arroyo Hondo.

Chloride concentrations in cores T1b and T1c are difficult to interpret because their profiles do not clearly indicate whether or not recharge is present (fig. 16). Chloride concentrations in core T1b are largest (18–24 μg/g) from zero to 1 m below land surface, decrease from 1 to 2 m, and remain less than about 9 μg/g. Chloride concentrations in core T1c are smallest (1.1 to 3.0 μg/g) from zero to 1.5 m, then increase to approximately 11 μg/g from about 2 to almost 5 m. A single sample from core T1c indicates an abrupt increase in chloride (and bromide) concentrations at about 5 m below land surface; the significance of this increase is unknown. The mass of chloride stored in the upper 5 m of cores T1b and T1c is 85 and 134 g/m2, respectively. The times required to accumulate these amounts of chloride are estimated to be 800 and 1,300 years, respectively (table 3). Although the chloride concentrations in cores T1b and T1c are small relative to those in T2c (fig. 16), the time required to accumulate the mass of chloride stored in T1b and T1c suggests that if recharge is occurring at these locations, it is at small rates.

Chloride concentrations in cores T1a, T2a, and T2b are relatively small (less than 9 μg/g) and generally show little variation with depth (fig. 16), indicating that recharge is presently occurring at these locations. Chloride concentrations in core T1a, located in the active channel of the upper ephemeral reach, vary from 1.1 to 2.8 μg/g. Chloride concentrations in core T2a, located in the arroyo channel of the lower ephemeral reach, vary from 1.1 to 6.1 μg/g. Chloride concentrations in core T2b, located 50 m from the arroyo channel, vary from 0.86 to 8.4 μg/g. Chloride profiles of cores T2a and T2b show a small bulge with maximum chloride concentrations at 4 and 5 m below land surface, respectively. Previous studies show that similar profiles with small chloride concentrations and little variation with depth indicate the presence of recharge (Anderholm, 1994; Izbicki and others, 2000). Anderholm (1994) reported similar profiles for two locations in active arroyo channels in the Española Basin.

Implications of Environmental Tracers

Interpretations of environmental tracers (table 3) generally agree with the conceptual model of recharge in the Arroyo Hondo watershed. Focused recharge is presently occurring in the upper ephemeral reaches of Arroyo Hondo (T1a). Direct recharge is presently occurring in the lower ephemeral reaches of Arroyo Hondo (T2a), and in other permeable areas of the Arroyo Hondo watershed (T2b). In the less permeable areas of the Arroyo Hondo watershed (T2c), recharge is not presently occurring.

Tracers indicate that recharge is occurring in the active channel of Arroyo Hondo (T1a and T2a) and at a site located

50 m from the active channel (T2b). Characterization of streamflow and investigation of streambed infiltration during this study (see sections on Streamflow and Streambed Infiltration) validate the presence of focused recharge in the active channel of the upper ephemeral reach (T1a). Results of this study suggest that focused recharge is not occurring in the active channel of the lower ephemeral reach; however, previous investigators have reported small amounts of direct recharge throughout the Arroyo Hondo watershed (Spiegel and Baldwin, 1963; Lee Wilson and Associates, 1978; McAda and Wasiolek, 1988).

Summary

This chapter presents the results of a three-year study of streamflow, infiltration, and recharge in Arroyo Hondo, New Mexico. Data were collected from October 1999 through October 2002 (WY 2000–02). Traditional and experimental methods were used to characterize streamflow in Arroyo Hondo. Traditional methods were used to characterize streamflow at a continuous-record stream gage. Experimental temperature-based methods were used to estimate the presence and duration of streamflow at selected sites along Arroyo Hondo. Streambed infiltration rates were estimated by using an inverse modeling technique that fits simulated to measured subsurface temperatures. Cumulative streambed infiltration rates were estimated from streambed infiltration rates, channel widths, and the downstream extent and duration of streamflow. Two environmental tracers (chloride and bromide) were used to investigate the presence of recharge at selected sites. Precipitation during the study period was below normal for two of three years.

Total annual streamflow in Arroyo Hondo ranged from zero to 474,000 m^3 during the study period. Annual streamflow was largest (474,000 m^3) in WY 2001 when annual precipitation at the Santa Fe 2 weather station was 103 percent of normal. Annual streamflow was smallest in WY 2002 (zero m^3) when annual precipitation at Santa Fe 2 was 57 percent of normal. Below-normal precipitation in the Santa Fe area during WY 2002 resulted in the smallest streamflows on record at streamflow-gaging stations Tesuque Creek above diversions near Santa Fe, N. Mex., and Santa Fe River above McClure Reservoir near Santa Fe, N. Mex. Snowmelt-induced streamflow events result in a larger total streamflow than monsoon-induced streamflow events.

Twelve surface-temperature probes were installed at selected locations in and near the arroyo channel; thermographs were constructed from data provided by surface-temperature probes. For each probe site, the presence and duration of streamflow was determined through inspection of thermographs. This information was used to ascertain the minimum downstream extent of continuous streamflow for every day in the study period. For a given daily mean streamflow (at the stream gage), monsoon-induced streamflow events extend a greater distance downstream from the mountain front than snowmelt-induced streamflow events. However, the duration of streamflow below the mountain front is greater during snowmelt-induced streamflow events than during monsoon-induced streamflow events. Throughout the study period, snowmelt-induced streamflow events produced more streamflow downstream from the mountain front than monsoon-induced streamflow events; the increased extent of streamflow may be due to higher residual moisture contents in streambed sediments during spring than during summer months. Snowmelt events are more likely than monsoon events to result in streambed infiltration because (1) a greater duration of streamflow below the mountain front, (2) a larger total volume of streamflow below the mountain front, (3) almost all streamflow is lost to infiltration, and (4) evapotranspiration rates are smaller during spring than summer and fall months.

A variably saturated, two-dimensional, heat transport model (VS2DI) was used to simulate streambed infiltration during streamflow events. The best fit of simulated and measured temperatures resulted in an effective saturated hydraulic conductivity of approximately 3 m/d and an estimated average infiltration rate of 1.4 m/d. The model domain required to achieve this fit consisted of three layers with varying hydraulic and transport properties. The estimated average infiltration rate (1.4 m/d) seems reasonable when compared with rates reported for the Santa Fe River.

Several simplifying assumptions were used to estimate cumulative streambed infiltration rates. Cumulative streambed infiltration was estimated to range from 17,100 m^3 to 230,000 m^3 during WY 2000, and from 58,500 m^3 to 246,000 m^3 during WY 2001. Cumulative streambed infiltration during water year 2002 was zero. Estimates of cumulative streambed infiltration do not equal measured streamflow, except during WY 2002; the differences are likely due to the simplifying assumptions used to estimate cumulative infiltration.

For every year of the study period, measured streamflow and estimates of cumulative streambed infiltration are lower than previous estimates of streamflow (660,000 m^3) and streambed infiltration (625,000 m^3). Below-normal precipitation during WY 2000–02 may account for the smaller measured streamflow and, in part, for smaller estimates of cumulative streambed infiltration.

Two environmental tracers (chloride and bromide) were used to investigate the presence of long-term recharge at selected locations in the Arroyo Hondo watershed. Interpretations of environmental tracers generally agree with the conceptual model of recharge (based on results of this study and those of previous investigations) in the Arroyo Hondo watershed. Tracers indicate that recharge is occurring in the active channel of Arroyo Hondo (T1a and T2a) and at a site located 50 m from the active channel (T2b). Characterization of streamflow and investigation of streambed infiltration conducted during this study indicate that focused recharge resulting from streambed infiltration is occurring in the upper portion of the ephemeral reach of Arroyo Hondo.

References Cited

Allison, G.B., Stone, W.J., and Hughes, M.W., 1985, Recharge in karst and dune elements of a semi-arid landscape as indicated by natural isotopes and chloride: Journal of Hydrology, v. 76, p. 1–26.

Anderholm, S.K., 1994, Ground-water recharge near Santa Fe, north-central New Mexico: U.S. Geological Survey Water-Resources Investigations Report 94–4078, 68 p.

Constantz, J., Stewart, A.E., Niswonger, R., and Sarma, L., 2002, Analysis of temperature profiles for investigating stream losses beneath ephemeral channels: Water Resources Research, v. 38, no. 12, p. 52(1)–52(13).

Constantz, J., and Thomas, C.L., 1996, The use of streambed temperature profiles to estimate the depth, duration, and rate of percolation beneath arroyos: Water Resources Research, v. 32, no. 12, p. 3597–3602.

Constantz, J., Tyler, S.W., and Kwicklis, E.K., 2003, Temperature-profile methods for estimating percolation rates in arid environments: Vadose Zone Journal, v. 2, p. 12–24.

Duke Engineering and Services, 2001, Water supply study, Jemez y Sangre Water Planning Region, New Mexico: Charlotte, North Carolina, Duke Engineering and Services, 235 p.

Healy, R.W., and Ronan, A.D., 1996, Documentation of computer program VS2DH for simulation of energy transport in variably saturated porous media—Modification of the U.S. Geological Survey's computer program VS2DT: U.S. Geological Survey Water-Resources Investigations Report 96–4230, 36 p.

Hsieh, P.A., Wingle, W., and Healy, R.W., 2000, VS2DI—A graphical software package for simulating fluid flow and solute or energy transport in variably saturated porous media: U.S. Geological Survey Water-Resources Investigations Report 99–4130, 16 p.

Izbicki, J.A., Radyk, J., and Michel, R.L., 2000, Water movement through a thick unsaturated zone underlying an intermittent stream in the western Mojave Desert, southern California, USA: Journal of Hydrology, v. 238 (3–4), p. 194–217.

Lapham, W.W., 1987, Use of temperature profiles beneath streams to determine rates of vertical ground-water flow and vertical hydraulic conductivity: U.S. Geological Survey Water-Supply Paper 2337, 35 p.

Lee Wilson and Associates, 1978, Santa Fe County water plan, Santa Fe County, New Mexico: Santa Fe, Lee Wilson and Associates, 162 p.

McAda, D.P., and Wasiolek, Maryann, 1988, Simulation of the regional geohydrology of the Tesuque aquifer system near Santa Fe, New Mexico: U.S. Geological Survey Water-Resources Investigations Report 87–4056, 71 p.

Niswonger, R.G., and Prudic, D.E., 2003, Modeling heat as a tracer to estimate streambed seepage and hydraulic conductivity, *in* Stonestrom, D.A., and Constantz, J., eds., Heat as a tool for studying movement of ground water near streams: U.S. Geological Survey Circular 1260, 96 p.

Ronan, A.D., Prudic, D.E., Thodal, C.E., and Constantz, J., 1998, Field study and simulation of diurnal temperature effects on infiltration and variably saturated flow beneath ephemeral streams: Water Resources Research, v. 34, no. 9, p. 2137–2153.

Scanlon, B.R., 1991, Evaluation of moisture flux from chloride data in desert soils: Journal of Hydrology, v. 128, p. 137–156.

Scanlon, B.R., 2000, Uncertainties in estimating water fluxes and residence times using environmental tracers in an unsaturated zone: Water Resources Research, v. 36, no. 2, p. 395–409.

Stonestrom, D.A., Prudic, D.E., Laczniak, R.J., Akstin, K.C., Boyd, R.A., and Henkelman, K.K., 2003, Estimates of deep percolation beneath irrigated fields, native vegetation, and the Amargosa River channel, Amargosa Desert, Nye County, Nevada: U.S. Geological Survey Open-File Report 03–104, 83 p.

Spiegel, Zane, and Baldwin, B., 1963, Geology and water resources of the Santa Fe area, New Mexico: U.S. Geological Survey Water-Supply Paper 1525, 258 p.

Stewart, A.E., 2003, Temperature based estimates of streamflow patterns and seepage losses in ephemeral channels: Stanford, Calif., Stanford University, Ph.D. dissertation, 248 p.

Thomas, C.L., Stewart, A.E., and Constantz, J., 2000, Determination of infiltration and percolation rates along a reach of the Santa Fe River near La Bajada, New Mexico: U.S. Geological Survey Water-Resources Investigations Report 00–4141, 65 p.

Western Regional Climate Center, 2003, Santa Fe 2, New Mexico, Period of record climate summary: http://www.wrcc.dri.edu/cgi-bin/cliMAIN.pl?nmsaf2, last accessed April 2003.

Ground-Water Recharge From Small Intermittent Streams in the Western Mojave Desert, California

By John A. Izbicki, Russell U. Johnson, Justin Kulongoski, and Steven Predmore

Abstract

Population growth has impacted ground-water resources in the western Mojave Desert, where declining water levels suggest that recharge rates have not kept pace with withdrawals. Recharge from the Mojave River, the largest hydrographic feature in the study area, is relatively well characterized. In contrast, recharge from numerous smaller streams that convey runoff from the bounding mountains is poorly characterized. The current study examined four representative streams to assess recharge from these intermittent sources. Hydraulic, thermal, geomorphic, chemical, and isotopic data were used to study recharge processes, from streamflow generation and infiltration to percolation through the unsaturated zone. Ground-water movement away from recharge areas was also assessed.

Infiltration in amounts sufficient to have a measurable effect on subsurface temperature profiles did not occur in every year in instrumented study reaches. In addition to streamflow availability, results showed the importance of sediment texture in controlling infiltration and eventual recharge. Infiltration amounts of about 0.7 meters per year were an approximate threshold for the occurrence of ground-water recharge. Estimated travel times through the thick unsaturated zones underlying channels reached several hundred years. Recharging fluxes were influenced by stratigraphic complexity and depositional dynamics. Because of channel meandering, not all water that penetrates beneath the root zone can be assumed to become recharge on active alluvial fans.

Away from study washes, elevated chloride concentrations and highly negative water potentials beneath the root zone indicated negligible recharge from direct infiltration of precipitation under current climatic conditions. In upstream portions of washes, generally low subsurface chloride concentrations and near-zero water potentials indicated downward movement of water toward the water table, driven primarily by gravity. Recharging conditions did not extend to the distal ends of all washes. Where urbanization had concentrated spatially distributed runoff into a small number of fixed channels, enhanced infiltration induced recharging conditions, mobilizing accumulated chloride.

Estimated amounts of ground-water recharge from the studied reaches were small. Extrapolating on the basis of drainage areas, the estimated aggregate recharge from small intermittent streams is minor compared to recharge from the Mojave River. Recharge is largely controlled by streamflow availability, which primarily reflects precipitation patterns. Precipitation in the Mojave Desert is strongly controlled by topography. Cool moist air masses from the Pacific Ocean are mostly blocked from entering the desert by the high mountains bordering its southern edge. Storms do, however, readily enter the region through Cajon Pass. These storms generate flow in the Mojave River that often reaches Afton Canyon, more than 150 kilometers downstream. The isotopic composition of ground water reflects the localization of recharge beneath the Mojave River. Similar processes occur near San Gorgonio Pass, 75 kilometers southeast from Cajon Pass along the bounding San Andreas Fault.

Introduction

The western Mojave Desert east of Los Angeles (fig. 1) is arid with hot, dry summers and cold winters. The population of the area, including the Palmdale/Lancaster areas to the west, the Victorville area, and the Yucca Valley area to the east, has increased rapidly from about 500,000 in 1990 to almost 670,000 in 2000 (California Department of Finance, 2002a,b). Water supply is derived almost entirely from ground water, and pumping has increased with population. As a result of pumping in excess of recharge, water levels throughout the area have declined in recent years (Smith, 2003; Stamos and others, 2001; Mendez and Christensen, 1997; Stamos and Predmore, 1995). Declining water levels and increased competition for ground-water supplies has resulted in a series of lawsuits and adjudications of parts of the area along the Mojave River (California Supreme Court, 2000) and in Yucca Valley (California Superior Court, 1977).

A better understanding of the physical processes that control the spatial and temporal distribution of natural recharge may help resolve questions about ground-water availability and enable agencies responsible for water supply to better manage ground-water resources. Ground-water recharge from larger streams such as the Mojave River has great economic value and has been extensively studied by traditional methods

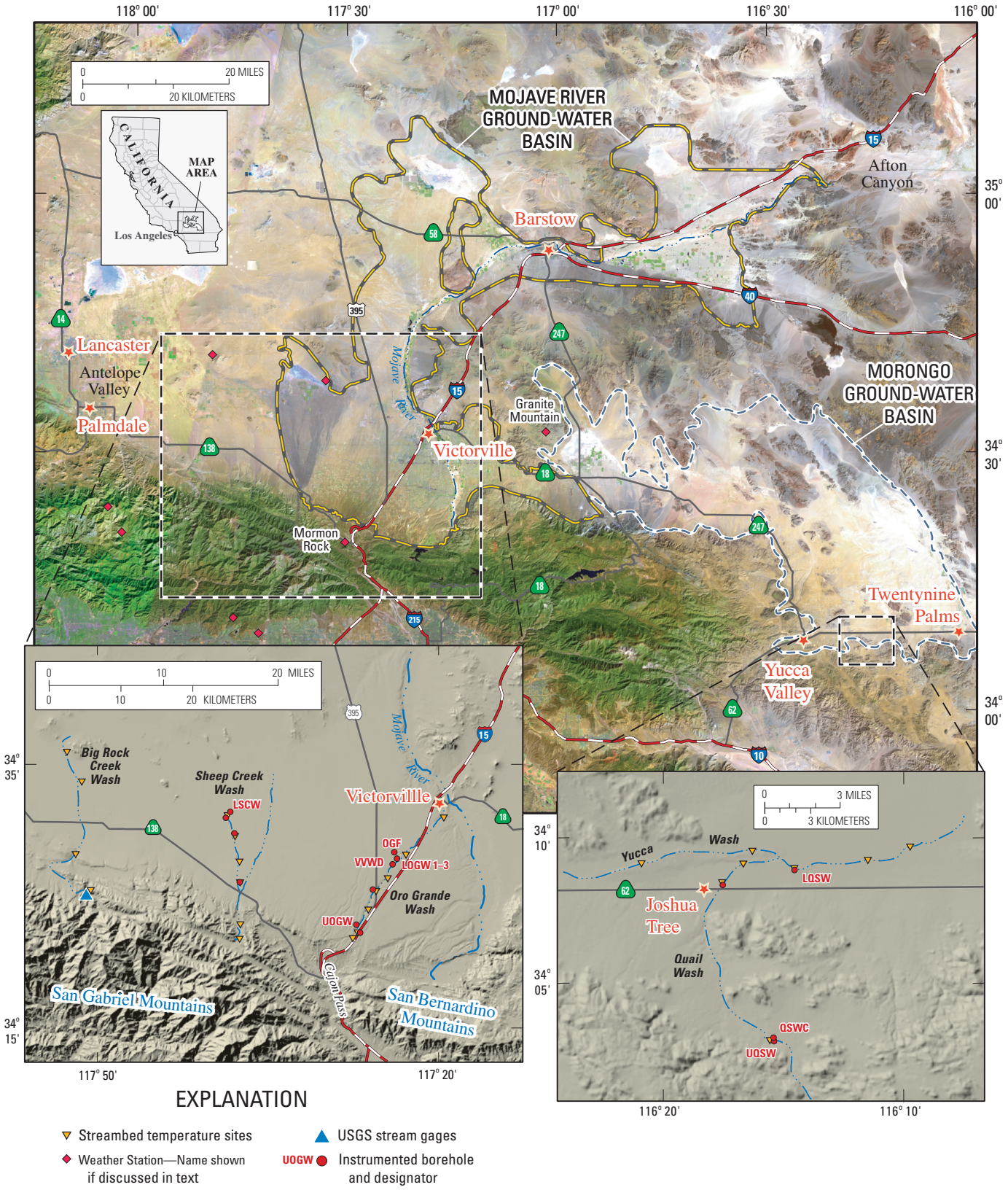

Figure 1. Location of study area in the western Mojave Desert, southern California.

(Thompson, 1929; California Department of Public Works, 1934; California Department of Water Resources, 1967; Hardt, 1971; Lines, 1996; Stamos and others, 2001). Recharge from small intermittent streams has not been as extensively studied but, in some areas, the aggregate recharge from these many small sources may represent a large part of the overall water budget in a basin. In addition, locations where even small amounts of natural recharge occur under present-day conditions may have value as potential sites for artificial recharge.

Purpose and Scope

The purpose of this paper is to describe the processes involved in focused recharge through thick unsaturated zones that underlie small intermittent streams in the western Mojave Desert. Understanding processes controlling recharge from small intermittent streams is important for assessing the regional water budget, and to determine if the aggregated recharge from the many small sources is greater or less than recharge from major sources such as the Mojave River.

Approach

This paper summarizes previously published results and ongoing work from a series of detailed U.S. Geological Survey studies addressing different aspects of natural recharge from intermittent streams in the western part of the Mojave Desert. In arid areas, natural recharge from these sources is typically small and difficult to study because it occurs intermittently at a wide range of temporal and spatial scales. A combination of physical, hydraulic, and chemical techniques were used to investigate different aspects of the recharge process—each technique constraining some aspect of the process. The use of multiple techniques was intended to describe the entire process, from frequency of streamflow and subsequent infiltration to the movement of water through the underlying unsaturated zone.

For the purpose of this study, the recharge process was divided into small increments on the basis of our understanding of natural recharge and our ability to measure and quantify each incremental step. Streamflow availability was determined from analysis of streambed temperature data. Infiltration of streamflow was determined from matric potential and borehole temperature data collected in the unsaturated zone beneath the stream channels. Stream reaches where deep infiltration (infiltration to depths below the root zone that presumably becomes ground-water recharge) occurred were determined from chloride profiles. Movement of water through the unsaturated zone to the underlying water table, in many cases several hundred meters below land surface, was evaluated of the basis of tritium data, numerical models, and a large-scale infiltration experiment.

Results from detailed studies along selected stream reaches were regionalized to the entire study area by using geomorphic techniques and isotopic data. The geomorphic techniques compared the stream drainage area to other stream drainage areas in the study area. The isotopic composition of ground water has preserved a record of the source, movement, and age of the water; interpretation of this record provides information on recharge from different sources within the basin through recent geologic time. As part of the interpretation of the isotopic record, large regional-scale sources of ground-water recharge were related to large-scale geologic features that focus precipitation, runoff, and subsequent ground-water recharge in a manner different from much of the arid southwestern United States.

Hydrogeologic Setting

The study area is the western Mojave Desert east of Los Angeles including the Mojave River Ground-Water Basin, the Morongo Ground-Water Basin and part of the Antelope Valley area along the northern slope of the San Bernardino and San Gabriel Mountains (fig. 1). The ground-water basins are defined on the basis of the contact between that alluvial valleys and the mountain front. The San Bernardino and Little San Bernardino Mountains to the east are composed largely of granitic rock. The San Gabriel Mountains are composed of granitic and metamorphic rock. For management purposes, these basins have been divided into smaller basins by the California Department of Water Resources (2003) on the basis of the areal extent of alluvial deposits, subsurface features such as faults and selected ground-water-flow divides.

The area is arid with hot, dry summers and cold winters (fig. 2). With the exception of the higher altitudes in the San Gabriel and San Bernardino Mountains, precipitation is generally about 150 mm/yr or less, but amounts may vary greatly from year to year. In most of the area, precipitation is greater during the winter rainy season (November-March) and occurs as a result of cyclonic storms moving inland from the Pacific Ocean. Although summer thunderstorms occur, especially in the southern part of the study area near Twentynine Palms, summer monsoonal precipitation that occurs throughout much of the southwestern United States is of lesser importance in this area.

With the exception of small streams—such as Big Rock Creek—that drain the higher altitudes of the San Gabriel and San Bernardino Mountains, and short reaches of the Mojave River —where ground water discharges at land surface—there are no perennial streams in the area. The Mojave River, the largest in the study area, drains about 5,500 km^2, about 540 km^2 of which are in the San Bernardino Mountains near Cajon Pass. Cajon Pass is a low altitude gap between the San Gabriel and San Bernardino Mountains. Moist air from the Pacific Ocean can enter the Mojave Desert through the pass without passing over the higher altitudes of the San Gabriel and San Bernardino Mountains and thus deliver precipitation to an otherwise rain-shadowed area. In some years winter precipitation near the pass gives rise to storm flow along the entire length of the Mojave River—reaching Afton Canyon, more than 156 km from the mountain front. A similar gap in the San Bernardino and San Jacinto Mountains forms San

Gorgonio Pass to the south of the study area and gives rise to winter precipitation in that area, although the effect is smaller than near Cajon Pass (Izbicki, 2004).

In the Mojave River Ground-Water Basin, two aquifers are pumped for water supply—the floodplain aquifer along the Mojave River and the surrounding and underlying regional aquifer. The floodplain aquifer consists of highly permeable sand and gravel deposited by the Mojave River. In most areas the deposits are less than 80-m thick and less than 2.5 km wide; however the deposits are thicker and more areally extensive in the Mojave Valley area downstream from Barstow (Stamos and others, 2001). Average annual recharge to the floodplain aquifer from infiltration of surface flow in the Mojave River is about 47.6 hm^3 (Stamos and others, 2001), but varies greatly from year to year in response to precipitation. The regional aquifer includes interconnected alluvial basins that drain toward the floodplain aquifer along the Mojave River and topographically closed basins that drain toward dry lakes. The deposits that compose the regional aquifer are less permeable than those of the floodplain aquifer, but may be more than 1,000-m thick in some areas. Annual recharge to the regional aquifer from the mountain block and from infiltration from small streams along the front of the San Gabriel and San Bernardino Mountains is about 13.2 hm^3 (Stamos and others, 2001). Although average annual recharge to the regional aquifer is smaller than recharge along the Mojave River, these deposits contain large amounts of ground water in storage.

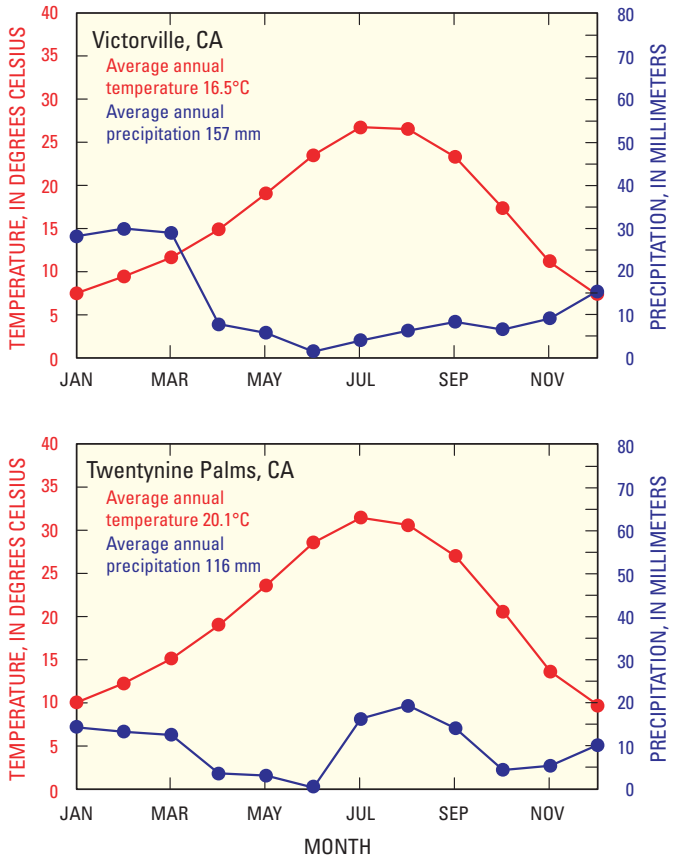

Figure 2. Monthly average temperature and precipitation for Victorville and Twentynine Palms, Calif. 1971–2000. Data from Western Regional Climate Center, http://www.wrcc.dri.edu, last accessed April 30, 2003.

The Morongo Ground-Water Basin contains a number of small, alluvial subbasins; each having separate ground-water flow systems typically terminating in dry lakes scattered throughout the area. These smaller alluvial basins are separated by faults and bedrock outcrops. Although the hydraulic properties of these subbasins vary spatially and with depth, they are more similar to those of the regional aquifer in the Mojave River Basin than to those of the floodplain aquifer along the Mojave River. In some areas, the alluvial subbasins may be more than 1,000 m thick and contain large amounts of ground water in storage. Aggregate recharge to the Morongo Ground-Water Basin due to infiltration from small streams at the front of the San Bernardino and Little San Bernardino Mountains has not been estimated.

The mechanisms by which surface flow from intermittent streams along the front of the San Gabriel and San Bernardino Mountains recharges underlying alluvial aquifers were studied along four washes—Oro Grande Wash and Sheep Creek Wash in the Mojave River Ground-Water Basin, Big Rock Creek Wash in Antelope Valley to the west of the Mojave River Ground-Water Basin, and Quail Wash in the southern part of the Morongo Ground-Water Basin. The total length of the selected washes is about 80 km. Each wash represents a range of climatic, geologic, and hydrologic conditions that control streamflow availability, infiltration of streamflow, movement of infiltrated water below the root zone (deep infiltration), and movement of water through the thick unsaturated zone to the water table, which varies up to several hundred meters below land surface.

Oro Grande Wash

Oro Grande Wash drains 6.2 km^2 at the downstream study site along the 22.7-km study reach. Oro Grande Wash is the smallest drainage included in this study and is representative of similar washes near Cajon Pass (fig. 3). Due to tectonic activity along the San Andreas Fault and subsequent erosion near the pass, Oro Grande Wash is no longer connected to the mountains, and flow in the wash is derived entirely as runoff from precipitation that falls on the alluvial fan surface. In some years precipitation on the alluvial fan near Cajon Pass can exceed 800 mm/yr (Izbicki and others, 2000a), but the average is less than 400 mm/yr. Precipitation decreases away from the pass and in most years is less than 150 mm/yr along the downstream parts of the study reach.

On the basis of channel-geometry data (Lines, 1996), average annual flow in Oro Grande Wash near LOGW is estimated to be about 0.5 hm^3 (table 1). Streamflow that occurs is brief in duration, typically lasting less than an hour. The channel of the wash is about 3-m wide and is incised about 10 to 20 m into the regional surface of the alluvial fan (fig. 4). As

Oro Grande Wash near LOQW-1 (December 2002). Channel sandy; width about 3 m. Infiltration rate about 0.28 m/hr.

Sheep Creek Wash near USCW, about 2 km downstream from mountain front (March 2004). Channel cobbly; width about 80 m (flows rarely span channel). Infiltration rate about 0.14 m/hr.

Sheep Creek Wash near LSCW, about 13 km downstream from mountain front (March 2004). Channel silty; width about 3 m. Infiltration rate about 0.04 m/hr.

Big Rock Creek gaging station, San Gabriel Mountains near Valyermo (10263500; March 2004). Channel is bedrock; width about 3 m. High flow is from snowmelt.

Quail Wash near LQSW (March 2004). Channel sandy; width about 20 m. Infiltration rate about 0.79 m/hr. Flow in August 2004 eroded more than five meters of left bank.

Figure 3. Photographs of selected intermittent streams in the western Mojave Desert study area, southern California. *A*, Oro Grande Wash; *B*, upstream reach of Sheep Creek Wash; *C*, downstream reach of Sheep Creek Wash; *D*, perennial reach of Big Rock Creek; *E*, downstream reach of Quail Wash. Locations are shown on figure 1. Infiltration rates are in meters per hour (m/hr).

a result, flow in the wash has followed nearly the same course, repeatedly wetting the underlying unsaturated zone, since incision of the wash after development of Cajon Pass, about 500,000 years ago (Meisling and Weldon, 1989). This repeated wetting has prevented development of the thick, impermeable caliche layers that underlie the alluvial fan away from the wash (Izbicki and others, 2000b, 2002). The bed of the wash is composed of sand along its entire length. Infiltration rates measured as part of this study by using a 1.2-m-diameter double-ring infiltrometer ranged from 1.3×10^{-2} to 2.2×10^{-2} cm/s (0.46–0.79 m/hr; table 2). Infiltration rates were lower near Cajon Pass and higher farther downstream.

The unsaturated zone underlying Oro Grande Wash ranges from more than 300-m thick near Cajon Pass to about 130 m along the downstream parts of the study reach. The alluvial deposits are composed of younger deposits of sand and gravel, reworked from the surrounding Victorville fan, that partly backfills the incision of the wash to a depth of about 7 m. These deposits are surrounded and underlain by older deposits of the Victorville fan (Meisling and Weldon, 1989) that consist of alternating layers of fluvially sorted sand, silt, and clay, with smaller amounts of gravel (Izbicki and others 2000a,b; Izbicki, 2002). The younger deposits are highly permeable, with saturated hydraulic conductivities of about 5.5×10^{-3} cm/s (Izbicki, 2002). The Victorville fan deposits are less permeable, and the saturated hydraulic conductivity of core material collected from the unsaturated zone along downstream reaches of Oro Grande Wash near instrumented borehole VVWD ranged from about 7×10^{-4} to 4×10^{-6} cm/s (fig. 5). Areally extensive clay layers having an average thickness of 1.2 m, but often less than 0.3 m thick, are present within the deeper, older deposits. These lower permeability layers are believed to be buried soil horizons (paleosols; Izbicki, 2002; fig. 6). They have lower permeability that impedes the downward movement of water and increases the lateral movement of water away from the wash (Izbicki, 2002; Nimmo and others, 2002). The statistical distribution of the low-permeability materials in the unsaturated zone along the downstream reaches of Oro Grande Wash was described by Izbicki (2002), and the effect of particle-size and sorting within the older deposits on unsaturated hydraulic properties was described by Winfield (2000).

Sheep Creek Wash

Sheep Creek Wash drains 36.8 km^2 in the San Gabriel Mountains west of Cajon Pass (fig. 3). The conical shape of the alluvial fan underlying the wash directs runoff away from the active channel of the wash (fig. 4), and the drainage area along the 18.8-km study reach from the mountain front to the downstream measurement site is only 2.4 km^2. Sheep Creek flows intermittently as a result of runoff from the higher altitudes in the mountains. Precipitation at the higher altitudes of the San Gabriel Mountains averages more then 1,000 mm/yr, with much of the precipitation falling as snow during the winter months. Precipitation decreases away from the mountain front and in most years is less than 150 mm/y along the downstream parts of the study reach.

On the basis of a relation between channel geometry and streamflow data (Lines, 1996), average annual flow in Sheep Creek Wash near the mountain front is estimated to be about 3.1 hm^3 (table 1). In some years, sustained flows, lasting as long as several weeks, may occur near the mountain front as a result of snowmelt after wet winters. The bank-to-bank width of the wash ranges from about 80 m near the mountain front to about 3 m as flows decrease downstream. Most flows near the mountain front do not fill the entire channel, and thus the active channel is much narrower. Under predevelopment conditions, streamflow in Sheep Creek Wash did not necessarily follow the same course each year; and occasionally flowed in different channels in response to deposition and subsequent changes in the slope of the fan (fig. 4). As a result, flow in Sheep Creek Wash did not repeatedly wet the same material year after year in the same manner as did flow in Oro Grande Wash (Izbicki and others, 2002). In recent years, a series of levees has restricted streamflow to fewer active channels. Near the mountain front the bed of the wash is composed of boulders and cobbles in a matrix of silt and sand. Farther downstream the bed of the wash is composed of fine silt. Infiltration rates measured as part of this study by using a 1.2-m-diameter double-ring infiltrometer ranged from 0.1×10^{-2} to 0.4×10^{-2} cm/s (0.04–0.14 m/hr; table 2). Infiltration rates were higher near the mountain front and lower farther downstream.

The thickness of the unsaturated zone underlying the wash ranges from more than 300 m near the mountain front to about 150 m along the downstream parts of the study reach (Izbicki and others, 2002). Much of the alluvial material comprising the Sheep Creek fan was deposited by debris flows and is poorly sorted. Near the mountain front, the deposits are composed of cobbles and gravel in a matrix of coarse sand. Although some cobbles and gravels are present in the deposits farther from the mountain front, the deposits there are finer grained and the matrix is composed of silt. Deposition on the Sheep Creek fan must have been fairly rapid and continuous, as evidence of paleosols within the deposits was not observed in test-drilling logs collected by Izbicki and others (1995, 2000a). Although the saturated hydraulic conductivity of the unsaturated deposits was not measured as part of this study, Winfield (2000) measured the physical properties, sorting, and water-retention characteristics. Winfield (2000) determined that differences in the water-retention characteristics between debris-flow deposits underlying Sheep Creek Wash and fluvially sorted deposits underlying Oro Grande Wash were determined primarily by the particle-size distribution of the material and not by a lack of fluvial sorting prior to deposition.

Big Rock Creek

Big Rock Creek drains 108 km^2 in the San Gabriel Mountains to the west of the Mojave River Basin in Antelope

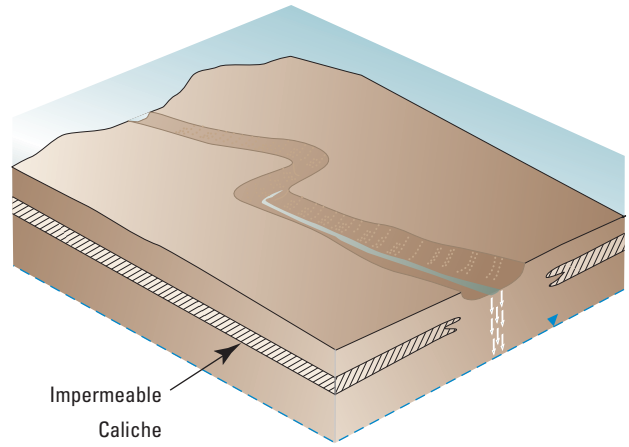

Oro Grande Wash

— Inactive alluvial fan; wash no longer drains mountain areas

— Channel locked in place by incision

— Infiltration has occured along the same reach in recent geologic time

— Heterogeneous unsaturated zone promotes lateral spreading of water

— Regional surface underlain by impermeable caliche

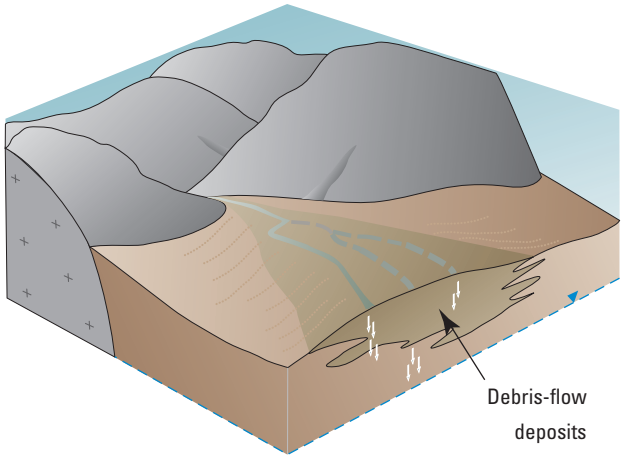

Sheep Creek Wash

— Active alluvial fan

— Active channel changes course in response to deposition on the fan

— Infiltration has occured along different reaches in recent geologic time

— Cobbles and gravel deposits near mountain front

— Debris-flow deposits inhibit infiltration along downstream reaches

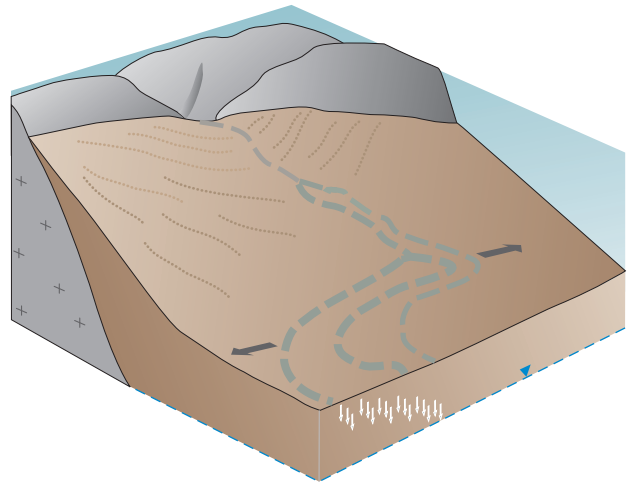

Quail Wash

— Active alluvial fan

— Upstream reaches locked in place by alluvial fan deposits

— Downstream reaches meander across low-slope alluvial deposits

— Relatively homogeneous unsaturated zone

— Downstream reaches affected by urbanization

Figure 4. Geomorphic and hydrologic features of selected intermittent streams, western Mojave Desert study area, southern California. Arrows represent recharging water.

Table 1. Physical characteristics along study reaches of Oro Grande Wash, Sheep Creek, Big Rock Creek, and Quail Wash, western Mojave Desert, southern California.

[Drainage areas and altitudes are measured above the mountain front. Average annual flow at the mountain front was estimated from a relation between channel geometry and annual flow developed by Lines (1996), except for Big Rock Creek, for which flow was estimated from streamflow data at Valyermo, Calif., five kilometers upstream of the mountain front. Abbreviations: —, not applicable (Oro Grande Wash no longer connects to an upstream watershed); km, kilometers; km^2, square kilometers; hm^3, cubic hectometers]

Stream	Drainage area at mountain front, in km^2	Altitude[1], in meters		Average annual flow, in hm^3	Length of study reach, in km	Channel width, in meters		Average slope of study reach, in percent
		Maximum	Average			At mountain front	At downstream site	
Oro Grande Wash	—	—	—	0.5	22.7	3.	3.	3.1
Sheep Creek Wash	36.8	2,594	1,948	3.1	18.8	80.	3.	4.9
Big Rock Creek	108.	2,829	1,769	16.	27.3	10.	40.	1.5
Quail Wash	237.	1,768	1,351	28.	15.2	10.	20.	1.7

[1]National Geodetic Vertical Datum of 1929.

Table 2. Streambed characteristics and infiltration along study reaches of Oro Grande Wash, Sheep Creek Wash, and Quail Wash, western Mojave Desert, southern California.

[Instantaneous infiltration measured using a 1.2-meter-diameter double-ring infiltrometer. Annual infiltration rate and infiltration along study reach estimated from temperature data (Kulongoski and Izbicki, 2008). Abbreviations: —, negligible (based on chloride accumulation; see text); m/hr, meters per hour; m/yr, meters per year; m^3, hm^3, cubic hectometers]

Stream	Description of stream channel	Instantaneous infiltration rate, in m/hr	Annual infiltration rate, in m/yr	Annual infiltration along study reach, in hm^3	Annual deep infiltration along study reach, in hm^3
Oro Grande Wash	Medium sand	0.28–0.72	0.7–2.0	0.1	0.04
Sheep Creek Wash	Cobbles near mountain front to silt downstream	0.04–0.14	0.7–1.3	0.58	0.51
Quail Wash	Coarse sand	0.46–0.79	[1]0.25	0.1	—

[1]Infiltration rate and annual infiltration calculated for 20-kilometer reach of Yucca Wash (Yucca Valley to Coyote [dry] Lake), which includes the confluence with Quail Wash.

Valley (fig. 3). The drainage area along the 27.3-km study reach from the mountain front to the downstream measurement site is 13.3 km^2. Precipitation amounts in the area are similar to those in the adjacent Sheep Creek area. Big Rock Creek flows perennially near the mountain front, and on the basis of streamflow gaging data, the average annual flow is 16.1 hm^3/yr. Flows are smaller and of shorter duration farther downstream. Streambed-temperature data and estimates of streamflow availability and frequency of flow from Big Rock Creek were included in this study for comparison with data from other streams having intermittent flow. Streambed-infiltration rates and the hydraulic properties of the underlying unsaturated zone were not characterized as part of this study.

Quail Wash

Quail Wash drains 237 km^2 in the Little San Bernardino Mountains in the Morongo Basin (fig. 3). Precipitation in the higher altitudes of the Little San Bernardino Mountains is as much as 350 mm/yr. Precipitation at the lower altitudes typically averages less than 100 mm/yr. Although it has the largest drainage area, Quail Wash is the driest of the study washes. Unlike the other study washes, more precipitation falls in the Quail Wash drainage during the summer months than during the winter months. The drainage area at the downstream site, LQSW, includes runoff from 185 km^2 in the San Bernardino and Little San Bernardino Mountains

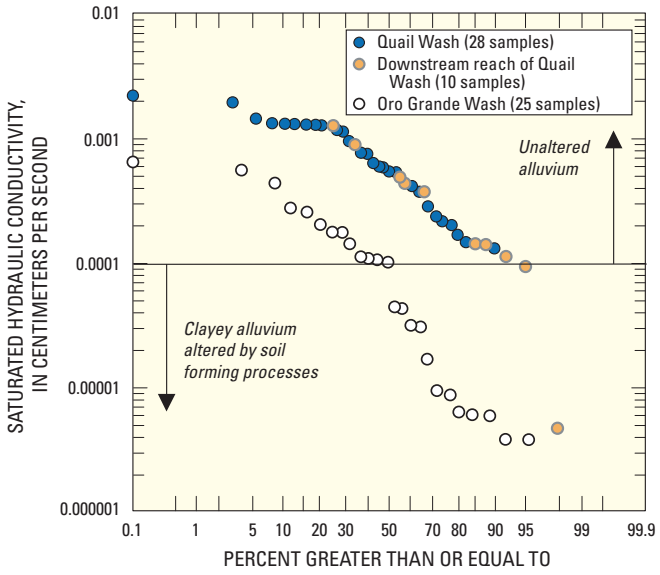

Figure 5. Distribution of saturated hydraulic conductivity values measured on core material collected from the unsaturated zone underlying the downstream reach of Oro Grande Wash (one site; total depth about 130 m) and Quail Wash (four sites; total depths about 15 m), western Mojave Desert, southern California. Figure 1 shows site locations.

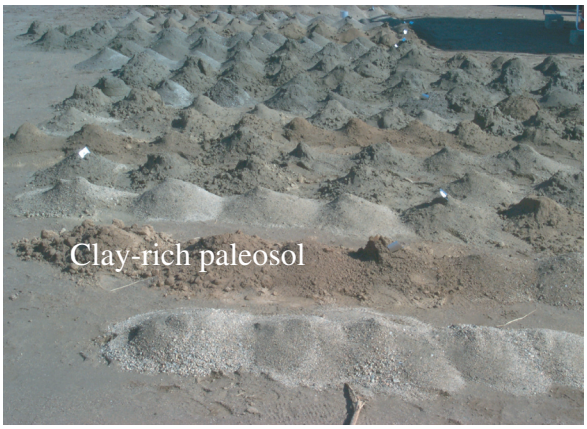

Figure 6. Heterogeneous alluvial deposits encountered during test drilling in the unsaturated zone underlying Oro Grande Wash near borehole VVWD, western Mojave Desert, California. Each pile represents the cuttings from a 0.3-m interval. Figure 1 shows the site location.

and alluvial valleys drained by Yucca Wash. Precipitation is greater in the area drained by Yucca Wash than in the area drained by Quail Wash, and more precipitation falls in this area during the winter months than during the summer months. Runoff from Yucca Wash has increased in recent years because of urbanization near Yucca Valley.

On the basis of a relation between channel geometry and streamflow data (Lines, 1996), average annual flow in Quail Wash was estimated to be about 28 hm^3 (table 1). Streamflow is more frequent and larger in magnitude along the downstream reach where flows from urban areas in Yucca Valley enter the wash. The channel of Quail Wash is about 10 m wide near the mountain front and about 20 m wide along downstream reaches where flows from urban areas are present. Streamflow along the downstream reach occurs more frequently during the winter rainy season than during the summer. Near the mountain front the position of the stream channel is constrained by alluvial fan deposits weathered from nearby hills. Farther from the mountain front the slope of the stream is small, about 0.3 percent, and the stream channel may change course as streamflow erodes the channel banks (fig. 4). The bed of the wash is composed of sand along its entire length. Infiltration rates measured as part of this study by using a 1.2 m diameter double-ring infiltrometer ranged from 1.3×10^{-2} to 2.2×10^{-2} cm/s (0.46–0.79 m/hr; table 2). Infiltration rates measured with the infiltrometer along Quail Wash decreased with distance from the mountain front to where it joins with Yucca Wash. Farther downstream, infiltration rates increased along stream reaches where the magnitude and frequency flow was increased by urbanization upstream.

The thickness of the unsaturated zone underlying the wash is about 150 m. The upper 15 m of these deposits were characterized by drilling as part of this study and are composed of fluvially sorted sand, with some gravel and silt. The sand was relatively homogeneous and lacked obvious paleosols. The saturated hydraulic conductivity of most core material collected from the unsaturated zone ranged from about 2×10^{-3} to 9×10^{-5} cm/s. The small range in hydraulic properties, in comparison with alluvial material underlying Oro Grande Wash, reflects the relatively homogeneous nature of the deposits, and the relatively continuous deposition with subsequent lack of soil development. Hydraulic-conductivity values were lower at the downstream site, where the deepest sample collected had a value similar to that of the paleosols beneath Oro Grande Wash. Additional clay layers may occur at greater depths within the unsaturated zone at Quail Wash (fig. 4).

Recharge Processes

For the purposes of this discussion, recharge has been divided into areal and focused recharge. Areal recharge occurs from direct infiltration of precipitation or snowmelt. Focused recharge occurs in areas, such as stream channels, where precipitation and subsequent runoff collects, however briefly, after storms. This study describes focused recharge from small intermittent streams present within the western Mojave Desert. Recharge from the Mojave River is discussed in a regional context to determine if the aggregated recharge from many small sources is as large as recharge from this single large source.

Areal Recharge

Previous studies have shown that direct infiltration of precipitation to depths below the root zone and subsequent ground-water recharge do not occur in many alluvial valley floors at rates significant for water supply through the thick unsaturated zones characteristic of arid areas in southern California (Prudic, 1994; Izbicki and others, 2000b, 2002) and in the southwestern United States (Phillips, 1994; Prudic, 1994). Analyses of core material collected from five boreholes as deep as 30 m at control sites away from study washes shows that the unsaturated zone underlying the Mojave Desert is very dry, with a median volumetric water content of 0.04 (Izbicki and others, 2000a). Volumetric water contents in coarse-grained material from some boreholes were less than 0.01. Water potentials, a measure of how tightly water is held within a material, were highly negative. Analysis of total potential (matric potential plus elevation potential) shows that gravity drainage does not occur at many of these sites and that the potential is for water to move upward as vapor towards shallower depths where soluble salts have accumulated beneath the surface (Izbicki and others, 2000a,b, 2002). The most negative water potentials, between –11,000 and –14,000 kPa, at depths of about 10 m, were associated with overlying high chloride concentrations (approaching 200 mg/g of alluvium) at depths between 5 and 10 m (site OGF, fig. 7). Because of its high solubility chloride, would move readily with infiltrating water if areal recharge were occurring (Allison and Hughes, 1978; Allison and others, 1985, 1994). Dry conditions and chloride accumulations in the unsaturated zone suggest that water is not infiltrating to greater depths and that areal recharge does not occur in the western Mojave Desert under present-day climatic conditions (Izbicki and others, 2000 and 2002).

Focused Recharge From Intermittent Streams

Analysis of core material from boreholes as deep as 200 m at 10 sites underlying Oro Grande Wash, Sheep Creek Wash, and Quail Wash shows that the unsaturated zone is much wetter beneath the washes than in the surrounding alluvial fans. Volumetric water contents are as high as 0.26 and matric potentials in many profiles are near zero (site UOGW and LOGW-1, fig. 7; Izbicki and others, 2000a). Calculations of total potential (matric potential plus gravitational potential) show downward movement of water under the influence of gravity at many of these sites (Izbicki and others, 2000b, 2002). Chloride concentrations in the alluvium are low, typically near 1 mg/g of alluvium, at sites where infiltration is sufficiently large for water to move below the root zone and ultimately recharge the underlying water table. Chloride has accumulated at depths of about 7 m at sites beneath the downstream reaches of Sheep Creek Wash (LSCW site, fig. 7) and Quail Wash (Nishikawa and others, 2005) suggesting that infiltration is not sufficient for water to move below the root zone and recharge the underlying water table along these stream reaches.

The following discussion examines the specific factors that control ground-water recharge, such as streamflow availability, infiltration of streamflow, deep infiltration below the root zone, and the movement of the water through the unsaturated zone into the underlying water table.

Streamflow Availability

Continuous-record stream gaging is the traditional method of assessing streamflow availability. The difference in flow between upstream and downstream gages can be used to estimate losses along stream reaches and infer infiltration losses into the streambed. However, stream gages are often impractical in desert settings because of the expense associated with the measurement of infrequent flows in channels that may scour or change course during streamflow. In addition, flows in some desert washes, although brief in duration, may be large in magnitude and destructive—precluding the installation of expensive monitoring equipment near stream channels. As a result of these limitations, with the exception of the perennial reach of Big Rock Creek near the mountain front, streams studied as part of this project were ungaged and alternate methods were used to assess streamflow availability for infiltration and ground-water recharge.

Streamflow availability was assessed by using streambed temperature data to estimating the frequency of days that had flow for study reaches along Oro Grande Wash, Sheep Creek Wash, and Big Rock Creek Wash between July 1998 and June 2000. Streambed temperature data also were collected along Quail Wash between October 2000 and July 2003. Streambed temperature data were collected by using inexpensive thermistors, equipped with internal data loggers, buried at shallow depths (10–20 cm) in the streambed (Constantz and Thomas, 1996; fig. 8). In most cases, the streambed temperature data were compared with similar data collected from instruments burried outside the stream channel, and streamflow was inferred from the difference between the two records. In some cases the presence of streamflow was inferred from the absence of daily temperature changes during streamflow. The streambeds were marked with paint to provide visible evidence of flow between site visits. Available precipitation and air temperature data from nearby weather stations, and streamflow in nearby gaged streams (fig. 1) also were used to constrain the interpretations. The approach assumes that certain changes in streambed temperature are caused by streamflow and works well in winter-dominated precipitation regimes or in streams having sustained flows from winter snowmelt that last from several days to several weeks (Constantz and Thomas, 1996, 1997).

Sustained flows lasting for more than several days did not occur along most fan and valley-floor reaches of Oro Grande Wash, Sheep Creek Wash, or Quail Wash during the study periods, and, except for Big Rock Creek, flows lasting for more than a few days were rare—even near the mountain fronts (fig. 9). An example of streambed temperature changes resulting from streamflow during winter runoff is shown for

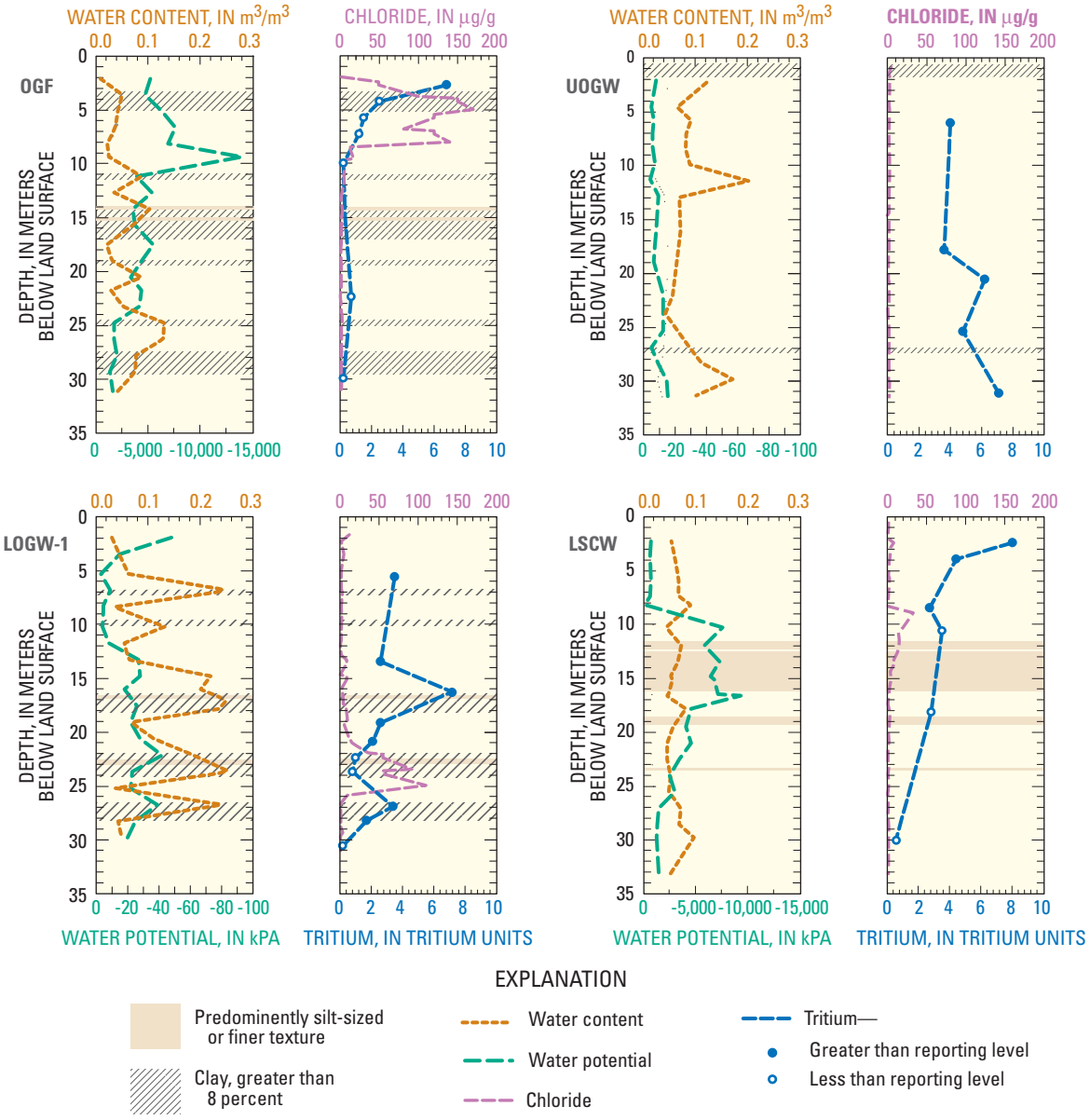

Figure 7. Water content, water potential, chloride, and tritium concentrations at representative sites in the unsaturated zone in an interchannel area (OGF), and beneath an intermittent stream (UOGW, LOGW-1, LSCW), western Mojave Desert study area, southern California. Unit designators are as follows: water content—cubic meters of water per cubic meter of bulk sediment (m^3/m^3); chloride [concentration]—micrograms of chloride per gram of pore water (µg/g); water potential [per volume of pore water]—kilopascals (kPa). Figure 1 shows site locations.

Figure 8. Streambed temperature site along Sheep Creek Wash near borehole USCW, western Mojave Desert, southern California. Inset shows close-up of temperature sensor. Figure 1 shows the site location.

Figure 9. Streamflow in Oro Grande Wash near VVWD, western Mojave Desert, southern California (January 28, 2001). Duration of flow from winter snowmelt was about 1 hour. Figure 1 shows the site location.

the upstream part of the study reach along Sheep Creek Wash from February 17 to 27, 2000 (fig. 10). Streamflow occurred twice during this period as a result of runoff from precipitation and snowmelt, although the duration of each flow was less than 2 days. The duration of streamflow inferred on the basis of temperature data for sites farther downstream was progressively less with increasing distance from the mountain front. Flow along Sheep Creek Wash during this period was confirmed by examination of the streambed.

Uncertainty about the occurrence of streamflow is larger for summer flows than winter flows because the duration of summer flows may be short and the streambed temperature change associated with summer flows are often small. An example of streambed temperature changes resulting from a brief flow after a summer thunderstorm is shown for Oro Grande Wash from July 5 to 11, 1999 in figure 11. Visits to the site and examination of the streambed confirmed that flow occurred during this period, but it was uncertain as to which changes in streambed temperature actually represented flow. Streambed temperature changes that occurred on July 10 and 11 were not interpreted as streamflow on the basis of numerical-model simulations that suggest that similar changes could result solely from infiltration of precipitation (Johnson and Izbicki, in review), although streamflow may have occurred.

The number of days having unexplained streambed temperature changes and streambed temperature changes interpreted as streamflow along Oro Grande Wash, Sheep Creek Wash, and Big Rock Creek Wash are shown in figure 12. The difference between the two lines in the graphs illustrates the magnitude of uncertainty associated with the interpretation of streamflow frequency in these channels. Although the magnitude of the uncertainty was nearly as great as the magnitude of the estimated flow frequency along much of Oro Grande Wash and Sheep Creek Wash, spatial patterns are apparent in the data.

Oro Grande Wash had the lowest estimated annual streamflow (table 1) and the lowest frequency of streamflow. Oro Grande Wash is no longer connected to the mountain front and flows only as a result of runoff from the surrounding alluvial fan deposits. Field observations and temperature data show that flows in Oro Grande Wash were brief in duration, typically lasting only an hour or less; therefore, a flow frequency of 0.05 days per year having flow probably represents a cumulative flow duration closer to 18 hours of flow rather than 18 days of flow (365 days per year times 0.05 days per year having flow).

Frequency of flow in Sheep Creek Wash and Big Rock Creek Wash was greater near the mountain front and decreased downstream as streamflow decreased—presumably due to infiltration into the unsaturated zone. The magnitude of the uncertainty associated with the technique was less near the mountain front where streamflow was more frequent and sustained for longer periods than farther downstream. This is particularly true for Big Rock Creek Wash where flow near the mountain front was perennial.

Farther from the mountain front, the flow frequency along Oro Grande Wash was similar to the flow frequency along both Sheep Creek Wash and Big Rock Creek Wash, except that small increases in flow frequency were observed along the downstream, urbanized reaches of Oro Grande Wash. Izbicki and others (2000b) inferred increased streamflow along this reach as a result of urbanization on the basis

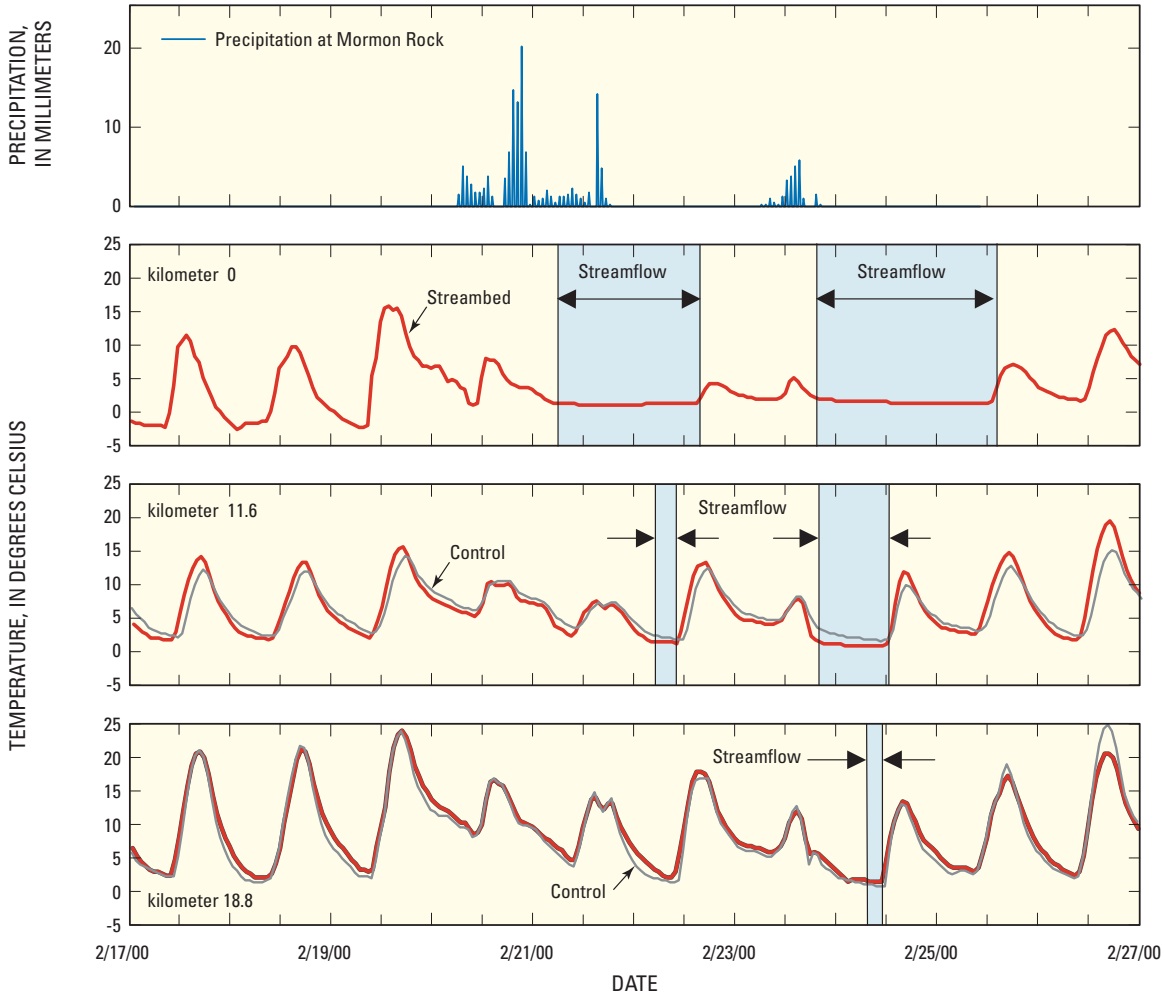

Figure 10. Precipitation, streambed temperature, control temperature (collected outside of streambed), and inferred duration of streamflow along Sheep Creek Wash, western Mojave Desert, southern California, February 17–27, 2000. Figure 1 shows the site location.

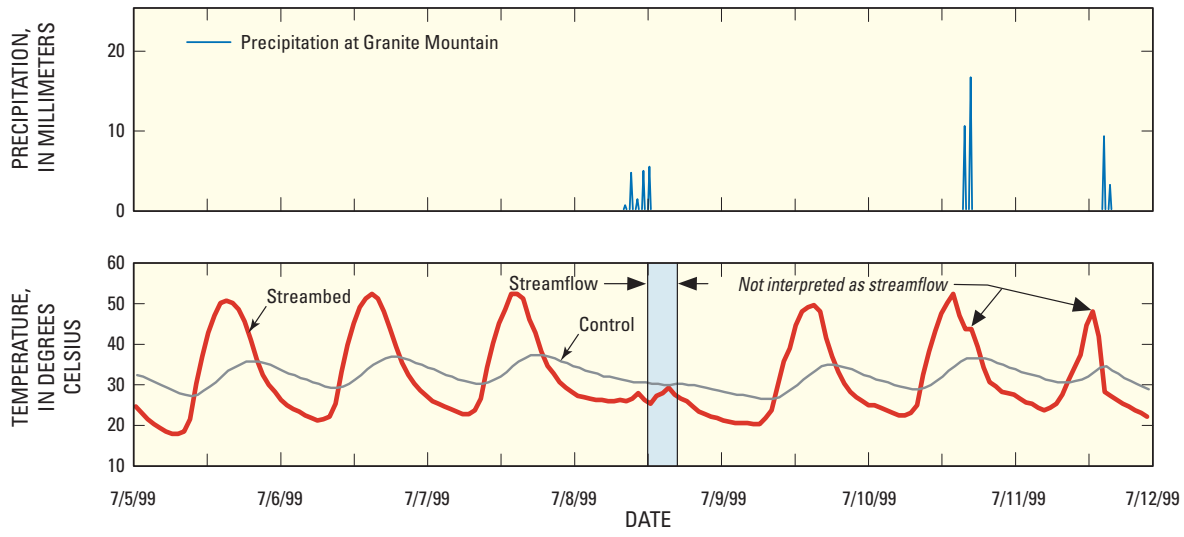

Figure 11. Precipitation, streambed temperature, control temperature (collected outside of streambed), and inferred duration of streamflow along Oro Grande Wash, western Mojave Desert, southern California, July 5–12, 1999. Figure 1 shows the site location.

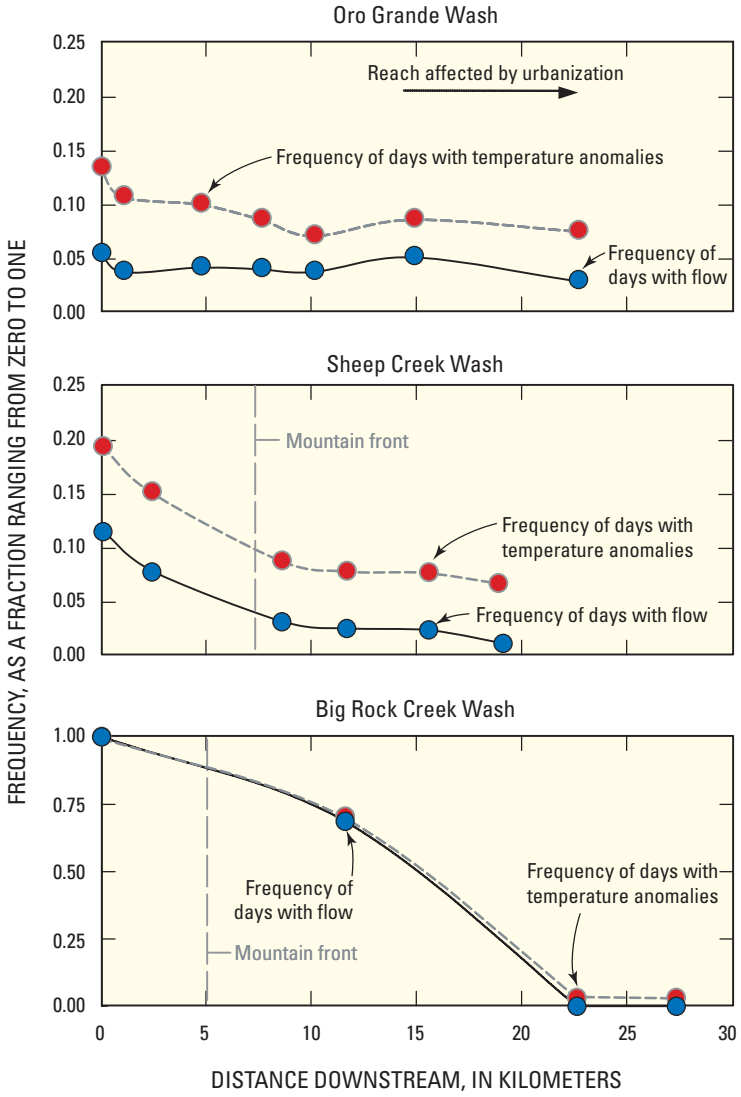

Figure 12. Frequency of temperature anomalies and frequency of days interpreted to have flow as a function of distance downstream in Oro Grande, Sheep Creek Wash, and Big Rock Creek Wash in the western Mojave Desert, southern California, July 1, 1998, to June 18, 2000. Figure 1 shows site locations.

of water content and chloride data collected from the unsaturated zone underlying the wash (LOGW-1, fig. 7).

Frequency and duration of flow are direct measures of streamflow available for infiltration and are important measures of the potential for ground-water recharge along a given stream reach. In principle, if the frequency and duration of flow are known with suitable precision, annual infiltration into the streambed can be calculated by multiplying the cumulative duration of individual streamflows by the hydraulic conductivity and wetted area of the streambed material, assuming a downward hydraulic gradient of 1. In practice, this approach was not used because it was not possible to measure the cumulative flow duration with suitable precision on the basis of streambed temperature data. Furthermore, the hydraulic properties of streambed material are not precisely known and may change during flow as a result of scour or deposition. Therefore, an indirect method was used to estimate infiltration from streamflow.

Infiltration from Streamflow

Continuous water-potential and temperature data collected from an instrumented borehole in the streambed along Oro Grande Wash illustrate infiltration of streamflow during the rainy season (fig. 13). The data are from instruments located about 6 m below the streambed. The instruments are especially responsive to the infiltration of water from the

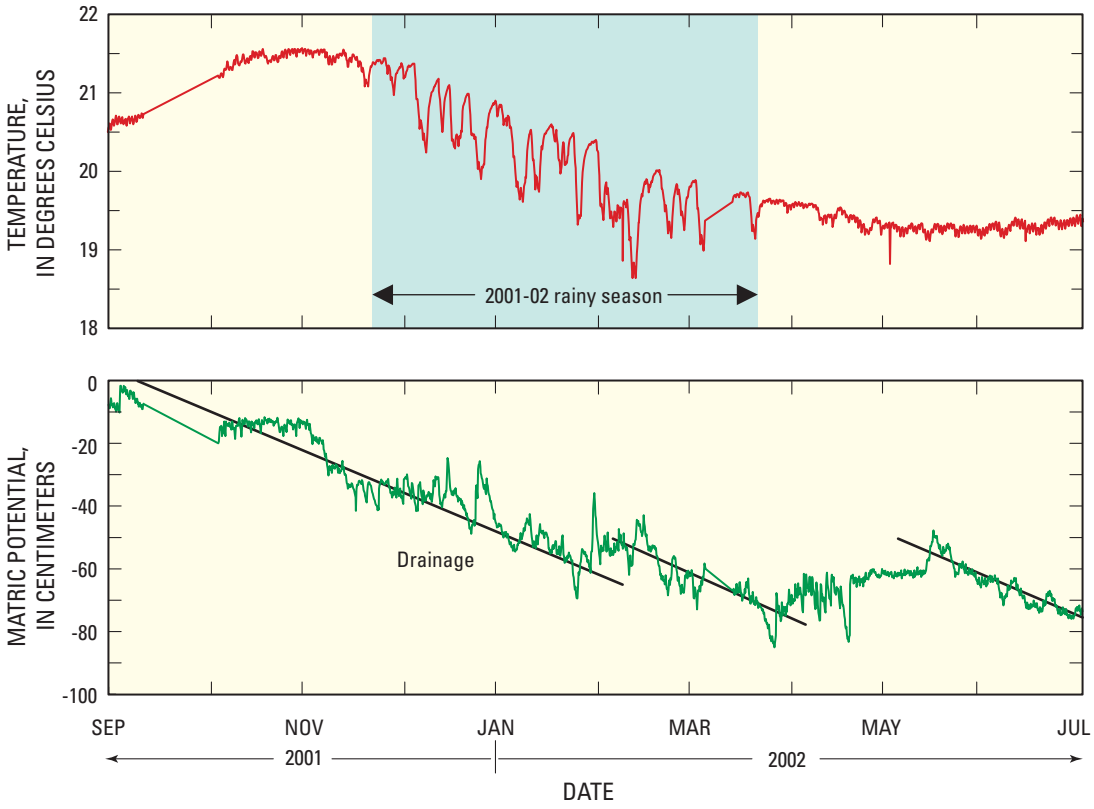

Figure 13. Temperature and matric potential about six meters below the streambed at site VVWD along Oro Grande Wash, western Mojave Desert, southern California. Figure 1 shows the site location.

stream because they are located above a 2-m thick clay layer that impedes the downward movement of water at the site.

As many as 16 distinct subsurface temperature changes, possibly associated with individual streamflows and subsequent infiltration of cold water along the wash, can be identified on the basis of the temperature data beneath Oro Grande Wash (fig. 13). The number and brief duration of these flows corresponds with the number of flows expected from frequency and duration data estimated on the basis of shallow streambed temperature data for this reach of Oro Grande Wash (fig. 8). Summer flows are less apparent in the data because temperature changes associated with summer streamflows are small. The cumulative infiltration from the rainy-season flows results in the increase in moisture apparent as less negative water potentials between January 24 and February 12, and between March 26 and April 15, 2002 (fig. 9). Changes in temperature and water potential at the site are dampened with depth, and although small seasonal changes in temperature of several tenths of a degree Celsius are apparent at depths as great as 26 m, water-potential data dampen to a constant value at the next instrument about 8 m below land surface.

The cumulative infiltration from rainy-season streamflows also results in a cooling of the unsaturated zone beneath the streambed in comparison with the surrounding material. This was measured as the difference in temperature between small-diameter (50 mm) air-filled access tubes at selected sites and nearby access tubes along Oro Grande Wash and Sheep Creek Wash between October, 1996, and September, 1997 (Izbicki and Michel 2002; fig. 14) and between October 2000 and July 2003 along Quail Wash. Comparison of temperature data (fig. 14) with chloride and data (fig. 7) shows that at sites such as UOGW and LOGW, where the temperature data suggest that a large amount of infiltration occurs, chloride is absent beneath the wash and tritium is present at great depths. In contrast, at sites, such as LSCW, where the temperature data suggest that only a small amount of infiltration occurs, chloride is present near the bottom of the root zone (about 7 m) and tritium is present only near the surface, typically about 1 m below land surface.

If the thermal properties of the underlying material can be estimated and one-dimensional downward movement of heat and water are assumed, temperature data can be converted into estimates of infiltration by using an approach described by Izbicki and Michel (2002). Numerical models, such as VS2DT (Lappala and others, 1987), also can be used to estimate infiltration (Kulongoski and Izbicki, 2008). The modeling approach incorporates advective and conductive movement of heat in two-dimensions and has the additional advantage of incorporating temporal changes in the distribution of infiltration. This information is important in areas where streamflow and subsequent infiltration do not occur every year. Hydraulic and thermal-property data, and details of model construc-

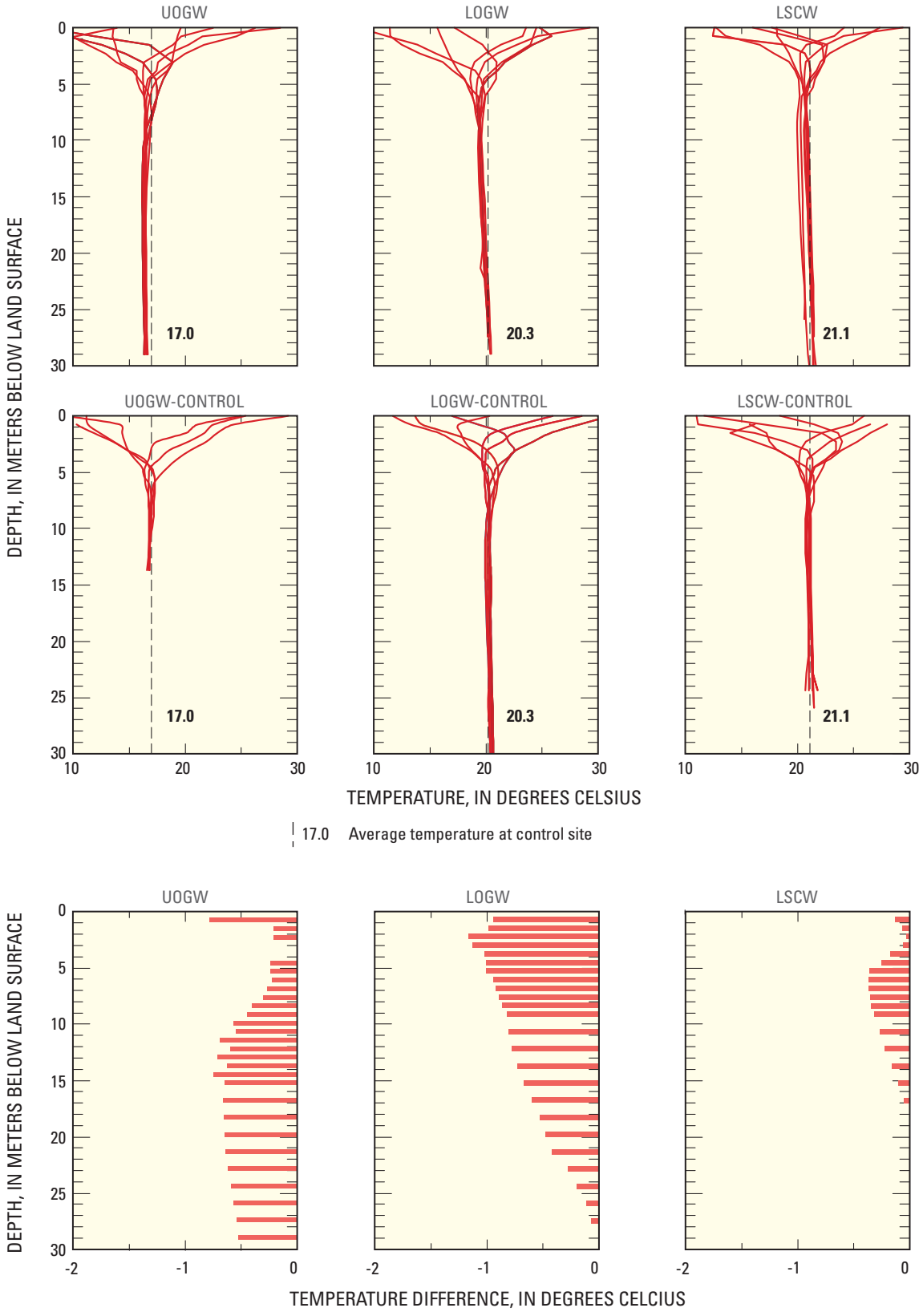

Figure 14. Temperature in small-diameter access tubes in intermittent streams and respective control sites along Oro Grande and Sheep Creek Washes in the western Mojave Desert, southern California, 1997–99 (modified from Izbicki and Michel, 2002). Figure 1 shows site locations.

tion used to estimate infiltration along selected study reaches, are discussed by Kulongoski and Izbicki (2008). Simulation results at selected sites show that the effect of different recharge rates and frequency of infiltration on the temperature profiles at selected sites along study washes (fig. 15).

The average infiltration rate at each site was estimated as the modeled infiltration rate divided by the number of years since infiltration occurred. The average infiltration rate was greatest along the upper reaches of Sheep Creek Wash near the mountain front. Although the bed of Sheep Creek Wash near the mountain front consists primarily of cobbles, instantaneous infiltration rates measured in this reach, by using a double-ring infiltrometer (table 2), were lower than rates measured along Oro Grande Wash; however, the average annual infiltration rate is greater along Sheep Creek Wash near the mountain front because the frequency of flow is greater along this reach (fig. 12). Model results showed that infiltration did not occur every year along most study reaches in sufficient magnitude to have a measurable effect on the subsurface temperature profile. However, infiltration was most consistent along the downstream reaches of Oro Grande Wash and Quail Wash. Runoff along these reaches has increased in recent years as a result of upstream urbanization. Infiltration was lowest along the downstream reach of Sheep Creek Wash; streamflow along this reach occurs infrequently for brief periods of time and the silty streambed along this reach has low permeability limiting the infiltration of streamflow.

Average annual infiltration along the study reaches of Oro Grande Wash, Sheep Creek Wash, and Quail Wash was estimated as the average infiltration rate times the width of the wash times the length of the wash reach between measurement points. Average annual infiltration along the study reaches was greater along Sheep Creek Wash than along Oro Grande Wash and Quail Wash (table 2). Along all three reaches, average annual infiltration was about 20 percent of the estimated annual streamflow, and more water is transmitted through the reach as surface flow than infiltrates into the streambed. Water infiltrated into the

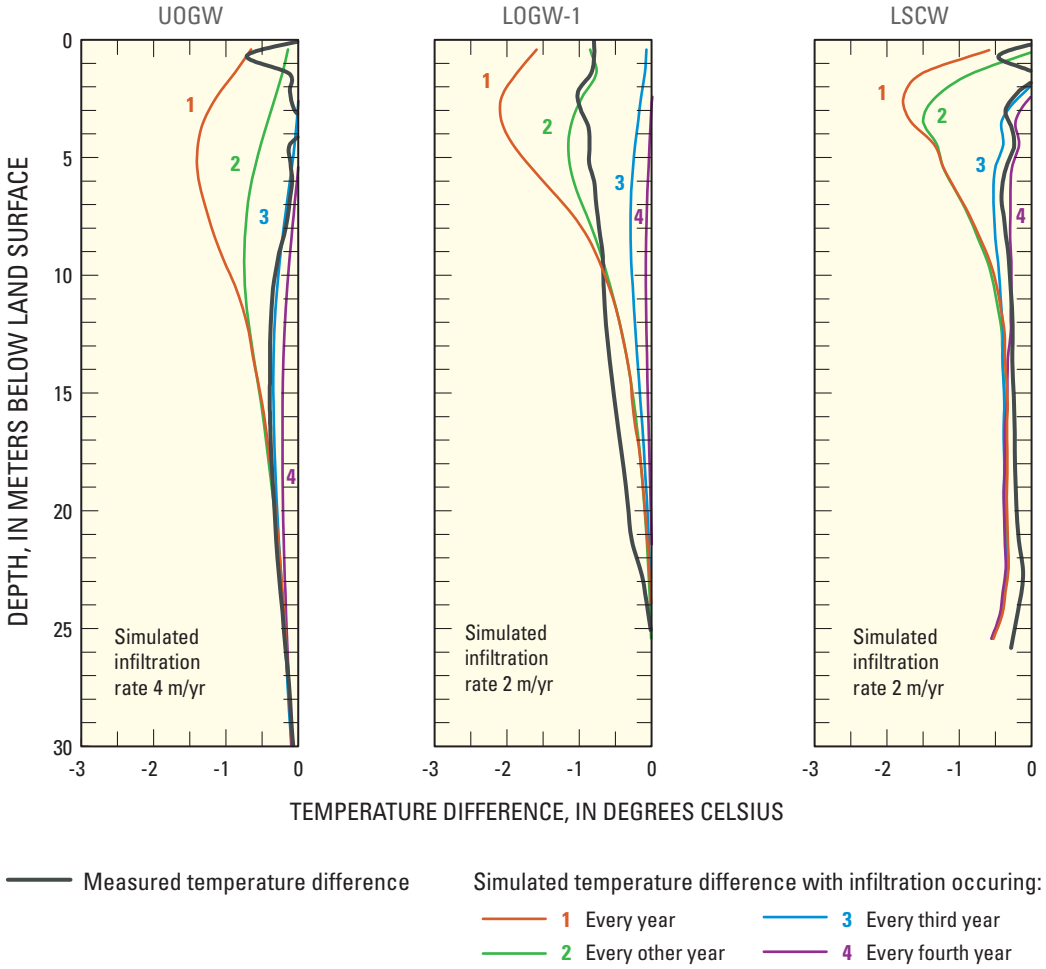

Figure 15. Measured and simulated temperature differences between selected wash sites and nearby control sites along Oro Grande (UOGW and LOGW-1) and Sheep Creek (LSCW) Washes, western Mojave Desert, southern California. Figure 1 shows site locations.

streambed may be transpired by plants along the stream channel or may infiltrate to depths below the root zone and ultimately become ground-water recharge.

Movement of Infiltrated Streamflow Below the Root Zone

Infiltration of streamflow below the root zone, also known as deep infiltration, was identified on the basis of chloride data in selected reaches of Oro Grande Wash, Sheep Creek Wash, and Quail Wash. As previously discussed, chloride is a tracer of the movement of water though unsaturated zones in arid environments. In areas where deep infiltration, and subsequent ground-water recharge do not occur, chloride in precipitation or dry deposition, may accumulate to high concentrations 5 to 10 m below land surface (fig. 7). In areas where recharge occurs, chloride—being highly soluble—will move with infiltrating water to depths below the root zone and ultimately to the underlying water table (Allison and Hughes, 1978; Allison and others, 1985, 1994; Prudic, 1994; Phillips, 1994).

The upstream site along Oro Grande Wash, UOGW (fig 7), is an example of a site where chloride is not present in the unsaturated zone underlying the wash, and ground-water recharge occurs under present-day climatic conditions (Izbicki and others, 2002). The downstream site along Oro Grande Wash, LOGW, is an example of a site where chloride that accumulated in the subsurface has been mobilized by increased infiltration of streamflow resulting from upstream urbanization (Izbicki and others 2000b, 2002). As discussed previously, streamflow along this reach of Oro Grande Wash has increased in recent years because of urbanization. Similar effects were observed along reaches of Sheep Creek Wash where levees have controlled streamflow, and subsequent infiltration, that under predevelopment conditions were distributed over time across the surface of the fan but are now restricted to a few active channels (Izbicki and others, 2002).

If water infiltrated at land surface is completely consumed by plants along a stream reach, chloride will accumulate at the base of the root zone. In these settings, although streamflow and infiltration occur, deep infiltration and subsequent ground-water recharge do not occur. The downstream site along Sheep Creek Wash, LSCW, is an example of a site where chloride has accumulated near the base of the root zone beneath the wash (Izbicki and others, 2002). Temperature data collected at this site suggest that streamflow and infiltration, while not occurring every year, average about 0.7 m/yr. This value may represent a threshold below which deep infiltration does not occur. Assuming that deep infiltration does not occur along reaches where chloride has accumulated, estimates of infiltration along Oro Grande Wash and Sheep Creek Wash can be reduced to provide an estimate of deep infiltration, and subsequent ground-water recharge (table 2). The threshold for deep infiltration is probably less in wider channels having less vegetation, or in channels composed of more permeable material.

Deep Movement to the Water Table

In many studies deep infiltration is presumed to ultimately become ground-water recharge because there are few processes that will remove water from the unsaturated zone other than plant roots, and because data from deeper depths are difficult and expensive to collect. However, before infiltrated water becomes ground-water recharge it must move through the unsaturated zone to the underlying water table. In the Mojave Desert the unsaturated zone may be as much as several hundred meters thick in some places and may be composed of many different layers having different hydraulic properties that ultimately control the rate of downward movement, lateral spreading, and flow of water through the unsaturated zone.

Rate of downward movement—The rate of downward movement of water through the unsaturated zone underlying Oro Grande Wash and Sheep Creek Wash was estimated on the basis of tritium data. Tritium is a radioactive isotope of hydrogen having a half-life of about 12.3 years. Although tritium is naturally occurring, the atmospheric testing of nuclear weapons beginning in 1952 increased its presence in the environment. Tritium concentrations reached a peak in about 1962 and decreased after the atmospheric testing of nuclear weapons ended (Michel, 1976). For the purpose of this paper, water in the unsaturated zone having measurable tritium was interpreted as water infiltrated after 1952 and the highest tritium concentrations were interpreted as water infiltrated in about 1962.

Tritium is not present in the unsaturated zone away from active stream channels at depths below the root zone where soluble salts have accumulated (fig. 5). In contrast, tritium was present at depths in excess of 30 m beneath Oro Grande Wash near Cajon Pass (UOGW and MOGW) and Sheep Creek Wash (USCW) near the mountain front. Downward rates of movement for infiltrating water at these sites must be at least 1.5 m/yr. Smaller rates of movement ranging from 0.8 to 0.3 m/yr were estimated for sites farther downstream where deep infiltration occurs (Izbicki and others, 2002). Given these rates of movement, and an unsaturated zone ranging from 130 m to more than 300 m thick near the mountain front, travel times of several hundred years may be required for infiltrating water to reach the water table beneath the sites (Izbicki and others, 2002). Given these long travel times, infiltration from infrequent streamflow dampens to a constant recharge rate by the time water reaches the water table. In settings such as the western Mojave Desert, recharge from small streams, such as Oro Grande Wash, Sheep Creek Wash, and Quail Wash, is not likely to be affected by short-term climatic cycles, such as El Niño or the Pacific Decadal Oscillation, even though infiltration at the streambed surface may greatly increase during these periods.

Lateral spreading—As infiltrated water moves downward through the unsaturated zone, it will spread laterally away from the wash. Lateral spreading decreases the flux and the rate of downward movement of the water (Izbicki and oth-

ers, 2000b; Nimmo and others, 2002). Lateral spreading of infiltrating water is controlled by the distribution and hydraulic properties of thin, often areally extensive, clay layers in the subsurface (Izbicki, 2002). These clay layers are believed to be soil horizons that developed during intervals when deposition was not occurring on the alluvial fan and were subsequently buried when deposition resumed. Given an infiltration rate of 1.3 m/yr applied to a 3-m wide wash, Izbicki (2002) simulated the movement of water through the heterogeneous unsaturated zone underlying Oro Grande Wash (fig. 16) to illustrate the effect of clay layers on the movement of water through the unsaturated zone. These simulations matched both the downward rate of movement of the infiltrating water calculated from tritium data and the lateral spreading of water measured in the unsaturated zone along a cross section perpendicular to the wash (Izbicki, 2002). Results were consistent with thin areally extensive clay layers from buried soils in the unsaturated zone rather than less extensive fine-grained fluvial deposits.

Flow of water through the unsaturated zone—The simulated movement of water shown in figure 16 assumes movement through the unsaturated porous media governed by Darcy's Law. Changes in the isotopic composition of water vapor after streamflow (Izbicki and others, 2000) show rapid movement of a small amount of water through preferential pathways, such as small cracks, in the unsaturated zone. If preferential flow occurs, some water may move in advance of the main wetting front and reach the water table faster than expected on the basis of Darcy flow.

Movement of water through the unsaturated zone was evaluated on the basis of a large-scale infiltration test at the VVWD site (fig. 1) along Oro Grande Wash near Victorville. Between October 1 and December 15, 2002, almost 190,000 m^3 of ground water was pumped from nearby public supply wells into a 0.4 ha pond and allowed to infiltrate into the unsaturated zone (fig. 17). An additional 72,000 m^3 was applied to the pond between February 10 and March 25, 2002. Measurement of infiltration from the pond provided a unique opportunity to evaluate the physical processes that control movement of water through a 130-m-thick, heterogeneous unsaturated zone, in the same manner that aquifer tests provide data on the physical movement of water through saturated aquifer material.

The site was selected because of its potential for artificial recharge resulting from its position on the alluvial fan overlying permeable material at the water table. Farther downslope the alluvial fan deposits are finer-grained—potentially impeding the downward movement of applied water through the unsaturated zone. Farther upslope the deposits are coarser grained but thicker; although water is likely to move downward through the unsaturated zone, permeable deposits pumped for water supply are not present at the water table in this area (fig. 18). The downward movement of water beneath the pond was monitored at a borehole instrumented with advanced tensiometers that measure both positive (saturated conditions) and negative (unsaturated conditions) pressure, and heat-dissipation probes that measure negative pressures.

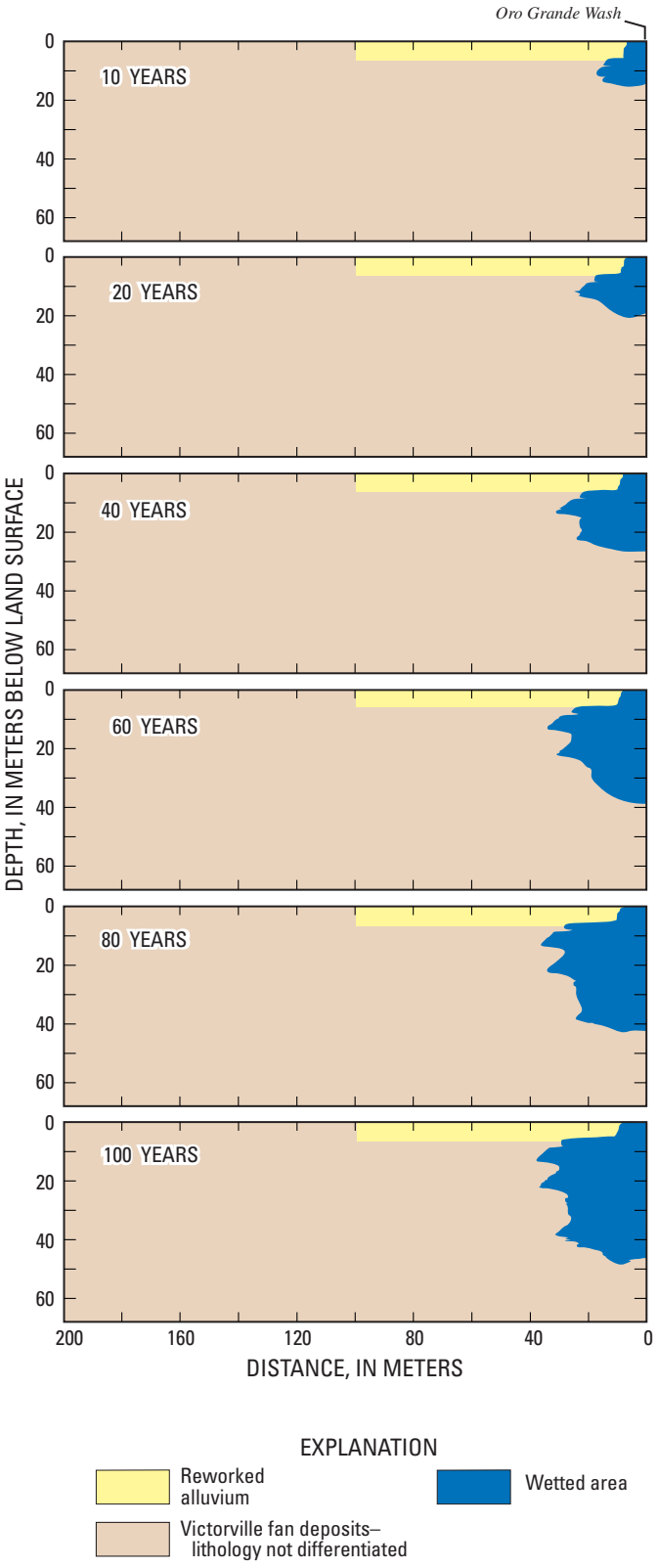

Figure 16. Simulated movement of water through a thick unsaturated zone having areally extensive clay layers, Oro Grande Wash, western Mojave Desert, southern California (modified from Izbicki, 2002).

Figure 17. Photograph of artificial recharge pond along Oro Grande Wash, western Mojave Desert, southern California. Flow from standpipe is about 50 liters per second.

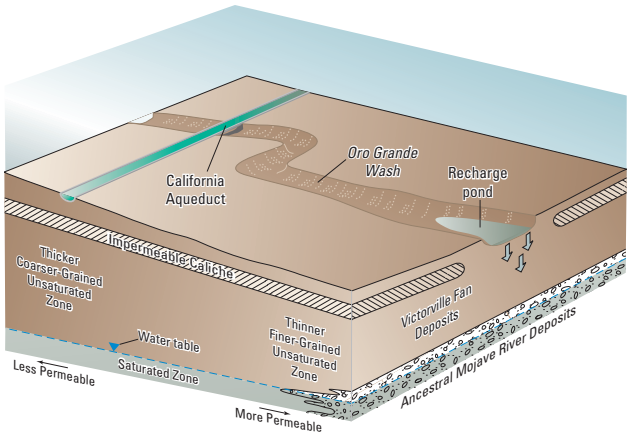

Figure 18. Subsurface geologic conditions in area of artificial recharge, Oro Grande Wash, southern California. Arrows represent recharging water.

Sequential electromagnetic logs were collected through a 50-mm-diameter access tube within the borehole to monitor the movement of applied water between instruments within the borehole and confirm tensiometer and heat-dissipation probe data. The borehole was sealed with low-permeability grout, except for short intervals near the instruments, by using procedures described in Izbicki and others (1995, 2000b, 2002) to minimize flow through the borehole during the infiltration test.

Results of data collection show rapid downward movement of water infiltrated from the pond. Changes in matric potential measured by using heat-dissipation probes between 6.7 and 26.2 m below land surface showed that on the basis of the arrival of the wetting front the rate of downward movement approached 1 m/d in October 2002 (fig.19). Slower rates of movement were recorded later in the test, in part because infiltrated water spread laterally away from the pond and because water was not infiltrated continuously from the pond.

Saturated conditions were measured beneath the pond in the tensiometer 6.4 m below land surface. This tensiometer is located above a fine-grained, clay-rich layer that impeded the downward flow and contributed to the lateral movement of water in the unsaturated zone (fig. 19). Water drained from this zone during periods when water was not present in the pond. Background data collected prior to the application of water from the pond showed that saturated conditions also developed on this clay layer from natural infiltration of streamflow at this site—although less water accumulated on the clay layer than during the infiltration test.

Saturated conditions also developed on a clay layer 84.7 m below land surface by late January 2003. Other instruments and geophysical log data show that at this time the main wetting front was still less than 60 m below land surface, and saturated conditions at this depth can only be explained by rapid movement of water, ahead of the main wetting front, through preferential pathways, such as cracks and large interconnected pore spaces. Increases in pressure between October and January are the result of increased air-pressure at this depth as air in the unsaturated zone was compressed by the downward-moving water, and from the cumulative weight of the infiltrated water on subsurface material.

Matric-potential data from heat-dissipation probes also show that small amounts of water moved ahead of the main wetting front through preferential pathways at rates approaching 2 m/d. For example, increases in pressure were recorded in the heat-dissipation probe at 53.6 m prior to the arrival of the main wetting front in February 2003 (fig. 19). This instrument, unlike the tensiometers, is not sensitive to increases in air pressure or the cumulative weight of the water and the measured changes in matric potential must represent the arrival of a small amount of water at the instrument prior to the arrival of the main wetting front.

Flow of water through preferential pathways was predicted for this site on the basis of changes in the isotopic composition of water vapor in the unsaturated zone after streamflow (Izbicki and others, 2000b). Although measurable, the amount of water that moved through preferential pathways in the unsaturated zone must under natural conditions have been small and probably did not significantly contribute to natural recharge at this site. However, this process may be important in areas where storage of hazardous waste in the unsaturated zone has been proposed.

Rates of movement between instruments and the position of the wetting front underlying the pond were confirmed on the basis of sequential electromagnetic logs (fig. 20). Increases in electromagnetic conductivity reflect increases in moisture content and decreases in electromagnetic conductivity reflect decreases in moisture content as infiltrated water moved through the unsaturated zone.

On the basis of electromagnetic log data, saturated conditions may have developed above coarse-grained layers in the unsaturated zone. This can occur because more pressure is required for water to enter the larger pore spaces between coarser-grained material than the smaller pore spaces in finer grained material. Electromagnetic logs done between

November 15, 2002, and December 4, 2002 (fig. 20), show that saturated conditions may also have developed above a coarse-grained layer at a depth near 30 m. Saturated conditions also occurred above a coarse-grained layer near 45 m between December 4 and December 22, 2002. After the entry pressure for water to enter the coarse-grained deposits was exceeded, water drained rapidly through the material at both depths (fig. 20).

Electromagnetic log data also show redistribution of water in the unsaturated zone between December 22, 2002, and May 6, 2003. After December 15, 2002, when less water was infiltrated from the pond, water in the upper part of the unsaturated zone continued to move downward under the influence of gravity; however, the rate of downward movement was significantly less.

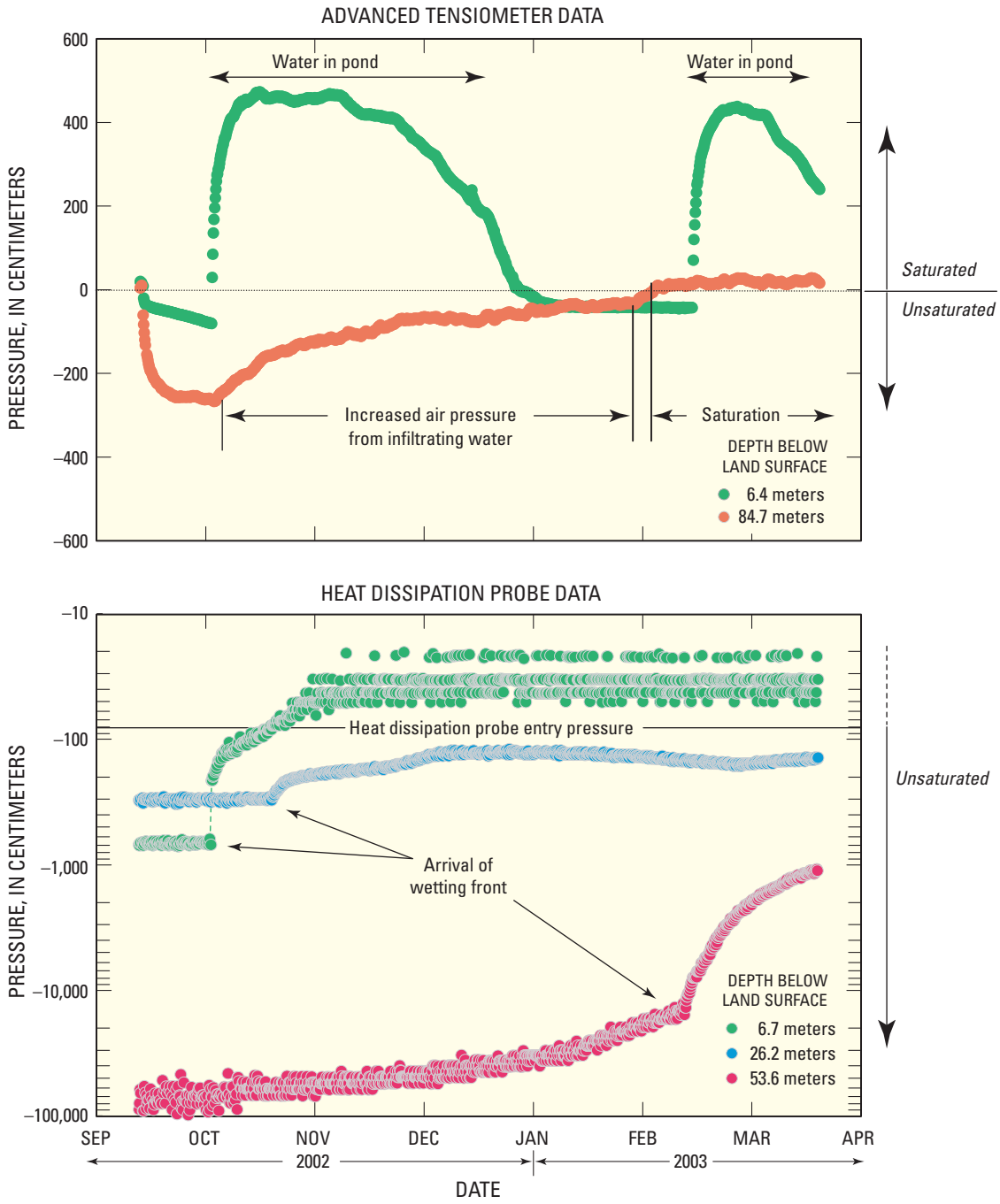

Figure 19. Response of selected instruments in the unsaturated zone to artificial recharge from a constructed pond near Oro Grande Wash (site VVWD), western Mojave Desert, southern California. Figure 1 shows the site location.

The results of the large-scale infiltration experiment show that the movement of water through thick, heterogeneous unsaturated zones is complex. Saturated conditions may develop above both fine-grained and coarse-grained layers, reducing the rate of downward movement of water. Saturated flow in these layers may increase the lateral spreading of water, further reducing the rate of downward movement of water. Although small amounts of water may move ahead of the main wetting front, after the water source is removed, downward movement continues at reduced rates as water is redistributed throughout the unsaturated zone. Given the time of travel and complex movement of water in thick, heterogeneous unsaturated zones, it may be unrealistic to assume that water infiltrated to depths below the root zone becomes ground-water recharge—especially in geomorphic settings, such as Sheep Creek Wash and Quail Wash, where channel abandonment processes on active alluvial fans may effectively strand water in the unsaturated zone above the water table.

Regionalization of Results

At the beginning of this study, it was unclear if the quantity of water infiltrated and recharged from a single large source, such as the Mojave River, was greater than the total quantity of water infiltrated from the many smaller sources, such as Oro Grande Wash, Sheep Creek Wash, Big Rock Creek Wash, Quail Wash and other small streams draining the San Gabriel, San Bernardino, and Little San Bernardino Mountains. Stamos and others (2001) estimated that annual recharge along the Mojave River averaged 47.6 hm^3 between 1930 and 1990. This value is much greater than the estimated infiltration and subsequent recharge (deep infiltration) from Oro Grande Wash, Sheep Creek Wash, and Quail Wash, which totals less than 0.8 hm^3 (table 2). A very large number of small streams, each contributing their small amount of recharge, would be required for the aggregated recharge from these sources to equal the recharge from a single large source such as the Mojave River.

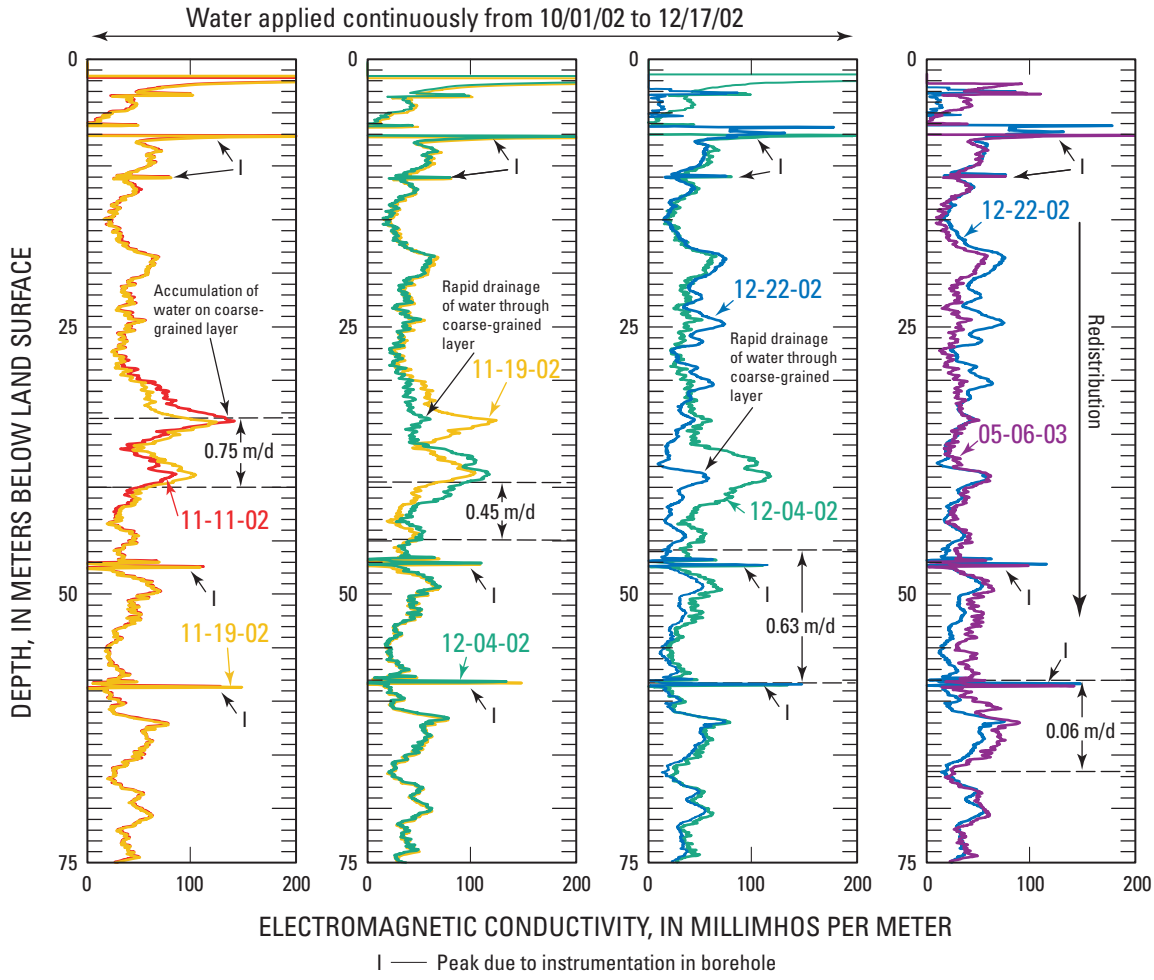

Figure 20. Sequential electromagnetic logs showing movement of water through the upper 75 m of the 120-m-thick unsaturated zone underlying an artificial-recharge pond near Oro Grande Wash, western Mojave Desert, southern California.

The rank-order distribution of streams draining the north-facing slope of the San Gabriel and San Bernardino Mountains, and east-facing slope of the Little San Bernardino Mountains is shown as a function of drainage area and stream order in figure 21 and table 3. The drainage area of each stream was calculated as the area upstream from the mountain front. A first-order stream is a stream having no tributaries, a second-order stream is formed at the confluence of two first-order streams, a third-order stream is formed at the confluence of two second-order streams, and so forth. The smallest area considered was 0.9 km^2. The largest basin considered was the headwaters of the Mojave River (including the West Fork of the Mojave River and Deep Creek), a fifth order stream draining 542 km^2 in the San Bernardino Mountains west of Cajon Pass. Oro Grande Wash (and other small streams near Cajon Pass) are not shown on figure 21 because they are not connected to the mountains as a result of erosion near Cajon Pass.

Quail Wash and Sheep Creek are among the larger streams draining the mountains. Results of this study show that deep infiltration and subsequent ground-water recharge from these streams are highly variable—ranging from 0.1 hm^3 for Quail Wash to 0.5 hm^3 (table 2) for Sheep Creek Wash—and not well-correlated to drainage area size (indicating heterogeneity of precipitation). In the case of Quail Wash, the second largest stream in the study area, much of the water that infiltrates may not reach the water table. Given that average annual recharge in the Mojave River has been estimated to be about 47.6 hm^3 (Stamos and others, 2001), there simply are not enough of the smaller streams to equal the large amount of recharge from a single large source such as the Mojave River. The smaller, more numerous first- and second-order streams, in aggregate, account for less than 20 percent of the total mountain drainage area. Furthermore, potential runoff, infiltration, and subsequent ground-water recharge from such sources are inherently smaller because low-order streams drain lower altitudes where precipitation is lower (due to orographic effects) than the higher altitudes drained by high-order streams.

Streams such as Sheep Creek are locally important sources of ground-water recharge. However, even for these relatively large secondary streams, the estimated recharge from infiltration that travels through the unsaturated zone is small compared to estimates made by Stamos and others (2001) by fitting a regional ground-water flow model. This difference suggests that most of the recharge to the regional aquifer in this area occurs as a result of infiltration of streamflow through coarse alluvium near the mountain front. Recharge in this fashion does not distribute water rapidly to large distances from the mountain front.

The isotopic composition of ground water was used to confirm interpretations of the cumulative ground-water recharge from small intermittent streams relative to other sources in the study area, especially the Mojave River. Isotopic data collected as part of this study included the stable isotopes of oxygen and hydrogen (oxygen-18 and deuterium, respectively), tritium, and carbon-14. These results are summarized below. More detailed discussions are presented in Izbicki and others (1995), Izbicki (2004), and Izbicki and Michel (2004).

Oxygen-18 and deuterium are naturally occurring stable isotopes of oxygen and hydrogen, respectively. Oxygen-18 and deuterium abundances are expressed as ratios in delta notation (δ) as per mil (parts per thousand) differences relative to the standard known as Vienna Standard Mean Ocean Water (VSMOW; Gonfiantini, 1978). Because the source of most of the world's precipitation is evaporation of seawater, the $\delta^{18}O$ and δD composition of precipitation is linearly correlated. This relation is known as the meteoric water line

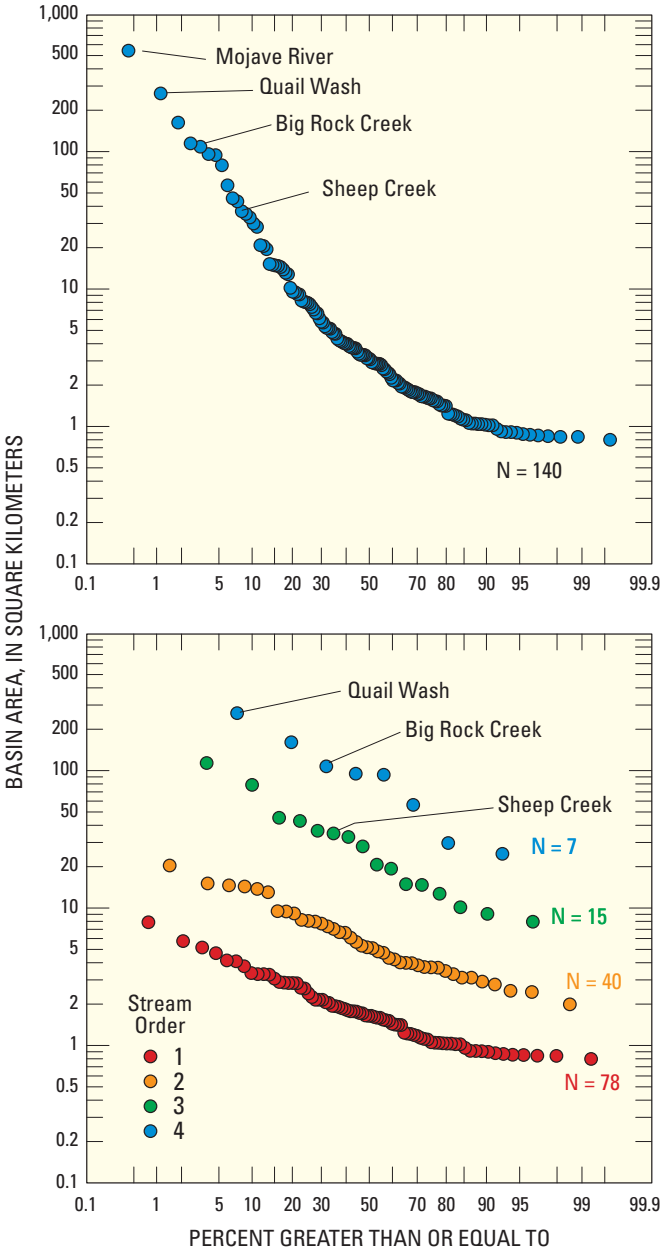

Figure 21. Rank-order distribution of selected basins on the north slope of the San Gabriel, San Bernardino, and Little San Bernardino Mountains, southern California.

Table 3. Drainage area of streams in the San Bernardino, Little San Bernardino, and San Gabriel[1] Mountains, southern California, by stream order.

[Abbreviations: —, not applicable (population consists of one value); km^2, square kilometers]

Stream order	Number of streams	Total drainage area, in km^2	Representative (50th percentile) drainage area, in km^2
5	1	543.	—
4	7	813.	96.
3	15	519.	28.
2	40	277.	5.2
1	78	155.	1.6

[1]Includes streams east of Amargosa Creek (near Palmdale) to Cajon Pass in the San Gabriel Mountains, and streams from Cajon Pass to Twenty-Nine Palms in the San Bernardino and Little San Bernardino Mountains.

(Craig, 1961). The $\delta^{18}O$ and δD composition of ground water relative to the meteoric water line and relative to the isotopic composition of water from other sources is an indication of the source and movement of the ground water. For example, water that condensed at cooler temperatures associated with higher altitudes has less of the heavier isotopes and more negative δ values than water that condensed at warmer temperatures associated with lower altitudes. In contrast, water than has been partly evaporated prior to recharge is enriched in the heavy isotopes relative to its original composition and plots to the right of the meteoric water line.

Orographic effects near Cajon Pass between the San Gabriel and San Bernardino Mountains allow air masses laden with moisture from the Pacific Ocean to enter the Mojave Desert during the winter rainy season and precipitate without uplift over the higher altitudes in the mountains (Izbicki, 2004). Winter precipitation near Cajon Pass gives rise to streamflow in the Mojave River, the largest stream in the study area. Because it condensed at lower altitudes and warmer temperatures, precipitation near Cajon Pass is isotopically heavier than precipitation that condensed over the mountains. Recharge from infiltration of streamflow along the Mojave River has resulted in a large body of isotopically heavy ground water extending for more than 100 km into the Mojave Desert (fig. 22). The isotopically heaviest water sampled in the study area is to the west of the Mojave River results from increased precipitation near the pass that has not been fractionated by orographic uplift over the mountains and subsequent runoff and infiltration of streamflow in Oro Grande Wash and other similar washes near the pass (Izbicki and others, 1995). These data demonstrate that, although the quantity of water from these sources is small, it is locally important. Similar processes have resulted in isotopically heavy ground water in the eastern part of the study area along Pipes Wash and in Yucca Valley near San Grogonio Pass (fig. 22), and along the western edge of Antelope Valley where the altitudes of the San Gabriel Mountains are lower (Smith and others, 1992). Precipitation, streamflow, and subsequent ground-water recharge associated with precipitation in low-altitude passes is different from conditions in most areas in the arid southwestern United States where precipitation, streamflow, and subsequent ground-water recharge are associated with higher altitudes in the mountains. This difference results from the cyclonic circulation of winter precipitation from west to east and proximity of the study area to the Pacific Ocean.

As previously discussed, tritium is a radioactive isotope of hydrogen having a half-life of 12.3 years. Although tritium is naturally occurring, the atmospheric testing of nuclear weapons beginning in 1952 greatly increased its presence in the environment. Tritium concentrations peaked about 1962 and decreased after nearly all atmospheric testing of nuclear weapons ended (Michel, 1976). Tritium concentrations in water that infiltrated before 1952 are below detection. Water with detectable amounts of tritium were thus interpreted as water that infiltrated during or after 1952. Where a tritium peak was present, the peak concentrations were interpreted as water that infiltrated in 1962.

Much of the water recharged along the Mojave River contains tritium (fig. 22) and was recharged after 1952. This water was distributed more than 150 km from Cajon Pass and the mountain front along the channel of the Mojave River by surface flow in the river. In contrast, only a small amount of recently recharged ground water containing tritium was present near Sheep Creek, Lucerne Valley, Pipes Wash, and Yucca Valley where small intermittent streams flow from the mountains. These data confirm that although infiltration from intermittent streams draining the San Gabriel and San Bernardino Mountains is locally important, especially in canyons near the mountain front; recent recharge from these sources is small and not distributed great distances by surface flow in small streams from the mountain front in comparison with recharge from a source such as the Mojave River.

Like tritium, carbon-14 also provides information on the age, or time since recharge, of ground water. Carbon-14 is a naturally occurring radioactive isotope of carbon having a half-life of about 5,730 years (Mook, 1980). Carbon-14 data are expressed as percent modern carbon by comparing carbon-14 activities to the specific activity of National Bureau of Standards oxalic acid: 12.88 disintegrations per minute per gram of carbon in the year 1950 equals 100 percent modern carbon. Carbon-14 was produced, as was tritium, by the atmospheric testing of nuclear weapons. As a result carbon-14 activities may exceed 100 percent modern carbon in areas where ground water contains tritium. Because of its longer half-life, carbon-14 preserves information on ground-water recharge over a longer time scale than does tritium. Unlike tritium, carbon-14 is not part of the water molecule,

and carbon-14 activities are affected by chemical reactions between ground water and aquifer material. In general, ground-water ages estimated from carbon-14 activity that do not account for these reactions overestimate the ground-water age and may be much as 30 percent greater than estimated ages that account for chemical reactions between the ground water and aquifer material (Izbicki and others, 1995). Because of its longer half-life, carbon-14 data illustrate the cumulative effect of ground-water recharge over longer times than do tritium data. For example, ground water having a carbon-14 activity of 50 percent modern carbon was recharged 5,730 years before present, and 30 percent modern carbon was recharged 9,950 years before present—assuming that there have been no chemical reactions between ground water and the alluvial deposits that compose the aquifer.

Carbon-14 activities near the mountain front are consistent with tritium data and show small amounts of ground-water recharge near Sheep Creek, Lucerne Valley, Pipes Wash, and Yucca Valley (fig. 22). Carbon-14 activities along the channel of Pipes Wash suggest that occasional flow in the wash is capable of supporting infiltration and subsequent ground-water recharge far into the Mojave Desert. Carbon-14 data also show recharge from intermittent streams near Cajon Pass, such as Oro Grande Wash (Izbicki and others, 1995), and show movement of water from the floodplain aquifer along the Mojave River into the surrounding regional aquifer. The data show that ground water in much of the study area has great age. In general, older ground water is found either at depth (Izbicki and Michel, 2004) or farther to the north—away from the front of the San Gabriel and San Bernardino Mountains.

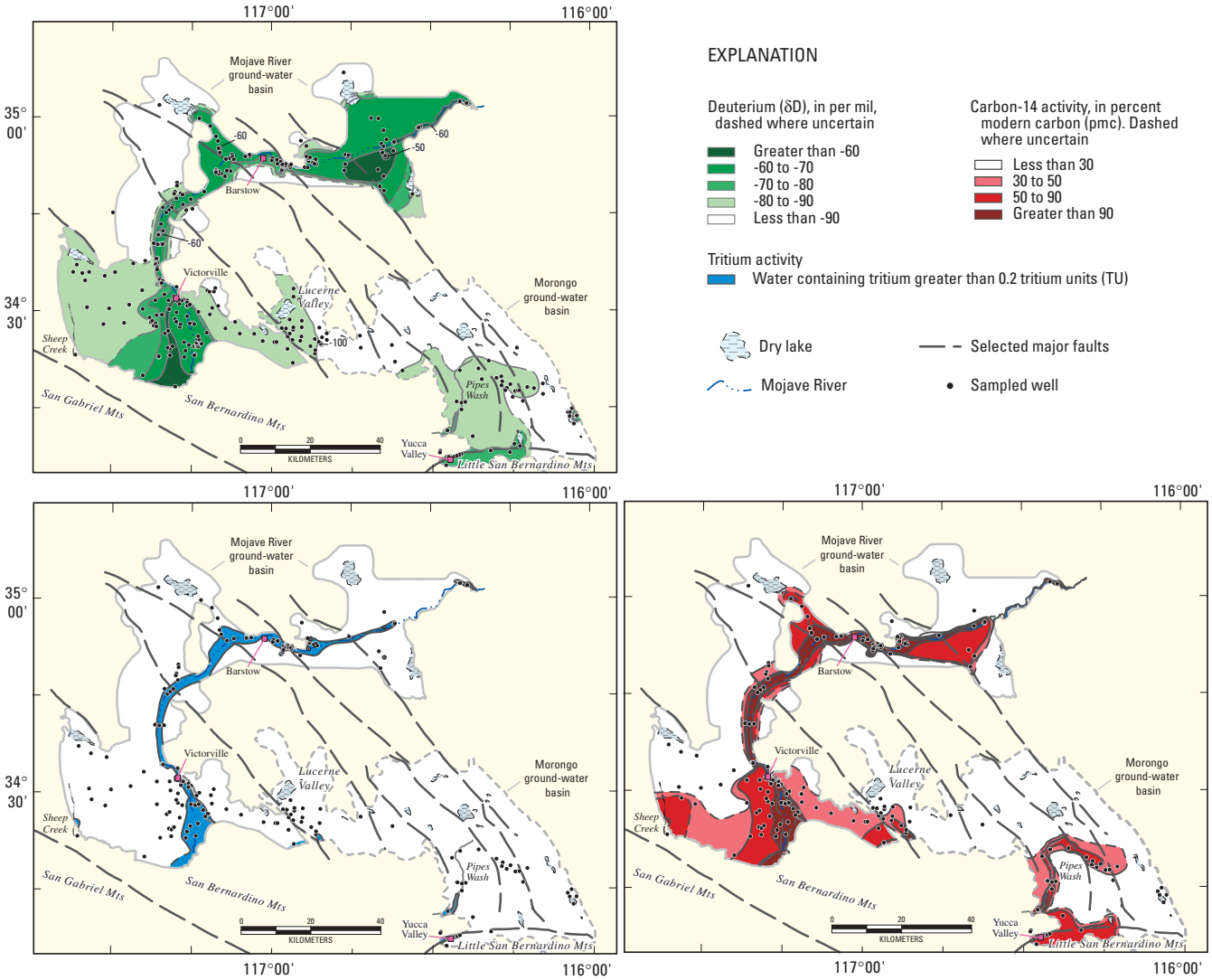

Figure 22. Deuterium, tritium, and carbon-14 composition of water from wells in the western part of the Mojave Desert, southern California (modified from Izbicki, 2003, and Izbicki and Michel, 2003).

Summary and Conclusions

Small amounts of water infiltrate into the unsaturated zone underlying intermittent streams in the western Mojave Desert. In some areas, infiltrated water moves to depths below the root zone and ultimately to the underlying water table where it becomes ground-water recharge. The amount of water that ultimately infiltrates along a given reach is a function of streamflow availability (the quantity of water available to infiltrate into the streambed), the physical properties of the streambed, and geomorphic features that control the spatial and temporal distribution of infiltration of water infiltrated from stream channels. In some settings infiltration along a stream reach did not result in deep infiltration and subsequent ground-water recharge. Presumably, infiltrated water is transpired by vegetation along the stream. On the basis of this study, infiltration of about 0.7 m/yr represents a threshold below which deep infiltration and subsequent ground-water recharge do not occur—although this value is likely to differ in response to a number of factors including geomorphology, vegetation type and density, and the hydraulic properties of the underlying alluvium. In addition, it may take several hundred years for water to infiltrate through thick, heterogeneous unsaturated zones underlying some intermittent streams. This long time period dampens annual variations in recharge and variations in recharge from longer-term climatic cycles, such as El Niño or the Pacific Decadal Oscillation, toward a constant value. Given the time of travel and complex movement of water in thick, heterogeneous unsaturated zones, it may be unrealistic to assume that water infiltrated to depths below the root zone becomes ground-water recharge—especially where channel-abandonment processes on active alluvial fans may effectively strand water in the unsaturated zone before it reaches the water table.

In contrast to the small amounts of ground-water recharge from numerous small streams that drain the San Gabriel, San Bernardino, and Little San Bernardino Mountains, the Mojave River is the largest single source of ground-water recharge in the western part of the Mojave Desert. Streamflow in the Mojave River recharges aquifers along the river throughout the study area to Afton Canyon more than 150 km from Cajon Pass and the mountain front. Cool moist air masses move inland from the Pacific Ocean and enter the Mojave Desert near the headwaters of the Mojave River near Cajon Pass generating precipitation, streamflow, and subsequent ground-water recharge. Similar processes also occur near San Gorgonio Pass in the southern part of the study area. These processes are different from recharge processes that occur elsewhere in the arid southwestern United States where streamflow, infiltration, and subsequent ground-water recharge are associated with precipitation and runoff in the higher altitudes of the mountains that surround the alluvial basins.

References Cited

Allison, C.B., and Hughes, M.W., 1978, The use of environmental chloride and tritium to estimate total recharge to an unconfined aquifer: Australian Journal of Soil Research, v. 16, p. 181–195.

Allison, C.B., Stone, W.J., and Hughes, M.W., 1985, Recharge in karst and dune elements of a semi-arid landscape as indicated by natural isotopes and chloride: Journal of Hydrology, v. 76, p. 1–26.

California Department of Finance, 2002a, Historical census populations of California state, counties, cities, places, and towns, 1850–2000: Sacramento, Calif.,http://www.dof.ca.gov/HTML/DEMOGRAP/ReportsPapers/CensusSurveys/Census-Historical/HISTTEXT.HTM

California Department of Finance, 2002b, Revised historical city, county and state population estimates, 1991–2000, with 1990 and 2000 census counts: Sacramento, Calif., http://www.dof.ca.gov/HTML/DEMOGRAP/ReportsPapers/Estimates/E4/E4-91-00/E-4text2.php

California Department of Public Works, 1934, Mojave River investigation: California Department of Public Works Bulletin 47, 249 p.

California Department of Water Resources, 1967, Mojave River ground-water investigation: California Department of Water Resources Bulletin 84, 151 p.

California Department of Water Resources, 2003, California's groundwater, Bulletin 118, Update 2003: Sacramento, California, http://www.groundwater.water.ca.gov/bulletin118/update2003/index.cfm.

California Superior Court, 1977, Hi-Desert Water District *v.* Yucca Water Company: Case number 172103.

California Supreme Court, 2000, City of Barstow and others (plaintiffs and respondents) *v.* Mojave Water Agency and others (defendants, cross-complainants and respondents) and Jess Ranch Water Company (cross-defendant and appellant): Case number S071728; Riverside County Superior Court, 2000, Mojave Water Agency and others *v.* Manuel Cardozo: Case number 208568.

Constantz, J., and Thomas, C.L., 1996, The use of streambed temperature profiles to estimate the depth, duration, and rate of percolation beneath arroyos: Water Resources Research, v. 32, p. 3597–3602.

Constantz, J., and Thomas, C.L., 1997, Streambed temperature profiles as indicators of percolation characteristics beneath arroyos in the Middle Rio Grande Basin, USA: Hydrological Processes, v. 11, p. 1621–1634.

Craig, H., 1961, Isotopic variation in meteoric waters: Science, v. 176, p. 187–222.

Gonfiantini, R., 1978, Standards for stable isotope measurements in natural compounds; Nature, v. 271, p. 534–536.

Hardt, W.F., 1971, Hydrologic analysis of Mojave River Basin, California, using electric analog model: U.S. Geological Survey Open-File Report 72–157, 84 p.

Izbicki, J.A., 2002, Geologic and hydrologic controls on the movement of water through a thick, heterogeneous unsaturated zone underlying an intermittent stream in the western Mojave Desert, southern California: Water Resources Research, v. 38, doi:10.1029/2000WR000197.

Izbicki, J.A., 2004, Source and movement of ground water in the western part of the Mojave Desert, southern California, USA: U.S. Geological Survey Water Resources Investigations Report 03–4313, 18 p.

Izbicki, J.A., Clark, D., Pimentel, I., Land M., Radyk, J., and Michel, R.L., 2000a, Data from a thick unsaturated zone underlying intermittent streams in the Mojave Desert, San Bernardino County, California: U.S. Geological Survey Open-File Report 00–262, 133 p.

Izbicki, J.A., Martin, P., and Michel, R.L., 1995, Source, movement and age of groundwater in the upper part of the Mojave River Basin, California, USA, *in* Adair, E.M., and Leibundgut, C., Application of tracers in arid zone hydrology: International Association of Hydrologic Sciences Publication Number 232, p. 43–56.

Izbicki, J.A., and Michel, R.L., 2002, Use of temperature data to estimate infiltration from intermittent streams in the western Mojave Desert, USA, *in* Foo, D.Y., ed., Balancing the Ground Water Budget, Proceedings of the International Association of Hydrologists Meeting in Darwin, Australia, May 12–14, 2002 (CD-ROM): IAH, Kenilworth, UK, 9 p.

Izbicki, J.A., and Michel, R.L., 2004, Movement and age of ground water in the western part of the Mojave Desert, southern California, USA: U.S. Geological Survey Water Resources Investigations Report 03–4314, 42 p.

Izbicki, J.A., Radyk, J., and Michel, R.L., 2000b, Water movement through a thick unsaturated zone underlying an intermittent stream in the western Mojave Desert, southern California, USA: Journal of Hydrology, v. 238, p. 194–217

Izbicki, J.A., Radyk, J., and Michel, R.L., 2002, Movement of water through the thick unsaturated zone underlying Oro Grande and Sheep Creek Washes in the western Mojave Desert, USA: Hydrogeology Journal, v. 10, p. 409–427.

Kulongoski, J.T., and Izbicki, J.A., 2008, Simulation of fluid, heat transport to estimate desert stream infiltration: Ground Water, doi:10.1111/j.1745-6584.2007.00403.x.

Lappala, E.G., Healy, R.W., and Weeks, E.P., 1983, Documentation of computer program VS2D to solve the equation of fluid flow in variably saturated porous media: U.S. Geological Survey Water Resources-Investigations Report 83–4099, 184 p.

Lines, G.C., 1996, Ground-water and surface water relations along the Mojave River, southern California: U.S. Geological Survey Water-Resources Investigations Report 95–4189, 43 p.

Meisling, K.E., and Weldon, R.J., 1989, Late Cenozoic tectonics of the northwest San Bernardino Mountains, southern California: Geological Society of America Bulletin, v. 101, p. 106–128

Mendez, G.O., and Christensen, A.H., 1997, Regional water table (1996) and water-level changes in the Mojave River, the Morongo, and the Fort Irwin Ground-Water Basins, San Bernardino County, California: U.S. Geological Survey Water-Resources Investigations Report 97–4160, 34 p.

Michel, R.L., 1976, Tritium inventories in the worlds oceans and their implications: Nature, v. 263, p. 103–106.

Mook, W.G., 1980, Carbon-14 in hydrogeological studies, *in*: Fritz, P., and Fontes, J.Ch., eds., Handbook of environmental isotope geochemistry, v. 1, p. 49–74.

Nimmo, J.R., Deason, J.A., Izbicki, J.A., and Martin, P., 2002, Evaluation of unsaturated zone water fluxes in heterogeneous alluvium at a Mojave Basin site: Water Resources Research, v. 38, doi:10.1029/2001WR000735.

Nishikawa, T., Izbicki, J.A., Hevesi, J.A., Stamos, C.L., and Martin, P., 2005, Evaluation of geohydrologic framework, recharge estimates and ground-water flow of the Joshua Tree area, San Bernardino County, California: U.S. Geological Survey Scientific Investigations Report SIR 2004–5267, 127 p.

Phillips, F.M., 1994, Environmental tracers for water movement in desert soils of the American southwest: Soil Science of America Journal, v. 58, p. 15–24.

Prudic, D.E., 1994, Estimates of percolation rates and ages of water in unsaturated sediments at two Mojave Desert sites, California-Nevada: U.S. Geological Survey Water-Resources Investigations Report 94–4160, 19 p.

Smith, G.A., 2003, Regional water table (2000) and ground-water-level changes in the Mojave River and Morongo Ground-Water Basins, southwestern Mojave Desert, southern California: U.S. Geological Survey Water-Resources Investigations Report 02–4277, 45 p.

Smith, G.I., and Friedman, I., Gleason, J.D., and Warden, A., 1992, Stable isotope composition of waters in southeast California—2, Groundwaters and their relation to modern precipitation: Journal of Geophysical Research, v. 97, p. 5813–5823.

Stamos, C.L., Martin, P., Nishikawa, T., and Cox, B.F., 2001, Simulation of ground-water flow in the Mojave River Basin, California: U.S. Geological Survey Water-Resources Investigations Report 01–4002, 129 p.

Stamos, C.L., and Predmore, S.K., 1995, Data and water-table map of the Mojave River Ground-Water Basin, San Bernardino County, California, November 1992; U.S. Geological Survey Water-Resources Investigations Report 95–4148, 1 sheet.

Thompson, D.G., 1929, The Mohave Desert region, California—A geographic, geologic, and hydrologic reconnaissance: U.S. Geological Survey Water-Supply Paper 578, 759 p.

Winfield, K.A., 2000, Factors controlling water retention of alluvial deposits, western Mojave Desert: San Jose, Calif., San Jose State University, master's thesis, 88 p.

Estimated Infiltration, Percolation, and Recharge Rates at the Rillito Creek Focused Recharge Investigation Site, Pima County, Arizona

By John P. Hoffmann, Kyle W. Blasch, Don R. Pool, Matthew A. Bailey, and James B. Callegary

Abstract

A large fraction of ground water stored in the alluvial aquifers in the Southwest is recharged by water that percolates through ephemeral stream-channel deposits. The amount of water currently recharging many of these aquifers is insufficient to meet current and future demands. Improving the understanding of streambed infiltration and the subsequent redistribution of water within the unsaturated zone is fundamental to quantifying and forming an accurate description of streambed recharge. In addition, improved estimates of recharge from ephemeral-stream channels will reduce uncertainties in water-budget components used in current ground-water models.

This chapter presents a summary of findings related to a focused recharge investigation along Rillito Creek in Tucson, Arizona. A variety of approaches used to estimate infiltration, percolation, and recharge fluxes are presented that provide a wide range of temporal- and spatial-scale measurements of recharge beneath Rillito Creek. The approaches discussed include analyses of (1) cores and cuttings for hydraulic and textural properties, (2) environmental tracers from the water extracted from the cores and cuttings, (3) seepage measurements made during sustained streamflow, (4) heat as a tracer and numerical simulations of the movement of heat through the streambed sediments, (5) water-content variations, (6) water-level responses to streamflow in piezometers within the stream channel, and (7) gravity changes in response to recharge events. Hydraulic properties of the materials underlying Rillito Creek were used to estimate long-term potential recharge rates. Seepage measurements and analyses of temperature and water content were used to estimate infiltration rates, and environmental tracers were used to estimate percolation rates through the thick unsaturated zone. The presence or lack of tritium in the water was used to determine whether or not water in the unsaturated zone infiltrated within the past 40 years. Analysis of water-level and temporal-gravity data were used to estimate recharge volumes. Data presented in this chapter were collected from 1999 though 2002. Precipitation and streamflow during this period were less than the long-term average; however, two periods of significant streamflow resulted in recharge—one in the summer of 1999 and the other in the fall/winter of 2000.

Flux estimates of infiltration and recharge vary from less than 0.1 to 1.0 cubic meter per second per kilometer of streamflow. Recharge-flux estimates are larger than infiltration estimates. Larger recharge fluxes than infiltration fluxes are explained by the scale of measurements. Methods used to estimate recharge rates incorporate the largest volumetric and temporal scales and are likely to have fluxes from other nearby sources, such as unmeasured tributaries, whereas the methods used to estimate infiltration incorporate the smallest scales, reflecting infiltration rates at individual measurement sites.

Introduction

The city of Tucson and surrounding areas obtain most of their municipal, agricultural, and industrial water from ground water that is withdrawn from thick, alluvial-basin aquifers. The amount of water currently recharging the aquifers within the Tucson area is insufficient to meet current and future demands. Resultant ground-water deficits are manifested in water-level declines of more than 60 m since the middle of the 20th century. These declines are largest where ground-water withdrawals are greatest.

The alluvial aquifers are recharged by infiltration from irrigation and industrial returns and by seepage losses through stream channels. In the Tucson area, where the climate is semiarid, diffuse recharge through the basin sediments from precipitation is considered a negligible component of total recharge owing to low precipitation rates and high evapotranspiration (ET) rates (Scott and others, 2000). For instance, annual precipitation averages 31.5 cm on the valley floor, and annual potential ET ranges from 90 to 190 cm (Yitayew, 1990). Additionally, depth to ground water in the underlying alluvial basin can be tens of meters, providing opportunity for ample storage of infiltrated water. Because of these conditions, concentrated infiltration repeated over time, such as infiltration from irrigation and industrial returns, is necessary for recharge to occur. A large fraction of ground water stored in the allu-

vial aquifer was recharged by water that percolated through ephemeral stream-channel deposits (Davidson, 1973; Hanson and Benedict, 1994).

Rillito Creek, located in the Upper Santa Cruz Basin in southern Arizona (fig. 1), is typical of a large, ephemeral stream in the Southwest. In many basins of the Southwest, such as in the Upper Santa Cruz Basin, streams originating at higher elevations coalesce downstream to form larger ephemeral streams. Streams originating near mountain fronts typically flow over thick, alluvial valleys, lose hydraulic connection with the underlying aquifer, and are ephemeral in their lower reaches. Underlying many of these ephemeral streams is a coarse-grained stream-channel deposit that overlies a basin-fill deposit. The coarse-grained stream-channel deposit typically has high permeability and infiltration rates (Anderson and others, 1992; Hanson and Benedict, 1994).

Although recharge from infiltration of streamflow is known to occur in ephemeral-stream channels in the Southwest, such as Rillito Creek, the processes that control the spatial distribution and volume of infiltration that recharges the underlying aquifers are poorly understood. The Rillito Creek focused recharge investigation site was selected as one of six sites to study recharge processes in the Southwest (see chapter C) as part of the U.S. Geological Survey (USGS) Ground-Water Resources Program and generally is representative of ephemeral washes within the Sonoran Desert. Improving the understanding of streambed infiltration and the subsequent redistribution of water within the unsaturated zone is fundamental to quantifying and forming an accurate description of streambed recharge. Improved estimates of recharge from ephemeral stream channels will reduce uncertainties in water-budget components used in current ground-water models. In addition, recharge augmentation has been proposed along several reaches of ephemeral streams in the Tucson area, including Rillito Creek, and understanding processes that control recharge is important to the construction of recharge facilities.

Purpose and Scope

The purpose of this chapter is to present a summary of findings related to a focused recharge investigation along Rillito Creek, Pima County, Arizona. One of the challenges of quantitatively studying recharge beneath ephemeral streams is the need to integrate measurements made over a wide range of spatial and temporal scales. No single method of measurement or analysis can resolve the complex physical processes that contribute to infiltration, percolation, and recharge beneath ephemeral streams; therefore, a variety of approaches are presented that provide a wide range of temporal- and spatial-scale measurements of recharge beneath Rillito Creek.

Six approaches were used to evaluate infiltration, percolation, and recharge to the aquifer beneath Rillito Creek. Cores and cuttings were collected during the drilling of five boreholes. Laboratory measurements used to determine physical and hydraulic properties of these cored subsurface materials (Hoffmann and others, 2002) represent the smallest spatial scale in this investigation. The core-based data typically are on the order of several centimeters, but are scaled up to meters in this report. Water content extracted from the cores, and environmental tracers measured in these waters, represent a temporal scale that is a function of the thickness and hydraulic properties of the unsaturated zone: in general, these data represent a time scale of less than 2 years in this investigation. Seepage measurements made during sustained streamflow represent portions of a streamflow event and typically have time scales of a few hours to several days. Measurements of temperature and water content in vertical (one-dimensional) and two-dimensional profiles represent spatial scales that are typically less than 5 m and have temporal scales that vary from seconds to several days. Vertically nested piezometers were installed in the boreholes drilled in the stream channel to monitor water-level responses to streamflow. These measurements also represent a temporal scale that is a function of the thickness and hydraulic properties of the unsaturated zone and, in general, represents a time scale of weeks to several months in this investigation. Measurements of ground-water storage changes using temporal-gravity measurements have the largest spatial and temporal scales spanning several square kilometers and a period of record of several months to years. Data presented in this chapter were collected from 1999 through 2002.

Previous Investigations

Smith (1910) probably was the first investigator to examine recharge along Rillito Creek. He concluded there was a difference in infiltration rates between the flashy, silt-laden summer flows, and the steady, long-duration flows of the winter snowmelt runoff. This conclusion was based partly on seasonal well hydrographs and ground-water temperature data. Investigators to follow, such as Schwalen and Shaw (1957) and Matlock (1965), also concluded that winter streamflow was the most effective source of recharge to the Tucson Basin. Burkham (1970) developed an empirical formula to estimate infiltration along a 15-km reach of Rillito Creek on the basis of streamflow losses between discharge measurement points. Davidson (1973) suggested that at least 90 percent of the amount of infiltrated water results in recharge. The remaining 10 percent is lost to ET. Although not necessarily specific to Rillito Creek, the work of Wallace and Lane (1978) related infiltration potential to stream-channel order. Wallace and Lane concluded that the greatest infiltration potential occurs in the large-order streams because these streams contain the greatest volume of alluvium. Hanson and Benedict (1994) summarized previous estimates of recharge and developed new estimates on the basis of work by previous investigators and numerical simulation.

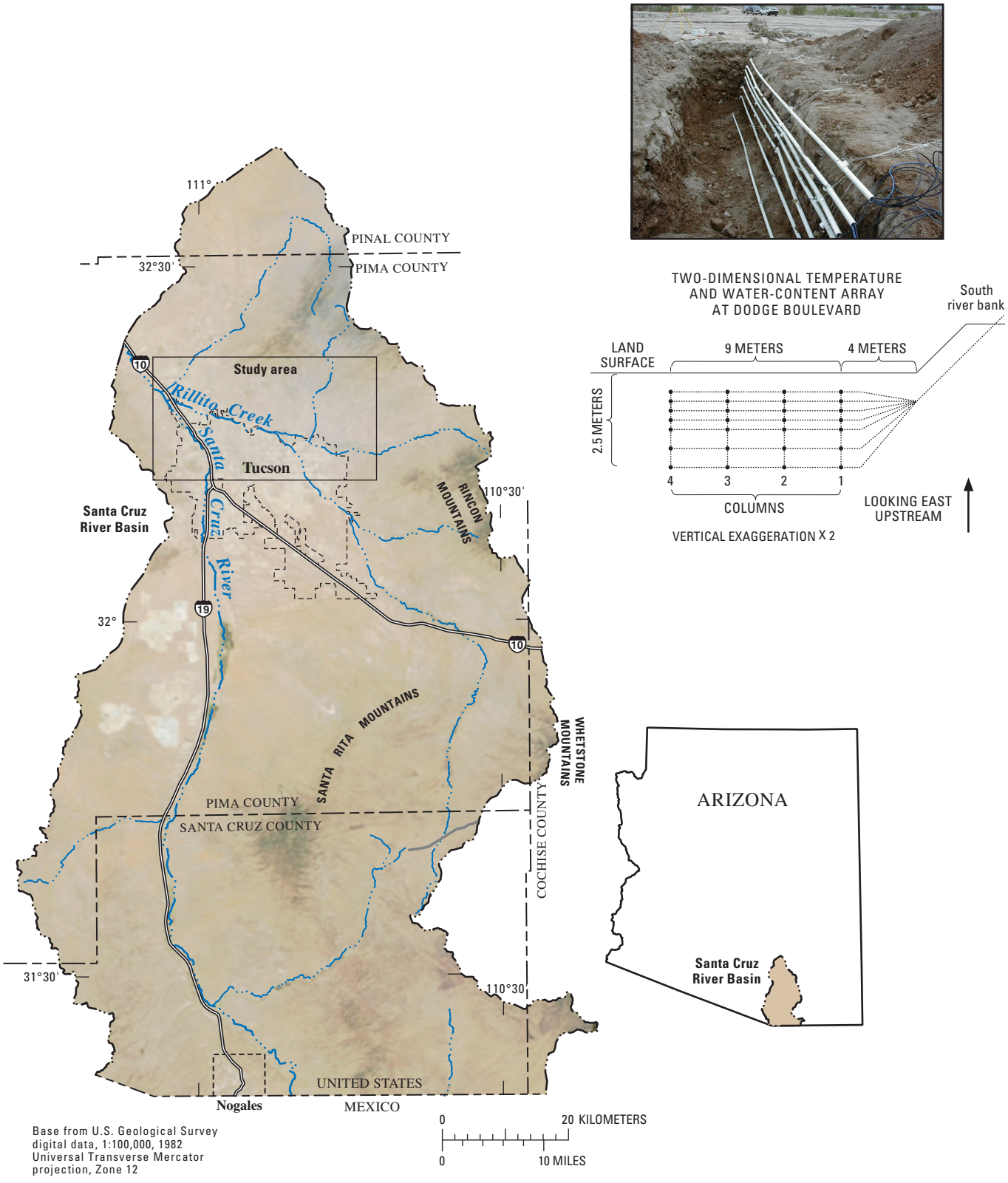

Figure 1. Location of study area, Pima County, Arizona.

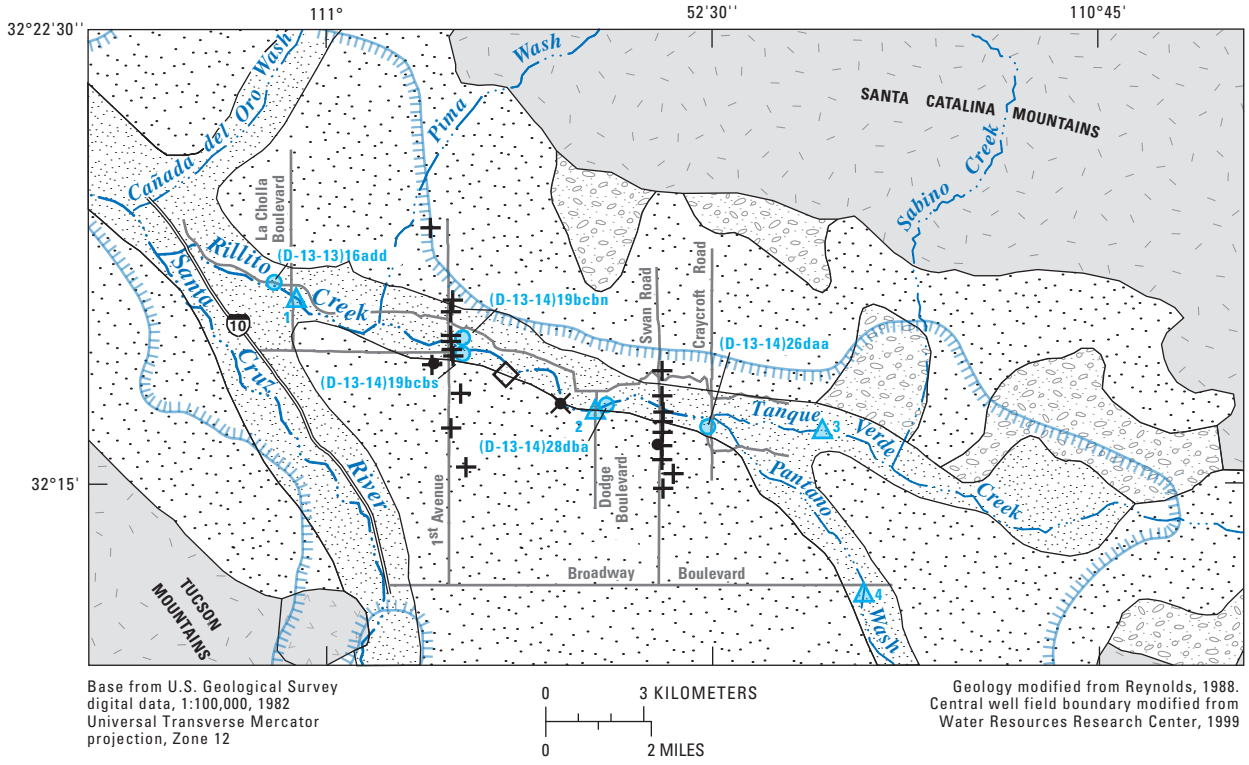

EXPLANATION

- STREAM ALLUVIUM
- QUATERNARY ALLUVIUM
- TERTIARY ALLUVIUM
- VOLCANIC ROCK
- CRYSTALLINE ROCK
- CENTRAL WELL FIELD
- PRECIPITATION STATION CAMPBELL AVENUE EXPERIMENTAL FARM
- (D-13-13)13add — BOREHOLE AND BOREHOLE IDENTIFICATION
- GRAVITY STATION
- 9486055 — STREAMFLOW-GAGING STATION AND STATION IDENTIFICATION
- VERTICAL-TEMPERATURE ARRAY
- TWO-DIMENSIONAL TEMPERATURE AND WATER-CONTENT ARRAY

IDENTIFICATION OF STREAMFLOW-GAGING STATIONS AND TEMPERATURE ARRAYS

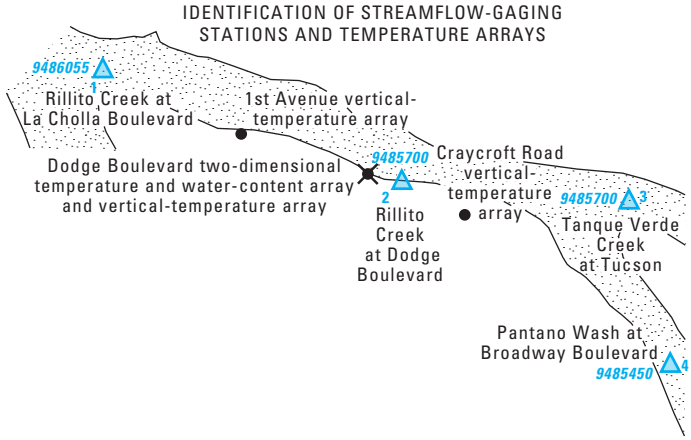

Figure 1.—Continued.

Hydrologic Setting

The climate of the study area is semiarid; annual rainfall averages 315 mm on the valley floor (fig. 2). There are two distinct seasons that account for most of the total precipitation; one (generally from July through September) is characterized by large summer convection and the other (generally from November through February) is characterized by frontal storms (fig. 2). The mean temperatures in January and July are 10°C and 29.6°C, respectively. To a lesser extent, there is a fall season of precipitation associated with tropical storms and climatic oscillations.

Rillito Creek is a tributary of the Santa Cruz River, which drains the Upper Santa Cruz Basin in southern Arizona. The Upper Santa Cruz Basin is in the Basin and Range Physiographic Province, which is characterized by block-faulted mountains separated by basins filled with alluvial sediments. The block-faulted mountains comprise Precambrian through Tertiary granitic, metamorphic, volcanic, and consolidated sedimentary rocks. The sediments that fill the basins are collectively termed alluvial basin-fill deposits and are composed of gravel, sand, silt, clay, and minor amounts of anhydrous sediments of Tertiary to Quaternary age. The basin-fill deposits generally are coarse grained along the basin margins and grade into finer-grained deposits and anhydrite deposits in the central parts of the basins. In the Upper Santa Cruz River Basin, thickness of the alluvium ranges from a thin veneer (a few meters) along the mountain fronts to as much as 3,400 m in the central parts of the basin (Davidson, 1973; Anderson, 1987, 1988; Hanson and Benedict, 1994).

Recent stream-channel deposits and basin-fill deposits underlie Rillito Creek. The recent stream-channel deposits, consisting of fine- to coarse-grained alluvium, are about 10 m thick and are detritus from the surrounding mountain ranges. The basin-fill deposits, which underlie the stream-channel deposits, are regionally extensive sedimentary units that form the regional aquifer system. Previous investigators have divided the basin-fill deposits into upper and lower basin-fill units on the basis of their general hydrogeologic characteristics (Pool, 1986; Hanson and Benedict, 1994). The upper basin-fill unit can be as much as 300 m thick. It consists mostly of unconsolidated to semiconsolidated gravel, sands, and clayey silt and is correlated to the upper Tinaja beds and the Fort Lowell Formation described by Anderson (1987, 1988). The lower basin-fill unit is a few thousand meters thick and consists of conglomerates, gravels, sands, silts, anhydritic clayey silts, and mudstones (Anderson, 1988). The lower basin-fill unit is represented by the Pantano Formation and the lower and middle Tinaja beds described by Anderson (1987, 1988).

Stream-channel infiltration is the predominant mechanism of recharge to the regional aquifer in the basin-fill deposits and, combined with contributions from other sources of recharge for the area, is less than the amount of water withdrawn to support the growing metropolitan population. As a result, water-level declines and related land subsidence have occurred in some areas. Depth to ground water immediately beneath Rillito Creek ranges from less than 6 m in the upper reach (near the mountain front) to 45 m near the Santa Cruz River (Hoffmann and others, 2002). Flow of ground water generally is northwestward; water-table elevations range from about 760 m in the southeast to 640 m in the northwest (Tucson Water, 2000). Ground water flows southwestward near the upper reach of Rillito Creek toward the major pumping center within the city of Tucson.

Rillito Creek has a drainage area of 2,256 km^2. It is ephemeral and most flows occur during the summer monsoon (July–September) and winter frontal storms (December–March; fig. 2). Characteristic monsoon streamflows result from localized short-duration convective storms, whereas winter streamflows are produced by longer-duration frontal storms and accumulated snowmelt. To a lesser extent, there also is a fall season in which tropical storms and climatic oscillations often result in streamflow.

The creek has two major tributaries, Tanque Verde Creek and Pantano Wash; Rillito Creek begins at the confluence of these two tributaries. Tanque Verde Creek drains a 702 km^2 area from the Santa Catalina and Rincon Mountains; Pantano Wash drains a 1,554 km^2 area between the Rincon, Santa Rita, and Whetstone Mountains. Several small washes divert runoff from the northeastern suburbs of Tucson into Rillito Creek. Rainfall runoff and snowmelt runoff from the Santa Catalina and Rincon Mountains contribute most of the flow to Rillito Creek. The creek flows westward to the Santa Cruz River from an elevation of 762 m at the confluence of Tanque Verde Creek and Pantano Wash to 657 m at its confluence with the Santa Cruz River. The creek is about 100 m wide and the channel slopes toward the Santa Cruz River at approximately 5.2 m/km with little variation in the slope. Flows in Rillito Creek typically are less than 28 m^3/s; the maximum recorded discharge was 680 m^3/s during the 1993 El Niño season (Tadayon and others, 2000). On average, Rillito Creek flows about 36 days per year at the streamflow-gaging station Rillito Creek at Dodge Boulevard (09485700). The average annual flow is approximately 33.3×10^6 m^3; about 44 percent of the flow occurs from the summer monsoonal storms, whereas about 56 percent of the flow occurs from the winter frontal storms.

The amount of water flowing in Rillito Creek, and therefore the amount available for recharge, is primarily related to precipitation frequency, distribution, and intensity, as well as to basin/channel runoff characteristics. The temporal distribution of flow in ephemeral streams is highly variable with observed decadal oscillations (Webb and Betancourt, 1992; Don Pool, Hydrologist, U.S. Geological Survey, written commun., 2003). Because of this, it is particularly difficult to estimate or predict recharge rates for ephemeral-stream channels on the basis of limited temporal observations. During the period of investigation there were two significant streamflow periods (fig. 3); one occurred in the summer of 1999 and the other in the fall of 2000 (mostly after September 30, or during water year 2001). Annual streamflow in Rillito Creek for the period of study was somewhat less frequent and smaller in volume than the long-term average (table 1). Prior to this study, a significant streamflow period occurred in the winter

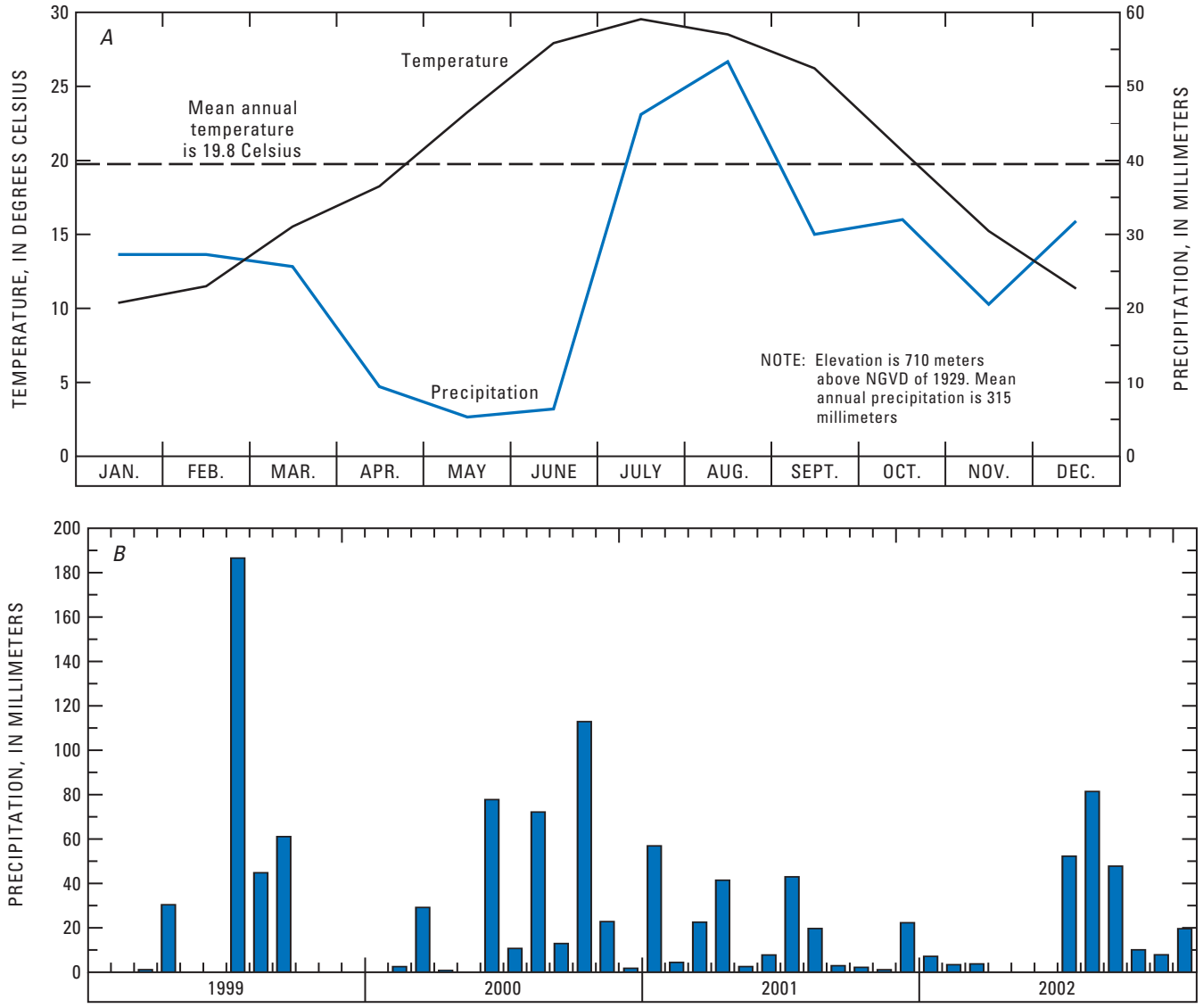

Figure 2. *A*, Monthly average temperature and precipitation, 1972–2002, at National Weather Service Station Campell Avenue Experimental Farm near Rillito Creek, Pima County, Arizona; *B*, monthly precipitation near Rillito Creek during period of study, 1999–2002.

and spring of 1998 (water year 1998) that was associated with El Niño precipitation and snowmelt. From February through April 1998, a total of 28.7×10^6 m^3 flowed past the streamflow-gaging station at Dodge Boulevard.

Infiltration, Percolation, and Recharge Rates

Physical and Hydraulic Properties of Stream-Channel and Basin-Fill Deposits

In March and April 1999, five boreholes were drilled at four sites in the active channel of Rillito Creek (fig. 1) to determine the physical and hydraulic properties of the stream-channel and basin-fill sediments down to about 10 m below the water table (Hoffmann and others, 2002). Each borehole was drilled using the ODEX air-hammer method, which is also known as the under-reamer method (Driscoll, 1986; Hammermeister and others, 1986). The ODEX method was used because it does not use fluids, thereby minimizing disturbance of the subsurface materials. At each hole, cuttings were collected about every 0.3 m. Fifty-one cores also were collected from these boreholes at 2- to 6-m intervals. The cores and cuttings were analyzed for physical properties, such as particle-size distribution, bulk density, particle density, porosity, volumetric water content, and percent saturation, and for hydraulic properties, such as saturated and unsaturated hydraulic conductivity, matric potential, and water-retention fitting terms. The detailed findings of these analyses are

described in Hoffmann and others (2002). This section of the chapter focuses on the hydraulic properties of the sediments and their role in infiltration rates, velocity of the wetting front, and potential recharge.

In order for ephemeral streamflow within Rillito Creek to recharge the underlying aquifer, the water must first infiltrate into the stream-channel deposits and percolate downward through the underlying deposits. The ability of water to infiltrate and percolate through these deposits is primarily a function of stream discharge and hydraulic properties of the deposits. One-dimensional steady-state vertical flow through a homogeneous, isotropic medium can be described by a form of Darcy's Law as:

$$q = -K(\theta)\left(\partial\psi/\partial z + 1\right), \quad (1)$$

where

q is the flux [L/T],
θ is the volumetric water content,
$K(\theta)$ is the hydraulic conductivity [L/T] as a function of the volumetric water content,
ψ is the pressure head of the water phase [L], and
z is the vertical dimension [L].

Determination of the rate of flow requires knowledge of the hydraulic conductivity and saturation of the porous media, and the head gradient. Water continues to move within the unsaturated zone after it has infiltrated across the ground surface. This subsurface redistribution is described by the unsaturated-flow equation:

$$\partial\theta/\partial t = \nabla q, \quad (2)$$

with the flux, q, as defined above. Because redistribution is inherently transient and multidimensional, fewer simplifying assumptions can be applied in the analysis of redistribution than can be applied to infiltration. To fully characterize subsurface redistribution, measurements of both water flux and changes in subsurface water storage must be made repeatedly throughout the unsaturated zone.

As shown in the section titled "Temperature and Water Content," vertical infiltration rates at the onset of infiltration were as high as 22 mm/s because of high hydraulic permeability, low antecedent water content, and resulting large capillary gradients. Two-dimensional flow is also evident, and lateral velocities were about the same as vertical velocities. Shortly after the onset of infiltration, however, the near-surface stream-channel deposits are saturated, and large capillary gradients decline. Flow of water becomes predominantly vertical, as gravity is the dominant process controlling the

Table 1. Annual streamflow measured at Rillito Creek at Dodge Boulevard (streamflow-gaging station 09485700), Pima County, Arizona, during period of study.

Water year[1]	Total annual streamflow, in cubic meters	Annual flow as a percentage of long-term annual streamflow	Percentage of annual stream-flow that occurred in summer	Percentage of annual stream-flow that occurred in winter
1999	11×10^6	33	98	2
2000	3.5×10^6	10.5	100	0
2001	19.6×10^6	59	5	95
2002	2×10^6	6	99	1

[1]Water year extends from October 1 through September 30 and is designated by the calendar year in which it ends.

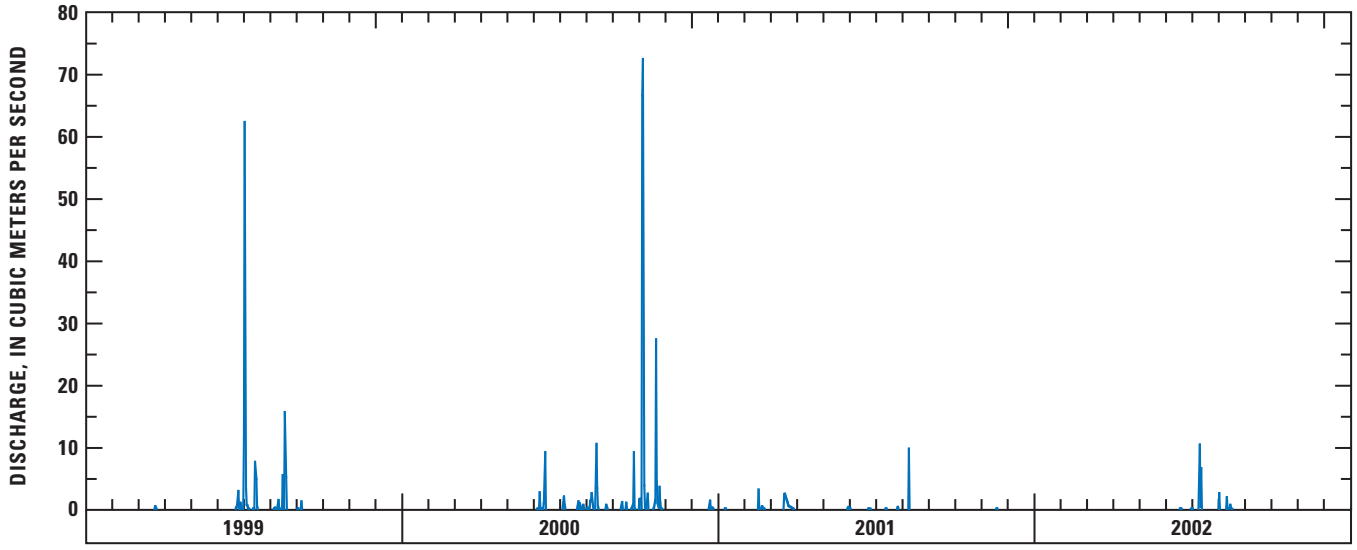

Figure 3. Mean discharge at Rillito Creek at Dodge Boulevard (streamflow-gaging station 09485700), 1999–2002, Pima County, Arizona.

direction of flow. From Darcy's Law, the flow rate through the sediments under saturated conditions is equal to the product of the hydraulic conductivity and the hydraulic gradient. If both hydraulic conductivity and gradient are known, then the flow rate can be calculated. This method of flow-rate estimation can be used for saturated and unsaturated conditions. Assuming properties of the pore water are constant, saturated hydraulic conductivity (K_{sat}) is a constant and is related to the texture and structure of the sediment. Unsaturated hydraulic conductivity is not a constant as it decreases rapidly as water content decreases. As surface flow proceeds, the infiltrated water moves farther below the surface of the streambed, capillary forces become less significant, and the hydraulic gradient approaches unity. If a unit gradient is assumed, the rate of infiltration becomes equivalent to the saturated hydraulic conductivity of the channel deposits.

On the basis of findings from the cuttings and cores, the stream-channel deposits beneath Rillito Creek are coarse grained, typically consisting of more than 95 percent gravel and sand. The underlying basin-fill deposits also are sandy gravels or gravelly sands, but typically contain more silt and clay than the stream-channel deposits.

Saturated vertical hydraulic conductivity of the deposits positively correlates with grain size (fig. 4). Values for the stream-channel deposits range from 0.3 to 2.5 m/d, whereas values for the basin-fill deposits tend to be less than about 0.6 m/d and in places are as low as 0.012 m/d. For heterogeneous media, such as the deposits beneath Rillito Creek, the equivalent vertical hydraulic conductivity is calculated as the harmonic mean of the K_{sat} for each layer within the deposits and is always less than the arithmetic mean (Freeze and Cherry, 1979). Although differing at each borehole, the overall average equivalent hydraulic conductivity of the stream-channel deposits is 1.2 m/d; the overall average equivalent hydraulic conductivity of the basin-fill deposits is 0.19 m/d; and the equivalent hydraulic conductivity of the combined sediments (stream-channel and basin-fill deposits) is 0.23 m/d. The calculated average vertical hydraulic conductivity for the basin-fill sediments reported by Hoffmann and others (2002) includes values associated with a fine-grained unit found in a lower reach of Rillito Creek near the Santa Cruz River. These values typically are as low as 0.012 m/d and may not be representative of the hydraulic conductivity in upstream reaches. Excluding the hydraulic-conductivity values for the basin-fill sediments in the lower reaches where the fine-grained unit was present, the average vertical hydraulic conductivity of the study area is 0.3 m/d. Assuming a unit gradient, equivalent vertical hydraulic conductivity values are equivalent to the rate of infiltration and provide an estimate of potential recharge rates under saturated conditions.

Saturated conditions will exist only after sustained periods of streamflow infiltration at a rate that enables water to fully saturate the underlying sediments from the streambed to the aquifer. Once a saturated hydraulic connection is achieved between the stream and underlying aquifer, the system behaves as though the stream were perennial. Unsaturated hydraulic-

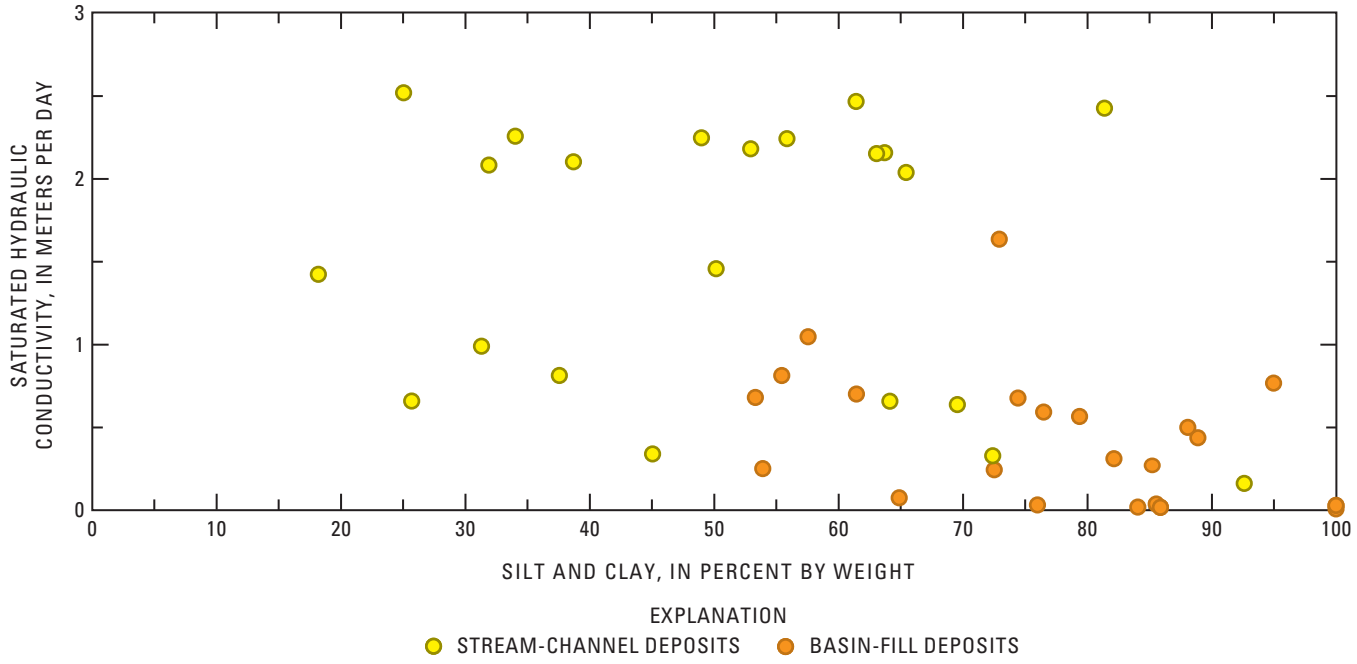

Figure 4. Relation of saturated hydraulic conductivity to sand, silt, and clay content for cores collected from boreholes drilled along Rillito Creek, Pima County, Arizona.

conductivity values need to be considered when estimating potential recharge rates for conditions prior to full saturation. Unsaturated hydraulic conductivity of the deposits beneath Rillito Creek varies by several orders of magnitude as a function of water content. For water-content conditions at the time of core collection, the unsaturated hydraulic conductivity was generally two or more orders of magnitude less than the saturated hydraulic conductivity (Hoffmann and others, 2002).

Antecedent pore water underlying Rillito Creek derives from streamflow infiltration and subsequent percolation. In this study, cores were collected in late March 1999; therefore, antecedent pore water was derived from streamflows prior to March 1999. Several flow events prior to 1999 could have been sources of the antecedent water. On the basis of streamflow records at the streamflow-gaging station at Dodge Boulevard, the most recent flow prior to core collection occurred in November 1998 and lasted for 2 days (average streamflow was less than 0.82 m^3/s). The last recorded flow prior to November 1998 occurred in the summer of 1998 and lasted for about 1 day. The most voluminous and long-lasting flow within a few years of the core collection was the sustained flow from February to April 1998, which was related to the 1998 El Niño precipitation.

Volumetric water content in the unsaturated zone ranged from 0.02 to 0.46 at the time of core collection (fig. 5). Variability in water content primarily is controlled by differences in sediment texture and is positively correlated with the percentage of fine-grained material (fig. 5). The stream-channel deposits averaged 17.8 percent water content and 57.6 percent saturation; the basin-fill deposits averaged 24 percent water content and 69.3 percent saturation. Integrating the water content over the thickness of the unsaturated zone, cumulatively, the unsaturated sediments beneath Rillito Creek contained 0.5 to 12.2 m of water. The smallest amount of water was in the upstream area at the borehole ((D-13-14)26daa) near Craycroft Road where the unsaturated zone was about 3 m thick; the largest amount of water was in the downstream area at the borehole ((D-12-14)26add) near La Cholla Boulevard where a 12-m thick fine-grained unit lies above the water table. The sites probably most representative of the unsaturated zone beneath Rillito Creek are in the middle reaches where the unsaturated zone was 30 to 40 m thick and had 6.1 m of water (boreholes (D-13-14)19bcbn, (D-13-14)19bcbs, and (D-13-14)28dba). The large amount of water stored in the unsaturated zone indicates that much of this water probably originated from the sustained flows prior to the summer of 1998, that the stored water is likely to be from several different streamflow and infiltration events, and that the sediments beneath Rillito Creek drain slowly.

Environmental Tracers

Environmental tracers of tritium (^3H), oxygen-18 (^{18}O), deuterium (^2H or D), and chloride from the pore waters in the unsaturated and saturated zones were analyzed to evaluate spatial variations in infiltration and recharge patterns along Rillito Creek. Tritium is a naturally occurring radioactive isotope of hydrogen with a half life of 12.43 years. Large concentrations of tritium were introduced into the atmosphere beginning in 1952 as a result of the atmospheric testing of nuclear

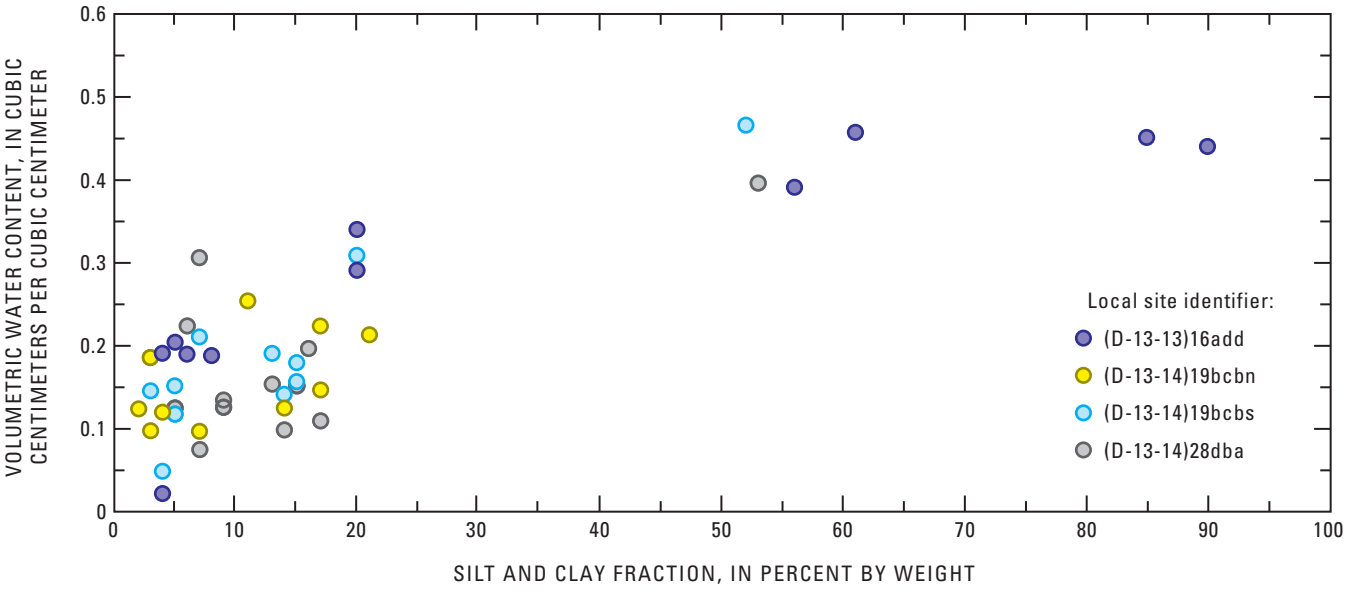

Figure 5. Relation of volumetric water content to sand, silt, and clay content for cores collected from boreholes drilled along Rillito Creek, Pima County, Arizona.

weapons. The input of tritium into the atmosphere related to nuclear weapon testing peaked at nearly 6,000 tritium units (TU) in 1963–64 prior to a ban on the tests. Atmospheric tritium concentrations returned to natural conditions by 1992 (Dr. Chris Eastoe, geochemist, University of Arizona, written commun., 2003), and the concentration of tritium in precipitation today is about 5 to 7 TU. Tritium concentrations are often used for dating ground water and to detect events, such as the 1963–64 peak. In this study, tritium was measured in water vacuum extracted from cores and analyzed by liquid scintillation with electrolytic enrichment (Thatcher and others, 1977) at the USGS laboratory in Menlo Park, California. Tritium was detected in pore water extracted from each core sample and ranged in concentration from 2 to 11 TU (fig. 6). The precision of individual measurements was ±0.3 TU. For the purposes of this study, waters having tritium concentrations in this range are interpreted as having infiltrated within the past 40 years. Tritium concentrations within a given profile could not be used to identify an event marker, such as the 1963 peak.

Given the presence of tritium in the unsaturated zone, the locally high vertical hydraulic conductivity values of more than 1 m/d in the stream-channel deposits, and depths to the water table of generally less than 40 m, it is likely that most of the pore water extracted from the cores was derived from runoff events during the few years prior to 1999.

Assuming negligible mixing of infiltrated waters, variations in isotopic signatures and chloride concentrations can be used to identify individual runoff and infiltration events. These unique signatures remain intact during infiltration and allow direct identification of runoff events as the infiltrated water migrates through the unsaturated profile. Sampling through the unsaturated zone at a point in time provides a snapshot of the isotopic and chemical signatures throughout the profile. This snapshot represents the composition of the water that infiltrated into the sediment over a period of time—the deepest water representing the beginning of the period. The downward rate of water movement at a particular site is calculated using the time elapsed between the runoff event and depth of infiltration of the water in the profile.

Oxygen and hydrogen isotopic compositions were determined for water extracted from cores by azeotropic distillation (Revesz and Woods, 1990) with toluene at the USGS laboratory in Reston, Virginia, using analytical methods described by Epstein and Mayeda (1953). Isotopic variations in water are expressed as a per mil ratio (δ value), which is a ratio of $^{18}O/^{16}O$ and $D/^{1}H$ in a sample relative to the ratio in an ocean water standard (Clark and Fritz, 1997). The delta symbol in this report is followed by the chemical symbol for the heavier isotope measured during isotopic analysis. Isotopic values are described as lighter or heavier in relation to each other. Lighter isotopic values are smaller or more negative per mil values, and heavier isotopic values are larger or more positive per mil values.

The source of precipitation is evaporation of seawater; therefore, the $\delta^{18}O$ and δD composition of precipitation is linearly correlated, which is known as the meteoric water line

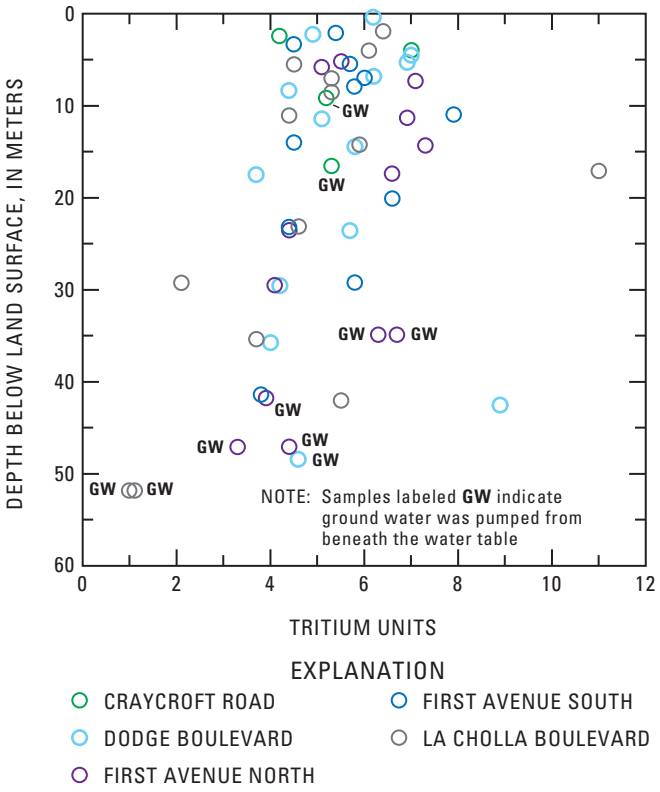

Figure 6. Profile of tritium content in water collected from boreholes drilled along Rillito Creek, Pima County, Arizona.

(MWL; Craig, 1961). Values of $\delta^{18}O$ and δD in precipitation vary from event to event and also seasonally. Many variables influence the isotopic signature of a precipitation event, including the origin, travel path, and duration of the storm, and the elevation and temperature of condensation prior to rainfall. In general, however, variations in isotopic signature are predominately temperature dependent. The cool, high-altitude precipitation events produce water having lighter isotopic ratios than water from the warm precipitation events. In addition, evaporation will result in $\delta^{18}O$–δD data for the remaining water that plot to the right of the MWL. A more detailed discussion on variations of isotopic ratios can be found in Clark and Fritz (1997).

Values of $\delta^{18}O$ and δD in waters extracted from the unsaturated zone range from about -12 to -6 per mil, and -80 to -37 per mil, respectively (fig. 7). Data for many of the samples indicate the effect of evaporation (fig. 7). Isotopic compositions from the Dodge Boulevard site generally indicate the greatest amount of evaporation, and isotopic data from a sample collected at First Avenue North from a depth of less than 1 m indicated the greatest amount of evaporation for any sample (fig. 7). Variations in isotopic compositions of water from the unsaturated zone beneath Rillito Creek are, therefore, attributed to both changes in the isotopic signatures of the source water and to evaporation. Those samples that lack an evaporative signal indicate that percolating waters were not exposed to significant evaporation prior to infiltration.

Several trends were evident in the isotopic ratios of Rillito Creek pore water. One trend is related to the location in the stream reach where the samples were collected. The water-weighted mean isotopic signature of the pore water in the unsaturated zone generally becomes lighter in the downstream direction (fig. 8). The water weighted mean uses the water content of the core as a weight that is multiplied by the isotopic ratio of the extracted water. Pore water in the borehole near Dodge Boulevard ((D-13-14)28dba) had $\delta^{18}O$ and δD values of -8.0 of -55.0 per mil, respectively, whereas pore water downstream in the borehole near LaCholla ((D-13-13)16add) had $\delta^{18}O$ and δD values of -9.5 and -64.0 per mil, respectively. At the intermediate boreholes near First Avenue ((D-13-14)bcbn and (D-13-14)19bcbs), $\delta^{18}O$ and δD values were -8.8 of -60.3 per mil, respectively. These variations are larger than the analytical precision (2-sigma values of 0.2 and 2 for $\delta^{18}O$ and δD, respectively; thus, in 95 percent of repeat analyses the same sample would result in $\delta^{18}O$ within 0.2 per mil of the originally reported value and the δD values would be within 2 per mil of the originally reported value). Evaporative effects would cause a trend opposite to the observed data; therefore, the trend is likely a function of the origin and season of precipitation events that resulted in streamflow and subsequent infiltration at the downstream sites. Specifically, for the time period represented by the unsaturated zone pore water, it is the longer duration and isotopically lighter winter storms that were more important contributors to infiltration in the downstream reaches than in the upstream reaches. The exception to this trend is at the uppermost borehole near Craycroft Road ((D-13-14)26daa) where the lightest values, a $\delta^{18}O$ of -10 per mil, and a δD of –65 per mil, were measured. Depth to water at this site, however, is commonly only a few meters below the streambed; therefore, water in the unsaturated zone at the time of core collection probably is representative of infiltration only from the most recent streamflows.

Another trend in the isotopic data is that water from the saturated zone has $\delta^{18}O$ and δD values that are consistently lighter than those in water from the unsaturated zone and do not reflect evaporation effects as do those in water from the

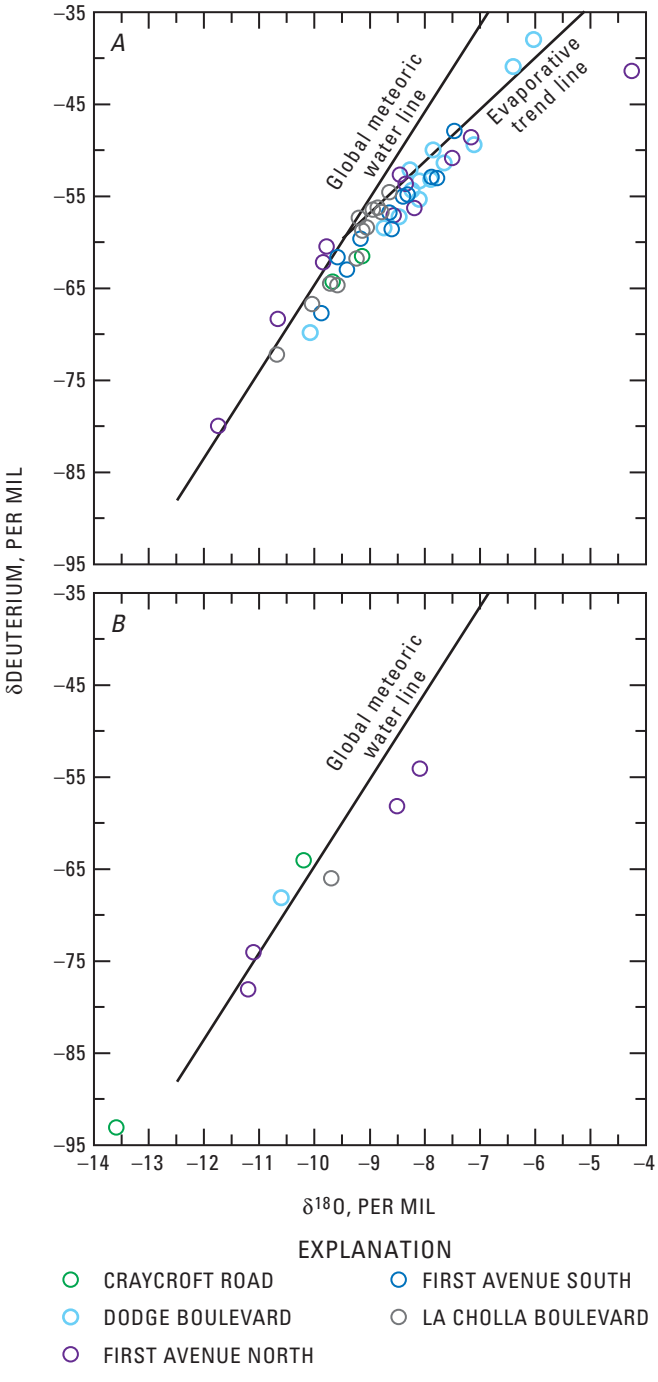

Figure 7. Stable isotope data of pore water collected from cores collected from boreholes drilled along Rillito Creek, Pima County, Arizona. *A*, unsaturated zone; *B*, below the water table.

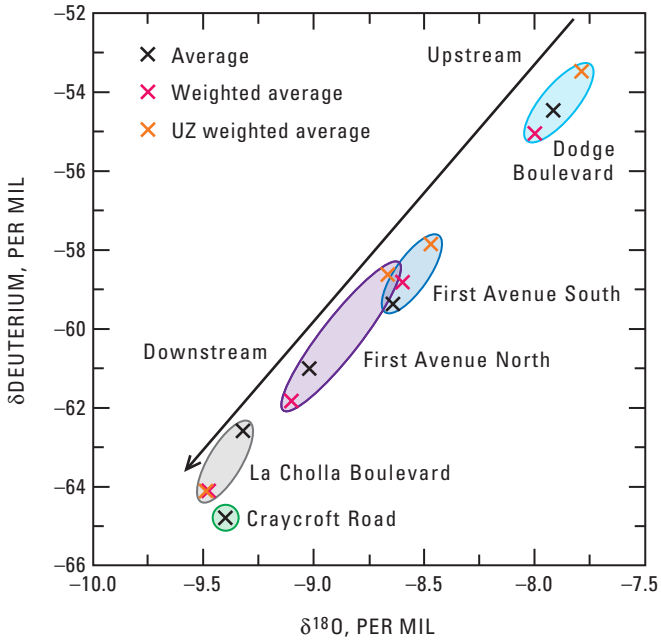

Figure 8. Weighted average of stable isotope values from pore water collected from boreholes along Rillito Creek Pima County, Arizona.

unsaturated zone (fig. 8). This lighter isotopic composition in the ground water from beneath the water table indicates a greater influence of winter and (or) higher elevation precipitation in the ground water than for the water in the unsaturated zone at the time of collection. The lack of an evaporative signal indicates that water that reaches the water table is exposed to minimal evaporation.

Oxygen-18 ($\delta^{18}O$) and δD data for precipitation in the Tucson Basin collected prior to the study period were analyzed to define a possible isotopic input function to the system. Isotopic compositions for precipitation in the Tucson Basin that resulted in Rillito Creek streamflow indicate that light compositions are associated with the winter 1998 El Niño weather pattern, whereas compositions are varied for the summer precipitation events of 1997 and 1998 (fig. 9).

A substantially heavy isotopic signal was associated with precipitation in April and August 1998. Assuming conservative behavior, isotopic compositions measured in the precipitation are possible event markers that might be identified in the unsaturated zone. In order to identify event markers in the unsaturated zone, vertical profiles of $\delta^{18}O$ and δD were compared to $\delta^{18}O$ and δD in samples of runoff (fig. 10). This analysis was done for the borehole near Dodge Boulevard because it is near the streamflow-gaging station at Dodge

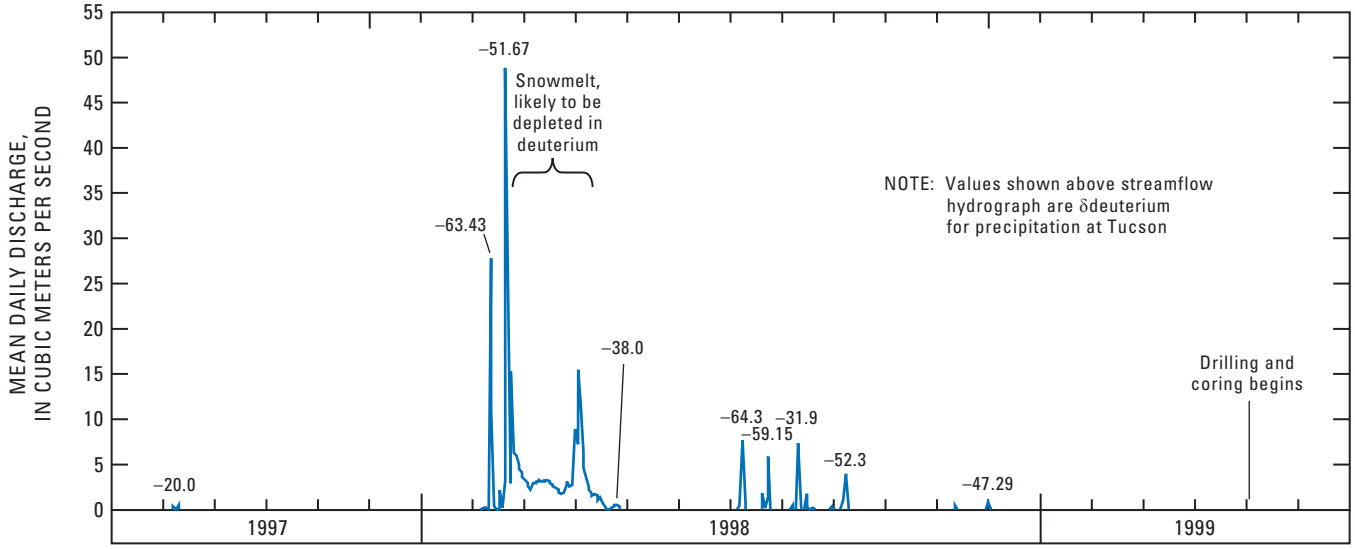

Figure 9. Hydrograph of streamflow gaging station 09485700 Rillito Creek near Dodge Boulevard (09485700) and associated stable isotope values determined for precipitation.

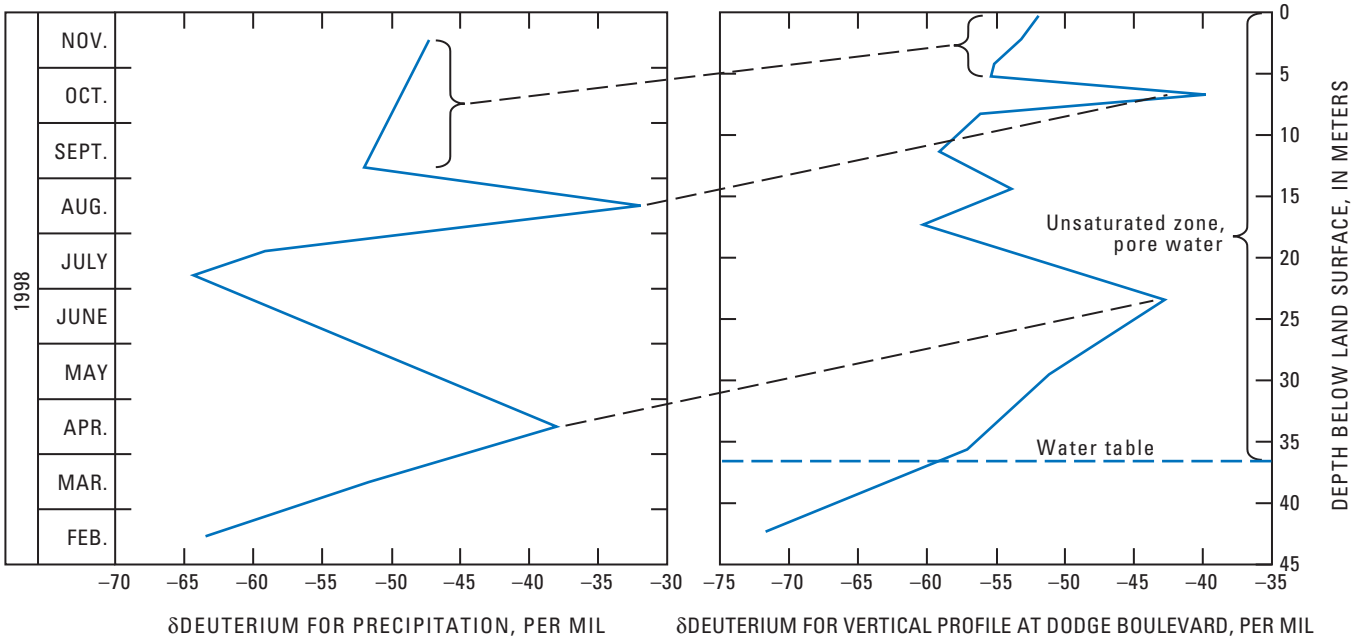

Figure 10. Comparison of stable isotope values in vertical profile to stable isotopic values of precipitation.

Boulevard (09485700). The hydrograph for this gaging station was used to determine timing of streamflow prior to drilling and coring. The trends in isotopic compositions measured in the pore-water cores approximately match the pattern of signatures in the basin precipitation from particular storms that occurred from February to November 1998. For instance, the heavy isotopic compositions in precipitation in April and August 1998 are possibly identified in pore water from depths of 6.5 and 23 m, respectively (fig. 10). Below 23 m, the compositions become lighter and are similar to those of the El Niño precipitation events about 14 months prior to the drilling and coring. If this interpretation is correct, water in the unsaturated zone below about 23 m is likely to have originated from sustained flows related to 1998 El Niño precipitation. Discrete pore-water sampling and minor mixing of pore water within the unsaturated zone can explain why the values for precipitation tend to have a wider range (-32 to -65 δD) than values for the unsaturated zone pore water (-40 to -61 δD). Correlation between the precipitation events and depths of infiltration, on the basis of corresponding isotopic signatures, indicates an average vertical linear velocity of approximately 0.049 m/d at the borehole near Dodge Boulevard. This velocity represents the downward percolation rate of water. Percolation is defined here as the flow of water that has infiltrated and is moving downward or lateral toward the water table. Note that infiltration connotes movement of water into sediments, in contrast to percolation, which connotes movement through sediments. Owing to the decrease in hydraulic conductivity with decreasing water content, the percolation rate is less than the measured saturated hydraulic conductivity.

Chloride concentrations in pore-water leachate were determined from drill cuttings at 0.3-m depth intervals. To derive the leachate, 50 mL of distilled water was mixed with 50 g of sieved cuttings having a particle size of less than 1 mm. The mixture was stirred and the specific conductance measured. An ion-specific probe was used to measure the chloride concentration after the specific conductance stabilized. Chloride concentrations are reported for the boreholes near Dodge Boulevard and near First Avenue (fig. 11).

Chloride concentrations at the borehole near La Cholla Boulevard between about 10 and 30 m are not presented because the fine-grained unit at this depth made leaching and sieving difficult, and therefore the results were suspect. Chloride concentrations are not presented for the borehole near Craycroft Road because of the shallow water table there.

Chloride concentration in runoff varies as a function of the precipitation location and the runoff travel path and surface-contact time. Chloride concentrations measured in the profile varied substantially through the upper 18 m at all sites (fig. 11). Below about 18 m, the variation in concentration declined considerably. On the basis of δ^{18}O and δD data discussed previously, this zone of smaller variation corresponds to the infiltration depth of the 1998 El Niño water. The small variation and low mean chloride concentration are attributed to infiltration from sustained streamflow having a low chloride concentration. In addition, the low chloride concentration indicates the water had little exposure to evaporation. The greater variation and higher concentration observed in post-El Niño pore water are likely due to mobilization of chloride from evaporative concentrates and dry fallout on the streambed and tributaries deposited between precipitation events. Calculation of a downward percolation rate using an event marker in the chloride profile at Dodge Boulevard yields an average linear velocity of 0.055 m/d, and corresponds closely to the rate calculated using the stable-isotope data. On the basis of the environmental tracers measured at the borehole near Dodge Boulevard, pore water in the unsaturated zone represents water that infiltrated into the sediments within the 12 to 14 months prior to drilling, and approximately half of the water (water in the deeper half of the unsaturated zone) infiltrated from the previous El Niño runoff event.

Multiplying the downward percolation rate by the volumetric water content results in the flux of recharge that reaches the water table. Using a percolation-rate estimate of 0.05 m/d, an average volumetric water content of 13 percent measured in the cores from the borehole near Dodge Boulevard borehole (Hoffmann and others, 2002), and a wetted perimeter of 25 m, results in a flux across the water table of 0.002 cubic meters per second per linear kilometer of streamflow ($m^3/s/km$).

Seepage Measurements

Seepage measurements were made at several sites along Rillito Creek during the El Niño-related sustained flows of March through April 1998 to determine infiltration rates for different stream reaches (Don Pool, hydrologist, U.S. Geological Survey, written commun., 2003). Findings from the 1998 seepage measurements are summarized here because, on the basis of stable-isotope ratios and chloride-concentration profiles, infiltration from the sustained El Niño flow is likely to have provided most of the water stored in the unsaturated zone at the time of borehole drilling and core collection. Streamflow losses owing to infiltration along Rillito Creek ranged from 0.07 to 0.9 $m^3/s/km$ and were largest downstream from Swan Road (fig. 1). The small streamflow losses in the upstream area were attributed to rejected recharge; depth to ground water upstream from Swan Road was near land surface after several days of sustained flow, whereas the depth downstream from Swan Road was typically greater than 30 m.

Seepage measurements were made again at four sites along Rillito Creek during an 8-hr period on October 24, 2000. Unlike the 1998 seepage measurements, the October 2000 seepage measurements did not isolate streamflow-infiltration rates relative to Swan Road; however, measured streamflow-infiltration rates generally agreed with those measured in 1998, as they ranged from 0.09 to 0.4 $m^3/s/km$ and averaged 0.22 $m^3/s/km$ (fig. 12). The October 2000 seepage measurements were made during an 8-hr period along a 14-km reach having an average wetted perimeter of about 25 m. Using a wetted perimeter of 25 m results in an average infiltration rate of 0.75 m/d, which is

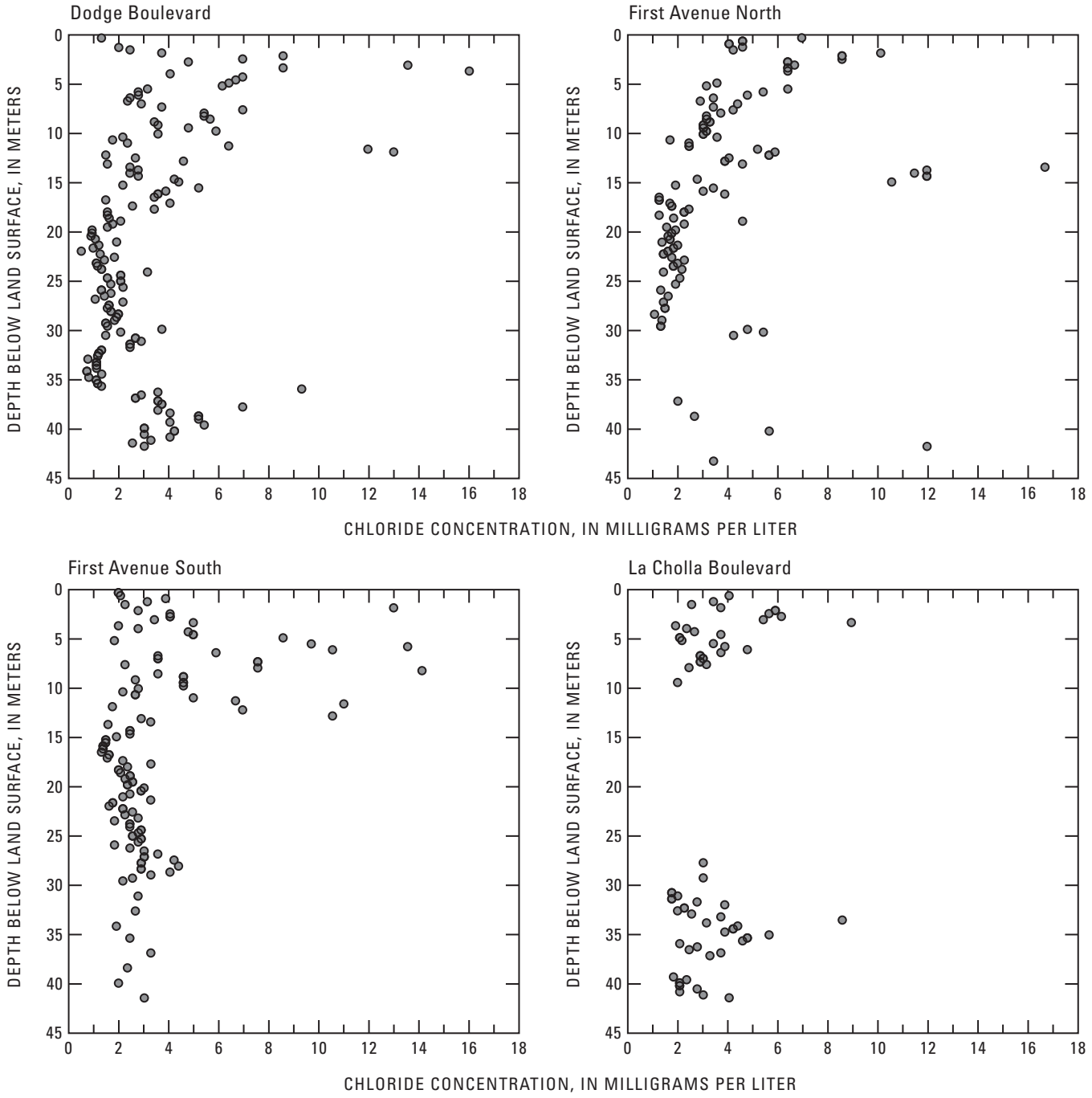

Figure 11. Profile of concentration of chloride from cuttings leachate from boreholes drilled along Rillito Creek, Pima County, Arizona.

similar to the measured saturated hydraulic conductivity of the stream-channel deposits (1.2 m/d), but more than an order of magnitude greater than percolation rates determined by tracers. The difference between the estimated infiltration and percolation rates probably is due to several factors, such as (1) the variably saturated nature of the sediments—the near-surface stream-channel deposits are likely to be nearly saturated during streamflow and, therefore, are approaching their saturated hydraulic conductivity, whereas the deeper sediments are less than fully saturated and will, therefore, have a lower hydraulic conductivity; (2) some water will spread laterally reducing the downward flux, and (3) percolation rates determined by tracers reflect average rates over longer periods of time than infiltration rates, including periods when the creek is not flowing.

Assuming 6 m of water in storage in the unsaturated zone beneath the creek (as determined by volumetric water-content measurements made on the cores; fig. 5) and a stream width of 100 m, the amount of pore water beneath every kilometer of the creek at the time of drilling and

coring was 6×10^5 m^3. There was less water in the upper reach where the unsaturated zone is shallower and more water in the downstream reach where there is an 18-m-thick fine-grained unit having high water content. Assuming an average streamflow loss rate of 0.22 $m^3/s/km$, about 33 days of streamflow infiltration would be needed to infiltrate the amount of water stored in the unsaturated zone. There were about 31 days of cumulative flow in the creek in the 12 months prior to drilling and coring; about two-thirds of the flow days were associated with the El Niño snowmelt runoff that occurred about 1 year before the drilling and coring. Assuming the water in the bottom two-thirds of the unsaturated zone collected in 1999 originated from surface water flowing a year earlier, the average downward percolation rate would be about 0.04 to 0.09 m/d, which brackets the percolation rate estimated by environmental tracers. This analysis of seepage and cumulative streamflow duration required to provide the amount of water held in storage in the unsaturated zone provides an independent method of estimating the age of water in the unsaturated zone, estimating infiltration and percolation rates, and substantiates the interpretation made on the basis of the environmental tracers.

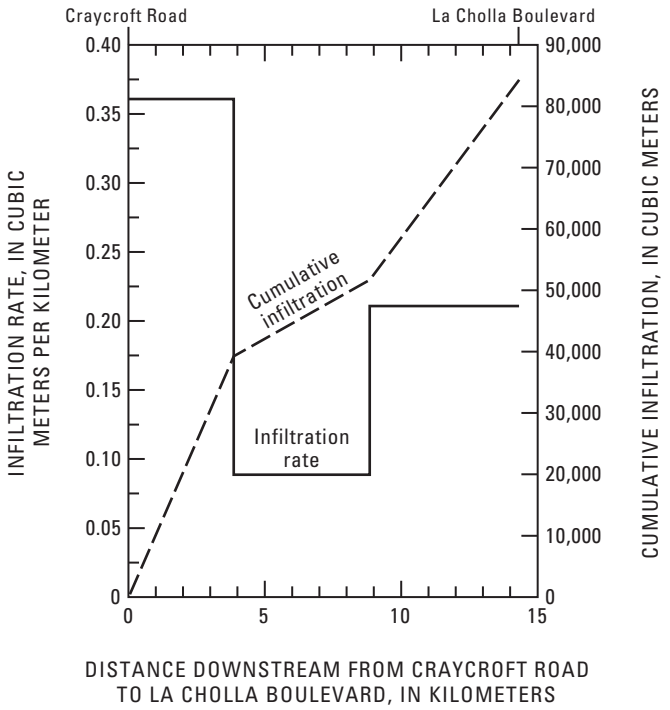

Figure 12. Seepage loses during October 8, 2000 streamflow in Rillito Creek, Pima County, Arizona.

Temperature and Water Content

One-Dimensional Temperature Monitoring and Modeling

Heat can be transferred through sediments by a combination of advection and conduction. Although both advective and conductive heat transport occur during infiltration, advective heat transport is more prevalent in high water-flux settings, whereas conductive heat transport is more prevalent in very low or no water-flux conditions. For most hydrologic applications related to infiltration through alluvial sediments, advection is the primary mechanism for the transport of heat by flowing water, and conductive heat transport is regarded as a negligible component of heat transfer (Constantz and others, 2003).

In this study, heat as a tracer was used to estimate one-dimensional vertical infiltration by inversely determining the vertical saturated hydraulic-conductivity profiles beneath the streambed. Stream-channel deposits were instrumented with vertical nests of thermistors at three sites along Rillito Creek (fig. 1). Thermographs predicted by numerical simulations were fitted to measured thermographs from the field by adjusting model parameters within appropriate ranges until the least error (best match) was found between simulated and measured thermographs. The three vertical-temperature arrays are buried in the stream-channel deposits near the boreholes (fig. 1). One array is near Craycroft Road in the upper reach of the study area; one is near Dodge Boulevard in the middle reach of the study area; and the other is near First Avenue also in the middle reach of the study area.

The simulation domains for the Rillito Creek models were represented numerically in one dimension, oriented vertically. The upper boundary and datum of the simulation domains was the streambed. The lower boundary was at or near the depth of the deepest measurements of temperature or pressure, or both. For the simulations, time-varying hydraulic and temperature potentials were defined at the upper- and lower-domain boundaries.

The hydraulic head at the streambed is equivalent to the stream stage. USGS streamflow-gaging stations provided measurements of stage after correction for the datum elevation. Streambed temperatures were measured by thermistors buried about 0.2 m below the streambed in the most active part of the channel. Pressure-head measurements from piezometers were used to define heads at the lower boundary of the three study sites. The lower-boundary temperatures for the Craycroft Road site were inferred from thermistor measurements near the lower-boundary depth. The lower-boundary temperatures coinciding with the water table for the Dodge Boulevard and First Avenue sites were approximated from ground-water temperatures measured within 5 meters of the water table at those sites. The inverse simulations were made with a numerical coupled water-flow and heat-transport model, VS2DH (Healy and Ronan, 1996), that was linked with parameter estimation software (PEST). A detailed description of the theory, modeling approach, and findings of this investigation is documented in Bailey (2002).

Infiltration at Craycroft Road Site

Infiltration for two periods of sustained streamflow were modeled for the upstream-most site (near Craycroft

Road). The first model period extends from July 20, 1999, to July 27, 1999. The second modeled period extends from July 29, 1999, to August 2, 1999. Streamflow and stage at the nearby streamflow-gaging station (Tanque Verde Creek at Tucson) fluctuated between 2.23 and 0.33 m^3/s, and between 0.26 and 0.11 m, respectively, during the first modeled flow period. Streamflow decreased from 1.11 to 0.05 m^3/s and stage decreased from 0.20 to 0.03 m during the second modeled flow period. The wetted perimeter of the streambed near the Craycroft Road site during these periods was about 10 m.

The measured thermograph at a depth of 1.2 m for the first modeled period shows a characteristic sinusoidal pattern that varies between about 24 and 26.5°C, whereas the thermograph for the second modeled period is generally flat and varies only between 25 and 25.5°C. Model simulation at the Craycroft Road site approximately reproduced the thermograph of the observed data for both model periods (fig. 13). Model simulations were optimized on vertical saturated hydraulic conductivity. Simulated vertical saturated hydraulic-conductivity values were in general agreement with those measured in the laboratory (Bailey, 2002; Hoffmann and others, 2002). A physical change within the streambed between flow periods at this site required the addition of a thin surface layer having a low vertical hydraulic conductivity within the model domain. The addition of this surface layer resulted in a lowering of the simulated equivalent saturated hydraulic conductivity by four orders of magnitude, from about 4 m/d to 3×10^{-4} m/d. The four orders of magnitude change in hydraulic conductivity is too large to result solely from changes in water viscosity owing to temperature changes. Given the tranquil flow conditions during the first flow period, it is possible that the change was the deposition of a fine-grained layer at the streambed surface. In fact, a thin layer of fine-grained material commonly was observed at the Craycroft Road site after small streamflow events.

Flow in the creek typically resulted in hydraulic connection between streamflows and ground water (see section titled "Water-Level Responses"). Thus, vertical gradients measured at the vertically nested piezometer at the borehole near Craycroft Road enabled estimation of infiltration rates using simulated equivalent vertical saturated hydraulic conductivity. Vertical hydraulic gradients measured from these piezometers typically ranged from 0.06 to 0.2 m/m and averaged 0.1 m/m. The highest gradients occurred during and shortly after streamflow. Assuming a typical gradient during and shortly after streamflow (0.2 m/m) and a wetted perimeter of 10 m, estimated infiltration rates ranged from 0.09 $m^3/s/km$ during the first modeled period to 8×10^{-6} $m^3/s/km$ during the second modeled period. The first modeled period is probably most representative of the typical ephemeral-streamflow conditions; the second period of streamflow modeled is probably most representative of small flows that occur after a layer of fine-grained deposits has been deposited. The infiltration rate of 0.09 $m^3/s/km$ for the first modeled period is about half of that estimated by seepage measurements (average of 0.21 $m^3/s/km$).

Infiltration at Dodge Boulevard and First Avenue sites

Infiltration also was modeled for two time periods at the Dodge Boulevard and First Avenue sites: the first modeled period extends from July 14, 1999, to July 17, 1999, and the second modeled period extends from July 25, 1999, to July 29, 1999. The proximity of the thermistors to the streamflow-gaging station 09485700 at Dodge Boulevard allowed direct use of the gaging-station measurements to define the hydraulic head at the upper boundary within the Dodge Boulevard model domain. These boundary conditions also were used for the First Avenue model domain. Discharge and stage for these two periods reached maximums of 254 m^3/s and 2.7 m, respectively. The wetted perimeter for these flows was about 10 m. An important difference between these sites and the site near Craycroft Road is that the depth to the water table near the Dodge Boulevard and First Avenue sites is greater than 30 m; therefore, ephemeral flow in the stream channel at these sites may never result in hydraulic connection between the stream and the aquifer.

Thermographs from a depth of 0.8 m at the Dodge Boulevard site for the two modeled periods have contrasting signals. The thermograph for the first period shows a decline in temperature associated with streamflow from about 29.5 to 20.5°C that is followed by a gradual increase to 26°C; the thermograph for the second period shows a rapid increase in temperature associated with streamflow from about 29 to 32°C that is followed by a gradual decrease to 27°C (fig. 14). The most accurate prediction of the observed thermograph for the first modeled time period at the Dodge Boulevard site resulted in an equivalent vertical saturated hydraulic conductivity of about 5 m/d, which is similar to, yet slightly higher than, the equivalent vertical saturated hydraulic conductivity simulated at the Craycroft Road site. Vertical hydraulic gradients were not measured at the Dodge Boulevard site, thus, infiltration rates can not be estimated; however, by assuming a vertical gradient of 0.2 m/m (on the basis of the measured gradient at the Craycroft Road site), an equivalent vertical hydraulic conductivity of 5 m/d, and a wetted perimeter of 10 m, the infiltration flux was calculated as 0.12 $m^3/s/km$.

To match the simulated thermograph to the measured thermograph for the second modeled period, a thin surface layer having a low-vertical hydraulic conductivity needed to be added during the modeled period. During the first part of the second simulation, the equivalent vertical saturated hydraulic conductivity was 0.7 mm/s, which, if sustained, would equate to 66 m/d. After about 3 hours of streamflow, the addition of the low-conductivity surface layer reduced the equivalent vertical hydraulic conductivity to about 0.25 m/d. The decrease in hydraulic conductivity during a flow event is consistent with the deposition and accumulation of fine sediments on the receding limb of a hydrograph.

Model simulations for the site near First Avenue relied on stage data from the streamflow gaging-station 09485700 at Dodge Boulevard (Bailey, 2002). Simulations for this site covered the same two time periods and resulted in equivalent

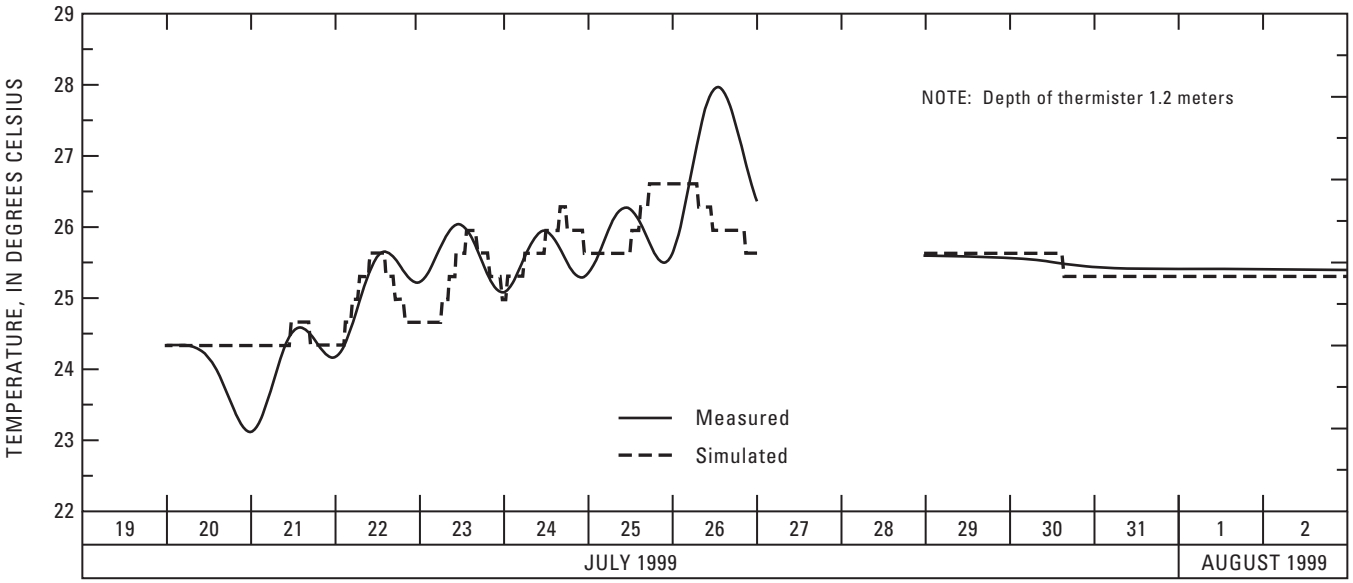

Figure 13. Measured and simulated thermographs in Rillito Creek near Craycroft Road, Pima County, Arizona.

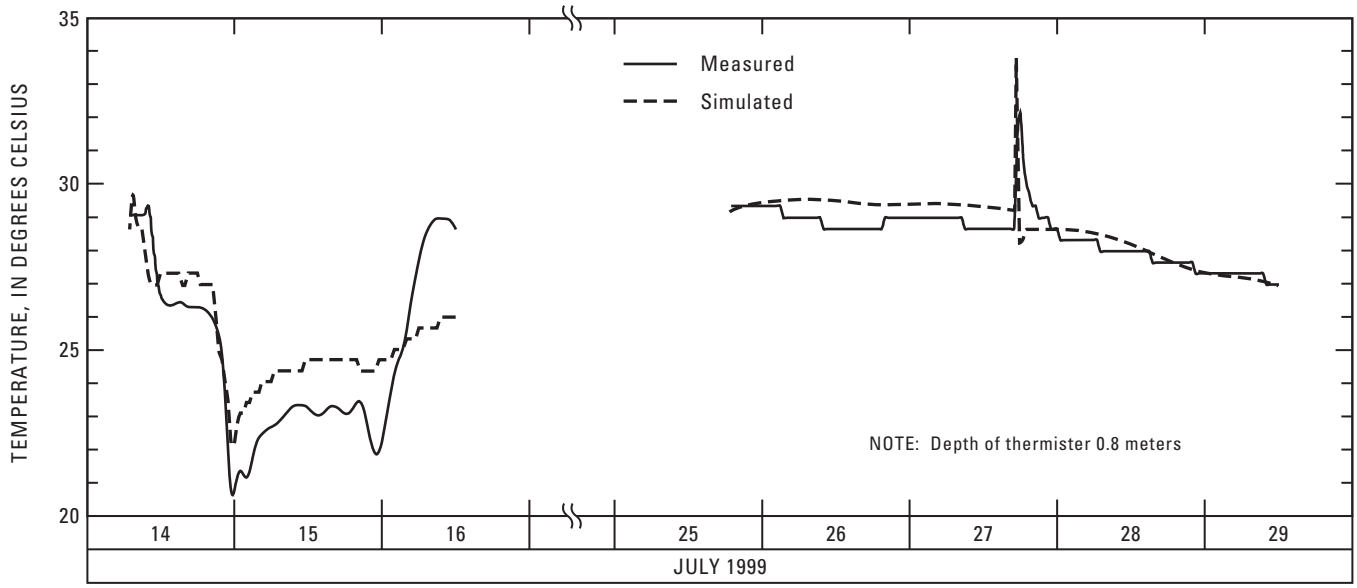

Figure 14. Measured and simulated thermographs in Rillito Creek near Dodge Boulevard, Pima County, Arizona.

vertical hydraulic conductivity values that were similar to those estimated for the site near Dodge Boulevard. In addition, the simulation for the second modeled period required the addition of a low vertical hydraulic conductivity surficial layer during the latter part of the period. The model simulations for the site near First Avenue, however, were less successful in matching the observed data than the simulations for the site near Dodge Boulevard. The inability of the simulations to match the magnitude and changes in the temperature measured at the site near First Avenue indicates the numerical model likely is not representing some of the infiltration processes, such as multidimensional flow beneath the streambed, the model has poorly constrained sediment and hydraulic parameters, or a combination of these factors.

Results of this investigation indicate that, under well-constrained conditions where predominantly vertical infiltration can be assumed, a one-dimensional inverse numerical model can be used to estimate infiltration rates. One-dimensional modeling, however, assumes lateral spreading does not occur. If lateral spreading does occur, the estimated rates predicted by one-dimensional modeling will be smaller than actual rates. The results also indicate that streambed hydraulic conductivity can limit infiltration and that hydraulic conductivity can vary significantly between and during flow events. Erosion

and deposition associated with low-frequency, high-intensity ephemeral streamflow can result in large variations in the hydraulic conductivity of the streambed surface owing to an accumulation or removal of fine-grained sediments. This variability affects the cumulative infiltration, which could vary greatly as a function of the amount of streamflow and a function of the nature of the streamflow and the accumulation or removal of fine-grained sediments. Additionally, these results indicate that simulation of streambed infiltration should allow for temporal variation of the streambed hydraulic conductivity or should be done using short time periods to account for rapid changes in the streambed hydraulic conductivity.

Two-Dimensional Temperature and Water-Content Monitoring

For the purpose of measuring infiltration fluxes at the onset and throughout the duration of streamflow events, Blasch and others (2003) instrumented the stream-channel deposits beneath Rillito Creek near Dodge Boulevard with a two-dimensional vertical array of 28 paired thermocouples, temperature probes, and time-domain reflectometry (TDR) water-content probes placed perpendicular to flow (fig. 1). The paired probes were arranged in four columns (profiles C1, C2, C3, and C4 in figure 1) spaced 3 m apart. There are seven rows (depths) within the array at depths of about 0.50, 0.75, 1.0, 1.25, 1.50, 2.0, and 2.5 m below the streambed. Depths of the probes varied by as much as 0.25 m owing to deposition and erosion during flow events. A near-surface temperature sensor also was placed adjacent to the paired two-dimensional array at a depth of 0.05 m.

The highly transient conditions that exist during the onset of streamflow are more difficult to simulate using temperature measurements exclusively than the saturated conditions presented in the previous section because of the rapid changes in water fluxes and increased multidimensional infiltration. Combined water-content and temperature measurements are needed to simulate initial transient infiltration rates in unsaturated sediments. Additionally, infiltration rates can be estimated using wetting-front arrival times and changes in water content at successive TDR probes.

Water-content data show rapid changes shortly after the onset of streamflow (fig. 15). Volumetric water content increases throughout the measured profiles from about 20 percent to 40 percent within minutes of the onset of streamflow. Initial infiltration rates measured as the change in volumetric water content over time per unit area were as high as 2 mm/s, which if sustained would be equivalent to 166 m/d. The high rates are likely to include vertical and lateral flow components. Temperature and water-content data for a September 2000 event indicate that infiltration occurs in both the horizontal and vertical directions at the onset of streamflow (figs. 16 and 17). Measured lateral wetting-front velocities between profiles were similar in magnitude to vertical velocities. The similar velocities measured at the onset of streamflow probably were due to tension gradients being much larger than the gravitational gradient. Water traveled laterally almost the entire 9-m

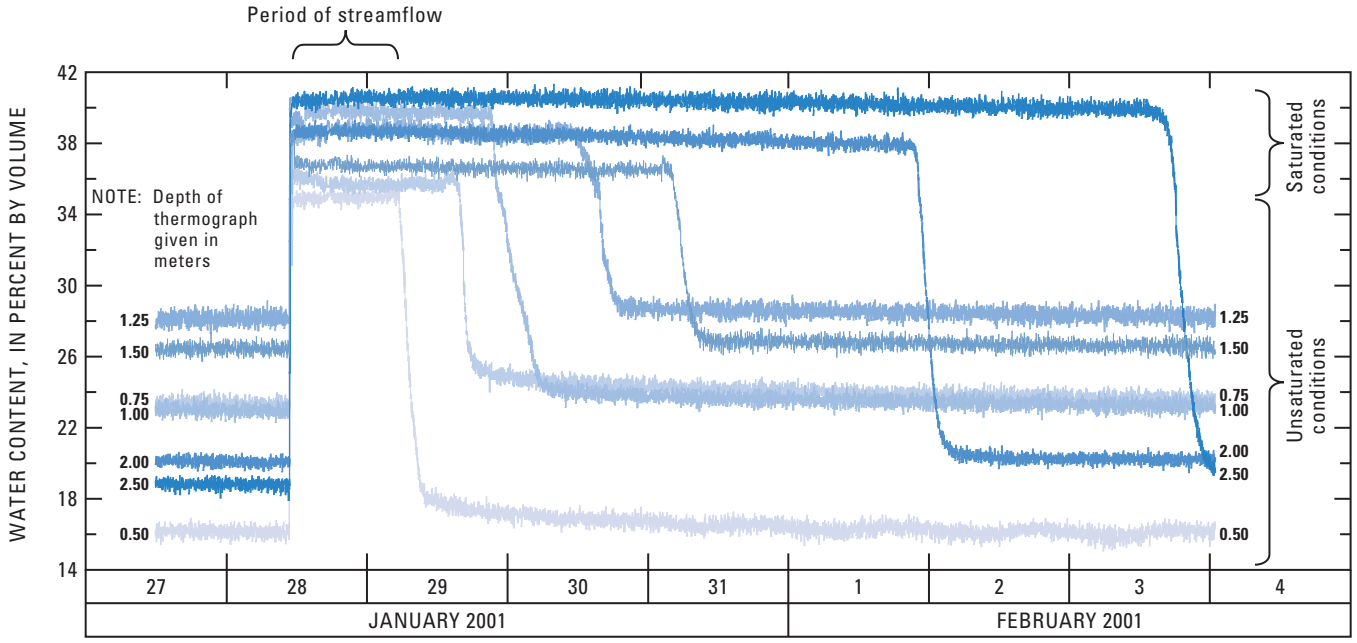

Figure 15. Water content of stream-channel sediments for duration of a streamflow event including onset and cessation, from within two-dimensional array in Rillito Creek near Dodge Boulevard, Pima County, Arizona.

distance between profiles within the first few minutes of the onset of streamflow.

Multidimensional-flow simulations are required to accurately represent the full volume of water infiltrating into a porous, heterogeneous medium near the margins of the advancing wetting front where capillary flow dominates. Infiltration, however, is increasingly vertical near the center of streamflow in a homogeneous medium, and lateral flow diminishes as capillary gradients decline with distance from the boundary of the wetted perimeter. The time from the onset of flow required for vertical infiltration to dominate varies depending on streamflow conditions and the texture of the streambed material. For instance, small braided-ribbon flows over fine material may never result in predominantly vertical infiltration, whereas large bank-to-bank flows over coarse material may produce predominantly vertical infiltration beneath the streambed within minutes on the basis of the large wetted perimeter and conductivity of the sediments.

A typical set of measured Rillito Creek thermographs from an April 2001 event and from a November 2000 event were simulated using a variably saturated heat and mass transport model, VS2DH (Healy and Ronan, 1996). The thermographs for the 0.5- and 2.5-m depths were used as boundary conditions, and the thermographs for the remaining five depths were used as observation points. One-dimensional models were created. Parameter optimization software, PEST, was used to calibrate thermal and hydraulic properties. Numerical simulations shown for data from the two-dimensional array are for a 10-m wide flow event starting on April 6, 2001 (fig. 18). The assumption of vertical one-dimensional flow was considered valid because temperature changes were predominantly in the vertical direction. The simulated infiltration rates varied from about 0.35 to 0.39 m/d throughout the initial 2 days of flow (fig. 19) and average 0.37 m/d. This represents a variation in predicted infiltration rates of less than 10 percent among the four columns, indicating that infiltration was uniform and predominantly vertical. Although the simulated and measured thermographs are in general agreement, departures do exist. Simulated temperatures differ from measured temperatures for several reasons, such as error in the measured boundary conditions, error in hydraulic and thermal property assignments, or an inability of the models to fully represent multidimensional infiltration.

The infiltration rate generally declines as the streamflow event proceeds. The declining infiltration rate is attributed to a declining pressure head and (or) development of a thin, fine-grained surface layer. Infiltration rates continued to decline during the flow event and averaged 0.32 m/d for the 12 days measured. By converting to flux units that are comparable with those estimates made at the vertical temperature nests described above and using a wetted perimeter of 10 m, an average infiltration rate of 0.32 m/d equates to a flux of 0.04 $m^3/s/km$. There are two important differences between these estimates and estimates made at the one-dimensional temperature-array sites near Craycroft Road and Dodge Boulevard. First, the estimated infiltration rates at the vertical-array sites near Craycroft Road and Dodge Boulevard are about twice that of the infiltration estimates made at the two-dimensional array. Second, the infiltration rates at the vertical-array sites required a low-hydraulic conductivity layer be incorporated into the model in the later stages of infiltration. The addition of a low-conductivity layer resulted in significantly reduced infiltration rates during the later stages of streamflow. The two-dimensional array was at the lowest part of the cross section, whereas the vertical nest was near a depositional fringe within the streambed, which may account for the deposition of the low-conductivity layer at the vertical nests.

An estimated sustained infiltration rate of about 0.32 m/d for the April 2000 streamflow event agrees with simulation results for a November 2000 event lasting 10 days. An average infiltration rate of 0.37 m/d was simulated for the November event. These rates show general agreement with infiltration rates of 0.41 to 0.50 m/d estimated by other investigators along Rillito Creek (Burkham, 1970; Katz, 1987). Simulations were also extended about 2 days beyond the periods of streamflow to estimate the redistribution of water in the subsurface. Redistribution rates, similar to infiltration rates, are determined from the elapsed time between sharp decreases in water content at each depth (fig. 15). After the cessation of streamflow, temperature measurements indicated the simulated dewatering flux was 0.33 and 0.30 m/d for the April and November events, respectively. Estimated redistribution rates using water-content changes were 0.08 and 0.1 m/d for the April and November events, respectively. Thus, redistribution rates were slightly less than infiltration fluxes during steady-state flow, and estimates of dewatering using water-content measurements were less than the simulated fluxes using temperature methods.

The variety of physical and chemical methods presented in this chapter (and elsewhere) are used to estimate rates of infiltration and percolation under steady-state conditions. For long-duration events (several days to months) steady-state conditions may be an accurate assumption, but for short-duration events (less than 24 hrs) typical of those in Rillito Creek and other streams in southern Arizona, infiltration fluxes that occur shortly after the onset of flow may differ substantially in magnitude from those throughout the duration of the event. For detailed water-budget analyses and hydrologic models dependent on infiltration flux estimates, the infiltration flux has to be estimated more accurately than is possible when using the assumption of steady-state conditions. Infiltration fluxes through the first 2 m of unsaturated sediments at the onset of streamflow calculated for 20 events ranged from 13 to 166 m/d. Variability in antecedent water content and fluid temperature were examined as possible factors contributing to the range in onset fluxes. Onset infiltration rates were inversely correlated to antecedent water content with a log-linear relation (fig. 20). Measured onset infiltration fluxes differed from those of the steady-state infiltration fluxes by four orders of magnitude. Infiltration rates after onset declined more quickly for events in which the antecedent water content was high; events starting with higher antecedent water content required 3.7 hours to achieve near steady-state conditions, whereas events with lower antecedent water content required 6.8 hrs.

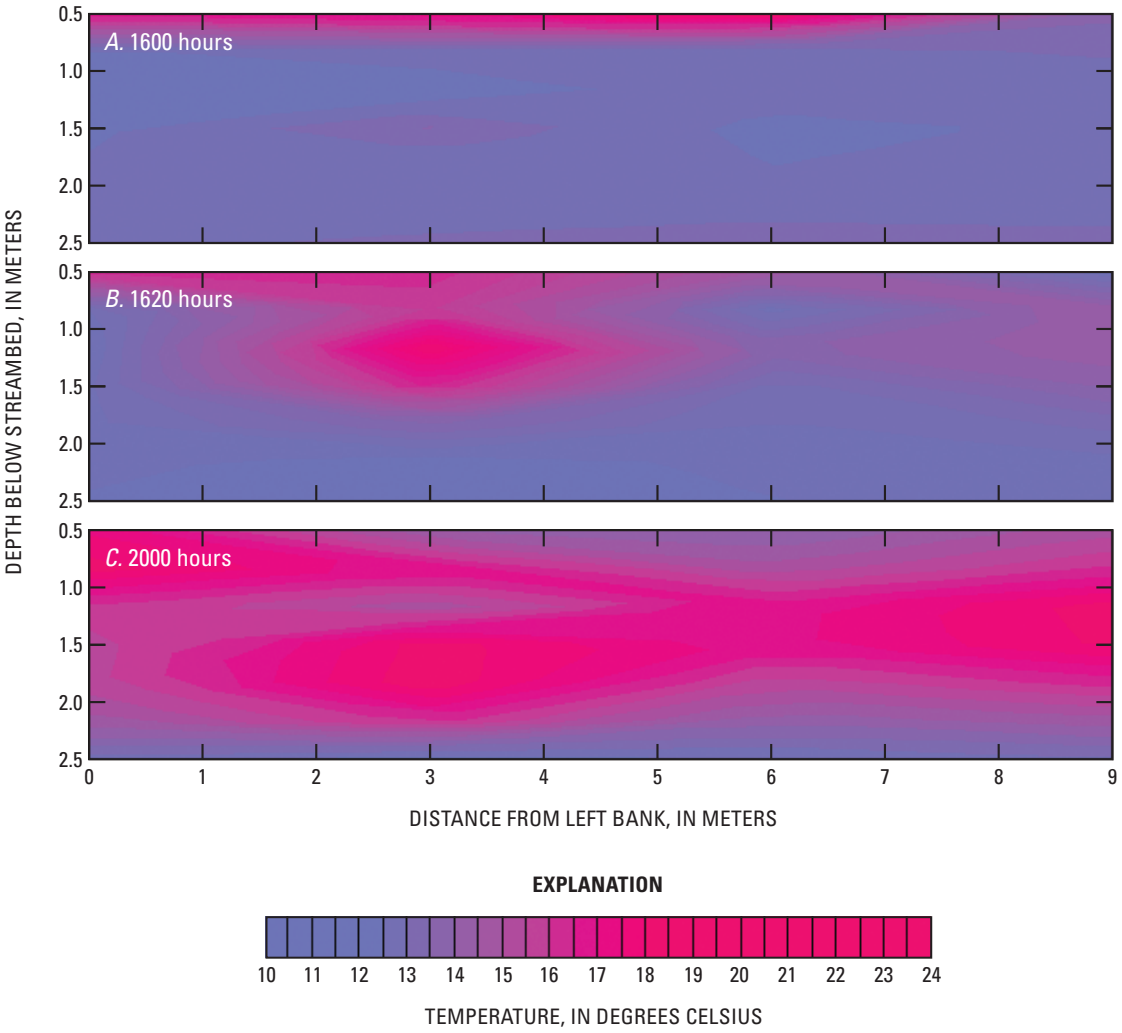

Figure 16. Two-dimensional distribution of temperature during different streamflow conditions in Rillito Creek on September 10, 2000, near Dodge Boulevard, Pima County, Arizona. *A*, Thermal transport through conduction before the onset of streamflow; *B*, thermal transport through a combination of advection and conduction at the onset of streamflow exhibiting multidimensional flow through the sediments; *C*, combined advection and conduction thermal transport to the deeper sediments several hours after the onset of streamflow.

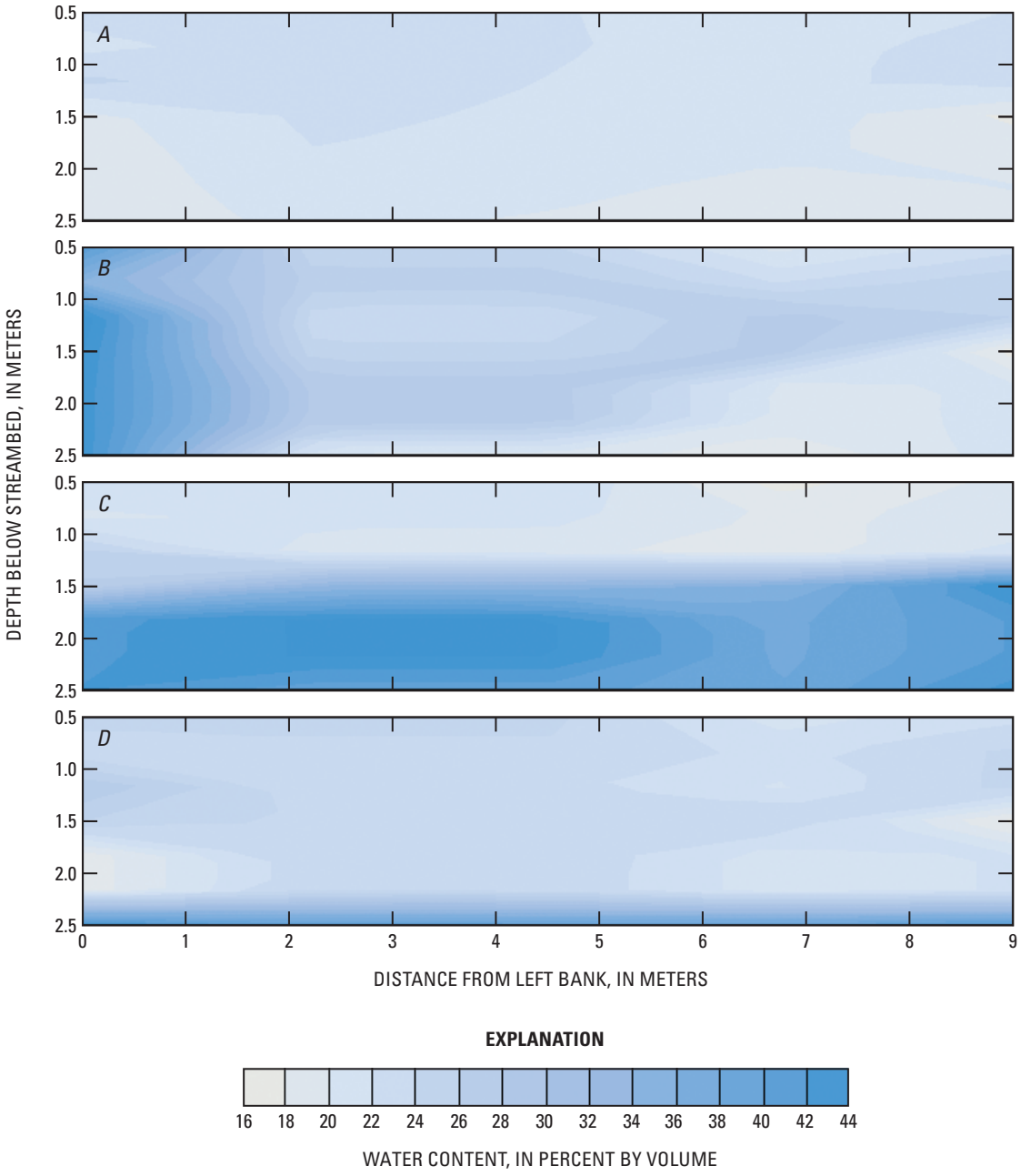

Figure 17. Two-dimensional plot of soil-water content during different streamflow conditions in Rillito Creek near Dodge Boulevard, Pima County, Arizona; *A*, Before the onset of streamflow, September 10, 2000, at 1600; *B*, 5 minutes after the onset of streamflow, September 10, 2000, at 1605; *C*, immediately after the cessation of streamflow September 12, 2000; *D*, approximately 2 days after the cessation of streamflow, September 14, 2000.

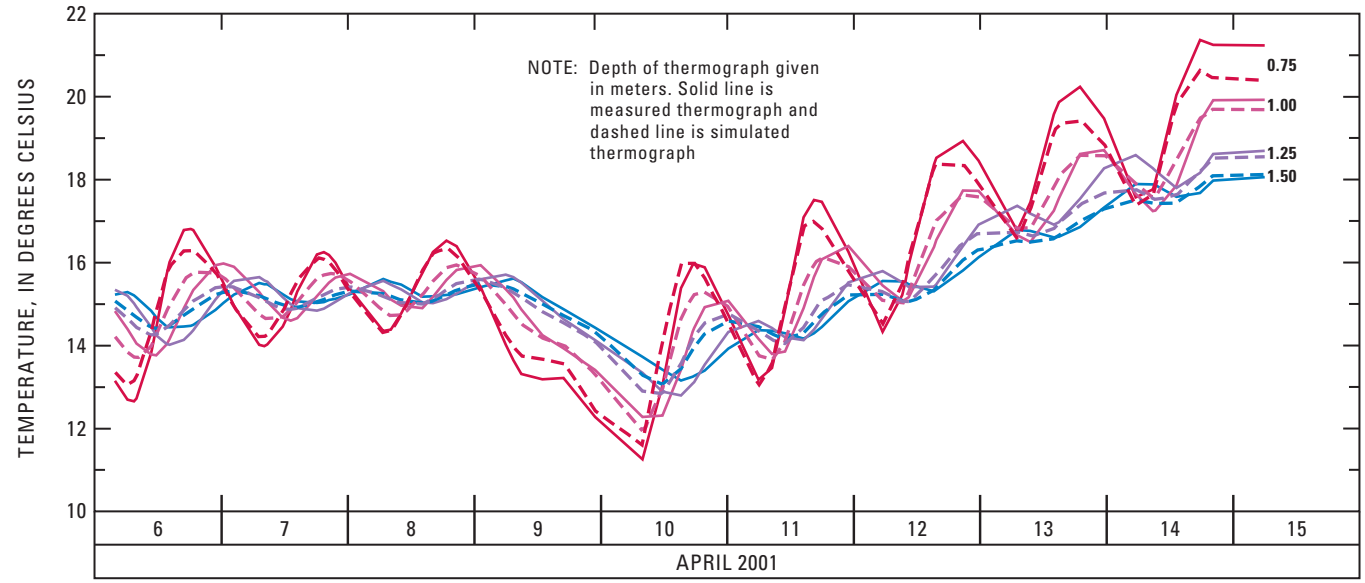

Figure 18. Typical measured and simulated thermographs from two-dimensional temperature array from column 1 (see fig. 1 for column location) in Rillito Creek near Dodge Boulevard, Pima County, Arizona.

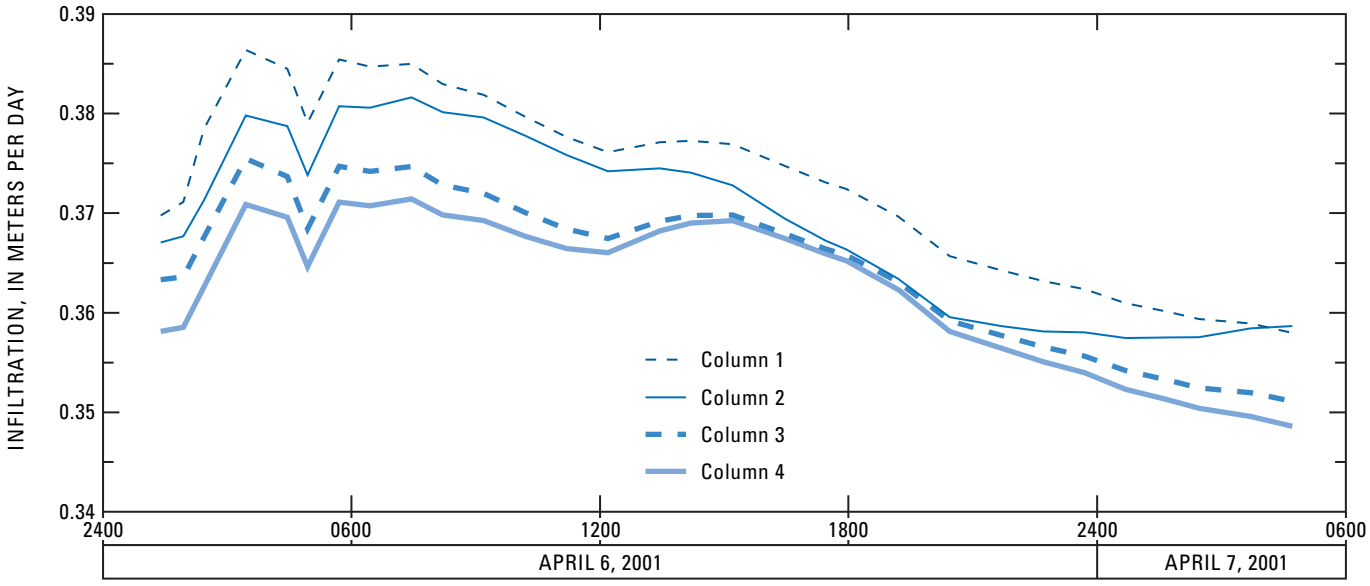

Figure 19. Simulated infiltration rates during period of flow at the two-dimensional temperature array near Dodge Boulevard, Pima County, Arizona.

The general agreement in infiltration estimates among these independent temperature and water-content methods indicates that these methods provide accurate estimates of infiltration. As such, vertical arrays of temperature probes can be located along stream reaches to estimate the potential for in-stream recharge and to provide guidance on citing recharge facilities. High infiltration rates at shallow depths, however, are not sufficient to ensure that water will percolate to deeper depths and recharge the deep aquifer at a high rate. Infiltration rates determined from shallow measurements should be considered an upper limit of the potential recharge rate for a particular site.

Water-Level Responses

Piezometer nests were installed in the stream-channel boreholes and monitored for water-level variations in response to streamflow. Nested piezometers included one shallow piezometer completed in what is usually the unsaturated zone,

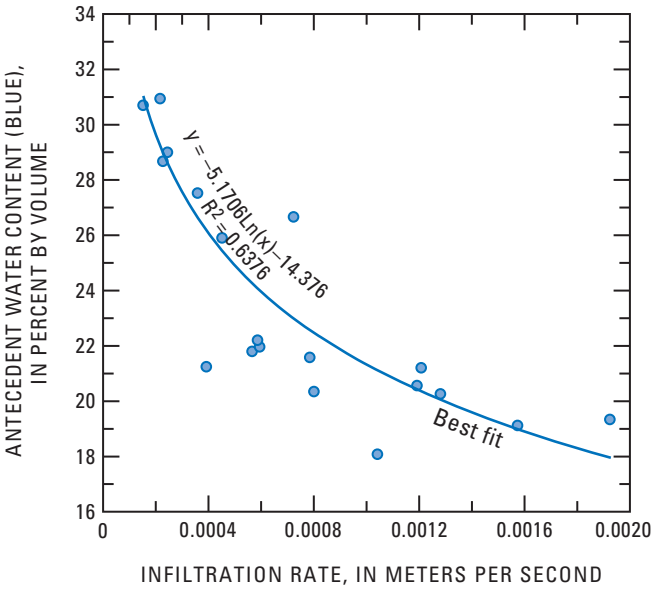

Figure 20. Correlation of onset infiltration rate to antecedent water content.

near the contact between the recent stream-channel alluvium and the basin-fill deposits, and a pair of deep piezometers—one near the water table and one about 10 m below the water table. With the exception of the piezometer near Craycroft Road, the shallow piezometers generally were dry except shortly after streamflow (fig. 21) and contained water for periods of days to several weeks. The magnitude of water-level variation and the period of time the shallow wells contained water varied. For instance, the water level in the shallow piezometer near Dodge Boulevard varied the least (usually less than 1 m), whereas the water level in the shallow piezometer near La Cholla Boulevard varied the most (usually between 6 and 7 m); water-level variations in the shallow piezometer near First Avenue were usually between 2 and 6 m. Duration in which the water level remained above the bottom of the piezometer was longest in the piezometer near La Cholla Boulevard where saturation persisted for 6 months after the summer 1999 streamflow and 12 months after the winter 2000 streamflow; saturation time was shortest at the shallow piezometer near Dodge Boulevard where it was typically less than 2 months (fig. 21). The long duration of saturation at the shallow piezometer near La Cholla Boulevard probably was due to the fine-grained unit at depth of about 12 to 30 m (Hoffmann and others, 2002).

Water levels in each of the pairs of deep piezometers responded several days to weeks later than the shallow piezometers and generally after the shallow piezometers became dry. There were little to no vertical gradients measured in the pairs of deep piezometers. These responses suggest gravity flow predominates, and that no hydraulic connection is established between streamflow and the underlying deep aquifer. Given the low-permeability of the basin-fill deposits, relative to that of the stream-channel deposits, it also is likely that temporary perched conditions existed near the contact between these two units for a period of several days to weeks after cessation of streamflow.

Water levels in the deep piezometers showed an overall decline during the period of investigation. Water-level declines between spring 1999 and summer 2002 ranged from about 2 m at the deep piezometer near Craycroft Road, to 8 m at the deep piezometer near Dodge Boulevard (fig. 21). The declines probably are related to ground-water pumpage from the basin-fill aquifer. Superimposed on the declines are a series of rises that range from about 0.5 to 3.9 m. These rises are in response to the two most significant streamflow periods that occurred in summer 1999 and fall/winter 2000.

The initial response of the water table in the deep piezometers lags the onset of streamflow by about 2 weeks at the piezometer nests near Dodge Boulevard and near First Avenue, whereas the initial response of the water table at the piezometer nests near Craycroft Road and near La Cholla Boulevard is more rapid—within about a day of streamflow in summer 1999. Lag time for the initial response at the piezometers near Dodge Boulevard and near First Avenue is related to the presence of a thick unsaturated zone at these sites. The short lag time between the onset of streamflow and the initial water-table response could be related to factors such as preferential flow and uniformly high water content throughout the unsaturated zone (Hoffmann and others, 2002). The occurrence of preferential flow is supported by the rapid response of the water table to streamflow despite the presence of the fine-grained unit.

Timing of the water-level peak also varies with location, and the peak occurs several weeks to months after the onset of streamflow. The longest lag time for the peak occurs near La Cholla Boulevard where it was about 7 months. Dissipation to prerecharge-event water levels also required several months at each site (fig. 21).

The magnitude of the water-table response in the deep piezometers is greatest at the piezometer nests near Dodge Boulevard and First Avenue. The water-table response in the piezometer nest near Craycroft Road is reduced relative to the water-table responses near Dodge Boulevard and First Avenue. Shallow piezometers near Craycroft Road indicate the water table often reaches land surface during streamflow events; therefore, the reduced water-level response probably is related to rejected recharge. The magnitude of the water-table response at the piezometer nest near La Cholla is the smallest and is related to a smaller recharge rate related to less frequent and smaller streamflows near La Cholla, relative to the other sites, and the presence of the fine-grained layer in the unsaturated zone. The lack of vertical gradients between the middle and deep piezometers at each nest indicates flow is predominantly horizontal in the saturated zone, except in the piezometer nest near Craycroft Road where the vertical gradient averages about 0.1m/m.

A series of recharge estimates were calculated on the basis of the water-level responses using an analyti-

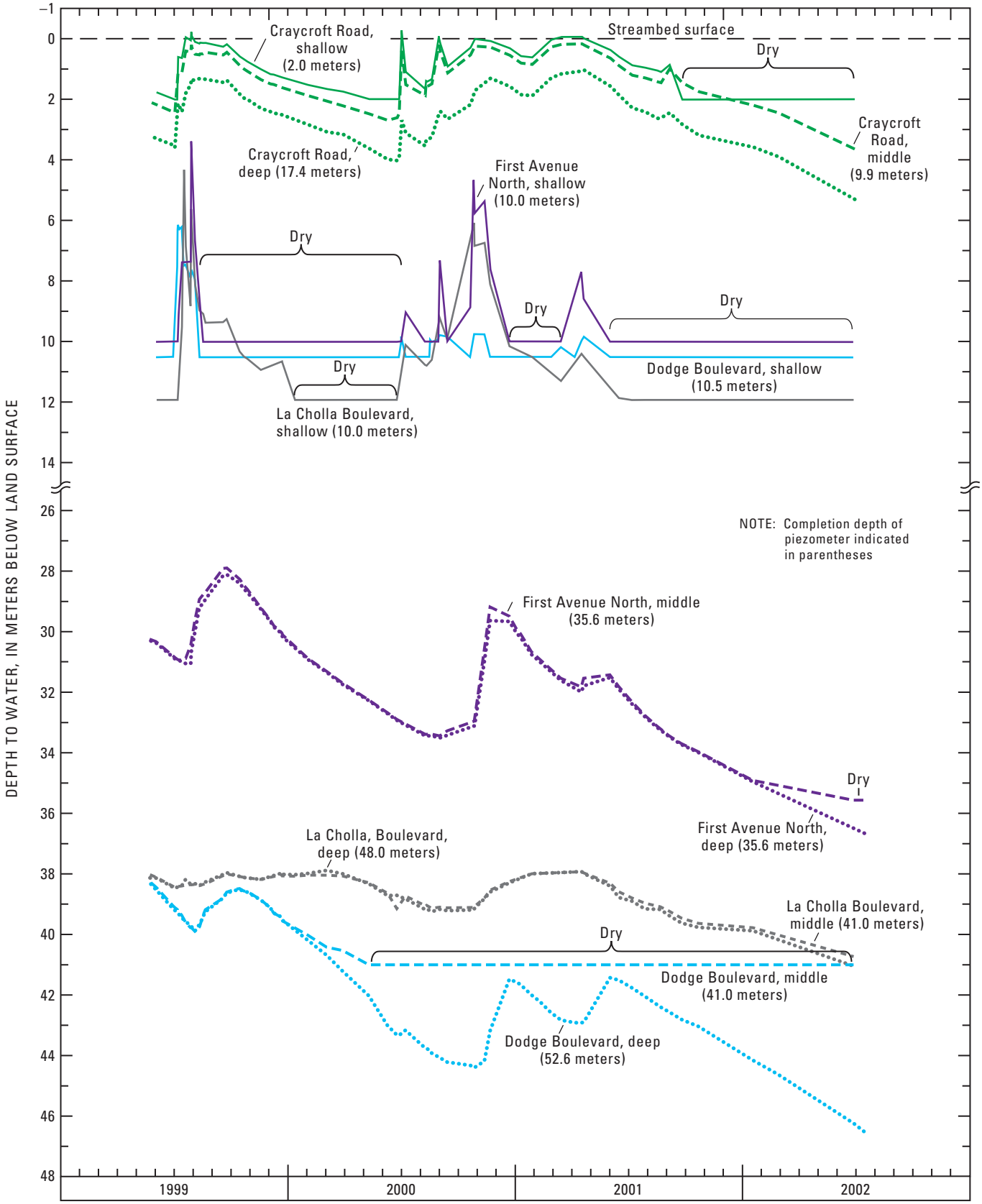

Figure 21. Hydrographs of selected piezometers within Rillito Creek, Pima County, Arizona.

cal approach developed by Moench and Kisiel (1970). In this analytical model, changes in water levels over time near an ephemeral-stream channel are assumed to reflect actual recharge. This is advantageous in that no information or assumptions regarding unsaturated-zone processes are required in order to make the calculations.

For any given streamflow event, a certain amount of water may recharge the aquifer and thereby cause water levels in nearby wells to rise. The water-level rise results in a mound that slowly dissipates normal to the line source. Subsurface sediments will act to slow the dispersal. The variation in rate and duration of recharge can thus be viewed as an input function, the aquifer as a filter or impulse-response function, and the water levels as output. The variation in the rate and duration of recharge can be calculated from a combination of water-level data and the impulse-response function, which is derived from parameters of aquifer geometry, aquifer storage, and hydraulic properties, using the groundwater flow equations. By summing these rates of recharge for the time period being studied, the volume of water recharged can be determined.

Various assumptions about the aquifer flow-system are required to implement the analytical model deveolpoed by Moench and Kisiel (1970). Flow is assumed to be one dimensional and horizontal. The aquifer is assumed to be homogeneous and isotropic, to be infinite in horizontal extent, and to receive recharge from a finite width source. Aquifer characteristics are assumed to be invariant with time and water-level fluctuations.

Input to the model includes temporal variations in water levels, channel width, distance of the well from the center of the stream channel, specific yield, and transmissivity. The output is recharge calculated as cubic meters per second per linear kilometer of stream channel ($m^3/s/km$) over the period of record. Variations in measured water levels were assumed to be recharge events superimposed upon a generally declining water table. In order to find the amount of water recharged without the bias of the decline, the data were detrended (fig. 22). Detrending consisted, first, of calculating the trend in the data using a linear regression. This trend was then removed from the data under the assumption that all other deviations from a constant water level were caused by recharge. The period of record for the recharge calculations was based on the time required for the water-level response to return to prerecharge levels; therefore, the period of record includes both the rise in water level associated with recharge and the dissipation of the water level. A specific yield of 0.15 was used on the basis of measurements made by Pool and Schmidt (1997). Bounding transmissivities of 1.6×10^{-3} and 6.5×10^{-3} m^2/s estimated from Hanson and Benedict (1994) were used to show the uncertainty in the recharge values. The only difference between input data for the various sites was the individual water-level records and the distance of the well from the stream channel (to which the model showed little sensitivity in comparison with its sensitivity to transmissivity).

Recharge estimates were calculated for the sites near Dodge Boulevard, First Avenue, and La Cholla Boulevard for the recharge events of 1999 and 2000. The recharge event in 1999 was caused by summer streamflows, whereas the recharge event in 2000 was due predominantly to fall and winter streamflows and only partly to summer flows (table 1). The site near Craycroft Road was excluded from this analysis because the presence of vertical water-level gradients violated the assumptions of the analytical model. The largest cumulative recharge estimates for the 1999 event at the site near First Avenue range from 3.0×10^5 to 6.0×10^5 m^3/km, which is about two to three times larger than those from the other two sites (near Dodge Boulevard, 1.7×10^5 to 3.4×10^5 m^3/km; near La Cholla Boulevard, 1.3×10^5 to 2.5×10^5 m^3/km; table 2). Cumulative recharge estimates for the 2000 recharge event were greatest at the site near Dodge Boulevard and decreased in the downstream direction. At the site near Dodge Boulevard, recharge estimates range from 7.1×10^5 to 1.4×10^6 m^3/km, which are slightly larger than those estimated at the site near First Avenue (5.3×10^5 to 1.1×10^6 m^3/km) and about three times larger than those estimated at the site near La Cholla Boulevard (2.2×10^5 to 4.3×10^5 m^3/km). The recharge estimates for the 2000 event at the sites near First Avenue and near La Cholla Boulevard were about twice those for the 1999 event at these sites and were more than five times that of the 1999 event at the site near Dodge Boulevard. The trends revealed in this analysis are consistent with the fact that the winter 2000 streamflows were more voluminous and longer in duration than the summer 1999 streamflows (table 1), and that water levels in the piezometers rose higher in response to the winter 2000 streamflows than to the summer 1999 flows (fig. 21).

Volumetric recharge rates were estimated by dividing the cumulative-recharge estimates by the cumulative duration of streamflow at each site during the period of record. Streamflow duration at the streamflow-gaging station at Dodge Boulevard totaled about 9 days between July 1, 1999 and September 30, 1999, whereas streamflow duration at streamflow-gaging station 09486055, near La Cholla Boulevard, for the same period totaled about 4.5 days. No streamflow-gaging station existed near First Avenue; however, in this analysis, a total of about 7 days of cumulative flow was assumed to have occurred at the site near First Avenue during 1999—a duration less than that at the upstream gage, at Dodge Boulevard, and greater than that at the downstream gage, near La Cholla Boulevard. Using the values of estimated cumulative-recharge determined using the Moench and Kisiel (1970) method and of cumulative-streamflow duration, recharge rates range from 0.2 to 1.0 $m^3/s/km$ for 1999 (table 2). During the period of June 15 to December 31, 2000, a span that includes most of the streamflow for the second recharge period, cumulative-streamflow duration ranged from a high of 43 days at the streamflow-gaging station at Dodge Boulevard, to a low of 14 days at the streamflow-gaging station near La Cholla Boulevard. In this analysis, a flow duration of 30 days was assumed to have occurred at the site near First Avenue. Using these values, volumetric-recharge rates range from 0.2 to 0.4 $m^3/s/km$ for 2000 (table 2). These rates are generally greater than volumetric-infiltration estimates

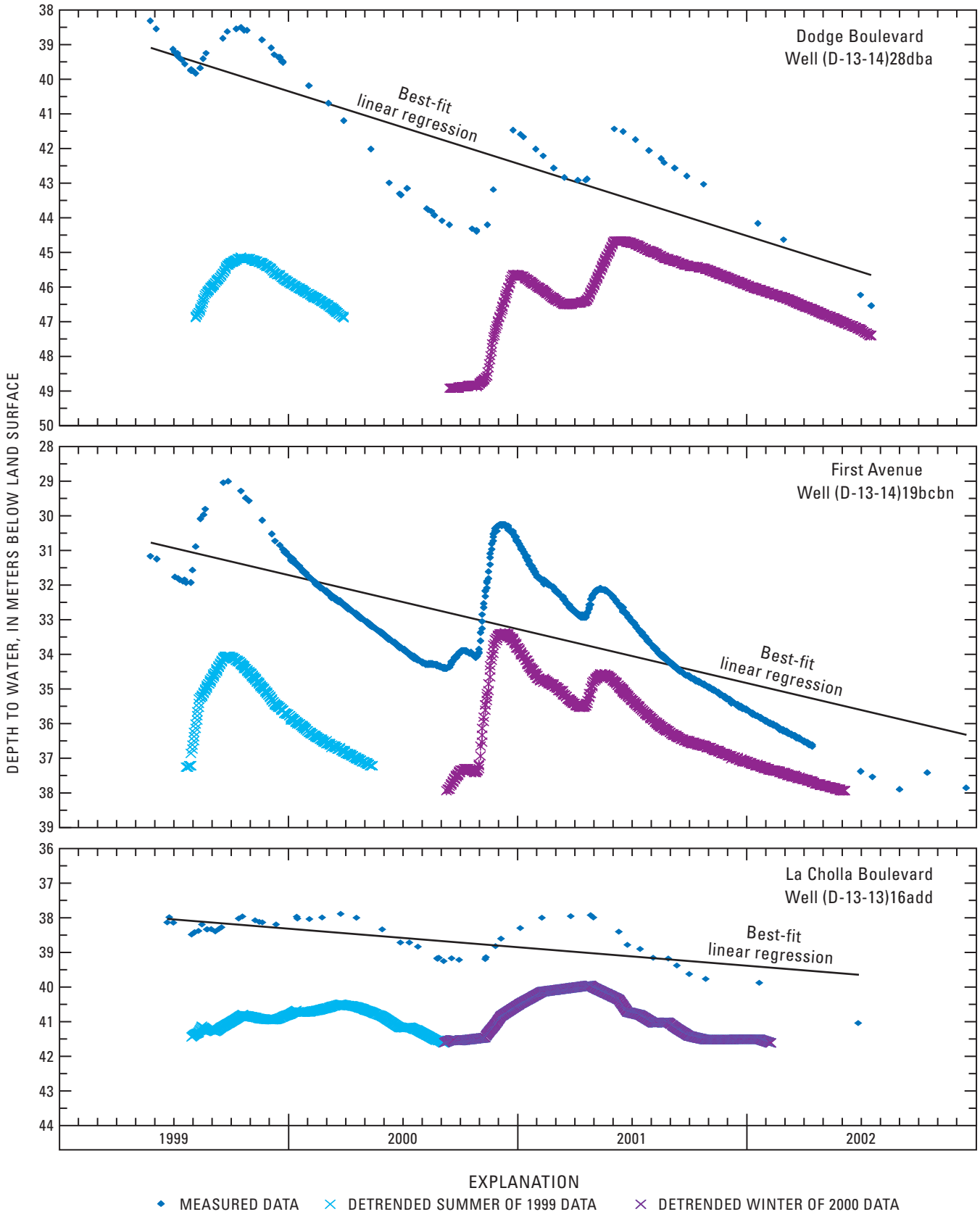

Figure 22. Measured and detrended hydrographs of selected piezometers within Rillito Creek, Pima County, Arizona.

Table 2. Recharge estimates for sites in Rillito Creek, Pima County, Arizona, using the Moench and Kisiel (1970) analytical-model method.

[m^2/sec, square meters per second; m^3/km, cubic meters per kilometer; m^3/s/km, cubic meters per second per kilometer]

Site location	Distance of well from center of Rillito Creek channel, in meters	Recharge	1999		2000	
			Transmissivity = 1.6×10^{-3} m^2/s	Transmissivity = 6.5×10^{-3} m^2/s	Transmissivity = 1.6×10^{-3} m^2/s	Transmissivity = 6.5×10^{-3} m^2/s
Dodge Boulevard	3	Length of recharge period, in days[1]	9		43	
		Total, in m^3/km	1.7×10^5	3.4×10^5	7.1×10^5	1.4×10^6
		Rate, in m^3/s/km	0.2	0.4	0.2	0.4
First Avenue	45.7	Length of recharge period, in days[1]	7		30	
		Total, in m^3/km	3.0×10^5	6.0×10^5	5.3×10^5	1.1×10^6
		Rate, in m^3/s/km	0.5	1	0.2	0.4
La Cholla Boulevard	3	Length of recharge period, in days[1]	4.5		14	
		Total, in m^3/km	1.3×10^5	2.5×10^5	2.2×10^5	4.3×10^5
		Rate, in m^3/s/km	0.3	0.7	0.2	0.4

[1]Refers to the cumulative time streamflow existed in Rillito Creek. Streamflow durations were calculated using data from the streamflow-gaging stations near Dodge and La Cholla Boulevards.

made using temperature, water-content, and seepage-loss methods. Because infiltrated water can be stored in the shallow subsurface it is available for subsequent evaporation and (or) transpiration; therefore, infiltration rates typically provide an upper bound for recharge rates. Estimated recharge rates in excess of infiltration rates indicate unaccounted sources of water. These unaccounted sources likely are inputs from adjacent tributaries, many of which drain the pediment north of Rillito Creek.

Temporal Gravity Measurements

Ground-water storage was monitored along two gravity profiles across Rillito Creek at Swan Road (5-km length) and First Avenue (6.4-km length). The profiles included 11 gravity stations that are closely spaced near Rillito Creek and at wells where water levels are monitored (fig. 1). Gravity changes along both profiles after summer 1999 show that increases in ground-water storage were primarily within the flood plain coincident with the stream alluvium (fig. 23). Gravity increases on the First Avenue profile were largest between these measurement dateswere at the station nearest Rillito Creek. The largest increase between June 199 and August 1999 was 48 microgals, which is equivalent to about 1.1 m of water, assuming the mass change occurs within a horizontal slab of infinite extent. Gravity increase on the Swan Road profile also was largest between the June 1999 and August 1999 measurements at the station about 0.5 km south of Rillito Creek. The greatest change between these measurement dates was 42 microgals (equivalent to about 1 m of water). The gravity changes and associated water-level rises indicate that the highly permeable stream-channel and flood-plain deposits act as a ground-water reservoir that readily accepts infiltrated streamflow.

Estimates of recharge through infiltration along Rillito Creek were made by assuming the storage changes measured by gravity at each profile were equivalent to recharge and by integrating the two-dimensional gravity change for the length of the creek. Similar to that shown with water-level trends, the overall storage-change estimates during the period of study steadily declined with two periods of recharge superimposed on the longer-term rate of decline (fig. 24). The long-term storage decline shown in figure 24 is related to the dissipation of a water-table mound produced in 1998, from sustained flows related to the El Niño precipitation, and to ground-water pumpage from nearby public and private wells. The periods of increased storage that reduce the rate of long-term declines were associated with the summer 1999 and fall/winter 2000 streamflows (figs. 3 and 24). The increase in storage for the summer 1999 period is about 7.5×10^6 m^3 ; for the fall/winter 2000–2001 period it is about 11.1×10^6 m^3 for the 14-km reach between Craycroft Road and La Cholla Boulevard. Although measurable, these seasonal storage increases are small compared to the storage increases associated with the 1998 El Niño event, which were about 5×10^7 m^3 (fig. 24).

Assuming that the increases in storage measured in summer 1999 and fall/winter 2000–2001 were uniform throughout the 14-km reach between Craycroft Road and La Cholla Boulevard, they would equate to 5×10^5 m^3/km and

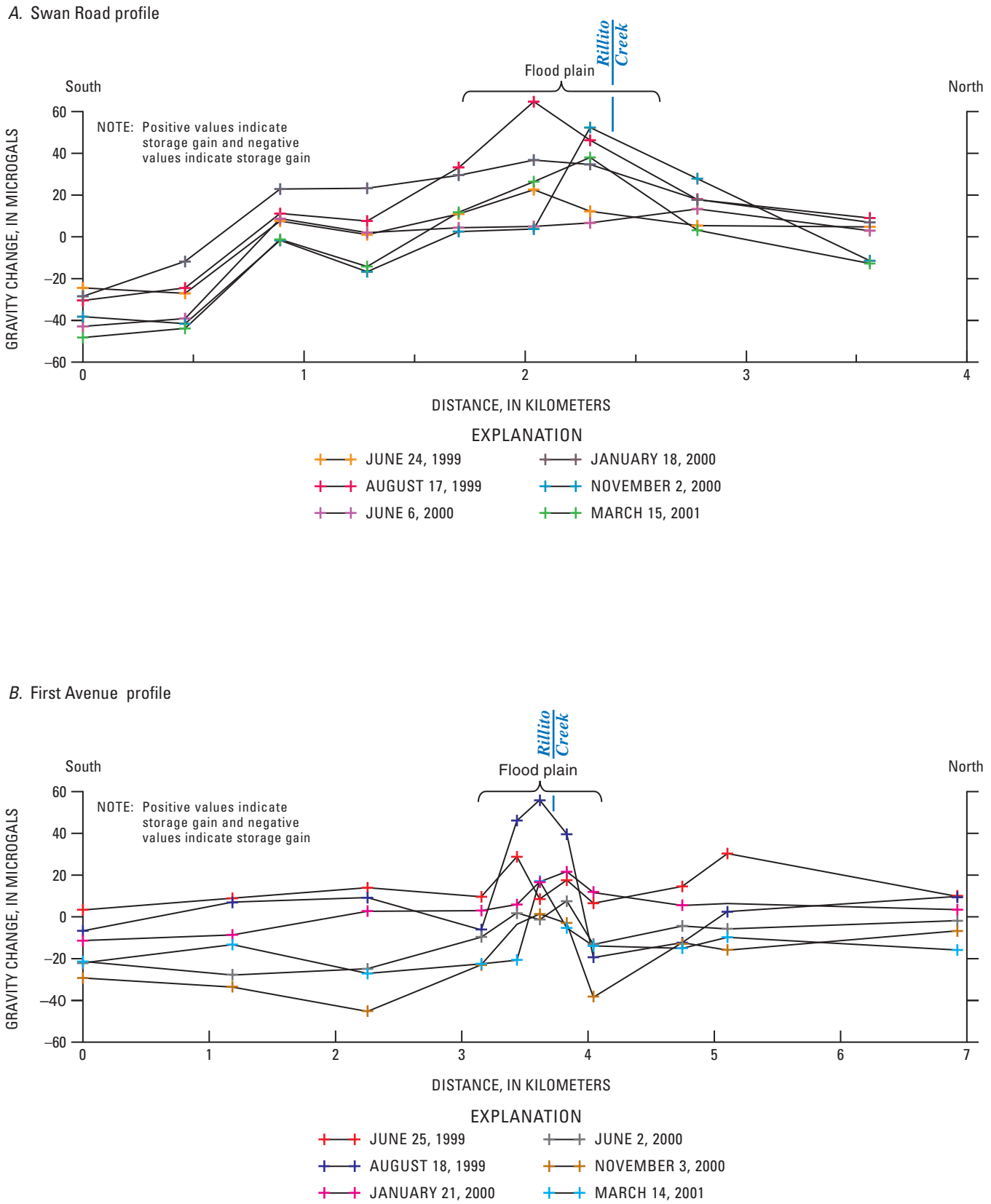

Figure 23. Gravity changes along profiles crossing Rillito Creek, Pima County, Arizona, since December 1997. *A*, Swan Road; *B*, First Avenue.

8×10^5 m^3/km, respectively. Using 7 days of flow (as estimated at First Avenue; table 2) for the summer 1999 event and 30 days of flow for the fall/winter 2000-2001 event, these recharge volumes equate to 0.9 m^3/s/km in the 1999 event, and 0.3 m^3/s/km in the 2000–2001 event.

These rates are generally similar to those estimated using water-level methods, yet greater than volumetric-infiltration estimates made using temperature, water-content, and seepage-loss methods. As discussed previously, recharge-rate estimates in excess of infiltration-rate estimates indicate unaccounted sources of water. These unaccounted sources likely are inputs from adjacent tributaries, many of which drain the mountain-front area north of Rillito Creek.

Two-dimensional simulations of the change in water distribution in the subsurface required to produce the change in gravity for the period June 24, 1999 to August 18, 1999, along both profiles are shown in figure 25. Simulations used GM-SYS software (version 4.6) developed by Northwest Geophysical Associates, Inc. The software calculates the gravity field response of polygonal features of variable subsurface density using the theory and algorithms of Talwani and others (1959), and Won and Bevis (1987). Simulation of the two-dimensional vertical polygons requires simplifying assumptions about the distribution of storage change in the third dimension, in this case along the stream channel, and at the margin of the simulated region. This application assumed the two-dimensional polygons of storage change extended in infinite length along the stream channel. Storage change in the crystalline rocks adjacent to the northern boundary of the aquifer was assumed to be insignificant. Storage change in the aquifer adjacent to the southern end of the profiles was assumed to extend laterally to an infinite distance. Each of these assumptions likely contributes little to no errors in the simulation. Available water-level data and gravity-derived estimates of specific yield were used to constrain the vertical distribution of saturated storage change at many gravity-station wells. Gravity changes along the First Avenue profile are explained by a combination of higher water levels and increases in water content in the unsaturated zone. A 10-percent increase in unsaturated water content was required to match the observed gravity change at gravity stations near the channel. The resulting model (fig. 25*A*) resulted in simulation errors of less than 1 microgal at each station.

Simulation of gravity change along the Swan Road profile could be explained by storage change within the zone of water-level change: no changes in water content in the unsaturated zone were required. Increases in gravity at all stations along the Swan Road profile during June 24, 1999, to August 17, 1999, (fig. 25*B*) indicated that infiltration and recharge during the intervening period between gravity surveys resulted in storage increases within about 2 km of the stream channel. The greatest increases in gravity occurred at the two stations within about 0.5 km south of the channel. Gravity increases at stations farther from the channel ranged from 2 to 23 microgal. The resulting model (fig. 25*B*) resulted in simulation errors of generally less than 1 microgal at each station.

Summary and Conclusions

The amount of water currently recharging the aquifers within the Tucson area is insufficient to meet current and future demands. Resultant ground-water deficits are manifested in water-level declines of more than 60 m since the middle of the twentieth century. The accurate determination of recharge is critical to establishing a sustainable water budget on the basin scale. In semiarid regions, recharge beneath ephemeral-stream

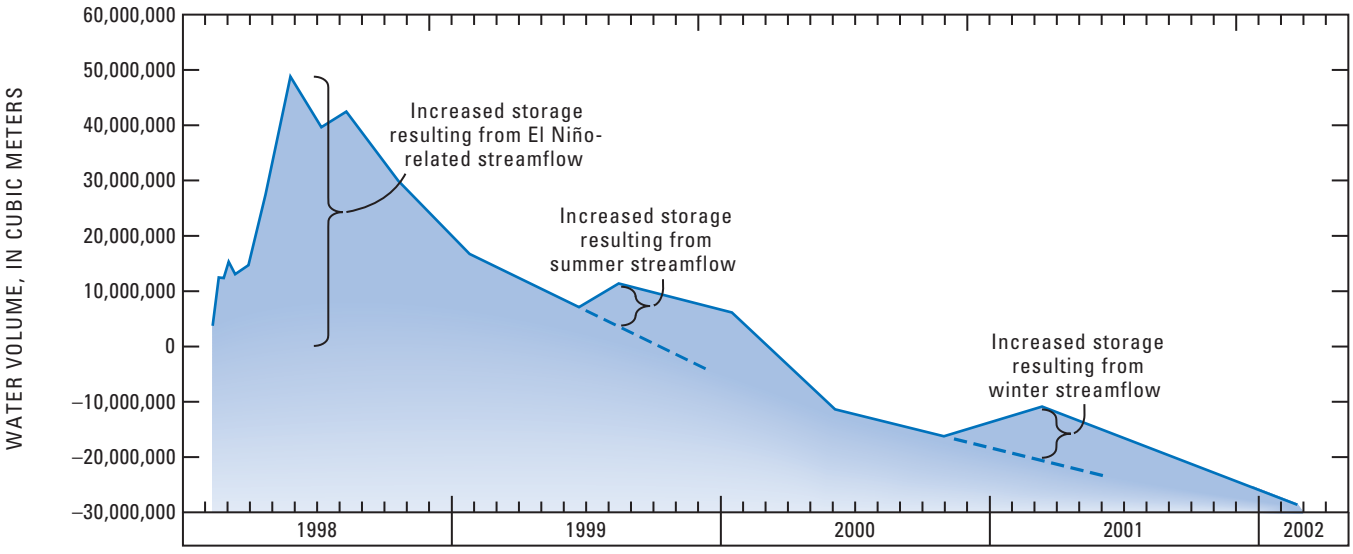

Figure 24. Storage changes measured along Rillito Creek, Pima County, Arizona, from Craycroft Road to La Cholla Boulevard relative to a measurement made in December 1997.

channels typically represents a major component of the total recharge. Improved understanding of streambed infiltration and the subsequent redistribution of water within the unsaturated zone is fundamental to quantifying and forming an accurate description of streambed recharge.

One of the challenges of quantitatively studying recharge beneath ephemeral-stream channels is the need to integrate measurements made over a wide range of spatial and temporal scales. No single method of measurement or analysis can resolve the complex physical processes that contribute to infiltration, percolation, and recharge beneath these channels; therefore, various approaches that provide a wide range of temporal and spatial scale measurements of recharge beneath Rillito Creek were used in this study. The approaches discussed in this chapter included analyses of cores and cuttings for hydraulic and textural properties, environmental tracers from the water extracted from the cores and cuttings, seepage measurements made during sustained streamflow, heat as a tracer and numerical simulations of the movement of heat through the streambed sediments, water-content variations within a two-dimensional array, water-level responses to streamflow in piezometers within the stream channel, and gravity changes in response to recharge.

The amount of water flowing in Rillito Creek, and therefore the amount available for ground-water recharge, is primarily related to precipitation frequency, distribution, and intensity, as well as to streamflow and basin/channel runoff characteristics. The temporal distribution of flow in ephemeral streams is highly varied. Because of this, estimating or predicting recharge rates for ephemeral-stream channels on the basis of limited temporal observations is particularly difficult. This investigation extended from 1999 through most of 2002 and represented a time of lower than average precipitation and streamflow on the basis of data from the previous 30 years. Estimates of cumulative infiltration and recharge during this study period may differ from long-term averages; however, estimates of infiltration and recharge rates for streamflow events during the study period can be extrapolated to a variety of climatic conditions.

In order for ephemeral streamflow within Rillito Creek to recharge the underlying aquifer, the water must first infiltrate into the stream-channel deposits and percolate downward through the underlying deposits. The ability of water to infiltrate and percolate through these deposits is a function of the availability of streamflow and the hydraulic properties of the deposits. Study results indicate that the ver-

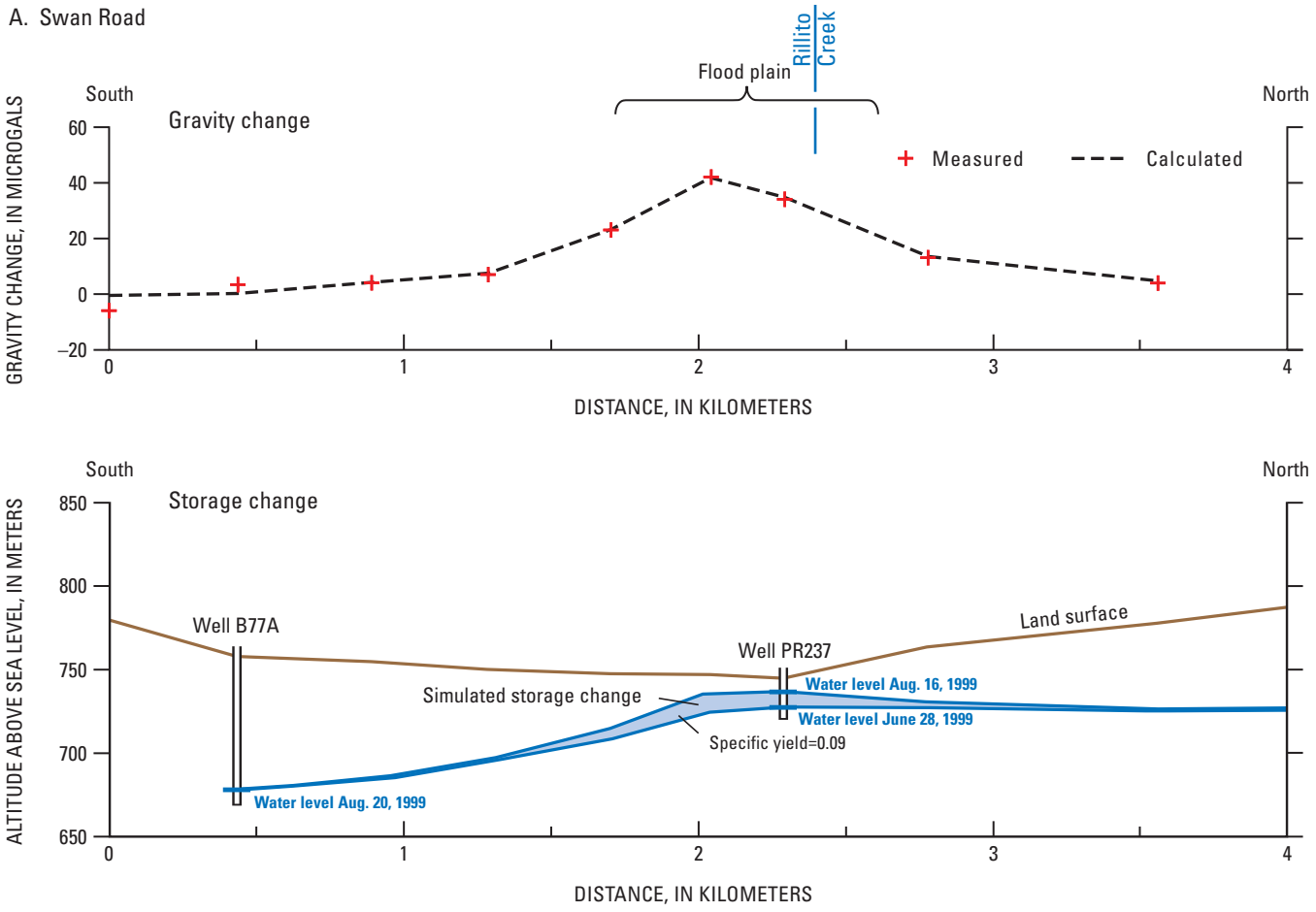

Figure 25. Gravity-model results for profiles crossing Rillito Creek, Pima County, Arizona. *A*, Swan Road; *B*, First Avenue.

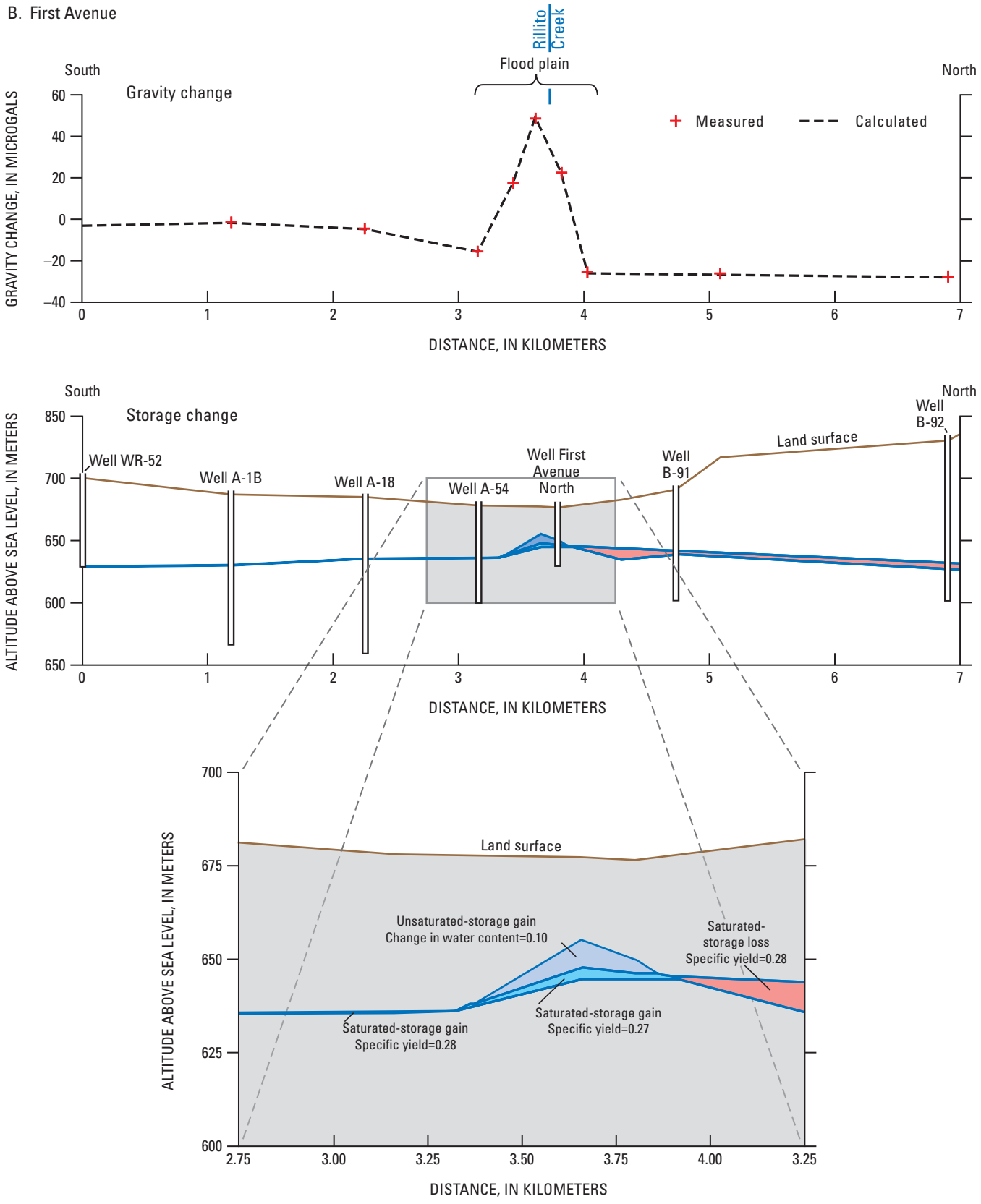

Figure 25.—Continued.

tical hydraulic conductivity of the stream-channel deposits ranges from 0.3 to 2.5 m/d, whereas hydraulic conductivity of the the basin-fill deposits ranges from 0.012 to 0.61 m/d. For heterogeneous media, such as the deposits beneath Rillito Creek, the equivalent vertical hydraulic conductivity is calculated as the harmonic mean of the Ksat for each textural layer within the deposits. Although differing at each borehole, the overall average equivalent saturated hydraulic conductivity of the stream-channel deposits is 1.2 m/d; the overall average equivalent saturated hydraulic conductivity of the basin-fill deposits is 0.19 m/d; and the equivalent hydraulic conductivity of the stream-channel and basin-fill deposits together is about 0.23 m/d (table 3). Assuming no preferential flow occurs and unit gradient conditions, these equivalent vertical hydraulic conductivity values provide an estimate of long-term potential recharge rates under saturated conditions. To convert these values into potential recharge volumes, assumptions of flow duration and average wetted perimeter and length must be made. For example, using an annual cumulative flow duration of 36 days per year for Rillito Creek, an average wetted perimeter of 20 m and a wetted length of 20 km, yields an annual volumetric recharge of 4.3×10^6 m^3/y, which is about two-thirds of the commonly reported long-term average recharge of 6×10^6 m^3/y (Hanson and Benedict, 1994).

Environmental tracers were used to evaluate spatial variations in infiltration and recharge patterns along Rillito Creek and estimate percolation rates through the unsaturated zone. Tritium was detected in pore water extracted from all core samples and ranged from 2 to 11 TU, indicating that water in the unsaturated zone infiltrated during the past 40 years. Given the presence of tritium in the unsaturated zone, the locally high vertical hydraulic conductivity values greater than 1 m/d in the stream-channel deposits, and a depth to the water table of generally less than 40 m, it is likely that most of the pore water extracted from the cores infiltrated during runoff events in the past few years. Variations in isotopic compositions of ground water beneath Rillito Creek are attributed to changes in the compositions of the source water and to evaporation. The lack of an evaporative signal for some samples indicates that percolating water was exposed to minimal evaporation.

Isotopic ratios measured in the pore water during the study are representative of the isotopic ratios in the infiltrating waters of the recent past. Isotopic ratios in Rillito Creek pore water become lighter in the downstream direction indicating that for the time period represented by the unsaturated-zone pore water, the longer duration and isotopically lighter winter storms were more important contributors to infiltration in the downstream reaches than in the upstream reaches. The trends in isotopic ratios measured in the pore-water cores approximately match the trends in ratios in the basin precipitation from particular storms during the year prior to drilling. Correlation between the precipitation events and depths of infiltration, on the basis of corresponding isotopic signatures, indicates an average vertical-percolation rate of approximately 0.049 m/d at the Dodge Boulevard borehole site (table 3). Chloride concentrations in pore-water leachate determined from drill cuttings varied substantially through the upper 18 m at all sites. Below about 18 m, variation in chloride concentration declined considerably. This zone of smaller variation is interpreted as corresponding to the infiltration depth of the 1998 El Niño water. The low variability and low mean value of chloride concentration is attributed to a constant supply of runoff having a low chloride concentration. In addition, the low chloride concentration indicates the water had little exposure to evaporation. The higher variability and concentration observed in post-El Niño pore water above 18 m likely is due to mobilization of chloride from evaporative concentrates and dry fallout deposited between precipitation events that resulted in runoff along a variety of surface-water flow paths. Calculation of a downward percolation rate using the El Niño event marker in the chloride profile yields an average percolation rate of 0.055 m/d (table 3). Although the estimates of recharge determined by hydraulic properties and environmental tracers required the assumption of no preferential flow, the water-level responses measured in the deep piezometers indicate that factors such as preferential flow likely influence recharge rates. Estimates made using these techniques, therefore, are likely representative of minimum values.

Infiltration rates are typically assumed to provide an upper bound for recharge rates. Infiltration rates were estimated using seepage-loss, temperature, and water-content methods. Seepage measurements made at several sites along Rillito Creek during the El Niño-related sustained flows of March through April 1998 and again on October 24, 2000, indicate that streamflow losses owing to infiltration along Rillito Creek ranged from 0.07 to 0.9 m^3/s/km and averaged 0.21 m^3/s/km (table 3). Streamflow losses were smallest in the upstream reaches. The losses in these reaches were attributed to a shallow water table and rejected recharge. Using a wetted perimeter of 25 m, which was the average width of the flow that occurred during October 2000, the calculated average infiltration rate is 0.7 m/d, (table 3) which is similar to the measured saturated hydraulic conductivity of the stream-channel deposits but more than an order of magnitude greater than percolation rates determined by tracers. The difference between the estimated infiltration and percolation rates probably is due to the variably saturated nature of the sediments. The near-surface stream-channel deposits are likely to be nearly saturated during streamflow and therefore are approaching their saturated hydraulic conductivity, whereas the deeper sediments are less saturated and will therefore have a lower hydraulic conductivity.

Infiltration-rate estimates made using temperature and water-content methods in this study are one dimensional; information on stream width and length are required to estimate volumetric rates from the infiltration estimates. Model simulations using streambed-temperature data indicate the likelihood of a thin surface layer having a low vertical

hydraulic conductivity at the site near Craycroft Road. The addition of this surface layer to the model domain resulted in a lowering of the simulated equivalent saturated hydraulic conductivity by four orders of magnitude from about 4 m/d to 3×10^{-4} m/d. The four orders of magnitude change is too large to result solely from changes in water viscosity owing to temperature changes. Given the tranquil flow conditions during the first modeled flow period near Craycroft Road, it is possible that the change resulted from the deposition of a fine-grained layer of sediment on the streambed surface. In fact, a thin layer of fine-grained material commonly was observed at the sites after small streamflows. Vertical hydraulic gradients measured in the nested piezometers at the site near Craycroft Road allowed for estimation of infiltration rates using simulated equivalent vertical saturated hydraulic conductivity. Vertical hydraulic gradients during and shortly after streamflow were typically 0.1 m/m. Estimated infiltration rates ranged from 0.09 $m^3/s/km$ during the period probably most representative of ephemeral-streamflow conditions. The infiltration rate of 0.09 $m^3/s/km$ (table 3) is about half of that estimated using seepage-measurement data. The difference between these methods is primarily the wetted-perimeter value used in the calculation. The seepage-measurement estimates used a wetted perimeter of 25 m that was based on measured stream width, whereas a wetted perimeter of 10 m was used for flows during the period modeled with the temperature method because flows during this period were smaller than those during the seepage measurements. If hydraulic conductivity and vertical gradient are assumed not to change with increasing wetted perimeter and these rates are extrapolated to a wetted perimeter of 25 m, infiltration rates estimated with the temperature method are 0.23 $m^3/s/km$—virtually the same that measured by the seepage-loss method.

Two-dimensional arrays of temperature and water-content sensors indicated that water-content measurements enable better estimates of rapid-infiltration rates associated with the onset of streamflow. Infiltration rates within the first few minutes after the onset of streamflow were as large as 166 m/d; however, saturation within the relatively homogeneous stream-channel deposits of Rillito Creek was established in less than 10 minutes and subsequent infiltration rates declined significantly. Simplified one-dimensional model simulations used to estimate infiltration as soon as the sediments were saturated indicate infiltration rates declined as streamflow duration increased and averaged 0.32 m/d for the 12-day event in April 2000 and 0.37 m/d for the 10-day event in November (table 3). The declining infiltration rate is attributed to a declining pressure head and (or) development of a thin fine-grained surface layer. On the basis of a wetted perimeter of 10 m, an average infiltration rate of 0.32 m/d equates to a flux of 0.04 $m^3/s/km$ (table 3).

Water levels in the stream-channel piezometers showed an overall decline during the period of investigation in relation to long-term records. The water-level decline probably is related to ground-water pumpage from the basin-fill deposits. Superimposed on the water-level decline is a series of water-level rises that range from about 0.5 to 3.9 m. These rises were in response to the two periods of greatest streamflow occurring in the summer of 1999 and the fall/winter of 2000. The water-level responses to streamflow were followed by gradual water-level dissipation.

Water-level responses were analyzed by using an analytical model to simulate cumulative recharge for the water-level rises measured in 1999 and 2000. The largest cumulative-recharge estimates for the 1999 event were for a piezometer site near the middle of the study reach and range from 3.0×10^5 to 6.0×10^5 m^3/km. This range is about two to three times as large as that for the other two sites. Estimates of recharge for 2000 were about two- to five-times that of the estimates for 1999. The trends revealed in this analysis are consistent with streamflow volumes and duration, and the magnitude of water-level changes that occurred in the piezometers in response to the streamflow. Cumulative-recharge estimates for the 2000 recharge event were greatest at the upstream-most site and decreased in the downstream direction. Recharge estimates for the upstream-most site range from 7.1×10^5 to 1.4×10^6 m^3/km; these values are slightly larger than those estimated for the middle-reach site and about three times greater than that estimated for the site farthest downstream. Recharge rates, estimated by dividing the cumulative-recharge estimates by the cumulative duration of streamflow, resulted in rates that range from 0.2 to 1.0 $m^3/s/km$ for 1999 and from 0.2 to 0.4 $m^3/s/km$ for 2000 (table 3).

Gravity methods used to estimate recharge through infiltration along Rillito Creek provide values similar to those made by using the water-level method. Both gravity- and water level-derived estimates, however, are higher than the infiltration-rate estimates made by using seepage, temperature, or water-content change methods. Typically, infiltration-rate estimates provide an upper bound for recharge-rate estimates as some of the infiltrated water is stored in the shallow subsurface and used by vegetation, or is subsequently evaporated. The relatively high estimates of recharge determined by the gravity and water-level methods compared to estimates of infiltration determined by use of the seepage, temperature, and water-content methods probably is due to recharge from ungaged tributaries. The ungaged tributaries provide additional wetted perimeter and channel length not accounted for in the recharge estimates made by using the seepage, temperature, and water-content methods.

Table 3. Summary of methods used and estimated rates of infiltration, percolation, and recharge along Rillito Creek, Pima County, Tucson, Arizona.

[m/d, meters per day; m^3/s, cubic meters per second; m^3/yr, cubic meters per year]

Method	One-dimensional infiltration rate, m/d	Vertical percolation rate, m/d	Volumetric rate, m^3/s per kilometer of streamflow (wetted perimeter of 25 meters is used for temperature-method estimates)	Potential annual average recharge; assumes 36 days of flow in the 20 kilometer reach, m^3/yr	Comments
Physical: equivalent saturated hydraulic conductivity	0.23	Not calculated	Not calculated	4.1×10^6	From Darcy's Law the flow rate through the sediments under saturated conditions is equal to the product of the hydraulic conductivity and the hydraulic gradient. This method uses the average vertical equivalent saturated hydraulic conductivity of the combined stream-channel and basin-fill deposits multiplied by a unit gradient to estimate a recharge rate in meters per day.
Stable-isotope profiles	Not calculated	0.049	Not calculated	Not calculated	Method uses isotopic signatures associated with specific streamflow events and correlates pore water at depth with timing of introduction of water to unsaturated zone.
Chloride profiles	Not calculated	0.055	Not calculated	Not calculated	Method uses chloride concentrations associated with streamflow seasons and correlates pore water at depth with season (timing) water was introduced to unsaturated zone.
Seepage losses	0.75	Not calculated	0.07 to 0.9; average of 0.21	13.7×10^6	Method uses differences in streamflow measurements to calculate streamflow losses. Seepage losses represent infiltration rates in cubic meters per kilometer per second of streamflow. The one-dimensional rate (0.75 meter per day) was calculated by using the average (0.21 cubic meters per kilometer per second).
One-dimensional temperature modeling	0.8 to 1.0	Not calculated	0.23	14.3×10^6	Rates shown are representative of infiltration rates prior to the reduced rates simulated to occur owing to the accumulation of fine sediments on the streambed surface. One-dimensional rates are based on a modeled hydraulic conductivity of 4 to 5 meters per day and a measured vertical hydraulic gradient of 0.2.
Temperature data from two-dimensional trench	0.32 (April 2000) 0.37 (November 2001)	Not calculated	0.09	5.8×10^6	Temperature modeling results in vertical infiltration rates of 0.32 to 0.37 meters per day; drainage-rate measurements after cessation of streamflow result in a vertical velocity of 0.46 meters per day.
Water level	Not calculated	Not calculated	0.2 to 1.0 for 1999; 0.2 to 0.4 for 2000–2001	Not calculated	Method uses an analytical solution to simulate recharge on the basis of a hydrograph response. Volumetric rates represent recharge rates for the period of streamflow in respective years.
Gravity integrated from Craycroft Road to La Cholla Boulevard	Not calculated	Not calculated	0.8 for 1999; 0.3 for 2000–2001	Not calculated	Method uses ground-water storage changes measured at Swan Road and First Avenue, and extents the storage changes upstream to Craycroft Road and downstream to La Cholla Boulevard. An average flow duration listed in table 2 is used to estimate the rate.

References Cited

Anderson, S.R., 1987, Cenozoic stratigraphy and geologic history of the Tucson basin, Pima County, Arizona: U.S. Geological Survey Water-Resources Investigations Report 87–4190, 20 p.

Anderson, S.R.,1988, Potential for aquifer compaction, land subsidence, and earth fissures in the Tucson basin, Pima County, Arizona: U.S. Geological Survey Hydrologic Investigations Atlas HA-713, 3 sheets, scale 1:250,000.

Anderson, T.W., Freethey, G.W., and Tucci, Patrick, 1992, Geohydrology and water resources of alluvial basins in south-central Arizona and parts of adjacent states: U.S. Geological Survey Professional Paper 1406-B, 67 p.

Bailey, M. A., 2002, Analysis of vertical hydraulic conductivity using heat as a tracer to estimate streambed infiltration in Rillito Creek, Tucson: University of Arizona, master's thesis, 158 p.

Blasch, K.W., Ferré, T.P., Hoffmann, J.P., Cordova, J.T., 2003, Field measured infiltration fluxes at the onset of ephemeral streamflow, EOS Transactions American Geophysical Union, v. 82, no. 47. p. F674.

Burkham, D.E., 1970, Depletion of streamflow by infiltration in the main channels of the Tucson basin, southeastern Arizona: U.S. Geological Survey Water-Supply Paper 1939-B, 36 p.

Clark, I.D. and Fritz, Peter, 1997, Environmental isotopes in hydrogeology: Boca Raton, Florida, CRC Press LLC, 328 p.

Craig, Harmon, 1961, Isotopic variations in meteoric waters: Science, v. 133, p. 1702–1703.

Constantz, J.E., Tyler, S.W., and Kwicklis, Ed, 2003, Temperature-profile methods for estimating percolation rates in arid environments: Vadose Zone Journal, v. 2, p. 12–24.

Davidson, E.S., 1973, Geohydrology and water resources of the Tucson basin, Arizona: U.S. Geological Survey Water-Supply Paper 1939-E, 81 p.

Driscoll, F.G., 1986, Groundwater and wells, 2nd ed.: St. Paul, Minnesota, Johnson Division, 1108 p.

Epstein, Samual, and Mayeda, T.K., 1953, Variations of ^{18}O content of waters from natural sources: Geochimica et Cosmochimica Acta, v. 4, no. 5, p. 213–224.

Freeze, R.A., and Cherry, J.A., 1979, Groundwater: Englewood Cliffs, New Jersey, Prentice-Hall, Inc., 604 p.

Hammermeister, D.P., Blout, D.O., and McDaniel, J.C., 1986, Drilling and coring methods that minimize the disturbance of cuttings, core, and rock formations in the unsaturated zone, Yucca Mountain, Nevada, in Klute, A.L., ed., Proceedings of the National Water Well Association Conference on Characterization and Monitoring of the Vadose (Unsaturated) Zone, Worthington, Ohio, National Water Well Association, USA, p. 507–541.

Hanson, R.T., and Benedict, J.F., 1994, Simulation of groundwater flow and potential for land subsidence, Upper Santa Cruz Basin, Arizona: U.S. Geological Survey Water-Resources Investigations Report 93–4196, 47 p.

Healy, R.W., and Ronan, A.D., 1996, Documentation of computer program VS2DH for simulation of energy transport in variably saturated porous media-modification of USGS computer program VS2DT: U.S. Geological Survey Water-Resources Investigations Report 96–4230, 36 p.

Hoffmann, J.P., Ripich, M.A., and Ellett, K.M., 2002, Characteristics of shallow deposits beneath Rillito Creek, Pima County, Arizona: U.S. Geological Survey Water-Resources Investigations Report 01–4257, 51 p.

Katz, L.T., 1987, Steady state infiltration processes along the Santa Cruz and Rillito Rivers, Ph.D. dissertation, Tucson, University of Arizona, 119 p.

Matlock, W.G., 1965, The effect of silt-laden water on infiltration in alluvial channels, Ph.D. dissertation, Tucson, University of Arizona, 109 p.

Moench, A.F. and Kisiel, C.C., 1970, Application of the convolution relation to estimating recharge from an ephemeral stream: Water Resources Research, v. 6, no. 4, p. 1087–1094.

Pool, D.R., 1985, Aquifer geology of alluvial basins of Arizona, in. Anderson T.W., and Johnson A.I., eds., Regional Aquifer Systems of the United States, Southwest Alluvial Basins of Arizona: American Water Resources Associations Monograph 7, p. 25–36

Pool, D.R., and Schmidt, Werner, 1997, Measurement of ground-water storage change and specific yield using the temporal-gravity method near Rillito Creek, Tucson, Arizona: U.S. Geological Survey Water-Resources Investigations Report 97–4125, 30 p.

Revesz, Kinga, and Woods, P.H., 1990, A method to extract soil water for stable isotopic analysis: Journal of Hydrology, v. 115, p. 397–406.

Schwalen, H.C., and Shaw, R.J., 1957, Ground water supplies of Santa Cruz Valley of southern Arizona between Rillito Station and the international boundary: Tucson, University of Arizona, Agricultural Experiment Station Bulletin 288, 119 p.

Scott, R.L., Shuttleworth, W.J., Keefer T.O., and Warrick, A.W., 2000, Modeling multiyear observations of soil moisture recharge in the semiarid American Southwest: Water Resources Research, v. 36, no. 8, p. 2233–2247.

Smith, G.E.P., 1910, Groundwater supply and irrigation in the Rillito Valley: Tucson, University of Arizona, Agricultural Experiment Station Technical Bulletin 64, 244 p.

Tadayon, Saeid, Duet, N.R., Fisk, G.G., McCormack, H.F., Partin, C.K., and Rigas, P.D., 2000, Water resources data—Arizona, water year 1999, U.S. Geological Survey Water-Data Report, AZ–99–1, 370 p.

Talwani, Manik, Worzel, J.L., and Landisman, Mark, 1959, Rapid gravity computations for two-dimensional bodies with application to the Mendocino submarine fracture zone: Journal of Geophysical Research, v. 64, no. 1, p. 49–59.

Thatcher, L.L., Janzer, V.J., and Edwards, K.W., 1977, Methods for determination of radioactive substances in water and fluvial sediments: U.S. Geological Survey Techniques of Water-Resources Investigations, Chapter A-5, 95 p.

Tucson Water, 2000, Annual static water level basic data report Tucson basin and Avra Valley Pima County, Arizona, 1997: City of Tucson, Tucson Water, Planning and Engineering Division.

Wallace, D.E., and Lane, L.J., 1978, Geomorphic features affecting transmission loss potential on semiarid watersheds, in Hydrology and Water Resources in Arizona and the Southwest—Proceedings of the 1978 Meetings of the Arizona Section, American Water Resources Association and the Hydrology Section, Arizona Academy of Science, April 14-15, 1978, Flagstaff, Arizona: American Water Resources Association, v. 8, p. 157–164.

Water Resources Research Center, 1999, Water in the Tucson area–Seeking sustainability: College of Agriculture, University of Arizona, Tucson, Arizona, 155 p.

Webb R.H., and Betancourt, J.L., 1992, Climatic variability and flood frequency of the Santa Cruz River, Pima County, Arizona: U.S. Geological Survey Water-Supply Paper 2379, 40 p.

Won, I.J. and Bevis, M., 1987, Computing the gravitational and magnetic anomalies due to a polygon: Algorithms and Fortran subroutines, Geophysics, v. 52, p. 232–238.

Yitayew, Muluneh, 1990, Reference evapotranspiration estimates for Arizona: Tucson, University of Arizona, College of Agriculture, Agricultural Experiment Station Technical Bulletin 266.

Infiltration and Recharge at Sand Hollow, an Upland Bedrock Basin in Southwestern Utah

By Victor M. Heilweil, D. Kip Solomon[1], and Philip M. Gardner

Abstract

Permeable bedrock aquifers in arid regions of the southwestern United States are being used increasingly as a source of water for rapidly growing populations, yet in many areas little is known about recharge processes and amounts available for sustainable development. Environmental tracers were used in this study to investigate infiltration and recharge to the Navajo Sandstone at Sand Hollow in the eastern Mojave Desert of southwestern Utah. Average annual precipitation is about 210 millimeters per year. Tracers included bromide, chloride, deuterium, oxygen-18, and tritium. The basin-wide average recharge rate, based on ground-water chloride mass balance, is about 8 millimeters per year, or 4 percent of precipitation. However, infiltration and recharge are highly variable spatially within Sand Hollow. Recharge primarily occurs both as focused infiltration of runoff from areas of outcropping bedrock and as direct infiltration beneath coarse surficial soils. Locations with higher rates generally have lower vadose-zone and ground-water chloride concentrations, smaller vadose-zone oxygen-18 evaporative shifts, and higher ground-water tritium concentrations. Infiltration rates estimated from vadose-zone tritium concentrations at borehole sites within Sand Hollow range from 1 to more than 57 millimeters per year; rates calculated from average vadose-zone chloride concentrations between land surface and the bottom of the chloride bulge range from 0 to 9 millimeters per year; rates calculated from average vadose-zone chloride concentrations below the chloride bulge range from 0.5 to 15 millimeters per year; and rates calculated from ground-water chloride concentrations range from 3 to 60 millimeters per year. A two-end-member deuterium-mixing model indicates that about 85 percent of ground-water recharge in Sand Hollow occurs in the 50 percent of the basin covered by coarser soils and bedrock. Vadose-zone chloride concentrations at individual boreholes represent as much as 12,000 years of accumulation, whereas vadose-zone tritium has only been accumulating during the past 50 years. Environmental tracers at Sand Hollow indicate the possibility of a cyclical recharge pattern from higher infiltration rates earlier in the Holocene to lower rates later in the Holocene, back again to higher infiltration rates during the past 50 years.

Introduction

The Jurassic-age Navajo Sandstone is a regionally important bedrock aquifer in the southwestern United States. It is part of the Dakota - Glen Canyon aquifer system and is the principal source of ground water in the easternmost part of the Mojave Desert and Colorado Plateau (Robson and Banta, 1995). This aquifer system covers an area of about 210,000 km^2 in Utah, Arizona, Colorado, and New Mexico.

The 50-km^2 Sand Hollow study area (fig. 1) is situated on the Navajo Sandstone in Washington County in the southwestern corner of Utah. The population of this county has nearly doubled from about 48,000 in 1990 to about 90,000 in 2000 (U.S. Census Bureau, 2003) and is expected to increase to nearly 230,000 by 2020 (Washington County Water Conservancy District, 1995). This rapid growth is pressuring water agencies to actively develop ground water from the Navajo aquifer. To better manage this resource, an understanding of vadose-zone infiltration processes is needed for evaluating spatial and temporal variations in ground-water recharge. This information is critical for determining sustainable amounts of ground-water withdrawal, establishing effective land-use zoning for aquifer-source protection, and evaluating the potential for artificial recharge.

Unlike net infiltration and recharge in clastic sediments of alluvial desert basins (Phillips, 1994; Prudic, 1994; Tyler and others, 1996; Andraski, 1997; Izbicki and others, 2002; chapters D–F and H, this volume), direct and focused infiltration of precipitation away from major drainages is often the primary source of recharge to bedrock aquifers in arid settings (Cordova, 1978; Eychaner, 1983; Rasmussen and Evans, 1993; Flint and others, 2002). Infiltration along losing stream reaches can be readily quantified with discharge measurements and combined temperature measurements and modeling. Direct and focused infiltration of precipitation away from major streams is difficult to quantify. Regional watershed and ground-water-flow modeling often use empiri-

[1] Department of Geology and Geophysics, University of Utah, Salt Lake City (solomon@earth.utah.edu).

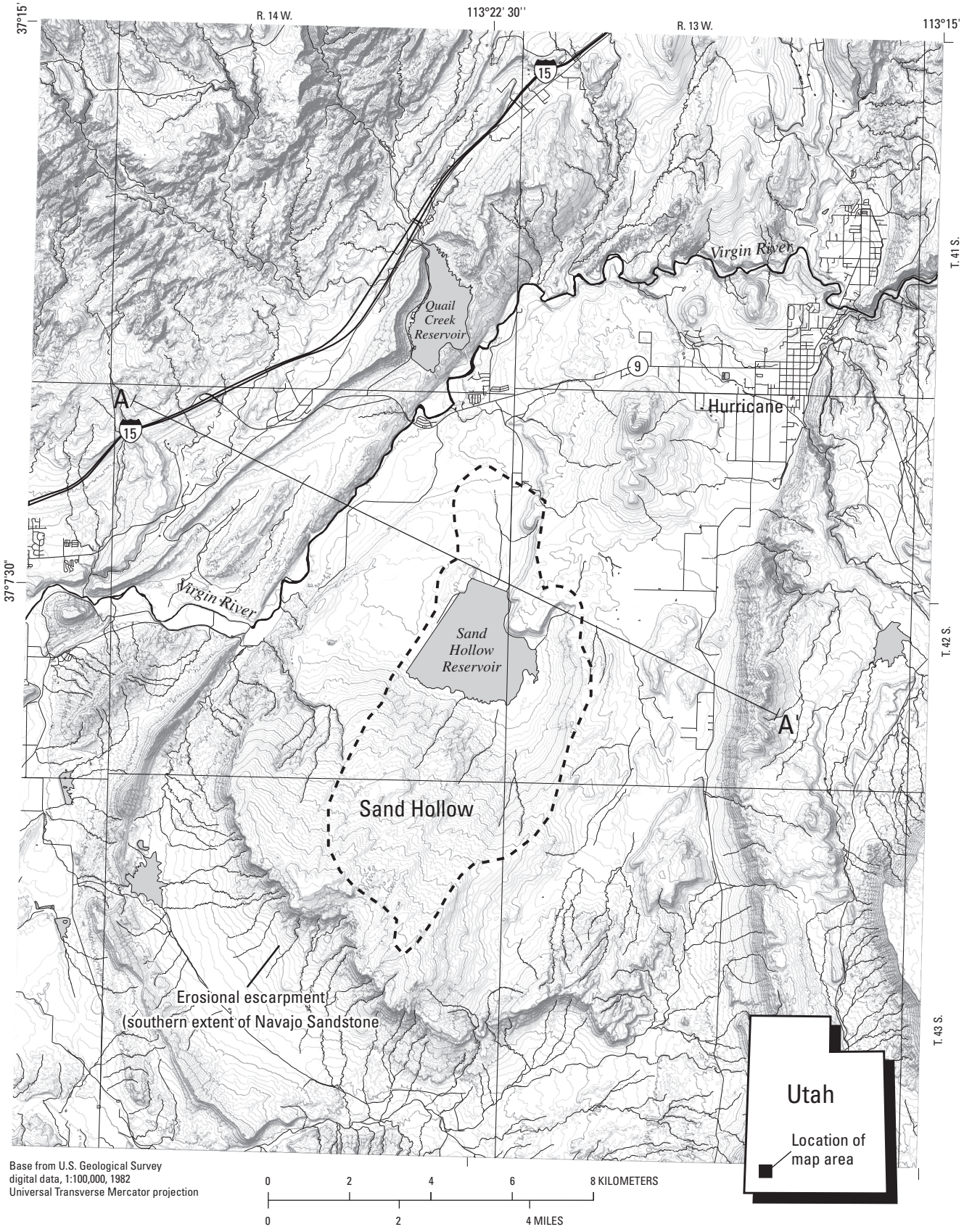

Figure 1. Location of the Sand Hollow ground-water-recharge study area, Washington County, Utah.

cal methods for estimating infiltration and runoff (Maxey and Eakin, 1950) that are not well suited for evaluating the spatial and temporal heterogeneity in recharge caused by localized climatic, geomorphologic, and geologic variables. Conversely, soil-physics methods such as soil moisture and Darcy flux measurements (Nimmo and others, 1994) are limited by their time- and site-specific nature. Such methods may not accurately represent long-term average moisture conditions at the basin scale.

The use of multiple environmental-tracer methods, however, can integrate a range of temporal and spatial scales in the evaluation of infiltration and recharge processes, including the ability to identify primary recharge areas, quantify vadose-zone travel times, and investigate seasonal variations in infiltration and recharge. Also, the application of multiple recharge-estimation methods may yield results at varying temporal and spatial scales, providing different but individually correct flux estimates (Allison, 1988; Allison and others, 1994; Flint and others, 2002; Scanlon and others, 2002).

Prior to this investigation, borehole environmental tracer methods had not been extensively utilized for examining desert recharge processes to an upland bedrock aquifer. The objective of this study is to apply such methods to quantify recharge to the Navajo aquifer. Tracers included chloride (Cl), bromide (Br), tritium (^{3}H), deuterium (^{2}H), and oxygen-18 (^{18}O). In this chapter, these tracer techniques are used to investigate both infiltration processes and recharge rates. An important objective of the investigation was to compare the results of different techniques to illustrate the variation in temporal and spatial scales of the different methods. Vadose-zone ^{3}H (depth-to-peak and mass balance), vadose-zone Cl mass-balance, and ground-water Cl mass-balance methods are applied to evaluate vadose-zone spatial and temporal variations of net infiltration and recharge. Basin-averaged recharge rates are also estimated by using the ground-water Cl mass-balance method. Vadose-zone and ground-water stable isotopes (^{2}H and ^{18}O) are used both to identify active recharge areas within the basin and to evaluate seasonal/millennial temporal recharge variations. Cl/Br ratios are used to investigate the possibility of nonatmospheric sources of Cl and preferential uptake processes in the root zone.

Previous Investigations

Focused and direct infiltration of precipitation on exposed outcrop or shallowly buried bedrock has been identified as the primary source of recharge to the Navajo aquifer of southern Utah and northern Arizona (Cordova and others, 1972, Cordova, 1981; Hood and Danielson, 1981; Eychaner, 1983; Hood and Patterson, 1984). Cordova (1978) concluded that most infiltration to the Navajo Sandstone of the central Virgin Basin in southwestern Utah occurs on or near the outcrop area where the sandstone is exposed or covered with thin deposits of coarser-grained soils. This observation was supported by vadose-zone solute distributions observed along shallow trenches in the Navajo Sandstone at Sand Hollow (Heilweil and Solomon, 2004), indicating a connection between infiltration rates and surficial characteristics, such as soil coarseness, topographic slope, and runoff from outcropping bedrock.

Studies of the Navajo aquifer in other parts of Utah and Arizona also have estimated recharge from infiltration of precipitation. A study of data from tensiometers and neutron probes in shallow boreholes drilled into exposed sandstone of the Lower Dirty Devil River Basin of south-central Utah shows that infiltration of summer precipitation ranged from less than 1 percent to as much as 25 percent on bare rock (Danielson and Hood, 1984). Other ground-water studies of the Navajo Sandstone in southern Utah and northern Arizona by Blanchard (1986a, b), Thomas (1986), Weiss (1987), Heilweil and Freethey (1992), and Heilweil and others (2000) used ground-water budgets and modeling to estimate recharge rates of between 0.5 and 15 percent of precipitation.

Zhu (2000) combined ^{14}C-based aquifer residence times with ground-water flow modeling to estimate temporal variability in recharge rates in the Shonto recharge area of the Navajo aquifer of Black Mesa, Ariz.: 13 to 19 mm/yr during the late Holocene (0 to 6 ka), lower rates during the mid Holocene (6 to 11 ka), and 2 to 3 times higher recharge during the late Pleistocene and early Holocene (31 to 11 ka). More recently, Zhu and others (2003) used the Cl mass-balance method with variable Cl deposition rates based on chlorine-36 data to estimate recharge rates ranging from about 10 mm/yr for the late Holocene (4 percent of the current 305 mm annual precipitation) to about 40 mm/yr for the late Pleistocene (8 percent of the estimated 540 mm annual precipitation estimated from 31 to 11 ka). These findings are consistent with lake-sediment core data from the Kaibab Plateau of Arizona that indicate wetter conditions at various times during the Holocene (Weng and Jackson, 1999).

Other recharge studies conducted in the Mojave Desert can be divided into two categories of surficial geology: fractured bedrock and unconsolidated (clastic) basin-fill sediments. A variety of techniques including Darcy flux, soil moisture, borehole temperature, and environmental tracers were used at the potential nuclear-waste repository site at Yucca Mountain, Nev., to estimate recharge rates through fractured tuff deposits; values ranged from 3 to 12 mm/yr, or between 2 and 7 percent of annual precipitation (Flint and others, 2002). The Yucca Mountain study determined that recharge was quite variable, mostly occurring on hill slopes with thin soil cover; there was little evidence of active recharge through the thicker sediments of the wash channels or terrace deposits. In contrast, studies of recharge through unconsolidated basin-fill deposits in the Mojave Desert have detected active recharge only beneath ephemeral stream channels; boreholes away from active wash sites showed that little or no active recharge is currently occurring (Phillips, 1994; Prudic, 1994; Tyler and others, 1996; Andraski, 1997; Hartsough and others, 2001; Izbicki and others, 2002; chapters E and G, this volume).

Hydrogeologic Setting

Climate

Although the geologic formations present in Sand Hollow are characteristic of the Colorado Plateau physiographic province, the study area is an upland basin within the lower-altitude and drier Mojave Desert ecosystem. Altitudes within Sand Hollow range from about 900 m to 1,300 m. Mean annual precipitation at St. George, Utah, from 1893 through 2003 was 210 ± 70 mm and ranged from 64 mm in 2002 to 419 mm in 1909. This historical precipitation record, along with precipitation measured at the Sand Hollow meteorological station during 1998 through 2002, is shown in figure 2. Total 5-year precipitation from 1998 through 2003 was 970 mm at Sand Hollow, compared with 1050 mm at St. George, about 10 miles to the southwest. Because of the close agreement (8 percent difference), it is assumed that long-term precipitation at St. George is representative of that at Sand Hollow.

Located in the northeastern part of the Mojave Desert, Sand Hollow is in the transitional area between winter Pacific-storm dominated precipitation to the north and west and a bimodal combination of winter Pacific storms and summer Gulf of California and Gulf of Mexico monsoon precipitation to the east and south (Brenner, 1974; Weng and Jackson, 1999). It receives about 55 percent of its precipitation during November through March and 35 percent of its precipitation during August through October (fig. 3). Spring is extremely dry, accounting for only 10 percent of the annual precipitation (Western Regional Climate Center, 2003). Since recharge at Sand Hollow is very episodic and driven by large precipitation events spanning several days, moving 30-day precipitation totals were calculated, showing that ten of the fifteen 30-day periods during the 20th century with more than 100 mm of precipitation occurred between 1957 and 1997. This is consistent with the greater-than-average precipitation that occurred in the region from 1977 through 1998 associated with the positive Pacific Decadal Oscillation (PDO; Gray and others, 2003).

Geology

Sand Hollow is underlain by the Navajo Sandstone, which has been folded into a bowl-like shape as part of the Hurricane Bench Syncline (fig. 4). The upper part of the formation has been eroded away, associated with uplift on the flank of the nearby Virgin Anticline, and remaining Navajo Sandstone at Sand Hollow is as much as 350 m thick (Hurlow, 1998). The sandstone is well sorted, fine-to-medium quartz sand held together by calcite cement (Cordova, 1978). It was deposited under eolian conditions and has prominent primary cross-bedding structures, along with secondary fracturing. The average dip of nonbedding-plane fractures within Sand Hollow is 75 degrees (Alpha Engineering,

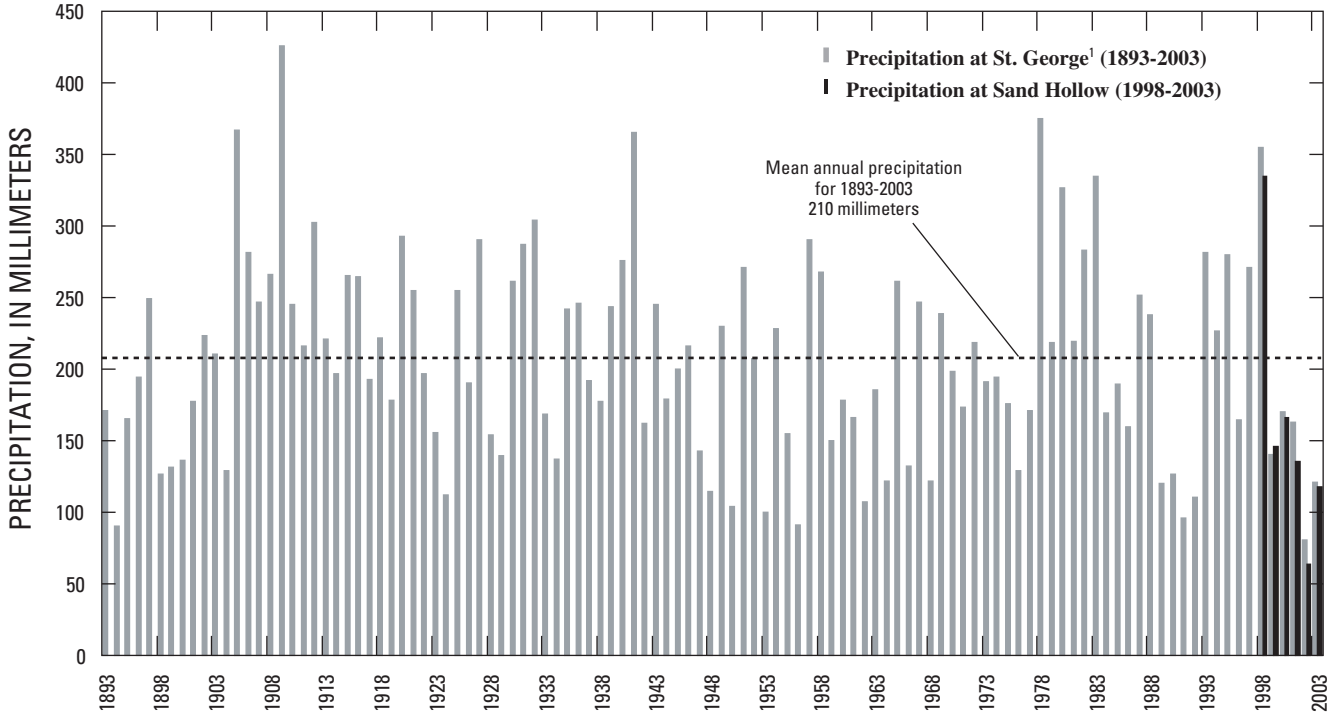

[1] St. George precipitation data from University of Nevada-Reno, Desert Research Institute, Western Region Climate Center (http://www.wrcc.sage.dri.edu), last accessed February 2003.

Figure 2. Annual precipitation at St. George, Utah, during 1893-2003, and at Sand Hollow, Utah, during 1998–2003.

Inc., written commun., 2001). Nonbedding-plane fractures in the Navajo Sandstone are unevenly distributed within the basin and occur in focused zones tens of meters wide, separated by areas with no fractures (Hurlow, 1998). The sandstone in Sand Hollow is either exposed at the surface or covered with a veneer of soils — generally less than 1.5 m. In the southern (upland) part of the basin where most of the sandstone outcrops occur, the soils are generally coarse-grained sands and sand-dune deposits. Finer grained loamy sand and sandy loams are present in the lower part of the basin. A thin layer of calcrete (generally less than 0.5 m) is often observed at the contact between the unconsolidated soils and the underlying sandstone, particularly beneath finer-grained soils.

Hydrology

The basin has a fairly gentle topographic relief. An erosional escarpment beyond the southern end of the drainage basin (fig. 1) marks the southern extent of the Navajo Sandstone. Most of the exposed sandstone is located along the perimeter of the basin. An ephemeral wash drains the higher-altitude southern part of the basin. Sand Hollow is essentially a closed basin under present climatic conditions. While the wash in the southern part of the basin flows during the largest storms, surface water spreads out and infiltrates into the permeable soils at the northern end (where the topographic slope decreases) rather than leaving the basin (L. Jessup, Washington County Water Conservancy District, oral commun., 2001).

As a porous medium, the fractured Navajo Sandstone shares characteristics of both clastic sediments and other consolidated rock formations. Because of its well-sorted nature and small amount of cementation, movement of water through the sandstone matrix is more similar to flow through unconsolidated soils than through other sedimentary formations with less primary permeability, such as siltstone, limestone, chalk, and tuff. Like other bedrock formations, the sandstone cannot be easily penetrated by roots, except where fractured. Therefore the sandstone matrix acts as a semipermeable medium, allowing moisture infiltration, but not root development. This limits transpiration losses, resulting in enhanced recharge compared to clastic sediments in similar arid settings.

The Navajo aquifer at Sand Hollow is unconfined, with depths to water in the central part of the basin ranging from 15 to 65 m below land surface. Ground water generally moves northward toward the Virgin River (fig. 5). The average horizontal hydraulic gradient is 0.006. Downward vertical hydraulic gradients calculated from nested piezometers at sites 14 and 43 (fig. 5) are 0.006 and 0.003, respectively. These downward gradients further support the conclusion that infiltration of precipitation through the vadose zone is the primary source of recharge to the Navajo aquifer in Sand Hollow.

Sample-Collection and Analytical Methods

Precipitation at Sand Hollow was measured from 1998 through 2003 at the Sand Hollow meteorology station (fig. 5) with a tipping bucket rain gauge connected to a data logger. Atmospheric-deposition samples for individual storms were collected for chemical analyses with a 150-mm-diameter brass funnel draining into a 250-mL high-density polyethylene bottle. Multiple-month composite atmospheric-deposition samples were collected with a 75-mm-diameter

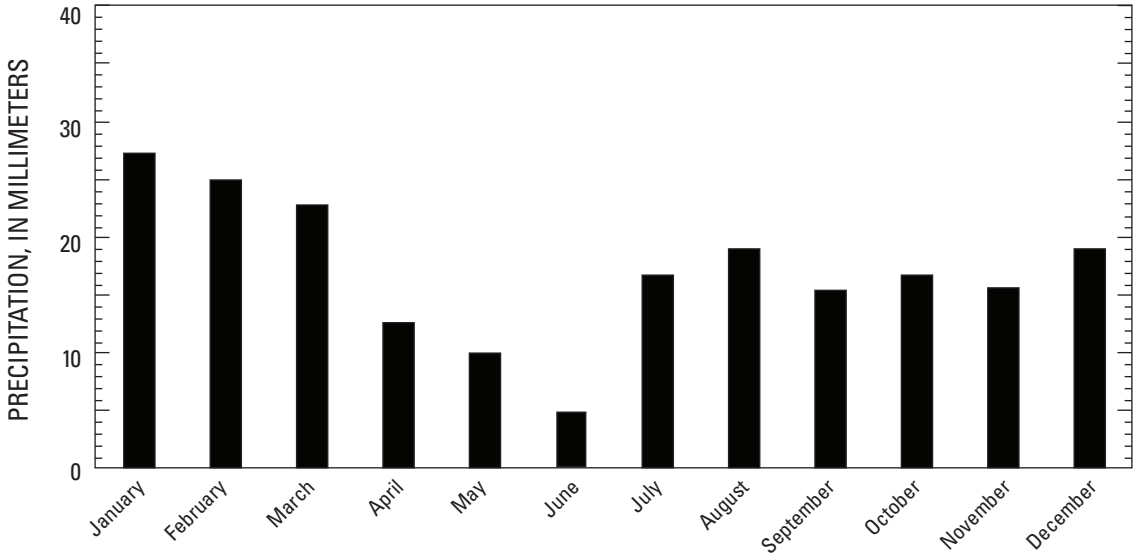

Figure 3. Monthly average precipitation at St. George, Utah, during 1893–2003.

straight-sided Buchner funnel at a height of about 1 m above ground supported by a stake and connected with copper tubing to a 1-L plastic sample bottle buried about 0.3 m below ground. A thin (10 mm) layer of mineral oil in the bottle was used to minimize evaporation of water (Friedman and others, 1992). To sample both wet fall and dust deposition between storms, the funnels for both the individual storms and the multiple-month composite samples were not rinsed between sample collections.

Vadose-zone core samples were collected at 18 sites in Sand Hollow (fig. 5) with an HQ-size triple-tube continuous coring system with air as the drilling fluid. The location of many of the boreholes was guided by a previous study of solute accumulations in shallow excavations within Sand Hollow (Heilweil and Solomon, 2004). Samples were immediately heat-sealed in a layered aluminum/plastic laminate. Pore waters were extracted for isotopic analysis by cryodistillation. Core samples for Cl and Br analysis were first oven-dried at 105ºC for 24 hours to determine moisture content and then mixed with an equal mass of de-ionized water to leach the salts. This leachate was centrifuged to remove silts and then filtered to 0.45 µm for anion analysis by ion chromatography. Pore-water Cl and Br concentrations were then calculated from the leachate-concentration and core-sample moisture-content measurements.

Ground-water samples for analysis of cations and anions, as well as trace elements, were collected by using U.S. Geological Survey procedures described by Wilde and others (1998). Cl, Br, and sulfate concentrations in precipitation, pore-water leachates, and ground water were analyzed by the U.S. Geological Survey in San Diego, Calif.; the U.S. Geological Survey National Water Quality Laboratory (NWQL) in Denver, Colorado; and the Los Alamos National Laboratory (LANL) in Los Alamos, N. Mex. Deuterium (^{2}H) and ^{18}O isotopic ratios of precipitation, vadose-zone pore waters, and ground water were analyzed with an isotope-ratio mass spectrometer at the University of Utah Stable Isotope Ratio Facility for Environmental Research (SIRFER). ^{3}H was analyzed at the University of Utah Dissolved Gas Service Center (DGSC). ^{3}H concentrations in precipitation, vadose-zone pore water, and ground water were analyzed on a mass spectrometer with the helium in-growth method (Clark and others, 1976), which was preferable to the conventional radiometric method because of its lower detection limit (0.05 TU) and smaller minimum sample volume requirements (40 ml).

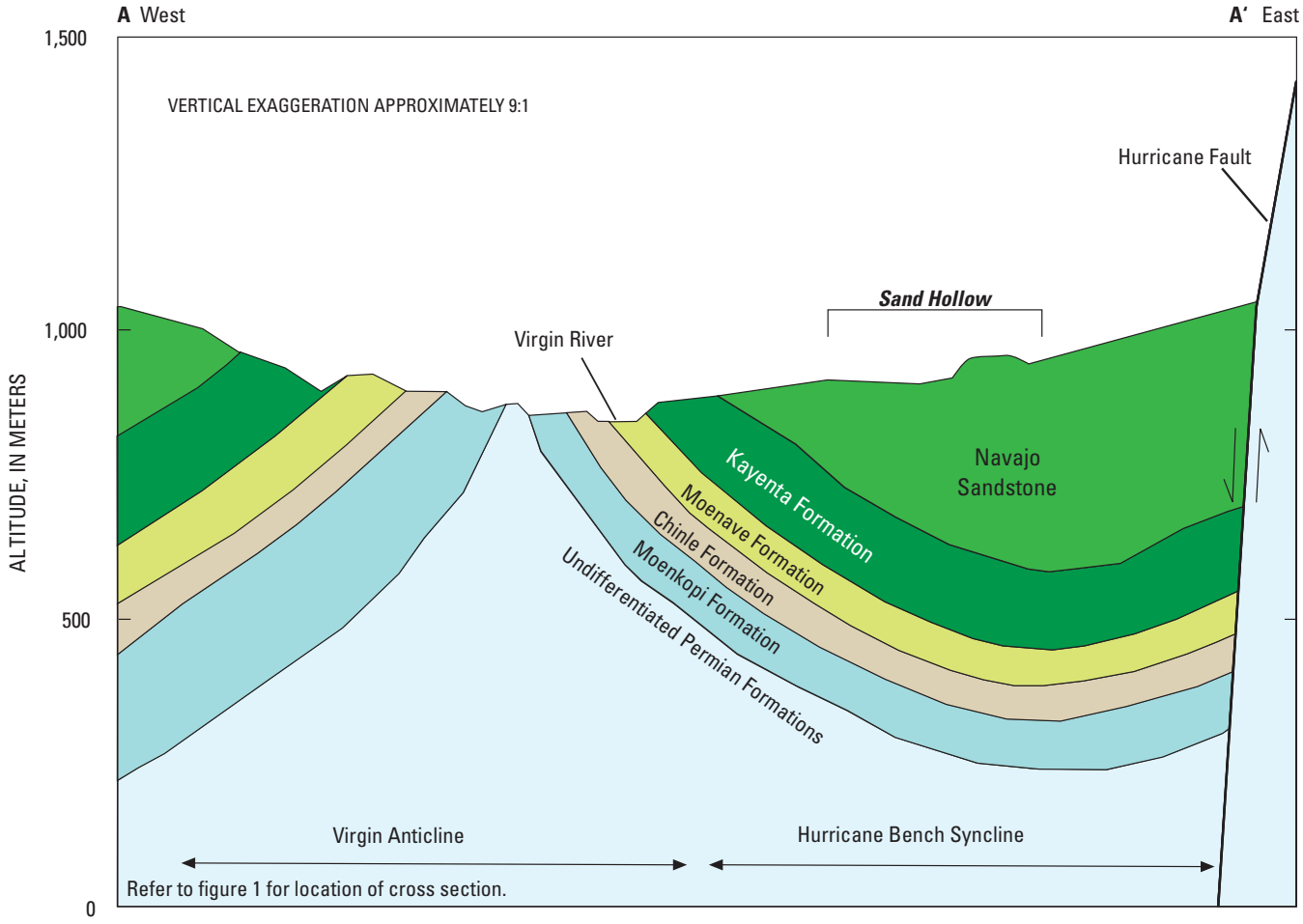

Figure 4. Generalized geologic cross section of the Navajo Sandstone and surrounding formations at the Sand Hollow ground-water-recharge study area, Utah. See figure 1 for location of **A**–**A'**.

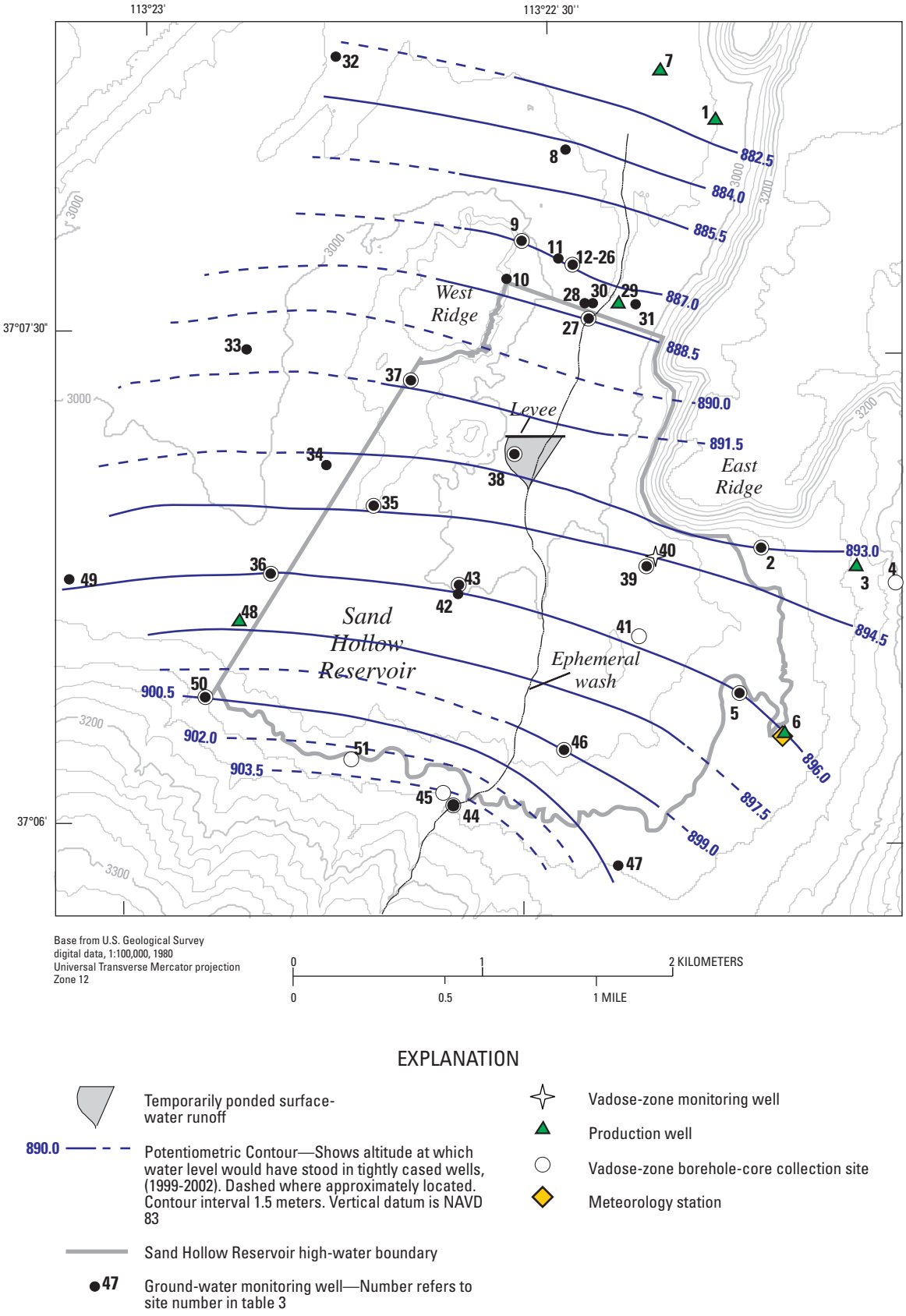

Figure 5. Location of wells, borehole-collection sites, meteorology station, and potentiometric surface of the Navajo Sandstone aquifer near the Sand Hollow ground-water-recharge study area, Utah.

Net Infiltration and Recharge Rates

Chloride

The ratio of the Cl concentrations in atmospheric deposition and ground water can be used with the Cl mass-balance method to provide an estimate of the recharge rate to an aquifer (Allison and Hughes, 1978; Allison, 1988; Dettinger, 1989; Wood and Sanford, 1995). Similarly, vadose-zone Cl concentrations beneath the root zone can be used to estimate rates of net infiltration (Allison and Hughes, 1978).

Chloride in Atmospheric Deposition

The precipitation-weighted mean concentration of atmospheric Cl deposition at Sand Hollow is 0.8 (± 0.3) mg/L from data collected during this study. This is based on the uncorrected Cl concentrations of eight multiple-month atmospheric-deposition samples collected between June 1999 and September 2004, which ranged from 0.5 to 1.2 mg/L (table 1). Three other multiple-month periods were excluded because of high sulfate concentrations (greater than 4.0 mg/L), which indicate possible contamination from bird droppings, decaying insect debris, or dust associated with construction. Because some evaporation from the sample container likely occurred, precipitation amounts from the atmospheric-deposition collector were often less than rain-gauge measurements at the same site. Therefore, a correction factor (the ratio of weather-station precipitation to atmospheric-deposition sample precipitation) was used to adjust the Cl concentration for this evaporative concentration of the sample. Similar Cl concentrations were measured in atmospheric-deposition samples collected during 12 individual storms from October 2000 to July 2001 (not including seven storms with sulfate concentrations greater than 4.0 mg/L), which ranged from 0.3 to 2.9 mg/L (table 1), with a mean of 0.8 mg/L. Assuming an average precipitation rate of 210 mm/yr, the mean 0.8 mg/L Cl concentration of atmospheric deposition corresponds to an average Cl deposition rate of 17 $\mu g/cm^2/yr$.

Chloride in the Vadose Zone

Leachates prepared from borehole-core samples show that accumulation of atmospheric Cl in the vadose zone at Sand Hollow is quite variable. Total Cl accumulation ranged from 4 mg/cm^2 at sites 9 and 35 to at least 230 mg/cm^2 at site 4. Assuming an annual Cl deposition rate of 17 ± 8.5 $\mu g/cm^2$, this mass of Cl in the vadose zone at Sand Hollow represents from 200 to at least 12,000 years of accumulation (table 2).

Pore-water chloride concentrations were calculated based on the mass of chloride in the leachate sample and the volumetric water content determined by oven-drying the core sample. Vadose-zone water content of the borehole-core samples is generally consistent with trends in Cl and ^3H accumulation (tables 2, 3). Mean vadose-zone volumetric water content, calculated from land surface to the capillary fringe, ranged from 1.7 to 7.8 percent. Site 4 had the lowest average vadose-zone moisture content, consistent with the largest Cl accumulation of the sites within Sand Hollow. Site 4 is located on the East Ridge (fig. 5) and is exposed to more wind, resulting in more bare-soil evaporation than at the other sites. Site 9 had the highest average vadose-zone moisture content, consistent with having very little Cl accumulation. Located along a small side wash, this site regularly receives focused infiltration of surface-water runoff from the exposed sandstone of the West Ridge.

The profiles generally show shallow Cl accumulations, with peak concentrations occurring less than 15 m below land surface. The peak concentrations range from 28 mg/L at site 35 to 29,900 mg/L at site 4 (table 2). The profiles generally have the characteristic bulge shape observed in many desert soils (figs. 6, 7).

Site-specific vadose-zone infiltration rates were calculated with the Cl mass-balance method (Phillips, 1994; Scanlon, 2004) by dividing the average Cl concentration of atmospheric deposition by either [1] the average vadose-zone Cl concentration of pore water from borehole samples between land surface and the bottom of the Cl bulge or [2] the average vadose-zone Cl concentration of pore water from borehole samples below the Cl bulge. In unconsolidated sediments, pore-water concentrations within the shallow Cl bulge generally are not used for calculating net infiltration rates because the depth of salt accumulation associated with root-zone transpiration often overlaps the depth of the bulge. However, at Sand Hollow there is minimal root penetration into the Navajo Sandstone, which is either exposed or covered by less than about 1.5 m of soil. Peak vadose-zone Cl concentrations are generally located in sandstone below the root zone at depths ranging from 1.2 to 14.5 m below land surface, with an average depth of about 5 m (table 2). Therefore, calculations based on Cl concentrations within the bulge should be representative of net infiltration rates. Infiltration rates ranged from 0.03 to 8 mm/yr based on pore-water Cl concentrations between land surface and the bottom of the Cl bulge; rates ranged from 0.5 to 13 mm/yr based on pore-water Cl concentrations below the bottom of the Cl bulge (table 4).

The boreholes can be divided into low- and high-recharge sites on the basis of total Cl accumulation, peak vadose-zone Cl concentration, and infiltration rates. Sites 2, 4, 12, 27, 37, 38, 39, and 46 have lower vadose-zone Cl net infiltration rates, with more than 20 mg/cm^2 total Cl accumulation and peak vadose-zone Cl concentrations of more than 300 mg/L. Conversely, sites 9, 35, 43, 44, and 50 have higher vadose-zone Cl net infiltration rates, with less than 20 mg/cm^2 total Cl accumulation and peak vadose-zone Cl concentrations of less than 200 mg/L (tables 2, 4).

Chloride in Ground Water

The mean Cl concentration from 31 ground-water sites in Sand Hollow (fig. 8) is 22.5 mg/L with a standard deviation of 12.5 mg/L. It is assumed that all of the Cl in the unsaturated zone and the underlying aquifer is of atmo-

Table 1. Selected chemical constituents in precipitation, Sand Hollow ground-water recharge study area, Utah.

[Site locations refer to figure 5. Anions analyzed by U.S. Geological Survey, San Diego, Calif., unless otherwise noted. Abbreviations: mg/L, milligrams per liter; δ^2H, deuterium; $\delta^{18}O$, 18-oxygen; ^3H, tritium; TU, tritium units; —, no data available; <, less than; ±, plus or minus]

Site number	Sample day or period	Chloride, in mg/L	[1] Bromide, in mg/L	[1] Sulfate, in mg/L	Chloride/ bromide ratio	δ^2H, in per mil	$\delta^{18}O$, in per mil	^3H, in TU
2	4/30/1999	—	—	4.7	—	—	—	21.0 ± 1.0
6	[2] 6/3/1999–10/12/1999	[3] 6	—	—	—	–76.0	–7.5	—
6	[2] 10/12/1999–4/13/2000	1.2	[4] 0.007	3.0	171	–82.0	–11.0	—
6	[2] 4/13/2000–10/11/2000	0.9	0.016	4.0	56	–21.0	–4.3	—
6	[2] 10/11/2000–4/30/2001	1.2	< 0.016	4.0	—	–86.0	–11.8	—
6	[2] 4/30/2001–10/3/2001	[3] 3.5	—	[3] 14	—	–1.0	2.8	—
6	[2] 10/3/2001–5/8/02	0.9	—	3.0	—	—	—	—
6	[2] 5/8/02–9/11/02	1.0	—	4.0	—	—	—	—
6	[2] 9/11/02–5/8/03	0.5	0.05	< 3.0	—	–97.6	–13.0	—
6	[2] 5/08/03–10/8/03	0.5	< 0.3	3.0	—	—	—	—
6	[2] 10/08/03–5/4/04	0.4	< 0.3	2.3	—	—	—	—
6	[2] 5/04/04–9/22/04	[3] 1.6	[3] < 0.3	[3] 11	—	—	—	—
12	10/10/2000	—	—	—	—	–43.0	–7.1	—
12	10/11/2000	1.7	[4] 0.007	2.6	243	–16.9	–2.6	—
12	10/23/2000	[3] 7.2	[3] 1.129	[3] 10.8	—	–122.1	–13.8	—
12	10/27/2000	—	—	—	—	–72.1	–11.1	—
12	10/28/2000	—	—	—	—	–116.9	–15.3	—
12	11/1/2000	—	—	—	—	–79.2	–10.7	—
12	11/10/2000	0.8	0.023	1.6	37	–52.3	–9.2	—
12	11/13/2000	—	—	—	—	–49.1	–8.8	—
12	12/12/2000	—	—	—	—	–84.6	–10.5	—
12	1/9/2001	0.8	—	3.95	—	–84.6	–10.8	—
12	1/12/2001	0.3	< 0.016	0.7		–91.0	–11.6	—
12	2/14/2001	—	—	—	—	–87.0	–12.7	9.14 ± 0.5
12	2/27/2001	—	—	—	—	–126.4	–15.5	—
12	3/1/2001	0.3	< 0.016	0.7	—	–104.1	–14.2	—
12	3/5/2001	0.4	< 0.016	1.3	—	—112.1	–15.1	—
12	3/7/2001	0.4	< 0.016	1.6	—	–104.5	–12.0	—
12	3/9/2001	—	—	—	—	–100.6	–13.7	9.28 ± 0.5
12	3/12/2001	0.4	< 0.016	1.3	—	–100.6	–13.7	—
12	4/6/2001	[3] 2.2	[3] < 0.016	[3] 11.2	—	–34.2	–6.2	—
12	4/9/2001	—	—	—	—	–51.6	–7.2	—
12	5/14/2001	[3] 16.6	[3] 0.615	[3] 29.9	—	4.2	0.5	—
12	5/17/2001	0.5	[4] 0.007	1.5	71	—	—	—
12	5/28/2001	[3] 1.8	0.020	4.7	—	—	—	—
12	6/26/2001	[3] 2.1	0.028	8.4	—	—	—	—
12	7/5/2001	0.6	[4] 0.007	2.2	84	—	—	—
12	7/9/2001	2.9	[4] 0.010	3.0	287	—	—	—
12	7/11/2001	[3] 16.7	[3] 0.620	[3] 28.4	—	—	—	—
12	10/7/2001	[3] 4.3	[3] 0.190	[3] 25.1	—	–54.3	–6.7	—
12	11/13/2001	—	—	—	—	–39.0	–5.6	—
12	11/25/2001	—	—	—	—	–73.0	–9.2	—
12	11/30/2001	—	—	—	—	–103.0	–14.6	—
12	12/4/2001	—	—	—	—	–59.0	–8.5	—
12	12/15/2001	—	—	—	—	–84.0	–11.5	—
12	12/23/2001	—	—	—	—	–103.0	–13.3	—
42	09/11/2001	—	—	—	—	–3.1	3.3	—
[5] 44	11/09/2002	0.32	[6] 0.006	2.3	53	–48.2	–6.6	2.3 ± 0.1

[1] Analyzed by Los Alamos National Laboratory, Los Alamos, New Mex.

[2] Multiple-month atmospheric deposition sample collected at meteorologic station.

[3] Value is suspect; high sulfate or phosphate concentration suggests contamination.

[4] Reported bromide concentration is less than the 0.016 parts per milion detection limit because of evaporative concentration.

[5] Sample of streamflow collected during ephemeral runoff.

[6] Analyzed by the USGS National Water-Quality Laboratory in Denver, Colo.

spheric origin. The Navajo Sandstone is a clean, well-sorted, eolian sandstone containing no evaporite or other salt deposits. However, because of the upward advective movement into the Navajo Sandstone of Cl-rich brines from underlying formations documented at other study sites (Kimball, 1992; Naftz and others, 1997; Heilweil and others, 2000), Cl-to-Br ratios were examined to evaluate potential Cl contributions from geologic sources. Such geologic sources of Cl typically have Cl-to-Br ratios exceeding 1,000 and the ratios increase with increasing Cl concentration (Davis and others, 1998). However, no such trend is evident in ground water from Sand Hollow and ground-water Cl-to-Br ratios are always less than 500 (fig. 9). Furthermore, vadose-zone pore water Cl-to-Br ratios generally increase from land surface to the water table (fig. 10; Heilweil, 2003), consistent with a doubling in the mean Cl-to-Br ratio from 120 for atmospheric-deposition samples to 230 for ground-water samples. This indicates that some unsaturated-zone process, such as preferential uptake of Br by plant roots, influences ground-water Cl-to-Br ratios rather than a geologic source of Cl.

By using mean Cl concentrations of 0.8 mg/L (with a standard deviation of 0.3 mg/L) for atmospheric deposition (Cl_{dep}) and 22.5 mg/L (with a standard deviation of 12.5 mg/L) for ground water (Cl_{gw}), along with the 210 mm (with a standard deviation of 70 mm) of mean annual precipitation (P) at Sand Hollow, the estimated Cl mass-balance recharge rate is 7.5 mm/yr (with a standard deviation of 5.6 mm/yr, or about 4 (± 3) percent of precipitation. The mean and variance (square of the standard deviation) in the recharge rate were evaluated with a truncated (linear terms only) Taylor series expansion (chapter appendix).

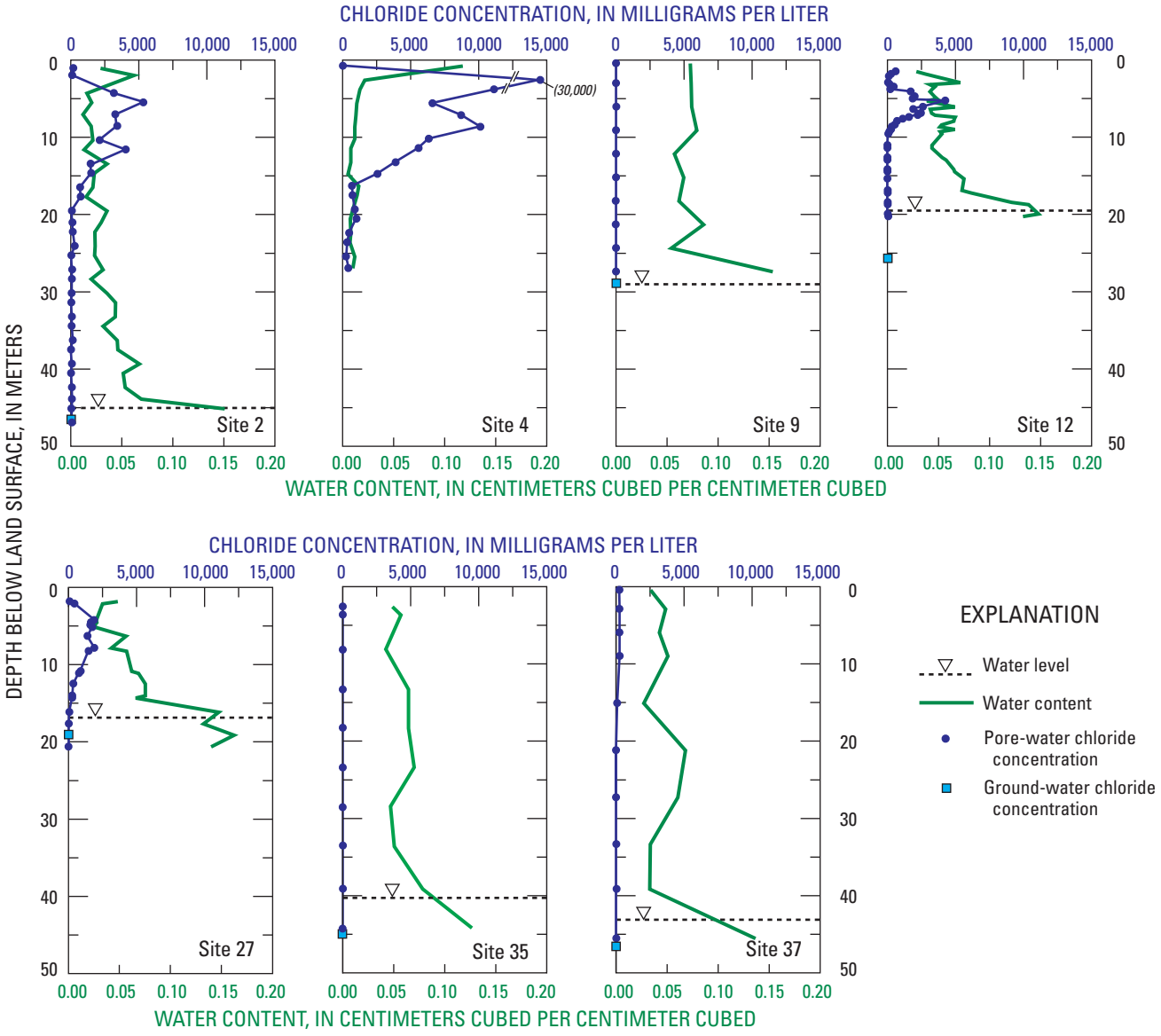

Figure 6. Chloride concentration and volumetric water content of pore-water and ground-water samples collected from selected boreholes at the Sand Hollow ground-water-recharge study area, Utah.

The wide range of Cl concentration in ground water, from 2.9 to 61.1 mg/L (fig. 8, table 4), indicates that the amount of evaporative concentration of infiltrating precipitation in the shallow root zone is quite spatially variable. The Cl mass-balance method can be applied to these individual ground-water sites, resulting in recharge rates ranging from 3 to 60 mm/yr (table 4), or about 1 to 28 percent of average annual precipitation.

Tritium

Tritium in Precipitation

The estimated ^{3}H concentration of precipitation in southwestern Utah from 1950 to 2000 is shown in figure 11. This estimation is based on a distance-weighted average from Global Network of Isotopes In Precipitation (GNIP) monitoring stations operated by the International Atomic Energy Agency (IAEA) at Albuquerque, N. Mex.; Flagstaff, Ariz.; and Salt Lake City, Utah. The maximum ^{3}H concentration of precipitation at Sand Hollow during the above-ground nuclear testing in the early 1960s was estimated to exceed 2,000 TU. Present ^{3}H concentrations in precipitation at Sand Hollow are near or slightly above the prebomb background levels. Three samples of recent precipitation (1999–2001) had measured ^{3}H concentrations ranging from 9.1 to 21.0 TU (table 1). A surface-water sample collected during a ephemeral flow event on 11/09/2002 had a ^{3}H concentration of only 2.3 TU, possibly caused by a dilution with older (lower ^{3}H) shallow vadose-zone pore waters flushed into the wash by the infiltrating precipitation.

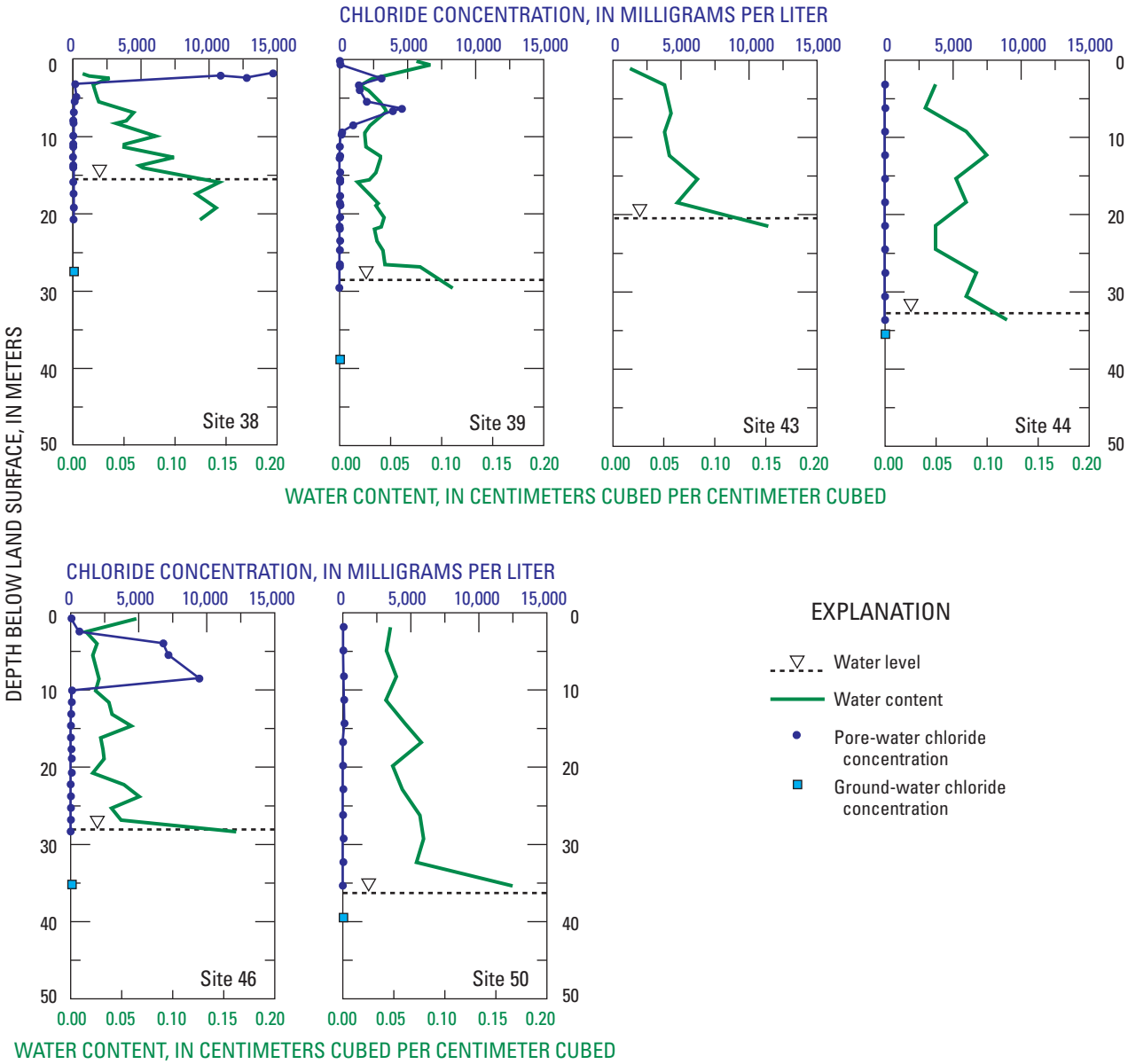

Figure 6.—Continued.

Table 2. Vadose-zone chloride parameters and water content from borehole samples, Sand Hollow ground-water-recharge study area, Utah.

[Site numbers refer to figure 5. Abbreviations: mg/cm^2, milligrams per centimeter squared; mg/L, milligrams per liter; m, meters; mm/yr, millimeters per year; —, no data available]

Site number	Total chloride accumulation, in mg/cm^2	[1] Chloride accumulation time, in years	[2] Peak chloride concentration, in mg/L	Depth of chloride peak concentration, in m	[3] Mean volumetric water content, in percent	Chloride accumulation time for bulge, in years	Mean chloride concentration in Cl bulge, in mg/L	Depth interval from chloride bulge to water table, in m	[4] Mean chloride concentration below bulge, in mg/L
High-recharge sites									
9	4	200	41	8	7.8	100	22	9 to 28.8	13
35	4	200	28	5	5.9	50	20	18 to 24.4	21
44	5	300	36	6	6.8	100	21	12 to 32.7	23
43	5	300	141	1	5.4	150	76	12 to 20.2	38
50	15	800	138	15	6.0	400	100	17 to 36.6	51
Low-recharge sites									
37	22	1,200	336	5	4.4	800	240	21 to 43.3	41
38	55	3,000	14,700	2	4.7	2,500	6,500	7 to 15.6	44
12	56	3,000	4,300	5	5.6	3,000	1,100	11 to 19.6	36
39	70	4,000	4,600	7	4.0	3,500	1,600	11 to 28.2	48
27	72	4,000	1,900	8	4.6	3,500	1,100	16 to 17.7	59
2	91	7,000	5,400	6	3.3	4,000	2,200	20 to 45.4	109
46	140	7,000	9,500	9	3.8	7,000	3,500	13 to 28.3	58
4	[5] 230	12,000	29,900	3	1.7	—	5,600	25 to [6] 137.0	354

[1] For entire vadose zone, assuming a 17 microgram per square centimeter annual chloride atmospheric deposition rate.

[2] Shown in figure 6.

[3] Calculated between land surface and the capillary fringe.

[4] For depths below the chloride bulge and above the water table, except for site 4, which did not reach water table.

[5] Minimum because borehole was not drilled to water table.

[6] Depth to water table extrapolated from potentiometric map (fig. 5).

Table 3. Vadose-zone tritium parameters and water content from borehole-core samples, Sand Hollow, Utah.

[Abbreviations: m, meters; mm/yr, millimeters per year; TU-m, tritium unit meters; —, no data available; >, greater than]

Site number	Borehole name	Collection date	Depth to tritium peak in vadose zone, in m	Mean volumetric water content to tritium peak, in percent	Time since peak atmospheric tritium concentration, in years	[1] Recharge rate from depth of tritium peak, in mm/yr	Total tritium in vadose zone, in TU-m	[2] Recharge rate from tritium mass balance, in mm/yr	Correction factor for mass balance recharge rate
High-recharge sites									
9	WD 6	2001/05/14	> 28.7	7.9	38	[3] > 57	12.9	[3] > 11	—
35	Hole N	2001/05/25	20.3	4.9	38	26	15.3	13.1	2.0
44	WD 8	2001/05/17	18.6	7.0	38	34	17.2	14.7	2.3
43	Hole O	2001/06/10	17.4	5.9	38	27	13.6	11.6	2.3
50	WD 7	2001/05/15	8.4	4.7	38	10	6.9	5.9	1.8
Low-recharge sites									
37	WD 9	2001/05/22	3.8	4.6	38	4.6	3.5	3.0	1.5
38	Basin 1	1999/04/22	—	—	—	—	1.5	1.2	—
12	IFP 1	1999/04/19	—	—	—	—	1.9	1.4	—
39	Slope 1a	1999/04/26	3.5	2.7	36	2.6	2.2	1.7	1.6
27	Wash 1	1999/04/15	—	—	—	—	2.7	2.0	—
2	WD 12	1999/05/03	—	—	—	—	2.8	2.1	—

[1] Based on equation 1.

[2] Based on equation 2; the decay-corrected tritium mass in precipitation since 1950 is 274 tritium-unit meters for wells drilled in 1999 and 246 tritium-unit meters for wells drilled in 2001.

[3] Based on assumption that tritium peak is already below water table.

Table 4. Summary of recharge rates and environmental-tracer data for individual borehole sites, Sand Hollow ground-water-recharge study area, Utah.

[Site numbers refer to figure 5. Abbreviations: mm/yr, millimeters per year; TU, tritium units; >, greater than; —, no data available]

Site number	Depth to bedrock, in m	Environmental tracer data					Infiltration or recharge rate				Site description
		Vadose-zone chloride accumulation time, in years	Ground-water chloride concentration, in mg/L	[1] Ground-water tritium concentration, in TU	Average vadose-zone 18-oxygen shift, in per mil	Ground-water deuterium ratio, in per mil	Chloride, land surface to bottom of bulge, in mm/yr	Chloride, bottom of bulge to water table, in mm/yr	Ground-water chloride, in mm/yr	Vadose-zone tritium, in mm/yr	
High-recharge sites											
9	0.0	200	2.9	6.9	2.1	–79	8	13	60	> 57	Fine sand/ exposed sandstone beneath wash
35	0.4	200	6.5	4.3	—	–82	8	8	26	26	Sand dunes
44	0.0	300	[2] 10.0	4.1	2.3	[2]–83	8	7	17	34	Fine sand/ exposed sandstone beneath wash
43	0.0	300	[2] 16.5	1.0	2.8	[2]–84	2	4	10	27	Exposed sandstone
50	1.2	800	18.0	0.21	3.4	–85	2	3	9	10	Loamy fine sand
Low-recharge sites											
37	0.2	1,000	[2] 20.4	0.00	3.0	[2]–88	0.7	4	8	4.6	Loamy very fine sand on ridge
38	0.9	3,000	[2] 61.1	0.07	2.2	[2]–86	0.03	4	3	[3] 2.4	Silty clay loam near wash
12	0.8	3,000	19.9	[4] 0.00	3.5	[2]–84	0.2	5	8	[3] 2.8	Loamy very fine sand
39	0.8	4,000	[2] 11.3	0.07	3.5	[2]–85	0.1	4	15	2.6	Fine sandy loam
27	0.8	4,000	28.1	0.27	4.1	[2]–86	0.2	3	6	[3] 4.0	Fine sandy loam beneath wash
2	1.5	7,000	[2] 21.0	0.02	3.8	[2]–85	0.08	2	8	[3] 4.2	Fine sandy loam
46	1.2	7,000	[2] 10.9	0.18	3.7	[2]–87	0.05	3	15	—	Fine sandy loam
[5] 4	1.5	12,000	—	—	4.7	—	0.03	0.5	—	—	Fine sandy loam on ridge
Mean											
	[2] 0.7	[6] 1,500	[6] 15	[2] 1.4	[2] 3.3	[2]–85	[6] 0.4	[6] 4	[6] 11	[6] 9	

[1] See table 5 for tritium precision; analysis with highest precision listed when multiple analyses available.

[2] Arithmetic mean of multiple values.

[3] Calculated using ^{3}H-mass-balance method multiplied by a correction factor of 2.

[4] From shallowest port (site 17) in same borehole.

[5] Borehole was not drilled to water table.

[6] Geometric mean.

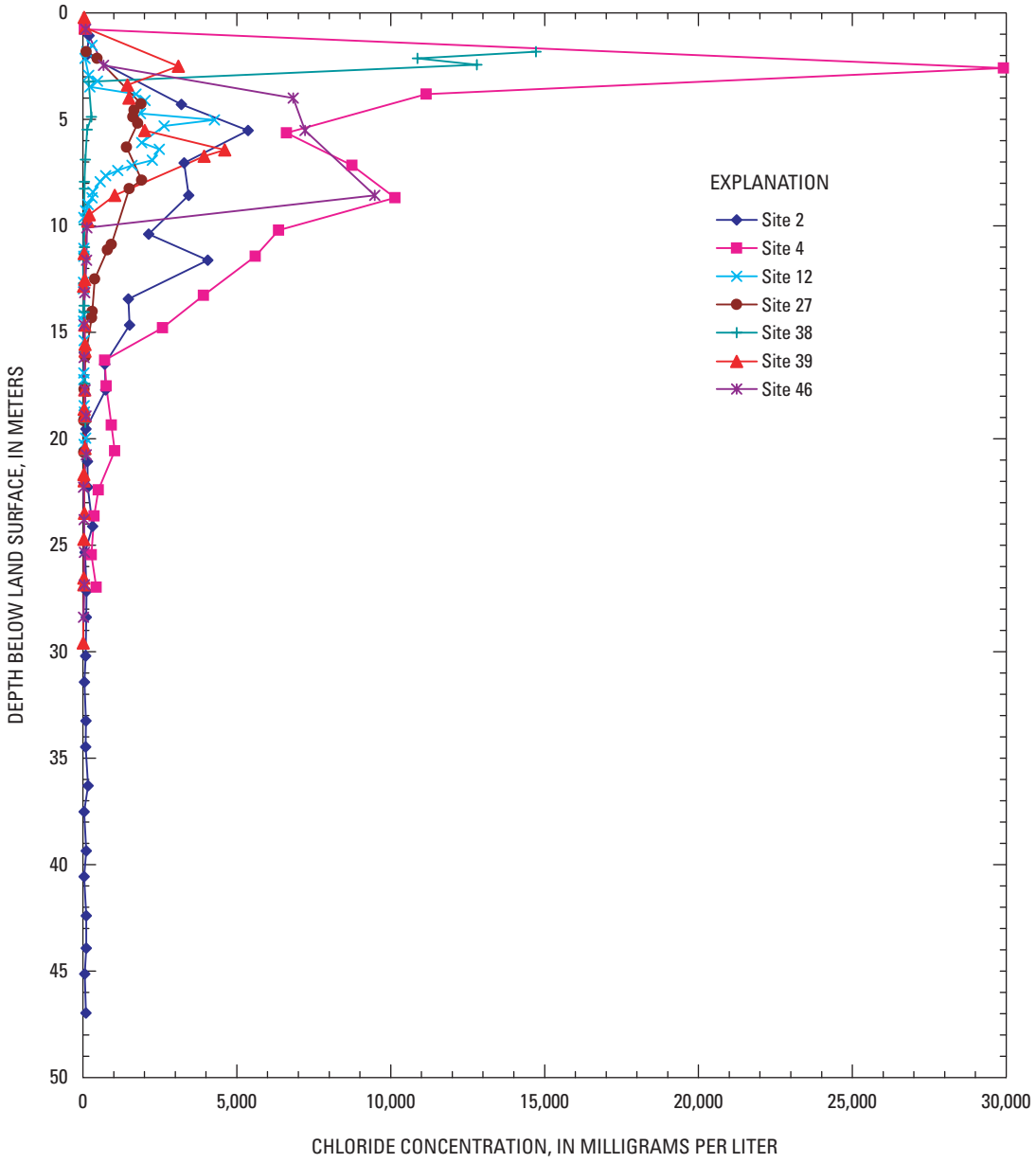

Figure 7. Vadose-zone chloride concentration obtained from borehole-core samples collected from locations with low values of recharge, Sand Hollow ground-water-recharge study area, Utah.

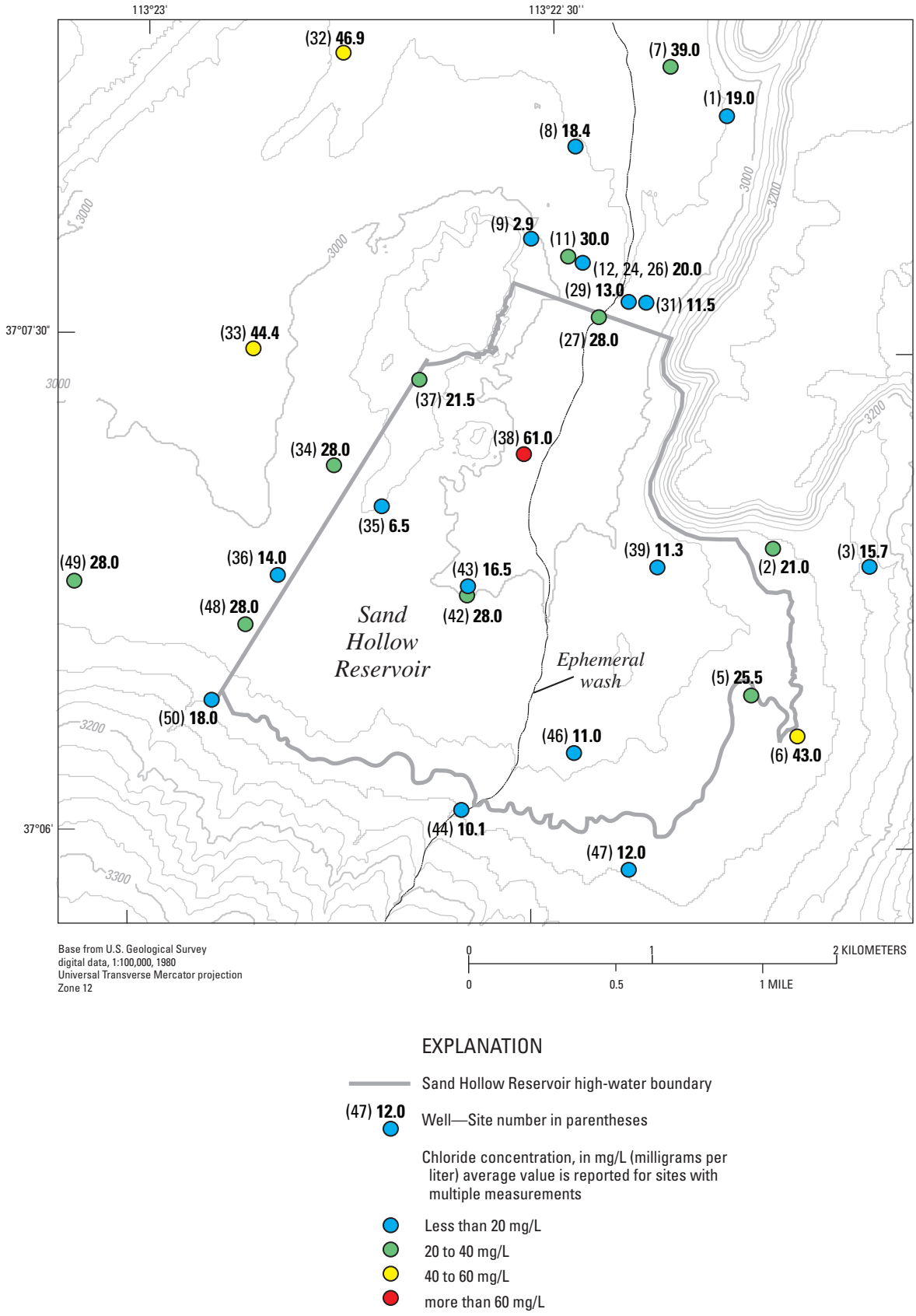

Figure 8. Chloride concentration in water from selected wells at the Sand Hollow ground-water-recharge study area, Utah.

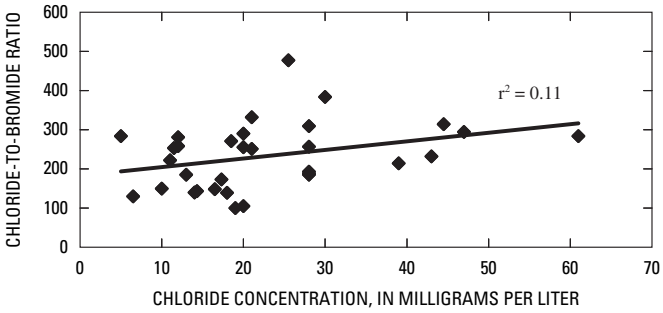

Figure 9. Relation of chloride-to-bromide ratio to chloride concentration in water from selected wells at the Sand Hollow ground-water-recharge study area, Utah.

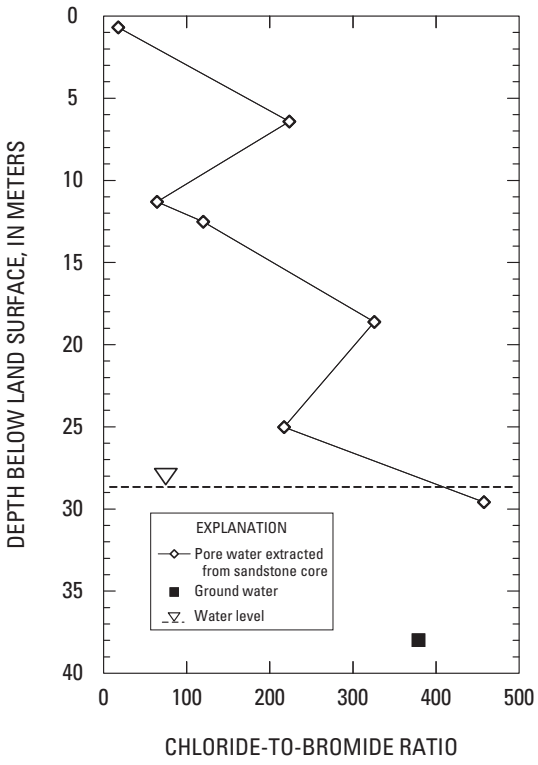

Figure 10. Chloride-to-bromide ratio with depth in vadose-zone pore-water and ground-water samples collected at site 39, Sand Hollow ground-water-recharge study area, Utah.

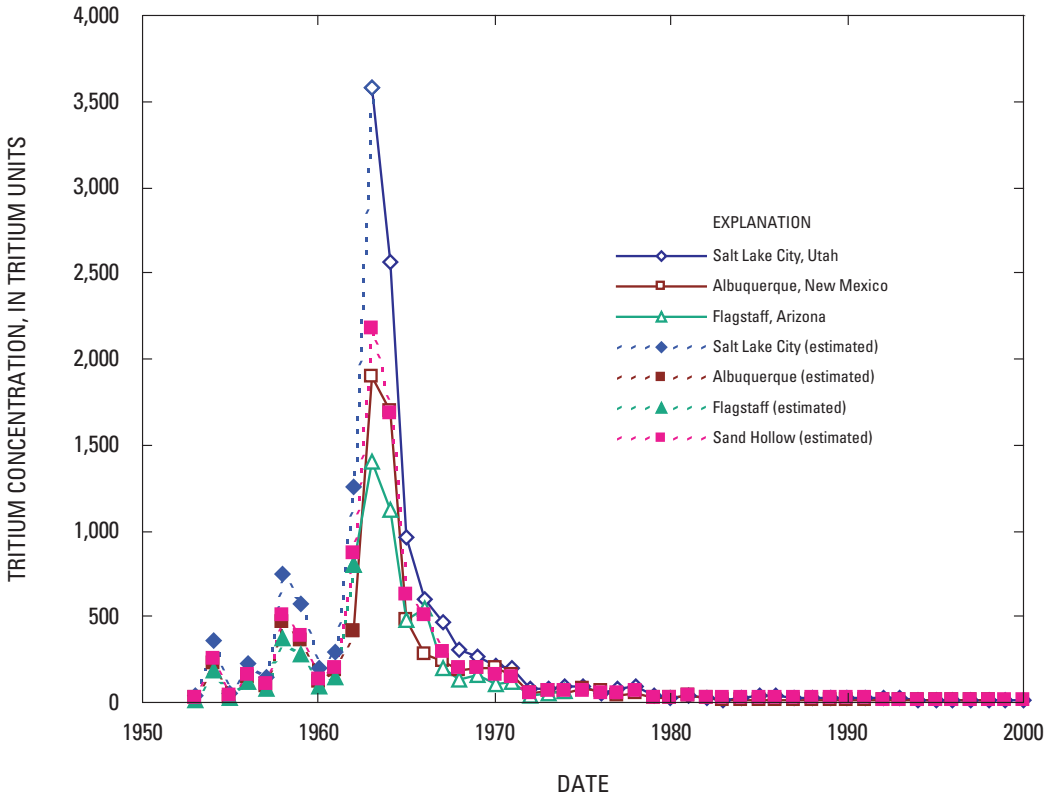

Figure 11. Estimated tritium concentration of precipitation at the Sand Hollow ground-water-recharge study area, Utah.

Tritium in the Vadose Zone

^{3}H concentrations in vadose-zone pore water from boreholes within Sand Hollow ranged from 0 to 17.9 TU (fig. 12). ^{3}H concentrations of 4 to 12 TU were typically measured within the first few meters of the boreholes and likely represent recent precipitation. Profiles at sites 35, 37, 39, 43, 44, and 50 show vadose-zone peaks consistent with the peak atmospheric-^{3}H concentrations of the early 1960s. Profiles at sites 2, 12, 37, and 38 do not display a subsurface ^{3}H peak. The profile at site 9 has consistently high concentrations throughout the entire vadose zone, indicating that the 1960s peak has already been flushed down to the water table. ^{3}H concentrations of ground-water at each site (also shown in fig. 12) are generally similar to concentrations in pore waters from borehole cores at or near the water table.

Both the ^{3}H depth-to-peak (TDTP) and ^{3}H mass-balance (TMB) methods were used to determine net infiltration rates at various borehole locations within Sand Hollow. The TDTP method uses the depth of the 1963 ^{3}H peak in the vadose zone and the average soil-moisture content to estimate a net infiltration flux rate, q (L T^{-1}), with the following equation (Cook and others, 1994):

$$q = \frac{z}{t}\theta_v \ , \qquad (1)$$

where z is the vertical distance between land surface and the 1963 ^{3}H peak (L),
υ is the length of time between the ^{3}H peak and the sample collection time (T),
and θ is the depth-weighted volumetric water content of the vadose zone between land surface and the ^{3}H peak.

Similar to the Cl mass-balance method, the ^{3}H mass-balance (TMB) method is based on the assumption that precipitation falling at the borehole site either becomes net infiltration or is lost from the site as evapotranspiration or runoff. The ratio of [1] the mass of ^{3}H between the root zone and the water table to [2] the mass of decay-corrected ^{3}H that fell as precipitation provides the percent of moisture that has infiltrated the subsurface. Multiplying this ratio by the average annual precipitation yields the average annual infiltration rate. The following TMB equation (Cook and others, 1994) was used to estimate net infiltration rates at Sand Hollow:

$$q = \frac{\int_0^{\infty} \theta(z)c\ (z)dz}{\sum_{i=1}^{\infty} w_i c_i e^{-i\lambda}} \ , \qquad (2)$$

where q is the net infiltration flux rate (L T^{-1}),
$c(z)$ is the pore-water ^{3}H concentration at depth z (M L^{-3}),
$\theta(z)$ is the volumetric moisture content at depth z (L^3 L^{-3}),
w_i is a weighting function to correct for variations in annual net infiltration flux (the weighting function used for Sand Hollow was the ratio of precipitation during each year (i) to mean annual precipitation),
and $c^i e^{-i\lambda}$ is the decay-corrected ^{3}H concentration in precipitation i years before present (M L^{-3}).

The TDTP method is considered more accurate than the TMB method. However, at borehole sites without the presence of a clearly discernable 1963 vadose-zone ^{3}H peak, the TMB method must be used to estimate net infiltration. The TMB method [1] requires knowledge of the ^{3}H input function (the historical record of ^{3}H in precipitation), which is generally not known for each site and must be interpolated from sparsely-located GNIP stations at other locations having different wind and climate patterns, [2] it may overpredict net infiltration at sites where surface-water runon has occurred, [3] part of the ^{3}H within the shallow root zone may eventually be recycled into the atmosphere rather than becoming net infiltration, causing an overestimate of net infiltration rates when ^{3}H in the root zone is included in the total mass of vadose-zone ^{3}H.

For estimating the ^{3}H input function at Sand Hollow, the nearest GNIP stations are Flagstaff, Ariz., Salt Lake City, Utah, and Albuquerque, N. Mex., located at distances of 270, 425, and 650 km, respectively. Also, since no early ^{3}H precipitation measurements were made at any of these stations, the Sand Hollow ^{3}H input function prior to the early 1960's is based only on correlations with the Ottawa, Canada station located more than 3,000 km to the northeast at a much more northerly latitude. Error associated with root zone ^{3}H in the mass-balance calculation is not considered an important factor at the borehole sites in Sand Hollow because of the exposed or shallowly buried sandstone, where minimal root penetration occurs.

Net infiltration was calculated at seven borehole sites by using the TDTP method, with rates ranging from 2.6 to more than 57 mm/yr (table 3). Net infiltration was calculated at 11 borehole sites by using the TNB method, with rates ranging from 1.2 to 14.7 mm/yr. At the seven sites where both ^{3}H methods were applied, the ratio of the mass-balance to depth-to-peak net infiltration rates was used as a correction factor for the sites where only the mass-balance method was applied. This correction factor ranged from 1.5 to 2.3. Therefore, the reported infiltration rates based on borehole ^{3}H in Table 4 for the four sites without TDTP rates (2, 12, 27, 38) are the TMB method rates of Table 3 multiplied by an average correction factor of 2.0. The use of this correction factor assumes that the TDTP method is more accurate than the TMB method, which requires an estimate of historical ^{3}H precipitation concentrations and may underestimate net infiltration because of runoff.

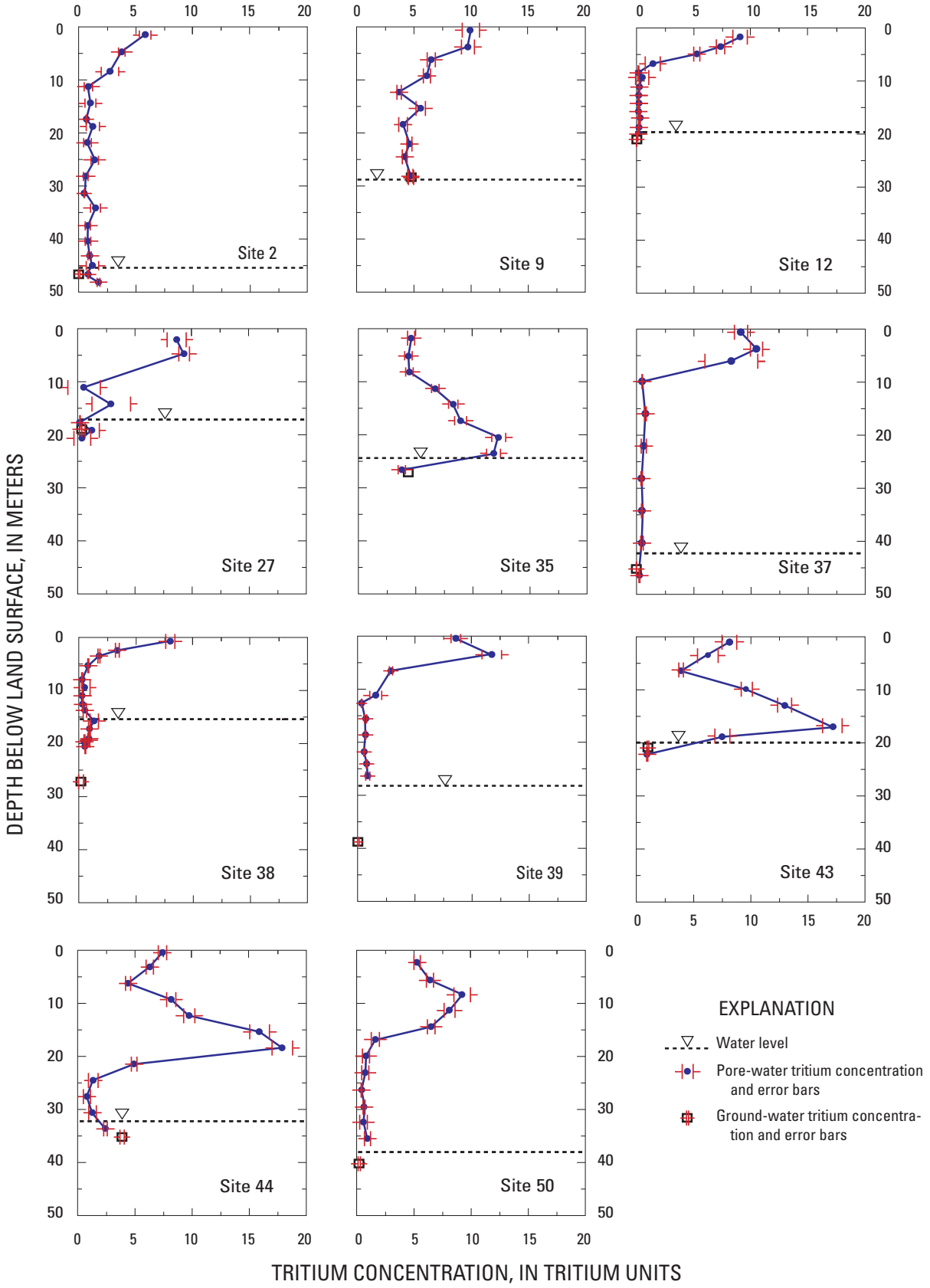

Figure 12. Tritium concentration of pore-water and ground-water samples collected from selected boreholes at the Sand Hollow ground-water-recharge study area, Utah.

The highest TDTP net infiltration rates were determined to be beneath exposed bedrock sites 9, 35, 43, and 44. Sites 9 and 44 are located in ephemeral washes or rivulets that receive surface-water runoff from nearby exposed sandstone during storms. Site 43 is located on nearly flat lying exposed sandstone away from the ephemeral wash channel, thus not receiving as much surface-water runoff. Site 35 is located on coarser-grained sand dune deposits. Because the 1960s ^{3}H peak has already been flushed out of the 29-m-thick vadose zone at site 9, a minimum TDTP net infiltration rate of 57 mm/yr is estimated from equation 6 with the mean water content of 7.9 percent. Sites 35, 43 and 44 have ^{3}H peaks at depths between 17 and 20 m (fig. 12) and water contents above the ^{3}H peaks of 5.9 to 7.0 percent, resulting in calculated TDTP net infiltration rates of 26 through 34 mm/yr. It is assumed that steeply dipping areas of exposed sandstone away from ephemeral wash channels in Sand Hollow would have net infiltration rates of less than about 25 mm/yr because of the potential for higher runoff than at site 43. Unfortunately, this could not be confirmed because of inaccessibility to drilling. TDTP net infiltration rates are lower at sites 35, 37, 39, and 50, which are covered by unconsolidated finer-grained soils. ^{3}H peaks at these sites are determined to be at depths of about 3 to 20 m and water contents ranged from 2.7 to 4.9 percent, resulting in net infiltration rates from 2.6 to 26 mm/yr. The other four sites without discernable ^{3}H peaks all have loamy very fine sand or fine sandy loam soil cover and low uncorrected TMB net infiltration rates, ranging from 1.2 to 2.1 mm/yr.

Tritium in Ground Water

The ^{3}H concentration of ground water within Sand Hollow ranged from below detection (0.01) to almost 7 TU (table 5; fig. 13). Higher concentrations of ^{3}H indicate areas where substantial amounts of recent precipitation have reached the water table. Because of its 12.3-year half-life, ground water originating as precipitation at Sand Hollow more than 50 years ago would likely have a ^{3}H concentration of less than 0.5 TU. Therefore, shallow ground-water ^{3}H concentrations greater than 0.5 TU indicate areas where active recharge has recently occurred either at or upgradient of the borehole. All of the wells that contain water with ^{3}H concentrations of more than 0.5 TU are screened within 10 m of the water table. A correlation of lower ground-water Cl concentration with higher ground-water ^{3}H concentration (fig. 14) indicates that areas of the aquifer receiving active recharge correspond to areas where infiltrating precipitation undergoes less solute enrichment in the root zone by evaporation and transpiration.

Stable Isotopes

Stable Isotopes in Precipitation

Stable-isotope ratios of precipitation at Sand Hollow range from +4.2 to –126.4 per mil for $\delta^{2}H$ and from +3.3 to –15.5 per mil for $\delta^{18}O$ (table 1). A local meteoric water line (LMWL) was constructed by linear curve-fitting to the stable-isotope ratios of precipitation samples collected at Sand Hollow between 1999 and 2002 (fig. 15; table 1). The equation for this LMWL is:

$$\delta^{2}H = 7.61\,\delta^{18}O - 0.03, \qquad (3)$$

This LMWL has a shallower slope and a smaller y-intercept than the global meteoric water line, which has a slope of 8 and a y-intercept of 10 (Craig, 1961). The slope and intercept of the LMWL is similar to other published precipitation-isotope data from other arid locations in the southwestern United States (Welch and Preissler, 1986).

Stable Isotopes in the Vadose Zone

Vadose-zone pore-water stable-isotope ratios range from –46 to –113 per mil for $\delta^{2}H$ and from +0.5 to –14.0 per mil for $\delta^{18}O$ (Heilweil, 2003). Although this range of values is smaller than the range in precipitation values, the vertical borehole profiles generally show much variability in the shallower part of the vadose zone, varying less and converging to the ground-water value at or near the water table (fig. 16). This indicates that little pore-water mixing occurs in the vadose zone.

Pore-water samples from high-recharge sites (9, 43, 44, 50) have a mean $\delta^{2}H$ concentration of –88 per mil, whereas pore waters from low-recharge sites (2, 4, 12, 27, 37, 38, 46) have a mean $\delta^{2}H$ concentration of –75 per mil and follow an evaporative trend below the LMWL (fig. 15). This evaporative shift was quantified by calculating the expected $\delta^{18}O$ concentration with the measured $\delta^{2}H$ concentration and the LMWL given in equation 3. The evaporative shift calculated for each site is the average value from land surface to the water table (table 4). The smallest shift of 2.1 per mil at the highest recharge site and the largest shift of 4.7 per mil at the lowest recharge site support the hypothesis that less evaporative loss occurs where infiltration can quickly move beneath the root zone in the more active recharge areas of the basin.

Stable Isotopes in Ground Water

Ratios of stable isotopes in ground water at Sand Hollow range from –79 to –94 per mil for $\delta^{2}H$ (mean of –86 per mil) and –9.7 to –11.9 per mil for $\delta^{18}O$ (mean of –11.1 per mil; table 5). These ratios are within a much narrower range than in precipitation and vadose-zone pore waters. These values also plot closer to the local meteoric water line, showing less evaporative effects than the vadose-zone pore waters (fig. 15).

Table 5. Isotope and chloride concentrations of ground-water samples collected at the Sand Hollow ground-water-recharge study area, Utah.

[Site numbers refer to figure 5. Abbreviations: δ^2H, deuterium; δ^{18}O, 18-oxygen; ^{3}H, tritium; TU, tritium units; mg/L, milligrams per liter; ±, plus or minus; —, no data available]

Site number	Well name	Date sampled	δ^2H, in per mil	δ^{18}O, in per mil	^{3}H, in TU	Chloride, in mg/L
1a	Well 1 (Wayne Wilson)	1/4/2000	–83	–11.5	0.03 ± 0.05	18.6
2	WD 12	[1] 4/30/1999	–85	–11.3	0.53 ± 0.38	22.0
2	WD 12	[1,2] 4/30/1999	–83	–11.0	—	—
2	WD 12	[1,2] 4/30/1999	–86	—	—	—
2	WD 12	9/12/2002	–85	–10.8	0.02 ± 0.06	20.0
3a	Well 2 (east side of reservoir) at 75 m	10/9/2002	–89	–11.7	0.33 ± 0.02	17.3
3b	Well 2 (east side of reservoir) at 122 m	10/10/2002	–89	–11.5	0.55 ± 0.20	17.8
3c	Well 2 (east side of reservoir) at 152 m	10/10/2002	–92	–11.7	—	—
3d	Well 2 (east side of reservoir) at 187 m	10/10/2002	–92	–11.8	0.02 ± 0.02	13.2
3e	Well 2 (east side of reservoir) at 229 m	10/10/2002	–94	–11.9	0.22 ± 0.06	14.3
5	WD 10	[1] 6/12/2001	–85	–11.0	0.45 ± 0.25	25.0
5	WD 10	[1,2] 6/12/2001	–84	–11.1	—	—
5	WD 10	9/13/2001	–85	–11.2	0.73 ± 0.35	25.6
6	Well 4 (Sky Ranch 2)	3/30/1999	–84	–11.6	0.52 ± 0.36	20.4
6	Well 4 (Sky Ranch 2)	8/29/2001	–85	–11.1	0.26 ± 0.21	44.4
6	Well 4 (Sky Ranch 2)	9/11/2002	–86	–11.0	—	42.0
7	Dale Wilson	4/28/1999	–84	–10.2	0.40 ± 0.26	39.0
7	Dale Wilson	[2] 4/28/1999	–83	—	—	—
8	WD 4	4/2/1999	–86	–11.0	0.22 ± 0.10	18.1
8	WD 4	2002/12/18	-85	–10.8	—	18.8
9	WD 6	2001/05/15	[3]–82	[3]–10.7	[3] 4.77 ± 0.24	[3] 7
9	WD 6	2001/08/28	–79	–10.5	6.88 ± 0.34	2.9
11	WD 2	1999/04/02	–90	–11.3	0.38 ± 0.45	30.0
12	IFP 1	[1] 4/20/1999	–86	–11.0	0.00 ± 0.66	19.9
12	IFP 1	[1,2] 4/20/1999	–82	–11.1	—	—
12	IFP 1	[1,2] 4/20/1999	–84	—	—	—
13	IFP 1 (port 1)	5/18/2002	—	—	0.12 ± 0.05	—
16	IFP 1 (port 4)	5/18/2002	—	—	0.03 ± 0.03	—
17	IFP 1 (port 5)	5/17/2002	—	—	0.00 ± 0.01	—
18	IFP 5 shallow	5/17/2002	–87	–10.5	0.08 ± 0.08	—
18	IFP 5 shallow	[2] 5/17/2000	–84	–10.7	—	—
18	IFP 5 shallow	[2] 5/17/2000	–85	–10.7	—	—
19	IFP 5 medium	5/17/2002	–85	–11.0	0.18 ± 0.14	—
20	IFP 5 deep	5/17/2002	–86	–11.0	0.08 ± 0.05	[4] 21.1
26	IFP 2	4/21/1999	–84	–11.6	—	21.3
26	IFP 2	[2] 4/21/1999	–85	—	—	—
27	Wash 1	4/20/1999	–86	–11.2	0.27 ± 0.10	28.1
27	Wash 1	[2] 4/20/1999	–85	—	—	—
29	Well 9 (east side of north dam)	8/30/1999	–86	–11.4	0.10 ± 0.04	13.0
31	WD 1	4/2/1999	–83	–10.6	0.37 ± 0.50	11.6
31	WD 1	[2] 4/2/1999	–84	—	—	—
31	WD 1	9/10/2002	–85	–10.9	—	—
32	WD RJ	4/2/1999	–83	–10.7	0.02 ± 0.05	46.0
32	WD RJ	12/17/2002	–84	–10.3	—	47.8
33	WD 5	4/3/1999	–85	–11.2	0.19 ± 0.06	43.5
33	WD 5	12/17/2002	–85	–10.6	—	44.8
34	WD 3	12/19/2000	–89	–10.6	0.28 ± 0.20	28.2
35	Hole N	5/25/2001	–82	–10.6	4.27 ± 0.21	6.6
36	WD 11	[1] 6/14/2001	–85	–9.7	1.19 ± 0.77	14.0
36	WD 11	9/14/2001	–86	–10.8	0.53 ± 0.08	22.5
37	WD 9	[1] 5/23/2001	–88	–11.5	0.00 ± 0.01	22.0
37	WD 9	9/14/2001	–86	–11.4	0.20 ± 0.15	17.9
37	WD 9	9/11/2002	–89	–11.5	—	21.4
38	Basin 1	[1] 7/22/1999	–88	–10.9	0.07 ± 0.21	58.3
38	Basin 1	9/10/2001	–84	–10.7	0.18 ± 0.21	64.0
39	Slope 1a	[1] 4/28/1999	–85	—	—	12.1
39	Slope 1a	7/20/1999	–85	–11.1	0.39 ± 0.18	—
39	Slope 1a	[2] 7/20/1999	–87	–11.1	—	—
39	Slope 1a	9/12/2001	–83	–11.4	0.44 ± 0.36	11.7
39	Slope 1a	9/9/2002	–86	–11.4	0.07 ± 0.06	10.1
42	Terracor 3	4/23/1999	–82	–10.9	0.53 ± 0.09	26.9
42	Terracor 3	[2] 4/23/1999	–82	—	—	—
42	Terracor 3	9/11/2001	–85	–11.0	0.28 ± 0.08	28.7
43	Hole O	[1] 6/11/2001	–84	–10.1	1.03 ± 0.07	21.0
43	Hole O	9/11/2001	–85	–10.3	1.09 ± 0.20	11.9
44	WD 8	[1] 5/21/2001	–81	–10.6	4.13 ± 0.38	9.2
44	WD 8	[1,2] 5/21/2001	–81	–10.6	—	—
44	WD 8	9/12/2001	–86	–10.9	2.98 ± 0.15	10.8
44	WD 8	9/9/2002	–85	–10.9	3.89 ± 0.19	10.1
46	Basin 2	[1] 5/5/1999	–87	—	—	—
46	Basin 2	7/21/1999	–86	–11.6	0.23 ± 0.35	11.8
46	Basin 2	[2] 7/21/1999	–86	–11.7	—	—
46	Basin 2	8/27/2001	–88	–11.1	0.18 ± 0.06	9.9
47	WD 13 (corral)	1/5/2000	–86	–11.6	0.43 ± 0.36	—
47	WD 13 (corral)	8/30/2001	–86	–11.4	0.29 ± 0.15	12.1
48	Well 17 (west dam)	5/18/2000	–87	–11.2	—	28.2
49	WD 14 (Terracor 2)	12/18/2002	–88	–11.4	0.32 ± 0.04	28.3
50	WD 7	9/10/2001	–85	–10.6	0.21 ± 0.09	18.0

[1] Collected prior to well installation.

[2] Replicate sample.

[3] Value affected by drilling and not considered representative.

[4] Collected on 11/29/2000.

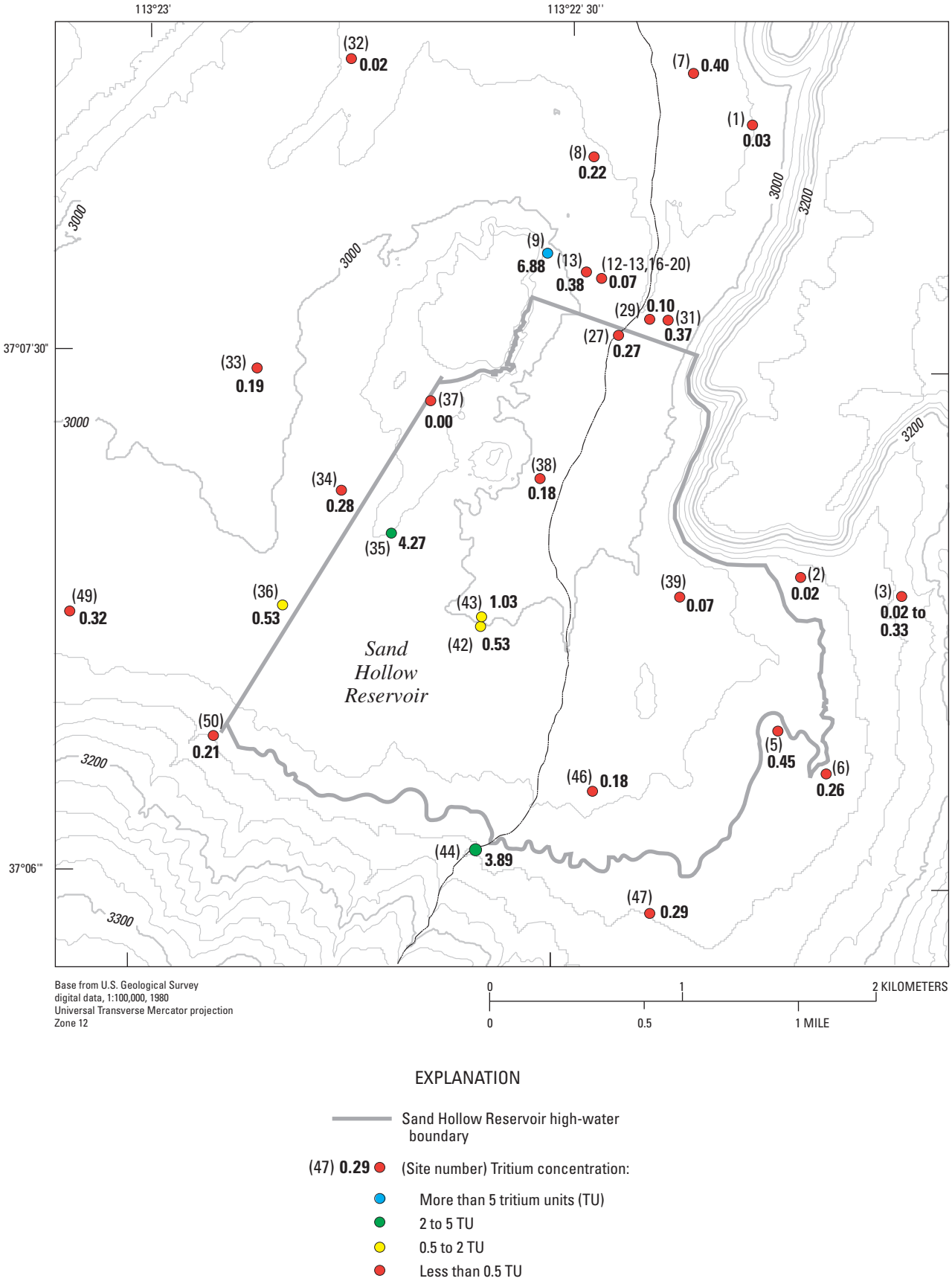

Figure 13. Tritium concentration in water from selected wells at the Sand Hollow ground-water-recharge study area, Utah.

Spatial and Temporal Variations in Recharge

Multiple environmental tracers were used at Sand Hollow in order to compare/contrast various independent lines of evidence regarding net infiltration and recharge rates. The combination of multiple tracer methods provides a higher level of confidence than any one method by itself. In addition, the individual methods can be used to investigate particular spatial and temporal patterns. Although both vadose-zone ^{3}H and Cl provide site-specific net infiltration estimates, ^{3}H targets modern (post 1950s) net infiltration whereas Cl provides a longer term record (up to about 12,000 years). Ground-water Cl yields more regionally averaged recharge estimates than vadose-zone methods because of horizontal hydraulic gradients and mixing in the well screen. Stable isotopes ($\delta^{2}H$ and $\delta^{18}O$), although not providing direct recharge rates, are useful for evaluating spatial and temporal differences in infiltration and recharge processes.

Spatial Variation in Recharge

Recharge within Sand Hollow is highly variable. Large differences likely are caused by local focusing of surface-water runoff, as well as variations in both surficial soil cover and topographic slope. This is illustrated by contrasting vadose-zone ^{3}H-based net infiltration rates at sites 12 (2.8 mm/yr) and 9 (more than 57 mm/yr), located less than 300 m apart. Site 9 is located along a small ephemeral wash with exposed sandstone and some coarse-grained sand deposits at the base of a steep sandstone outcrop that regularly receives surface-water runoff. Conversely, site 12 is located away from any potential pathway of surface-water runoff and is covered by relatively fine-grained soil (loamy fine sand, table 4). In general, relatively high net infiltration and recharge rates were observed at sites with focused surface-water runoff, coarse-grained soils, or shallowly sloping exposed bedrock. Low net infiltration and recharge rates were observed at sites with no surface-water runoff and fine-grained soils.

An initial hypothesis of infiltration and recharge at Sand Hollow, based on other vadose-zone bedrock studies, was that water would move preferentially along sandstone fractures to the water table. However, there is no correlation between higher net-infiltration rates, based on vadose-zone ^{3}H, and fracture density (fig. 17). To the contrary, rates are higher at borehole sites with less fracturing. This finding is supported by a recent modeling study of vadose-zone fracture flow (Ludwig, 2003), which determined that an open sandstone fracture with an aperture of 1 mm (typical of those measured in trenches in Sand Hollow) would not saturate and become preferential flow conduits, even during periods of intense precipitation. Rather, the numerical simulations showed that [1] surface infiltration through fractures is quickly imbibed by the highly porous sandstone; and [2] the larger pore-throat diameters of fractures act as capillary barriers to flow, especially in arid settings.

Although recharge rates at individual sites vary depending on the particular environmental-tracer method, the various environmental tracers used in this study generally show similar trends. Higher recharge rates are generally correlated with smaller vadose-zone $\delta^{18}O$ shifts, smaller vadose-zone Cl accumulation, higher shallow ground-water ^{3}H concentrations, and less depleted $\delta^{2}H$ values (table 4).

Net infiltration and recharge rates based on all three Cl mass-balance methods generally were well correlated, although the vadose-zone Cl rates were generally lower than the ground-water Cl rates. Two exceptions to this were sites 39 and 46, which had much higher ground-water Cl rates (15 mm/yr) than those based on vadose-zone Cl within the bulge (0.05 to 0.1 mm/yr), vadose-zone Cl beneath the bulge (4 mm/yr and 3 mm/yr, respectively), and vadose-zone tritium (2.6

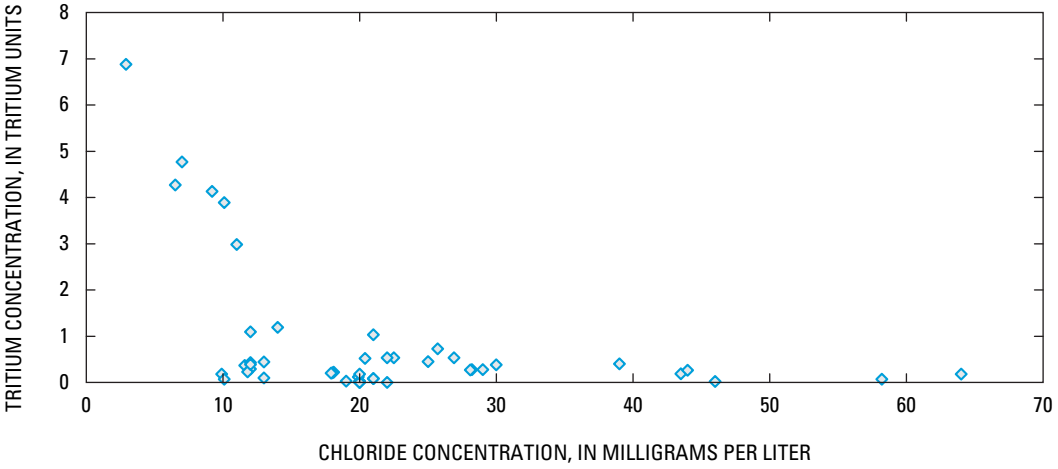

Figure 14. Relation of tritium concentration to chloride concentration in water from selected wells at the Sand Hollow ground-water-recharge study area, Utah.

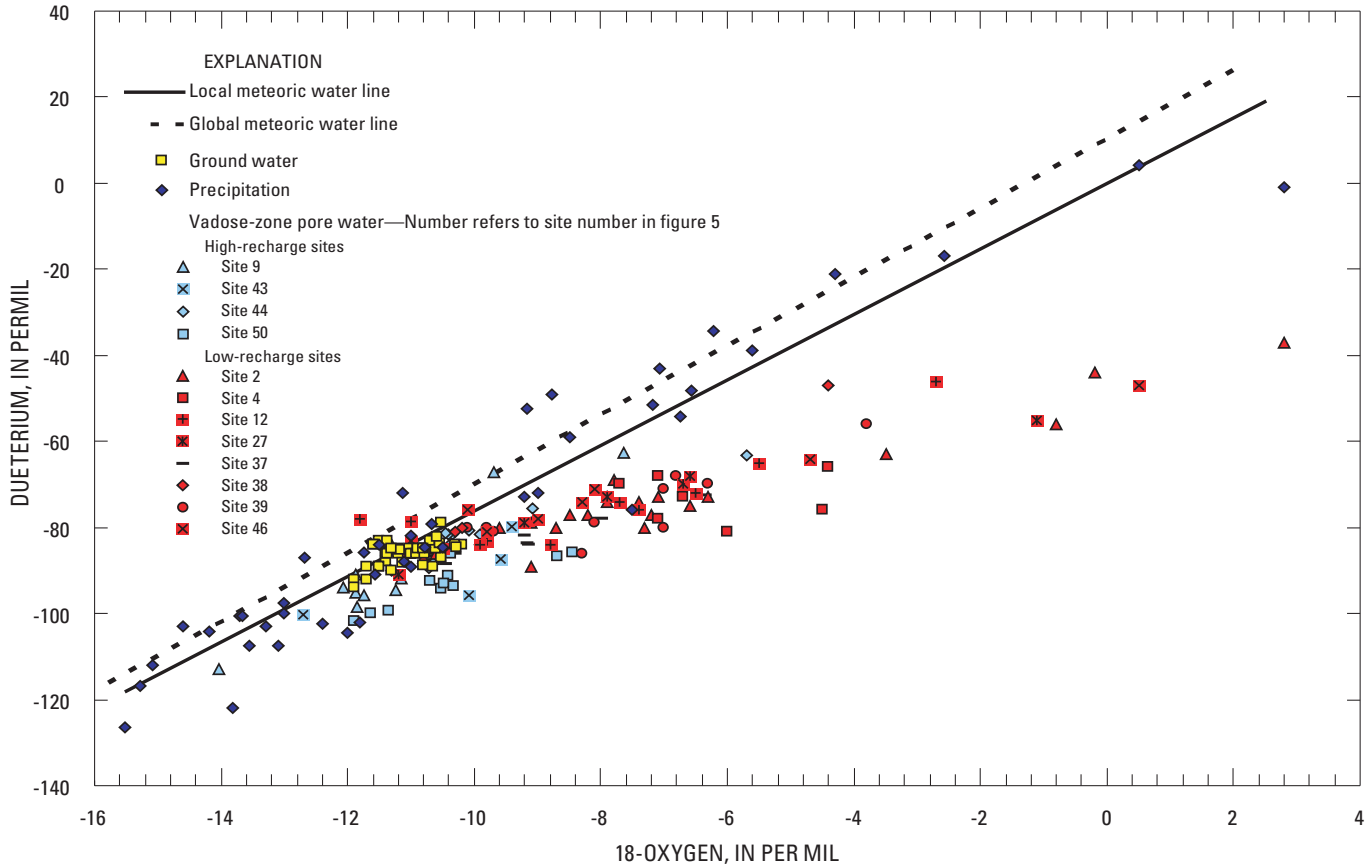

Figure 15. Relation between the stable-isotope ratios of hydrogen and oxygen in vadose-zone pore water, water samples from selected wells, and precipitation at the Sand Hollow ground-water-recharge study area, Utah.

mm/yr at site 39). Vadose-zone water potential measurements at four depths at site 39 were consistent with these low vadose zone environmental tracer-based recharge rates, showing no substantial infiltration events between January 2000 and September 2002 (fig. 18). At both sites, pore-water Cl concentrations decrease dramatically when crossing from the deep vadose zone into the underlying water table (Heilweil, 2003). These anomalies may be caused by upgradient areas having higher recharge rates than the vadose zones at each of these two sites. An upgradient high-recharge area would result in ground-water mounding and a large horizontal component of flow beneath the water table at the downgradient site. Therefore, the low Cl concentration of shallow ground water at these two sites likely represents upgradient recharge conditions, whereas the higher Cl concentration of the deep vadose-zone represents in-situ recharge conditions.

Stable-isotope ratios were also used for evaluating spatial variability of recharge in Sand Hollow. Assuming average δ^2H values of –75 per mil for the low-recharge site vadose-zone pore waters, –88 per mil for the high-recharge site vadose-zone pore waters, and –86 per mil for ground water, a two-end-member mixing model indicates that about 85 percent of ground-water recharge in Sand Hollow occurs at high-recharge sites.

Temporal Variations in Recharge

The vadose zone at Sand Hollow is an archive of past climate. Vadose-zone Cl bulges characteristic of those occurring in unconsolidated desert soils were observed in many of the boreholes, an unusual finding for bedrock. This Cl has been accumulating in the vadose zone of Sand Hollow for as much as 12,000 years (since the early Holocene; table 2), whereas ^3H has only been accumulating for the past 50 years. Thus, the two tracers can be used for looking at net infiltration during different time intervals.

For the group of 11 sites having vadose-zone tritium information, vadose-zone ^3H-based infiltration rates are always higher (2.4 to more than 57 mm/yr; geometric mean of 9 mm/yr) than infiltration rates calculated by using shallow vadose-zone Cl within the bulge (0.08 to 8 mm/yr; mean of 2.1 mm/yr; table 4). Since the total mass of Cl within the bulge represents from 50 to 12,000 years of accumulation, this implies that infiltration rates during the past few decades were generally higher than during previous centuries to millennia. Such recently higher net infiltration may have flushed down Cl that previously accumulated in the shallow root zone, a possible reason why the average depth

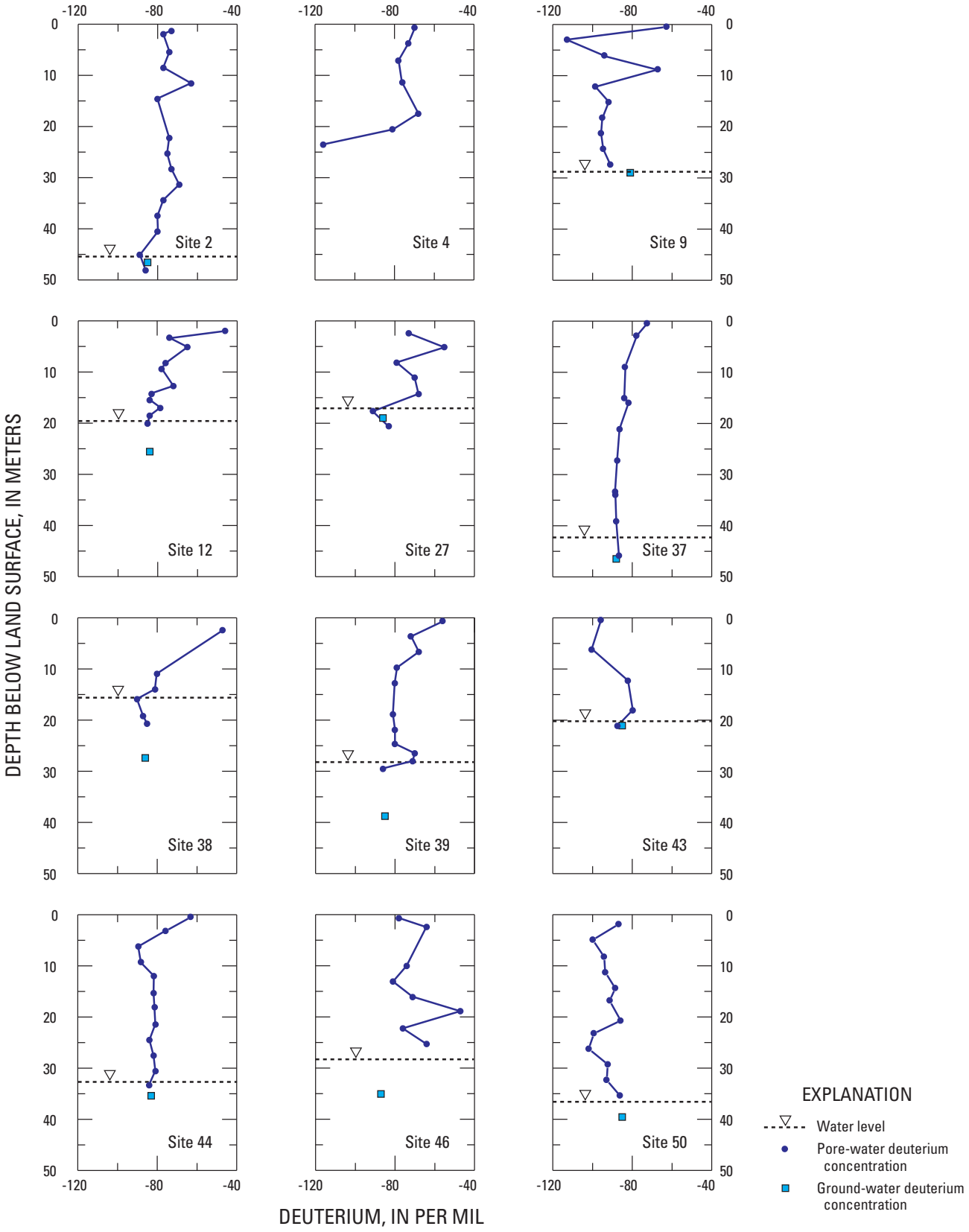

Figure 16. Stable-isotope ratio of hydrogen in pore-water and ground-water samples collected from selected boreholes at the Sand Hollow ground-water-recharge study area, Utah.

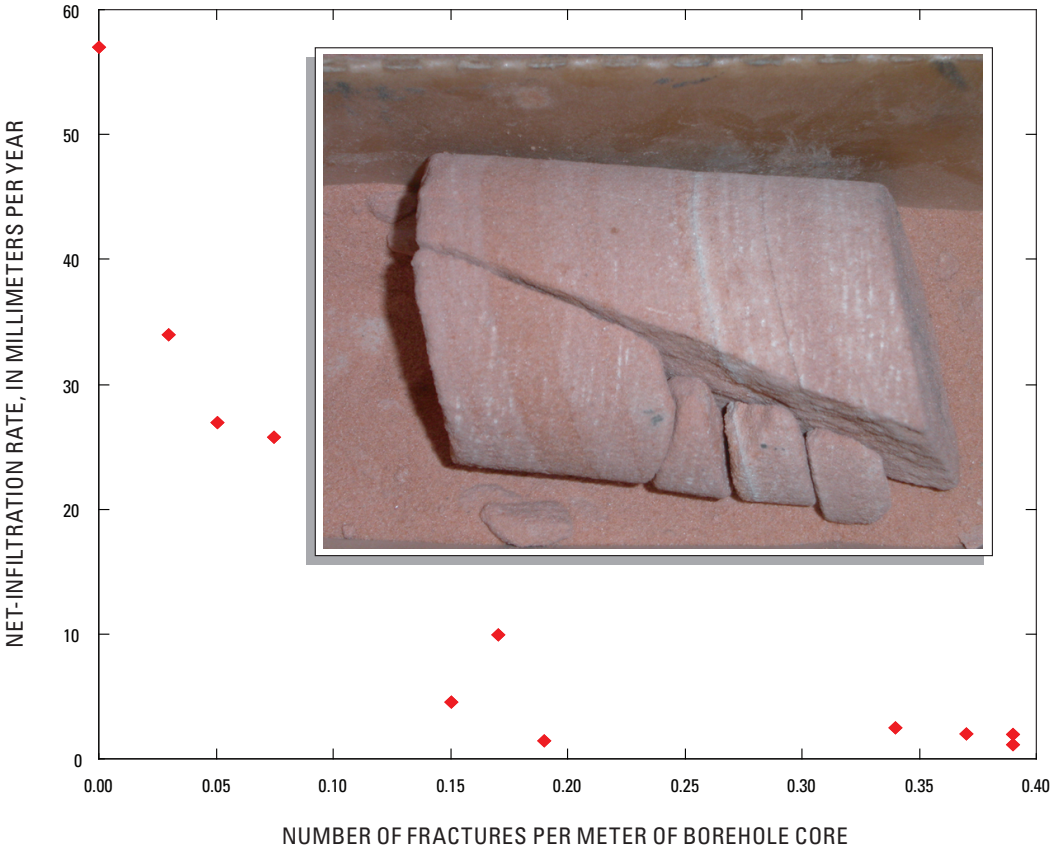

Figure 17. Relation of net infiltration rate, based on vadose-zone tritium concentration, to fracture density obtained from core samples at the Sand Hollow ground-water-recharge study area, Utah.

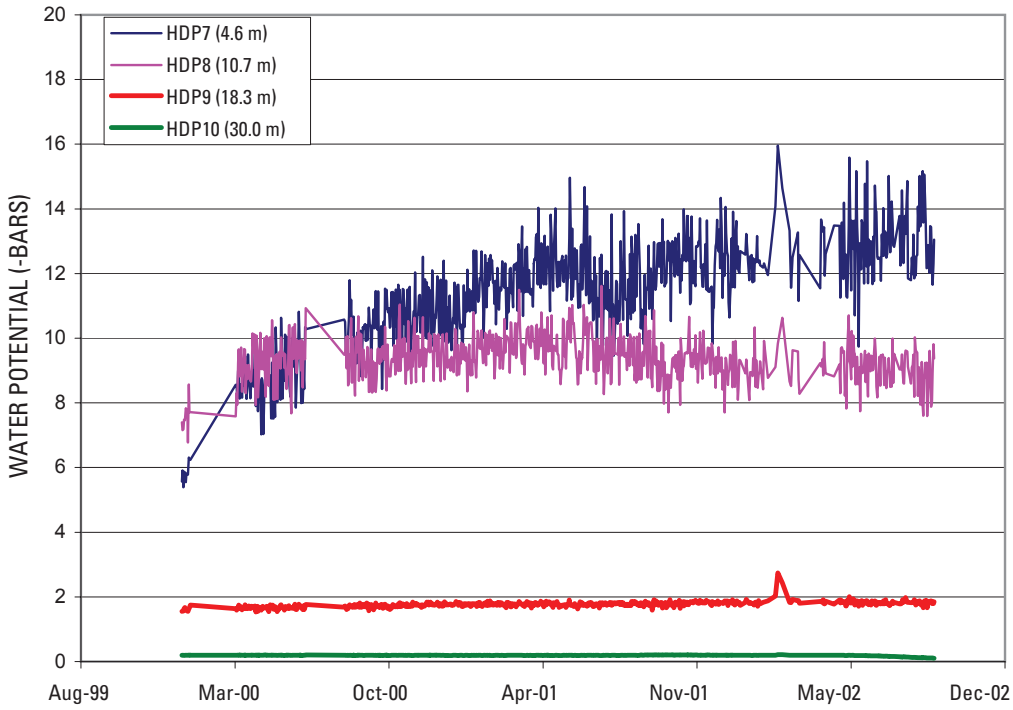

Figure 18. Vadose-zone water potential measured with heat dissipation probes at various depths below land surface at site 39, Sand Hollow ground-water-recharge study area, Utah.

of 5 m to the Cl bulge peaks at the borehole sites is much greater than the maximum soil thickness and root zone depth of about 1.5 m.

Comparison of ^{3}H-based net infiltration rates to deeper vadose-zone Cl-based net infiltration rates beneath the bulge is not as straightforward. For the group of high-recharge sites (9, 35, 43, 44, 50), vadose-zone ^{3}H-based infiltration rates are higher (9 to more than 57 mm/yr) than vadose-zone Cl-based rates from beneath the bulge (3 to 13 mm/yr; table 4). These sites contain up to about 800 years of total vadose-zone Cl accumulation and this deeper Cl represents 50 to 80 percent of this accumulation, indicating that infiltration rates in high-recharge settings during recent decades was higher than during previous centuries. However, for the group of low-recharge sites (2, 12, 27, 37, 38, 39), vadose-zone ^{3}H-based infiltration rates (2.4 to 4.6 mm/yr) are similar to vadose-zone Cl-based rates from beneath the bulge (2 to 5 mm/yr). The total amount of Cl beneath the bulge at these low-recharge sites represents only a small fraction of the total vadose-zone Cl accumulation (0 to 40 percent), but represents the oldest preserved vadose-zone information regarding infiltration and indicates that rates earlier in the Holocene were similar to the higher rates of recent decades.

Eight of the 12 borehole sites drilled to the water table have shallow ground-water ^{3}H concentrations of less than 0.5 TU, indicating recharge that occurred more than 50 years ago. Modern ^{14}C ages indicate that these ground waters are of Holocene age (Heilweil, 2003). Recharge rates based on ground-water Cl concentrations at these 8 boreholes range from 3 to 15 mm/yr, much higher than the 0.05 to 0.7 mm/yr vadose-zone Cl bulge recharge rates or the 2 to 5 mm/yr Cl-based net infiltration rates below the bulge (table 4). Higher ground-water Cl-based recharge rates may be caused by higher recharge in upgradient areas. However, another possibility is that the ground-water Cl-based recharge rates indicate a wetter climatic period earlier in the Holocene than recharge rates represented by both the shallow and deep vadose-zone Cl. If so, this implies that a full swing in climatic cycle has occurred, with higher recharge rates earlier in Holocene changing to lower rates in the later Holocene, returning again to higher rates during the past 50 years. This is consistent with Holocene variations in recharge to the Navajo Sandstone observed at Black Mesa, Ariz. (Zhu, 2000) and is supported by the meteorological record, which shows an anomalously large number of 30-day periods between 1957 and 1997 with over 100 mm of precipitation at St. George.

Recent changes in infiltration rates resulting from changing soil cover or land use may have occurred at sites 27 and 38, resulting in vadose-zone environmental tracer concentrations that are not in equilibrium with current net infiltration conditions. Unlike the other 11 boreholes in table 2, these sites are located in or near the main ephemeral wash of Sand Hollow and do not fit the trend of increasing peak concentration of the shallow Cl bulge with increasing total vadose-zone Cl accumulation. Considering the total accumulation of Cl in the vadose zone, the peak Cl concentration of 1,900 mg/L at site 27 is lower than expected. Although this site is presently situated in the ephemeral wash, solute distributions in nearby trench excavations indicate that the wash had recently migrated from a location farther to the east (Heilweil and Solomon, 2004). The lower-than-expected peak concentration of the shallow Cl bulge at this site is consistent with a recent shift to higher net infiltration beneath the active wash channel, which would push downward and dilute a preexisting shallow Cl bulge. The high cumulative vadose-zone Cl at the site indicates that the previously accumulated Cl has not yet been flushed out of the vadose zone.

The very shallow (1.8 m depth) and higher-than-expected peak Cl concentration of 14,700 mg/L (table 2) at site 38 may indicate a recent change to lower net infiltration rates and increased runon of Cl. This site is located adjacent to a section of the ephemeral wash that was impounded by a small levee built by cattle ranchers about 50 years ago (L. Jessup, Washington County Water Conservancy District, oral commun., 2001) and is now covered with about 0.5 m of fine-grained silts that have settled out of surface-water runoff. Prior to the existence of the levee, the site was likely a higher recharge site on the natural wash channel. This would explain the low Cl concentrations measured below a 3-m depth, the poor correlation between total Cl accumulation and peak Cl concentration, the low vadose-zone ^{3}H-based net infiltration rate, and a small average vadose-zone $\delta^{18}O$ evaporative (2.2 per mil) similar to the highest recharge sites (table 4). The very high Cl concentration in the shallow subsurface likely represents a combination of salt accumulation from runon and evaporative enrichment associated with decreased infiltration through the shallow, low-permeability silts at the site.

The uniformity of ground-water stable-isotope ratios at the more negative end of the range of precipitation values indicates that most of the net infiltration reaching the water table comes from cooler-season precipitation. The more depleted $\delta^{2}H$ values (–84 to –88 per mil) of ground water having ages between about 50 years and a few thousand years (based on ^{3}H concentrations less than 0.5 TU and modern apparent ^{14}C ages) from the low-recharge sites compared to less depleted $\delta^{2}H$ values (–79 to –85 per mil) of ground water at high-recharge sites (table 4) may indicate that the source of this older shallow ground water was cooler-temperature recharge. One scenario hypothesis for this is a higher percentage of winter precipitation prior to the 1950s, indicating less summer monsoonal precipitation relative to winter Pacific storms than at present.

Conclusions

The combination of multiple vadose-zone and ground-water environmental tracer techniques is used to evaluate various aspects of infiltration and recharge at Sand Hollow, including basin-average rates, site-specific (spatial) processes, and seasonal to millennial temporal variations. Spatial variations in

infiltration and recharge rates show that most recharge occurs in areas with coarse soils or exposed bedrock that receive focused runoff. However, substantial amounts of direct infiltration and recharge also occur beneath coarse-grained sandy soils away from washes. This is contrary to findings generally reported from alluvial desert basins receiving similar amounts of precipitation, where little or no basin-floor recharge away from washes is generally thought to occur. This indicates that more moisture is able to pass beyond the maximum rooting depth and become net infiltration where permeable bedrock formations are exposed or shallowly buried. Bedrock prevents substantial root penetration and plant transpiration. Also, lower ground-water Cl concentrations are clearly correlated with higher ground-water ^{3}H concentrations, indicating that areas of the aquifer receiving active recharge correspond to areas where infiltrating precipitation is able to bypass the concentration of solutes in the shallow root zone.

Tritium and chloride were also used to explore temporal variations in infiltration and recharge. Vadose-zone Cl concentrations at some borehole locations represent up to 12,000 years of accumulation, whereas vadose-zone ^{3}H has only been accumulating during the past 50 years. Net-infiltration rates at individual borehole sites range from 2.4 to at least 57 mm/yr calculated from vadose-zone ^{3}H concentrations, 0.03 to 8 mm/yr from vadose-zone Cl concentrations within the Cl bulge, 0.5 to 13 mm/yr from vadose-zone Cl concentrations beneath the Cl bulge, and 3 to 60 mm/yr from ground-water Cl concentrations. Because of the different time periods represented by these environmental tracers, it is inferred that recharge rates at Sand Hollow have changed from higher rates during the early Holocene to lower rates during the past few centuries/millenia, back to higher rates during the latter part of the 20th century, illustrating the cyclical nature of desert bedrock recharge.

Ground-water tracer concentrations provide a more spatially averaged recharge flux than vadose-zone tracers. The basin-wide average recharge rate calculated from the ground-water Cl mass-balance method is about 8 mm/yr, or about 4 percent of precipitation. Ground-water stable-isotope ratios are generally more depleted (isotopically lighter) than the seasonally weighted mean value of local precipitation samples, indicating that net infiltration and recharge occurs predominantly during the cooler winter months. The seasonally weighted mean value of $\delta^{2}H$ in precipitation is -79 per mil, compared to the -86 per mil mean of shallow ground water. A two-end-member mixing model of stable-isotope ratios from vadose-zone pore waters indicates that about 85 percent of recharge occurs in high-infiltration areas of Sand Hollow. Similarly, calculated $\delta^{18}O$ evaporative shifts of pore waters from low-infiltration sites are larger than from the high-infiltration sites. Stable isotopes in ground water show that most infiltration occurs during cooler months and that a larger percent of cooler-season recharge occurred prior to the 1950s than during recent decades.

References Cited

Allison, G.B., 1988, A review of some of the physical, chemical, and isotopic techniques available for estimating groundwater recharge, *in* Simmers, I., ed., Estimation of natural groundwater recharge: Norwell, Mass., D. Riedel Publishers, p. 49–72.

Allison, G.B., Gee, G.W., and Tyler, S.W., 1994, Vadose-zone techniques for estimating groundwater recharge in arid and semi-arid regions: Soil Science Society of America Journal, v. 58, p. 6–14.

Allison, G.B., and Hughes, M.W., 1978, The use of environmental chloride and tritium to estimate total recharge to an unconfined aquifer: Australian Journal of Soil Resources, v. 16, p. 181–195.

Andraski, B.J., 1997, Soil-water movement under natural-site and waste-site conditions, A multiple-year field study in the Mojave Desert, Nevada: Water Resources Research, v. 33, p. 1901–1916.

Ang, A., H-S., and Tang, W.H., 1975, Probability concepts in engineering planning and design, volume 1—basic principles: New York, John Wiley & Sons, 409 p.

Blanchard, P.J., 1986a, Ground-water conditions in the Kaiparowits Plateau area, Utah and Arizona, with emphasis on the Navajo Sandstone: Utah Department of Natural Resources Technical Publication 81, 87 p.

Blanchard, P.J.,1986b, Ground-water conditions in the Lake Powell area, Utah: Utah Department of Natural Resources Technical Publication 84, 64 p.

Brenner, I.S., 1974, A surge of maritime tropical air—Gulf of California to the southwestern United States: Monthly Weather Reviews, v. 102, p. 375–389.

Clark, W.B., Jenkins, W.J., and Top, Z., 1976, Determination of tritium by mass spectrometric measurements of ^{3}He: International Journal of Applied Radiation and Isotopes, v. 27, p. 515–522.

Cook, P.G., Jolly, I.D., Leaney, F.W., Walker, G.R., Allan, G.L., Fifield, L.K. and Allison, G.G., 1994, Unsaturated zone tritium and chlorine 36 profiles from southern Australia—Their use as tracers of soil water movement: Water Resources Research, v. 31, p. 1709–1719.

Cordova, R.M., 1978, Ground-water conditions in the Navajo Sandstone in the Central Virgin River Basin, Utah: Utah Department of Natural Resources Technical Publication 61, 66 p.

Cordova, R.M., 1981, Ground-water conditions in the Upper Virgin River and Kanab Creek Basins area, Utah, with emphasis on the Navajo Sandstone: Utah Department of Natural Resources Technical Publication 70, 87 p.

Cordova, R.M., Sandberg, G.W., and McConkie, W., 1972, Ground-water conditions in the Central Virgin River Basin, Utah: Utah Department of Natural Resources Technical Publication 40, 64 p.

Craig, H., 1961, Isotopic variations on meteoric waters: Science, v. 133, p. 1702–1703.

Davis, S.N., Whittemore, D.O., and Fabryka-Martin, J., 1998, Uses of chloride/bromide ratios in studies of potable water: Ground Water, v. 36, p. 338–350.

Danielson, T.W., and Hood, J.W., 1984, Infiltration to the Navajo Sandstone in the Lower Dirty Devil River Basin, Utah, with emphasis on techniques used in its determination: U.S. Geological Survey Water-Resources Investigation Report 84–4154, 45 p.

Dettinger, M.D., 1989, Reconnaissance estimates of natural recharge to desert basins in Nevada, U.S.A., by using chloride-balance calculations: Journal of Hydrology, v. 106, p. 55–78.

Eychaner, J.H., 1983, Geohydrology and effects of water use in the Black Mesa area, Navajo and Hopi Indian Reservations, Arizona: U.S. Geological Survey Water-Supply Paper 2201, 26 p.

Flint, A.L., Flint, L.E., Kwickless, E.M., Fabryka-Martin, J.T., and Bodvarsson, G.S., 2002, Estimating recharge at Yucca Mountain, Nevada, USA, Comparison of methods: Hydrogeology Journal, v. 10, p. 180–204.

Friedman, I., Smith, G.I., Gleason, J.D., Warden, A., and Harris, J.M., 1992, Stable isotope composition of waters in southeastern California, 1—Modern precipitation: Journal of Geophysical Research, v. 97, no. D5, p. 5795–5812.

Gray, S.T., Betancourt, J.L, Fastie, C.L., and Jackson, S.T., 2003, Patterns and sources of multidecadal oscillations in drought-sensitive tree-ring records from the central and southern Rocky Mountains: Geophysical Research Letters, v. 30, no. 6, p. 49-1 through 49-4.

Hartsough, P., Tyler, S.W., Sterling, J., and Walvoord, M., 2001, A 14.6 kyr record of nitrogen flux from desert soil profiles as inferred from vadose zone pore waters: Geophysical Research Letters, v. 28, no. 15, p. 2955–2958.

Heilweil, V.M., 2003, Recharge to the Navajo Sandstone aquifer of southwestern Utah: Salt Lake City, Utah, Ph.D. dissertation, 278 p.

Heilweil, V.M., and Freethey, G.W., 1992, Simulation of ground-water flow and water-level declines that could be caused by proposed withdrawals, Navajo Sandstone, southwestern Utah and northwestern Arizona: U.S. Geological Survey Water-Resources Investigation Report 90–4105, 51 p.

Heilweil, V.M., Freethey, G.W., Stolp, B.J., Wilkowske, C.D., and Wilberg, D.E., 2000, Geohydrology and numerical simulation of ground-water flow in the central Virgin River Basin of Iron and Washington Counties, Utah: Utah Department of Natural Resources Technical Publication 116, 139 p.

Heilweil, V.M., and Solomon, D.K., 2004, Millimeter- to kilometer- scale variations in vadose-zone bedrock solutes, implications for estimating recharge in arid settings, *in* Hogan, J.F., Phillips, F.M., and Scanlon, B.R., eds., Groundwater recharge in a desert environment—The Southwestern United States: American Geophysical Union, Water Science and Applications Series, v. 9, p. 49–67, doi:10.1029/0009WSA04.

Hood, J.W., and Danielson, T.W., 1981, Bedrock aquifers in the Lower Dirty Devil River Basin area, Utah, with special emphasis on the Navajo Sandstone: Utah Department of Natural Resources Technical Publication 68, 143 p.

Hood, J.W., and Patterson, D.J., 1984, Bedrock aquifers in the northern San Rafael Swell area, Utah, with special emphasis on the Navajo Sandstone: Utah Department of Natural Resources Technical Publication 78, 128 p.

Hurlow, H.A., 1998, The geology of the Central Virgin River Basin, southwestern Utah, and its relation to ground-water conditions: Utah Department of Natural Resources Water Resources Bulletin 26, 53 p.

Izbicki, J.A., Radyk, J., and Michel, R.L., 2002, Movement of water through the thick unsaturated zone underlying Oro Grande and Sheep Creek Washes in the western Mojave Desert, USA: Hydrogeology Journal, v. 10, p. 409–427.

Kimball, B.A., 1992, Geochemical indicators used to determine source of saline water in Mesozoic aquifers, Montezuma Canyon area, Utah, *in* Subitzky, S., ed., Selected papers in the hydrologic sciences, 1988–1992: U.S. Geological Survey Water Supply Paper 2340, p. 89–106.

Ludwig, D.E., 2003, Numerical simulation of tritium transport in an unsaturated fractured sandstone: Salt Lake City, Utah, master's thesis, 84 p.

Maxey, G.B., and Eakin, T.E., 1950, Groundwater in the White River Valley, White Pine, Nye and Lincoln Counties, Nevada: Nevada State Engineer, Water Resources Bulletin 8, 59 p.

Naftz, D.L., Peterman, Z.E., and Spangler, L.E., 1997, Using $\delta^{87}Sr$ values to identify sources of salinity to a freshwater aquifer, greater Aneth Oil Field, Utah, USA: Chemical Geology, v. 141, p. 195–209.

Nimmo, J.R., Stonestrom, D.A., and Akstin, K.C., 1994, The feasibility of recharge rate determinations using the steady-state centrifuge method: Soil Science Society of America Journal, v. 58, p. 49–56.

Phillips, F.M., 1994, Environmental tracers for water movement in desert soils of the American Southwest: Soil Science Society of America Journal, v. 58, p. 15–24.

Prudic, D.E., 1994, Estimates of percolation rates and ages of water in unsaturated sediments at two Mojave Desert sites, California-Nevada: U.S. Geological Survey Water-Resources Investigation Report 94–4160, 19 p.

Rasmussen, T.C., and Evans, D.D., 1993, Water infiltration into exposed fractured rock surfaces: Soil Science Society of America Journal, v. 57, p. 324–329.

Robson, S.G., and Banta, E.R., 1995, Ground water atlas of the United States, segment 2—Arizona, Colorado, New Mexico, Utah: U.S. Geological Survey Hydrologic Investigations Atlas 730–C.

Scanlon, B.R., Healy, R.W., and Cook, P.G., 2002, Choosing appropriate techniques for quantifying groundwater recharge: Hydrogeology Journal, v. 10, p. 18–39.

Scanlon, B.R., 2004, Evaluation of methods of estimating recharge in semiarid and arid regions in the southwestern U.S., *in* Hogan, J.F., Phillips, F.M., and Scanlon, B.R., eds., Groundwater Recharge in a Desert Environment—The Southwestern United States: American Geophysical Union, Water Science and Applications Series, v. 9, p. 235–254, doi:10.1029/0009WSA13.

Thomas, B.E., 1986, Simulation analysis of water-level changes in the Navajo Sandstone due to changes in the altitude of Lake Powell near Wahweap Bay, Utah and Arizona: U.S. Geological Survey Water-Resources Investigation Report 85–4207, 45 p.

Tyler, S.W., Chapman, J.B., Conrad, S.H., Hammermeister, D.P., Blout, D.O., Miller, J.J., Sully, M.J. and Ginnani, J.M., 1996, Soil-water flux in the southern Great Basin, United States—Temporal and spatial variations over the last 120,000 years: Water Resources Research, v. 32, p. 1481–1499.

U.S. Census Bureau, 2003, United States Census 2000 State and County Quick Facts, accessed February 11, 2003 at http://quickfacts.census.gov.

Washington County Water Conservancy District, 1995, Purpose and need executive summary: Saint George, Utah, 84 p.

Weiss, E., 1987, Ground-water flow in the Navajo Sandstone in parts of Emery, Grand, Carbon, Wayne, Garfield, and Kane Counties, southeast Utah: U.S. Geological Survey Water-Resources Investigations Report 86–4012, 41 p.

Welch, A.H., and Preissler, A.M., 1986, Aqueous geochemistry of the Bradys Hot Springs geothermal area, Churchill County, Nevada, *in* Subitzky, S., ed., Selected papers in the hydrologic sciences, U.S. Geological Survey Water-Supply Paper 2290, p. 17–36.

Weng, C., and Jackson, S.T., 1999, Late Glacial and Holocene vegetation history and paleoclimate of the Kaibab Plateau, Arizona: Paleogeography, Paleoclimatology, Paleoecology, v. 153, p. 179–201.

Western Regional Climate Center, 2003, Monthly and annual precipitation at St. George, Utah (station 427516), accessed February 11, 2003 at http://www.wrcc.dri.edu.

Wilde, F.D., Radtke, D.B., Gibs, J., and Iwatsubo, R.T., eds., 1998, Collection of Water Samples, *in* National field manual for the collection of water-quality data: U.S. Geological Survey Techniques of Water-Resources Investigations Book 9 Chapter 4, 103 p.

Wood, W.W., and Sanford, W.E., 1995, Chemical and isotopic methods for quantifying ground-water recharge in a regional, semi-arid environment: Ground Water, v. 33, p. 458–468.

Zhu, C., 2000, Estimate of recharge from radiocarbon dating of groundwater and numerical flow and transport modeling: Water Resources Research, v. 36, p. 2607–2620.

Zhu, C., Winterle, J.R., and Love, E.I, 2003, Late Pleistocene and Holocene groundwater recharge from the chloride mass balance method and chlorine-36 data, Water Resources Research, v. 39, 1182, p. SBH4:1–15.

Chapter I Appendix—Determination of Mean and Variance of Ground-Water Recharge

For a function Y composed of n statistically independent variables:

$$Y = f(X_1, X_2, ..., X_n), \tag{I–1}$$

the first order approximation of the mean, $\overline{Y}$, and variance, $Var\,(Y)$ can be defined, respectively, as

$$\overline{Y} \approx f\ (\overline{X}_1, \overline{X}_2, ..., \overline{X}_n), \text{ and} \tag{I–2}$$

$$Var(Y) = \left[\frac{\partial Y}{\partial X_1}\right]^2 Var(X_1) + \left[\frac{\partial Y}{\partial X_2}\right]^2 Var(X_2) + ... + \left[\frac{\partial Y}{\partial X_n}\right]^2 Var(X_n), \tag{I–3}$$

where the partial derivatives are evaluated at the mean value of the respective parameter (Ang and Tang, 1975).

Therefore, the variance in the net infiltration or recharge rate, q, is defined as

$$Var(q) = \left[\frac{\partial q}{\partial [Cl_{dep}]}\right]^2 Var[Cl_{dep}] + \left[\frac{\partial q}{\partial [Cl_{gw}]}\right]^2 Var[Cl_{gw}] + \left[\frac{\partial q}{\partial P}\right]^2 Var[P]. \tag{I–4}$$

Ephemeral-Stream Channel and Basin-Floor Infiltration and Recharge in the Sierra Vista Subwatershed of the Upper San Pedro Basin, Southeastern Arizona

By Alissa L. Coes and Donald R. Pool

Abstract

The timing and location of streamflow in the San Pedro River are partially dependent on the aerial distribution of recharge in the Sierra Vista subwatershed. Previous investigators have assumed that recharge in the subwatershed occurs only along the mountain fronts by way of stream-channel infiltration near the contact between low-permeability rocks of the mountains and the basin fill. Recent studies in other alluvial basins of the Southwestern United States, however, have shown that significant recharge can occur through the sediments of ephemeral stream channels at locations several kilometers distant from the mountains. The purpose of this study was to characterize the spatial distribution of infiltration and subsequent recharge through the ephemeral channels in the Sierra Vista subwatershed.

Infiltration fluxes in ephemeral channels and through the basin floor of the subwatershed were estimated by using several methods. Data collected during the drilling and coring of 16 boreholes included physical, thermal, and hydraulic properties of sediments; chloride concentrations of sediments; and pore-water stable-isotope values and tritium activity. Surface and subsurface sediment temperatures were continuously measured at each borehole.

Twelve boreholes were drilled in five ephemeral stream channels to estimate infiltration within ephemeral channels. Active infiltration was verified to at least 20 meters at 11 of the 12 borehole sites on the basis of low sediment-chloride concentrations, high soil-water contents, and pore-water tritium activity similar to present-day precipitation. Consolidated sediments at the twelfth site prevented core recovery and estimation of infiltration. Analytical and numerical methods were applied to determine the surface infiltration flux required to produce the observed sediment-temperature fluctuations at six sites. Infiltration fluxes were determined for summer ephemeral flow events only because no winter flows were recorded at the sites during the monitoring period.

Four boreholes were drilled in the basin floor to estimate infiltration in areas between ephemeral channels. Infiltration fluxes through the basin floor ranged from less than 1 centimeter to 6 centimeters per year. At a site in semiconsolidated to consolidated basin-fill conglomerate, the long-term infiltration fluxes were very low (less than 1 centimeter per year). Chloride, tritium, and stable-isotope data indicate long periods of no net deep downward percolation flux beneath the basin floor. At a site in unconsolidated to semiconsolidated basin-fill sand and gravel, infiltration fluxes were high (2 to 6 centimeters per year). Chloride, tritium, and stable-isotope data indicate active infiltration to 8 meters, and a decrease in infiltration below 8 meters. The change in the infiltration rate below 8 meters is controlled by an increase in the silt and clay content of the sediment.

Ephemeral-channel recharge for the entire subwatershed was estimated by upscaling the calculated infiltration fluxes and weighting the fluxes by streamflow duration, evaporation, and transpiration. In contrast to previous assumptions, recharge from ephemeral-streamflow infiltration occurs not only near the mountain fronts, but also along significant lengths of ephemeral channels. Although most of the ephemeral streams in the subwatershed flow less than a few days per year, the available streamflow quickly infiltrates past depths where it is available for evapotranspiration. This water likely stays in the unsaturated zone until it is vertically displaced by infiltrated water from subsequent streamflows and eventually recharges the regional aquifer. Ephemeral-channel infiltration during 2001 and 2002 was estimated to account for about 12 to 19 percent of the estimated average annual recharge in the Sierra Vista subwatershed.

Introduction

An improved understanding of the recharge distribution in the Sierra Vista subwatershed of the Upper San Pedro ground-water basin was needed to better estimate the effects of ground-water withdrawals on natural discharges from the system through base flow and riparian vegetation. The interception of ground water that would flow naturally from recharge areas to the San Pedro River by pumping could result in decreased streamflows in the river. The timing and location of the reduced streamflow are dependant on the location of the withdrawal wells, the hydraulic properties of the aquifer, and the aerial distribution of recharge. Recharge occurring downgradient of withdrawal wells is less likely to be cap-

tured by withdrawal wells and more likely to discharge to the river. Improved understanding of recharge distributions will enable local, State, and Federal organizations and agencies to effectively manage available water resources to meet water needs in the basin. Toward this goal, the U.S. Geological Survey (USGS), in cooperation with the Bureau of Land Management (BLM) and the Upper San Pedro Partnership, has collected and analyzed hydrologic information describing infiltration and recharge, ground- and surface-water interactions, water-level and ground-water storage trends, and geometry and lithology of the aquifer. This report documents the results of investigations of recharge by stream-channel and basin-floor infiltration, potentially important recharge mechanisms in the basin.

The Sierra Vista subwatershed encompasses about 2,460 square kilometers (km^2) in the southern part of the San Pedro River Basin in southeastern Arizona (fig. 1) and extends about 43 km north from the international boundary with Mexico to near Fairbank, Ariz. The subwatershed is part of a broad alluvial basin and is bounded on the west by the Huachuca Mountains and on the east by the Mule Mountains and the Tombstone Hills. Elevations of the basin floor vary from about 1,150 to 1,310 m; mountain elevations range from about 1,520 to 2,900 m.

The San Pedro River flows northward through the subwatershed (fig. 1). The river and its associated ground-water system support a corridor of riparian vegetation that hosts several endangered species and is an important habitat for American migratory birds. About 64 km of the river and riparian area has been protected by designation as the San Pedro Riparian National Conservation Area (SPRNCA; fig. 1), and is managed by the BLM.

Sierra Vista, with a population of 37,775 in 2000, is the largest city in the subwatershed (U.S. Census Bureau, 2000). By 2020, the population of Sierra Vista is projected to be 52,571 (Arizona Department of Economic Security, 1997), an increase of 39 percent. Populations of other cities in the subwatershed in 2000 were 6,090 in Bisbee, 1,751 in Huachuca City, and 1,504 in Tombstone (U.S. Census Bureau, 2000).

Ground water is the primary source for municipal, domestic, livestock, and irrigation water needs in the subwatershed. As the population has increased, ground-water withdrawals have increased. The magnitude of the effect that these increasing withdrawals have on the river and its associated riparian vegetation is proportional to the amount and distribution of recharge to the ground-water system. Ground-water pumping intercepts part of the natural flow of water through the aquifer before the water reaches natural discharge areas. Therefore, to better understand and predict the effects of historic, present, and future ground-water withdrawals on natural discharge, the spatial and temporal variability of recharge rates must be adequately understood.

Previous investigators have assumed that recharge in the Sierra Vista subwatershed occurs only near the mountain fronts (Freethey, 1982; Corell and others, 1996; Goode and Maddock, 2000). They envisioned recharge occurring as stream-channel infiltration near the contact of the low-permeability rocks of the mountains and the basin fill. Recent studies in other alluvial basins of the Southwestern United States, however, have shown that significant recharge can occur through the sediments of stream channels far from the mountains (Blasch and others, 2000; Izbicki and others, 2000; Constantz and others, 2003). Direct infiltration of precipitation through the floors of alluvial basins in the Southwest has been considered negligible because of high evapotranspiration and low precipitation. The possibility of significant recharge along ephemeral stream channels far from the mountains or through direct infiltration on the basin floor places uncertainty on the adequacy of previous recharge concepts for use in the development of water-management plans.

Purpose and Scope

This report presents estimates of infiltration and recharge through the ephemeral channels and the basin floor of the Sierra Vista subwatershed, and documents the data collection and analysis. Data resulted from drilling and coring of 16 boreholes and included physical, hydraulic, and thermal properties of sediment; chloride concentrations of sediment; pore-water stable-isotope values and tritium activity; neutron-soil moisture and electromagnetic induction (EMI) logs; and continuous sediment-temperature profiles and water levels during 2001 and 2002. Unsaturated-zone infiltration processes at six ephemeral-stream channel sites were modeled to estimate infiltration and percolation fluxes during and following streamflows.

Land Cover

Major types of land cover include grassland (32.6 percent), desert scrub (28.8 percent), mesquite woodland (13.5 percent), and urban (5.3 percent; fig. 2; U.S. Environmental Protection Agency, 2003). The remaining 19.8 percent includes oak woodlands (15.2 percent) and forest (2.2 percent) in and near the mountains and the riparian (0.9 percent) and agricultural (0.8 percent) areas near the San Pedro and Babocomari Rivers (U.S. Environmental Protection Agency, 2003). Although the urban percentage is small, most of the urban land is concentrated in the north-central part of the subwatershed.

The hydrologic influence of each major land-cover type on the portion of precipitation that is transported to ephemeral stream channels has not been qualified. Some basic assumptions can, however, be inferred. Runoff produced in mesquite woodlands and desert scrub areas most likely is a small percentage of precipitation because leaves and branches can intercept precipitation and the high soil temperatures and low soil-moisture contents and potentials result in high soil permeability. Runoff from grasslands likely is a greater percentage of precipitation because the lower soil temperatures and higher soil-moisture contents result in lower soil permeability than that in mesquite woodlands and desert scrub areas. Urban

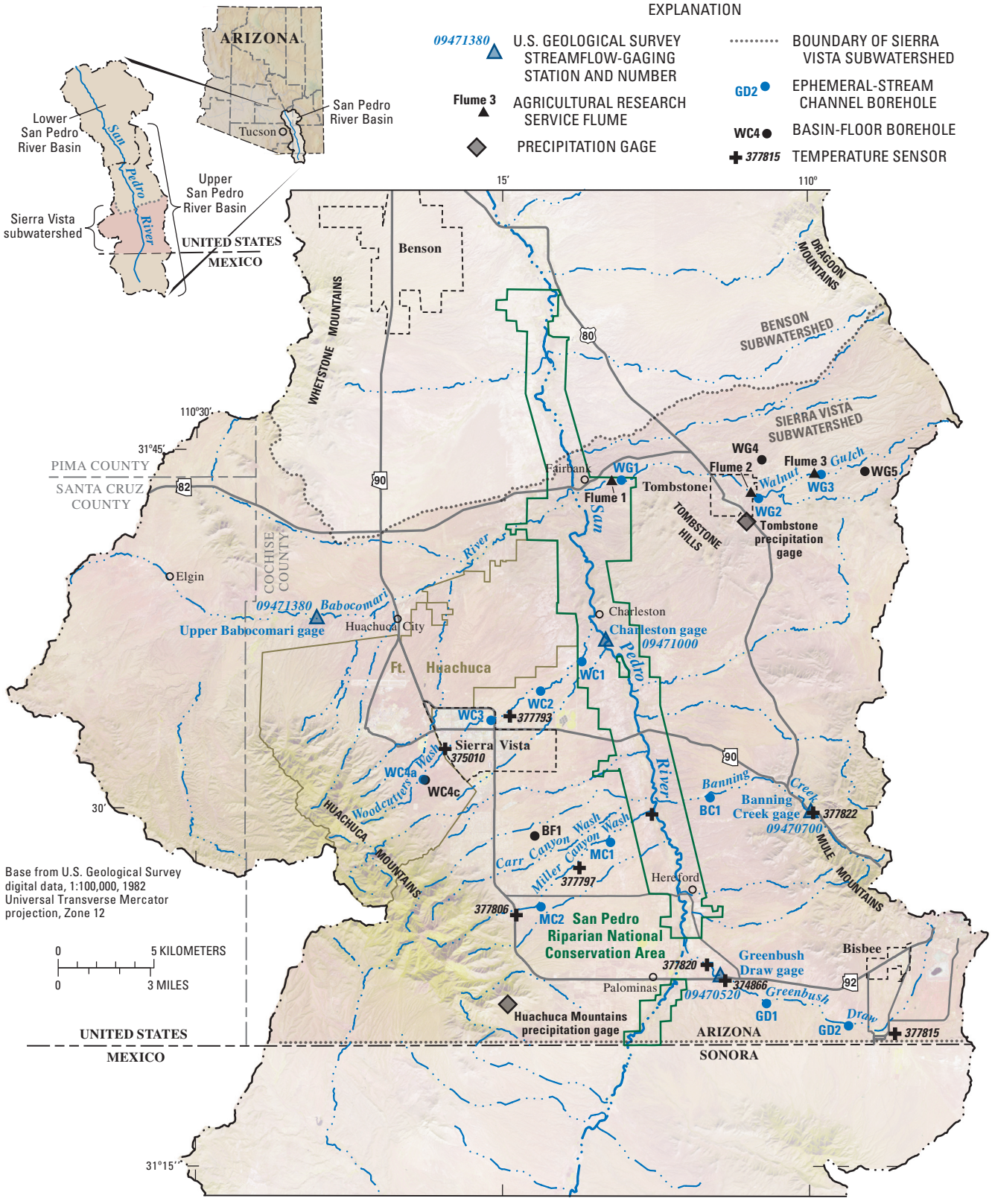

Figure 1. Map of the Sierra Vista ground-water-recharge study area, southeastern Arizona and northeastern Sonora, Mexico, showing the locations of boreholes, temperature sensors, Agricultural Research Service flumes, U.S. Geological Survey streamflow-gaging stations, and precipitation stations.

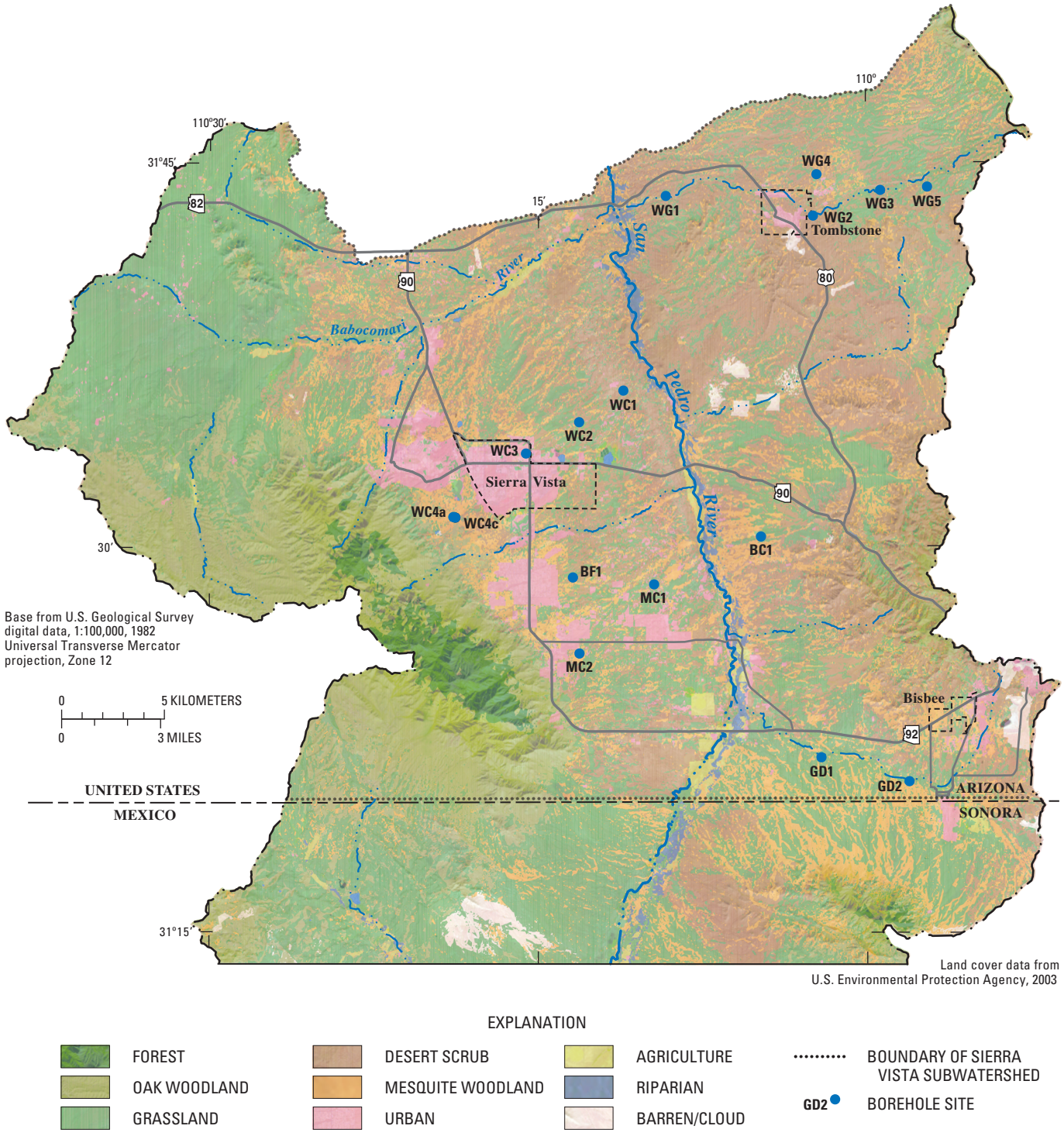

Figure 2. Land cover and locations of boreholes, Sierra Vista ground-water-recharge study area, Arizona and northeastern Sonora, Mexico.

areas produce the highest percentage of runoff into stream channels because of large expanses of impermeable surfaces that prevent soil infiltration and engineered drainage infrastructures that concentrate and focus runoff.

Soils

The distribution of soil types in the Sierra Vista subwatershed is dominated by lithic, loamy, and fine paleosoils near the mountains, and clayey soils and calcium carbonate soils along the lower reaches of the watersheds (fig. 3; U.S. Environmental Protection Agency, 2003). Narrow ribbons of sandy loam typically lie along ephemeral-stream channels; sandy, clayey, and calcium carbonate soils typically lie between the channels. Calcium carbonate soils dominate areas below the mountains across much of the eastern part of the subwatershed. A wedge of calcium carbonate soils also extends nearly to the mountains in the central part of the study area west of the San Pedro River. The southwestern part of the subwatershed is dominated by clayey and sandy soils.

Soil types can also have a strong influence on the fraction of precipitation that is transported to ephemeral-stream channels. Sandy loam soils likely are the most permeable, enabling direct infiltration of precipitation and limiting runoff into stream channels. Clayey soils can limit deep infiltration where they underlie channels. Soils having secondary calcium carbonate are less permeable and enhance runoff. Shallow lithic soils underlain by bedrock or rocky layers promote runoff into stream channels and limit infiltration.

Precipitation

The subwatershed climate is arid to semiarid. Precipitation data are available from the Western Regional Climate Center (2003) from a station in Tombstone, at an elevation of 1,384 m, from 1905 to 2002; and from a station in the Huachuca Mountains, at an elevation of 1,692 m, from 1956 to 2002 (figs. 1 and 4). Historically, July through September are the wettest months; precipitation during this period averages 21 cm at the Tombstone station and 27 cm at the Huachuca Mountains station. Precipitation from October through March averaged 12 and 23 cm at the Tombstone and Huachuca Mountains stations, respectively; and precipitation from April through June averaged less than 3 cm at both stations.

Long-term monitoring indicates that annual precipitation rates were above average before about 1940 and during the early to mid-1980s and below average from about 1940 to 1980; and annual precipitation was about average after the mid-1980s (Pool and Coes, 1999). Trends in seasonal precipitation, however, are different from trends in annual precipitation. From 1956 to 1997, winter (November–February) precipitation rates increased while wet-season (June 10–October) precipitation rates decreased (Pool and Coes, 1999).

Estimates of recharge in this report are biased by precipitation immediately prior to and during the monitoring period. Precipitation during the year that preceded the monitoring period, 2000, was normal (36 cm) at the Tombstone station, but wetter than normal (78 cm) at the Huachuca Mountains station (fig. 4). During 2000, the Huachuca Mountain station recorded an abnormally wet June and August, and October was the wettest month on record (32 cm). Precipitation during the monitoring period, 2001 and 2002, was dominated by dry winters and slightly drier than normal summers (fig. 4). During July through September of 2001 and 2002, precipitation was below average at the Tombstone station (16 and 17 cm, respectively) and slightly above average at the Huachuca Mountains station (29 cm during both years). Precipitation in October through June of 2001 and 2002 was below average at both stations.

Surface-Water Drainage System

The San Pedro River, an intermittent stream, drains the Sierra Vista subwatershed (fig. 1). Annual and wet-season runoff in the San Pedro River have declined since the mid-1910s, probably as a result of reduced precipitation duration and intensity, increased vegetation, and increased streamflow infiltration along ephemeral reaches of the river and its tributary streams (Pool and Coes, 1999). Base flow in the river is lowest during the summer, when rates of near-stream groundwater withdrawals by wells and phreatophytes are highest. Long-term records indicate that summer base flows have been declining since 1937 (Pool and Coes, 1999).

Tributaries of the San Pedro River are ephemeral except for the Babocomari River, which is perennial in some areas (fig. 5). Flow occurs only in direct response to rainfall or snowmelt, and the amount of flow is generally dependant on the spatial distribution and intensity of precipitation and the runoff characteristics of the channel and the associated drainage area. The temporal distribution of flow in ephemeral-stream channels in the arid Southwest generally is the result of monthly, annual, and decadal oscillations in precipitation frequency (Redmond and Koch, 1991; Webb and Betancourt, 1992).

The majority of tributaries to the San Pedro River originate in the mountains bounding the subwatershed and coalesce downstream to form higher-ordered ephemeral-stream channels (fig. 5). Tributaries generally have narrow, shallow channels close to the mountain fronts that become wide, deep channels below a knick point. Channels draining the east side of the Huachuca Mountains typically have long and narrow drainage areas and few channels coalescing downstream; the southern tributaries become wider and less incised towards the San Pedro River. Channels draining the western side of the Mule Mountains typically have much wider drainage areas and multiple channels coalescing downstream.

Ground-Water System

The ground-water system of the Sierra Vista subwatershed has been described by previous investigators (Brown

and others, 1966; Pool and Coes, 1999); an overview is given here. The primary aquifer in the subwatershed is within basin fill that overlies crystalline and sedimentary rocks. Secondary aquifers comprise stream alluvium beneath the flood plains of the San Pedro and Babocomari Rivers, and pre-basin fill and limestones that crop out in the mountains and hills surrounding the subwatershed. Ground water generally flows from recharge areas to discharge areas along the San Pedro and Babocomari Rivers. Ground water also discharges from the aquifer through ground-water withdrawals, evapotranspiration, springs, and ground-water underflow to the north.

Aquifers

The Pantano Formation, a consolidated to semiconsolidated conglomerate, overlies the bedrock in the subwatershed and is the oldest of the basin sediments. The formation probably is greater than 900 m thick in some areas (Halverson, 1984; Gettings and Houser, 1995). The Pantano Formation is a locally important water-bearing unit, as it yields water through fractures to many wells in the Sierra Vista area (Pool and Coes, 1999).

The basin fill that overlies the Pantano Formation has been divided into upper and lower units on the basis of com-

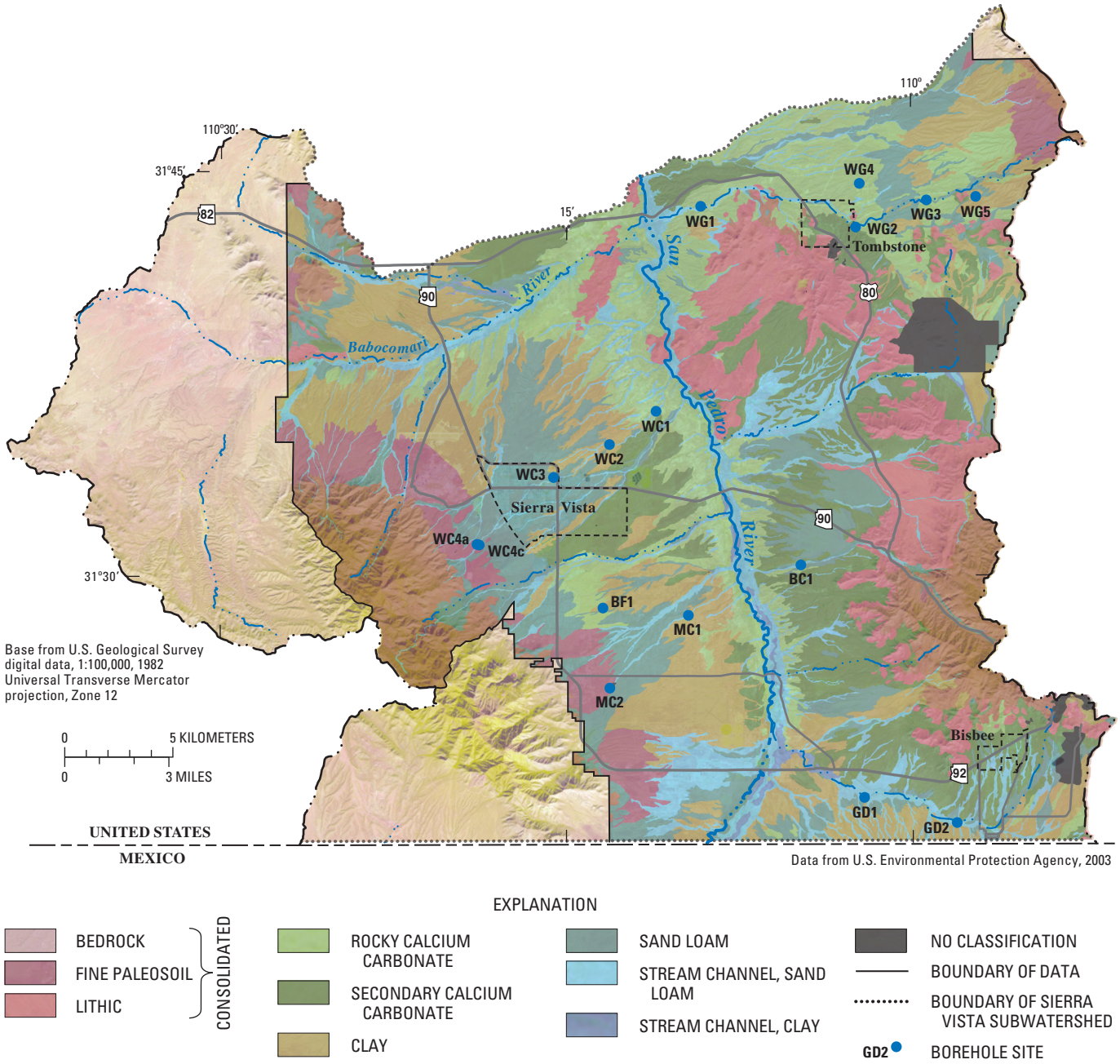

Figure 3. Soil type and locations of boreholes, Sierra Vista ground-water-recharge study area, Arizona and northeastern Sonora, Mexico.

positional, textural, and depositional differences. The lower unit consists of partially cemented interbedded gravel, sand, silt an clay that is often described as conglomerate, and ranges in thickness from about 45 to 90 m (Pool and Coes, 1999). Permeability of the lower unit varies because of variability in sediment size, sorting, and cementation (Brown and others, 1966). The upper unit consists of poorly cemented gravel, sand, silt, and clay (Brown and others, 1966), and is generally less than 120 m thick (Pool and Coes, 1999). The upper unit includes a permeable fan-gravel facies near the mountain fronts that grades to a poorly permeable silt and clay facies with interspersed sand and caliche beds near the basin center (Pool and Coes, 1999). Between the city of Sierra Vista and the San Pedro River, and between the city of Hereford and Highway 90, the upper unit is primarily a saturated confining bed of silt and clay (Pool and Coes, 1999). The upper and lower basin-fill units are the major water-yielding units in the Sierra Vista subwatershed and constitute the basin-fill aquifer. Water levels in the basin-fill aquifer range from less than 1 m to as much as 165 m (USGS data).

Terrace deposits of clay, silt, sand, and gravel overlie the upper basin fill in most areas. The deposits form a veneer of stream alluvium that is thin near the mountain fronts but is as much as 15 to 30 m thick in erosional channels that parallel the San Pedro River (Pool and Coes, 1999). Older terrace deposits include lakebed deposits of silt, clay, and marl (Haynes, 1968) that are local confining layers where they occur near the San Pedro River; erosion has removed most of the lakebed deposits along tributaries (Pool and Coes, 1999). Younger terrace deposits include stream alluvium along the San Pedro River and some of its tributaries (Pool and Coes, 1999). The older deposits are rarely saturated outside of the flood plains of the San Pedro and Babocomari Rivers; the younger deposits are saturated in some areas near the San Pedro and Babocomari Rivers and along some tributaries near the base of the mountains, and are locally important water-bearing units (Pool and Coes, 1999).

Recent stream alluvium lies along the San Pedro and Babocomari Rivers. Stream alluvium deposited prior to the entrenchment of the San Pedro River consists of clay, silt, and fine sand interbedded with coarse sand and gravel, and is as much as 6 m deep and 1.5 km wide (Pool and Coes, 1999). Stream alluvium deposited after the entrenchment of the San Pedro River consists of sand and gravel, and is less than 6 m

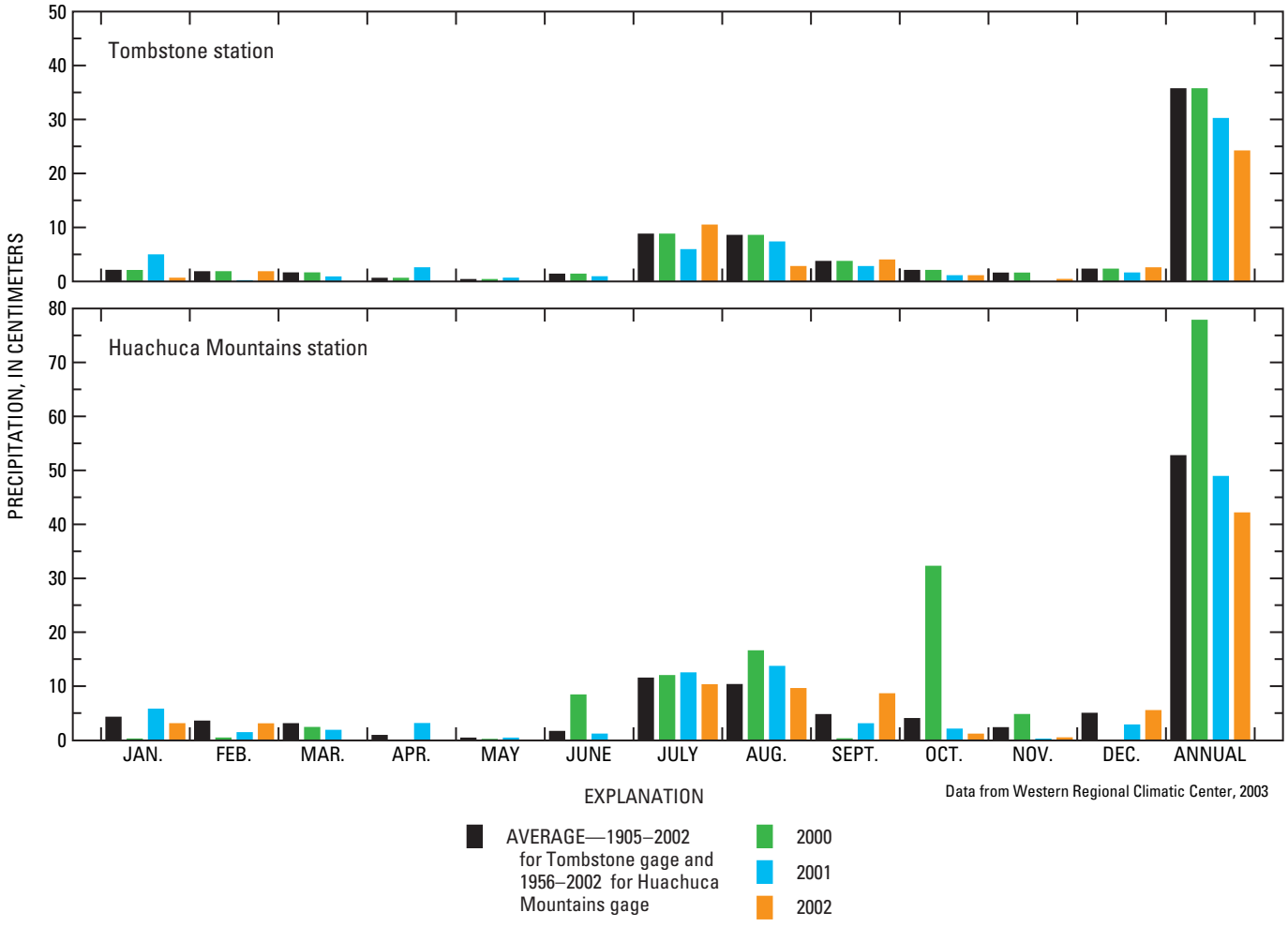

Figure 4. Monthly and annual precipitation at the Tombstone and Huachuca Mountains meteorologic stations.

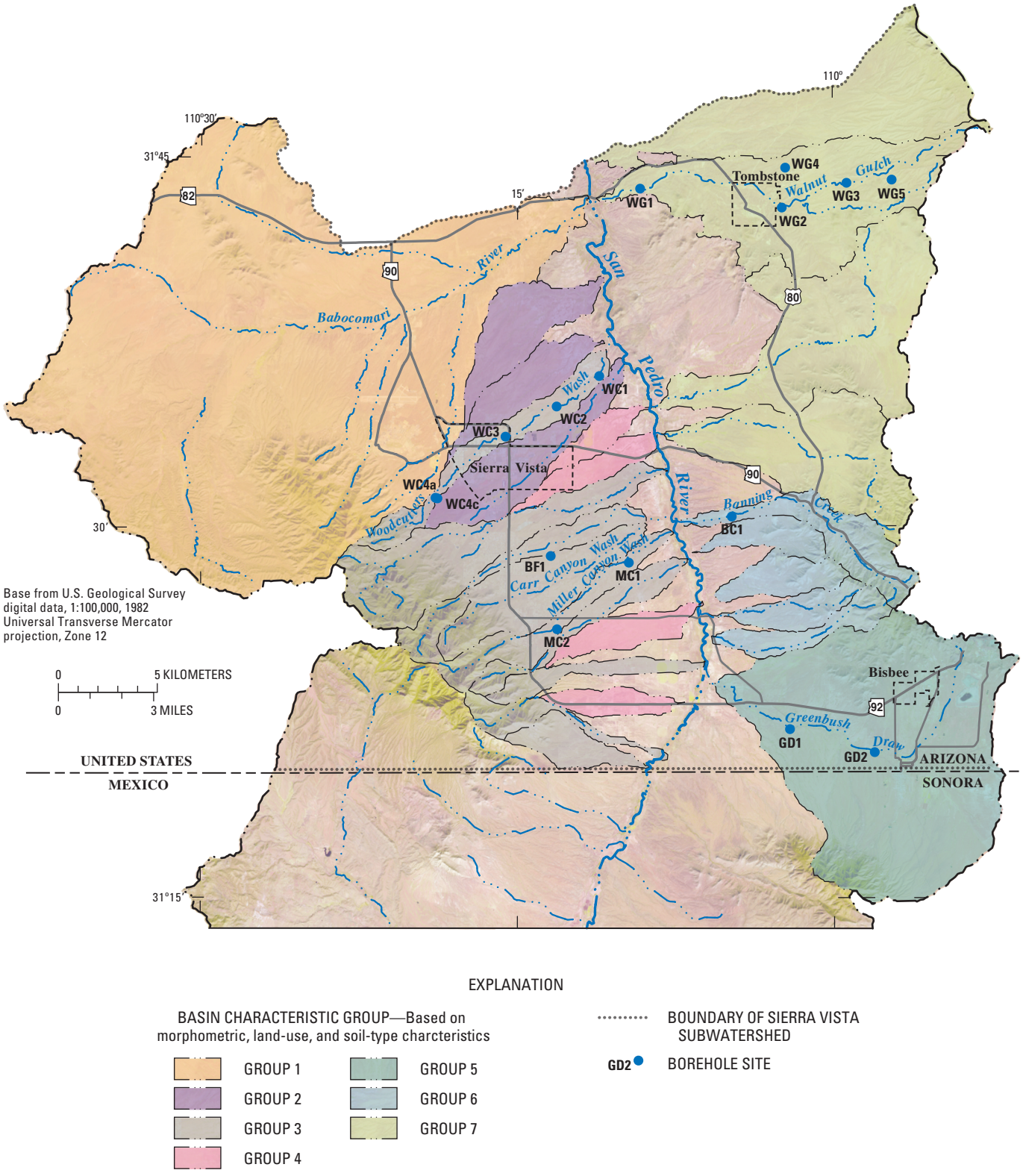

Figure 5. Tributary drainage basins and locations of boreholes, Sierra Vista ground-water-recharge study area, Arizona and northeastern Sonora, Mexico.

deep and only about 1 km wide (Pool and Coes, 1999). The post-entrenchment stream alluvium is highly permeable; the pre-entrenchment stream alluvium is less so (Pool and Coes, 1999). The pre- and post-entrenchment stream alluvium forms a long, narrow, shallow aquifer along the San Pedro River that is referred to as the flood-plain aquifer. Water levels in the flood-plain aquifer range from less than 1 to as much as 6 m below land surface (USGS data), and water levels in this aquifer are a major influence on river discharges and show seasonal trends reflecting cycles of surface-water runoff and evapotranspiration.

Recharge Mechanisms

Historically, recharge to the basin-fill aquifer in the Sierra Vista subwatershed was thought to primarily occur near the mountain fronts through ephemeral-stream channel infiltration of runoff from the relatively impermeable rocks of the mountains. Previous conceptual models of the ground-water flow system included annual recharge rates of 15 to 23 cubic hectometers per year (hm^3/yr), all of which was distributed within about 1.5 km of the mountains (Freethey, 1982; Corell and others, 1996; Goode and Maddock, 2000). Infiltration and recharge could, however, be distributed along much greater lengths of the channels. Recent studies (Blasch and others, 2000; Izbicki and others, 2000; Constantz and others, 2003) have shown that significant recharge can occur through the beds of ephemeral streams far from mountain fronts. In the Sierra Vista subwatershed, Corell and others (1996) estimated that infiltration along the length of Greenbush Draw contributed about 1.20 hm^3/yr of recharge. Goodrich and others (2004) estimated that a 6.8-km reach of Walnut Gulch contributed about 0.14 to 0.47 hm^3 of recharge in 1999 and about 0.13 to 0.37 hm^3 of recharge in 2000. The occurrence of similar rates of recharge along other major ephemeral streams would result in significant alterations to the preexisting conceptual model of recharge distributions in the subwatershed. Recharge through direct infiltration of precipitation through the basin floor is thought to rarely occur because of high evaporation, low precipitation, and water use by desert vegetation in the semiarid Southwest (Anderson and others, 1992; Scott and others, 2000). Rare basin-floor recharge could, however, be a significant source of recharge during extended periods of high precipitation and low evapotranspiration.

The occurrence of significant recharge along the lengths of ephemeral stream channels or through the basin floor, however, would not result in increased estimates of average annual basin-wide recharge rates. Water-budget analysis requires that estimates of recharge rates be maintained to balance inflows and outflows. The change would simply be in the conceptual model of recharge distribution: less concentrated near the mountains and more extensive downstream in tributary channels.

Previous recharge estimates for the Sierra Vista subwatershed have generally assumed that recharge rates are constant with time. Trends in seasonal and annual precipitation (Pool and Coes, 1999), however, likely result in long-term variations in recharge rates. Water-chemistry data for the Sierra Vista subwatershed and the adjacent Tucson Basin indicate that a greater percentage of precipitation infiltrates during winter streamflow than during summer streamflow (Gallaher, 1979; Keith, 1981; Pool and Coes, 1999). Rates of summer streamflow have varied randomly from year to year, but rates of winter streamflow vary over decadal periods with Pacific Ocean climate indicators (Cayan and Webb, 1992; Webb and Bentancourt, 1992; Cayan and others, 1999; McCabe and Dettinger, 1999).

Ground-Water Flow System

Ground water in the basin-fill aquifer is transmitted from recharge areas to discharge areas primarily through the sands and gravels of the upper and lower basin-fill units. Near the mountain fronts, shallow bedrock and relatively impermeable sediments support perched aquifers. Silt and clay layers within the upper and lower basin-fill units on the western side of the subwatershed split ground-water flow in the regional aquifer into deep and shallow flow systems (Pool and Coes, 1999). Exceptions to the regional directions of ground-water flow exist near the Sierra Vista-Fort Huachuca area, where withdrawals have removed ground water from aquifer storage and altered pre-development ground-water flow paths (Pool and Coes, 1999).

Post-development discharge from the basin-fill aquifer in the Sierra Vista subwatershed occurs primarily as ground-water withdrawals, discharge to the San Pedro and Babocomari Rivers (base flow), and evapotranspiration. Ground-water withdrawals in the subwatershed began in about 1940 and peaked in the early 1980s at about 18.5 hm^3/yr (Freethey, 1982; Corell and others, 1996). Withdrawals declined to about 13.5 hm^3/yr by 1991 (Corell and others, 1996). Post-development discharge to streams is about 7.4 hm^3/yr, and post-development evapotranspiration is estimated to be about 7.0 hm^3/yr (Freethey, 1982). About 3.7 to 4.9 hm^3/yr discharges from the subwatershed as underflow through basin fill and stream alluvium in the Fairbank area (Freethey, 1982; Corell and others, 1996). In addition, a small amount of ground water discharges as springs near the San Pedro River.

Pool and Coes (1999) identified four types of long-term water-level changes in the Sierra Vista subwatershed. The first type is periodic decline and recovery of water levels near the mountains related to variations in precipitation and rates of recharge. The second is a decline of 0.2 to more than 0.3 m/yr in the Sierra Vista-Fort Huachuca area caused by ground-water withdrawals. The third is a regional decline of 0.1 to 0.2 m/yr during 1940 through the mid-1960s to early 1980s followed by a period of no decline or slight recovery. This regional decline could be caused by variations in recharge rates or regional response to incision of the San Pedro River. The fourth type of long-term water-level change is recovery near the San Pedro River after the mid-1980s that is probably due to a decrease in agricultural ground-water withdrawals.

Methods of Investigation

Multiple methods were used to estimate infiltration through ephemeral channels and the basin floor in the Sierra Vista subwatershed. Information gathered through unsaturated-zone borehole drilling and monitoring was used to better describe infiltration through the unsaturated zone. Tritium data were used to describe the extent to which water has moved through the unsaturated zone since the 1950s. Ratios of the stable isotopes of oxygen and hydrogen were used to identify evaporative and seasonal signatures of pore water. The distribution of chloride in the subsurface was used to identify active or inactive recharge areas, and where possible, was balanced to determine infiltration fluxes and water residence times. The transport of heat with infiltrating water was used to quantify infiltration rates from individual ephemeral streamflow events.

Field and Laboratory Methods

To characterize ephemeral-stream channel and basin-floor recharge in the Sierra Vista subwatershed, 12 tributary sites and 4 intertributary sites were chosen for intensive unsaturated-zone data collection. At each site, a borehole was drilled into the subsurface and sediment cuttings and cores were collected. Of the 16 boreholes, 15 were completed with casing for subsurface monitoring. Sediment textures were described in the field, and sediment-chloride concentrations were measured. Sediment cores were measured for hydraulic, physical, and thermal properties; pore-water stable-isotopes values; and tritium activity. Twelve of the completed boreholes were instrumented for continuous monitoring of sediment temperature. Ground-water levels of saturated intervals were continuously monitored in three of the completed boreholes.

Borehole Site Selection

Tributary and intertributary borehole locations were chosen by using a multistep approach. First, the Automated Geospatial Watershed Assessment (AGWA) tool (Miller and others, 2002), an extension to the Environmental Systems Research Institute's ArcView version 3, was used to delineate the drainage basins of the major tributaries of the San Pedro River (fig. 5). For each basin, the main channel length, main channel slope, total basin area, mean basin elevation, basin perimeter, basin length, major land use, and major soil type were quantified by using the Xtools and Spatial Analyst extensions to ArcView (table 1). The basins were then divided into seven groups on the basis of similar morphometric, land-use, and soil-type characteristics (fig. 5). Twelve tributary sites were chosen in five drainage basins that represent four of the seven groups: four sites in Woodcutters Wash, two sites in Miller Canyon Wash, two sites in Greenbush Draw, one site in Banning Creek, and three sites in Walnut Gulch. In addition, four intertributary (basin floor) sites were chosen in three drainage basins: two sites in Walnut Gulch, one site in Woodcutters Wash, and one site in Carr Canyon.

Borehole Drilling and Completion

Unsaturated-zone boreholes were drilled and completed in January 2001 and November – December 2001 (table 2). All boreholes were drilled by using the ODEX air-hammer method, also known as the under-reamer method (Driscoll, 1986; Hammermeister and others, 1986). This drilling method minimized disturbance of the formation near the borehole, and enabled collection of representative cuttings and cores at predetermined intervals. Boreholes were drilled to depths of less than 30.0 m and were either 15.2 or 20.3 cm in diameter. At each borehole, drill cuttings were collected every 0.3 m, and 0.6-m-long cores were collected at differing intervals by using a 10.2-cm-diameter piston core barrel. The 0.6-m-long core barrel was lined with three 15.2-cm-long sleeve liners and two 7.6-cm-long sleeve liners. Upon core collection, each of the liners was immediately capped, taped, plastic wrapped, and placed in an aluminum pouch, which was then heat-sealed, following the procedure described by Hammermeister and others (1986), to preserve the integrity of each core sample.

Of the 16 boreholes, 15 were completed to enable future subsurface monitoring (table 2). Permission was not granted from the land owner to complete the borehole at WC2. Each borehole was completed with 5.1-cm-diameter schedule-40 polyvinyl chloride (PVC) pipe. Twelve of the completed boreholes were completed with solid-walled PVC, and capped at the bottom and top. During drilling, three of the completed boreholes intercepted saturated intervals. These three boreholes were completed with solid-walled PVC above the saturated interval and a 1.5-m section of slotted PVC spanning the unsaturated/saturated interface. The annular space of the 12 boreholes completed with solid-walled PVC was filled with a mixture of cuttings from the boreholes and sand. The annular space of the three boreholes completed with slotted PVC was filled with gravel in the slotted interval, bentonite above the slotted interval, and a mixture of cuttings and sand above the bentonite. Surface casing consists of 10.2-cm-diameter schedule-80 PVC pipe from above land surface to 0.9 to 1.5 m depth around the 5.1-cm-diameter PVC casing. The uppermost 0.9 to 1.5 m of annular space was filled with cement. The surface casing was capped with a watertight, locking, aluminum cap. Completion of the 15 boreholes with PVC casing resulted in 12 unsaturated-zone monitoring access points and 3 wells. Use of the term "borehole" is retained, however, for convenience of discussion in this report.

Sediment Analysis

Cuttings—Cuttings from each borehole were visually described for grain-size distribution at 0.3-m intervals (fig. 6). Cuttings from three boreholes were also analyzed in the laboratory for particle-size distribution (fig. 6).

Table 1. Geomorphic, land-cover, and soil-type characteristics of tributary drainage basins, Sierra Vista ground-water recharge study area, Arizona.

[Group numbers refer to figure 5. Abbreviations: km, kilometers; m/km, meters per kilometer; km^2, square kilometers; ND, not determined]

Tributary name	[1] Main channel length, in km	Main channel slope, in m/km	[2] Total basin area, in km^2	Mean basin elevation, in m	Basin perimeter, in km	Basin length, in km	[2] Major land cover, in percent	[2] Major soil type, in percent
				Group 1				
Babocomari River	47.8	7.9	528.0	1,512	187.5	48.2	Grassland (48.3)	ND
				Group 2				
Unnamed Wash 1	15.4	10.9	41.8	1,288	39.2	14.4	Desert scrub (44.1)	Loam (27.9)
Graveyard Gulch	14.4	12.3	30.9	1,310	35.1	12.7	Desert scrub (38.3)	Loam (49.7)
Escapule Wash	20.7	13.8	50.3	1,370	44.8	19.4	Urban (37.9)	Loam (54.8)
				Group 3				
Woodcutters Wash	23.0	13.9	37.5	1,434	54.7	32.6	Desert scrub (26.7)	Loam (34.4)
Garden Canyon Wash	21.7	13.5	86.4	1,651	63.8	33.5	Oak woodland (37.0)	Loam (17.3)
Ramsey Canyon Wash	17.4	18.1	32.5	1,701	51.5	25.2	Forest (31.0)	Clay (22.6)
Carr Canyon Wash	16.8	18.1	57.2	1,590	42.5	23.0	Urban (23.1)	Loam (26.9)
Miller Canyon Wash	16.2	20.5	32.8	1,693	48.1	27.9	Forest (25.2)	Loam (23.3)
Hunter Canyon Wash	15.5	19.1	24.1	1,478	43.0	23.9	Grassland (38.5)	Loam (32.9)
Stump Canyon Wash	14.6	19.5	18.5	1,624	36.3	16.4	Grassland (35.3)	Clay (41.5)
Ash Canyon Wash	12.9	23.7	17.5	1,818	37.5	15.6	Oak woodland (67.2)	Paleosoil (13.3)
Brown-Bob Thompson Wash	9.5	23.3	21.0	1,536	25.7	11.0	Grassland (38.4)	Loam (31.9)
				Group 4				
Lewis Springs Wash	12.1	12.0	13.0	1,300	22.0	12.5	Desert scrub (46.7)	Secondary calcium carbonate (71.8)
Bakarich-McCool Wash	11.8	12.6	18.5	1,320	28.5	13.2	Desert scrub (52.0)	Secondary calcium carbonate (58.8)
Three Canyons Wash	6.6	12.7	21.2	1,354	29.1	12.7	Grassland (41.7)	Clay (85.0)
Palominas Wash	11.1	19.6	15.4	1,385	23.6	17.2	Desert scrub (47.3)	Sandy stream channel (52.3)
				Group 5				
Greenbush Draw	19.5	8.8	306.3	1,476	81.6	23.9	Grassland (38.6)	ND
				Group 6				
Banning Creek	8.6	15.6	41.3	1,655	47.8	21.2	Desert scrub (46.4)	Secondary calcium carbonate (11.0)
Unnamed Wash 2	10.1	24.1	19.0	1,436	24.7	13.3	Desert scrub (51.7)	Secondary calcium carbonate (59.4)
Stagg Ranch Wash	10.5	25.7	21.9	1,456	25.0	10.2	Desert scrub (63.3)	Secondary calcium carbonate (53.8)
Little Dry Creek	10.6	23.4	19.2	1,466	27.6	13.4	Desert scrub (40.5)	Secondary calcium carbonate (61.1)
Spring Creek	11.4	22.9	22.6	1,527	33.3	14.6	Desert scrub (43.3)	Loam (29.0)
				Group 7				
Willow Creek	20.9	16.0	130.8	1,531	76.6	23.1	Grassland (40.1)	Rocky calcium carbonate (29.0)
Walnut Gulch	26.5	12.1	152.1	1,411	86.1	34.1	Desert scrub (57.6)	Rocky calcium carbonate (35.2)
Government Draw	17.8	7.6	148.4	1,399	80.8	20.5	Desert scrub (65.0)	Lithic (26.4)
High Knolls Canyon Wash	18.7	12.5	98.9	1,443	56.5	29.4	Desert scrub (45.2)	Lithic (43.6)

[1]From the mountain front.

[2]U.S. Environmental Protection Agency, 2003.

Table 2. Borehole construction and instrumentation, Sierra Vista ground-water-recharge study area, Arizona.

[Abbreviations: km, kilometers; m, meters; cm, centimeters; ", ditto; NA, not applicable; NC, not completed; PVC, slotted polyvinyl chloride; Surface TidbiT: Y, yes; N, no]

Borehole identifier	Borehole identification number	Distance downstream from mountain front, in km	Approximate channel width, in m	Construction information								Instrumentation information		
				End drill date	Borehole diameter, in cm	Borehole depth, in m	Casing diameter, in cm	Casing depth, in m	Opening type	Depth to top of opening, in m	Depth to bottom of opening, in m	Transducer depth, in m	Surface TidbiT	Down-hole TidbiT depths, in m
Ephemeral-channel boreholes														
BC1	(D-22-22)23bbd	3.9	4	01/17/01	20.3	26.3	5.1	26.3	None	NA	NA	NA	Y	1.5, 3.0, 4.6, 6.1, 7.6, 9.1, 12.2
GD1	(D-24-23)06dbd	12.4	14	11/30/01	15.2	19.5	"	19.5	None	NA	NA	NA	N	1.5, 3.0, 6.1, 9.1
GD2	(D-24-23)14aba	5.6	2	11/29/01	"	28.2	"	28.2	None	NA	NA	NA	Y	1.5, 3.0, 4.6, 6.1, 7.6, 9.1, 12.2
MC1	(D-22-21)36bad	7.1	4	11/18/01	"	23.0	"	23.0	None	NA	NA	NA	Y	1.5, 3.0, 4.6, 6.1, 9.1
MC2	(D-23-21)bca2	0.0	2	11/20/01	"	16.0	"	16.0	None	NA	NA	NA	N	1.5, 3.0, 4.6, 6.1, 7.6, 9.1, 12.2
WC1	(D-21-21)14dbc1	16.4	10	01/14/01	20.3	9.4	"	9.4	None	NA	NA	NA	Y	1.5, 3.0, 4.6, 6.1, 7.6, 9.1
do.	(D-21-21)14dbc2	"	"	"	"	"	"	8.5	PVC	7.3	8.8	8.8	N	NA
WC2	(D-21-21)28bbb	12.3	22	01/12/01	"	12.5	NC	NC	NC	NC	NC	NA	N	NA
WC3	(D-21-20)36caa	7.2	8	11/09/01	15.2	22.6	5.1	22.6	None	NA	NA	NA	N	1.5, 3.0, 4.6, 6.1, 7.6, 9.1, 12.2
WC4a	(D-22-20)16abc1	0.4	0.5	01/10/01	20.3	12.5	"	12.7	None	NA	NA	NA	Y	1.5, 3.0, 4.6, 6.1, 7.6, 9.1, 12.2
do.	(D-22-20)16abc2	"	"	"	"	"	"	5.3	PVC	3.8	5.3	4.6	N	NA
WG1	(D-20-21)01aba	25.6	31	11/11/01	15.2	23.0	"	23.0	None	NA	NA	NA	N	1.5, 3.0, 4.6, 6.1, 9.1
WG2	(D-20-22)01bdc	13.2	13	11/16/01	"	12.2	"	11.4	None	NA	NA	NA	N	1.5, 3.0, 4.6
WG3	(D-19-23)33aad	7.2	2	11/15/01	"	12.3	"	12.3	None	NA	NA	NA	N	NA
Basin-floor boreholes														
BF1	(D-22-21)32dad	NA	NA	12/01/01	15.2	15.8	5.1	15.1	None	NA	NA	NA	Y	1.5, 3.0, 4.6, 6.1, 7.6, 9.1, 12.2
WC4c	(D-22-20)16acb	NA	NA	01/08/01	20.3	12.5	"	12.5	PVC	4.3	5.8	9.1	Y	1.5, 3.0, 4.6, 6.1, 7.6, 9.1, 12.2
WG4	(D-19-22)36abb	NA	NA	11/12/01	15.2	13.4	"	13.4	None	NA	NA	NA	N	NA
WG5	(D-19-23)36dbc	NA	NA	11/13/01	"	12.3	"	12.3	None	NA	NA	NA	N	NA

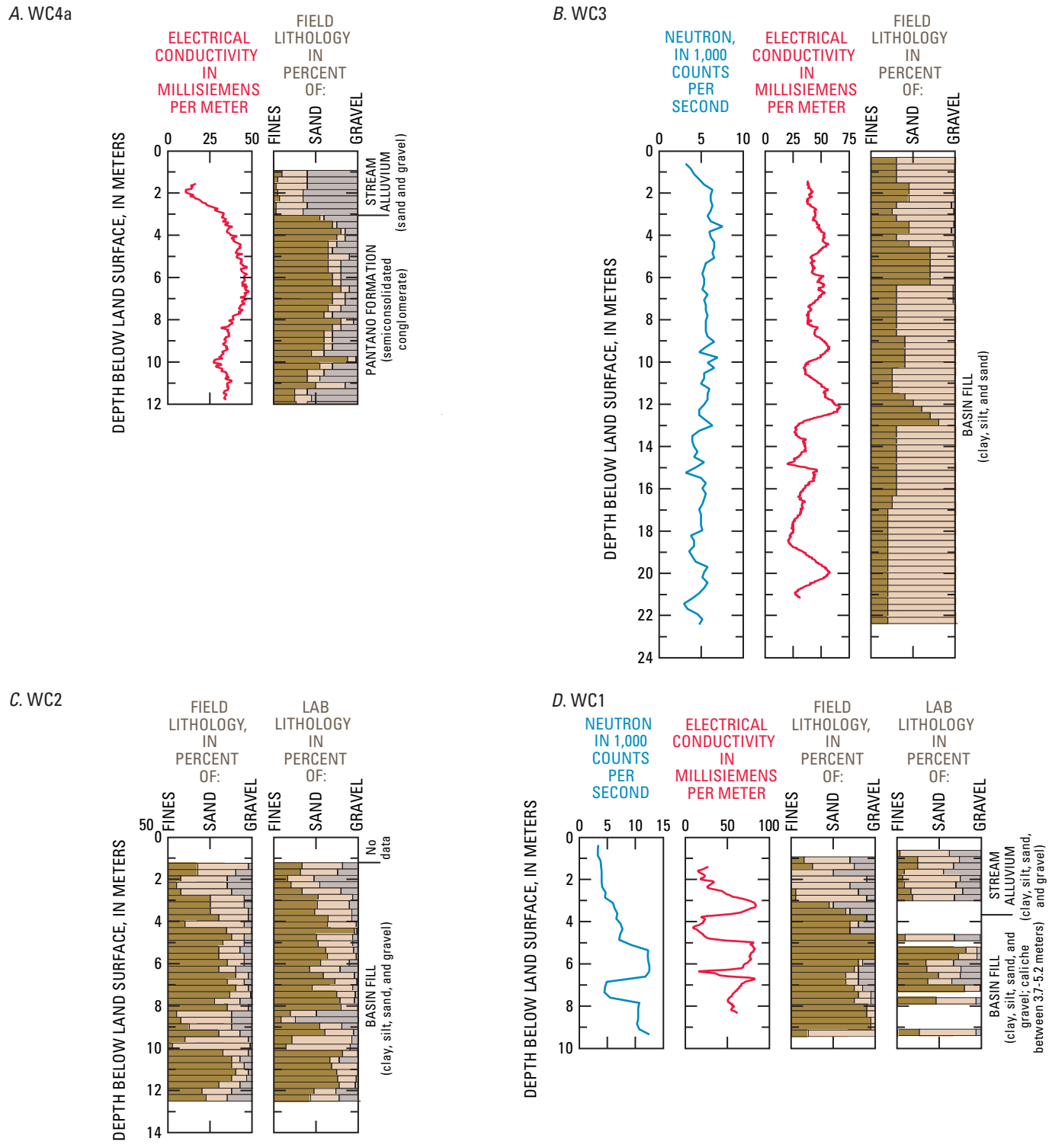

Figure 6. Neutron soil-moisture, electrical conductivity, field grain-size, and laboratory grain-size data for boreholes in the Sierra Vista ground-water-recharge study area, Arizona and northeastern Sonora, Mexico: *A*, WC4a; *B*, WC3; *C*, WC2; *D*, WC1; *E*, MC2; *F*, MC1; *G*, WG3; *H*, WG2; *I*, WG1; *J*, BC1; *K*, GD2; *L*, GD1; *M*, WG4; *N*, WG5; *O*, BF1; *P*, WC4c.

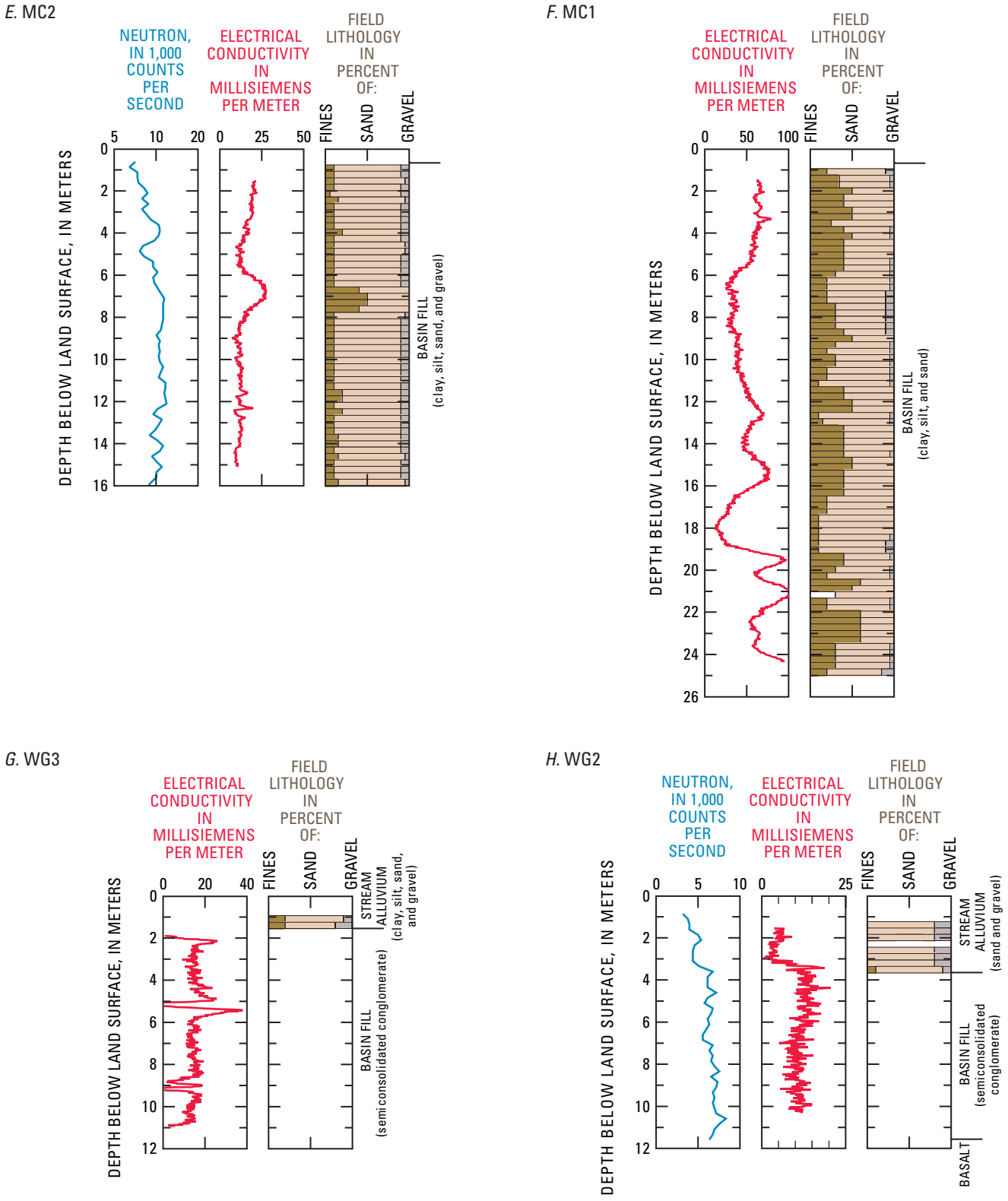

Figure 6. —Continued.

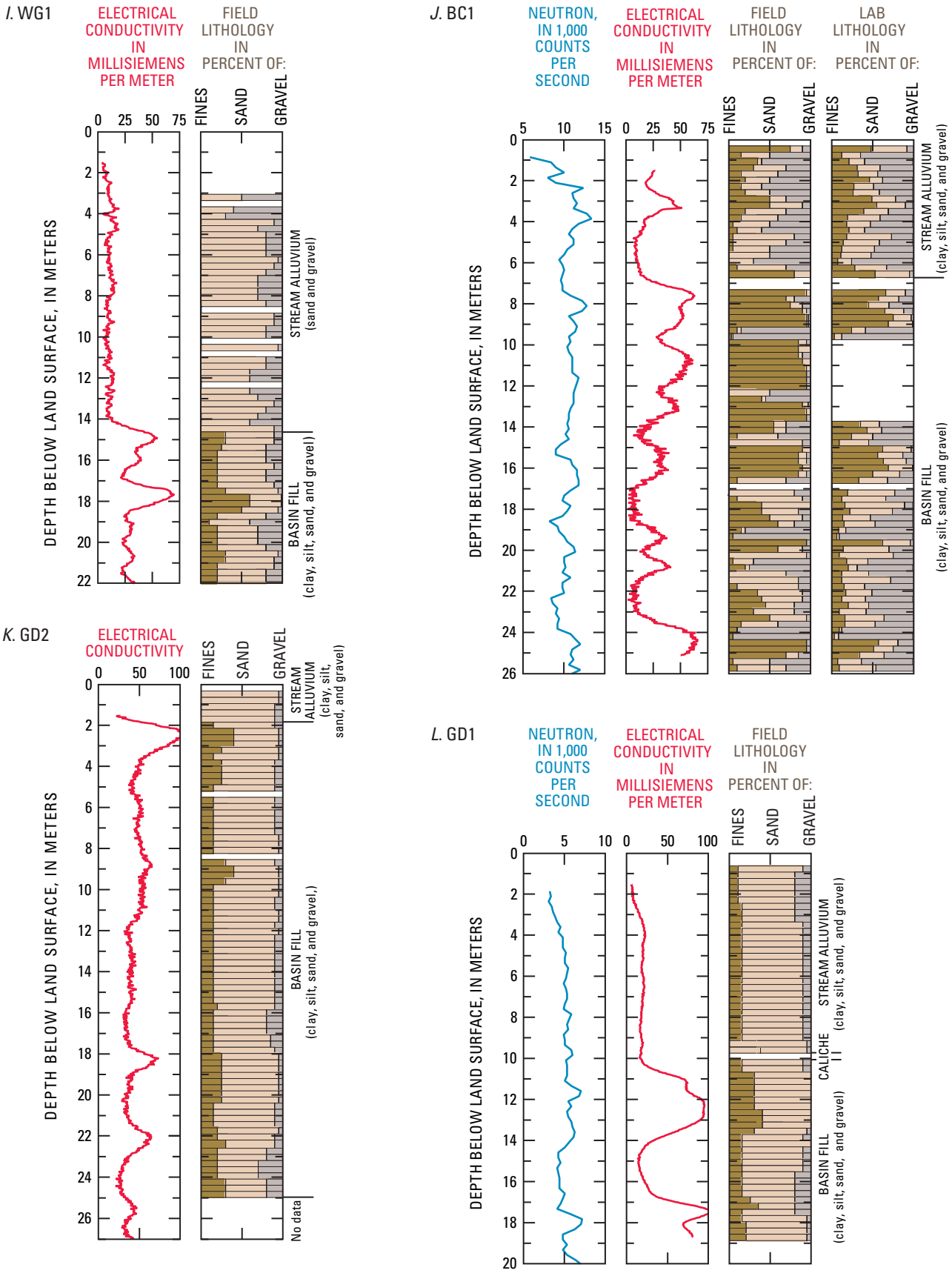

Figure 6. —Continued.

M. WG4

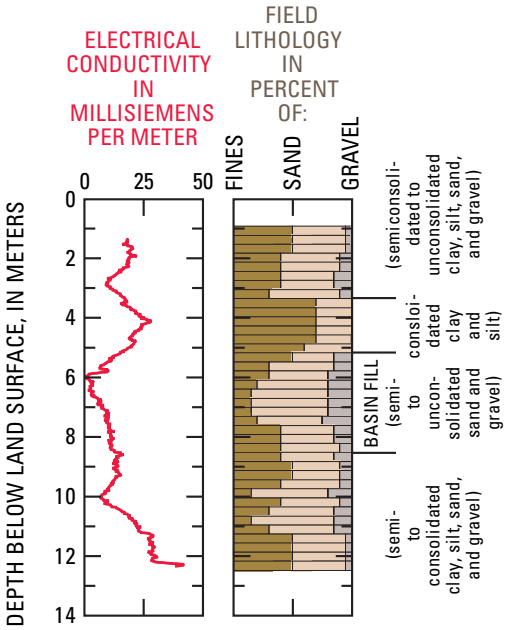

N. WG5

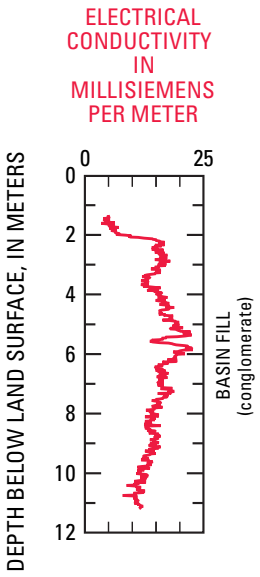

O. BF1

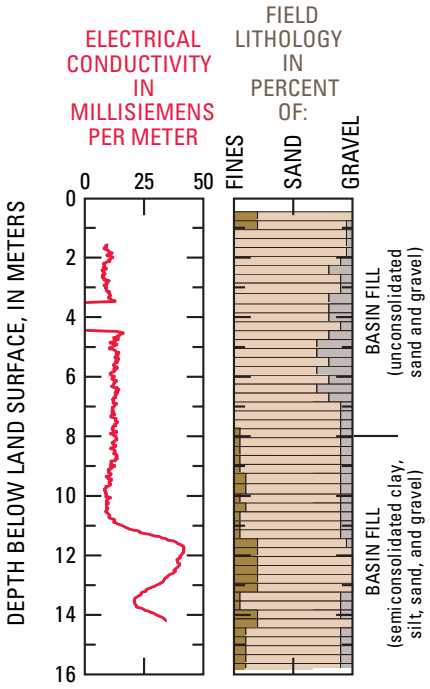

P. WC4c

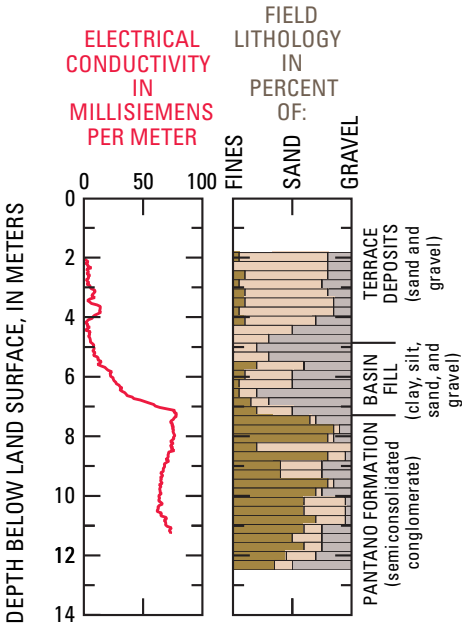

Figure 6. —Continued.

Sediment-chloride concentrations of borehole cuttings collected at 0.3-m intervals were determined in the field (table 3) (tables 3-13 are placed at the end of this chapter). A subsample of cuttings representative of each 0.3-m interval was sieved to obtain particles less than 2 mm in diameter. Fifty grams of the sieved subsample was mixed well with 50 mL of deionized water and allowed to settle. The chloride concentration of the leachate was then measured by using an Orion chloride-specific electrode, Model 96-17 (Thermo Electron Corporation, 2000). This electrode measures chloride concentrations of 1.8 to 35,500 mg/L with a reproducibility of ±2 percent. The electrode was calibrated in the field at the beginning of each set of measurements; calibration was checked every 1 to 2 hours. Chloride is reported in milligrams of chloride per kilogram of soil (mg/kg; M_{Cl}, in M/M):

$$M_{Cl} = Cl_{samp} \frac{V_w}{M_s} \quad , \qquad (1)$$

where

Cl_{samp} = chloride concentration of leachate [M/L^3],

V_w = volume of deionized water in leachate [L^3]

M_s = mass of sediment in leachate [M].

Cores—Cores were analyzed to determine pore-water stable-isotope values and tritium activity; thermal, physical, and hydraulic properties; and particle-size distributions. Pore water was extracted and analyzed for the stable isotopes of oxygen and hydrogen at the USGS Isotope Fractionation Project Laboratory in Reston, Virginia (table 4). Pore water was extracted and analyzed for tritium activity at the USGS Water-Quality Laboratory in Menlo Park, Calif. (table 4). The precision of individual tritium measurements is a function of the volume of water extracted from the core material and ranged from ±0.2 tritium units (TU) for moist cores to ±5.0 TU for an extremely dry core. Thermal properties (heat capacity, thermal conductivity, and thermal diffusivity; all at field soil-water content; table 5) were measured at the USGS Hydrologic Research Laboratory in Sacramento, Calif., by using a dual-needle, line-heat source probe and a ThermoLink measurement system (Campbell and others, 1991; Decagon Devices, Inc., 1999).

Core analyses for hydraulic properties (saturated hydraulic conductivity and van Genuchten parameters) and physical properties (bulk density, volumetric soil-water content, porosity, and particle density) were completed in a laboratory at the University of Arizona in Tucson, Ariz. (table 6). Initially, each core's weight was measured and its volume calculated. Cores were then fully saturated and weighed again. Saturated hydraulic conductivity (K_s, in L/t) was measured by the falling-head method (Klute and Dirksen, 1986). Reported K_s values are the average of two to five falling-head tests run sequentially. Van Genuchten parameters (alpha (α), in 1/L; n, dimensionless; residual soil-water content (θ_R), in L^3/L^3; saturated soil-water content (θ_S), in L^3/L^3) were determined from moisture-release data measured by the pressure-step outflow method (Gardner, 1956) from about 15 to 15,000 cm water pressure. Cores were then oven dried at 105ºC for 24 hours, and weighed a third time. Dry bulk density (ρ_b, in M/L^3) was determined by dividing the weight of the core after oven drying by the calculated volume of the core. Gravimetric field soil-water content (θ_g, in M/M) was calculated as the difference between the initial core weight and the weight of the core after oven drying, divided by the weight of the core after oven drying. Volumetric field soil-water content (θ_v, in L^3/L^3) was calculated as the product of the gravimetric soil-water content and the bulk density. Porosity (φ, dimensionless) was assumed equal to the saturated soil-water content and was calculated as the product of the bulk density and the difference between the saturated core weight and the dry core weight, divided by the dry core weight. Particle density (ρ_p, in M/L^3) was calculated by (Danielson and Sutherland, 1986):

$$\rho_p = \frac{\rho_b}{1-\varphi} \quad , \qquad (2)$$

The Soil, Water, and Plant Analysis Laboratory at the University of Arizona measured particle-size distributions for the cores (table 6). Gravel-size fractions (greater than 2 mm) were determined by sieve analysis. Sand-, silt-, and clay-sized fractions were determined by hydrometer analysis (Gee and Bauder, 1986).

Borehole Logging

Electromagnetic-induction (EMI) and neutron soil-moisture geophysical borehole tools were used to augment subsurface sampling of borehole cuttings and core (fig. 6). EMI measures the electrical conductivity of the sediments near the borehole by measuring the strength of a secondary magnetic field induced in the sediments by a primary electromagnetic field. The EMI tool has a variable radius of investigation dependent on the frequency of the primary field, the spacing between the primary and secondary magnetic coils, and the subsurface conductivity. The tool used in this investigation used a frequency of about 40 kiloHertz and a coil spacing of 0.5 m. At this setting, about 90 percent of the secondary magnetic field results from materials within a radius of about 1.3 m from the center of the coil spacing (Peterson, 1999). Variations in subsurface electrical conductivity are primarily caused by variations in amounts of electrically conductive silt, clay, and dissolved ions in water. Electrical conductivity is proportional to silt, clay, and soil-water contents. Dry zones with little silt and clay can have electrical conductivity values well below 10 millisiemens per meter (mS/m), but saturated clay can have values greater than 100 mS/m. Variations in electrical conductivity can also be related to variations in electrically conductive salts; however, the salt contents in most of the boreholes drilled for this investigation were very low and did not likely contribute significantly to variations in electrical conductivity.

The neutron tool used in this study contained a 50-millicurie americium-241/beryllium neutron source and detector

to measure variations in the amount of water molecules near the borehole. The tool had a radius of investigation of about 60 to 75 cm. Response of the neutron tool is reported as measured neutron counts at the detector; higher neutron counts indicate greater amounts of water near the borehole. Neutron counts can be converted to soil-water content by using a soil-dependent calibration; however, calibration was not attempted for this investigation, and the resultant neutron counts from different boreholes can only be compared in a relative sense.

Borehole Monitoring

Onset StowAway TidbiT temperature sensors were installed in boreholes WC1, WC4a, WC4c, and BC1 in February 2001, and in boreholes WC3, MC1, MC2, BF1, GD1, GD2, WG1, and WG2 from January to May 2002. Sensors were installed from land surface to a maximum depth of 12.2 m at intervals of 1.5 to 3.0 m (table 2). Additionally, at most boreholes, a sensor was buried about 15 cm below land surface next to the borehole surface casing. Temperature was measured and recorded every 30 minutes. The TidbiT sensors measure temperatures of –5ºC to +37ºC with an accuracy of ±0.2ºC.

In-Situ Inc. miniTROLL pressure transducers were installed in the three boreholes that intercepted saturated intervals (WC1, WC4a, and WC4c) during February 2001. Depth to water was measured and recorded every 30 minutes.

Precipitation Collection and Analysis

Composite atmospheric deposition samples were collected twice a year after the summer (April to October) and winter (October to April) rains at the Upper Babocomari River and Greenbush Draw streamflow-gaging stations (fig. 1). Sample collection began in June 2000 and continued through April 2003. Samples were analyzed for bulk chloride concentrations, stable-isotope values, and tritium activity (table 7). Bulk chloride was determined by ion chromatography at the USGS laboratory in San Diego, Calif.. The stable isotopes of oxygen and hydrogen were analyzed at the USGS Isotope Fractionation Project Laboratory in Reston, Virginia. Tritium activity was determined at the Laboratory of Isotope Geochemistry at the University of Arizona in Tucson.

Streamflow-Data Collection and Analysis

Knowledge of ephemeral streamflow timing and duration in the tributaries was needed to determine the availability of water for ephemeral-stream channel infiltration. In this study, streamflow availability was estimated by using frequency and duration of flow determined by USGS streamflow-gaging stations, ARS flumes, and temperature methods. Onset StowAway TidbiT temperature sensors were buried about 15 cm below the surface of streambed sediments at 7 of the 12 tributary borehole sites (table 2) and at selected channel locations between boreholes (fig. 5). Sediment temperatures were logged every 15 to 30 minutes. A rapid drop in temperature of more than 0.2ºC indicated onset of streamflow; a low-temperature inflection point in the thermograph was interpreted as the cessation of streamflow (Constantz and others, 2001; Gungle, 2003). Durations of individual ephemeral-streamflow events ranged from 15 minutes to 48 days (table 8).

Data-Analysis Methods

Infiltration is defined as the flow of water from above ground into the unsaturated zone; recharge is defined as the flow of water across the regional water table. The rate of infiltration, or infiltration flux, is strongly dependent on the spatial and temporal distribution of source water and the hydraulic and physical properties of the subsurface sediments. At the onset of infiltration, the initial infiltration flux is at its highest and is extremely transient. As infiltration continues over time, the infiltration flux decreases to a nearly constant rate approaching the effective mean saturated hydraulic conductivity of the subsurface sediments.

Infiltration can lead directly to recharge when the wetting front reaches the regional water table while infiltration is still occurring. In the arid and semiarid Southwest, however, deep water tables and short infiltration times lead to infiltration ending long before the wetting front crosses the water table. In these instances, water that has infiltrated into the unsaturated zone can be removed by evapotranspiration or, if the water has moved past the root zone, remain in storage until it is displaced by water from a subsequent infiltration event. Unsaturated-zone water in storage below the root zone can continue to redistribute over time. This long-term movement of water, or percolation flux, occurs both vertically, by drainage, and horizontally in response to heterogeneity or anisotropy of the sediments. Long-term percolation can result in recharge.

Unsaturated Hydraulic Properties

Moisture-release curves describe the nonlinear decrease in soil-water content at decreasing matric potentials. The van Genuchten (1980) algebraic expression relates soil-water content to matric potential by:

$$\theta_v = (1+(\alpha|h_p|)^n)^{-m}, \quad (3)$$

where

θ_v = volumetric soil-water content [L^3/L^3],
α = van Genuchten fitting parameter [1/L],
h_p = matric potential [L],
n = van Genuchten fitting parameter (dimensionless), and
m = van Genuchten fitting parameter equal to $1–1/n$ (dimensionless).

For this study, the pressures (in cm water) at which soil-water contents were determined are considered equivalent to matric potentials.

The RETC (RETention Curve) computer code (van Genuchten and others, 1991) was used to fit moisture-release curves to the induced-pressure and measured water-content data to determine the van Genuchten fitting parameters of α and n (table 6). All curves were fit so that their coefficients of determination (R^2) for the regression of the measured values versus the fitted values were greater than 0.95. Volumetric residual and saturated soil-water contents (θ_R and θ_S, in L^3/L^3) were also determined by using the RETC code.

Unsaturated-Zone Chloride Mass Balance

The mass of chloride (Cl) in the unsaturated zone can be used to estimate long-term vertical water movement. Chloride is continuously deposited on the land surface by precipitation and dry fallout. The high solubility of Cl enables its transport into the subsurface by infiltrating water. Because Cl is essentially nonvolatile and Cl uptake by plants is minimal, Cl is retained in the sediment when water is removed by evaporation and transpiration. Therefore, an increase in Cl within the root zone of the shallow subsurface is proportional to the amount of water lost by evapotranspiration (Allison and Hughes, 1978). In areas where active infiltration is occurring, an increase in Cl in the shallow subsurface will generally be absent, and concentrations will be very low through the unsaturated zone. In areas where little to no active infiltration is occurring, an increase in Cl in the shallow subsurface will be present, and concentrations will be relatively high through the unsaturated zone.

If the Cl deposition rate on the land surface is known, the average travel time of Cl (t_{Cl}; in t) to a depth in the unsaturated zone (z, in L) can be calculated by:

$$t_{Cl} = \frac{\int_0^z Cl_{soil}\,dz}{Cl_{dep}} \quad , \tag{4}$$

where

Cl_{soil} = chloride mass in the sample interval [M/L^3], and

Cl_{dep} = chloride deposition rate [$M/L^2/t$].

The above calculations entail several assumptions: (1) flow in the unsaturated zone is downward-vertical and piston type, (2) bulk precipitation (precipitation plus dry fallout) is the only source of Cl and there are no mineral sources of Cl, (3) the Cl deposition rate has stayed constant over time, and (4) there is no recycling of Cl within the unsaturated zone.

This model of Cl movement predicts that in interdrainage areas with little to no infiltration, Cl concentrations should increase through the root zone and then remain constant down to the water table. Numerous published chloride profiles, however, show that Cl concentrations commonly decrease below the peak concentration in the root zone. Therefore, some of the above assumptions may not be valid for all unsaturated-zone systems. The decrease in Cl concentrations below the peak has been attributed to nonpiston flow (Sharma and Hughes, 1985), ground-water dilution (Allison and others, 1985), or nonsteady flow as a result of paleoclimatic variations (Phillips and Stone, 1985; Scanlon, 1991).

For some geomorphic settings, such as ephemeral streams, assumption 2 is not valid because streamflow provides an additional source of Cl to the subsurface. To correctly determine percolation flux below ephemeral streams with the Cl mass balance method, the mass of Cl in streamflow needs to be included in equation 5. In this study, ephemeral streamflow discharges and Cl concentrations were not quantified; therefore, the Cl mass method was not used to determine percolation fluxes below ephemeral streams.

Chloride deposition rates in the Sierra Vista subwatershed were determined from the composite precipitation samples collected for this study (table 7). Annual rates ranged from 0.011 to 0.032 mg/cm^2 yr. The average annual Cl deposition rate for the subwatershed was determined to be 0.022 mg/cm^2 yr.

Meteoric Tritium

Tritium (^{3}H), a naturally occurring radioactive isotope of hydrogen, can be used to estimate the age of subsurface water and infiltration fluxes into the subsurface. Large quantities of tritium were released to the atmosphere during thermonuclear-weapons testing from 1952 until the late 1960s; maximum releases occurred in the early 1960s. As a result, the amount of tritium in precipitation sharply increased during testing as tritium was introduced into the water cycle, and decreased after testing ended. The amount of tritium in subsurface water at a given time is a function of the amount of tritium in the atmosphere when infiltration occurred and the radioactive-decay rate of tritium. If flow in the unsaturated zone is assumed to be downward-vertical and piston type, the average infiltration flux (q_i, in L/T) can be estimated by:

$$q_i = \frac{\Delta z}{\Delta t}\theta_v \quad , \tag{5}$$

where

Δz = depth of maximum tritium activity [L],

Δt = elapsed time between sampling and maximum atmospheric tritium activity [t] (38 years for this study), and

θ_v = volumetric soil-water content [L^3/L^3].

Tritium activity in the composite precipitation samples collected during this study ranged from 1.7 to 4.2 tritium units (TU) for winter precipitation and 4.6 to 4.8 TU for summer precipitation (table 7). Therefore, pore water having a tritium

activity within this range was considered to be recent infiltration. Pore water having an activity of less than 0.5 TU was considered to have infiltrated prior to 1952.

Stable Isotopes

The stable-isotope ratios of oxygen ($^{18}O/^{16}O$) and hydrogen ($^{2}H/^{1}H$) can be used to estimate seasonal cycles of infiltration and to determine if pore water has undergone evaporation. Ratios determined in this study are reported relative to Vienna Standard Mean Ocean Water (VSMOW). Differences from the standard are expressed by delta notation (δ), in per mil. The delta notation is computed by:

$$\delta = \left[\frac{R_x - R_{Std}}{R_{Std}} \right] \times 1{,}000 , \quad (6)$$

where

R_x = ratio of isotopes measured in sample, and

R_{Std} = ratio of same isotopes in standard.

The relation between $\delta^{18}O$ and $\delta^{2}H$ in precipitation can be represented by the global meteoric water line (Craig, 1961):

$$\delta^2 H = 8\ \delta^{18} O + 10 , \quad (7)$$

The amount of each isotope in precipitation is dependant on the temperature and source location of the precipitation. Because precipitation temperatures and sources vary by season in the Sierra Vista subwatershed, stable-isotope values in precipitation show seasonal variation. The $\delta^{18}O$ for the composite precipitation samples collected for this study ranged from –5.23 to –8.17 per mil for summer precipitation and from –10.37 to –17.71 per mil for winter precipitation (table 7). The $\delta\ ^{2}H$ ranged from –34.0 to –54.7 per mil for summer precipitation and from –65.6 to –133.4 per mil for winter precipitation (table 7).

Mass differences between ^{18}O and ^{16}O and between ^{2}H and ^{1}H enable isotopic fractionation during phase changes, such as evaporation. Water molecules consisting of ^{16}O and ^{1}H evaporate preferentially, resulting in water enriched in ^{18}O and ^{2}H. Lines describing the relation between $\delta^{18}O$ and $\delta^{2}H$ in enriched water have smaller slopes than the slope of the global meteoric water line.

Heat as a Tracer

Sediment-temperature profiles can be used to estimate one-dimensional infiltration fluxes in the unsaturated zone below the beds of ephemeral-stream channels (Constantz and Thomas, 1996; Constantz and others, 2003). Temperatures of streambed surfaces are predominantly influenced by heating from solar radiation and ambient air temperatures. Beneath dry streambeds, shallow sediment temperatures vary diurnally and seasonally in response to downward conductive heat transport. Deeper sediment temperatures are less affected by diurnal or seasonal air temperatures, and therefore do not greatly vary over time. During periods of stream-channel infiltration, heat transport into the subsurface by advection predominates and transport by conduction is considered negligible.

An analytical method (Taniguchi and Sharma, 1990; Constantz and Thomas, 1996) was used as a first approximation to calculate infiltration flux (q_i, in L/t) from measured sediment temperatures at each ephemeral-stream site (table 9):

$$q_i = \frac{\Delta z}{\Delta t} \frac{\rho_{b_{soil}} C_s}{\rho_{b_{water}} C_w} , \quad (8)$$

where

Δz = vertical distance between temperature sensors [L],

Δt = travel time of the temperature perturbation between sensors [t],

$\rho_{b_{soil}}$ = bulk density of sediment [M/L^3],

C_s = heat capacity of the dry sediment [E/L^3/T],

$\rho_{b_{water}}$ = bulk density of water [M/L^3], and

C_w = heat capacity of water [E/L^3/T].

Onset of streamflow was determined from streambed-temperature data. The distance between temperature sensors was known for each borehole, and the travel time of the temperature signal was measured. The ρ_b and C_S of the sediment were determined from cores. For depth intervals where more than one property value was available, average values were used. The ρ_{bwater} is a constant 1.0 g/cm^3, and the C_W is a constant 4.2×10^6 J/m^3 C.

The infiltration flux determined by the use of the analytical method represents the initial, transient infiltration flux. This method is only valid for cases where pore-water velocities are high enough such that heat transport by conduction is negligible compared with heat transport by advection. The high K_s values determined for stream-alluvium cores indicate that this situation is typical for most of the subsurface sediments beneath ephemeral-stream channels in the Sierra Vista subwatershed. The analytical method is also only valid for infiltration under nonisothermal, continuous streamflow loss; this condition is assumed in the ephemeral-stream channels. A more comprehensive, rigorous numerical approach was used to account for heat transport with water flow in the unsaturated zone. Convective and advective heat transport can be expressed by (Kipp, 1987):

$$\frac{d}{dt}\left[\theta_v C_w + (1-\varphi) C_s\right] = \frac{d}{dz}\left[K_t(\theta_v)\frac{dT}{dz}\right] + \frac{d}{dz}\left(\theta_v C_w D_h \frac{dT}{dz}\right) - \frac{d}{dz}\left(\theta_v C_w T q_w\right), \quad (9)$$

where

θ_v = volumetric soil-water content [L^3/L^3],

K_t = thermal conductivity [E/t/L/T],

T = temperature [T], and

D_h = a thermomechanical dispersion tensor [L^2/t].

To describe water flow in the unsaturated zone, variably saturated ground-water flow can be expressed by (Richards, 1931):

$$\frac{d\theta(z,t)}{dt} = \frac{d}{dz}\left[K_u(h_p, z)\frac{dh(z,t)}{dz}\right], \quad (10)$$

where

K_u = unsaturated hydraulic conductivity [L/t],

h_p = matric potential [L], and

h = total head [L].

The numerical code VS2DH (Healy and Ronan, 1996) and its graphical user interface (Hsieh and others, 2000) were used to solve equations (9) and (10) simultaneously.

One-dimensional numerical models were developed to represent conceptual fluid flow and heat transfer at each ephemeral-stream site (tables 10 and 11). Models were created only for sites and times where temperature perturbations were detected at depth during streamflow events. Models were not created for sites and events where temperature perturbations were not detected until after streamflow ended. Similarly, simulations were terminated at the end of streamflow because at that point, heat transfer is dominated by both water and vapor flux, a condition VS2DH cannot simulate.

Sediment properties were determined from core measurements. For depth intervals where more than one property value was measured, average values were used in the calculation. Thermal conductivities at saturation were estimated on the basis of measured thermal conductivities at ambient conditions (table 5). All layers were assumed to be isotropic and to have a specific storage of zero. Streamflow water temperatures were determined from values measured by the surface temperature sensors. Upper boundaries were defined as no flow for the hour prior to the onset of flow, and then as specified normal-flux boundaries during streamflow. Initial sediment temperatures were determined from values measured by temperature sensors at depth. Initial hydraulic conditions were estimated as soil-water contents. Lower boundaries were defined as possible seepage faces. Onset and length of streamflow were determined from streambed sediment-temperature data.

The model simulations yielded subsurface sediment temperatures due to advective heat transport. In all cases, the saturated hydraulic conductivity had to be adjusted to accurately simulate the temperature inflection point identifying streamflow arrival time (table 12). The models were calibrated by adjusting the specified infiltration flux at the upper boundary to minimize the difference between the calculated and the measured sediment temperatures at depth.

The infiltration flux calibrated for the upper boundary represents an average value of the initial, transient infiltration flux. The model simulations represent infiltration from streamflow events ranging in duration from 1 to 5.5 hours; long-term constant infiltration rates were probably not achieved during these ephemeral streamflows.

Rates of Ephemeral-Channel Recharge

Recharge deriving from ephemeral streamflow along the length of a channel can be estimated by:

$$R = \int_0^{\ell} (S\, w\, q_i - EV - T)\, d\ell, \quad (11)$$

where

R = recharge [L^3],

S = streamflow duration [t],

w = wetted width of channel [L],

q_i = infiltration flux [L/t],

EV = water lost to channel evaporation per channel length [L^3/L],

T = water lost to near-channel transpiration per channel length [L^3/L], and

l = length of channel containing alluvial sediments [L].

Average annual recharge was determined by dividing the calculated recharge rate for the 2001–2002 period by the number of years in the time period (2 years for this study). The total streamflow duration was determined for the 2-year period at each streambed-temperature sensor, ARS flume, and USGS streamflow-gaging station (table 8), and an exponential best-fit relation between streamflow duration and distance in the channel downstream from the mountain front was then developed for each channel (fig. 7); only sites having streamflow-duration data for the entire 2001–2002 period were used. The width of the channel at each borehole was known (table 2), and was linearly extrapolated between boreholes. The averaged wetted-channel width during flow events was determined

to be between 10 and 20 percent of the channel width on the basis of the effective wetted channel width along a portion of Walnut Gulch as estimated by Goodrich and others (2004). An average wetted-channel width of 15 percent of the channel width was used in the calculations. Goodrich and others (2004) also estimated channel evaporation losses and near-channel transpiration losses for 1999 and 2000 along a 6.8-km reach of Walnut Gulch. The average losses were scaled so that channel evaporation was represented by 3.0×10^{-4} hm^3/km/2yr and near-channel transpiration was represented by 1.4×10^{-2} hm^3/km/2yr. These values were used for all the channels in the 2001–2002 calculations

Ephemeral-stream channel recharge rates determined with equation 11 were compared with rates derived by using other independent methods (channel-reach water balance, chloride mass balance, ground-water mounding model, and microgravity measurements) for a 6.8-km reach of Walnut Gulch (Goodrich and others, 2004). The infiltration flux used in this comparison was the lowest one calculated for Walnut Gulch by sediment-temperature analysis. As previously stated, streamflow events for which infiltration fluxes could be determined were all less than 5.5 hours in duration; the calculated infiltration fluxes represent an average value of the initial, transient infiltration fluxes. The lowest calculated infiltration fluxes are assumed to best represent the steady-state infiltration rate. Calculations of recharge for 1999 were 0.44 hm^3 from the use of equation 11 and 0.14 to 0.47 hm^3 from the use of other methods; recharge for 2000 was 0.16 hm^3 from the use of equation 11 and 0.13 to 0.37 hm^3 from the use of other methods. These results validate the assumption that the lowest calculated infiltration flux can represent the steady-state infiltration flux when determining ephemeral-stream channel recharge.

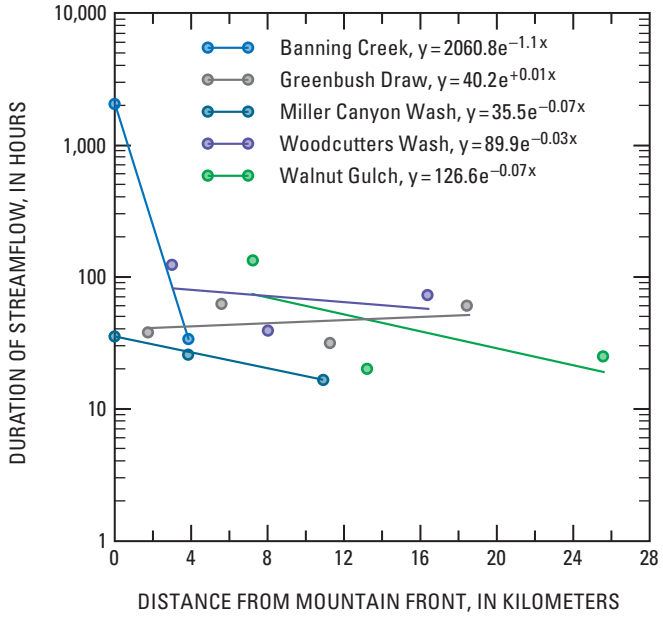

Figure 7. Regression of streamflow duration to distance from the mountain front for 2001 and 2002, Sierra Vista ground-water-recharge study area, Arizona and northeastern Sonora, Mexico. In the equations, y is the duration of streamflow, in hours; x is distance from the mountain front, in kilometers; and e is the base of the natural log.

Ephemeral-Stream Channel Infiltration

Infiltration fluxes during, and percolation fluxes immediately following, streamflow events were determined for sites in Woodcutters Wash, Miller Canyon Wash, Walnut Gulch, Banning Creek, and Greenbush Draw. Data used in the determination of fluxes included physical, hydraulic, and thermal properties of sediment; chloride concentrations of sediment; pore-water stable isotope values and tritium activity; neutron soil-moisture and EMI logs; and sediment-temperature and water-level monitoring. Where possible, fluxes through the upper 1.5 to 12.2 m of sediments were estimated.

Woodcutters Wash

Woodcutters Wash is a northeastward-trending channel with headwaters in the Huachuca Mountains. The channel is 23.0 km long and has an average slope of 13.9 m/km. The channel widens from less than 1 m along the upper reaches to more than 20 m along the lower reaches. It is incised less than 0.5 m along the upper reaches and 2 m or more along the lower reaches. Several knickpoints occur along the lower one-half of the channel in an area where the stream has cut through several layers of clay and caliche.

The channel drains a 37.5-km^2 area that ranges in elevation from 1,204 to 2,488 m. Desert scrub and grassland are the primary land-cover types in the drainage basin; mesquite is dominant along the mountain fronts, and oak woodland is dominant in the mountainous areas (fig. 2). About 21 percent of the drainage basin, the central part, is urban. The banks of Woodcutters Wash have been stabilized in this area.

Soils in the drainage basin vary from loamy near the mountains to calcium carbonate and clayey downgradient; soils are sandy along the stream channel (fig. 3). Thickness of permeable stream alluvium is about 1 m near the mountains, a few centimeters within the city of Sierra Vista, and about 3 m in the lower reaches of Woodcutters Wash. The stream alluvium is underlain by the compacted clayey gravels of the Pantano Formation near the mountains; the poorly sorted sand, silt, and clay of the basin fill in the Sierra Vista area; and the low-permeability silt and clay and calcium carbonate of the basin fill along the lower reaches of the wash.

Ephemeral streamflows recorded from 2001 to 2002 in Woodcutters Wash ranged in duration from about 15 min to 22 hr (table 8). Flows in the upper reaches generally were more frequent and were of a longer duration than flows in reaches downstream (fig. 7). The farthest upstream temperature sensor,

375010, detected 19 flows, which had an average duration of 6.5 hr. The farthest downstream temperature sensor, at site WC1, detected 18 flows, which had an average duration of 4.0 hr.

Borehole WC4a is the farthest upstream site in Woodcutters Wash and is about 0.4 km from the base of the Huachuca Mountains. The site is in a reach about 0.5 m wide and incised less than 1 m into terrace deposits, basin fill, and the Pantano Formation. The highly permeable sand and gravel stream alluvium extends from the land surface to a depth of 3.4 m, and the less permeable semiconsolidated conglomerate of the Pantano Formation extends from 3.4 to 12.5 m (fig. 6*A*). Electrical conductivities of the stream alluvium and the Pantano Formation ranged from about 10 to 30 mS/m, and from about 25 mS/m to 45 mS/m, respectively (fig. 6*A*). A neutron soil-moisture log was not recorded at this site.

Physical and hydraulic properties were determined for two core samples from WC4a collected at depths of 2.1 and 11.3 m (table 6). For the stream alluvium and the Pantano Formation, measured saturated hydraulic conductivity was 6.4×10^{-2} and 4.2×10^{-4} cm/s, respectively; porosity was 0.43 and 0.33 cm^3/cm^3, respectively; and soil-water content was 0.09 and 0.07 cm^3/cm^3, respectively.

When borehole WC4a was drilled in in January 2001, a saturated interval was penetrated above the Pantano Formation at a depth of 2.0 to 3.4 m (fig. 8*A*). Sediment-chloride concentrations were lower than 8 mg/kg in the stream alluvium and generally lower than 3 mg/kg in the Pantano Formation (fig. 9*A*). Tritium activity in the stream alluvium pore water was similar to activity in present-day precipitation (between 3.4 and 3.7 TU; fig. 9*A*). Tritium activity was 10.1 TU in the upper 1.7 m of the Pantano Formation and was between 1 and 2 TU from a depth of 6.6 to 11.1 m. This pattern indicates that recent precipitation has likely infiltrated through the stream alluvium to the Pantano Formation. Water is infiltrating into the semiconsolidated, unsaturated Pantano Formation slowly, at a rate of about 0.9 cm/yr (assuming an average volumetric soil-water content of 0.20 cm^3/cm^3). Pore water within the Pantano Formation was depleted in heavy isotopes, similar to winter precipitation (fig. 10). This could indicate that the Pantano Formation receives infiltration primarily during winter streamflows or that the existing pore water was derived from infiltration received when the climate was cooler than at present.

Temperature methods detected only one summer flow event (30 minutes in duration) at WC4a between January 2001 and April 2002 (table 8). Water levels in the saturated zone, however, rose at least six times during the summer of 2001 (fig. 8*A*). The lack of sediment-temperature signals may be caused by a retention basin about 260 m upstream from the borehole. Water-level recovery was likely the result of infiltration at the retention basin and subsequent downgradient subflow above the contact between the Pantano Formation and the stream alluvium. A recharge flux could not be calculated from the detected flow event because the water level began to rise before the onset of temperature-detected flow in the channel.

Borehole WC3 is about 7.2 km downstream from the mountain front. This site is within the city limits of Sierra Vista, just downstream from an area where the banks and streambed of Woodcutters Wash have been stabilized. The site is in a reach about 8 m wide and incised 1.8 to 3.0 m into terrace deposits and basin fill. Stream alluvium in the channel bed is only a few centimeters thick. The poorly sorted sand, silt, and clay of the upper basin fill extends from the land surface to a depth of 22.6 m (fig. 6*B*). The silt and clay content of the upper basin fill is generally 30 to 60 percent. Electrical conductivity of the sediments ranged from about 25 to 60 mS/m (fig. 6*B*). Neutron soil-moisture counts ranged from 6,000 to 9,000 in the borehole (fig. 6*B*).

Physical and hydraulic properties were determined for five core samples from WC3 collected at depths of 0.9, 1.5, 8.2, 13.7, and 19.8 m (table 6). The measured saturated hydraulic conductivity of the basin fill ranged from 1.7×10^{-4} to 9.9×10^{-3} cm/s. Porosity ranged from 0.33 and 0.40 cm^3/cm^3, and soil-water content ranged from 0.11 to 0.19 cm^3/cm^3.

Sediment-chloride concentrations ranged from 3 to 70 mg/kg from the surface to 4.9 m, and were below 4 mg/kg from 5.2 to 22.6 m (fig. 9*B*). Stable-isotope data indicate that the high chloride concentrations near the surface are not the result of chloride accumulation due to evapotranspiration; stable-isotope values in pore water at 0.2 m had evaporative signatures, but the values at 0.8 m and below did not (fig. 10). The high chloride concentrations in the shallow part of the unsaturated zone are probably indicative of chloride concentrations in runoff from Sierra Vista. Pore-water tritium activity values from the surface to 16.6 m were similar to those of present-day precipitation (between 1.0 and 6.3 TU; fig. 9*B*). The tritium activity at 19.7 m was 0.4 TU. Five flow events were detected at WC3 between January 2002 and December 2002 (table 8). There were no sediment-temperature perturbations, however, at 1.5 m and below during or after flow events.

The temperature data indicate that the infiltration flux at WC3 is too low to perturb the sediment-temperature profile during and after individual flow events. Tritium data indicate an infiltration rate of about 4.1 cm/yr (assuming an average volumetric soil-water content of 0.15 cm^3/cm^3). Stable-isotope values in pore water were between the ranges for summer and winter precipitation, indicating that infiltration may have occurred during both summer and winter streamflow events in the past (fig. 10).

Borehole WC2 is about 12.3 km downstream from the mountain front. The site is in a 22-m wide channel reach that is incised about 1.8 m into terrace deposits and basin fill. The channel bed is floored with only a veneer of stream alluvium and is underlain by less permeable, poorly sorted sand, silt, and clay of the basin fill (fig. 6*C*). The silt and clay content of the basin fill is generally 50 to 80 percent. Geophysical borehole logs were not recorded in this borehole.

Physical and hydraulic properties were determined for five core samples from WC2 collected at depths of 2.1, 3.7, 6.7, 8.2, and 9.8 m (table 6). The measured saturated hydraulic conductivity of the basin fill ranged from 9.8×10^{-6} to $2.2 \times$

10^{-2} cm/s. Porosity of the basin fill ranged from 0.34 to 0.52 cm^3/cm^3. The soil-water content of the basin fill ranged from 0.15 to 0.47 cm^3/cm^3.

Sediment-chloride concentrations to 12.5 m were low (less than 7 mg/kg), and tritium activity to 11.1 m was comparable to that of present-day precipitation (between 3.9 and 5.7 TU), indicating that recent infiltration has occurred to at least 11.1 m (fig. 9*C*). Pore-water stable-isotope values at 2.0 m had a slight evaporative signature and indicate infiltration of both summer and winter streamflow (fig. 10). This borehole was not completed with a casing; therefore, sediment-temperature data are not available and infiltration fluxes could not be determined.

Borehole WC1 is at the SPRNCA boundary 16.4 km downstream from the Huachuca Mountains. The site is in a reach 10-m wide and incised several meters into the basin fill. The highly permeable stream alluvium, consisting of sand and gravel, extends from land surface to 3.7 m; basin fill, consisting of silt and clay, extends from 3.7 to 9.1 m; and basin fill, consisting of sand, extends from 9.1 to 9.4 m (fig. 6*D*). The basin fill includes a large amount of calcium carbonate from 3.7 to 5.2 m, and a slightly sandy zone from 6.4 to 7.0 m. Electrical conductivity of the sediments was about 10 mS/m within the stream alluvium and 60 to 100 mS/m within the basin fill (fig. 6*D*). The higher electrical conductivity in the basin fill is likely due to both higher soil-water content and a higher silt and clay content than the stream alluvium.

During drilling in January 2001, the borehole penetrated saturated sediments at 7.5 m. Water levels were highly variable during the monitoring period, from 6.6 to 8.3 m below the land surface, and rose as much as 0.5 m in 2 days following a single flow event (fig. 8*B*). Neutron soil-moisture counts ranged from 5,000 to 7,000 in the stream alluvium and 7,000 to nearly 20,000 in the basin fill (fig. 6*D*). The highest counts correspond to saturated or near-saturated sediments.

Physical and hydraulic properties were determined for four core samples from WC1 collected at depths of 0.3, 2.1, 3.7, and 6.7 m (table 6). The measured saturated hydraulic conductivity of the stream alluvium ranged from 3.6×10^{-2} to 7.2×10^{-2} cm/s, and that of the basin fill ranged from 2.1×10^{-6} to 3.2×10^{-3} cm/s. Porosity of the stream alluvium ranged from 0.37 to 0.46 cm^3/cm^3; porosity of the basin fill was not determined. Soil-water contents of the stream alluvium ranged from 0.07 to 0.13 cm^3/cm^3, and the soil-water content at one depth in the basin fill was 0.37 cm^3/cm^3. Sediment-chloride concentrations to 8.8 m were low (less than 6 mg/kg) and tritium activity values to 8.1 m were between 3.9 and 7.2 TU (fig. 9*D*), indicating that recent infiltration has occurred to at least 9.1 m. Stable-isotope values in pore water were between the isotope ratio ranges for summer and winter precipitation, indicating that infiltration prior to drilling may have occurred during both summer and winter streamflow events (fig. 10). An evaporative signature is not evident in the stable-isotope data.

Eighteen flow events occurred at WC1 between January 2001 and December 2002 (table 8). During four events, temperature perturbations were detected at 1.5 and 3.0 m, but not below 3.0 m (table 9). The water level in the saturated zone, however, rose sharply following each event, indicating that the infiltrating streamflow is recharging the saturated zone. The lack of temperature variation below 3.0 m, coupled with the substantial water-level response, supports the occurrence of recharge from nearby areas but not directly through the silt and clay at the site. The water-level response may represent a confined response in sandy stringers within the silt and clay that are hydraulically connected to upstream areas where infiltration occurs.

Infiltration fluxes to 3.0 m below the land surface during flow events ranged from 1.3 to 1.5 m/hr (fig. 11 and tables 9 and 11). Percolation fluxes to 3.0 m after flow events ranged from 0.4 to 1.5 m/hr (table 9).

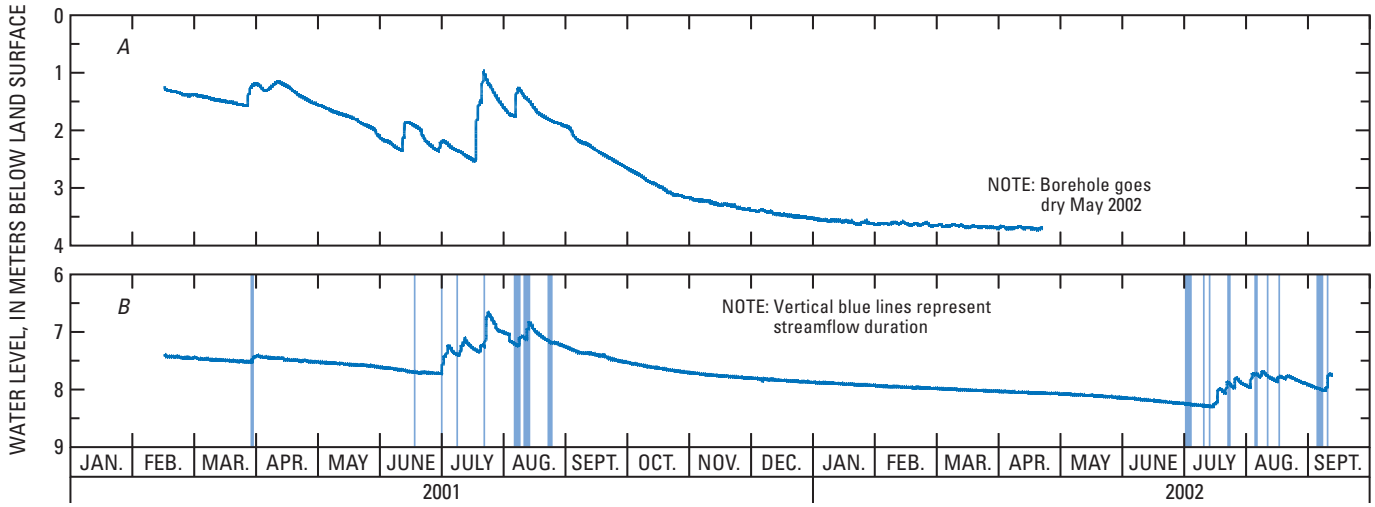

Figure 8. Water levels and streamflow durations from temperature sensors, Woodcutters Wash boreholes: *A*, WC4a; *B*, WC1.

Miller Canyon Wash

Miller Canyon Wash is a northeastward-trending channel with headwaters in the Huachuca Mountains. The channel is 16.2 km long and has an average slope of 20.5 m/km. The channel widens from less than 1 m along the upper reaches to more than 4 m along the lower reaches. It is incised less than 1 m along the upper reaches and 1 m or more along the lower reaches. The channel drains a 32.8-km^2 area that ranges in elevation from 1,252 to 2,859 m. Desert scrub, grassland, and mesquite are the primary land-cover types in the drainage basin; oak woodland and forest are dominant in the mountainous areas (fig. 2). About 15 percent of the basin, along the mountain front, is urban. The urban areas, however, generally have less paved areas than the urban areas in the Woodcutters Wash drainage basin.

Soils in the drainage basin vary from loamy and fine paleosoils below the mountains to clayey downgradient; soils are sandy along the stream channel (fig. 3). The permeable stream alluvium ranges in thickness from a few centimeters near the mountains to a few meters in the lower reaches. The stream alluvium is underlain by low permeability basin fill that has variable amounts of clay, silt, sand, and gravel.

Ephemeral streamflows recorded in 2001–2002 ranged in duration from about 30 min to 19.8 hr (table 8). Flows in the upper reaches were less frequent but generally were of longer duration than those farther downstream (fig. 7). The farthest upstream site, temperature sensor 377806, detected four flows,

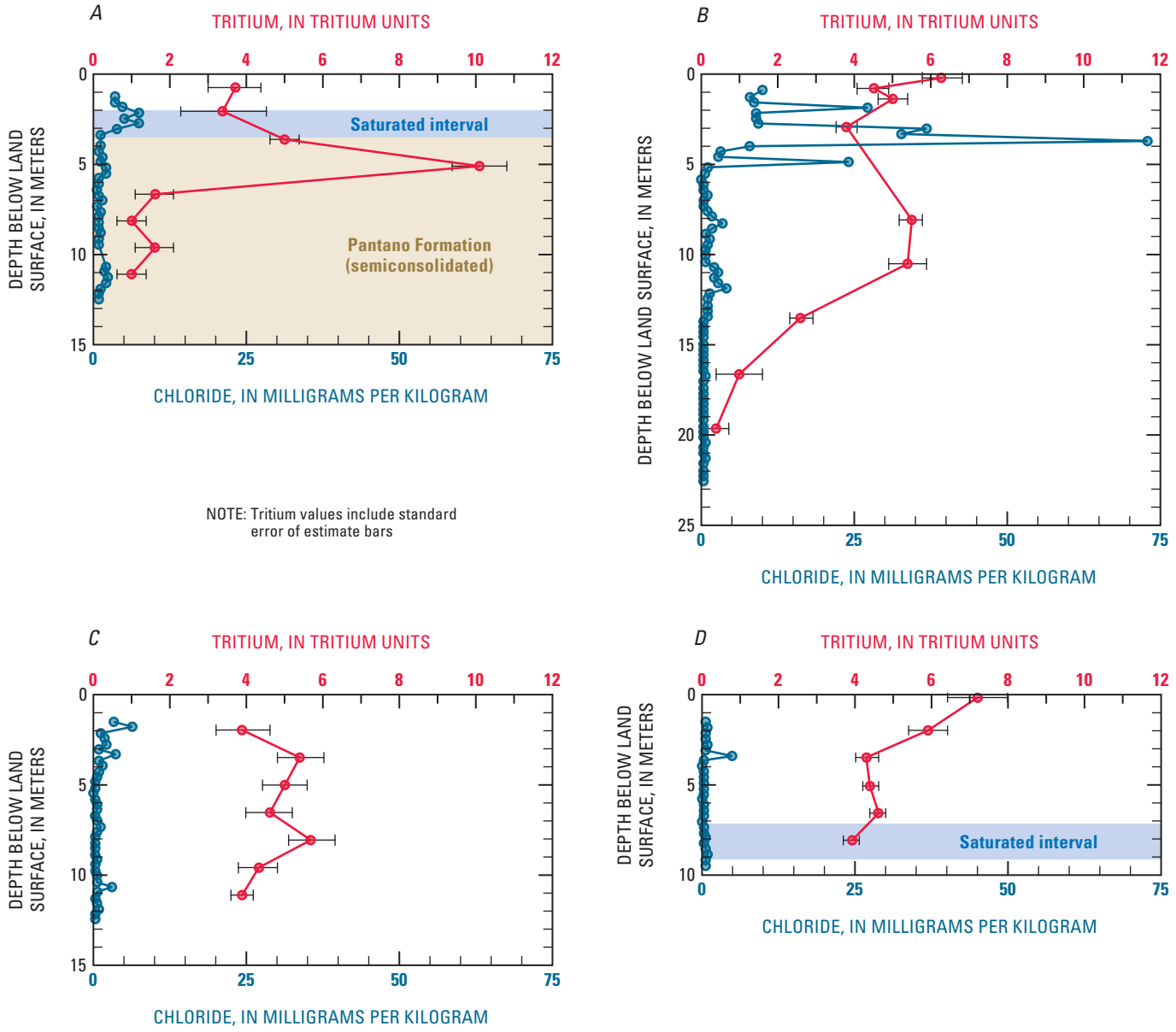

Figure 9. Sediment-chloride and pore-water tritium data, Woodcutters Wash boreholes: *A*, WC4a; *B*, WC3; *C*, WC2; *D*, WC1.

which had an average duration of 9.1 min. The farthest downstream site, temperature sensor 374919, detected six flows, which had an average duration of 2.8 hr.

Borehole MC2 is at the contact between the crystalline rocks of the Huachuca Mountains and the basin fill. The site is in a reach about 2 m wide and incised less than 1 m into the basin fill. The borehole penetrated a layer of predominantly poorly sorted gravel and sand of the basin fill from the land surface to 15.8 m that included a layer of silt and clay from 6.4 to 7.6 m (fig. 6*E*). Electrical conductivity of the sediments at MC2 ranged from about 20 to 40 mS/m (fig. 6*E*). Borehole MC1 is at the SPRNCA boundary 7.1 km downstream from the mountain front. The site is in a reach about 4 m wide and incised several meters into the basin fill. The borehole penetrated poorly sorted sand, silt, and clay of the basin fill from the land surface to 25.0 m (fig. 6*F*). Electrical conductivity of the sediments ranged from about 20 to 100 mS/m (fig. 6*F*). Neutron soil-moisture counts ranged from about 7,000 to 11,000 for MC2 (fig. 6*E*); a neutron soil-moisture log was not completed in MC1.

Physical and hydraulic properties of the basin fill were determined for three core samples from MC2 collected at depths of 1.8, 7.0, and 10.1 m; and for four core samples from MC1 collected at depths of 0.9, 4.0, 8.5, and 19.2 m (table 6). The measured saturated hydraulic conductivity ranged from 1.7×10^{-2} to 3.2×10^{-6} cm/s at MC2 and from 9.3×10^{-3} to 1.8×10^{-6} cm/s at MC1. Porosities ranged from 0.36 to 0.42 cm^3/cm^3 at MC2 and from 0.36 to 0.39 cm^3/cm^3 at MC1. Soil-water contents ranged from 0.18 to 0.30 cm^3/cm^3 at MC2 and from 0.28 to 0.31 cm^3/cm^3 at MC1.

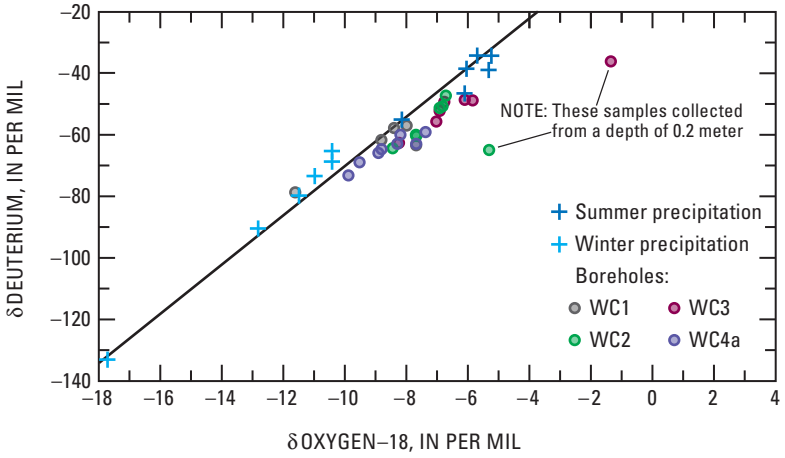

Figure 10. Stable-isotope data for pore water collected from Woodcutters Wash boreholes and for precipitation.

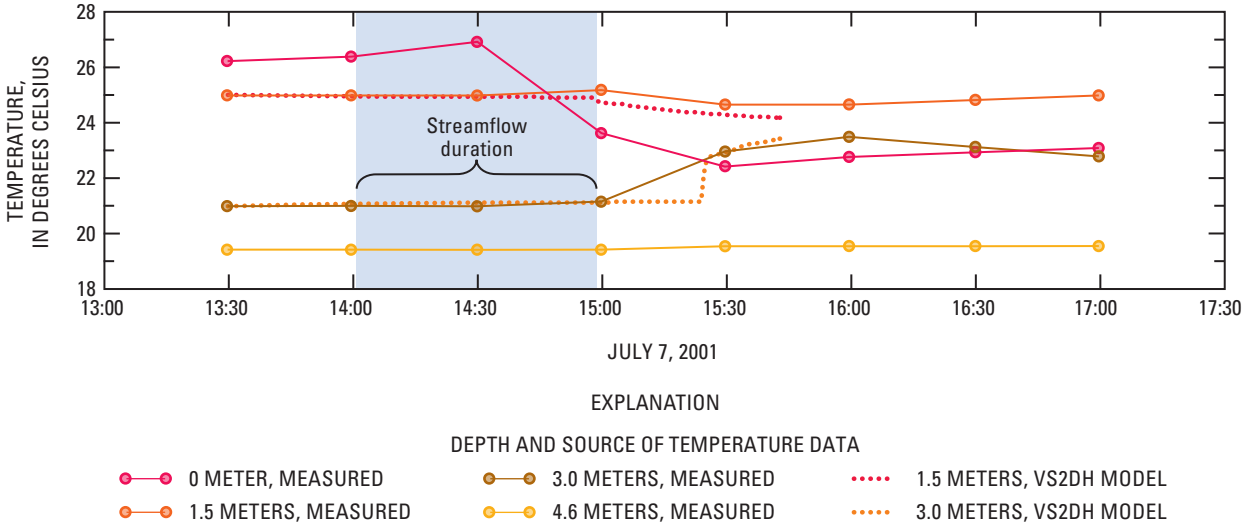

Figure 11. Streamflow duration and sediment temperatures from sensors and from VS2DH model output, Woodcutters Wash borehole WC1, July 7, 2001.

Sediment-chloride concentrations were lower than 5 mg/kg in the upper 15.8 m of MC2 and in the upper 21.9 m of MC1. Tritium activity in the upper 9.9 m of MC2 and in the upper 22.1 m of MC1 were comparable to activity in present-day precipitation (1.9 to 7.8 TU; fig. 12).Recent infiltration has occurred to at least 9.9 m at MC2 and 22.1 m at MC1. Stable-isotope values for the pore water at both sites indicated that infiltration occurred during summer and winter; pore water below 0.2 m did not show evaporative signatures (fig. 13).

One, 18-hour, streamflow event was detected between January 2002 and December 2002 at MC2; streamflow was not detected between April 2002 and December 2002 at MC1 (table 8). There were no sediment-temperature perturbations at or below 1.5 m during or after flow events at MC2. The temperature data suggest that the infiltration flux at MC2 is too low to perturb the sediment-temperature profile during and after individual events. Because of a lack of data, infiltration fluxes could not be calculated from sediment-temperature profiles at either site.

Walnut Gulch

Walnut Gulch is a westward-trending channel with headwaters in the Tombstone Hills and the Mule and Dragoon Mountains. The main channel is about 26.5 km long and has an average slope of 12.1 m/km. The channel widens from less than 2 m along the upper reaches to more than 40 m along the lower reaches. It is incised less than 1 m along the upper reaches and 4 m or more along the lower reaches. The channel drains a 152.1-km^2 area that ranges in elevation from 1,164 to 1,939 m. Desert scrub, grassland, and mesquite are the primary land-cover types in the drainage basin (fig. 2). Approximately 3 percent of the Walnut Gulch drainage basin, near the northern extent of the Tombstone Hills, is urbanized.

Soils in the drainage basin range from clayey near the mountains to secondarily developed calcium carbonate downgradient; soils are sandy along the stream channel. The permeable stream alluvium ranges in thickness from about 1 m near the mountains to 15 m in the lower reaches of the channel. The stream alluvium is underlain by low-permeability consolidated to semiconsolidated conglomerate of the lower basin fill near the mountains and by upper basin fill in the lower reaches of the channel.

The ARS has monitored ephemeral streamflows in Walnut Gulch since the 1950s by using a series of flumes. Ephemeral streamflows recorded in 2001–2002 at flumes 1, 6, and 11 ranged in duration from 12 min to 82.2 hr (table 8). Flows generally were more frequent and of longer duration near the mountain front than in areas downstream (fig. 7). The farthest upstream site, flume 11, had 12 flows, which had an average duration of 11.1 hr. The farthest downstream site, flume 1, had eight flows, which had an average duration of 3.2 hr.

Borehole WG3 is just upstream from flume 11 and is 7.2 km downstream from the mountain front. The site is in a reach about 2 m wide and incised less than 1 m into the basin fill. The borehole penetrated unconsolidated stream alluvium of sand and gravel to 1.8 m, and semiconsolidated conglomerate of the lower basin fill from 1.8 to 13.1 m (fig. 6*G*). The electrical conductivity of the conglomerate was about 5 to 10 mS/m (fig. 6*G*). A neutron soil-moisture log was not recorded in this

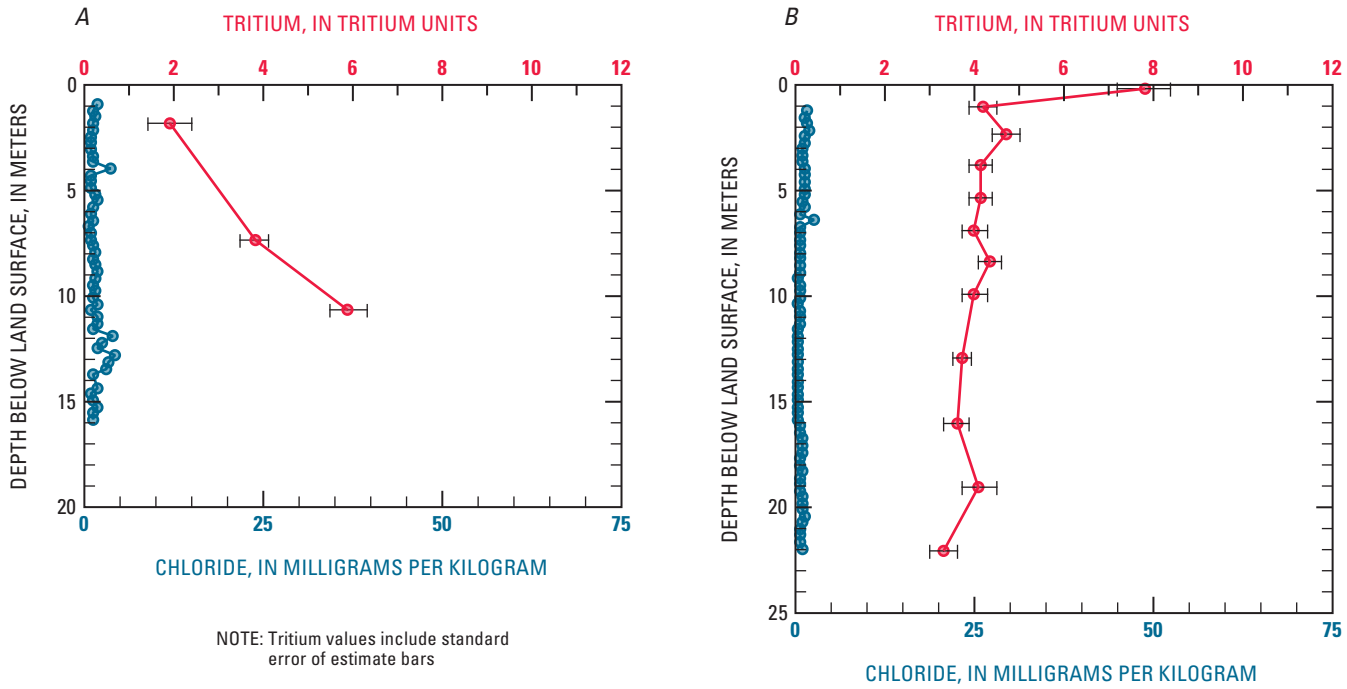

Figure 12. Sediment-chloride and pore-water tritium data, Miller Canyon Wash boreholes: *A*, MC2; *B*, MC1.

borehole. The high degree of induration of the conglomerate and basalt prevented the collection of cores below 1.8 m, and physical and hydraulic properties were not determined for the stream alluvium above 1.8 m.

Sediment-chloride concentrations were less than 4 mg/kg in the upper 1.8 m, and tritium activity in the upper 0.8 m was comparable to activity for present-day precipitation (6.5 to 8.5 TU; fig. 14*A*), indicating that recent infiltration has occurred to at least 0.8 m. Although the primary porosity of the semiconsolidated conglomerate is small, infiltration can occur through secondary fractures. The stable-isotope values of the pore water at 0.2 and 0.8 m had a strong evaporative signature (fig. 15). Sediment temperatures were not monitored at this site, and therefore, infiltration fluxes were not calculated.

Borehole WG2 is just upstream from flume 6 and is 13.2 km downstream from the mountain front. The site is in a reach about 13 m wide and incised several meters into the basin fill. The borehole penetrated unconsolidated stream alluvium of sand and gravel to 3.7 m, semiconsolidated conglomerate of the lower basin fill from 3.7 to 11.6 m, and basalt from 11.6 to 12.2 m (fig. 6*H*). Electrical conductivity of the sediments was less than 5 mS/m in the stream alluvium and from 10 to 15 mS/m in the conglomerate (fig. 6*H*). Neutron soil-moisture counts in the borehole ranged from about 6,000 to 10,000. As at WG3, the high degree of induration of the conglomerate and basalt prevented the collection of cores below 3.7 m, and physical and hydraulic properties were not determined for the stream alluvium above 3.7 m.

Sediment-chloride concentrations in the upper 3.4 m were less than the detection limit of 1.80 mg/kg, and tritium activity in the upper 2.3 m was comparable to values for present-day precipitation (4.7 to 6.7 TU; fig. 14*B*), indicating that recent infiltration has occurred to at least 2.3 m. The stable-isotope values for the pore water at 0.5 and 0.8 m had a strong evaporative signature; however, the pore water at 2.3 m did not (fig. 15). Although the primary porosity of the consolidated conglomerate is small, infiltration can occur through secondary fractures.

Seven flow events occurred at flume 6 between May 2002 and December 2002 (table 8). Borehole WG2 was damaged sometime after mid-July 2002, however, and therefore only sediment temperatures from the flow on July 19, 2002, can be used to determine infiltration fluxes at this site. During this flow, a temperature perturbation was detected at a depth of 3.0 m (table 9). The temperature sensor at 1.5 m malfunctioned during this time and all data were lost. The calculated infiltration fluxes to 3.0 m during flow ranged from 0.4 to 1.0 m/hr (fig. 16*A* and tables 9 and 11).

Borehole WG1 is just upstream from flume 1 and 25.6 km downstream from the mountain front. The site is in a reach about 31 m wide and incised several meters into the basin fill. The borehole penetrated stream alluvium of sand and gravel in the upper 14.5 m underlain by basin fill that is 20 to 55 percent silt and clay (fig. 6*I*). Electrical conductivity of the sediments ranged from less than 20 mS/m within the stream alluvium to 25 to 65 mS/m within the basin fill (fig. 6*I*). A neutron soil-moisture log was not recorded in this borehole.

Physical and hydraulic properties were determined for four core samples from WG1 collected at depth of 3.0, 3.7, 13.4, and 22.6 m (table 6). The data indicate little variation of properties between the stream alluvium and the upper basin fill. The measured saturated hydraulic conductivity of the cores ranged from 2.0×10^{-2} to 4.6×10^{-2} cm/s; porosity ranged from 0.35 to 0.47 cm^3/cm^3; and soil-water content ranged from 0.10 to 0.25 cm^3/cm^3.

Sediment-chloride concentrations in the upper 22.3 m were less than 3 mg/kg, and tritium activity in the upper 22.4 m was comparable to present-day precipitation (2.9 to 4.5 TU; fig. 14*C*), indicating that recent infiltration has occurred to at least 22.4 m. Stable-isotope values at 2.9 m had a slight evaporative signature (fig. 15) and also indicated that water in the unsaturated zone infiltrated during both summer and winter streamflow events.

Three flow events occurred at flume 1 between April 2002 and December 2002 (table 8). All were during the summer and had durations from 12 min to about 10 hr. During each event, sediment-temperature perturbations in WG1 were detected at 1.5, 3.0, and 4.6 m (table 9). Temperature perturbations were detected at 6.1 m after the end of each flow event (table 9), but no perturbations were detected below 6.1 m.

Calculated infiltration fluxes to 4.6 m below the land surface during flow events ranged from 0.4 to 2.1 m/hr (figs. 15*B* and 15*C* and tables 9 and 11). Percolation fluxes to 6.1 m after flow ended ranged from 0.1 to 1.0 m/hr (table 9).

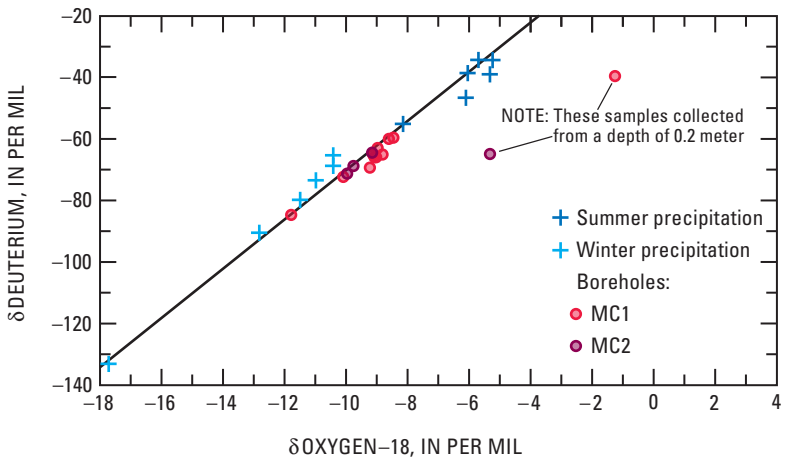

Figure 13. Stable-isotope data for pore water collected from Miller Canyon Wash boreholes and for precipitation.

Banning Creek

Banning Creek is a westward-trending channel with headwaters in the Mule Mountains. The channel is 8.6 km long and has an average slope of 15.6 m/km. The creek drains a 41.3-km^2 area that ranges

in elevation from 1,257 to 2,217 m. Desert scrub, grassland, and mesquite are the primary land-cover types in the drainage basin; oak woodland dominates the mountainous areas (fig. 2). Less than 1 percent of the basin is urbanized land.

Soils in the drainage basin vary from lithic rock near the mountains to calcium carbonate downgradient; soils are sandy along the stream channel (fig. 3). The permeable stream alluvium ranges in thickness from less than 1 m near the mountains to more than 7 m in the lower reaches of the creek. The stream alluvium is underlain by limestone in the upper reaches and unconsolidated basin fill of clay, silt, sand, and gravel in the lower reaches.

Ephemeral streamflows recorded during 2001–2002 ranged in duration from 1 hr to 48 days (table 8). Flows in the upper reaches were not more frequent but were of a longer duration than flows farther downstream (fig. 7). The farthest upstream streamflow-gaging station, 09470700, and temperature sensor, 377822, detected two flows in 2001 to 2002. The flows had an average duration of 42.9 days. The farthest downstream temperature sensor, at site BC1, detected eight flows, which had with an average duration of 4.6 hr.

Borehole BC1 is 3.9 km downstream from the crystalline rocks of the Mule Mountains. The channel at the site is about 4 m wide and is incised several meters into the basin fill. The borehole penetrated unconsolidated stream alluvium of clay, silt, sand, and gravel from the land surface to 6.4 m (fig. 6*J*). Basin fill, which includes greater amounts of clay and silt than the stream alluvium, was penetrated from 6.4 to 25.9 m. Electrical conductivity ranged from 10 to 50 mS/m in the stream alluvium and from 10 to 70 mS/m in the basin fill (fig. 6*J*). Neutron soil-moisture counts ranged from 6,000 to 10,000 in the borehole (fig. 6*J*).

Physical and hydraulic properties were determined for six core samples from BC1 collected at depths of 2.1, 5.2, 8.2, 14.3, 15.8, and 20.4 m (table 6). The measured saturated hydraulic conductivity ranged from 9.6^{-3} to 1.2^{-1} cm/s for the stream alluvium and from 4.1^{-7} to 8.9^{-3} cm/s for the basin fill. Porosity of the two units ranged from 0.25 to 0.43 cm^3/cm^3, and soil-water content ranged from 0.08 to 0.29 cm^3/cm^3.

Sediment-chloride concentrations in the upper 25.9 m were less than 12 mg/kg, and tritium activity in the upper 23.3 m were comparable to values for present-day precipitation (3.2 to 6.7 TU; fig. 17), indicating that recent infiltration has occurred to at least 23.3 m. Stable-isotope values for pore water were between bulk precipitation ranges for summer and winter (fig. 18), indicating that infiltration occurs during summer and winter streamflow events.

Eight flow events occurred at BC1 between January 2001 and December 2002 (table 8). During seven of the events, temperature perturbations were detected at 1.5 and 3.0 m; temperature perturbations were also detected at 4.6 and 6.1 m after the end of each event (table 9).

Calculated infiltration fluxes to 3.0 m during flow events ranged from 0.4 to 2.8 m/hr (fig. 19 and tables 9 and 11). Percolation fluxes to 6.1 m after flow ended ranged from 0.7 to 2.8 m/hr (tables 9 and 11).

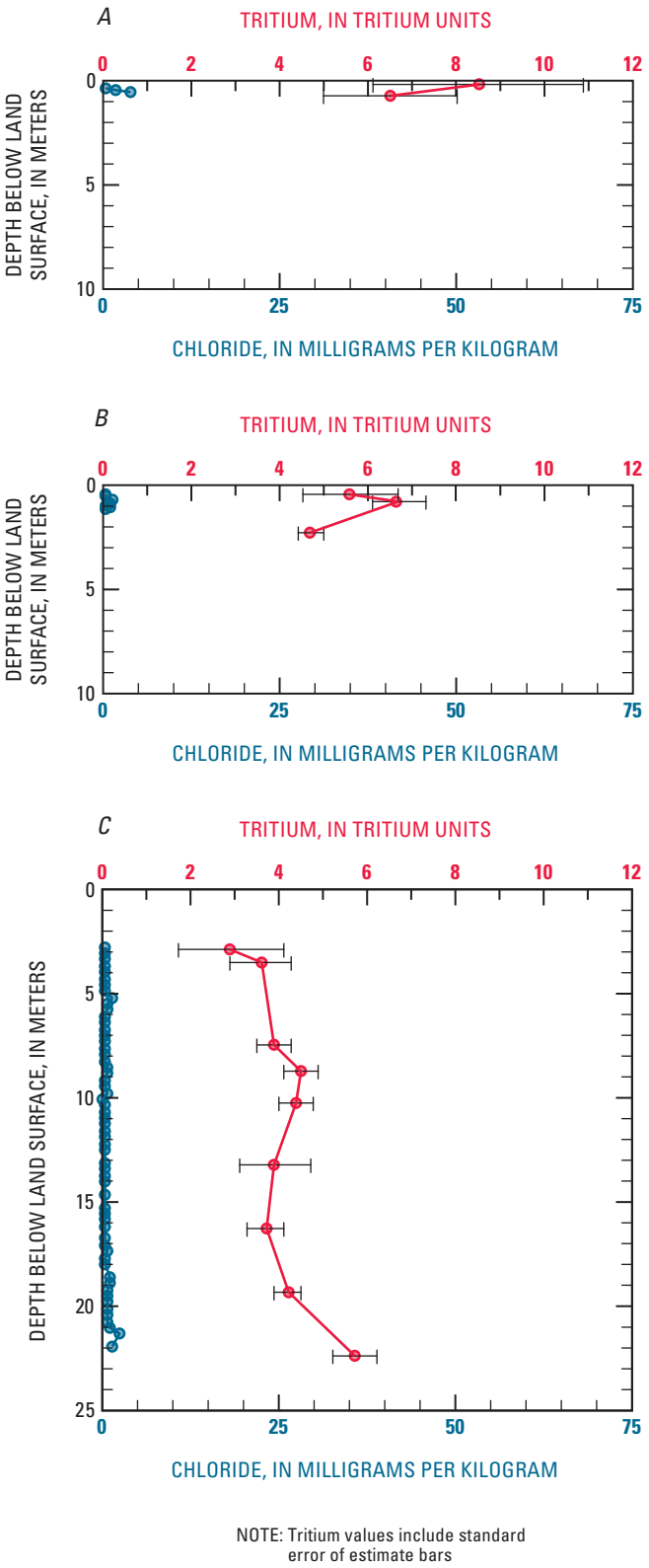

Figure 14. Sediment-chloride and pore-water tritium data, Walnut Gulch boreholes: *A*, WG3; *B*, WG2; *C*, WG1.

Greenbush Draw

Greenbush Draw is a northwestward-trending channel with headwaters in the Mule Mountains and in parts of Mexico. The main channel is 19.5 km long and has an average slope of 8.8 m/km. The channel widens from less than 2 m along the upper reaches to more than 14 m along the lower reaches of the draw. It is incised 2 m or more along the lower reaches. The draw drains a 306.3-km^2 area that ranges in elevation from 1,280 to 2,258 m. Grassland, mesquite, and desert scrub are the primary land-cover types in the drainage basin (fig. 2). About 4 percent of the basin is urbanized land.

Soils in the drainage basin are primarily sandy along the stream channels and clayey and calcium carbonate elsewhere (fig. 3). Secondary calcium carbonate soils dominate the lower downgradient areas to the north of Greenbush Draw, and clayey soils dominate the downgradient areas to the south of Greenbush Draw. The stream alluvium ranges in thickness from 2 m or less in the upper reaches to 10 m along the lower reaches. The stream alluvium is underlain by unconsolidated to semiconsolidated upper basin fill that includes interbedded sand, gravel, silt, and clay.

Ephemeral streamflows recorded during 2001–2002 ranged in duration from 30 min to 19 hr (table 8). Flows in the upper reaches of Greenbush Draw were not more frequent or of a longer duration than flows at sites farther downstream (fig. 7). The farthest upstream temperature sensor, 377815, detected five flows in 2001 and 2002, which had an average duration of 7.5 hr. The farthest downstream temperature sensor, 377820, detected six flows, which had an average duration of 10.0 hr.

Borehole GD2 is 5.6 km downstream from the limestone and crystalline rocks of the mountains. The channel at the site is about 2 m wide and is incised less than 1 m into the basin fill. The borehole penetrated unconsolidated stream alluvium of clay, silt, sand, and gravel from the surface to 2.0 m and basin fill from 2.0 to 25.0 m (fig. 6*K*). The basin fill has greater percentages of clay and silt than the stream alluvium. Electrical conductivity of the sediments ranged from 10 to 70 mS/m in the stream alluvium and from 10 to 100 mS/m in the basin fill (fig. 6*K*). Thin saturated intervals (less than 1.2 m in thickness) were penetrated at depths of 8.2, 12.8, and 24.1 m during drilling. A neutron log was not recorded in this borehole.

Physical and hydraulic properties were determined for three core samples from GD2 collected at depths of 2.4, 5.3, and 13.1 m (table 6). All the cores were from basin fill. The saturated hydraulic conductivity ranged from 5.9×10^{-3} to 5.3×10^{-2} cm/s. Porosity ranged from 0.41 to 0.53 cm^3/cm^3, and soil-water content ranged from 0.14 to 0.44 cm^3/cm^3.

Sediment chloride concentrations in the upper 25.0 m were less than 3 mg/kg, and tritium activity in the upper 19.1 m were similar to values for present-day precipitation (3.5 to 4.3 TU; fig. 20*A*), indicating that recent infiltration has occurred to at least 19.1 m. Stable-isotope values for pore water were between ranges for summer and winter precipitation (fig. 21), indicating that infiltration occurs during summer and winter streamflow events.

Three flow events occurred at GD2 between January 2002 and December 2002 (table 8). During two of the events, temperature perturbations were detected at 1.5 m; temperature perturbations were detected at 3.0, 6.1, 9.1, and 12.2 m after flow ended (table 9). Infiltration fluxes to 1.5 m during flow ranged from 0.7 to 0.9 m/hr. Percolation fluxes after flow ended ranged from 0.3 to 1.8 m/hr.

Borehole GD1 is 12.4 km downstream from the limestone and crystalline rocks of the mountains. The channel at the site is about 14 m wide and is incised several meters into the basin fill. The borehole penetrated unconsolidated stream alluvium of clay, silt, sand, and gravel from the land surface to 10.0 m and basin fill from 10.0 to 19.5 m (fig. 6*L*). The basin fill has a greater percentage of clay and silt than the stream alluvium and includes a large amount of calcium carbonate from 10.1 to 10.4 m. Electrical conductivity of the sediments ranged from 10 to 20 mS/m in the stream alluvium and from 15 to 100 mS/m in the basin fill (fig. 6*L*). Neutron counts did not vary greatly (7,000 to 12,000) in the borehole (fig. 6*L*).

Physical and hydraulic properties were determined for four core samples from GD1 collected at depths of 4.0, 7.0, and 13.1 m (table 6). The measured saturated hydraulic conductivity ranged from 4.6×10^{-3} to 1.4×10^{-2} cm/s for the stream alluvium and was 6.8×10^{-8} cm/s for the basin fill. Porosity was determined only for one core, from the stream alluvium, and was 0.27 cm^3/cm^3. Soil-water content was determined only for the stream alluvium, and ranged from 0.11 to 0.15 cm^3/cm^3.

Sediment-chloride concentrations in the upper 18.9 m were less than the detection limit of 1.80 mg/kg, and tritium activity in the upper 19.1 m was similar to values for present-day precipita-

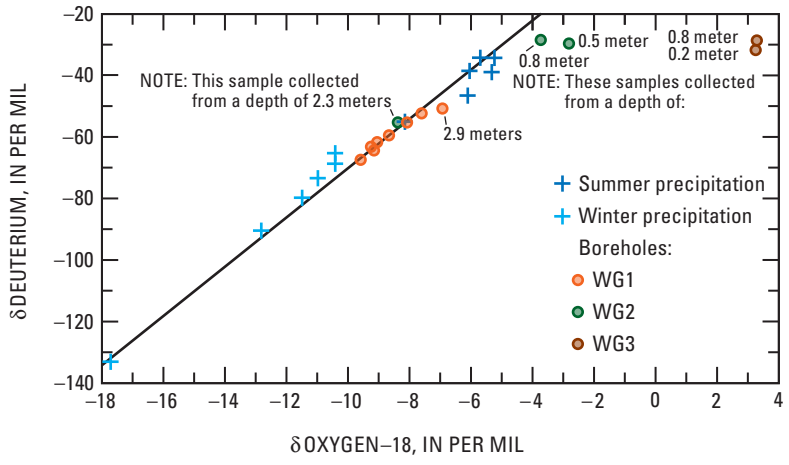

Figure 15. Stable-isotope data for pore water collected from Walnut Gulch boreholes and for precipitation.

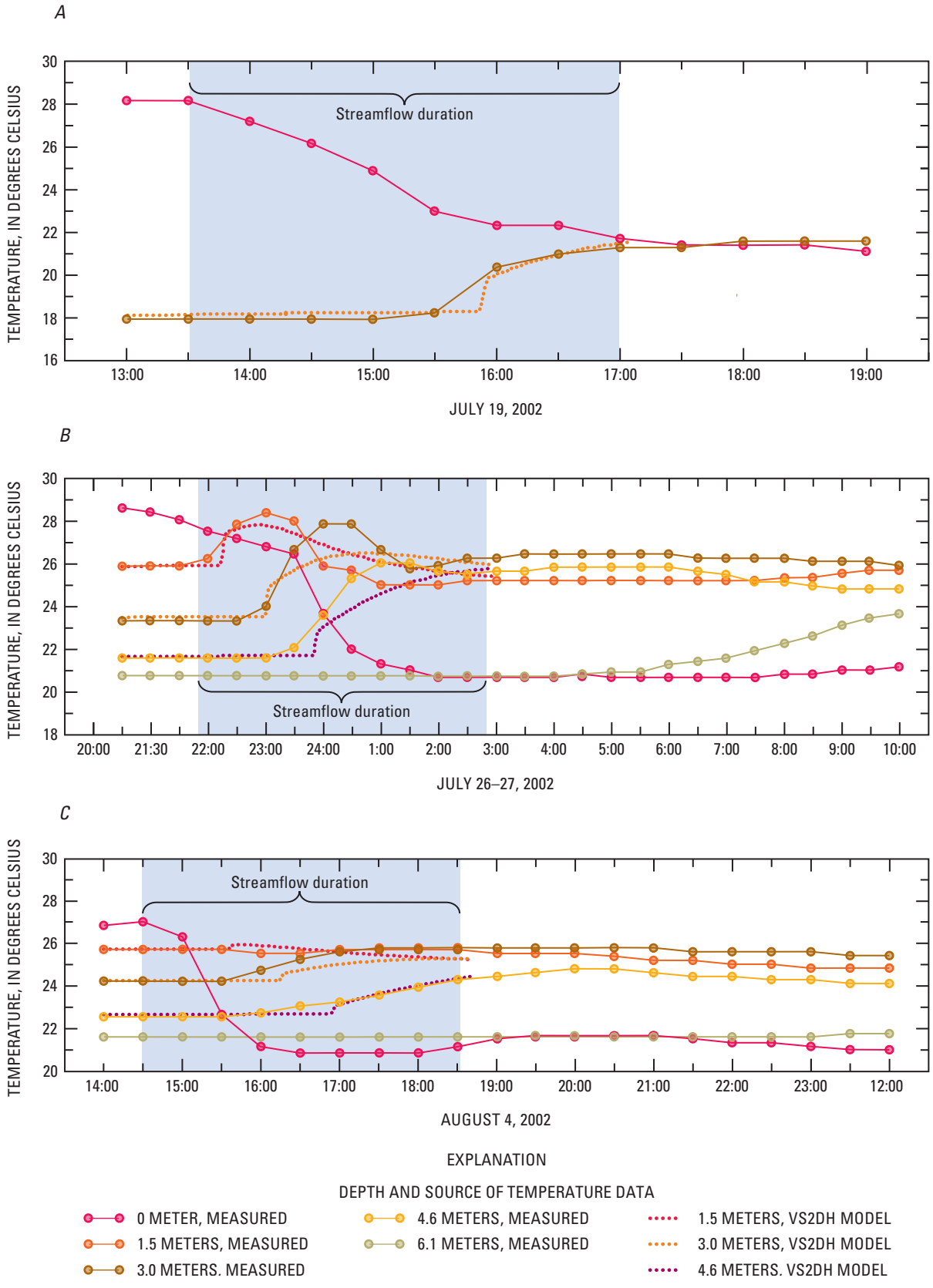

Figure 16. Streamflow durations and sediment temperatures from sensors and from VS2DH model output, Walnut Gulch boreholes: *A*, WG2, July 19, 2002; *B*, WG1, July 26–27, 2002; *C*, WG1, August 4, 2002.

tion (3.3 to 4.6 TU; fig. 20*B*), indicating that recent infiltration has occurred to at least 19.1 m. Stable-isotope values for pore water at 0.5 m had strong evaporative signatures; the remaining values were between bulk precipitation ranges for summer and winter (fig. 21), indicating that infiltration occurs during summer and winter streamflow events.

One flow event was detected at GD1 between May 2002 and December 2002 (table 8). Temperature perturbations, at depths of 1.5, 3.0, 6.1, and 9.1 m, were detected only after flow ended (table 9). Percolation fluxes to 9.1 m after flow ended ranged from 0.1 to 0.8 m/hr (table 9).

Basin-Floor Infiltration

Infiltration fluxes were determined for basin-floor sites in the Walnut Gulch, Carr Canyon Wash, and Woodcutters Wash drainage basins. Data used in the determination of infiltration fluxes included physical and hydraulic properties of sediments, chloride concentrations of sediments, and pore-water stable-isotope values and tritium activity. Where possible, infiltration fluxes through the upper 4.0 to 9.8 m of sediments were estimated.

Borehole WG4 is within the Walnut Gulch drainage basin on a hilltop in the ARS Lucky Hills research station. Mesquite woodland is the primary land-cover type at the site (fig. 2). Basin fill penetrated by the borehole consists of semiconsolidated to unconsolidated sand and gravel from the surface to 3.4 m, consolidated clay and silt from 3.4 to 5.5 m, semiconsolidated to unconsolidated sand and gravel from 5.5 to 9.8 m, and semiconsolidated to consolidated clay, silt, and sand from 9.8 to 13.4 m (fig. 6*M*). Electrical conductivity of the sediments ranged from 0 to 30 mS/m (fig. 6*M*). A neutron soil-moisture log was not recorded in this borehole.

Physical and hydraulic properties were determined for two core samples collected at depths of 4.3 and 13.4 m in the borehole (table 6). Saturated hydraulic conductivity was 1.3×10^{-2} and 1.7×10^{-2} cm/s. Porosity was 0.48 and 0.50 cm^3/cm^3, and soil-water content was 0.10 and 0.19 cm^3/cm^3.

Sediment-chloride concentrations increased sharply to 226 mg/kg from 1.5 to 2.1 m as a result of evapotranspirative enrichment (fig. 22*A*). Concentrations then decreased sharply to 34 mg/kg from 2.4 to 3.4 m, probably as a result of no downward water movement or preferential transport past the root zone. Below 3.4 m, the chloride concentration ranged from 3 to 90 mg/kg. Chloride below 2.1 m was likely emplaced by infiltration during a wetter period.

Tritium activity of the pore water indicates that water has infiltrated to at least 7.5 m since 1952 (fig. 22*A*). No anthropogenic tritium was detected at 13.3 m. The location of the tritium peak at 2.0 m indicates an infiltration flux of about 1.0 cm/yr (assuming an average volumetric soil-water content of 0.19 cm^3/cm^3) to 2.0 m. The chloride data indicate that about 694 years is required for water to infiltrate to this depth, at a flux of about 0.2 cm/yr (fig. 22*B*). Deeper penetration of tritium relative to that of chloride was previously identified in desert soils; possible explanations have included the downward movement of tritium in the vapor phase (Phillips and others, 1988; Scanlon, 1991) and the downward preferential flow of tritium through cracks and macropores (Izbicki and others, 2000).

Pore-water stable-isotope values to 13.3 m plot along an evaporative trend line that has a slope of 2.5 (fig. 23). The point of intersection between the evaporative trend line and the meteoric water line indicates that historical infiltration at WG4 was

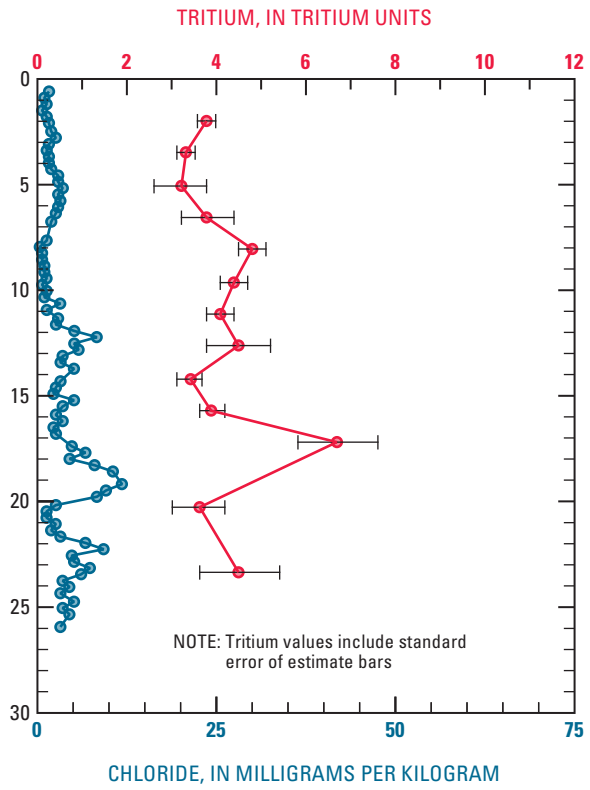

Figure 17. Sediment-chloride and pore-water tritium data, Banning Creek borehole BC1.

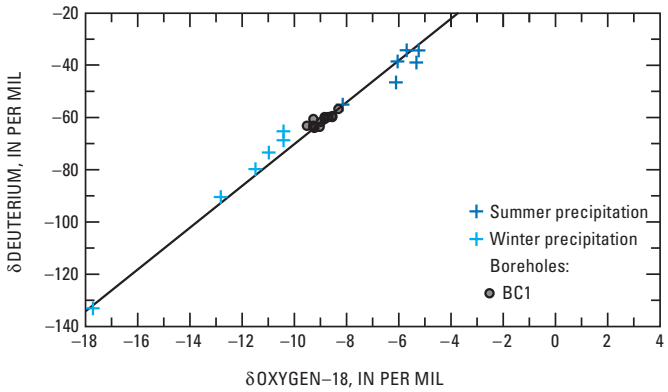

Figure 18. Stable-isotope data for pore water collected from Banning Creek borehole BC1 and for precipitation.

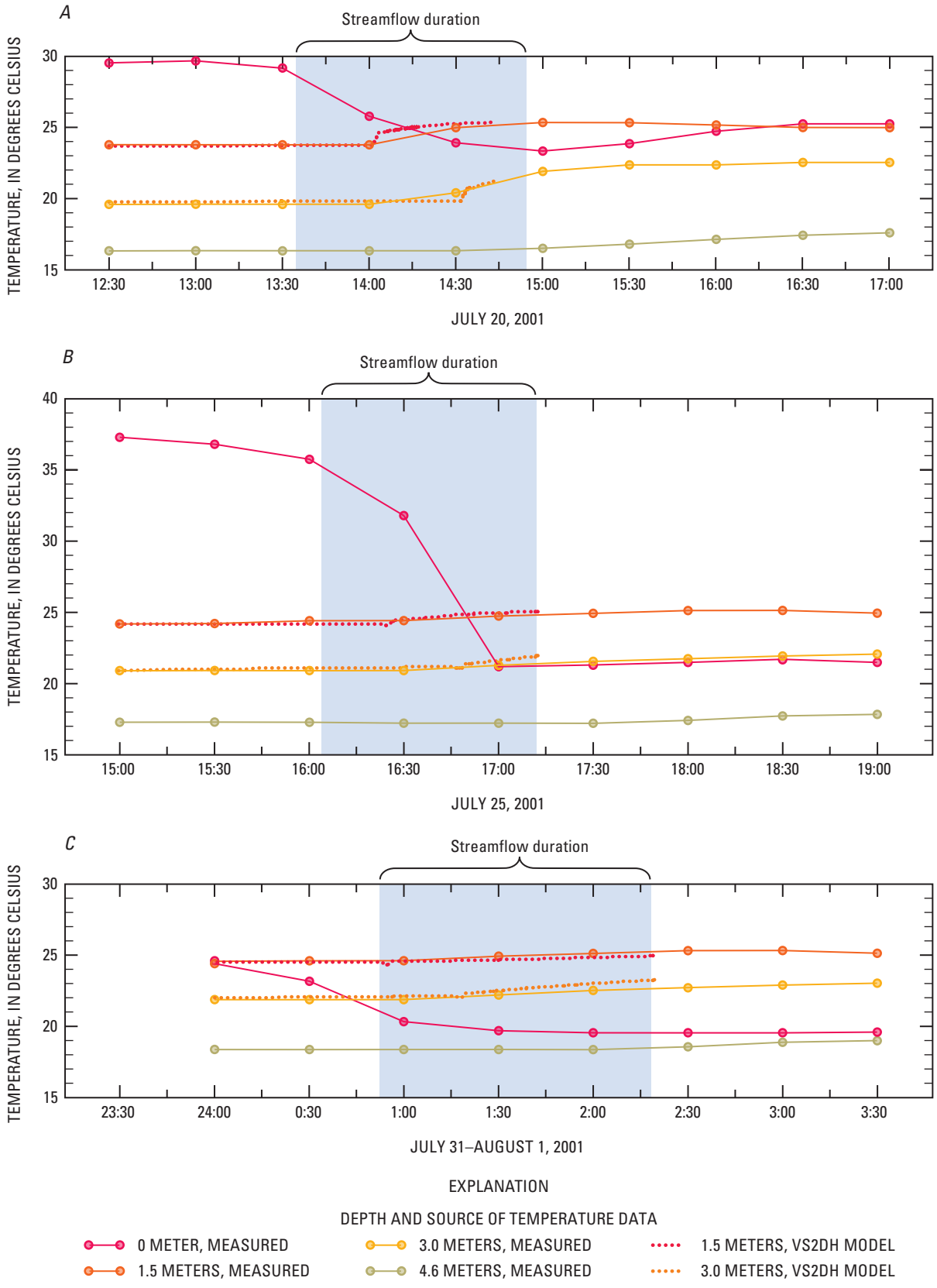

Figure 19. Streamflow durations and sediment temperatures from sensors and from VS2DH model output, Banning Creek borehole BC1: *A*, July 20, 2001; *B*, July 25, 2001; *C*, August 1, 2001.

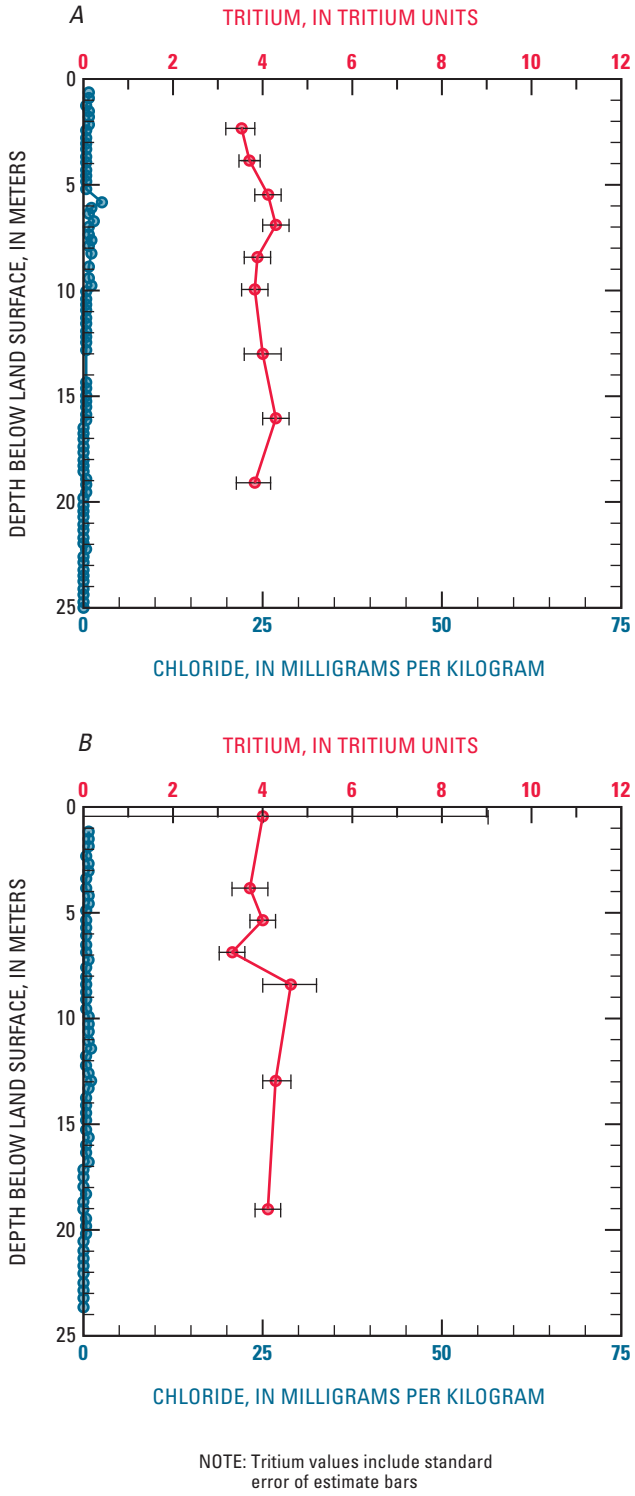

Figure 20. Sediment-chloride and pore-water tritium data, Greenbush Draw boreholes: *A*, GD2; *B*, GD1.

isotopically similar to recent winter precipitation. The chloride, tritium, and stable-isotope data indicate that little to no recent infiltration has occurred past shallow depths at site WG4.

Borehole WG5 is also within the Walnut Gulch drainage basin. The borehole is on a hilltop within the ARS Kendall research station. Grassland is the primary land-cover type at the site (fig. 2). The borehole penetrated consolidated basin-fill conglomerate from the surface to 12.2 m (fig. 6*N*). The electrical conductivity ranged from 10 to 20 mS/m (fig. 6*N*). A neutron soil-moisture log was not recorded in this borehole. The degree of consolidation of the sediments precluded collection of complete cores; therefore, physical and hydraulic properties of the conglomerate were not determined.

Sediment-chloride concentrations were not measured at this site. Stable-isotope values of pore water at 0.2 m showed a slight evaporative signature, but were not as enriched as at similar depths at other basin-floor sites (fig. 23). The tritium activity of pore water at 0.2 m was 0.4 TU. These isotopic data indicate that recent infiltration at this site has not extended past shallow depths.

Borehole BF1 is within the Carr Canyon drainage basin on a flat area of the basin floor between the Carr Canyon and Ramsey Canyon Washes. Vegetation at the site is sparse and the primary land-cover types are mesquite woodland and grassland (fig. 2). The borehole penetrated two primary lithologic layers within the basin fill: unconsolidated sand and gravel from the surface to about 8 m; and semiconsolidated clay, silt, sand, and gravel from 8 m to 15.8 m (fig. 6*O*). The electrical conductivity of the sediments were about 15 to 25 mS/m from the surface to 11 m, and about 30 to 60 mS/m from 11 to 15.8 m. The higher values below 11 m are indicative of a higher soil-water content or higher silt and clay content below 11 m (fig. 6*O*). A neutron soil-moisture log was not recorded in this borehole.

Physical and hydraulic properties were determined for seven core samples from BF1 collected at depths of 0.3, 4.0, 5.5, 7.0, 8.5, 10.1, and 13.1 m (table 6). Saturated hydraulic conductivity at 0.3 and 7.0 m was 2.1×10^{-2} and 1.4×10^{-2} cm/s, respectively. Porosity was 0.39 and 0.35 cm^3/cm^3, and soil-water content was less than 0.02 cm^3/cm^3 and 0.11 cm^3/cm^3, respectively. The silt and clay content of the cores from 0.3 to 7.0 m was less than 15 percent. The silt and clay content at 8.5 m, however, was 30.7 percent. The saturated hydraulic conductivity of this core was 5.1×10^{-3} cm/s, the porosity was 0.45 cm^3/cm^3, and the soil-water content was 0.26 cm^3/cm^3. The silt and clay content from 10.1 and 31.1 m was less than 15 percent.

Sediment-chloride concentrations were less than 5 mg/kg from the surface to 5.8 m (fig. 24*A*) and were between 10 and 32 mg/kg from 6.1 to 14.3 m. Below 14.3 m, concentrations were less than 10 mg/kg. This chloride profile is not typical for desert soils in that the chloride peak is not near the land surface; is broad, extending almost 8 m; and has a low concentration.

Tritium activity of the pore water indicates that water has infiltrated to at least 5.3 m, and possibly to 10.2 m, since 1952

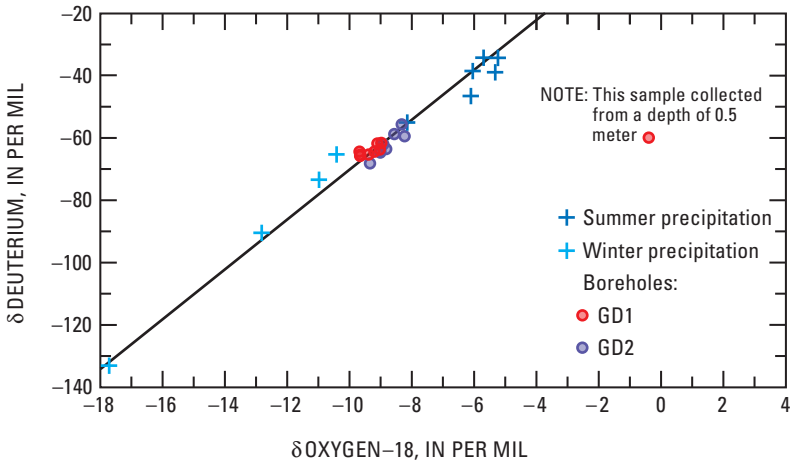

Figure 21. Stable-isotope data for pore water collected from Greenbush Draw boreholes and for precipitation.

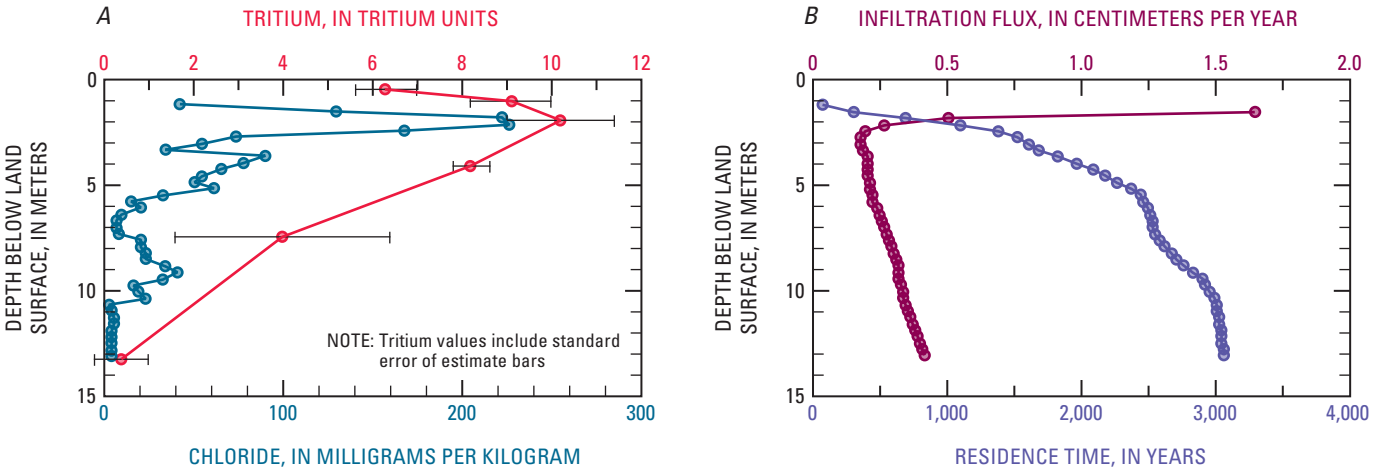

Figure 22. Walnut Gulch borehole WG4: *A*, Sediment-chloride and pore-water tritium data; *B*, Residence time and infiltration flux, calculated from chloride data.

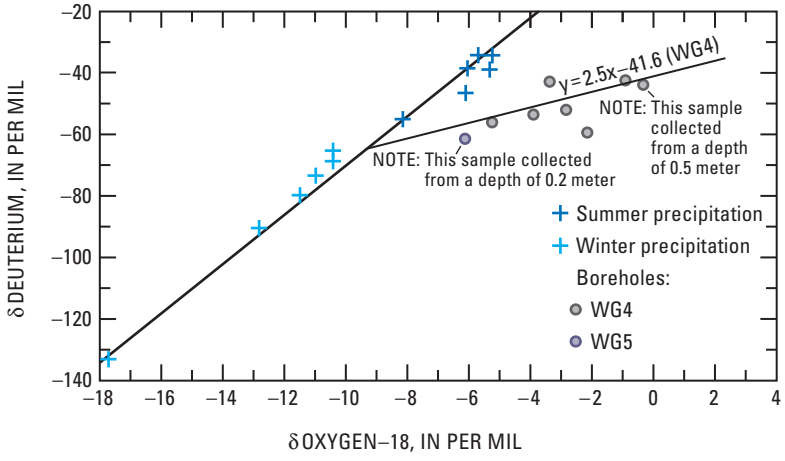

Figure 23. Stable-isotope data for pore water collected from Walnut Gulch basin-floor boreholes WG4 andWG5 and for precipitation.

(fig. 24*A*). An infiltration flux could not be calculated by using the tritium data because there is not a clear depth of maximum tritium activity. The presence of tritium to 5.3 m, however, corresponds well with the chloride profile, which indicates that about 75 years is required for water to infiltrate to this depth.

Pore-water stable-isotope values show strong evaporative enrichment at 0.5 m and a slight evaporative enrichment from 3.8 to 13.0 m; values plot along an evaporative trend line that has a slope of 2.0 (fig. 25). The point of intersection between the evaporative trend line and the meteoric water line indicates that historical infiltration at BF1 was isotopically similar to recent winter precipitation.

The chloride, tritium, and stable-isotope data indicate that infiltration occurs at a rate of about 6 cm/yr through the more permeable upper zone of sediments to a depth of about 8 m. Infiltration is much slower through the less permeable sediments at depths of 8 to 15.8 m. Infiltration through the upper sediments maintains a low chloride content and high tritium activity. The water that infiltrates the upper permeable sediments slowly infiltrates and transports chloride to the deeper zone. The chloride content in the deep zone is enriched through transport of water to the atmosphere by plant roots.

Borehole WC4c is within the Woodcutters Wash drainage basin. The borehole is about 150 m south of borehole WC4a on an area of the basin floor that slopes northward towards Woodcutters Wash (fig. 26). Grassland is the primary land-cover type at the site (fig. 2). The borehole penetrated terrace deposits of mostly unconsolidated sand and gravel from the surface to 5.8 m; basin fill of clay, silt, sand, and gravel from 5.8 to 7.6 m; and a semiconsolidated conglomerate, the Pantano Formation, from 7.6 to 12.5 m (fig. 6*P*). Electrical conductivity of the terrace and basin fill ranged from less than 10 to 50 mS/m, and the electrical conductivity of the Pantano Formation ranged from 50 to 75 mS/m (fig. 6*P*). A neutron soil-moisture log was not recorded in this borehole.

Physical and hydraulic properties were determined for five core samples from WC4c collected from depths of 1.1, 2.4, 3.8, 9.9, and 11.3 m (table 6). The saturated hydraulic conductivity ranged from 5.1×10^{-3} to 1.5×10^{-2} cm/s for the terrace deposits and from 7.2×10^{-6} to 1.9×10^{-5} cm/s for the Pantano Formation. Porosity ranged from 0.33 to 0.40 cm^3/cm^3 for both units. Soil-water content ranged from 0.07 to 0.15 cm^3/cm^3 for the terrace deposits and was 0.24 in the Pantano Formation.

During drilling in January 2001, the borehole intersected a saturated interval within the terrace deposits and basin fill above the Pantano Formation at 4.7 m (fig. 27). Sediment-chloride concentrations were 17 mg/kg at 1.5 m and generally were less than 6 mg/kg below 2.7 m (fig. 28*A*). Tritium activity of 2.6 to 7.0 TU in pore water to 3.7 m indicated that recent water is present in the unsaturated zone above the saturated interval (fig. 28*A*). The chloride data, however, indicate that about 150 years is required for water to infiltrate to the saturated interval, at a flux of about 3 cm/yr (fig. 28*B*). Similar to conditions at site WC4a, the saturated interval at WC4c is probably controlled by infiltration from an upgradient retention basin and subsequent downgradient subflow above the contact of the Pantano Formation with terrace and basin fill.

Pore-water tritium activity indicates that the perched water is infiltrating into the semiconsolidated Pantano Formation very slowly, at about 0.4 cm/yr (assuming an average soil-water content of 0.07 cm^3/cm^3). This flux is comparable to

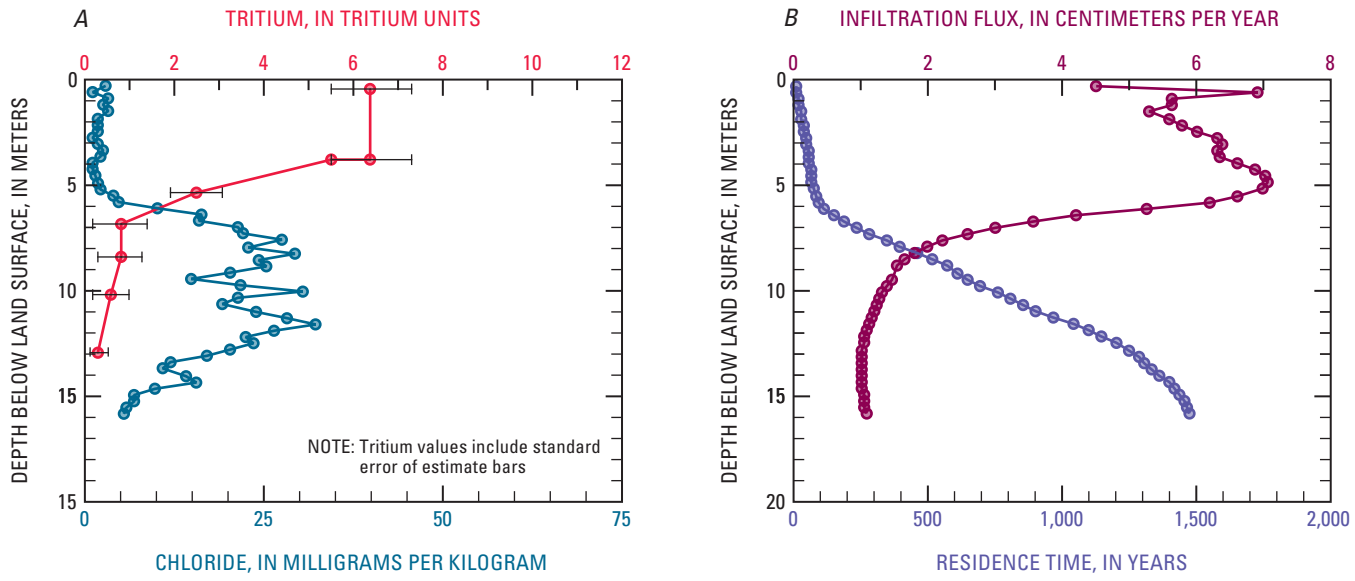

Figure 24. Carr Canyon borehole BF1: *A*, Sediment-chloride and pore-water tritium data; *B*, Residence time and infiltration flux, calculated from chloride data.

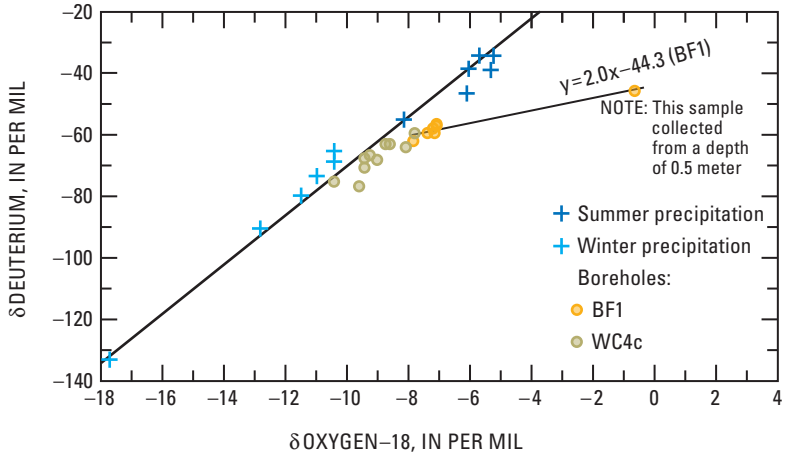

Figure 25. Stable-isotope data for pore water collected from basin-floor boreholes BF1 and WC4c and for precipitation.

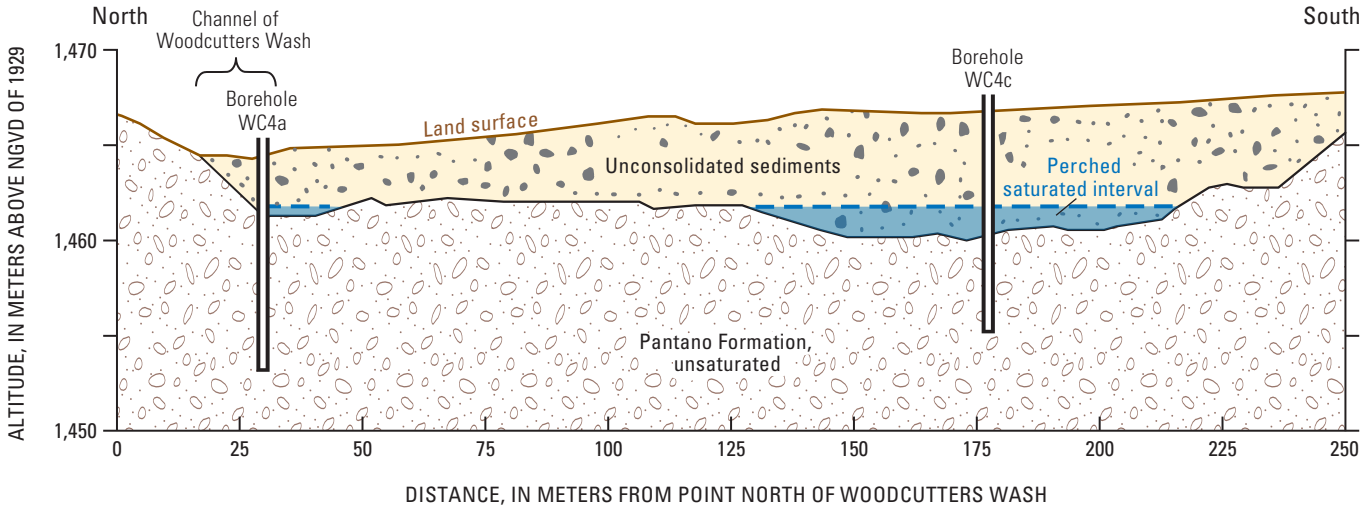

Figure 26. Generalized hydrogeologic section in the area of Woodcutters Wash boreholes WC4a and WC4c.

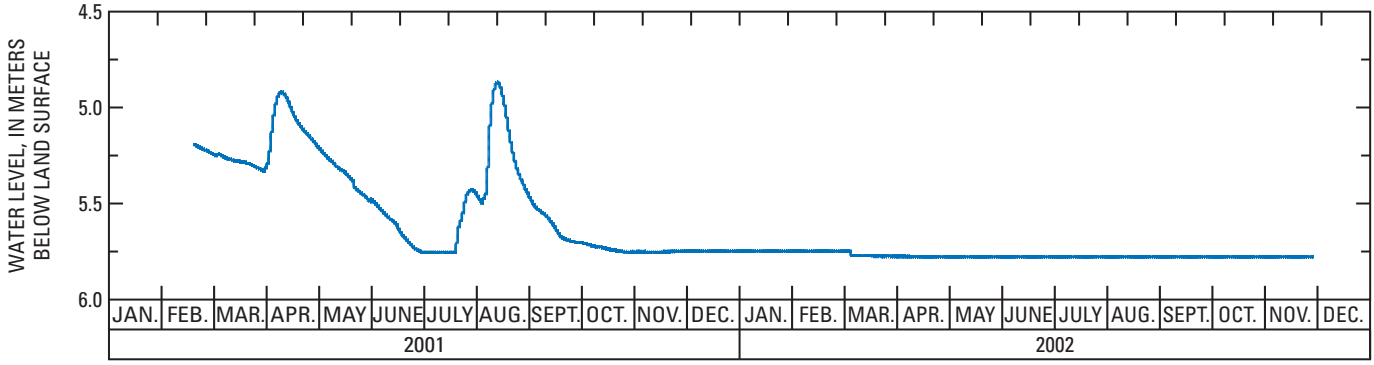

Figure 27. Water level in Woodcutters Wash borehole WC4c.

the percolation flux for the Pantano Formation at WC4a of 0.3 cm/yr. Pore-water stable-isotope values above the water table and within the Pantano Formation did not have an evaporative signature, but rather fell within the range of values for winter precipitation (fig. 25). This indicates that infiltration at WC4c could be dominated by winter precipitation.

Subwatershed Ephemeral-Stream Channel and Basin-Floor Recharge

Average annual recharge during 2001–2002 was estimated for the Sierra Vista subwatershed by upscaling the infiltration fluxes determined for the basin-floor and ephemeral-stream channel sites. This recharge estimate does not include mountain-front recharge; this study did not monitor streamflow or infiltration near the contact between the hard rock of the mountains and the basin fill. Precipitation during the period of study was slightly below average and primarily occurred during July through September (fig. 4). As a result, the calculated annual recharge represents recharge under drier-than-normal conditions.

At the basin-floor sites in the Walnut Gulch drainage basin, the long-term infiltration fluxes were very low (less than 1 cm/yr). Chloride, tritium, and stable-isotope data indicate long periods of no net deep downward percolation flux beneath the basin floor. Previous investigators have shown that infiltration of precipitation through the basin floor and past the root zone may not be significant in arid areas of the Southwestern United States that have thick unsaturated zones (Phillips, 1994; Walvoord and others, 2002). Additionally, Scott and others (2000) reported that moisture fronts in the unsaturated zone at WG4 and WG5 reach a maximum depth of only 0.5 m in the summer and only 1.3 m in the winter. The chloride, tritium, and stable-isotope data, coupled with the work done by previous investigators, support the conclusion that recharge through the basin floor area is negligible. Infiltration rates could also be negligible in other areas of the basin floor that have soil and vegetation that are similar to those at WG4 and WG5.

Infiltration fluxes were higher at the basin-floor site in the Carr Canyon Wash drainage basin (2 to 6 cm/yr) than at other basin-floor sites. Chloride, tritium, and stable-isotope data indicate active infiltration to 8 m and a decrease in infiltration below 8 m. The change in the infiltration rate below 8 m is controlled by an increase in the silt and clay content of the soil. Relatively high infiltration rates could occur in other areas of the basin floor that have soil and vegetation that are similar to those at BF1. The depth that infiltrating water moves through the unsaturated zone, and whether the infiltrating water will ultimately become recharge, however, are strongly dependant on the silt and clay content of limiting soil horizons in the unsaturated zone.

Recharge through ephemeral-stream channels is strongly influenced by the thickness and hydraulic properties of stream alluvium and the permeability of the underlying basin fill. Steamflow infiltration readily occurs through the highly permeable stream alluvium and the unconsolidated basin fill that do not have thick intervals of silt and clay. Infiltration is limited by shallow low-permeability layers, such as bedrock, silt and clay, caliche, or consolidated basin fill. Where the contact between unconsolidated sediments and low-permeability layers is deeper than the depth of root penetration, streamflow infiltrates to depths at which water is probably not removed by evapotranspiration. This water will remain in storage within the unsaturated zone until it is vertically displaced by subse-

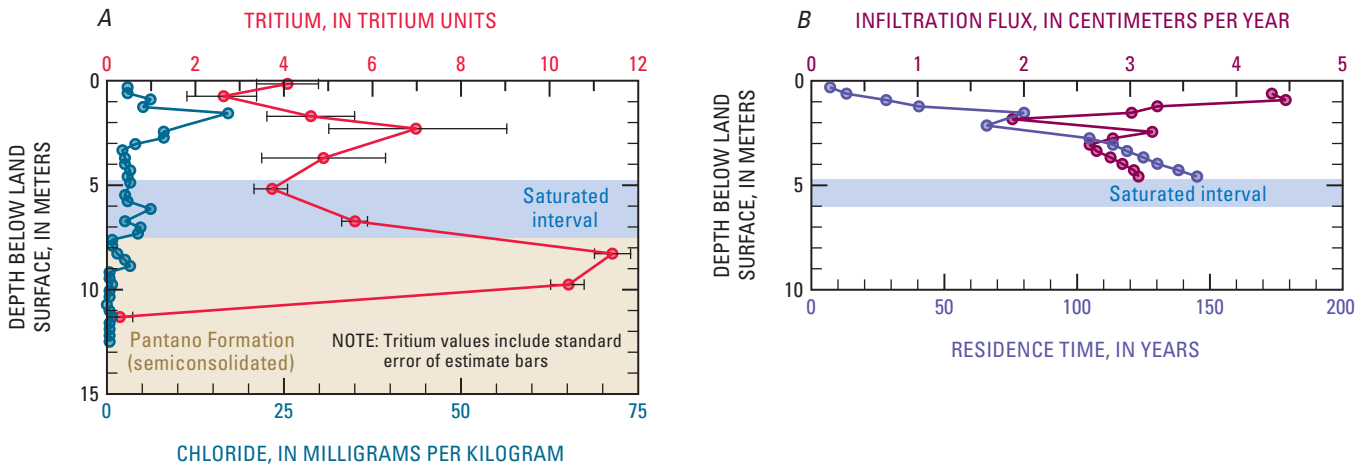

Figure 28. Woodcutters Wash borehole WC4c: *A*, Sediment-chloride and pore-water tritium data; *B*, Residence time and infiltration flux, calculated from chloride data.

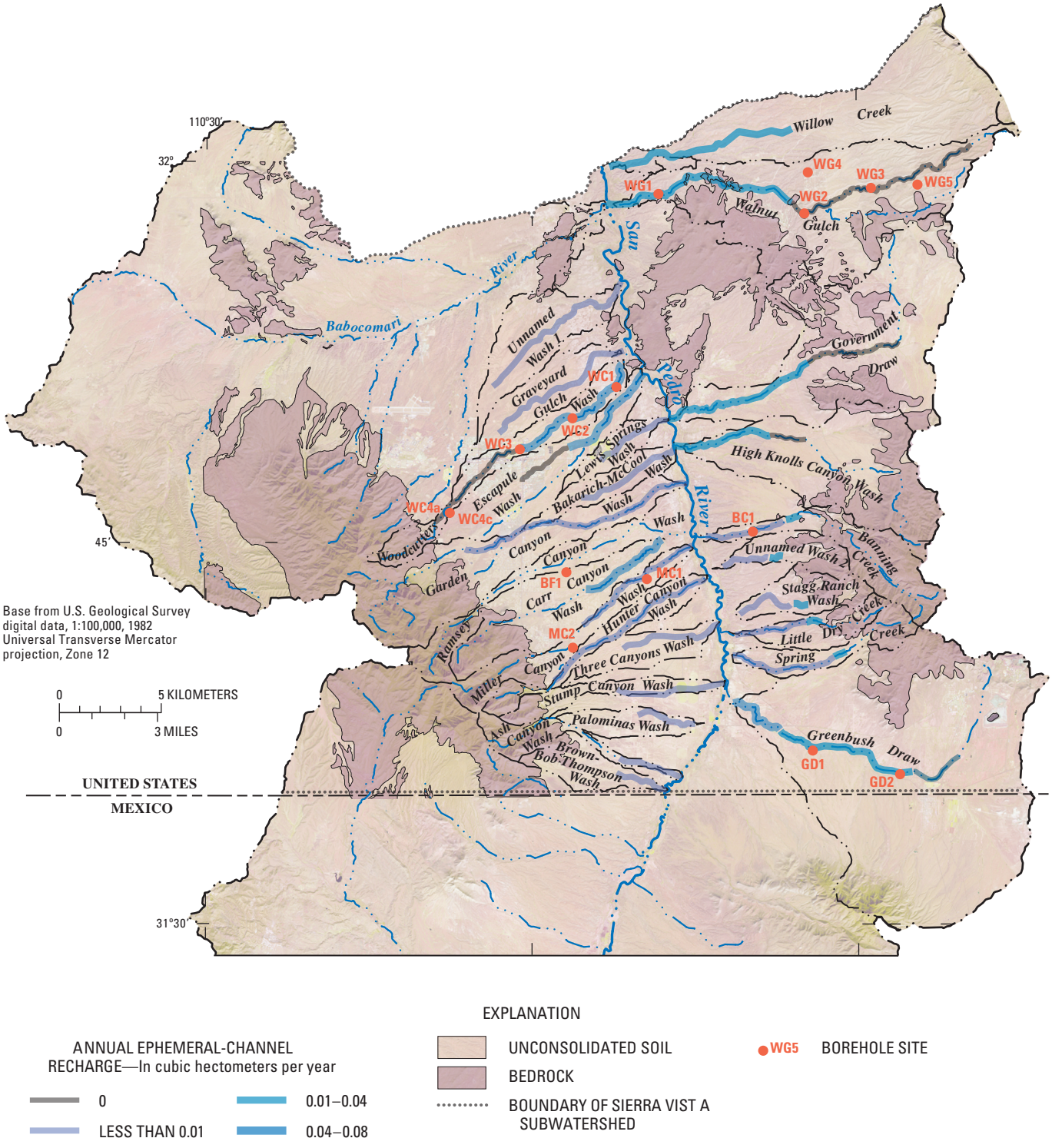

Figure 29. Approximate distribution of annual ephemeral-stream channel recharge, 2001–2002, Sierra Vista subwatershed, Arizona.

quent infiltration and eventually recharges the regional aquifer. Where the contact between unconsolidated sediments and low-permeability layers is shallow, however, aquifer recharge may be minimal because the infiltrated water is available for upward transport by evapotranspiration. Water not lost by evapotranspiration likely flows laterally above the contact until it encounters the limit of the low-permeability layer, reaches permeable fractures, or recharges the aquifer where the water table intersects the top of the low-permeability layer.

Infiltration fluxes at the ephemeral-stream channel sites were very high (0.4 to 2.8 m/hr) during streamflow events. Percolation fluxes were also high (0.1 to 2.8 m/hr) immediately following streamflow events. Chloride data indicate that in areas where low-permeability layers are absent in the shallow subsurface, infiltrated water moves past depths where it is available for evapotranspiration, resulting in a net downward water flux. Tritium data indicate that water that has infiltrated since 1952 is reaching depths of more than 20 m. We assume that the net water flux below 20 m continues to be downward and that infiltrated streamflow ultimately recharges the regional aquifer. Stable-isotope data indicate that both summer and winter streamflows contribute to ephemeral-channel recharge.

Subwatershed recharge during 2001–2002 from ephemeral-stream channel infiltration was estimated by upscaling the calculated infiltration fluxes to the area covered by each ephemeral-stream channel in the watershed and weighting the fluxes by streamflow duration, evaporation, and transpiration for the 2-year period, per equation 11 (table 12 and fig. 29). Recharge estimates were not derived for channels in the

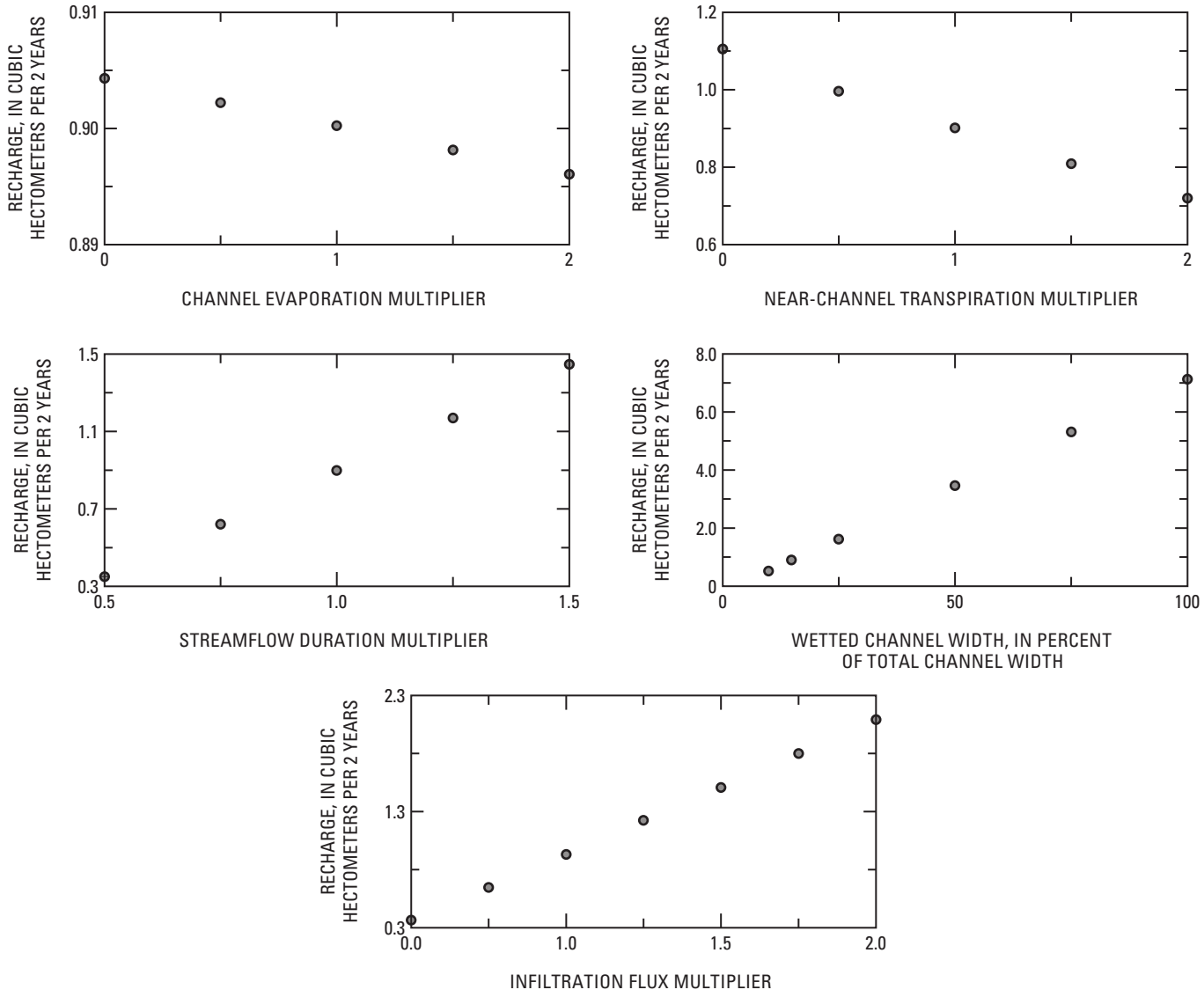

Figure 30. Examples of sensitivity analysis results, Greenbush Draw, 2001–2002.

Babocomari River drainage basin (group 1) because the river is perennial over much of its length and, therefore, use of the infiltration parameters derived for the ephemeral channels is not appropriate.

The infiltration flux used in equation 11 was the lowest flux calculated for each channel by sediment-temperature analysis. The calculated infiltration fluxes represent average values of the initial transient infiltration fluxes during each ephemeral-flow event. Consequently, we assume that the lowest calculated infiltration flux best represents the steady-state infiltration flux when determining ephemeral-stream channel recharge. This assumption was validated by comparing ephemeral-stream channel recharge rates determined by use of equation 11 with rates determined by using other independent methods (channel-reach water balance, chloride mass balance, ground-water mounding model, and microgravity measurements) for a 6.8-km reach of Walnut Gulch (Goodrich and others, 2004).

Groups 3, 5, 6, and 7 contain ephemeral-stream channels for which infiltration fluxes were determined. We assume that these infiltration fluxes are the same in other ephemeral channels within each group. The infiltration flux determined for Woodcutters Wash was also used for channels in groups 2 and 4, which did not contain instrumented borehole sites. Infiltration fluxes for periods of streamflow were not calculated for Greenbush Draw; therefore, the average percolation flux for periods after cessation of streamflow was used in the Greenbush Draw calculation. Channel segments in Woodcutters Wash and Walnut Gulch underlain at shallow depths by the low-permeability sediments of the lower basin fill were not included in the recharge calculations; it was assumed that similar conditions exist in Escapule Wash, because of its location relative to Woodcutters Wash, and Government Draw and High Knolls Canyon Wash, because of their locations relative to Walnut Gulch (fig. 29).

The streamflow durations measured in Woodcutters Wash during 2001–2002 were greater than those measured in Miller Canyon Wash (table 8 and fig. 7); the longer durations are assumed to be related to the corresponding higher percentage of urban land cover in the drainage basin. Therefore, the streamflow-duration and wetted-channel-width regressions determined for Woodcutters Wash were also used for Escapule and Carr Canyon Washes, whose drainage basins have similar amounts of urban land cover as that in Woodcutters Wash and, therefore, likely have similar runoff characteristics. The streamflow-duration and wetted-channel-width regressions determined for Miller Canyon Wash were used for the remaining channels in groups 2, 3, and 4.

The estimated annual recharge derived from ephemeral-stream channel infiltration during 2001–2002 is 2.95 hm^3/yr. This rate is slightly lower than average recharge rates of 3.4 to 9.7 hm^3 determined by Goodrich and others (2004) for 1999–2000. The rate calculated during this study is lower probably because fewer streamflow events occurred during the 2001–2002 monitoring period than during 1999–2000. At the Tombstone and Huachuca Mountains stations, precipitation during 2001–2002 averaged 36.4 cm/yr, whereas precipitation during 1999–2000 averaged 47.4 cm/yr.

This calculated ephemeral-stream channel recharge rate is about 12 to 19 percent of previous total recharge estimates for the Sierra Vista subwatershed of 15 to 23 hm^3/yr (Freethey, 1982; Corell and others, 1996; Goode and Maddock, 2000), indicating that ephemeral-stream channel recharge is a significant component of total recharge. These previous investigators have assumed that recharge occurred only within about 1.5 km of the mountains; however, the borehole data clearly indicated that when streamflow is available, a significant portion of recharge is distributed along the entire lengths of ephemeral-stream channels (fig. 29). During this study, most of the streamflow, and therefore most of the recharge, occurred during the summer; however, stable-isotope data from most of the ephemeral-stream channel boreholes indicate infiltration from past summer and winter streamflow events.

Sensitivity Analysis

A sensitivity analysis was done to quantify bounds on the calculated ephemeral-stream channel recharge rates by independently varying the recharge calculation parameters in equation 11 within reasonable limits and recalculating recharge over the length of each channel (table 13). Channel evaporation and near-channel transpiration were increased and decreased by 100 percent. Streamflow duration was increased and decreased by 50 percent. The wetted channel width was increased to 100 percent, and decreased to 10 percent, of the total channel width. Calculated infiltration fluxes were increased by 100 percent and decreased by 50 percent.

Recharge rates were most sensitive to the wetted channel width (fig. 30 and table 13) — average annual recharge for the subwatershed increased by 937 percent with the assumption that 100 percent of the channel widths are wetted during streamflow events. Although there is a high degree of uncertainty associated with the wetted channel width value, the assumption that the total channel width is wetted during streamflow is most likely not valid. Recharge was less sensitive to other parameters (fig. 30 and table 13). The highest and lowest annual recharge rates determined through the sensitivity analysis (excluding the rate determined for 100 percent wetted channel width) produce bounds of +4.84 hm^3/yr and –1.79 hm^3/yr on annual ephemeral-stream channel recharge for 2001–2002.

Summary and Conclusions

As part of a project to better understand the hydrologic system in the Sierra Vista subwatershed, infiltration and recharge fluxes through the subwatershed's ephemeral channels and basin floor were investigated. Data used in this study include information resulting from the drilling and coring

of 16 boreholes: 12 within ephemeral channels and 4 on the basin floor. The collected data includes physical, hydraulic, and thermal properties of sediment; chloride concentrations of sediment; pore-water stable-isotope values and tritium activity; neutron soil-moisture and EMI logs; continuous sediment-temperature profiles; and continuous water levels.

Infiltration fluxes through the basin floor were 0.2 to 6 cm/yr. At the basin-floor sites in the Walnut Gulch drainage basin, long-term infiltration fluxes were very low (less than 1 cm/yr). Chloride, tritium, and stable-isotope data indicate long periods of no net deep downward percolation flux beneath the basin floor. The sediment-chloride profiles coupled with previous studies in the arid Southwestern United States indicate that water infiltrated through the basin floor does not move downward past the root zone for long periods of time. Infiltration rates could also be negligible in other areas of the basin floor that have soil and vegetation similar to those at WG4 and WG5.

Infiltration fluxes in the Carr Canyon drainage basin (2 to 6 cm/yr) were higher than at other basin-floor sites. Chloride, tritium, and stable-isotope data indicate active infiltration to 8 m, and a decrease in infiltration below 8 m. The change in the infiltration rate below 8 m is controlled by an increase in the silt and clay content of the sediment. At this site, the depth that infiltrating water moves through the unsaturated zone and whether the infiltrating water will ultimately become recharge are strongly dependant on the silt and clay content of limiting soil horizons in the unsaturated zone. Relatively high infiltration rates could occur in other areas of the basin-floor that have soil and vegetation similar to those at BF1, but detailed subsurface soil data are necessary to determine if infiltrated water will become recharge.

Infiltration through ephemeral-stream channels in the Sierra Vista subwatershed is rapid, occurs to depths of at least 20 m, and occurs from the edge of the mountain front to as far as 25.6 km downstream. During streamflow events, infiltration fluxes ranged from 0.4 to 2.8 m/hr. After streamflow ended, percolation fluxes ranged from 0.1 to 2.8 m/hr. In areas where low-permeability layers are absent in the shallow subsurface, infiltrated water moves past depths where it is available for evapotranspiration, resulting in a net downward flux. This deep downward water flux is assumed to ultimately recharge the regional aquifer.

Recharge from ephemeral-stream channel infiltration is highly dependant on the thickness and hydraulic properties of the stream alluvium, the permeability of the sediments underlying the stream alluvium, the streambed geomorphology, the runoff characteristics of the contributing drainage basin, and the availability of streamflow. Ephemeral-stream channel recharge for the entire Sierra Vista subwatershed was estimated by upscaling the calculated infiltration fluxes to the area covered by each ephemeral-stream channel and weighting the fluxes by streamflow duration, evaporation, and transpiration. The resulting average annual recharge during 2001–2002 is 2.95 hm^3/yr. Analysis indicates that the calculated recharge rates are most sensitive to wetted channel width and are less sensitive to the other parameters of evaporation, transpiration, streamflow duration, and infiltration flux. The upper and lower bounds for the annual recharge estimate determined from the sensitivity analysis are +4.84 hm^3/yr and –1.79 hm^3/yr, respectively.

The calculated annual ephemeral-stream channel recharge rate indicates that ephemeral-stream channel infiltration is a significant contributor to total recharge in the subwatershed. When streamflow is available, recharge is significant along the entire length of the ephemeral-stream channels. In addition, ephemeral-stream channel recharge occurs during both summer and winter streamflow events.

References Cited

Allison, G.B., and Hughes, M.W., 1978, The use of environmental chloride and tritium to estimate total recharge to an unconfined aquifer: Australian Journal of Soil Resources, v. 16, p. 181–195.

Allison, G.B., Stone, W.J., and Hughes, M.W., 1985, Recharge in karst and dune elements of a semi-arid landscape as indicated by natural isotopes and chloride: Journal of Hydrology, v. 76, p. 1–26.

Anderson, T.W., Freethey, G.W., and Tucci, P., 1992, Geohydrology and water resources of alluvial basins in south-central Arizona and parts of adjacent states: U.S. Geological Survey Professional Paper 1406–B, 67 p.

Arizona Department of Economic Security, 1997, July 1, 1997 to July 1, 2050 Arizona subcounty population projections: Population Statistics Unit, Research Administration, http://www.workforce.az.gov/?PAGEID=67&SUBID=138subco97.html, last accessed February 21, 2003.

Blasch, K.W., Fleming, J.B., Ferré, P.A., and Hoffmann, J.P., 2000, One- and two-dimensional temperature and moisture-content profiling of an ephemeral stream channel in a semiarid watershed [abstract]: Eos (Transactions, American Geophysical Union), v. 81, no. 48, p. F502.

Brown, S.G., Davidson, E.S., Kister, L.R., and Thomsen, B.W., 1966, Water resources of Fort Huachuca Military Reservation, southeastern Arizona: U.S. Geological Survey Water-Supply Paper 1819–D, p. D1–D57.

Campbell, G.S., Calissendorff, C., and Williams, J.H., 1991, Probe for measuring soil-specific heat using a heat-pulse method: Soil Science Society of America Journal, v. 55, no. 1, p. 291–293.

Cayan, D.R., and Webb, R.H., 1992, El Niño/southern oscillation and streamflow in the Western United States, *in* Diaz, H.F., and Markgraf, V., eds., El Niño historical and paleoclimatic aspects of the southern oscillation: Cambridge, United Kingdom, Cambridge University Press, p. 29–68.

Cayan, D.R., Redmond, K.T., and Riddle, L.G., 1999, ENSO and hydrologic extremes in the western United States: Journal of Climate, v. 12, no. 9, p. 2881–2893.

Constantz, J., Tyler, S.W., and Kwicklis, E., 2003, Temperature-profile methods for estimating percolation rates in arid environments: Vadose Zone Journal, v. 2, p. 12–24.

Constantz, J., Stonestrom, D., Stewart, A.E., Niswonger, R., and Smith, T.R., 2001, Analysis of streambed temperatures in ephemeral channels to determine streamflow frequency and duration: Water Resources Research, v. 37, no. 2, p. 317–328.

Constantz, J., and Thomas, C.L., 1996, The use of streambed temperature profiles to estimate the depth, duration, and rate of percolation beneath arroyos: Water Resources Research, v. 32, no. 12, p. 3597–3602.

Corell, S.W., Corkhill, F., Lovvik, D., and Putman, F., 1996, A groundwater flow model of the Sierra Vista Subwatershed of the Upper San Pedro Basin, southeastern Arizona: Arizona Department of Water Resources Modeling Report No. 10, 107 p.

Craig, H., 1961, Isotopic variations in meteoric waters: Science, v. 133, p. 1702–1703.

Danielson, R.E., and Sutherland, P.L., 1986, Porosity, *in* Klute, A., ed., Methods of soil analysis, Part I, Physical and mineralogical methods (2d ed.): Madison, Wisc., American Society of Agronomy and Soil Science Society of America, p. 443–461.

Decagon Devices, Inc., 1999, Thermolink System Manual (version 2.5): Pullman, Wash., Decagon Devices, Inc., variously paginated.

Driscoll, F.G., 1986, Groundwater and wells, 2d ed.: St. Paul, Minnesota, Johnson Division, 1108 p.

Freethey, G.W., 1982, Hydrologic analysis of the upper San Pedro Basin from the Mexico-United States international boundary to Fairbank, Arizona: U.S. Geological Survey Open-File Report 82–752, 52 p.

Gallaher, B.M., 1979, Recharge properties of the Tucson Basin aquifer as reflected by the distribution of a stable isotope: Tucson, University of Arizona, master's thesis, 92 p.

Gardner, W.R., 1956, Calculation of capillary conductivity from pressure plate outflow data: Soil Science Society Proceedings, v. 20, p. 317–320.

Gee, G.W., and Bauder, J.W., 1986, Particle-size analysis, *in* Klute, A., ed., Methods of soil analysis, Part I, Physical and mineralogical methods (2d ed.): Madison, Wisc., American Society of Agronomy and Soil Science Society of America, p. 383–411.

Gettings, M.E., and Houser, B.B., 1995, Preliminary results of modeling the gravity anomaly field in the upper San Pedro Basin, southeastern Arizona: U.S. Geological Survey Open-File Report 95–76, 9 p.

Goode, T.C., and Maddock, T., 2000, Simulation of groundwater conditions in the Upper San Pedro Basin for the evaluation of alternative futures: University of Arizona Hydrology and Water Resources Report no. 00–030, 113 p.

Goodrich, D.C., Williams, D.G., Unkrich, C.L., Hogan, J.F., Scott, R.L., Hultine, K.R., Pool, D.R., Coes, A.L., and Miller, S., 2004, Comparison of methods to estimate ephemeral channel recharge, Walnut Gulch, San Pedro River Basin, Arizona, *in* Hogan, J.F., Phillips, F.M., and Scanlon, B.R., eds., Groundwater recharge in a desert environment—The southwestern United States: American Geophysical Union, Water Science and Applications Series, v. 9, p. 77–99.

Gungle, B., 2003, Estimation of ephemeral streamflow duration using temperature methods in the Upper San Pedro River Basin, Arizona, *in* Proceedings of first interagency conference on research in watersheds, October 27–30, 2003: Benson, Arizona, p. 146–151.

Halverson, P.H., 1984, An exploratory gravity survey in the upper San Pedro Valley, southeastern Arizona: Tucson, University of Arizona, master's thesis, 85 p.

Hammermeister, D.P., Blout, D.O., and McDaniel, J.C., 1986, Drilling and coring methods that minimize the disturbance of cuttings, core, and rock formations in the unsaturated zone, Yucca Mountain, Nevada, *in* Klute, A.L., ed., Proceedings of the National Water Well Association Conference on Characterization and Monitoring of the Vadose (Unsaturated) Zone: Worthington, Ohio, National Water Well Association, USA, p. 507–541.

Haynes, C.V., 1968, Preliminary report on the Late Quaternary geology of the San Pedro Valley, Arizona, *in* Arizona Geological Society guidebook III: Tucson, Ariz., Arizona Geological Society, p. 76–96.

Healy, R.W. and Ronan, A.D., 1996, Documentation of computer program VS2DH for simulation of energy transport in variably saturated porous media Modification of the U.S. Geological Survey's computer program VS2DT: U.S. Geological Survey Water-Resources Investigations Report 96–4230, 36 p.

Hsieh, P.A., Wingle, W., and Healy, R.W., 2000, VS2DI A graphical software package for simulating fluid flow and solute or energy transport in variably saturated porous media: U.S. Geological Survey Water-Resources Investigations Report 99–4130, 16 p.

Izbicki, J.A., Radyk, J., and Michel, R.L., 2000, Water movement through a thick unsaturated zone underlying an intermittent stream in the western Mojave Desert, southern California, USA: Journal of Hydrology, v. 238, p. 194–219.

Keith, S.J., 1981, Stream channel recharge in the Tucson Basin and its implications for groundwater management: Tucson, Ariz., University of Arizona, master's thesis, 84 p.

Kipp, K.L., 1987, HST3D: A computer code for simulation of heat and solute transport in three-dimensional ground-water systems: U.S. Geological Survey Water-Resources Investigations Report 86–4095, 517 p.

Klute, A., and Dirksen, C., 1986, Hydraulic conductivity and diffusivity: Laboratory Methods, *in* Klute, A., ed., Methods of soil analysis, Part I, Physical and mineralogical methods (2d ed.): Madison, Wisc., American Society of Agronomy and Soil Science Society of America, p. 687–734.

McCabe, G.J., and Dittinger, M.D., 1999, Decadal variations in the strength of ENSO teleconnections with precipitation in the western United States: International Journal of Climatology, v. 19, no. 13, p.1399–1410.

Miller, S.N., Semmens, D.J., Miller, R.C., Hernandez, M., Miller, P., Goodrich, D.C., Kepner, W.G., and Ebert, D., 2002, Automated Geospatial Watershed Assessment (AGWA) – A GIS-based hydrologic modeling tool Documentation and user manual: U.S. Department of Agriculture, Agricultural Research Service, ARS–1446, 69 p.

Peterson, B., 1999, [Model] 9510 slim hole induction tool test results and field application to groundwater monitoring wells: Tulsa, Okla., Century Geophysical Corp., User guide no. 317, 4 p.

Phillips, F.M., and Stone, W.J., 1985, Chemical considerations in groundwater recharge, Socorro, New Mex.: Symposium on Water and Science, New Mexico Water Resources Research Institute, Las Cruces, New Mex., p. 109–125.

Phillips, F.M., Mattick, J.L., and Duval, T.A., 1988, Chlorine-36 and tritium from nuclear weapons fallout as tracers for long-term liquid movement in desert soils: Water Resources Research, v. 24, p. 1877–1891.

Phillips, F.M., 1994, Environmental tracers for water movement in desert soils of the American Southwest: Soil Science of America Journal, v. 58, p. 15–24.

Pool, D.R., and Coes, A.L., 1999, Hydrogeologic investigations of the Sierra Vista subwatershed of the Upper San Pedro Basin, Cochise County, Southeast Arizona: U.S. Geological Survey Water-Resources Investigations Report 99–4197, 41 p.

Redmond, K.T., and Koch, R.W., 1991, Surface climate and streamflow variability in the western United States and their relationship to large-scale circulation indices: Water Resources Research, v. 27, no. 9, p. 2381–2399.

Richards, L.A., 1931, Capillary conduction of liquids through porous mediums: Physics, v. 1, p. 318–333.

Scanlon, B.R., 1991, Evaluation of moisture flux from chloride data in desert soils: Journal of Hydrology, v. 128, p. 137–156.

Scott, R.L., Shuttleworth, W.J., Keefer, T.O., and Warrick, A.W., 2000, Modeling multiyear observations of soil moisture recharge in the semiarid American Southwest: Water Resources Research, v. 36, no. 8, p. 2233–2247.

Sharma, M.L., and Hughes, M.W., 1985, Groundwater recharge estimation using chloride, deuterium and oxygen-18 profiles in the deep coastal sands of western Australia: Journal of Hydrology, v. 81, p. 93–109.

Taniguchi, M., and Sharma, M.L., 1990, Solute and heat transport experiments for estimating recharge rate: Journal of Hydrology, v. 119, pp. 57–96.

Thermo Electron Corporation, 2000, Orion chloride electrode instruction manual: Waltham, Mass., Thermo Electron Corporation, 39 p.

U.S. Census Bureau, 2000, Census 2000 summary file 1, http://factfinder.census.gov/servlet/GCTTable?ds_name=DEC_2000_SF1_U&geo_id=04000US04&_box_head_nbr=GCT-PH1&format=ST-7, last accessed February 21, 2003.

U.S. Environmental Protection Agency, 2003, Upper San Pedro Watershed geodata, http://www.epa.gov/esd/landsci/san_pedro/geodata/subws.html, last accessed June 1, 2003.

van Genuchten, M.T., 1980, A closed-form equation for predicting the hydraulic conductivity of unsaturated soil: Soil Science Society of America Journal, v. 44, p. 892–898.

van Genuchten, M.T., Leij, F.J., and Yates, S.R., 1991, The RETC code for quantifying the hydraulic functions of unsaturated soils: U.S. Salinity Laboratory, 85 p.

Walvoord, M.A., Phillips, F.M., Tyler, S.W., and Hartsough, P.C., 2002, Deep arid system hydrodynamics 2. Application to paleohydrologic reconstruction using vadose zone profiles from the northern Mojave Desert: Water Resources Research, v. 38, no. 12, p.

Webb, R.H., and Betancourt, J.L., 1992, Climatic variability and flood frequency of the Santa Cruz River, Pima County, Arizona: U.S. Geological Survey Water-Supply Paper 2379, 40 p.

Western Regional Climate Center, 2003, Arizona Climate summaries, http://www.wrcc.dri.edu/summary/climsmaz.html, last accessed June 1, 2003.

Tables 3–13

Table 3. Sediment-chloride concentrations, Sierra Vista ground-water recharge study area, Arizona.

[cm, centimeters; mg/kg, milligrams chloride per kilograms sediment; m, meters; —, below the 1.8 mg/kg detection limit; blank cell, no data]

Depth to top of 15.2 cm interval, in m	Chloride, in mg/kg													
	Basin-floor boreholes			Ephemeral-channel boreholes										
	BF1	WC4c	WG4	BC1	GD1	GD2	MC1	MC2	WC1	WC2	WC3	WC4a	WG1	WG2	WG3
0.3	3.1	3.0													
0.6	—	2.8		—		—									
0.9	3.3	6.1		—	—	—		1.9			9.9				
1.2	2.4	5.2	42.2	—	—	—	—	—			7.9	3.5			—
1.5	3.3	17.1	130.0	—	—	—	—	—	—	3.3	8.5	3.6		—	—
1.8	—		222.0	—	—	—	—	—	—	6.5	27.3	4.6		—	3.8
2.1	2.0	11.1	226.0	—	—	—	2.1	—	—	—	9.1	7.5		—	
2.4	—	8.1	168.0	1.8	—	—	—	—	—	—	8.9	5.1			
2.7	—	8.2	73.6	2.4	—	—	—	—	5.0	2.2	9.3	7.3		—	
3.0	1.9	3.8	54.6	—	—	—	—	—	—	—	36.9	3.9	—	—	
3.4	2.5	2.4	34.2	—	—	—	—	—	—	3.6	32.6	—		—	
3.7	2.1	2.5	90.3	—	—	—	—	—	—	—	73.1	—	2.6		
4.0	—	2.4	77.5	—	—	—	—	3.7	—	—	7.8	—	—		
4.3	—	3.3	66.1	1.9	—	—	—	—	—	—	3.0	—	—		
4.6	—	2.8	54.8	2.7	—	—	—	—	—	—	2.7	—	—		
4.9	1.8	3.2	50.3	2.8	—	—	—	—	—	—	24.2	—	—		
5.2	2.3		61.7	3.4	—	—	—	—	—	—	—	2.0	—		
5.5	3.9	2.4	33.2	3.0	—		—	—	—	—	—	1.9	—		
5.8	4.8	3.0	15.0	3.2	—	2.6	—	—	—	—	—	—	—		
6.1	10.1	6.0	20.0	2.9	—	—	—	—	—	—	—	—	—		
6.4	16.4	4.4	9.1	2.5	—	—	2.6	—	—	—	—	—	—		
6.7	15.8	2.5	7.3	2.0	—	—	—	—	—	—	—	—	—		
7.0	21.2	4.8	6.7		—	—	—	—	—	—	—	—	—		
7.3	22.1	4.4	7.7		—	—	—	—	—	—	—	—	—		
7.7	27.7	—	20.1	—	—	—	—	—	—	—	—	—	—		
7.9	22.8	—	21.1	—	—	—	—	—	—	—	—	—	—		
8.2	29.3	—	22.6	—	—	—	—	—	—	—	3.3	—	—		
8.5	24.2	2.7	23.4	—	—		—	—	—	—	—	—			
8.8	25.2	3.2	34.3	—	—	—	—	—	—	—	—	—	—		
9.1	20.2	—	40.7	—	—		—	—		—	—	—	—		
9.4	15.0	—	32.5	—	—	—	—	—		—	—	—	—		
9.8	21.7	—	16.1	—	—	—	—	—		—	—		—		
10.1	30.4	—	18.8	—	—	—	—	—		—	—				
10.4	21.2	—	22.7	—	—	—	—	—		—	—		—		
10.7	19.3	—	3.2	3.2	—	—	—	—		2.9	2.0	2.1			
11.0	23.8	—	4.3	—	—	—	—	1.8		—	2.9	—	—		
11.3	28.1	—	5.8	2.8	—	—	—	1.9		—	2.2	2.3	—		
11.6	32.1	—	5.6	2.5	—	—	—	—		—	2.7	2.1	—		
11.9	26.4	—	4.3	5.2	—	—	—	3.9		—	4.1	—	—		
12.2	22.6	—	4.3	8.4	—	—	—	2.3		—	—	—			
12.5	23.5	—	4.1	5.1	—	—	—	1.9		—	—	—	—		
12.8	20.4		3.7	5.9	—	—	—	4.2			—		—		
13.1	17.1		3.6	3.5	—		—	3.4			—		—		
13.4	11.8			3.2	—		—	3.2			—		—		
13.7	10.7			5.1	—		—	—			—		—		
14.0	14.3			4.1	—		—	—			—		—		
14.3	15.5			3.2	—	—	—	1.9			—		—		
14.6	9.9			2.6	—	—	—	—			—		—		
14.9	7.1			2.3	—	—	—	—			—		—		
15.2	7.1			5.2	—	—	—	1.9			—		—		
15.5	6.0			3.6	—	—	—	—			—		—		
15.8	5.5			2.7	—	—	—	—			—		—		
16.2				3.6	—	—	—				—		—		
16.5				2.4	—	—	—				—		—		
16.8				2.5	—	—	—				—		—		
17.1					—	—	—				—		—		
17.4				4.9	—	—	—				—		—		
17.7				6.6	—	—	—				—		—		

Table 3. Sediment-chloride concentrations, Sierra Vista ground-water recharge study area, Arizona.—Continued

[cm, centimeters; mg/kg, milligrams chloride per kilograms sediment; m, meters; —, below the 1.8 mg/kg detection limit; blank cell, no data]

Depth to top of 15.2 cm interval, in m	Chloride, in mg/kg													
	Basin-floor boreholes			Ephemeral-channel boreholes										
	BF1	WC4c	WG4	BC1	GD1	GD2	MC1	MC2	WC1	WC2	WC3	WC4a	WG1	WG2	WG3
18.0				4.5	—	—	—				—		—		
18.3				8.1	—	—	—				—		—		
18.6				10.5	—	—	—				—		—		
18.9				11.1	—	—	—				—		—		
19.2				11.9		—	—				—		—		
19.5				9.6		—	—				—		—		
19.8				8.2		—	—				—		—		
20.1				2.4		—	—				—		—		
20.4				—		—	—				—		—		
20.7				—		—	—				—		—		
21.0				2.5		—	—				—		—		
21.3				2.0		—	—				—		—		
21.6				3.1		—	—				—		—		
21.9				6.8		—	—				—		—		
22.3				9.4		—					—		—		
22.6				4.8		—					—				
22.9				5.0		—									
23.2				7.2		—									
23.5				6.2		—									
23.8				3.5		—									
24.1				4.5		—									
24.4				3.1		—									
24.7				5.1		—									
25.0				3.5		—									
25.3				4.5											
25.6				3.7											
25.9				3.3											

(NO DATA BELOW 16 METERS)

Table 4. Stable-isotope and tritium data for pore water, Sierra Vista ground-water recharge study area, Arizona.

[Abbreviations: cm, centimeters; m, meters; δD, delta dueterium; $\delta^{18}O$, delta oxygen-18; ‰, per mil; TU, tritium units; —, no data]

Depth to top of 15.2-cm interval, in m	δD, in ‰	$\delta^{18}O$, in ‰	^{3}H, in TU	^{3}H error, in TU
Ephemeral-channel boreholes				
BC1				
2.0	-63.5	-9.50	3.8	0.2
3.5	-64.0	-9.22	3.3	.2
5.0	-60.8	-8.80	3.2	.6
6.6	-61.8	-8.96	3.8	.6
8.1	-60.8	-9.23	4.8	.3
9.6	-60.0	-8.52	4.4	.3
11.1	-63.4	-9.25	4.1	.3
12.6	-60.0	-8.81	4.5	.7
14.2	-63.8	-9.24	3.4	.3
15.7	-63.6	-9.00	3.9	.3
17.2	-59.5	-8.51	6.7	.9
20.3	-57.0	-8.30	3.6	.6
23.3	-60.0	-8.65	4.5	.9
GD1				
0.5	-60.0	-.41	4.0	5.0
.8	-65.6	-9.64	3.7	.4
5.3	-64.7	-9.67	4.0	.3
6.9	-65.1	-9.41	3.3	.3
8.4	-64.4	-9.18	4.6	.6
9.9	-62.0	-9.09	4.3	.3
19.1	-65.6	-9.68	4.1	.3
GD2				
2.3	-55.5	-8.32	3.5	.3
3.8	-58.4	-8.57	3.7	.2
5.5	-59.3	-8.24	4.1	.3
6.9	-62.0	-8.89	4.3	.3
8.4	-64.5	-9.02	3.9	.3
9.9	-67.9	-9.34	3.8	.3
13.0	-63.5	-8.83	4.0	.4
16.0	-63.7	-9.02	4.3	.3
19.1	-67.0	-9.03	3.8	.4
MC1				
.2	-39.4	-1.25	7.8	.6
1.1	-59.8	-8.59	4.2	.3
2.3	-59.5	-8.44	4.7	.3
3.8	-65.8	-9.07	4.2	.3
5.3	-69.3	-9.23	4.1	.3
6.9	-63.1	-8.96	4.0	.3
8.4	-64.9	-8.94	4.4	.3
9.9	-64.9	-9.10	4.0	.3
13.0	-72.5	-10.09	3.7	.2
16.0	-66.0	-9.00	3.6	.3
19.1	-64.9	-8.81	4.1	.4
22.1	-84.6	-11.77	3.3	.3
MC2				
.2	-65.1	-5.28	—	—
1.7	-64.7	-9.14	1.9	.5
6.9	-71.3	-9.93	3.8	.3
9.9	-69.1	-9.71	5.9	.4
WC1				
.2	-63.5	-7.70	7.2	.8
2.0	-78.7	-11.60	5.9	.5
3.5	-57.1	-8.02	4.3	.3
5.0	-61.7	-8.80	4.4	0.2
6.6	-57.8	-8.40	4.6	.2
8.1	-57.8	-8.30	3.9	.2
WC2				
2.0	-59.2	-6.29	3.9	.7
3.5	-60.0	-7.70	5.4	.6
5.0	-59.5	-7.70	5.0	.6
6.6	-46.8	-6.70	4.6	.6
8.1	-50.5	-6.90	5.7	.6
9.6	-50.0	-6.80	4.3	.5
11.1	-63.8	-8.43	3.9	.3
WC3				
.2	-36.1	-1.36	6.3	.5
0.8	-48.8	-5.83	4.5	.4
1.4	-48.6	-6.10	5.0	.4
2.9	-55.9	-7.05	3.8	.3
8.1	-52.2	-6.90	5.5	.3
10.5	-49.4	-6.75	5.4	.5
13.6	-59.9	-7.84	2.6	.3
16.6	-62.5	-8.26	1.0	.6
19.7	-62.1	-8.04	0.4	.3
WC4a				
.8	-63.0	-7.70	3.7	.7
2.1	-59.0	-7.38	3.4	1.1
3.6	-64.6	-8.82	5.0	.4
5.1	-60.0	-8.20	10.1	.7
6.6	-66.0	-8.90	1.6	.5
8.2	-63.0	-8.30	1.0	.4
9.6	-73.0	-9.90	1.6	.5
11.1	-68.8	-9.55	1.0	.4
WG1				
2.9	-50.9	-6.94	2.9	1.2
3.5	-67.7	-9.60	3.6	.7
7.5	-64.7	-9.14	3.9	.4
8.7	-62.0	-9.06	4.5	.4
10.2	-63.3	-9.24	4.4	.4
13.3	-52.3	-7.60	3.9	.8
16.3	-55.5	-8.10	3.7	.4
19.4	-54.6	-8.14	4.2	.3
22.4	-59.6	-8.66	5.7	.5
WG2				
.5	-29.9	-2.80	5.6	1.1
.8	-28.5	-3.72	6.7	.6
2.3	-55.3	-8.38	4.7	.3
WG3				
.2	-32.0	3.27	8.5	2.4
.8	-29.1	3.32	6.5	1.5
Basin-floor boreholes				
BF1				
.5	-45.8	-.60	6.4	.9
3.8	-62.2	-7.82	6.4	.9
5.3	-59.5	-7.34	2.5	.6
6.9	-57.2	-7.03	.8	.6

Table 4. Stable-isotope and tritium data for pore water, Sierra Vista ground-water recharge study area, Arizona.—Continued

[Abbreviations: cm, centimeters; m, meters; δD, delta dueterium; $\delta^{18}O$, delta oxygen-18; ‰, per mil; TU, tritium units; —, no data]

Depth to top of 15.2-cm interval, in m	δD, in ‰	$\delta^{18}O$, in ‰	^{3}H, in TU	^{3}H error, in TU
Basin-floor boreholes—Continued				
BF1—Continued				
8.4	-59.8	-7.11	0.8	0.5
10.2	-58.0	-7.18	.6	.4
13.0	-56.5	-7.04	.3	.2
WC4c				
.2	-67.0	-9.20	4.1	.7
.8	-75.5	-10.37	2.6	.8
1.7	-68.0	-9.40	4.6	1.0
2.3	-68.4	-8.99	7.0	2.0
3.7	-77.0	-9.60	4.9	1.4
5.2	-64.4	-8.07	3.7	.4
6.7	-59.8	-7.74	5.6	.3
8.2	-63.0	-8.56	11.4	.4
9.8	-63.0	-8.68	10.4	.4
11.3	-71.0	-9.40	.3	.3
WG4				
.5	-44.1	-0.32	6.3	.7
1.1	-42.5	-0.94	9.1	.9
2.0	-52.2	-2.82	10.2	1.2
4.1	-53.8	-3.91	8.2	.4
7.5	-43.1	-3.37	4.0	2.4
13.3	-55.9	-5.23	.4	.6
WG5				
.2	-60.0	-6.12	.4	.4

Table 5. Thermal properties of sediment, Sierra Vista ground-water recharge study area, Arizona.

[Abbreviations: cm, centimeters; m, meters; MJ, megajoules; J/m^3·°C, joules per cubic meter degree Celsius; J/s·m·°C, joules per second meter degree Celsius; —, no data]

Depth to top of 15.2-cm interval, in m	Field water content, in cm^3/cm^3	Volumetric specific heat, field water content, in MJ/m^3·°C	Thermal conductivity, field water content, in J/s m °C
Ephemeral-channel boreholes			
BC1			
2.3	0.20	2.06	2.25
3.8	—	2.24	2.03
5.3	.09	1.94	2.87
6.9	—	1.68	2.32
8.4	—	3.93	2.30
9.9	—	2.78	4.11
11.4	—	3.46	2.11
14.5	.27	2.15	2.59
16.0	.29	1.07	1.76
17.5	—	2.54	1.50
20.6	.08	2.32	2.61
23.6	—	1.34	1.74
GD1			
6.7	.11	1.74	1.56
18.9	—	2.42	1.63
GD2			
2.1	.44	2.54	1.66
9.8	—	2.30	1.63
18.9	—	2.58	.77
MC1			
0	—	1.34	1.09
8.2	.28	3.01	1.99
18.9	—	2.76	1.54
MC2			
6.7	.30	1.90	2.08
WC1			
.5	.13	1.37	.95
2.3	.07	1.11	.60
3.8	—	5.08	1.32
5.3	—	4.41	1.22
6.9	.37	3.41	2.00
8.4	—	2.60	1.57
WC2			
2.3	.15	1.34	1.20
3.8	.33	1.75	1.00
5.3	—	2.71	1.93
6.9	.47	2.79	1.33
8.4	.40	1.27	1.50
9.9	.18	2.22	1.50
11.4	—	3.02	1.63
WC3			
0	—	2.72	1.35
10.4	—	1.23	1.03
WC4a			
1.1	—	1.71	1.38
2.4	.25	1.36	.79
3.9	—	1.63	1.64
5.4	—	2.98	1.66
6.9	—	3.25	2.94
Ephemeral-channel boreholes—Continued			
WC4a—Continued			
8.4	—	3.33	2.32
9.9	—	1.94	.90
11.4	.20	1.43	1.91
WG1			
2.7	0.25	1.63	0.86
10.1	—	1.41	.93
19.2	—	2.40	1.55
WG2			
2.1	—	1.23	.80
WG3			
.6	—	1.15	.27
Basin-floor boreholes			
BF1			
6.7	.11	2.47	1.73
12.8	—	2.42	1.45
WC4c			
.5	—	1.22	.56
1.1	.09	1.25	.53
2.0	—	1.48	.69
2.6	.07	9.70	.42
4.0	.15	1.55	.67
5.5	—	2.67	1.49
7.0	—	3.20	2.31
8.5	—	2.42	2.05
10.1	—	2.00	1.89
11.6	.24	1.44	1.12
WG4			
0	—	1.49	.31
13.1	.10	1.33	.89
WG5			
0	.10	1.24	.34

Table 6. Physical and hydraulic properties of sediments, Sierra Vista ground-water recharge study area, Arizona.

[Abbreviations: cm, centimeters; m, meters; %, percent; g/cm^3, grams per cubic centimeter; m^3/m^3, cubic meter per cubic meter; cm/s, centimeters per second; e, base-10 exponent (1.2e–1 = 1.2 × 10^{-1}, for example); —, no data]

Depth to top of 7.6-cm interval, in m	Gravel, in %	Sand, in %	Silt, in %	Clay, in %	Bulk density, in g/cm^3	Particle density, in g/cm^3	Porosity, in m^3/m^3	Field water content, in m^3/m^3	Saturated hydraulic conductivity, in cm/s	van Genuchten parameters					
										α, in cm^{-1}	n (dimensionless)	m (= 1-1/n)	Residual water content, in m^3/m^3	Saturated water content, in m^3/m^3	R^2
Ephemeral-channel boreholes															
BC1															
2.1	63.7	22.6	8.9	4.8	1.85	2.81	0.34	0.20	9.6e-3	0.145	1.86	0.46	0.19	0.34	0.99
5.2	79.7	16.2	2.6	1.5	1.82	2.65	.31	.09	1.2e-1	.122	2.01	.50	.11	.31	1.00
8.2	—	—	—	—	—	—	—	—	4.1e-7	—	—	—	—	—	—
14.3	70.8	19.9	7.4	1.9	1.82	3.00	.39	.27	1.7e-6	.138	1.45	.31	.07	.39	1.00
15.8	35.3	37.8	23.5	3.4	1.63	2.88	.43	.29	3.3e-5	.009	1.62	.38	.16	.42	1.00
20.4	77.7	19.5	1.9	.9	2.02	2.70	.25	.08	8.9e-3	.145	1.96	.49	.08	.25	1.00
GD1															
4.0	47.6	48.3	2.2	1.9	1.82	2.49	.27	.15	1.4e-2	.145	2.19	.54	.11	.26	.95
7.0	46.1	47.6	2.8	3.5	1.89	—	—	.11	4.6e-3	.145	1.29	.23	.06	.36	1.00
13.1	19.4	38.9	27.3	14.4	—	—	—	—	6.8e-8	—	—	—	—	—	—
GD2															
2.4	2.7	66.1	21.9	9.3	1.47	3.11	.53	.44	5.9e-3	.067	1.11	.10	.20	.50	.99
5.3	50.7	33.0	4.2	12.1	1.44	2.60	.45	.14	5.3e-2	.145	2.54	.61	.18	.44	.97
13.1	70.9	12.5	4.2	12.4	1.57	2.64	.41	.27	1.6e-2	.145	2.40	.58	.25	.40	.97
MC1															
0.9	4.2	60.1	22.9	12.8	1.84	2.87	.36	—	9.3e-3	.145	1.20	.17	.11	.36	.99
4.0	18.9	44.6	19.1	17.4	1.84	2.91	.37	.31	3.5e-6	.005	1.33	.25	.12	.35	.95
8.5	4.2	57.6	25.3	12.9	1.78	2.92	.39	.28	1.3e-3	.005	1.21	.17	.12	.39	.95
19.2	4.5	31.5	32.1	31.9	—	—	—	—	1.8e-6	—	—	—	—	—	—
MC2															
1.8	36.4	42.7	12.2	8.7	1.37	2.35	.42	.18	3.3e-3	.066	1.22	.19	.08	.41	.99
7.0	3.7	63.7	21.0	11.6	1.87	2.92	.36	.30	3.2e-6	.013	1.37	.27	.16	.36	.95
10.1	73.0	19.0	4.9	3.1	1.60	2.76	.42	.22	1.7e-2	.136	1.33	.25	.14	.42	.97
WC1															
0.3	25.6	72.5	<.7	1.9	1.49	2.74	.46	.13	7.2e-2	.145	2.44	.59	.05	.45	.98
2.1	53.0	43.5	1.0	2.5	1.84	2.90	.37	.07	3.6e-2	.145	2.32	.57	.07	.36	.97
3.7	45.1	36.1	13.0	5.8	—	—	—	—	3.2e-3	.006	1.23	.19	.28	.54	1.00
6.7	61.1	20.8	12.1	6.0	1.69	—	—	.37	2.1e-6	.008	1.59	.37	.22	.52	.98
WC2															
2.1	34.7	61.8	.2	3.3	1.71	2.64	.35	.15	6.3e-3	.145	2.56	.61	.07	.35	.97
3.7	22.0	39.5	22.7	15.8	1.64	3.18	.48	.33	2.2e-2	.106	1.25	.20	.22	.48	.96
6.7	59.0	14.5	12.7	13.8	1.43	2.95	.52	.47	5.0e-4	.028	1.15	.13	.20	.52	.95
8.2	27.4	30.1	30.7	11.8	1.52	2.92	.48	.40	9.8e-6	.014	1.41	.29	.21	.47	.95
9.8	15.9	76.1	3.7	4.3	1.65	2.48	.34	.18	3.0e-3	.068	1.51	.34	.10	.32	.97
WC3															
0.9	38.7	45.3	4.8	11.2	1.64	2.48	.34	.11	8.5e-3	.145[1]	2.03	.51	.13	.34	1.00
1.5	—	—	—	—	—	—	—	—	1.7e-4	—	—	—	—	—	—
8.2	92.4	5.0	1.7	.9	1.75	2.60	.33	.21	2.3e-3	.043	1.36	.27	.08	.32	.97
13.7	20.7	62.4	9.8	7.1	1.64	2.71	.39	.11	9.9e-3	.162	1.53	.35	.10	.39	1.00
19.8	11.3	58.9	22.6	7.2	1.72	2.88	.40	.19	5.8e-3	.068	1.37	.27	.13	.39	.98
WC4a															
2.1	78.7	15.9	1.9	3.5	1.81	3.16	.43	.25	6.4e-2	.145[1]	2.03	.51	.15	.42	.99
11.3	48.5	32.7	11.7	7.1	1.80	2.69	.33	.20	4.2e-4	.049	1.48	.32	.22	.33	1.00
WG1															
3.0	68.5	27.9	1.4	2.2	1.68	2.97	.43	.25	2.0e-2	.146	1.39	.28	.05	.43	1.00
3.7	72.8	24.0	1.6	1.6	1.84	2.81	.35	.13	4.6e-2	.145	1.51	.34	.04	.34	.98
13.4	43.9	52.9	.7	2.5	1.37	2.58	.47	.10	4.0e-2	.145	1.98	.50	.07	.47	.99
22.6	66.0	27.8	5.7	.5	1.59	2.66	.40	.19	2.0e-2	.145	1.29	.23	.05	.39	.97

Table 6. Physical and hydraulic properties of sediments, Sierra Vista ground-water recharge study area, Arizona.—Continued

[Abbreviations: cm, centimeters; m, meters; %, percent; g/cm^3, grams per cubic centimeter; m^3/m^3, cubic meter per cubic meter; cm/s, centimeters per second; e, base-10 exponent (1.2e–1 = 1.2 × 10^{-1}, for example); —, no data]

Depth to top of 7.6-cm interval, in m	Gravel, in %	Sand, in %	Silt, in %	Clay, in %	Bulk density, in g/cm^3	Particle density, in g/cm^3	Porosity, in m^3/m^3	Field water content, in m^3/m^3	Saturated hydraulic conductivity, in cm/s	van Genuchten parameters					
										α, in cm^{-1}	n (dimensionless)	m (= 1-1/n)	Residual water content, in m^3/m^3	Saturated water content, in m^3/m^3	R^2
Basin-floor boreholes															
BF1															
0.3	41.7	43.3	7.0	8.0	1.52	2.51	0.39	<.02	2.1e-2	0.076	2.11	0.53	0.09	0.40	1.00
4.0	68.0	25.8	2.5	3.7	—	—	—	—	—	—	—	—	—	—	—
5.5	76.5	16.5	1.7	5.3	—	—	—	—	—	—	—	—	—	—	—
7.0	64.1	28.5	3.1	4.3	1.77	2.72	.35	.11	1.4e-2	.137	1.72	.42	.14	.35	.99
8.5	34.8	34.5	21.0	9.7	1.60	2.92	.45	.26	5.1e-3	.073	1.28	.22	.18	.46	.95
10.1	77.0	18.5	2.4	2.1	—	—	—	—	—	—	—	—	—	—	—
13.1	60.7	24.6	7.7	7.0	—	—	—	—	—	—	—	—	—	—	—
WC4c															
1.1	41.1	54.4	1.0	3.5	1.70	2.54	.33	.09	1.5e-2	.166	1.58	.37	.03	.33	.98
2.4	51.6	43.9	1.7	2.8	1.69	2.57	.34	.07	5.1e-3	.145	1.81	.45	.05	.34	.99
3.8	23.9	68.5	2.1	5.5	1.66	2.76	.40	.15	1.5e-3	.071	1.89	.47	.06	.40	1.00
9.9	68.3	19.1	9.3	3.3	—	—	—	—	1.9e-5	.025	3.89	.74	.27	.40	.99
11.3	56.6	31.0	9.6	2.8	1.83	2.87	.36	.24	7.2e-6	.021	2.09	.52	.27	.36	.97
WG4															
4.3	47.6	26.0	17.2	9.2	1.24	2.38	.48	.19	1.3e-2	.122	1.21	.17	.15	.48	1.00
13.4	36.3	37.2	18.6	7.9	1.30	2.61	.50	.10	1.7e-2	.077	1.63	.39	.17	.47	.96
WG5															
0.3	34.0	47.2	15.6	3.2	1.41	2.71	.48	.10	1.5e-2	.126	1.40	.29	.10	.48	.98

Table 7. Isotope and chloride data for composite precipitation, Sierra Vista ground-water recharge study area, Arizona.

[Abbreviations: cm, centimeters; mg/cm²/yr, milligrams per square centimeter per year; ‰, per mil; TU, tritium units; —, no data]

Begin collection date	End collection date	Precipitation amount, in cm	Chloride deposition rate, in mg/cm²/yr	Delta deuterium, in ‰	Delta oxygen-18, in ‰	Tritium, in TU	Tritium error, in TU
Upper Babocomari site							
07/27/00	10/17/00	25.7	0.021	-34.0	-5.72	—	—
10/17/00	04/11/01	19.1	.011	-73.6	-10.97	3.3	0.4
04/11/01	10/11/01	26.4	.013	-38.7	-5.31	4.7	.3
10/11/01	04/25/02	5.3	.004	-90.7	-12.80	3.3	.3
04/25/02	10/17/02	24.1	.010	-54.7	-8.17	4.8	.3
10/17/02	04/23/03	—	—	-80.1	-11.47	4.2	.3
Greenbush Draw site							
07/26/00	10/18/00	27.2	.011	-38.5	-6.05	—	—
10/18/00	04/11/01	15.5	.017	-65.6	-10.41	3.2	.3
04/11/01	10/11/01	14.5	.010	-46.5	-6.12	4.6	.3
10/11/01	04/25/02	4.3	.001	-133.4	-17.71	2.6	.3
04/25/02	10/17/02	15.0	.012	-34.2	-5.23	4.8	.3
10/17/02	04/21/03	—	—	-68.8	-10.37	1.7	.3

Table 8. Streamflow durations at streambed-temperature sensors, Agricultural Research Service flumes, and U.S. Geological Survey streamflow-gaging stations; and distance of duration-measurement locations from the mountain front, Sierra Vista ground-water recharge study area, Arizona.

[Abbreviations: hr, hours; km, kilometers; —, no data; header numbers are streamgaging-station identifiers; values in parentheses are distance from the mountain front in kilometers]

Stream-flow starting	Streamflow duration, in hr				
	Greenbush				
	377815 (1.8 km)	GD2 (5.6 km)	374866 (11.3 km)	GD12 (12.4 km)	377820 (18.5 km)
01/09/01	1.0	0.0	0	—	0
04/06/01	7.5	0	0	—	0
07/09/01	0	2.0	0	—	0
07/10/01	0	3.0	0	—	0
07/13/01	0	.5	12	—	0
07/17/01	0	0	15	—	0
07/18/01	0	0	.8	—	2.5
07/21/01	0	13	0	—	5.3
07/24/01	0	2.3	0	—	0
07/25/01	0	6.0	0	—	0
07/28/01	0	0	1.8	—	16
08/05/01	0	16	1.0	—	0
08/11/01	0	3.3	0	—	0
08/12/01	0	5.3	0	—	0
08/13/01	0	7.0	.8	—	0
09/12/01	0	0	0	—	16
07/14/02	0	0	0	0	1.5
07/21/02	17	0	0	0	0
08/01/02	0	2.0	.5	0	0
08/02/02	0	0	0	1.0	0
08/03/02	0	.8	0	0	0
08/18/02	0	0	0	0	19
08/29/02	0	0	0	0	0
09/09/02	7.0	0	0	0	0
09/10/02	0	1.3	0	0	0
Total	37.5	62.5	94.4	1	60.3

Stream-flow starting	Miller Canyon Wash				
	377806 (0.0 km)	MC2[1] (0.0 km)	377797 (3.9 km)	MC1[1] (7.1 km)	374919 (10.9 km)
04/06/01	0	—	6.0	—	0
06/25/01	0	—	2.0	—	0
07/18/01	0	—	2.3	—	0
07/28/01	.5	—	3.5	—	0
08/01/01	0	—	1.8	—	0
08/05/01	15	—	3.0	—	1.5
08/16/01	.8	—	0	—	3.5
08/17/01	0	—	0	—	2.5
10/03/01	0	—	0	—	2.5
07/16/02	20	18	0	0	0
07/25/02	0	0	0	0	2.3
08/19/02	0	0	1.0	0	0
09/03/02	0	0	2.0	0	0
09/09/02	0	0	1.3	0	4.5
09/10/02	0	0	3.5	0	0
Total	36.3	18	26.4	0	16.8

Stream-flow starting	Streamflow duration, in hr				
	Woodcutters Wash				
	WC4a2 (0.4 km)	375010 (3.1 km)	WC32 (7.2 km)	377793 (8.0 km)	WC1 (16.4 km)
04/05/01	0	0	—	13	0
04/06/01	0	.5	—	0	3.0
06/19/01	0	16	—	12.5	0
06/25/01	0	0	—	2.0	.3
07/05/01	0	13	—	0	0
07/07/01	0	22	—	1.5	.5
07/09/01	0	5.0	—	1.3	0
07/16/01	0	0	—	0	.8
07/24/01	0	5.0	—	0	0
07/25/01	0	7.5	—	0	0
07/28/01	0	13	—	2.8	.3
08/01/01	0	1.0	—	0	0
08/05/01	0	2.0	—	0	0
08/11/01	0	7.5	—	0	0
08/13/01	.5	6.5	—	0	14
08/14/01	0	1.5	—	0	0
08/16/01	0	2.0	—	0	0
08/17/01	0	8.5	—	0	4.5
08/29/01	0	5.5	—	0	12
09/12/01	0	6.5	—	0	0
07/08/02	0	1.0	2.5	.8	12
07/16/02	0	.5	1.5	1.0	.5
07/18/02	0	0	0	0	.8
07/26/02	0	0	0	0	2.0
08/03/02	0	0	2.0	0	0
08/08/02	0	0	0	0	1.8
08/16/02	0	0	0	0	.8
08/19/02	0	0	1.0	1.0	.8
09/08/02	0	0	0	0	15
09/09/02	0	0	0	0	3.3
10/07/02	0	0	1.5	2.5	1.0
Total	0.5	124.5	8.5	38.4	73.4

Stream-flow starting	Banning Creek		
	094707001 (0.0 km)	377822[2] (0.0 km)	BC1 (3.9 km)
07/15/01	1,152	—	0.0
07/20/01	0	—	1.5
07/22/01	0	—	11.
07/25/01	0	—	1.0
08/01/01	0	—	1.5
10/03/01	0	—	2.3
08/03/02	—	909	13.
08/04/02	—	0	1.0
08/05/02	—	0	5.8
Total	1,152	909	37.1

[1] Data not used in analysis of streamflow duration versus distance from the mountain front.

[2] Streamflow-gaging station 09470700 and temperature sensor 377822 are at the same location.

Table 8.—Continued.

Stream-flow starting	Streamflow duration, in hr		
	Walnut Gulch[3]		
	Flume 11 (7.2 km)	Flume 6 (13.2 km)	Flume 1 (25.6 km)
01/06/01	0	0	.7
01/13/01	38	0	0
01/16/01	82	0	0
07/07/01	1.2	0	0
07/13/01	.5	0	0
08/11/01	1.7	0	0
08/13/01	.8	0	2.6
08/14/01	0	0	2.9
08/17/01	0	0	.4
09/14/01	0	0	3.4
07/08/02	1.2	0	0
07/16/02	0	.5	0
07/19/02	1.2	2.8	0
07/26/02	0	1.3	10
08/01/02	.6	5.0	0
08/04/02	3.0	6.0	5.0
08/06/02	1.0	0	0
09/08/002	0	0	.2
09/09/02	0	3.5	0
09/11/02	1.3	1.0	0
Total	132.5	20.1	25.2

[3] Provisional data provided by the U.S. Department of Agriculture, Agricultural Research Service, Southwest Watershed Research Center.

Table 9. Stream parameters used in the infiltration-flux analytical method, Sierra Vista ground-water recharge study area, Arizona.

[Abbreviations: m, meters; h, hour; g/cm^3, grams per cubic centimeter; MJ/m^3 °C, megajoules per cubic meter degree Celsius; m/hr, meters per hour; ", ditto; —, not calculated]

Date of flow event	Upper measuring point, in m	Lower measuring point, in m	Travel time, in hr	Bulk density, in g/cm^3	Heat capacity, dry soil, in MJ/m^3 °C	Calculated transient flux, in m/h	Flux type
			BC1 (borehole identifier)				
07/20/01	0.0	1.5	1.0	1.84	2.08	1.4	Infiltration
	1.5	3.0	0	"	"	—	—
	3.0	4.6	.5	"	"	2.8	Percolation
	4.6	6.1	2.0	"	"	.7	Percolation
07/22/01	0	1.5	.5	"	"	2.8	Infiltration
	1.5	3.0	.5	"	"	2.8	Infiltration
	3.0	4.6	1.5	"	"	.9	Percolation
	4.6	6.1	1.0	"	"	1.4	Percolation
07/25/01	0	1.5	1.0	"	"	1.4	Infiltration
	1.5	3.0	0	"	"	—	—
	3.0	4.6	1.0	"	"	1.4	Percolation
	4.6	6.1	1.5	"	"	.9	Percolation
08/01/01	0	1.5	1.0	"	"	1.4	Infiltration
	1.5	3.0	0	"	"	—	—
	3.0	4.6	1.0	"	"	1.4	Percolation
	4.6	6.1	1.0	"	"	1.4	Percolation
10/03/01	0	1.5	1.0	"	"	1.4	Percolation
	1.5	3.0	0	"	"	—	—
	3.0	4.6	.5	"	"	2.8	Percolation
	4.6	6.1	1.5	"	"	.9	Percolation
08/03/02	0	1.5	1.0	"	"	1.4	Percolation
	1.5	3.0	0	"	"	—	—
	3.0	4.6	1.0	"	"	1.4	Percolation
	4.6	6.1	1.5	"	"	.9	Percolation
08/04/02	0	1.5	1.0	"	"	1.4	Percolation
	1.5	3.0	0	"	"	—	—
	3.0	4.6	1.0	"	"	1.4	Percolation
	4.6	6.1	.5	"	"	2.8	Percolation
			GD1				
08/02/02	0	1.5	1.5	1.86	1.74	.8	Percolation
	1.5	3.0	0	"	"	—	—
	3.0	6.1	3.5	"	"	.7	Percolation
	6.1	9.1	17.5	"	"	.1	Percolation
			GD2				
08/01/02	0	1.5	1.5	1.46	2.54	.9	Percolation
	1.5	3.0	1.5	"	"	.9	Percolation
	3.0	6.1	5.0	"	"	.5	Percolation
09/10/02	0	1.5	2.0	"	"	.7	Percolation
	1.5	3.0	2.5	"	"	.5	Percolation
	3.0	6.1	1.5	"	"	1.8	Percolation
	6.1	9.1	1.5	"	"	1.8	Percolation
	9.1	12.2	10	"	"	.3	Percolation
			WC1				
07/07/01	0	1.5	.5	1.67	1.24	1.5	Infiltration
	1.5	3.0	.5	"	"	1.5	Infiltration
07/16/01	0	1.5	.5	"	"	1.5	Percolation
	1.5	3.0	.5	"	"	1.5	Percolation
07/28/01	0	1.5	.5	"	"	1.5	Percolation
	1.5	3.0	.5	"	"	1.5	Percolation
07/16/02	0	1.5	2.0	"	"	.4	Percolation
	1.5	3.0	2.0	"	"	.4	Percolation
			WG1				
07/26/02	0	1.5	1.0	1.76	1.63	1.0	Infiltration
	1.5	3.0	.5	"	"	2.1	Infiltration
	3.0	4.6	.5	"	"	2.1	Infiltration
	4.6	6.1	5.5	"	"	.2	Percolation
08/04/02	0	1.5	1.0	"	"	1.0	Infiltration
	1.5	3.0	0	"	"	—	—
	3.0	4.6	0	"	"	—	—
	4.6	6.1	7.4	"	"	.1	Percolation
09/08/02	0	1.5	1.0	"	"	1.0	Percolation
			WG2				
07/19/02	0	3.0	1.5	1.76[1]	1.23	1.0	Infiltration

[1] Estimated on the basis of the value for borehole WG1.

Table 10. Sediment properties used for the VS2DH numerical simulations, Sierra Vista ground-water recharge study area, Arizona.

[Abbreviations: m, meters; cm/s, centimeters per second; cm^3/cm^3, cubic centimeters per cubic centimeters; W/m °C, watts per meter degree Celsius; $J/m^3 \cdot °C$, joules per cubic meter degree Celsius; e, base-10 exponentiation (9.6e–3 = 9.6×10^{-3}, for example)]

Borehole identifier	Depth to top of domain, in m	Depth to bottom of domain, in m	Saturated hydraulic conductivity, in cm/s		Porosity, in cm^3/cm^3	Residual water, in cm^3/cm^3	α, in cm^{-1}	n (dimensionless)	Thermal conductivity, in W/m °C		Heat capacity, dry soil, in MJ/m^3 °C
			Initial	Adjusted					Saturation water content[1]	Residual water content	
BC1	0.0	3.0	9.6e-3	1.5e-2	0.34	0.10	0.145	1.9	2.5	2.1	2.08
WC1	0	3.0	5.4e-2	4.0e-2	.42	.03	.145	2.4	2.0	.8	1.24
WG1	0	4.6	3.3e-2	3.5e-2	.39	.05	.145	1.4	2.5	.9	1.63
WG2	0	3.0	[2]3.3e-2	3.5e-2	[2].39	[2].05	[2].145	[2]1.4	2.5	.8	1.23

[1] Estimated from thermal conductivity at field water content.

[2] Estimated on the basis of values for borehole WG1.

Table 11. Initial and boundary conditions for the VS2DH numerical simulations, Sierra Vista ground-water recharge study area, Arizona.

[Abbreviations: m, meters; °C, degrees Celsius; cm^3/cm^3, cubic centimeter per cubic centimeter; m/hr, meters per hour; —, no data]

Borehole identifier	Simulation date	Initial sediment temperature, in °C					[1] Initial water content, in cm^3/cm^3	Transport boundary condition	
		0.0 m	1.5 m	3.0 m	4.6 m	6.1 m		Inlet temperature, in °C	[2] Flux into domain, in m/hr
BC1	07/20/01	29.5	23.7	19.6	—	—	0.15	24.0	0.5
	07/25/01	37.3	24.1	20.9	—	—	.25	22.0	.4
	08/01/01	25.0	24.6	21.9	—	—	.25	20.0	.4
WC1	07/07/01	26.2	25.0	21.0	—	—	.07	24.0	1.3
WG1	07/26/02	28.7	25.9	23.4	21.5	—	.10	25.0	.5
	08/04/02	26.8	25.7	24.2	22.6	—	.20	25.0	.4
WG2	07/19/02	28.2	—	18.0	—	—	.15	21.0	.4

[1] Estimated from soil-water content at time of sampling.

[2] Determined through calibration.

Table 12. Estimated annual ephemeral-stream channel recharge, 2001 and 2002, Sierra Vista ground-water recharge study area, Arizona.

[Group numbers refer to figure 5. Abbreviations: $hm^3/km/2yr$, cubic hectometers per kilometer per 2-year period; hr/2yr, hours per 2-year period; m, meters; m/hr, meters per hour; km, kilometer; $hm^3/2yr$, cubic hectometers per 2-year period; x, distance from mountain front, in kilometers; e, base of the natural logarithm; ", ditto; <, less than]

Tributary name	Channel evaporation, in $hm^3/km/2yr$	Near-channel transpiration, in $hm^3/km/2yr$	Stream-flow duration vs. distance from mountain front, in hr/2yr	Wetted channel width vs. distance from mountain front, in m	Infiltration flux, in m/hr	Channel length in alluvium, in km	Ephemeral channel recharge, in $hm^3/2yr$
			Group 2				
Unnamed Wash 1	$3.0 \cdot 10^{-4}$	$1.4 \cdot 10^{-2}$	$35.5 \cdot e^{-0.07x}$	$0.15 \cdot (0.2x+2.0)$	1.3	15.4	0.01
Graveyard Gulch	"	"	"	"	"	14.4	.01
Escapule Wash	"	"	$89.9 \cdot e^{-0.03x}$	$0.15 \cdot (0.9x+1.9)$	"	18.5	1.16
			Group 3				
Woodcutters Wash	"	"	"	"	"	18.5	1.16
Garden Canyon Wash	"	"	$35.5 \cdot e^{-0.07x}$	$0.15 \cdot (0.2x+2.0)$	"	21.7	.01
Ramsey Canyon Wash	"	"	"	"	"	17.4	.01
Carr Canyon Wash	"	"	$89.9 \cdot e^{-0.03x}$	$0.15 \cdot (0.9x+1.9)$	"	16.8	.88
Miller Canyon Wash	"	"	$35.5 \cdot e^{-0.07x}$	$0.15 \cdot (0.2x+2.0)$	"	16.2	.01
Hunter Canyon Wash	"	"	"	"	"	15.5	.01
Stump Canyon Wash	"	"	"	"	"	14.6	.01
Ash Canyon Wash	"	"	"	"	"	12.9	.01
Brown-Bob Thompson Wash	"	"	"	"	"	9.5	.01
			Group 4				
Lewis Springs Wash	"	"	"	"	"	12.1	.01
Bakarich-McCool Wash	"	"	"	"	"	11.8	.01
Three Canyons Wash	"	"	"	"	"	6.6	<.01
Palominas Wash	"	"	"	"	"	11.1	.01
			Group 5				
Greenbush Draw	"	"	$40.2 \cdot e^{0.01x}$	$0.15(1.8x-8.2)$	0.8	19.5	.9
			Group 6				
Banning Creek	"	"	$2060.8 \cdot e^{-1.1x}$	$0.15(0.8x+0.9)$	.4	8.6	.15
Unnamed Wash 2	"	"	"	"	"	10.6	.15
Stagg Ranch Wash	"	"	"	"	"	10.1	.15
Little Dry Creek	"	"	"	"	"	10.5	.15
Spring Creek	"	"	"	"	"	11.4	.15
			Group 7				
Willow Creek	"	"	$126.6 \cdot e^{-0.07x}$	$0.15 \cdot (1.6x-8.5)$	"	7.7	.23
Walnut Gulch	"	"	"	"	"	7.7	.23
Government Draw	"	"	"	"	"	7.7	.23
High Knolls Canyon Wash	"	"	"	"	"	7.7	.23
					Total ephemeral-stream channel recharge, 2001 and 2002 , in $hm^3/2$ yr		5.89
					Average annual ephemeral-stream channel recharge, in hm^3/yr		2.95

Table 13. Sensitivity of estimated annual ephemeral-stream channel recharge to calculation parameters, 2001 and 2002, Sierra Vista ground-water recharge study area, Arizona.

[Group numbers refer to figure 5. Abbreviations: hm3/2yr, cubic hectometers per 2-year period; %, magnitude of change, in percentage of base value; <, less than]

Tributary name	Resulting recharge for 2001–2002, in hm^3/2yr, after indicated change									
	Channel evaporation, in %		Near-channel transpiration, in %		Stream-flow duration, in %		Wetted channel width, in %		Infiltration flux, in %	
	+100	-100	+100	-100	+50	-50	100	10	+100	-50
Group 2										
Unnamed Wash 1	<0.01	0.01	<0.01	0.23	0.12	<0.01	1.34	<0.01	0.24	<0.01
Graveyard Gulch	<.01	0.01	<0.01	0.22	0.12	<0.01	1.27	<0.01	0.23	<0.01
Escapule Wash	.15	1.16	1.06	1.26	1.79	0.53	8.30	0.74	2.42	0.53
Group 3										
Woodcutters Wash	1.15	1.16	1.06	1.26	1.79	.53	8.30	.74	2.42	.53
Garden Canyon Wash	<.01	.01	<.01	.31	.15	<.01	1.79	<.01	.31	<.01
Ramsey Canyon Wash	<.01	.01	<.01	.26	.14	<.01	1.52	<.01	.27	<.01
Carr Canyon Wash	.87	.88	.80	.95	1.35	.40	6.29	.56	1.83	.40
Miller Canyon Wash	<.01	.01	<.01	.24	.13	<.01	1.40	<.01	.25	<.01
Hunter Canyon Wash	<.01	.01	<.01	.23	.12	<.01	1.34	<.01	.24	<.01
Stump Canyon Wash	<.01	.01	<.01	.22	.12	<.01	1.27	<.01	.23	<.01
Ash Canyon Wash	<.01	.01	<.01	.20	.11	<.01	1.14	<.01	.21	<.01
Brown-Bob Thompson Wash	<.01	.01	<.01	.15	.08	<.01	.87	<.01	.16	<.01
Group 4										
Lewis Springs Wash	<.01	.01	<.01	.19	.10	<.01	1.08	<.01	.19	<.01
Bakarich-McCool Wash	<.01	.01	<.01	.19	.10	<.01	1.08	<.01	.19	<.01
Three Canyons Wash	<.01	<.01	<.01	.10	.05	<.01	.59	<.01	.11	<.01
Palominas Wash	<.01	.01	<.01	.17	.09	<.01	1.01	<.01	.18	<.01
Group 5										
Greenbush Draw	.90	.90	.72	1.11	1.45	.36	7.15	.54	2.00	.36
Group 6										
Banning Creek	.15	.15	.10	.21	.25	.05	1.32	.08	.35	.05
Unnamed Wash 2	.15	.15	.10	.21	.25	.05	1.32	.08	.35	.05
Stagg Ranch Wash	.15	.15	.10	.21	.25	.05	1.32	.08	.35	.05
Little Dry Creek	.15	.15	.10	.21	.25	.05	1.32	.08	.35	.05
Spring Creek	.15	.15	.10	.21	.25	.05	1.32	.08	.35	.05
Group 7										
Willow Creek	.23	.24	.12	.35	.41	.06	2.21	.12	.58	.06
Walnut Gulch	.23	.24	.12	.35	.41	.06	2.21	.12	.58	.06
Government Draw	.23	.24	.12	.35	.41	.06	2.21	.12	.58	.06
High Knolls Canyon Wash	.23	.24	.12	.35	.41	.06	2.21	.12	.58	.06
Total recharge, 2001–2002	5.74	5.93	4.62	9.74	10.70	2.31	61.18	3.46	15.55	2.31
Average annual recharge	2.87	2.97	2.31	4.87	5.35	1.16	30.59	1.73	7.78	1.16
Change, in percentage	−2.7	.7	−21.7	65.1	81.4	−60.7	937	−41.4	164	−60.7

Streambed Infiltration and Ground-Water Flow From the Trout Creek Drainage, an Intermittent Tributary to the Humboldt River, North-Central Nevada

By David E. Prudic, Richard G. Niswonger, James R. Harrill, and James L. Wood

Abstract

Ground water is abundant in many alluvial basins of the Basin and Range Physiographic Province of the western United States. Water enters these basins by infiltration along intermittent and ephemeral channels, which originate in the mountainous regions before crossing alluvial fans and piedmont alluvial plains. Water also enters the basins as subsurface ground-water flow directly from the mountains, where infiltrated precipitation recharges water-bearing rocks and sediments at these higher elevations. Trout Creek, a typical intermittent stream in the Middle Humboldt River Basin in north-central Nevada, was chosen to develop methods of estimating and characterizing streambed infiltration and ground-water recharge in mountainous terrains. Trout Creek has a drainage area of about 4.8×10^7 square meters. Stream gradients range from more than 1×10^{-1} meter per meter in the mountains to 5×10^{-3} meter per meter at the foot of the piedmont alluvial plain. Trout Creek is perennial in short reaches upstream of a northeast-southwest trending normal fault, where perennial springs discharge to the channel. Downstream from the fault, the water table drops below the base of the channel and the stream becomes intermittent.

Snowmelt generates streamflow during March and April, when streamflow extends onto the piedmont alluvial plain for several weeks in most years. Rates of streambed infiltration become highest in the lowest reaches, at the foot of the piedmont alluvial plain. The marked increases in infiltration are attributed to increases in streambed permeability together with decreases in channel-bed armoring, the latter which increases the effective area of the channel. Large quartzite cobbles cover the streambed in the upper reaches of the stream and are absent in the lowest reach. Such changes in channel deposits are common where alluvial fans join piedmont alluvial plains. Poorly sorted coarse and fine sediments are deposited near the head of the fan, while finer-grained but better sorted gravels and sands are deposited near the foot.

All flow in Trout Creek is lost to infiltration in the upper and middle reaches of the channel during years of normal to below-normal precipitation. During years of above-normal precipitation, streamflow extends beyond the piedmont alluvial plain to the lower reaches of the channel, where high rates of infiltration result in rapid stream loss. The frequency and duration of streambed infiltration is sufficient to maintain high water contents and low chloride concentrations, compared with interchannel areas, to depths of at least 6 m beneath the channel. Streamflow, streambed infiltration, and unsaturated-zone thickness are all highly variable along intermittent streams, resulting in recharge that is highly variable as well.

Average annual ground-water recharge in the mountainous part of the Trout Creek drainage upstream of Marigold Mine was estimated on the basis of chloride balance to be 5.2×10^5 cubic meters. Combined with an average annual surface runoff exiting the mountains of 3.4×10^5 cubic meters, the total annual volume of inflow to alluvial-basin sediments from the mountainous part of the Trout Creek is 8.6×10^5 cubic meters, assuming that all runoff infiltrates the stream channel. This equates to about 7 percent of average annual precipitation, which is about the same percentage estimated for ground-water recharge using the original Maxey-Eakin method.

Introduction

Nevada is the driest state in the nation, receiving an average of 230 mm (9 inches) of precipitation annually (Houghton and others, 1975, p. 4). Most of Nevada is in the Great Basin, an area of the Basin and Range Physiographic Province where streams have no connection to the ocean (Eakin and others, 1976). Water is an important but limited resource that is used for a variety of purposes. Traditionally, most of the water was used for agricultural purposes on the valley lowlands. Agricultural water use predominantly involved diverting streamflows for the production of native grass and alfalfa, and pumping ground water from alluvial aquifers for irrigation, also principally of alfalfa. Recently, the rapidly increasing population, development of electric power plants, and expansion of gold-mining operations have placed additional and sometimes conflicting demands on water resources.

Estimating the quantity of water that enters the alluvial aquifers from adjacent mountains is important in assessing

the water resources in the Middle Humboldt River Basin. Most of the streams that enter the basin are intermittent and flow from the mountains across large piedmont alluvial plains during periods of snowmelt (fig. 1). Piedmont alluvial plains are formed when several alluvial fans coalesce to form one large plain between the mountain front and valley floor. The distribution of recharge along these streams and the amounts of ground-water flow across the mountain front is largely unknown. Trout Creek was selected for study as a typical intermittent stream in the Middle Humboldt River Basin (fig. 2). Trout Creek is intermittent over most of its reach, but perennial where mountain springs discharge directly into the channel at higher elevations.

Purpose and Scope

The purpose of Trout Creek study was to determine the frequency, duration, and quantity of runoff and streambed infiltration from a mountain drainage that crosses a piedmont alluvial plain, and to estimate the quantity of ground-water recharge originating at various elevations of the drainage. This recharge provides subsurface flow from the mountainous part of the drainage into the adjacent alluvial basin. The scope of the study included obtaining data on streamflow, channel characteristics, geology, ground water, and precipitation, as well as developing a numerical model to simulate streamflow and streambed infiltration on the piedmont alluvial plain. Data were collected from May 1999 through October 2002.

Description of Trout Creek Drainage

Location and Drainage Area

Trout Creek drains the northwest flank of Battle Mountain near the town of Valmy, about 25 km west of the town of Battle Mountain in north-central Nevada (fig. 1). Trout Creek generally parallels Cottonwood Creek, which is immediately to the west (fig. 2). The drainage area of Trout Creek at its entrance to the Humboldt River floodplain is about 4.8×10^7 m^2 (fig. 2). North Peak of Battle Mountain is the highest point in the drainage, with an elevation of about 2,600 m above sea level. The elevation of the entrance to the Humboldt River floodplain is about 1,360 m above sea level. Stream gradients range from more than 1×10^{-1} m/m in the mountains to 5×10^{-3} m/m near the foot of the piedmont alluvial plain.

The channel of Trout Creek near Marigold Mine was relocated prior to 1999. The channel was moved westward around the mine to accommodate expansion (John Barber, Glamis Marigold Mining Company, Valmy, Nev., written commun., 2003). Originally, the stream passed through a narrow opening in Paleozoic-age rock before flowing northward onto the piedmont alluvial plain (Roberts, 1964). The original channel was incised less than a meter throughout the piedmont alluvial plain. The new channel was excavated across a narrow divide and onto the piedmont alluvial plain. The new channel reenters its original channel about 2 km downstream from Marigold Mine (fig. 2). Further downstream, the channel has been altered beneath Interstate 80 where concrete culverts are used to route streamflow beneath the highway. The channel was broadened and straightened downstream of Interstate 80 to where it passes beneath the adjacent railroad tracks. The natural stream channel continues northward until it reaches the floodplain of the Humboldt River where the channel braids into many small channels on the heavily vegetated floodplain of the Humboldt River.

Trout Creek was divided into six reaches for purposes of analysis—three mountain reaches and three piedmont alluvial-plain reaches (fig. 2). Reaches in each group are designated as upper, middle, and lower.

Climate

The climate of the Trout Creek drainage is typical of much of Middle Humboldt River Basin. Houghton and others (1975, p. 3) classified the study area as mid-latitude steppe, which is semi-arid with cold winters and hot summers. The climate is semi-arid because much of the moisture from the prevailing westerly winds from the Pacific Ocean condenses on the western slopes of the Sierra Nevada and Cascade Range in California and Oregon (Houghton and others, 1975) prior to reaching northern Nevada (fig. 1). Additionally, the mountain ranges within northern Nevada have a similar orographic effect on local climate whereby the mountains receive, on average, more precipitation than the adjacent valleys (chapter A, this volume).

Temperature

The mean annual temperature at the nearest long-term weather station (in the town of Battle Mountain, about 20 km east of Marigold Mine) was 10.3°C for the period 1971–2000. Monthly means ranged from –1.2°C in December and January to 23.1°C in July (fig. 3; U.S. Department of Commerce, 2003). The highest temperature recorded at Battle Mountain was 44.4 °C on July 12, 2002, whereas lowest temperature recorded was –39.4°C on December 22, 1990. A daily range of more than 20 °C is not uncommon. The large daily range in temperature is typical of dry continental-type climates in mountainous areas (Houghton and others, 1975, p. 26).

Precipitation

The mean annual precipitation at the town of Battle Mountain was 223 mm for the 30-year period 1971–2000 (U.S. Department of Commerce, 2003). Mean monthly precipitation ranged from a low of 7.1 mm in July to a high of 33 mm in May (fig. 3). Precipitation is generally less in the valleys than in the adjacent mountains. Mean annual precipitation in the Trout Creek drainage ranges from about 200 mm along the Humboldt River floodplain north of Marigold Mine

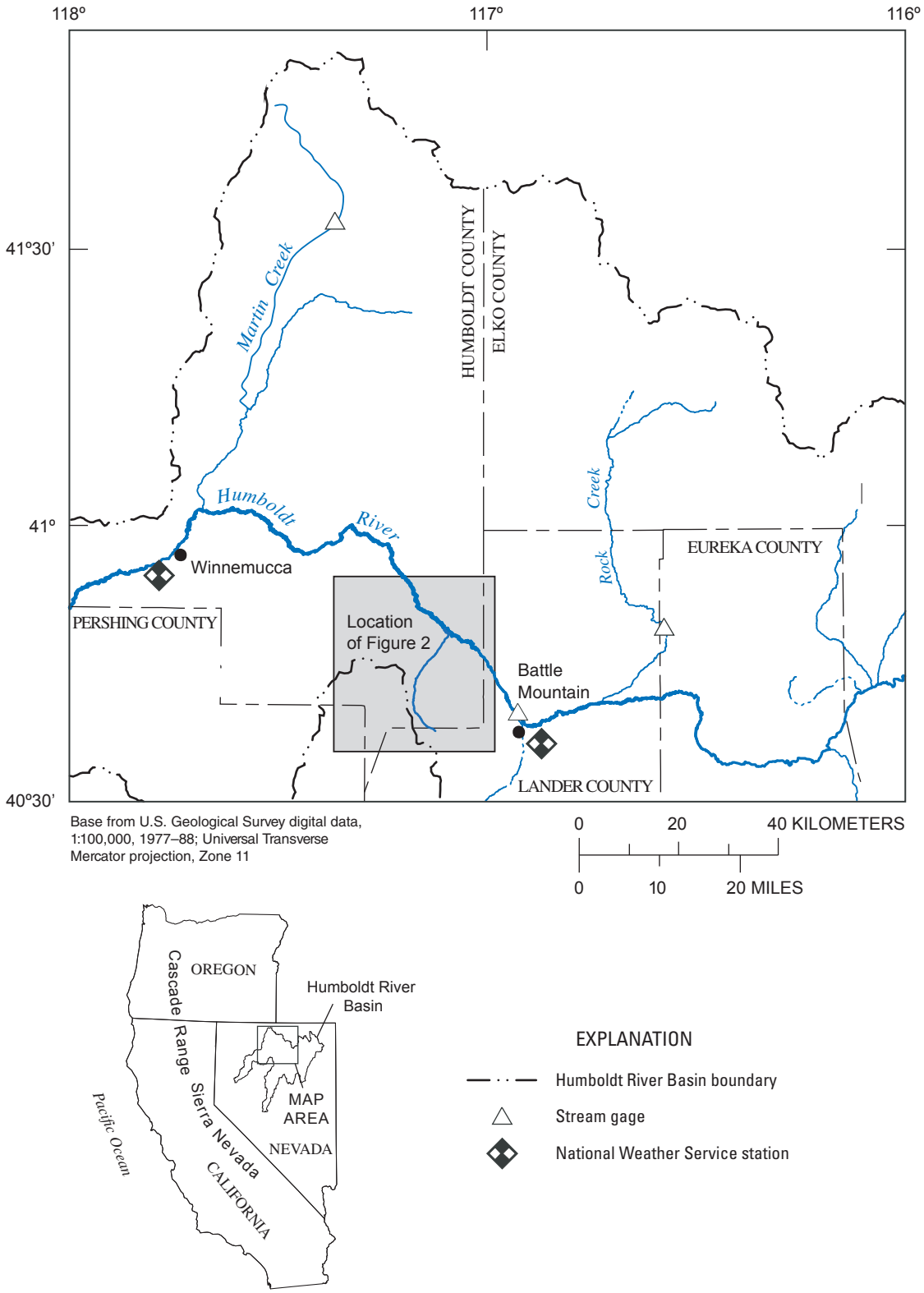

Figure 1. General features, selected stream gages and precipitation stations, and location of Trout Creek study area in north-central Nevada.

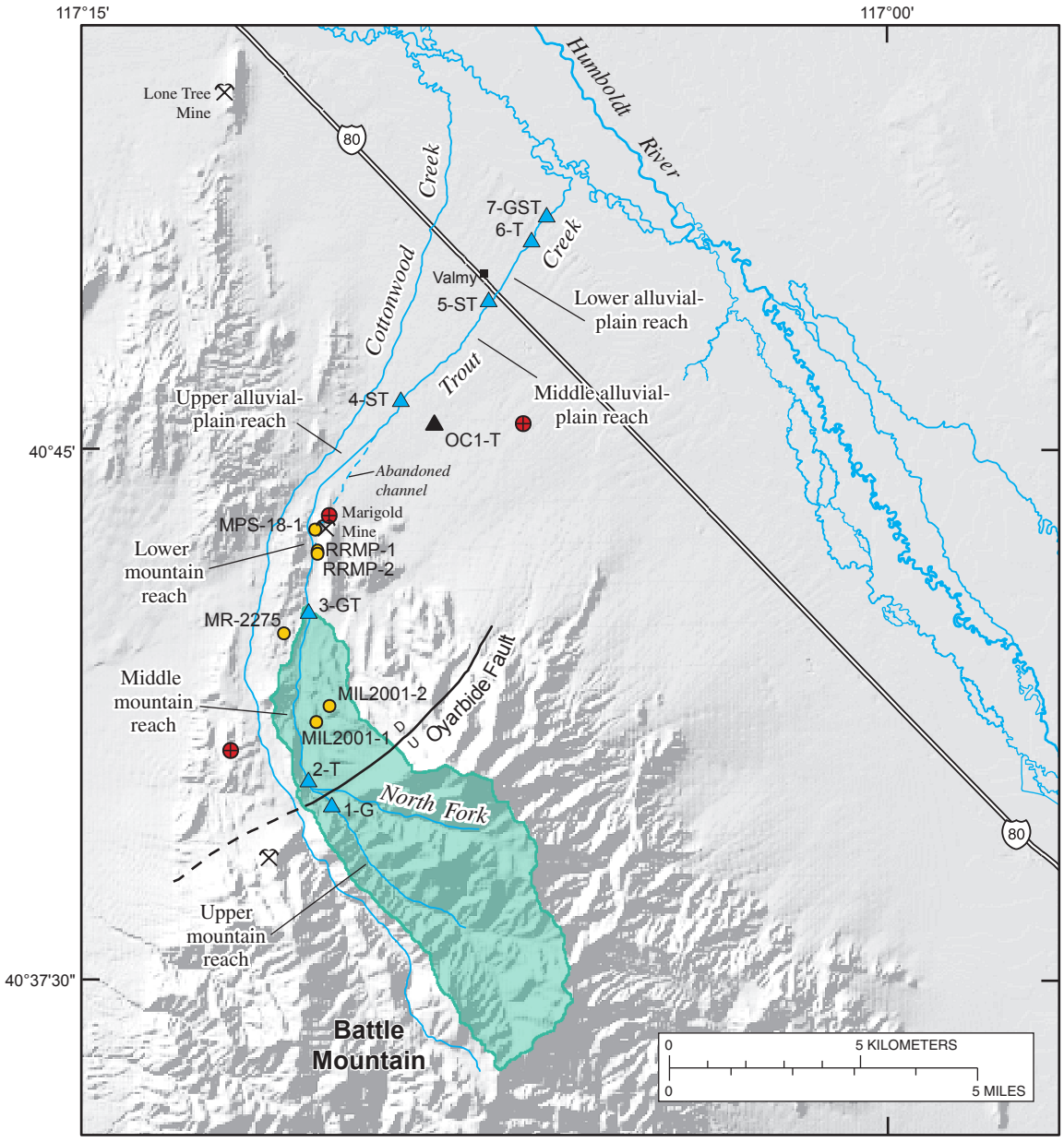

Base prepared by U.S. Geological Survey from digital data, 1:100,000 and 1:250,000
Universal Transverse Mercator projection, Zone 11

EXPLANATION

- Drainage area
- D/U — Fault—D is downthrown side, U is upthrown side. Dashed where concealed
- Mine
- Weather station
- MR-2275 — Well with local well name
- 7-GST — Channel measurement site and identification—G is stream gage, T is surface temperature recorder, and S is subsurface temperature recorder
- OC1-T — Off-channel measurement site and identification—T is surface temperature recorder

Figure 2. General features, drainage area, active mines, channel measurement sites, selected wells, and precipitation stations in vicinity of Trout Creek, north-central Nevada (modified from Prudic and others, 2003). Location of figure 2 is shown in figure 1. Reaches along the piedmont alluvial plain are abbreviated to alluvial-plain reach.

to about 350 mm in the highest parts of Battle Mountain (Daly and others, 1994). Precipitation usually accumulates as snow in the mountains or as increased soil moisture in the valleys because much of the precipitation falls during the winter months when temperatures are near or below freezing and evapotranspiration is at a minimum. Snow accumulation in the valleys may remain for a few days to weeks, but snow usually accumulates in the mountains until March when daily temperatures increase above freezing. Precipitation ranges from zero on most days to more than 50 mm on rare occasions.

Annual precipitation at the Marigold Mine during water years 2000 through 2002 was consistently less than that at the weather station in Battle Mountain (station Battle Mountain4SE, Western Climate Center, 2003) but greater than that at Winnemucca (station Winnemucca WSO Airport, Western Climate Center, 2003; fig. 4). Monthly precipitation at Marigold Mine, however, was sometimes more and sometimes less than that at the weather stations. Precipitation at the Marigold Mine ranged from 232 mm in water year 2000 to 167 mm in water year 2002 (John Barber, Glamis Gold Mining Company, Valmy, Nev., written commun., 2003). Precipitation during water year 2000 was slightly above normal to normal on the basis of comparing the 30-year mean annual from 1971–2000 with precipitation during water year 2000 at Battle Mountain and Winnemucca (115 and 100 percent, respectively). Precipitation during water years 2001 and 2002 was below normal (89 and 81 percent at Battle Mountain; and 62 and 75 percent at Winnemucca, respectively). In contrast, precipitation during water year 1998 was 414 mm or 186 percent of the 30-year mean annual precipitation at Battle Mountain and 367 mm or 173 percent at Winnemucca.

Vegetation and Evapotranspiration

The mid-latitude steppe climate in Nevada has sufficient precipitation to support a cover of big sagebrush (*Artemisia tridentate*) and a variety of grasses in the valleys and dwarf pinyon (*Pinus monophylla*), juniper trees (*Juniperus osteosperm*) and grasses in the mountains (Houghton and others, 1975, p. 69). This same pattern occurs in the Trout Creek drainage (fig. 5). Dwarf pinyons and junipers are present at the higher elevations on Battle Mountain (fig. 5*A*) and give way to sagebrush and grasses on the lower slopes and on the piedmont alluvial plain that extends to the Humboldt River floodplain (fig. 5*B*). Depth to ground water is less than 15 m along the Humboldt

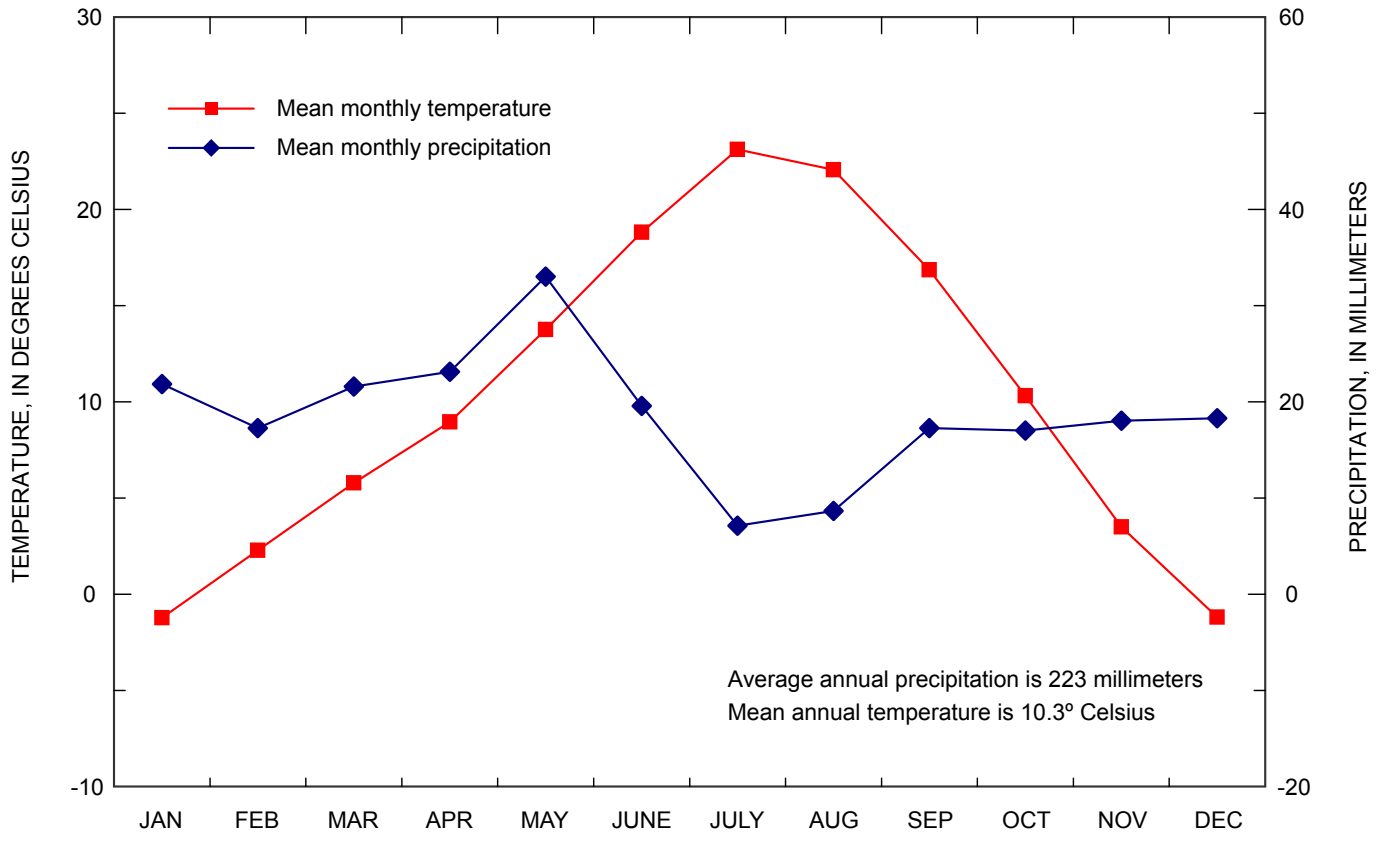

Figure 3. Mean monthly temperature and precipitation at National Weather Service Cooperative Network station Battle Mountain4SE, north-central Nevada. Location of weather station near Battle Mountain is shown in figure 1. Data are from U.S. Department of Commerce (2003).

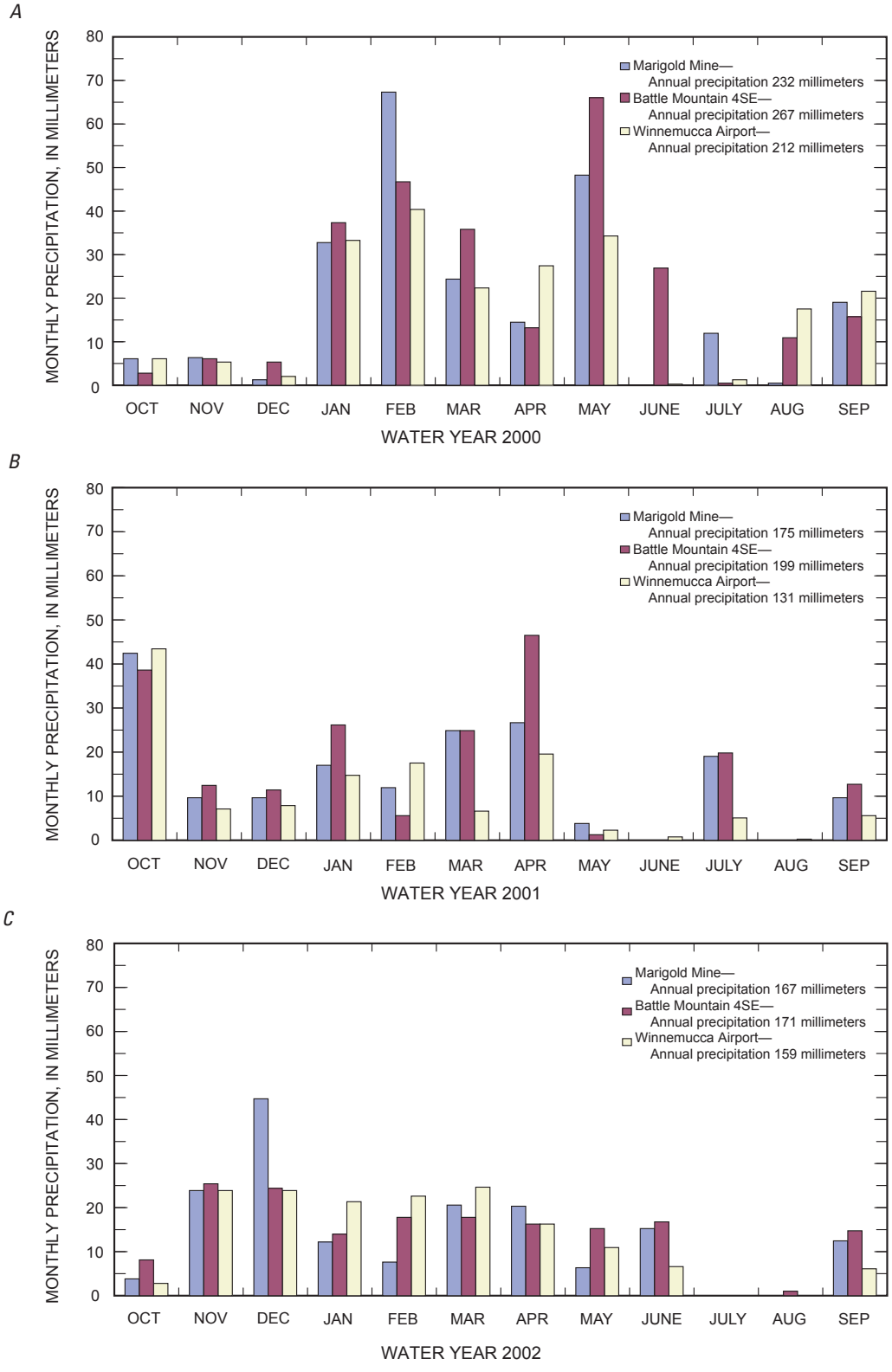

Figure 4. Comparison of monthly precipitation at Marigold Mine (John Barber, Glamis Gold Mining Company, Valmy, Nevada, written commun., 2003) with monthly precipitation at National Weather Service Cooperative Network stations near Battle Mountain and Winnemucca, Nevada for water years 2000–2002. Location of weather stations is shown in figures 1 and 2. Data for National Weather Service Cooperative Network stations are from Western Regional Climate Center (2003).

River floodplain and helps support a different plant community that consists primarily of greasewood (*Sarcobatus vermiculatus*), shadscale (*Atriplex canescens*), and rabbitbrush (*Chrysothamnus nauseosus*) along with native grasses. Various types of Willows (*Salix sp.*) are common along the active and abandoned channels of the Humboldt River. Similarly, various types of willows, chokecherry (*Prunus virginiana var. demissa*), and mountain alder (*Alnus incana sp. Tenuifolia*) are present along Trout Creek at the higher elevations on Battle Mountain (fig. 5*A*), particularly near springs where water is more prevalent.

Geology

Geology in the Trout Creek drainage is an important factor in controlling runoff to the piedmont alluvial plain and ground-water flow from the mountain into the alluvial basin. The upper mountain reach of the Trout Creek drainage (including its major tributary North Fork) is underlain by Paleozoic-age rocks that have been extensively folded and faulted (Roberts, 1964). The rocks generally have low permeability except where highly fractured (table 1). Consequently, infiltration of precipitation is limited to areas where the rocks are highly fractured or where alluvium overlies the rocks.

Both Trout Creek and its major tributary North Fork cross the northeast-southwest trending normal fault (named the Oyarbide Fault by Roberts, 1964; fig. 6) near their confluence and continue over a thin layer of younger alluvium (too thin to show on fig. 6) that covers older alluvium and Tertiary-age volcanic rocks (fig. 6, table 1). The volcanic rocks were described by Roberts (1964, p. A64) as a sequence of volcanic welded tuff and pyroclastic rocks as much as 40-m thick that extend across the drainage divide with Cottonwood Creek and are overlain by older alluvium. Springs discharge at the base of the welded tuff and pyroclastic rocks that are in contact with older alluvium just downstream of the confluence with North Fork (fig. 6).

The older alluvium is part of an alluvial fan that was deposited over a long period that probably extended through much of the Pleistocene (Roberts, 1964). The channel continues over a thin layer of younger alluvium deposited by streams that began to cut downward into the older alluvium near the end of the Pleistocene. The older alluvium near the confluence of Trout Creek with North Fork consists of layers of unsorted coarse and fine gravels in a sandy and clayey matrix that represent interlayered mudflows and fluvial deposits (Roberts, 1964, p. A50). The older alluvium beneath the channel downstream of its confluence with North Fork is generally less than 20-m thick (fig. 7).

Both younger and older alluvium are divided into two groups, alluvial-fan and valley-floor deposits (fig. 7). Although younger alluvial-fan deposits extend to the Oyarbide Fault, they are too thin to show on figure 7. Neither the younger nor older alluvial deposits are shown upstream of the fault because only a thin veneer of younger alluvium associated with the stream overlies the Paleozoic-age rocks. The older alluvial fan-deposits beneath the channel are relatively thin (about 20-m thick) upstream of the Marigold mine (fig. 7). There alluvial-fan deposits begin to thicken until they merge with floodplain deposits associated with the Humboldt River. The thickness of the younger alluvial-fan deposits is poorly constrained in the Trout Creek area but probably does not exceed 30 m on the basis of work by Cohen (1963), who found that younger alluvium (ranging from Holocene to Pleistocene age Lake Lahontan deposits) generally less than 30-m thick elsewhere in the Humboldt River floodplain.

Ground Water

Springs near the channel upstream of the Oyarbide Fault result in short perennial reaches along Trout Creek. These springs likely result from numerous localized ground-water flow systems created during the extensive folding and faulting of the rocks. Ground-water flow is generally restricted by the Oyarbide Fault as evidenced by the fact that water levels in test holes south of the fault (higher in the mountain) in the adjacent Cottonwood Creek drainage are much higher than in wells north of the fault (lower in the mountain) in the Cottonwood Creek and Trout Creek drainages. Water levels in monitoring wells north of Oyarbide Fault are far below the elevation of the stream channel, within the Paleozoic-age rocks (fig. 7). Springs that discharge at the base of welded tuffs and pyroclastic rocks downstream of the fault likely form as a result of flow through the volcanic rocks. Some of the water that discharges from the springs may originate in adjacent Cottonwood Creek, as the welded-tuff and pyroclastic-rock units both straddle the drainage between the two streams.

The water table is located in Paleozoic-age rocks until about 6 km downstream of Marigold Mine, where the deep alluvium becomes saturated and the water table is about 50 m below the channel (fig. 7). Depth to ground water gradually decreases to less than 15 m where Trout Creek enters the Humboldt River floodplain. Dewatering of the Lone Tree Mine northwest of Trout Creek (fig. 2), which began in 1992, has lowered the water table beneath Trout Creek by about 20 m at Marigold Mine (as of 2002; fig. 7).

Streamflow and Streambed-Infiltration Rates

Extent and Duration of Streamflow

Trout Creek is generally an intermittent stream. It is perennial only for short reaches where springs discharge into the channel in the upper mountain reach upstream of Oyarbide Fault. The extent and duration of streamflow was determined using stream gages and streambed temperatures.

A. Trout Creek at confluence with North Fork; view is to south

D.E. PRUDIC, U.S. GEOLOGICAL SURVEY

B. Trout Creek on piedmont alluvial plain below Marigold Mine; view is to north

J.L. WOOD, U.S. GEOLOGICAL SURVEY

Figure 5. Typical vegetation along Trout Creek drainage *A,* in the mountains near site 2-T where North Fork joins Trout Creek, and *B*, on piedmont alluvial plain at site 4-ST below Marigold Mine. Locations of sites 2-T and 4-ST are shown in figure 2.

Table 1. Generalized description of geologic units and hydrologic characteristics in vicinity of Trout Creek drainage, north-central Nevada.

	Age	Geologic unit	General hydrologic characteristics
Cenozoic	Quaternary	Qya – Younger alluvium, primarily valley alluvium and stream deposits. Sand and gravel deposits are interbedded with fine-grained deposits.	Sand and gravel aquifers readily yield water to wells.
	Quaternary	Ooa – Older alluvium, primarily alluvial-fan deposits, also includes some upland alluvial deposits and bench deposits. Upper parts of alluvial-fan deposits are incised. Deposits are typically poorly sorted with sand, gravel and small boulders being mixed with fine-grained materials on the upper alluvial-fans. Deposits become finer grained and better sorted on middle and lower parts of the fans. Older alluvium also underlies younger alluvium on valley floor (Cohen, 1963)	Sand and gravel deposits yield water to wells.
	Quaternary	Qtb – Basalt and olivine basalt lava flows, cinder cones, and shallow dikes.	May transmit water through fractures and interflow zones.
	Tertiary	Twt – Welded tuff and pyroclastics.	Welded tuffs have little primary porosity but may transmit water where jointed and fractured.
Cenozoic/ Mesozoic	Tertiary and Cretaceous	TKg – Granodiorite, includes all quartz bearing pre-late-Tertiary intrusive rocks.	Acts primarily as a confining unit but may transmit some water through fractures.
Paleozoic	Pennsylvanian and Permian	PPah – Antler and Havallah Sequences. Consists of Battle Formation, Middle Pennsylvanian conglomerate, minor sandstone, shale, and limestone; Antler Peak Limestone, Upper Pennsylvanian limestone and shaley limestone; and Edna Mountain Formation, Upper Permain calcareous sandstone with conglomerate and limestone. Havallah Formation, Middle Pennsylvanian and Lower Permain; shale, sandstone (or quartzite), chert, limestone, and conglomerate and Pumpernickel Formation, Pennsylvanian (?) chert, shale, and greenstone	May transmit some water if highly fractured.
	Ordovician	Ov – Valmy Formation, dark gray, black, green, and red chert, vitreous quartzite, and subordinate greenstone pillow lavas and shale.	Primarily acts as a confining unit but may transmit some water through fractures.
	Cambrian	Chsc – Consists of Harmony Formation, micaceous sandstone, arkose, shale, and subordinate calcareous shale and limestone; and Scott Canyon Formation, chert, shale, and argillite, subordinate greenstone flows, pillow lavas and pyroclastic rocks.	Primarily acts as a confining unit but may transmit some water through fractures.

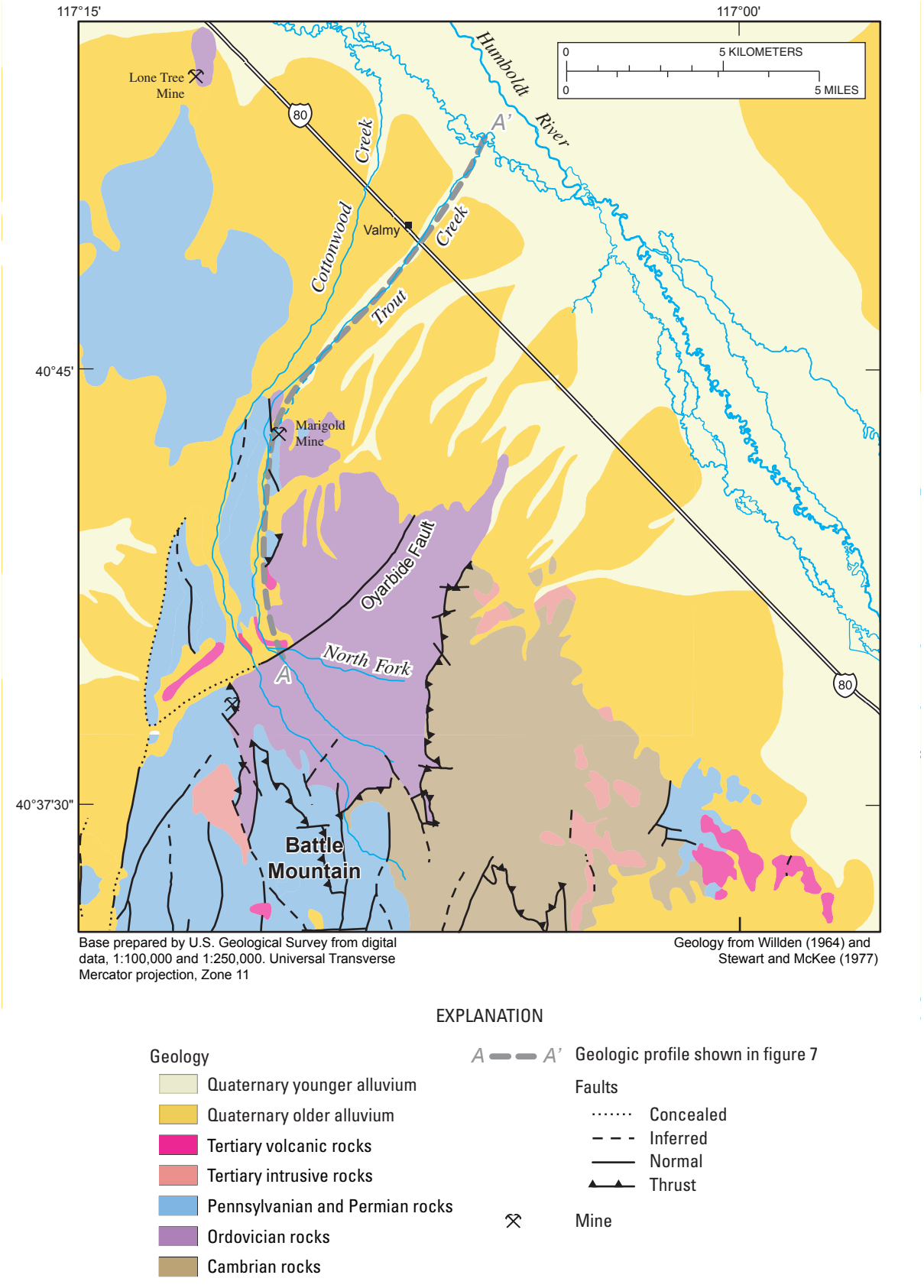

Figure 6. Geology in the vicinity of Trout Creek drainage, north-central Nevada. Geology modified from Willden (1964) and Stewart and McKee (1977).

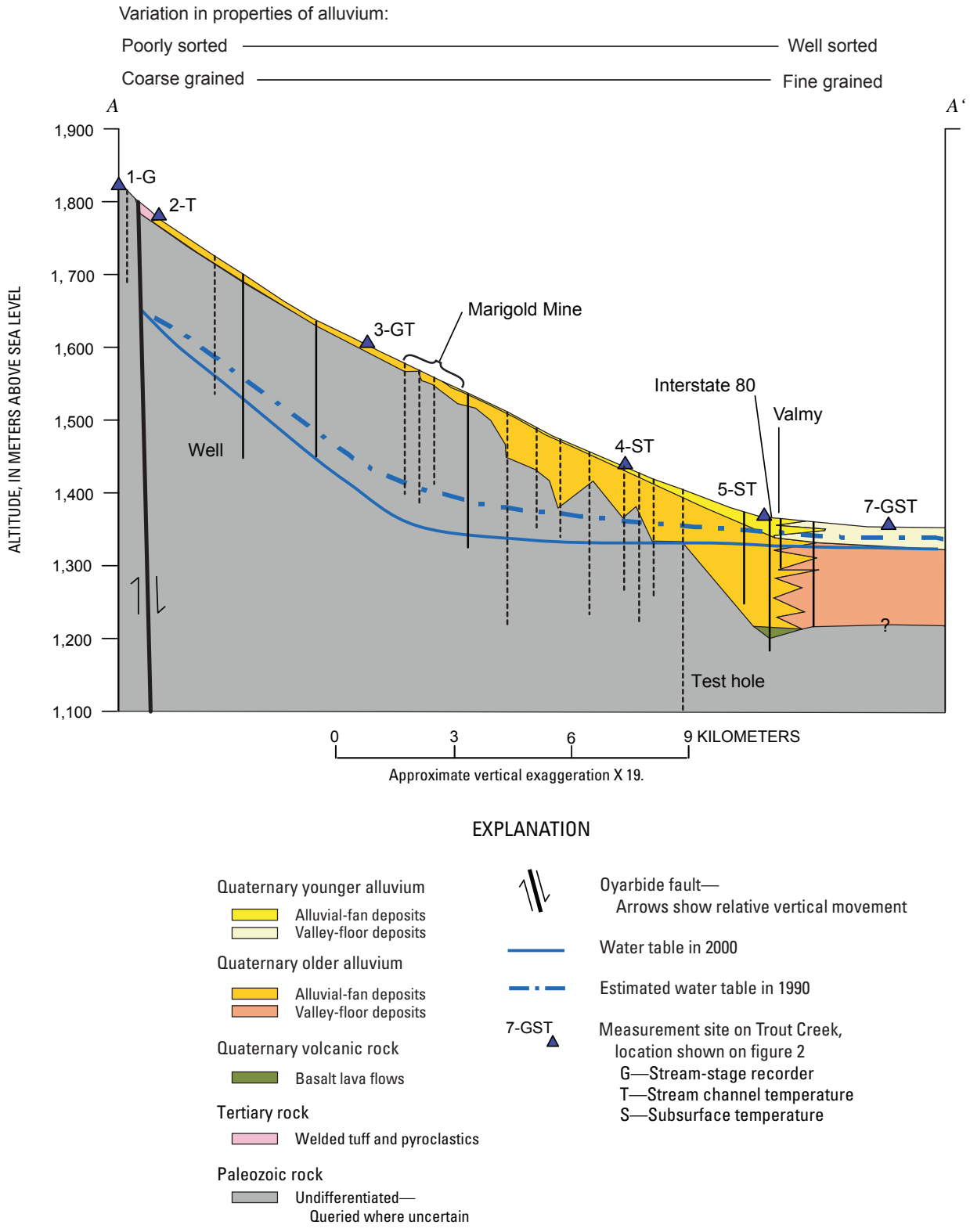

Figure 7. Geologic profile along Trout Creek, north-central Nevada (modified from Prudic and others, 2003). Geologic information is from test holes and wells drilled near Trout Creek (Glamis Gold Mining Company, Valmy, Nev., written commun., 2002 and Nevada State Engineers Office, Carson City, Nev., written commun., 2002). Water-level data are from Glamis Gold Mining Company, Nevada State Engineers Office, Newmont Mining Corporation (Winnemucca, Nev., written commun., 2002), and U.S. Geological Survey. Location of profile is shown in figure 6.

Stream Gages

A stream gage was installed at site 1-G (fig. 2) in October 1999 by Newmont Mining Corporation. Additional gages were installed as part of this project at sites 3-GT and 7-GST in March 2000 and November 1999, respectively (fig. 2). The stream gage at site 1-G was operated and maintained by personnel from Newmont Mining Corporation. Stream gages at sites 3-GT and 7-GST were operated and maintained by USGS personnel. Stage was measured every 15 minutes at site 1-G and every 30 minutes at sites 3-GT and 7-GST, using recording pressure transducers. Relationships between stage and discharge were determined on the basis of periodic discharge measurements at sites 1-G and 3-GST. A square-notch weir was installed at site 7-GST, but no streamflow was recorded at the site from November 1999 through October 2002, although streamflow had been observed at the site in April and May 1999.

Streamflow from October 1999 through September 2002 was intermittent at sites 1-G and 3-GT, with more-persistent flows at site 1-G (fig. 8). Streamflow duration at both sites was less in 2001 and 2002 as compared with 2000 because of lower than normal precipitation. Peak discharges at site 3-GT during 2000 and 2002 lagged behind the corresponding peak discharges at site 1-G such that the daily mean discharge at site 3-GT occasionally exceeded that at site 1-G. The occasional higher discharges at site 3-GT could result from intermittent flow in North Fork and from increased discharge from springs at the base of the volcanic rocks near the confluence of Trout Creek with North Fork.

The estimated annual volume of runoff at site 1-G was 5.5×10^5 m^3, 1.3×10^5 m^3, and 1.8×10^5 m^3 for water years 2000–2002, respectively. These estimated volumes are approximate because the relation between stage and discharge is poor. The estimated volume of runoff from site 3-GT was 2.1×10^5 m^3 and 1.2×10^5 m^3 for water years 2000 and 2002, respectively. No estimate of runoff was made for water year 2001 because the recording pressure transducer failed during much of the runoff period. The smaller runoff at site 3-GT compared to site 1-G is caused by streambed infiltration downstream of the fault, particularly during low-flow periods when spring discharge upstream of site 1-G maintained streamflow at the gage that was insufficient to reach site 3-GT. During low-flow periods, discharge at the spring near site 2-T was reduced to a small seep.

Streambed Temperature as Indicator of Streamflow

Streambed temperatures were used to estimate the duration of streamflow at selected locations on Trout Creek including four locations that were not instrumented with pressure transducers. Self-contained temperature loggers (Stonestrom and Blasch, 2003, p. 75) were placed at seven sites, one of which was outside the channel for reference (fig. 2). The intent of the temperature loggers was to inexpensively obtain additional information on the duration of flow along Trout Creek. Initially, temperature loggers were placed in polyvinyl chloride (PVC) housings directly on the streambed. This resulted in excessive heating during the summer. Subsequently, in March 2000, temperature loggers were buried about 7 cm below the channel or land surface.

Although streambed temperatures were generally reliable in estimating the onset of flow along Trout Creek, it was not always easy to estimate the cessation of flow. Considerable interpretation was needed to estimate the duration of streamflow from streambed temperatures alone (Prudic and others 2003). The analysis was complicated by the changing character of the temperature offset (streambed temperature minus flowing-water temperature) at the onset of flow, which generally was continuous, compared to the cessation of flow, which involved daily periods of intermittent streamflow.

An analysis of streambed temperatures at the onset of flow in March 2000 at site 3-GT was compared with available pressure-transducer data and with streambed temperature at site 2-T, where flow was continuous during the periods of intermittent flow at site 3-GT (fig. 9*A*). Minimum nightly temperatures at site 3-GT during mid-March routinely dropped below freezing, whereas the temperature of the streambed in a reach at site 2-T (upstream from 3-GT) remained above freezing. If flowing water was in the channel at site 3-GT, minimum temperatures during mid-March would also have been at or above freezing. Minimum temperatures at site 3-GT became constant at 0 °C during the early morning hours of March 22, 2000, marking the onset of flow. Once flow began, minimum temperatures at site 3-GT generally mimicked those at the upstream site 2-T. Freezing conditions in the channel during the early morning hours on March 30 and 31, 2000 were accompanied by large apparent increases in stream stage recorded by the pressure transducer installed on March 29, 2000. The large apparent increases in stream stage were an artifact of water freezing in the instrument and do not reflect streamflow (fig. 9*A*).

The minimum streambed temperatures at site 3-GT were higher than at site 2-T prior to the onset flow on April 3, 2001 at site 3-GT (fig. 9*B*), which differs from the lower minimum temperatures prior to flow in March 2000. A marked increase in stream stage was recorded at 10:30 a.m. Pacific Standard Time (PST) on April 3, 2001 during a period of above freezing temperatures. Streamflow continued until early afternoon on April 3, 2001 when the stream stage at the transducer decreased to zero. Negative pressures developed as water evaporated from the protective screen. This pattern of intermittent flow was repeated daily until April 7, 2001 when the water temperature dropped to 0 °C. High pressures caused by freezing water in the transducer caused it to fail. Minimum temperatures at site 3-GT became lower than those at site 2-T after the onset of intermittent flow and continued to be lower until April 16, 2001 when the pattern of minimum temperatures mimicked those at site 2-T. Flow was continuous after April 16. When flow became continuous is not precisely known.

The cessation of streamflow at site 3-GT was also difficult to assess from temperature data alone because of daily periods of intermittent streamflow. Streamflow at site 3-GT became intermittent in the afternoon of June 4, 2000 as indicated by the pressure transducer readings, which resulted in a slight deflection in the temperature profile (fig. 10*A*). However, the minimum temperatures during these periods of no streamflow remained similar to those at site 2-T because of residual moisture in the sediments following the period of daily streamflow. The onset of flow on June 5, 2000 also resulted in a slight increase in temperature during the morning hours, although it is not as pronounced as when flow ceased. The slight changes in temperature associated with the onset and cessation of flow on the basis of the pressure transducer readings from June 4 through June 6, 2000 were used to evaluate intermittent flow from June 7 to June 17, 2000 (fig. 10*B*) during the period without data from the pressure transducer. The onset of flow in the morning generally resulted in a subtle increase in the streambed temperature whereas the cessation of flow generally resulted in a marked decrease in the slope of the streambed temperature. Although the precise timing of intermittent flow each day is uncertain, streambed temperatures suggest that intermittent flow continued daily through June 13. Afterwards the streambed dried sufficiently that minimum temperatures at site 3-GT were consistently higher than those at site 2-T, where flow was continuous.

Duration of streamflow also was estimated at three locations using nested thermocouple wires placed at 5 depths between 10 and 150 cm beneath the channel (sites 4-ST, 5-ST, and 7-GST; fig. 2; Prudic and others, 2003). Temperatures from the thermocouple wires were measured every 30 minutes using dataloggers. During streamflow, heat in the stream is advected downward as water infiltrates into the stream channel. Streamflow in Trout Creek reached site 4-ST in April 2000 and again in April 2002, based on subsurface temperatures. No streamflow was observed throughout the study at sites 5-ST or 7-GST. Streambed temperatures generally showed a consistent diurnal pattern in maximum and minimum temperatures prior to the onset of streamflow at site 4-ST on April 9, 2000 (fig. 11*A*), whereas temperatures began to fluctuate in response to temperature in the stream after the onset of streamflow.

Although all temperatures in the subsurface beneath site 4-ST responded to periods of streamflow, temperatures

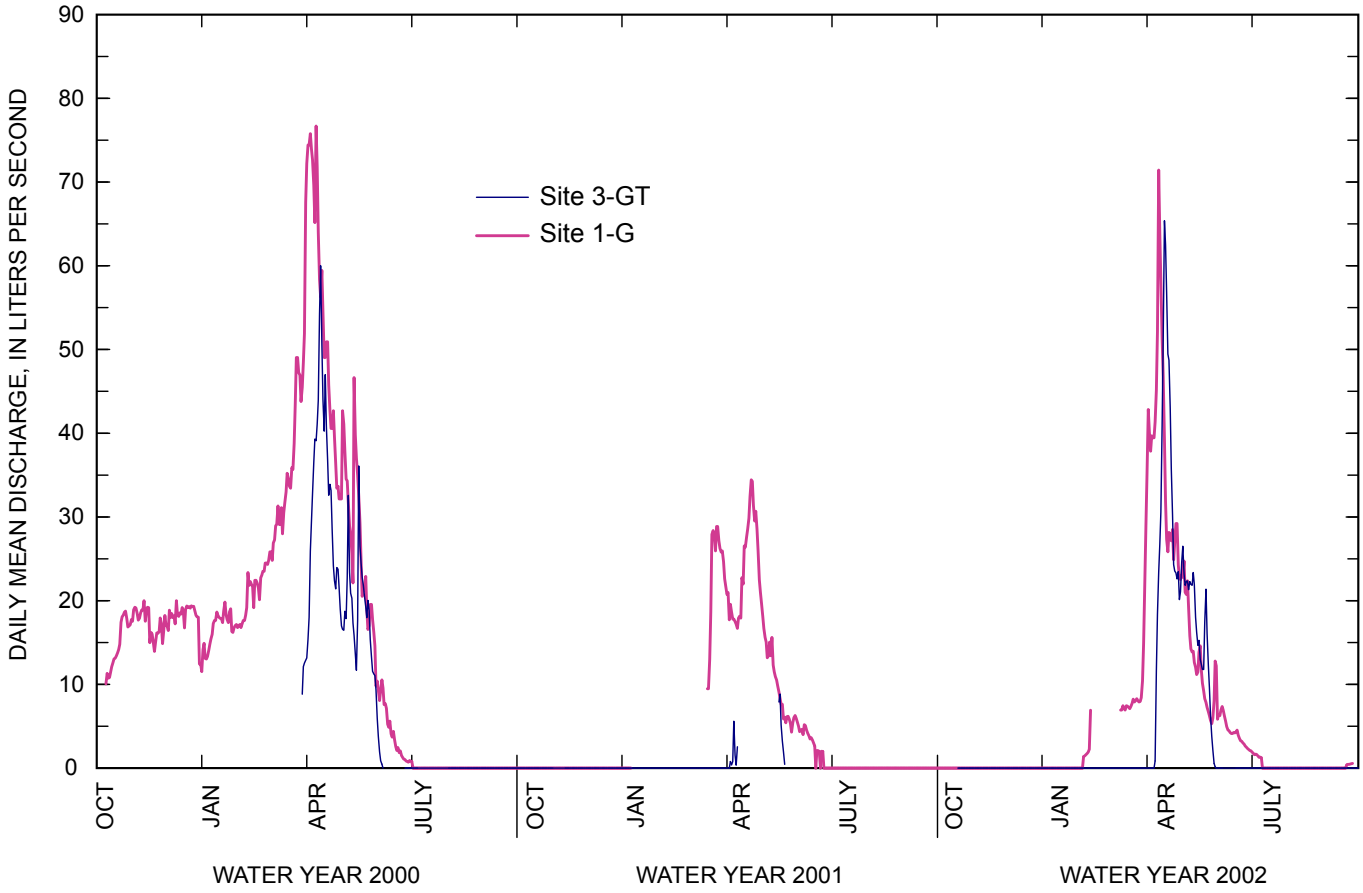

Figure 8. Daily mean discharge at sites 1-G and 3-GT on Trout Creek during water years 2000 through 2002. Daily mean discharge estimated from pressure measurements recorded every 15 minutes at site 1-G and every 30 minutes at 3-GT. Data at site 1-G is from Newmont Mining Corporation (Winnemucca, NV, written commun., 2002). Location of sites is shown in figure 2.

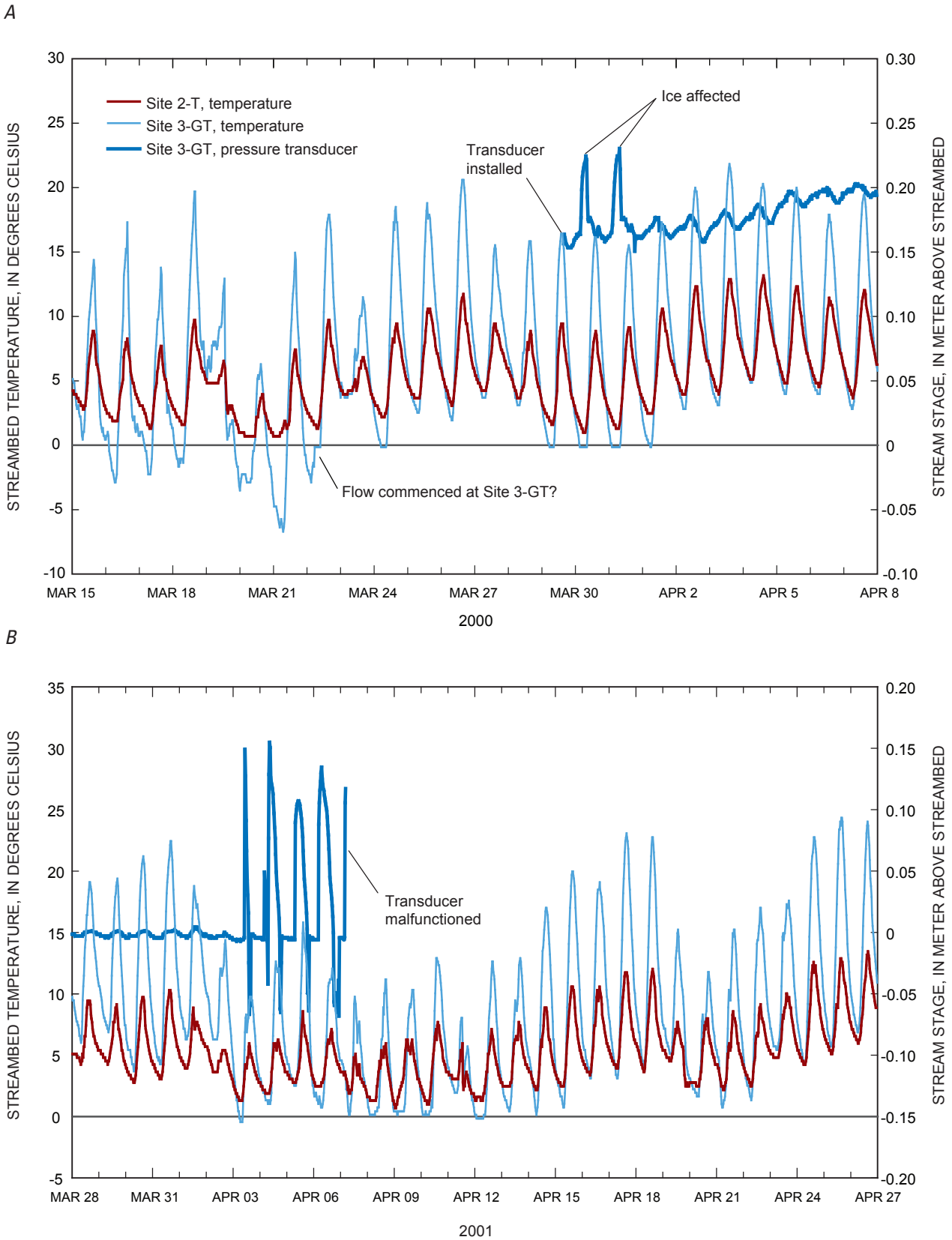

Figure 9. Commencement of streamflow at site 3-GT evaluated using stream stage measured by a pressure transducer and streambed temperatures at sites 2-T and 3-GT in *A,* March 2000 and *B,* April 2001. Location of sites 2-T and 3-GT is shown in figure 2.

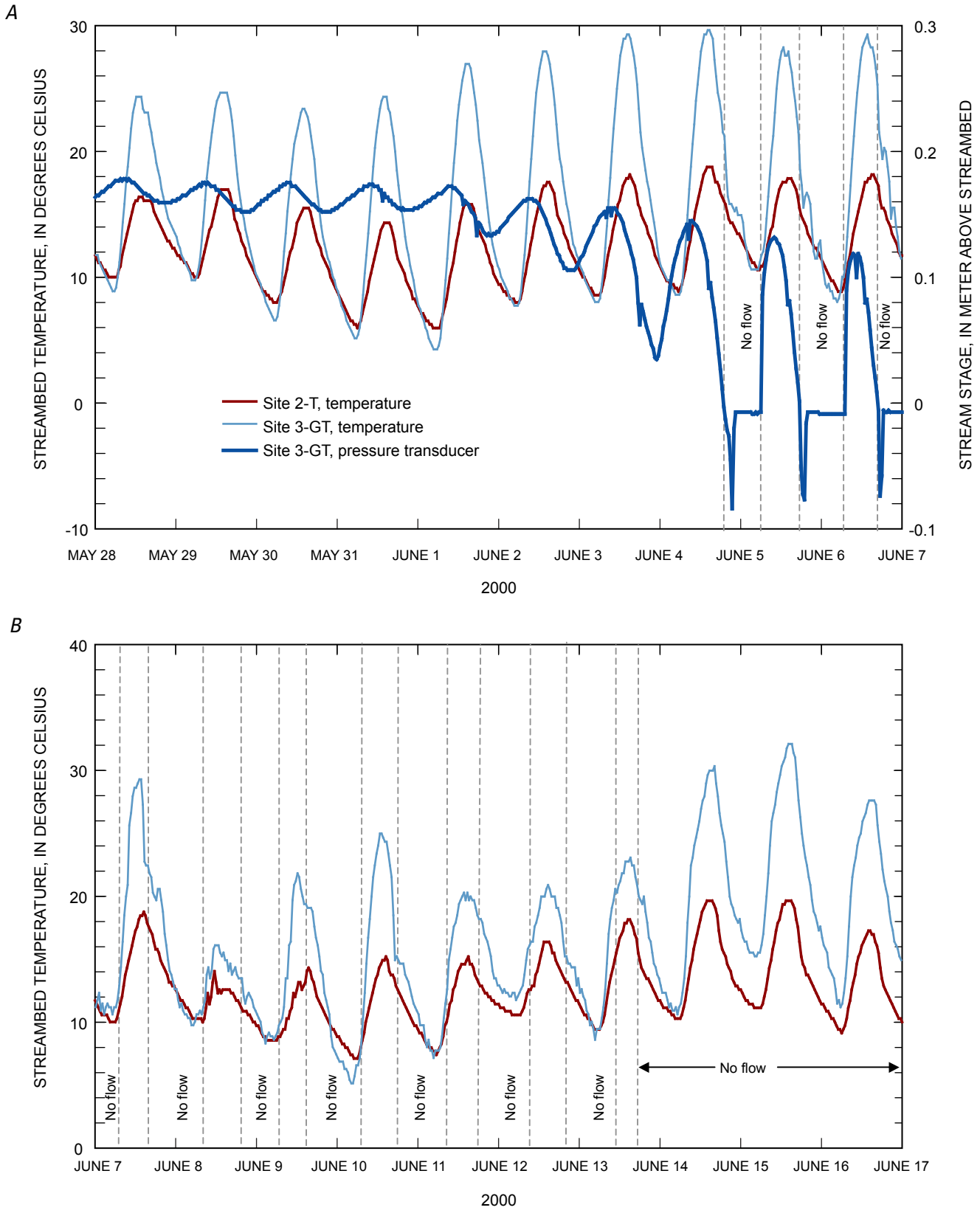

Figure 10. Cessation of streamflow at site 3-GT evaluated using *A*, streambed temperature at sites 2-T and 3-GT and stream stage from pressure transducer at site 3-GT during first week of June 2000, and *B*, estimates of periods of no flow from streambed temperature during second week of June 2000. Location of sites 2-T and 3-GT is shown in figure 2.

between depths of 20 and 138 cm were used to assess general periods of intermittent or discontinuous flow in the channel because changes in air temperature (caused by clouds and rain) affected the response of the shallowest thermocouple. When flow became intermittent is uncertain because gravity drainage continued through the sediments after flow ceased in the channel. However, diurnal fluctuations at depths of 100 and 138 cm decreased noticeably after April 27, 2000, suggesting streambed infiltration had ceased prior to this date. Temperature fluctuations increased again on May 1, which may indicate intermittent streamflow on that date.

The duration of streamflow was also estimated at site 4-ST from subsurface temperatures for 2002. The subsurface temperature data in 2002 were affected by the heating of the data logger inside of its shelter, which caused the temperature readings to have an additional, but spurious, diurnal signal at all depths due to the transient offset between the temperature of the wiring panel and the data-logger's internal thermocouple reference temperature (Stonestrom and Blasch, 2003, p. 77-79). The signal was removed by fitting polynomial equations to the temperature at a depth of 138 cm during the early morning hours (4:30 to 6:30 PST), when temperatures were near their minimums. The removal of the natural diurnal signal at the depth of 138 cm also removed the diurnal signal at the 100 m depth but did not greatly affect the diurnal signals at the shallower depths (fig. 11*B*). The overall effect of removing the signal from heating of the datalogger inside its shelter was to reduce the sensitivity of the subsurface temperature to changes in stream temperatures. Thus, the data in 2002 was used only to estimate the duration of flow.

Streamflow began April 14 and continued until April 23 on the basis of sudden decreases in the surface and subsurface temperatures. Another brief period from May 1 to May 3 may have been a period of intermittent streamflow. Estimating brief periods of discontinuous streamflow or the exact moment when streamflow in the channel ceases entirely is difficult using subsurface temperature profiles because drainage through the sediments beneath the streambed continues for some time after streamflow ceases.

No streamflow was observed at sites 5-ST, 6-T, and 7-GST during water years 2000–2002. However, streamflow was observed and measured along the entire channel during May 1999. Streamflow extended past site 7-GST during an initial reconnaissance on April 28, 1999. Discharge measurements were made along the channel from site 2-T to 7-GST on May 12, 1999, and self-contained temperature loggers were placed in the channel on May 13, 1999. Streamflow remained continuous at the uppermost temperature site (2-T) from May to October 1999, but further downstream, streamflow was intermittent at sites 3-GT, 4-ST, 5-ST, 6-T, and 7-GST.

The minimum-daily streambed temperatures at all sites generally followed the same pattern as that at site 2-T during May 1999, although the minimum-daily temperature increased downstream. This pattern continued until June 11, 1999 when the minimum-daily temperature at site 7-GST began to deviate markedly from the minimum-daily temperature of the upstream sites, and was followed by similar deviations at sites 6-T, 5-ST, 4-ST, and 3-GT. The deviation of the minimum-daily temperature was used to indicate when flow ceased at each site (fig. 12). The rapid rate of retreat of streamflow between sites 7-GST and 5-ST, in about 2 days, as compared with the rate between sites 5-ST and 4-ST and between sites 4-ST and 3-GT (both in about 8 days) suggests that streambed-infiltration rates are higher downstream of site 5-ST (Interstate 80). The more rapid retreat downstream of site 5-ST also is consistent with a marked increase in streambed infiltration rates estimated from discharge measurements on May 12, 1999, as discussed in the following section. Estimates of the duration of streamflow at the different sites are summarized in table 2. The duration of streamflow lasted longer at sites 1-G and 2-T than further downstream.

Streambed-Infiltration rates

Streambed-infiltration rates were estimated by subtracting discharge measurements between selected reaches of the channel and from subsurface temperatures at site 4-ST. Discharge measurements were made at all sites on May 12, 1999; at sites 2-T, 3-GT, and 4-ST on April 13, 2000; and at sites 3-GT and 4-ST on April 19, 2000 and May 11, 2000. Measurements of streamflow during 2001 and 2002 were limited to sites 1-G, 2-T, and 3-GT because streamflow was insufficient to reach the lower sites.

Estimates from Discharge Measurements

Discharge measurements for May 12, 1999, and April 13, April 19, and May 11, 2000 are plotted in relation to the distance downstream of site 1-G (fig. 13). The discharge measurements that were made on May 12, 1999 were during a period when there had been sustained flow in the channel for at least 2 weeks prior to the measurement and flow continued along the channel for several weeks following the measurement (table 2). Similarly, flow commenced at site 3-GT on March 22, 2000 and from the pressure transducer, flow peaked near the discharge measurement on April 13, 2000, and declined through the measurements on April 19, and May 11, 2000.

Discharge measurements for May 12, 1999 show a slight increase in streamflow between site 2-T and site 3-GT because of tributary inflow from North Fork of Trout Creek and from a spring immediately downstream of site 2-T. Stream discharge decreases proportionately with distance downstream of site 3-GT for all dates until site 5-ST. Discharge decreased dramatically downstream of site 5-ST on May 12, 1999, indicating a substantial increase in the streambed-infiltration rate at the foot of the piedmont alluvial plain. Estimated uncertainty in the discharge measurements are about 5 percent for measured discharges exceeding 100 L/s, 8 percent for discharges between 50 and 100 L/s and 10 percent for discharges less than 50 L/s.

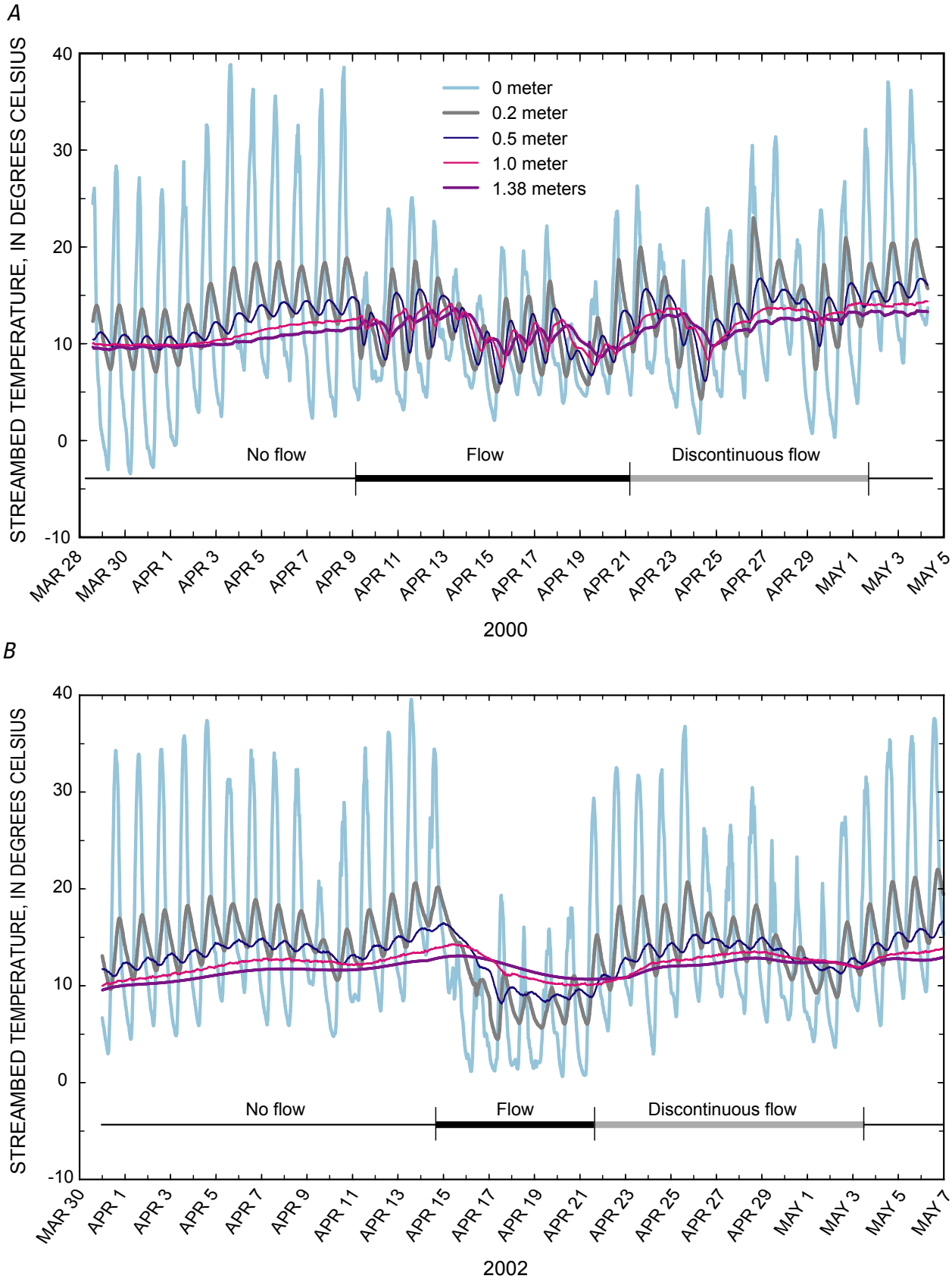

Figure 11. Streamflow duration estimated from subsurface temperatures beneath streambed at site 4-ST for *A*, April-May 2000 and *B*, April-May 2002. Location of site 4-ST is shown in figure 2.

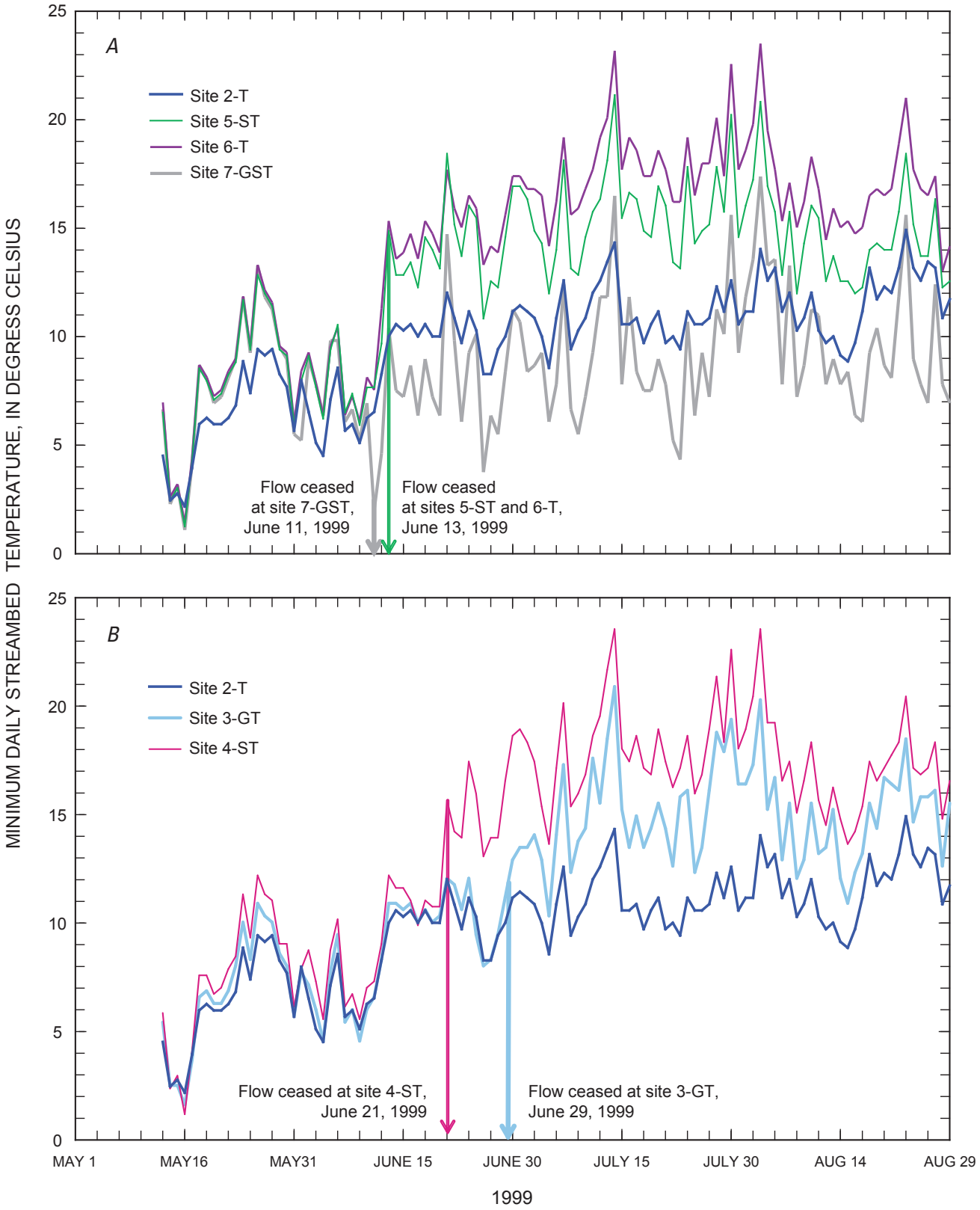

Figure 12. Estimates of flow cessation along Trout Creek between sites 2-T and 7-GST from May 13, 1999 to August 29, 1999 determined from daily minimum streambed temperatures. Flow was continuous at site 2-T through September 30, 1999. Self-contained temperature loggers in Trout Creek were placed on streambed in polyvinyl chloride (PVC) housing attached to a cable secured to a metal stake. Location of sites is shown in figure 2.

Table 2. Estimates of streamflow duration at selected locations along Trout Creek from May 1999 to October 2002, north-central Nevada.

[Site locations are shown in figure 2. Letters following site numbers denote: G, recording pressure transducer (stream gage); T, surface-temperature logger; S, subsurface-temperature logger. Other abbreviations: <, less than; (?), uncertain. Flow durations may include brief periods of intermittent flow]

Sites	Water Year			
	[1] 1999	[2] 2000	[3] 2001	[4] 2002
1-G	(?)	Oct. 1 – July 7	Mar. 20 – June 29	Sept. 30 – July 12
2-T	<Apr. 28 – Sept. 30	Oct. 1 – July 20(?)	Mar. 20 – June 27	(?) – July 10
3-GT	<Apr. 28 – June 29	Mar. 22 – June 14	Apr. 5 – May 23	Apr. 7 – May 29
4-ST	<Apr. 28 – June 21	Apr. 9 – May 19	No flow	Apr. 14 – Apr. 23 May 1 – May 3
5-ST	<Apr. 28 – June 13	No flow	No flow	No flow
6-T	<Apr. 28 – June 13	No flow	No flow	No flow
7-GST	<Apr. 28 – June 11	No flow	No flow	No flow

[1] Duration for water year 1999 was compiled from an initial reconnaissance on April 28 and from minimum daily temperatures from surface-temperature loggers installed May 13.

[2] Pressure transducer at 1-G installed October 13, 1999, by Newmont Mining Corporation. Flow duration during October 1–October 13 was estimated from surface-temperature logger at site 2-T. Although flow ceased at site 1-G on July 7, water remained ponded at gage for several days. End of flow at site 2-T is difficult to determine because streambed at logger was shaded by willows. Flow at site 4-ST was intermittent during the period between April 20 and May 19.

[3] Surface-temperature and subsurface-temperature loggers malfunctioned at site 4-ST during April and May 2001. Neutron-moisture measurements indicate flow did not reach site 4-ST during the period of missing record.

[4] No data from surface-temperature logger at site 2-T from October 1, 2001 to June 4, 2002.

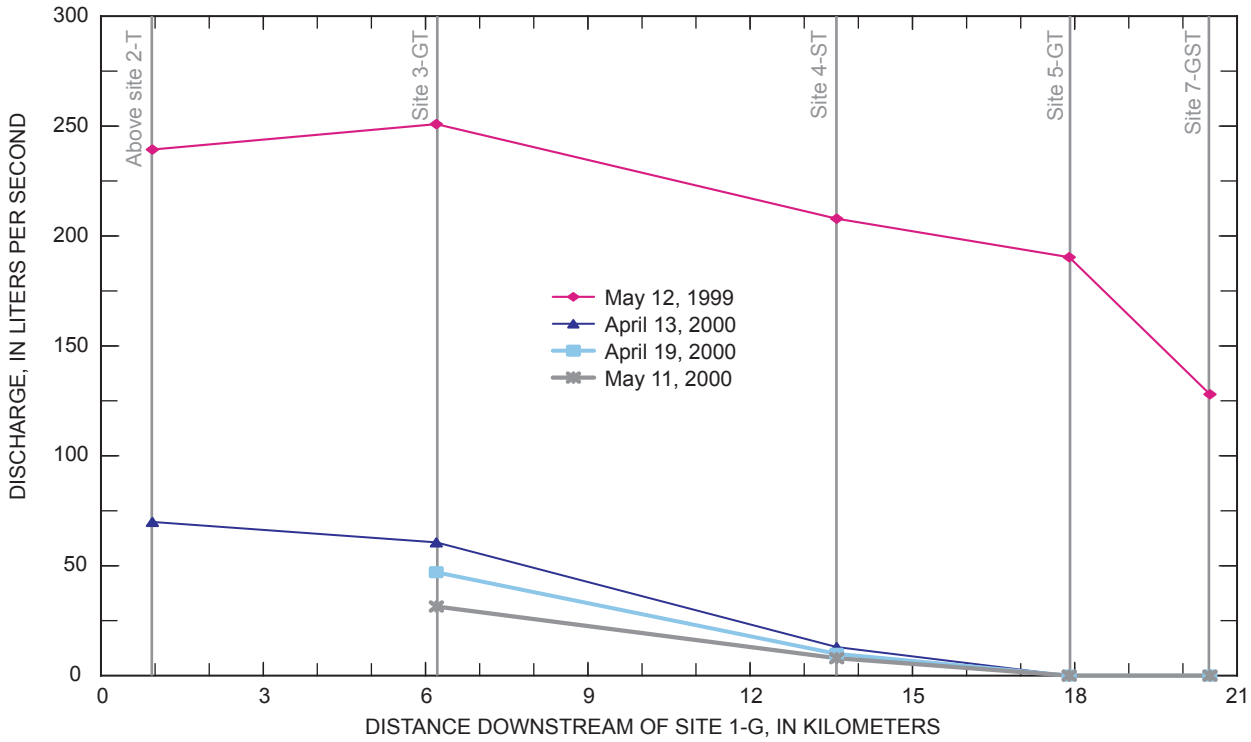

Figure 13. Measured discharge along Trout Creek on May 12, 1999; April 13 and 19, 2000; and May, 11, 2000. Measurements were made between 7:30 a.m. and 12:00 pm on May 12, 1999; 7:00 a.m. and 9:00 a.m. on April 13, 2000; 12:45 pm and 1:45 pm on April 19, 2000; and 10:00 a.m. and 11:30 a.m. on May 11, 2000. All times are Pacific Standard Time and measurements were made starting at upstream site except on May 11, 2000 when measurements started at downstream site. Location of sites is shown in figure 2.

Streambed-infiltration rates (volumetric flow per unit area) were estimated for stream reaches downstream of site 3-GT because of unknown contributions to the channel between sites 2-T and 3-GT. The estimates were made by dividing the measured loss with the streambed area. Streambed area was estimated by multiplying the channel length between sites with the average stream width (table 3). The average stream width was estimated as the average stream width measured at the sites because channel cross sections do not vary greatly between sites 3-GT and 7-GST (Niswonger and others, 2005). Loss rates in percent of flow at the upstream site are summarized in table 3. Although loss rates between sites 3-GT and 5-ST were similar for all dates, the loss rate in percent of flow at the upstream site for May 12, 1999 was less than those for the three measurements made in April and May, 2000 because of the much higher discharges. The percent of flow loss between sites exceeded the estimated uncertainty in discharge measurements except between sites 4-ST and 5-ST on May 12, 1999 where the loss was about the same as the sum of the uncertainty in the two measurements.

The streambed-infiltration rate on May 12, 1999 was estimated between 0.1 and 0.2 m/d upstream of site 5-ST, whereas it increased nearly an order of magnitude to 1.1 m/d downstream. The streambed-infiltration rate between sites 3-GT and 4-ST was about 0.46 m/d on April 13, 2000 near the peak discharge period and decreased to 0.22 m/d on May 11, 2000 (table 3). This decrease in the streambed-infiltration rate may result from errors in the measured discharges, which were estimated to be about 10 percent of the measured discharge or in the estimate of the average stream width. Streambed-infiltration rates can also be affected by the natural diurnal variation in streamflow along the channel, which is more pronounced during periods of less streamflow. Additionally, accumulation of fines on the streambed during flow recession can also reduce infiltration rates (Burkham, 1970). Even though the streambed-infiltration rate estimated on May 11, 2000 was similar to that estimated for May 12, 1999, uncertainty in the streambed-infiltration rates make it difficult to assess if the decrease in rates estimated during 2000 are real or the result of measurement errors.

The much greater streambed-infiltration rate along the lower reach of the piedmont alluvial plain (downstream of site 5-ST) was not initially anticipated because finer-grained sediment is normally deposited after the break in slope on alluvial fans and piedmont alluvial plains, and coarse-grained sediment is normally associated with the upper, steeper parts (Rachocki, 1981). Greater distal streambed-infiltration rates also were observed during the spring of 2004 (Niswonger and others, 2005). Two factors are likely responsible for the increased streambed-infiltration rates in the lower reaches of the channel. First, the streambed along the upper reach of the piedmont alluvial plain is armored with large quartzite cobbles (up to 15 cm in diameter), whereas the lower reach is primarily sand and gravel (up of 2 cm in diameter). The space between the larger cobbles is generally filled with fine-grained materials (sand and silt) through which infiltration occurs. Because the large cobbles are impermeable, the effective area for infiltration is less in the upper reach than in the lower reach. Second, the deposits in the upper reach are less sorted and more heterogeneous than those on the lower reach. Poorly sorted heterogeneous deposits generally have a lower effective hydraulic conductivity than better sorted and more homogeneous deposits. This implies that greater streambed-infiltration rates could occur near the base of the alluvial fans or piedmont alluvial plains in many areas of the desert Southwest.

Estimates From Subsurface Temperature Profiles

Streambed-infiltration rate from subsurface temperature profiles was estimated at site 4-ST on April 13 through April 19, 2000, several days after the commencement of streamflow. Estimates were not made at the other temperature sites 5-ST and 7-GST because no streamflow occurred at these locations. A two-dimensional, variably saturated, water-flow and heat-transport model developed by Healy and Ronan (1996) was used in the analysis, as described in Niswonger (2001) and Niswonger and Prudic (2003). The modeled region included no-flow vertical boundaries located 15 m on either side of the channel, a specified stream depth and temperature within channel, and a constant-elevation water table (zero matric pressure) and temperature (17 °C) at a depth of about 30 m. The bottom boundary conditions were based on measurements in well MPS-18-1 (fig. 2). The lateral boundaries were extended 15 m beyond the channel so as not to inhibit lateral ground-water flow. Thermal and hydraulic properties used in the model are listed in table 4.

Hydraulic conductivity was adjusted until the modeled temperature at depths of 20 and 50 cm approximated the measured temperatures. The best-fit simulation to the measured temperatures at depths of 20 and 50 cm (fig. 14) resulted in the simulated peak arrival times that were consistently earlier than measured, however decreasing the arrival time in the model resulted in a worse fit to the diurnal amplitude. The resultant streambed-infiltration rate was 0.46 m/d and the saturated streambed hydraulic conductivity was 0.56 m/d (Niswonger, 2001; and Prudic and others, 2003). This streambed-infiltration rate is the same as that estimated from discharge measurements on April 13, 2000 (table 3).

Uncertainty in the estimate of the rate of streambed infiltration was analyzed using a Monte Carlo technique (Niswonger and Rupp, 2000). An analysis was done to evaluate the error in sediment thermal properties on the predicted streambed-infiltration rate. Thermal conductivity of the sediment was assumed normally distributed with a mean and standard deviation of 2.3 and 0.63 W/m °C, respectively. The volumetric heat capacity of the dry sediments also was assumed normally distributed with a mean and standard deviation of 2.6×10^6 and 0.21×10^6 J/m^3 °C, respectively. The mean for the volumetric heat capacity differed from the manually calibrated value listed in table 4 because the Monte Carlo technique included the effects of correlation with the thermal conductivity (Niswonger and Rupp, 2000). The standard deviation of

Table 3. Estimates of streambed-infiltration rates from discharge measurements along Trout Creek between May 1999 and May 2000, north-central Nevada.

[Site locations are shown in figure 2. Letters following site numbers denote: G, recording pressure transducer (stream gage); T, surface-temperature logger; S, subsurface-temperature logger. Multiple instruments were deployed at most sites. All values are rounded to two significant figures. Abbreviations: m, meters; L/s, liters per second; %, percent; m^3/m^2 d, cubic meters per square meter per day; —, flow did not reach downstream site]

Selected reach		Channel length, in m	Streamflow loss,		[1] Average channel width, in m	[2] Streambed infiltration rate, in m^3/m^2 d
Upstream site	Downstream site		in L/s	in % of flow		
May 12, 1999						
3-GT	4-ST	7,400	43	17	2.7	0.19
4-ST	5-ST	4,300	18	8	2.7	0.13
5-ST	7-GST	2,600	62	32	2.0	1.1
April 13, 2000						
3-GT	4-ST	7,400	47	79	1.2	0.46
4-ST	5-ST	—	13	100	—	—
April 19, 2000						
3-GT	4-ST	7,400	37	79	1.3	0.33
4-ST	5-ST	—	10	100	—	—
May 11, 2000						
3-GT	4-ST	7,400	24	75	1.3	0.22
4-ST	5-ST	—	8	100	—	—

[1] Average width for each reach was estimated as the average width of the upstream and downstream measurement site. Channel cross sections vary little between sites 3-GT and 7-GST (Niswonger and others, 2005).

[2] Streambed infiltration rate was estimated first by multiplying the loss (in liters per second) between sites with the product of 1,000 liters per cubic meter and 86,400 seconds per day to obtain cubic meters per day, and then by dividing the loss in cubic meters per day with the product of the channel length and average width to obtain a volumetric streambed infiltration rate per unit area of channel.

Table 4. Unsaturated zone properties used to determine hydraulic conductivity and streambed-infiltration rate from subsurface temperatures at site 4-ST during April 2000 (Niswonger, 2001; and Niswonger and others, 2005).

[Thermal dispersivity assumed analogous to solute dispersivity. Abbreviations: m, meters; J/m^3 ºC, joules per cubic meter per degree Celsius; W/mºC, watts per square meter per degree Celsius per meter]

Unsaturated property	Value	Source
van Genuchten/Mualem alpha, in m^{-1}	0.847	Kosugi and others (2002)
van Genuchten/Mualem *n* (dimensionless)	4.8	Kosugi and others (2002)
Residual water content, in m^3/m^3	0.072	Kosugi and others (2002)
Porosity, in m^3/m^3	0.36	Core samples
Dispersivity, in m	0.1	Fetter (1993)
Volumetric heat capacity of dry sediment, in J/m^3 ºC	2.0×10^6	Stonestrom and Blasch (2003)
Thermal conductivity of sediment at residual water content, in W/mºC	1.4	Hopmans and Dane (1986)
Thermal conductivity of sediment at saturation, in W/mºC	2.3	Stonestrom and Blasch (2003)

the streambed-infiltration rate converged to a value of 0.12 m/d after 180 realizations. The ninety-five percent confidence interval in the predicted streambed-infiltration rate was ±0.24 m/d or about half the estimated rate.

A similar analysis tested the temperature-measurement error on the predicted streambed-infiltration rate. The normal distribution of temperature error was estimated on the basis of manufacturer specifications and from instrument installation. The mean and standard deviations for the temperature-measurement error were 0 and 0.2 °C, respectively (Niswonger and Rupp, 2000). The ninety-five percent confidence interval in the predicted streambed-infiltration rate was only ±0.07 m/d indicating the greatest error was caused by uncertainty in the sediment thermal properties. These analyses suggest that estimates of streambed-infiltration rates from subsurface temperature profiles may have errors similar in magnitude as those from discharge measurements. Finally, extrapolation of streambed-infiltration rates from subsurface temperature profiles may be difficult where hydraulic conductivity is variable along the channel.

Modeling Streambed Infiltration Along Trout Creek

This section briefly summarizes the development of and results from a numerical model that was used to simulate streamflow losses along Trout Creek from streambed infiltration. Additional details are given in Niswonger (2001) and Niswonger and others (2005). The model was used to estimate the duration of flow and volumes of infiltration along the channel in water years 2000 and 2002. The underlying approach could be used for any stream that is separated from the underlying ground water by an unsaturated zone. The minimum requirements for simulating duration of streamflow and quantity of streambed infiltration with the model include data on: (1) streamflow at the mountain front, (2) channel length and cross sectional areas, (3) streambed-infiltration rates in relation to stream stage, and (4) streambed hydraulic properties.

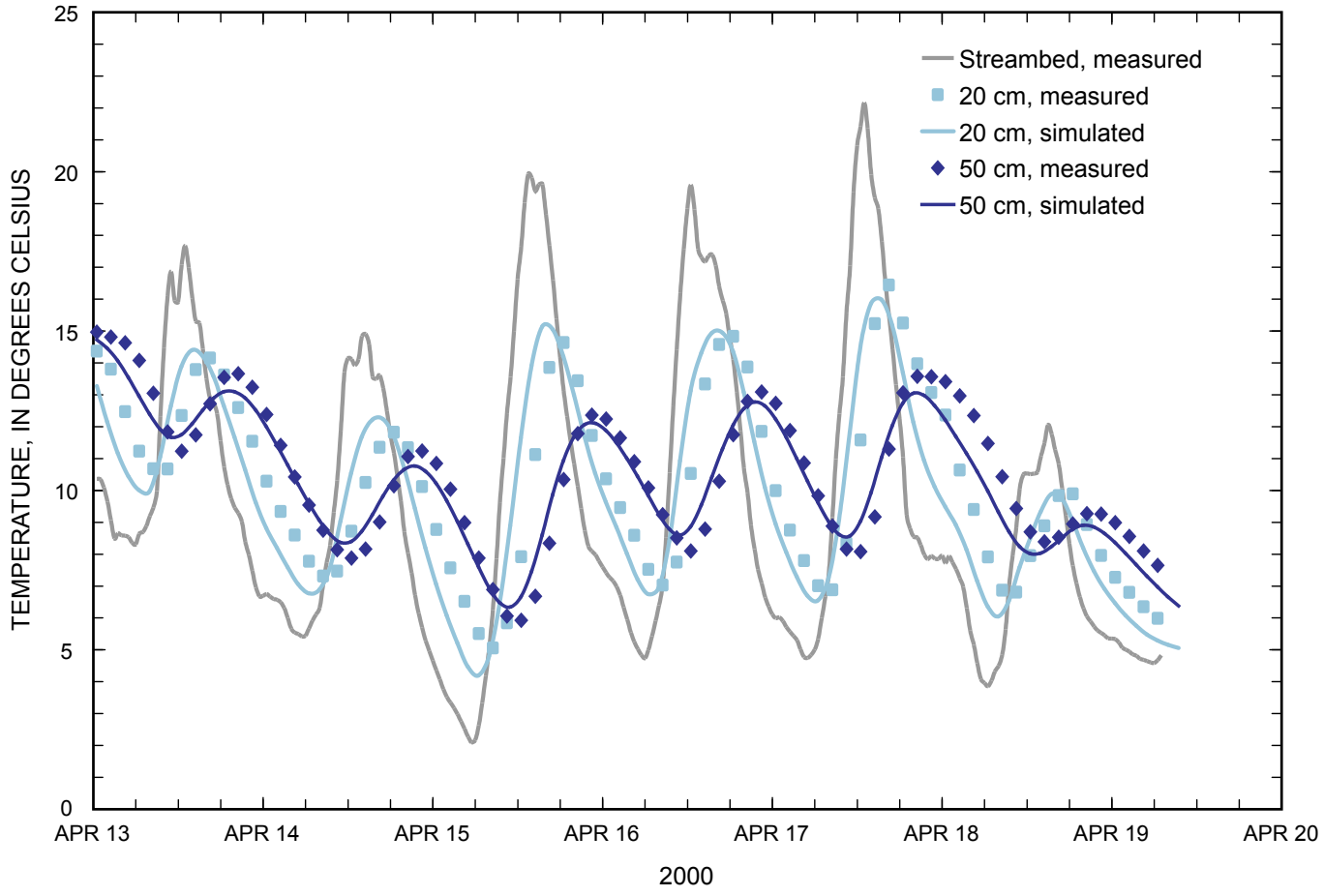

Figure 14. Comparison of simulated to measured temperatures for depths 20 and 50 centimeters beneath Trout Creek at site 4-ST from April 13 to April 20, 2000 (from Prudic and others, 2003). Location of site 4-ST is shown in figure 2.

Description of Model

The numerical model was specifically formulated to treat the case of a stream separated from its underlying aquifer by a thick unsaturated zone, which is typical for most streams that flow across alluvial fans or piedmont alluvial plains in the Middle Humboldt River Basin. The model was used to evaluate the duration and quantity of infiltration along the channel during periods of streamflow.

The model solves the one-dimensional form of the Saint-Venant equations for surface-water flow (Strelkoff, 1970), modifying streamflow to account for infiltration losses into the streambed. The Saint-Venant equations can be written (modified from Chow and others, 1988):

$$\frac{\partial y}{\partial t}+\frac{1}{B}\frac{\partial Q}{\partial x}=0\ , \tag{1}$$

$$\frac{\partial Q}{\partial t}+\frac{\partial}{\partial x}\left(\frac{\beta\, Q^2}{A}\right)+g\,A\frac{\partial y}{\partial x}+g\,A\frac{Q|Q|}{S^2}=0\ , \tag{2}$$

where

y = water-surface elevation, in meters,

t = time, in seconds,

B = channel width at water surface, in meters,

Q = streamflow, in cubic meters per second,

x = distance down the channel, in meters,

β = momentum correction factor, dimensionless,

g = gravity, in meters per second per second,

A = cross-sectional area, in square meters, and

S = stream hydraulic conveyance, in cubic meters per second.

The momentum correction factor, β, is used to correct the overall momentum flux for non-uniform velocity distributions (Strelkoff, 1970). The stream hydraulic conveyance, S, is a composite of stream-geometric parameters—area, roughness, and hydraulic radius—equal to the ratio of stream discharge to square root of friction slope in the Manning equation (Dalrymple and Benson, 1968; see equation 4 for definition).

Spatial derivatives of streamflow, which include losses from streambed infiltration, were estimated using the Preissman four-point finite-difference method (Cunge and others, 1980). The spatial derivative for streamflow in equation 1 was represented as:

$$\frac{1}{B}\frac{\partial Q}{\partial x}=\left\{\frac{\sum_{j\in I_{ju}} Q_j^{k+1}-\sum_{j\in O_{ju}} Q_j^{k+1}}{F_{ju}^{k+1}}+\frac{\sum_{j\in I_{jd}} Q_j^{k+1}-\sum_{j\in O_{jd}} Q_j^{k+1}}{F_{jd}^{k+1}}\right\}, \tag{3}$$

where

$\sum_{j\in I_{ju}} Q_j^{k+1}$ = sum of inflows between midpoints of reach j–1 and reach j,

$\sum_{j\in O_{ju}} Q_j^{k+1}$ = sum of outflows between midpoints of reach j–1 and reach j,

$\sum_{j\in I_{jd}} Q_j^{k+1}$ = sum of inflows between midpoints of reach j and reach j+1,

$\sum_{j\in O_{jd}} Q_j^{k+1}$ = sum of outflows between midpoints of reach j and reach j+1,

F_{ju}^{k+1} = area (plan view) between midpoints of reach j–1 and reach j, and

F_{jd}^{k+1} = area (plan view) between midpoints of reach j and reach j+1.

The sum of all outflows between reach midpoints in equation 3 includes the streambed infiltration.

The stream hydraulic conveyance (S) in metric form is (Chow and others, 1988):

$$S=\frac{AR^{2/3}}{n}\ , \tag{4}$$

where R is hydraulic radius (meters), and n is Manning's roughness coefficient (dimensionless). Manning's roughness coefficient was estimated from channel characteristics (Phillips and Ingersoll, 1998). Trout Creek was characterized with a single value of Manning's roughness coefficient equal to 0.03.

Trout Creek was divided into reaches between adjacent cross sections (fig. 15). Streamflow was computed at the midpoint (or node) of each reach, and streambed infiltration was calculated over a reach as a function of stream depth and wetted area of the channel. Irregular stream cross sections were used in the model to account for changes in the channel dimensions along the channel. All model variables dependent on stream depth were determined in the model using tables that relate the value of each variable to stream depth. The system of non-linear algebraic equations resulting from the finite-difference approximations was solved using Newton Raphson and lower-upper (LU) decomposition matrix-solution techniques (Burden and Faires, 1997).

The upstream boundary at site 3-GT was specified as time-variable discharge and stage (depth plus elevation of streambed). During periods of supercritical streamflow, the downstream boundary was not required. During periods of subcritical streamflow, the streambed elevation was assigned to the next cross section downstream of streamflow cessation.

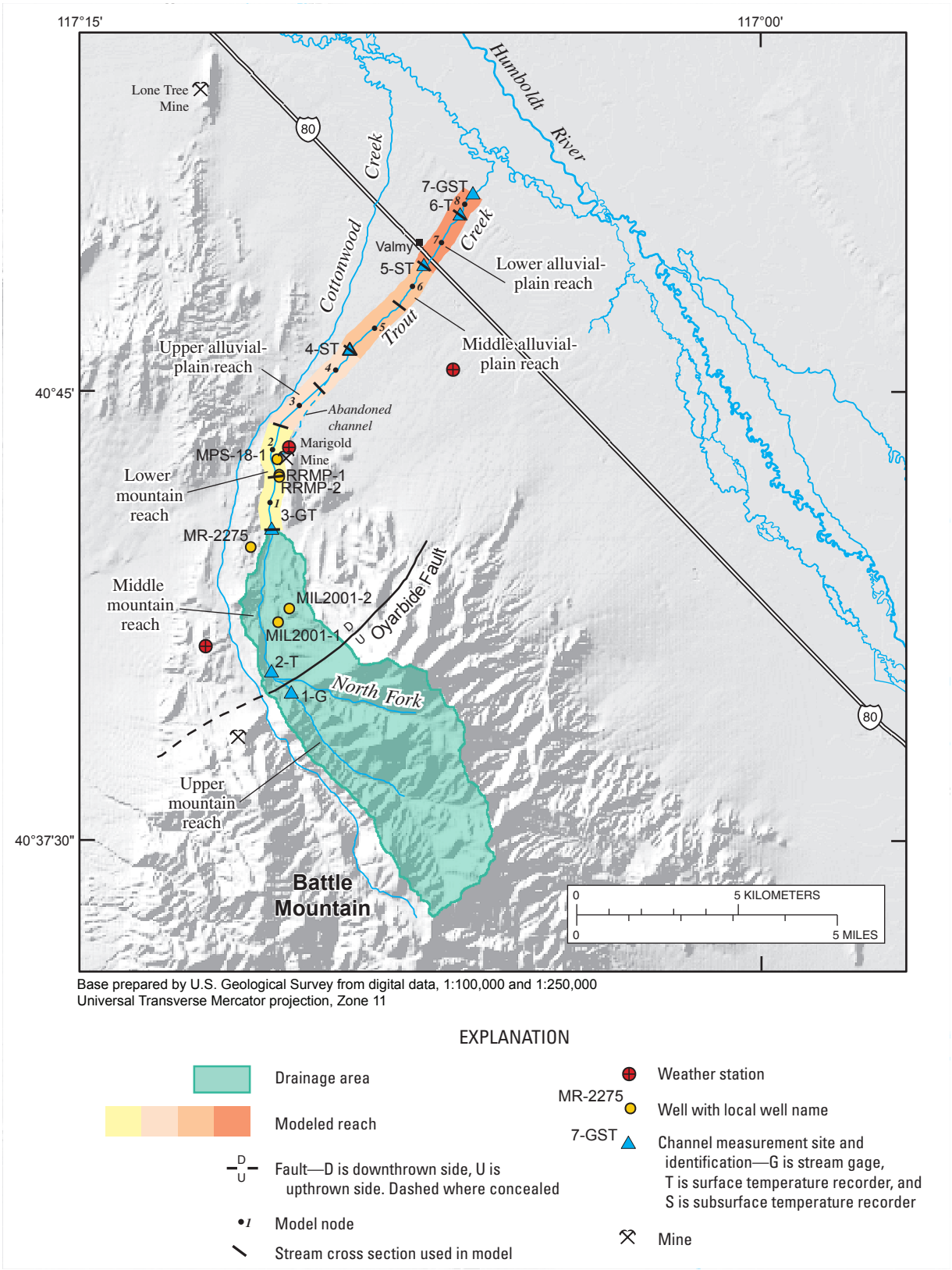

Figure 15. Location of cross sections, and modeled nodes and reaches used to simulate streamflow and streambed infiltration along Trout Creek, north-central Nevada (modified from Prudic and others, 2003). Reaches along the piedmont alluvial plain are abbreviated to alluvial-plain reach.

Tables relating streambed infiltration to stream depth were estimated for each of nine cross sections using a variably saturated two-dimensional model (VS2DT; Healy, 1990; locations of cross sections are shown in fig. 15). Streambed infiltration as a function of depth was computed using twenty simulations at each cross section. Stream depth was held constant in each simulation until infiltration across the streambed became approximately constant. Vertical no-flow boundaries at the end of each cross section were extended 15 m on either side of the channel to allow for ground-water flow away from the channel. A zero pressure head was assigned at the water-table elevation. Initial conditions for the unsaturated zone were assigned on the basis of residual water content of 0.07 m^3/m^3 (Niswonger, 2001) estimated from the water content in core samples. Hydraulic conductivity of 0.56 m/d estimated from the subsurface temperature profile at site 4-ST was initially assigned to the unsaturated zone at all cross sections.

Distribution of Streambed Infiltration

The initial simulation assumed a steady discharge at site 3-GT equal to the measured discharge on May 12, 1999. The simulation reproduced the measured stream discharges upstream of site 5-ST but could not reproduce the measured discharges and streambed-infiltration rates between sites 5-ST and 7-GST (lower reach of the piedmont alluvial plain). Thus the hydraulic conductivity for this reach was increased to 1.2 m/d in order to match the measured discharge at site 7-GST. The hydraulic conductivity was only slightly greater than the 1.1 m/d estimated for the streambed-infiltration rate from discharge measurements and average stream widths (table 3). Tables relating streambed infiltration to stream depth for cross sections between sites 5-ST and 7-GST were revised on the basis of the higher estimate of hydraulic conductivity and model results for May 12, 1999 closely matched the measured streamflows (fig. 16). The correlation coefficient of simulated to measured streamflows was 0.98. The distribution of hydraulic conductivities used for the May 12, 1999 simulation was used for the simulation of streamflow from March 31 to April 27, 2000. The simulation of streamflow for April 13, 2000 also closely matched the measured streamflows during the time period that streamflows were measured on that date (fig. 16).

The simulation of May 12, 1999 was further evaluated by comparing simulated and measured stream depth and velocity at each measurement site. Simulated stream depths ranged

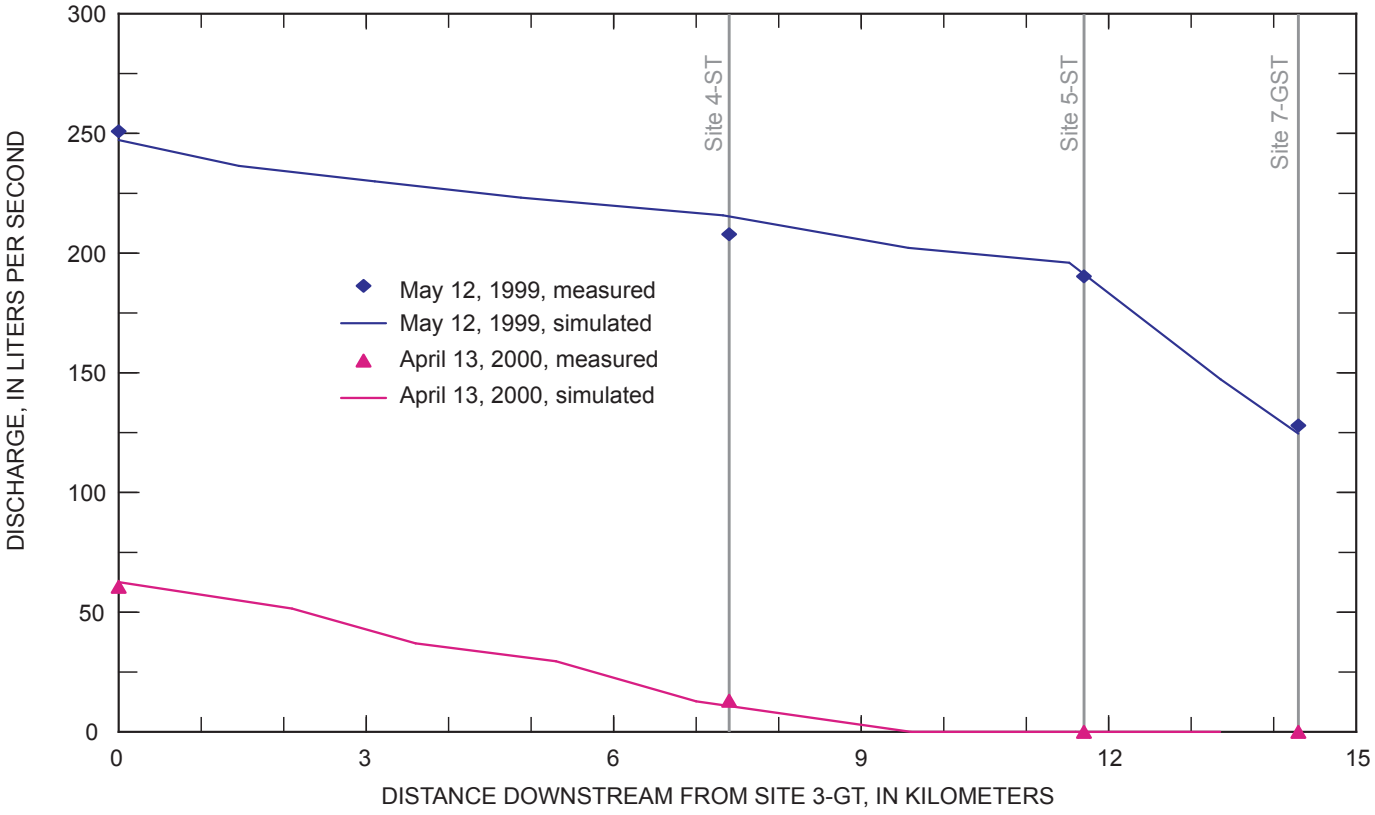

Figure 16. Comparison of simulated with measured discharge along Trout Creek for May 12, 1999 and April 13, 2000 (modified from Prudic and others, 2003). Simulated discharge on each date was calculated at the end of each cross section during the same time period as the measured discharge. Location of measurement sites, cross sections, and model nodes and reaches are shown in figure 15.

from 0.07 to 0.17 m at the nine cross sections (median value was 0.11 m) whereas, measured stream depths ranged from 0.11 to 0.15 m at the four measurement sites (median value was 0.13 m). Simulated stream velocities ranged from 0.57 to 1.3 m/s at the nine cross sections (median value was 0.84 m/s), whereas the measured velocity ranged from 0.52 to 0.80 m/s at the four measurement sites (median value was 0.65 m/s). Matches between simulated and observed depths and velocities are reasonably good given the uncertainties in channel characteristics over the relatively long reaches that were being simulated. No attempt was made to adjust Manning's roughness coefficient or the momentum correction factor (β), the latter which was assigned a value of one. Increasing Manning's roughness coefficient or decreasing the momentum correction factor would have decreased the velocities and increased stream depths in a manner that could have better matched the measured depths and velocities. However, this adjustment also would have resulted in slightly increased streambed-infiltration rates that would have decreased the simulated streamflow.

The simulation of streamflow from March 29 to June 7, 2000 and 2002 approximately matched the observed distribution of streamflow along the channel during both years (fig. 17). Streambed infiltration was limited to the lower mountain and upper and middle reaches of the piedmont alluvial plain, as simulated streamflow did not extend to site 5-ST. The terminus of simulated streamflow was between nodes 5 and 6 during the period of peak flow in 2000 and 2002. The simulated streamflow at node 5, just downstream of site 4-ST, began on April 5 in 2000 and on April 12 in 2002, slightly earlier than indicated by the temperature data at 4-ST (table 2). The model does not account for initially higher infiltration rates caused by capillary pressure gradients when the leading edge of streamflow encounters a dry streambed, which creates a bias towards early arrivals when the streambed moisture content is low. Continuous flow was simulated from April 5 to April 24, 2000 and from April 15 to April 20, 2002, generally replicating the period of continuous flow inferred from the temperature data at site 4-ST.

Diurnal variation in streamflow was observed at site 3-GT and likely results from daily variations in snowmelt. The diurnal variation in streamflow at site 3-GT propagated downstream in a manner that produced a time-varying change in the location of streamflow cessation. Simulated streamflows at different places along the channel profile show this time-dependent migration in the location of streamflow cessation (fig. 17).

The simulation of streamflow down the channel during the period of flow from March 29 through June 7, 2000 and 2002 was used to estimate the cumulative percentage of streambed infiltration for the lower-mountain and upper and middle piedmont alluvial-plain reaches (fig. 18). Total simulated streambed infiltration for the period was 2.0×10^5 and 1.2×10^5 m^3 for water years 2000 and 2002, respectively. Because the simulation period did not include the onset of flow on March 22, 2000, the estimated total streambed infiltration for the water year was slightly lower than the estimated annual runoff (2.1×10^5 m^3). Although the pressure transducer was not installed until March 29, 2000, annual runoff includes an estimate of flow for the period between the onset of flow and March 29, 2000.

The model of unsteady streamflow with infiltration provides a means for estimating cumulative volumes of streambed infiltration and flow durations for different conditions of peak discharge and runoff. Streambed infiltration is limited to the lower mountain section at the onset and cessation of flow each spring, as shown for 2002 at site 3-GT (fig. 18*B*). Cumulative simulated streambed infiltration for a given reach along the channel varies as a function of flow at site 3-GT. Cumulative simulated streambed infiltration for 2000 was initially divided equally between the lower-mountain and upper piedmont alluvial-plain reaches because the model simulation began when the pressure transducer was installed rather than the beginning of flow, as in 2002. Slightly less than half of the cumulative streambed infiltration was simulated along the lower mountain section during 2000, whereas slightly more than half was simulated during 2002, when runoff was less. Modeled cumulative streambed infiltration in the middle piedmont alluvial-plain reach gradually increased in both years until streamflow became smaller than streambed losses in the higher reaches.

Streamflow measured at site 3-GT and simulated at model nodes 2–5 for water year 2000 lasted longer than the streamflow at the same locations for water year 2002, even though peak discharges were nearly the same (fig. 19). The difference in flow duration along Trout Creek for water years 2000 and 2002 is reflected in the simulated streamflows shown in figure 19 whereby a longer period of low flow following the peak discharge during spring snowmelt was measured at site 3-GT during 2000 than during 2002. The extended period of runoff measured during the spring of 2000 was in part caused by a single large storm in May that produced 48 mm of precipitation at the Marigold Mine (fig. 4). The difference in May precipitation accounts for much of the difference in annual precipitation between 2000 and 2002 and illustrates the importance of precipitation in winter and spring on the duration of flow in the Trout Creek drainage.

Runoff in 1999 was relatively high. Flow was observed along the entire channel in April and May. On May 11, 1999, streamflow losses measured by sampling cross sections with a hand-held flow meter were higher in the lower reach of the piedmont alluvial plain (5-ST to 7-GST, fig. 16) than those measured upstream, indicating a higher streambed-infiltration rate on the lower alluvial plain. Greater streamflow losses on the lower plain were again observed throughout a series of repeated measurements in March and April of 2004 (Niswonger and others, 2005). About 50 percent of the simulated cumulative streambed infiltration occurred on the lower piedmont alluvial plain (Niswonger and others, 2005). Thus, during years of above-average runoff, as in May 1999 and March and April 2004, a large percentage of streambed infiltration occurs there. Greater streambed infiltration combined

with an unsaturated zone that is less than 15-m thick likely results in more rapid recharge than higher on the piedmont alluvial plain where the streambed-infiltration rate is less and the unsaturated zone can exceed 50 m in thickness.

Ground-Water Recharge

The source of ground water in the Trout Creek drainage is probably limited to precipitation that falls within its drainage area. Little ground water can flow into the Trout Creek drainage upstream of Oyarbide Fault from adjacent drainages because the underlying rocks are relatively impermeable and because the land surface drops quickly in all of the surrounding drainages. However, older alluvium, welded tuff and pyroclastic rocks are continuous across the drainage divide between Trout and Cottonwood Creeks just downstream of the Oyarbide Fault (Roberts, 1964, plate 7). Limited data on ground-water levels upstream and downstream of the fault in the Cottonwood drainage, together with the elevation of springs at the base of the volcanic rocks in the Trout Creek drainage, suggest that the springs could represent ground-water discharge from the Cottonwood Creek drainage. Additionally, rocks of the Havallah Sequence (table 1) are exposed along the divide between the two drainages and could

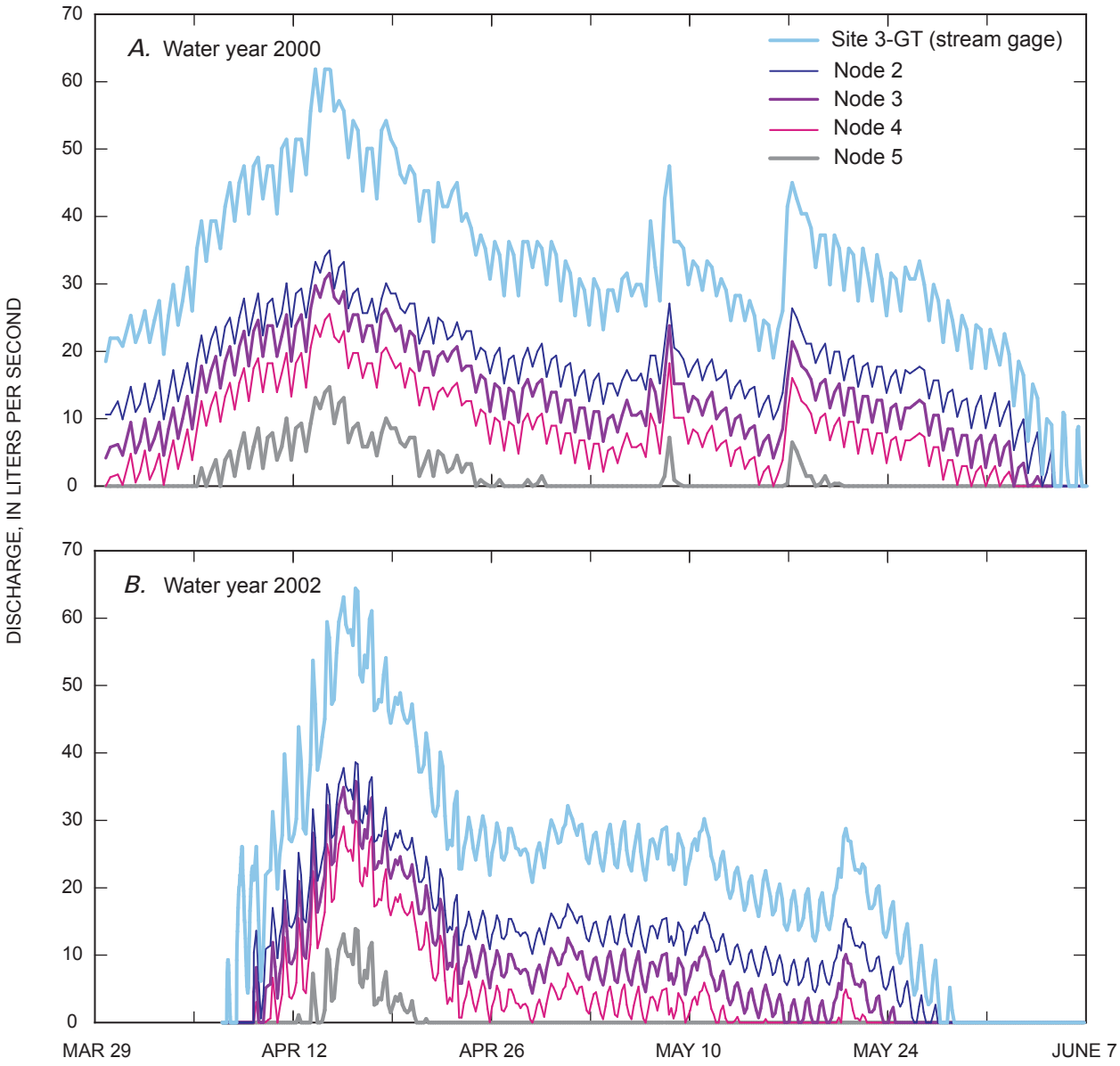

Figure 17. Discharge at site 3-GT and discharge at model nodes 2, 3, 4, and 5 simulated from *A*, March 29–June, 2000, and *B*, March 29–June 7, 2002. Locations of site 3-GT and model nodes are shown in figure 15.

allow ground water flow from the parallel Cottonwood Creek drainage to encroach along the northwestern boundary of the Trout Creek drainage. Test hole MR-2275, drilled near the crest between the two drainages into the Havallah Sequence, yielded more water than test holes and wells drilled into the Valmy Formation in the Trout Creek drainage.

Ground-water recharge in the Trout Creek drainage primarily occurs as concentrated infiltration along Trout Creek and its tributaries and as diffuse recharge from infiltration of precipitation higher on the mountain. Ground-water recharge occurs from these sources only after percolation through the unsaturated zone. Precipitation on the piedmont alluvial plain is insufficient to result in ground-water recharge because any deficits in soil-water storage must be satisfied before deep percolation leading to recharge can occur. Potential soil-water storage on the alluvial plain is large, and virtually all water added to soil storage during periods of precipitation is lost to evapotranspiration during spring and summer.

Evidence for Deep Percolation beneath Trout Creek

Although streambed-infiltration rates were estimated from discharge measurements and from subsurface temperature profiles at shallow depths beneath the channel, they are

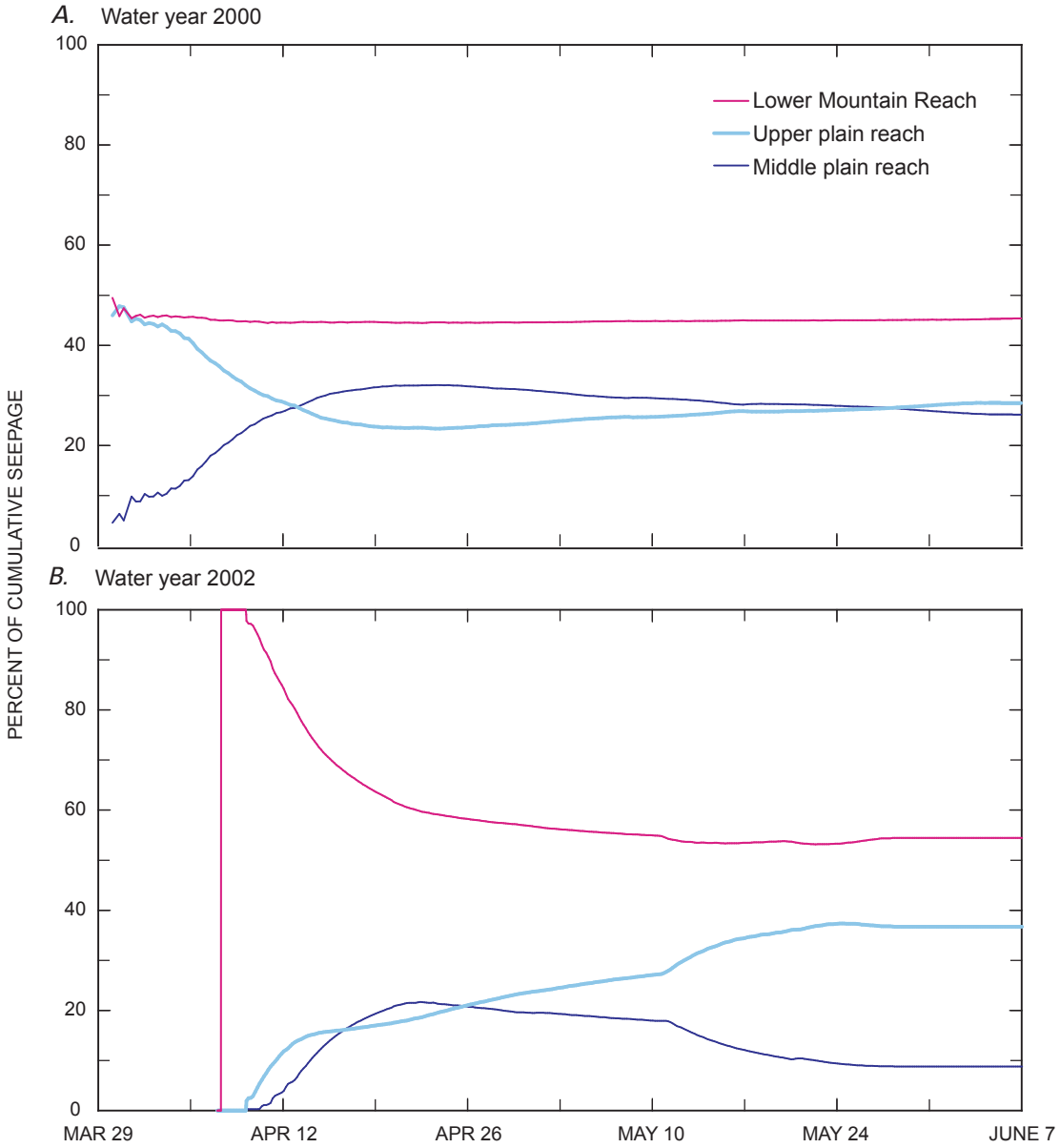

Figure 18. Percentage of cumulative streambed infiltration along lower mountain and upper and middle piedmont alluvial-plain reaches simulated for *A*, March 29–June 7, 2000, and *B*, March 29–June 7, 2002. Location of reaches is shown in figure 15.

only an estimate of the quantity of water that infiltrates through the streambed and not the rate of recharge at the water table. Percolation through the unsaturated zone beneath the stream channel from intermittent streamflow results in delay and attenuation of streamflow-infiltration transients. The dynamics of percolation depend on the hydraulic and storage properties of the unsaturated zone. Lateral spreading of percolating water will further delay and attenuate recharge by spreading infiltrated water over a larger area than the channel width. If lateral spreading of infiltrated water occurs at sufficiently shallow depths, additional water will be lost to evapotranspiration.

Direct evidence for deep percolation along and adjacent to the channel was obtained by drilling holes to depths of 6 to 8 m, collecting samples for water content and chloride concentration, and installing access tubes for neutron-moisture measurements. In November 1999, two test holes were drilled at site 5-ST, one in the channel and one 20 m from the channel. An additional test hole was drilled in the channel at site 7-GST (fig. 15). Test holes were drilled with a hollow-stem auger. Core samples were collected every 1.5 m using a 5-cm diameter by 60-cm long split-spoon sampler. Coring was not always successful because of coarse gravels. Grab samples were usually obtained where coring was not possible. When each hole reached its final depth, thin-wall aluminum tubing having a diameter of 5 cm and sealed at the bottom was placed inside the hollow-tube auger. Augers were removed and the annular space around the tubing filled with polyurethane foam, following the procedure of Zawislanski and Faybishenko (1999).

The trailer-mounted auger rig was not sufficiently robust to penetrate the first meter of large cobbles at site 4-ST, at which

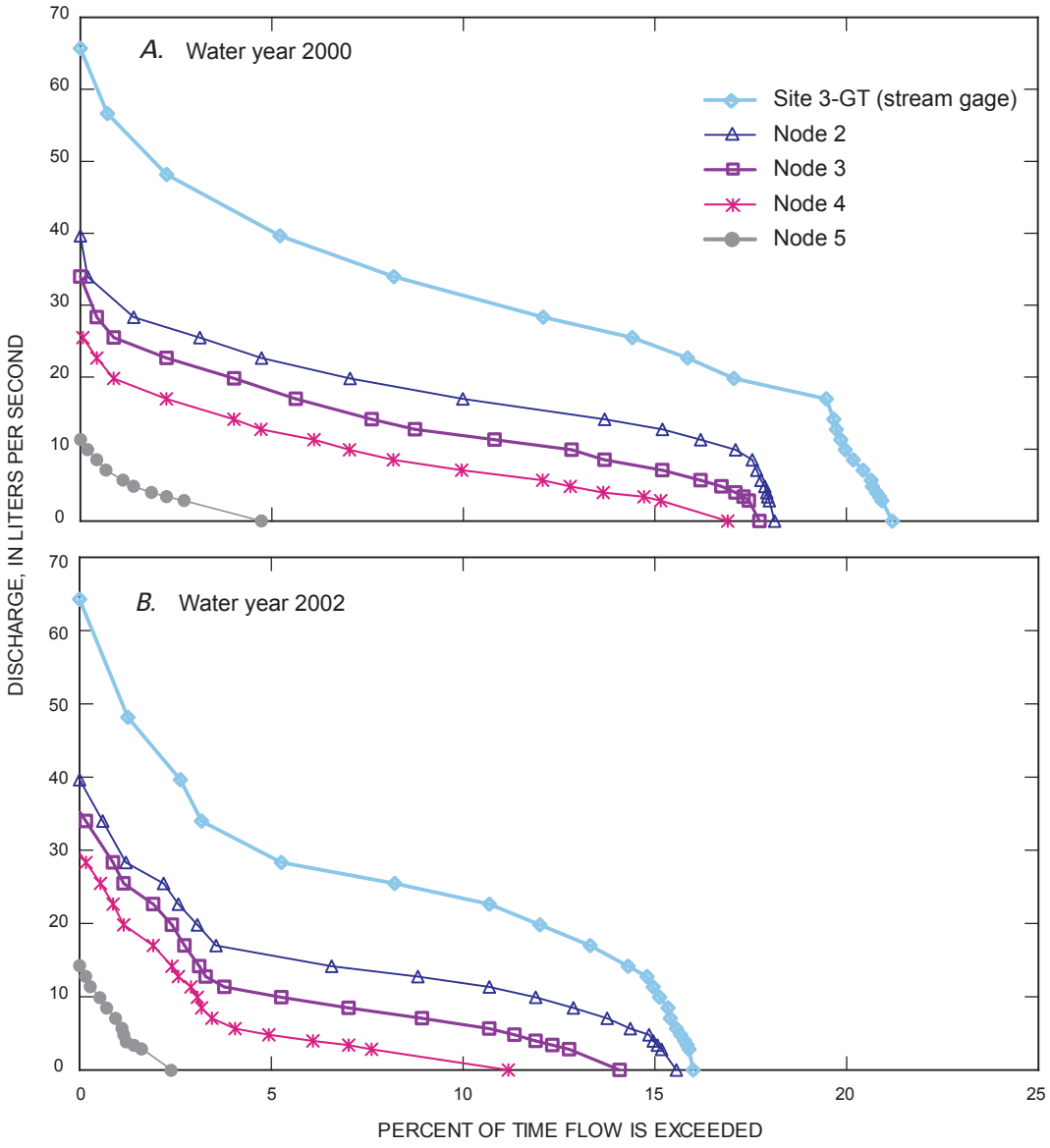

Figure 19. Flow duration at site 3-GT and selected model nodes for water years *A*, 2000 and *B*, 2002. Location of site 3-GT and model nodes is shown in figure 15.

point drilling efforts were suspended. A rotary exploration drill rig from the Marigold Mine became available the following November that was capable of penetrating solid rock. One test hole each was drilled to a depth of 6.6 m in the channel at sites 3-GT and 4-ST. The drill bit was roughly 10-cm in diameter. Air was used to circulate cuttings to the surface that were collected in bags at 0.75 m intervals, starting from land surface. Saturated sediment was not encountered in either hole. Thin-walled aluminum tubing was placed into each hole and the space around the tubing filled with polyurethane foam, as before.

Neutron measurements were related to water content by developing a relation between neutron count ratios (ratio of the number of counts at a given depth in the access tube to the standard shielded count) to water content for the three access holes at or near sites 5-ST and 7-GST. The exploration rig used for install the access tubes at sites 3-GT and 4-ST was not equipped to collect core samples and thus, the neutron count ratios for these holes could not be directly related to water content. Instead, a general relation was developed by comparing neutron count ratios in a similar installation placed next to a calibrated neutron access hole at Eagle Valley in Carson City, Nev. Volumetric water contents are shown in figure 20. Water-content profiles from borehole to borehole are only approximately comparable, due to uncertainties of calibration. In contrast, temporal changes are fairly robust.

Neutron measurements at site 3-GT showed marked changes in water content throughout the profile beneath the channel during periods of streamflow (April and May 2001 and May 2002). The relatively deep percolation at site 3-GT is consistent with the periodic appearance of water in two wells located about 500 m downstream of site 3-GT and in the upstream end of the original channel at Marigold Mine. The wells were drilled to depths of 13 and 58 m and were dry except each spring during and after runoff events in Trout Creek (fig. 21). The quick response of water levels in the wells near site 3-GT to streamflow indicates that infiltration in the lower mountain channel forms temporarily perched zones above the regional water table and that deep percolation is rapid.

Neutron measurements at site 4-ST were consistent with temperature data indicating that streamflow between November 2000 and October 2002 was limited to one brief period, during the spring of 2002. The water content in the channel at sites 5-ST and 7-GST decreased from March 2000 to October 2002, indicating that the channel was mostly dry during the study period. These data are also consistent with pressure-transducer data at site 7-GST, which indicated that no streamflow occurred during the study.

The neutron access hole in the channel at site 5-ST revealed water contents that were considerably higher than those 20 m away from the channel (fig. 20*E*), indicating that flow at 5-ST, though infrequent, was sufficient to maintain higher water contents in the unsaturated zone beneath the channel even after long periods without flow. The lower water contents in the access tube 20 m west of site 5-ST also suggests that lateral spreading in near-surface layers does not extend far from the channel. This observation is supported by a general lack of vegetation next to the channel downstream of 3-GT (fig. 5*B*).

Chloride concentrations in the subsurface were low and uniform beneath the channel, even at sites on the lower piedmont alluvial plain, whereas the subsurface chloride concentrations measured 20 from the channel at site 5-ST were high and displayed a distinct peak at about 1.5 m (fig. 22). Expressed in terms of pore-water concentration, the peak value was about 1,800 mg/L. The lowest value, measured at a depth 6 m beneath the channel, was 70 mg/L. The median chloride concentration at the off-channel site was 250 mg/L, considerably higher than the 17.5 mg/L median value at sites 5-ST and 7-GST.

Chloride concentration in pore water beneath the channel was nearly the same as the average of 7 surface-water samples collected from Trout Creek near Marigold Mine, and 6 samples collected near site 4-ST. Samples were collected between March 1998 and May 2002. No sample was collected May 2002 at the downstream site. Chloride concentrations ranged from 10.2 to 18.8 mg/L at the upstream site, and from 9.8 to 20.2 mg/L at the downstream site (U.S. Department of Interior, Bureau of Land Management, 2003, p. 3–33). Median (mean) concentrations were 14.9 (15.2) mg/L at the upstream site and 14.6 (15.1) mg/L at the downstream site.

Chloride concentrations at the two upper sites (3-GT and 4-ST) likely are similar to those in Trout Creek and at the lower sites because the chloride concentration per gram of sediment was nearly the same. These results suggest that the frequency of streamflow in the channel along the lower reach of the piedmont alluvial plain, and associated quantity of deep percolation, is sufficient to prevent the accumulation of salts observed away from the channel.

Mountain Recharge

Ground-water heads in wells upstream of site 3-GT indicate that diffuse ground-water recharge occurs high in the mountains. Because data are not available to accurately determine ground-water recharge from hydraulic considerations, an estimate of average annual ground-water recharge in the Trout Creek drainage upstream of site 3-GT was made using the chloride mass-balance method (see, for example, Dettinger, 1989). The chloride mass-balance method assumes that: (1) all chloride in ground water comes from precipitation and dry fall in the drainage upstream of site 3-GT, (2) no chloride is derived from rocks as water percolates to the water table, and (3) a balance exists between chloride deposited from the atmosphere in the drainage upstream of site 3-GT and chloride that exits in the drainage downstream of site 3-GT, both in streamflow and in ground-water flow (that is, annualized fluxes of chloride and water are approximately in steady state, with no changes in storage). Ground-water recharge (in cubic meters per year) can be estimated using the following equation (modified from Dettinger, 1989):

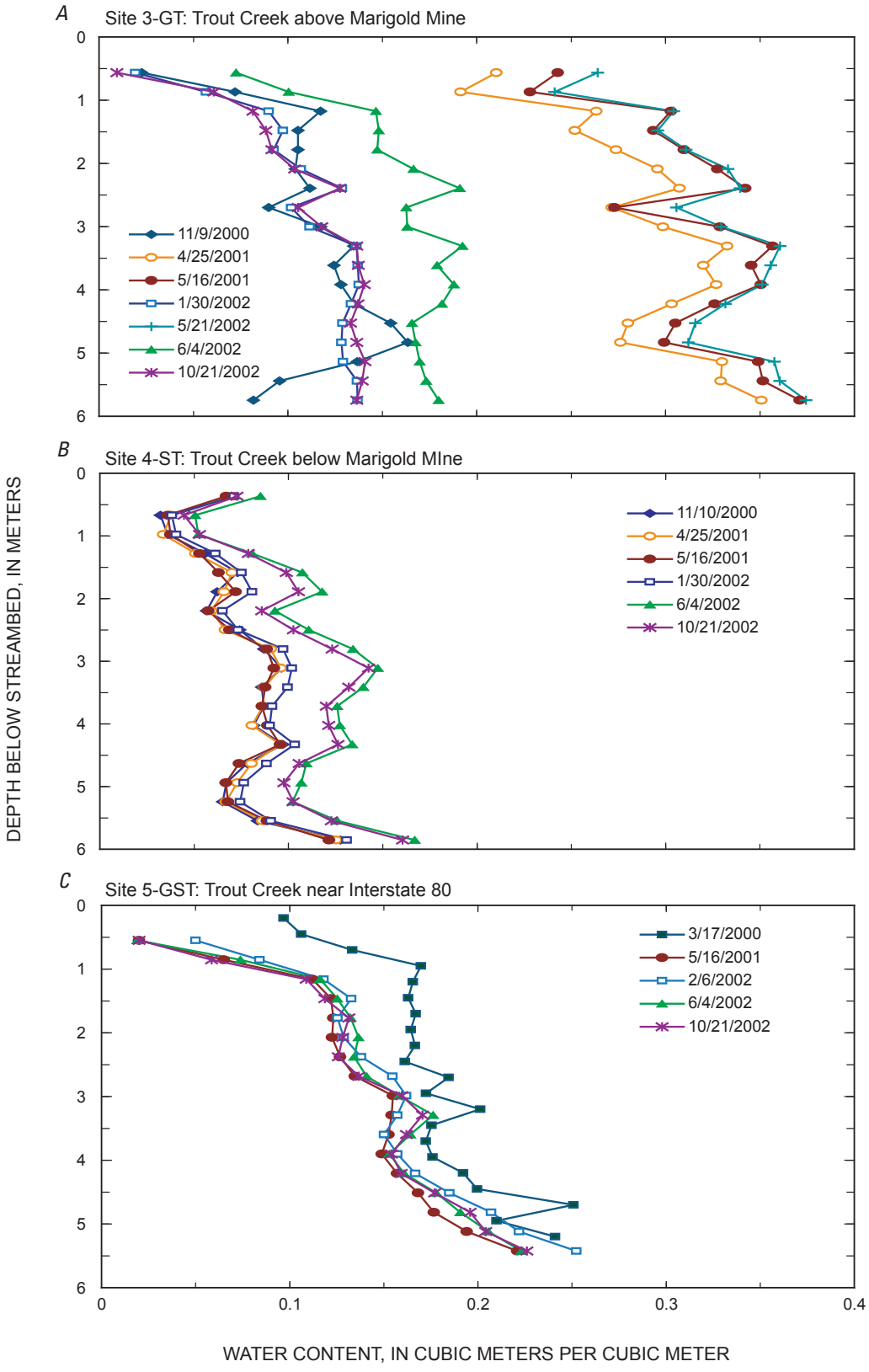

Figure 20. Approximate water content in unsaturated zone beneath and next to Trout Creek estimated from neutron-moisture measurements taken from March 2000 to October 2002 at *A*, site 3-GT, *B*, site 4-ST, *C*, site 5-ST, *D*, site 7-GST, and *E*, twenty meters west of site 5-ST. Location of sites is shown in figure 15.

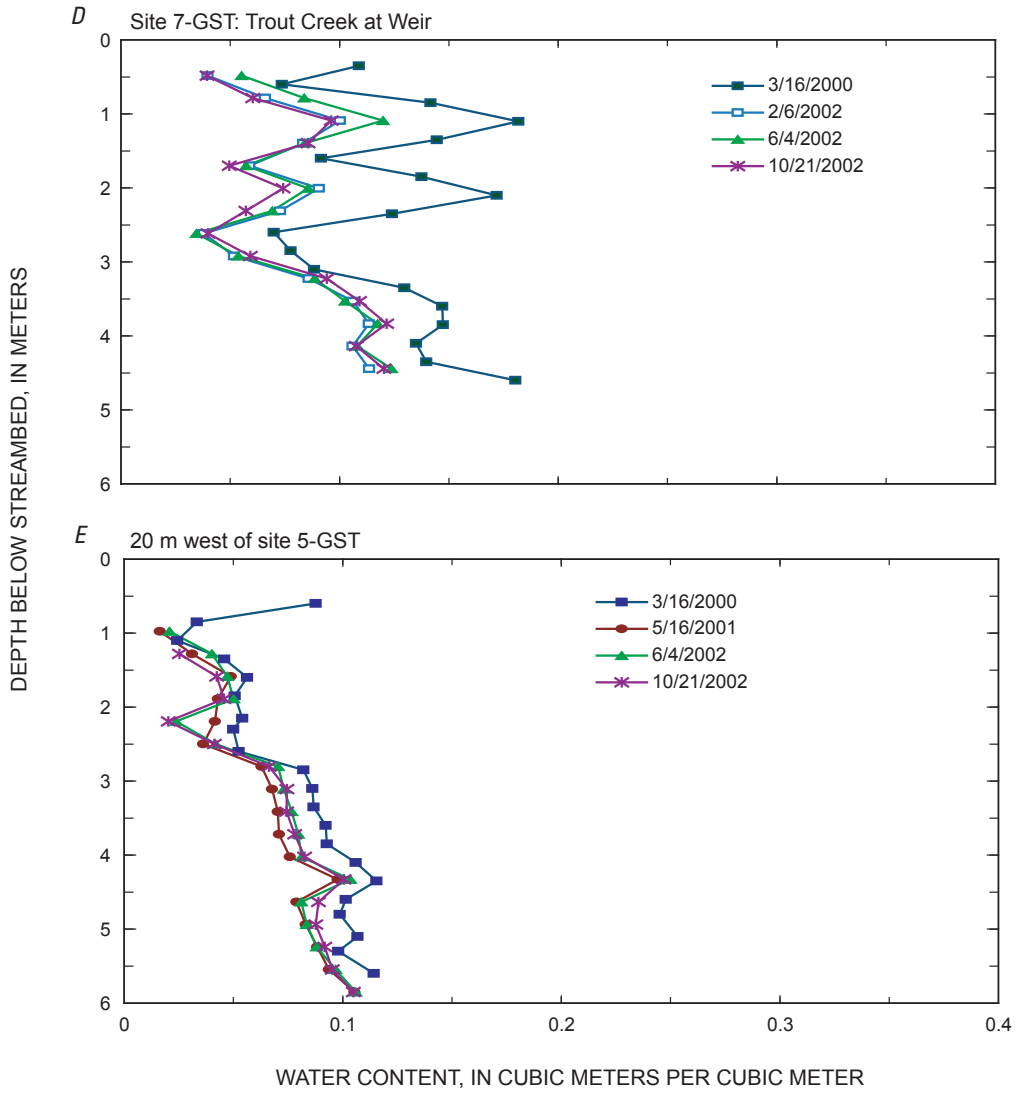

Figure 20.—Continued.

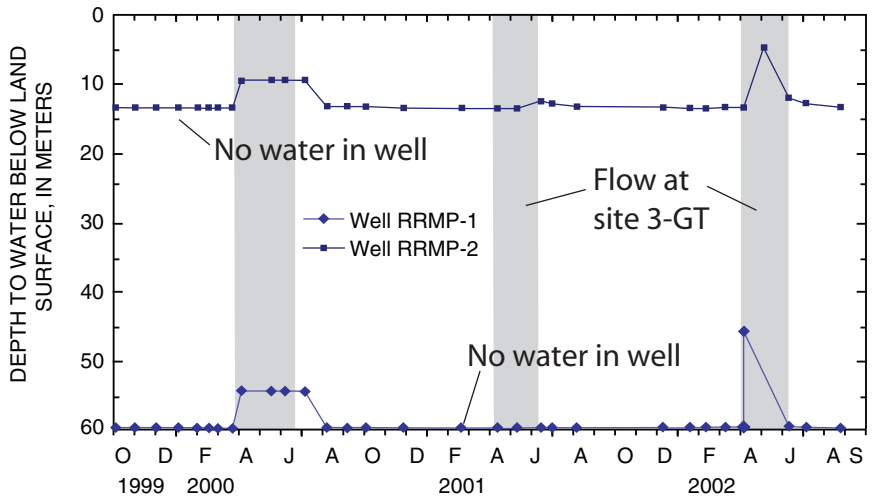

Figure 21. Depth to water in two wells near Trout Creek and Marigold Mine for water years 2000 to 2002. Location of site is shown in figure 15. Data are from Jonn Barber, Glamis Marigold Mining Company, written commun., 2003.

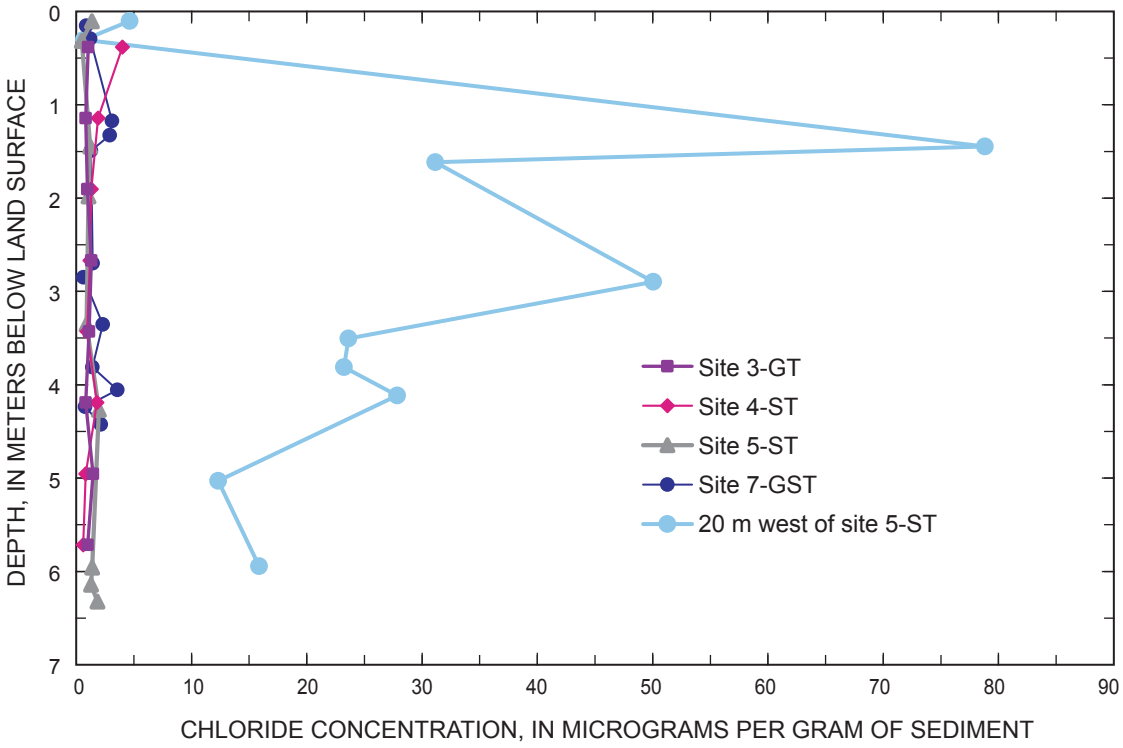

Figure 22. Chloride concentrations in cores and cuttings collected from test holes drilled into unsaturated alluvium beneath and adjacent to Trout Creek. Core samples and cuttings were collected from test holes drilled November 1999 at sites 5-ST and 7-GST and cuttings were collected from test holes drilled November 2000 at sites 3-GT and 4-ST. Location of sites is shown in figure 15.

$$Q_{gw} = \frac{Q_p \ (C_p)}{C_{gw}} - \frac{Q_{sr} \ (C_{sr})}{C_{gw}}, \qquad (5)$$

where

Q_{gw} = average annual ground-water recharge, in millions of cubic meters,

C_{gw} = average chloride concentration in ground water, in milligrams per liter,

Q_p = average annual volume of precipitation, in millions of cubic meters,

C_p = average chloride concentration of precipitation, in milligrams per liter,

Q_{sr} = average annual surface runoff, in millions of cubic meters, and

C_{sr} = average chloride concentration of surface runoff, in milligrams per liter.

Separate estimates of the mass of chloride in precipitation and runoff are needed because ground-water recharge is calculated from the difference. The chloride in precipitation is an effective value that includes chloride in dust (dry deposition).

The average annual volume of precipitation was estimated from a precipitation map derived from a statistical topographically based model (Daly and others, 1994), which uses average annual precipitation from surrounding meteorologic stations over a 30-year period (1961–1990). This approach was advantageous because it produced orographically realistic estimates even for the highest elevations in the Trout Creek drainage. The estimates compare well with the independently measured data from the precipitation stations already discussed in this report.

The drainage area upstream of site 3-GT is 38 km^2, where the average annual precipitation ranged from 267 to 368 mm. The total annual volume of precipitation was determined by dividing the precipitation range into four equal zones, and estimating the area of each. The estimated volume of precipitation for the drainage upstream of site 3-GT was 1.28×10^7 m^3/yr (table 5).

An estimate of long-term average runoff for the Trout Creek gage, with two years of record, can sometimes be made on the basis of correlations with nearby streams having similar characteristics and longer periods of record. Long-term gages on small streams to the northwest and northeast—Martin Creek near Paradise Valley, about 100 km northwest, and Rock Creek near Battle Mountain, about 50 km northeast—showed greater annual runoff in 2002 than in 2000 (Allander and others, 2001 and Berris and others, 2003). Thus precipitation patterns in those watersheds can differ substantially from the precipitation pattern in the Trout Creek drainage.

Consequently, average annual runoff at site 3-GT was estimated by adjusting annual runoff for 2000 and 2002 at site 3-GT on the basis of annual runoff of the Humboldt River near Battle Mountain (about 25 km east of site 3-GT). Humboldt River data were obtained from Allander and others, 2001; Berris and others, 2003; and Stockton and others, 2004. The annual runoff of the Humboldt River during water year 2000 was 53 percent of the long-term average (1886–1897, 1921–1924, 1945–1981, and 1991–2003). Annual runoff during 2002 was 42 percent of the long-term average. Since these data approximately matched the record at Trout Creek, the average annual runoff at site 3-GT was estimated by assuming that the ratio of annual runoff in the Trout Creek basin to annual runoff at the Humboldt River near Battle Mountain was roughly representative of the longer period of Humboldt River record. With this assumption, the estimated long-term average annual runoff for Trout Creek at site 3-GT was 3.4×10^5 m^3.

Chloride concentrations in precipitation (including dryfall) were determined on the basis of two chloride collectors—one on the piedmont alluvial plain east of Trout Creek and the other near the fault in the Cottonwood Creek drainage, west of Trout Creek (fig. 15 and table 6). The chloride concentrations in precipitation and dryfall from the two sites were assumed to represent an average annual chloride concentration. The chloride collectors consisted of a 2-liter polyethylene bottle connected by silicone-rubber tubing to an 8-cm diameter funnel, which was attached to the top of a fence post. Mineral oil was placed in the bottom of the bottle to prevent evaporation. The collectors were located at the weather stations operated by the mines. Samples were retrieved in the spring and fall of each year, starting in April 2000.

Volumetrically averaged chloride concentrations in precipitation for the period November 1999 to November 2002 was 1.3 mg/L at site 1 on the piedmont alluvial plain north of Marigold Mine and 2.1 mg/L at site 2, on the mountain south of Marigold Mine. Omitting the first sample collected at site 2, which had a concentration of 7.4 mg/L that was never approached by subsequent samples, resulted in the same volumetrically averaged chloride concentration as site 1(table 6). The concentration is roughly twice the average 0.6 mg/L of chloride in bulk-precipitation reported by Dettinger (1989) for stations in Nevada but within the range of measured values. On the basis of the similarity in the volumetrically averaged chloride at the two sites during the study period, average annual bulk chloride in precipitation was assumed to be 1.3 mg/L throughout the Trout Creek drainage.

The average chloride concentration of runoff is about 15 mg/L, based on thirteen chloride samples collected between March 1998 and May 2002 (U.S. Department of Interior, Bureau of Land Management, 2003, p. 3–33). Ground-water samples were collected from three monitoring wells and one test hole, in October 2002. Chloride concentrations in the wells nearest the fault (MIL2001-1 and MIL2001-2; fig. 15) were 23.1 and 24.4 mg/L, respectively. The other two sites (well MPS-18 and test hole MR-2275; fig. 15), near site 3-GT, had chloride concentrations of 20.9 and 18.4 mg/L, respectively (table 7). The average chloride concentration from all wells was 22 mg/L, rounded to two significant figures.

Average annual ground-water recharge in Trout Creek drainage upstream of site 3-GT was estimated using equation 5. Estimates of average annual precipitation, runoff, and volume-averaged chloride concentrations of precipitation, runoff, and ground water are given in table 8. The resulting ground-water recharge upstream of site 3-GT is 5.2×10^5 m^3. The estimated quantity of ground-water recharge within the entire Trout Creek drainage is assumed equal to ground water flow from the mountain block to the adjacent alluvial basin because the water table is far below land surface (fig. 7). This calculation neglects any net changes in ground-water storage caused by operations at the Lone Tree Mine. If all the average annual runoff is assumed to infiltrate prior to reaching the Humboldt River floodplain, the total water yield from the Trout Creek drainage upstream of site 3-GT is 8.6×10^5 m^3, or 7 percent of the average annual precipitation (table 8).

This percentage is the same as that estimated by using the original Maxey-Eakin method (Maxey and Eakin, 1949), given that the mean annual precipitation in the drainage is roughly 340 mm (13.3 inches). Additionally, the total water yield from the Trout Creek drainage is about the same as that estimated for two watersheds entering Eagle Valley in greater Carson City, Nev., which have similar values of average annual precipitation (Maurer and Berger, 1997, p. 34).

The fact that more than half of the recharge to ground water occurs in the mountains indicates that the consolidated rocks making up the mountain block have a higher permeability than initially expected on the basis of the geologic descriptions of the units (table 1), at least near the surface. Evidence of high near-surface permeability in the consolidated rocks can be seen in the ground-water gradient shown on figure 8. In 2002, the ground-water gradient between the fault and Marigold Mine was about $4x10^{-2}$ m/m, whereas the gradient on the piedmont alluvial plain north of the mine was less than $4x10^{-3}$ m/m. Assuming that ground-water flow in the Trout Creek drainage upstream of Marigold Mine is limited to the upper 300 m of saturated consolidated rocks and that the width of the ground-water-flow system is 1.5 km at site 3-GT, the bulk hydraulic conductivity of the consolidated rocks in the drainage upstream of Marigold Mine is estimated to be 0.08 m/d. The lower hydraulic gradient in the consolidated rocks below Marigold Mine indicates an increase in permeability.

Tritium (^3H), a cosmogenically produced isotope of hydrogen with a half-life of 12.3 years, was detected in water from wells MIL2001-1 and MPS-18 at 140 and 86 Bq/L, respectively (table 7). Depth to ground water in these wells exceeded 135 m below land surface (table 7). The presence of tritium at these levels indicates that a substantial portion of ground water at these locations represents recharge that occurred after 1950.

Table 5. Average annual volume of precipitation in Trout Creek drainage upstream of site 3-GT, north-central Nevada.

[Location of site 3-GT is shown in figure 15. Precipitation from the statistical-topographic model of Daly and others (1994) using data from 1961—1990. Abbreviations: mm, millimeters; m^2, square meters; m^3, cubic meters]

Annual precipitation range, in mm	Average annual precipitation, in mm		Area, in m^2	Volume, in m^3
267–292	279		4.07×10^6	1.14×10^6
292–318	305		4.43×10^6	1.35×10^6
318–343	330		6.30×10^6	2.08×10^6
343–368	356		2.31×10^7	8.21×10^6
		Total	3.79×10^7	1.28×10^7

Table 6. Chloride concentration of precipitation in the vicinity of Trout Creek drainage, north-central Nevada.

[Locations of precipitation sites are shown in figure 15. All samples analyzed at the U.S. Geological Survey laboratory in San Diego, Calif., using ion chromatography. Abbreviations: mL, milliliters; mg, milligrams; mg/L, milligrams per liter; NWIS #, National Water Information System site identifier; <, less than; —, not applicable]

Sample period: Starting date	Sample period: Ending date	Volume of precipitation, in mL	Mass of chloride, in mg	Chloride, dissolved, in mg/L	Precipitation, in mm: at indicated site	Precipitation, in mm: [1] at Marigold Mine
Site 1, piedmont alluvial plain, north of Marigold Mine (NWIS 404522117074801)						
11/09/1999	04/18/2000	215	0.09	0.4	56	147
04/18/2000	10/10/2000	237	0.38	1.6	62	80
10/10/2000	04/04/2001	254	0.18	0.7	66	116
04/04/2001	10/18/2001	124	0.26	2.1	32	36
11/07/2001	05/21/2002	299	0.48	1.6	78	136
05/21/2002	11/20/2002	135	0.20	1.5	35	33
	Totals	1,264	1.59		329	548
		Volume-averaged chloride concentration		1.3		
Site 2, mountain reach of Cottonwood Creek, near Oyarbide Fault (NWIS 404034117114501)						
11/09/1999	04/19/2000	235	1.7 (?)	7.4 (?)	61	147
04/19/2000	10/10/2000	345	<0.14	<0.4	90	80
10/10/2000	04/04/2001	304	0.43	1.4	79	116
04/04/2001	10/18/2001	210	0.40	1.9	55	36
11/07/2001	05/21/2002	448	0.81	1.8	117	136
05/21/2002	11/20/2002	242	0.31	1.3	63	33
	Totals	1,784	3.79	—	465	548
		Volume-averaged chloride concentration		2.1		
	[2] Totals	1,549	2.09	—	404	401
		Volume-average chloride concentration		1.3		

[1] Precipitation at Marigold Mine, from monthly totals, shown for comparison.

[2] Omitting sample period 11/09/1999–04/19/2000.

Table 7. Selected water-quality data from wells in Trout Creek drainage near or upstream of site 3-GT, north-central Nevada.

[Location of wells and test hole shown in figure 15. All samples processed through U.S. Geological Survey laboratory in Arvada, Color. Abbreviations: m, meters; mg/L, milligrams per liter, ^{3}H, tritium activity and 2-standard deviation counting uncertainty; Bq/L, becquerels per liter; δD, delta dueterium; δ^{18}O, delta oxygen-18; ‰, per mil deviation from sea water (Gonfiantini, 1978)]

[1] Well or test hole name	Date sampled	Depth below land surface: well screen, in m	Depth below land surface: water level, in m	Chloride, in mg/L	^{3}H, in Bq/L	δD, in ‰	δ^{18}O, in ‰
MPS-18-1	10/21/2002	204–229	217.6	18.4	86 ± 51	−124.5	−16.14
[2] MR-2275	10/23/2002	Open hole	135.0	20.9	−8 ± 51	−125.0	−15.95
MIL2001-1	10/22/2002	283–307	213.0	23.1	140 ± 51	−123.3	−15.80
MIL2002-2	10/23/2002	277–302	257.9	24.4	27 ± 27	−124.7	−16.04
			Average	22			

[1] National Water Information System (NWIS) site-identification numbers are: 404357117103301 (well MPS-18-1), 404228117113201 (test hole MR-2275), 404105117104101 (well MIL2001-1), and 404115117102001(well MIL2002-2).

[2] Ground-water sample was collected when depth of hole reached 317 meters. The polymer drilling mud and several well-bore volumes of water were pumped from the hole the day before sampling. Additional water was pumped at 360 liters per minute for 15 minutes immediately before sampling.

Table 8. Estimate of ground-water recharge in mountain part of drainage upstream of site 3-GT using chloride-balance method, Trout Creek drainage, north-central Nevada.

[Location of streamflow-gaging station is shown in figure 15. Abbreviations: PTTN, precipitation; GW, ground water; mg/L, milligrams per liter; m^{3}, cubic meters; %, percent]

Average chloride concentration in: [1] PTTN, in mg/L	[2] Runoff, in mg/L	[3] GW, in mg/L	Estimated average annual volume of: [4] PTTN, in m^{3}	[5] Runoff, in m^{3}	[6] GW recharge, in m^{3}	Average annual runoff plus GW flow, in m^{3}	in % PTTN
1.3	15.	22.	$128. \times 10^{5}$	3.4×10^{5}	5.2×10^{5}	8.6×10^{5}	7

[1] Volume-averaged bulk chloride concentration in precipitation (wetfall plus dryfall) from samples collected between April 2000 and November 2002 (table 6).

[2] Average chloride concentration in runoff from thirteen Trout Creek samples collected upstream of Marigold Mine between March 1998 and May 2002 (U.S. Department of Interior, Bureau of Land Management, 2003, p. 3-33).

[3] Average chloride concentration in ground water from samples collected in October 2002 (table 7).

[4] From table 6.

[5] Average annual volume of runoff was from annual runoff at site 3-GT for water years 2000 and 2002, adjusted to long-term average annual runoff using gage on Humboldt River near Battle Mountain, about 25 kilometers to the east.

[6] Average annual volume of ground-water recharge upstream of site 3-GT, calculated on the basis of equation 5.

The stable isotopes of hydrogen, expressed as δD (delta deuterium, the normalized difference, relative to sea water, of the ratio of deuterium, ^{2}H, to ordinary hydrogen, ^{1}H), ranged from 123 to 125 per mil. The stable isotopes of oxygen, expressed as $\delta^{18}O$ (the similarly normalized difference in the ratio of ^{18}O to ^{16}O), ranged from 15.8 to 16.1 per mil. The range was within the uncertainty of each estimate (± 2 per mil for δD and ± 0.2 per mil for $\delta^{18}O$). The δD values are similar to those measured in winter precipitation in central Nevada (Smith and others, 2002) again suggesting that ground-water recharge is from modern-day precipitation.

Summary and Conclusions

Trout Creek has an actively recharged ground-water system, controlled by the combination of geologic features and precipitation. Much of the precipitation in the Trout Creek drainage falls during winter months, when temperatures are near or below freezing and evapotranspiration is small. Precipitation therefore generally accumulates as snow at the higher elevations in the watershed. Streamflow produced by precipitation and snowmelt was observed near the mountain front for periods of 4 to 8 weeks during water years 1999 through 2002. Streamflow commenced in March or April and ceased in May or June. Streamflow in Trout Creek in 1999 reached the Humboldt River floodplain from April to June, following a winter of above-normal precipitation. In contrast, streamflow reached only the middle reach of the piedmont alluvial plain during the normal to below-normal precipitation years of 2000 through 2002.

The extent and duration of flow along the channel was determined using several methods, including analysis of streambed temperatures obtained with single-channel data loggers, subsurface temperature profiles obtained with a thermocouple nest, and pressure transducers. The pressure transducers provided the most reliable estimates of the duration of flow, although they were damaged by freezing. The onset of flow could be reasonably estimated from the self-contained temperature loggers and subsurface temperature profiles. Long periods of no flow generally could be determined by evaluating differences in minimum daily temperatures. However, estimating brief periods of intermittent flow that often occurred each day near the end of runoff was difficult because the thermal signal of drainage cessation is indistinct.

A numerical model that simulated unsteady streamflow with streambed infiltration was used to estimate the duration of streamflow and the annual percentage of streambed infiltration for selected reaches of Trout Creek. Analysis of simulation results indicate that cumulative streambed infiltration along the channel varied as a function of runoff in the mountain drainage upstream of site 3-GT. Simulated flow did not extend past the middle reach of the piedmont alluvial plain during 2000 and 2002, consistent with field observations. The model was also used to simulate streambed infiltration losses for May 12, 1999. Model results matched measured flows in the lower reaches of the piedmont alluvial plain when streambed-infiltration rates were increased by a factor of two.

The model has utility in evaluating streambed infiltration along similar intermittent streams provided that streamflow is measured near the mountain front, that channel lengths and cross-sectional areas characterized reasonably well, and that the relation between stream stage and streambed-infiltration rate is known for each reach with distinctive properties.

Although the upper and middle reaches on the piedmont alluvial plain constituted the greatest area of channel, more streambed infiltration occurred along the lowest reach whenever flow extended to it. The marked increase in streambed infiltration along the lower reach of the piedmont alluvial plain was attributed to the combination of an increase in the permeability and to a decrease in channel armoring. Armoring of the upstream portion of the channel by large quartzite cobbles embedded in a sand matrix decreased the effective area for streambed infiltration. Channel deposits in the lower reaches lack armoring, consisting only of fine gravels and sands. The armoring of the upper reaches is a nearly ubiquitous feature of fan deposition in which poorly sorted coarse sediments are deposited near the head of a fan and better-sorted and finer-grained sediments are deposited near the foot.

Percolation beneath the channel in areas of streamflow was indicated by increased water content to depths of 6 m, as determined by neutron logging. Water contents beneath the channel were higher and more variable than water contents 20 m away from the channel. Chloride concentrations beneath the channel to depths of at least 6 m were substantially lower than those away from the channel. The data indicate active recharge beneath the channel stemming from infiltration that remains relatively focused during subsequent percolation. The frequency and duration of streambed infiltration is sufficient to maintain relatively high water contents and low chloride concentrations to depths of at least 6 m beneath the channel, compared with interchannel areas.

Variability in climate affects discharge and duration of streamflow onto the piedmont alluvial plain, which shifts the balance between downstream infiltration losses and mountain-block ground-water recharge. During years of normal to below-normal precipitation, all streamflow is lost to streambed infiltration along the lower mountain reach and upper to middle reaches of the piedmont alluvial plain. During periods of above-normal precipitation, streambed infiltration is greater along the lower reaches of the drainage. This result is likely typical for other watersheds in the Middle Humboldt River Basin. The timing, duration, magnitude, and location of annual streambed infiltration and ground-water recharge from intermittent streams that flow across alluvial fans and piedmont alluvial plains vary strongly, but in a systematic way, with variations in precipitation patterns.

Average annual ground-water recharge in the mountainous portion of the Trout Creek drainage was estimated on the basis of chloride mass balance to be roughly 5.2×10^{5} m^{3}. Near the mountain front, the average annual volume of

runoff was 3.4×10^5 m^3. This latter estimate was based on two years of record from Trout Creek (water years 2000 and 2002) adjusted by the variation in long-term runoff of the Humboldt River near Battle Mountain, Nev. Annual runoff from Trout Creek in water years 2000 and 2002 was 2.1×10^5 and 1.2×10^5 m^3, respectively. Annual runoff of the Humboldt River for those two years was 53 and 42 percent of the long-term average runoff. The combined annual volume of ground-water recharge and surface runoff from the Trout Creek drainage near the mountain front was 8.6×10^5 m^3, which is about 7 percent of the estimated average annual precipitation in the mountain-block part of the drainage. The sum of mountain-block runoff plus ground-water recharge to annual precipitation estimated in this study, on an average annual basis, closely matches the original Maxey-Eakin estimate for ground-water recharge.

Acknowledgments

We are grateful for support received from the Nevada Department of Conservation and Natural Resources, Carson City, Nev., and to Glamis Marigold Mining Company, Valmy, Nev., and Newmont Mining Corporation, Carlin, Nev., for assistance and access to property. Douglas McGibbon and John Barber (Glamis Marigold Mining Company) provided geologic logs of test borings and wells, ground-water levels, meteorological data, and data on ground-water and surface-water chemistry. Paul Pettit and Patricia Cannon (Newmont Mining Corporation) provided streamflow and meteorological data. Glamis Marigold Mining Company provided two neutron-access holes in the channel near the mine that were installed by Eklund Drilling Company, Inc., Elko, Nev. Paul Pettit and Johnny Zhan (Barrick Gold Corporation) provided many helpful comments and suggestions on an early draft of this report.

References Cited

Allander, Kip, Gortsema, Gary, Hutchinson, Douglas, and Schwartzenberger, James, 2001, Water resources data Nevada water year 2000: U.S. Geological Survey Water-Data Report NV–00–1, 570 p.

Berris, S.N., Crompton, E.J., Joyner, J.D., and Ryan, Roslyn, 2003, Water resources data Nevada water year 2002: U.S. Geological Survey Water-Data Report NV–02–1, 600 p.

Burden, R.L., and Faires, J.D., 1997, Numerical analysis (6th ed.): Pacific Grove, Calif., Brooke/Cole Publishing Co., 811 p.

Burkham, D.E., 1970, A method for relating infiltration rates to streamflow rates in perched streams, U.S. Geological Survey Professional Paper 700–D, p. D266–D271.

Cohen, Philip, 1963, An evaluation of the water resources of the Humboldt River Valley near Winnemucca, Nevada: Nevada Department of Conservations and Natural Resources, Water Resources Bulletin 24, 104 p.

Chow, V.T., Maidment, D.R., and Mays, L.W., 1988, Applied hydrology: New York, McGraw-Hill, Inc., 572 p.

Cunge, J. A., Holly, F.M., and Verway A., 1980, Practical aspects of computational river hydraulics: Pitman Publishing, London, 420 p.

Dalrymple, Tate, and Benson, M.A., 1968, Measurement of peak discharge by the slope-area method: U.S. Geological Survey Techniques of Water-Resource Investigations, Book 3, Chapter A3, 12 p.

Daly, Christopher, Neilson, R.P., and Phillips, D.L., 1994, A statistical-topographic model for mapping climatological precipitation over mountainous terrain: Journal of Applied Meteorology, v. 33, no. 2, p. 140–158.

Dettinger, M.L., 1989, Reconnaissance estimates of natural recharge to desert basins in Nevada, U.S.A., by using chloride-balance calculations: Journal of Hydrology, v. 106, no. 1/2, p. 55–78.

Eakin, T.E., Price, Don, and Harrill, J.R., 1976, Summary appraisals of the Nation's ground-water resources—Great Basin region: U.S. Geological Survey Professional Paper 813–G, 37 p.

Fetter, C.W., 1993, Contaminant hydrogeology: New York, Macmillan Publishing Company, 458 p.

Gionfiantini, R., 1978, Standards for stable isotope measurements in natural compounds: Nature, v. 271, p. 534–536.

Healy, R.W., 1990, Simulation of solute transport in variably-saturated porous media with supplemental information on modification of the U.S. Geological Survey's computer program VS2D: U.S. Geological. Survey Water-Resources Investigations Report 90–4025, 125 p.

Healy, R.W., and Ronan, A.D., 1996, Documentation of the computer program VS2DH for simulation of energy transport in variable saturated porous media—Modification of the U.S. Geological Survey's computer program VS2DT: U.S. Geological. Survey Water-Resources Investigations Report 96–4230, 36 p.

Hopmans, J.W., and Dane, J.H., 1986, Thermal conductivity of two porous media as a function of water content, temperature, and density: Soil Science, v. 142, no. 4, p. 187–195.

Houghton, J.G., Sakamoto, C.M., and Gifford, R.O., 1975, Nevada's weather and climate: Nevada Bureau of Mines and Geology Special Publication 2, 78 p.

Kosugi, K., Hopmans, J.W., and Dane, J.H., 2002, Parametric models, *in* Dane, J.H., and Topp, G.C., eds., Methods of soil analysis, part 4, physical methods: Madison, Wis., Soil Science Society of America, Inc., p. 739–757.

Maurer, D.K., and Berger, D.L., 1997, Subsurface flow and water yield from watersheds tributary to Eagle Valley hydrographic area, west-central Nevada: U.S. Geological Survey Water Resources Investigations Report 97–4191, 56 p.

Maxey, G.B., and Eakin, T.E., 1949, Ground water in White River Valley, White Pine, Nye, and Lincoln Counties, Nevada: Nevada State Engineer, Water Resources Bulletin 8, 59 p.

Niswonger, R.G., 2001, Assessing streamflow processes in mountain front streams using surface/groundwater modeling: Reno, Nev., University of Nevada, Reno, unpublished master's thesis, 91 p.

Niswonger, R.G., and Rupp, J.L., 2000, Monte Carlo analysis of streambed seepage rates, *in* Wigington, P.J., and Beschta, R.C., (eds.), Riparian ecology and management in multiland use watersheds: American Water Resources Association, p. 161–166.

Niswonger, R.G., and Prudic, D.E., 2003, Appendix B—Modeling heat as a tracer to estimate streambed seepage and hydraulic conductivity, *in* Stonestrom, D.A., and Constantz, Jim, eds., Heat as a tool for studying the movement of ground water near streams: U.S. Geological Survey Circular 1260, p. 81–89.

Niswonger, R.G., Prudic, D.E., Pohll, G., and Constantz, Jim, 2005, Incorporating seepage losses into the unsteady streamflow equations for simulating intermittent flow along mountain-front streams: Water Resources Research, doi: 2004/WR003677.

Phillips, J.V., and Ingersoll, T. L., 1998, Verification of roughness coefficients for selected natural and constructed stream channels in Arizona: U. S. Geological Survey Professional Paper 1584, 77 p.

Prudic, D.E., Niswonger, R.G., Wood, J.L., and Henkelman K.K., 2003, Trout Creek—estimating flow duration and seepage losses along an intermittent stream tributary to Humboldt River, Lander and Humboldt Counties, Nevada, *in* Stonestrom, D.A., and Constantz, Jim, eds., Heat as a tool for studying the movement of ground water near streams: U.S. Geological Survey Circular 1260, p. 57–71.

Rachocki, A.H., 1981, Alluvial fans: John Wiley and Sons, Ltd., New York, 161 p.

Roberts, R.J., 1951, Geologic of the Antler Peak quadrangle, Nevada: U.S. Geol. Survey Quad. Map GQ–10.

Roberts, R.J., 1964, Stratigraphy and structure of the Antler Peak Quadrangle, Humboldt and Lander Counties, Nevada: U.S. Geological Survey Professional Paper 459–A, 93 p.

Smith, G.I., Friedman, Irving, Veronda, Guida, and Johnson, C.A., 2002, Stable isotope compositions of waters in the Great Basin, United States, 3. Comparison of groundwaters with modern precipitation: Journal of Geophysical Research, v. 107, no. D19, p. ACL 16-1 to 16-5.

Stewart, J.H., and McKee, E.H., 1977, Geology and mineral deposits of Lander County, Nevada: Nevada Bureau of Mines and Geology Bulletin 88, p. 1–59.

Stockton, E.L., Jones, C.Z., Rowland, R.C., and Medina, R.L., 2004, Water resources data Nevada water year 2003: U.S. Geological Survey Water-Data Report NV–03–1, 679 p.

Stonestrom, D.A., and Blasch, K.W., 2003, Appendix A—Determining temperature and thermal properties of heat-based studies of surface-water ground-water interactions, *in* Stonestrom, D.A., and Constantz, Jim, eds., Heat as a tool for studying the movement of ground water near streams: U.S. Geological Survey Circular 1260, p. 75–80.

Strelkoff, T., 1970, Numerical solution of Saint-Venant equations: Journal of Hydraulic Engineering, v. 96, p. 223–252.

U.S. Department of Interior, Bureau of Land Management, 2003, Final supplemental environmental impact statement, Glamis Marigold Mining Company's millennium expansion project: Bureau of Land Management Field Office, Winnemucca, Nevada, 409 p.

U.S. Department of Commerce, 2003, Monthly station normals of temperature, precipitation, heating and cooling degree days, 1971–2000: National Oceanic and Space Administration, National Climatic Data Center, Asheville, North Carolina, Climatography of the United States No. 81, 26 Nevada , 26 p.

Willden, Ronald, 1964, Geology and mineral deposits of Humboldt County, Nevada: Nevada Bureau of Mines and Geology Bulletin 59, 154 p.

Western Region Climate Center, 2003, Monthly Total Precipitation for Battle Mountain SE and Winnemucca WSO Airport, Nevada accessed December 2003 at url http:/www.wrcc.dri.edu/summary.

Zawislanski, P. T., and Faybishenko, Boris, 1999, New casing and backfill design for neutron logging access boreholes, Ground Water, v. 37, no. 1, p. 33–37.

Thermal Methods for Investigating Ground-Water Recharge

By Kyle W. Blasch, Jim Constantz, and David A. Stonestrom

Introduction

Recharge of aquifers within arid and semiarid environments is defined as the downward flux of water across the regional water table. The introduction of recharging water at the land surface can occur at discreet locations, such as in stream channels, or be distributed over the landscape, such as across broad interarroyo areas within an alluvial ground-water basin. The occurrence of recharge at discreet locations is referred to as focused recharge, whereas the occurrence of recharge over broad regions is referred to as diffuse recharge. The primary interest of this work is focused recharge, but regardless of the type of recharge, estimation of downward fluxes is essential to its quantification.

Direct measurement of water flux in the subsurface is difficult, prompting investigators to pursue indirect methods. Geophysical approaches that exploit the coupled relation between heat and water transport provide an attractive class of methods that have become increasingly reliable and widely used in investigations of recharge—for example, in chapters D–H, J, and K of this volume. This appendix reviews the application of heat to the problem of recharge estimation. Geophysical methods other than heat are presented in appendix 2.

Tutorials on measuring and modeling heat as a tracer of hydrologic processes have appeared elsewhere (Stonestrom and Blasch, 2003; Niswonger and Prudic, 2003). The objective of this appendix is to provide a fairly complete account of the theoretical underpinnings together with a comprehensive review of thermal methods in practice.

Like chemical tracers, heat can come from natural sources or be intentionally introduced to infer transport properties and aquifer recharge. The admission and redistribution of heat from natural processes such as insolation, infiltration, and geothermal activity can be used to quantify subsurface flow regimes (fig. 1). Heat is well suited as a ground-water tracer because it provides a naturally present dynamic signal and is relatively harmless over a useful range of induced perturbations; however, artificially exchanging heat with ground-water systems can change the hydraulic properties and fluid fluxes of interest. Specific properties that depend on temperature include viscosity, density, and surface tension, all of which affect hydraulic conductivity and fluid flow.

Thermal methods have proven valuable for recharge investigations for several reasons. First, theoretical descriptions of coupled water-and-heat transport are available for hydrologic processes most often encountered in practice. These include land-surface mechanisms such as radiant heating from the sun, radiant cooling into space, and evapotranspiration, in addition to the advective and conductive mechanisms that usually dominate at depth. Second, temperature is theoretically well defined and readily measured. Third, thermal methods for depths ranging from the ground surface to depths of hundreds of meters are based on the same physical principles. Finally, numerical codes for simulating heat and water transport are widely available.

Investigators began using subsurface temperatures to delineate recharge areas and infer directions of ground-water flow about the turn of the 20th century. During the 1960s, analytical and numerical solutions for simplified heat- and fluid-flow problems became available. These solutions, though one-dimensional and otherwise restricted, provided a strong impetus for applying thermal methods to problems of liquid and vapor movement in systems ranging from soils to geothermal reservoirs.

The combination of fast processors, massive data storage, and efficient matrix techniques now provide numerical solutions to complex, three-dimensional transport problems. These solutions allow researchers to take advantage of the considerable information content routinely achievable in high-accuracy temperature work.

Theoretical Framework

Darcy (1856) demonstrated that the movement of water through a porous medium is the product of the medium's hydraulic conductivity and the gradient of total head, where total head is composed of a gravitational and a pressure component. Electrical, chemical, and thermal gradients represent potential-energy fields that also are capable of inducing fluid flow. In most cases, induced fluid, chemical, and energy fluxes can be approximately conceptualized as linearly independent summations of the products of gradients acting on a given domain times a set of corresponding coupling ("phenomenological") coefficients, or constants of proportionality (Freeze and Cherry, 1979; Warrick, 2003). Following Warrick (2003), the hydraulic flux Q (L t^{-1}) is given as the summation of pressure, gravitational, and thermal gradients, X (L L^{-1}), multiplied by the coupling coefficients, L (L t^{-1}):

$$Q_i = \sum_{j=1}^{3} L_{ij} X_j \ , \qquad (1)$$

where the subscript j denotes pressure, gravitational, and thermal gradients, and the subscript i denotes water in the present case or, with appropriate changes to units, heat.

Darcy's law is thus a special case of equation 1. The flow of liquid water through isothermal but variably saturated media is induced by a hydraulic gradient composed of pressure and gravitational terms:

$$Q = L_{11} X_1 + L_{12} X_2 \ . \qquad (2)$$

Substitution of gradients and coupling coefficients produces:

$$Q = -K_H(\theta)\nabla\psi - K_H(\theta)\nabla z \ , \qquad (3)$$

where K_H is the hydraulic conductivity (L t^{-1}), which depends strongly on soil-water content θ (L^3 L^{-3}), ψ is pressure head (L), and z is elevation head (L). The symbol ∇ is the del operator denoting (here) the gradient of a scalar in three dimensions.

Equation 3 can be generalized to include temperature gradients and vapor flow:

$$Q = -D_\theta \nabla\theta - D_T \nabla T - K_H(\theta)\nabla z \ , \qquad (4)$$

where Q is now the total water flux (vapor plus liquid) due to hydraulic, thermal, and temperature gradients (L t^{-1}), D_θ is the moisture diffusivity (L^2 t^{-1}), and D_T is the sum of vapor and liquid thermal moisture diffusivity ($L^2 t^{-1} T^{-1}$). The first term on the right-hand side of equation 4 is a diffusion-formalized hydraulic flux that is actually driven by a gradient in pressure head, which—with some restrictions—can be related to the gradient in moisture content by means of the soil-moisture characteristic $\theta(\psi)$. The second term is a liquid-plus-vapor diffusive flux driven by the temperature gradient. The third term is the gravitational hydraulic flux, written here for liquid water only. This latter simplification is possible because the specific density of liquid water is some 40-thousand times higher than water vapor at standard temperature and pressure.

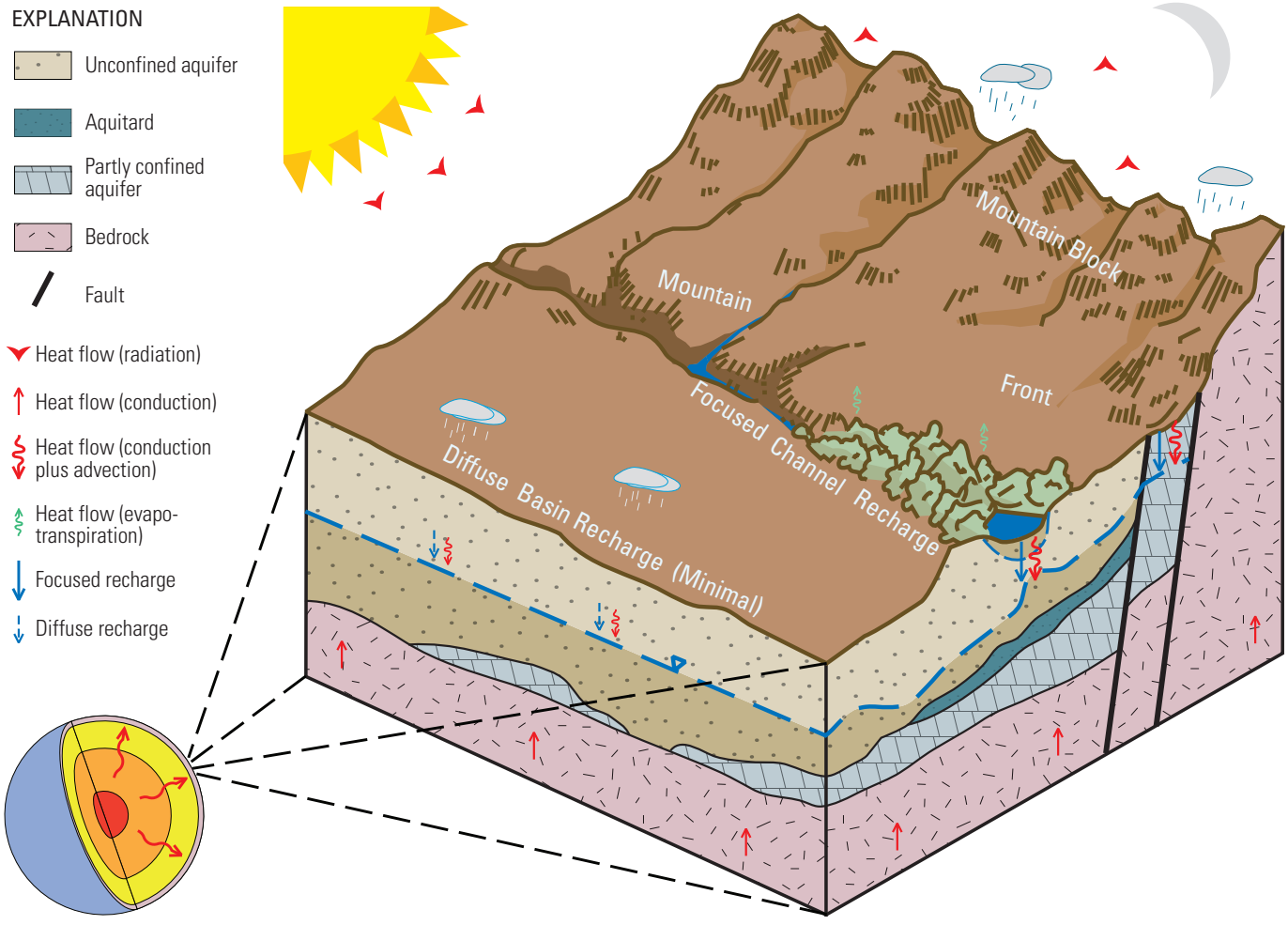

Figure 1. Conceptual model of coupled water and heat transport through focused (for example, channel and mountain block) recharge and diffuse (for example, basin) recharge processes. Thermal energy is sustained by radiant heating from the sun and geothermal heating from the Earth's interior.

Temperature Gradients

Conditions frequently encountered in nature produce large gradients in hydraulic head that cause water at an initial temperature to flow into a new location with a contrasting temperature. For example, alpine streams can rapidly transport near-freezing meltwater to warmer portions of the channel at lower altitudes. Irrigation water applied to agricultural fields often has a sharply contrasting temperature from that of ambient soils and subsoil sediments.

Fluid movement is usually dominated by pressure and elevation gradients rather than by temperature gradients, at least for high-to-medium water contents. Nevertheless, Hoekstra and Miller (1967) documented thermally induced migration of liquid water at the pore scale in partially frozen soils. And at larger scales, Bredehoeft and Papadopulos (1965) described redistribution of water in the saturated zone due to density gradients arising from spatial variation in temperature.

Arid and semiarid sediments are often far from saturation. Because the hydraulic conductivity of dry materials is many orders of magnitude below that of water-saturated materials, naturally occurring hydraulic gradients—though often large—are insufficient to drive appreciable amounts of liquid movement. Over an appreciable range of low-to-intermediate water contents, temperature gradients tend to dominate the movement of water, predominantly as vapor (Philip and de Vries, 1957; Rose, 1963; Walvoord and others, 2004). Scanlon and Milly (1994) simulated thermally driven vapor fluxes in near-surface sediments of a semiarid basin in the Chihuahuan Desert. Acting over many years, thermally induced vapor movement accounted for the deepening of tritiated water ($^{3}H–O–^{1}H$) relative to radioactive chloride ions ($^{36}Cl^{-}$) generated by above-ground nuclear-weapons testing in the 1950s and 1960s (Scanlon, 1994; Scanlon and Milly, 1994). As a practical matter, early designs for heat-pulse probes produced problematic amounts of moisture movement due to induced temperature gradients (Ren and others, 1999; Ren and others, 2000).

Distribution of Heat in the Subsurface

The background distribution of temperature in the subsurface reflects the flows of thermal energy from two primary sources—the cyclic radiant heating and cooling from above, and nearly constant geothermal heating from below (fig. 1). Spatial flows of heat are strongly influenced by climate and geology. Shallow temperature regimes vary with latitude, altitude, topography, soil and sediment properties, shading, and vegetation, in addition to sources and sinks of heat. Soil and sediment properties include composition—particularly soil-organic-matter content—and structure, layering, and water content.

Subsurface sources of heat include microbial metabolism, radioactive decay, magmatic intrusions, and tectonic activity. Geothermal energy provides heating from deep within the Earth's crust, mantle, and core. The outward propagation of heat from the planet's interior results in a characteristic geothermal gradient. The shape of the geothermal profile reflects (1) the local thickness and thermal properties of the crustal rocks through which the heat is escaping towards space, (2) radiogenic additions of heat from local crustal rocks, and (3) regional magmatic emplacement (Lachenbruch and Sass, 1977).

At the land surface, temporal fluctuations in temperature due to changes in deep geothermal heating are negligible compared to those due to (1) diurnal fluctuations in incoming (predominantly shorter wave) and outgoing (predominantly longer wave) radiation and (2) sensible heat exchanges with overlying air. Bare-soil surface temperatures typically lag the radiant diurnal cycle by approximately one hour. Surface heating of wet soils is decreased appreciably by the large latent heat of evaporating water. For soils with vegetative cover, soil surface temperatures are reduced as a consequence of shade, transpiration, and the thermal mass of the canopy. Under a vegetated canopy, soil-surface temperatures change mostly by contact with air, and thus lag the daily cycle of air temperature rather than the radiant diurnal cycle.

The cyclical nature of vertical heat exchange is manifested in characteristic downward-pinching temperature envelopes (Heath, 1964; Lapham, 1987). As oscillating temperature signals propagate downward from the surface, heat is exchanged with a progressively greater mass of sediments. This results in signal attenuation manifested in a decrease in the width of temperature envelopes with depth (fig. 2). Annual temperature envelopes capture the range and persistence of annual cooling and heating and extend wider and deeper than diurnal temperature envelopes. Temperature envelopes at depth narrow to a point where cyclic variations are no longer detectable. As shown in subsequent sections, the depths of temperature envelopes depend sensitively on hydraulic fluxes within the sediments (fig. 2).

Heat Propagation Through Conduction

If the movement of fluids is temporarily not considered, then the flow of thermal energy from a radiatively heated or geothermal source, for example, can be described by Fourier's first two laws of heat conduction. Fourier's first law states that heat flow in a homogeneous material is directly proportional to the temperature gradient:

$$q_T = -K_T(\theta)\nabla T \ , \qquad (5)$$

where q_T is the thermal (heat) flux (E L^{-2} t^{-1}) and K_T is the thermal conductivity (E L^{-1} t^{-1} T^{-1}). Dimensions E, L, T, and t represent energy, length, temperature, and time. The thermal conductivity is approximately independent of temperature but varies with water content, as indicated. Equation 5 is analogous to Darcy's law (eqn. 3).

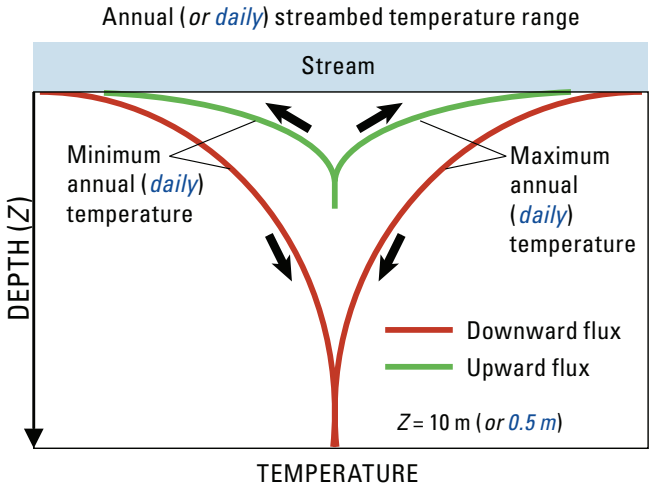

Figure 2. Ranges of sediment temperatures versus depth, *Z*, for gaining stream conditions (green lines) compared with losing stream conditions (red lines), over daily or annual cycles. The depth at which the temperature becomes constant depends upon the upward or downward flow of water through the sediments. For annual profiles, this depth may be 10 meters or more for downward flow versus less than a few meters for upward flow. For diurnal cycles, the depths at which temperatures become constant are shallower by the square root of (365/1) for a neutral flux. (Modified from Constantz and Stonestrom, 2003.)

Fourier's second law of heat conduction states that the rate of change in thermal energy stored in a volume element of thermally conducting medium is equal to the divergence of the heat flux:

$$\rho_s c_s \frac{\partial T}{\partial t} = -\nabla \cdot q_T \ , \qquad (6)$$

where ρ_s is the mass density (M L^{-3}) and c_s is the specific heat capacity (E M^{-1} T^{-1}) of the medium (in this case soil or sediment).

Combining equations 5 and 6, and defining thermal diffusivity as

$$\alpha_T = \frac{K_T(\theta)}{\rho_s c_s} \ , \qquad (7)$$

produces an equation for the conductive flow of heat in four dimensions:

$$\frac{\partial T}{\partial t} = \frac{K_T(\theta)}{\rho_s c_s} \nabla^2 T = \alpha_T(\theta) \nabla^2 T \ . \qquad (8)$$

Conductive heat transport occurs by molecule-to-molecule transfer of thermal energy in solids and semi-solids, in which the molecules have no long-range motion. As with all forms of heat, the movement of energy is from higher temperature to lower temperature.

Equation 8 can be solved analytically or numerically depending on the complexity of the boundary conditions and system geometry. In one dimension, the governing equation can be written (Carslaw and Jaeger, 1959; van Wijk and de Vries, 1963a):

$$\frac{\partial T}{\partial t} = -\frac{K_T}{\rho_s c_s} \frac{\partial^2 T}{\partial z^2} \ , \qquad (9)$$

where z is the depth below the land surface (L). Equation 9 assumes a homogeneous, isotropic medium in which the thermal conductivity is constant. The diurnal temperature signal at the upper boundary, $T(z_o, t)$, is frequently approximated by a sinusoidal forcing function:

$$T(z_o, t) = T_m + T_a \sin\left[\left(\frac{2\pi}{P}\right) \cdot (t - t_o)\right] , \qquad (10)$$

where T_a is the amplitude of the temperature wave at the surface (T), T_m is the mean temperature (T), P is the period of the wave (t), and t_o is the time that the amplitude is zero (t).

The solution to equation 9 with an upper-boundary condition represented by equation 10 and a lower-boundary condition $T = T_m$ at infinite depth is:

$$T(z,t) = T_m + T_a \exp\left(\frac{-z}{D}\right) \cdot \sin\left[\left(\frac{2\pi}{P}\right) \cdot (t - t_0) - \frac{z}{D}\right] , \qquad (11)$$

where D is the damping depth (L):

$$D = \left(\frac{P\alpha_s}{\pi}\right)^{1/2} . \qquad (12)$$

The damping depth conveys several useful attributes of the thermal wave, including its speed of propagation:

$$v = 2\pi \frac{D}{P} \ . \qquad (13)$$

In addition, the amplitude of the temperature wave falls to e^{-1} (≈ 0.37) at a depth D. The phase of the temperature wave shifts 180 degrees with respect to the surface at a depth $z = D\pi$.

Equation 13 is suitable for describing annual as well as diurnal cycles. The thermal wave described by the annual cycle can penetrate about 19 times deeper than the diurnal wave, the square root of 365 being approximately 19. Peerklamp (1944) provides solutions for amplitude and phase of thermal waves as a function of depth for the case of layered systems.

The addition of nonflowing water in the pore space causes an increase in the volumetric heat capacity as well as the thermal conductivity. To the degree that heat is transported only by conduction, the solution just given remains applicable. The change in thermal conductivity is more pronounced than the change in the thermal heat capacity, resulting in an

increased thermal diffusivity. As shown above, the damping depth of the thermal wave is directly proportional to the square root of the thermal diffusivity. Thus, contrary to what might be expected, increasing saturations result in a faster (and deeper) propagation of a thermal signal into the profile (fig. 3).

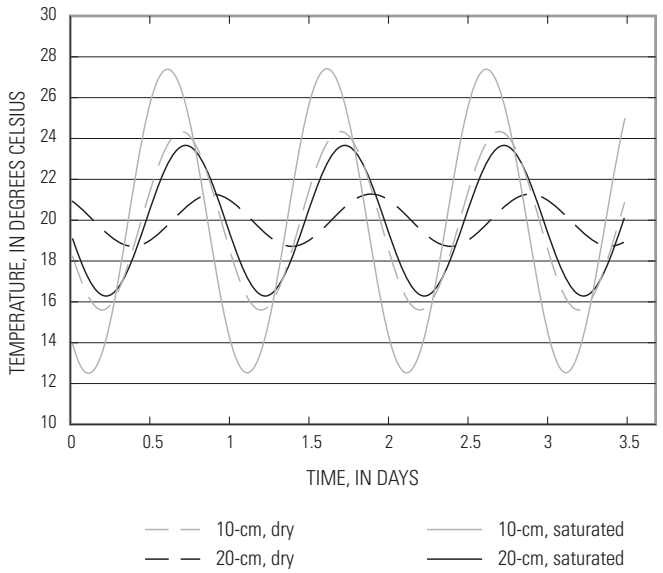

Figure 3. Conductive heat transport in a sandy soil at 10-cm and 20-cm depths for dry (dashed lines) and saturated (solid lines) water contents, computed with typical thermal properties of Rillito Creek sediments (chapter H, this volume).

Heat Propagation Through Conduction plus Advection

The previous section considered only conductive heat transport. Advective heat transport associated with pore-water movement changes the distribution of temperatures described by equation 11. Advection is the transport of heat by the organized movement of fluid from one location to another. The term "convection" as used especially in the older literature is synonymous with the term "advection" as used here. In the context of ground-water recharge, the advection of heat is primarily through the flow of liquid water and thus depends primarily on hydraulic-flux density, water content, and initial and boundary conditions.

The nonisothermal transport of water through a variably saturated porous medium can be described by the following generalization of the Richards equation:

$$\frac{\partial \theta}{\partial t} = \nabla \cdot \left(D_T \nabla T \right) + \nabla \cdot \left(D_\theta \nabla \theta \right) - \frac{\partial K(\theta)}{\partial z} \quad , \qquad (14)$$

where D_T is the thermal moisture diffusivity ($L^2 t^{-1} T^{-1}$), D_θ is the hydraulic moisture diffusivity ($L^2 t^{-1}$), and t is time. Richards' original equation combined the equation of continuity with Darcy's law for isothermal conditions to describe the change of water content due to capillary and gravitational gradients alone (Richards, 1931).

The corresponding heat-transport equation balances the change in stored thermal energy with the inflow and outflow of heat through conduction, advection, dispersion, and sources and sinks within the porous medium (Kipp, 1987; Nasser and Horton, 1992; Healy and Ronan, 1996). The following equation represents contributions from these sources in homogeneous and isotropic sediments:

$$\left[\theta C_w + (1-\varphi) C_s \right] \frac{\partial T}{\partial t} = \nabla \cdot \left[K_T(\theta) \nabla T \right] + \nabla \cdot \left(\theta C_w D_H \nabla T \right) - \nabla \theta C_w Q T + q^* C_w T^* \quad , \qquad (15)$$

where φ is the sediment porosity ($L^3 L^{-3}$), C_w and C_s are the volumetric heat capacities of water and bulk sediment, respectively, K_H is the bulk thermal conductivity, D_H is the hydrodynamic dispersion tensor ($L^2 t^{-1}$), Q is the hydraulic flux ($L t^{-1}$), q^* is the rate of water added per volume of porous medium from an external or internal source (t^{-1}), and $T^*$is the temperature of that water source (T).

The left-hand side of equation 15 represents the change in thermal energy stored in the liquid and solid phases; heat stored in the gas phase is assumed to be negligible. The change in stored thermal energy is balanced by the terms on the right, beginning with the energy transported by thermal conduction followed by the energy transported by thermomechanical dispersion. The remaining two terms represent the energy transported by advection and sources or sinks of heat within the domain. Thermomechanical dispersion caused by mixing of water within the porous medium is treated by a hydrodynamic dispersion tensor term D_H analogous to that from solute-transport theory, defined as follows (Healy and Ronan, 1996):

$$D_{H_{i,j}} = \alpha_T |v| \delta_{ij} + (\alpha_L - \alpha_T)(v_i v_j) / |v| \quad , \qquad (16)$$

where α_T is the transverse dispersivity of the porous medium (L), $|v|$ is the magnitude of the hydraulic flux-density vector ($L t^{-1}$), v_i is the ith component of the hydraulic flux-density vector ($L t^{-1}$), δ_{ij} is the Kronecker delta operator (equal to 1 if $i=j$; otherwise equal to 0), α_L is the longitudinal dispersion (L), and i and j are indices (i = 1, 2, 3; j = 1, 2, 3) representing the orthogonal Cartesian directions. Heat transport is coupled to fluid flow not only through the thermal and hydraulic gradients, but also through the water-content- and temperature-dependent phenomenological coefficients.

The equations for coupled water and heat transport, 14–16, provide the mathematical foundation for the application of thermal methods to recharge investigations. Thermal methods can be grouped into shallow-, intermediate-, and deep-application ranges, although the boundaries between the depth ranges are not distinct. Similar mechanisms and principles apply to all ranges.

A key factor differentiating shallow, intermediate, and deep thermal profiles with respect to recharge analysis is the periodicity or stability of the temperature profile. At shallow depths, aperiodic fluctuations in weather and radiation along with periodic fluctuations on diurnal and annual periods generate large transients in temperature. At intermediate depths temperature profiles are more stable, changing cyclically with the seasons, such that changes due to vertical water fluxes combine with the annual temperature cycle to produce temperature profiles intermediate between those of shallow, diurnally varying profiles and the nearly constant temperature profiles at depth (fig. 4). Temperature profiles at depth are mostly controlled by the interplay of water movement with deep-seated, upwardly directed geothermal gradients. Deep profiles tend to be stable, changing only on decadal or longer time scales in most cases. Shifts in temperature regimes at large depths indicate substantial changes in recharge conditions.

Emergence of Thermal Methods

Thermal methods of soil-moisture and ground-water investigations came into widespread use in the early to mid 1960s. Whereas earlier investigations, such as those of Smith (1910) and Rorabaugh (1956), used heat qualitatively to locate sources of ground-water recharge and ground-water flow paths, it was not until Suzuki (1960), Stallman (1965), and Bredehoeft and Papadopulos (1965) published analytical solutions to the coupled heat and water transport equations that thermal methods for estimating rates of subsurface water movement came into general use. Suzuki (1960) used temperature measurements to estimate infiltration and deep percolation in rice paddies by assuming saturated, vertical, steady state flow in a homogeneous medium with a sinusoidal daily surface temperature. Suzuki presented an approximate analytical solution to a simplified form of equation 15, assuming the temperature at depth was equal to the mean surface temperature. For one-dimensional, vertical transport, the governing equation is (Suzuki, 1960):

$$\frac{\partial T}{\partial t} = \frac{K_T}{c_s \rho_s}\frac{\partial^2 T}{\partial z^2} - \frac{c_w \rho_w}{c_s \rho_s} v_z \left(\frac{\partial T}{\partial z}\right). \qquad (17)$$

Stallman (1960; as reported in Stallman, 1963) independently developed a three-dimensional generalization of equation 17 from first principles and remarked that an analytical solution was available for the one-dimensional case, attributed to Robert E. Glover. Stallman (1965) published an exact solution for the one-dimensional problem solved approximately by Suzuki. Like Suzuki, Stallman represented the upper boundary condition as a sinusoidal temperature fluctuation; however, Stallman investigated the propagation of annual as well as diurnal temperature signals. Stallman estimated that his exact analytical solution could be used to detect percolation rates as low as 0.1 cm/d by using annual temperature signals and 0.3 cm/d by using diurnal signals. At lower velocities, heat transport through conduction would become dominant. Taniguchi and Sharma (1993) employed Stallman's (1965) one-dimensional solution to determine recharge beneath two forested sites near Perth, Australia. Ground-water recharge rates obtained by this method were consistent with results obtained with chemical tracers.

Additional early approaches to solving the one-dimensional coupled transport equation include a type-curve method developed by Bredehoeft and Papadopulos (1965), discussed in the following section, and a heat-balance method developed by Wierenga and others (1970). Wierenga developed the heat-balance method to model temperatures in irrigated soils. For purposes of analysis the soil is discretized into horizontal layers, and different mathematical approaches are used to simulate early and late-time behavior. For periods of infiltration and appreciable soil-water redistribution, interlayer transfers of heat are adjusted to match measured temperatures by algebraically adjusting transfers of water. After the transfer of water between layers becomes negligible, subsequent (conductive-only) heat flow is modeled with an explicit finite-difference form of the one-dimensional heat equation. Taniguchi and Sharma (1993) evaluated the heat-balance method and found that, while useful for estimating water fluxes near the surface, its accuracy deteriorated quickly with depth. They concluded that the heat-balance method is limited to the upper two meters because changes in temperature below this depth could not be resolved with sufficient accuracy.

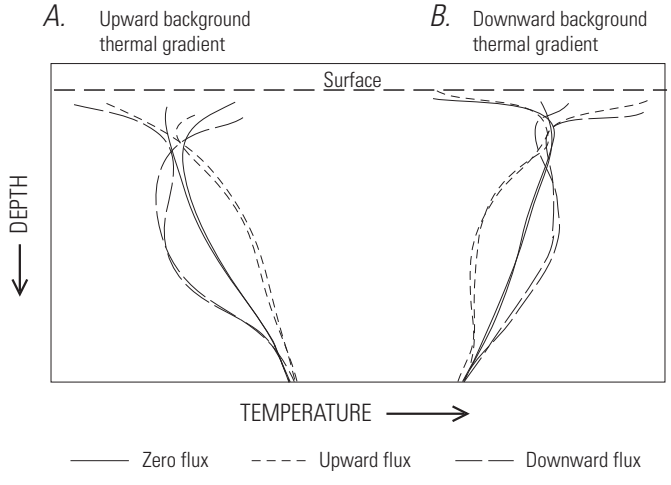

Figure 4. The influence of vertical water flow on the shape of background thermal gradients. Upward, zero, or downward fluxes of water superimposed on *A*, an upward (geothermal) background gradient, or *B*, a downward background thermal gradient. Example constructed from data obtained at Rillito Creek, Arizona (chapter H, this volume).

Early Thermal Methods for Estimating Deep Recharge

The fact that ground-water movement in deep sediments causes anomalies in the Earth's geothermal gradients was realized by the 1930s (Van Orstrand, 1934; Bullard, 1939). Deviations from linearity in vertical thermal profiles were proposed as a means to identify the extent and thickness of low-permeability layers near the production interval of an aquifer (Norris and Spieker, 1962). The discovery of subterranean hot springs thousands of feet below land surface enabled Lovering and Morris (1965) to estimate amounts of fresh water coming from the surface versus geothermal water coming from depth on the basis of a simple conductive heat-flow and water-mixing model. Schneider (1972) used deviations in thermal profiles to qualitatively infer the presence of aquifer recharge beneath a losing reach of a river in the presence of ground-water pumpage.

Bredehoeft and Papadopulos (1965) presented a general analytical solution to the differential equation describing the steady flow of heat and fluid in the deep subsurface and showed how it could be used to estimate vertical ground-water velocities in and hydraulic conductivities of confining layers. The solution assumes vertical steady-state ground-water flow through a homogeneous layer. The authors presented type curves corresponding to various combinations of medium properties and flow rates. They estimated that with available thermometry one could detect Darcian water fluxes as small as 0.1 cm/d in a 10-m thick semiconfining layer. The type-curve method quickly became popular for determining ground-water velocities because it required minimal data collection and was easy to apply (Cartwright, 1970; Sorey, 1971; Cartwright, 1979, Boyle and Saleem, 1979).

Cartwright (1970) constructed contour maps of temperatures at 500 feet by linear interpolation of surface data and data from deep exploration boreholes throughout Illinois and compared them with theoretical maps derived from extrapolations of geothermal gradients measured at the bottom of the boreholes and the assumption of no fluid flow. The residuals of predicted minus interpolated temperatures showed regions of positive and negative anomalies corresponding to areas of inferred recharge and discharge. Cartwright (1970) applied the analysis of Bredehoeft and Papadopulos to estimate water movement at the basin scale and, in later work, to estimate ground-water movement between two aquifers (Cartwright, 1979). Similarly, Sorey (1971) calculated vertical flow velocities on the order of 0.3 m/yr hundreds of feet below the land surface in semiarid basins in New Mexico and Colorado. Velocities from the type-curve method were similar to those from water-budget and pump-test analyses. Sorey recommended that the type-curve method be restricted to cases where the geology was well characterized and relatively simple. Stevens and others (1975) recommended that temperature profiles used in thermal analysis be measured in a borehole that has sat idle for several years, allows no circulation from one interval to another inside or along the outside of the casing, and has a diameter no greater than 5 cm. Furthermore, they warned against using metal casing, which conducts heat preferentially, and cement-based grout, which generates heat while curing.

Numerical methods were also introduced starting in the 1970s to interpret temperature anomalies in terms of water movement. Supko (1970) measured temperatures in the unsaturated zone to delineate ground-water flow in the Tucson Basin of Arizona by using a "valley mapping function" developed from a numerical heat- and fluid-transport model. Areas of recharge and paths of subsequent ground-water movement were delineated by tracks of relatively low ambient subsurface temperatures.

Expansion of Thermal Methods

During the 1970s and early 1980s, field and numerical studies were conducted in Europe and the United States to determine the feasibility of storing thermal energy in confined and unconfined aquifers (Tsang and Hopkins, 1982). Data from field experiments greatly improved the understanding of fluid flow resulting from temperature gradients. Sophisticated numerical models of multiphase heat and fluid transport emerged. A large number of thermal investigations undertaken during this period, including modeling techniques and calibration methods, are summarized in Beck and others (1989).

During the past two decades, thermal methods have been increasingly applied to problems of water availability in arid and semiarid communities. Many of these communities depend on ground water as a primary source for agricultural, domestic, and industrial uses. As shown by the examples in chapters D–H, J, K (this volume), thermal methods have been increasingly applied to identify and enumerate channel infiltration and basin recharge. A major factor has been the improvement in field instrumentation, including temperature sensors and data-storage technology. A recent development is the use of fiber-optic-cable techniques—which, while relatively expensive, allow nearly continuous measurements of temperature in space and time (Day-Lewis and others, 2006; Selker and others, 2006; Gungle, 2007).

Investigations of Channel Infiltration and Recharge

Channel recharge is defined as recharge that originates as channel infiltration. Infiltration rates measured at the streambed provide upper bounds for channel recharge. They are upper bounds because some of the infiltrating water will be subsequently lost to evapotranspiration. Water evaporates directly from the channel following the cessation of ephemeral flow. In addition, water that moves laterally from the channel may also not reach the water table, returning instead to the atmosphere through evapotranspiration adjacent to the channel.

Thermal methods are advantageous for determining seepage losses because useful measurements can be obtained from

the sediments beneath the channel surface. Buried sensors are less prone than surface instruments to loss by scour and deposition or damage by flood-borne debris. Measurements can be obtained during large flows that render surface measurements impractical and unsafe. Infrequent events are more easily captured. Traditional seepage losses are determined as the difference in stage-based discharge at two or more points along a reach. Stage-based estimates of discharge tend to be inaccurate, especially for large, non-steady flow events. Infiltration rates inferred by using thermal methods are essentially point measurements, differentiating them from seepage losses inferred by discharge measurements, which involve integration of infiltration rates along a reach.

Lapham (1987) monitored temperature profiles beneath streams to determine the magnitude and direction of water exchanges between streams and underlying aquifers. He modeled the coupled transport of water and heat by obtaining solutions to explicit finite-difference representations of equation 17. This approach allowed the use of measured (nonsinusoidal) temperature boundary conditions at the channel surface as well as a ground-water temperature not equal to the mean surface value. Lapham's approach provided simultaneous estimates of effective hydraulic conductivities and vertical flow rates for water.

Silliman and Booth (1993) identified characteristic thermographs of gaining and losing reaches of channels by measuring streamflow and sediment temperatures along a stream in Indiana. Gaining and losing reaches were readily identified by inspection of the amplitude of the diurnal temperature signal in the streambed versus in flowing water. Losing reaches were characterized by large thermal amplitudes associated with radiant daytime heating and nighttime cooling (fig. 5). Gaining reaches were characterized by much smaller thermal amplitudes because ground water entering the stream from an underlying aquifer is buffered from diurnal forcing. Thus, temperature profiles within the streambed of a channel provide immediate information on gaining and losing portions of streams. Lee (1985) had previously used a similar analysis to identify areas of ground-water inflow and discharge in lakes. Constantz (1998) applied a similar analysis to identify gaining and losing reaches in alpine environments. Lawler (2002) identified reaches in a semiarid stream that were gaining and losing during different parts of the year. During winter the water table was above the altitude of the streambed, producing gaining conditions. During spring and summer ground-water pumping for agriculture together with riparian evapotranspiration dropped the water table below the streambed, producing losing conditions.

Silliman and others (1995) developed solutions to equation 17 for arbitrarily varying upper-boundary conditions by using the mathematical technique of superposition. The approach required the assumption of fully saturated conditions. Silliman and others used this approach in estimating stream-bed losses from temperatures measured at the base of the water column and at a depth of 25 cm in underlying stream-bed sediments.

Pure Advection Solution

Infiltration rates in the streambed vary widely. Wankiewicz (1984) analyzed thermal profiles beneath two streams in the Northwest Territories of Canada and concluded that thermal transport beneath one stream was almost entirely by conduction, whereas thermal transport beneath another stream was almost entirely by advection. The Peclet number can be used to assess the relative magnitude of advection and conduction for heat transport in ground-water recharge applications. The Peclet number is defined as follows (van der Kamp and Bachu, 1989):

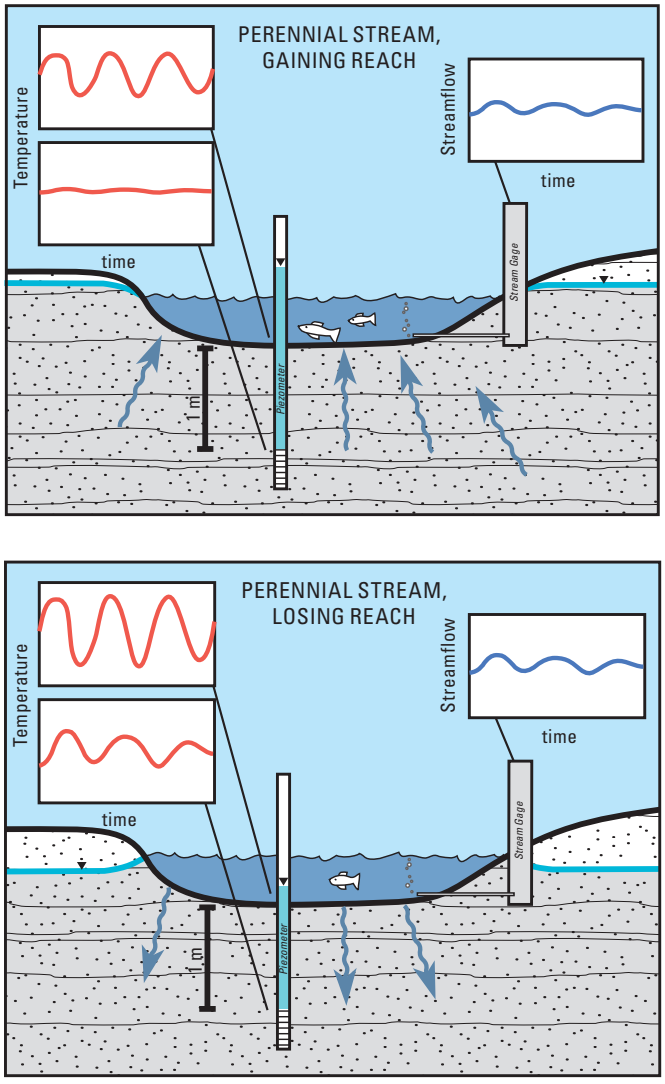

Figure 5. Idealized stream interactions with ground water, with sediment thermographs. *A*, A perennial stream gaining water from the underlying sediments. *B*, A perennial stream losing water to the underlying sediments (modified from Constantz and Stonestrom, 2003).

$$P_e = \frac{1}{\alpha}\frac{\rho_w c_w}{\rho_s c_s} Q\varphi l \ , \qquad (18)$$

where l is the characteristic length of the medium (mean grain diameter) (L), α is the thermal diffusivity of the saturated soil sediments ($L^2\ t^{-1}$), φ is the porosity ($L^3\ L^{-3}$), and Q is the hydraulic flux density ($L\ t^{-1}$). Values much less than 2×10^{-4} indicate that heat transport is dominated by conduction (Silliman and others, 1995). Conversely, values much greater than 2×10^{-4} indicate that heat transport is dominated by advection.

Several investigators considered the limiting case of purely advective heat transport (Nightingale, 1975; Taniguchi and Sharma, 1990; Constantz and Thomas, 1996). These studies determined water fluxes from measurements of the vertical propagation velocity of temperature fluctuations into saturated or nearly saturated sediments. Constantz and Thomas (1996) used the propagation velocity of diurnal temperature signals to estimate seepage rates beneath a strongly losing channel. Their analysis starts by expressing equation 17 as (Stallman, 1965):

$$K_T \frac{\partial^2 T}{\partial z^2} - Q\rho_w c_w \frac{\partial T}{\partial z} = \rho_s c_s \frac{\partial T}{\partial t} \ , \qquad (19)$$

where the first term is the gain or loss of heat by conduction (the divergence of the conductive heat flux given by Fourier's first law), the second term is the gain or loss of heat by water movement (advection), and the right-hand side is the change in stored heat per unit volume of sediment per unit time. Here Q is the component of the hydraulic flux density in the z direction (volume of water crossing a unit area of sediment per unit time; $L\ t^{-1}$). If the conductive flux of heat is negligible in comparison to the advective flux of heat, equation 19 can be simplified by eliminating the first term and solving for hydraulic flux Q (Constantz and Thomas, 1996):

$$Q = \left(\rho_s c_s / \rho_w c_w\right) V_T \ , \qquad (20)$$

where V_T is the propagation velocity of the temperature signal ($L\ t^{-1}$). Note that the specific heat capacity of sediment $\rho_s c_s$ in equations 19 and 20 is expressed per unit volume of bulk (wet) sediment (total bulk volume of all phases), whereas the specific heat capacity of water $\rho_w c_w$ is per unit volume of water (liquid only). Thus the term in parenthesis in equation 20 has the units of volumetric water content, making equation 20 parallel to the well-known equation relating the Darcy flux (hydraulic flux density) to the (macroscopic) propagation velocity V_C of an ideal chemical tracer, $Q=\theta V_c$ (see chapter E, this volume, for example). Here θ is the volume of water per bulk volume of sediment (water content). The propagation velocity of a chemical tracer will thus exceed that of the temperature signal by a factor of about two:

$$V_C / V_T = \left(1/\theta\right)\left(\rho_s c_s / \rho_w c_w\right), \qquad (21)$$

with parameter values typical of saturated sandy sediments ($\rho_s c_s$ = 2.6 MJ m^{-3} $°C^{-1}$; $\rho_w c_w$ = 4.2 MJ m^{-3} $°C^{-1}$; and θ = 0.3; see table 1 in Stonestrom and Blasch, 2003).

Constantz and Thomas calculated seepage losses from the arrival times of the daily temperature peak measured in the upper 3 m of channel sediments. Infiltration rates determined with equation 20 were about twice estimates determined from streamflow losses measured in the adjacent (upstream) reach of the channel, after correcting for evaporation. Analysis of the temperature data showed that seepage losses from intermittent streamflows were rapidly converted to deep percolation, rather than spreading laterally into near-surface storage that could later be lost to evapotranspiration.

The pure advection solution is readily applicable to multiday streamflow events with small variations in flow rate and large variations in diurnal temperature (fig. 6). Analysis becomes increasingly difficult as flow rates become more highly variable and as temperature variations at the land surface diminish. Stream segments receiving contributions from tributaries, surface runoff, and snowmelt can have erratic temperature signatures in the flowing water. As a consequence, subsurface thermographs are also erratic, making it difficult to conduct an analysis based on diurnal peaks.

Numerical Techniques for Variably Saturated Flow, Multiple Layers, and Nonperiodic Forcing

Numerical solutions to the coupled heat- and fluid-transport equations are required for most cases involving variably saturated flow, nonperiodic boundary temperatures, or non-trivial geometries. Sophocleous (1979) used a numerical model to simulate variably saturated flow of water and temperature through laboratory and field plots. Jaynes (1990) employed a similar model to evaluate the influence of layering on infiltration in agricultural soils.

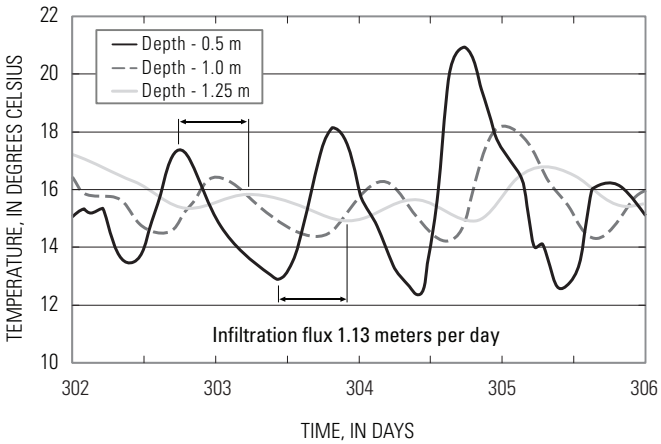

Figure 6. Example of the use of thermal amplitudes to estimate Darcy flux for predominantly advective heat transport with negligible conductive heat transport (unpublished data from Rillito Creek, Arizona).

The ability to simulate the transport of heat has been incorporated into popular numerical models for solving problems of variably saturated water movement. Well-documented, publicly accessible examples include VS2DH (Healy and Ronan, 1996), SUTRA (Voss, 1984) and HYDRUS (Simunek and others, 1998). These models solve the Richards (1931) equation for unsaturated water movement coupled to the advection-diffusion equation for heat transport by either finite-difference or finite-element methods. Because of nonlinearities, solutions are obtained by iterative approximation. The models differ somewhat in their treatment of conduction, advection, and dispersion, and they differ considerably in their representation of thermal and hydraulic parameters. Comparing results from independently developed codes thus reduces uncertainties related to the numerical solution of governing equations.

Thermal and Hydraulic Properties

Applying thermal methods to problems of water-flux measurement requires the specification of thermal and hydraulic properties. The study of Lapham (1987) included a sensitivity analysis of stream-aquifer interactions to thermal and hydraulic properties. Thermal properties depend on the water content of the sediments, with thermal conductivity and volumetric heat capacity both increasing as soil-water content increases (fig. 7). Stonestrom and Blasch (2003) present tables of thermal conductivity, thermal diffusivity, and volumetric heat capacity for several water contents and discuss techniques for measuring and calculating thermal properties. Hydraulic properties are discussed at length in van Genuchten and others (1992).

Because the viscosity and surface tension of water both vary with temperature, hydraulic properties vary with temperature as well. For example, hydraulic conductivity increases with increasing temperature. The dependence of hydraulic properties on temperature was investigated in the laboratory by Constantz (1982) and Nimmo and Miller (1986). These studies found that temperature dependencies of unsaturated hydraulic parameters tend to be larger than predicted by viscosity and surface tension alone. Jaynes' (1990) study of infiltration in field plots included an evaluation of temperature-dependent hydraulic conductivities on infiltration rates. Mitchell and others (1990) and Duke (1992) documented large temperature effects on infiltration fluxes in agricultural settings. Despite the greater-than-expected temperature sensitivity of hydraulic properties, the water-content dependence still dominates (van Genuchten and others, 1992).

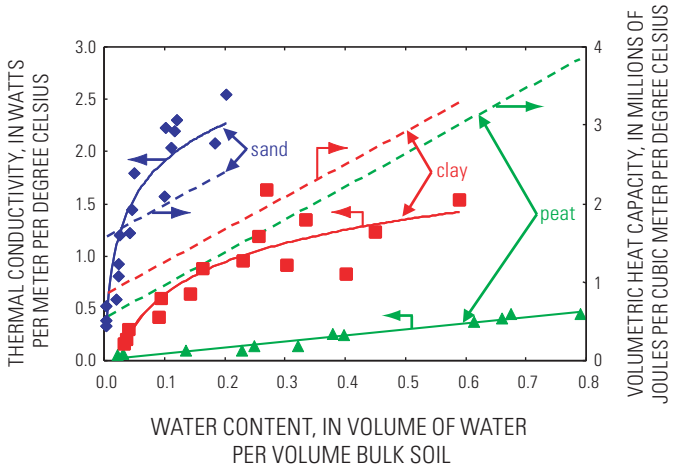

Figure 7. Dependence of volumetric heat capacity and thermal conduction on water content for selected materials. Dashed lines are volumetric heat capacities calculated as described in Stonestrom and Blasch (2003). Points are experimentally determined thermal conductivities from de Vries (1963). Solid curves are empirical fits to the thermal-conductivity data. (Modified from Stonestrom and Blasch, 2003.)

A main reason that thermal techniques are well suited to determining water fluxes is the relative lack of dependence of thermal conductivity on sediment texture and water content relative to the large dependencies of hydraulic conductivity on these same parameters (fig. 8; Constantz and Stonestrom, 2003). Because of this, hydraulic conductivity largely controls both the percolation flux and the propagation of thermal signals in strongly advective systems (Niswonger and Prudic, 2003).

The large diurnal variations in stream temperature typical of arid and semi-arid environments strongly influence streamflow losses and associated ground-water recharge. Constantz and others (1994) showed that seepage losses from streams in Colorado and New Mexico closely tracked diurnal variations in stream temperature, with loss rates fluctuating on the order of 25 percent with daily temperature cycles that fluctuated in the range of 4–18˚C and 10–25˚C for Colorado and New Mexico streams, respectively. These changes were attributed to the inverse temperature dependencies of both water viscosity and water density. Both streams were located near mountain fronts. Measurements of streamflow loss and evapotranspiration at the New Mexico site indicated that 95 percent of the seepage loss became ground-water recharge. Decreased temperatures at night simultaneously reduced infiltration and extended the distal range of streamflow. Similar effects were observed in a stream in Nevada by Ronan and others (1998) and in a stream in Arizona by Blasch and others (2000). In the latter study, post-flow drainage and redistribution rates increased as much as 50 percent with a change in temperature from 14˚C to 28˚C. The temperature effects on seepage velocities were modeled using VS2DH by Ronan and others (1998), Bartolino and Niswonger (1999), and Bailey (2002). Bailey (2002) showed that seepage velocities were more sensitive to hydraulic conductivity than stage for conditions encountered in Rillito Creek, Arizona.

Further Considerations for Investigation of Specific Recharge Processes

Thermal methods offer a variety of approaches for investigating recharge processes, whether it involves infiltration at

the land surface or percolation at depth. The following section reviews pertinent considerations for three main applications of thermal methods, the first two of which involve measurements at relatively shallow depths—the characterization of ephemeral streamflow, and the estimation of streambed seepage fluxes. The third section discusses considerations involving the application of thermal techniques to the deep unsaturated zone.

Streamflow Detection

Measuring the duration and extent of streamflow in large semiarid and arid basins is important for identifying channels that contribute to ground-water recharge. Methods employed for monitoring inputs to basin-scale and regional-scale sized recharge models need to be inexpensive and reliable. Traditional streamflow-gaging techniques are generally inapplicable because of the flashy nature of streamflow, shifting channel- geometries, the wide dynamic range of flow rates, and the potential importance of low-flow conditions. Transients in flow rates and shifting channel geometries invalidate stage-discharge relations.

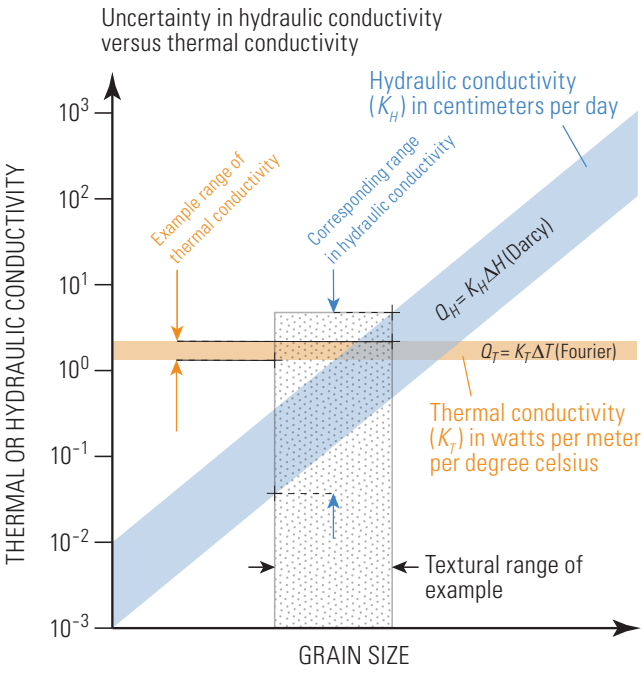

Figure 8. Uncertainty in hydraulic conductivity versus thermal conductivity. The hydraulic conductivity of saturated sediments (blue band) is strongly dependent on sediment texture (represented here by the stippled 10–90 percent range in grain-size distribution), whereas the thermal conductivity (tan band) is almost independent of texture. The vertical width of the hydraulic and thermal conductivity bands gives an approximate range of each parameter for the example texture. (From Constantz and Stonestrom, 2003).

Constantz and others (2001) used streambed temperatures to indicate the presence of streamflow in central New Mexico and southeastern Nevada. The presence of streamflow was identified with large perturbations in temperatures in the shallow subsurface due to the transport of heat by advection. Benchmark temperature measurements made at similar depths adjacent to channel helped identify false positives caused, for example, by precipitation without streamflow.

Subsequent studies of ephemerally and intermittently flowing channels in the Southwest refined methodologies of sensor placement in streambed sediments and developed automated techniques for interpreting thermographs (Lawler, 2002; Stewart, 2003; Blasch and others, 2004). Optimal placement of sensors depends on the details of flow geometry and thermal forcing as well as general meteorologic, geomorphologic, and hydrologic conditions. The following section describes optimal placement for inferring streamflow timing and extent. These considerations are largely the same as for measuring sediment temperatures to estimate percolation fluxes.

Optimizing Sensor Placement

When streamflow is not present, the thermal signal from radiant heating and cooling of the streambed sediments travels into the profile primarily by conduction (fig. 9). As this signal—idealized as a sinusoidal wave—propagates into the sediments, its amplitude decreases and its time lag increases with respect to the surface forcing (van Wijk and de Vries, 1963a). The magnitude of the ideal diurnal temperature wave as a function of depth for a homogenous single layer is (van Wijk and de Vries, 1963a):

$$T_{conduction}(z) = T_o \, e^{-z/D}, \qquad (22)$$

where $T_{conduction}(z)$ is the amplitude of the sediment temperature variation at depth z, T_o is the amplitude of the diurnal temperature wave at the sediment surface, and D is the damping depth (eq. 12). The typical damping-depth value for diurnal fluctuations in sandy soils is about 0.15 m, and in clay soils about 0.12 m (van Wijk and de Vries, 1963b).

When streamflow is present, the amplitude of the diurnal temperature fluctuation at the streambed surface is almost always reduced (fig. 9). During daylight hours, a portion of the thermal energy from incoming solar radiation is used to raise the temperature of the water column and to drive evaporation. The result is a lower maximum temperature at the sediment surface when streamflow is present compared to dry channel conditions. Similarly, during the evening, an overlying water column buffers the sediment surface from cool air temperatures, resulting in higher minimum temperatures than when streamflow is absent. In addition, infiltration and percolation of water through streambed sediments increases the amount of heat transported downward due to the advection of heat. As a result, thermographs at greater depths show a marked increase in the diurnal temperature amplitude in the presence of streamflow (fig. 9).

As mentioned earlier, Stallman (1965) developed an exact analytical solution to the coupled heat- and water-transport equation for one-dimensional vertical transport in a uniform medium with a steady percolation rate and a sinusoidal temperature variation at the land surface. The diurnal temperature-wave amplitude for the advection-conduction equation 17 is (Stallman, 1965):

$$T_{advection}(z) = T_o\, e^{-az}\,, \tag{23}$$

where $T_{advection}$ is the amplitude of the sediment temperature variation due to the combined influence of advection plus conduction, and a (L) is a coefficient based on the hydraulic flux density (Darcy velocity) as well as the thermal properties of the sediment:

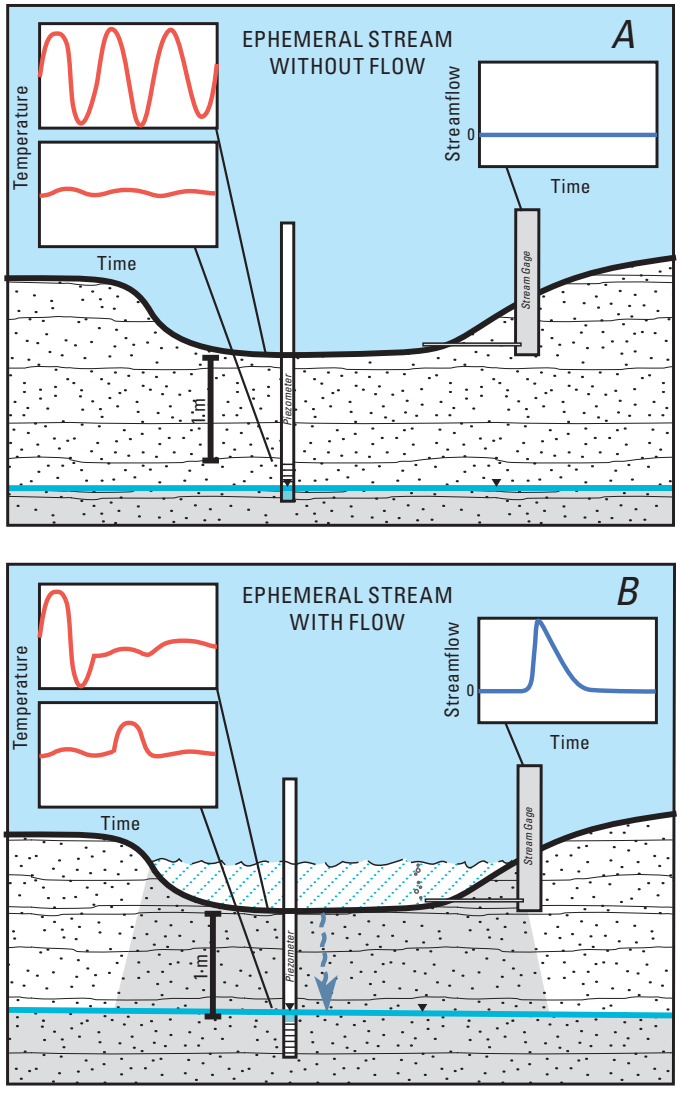

Figure 9. Streamflow hydrographs and corresponding streambed thermographs for an idealized ephemeral-stream channel *A*, before, and *B*, after onset of flow (from Constantz and Stonestrom, 2003).

$$a = \left[\left(\beta^2 + Q^4/4\right)^{1/2} + \left(\beta^2/2\right)\right]^{1/2} - Q\,, \tag{24}$$

where

$$\beta = \frac{\pi \rho_s c_s}{\lambda P}\,, \tag{25}$$

and

$$\lambda = \frac{Q \rho_w c_w}{2K_T}\,. \tag{26}$$

As discussed previously, the variable c_w is the specific heat of the fluid and sediment in combination (E M^{-1} T^{-1}), ρ_s is the density of the fluid and sediment in combination (M L^{-3}), K_T is the thermal conductivity of the fluid and sediment in combination (E L^{-1} t^{-1} T^{-1}), Q is the hydraulic flux density (L t^{-1}), c_w is the specific heat of pore water (E L^{-3} T^{-1}), and ρ_w is the density of pore water (M L^{-3}). If Q is zero, then equation 24 reduces to the conduction equation and $\beta = D^{-2}$. As Q increases, the transport of heat due to advection increases. The predominant heat-transport mechanism within the sediments depends upon percolation rate, thermal parameters, and depth. For simplicity the following discussion will refer to the transport of heat during the presence of percolation as "advection" even though conduction contributes to transport of heat.

Figure 10 contrasts the purely conductive case (conduction without water movement) to the advective case (conduction with water movement). The profiles were generated using equations 22–26 with assumed hydraulic and thermal parameters for coarse-grained sediments typical of ephemeral streams. The same thermal and hydraulic properties were used in each case. Material properties were assumed to be homogeneous.

The attenuation of diurnal temperature waves are plotted as a function of depth for three different cases of streamflow in figure 10*A*. The first (no-damping) case assumes no reduction in the amplitude of diurnal temperature at the streambed surface compared to the air-sediment interface outside of the channel. The 50-percent-damping case assumes that the amplitude of the diurnal temperature signal at the streambed surface is reduced by 50 percent in the presence of streamflow. The third case assumes a 50-percent reduction in fluid flux in addition to the 50-percent water-column damping to investigate the relative importance of advective heat flux. Comparison of the conductive (no percolation) and advective (percolation) diurnal temperature waves as a function of depth shows that the conductive thermal amplitude is larger than the advective thermal amplitude, but only near the surface (fig. 10). It is also shows that percolating water transports heat deeper into the profile than conduction alone. Obviously, a requirement for using thermographs at any depth to infer streamflow is that the hydrologic flux be sufficiently large to cause measurable deviations in the amplitude of the diurnal temperature wave at that depth when streamflow is present compared to when streamflow is absent.

To characterize depth-dependent changes in amplitude of the temperature wave resulting from percolation, the conductive temperature wave amplitude ($T_{conducton}$) at each depth is subtracted from the advective temperature wave amplitude ($T_{advection}$) (fig. 10*B*). When there is no reduction (damping) in the amplitude of the temperature wave at the sediment surface due flowing water in the channel, the difference in conductive and advective temperature-wave amplitudes at the surface is zero. At depth, however, there is a marked change between conductive and advective temperature-wave amplitudes. When the overlying water column damps the amplitude of the temperature wave at the sediment surface, there is a change in the amplitude of the temperature wave both at the surface and at depth. Thus, temperature monitoring within the profile is in general more reliable and informative than monitoring at the surface, because changes in the sign of the temperature-wave amplitude are less sensitive to possible thermal buffering by the overlying water column. This is especially true for ephemeral streams in which stage can quickly vary over a large range.

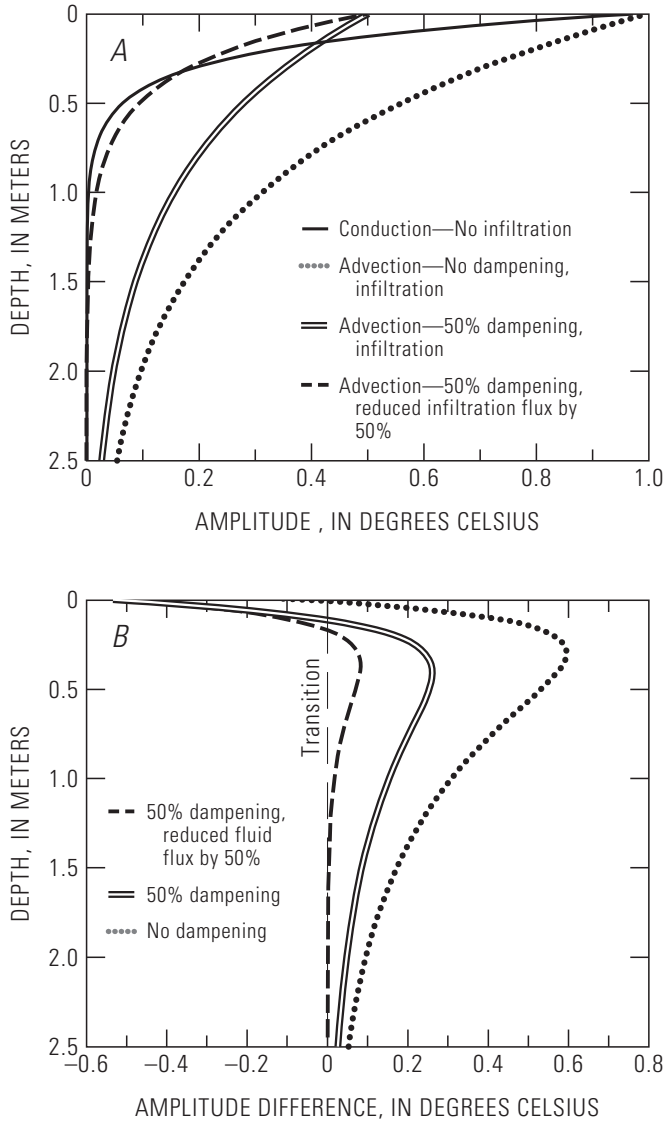

Figure 10. Amplitudes of thermal waves in a coarse-grained streambed. *A*, Conductive-only (dry channel) and advective-plus-conductive (flowing channel) thermal-wave amplitudes (single solid line and dotted line, respectively). The amplitude at the surface is 1°C. The 50-percent dampening case assumes that half of the heat signal is lost to flowing water. The 50-percent dampening–50-percent fluid-flux reduction considers in addition a fluid flux that is half of the previous two cases. *B*, Difference between advective and conductive thermal wave amplitudes as a function of depth (from Blasch and others, 2004).

Equations 22–26 can be used with knowledge of the sediment profile and percolation range to estimate optimal measurement depths for inferring streamflow. The optimal measurement depth for inferring streamflow is that depth at which streamflow-induced percolation causes the greatest change in temperature-wave amplitude relative to no-flow conditions. For the case illustrated, the optimal depth is about 0.45 m (fig. 10*B*). The least-optimal depth is that for which the presence of streamflow does not appreciably change the temperature amplitude ($T_{conduction} \approx T_{advection}$). For a given percolation rate, transition depths z_t can be identified as the shallowest depth at which the conduction and advection temperature-wave amplitudes are equal with and without streamflow. The transition depth represents the depth at which the temperature-wave amplitude with flow becomes larger than the amplitude without flow.

Depths closer to the surface than z_t may be subjected to scour or influenced by temperature anomalies induced by precipitation or cloud shadowing in the absence of flow. In extreme scour conditions, sensors can be removed entirely from the channel. Even in less extreme cases, scour and deposition complicate analysis of streambed thermographs (Constantz and others, 2001; Stewart, 2003; Gungle, 2006). Scour and fill during flow events dynamically affects the depth of the sensors below the sediment surface. This variable depth introduces uncertainty into the analysis even if sensor depths are surveyed after each flow event.

In addition to considerations just discussed, optimal depth selection for temperature sensors depends on channel cross-sectional shape, wetted perimeter, and location of adjacent vegetation and bank features. Stewart (2003) used a numerical two-dimensional model to determine the influence of cross-sectional shape on the propagation of heat both vertically and horizontally into the sediments. Rectangular-shaped channels produced more transport of heat through a combination of advection and conduction than triangular-shaped channels for the same constant-head upper boundary conditions. Blasch and others (2004) suggested placement of sensors in channel constrictions after observing timing errors caused by channel migration in otherwise optimal locations. Additionally, shading by vegetation, bridges, and steep banks anomalously reduced the diurnal amplitude, obscuring analysis (Lawler, 2002; Stewart, 2003).

Constantz and others (2001) monitored temperature at the near surface (15 cm depth) to successfully infer the presence of streamflow. The method was appropriate for the streams studied because two essential conditions for the success of this method were met. First, the diurnal temperature-wave amplitude at the surface was sufficiently large that temperature fluctuations caused by the passage of clouds, for example, did not obscure the diurnal signal. Second, during the presence of streamflow, the overlying water column produced a large reduction of the amplitude of the diurnal temperature wave at the streambed surface compared to the magnitude of the diurnal temperature wave in the dry streambed. The magnitudes of flow-induced perturbations can be quite large, especially for summer-monsoonal flows (fig. 11). On the other hand, changes in the near-surface diurnal temperature-wave amplitude during streamflow alone are often insufficient to infer the presence of streamflow. If antecedent pore-water temperatures in the bed sediments match temperatures in the flowing water too closely, it can become difficult to detect streamflow (Stewart, 2003).

Constantz and others (2001) and Stewart (2003) considered the effects of precipitation, cloud cover, and sudden changes in air temperature on heat transport through the bed sediments. In general, precipitation-induced fluid fluxes and abrupt air temperature changes do not penetrate as deeply below the sediment surface or as quickly as streamflow events, so will have a greater influence on sensors near the surface. Stewart (2003) compared sensors placed at 0-, 15-, 30-, 50-, and 100-cm depths and showed that burial to 15 cm was sufficient to differentiate rainfall infiltration from streamflow infiltration in the cases considered.

Analysis of Streamed Thermographs to Detect Presence of Streamflow

Analysis of streambed thermographs to detect streamflow can be as simple as visual identification of streamflow-induced temperature anomalies. Although visual inspection has proven useful, the technique is subjective and is time consuming for large data sets. Also, visual inspection is less effective for identifying streamflow events shorter than 24 hours in duration, which are typical of ephemeral flows in southern Arizona (Blasch, 2003; chapters H and J, this volume). To overcome these limitations, automated techniques were developed that incorporate comparative and statistical analyses.

Benchmark measurements made outside of the flowing portion of the channel were evaluated by Stewart (2003) for automating detection of streamflow. Benchmark comparison requires that environmental conditions for the in-channel and benchmark sensors be similar. Differences caused by shading, precipitation rates, soil types, and exposure to wind can obscure interpretation (Lawler, 2002; Stewart, 2003). Benchmark methods proved less useful for short duration events than for long-term events. Data from in-channel probes during dry periods were also evaluated for their ability to provide a virtual or surrogate benchmark. Recorded diurnal oscillations and amplitudes during known dry periods were used to construct monthly and seasonal dry-benchmark signatures, which were then compared to the remaining record. However, variations caused by short-term meteorological events proved even more difficult to distinguish from streamflow events with in-channel benchmarks than with out-of-channel benchmarks (Stewart, 2003).

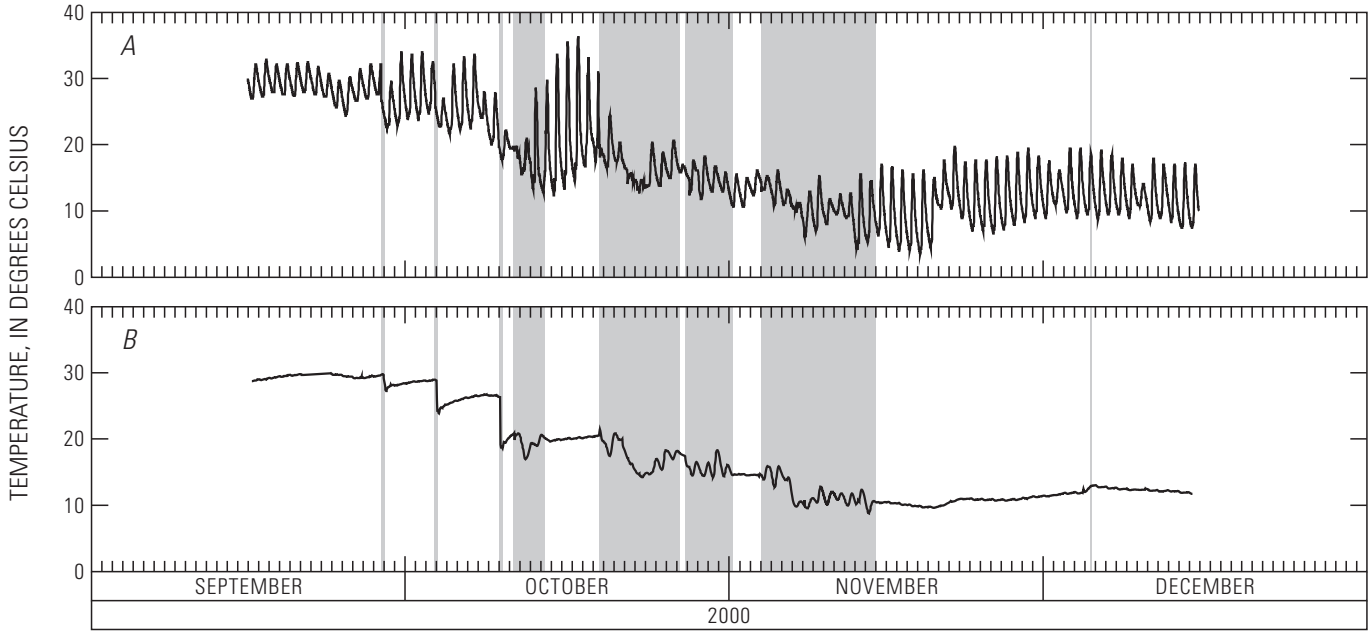

Figure 11. Thermographs for *A*, a depth above the transition depth, and *B*, a depth below the transition depth. The gray areas represent periods of streamflow (from Blasch and others, 2004).

Analysis of a streambed thermograph to infer the timing of flow is based on identification of the aforementioned temporal changes in the thermograph (fig. 9). As an example, two thermographs for a coarse-grained alluvial stream at depths above and below the transition depth are presented in figure 11. When streamflow is present (indicated in this case from a nearby streamflow-gaging station), the diurnal temperature-wave amplitudes in the sensor above the transition depth decrease, whereas below the transition depth the diurnal amplitudes increase. Streamflow timing can be inferred from the thermographs by identifying these changes in thermal amplitude above and below the transition depth. The analysis can be conducted visually (Constantz and others, 2001) or by using statistical analysis (Stewart and Constantz, 1999; Stewart, 2003; Blasch, 2003).

Gungle (2006) reported a small but distinctive additional temperature drop in the sediments of ephemeral channels immediately after at the cessation of streamflow, which dissipated as the sediments regained the diurnal temperature pattern in effect before streamflow began (fig. 12). He attributed this brief temperature minimum to evaporative cooling of freshly exposed wet sediments. Gungle used the local temperature minimum as a marker for the cessation of streamflow. Similar observations had been previously reported by Geiger (1965) and Wierenga and others (1970).

Analysis of Sensor Networks to Detect Extent of Streamflow

The deployment of multiple sensors along a single channel or within a network of channels allows relatively inexpensive detection of the geographic extent and temporal duration of ephemeral flow events. Several examples have already been discussed (Lawler, 2002; Stewart, 2003; Gungle, 2006; chapters D–H, J, and K, this volume). Exemplifying this approach, Coes and Pool installed temperature sensors at many locations in stream channels draining the Huachuca and Mule Mountains in southeastern Arizona (chapter J, this volume). Information on the temporal and spatial extent of ephemeral streamflow was used to estimate the total mountain-front recharge for the basin.

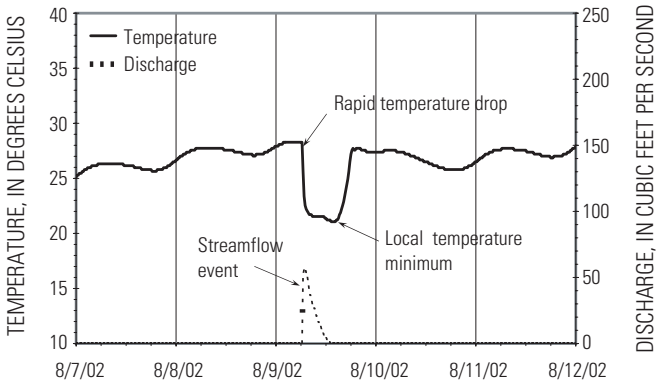

Figure 12. Thermograph and streamflow record from Greenbush Draw, southeastern Arizona, indicating the decline in temperature at the cessation of streamflow (data and interpretation from Bruce Gungle, U.S. Geological Survey, written commun., 2005).

Estimation of Percolation Fluxes

While streamflow timing alone provides qualitative information on stream-channel infiltration losses, quantifying infiltration rates and subsequent percolation fluxes and ground-water recharge amounts requires additional analysis. Of interest are not only the easily measured infiltration losses from the wetted channel but also the net (or recharging) percolation flux (infiltration minus subsequent evapotranspiration losses). Thermal methods have been widely used for estimating infiltration and percolation fluxes in small to large channels across a range of flow regimes—ephemeral, intermittent, and perennial (Constantz and Thomas, 1996; Constantz and Thomas, 1997; Ronan and others, 1998; Bartolino and Niswonger, 1999; Constantz and others, 2002; Blasch, 2003; Conlon and others, 2003).

Ronan and others (1998) developed a method to determine the vertical percolation flux beneath a streambed by solving the coupled equations for heat and water flow within the context of a publically accessible numerical model. Adaptation of the model required assigning appropriate thermal and hydraulic parameters to the bed sediments and establishing boundary conditions. As a simplification, the modeled domains were limited to fully saturated conditions, which eliminated the need to specify unsaturated parameters and the dependence of thermal and hydraulic parameters on soil-water content.

A common additional simplification is the restriction to that portion of the domain characterized by one-dimensional vertical fluxes. This restriction is often assumed to be met at all times beneath the center of the channel, and elsewhere after fully saturated conditions have been established and horizontal pressure gradients have decayed. Nevertheless, infiltration at the onset of streamflow is multidimensional, as the wetting front initially travels subhorizontally into the stream bank as well as downward. Water-content measurements in sediments of Rillito Creek at the beginning of ephemeral flow showed an initially quasi-radial progression of the wetting front, with lateral flow velocities nearly as large as vertical flow velocities (chapter H, this volume).

Instrumentation for Percolation-Flux Estimates

Estimation of vertical fluxes requires deployment of temperature sensors at multiple depths to obtain spatial and temporal coverage (fig. 13). Stream temperatures or sediment-surface temperatures are required to provide data on the upper boundary condition for subsequent analysis. Constantz and Thomas (1996, 1997) installed probes at five depths within the streambed sediments in the Middle Rio Grande Basin in

addition to water-temperature probes at the surface. Sensors were installed directly into streambed sediments at depths of 30, 60, 105, 150, and 300 cm by auger. Temperatures were recorded every 30 minutes. Because the optimal installation depths of sensors depend on factors that are unknown a-priori, the number of depths in vertical sampling arrays is typically about five to seven. A larger number of observation depths reduces inaccuracies caused by heterogeneity and also provides insurance against the loss of data due to sensor failure or removal by scour.

Bartolino and others installed lines of nested piezometers crossing the perennial Rio Grande and manually monitored ground-water temperatures over a 24-month period (Bartolino and Niswonger, 1999; Bartolino, 2003). An advantage to using a cable-logging temperature sensor was the ability to obtain high spatial resolution. Measurements were obtained at 15-cm intervals for piezometers about 9–16 meters in depth. An assumption of this method is that the water temperature inside the piezometers equaled the temperature of saturated sediments outside the piezometers.

Bailey (2002) and Coes and Pool (chapter J, this volume) applied a similar approach to the unsaturated zone beneath an ephemeral stream prone to scour and deposition. Piezometers were installed about 10 m into the bed sediments, and an array of self-contained temperature sensors was mounted on a cable and inserted into the piezometers. The temperature sensors included self-contained data loggers. This system enabled continuous data collection within the sediments and ready access to probes without having to repeatedly disturb the sediments. Temperatures inside the borehole were assumed to be equal to temperatures outside the borehole.

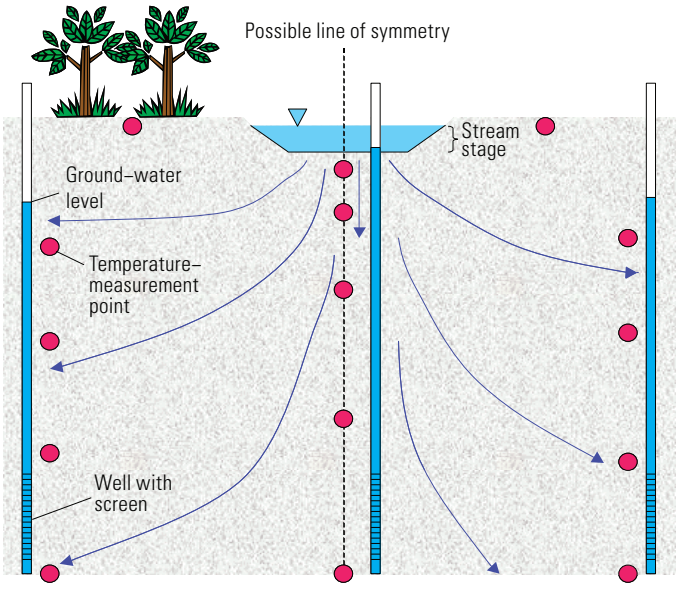

Figure 13. Conceptual modeling framework when flow through streambed is downward and outward (from Niswonger and Prudic, 2003.)

To investigate installation considerations related to the assumption of vertical fluxes, Ronan and others (1998) deployed two-dimensional arrays of temperature sensors beneath an ephemeral stream and used thermal modeling techniques to estimate two-dimensional infiltration and percolation fluxes. The authors observed vertical and lateral flow variations within the sediments due to layering as well as to the geometry of channel meandering relative to hillslope direction. As previously discussed, Stewart (2003) simulated two-dimensional flow in a rectangular channel bottom and a triangular channel bottom. Flow was predominantly vertical beneath most of the width of the rectangular channel, with lateral components of flow increasing near the edges of channel flow. The same pattern was observed beneath the triangular channel. Comparison of the two channel geometries indicated a greater proportion of vertical flow beneath the rectangular channel than beneath the triangular channel for a given head or wetted channel cross-sectional area.

Hydraulic and Energy Transport Properties

Hydraulic parameters required for numerical modeling of saturated conditions include hydraulic conductivity (a tensor for anisotropic materials), specific storage, and porosity, whereas modeling unsaturated conditions requires additional parametric functions describing soil-moisture retentivity and unsaturated hydraulic conductivity. Required thermal-transport parameters include heat capacity and thermal conductivity of the sediment, both as functions of water content, as well as thermal dispersivity. Hydraulic and energy-transport parameters can be determined from core samples (Bailey, 2002; chapter J, this volume), literature values (Bartolino and Niswonger, 1999), expert judgment (Ronan and others, 1998), or model calibration (Bartolino and Niswonger, 1999). Often a combination of methods is used to obtain the full set of required parameters.

Sensitivity analysis has shown that hydraulic conductivity is the most important parameter controlling infiltration flux (Smith and others, 1989; Wang and others, 1989; Ronan and others, 1998; Bartolino and Niswonger, 1999). Inverse calibration using automated procedures, such as PEST (Doherty and others, 1994) and UCODE (Poeter and Hill, 1998) have become routine in channel-recharge investigations (Bartolino and Niswonger, 1999; Bailey 2002; Stewart, 2003; Constantz and others, 2003). Niswonger and Prudic (2003) provide guidance on the application of inverse calibration for thermal studies of surface-water–ground-water interactions.

Boundary and Initial Conditions

Infiltration and associated percolation fluxes largely depend on the product of the hydraulic gradient and the hydraulic conductivity of the sediments. Temperature data alone can be insufficient to determine both hydraulic conductivity and water fluxes through inverse modeling procedures.

Solutions become better constrained with the consideration of additional types of data. Pressure observations are the most commonly used auxiliary data for constraining solutions of the coupled transport equations. Piezometers (often outfitted with recording transducers) can be used to measure pressure gradients in saturated sediments. Similarly, tensiometers can be used in unsaturated sediments. Measurement of matric pressure or water content is often required to obtain the required parameters for partially saturated conditions. At a minimum, hydraulic—as well as thermal—initial and boundary conditions must be specified to run the transport model.

The measured depth of water in the stream channel, if available, is usually used as the upper hydraulic boundary condition (Ronan and others, 1998; Bailey, 2002). As discussed above, Bartolino and Niswonger (1999) employed rows of piezometers to study surface-water–ground-water exchanges along the Rio Grande. Hoffmann and others (chapter H, this volume) used subsurface pressure sensors to measure hydraulic head during ephemeral flow of Rillito Creek.

The bottom boundary condition can be represented in several ways. The bottom boundary is often represented as a zero-pressure head boundary corresponding to the measured or assumed location of the water table (Ronan and others, 1998; Bailey, 2002). Another option is the use of measured pressure heads at the bottom of the model domain (Bartolino and Niswonger, 1999). Alternative approaches are to place the lower boundary at a great enough distance from the active domain that assumed stationary conditions do not affect the active domain, or to assume constant vertical gradients of temperature and pressure at depth. The latter two approaches simulate percolation as occurring into a semi-infinite half-space.

Initial conditions include pressure-head and temperature profiles in the sediments. For unsaturated media, initial water-content conditions have been determined directly from core samples (Ronan and others, 1998). Initial water-content conditions can also be determined from time-domain-reflectometry measurements (Blasch, 2003; appendix 2, this volume).

Sensitivity of Fluxes to Hydraulic Conductivity

Since modeled fluxes reflect hydraulic gradient and hydraulic conductivity, solutions are sensitive to fluctuations in stream stage and hydraulic conductivity. While stream stage can be measured independently, changes in hydraulic conductivity over the course of an ephemeral flow event can be difficult to monitor. Bailey (2002) estimated infiltration rates along Rillito Creek by using temperature monitoring and inverse simulation of heat and water transport through stream sediments. Modeling of two sequential streamflow events suggested that the hydraulic conductivity of the streambed surface layer changed by four orders of magnitude due to sediment redistribution from one event to the next. During a single event, the hydraulic conductivity changed by two orders of magnitude.

The data of Ronan and others (1998) showed generally decreasing infiltration rates throughout the duration of a multiple-day ephemeral flow event with superimposed diurnal oscillations, representing the net effect of several influences. The dominant influence was the rapid decrease in hydraulic gradient at the sediment-water column interface as infiltration proceeds. An opposing influence was the initial increase of hydraulic conductivity as water content increases from preflow to saturated conditions. Hydraulic conductivity fluctuated diurnally with fluctuating streamflow temperature.

Blasch and others (2006) simulated transient infiltration fluxes at the onset of the streamflow events by using measured field data from alluvial channels (fig. 14). The multiple transient and steady-state fluxes observed after the onset of streamflow were attributed to the layering of streambed sediments. The time between transient and steady-state periods was inversely proportional to the antecedent moisture content. The results of Coes and Pool (chapter J, this volume) indicated that even their longest recorded streamflow event, 5.5 hrs, was not long enough for infiltration to reach steady state.

Accuracy of Infiltration and Percolation Fluxes

Infiltration and percolation fluxes calculated from thermal monitoring and numerical models have been compared to fluxes calculated by using data from streamflow-gaging stations, stage recorders, chemical tracers, and soil-water content measurements. Constantz and Thomas (1996) estimated a factor-of-two difference between vertical fluxes calculated by using a thermal method and fluxes calculated from streamflow data. Ronan and others (1998) reported simulated infiltration rates that were within an order of magnitude of seepage rates determined from flume data. The difference was partially attributed to the difference in the point-scale measurements of the thermal method and reach-scale measurements of the seepage runs. To evaluate the accuracy of simple heat-based flux estimates, Blasch and others (2006) compared thermally-determined infiltration fluxes near the onset of streamflow with continuously monitored soil-water content data. Because initial transient rates are higher than eventual quasi-steady state rates, errors in cumulative infiltration caused by considering only the quasi-steady behavior ranged from 9 to 25 percent for the cases tested. Cumulative error for more typical, short-duration (8-hour) events was about 90 percent.

Niswonger and Prudic (2003) provide guidance for collecting field data and modeling measured temperatures to infer hydraulic fluxes. These procedures are designed to broaden the applicability of thermal methods while reducing measurement uncertainty.

Thermal Methods for Quantifying Deeper Recharge

Focused recharge occurs at discreet locations, such as stream channels, whereas diffuse recharge is spread over the landscape. Percolating water generally becomes more diffuse with depth (Nimmo and others, 2002); however, focused recharge in arid settings can reach great depths. This is par-

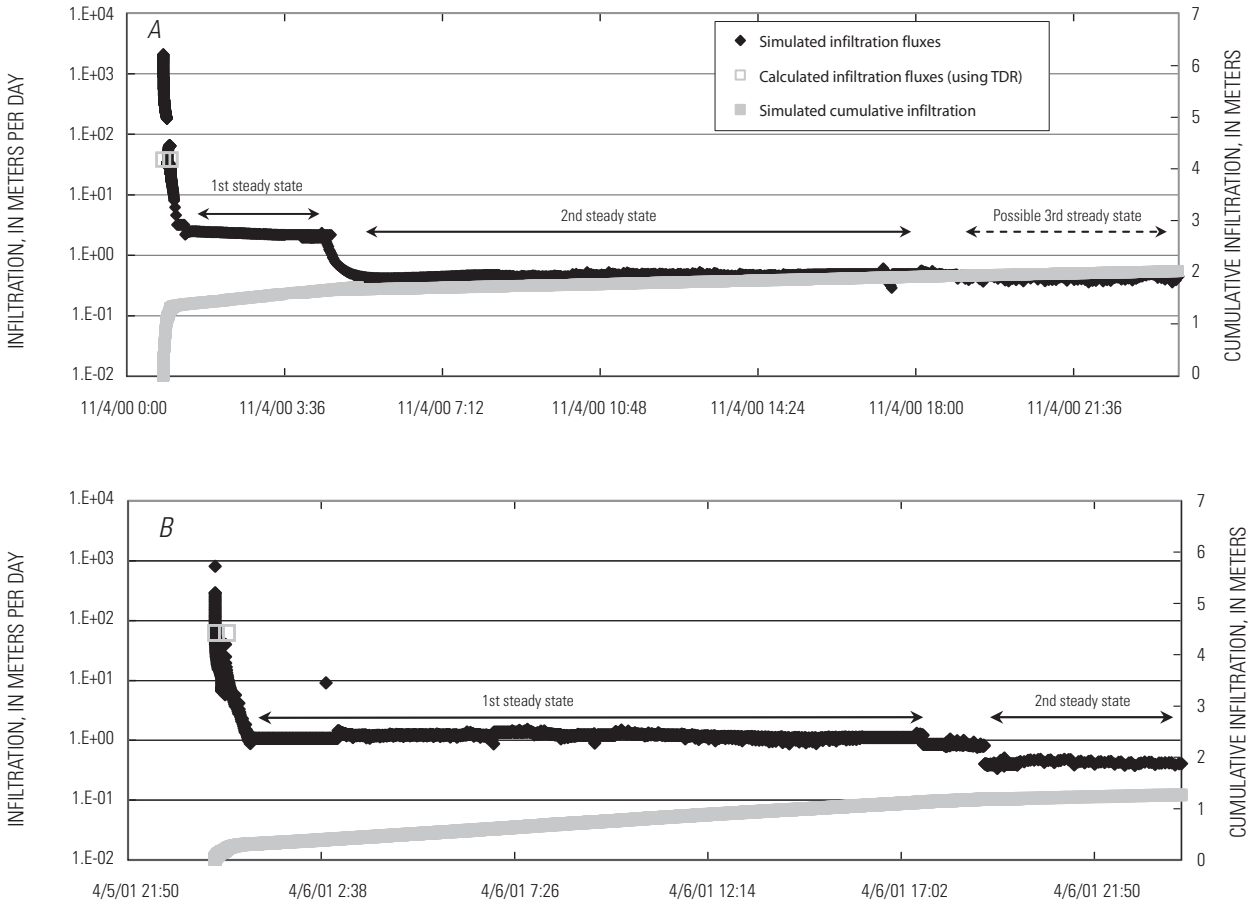

Figure 14. Simulated infiltration fluxes and cumulative infiltration for *A*, November 4, 2000 and *B*, April 6, 2001. Infiltration fluxes at the onset of streamflow were calculated by using time-domain reflectometry (TDR) water-content measurements (from Blasch and others, 2006).

ticularly true for large volume, spatially discreet inputs, such as those that occur within large ephemeral streams, and areas that receive large volumes of artificial recharge from irrigation (Stonestrom and others, 2004) and percolation ponds (Izbicki and others, chapter G, this volume). Nimmo and others (2005) provide an overview of thermal methods for the investigation of deeper recharge.

A comparison of thermal methods to track shallow, moderate, and deep percolating water on progressively slower paths toward recharge was presented by Constantz and others (2003). Temperature-estimated fluxes were as large as 20 m/d for shallow depths immediately beneath a stream channel and as small as 0.01 m/d for depths greater than 100 m below the surface beneath an alluvial fan. A trend to smaller fluxes with increasing depth was partly explained by the spreading of downward percolating moisture with depth, although deep percolation rates may reflect arrested paleorecharge (Walvoord and others, 2004). In any case, flux divergence beneath focused sources of water due to sediment layering generates additional attenuation of thermal signals beyond the amount expected in homogeneous sediments. The greater the depth of the recharge investigation, the greater the need for precision in temperature measurements. A precision of 0.1°C is usually more than adequate for estimating fluxes near the land surface, whereas a precision of at least 0.01°C is required to detect thermal perturbations at depths greater than a few tens of meters.

Studies that used thermal data to examine recharge in moderate-to-deep unsaturated zones include those of Reiter (1999, 2001), Izbicki and Michel (2002), Constantz and others (2003), and Dowman and others (2003). Examining unsaturated zones to depths of 100 m and saturated zones to depths of 350 m, Reiter used high-precision temperature logs to evaluate vertical moisture fluxes in the Rio Grande Rift in central and southern New Mexico. Thermal gradients were measured with precisions of 0.005°C/m. Vertical water fluxes as low at 1×10^{-6} m/yr were obtained by fitting quadric and cubic polynomials to measured temperature data and matching analytical solutions.

Izbicki and Michel (2002) used temperature profiles to depths of 30 m for estimating recharge rates and cumulative recharge volumes beneath ephemeral and intermittent streams across the western Mojave Desert. Air temperatures were monitored in cased and grouted boreholes in normally dry

washes to estimate the sediment-temperature profiles. Companion boreholes outside the channel were used for no-flow controls. Average annual temperatures beneath the washes were as much as 1.5°C lower than the average temperatures for the control sites. Assuming one-dimensional heat transport by conduction and advection, calculated recharging fluxes from intermittent runoff ranged from 0.22 to 0.84 m/yr depending on distance downstream from the mountain front.

In the study alluded to above, Constantz and others (2003) used thermal geophysical logs from boreholes as deep as 300 m to estimate recharge in southern Nevada beneath an alluvial-fan surface. Recharging fluxes were estimated from perturbations of assumed geothermal profiles on the basis of analytical solutions to the coupled heat-and-water flow equations as well as numerical solutions generated by TOUGH2 (Preuss and others, 1999). Estimates of recharging fluxes ranged from undetectable to 0.011 m/yr.

Dowman and others (2003) investigated temperature perturbations beneath Rillito Creek during constant-flux streambed infiltration experiments. A 5-m by 5-m bermed area was instrumented with buried thermocouples to a depth of 5 m, and a 15 m-borehole adjacent to the buried area was logged for temperature using a cable-mounted logging thermistor. Temperatures measured by the buried sensors agreed with borehole temperatures at depths greater than about 1 m. An imposed percolation flux of 0.34 m/d produced a thermal anomaly that reached 11°C of cooling at shallow depth (above the transition point) and 0–2°C of heating between 4 and 10 m depth (below the transition point). Numerical sensitivity analysis using VS2DH showed that the temperature of the percolating water and percolation rate were the most important factors in determining the temperature-profile perturbation. The analysis also showed that having the deeper temperature measurements substantially reduced the uncertainty of recharge-rate estimates compared to estimates that were based on shallow temperature measurements alone.

Conclusions

Thermal methods have emerged as a versatile class of geophysical tools for monitoring focused recharge in arid and semiarid settings. Compared to other geophysical techniques and chemical tracers, thermal methods are relatively simple and inexpensive. Heat flows through hydrologic systems naturally. Heat can also be artificially introduced and is benign over a useful range of applications. The theory for coupled heat-and-water transport is well established and incorporated into numerical models of variably saturated flow.

Recent investigations have led to improved methods for experimental design and data collection. Instrumentation has been steadily improving. Additionally, the treatment of unsaturated thermal- and hydraulic-transport processes through numerical models provides flexibility not possible 50 years ago, when Suzuki first estimated percolation rates beneath a field of rice (Suzuki, 1960).

Like other methods for determining recharge rate, thermal techniques are limited by sampling accessibility and scale of measurement, which often become limiting factors in recharge investigations. Nevertheless, thermal methods are particularly well suited for monitoring focused recharge beneath unconsolidated alluvial channels that remain dry much of the time.

The coupled relation between heat and water transport has been used to identify the occurrence, extent, and timing of streamflow. Temperature measurements have also been used to indicate gaining and losing reaches of stream channels as well as of areas of inflow to lakes. Temperature observations beneath the depth of seasonal fluctuations have been used to identify the presence and direction of water movement through analyses of anomalies in the background geothermal gradient.

Infiltration and percolation estimates determined by thermal techniques are similar to values determined by channel-flow-loss measurements and chemical tracers. In addition, thermal techniques provide the ability to continuously monitor infiltration and percolation fluxes throughout streamflow events. Thermal studies have shown that infiltration rates can vary by four orders of magnitude from the onset to late stages of ephemeral streamflow—not only because of hydraulic-gradient decay, but also because of flow-induced changes in the hydraulic conductivity of streambed sediments. Fluxes as high as 100 m/d have been detected in coarse alluvial sediments, whereas fluxes as low as 0.01 m/d have been detected in clayey sediments.

Thermal methods have been used to estimate ground-water recharge rates hundreds of meters beneath stream channels and basin floors. Lateral spreading of percolating water often reduces local vertical-flux densities to values substantially lower than those prevailing near the surface. Estimated fluxes at depths exceeding 100 m determined by thermal methods range from 0–0.01 m/d. Detecting small fluxes at such great depths requires extraordinary precision. Measurement depth is, therefore, a major consideration when applying thermal methods to estimate recharge in arid environments.

References Cited

Bailey, M.A., 2002, Analysis of one-dimensional vertical infiltration using heat as a tracer in Rillito Creek, Tucson, Arizona: Tucson, University of Arizona, master's thesis, 152 p.

Bartolino, J.R., 2003, The Rio Grande—Competing demands for a desert river, *in* Stonestrom, D.A., and Constantz, J., eds., Heat as a tool for studying the movement of ground water near streams: U.S. Geological Survey Circular 1260, p. 7–16.

Bartolino, J.R., and Niswonger, R.G., 1999, Numerical simulation of vertical ground-water flux of the Rio Grande from ground-water temperature profiles, central New Mexico: U.S. Geological Survey Water-Resources Investigations Report 99–4212, 34 p.

Beck, A.E., Garven, G., and Stegena, L., eds., 1989, Hydrogeological regimes and their subsurface thermal effects: American Geophysical Union, Geophysical Monograph, v. 47, 158 p.

Blasch, K.W., 2003, Streamflow timing and estimation of infiltration rates in ephemeral stream channels using variably saturated heat and fluid transport methods: Tucson, University of Arizona, Ph.D. dissertation, 204 p.

Blasch, K.W., Ferré, P.A., and Hoffmann, J.P., 2004, A statistical technique for interpreting streamflow timing using streambed sediment thermographs: Vadose Zone Journal, v. 3, p. 936–946.

Blasch, K.W., Ferré, T.P.A., Hoffmann, J.P., and Fleming, J.B., 2006, Relative contributions of transient and steady state infiltration during ephemeral streamflow: Water Resources Research, v. 42, no. 8, doi:10.1029/2005WR004049.

Blasch, K.W., Fleming, J.B., Hoffmann, J.P, and Ferré, P.A., 2000, Temperature and moisture content profiling of an ephemeral stream channel in a semiarid watershed—Comparison of vertical infiltration velocities at the onset and cessation of flow [abs.]: Eos (American Geophysical Union Transactions), Fall Meeting Supplement, v. 81, no. 48, p. F502.

Boyle, J.M., and Saleem, Z.A., 1979, Determination of recharge rates using temperature depth profiles in wells: Water Resources Research, v. 15, no. 6, p. 1616–1622.

Bullard, E.C., 1939, Heat flow in South Africa: Proceedings of the Royal Society of London A, v. 173, p. 474–502.

Bredehoeft, J.D., and Papadopulos, I.S., 1965, Rates of vertical groundwater movement estimated from the Earth's thermal profile: Water Resources Research, v. 1, no. 2, p. 325–328.

Carslaw, H.S., and Jaeger, J.C., 1959, Conduction of heat in solids (2d ed.): New York, Oxford University Press, 510 p.

Cartwright, K., 1970, Groundwater discharge in the Illinois Basin as suggested by temperature anomalies: Water Resources Research, v. 6, no. 3, p. 912–918.

Cartwright, K., 1979, Measurement of fluid velocity using temperature profiles—experimental verification: Journal of Hydrology, v. 43, p. 185–194.

Conlon, T., Lee, K., and Risley, J., 2003, Heat tracing in streams in the Central Willamette Basin, Oregon, *in* Stonestrom, D.A., and Constantz, J., eds., Heat as a tool for studying the movement of ground water near streams: U.S. Geological Survey Circular 1260, p. 29–34.

Constantz, J., 1982, Temperature dependence of unsaturated hydraulic conductivity of two soils: Soil Science Society of America Journal, v. 46, p. 466–470.

Constantz, J., 1998, Interaction between stream temperature, streamflow, and groundwater exchanges in alpine streams: Water Resources Research, v. 34, no.7, p. 1609–1615.

Constantz, J., Stewart, A.E., Niswonger, R., and Sarma, L., 2002, Analysis of temperature profiles for investigating stream losses beneath ephemeral channels: Water Resources Research, v. 38, no. 12, p. 51–2 to 51–13.

Constantz, J., and Stonestrom, D.A., 2003, Heat as a tracer of water movement near streams, *in* Stonestrom, D.A., and Constantz, J., eds., Heat as a tool for studying the movement of ground water near streams: U.S. Geological Survey Circular 1260, p. 1–6.

Constantz, J., Stonestrom, D., Stewart, A.E., Niswonger, R., and Smith, T.R., 2001, Analysis of streambed temperature in ephemeral stream channels to determine streamflow frequency and duration: Water Resources Research, v. 37, no. 2, p. 317–328.

Constantz, J., and Thomas, C.L., 1996, The use of streambed temperature profiles to estimate depth, duration, and rate of percolation beneath arroyos: Water Resources Research v. 32, no. 12, p. 3597–3602.

Constantz, J., and Thomas, C.L., 1997, Streambed temperature profiles as indicators of percolation characteristics beneath arroyos in the Middle Rio Grande Basin, USA: Hydrologic Processes, v. 11, p. 1621–1634.

Constantz, J., Thomas, C.L., and Zellweger, G., 1994, Influence of diurnal variations in stream temperature on streamflow loss and groundwater recharge: Water Resources Research, v. 30, no.12, p. 3253–3264.

Constantz, J., Tyler, S.W., and Kwicklis, E., 2003, Temperature-profile methods for estimating percolation rates in arid environments: Vadose Zone Journal, v. 2, p. 12–24.

Darcy, H., 1856, Les fontaines publiques de la ville de Dijon: Paris, Victor Dalmont, 647 p.

Day-Lewis, F.D., Karam, H.N., Harvey, C.F., Lane, J.W., 2006, Monitoring submarine ground-water discharge using a distributed temperature sensor, Waquoit Bay, Massachusetts [abs.]: Eos (American Geophysical Union Transactions), v. 87, no. 52, NS24A–02.

de Vries, D.A., 1963, Thermal properties of soils, *in* van Wijk, W.R., ed., Physics of plant environment (2d ed.): Amsterdam, North-Holland Publishing Co., p. 210–235.

Doherty, J., Brebber, L., and Whyte, P., 1994, PEST—Model independent parameters estimation: Brisbane, Australia, Watermark Computing, 160 p.

Dowman, C.E., Ferre, T.P.A., Hoffmann, J.P., Rucker, D.F., and Callegary, J.B., 2003, Quantifying ephemeral streambed infiltration from downhole temperature measurements collected before and after streamflow: Vadose Zone Journal, v. 2, p. 595–601.

Duke, H.R., 1992, Water temperature fluctuations and effect on irrigation infiltration: Transactions of the American Society of Agricultural Engineers, v. 35, no. 1.

Freeze, R.A., and Cherry, J.A., 1979, Groundwater: Englewood Cliffs, N.J., Prentice-Hall, p. 25–26.

Geiger, R., 1965, The climate near the ground: Cambridge, Mass., Harvard University Press, 611 p.

Gungle, B., 2006, Timing and duration of flow in ephemeral streams of the Sierra Vista subwatershed of the Upper San Pedro River Basin, Cochise County, southeast Arizona: U.S. Geological Survey Scientific Investigations Report 2005–5190, 47 p.

Gungle, B., 2007, Investigation of ground-water/surface-water interactions in the San Pedro River near Charleston using fiber-optic distributed temperature methods [abs.], in Sustainable water, unlimited growth, quality of life: Can we have it all?, Arizona Hydrological Society, Proceedings of the 20th Annual Symposium, August 29–September 1, 2007, Tucson, Arizona [electronic medium).

Healy, R.W., and Ronan, A.D., 1996, Documentation of computer program VS2DH for simulation of energy transport in variably saturated porous media—Modification of the U.S. Geological Survey computer program VS2DT: U.S. Geological Survey Water-Resources Investigations Report 96–4230, 36 p.

Heath, R.C., 1964, Seasonal temperature fluctuations in surficial sand near Albany, New York: U.S. Geological Survey Professional Paper 475–D, p. D204–D208.

Hoekstra, P., and Miller, R.D., 1967, On the mobility of water molecules in the transition layer between ice and a solid surface: Journal of Colloid Interface Science, v. 25, p.166–173.

Izbicki, J.A., and Michel, R.L., 2002, Use of temperature data to estimate infiltration from intermittent streams in the western Mojave Desert, USA, *in* Foo, D.Y., ed., Balancing the ground water budget, Proceedings of the International Association of Hydrogeologists Meeting in Darwin, Australia, May 12–14, 2002 [CD-ROM): Kenilworth, UK, IAH, 9 p.

Jaynes, D.B., 1990, Temperature variation effects on field measured infiltration: Soil Science Society of America Journal, v. 54, no. 2, p. 305–312.

Kipp, K.L., 1987, HST3D—A computer code for simulation of heat and solute transport in three-dimensional ground-water flow systems: U.S. Geological Survey Water-Resources Investigations Report 86–4095, 517 p.

Lachenbruch, A.H., and Sass, J.H., l977, Heat flow in the United States and the thermal regime of the crust, *in* Heacock, J.G., ed., The Earth's crust: American Geophysical Union, Geophysical Monograph 20, p. 626–675.

Lapham, W.W., 1987, Use of temperature profiles beneath streams to determine rates of vertical ground-water flow and vertical hydraulic conductivity: U.S. Geological Survey Water Supply Paper 2337, 35 p.

Lawler, David, 2002, Using streambed temperature sensors to monitor flow events in the San Pedro River, southeastern Arizona, and north-central Sonora, Mexico: Tucson, University of Arizona, master's thesis, 68 p.

Lee, D.R., 1985, Method for locating sediment anomalies in lakebeds that can be caused by groundwater flow: Journal of Hydrology, v. 79, p.187–193.

Lovering, T.S., and Morris, H.T., 1965, Underground temperatures and heat flow in the East Tintic District, Utah: Geological Survey Professional Paper 504–F, 27 p.

Mitchell, K.C., James, L.G., Elgar, S., and Pitts, M.J., 1990, Characterizing cyclic water-level fluctuations in irrigation canals: Journal of Irrigation and Drainage Engineering, v. 116, no. 2, p. 261–272.

Nasser, I.N., and Horton, R., 1992, Simultaneous transfer of heat, water, and solute in porous media—I. Theoretical development and II. Experiment and analysis: Soil Science Society of America Journal, v. 56, p. 1350–1365.

Nightingale, H.I., 1975, Groundwater recharge rates from thermometry, Ground Water, v. 18, no. 4, p. 340–344.

Nimmo, J.R., Deason, J.A., Izbicki, J.A., and Martin, P., 2002, Evaluation of unsaturated zone water fluxes in heterogeneous alluvium at a Mojave Basin site: Water Resources Research, v. 38, no. 10, p. 33–1 to 33–13.

Nimmo, J.R., Healy, R.W., and Stonestrom, D.A., 2005, Chapter 170, Aquifer recharge, *in* Anderson, M.G., ed., Encyclopedia of hydrological sciences: New York, John Wiley & Sons, p. 2229–2246, doi:10.1002/0470848944.hsa161a.

Nimmo, J.R., and Miller, E.E., 1986, The temperature dependence of isothermal moisture vs. potential characteristics of soils: Soil Science Society of America Journal, v. 50, no. 5, p. 1105–1113.

Niswonger, R.G., and Prudic, D.E., 2003, Modeling heat as a tracer to estimate streambed seepage and hydraulic conductivity, *in* Stonestrom, D.A., and Constantz, J., eds., Heat as a tool for studying the movement of ground water near streams: U.S. Geological Survey Circular 1260, p. 81–89.

Norris, S.E., and Spieker, A.M., 1962, Temperature-depth relations in wells as indicators of semiconfining beds in valley-train aquifers: U.S. Geological Survey Professional Paper 450–B, p. B103–B105.

Peerklamp, P.K., 1944, Bodenmeteorologische onderzoekingen te Wageningen: Meded Landbouwhogeschool Wageningen, v. 47, no.3, p. 1–96.

Philip, J.R., and de Vries, D.A., 1957, Moisture movement in porous materials under temperature gradients: Eos (American Geophysical Union Transactions), v. 38, p. 222–232.

Poeter, E.P., and Hill, M.C., 1998, Documentation of UCODE, a computer code for universal inverse modeling: U.S. Geological Survey Water-Resources Investigations Report 98–4080, 116 p.

Pruess, K., Oldenburg, C., and Moridis, G., 1999, TOUGH2 User's guide, version 2.0: Berkeley, Calif., Lawrence Berkeley National Laboratory Report LBNL–43134, 196 p.

Ren, T., Kluitenberg, G.J., and Horton, R., 2000, Determining soil water flux and pore water velocity by a heat pulse technique: Soil Science Society of America Journal, v. 64, p. 552–560.

Ren, T., Noborio, K., and Horton, R., 1999, Measuring soil water content, electrical conductivity and thermal properties with a thermo-TDR probe: Soil Science Society of America Journal, v. 63, p. 450–457.

Reiter, M., 1999, Hydrogeothermal studies on the southern part of Sandia National Laboratories/Kirtland Air Force Base—Data regarding ground-water flow across the boundary of an intermontane basin, *in* Haneberg, W.C., Mozley, P.S., Moore, J.C., and Goodwin, L.B., eds., Faults and subsurface fluid flow in the shallow crust: Geophysical Monograph Series, v. 113, p. 207–222.

Reiter, M., 2001, Using precision temperature logs to estimate horizontal and vertical groundwater flow components: Water Resources Research, v. 37, no. 3, p. 663–674.

Richards, L.A., 1931, Capillary conduction of liquids in porous mediums: Physics, 1, p. 318–333.

Ronan, A.D., Prudic, D.E., Thodal, C.E., and Constantz, J., 1998, Field study and simulation of diurnal temperature effects on infiltration and variably saturated flow beneath an ephemeral stream: Water Resources Research, v. 34, no. 9, p. 2137–2153.

Rorabaugh, M.I., 1956, Ground water in northwestern Louisville, Kentucky: U.S. Geological Survey Water Supply Paper 1360–B, p. 101–169.

Rose, D.A., 1963, Water movement in porour materials, part 2—The separation of the components of water movement: British Journal of Applied Physics, v. 14, p. 491–496.

Scanlon, B.R., 1994, Water and heat fluxes in desert soils—1. Field studies: Water Resources Research, v. 30, no. 3, p. 709–719.

Scanlon, B.R., and Milly, P.C.D., 1994, Water and heat fluxes in desert soils—2. Numerical simulations: Water Resources Research, v. 30, no. 3, p. 721–733.

Schneider, R., 1972, Distortions of the geothermal field in aquifers by pumping: U.S. Geological Survey Professional Paper 800–C, p. 267–270.

Selker, J.S., Thévenaz, L., Huwald, H., Mallet, A., Luxemburg, W., van de Giesen, N., Stejskal, M., Zeman, J., Westhoff, M., and Parlange, M.B., 2006, Distributed fiber-optic temperature sensing for hydrologic systems: Water Resources Research, v. 42, doi:10.1029/2006WR005326.

Silliman, S.E., and Booth, D.F., 1993, Analysis of time-series measurements of sediment temperature for identification of gaining versus losing portions of Juday Creek, Indiana: Journal of Hydrology, v. 146, p. 131–148.

Silliman, S.E., Ramirez, J., and McCabe, R., 1995, Quantifying downflow through creek sediments using temperature time series—One-dimensional solution incorporating measured surface temperature: Journal of Hydrology, v. 167, p. 99–119.

Simunek, J., Sejna, M., and van Genuchten, M.T., 1998, The Hydrus-1D software package for simulating the one-dimensional movement of water, heat, and multiple solutes in variably-saturated media—version 2.0: Riverside, Calif., U.S. Salinity Laboratory, Agricultural Research Service, U. S. Department of Agriculture, 178 p.

Smith, G.E.P., 1910, Groundwater supply and irrigation in the Rillito Valley: Tucson, Ariz., University of Arizona Agricultural Experiment Station, Bulletin no. 64, p. 81–243.

Smith, L., Forster, C., and Woodbury, A., 1989, Numerical simulation techniques for modeling advectively-disturbed thermal regimes, *in* Beck, A.E., Garven, G., and Stegena, L., eds., Hydrogeological regimes and their subsurface thermal effects: American Geophysical Union, Geophysical Monograph 47, p. 7–21.

Sophocleous, M., 1979, Analysis of water and heat flow in unsaturated-saturated porous media: Water Resources Research, v. 15, no. 5, p. 1195–1206.

Sorey, M.L., 1971, Measurement of vertical ground-water velocity from temperature profiles in wells: Water Resources Research, v. 7, no. 4, p. 963–970.

Stallman, R.W., 1960, Notes on the use of temperature data for computing ground-water velocity: Nancy, France, 6th Assembly on Hydraulics, Societe Hydrotechnique de France, question 1, report 3, p. 1–7.

Stallman, R.W., 1963, Computation of ground-water velocity from temperature data, *in* Bentall, R., ed., Methods of collecting and interpreting ground-water data: U.S. Geological Survey Water-Supply Paper 1544–H, p. 36–46.

Stallman, R.W., 1965, Steady one-dimensional fluid flow in a semi-infinite porous medium with sinusoidal surface temperature: Journal of Geophysical Research, v. 70, no. 12, p. 2821–2827.

Stevens, H.H. Jr., Ficke, J.F., and Smoot, G.F., 1975, Water temperature—Influential factors, field measurement, and data presentation: U.S. Geological Survey Techniques of Water-Resource Investigations, book 1, chap. D1, 65 p.

Stewart, A.E., and Constantz, J.E., 1999, Measurement techniques to identify spatial and temporal patterns of streamflow in large ephemeral streams [abs.]: GSA Abstracts with Programs, v. 31, no. 7, p. A150–A151.

Stewart, A.E., 2003, Temperature based estimates of streamflow patterns and seepage losses in ephemeral channels: Stanford, Calif., Stanford University, Ph.D. dissertation, 248 p.

Stonestrom, D.A., and Blasch, K.W., 2003, Determining temperature and thermal properties for heat-based studies of surface-water ground-water interactions, *in* Stonestrom, D.A., and Constantz, J., eds., Heat as a tool for studying the movement of groundwater near streams: U.S. Geological Survey Circular 1260, p. 73–80.

Stonestrom, D.A., Prudic, D.E., Laczniak, R.J., and Akstin, K.C., 2004, Tectonic, climatic, and land-use controls on ground-water recharge in an arid alluvial basin: Amargosa Desert, U.S.A., *in* Hogan, J.F., Phillips, F.M., and Scanlon, B.R., eds., Groundwater recharge in a desert environment—The southwestern United States: American Geophysical Union, Water Science and Applications Series, v. 9, p. 29–47, doi:10.1029/0009WSA03.

Supko, D. J., 1970, Subsurface heat flow as a means for determining aquifer characteristics in the Tucson Basin, Pima County, Arizona: Tucson, Ariz., University of Arizona, unpublished Ph.D. dissertation, 184 p.

Suzuki, S., 1960, Percolation measurements based on heat flow through soil with special reference to paddy fields: Journal of Geophysical Research, v. 65, no.9, p. 2883–2885.

Taniguchi, M., and Sharma, M.L., 1990, Solute and heat transport experiments for estimating recharge: Journal of Hydrology, v. 119, p. 57–69.

Taniguchi, M., and Sharma, M.L., 1993, Determination of groundwater recharge using the change in soil temperature: Journal of Hydrology, v. 148, p. 219–229.

Tsang, C.F., and Hopkins, D.L., 1982, Aquifer thermal energy storage—A review, *in*, Narasimham, T.N., ed., Recent trends in hydrogeology: Geological Society of America, Special Paper 189, p. 427–441.

van Genuchten, M.T., Leij, F.J., and Lund, L.J., eds., 1992, Indirect Methods for Estimating the Hydraulic properties of Unsaturated Soils: Riverside, University of California at Riverside, 718 p.

van der Kamp, G., and Bachu, S., 1989, Use of dimensional analysis in the study of thermal effects of various hydrogeological regimes, *in* Beck, A.E., Garven, G., and Stegena, L., eds., 1989, Hydrogeological regimes and their subsurface thermal effects: American Geophysical Union, Geophysical Monograph 47, p. 23–28.

van Orstrand, C.E., 1934, Temperature gradients, *in* Wrather, W.E., and Lahee, F.H., eds., Problems of Petroleum Geology: Tulsa, Okla., American Association of Petroleum Geologists, p. 989–1021.

van Wijk, W.R., and de Vries, D.A., 1963a, Periodic temperature variations, *in* van Wijk, W.R., ed., Physics of plant environment (2d ed.): Amsterdam, North-Holland Publishing Co., p. 102–143.

van Wijk, W.R., and de Vries, D.A., 1963b, The atmosphere and the soil, *in* van Wijk, W.R., ed., Physics of plant environment (2d ed.): Amsterdam, North-Holland Publishing Co., p. 17–61.

Voss, C.I., 1984, A finite-element simulation model for saturated-unsaturated, fluid-density dependent groundwater flow with energy transport or chemically-reactive single-species solute transport: U.S. Geological Survey Water-Resources Investigations Report, 84–4369, 409 p.

Walvoord, M.A., Stonestrom, D.A., Andraski, B.J., and Striegl, R.G., 2004, Constraining the inferred paleohydrologic evolution of a deep unsaturated zone in the Amargosa Desert: Vadose Zone Journal, v. 3, no. 2, p. 502–512.

Wang, K., Shen, P., and Beck, A.E., 1989, A solution to the inverse problem of coupled hydrological and thermal regimes, *in* Beck, A.E., Garven, G., and Stegena, L., eds., 1989, Hydrogeological regimes and their subsurface thermal effects: American Geophysical Union, Geophysical Monograph 47, p. 7–21.

Wankiewicz, A., 1984, Hydrothermal processes beneath Arctic river channels: Water Resources Research, v. 20, no. 10, p. 1417–1426.

Warrick, A.W., 2003, Soil water dynamics: New York, Oxford University Press, 391 p.

Wierenga, P.J., Hagan, R.M., and Nielsen, D.R., 1970, Soil temperature profiles during infiltration and redistribution of cool and warm irrigation water: Water Resources Research, v. 6, no. 1, p. 230–238.

Geophysical Methods for Investigating Ground-Water Recharge

By Ty P.A. Ferré[1], Andrew M. Binley[2], Kyle W. Blasch, James B. Callegary, Steven M. Crawford, James B. Fink[3], Alan L. Flint, Lorraine E. Flint, John P. Hoffmann, John A. Izbicki, Marc T. Levitt[3], Donald R. Pool, and Bridget R. Scanlon[4]

Introduction

Numerical models of water flow have revolutionized our understanding of basin-scale hydrologic processes. To date, these models have relied primarily on traditional hydrologic monitoring—of rainfall, streamflow, and water-table elevations, for example—for calibration and performance testing. Calibration provides initial estimates of the rates and distribution of ground-water recharge, and the calibrated models that result provide important tools for addressing recharge questions. This inverse approach has been preferred over monitoring of recharge due to the inherent difficulties of making direct measurements of flow across the water table. The difficulty is magnified because recharge fluxes are typically small and because the location of the water table changes with time. In arid and semiarid regions, deep water tables make recharge monitoring especially challenging. Despite the challenges, recharge monitoring must advance to allow for continued improvement in our understanding of basin-scale hydrologic processes. Such understanding is crucial for future water resource characterization and planning.

The difficulties associated with measuring recharge directly have led to growing interest in the adoption and development of indirect methods to measure or estimate recharge. The mass balance approach of estimating recharge as the residual of other (generally larger) terms has advanced through the use of more complex and more complete basin-scale hydrologic models. Improved measurements of recharge rates, timing, and patterns can be used to improve these modeling efforts by providing boundary conditions, constraints on model inputs, data for the testing of simplifying assumptions, and identification of spatial and temporal resolution of model inputs necessary to predict recharge to specified tolerances in space and in time. Under some conditions, improved measurements may provide a direct measure of recharge or changes in water storage, largely eliminating the need for indirect estimates of recharge.

This appendix presents an overview of physically based, indirect, geophysical methods that are available or in development for recharge monitoring. The material is written primarily for hydrologists. It is not intended to be an exhaustive review of geophysical methods; rather, the intent is to introduce the possible uses of geophysical methods for improved recharge monitoring through brief discussions and case studies. The focus is to present an approach to determine how geophysical methods can be used most effectively in quantifying recharge and studying recharge processes. As such, it is presented as a conceptual framework for matching the strengths of individual geophysical methods with the manners in which they can be applied for hydrologic analyses. For further information on individual geophysical methods, readers are referred to excellent texts describing the theory and practice of geophysics including Telford and others (1990) and Reynolds (1997). A 2002 workshop on advanced hydrogeophysics led to a well-organized collection of papers describing classical concepts and emerging techniques (Rubin and Hubbard, 2005). An illustrated introduction to the geophysical techniques most commonly used in alluvial deposit characterization appears in a recent USGS circular (Lucius and others, 2007).

This appendix is organized in three sections. First, the key hydrologic parameters necessary to determine the rates, timing, and patterns of recharge are identified. Second, the basic operating principals of selected geophysical methods are presented. The methods are grouped by the physical property that they measure directly (table 1). Each measured property is related to one or more of the key hydrologic properties for recharge monitoring. Third, the emerging conceptual framework for applying geophysics to recharge monitoring is summarized in the closing remarks.

Examples of the application of selected geophysical methods to recharge monitoring are presented in sidebars. These case studies illustrate hydrogeophysical applications under a range of conditions and measurement scales, which vary from tenths of a meter to hundreds of meters (table 1).

[1]Department of Hydrology and Water Resources, University of Arizona, Tucson, Arizona (ty@hwr.arizona.edu).

[2] Department of Environmental Science, Lancaster University, Lancaster, United Kingdom (A.Binley@lancaster.ac.uk).

[3] hydroGEOPHYSICS Inc., Tucson, Arizona (mail@hydrogeophysics.com).

[4]Jackson School of Geosciences, University of Texas at Austin, Austin, Texas (Bridget.Scanlon@beg.utexas.edu).

Table 1. Geophysical methods available or in development for recharge monitoring—comparison of directly measured properties or parameters, approximate measurement scales, and primary applications (×).

Method	Measured property or parameter	Measurement scale (meters)	Primary recharge monitoring application(s)			
			Hydrogeologic framework	Water mass balance	Direct flux measurement	Vadose zone model calibration
Seismic	Seismic velocity	10s–100s	×			
Time-domain reflectometry (TDR)	Dielectric permittivity	0.1–1				×
Time-domain transmission (TDT)	ditto	0.1–1				×
Ground penetrating radar (GPR)	ditto	1–10	×	×		×
Capacitance	ditto	0.1–1				×
Electrical resistance tomography (ERT)	Electrical conductivity	10s–100s	×	×		×
Electromagnetic induction (EMI)	ditto	1–10s	×	×		×
Time-domain electromagnetics (TEM)	ditto	10s–100s	×	×		×
Streaming potential (SP)	ditto	10s–100s			×	
Controlled source audio magnetotellurics (CSAMT)	ditto	10s–100s	×			
Nuclear magnetic resonance (NMR)	Proton precession	10s–100s	×	×		×
Gravity	Mass change	10s–100s	×	×		
Neutron	Hydrogen density	0.1–1	×	×		×
Temperature[1]	Temperature	1–10s			×	×

[1]Temperature methods are discussed in appendix 1 of this volume.

In addition, case studies have been selected to show practice-proven as well as recently emerging applications of geophysical methods to recharge monitoring. Because these recent applications have received testing in relatively few locations, the case studies on emerging techniques involve applications relatively far from the study area—including one in the United Kingdom and one in south-central Washington State.

Key Hydrologic Parameters for Recharge Monitoring

Recharge in granular media can be identified in one of three ways: (1) changes in water storage in the saturated zone can be measured and attributed to recharge, (2) the water flux past a fixed depth can be measured and equated to recharge, or (3) calibrated numerical variably saturated water-flow models can be constructed and used to infer the rates and patterns of water movement throughout the subsurface. Each of these approaches to recharge characterization is discussed briefly to give a context for considering the use of geophysical methods for recharge estimation. Note that this appendix is limited to the topic of recharge in unconfined, granular media. At this time, quantitative application of geophysical methods to monitoring recharge in fractured media or to confined aquifers is limited.

Monitoring Changes in Water Storage in the Saturated Zone

Changes in water storage in the subsurface occur due to the following processes: natural and artificial infiltration at the ground surface, evapotranspiration, lateral inflow and outflow, and withdrawal or addition from pumping wells and injection wells. Typically, basin-scale hydrologic models lump the processes of infiltration, evapotranspiration, and redistribution within the unsaturated zone, expressing the net result as a recharge flux across the water table. Subsurface water flow is then treated by only considering water flow through a saturated medium. If water withdrawals by pumping, inflows/outflows, and the storage characteristics of the medium near the

water table are well-characterized, then spatial and temporal changes in the water table elevation can be used to constrain a saturated flow model to infer the rates, patterns, and timing of recharge. This can be simplified further by ignoring the rates of inflow and outflow and equating measured changes in water table elevation with recharge. This simple approach, while lacking the explanatory capabilities of a calibrated flow numerical model, is particularly useful for rapid water-resource evaluation. More complex basin-scale analyses may rely on calibrated saturated-flow numerical models. However, these also have limited predictive capabilities because they do not explicitly represent unsaturated zone processes. As a result, these models should only be applied for recharge prediction under climatic conditions that are similar to those used for model calibration.

Numerical saturated-flow models are usually calibrated by using measurements of water-table elevation or estimates of subsurface storage within the basin. These models also require estimates of inflow and outflow across the boundaries. To relate the timing and patterns of water table elevation change to the rates, timing, and patterns of recharge, the distribution of hydraulic properties also must be defined throughout the domain. The key properties that control the accuracy of recharge estimation based on saturated-flow numerical modeling are hydraulic property distributions, the water flux across the water table, and the water content or pressure head change in the vicinity of the water table.

Monitoring Water Flux Over a Fixed-Depth Interval

Recharge to an unconfined aquifer is defined as the positive downward flux across the water table. Therefore, measurements of water flux at the water table provide the only direct measure of recharge. Direct recharge monitoring may be possible at a limited number of sites within a well-instrumented watershed with relatively shallow water tables. However, given that the water-table elevation changes in time, it is more practical to conceive of measurements that are made at some fixed depth (or depths) either above the water table or spanning the water table. The closer the measurement depth is to the water table, the more faithfully the measured or inferred flux will represent the recharge flux, both in magnitude and in timing. However, shallower measurements are typically less expensive, with the least costly measurements being remote sensing of ground surface. These reduced costs translate to greater spatial coverage. As a result, flux monitoring over a fixed depth interval is a balance between relatively sparse measurements of the local recharge flux versus greater spatial coverage of the water flux at some point at a shallower depth within the unsaturated zone. As with the saturated-zone modeling approach described above, fixed-depth interval monitoring requires significant simplifying assumptions regarding flow processes within the unsaturated zone. Therefore, these measurements cannot be used to link surface and unsaturated-zone processes with the timing and pattern of recharge. Rather, this approach provides either improved estimates of the local recharge flux (by using deep measurements), or improved spatial representation of water fluxes within the unsaturated zone (by using shallow measurements) when compared to saturated-flow numerical models. As a result, fixed-depth interval monitoring is amenable to both water-resource planning and to some large-scale scientific analyses.

Fixed-depth interval flux monitoring can be applied to either transient or steady-state infiltration and recharge. Monitoring transient infiltration processes can take advantage of changes in water content that are associated with transient flow through unsaturated media. During the advance of a wetting front, changes in the volume (or length, in one dimension) of water between the wetting front and the ground surface can be related directly to changes in the volume (or length) of water stored in the unsaturated zone. Simultaneous volumetric water-content measurements throughout the unsaturated zone can be used to determine directly the volume (or length) of water stored. Changes in the water stored with time can be related to the cumulative net infiltration (infiltration less evapotranspiration) until the wetting front reaches a zone of full saturation. Alternatively, water-content or pressure-head measurements made at specific points can be used to constrain unsaturated-flow models to infer the flux past the deepest observation point as a function of time. Inference of the flux using this approach requires characterization of the unsaturated hydraulic properties throughout the zone of measurement. Monitoring steady-state infiltration and recharge is more challenging. Under steady-state conditions, there is no change in water content associated with infiltration. As a result, steady-state flux can only be estimated by using direct measurements of water flux at a fixed depth, or by measuring vertical pressure-head gradients and calculating flux from known hydraulic conductivity functions for the site materials. Alternatively, the water velocity can be measured and related to the water flux through the measured volumetric water content.

Characterizing Water Flow Throughout the Unsaturated Zone

Full characterization of the rates, timing, and patterns of recharge requires complete analysis of water movement throughout the unsaturated zone. Ideally, this analysis would be conducted by using a multidimensional numerical model that accounts for liquid and vapor movement, preferential flow, and root uptake, among other processes. In addition, the subsurface hydraulic property distribution would be characterized with high spatial resolution throughout the domain. Such a model could then be calibrated by using measurements of water content and water pressure at multiple depths, at many times, and at many locations throughout a basin. This well-calibrated model could then be used to infer recharge rates

and to predict the impact of processes at the ground surface and throughout the unsaturated zone on recharge rates, timing, and patterns. It is impractical to construct and calibrate such a model for each basin of interest. Rather, these models can be used to improve our understanding of the dependences of fluxes at fixed depths and changes in water storage on processes that occur at the ground surface and throughout the unsaturated zone. These insights can then be used to improve recharge analyses based on saturated-flow models or flux measurements made at limited depths. For example, it would be useful to identify and characterize the systematic errors of these simpler approaches and to determine the conditions for which they can be used with acceptable error or uncertainly of recharge estimates. Similarly, more complete models of water flow throughout the unsaturated zone could be used to design a monitoring network that combines measurements within the saturated zone and at selected locations within the unsaturated zone to produce the most accurate recharge estimates within an available budget. Stochastic approaches may play a key role in characterizing the uncertainty of recharge estimates and in identifying optimal monitoring networks for specific applications (for example, Yeh and Simunek, 2002).

Geophysical Methods for Recharge Monitoring—Principles

Four key hydrologic parameters for recharge monitoring have been identified: hydraulic property distributions in space, water content distributions in space and time, water pressure distributions in space and time, and water flux distributions in space and time. To date, geophysical methods have only seen limited use in direct measurement and monitoring of water flow in the subsurface. More commonly, geophysics fills its traditional role of characterization of subsurface hydrologic properties either by using surface-based methods or borehole methods. This role can be expanded and improved through the routine incorporation of geophysical data in constructing domains for numerical models of water flow. However, this will likely require new approaches to the interpretation and application of geophysical methods to highlight the heterogeneity and anisotropy of hydraulic conductivity that are of particular importance to hydrologic investigations. Similarly, expanded use of geophysics for flux monitoring will require new approaches to geophysical survey design and geophysical data interpretation that are aimed specifically at hydrologic applications. Furthermore, improvements in the application and interpretation of geophysical data for hydrologic applications must be made with consideration of the scales of measurement and the costs of geophysical surveys. For the near future, the use of geophysics for hydrologic monitoring will expand only if there are clear cost savings or significantly improved framework data that balance the added costs. As a result, the conceptual framework for the application of geophysical methods to recharge monitoring presented here is focused on practically achievable contributions that likely can be made by geophysics within the next decade rather than on the eventual possibilities of geophysical monitoring.

Geophysical methods vary widely in their physical bases and methods of application. However, the expected contributions of geophysical methods to recharge monitoring can be assessed based on three common factors: the sensitivity of the instrument response to changes in hydrologically relevant properties, the ability of the method to provide measurements with sufficient spatial and temporal resolutions to characterize hydrologically relevant properties, and practical limitations to field applications of the method. In this section, geophysical methods are introduced that are currently available or in late-stage development for recharge monitoring. The methods are grouped by the physical property measured, seismic velocity, dielectric permittivity, electrical conductivity, proton precession, mass change, hydrogen density, or temperature. Each physical property is related to hydrologically relevant properties. Then, the physical basis of each method is presented. Finally, the resolution and applicability of each method for recharge monitoring are discussed. Case studies demonstrating the application of selected geophysical methods to recharge monitoring are shown as illustrative sidebars. To highlight geophysical methods, traditional hydrologic methods such as thermogravimetric soil water content measurement, piezometry, and tensiometry are not discussed. Readers are encouraged to refer to complete texts such as Methods of Soils Analysis (Dane and Topp, 2002) for more complete discussion of these methods. In addition, some methods that can contribute to recharge studies exclusively through geologic mapping (for example, geomagnetic methods) are not discussed here—only seismic methods are presented for structural geologic characterization. Finally, temperature methods, which have seen great recent success in recharge monitoring, are not discussed here because they are presented in detail in appendix 1.

Seismic Velocity

The density and elastic properties of a porous medium control the speed with which seismic waves will propagate through the medium, which is known as the seismic velocity of the medium (with units of length divided by time). Specifically, the seismic velocity of a medium is directly related to the square root of the ratio of the elastic modulus to the density. That is, increased rigidity and decreased density lead to an increased seismic velocity. The seismic velocities in air and water are 0.35 kilometers per second (km/s) and 1.5 km/s, respectively. The seismic velocity in rocks ranges from 1.75 km/s in porous shale to more than 7 km/s in low porosity dolomite (Birch, 1966). The seismic velocity in a partially saturated porous medium increases with increasing water content. This increase is a balance of the effects of the higher velocity of propagation through water filled pores and the increased density due to water displacing air within the medium. Similarly, seismic velocity decreases in a linear fashion as oil replaces water in a porous medium (Geller and Myer, 1995).

Kohnen (1974) reported seismic velocities ranging from 0.2 to 2 km/s in sands variably saturated with air and water.

Because the seismic velocity depends on both the elastic properties and density of the solid matrix and the volumetric water content, it would appear that this method could be used to map water content distributions as well as hydrogeologic structure. Time-lapse seismic monitoring of water-content change has been applied successfully at the laboratory scale (for example, Geller and Myer, 1995). However, the typical mode of application of seismic methods at the field scale precludes water content mapping. Specifically, seismic methods are typically operated in reflection or refraction mode wherein a seismic source is activated, commonly at or near the ground surface, and seismic waves are recorded with time at or near the ground surface. Seismic energy travels along multiple paths including a direct path between the source and receiver and indirect paths of reflected and refracted rays. Direct arrivals can potentially be useful for characterizing the seismic velocity between the source and receiver. The simultaneous inversion of data recorded from multiple source and receiver locations within boreholes can potentially be used to construct a two- or three-dimensional image of the velocity distribution. This might then be used, together with supporting information, to characterize the water-content distribution. However, current field applications rarely use multiple down-hole source and recording positions, primarily due to difficulties with coupling the source and receivers to the medium within the unsaturated zone. It is far more common to conduct surveys at the ground surface and to interpret structure based on reflected or refracted energy. This survey approach relies on sharp changes in the seismic velocity in the subsurface to give rise to reflections and refractions. The responses from these different travel paths can be separated on a seismograph due to their different travel path lengths and propagation velocities. However, this typically requires that seismic surveys be applied at scales of meters to tens of meters between measurement points. This scale of application, together with the relatively large minimum resolvable bed thicknesses achievable with seismic waves, limits the ability of seismic methods to characterize water content distributions with sufficient resolution to constrain unsaturated water flow models. As a result, high-resolution applications of seismic methods for water content mapping will likely remain limited to the laboratory for the near future. While the relatively large measurement scale of seismic methods is a limitation for water content mapping, it is an advantage for defining the hydrogeologic structure of relatively deep unsaturated zones. Hydraulic and physical properties often most commonly obtained from drill cuttings and cores; however, these data typically are sparse owing to their associated costs and, thus, are limited in defining the geometry of subsurface deposits. Seismic data can be used to extend the limited hydraulic and physical properties of the shallow subsurface sediments and to define vertical and lateral extents of subsurface layers. An example of this application is shown in the sidebar "Estimating stream-channel deposit geometry with seismic-refraction surveys." The ready availability of seismic instruments and the wealth of expertise in the use and interpretation of seismic methods from the minerals and petroleum exploration industries suggest that the use of seismic methods should be a standard for the definition of hydrogeologic structure for basin-scale hydrologic models. High-resolution seismic methods may also contribute to the definition of hydrologic structure for detailed models of water flow throughout the unsaturated zone.

Dielectric Permittivity

The dielectric permittivity (farads per meter) describes the ability of a medium to store charge in an alternating electromagnetic field. In general, the bulk dielectric permittivity of a medium depends on the dielectric permittivities, electrical conductivities, and magnetic permeabilities of the constituents of the medium, weighted by their volume fractions. Furthermore, the dielectric permittivity depends upon the frequency of the applied electromagnetic field. Researchers are currently exploring the use of multifrequency analyses of complex dielectric permittivity measurements to infer soil-specific properties, such as mineral composition and water-air interfacial areas. However, most dielectric permittivity methods that will be applied to recharge monitoring in the near future operate in a frequency range over which the dielectric permittivity of water can be considered nearly independent of frequency. Furthermore, most of these applications will be conducted in nonmagnetic media, eliminating complications due to high magnetic permeability materials. Typically, dielectric methods applied to recharge studies will rely on determination of the apparent dielectric permittivity relative to the permittivity of a vacuum. Use of this dimensionless lumped parameter assumes that the imaginary component of the complex dielectric permittivity, which is related to conductive and dielectric losses, does not contribute significantly to the medium's dielectric response. With this assumption, the velocity of propagation of an electromagnetic wave can be related directly to the inverse of the square root of the relative apparent dielectric permittivity.

The bulk dielectric permittivity can be related to the dielectric permittivity of the soil components through variations of the complex refractive index model:

$$\sqrt{\kappa} = (1-\varphi)\sqrt{\kappa_s} + \theta\sqrt{\kappa_w} + (\varphi-\theta)\sqrt{\kappa_a} \quad , \qquad (1)$$

where

κ_s = the dielectric constant of the sediment grains,

κ_w = the dielectric constant of water (assumed to be 81),

θ = the volumetric water content, and

φ = the porosity.

The relatively high dielectric constant of water compared to other soil components imparts the strong dependence of the bulk dielectric permittivity on the volumetric water content of the medium. In fact, the bulk dielectric permittiv-

Estimating Stream-Channel Deposit Geometry with Seismic-Refraction Surveys

By John P. Hoffmann

The amount of water that recharges many aquifers in the Southwest is insufficient to meet current and future demands. As a result, water levels have declined tens of meters in the past several years. For instance, in the Tucson area, water levels have declined by as much as 60 meters over the past 50 years (Tucson Water, 2000). Many ephemeral streams in the Southwest, such as Rillito Creek, are being considered as artificial-recharge sites to help mitigate the deficit. Design and construction of in-channel recharge facilities, in the absence of information that can be used to estimate performance and optimize design, constitute an expensive and uncertain venture.

Infiltrated water within the Rillito Creek stream-channel deposits is a primary source of recharge for the alluvial aquifer underlying the city of Tucson and surrounding areas. Rillito Creek, located in Upper Santa Cruz Basin in southern Arizona, is typical of a large ephemeral-stream channel in the Southwest. In many of the Southwest basins, such as in Upper Santa Cruz Basin, streams originating at higher elevations coalesce downstream to form larger ephemeral streams. Streams originating near mountain fronts typically flow over thick alluvial valleys, lose hydraulic connection with the underlying aquifer, and become ephemeral in their lower reaches. Underlying many of these ephemeral streams is a coarse-grained stream-channel deposit that overlies a basin-fill deposit. The coarse-grained stream-channel deposit typically has high permeability that enables high infiltration rates and provides storage capacity for subsequent ground-water recharge. In places, Rillito Creek has an unsaturated zone that is 40 meters thick (Hoffmann and others, 2002).

The stream-channel deposits are predominantly sand and gravel with less than 5 percent clay and silt, while the underlying basin-fill deposits are finer grained, typically having 10 percent or more of silt and clay (Hoffman and others, 2002). The difference in grain size between the deposits results in differing hydraulic and physical values for the deposits. For instance, the average hydraulic conductivity of the stream-channel deposits is about 1.2 meters per day (m/d), whereas the average hydraulic conductivity of the basin-fill deposit is 0.2 m/d. In addition, the field capacity of the stream-channel deposits is about 18 percent by volume and about 24 percent by volume in the basin-fill deposits. Porosity of both deposits is close to 30 percent. Given the hydraulic and physical differences between the deposits that underlie Rillito Creek, it is important to accurately characterize the geometry of these deposits to better estimate infiltration, storage, and subsequent recharge capacity of the sediments.

As part of an investigation of the hydrogeology of Rillito Creek, 51 core samples from five boreholes were collected and analyzed for hydraulic and physical properties (Hoffmann and

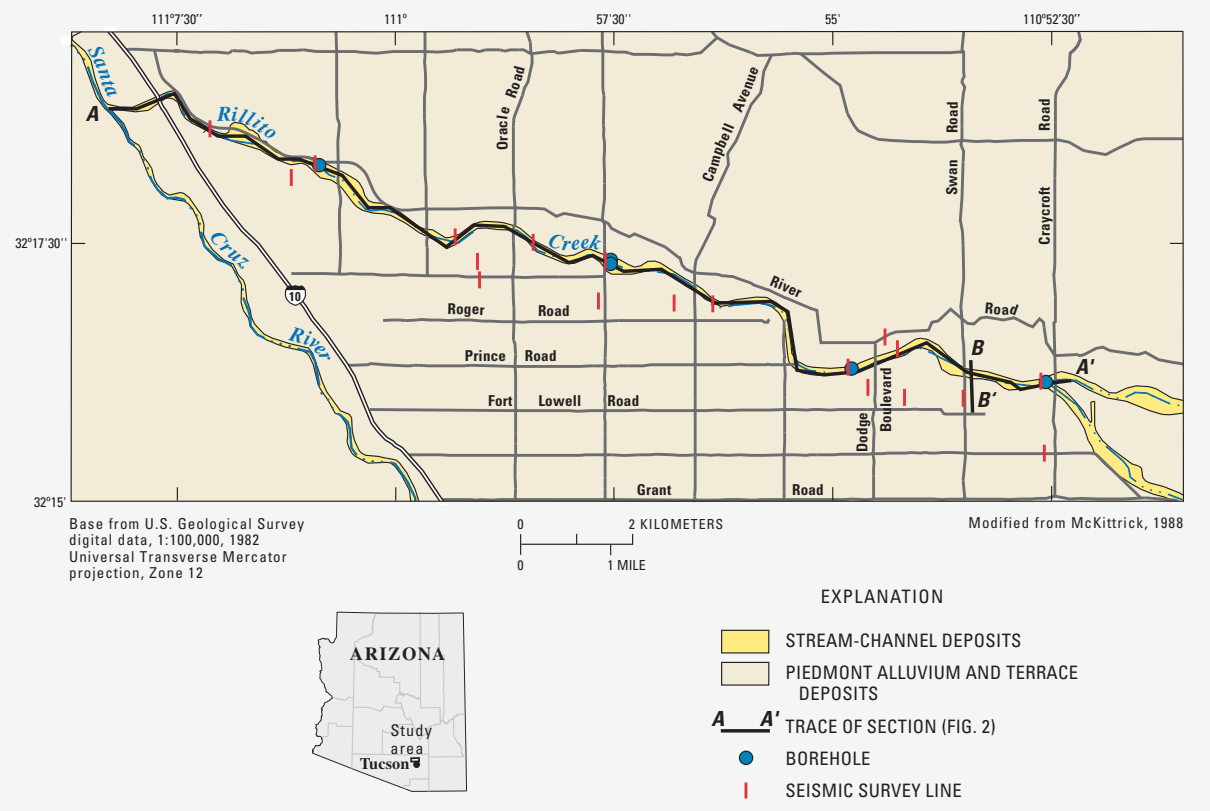

Figure 1. Location of study area showing borehole and seismic-survey locations, Rillito Creek, Pima County, Ariz.

others, 2002). In addition, seismic-refraction surveys were done at each borehole and at several intermediate locations between boreholes and on the adjacent stream-channel terrace. Twelve surveys were conducted within the stream channel along a 20-km reach and 12 surveys were conducted on the adjacent terrace deposits (fig. 1). Four of the in-channel surveys were near boreholes having geologic logs; therefore, the wells could be used as ground truth for the seismic surveys. Seismic-velocity values for the unsaturated recent stream alluvium averaged 400 m/s and ranged from 350 to 500 m/s, whereas the velocities for unsaturated basin-fill deposits averaged about 840 m/s and ranged from 600 to 1,400 m/s. In locations where the saturated zone was generally less than 10 m below ground surface, seismic-refraction surveys were capable of detecting the water table—seismic velocity values for the saturated basin-fill deposit averaged 2,400 m/s and ranged from 1,500 to 3,500 m/s. Thickness of stream-channel deposits estimated by the refraction surveys generally agreed with geologic logs at adjacent wells to within about a meter allowing for confident extension of the definition of the basin-fill contact. Thickness of the stream-channel deposits averaged approximately 7 m and ranged from 3 to 9 m along the 20-km reach (fig. 2*A*). Cross-channel surveys were used to estimate the width of the stream-channel deposit, such as shown in the cross section in figure 2*B*.

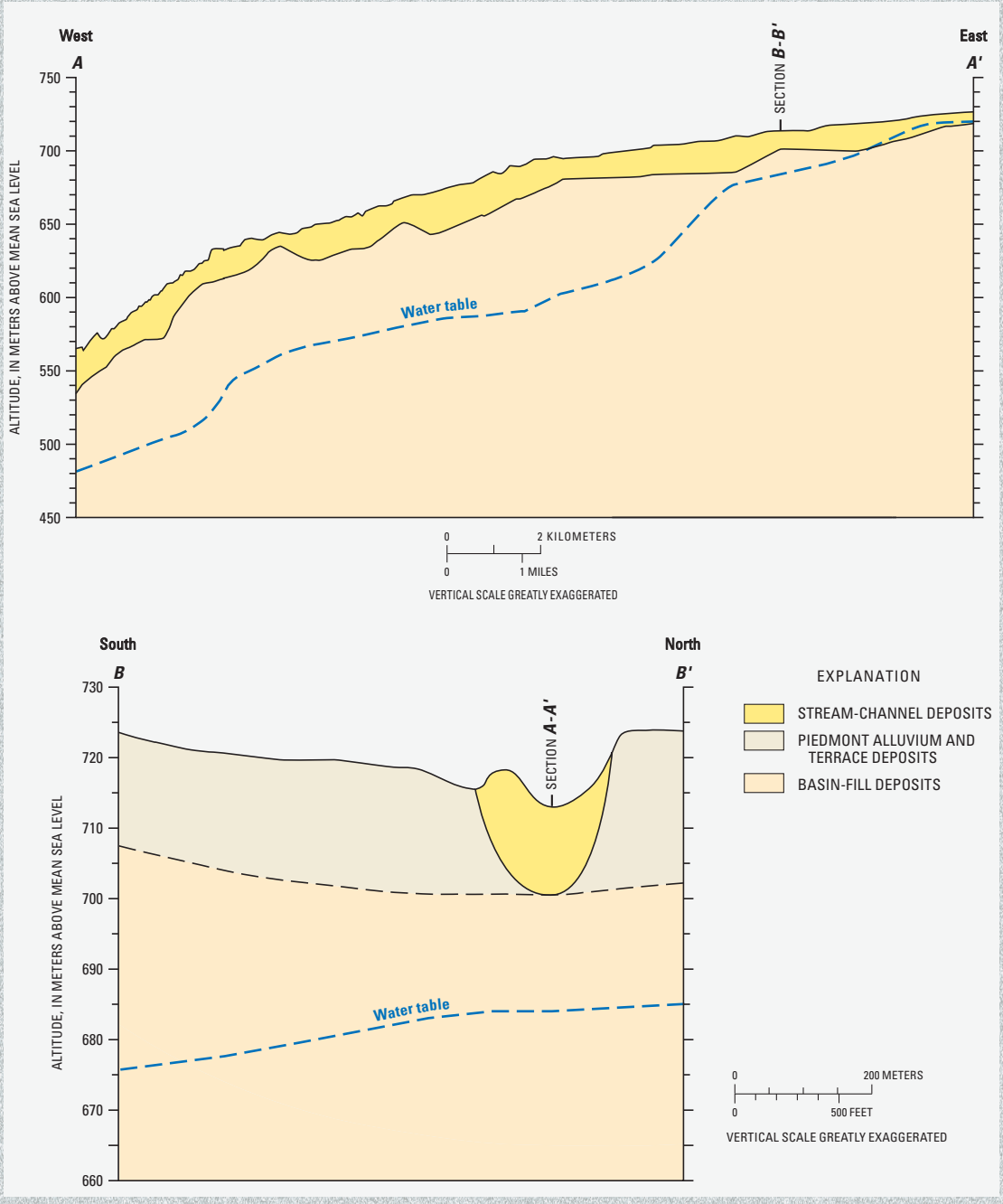

Figure 2. *A,* Section of longitudinal section based on seismic and borehole data; *B,* Cross-channel section based on seismic data, Rillito Creek, Pima County, Ariz.

ity of most unconsolidated geologic materials depends upon the volumetric water content with only minor dependence on the volume fraction or the composition of the solids or of the composition of the water and other pore fluids. As a result of this insensitivity to medium-specific properties, the volumetric water content can be determined with reasonable accuracy by using a general calibration equation, such as that presented by Topp and others (1980). Examining the change in bulk dielectric permittivity with time and relating this to the change in water content can reduce the dependence on the bulk dielectric permittivity of the soil solids further. While general relationships relating dielectric permittivity (change) and volumetric water content (change) can be applied under most conditions, two limitations must be considered. First, measurements in highly electrically conductive environments can lead to systematic measurement errors and increased measurement uncertainties (Hook and others, 2004). Second, clay-rich soils can have a large fraction of water that is bound to solid surfaces. The dielectric permittivity of bound water is lower than that of free water and can be temperature dependent (Or and Wraith, 1999). As a result, clay-rich soils may require soil-specific calibration and temperature corrections.

Point-scale measurements of water content can be made by using capacitance probes, time domain reflectometry (TDR), or time domain transmission (TDT) methods. Capacitance methods compare the capacitance of a circuit including a sample of soil to the capacitance of the circuit without the soil present to determine the relative apparent dielectric permittivity. TDR and TDT methods measure the velocity of propagation of a fast rise time electromagnetic signal through the medium along waveguides of known length to infer the relative apparent dielectric permittivity. Capacitance and TDR probes are used widely in hydrology and related fields because they allow for rapid, automated monitoring of water content within a small sample volume. In addition, TDR probes can be multiplexed readily and the probes can be designed to fit specific monitoring needs. TDT probes are not used as widely due to the need to connect wires to each end of the probe, making installation more difficult. However, due to the small sample volumes (tens of cubic centimeters) of TDR and capacitance instruments, individual probes cannot be used to monitor changes in water storage throughout the unsaturated zone. Rather, many of these probes must be used together to define the volumetric water content profile through time. However, automated depth profiling requires that each TDR or capacitance probe be connected, individually, to an instrument or data logger. While both TDR and capacitance probes have been designed to measure through access tubes, in practice this greatly restricts the sample volume of the instruments to the region immediately adjacent to the access tube. As a result, both the depth of investigation and the spatial resolution of the water content profile achievable with capacitance, TDR and TDT probes are limited. The primary contribution of capacitance, TDR and TDT probes to recharge monitoring lies in ability to collect their high temporal resolution data at single depths for calibration of unsaturated flow models. The case study, "Monitoring temporal changes in water storage with time domain reflectometry," provides an example where the high time resolution and ability to make automated measurements made TDR the ideal choice for recharge monitoring beneath an ephemeral stream. Robinson and others (2003) provide an extensive review of TDR.

Unlike TDR and TDT methods, ground-penetrating radar (GPR) instruments measure the velocity of propagation of unguided electromagnetic waves. Separate transmitting and receiving antennae generate and detect the electromagnetic (EM) energy. Antennae can be deployed either on or above the ground surface or in parallel boreholes. Surface applications typically produce radargrams, which show the strength of the received signal as a function of time since the source signal was produced. Analysis follows that developed for seismic methods, leading to images of subsurface reflectors that are associated with locations of sharp dielectric permittivity contrasts. Because GPR uses higher frequency sources than seismic methods, GPR offers greater spatial resolution than seismic methods; however, the maximum depth of penetration is much smaller. For example, while surface-based GPR can penetrate many tens of meters through ice, it may be limited to the shallowest several meters in clay-rich soils. Surface GPR methods are well suited to characterizing geologic structure in relatively shallow unsaturated zones. However, the method currently lacks sufficient spatial resolution and sensitivity to quantify changes in water content throughout the unsaturated zone to constrain unsaturated flow models. The spatial resolution of GPR may improve with advances in equipment and signal processing, but there is an inherent limitation of the depth of investigation of any surface-based method. In contrast, borehole GPR (BGPR) has been shown to be able to resolve the water content profile with very high spatial resolution to great depths. The ability of BGPR to characterize the water content profile rapidly and to great depths will likely lead to expanded use of the method for monitoring changes in water storage and for calibrating unsaturated flow models. An example of quantitative monitoring with BGPR is given in the case study "Monitoring infiltration and redistribution with borehole ground-penetrating radar." The primary limitation on the use of BGPR is the need for two parallel boreholes for each measurement location. The cost of borehole installation will likely relegate this method to limited application in areas of particular interest within a basin. Huisman and others (2003) provide an excellent review of GPR.

Electrical Conductivity

The electrical conductivity describes the ability of a medium to transmit electric current in accordance with Ohm's law applied to a multiphase porous medium. In general, the bulk electrical conductivity of a medium depends

Monitoring Temporal Changes in Water Storage With Time Domain Reflectometry

By Kyle W. Blasch

A two-dimensional array of time-domain reflectometry (TDR) probes was installed perpendicular to the path of streamflow in a 60-m wide, coarse-grained alluvial channel. The study site was located where Dodge Boulevard crosses Rillito Creek, about 3 km west of Swan Road (fig. 1). The array was used to measure changes in soil water content at the onset and cessation of ephemeral streamflow events. The changes in the water-content profiles with time were used to quantify infiltration at the onset of streamflow and redistribution at the cessation of streamflow. In addition, the data were used to infer the timing of onset and cessation of streamflow. TDR was selected because it provides rapid, automated measurements of water content with little need for medium-specific calibration. For this study, it was also critical that the TDR probes could be installed in the streambed beneath the zone of scour.

The volumetric water content was measured at 2-minute intervals from July 2000 through December 2002 using 28 TDR probes installed in a trench, arranged in four vertical profiles, spaced 3 m apart (fig. 3). Twenty-eight type-T thermocouple probes were collocated with the TDR probes. The southernmost instrument profile was installed at the point of lowest elevation in the channel cross section, approximately 4 m from the south bank. TDR probes were placed at depths of approximately 0.50, 0.75, 1.0, 1.25, 1.50, 2.0, and 2.5 m below the stream channel surface. A Campbell Scientific TDR100 time domain reflectometer was used in conjunction with a Campbell Scientific CR10X data logger to transmit, receive, and convert waveforms into volumetric water content. TDR probes were constructed from two stainless steel wave-guides 0.20 m in length, spaced 0.03 m apart. Probes were connected by coaxial cable (RG-8; 50-ohm impedance, 2.6-millimeter diameter center conductor) to minimize signal attenuation between the probes and the TDR100 instrument. Cable lengths ranged from 11 to 26 m. Each probe was calibrated in the laboratory with the RG-8 cable attached. The precision of the water-content measurements was approximately 0.03 cubic meter of water per cubic meter of bulk sediment (m^3/m^3). Copper-constantan thermocouple probes were operated using a Campbell Scientific CR10X. Temperature sensors were programmed to measure temperature every 5 seconds and to record a time-averaged temperature at 5-minute intervals with a precision of 0.1°C.

The water content generally increased from about 0.20 to 0.35–0.40 m^3/m^3 within 10 minutes of the onset of streamflow (fig. 4). Vertical infiltration rates were estimated from the velocity of the wetting front and from the measured water contents. The wetting front velocity was determined by dividing the depth of the deepest probe minus

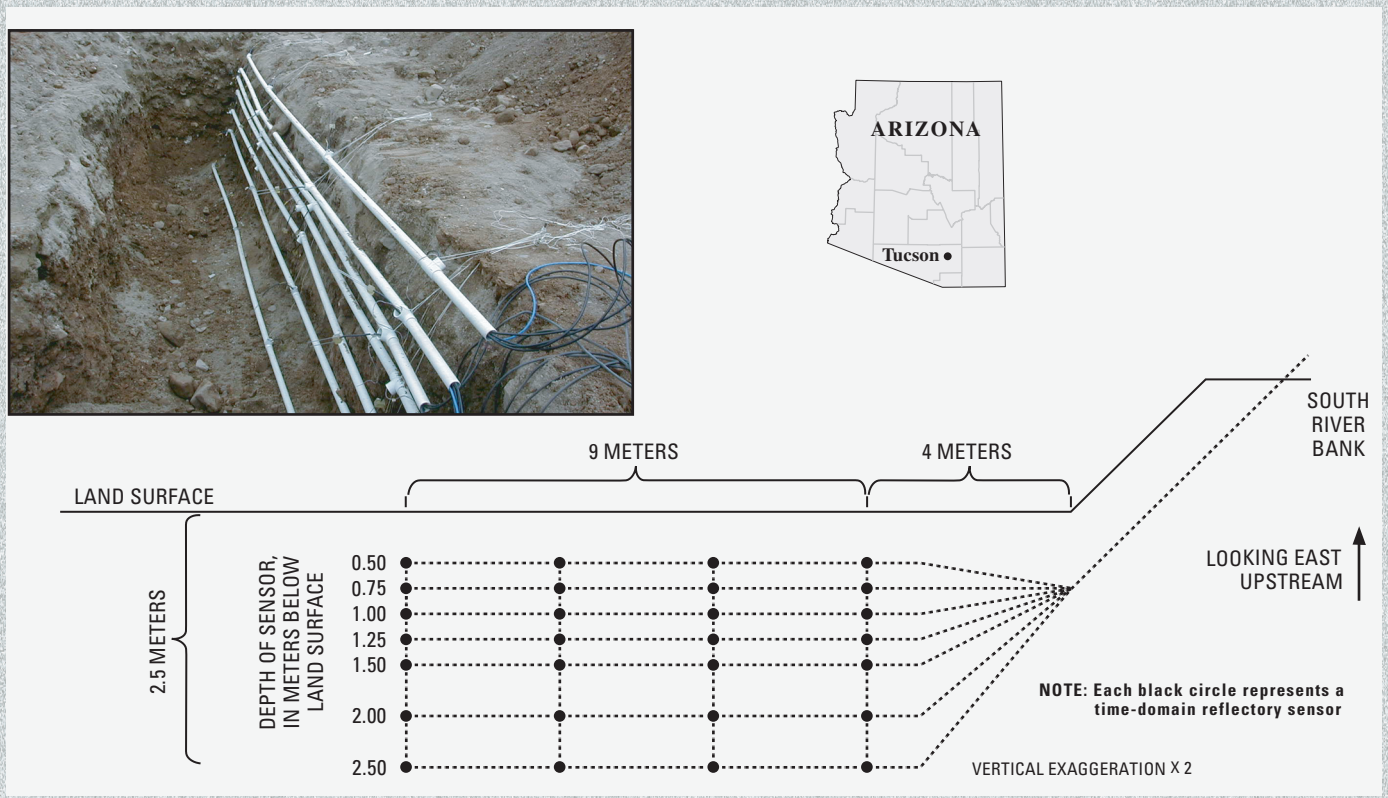

Figure 3. Photograph and schematic of two-dimensional array of sensors within the Rillito Creek stream-channel deposits, Tucson, Ariz.

0.5 m by the elapsed time between an increase in water content exceeding 0.05 m^3/m^3 at 0.5 m and an increase in water content to more than 0.30 m^3/m^3 at the deepest probe. The infiltration flux at the onset of flow was as high as 300 m/d, with higher infiltration rates associated with lower antecedent water contents, which agrees with the values reported in a previous investigation in Rillito Creek (Wilson, 1980). The infiltration rate reduced by an order of magnitude within minutes and continued to decrease as water percolated to greater depths. Late-time redistribution occurred at a rate of approximately 0.12 m/d, which is lower than the reported range of 0.34 to 1.1 m/d for steady state infiltration flux reported previously for this site (Turner, 1943; Katz, 1987).

Vertical redistribution fluxes at the cessation of streamflow averaged about 0.12 m/d. Variability among redistribution fluxes shows strong correlation with temperature, with the magnitude of the redistribution flux increasing with increasing temperatures. Specifically, redistribution fluxes ranged from about 0.07 m/d for sediment and fluid temperatures near 10°C to 0.17 m/d for temperatures near 30°C. Water content measurements were used in conjunction with temperature and pressure measurements to constrain a variably saturated heat and fluid flow model of the upper 2.5 meters of the subsurface. This model was used to infer hydraulic properties of the soil (Blasch, 2003).

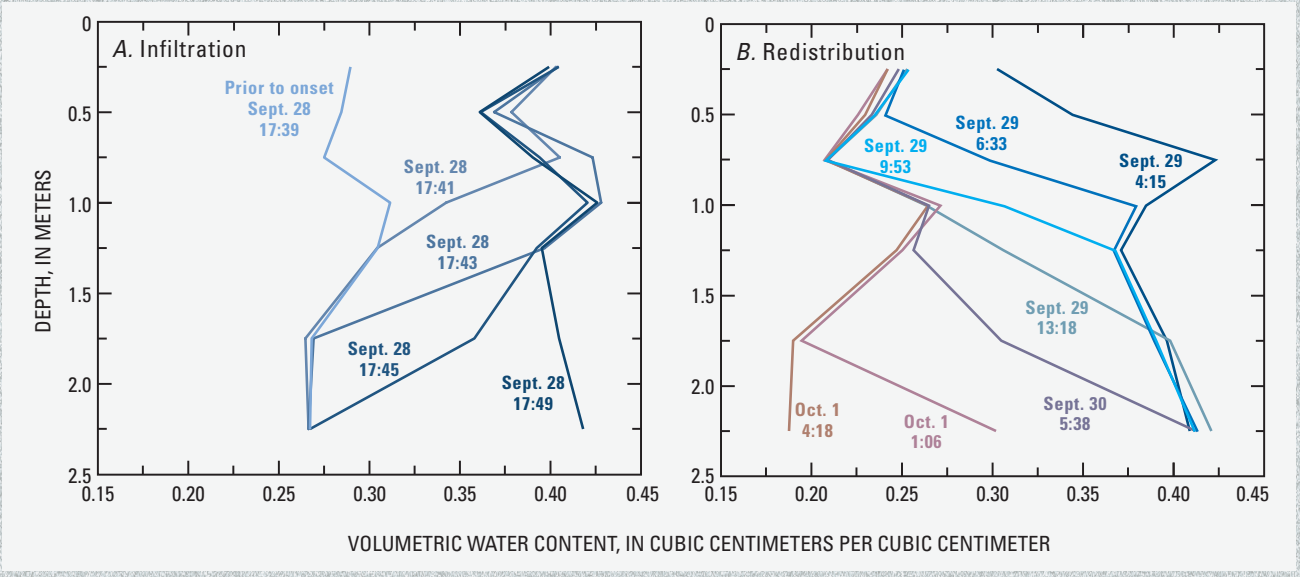

Figure 4. Change in volumetric water content of the stream-channel deposits at: *A*, The onset of an ephemeral event on September 28, 2000; and *B*, The cessation of the ephemeral event.

Monitoring Infiltration and Redistribution With Borehole Ground-Penetrating Radar

By Andrew M. Binley

Borehole ground-penetrating radar shows promise for investigating focused ground-water recharge in arid and semi-arid environments. This sidebar illustrates its potential by summarizing results of borehole ground penetrating radar (BGPR) surveys conducted at a field site in the United Kingdom.

The Permo-Triassic Sherwood Sandstone is a major groundwater resource subject to increasing demand for public and private water supply. The aquifer is threatened by heavy chemical loading from agricultural practices. Consequently, models are required in order to assess travel times and attenuation within the unsaturated zone. Recent work demonstrated the value of borehole geophysical methods for monitoring water flow through the unsaturated zone (induced by natural and tracer loading) at two sites (Binley and others, 2001; Binley, Cassiani, and others, 2002, Binley, Winship, and others, 2002). Results for one of the sites are shown here.

The site, near Hatfield, South Yorkshire at the Lings Farm smallholding (National Grid Reference SE 653 079), was instrumented during June and July of 1998. The site is an example of potentially vulnerable sandstone islands, a term used by UK environmental regulators to indicate areas of relatively clay-free drift deposits that allow direct and rapid recharge to the underlying sandstone aquifer relative to clay-covered areas. Because such areas permit potentially rapid, poorly attenuated, contaminant transport to the water table, the hydrological characterization is essential for accurate vulnerability evaluation.

Two boreholes (H-R1 and H-R2) were drilled 5 m apart at the site for deployment of borehole radar. Two 102-millimeter (mm) diameter cores (H-M and H-AC) were drilled near to H-R1 and H-R2 by Leeds University, UK. Drift thickness at the site is typically 2–3 m and consists of mainly fluvio-glacial sand and gravel. From analysis of the cores, the sandstone sequence at the site consists of fluvially derived fining upwards sequences 1–3 m thick, grading from medium-grained to fine-grained sandstone. Pokar and others (2001) present physical and hydraulic analysis of samples extracted from a core at the site. Two main distinguishable lithologies are medium-grained sandstone, which comprises the bulk of the core, and fine and medium sandstone, subhorizontally laminated on a millimeter scale.

Specimens from the core were extracted by Leeds University for measurement of the dielectric permittivity under varying volumetric water contents. West and others (2003) show that for 100 MHz frequency measurements, a value of relative permittivity $\kappa = 5$ is appropriate for the main lithological unit of the core.

To determine dielectric properties at the field scale, borehole-to-borehole surveys may be conducted in two transmission modes. In both cases, a radar signal is generated from a transmitter placed in one borehole with a receiver deployed in the other. Measurement of the travel time of the received wave permits determination of the first arrival and, hence, the apparent velocity of the electromagnetic wave. In one mode, using a multiple offset gather (MOG), the receiver is moved to different locations in one borehole whilst the transmitter remains fixed. The transmitter is then moved and the process repeated. Following collection of all data in this mode and determination of the travel time for each wave path-line it is possible to derive a tomogram of velocity within the plane of the borehole pair. In contrast, a zero offset profile (ZOP) may be determined by placing the transmitter and receiver common depths for each measurement. By systematically lowering or raising the pair of antennae in the two boreholes, it is possible to obtain a one-dimensional profile of travel time over the entire borehole length. Typically, MOG surveys offer two-dimensional discrimination of the water content or change in water content at the expense of greater measurement times.

Borehole-to-borehole radar measurements in ZOP mode were conducted at the Hatfield site between February 1, 1999, and November 19, 2000, at approximately monthly intervals. During 1999, a number of MOG surveys were also carried out at the site. For all surveys, the Sensors and Software (Mississauga, ON, Canada) PulseEKKO borehole radar system was used with 100 MHz borehole antennae. Surveys were conducted using 0.25-m depth intervals between antennae positions over the range 1–12 m below ground level. Typical survey times were 2 hours for MOG mode and 5 minutes for ZOP mode. Instrument calibration was carried out

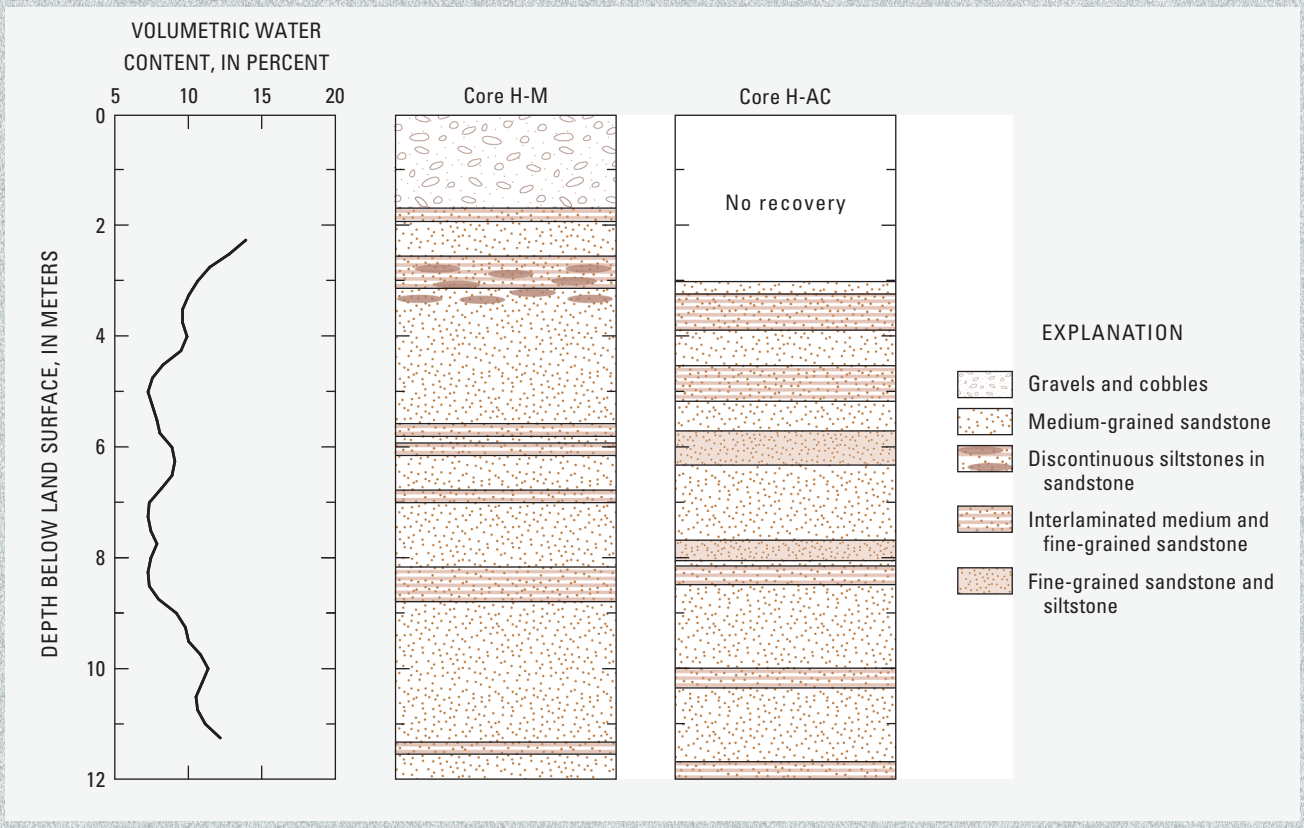

Figure 5. Radar derived volumetric water contents on February 1, 1999, at the Hatfield site together with core lithologic logs.

prior to and following each mode of survey and regularly during each MOG survey to remove instrument drift. For both survey modes first time arrivals were picked manually. Tomographic analysis of the MOG data was carried out by using the straight-ray inversion procedure of Jackson and Tweeton (1994) using a discretization of 0.5 m in the horizontal and 0.25 m in the vertical. A repeat set of measurements was made for each ZOP survey. The average, manually picked, first arrival travel time from the two measurements at each depth was used to define the volumetric water content profile with depth.

The volumetric water content profile was collected on February 1, 1999, at the Hatfield site with a ZOP BGPR survey (fig. 5). The volumetric water content varied from 0.6 to 0.16 m^3/m^3 and showed some correlation with the lithologic information provided by the core logs (J. West, oral commun., 1999). A comparison of the core logs illustrates that the tops of the fine-grained units are not necessarily horizontal because these are erosional contacts (fig. 5). The logs do show, however, similar larger scale characteristics, see for example the fine-grained units at approximately 6-, 8- and 10-m depths. The layers at 6 and 10-m depth are also associated with zones of higher volumetric water content.

Seasonal characteristics of precipitation at the Hatfield site are the occurrence of main net inputs during September to January with a number of spring events during March or April, followed by relatively high evapotranspiration during summer. The monthly net rainfall estimates at the Hatfield site for the period July 1, 1998, to December 31, 2000, and the temporal dynamics of water content change throughout the profile are compared in figure 6. The shape of the response in the upper sandstone follows the seasonal pattern of the net rainfall. Note the reduction in

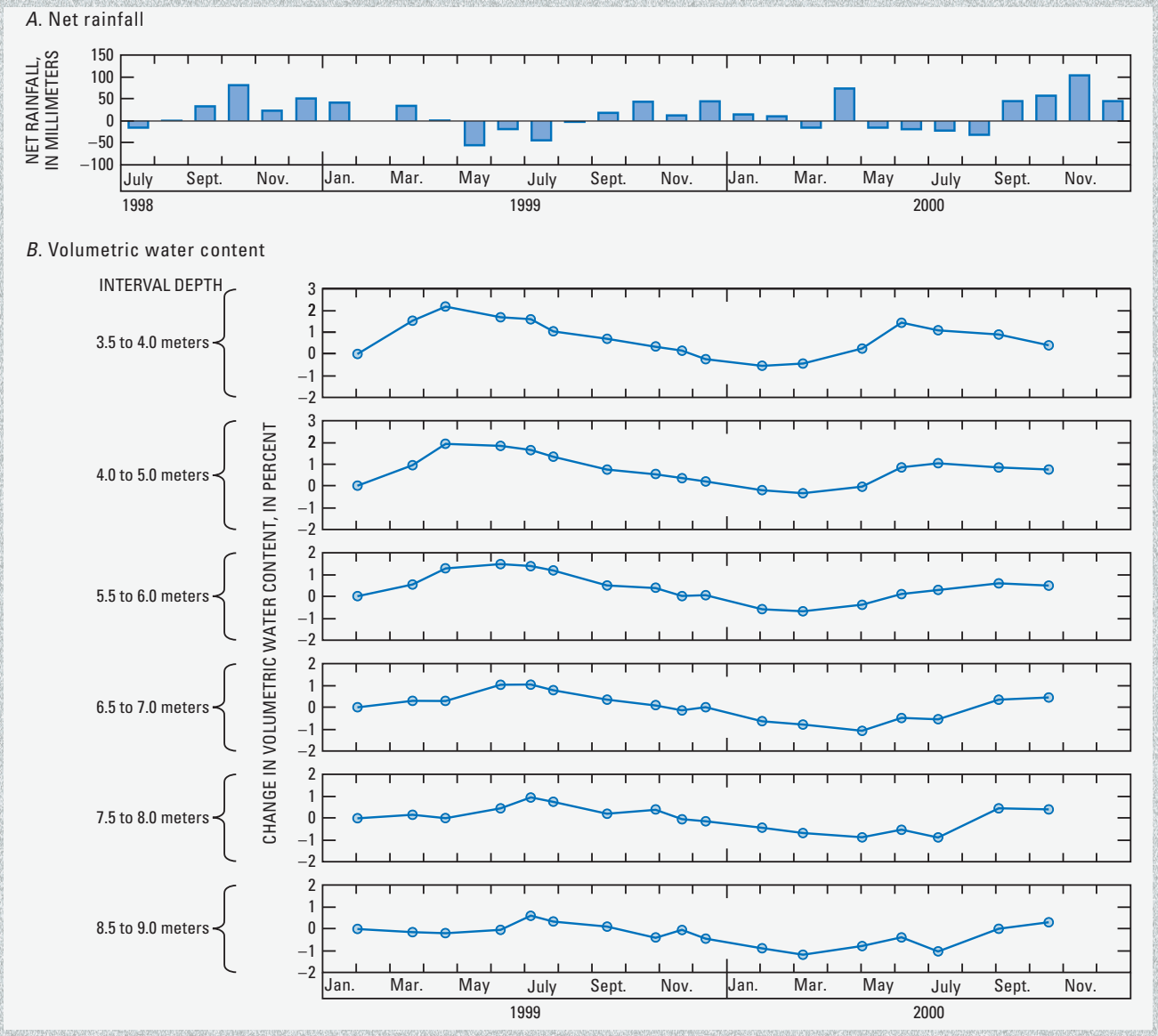

Figure 6. *A*, Net rainfall series, and; *B*, Change in volumetric water content over selected depth intervals using zero offset profile (ZOP) radar estimates, Hatfield site. All differences are relative to February 1, 1999.

volumetric water content changes for the peak in 2000 in comparison to the peak in 1999 because of significantly reduced rainfall during winter 1999. The delays in wetting and drying patterns are also clearly visible over this interval when compared with the rainfall input series, as is the smooth cyclic pattern, both demonstrating the impact of drift cover. More significant, however, is the transmission of this signal throughout the profile. A delay of two to three months in the initial peak is apparent when comparing series at 3.5 to 4 m and 6.5 to 7 m. A similar delay is also apparent in the propagation of the drying front. It is interesting to note the marked change in the time series for the 5.5 to 6 m and 6.5 to 7 m intervals, indicating that the transmission of the wetting front appears geologically controlled at about 6 m. This may be due to the low permeability unit identified on the core logs (fig. 5). This is also consistent with the observed response during tracer experiments at the site (Binley and others, 2001).

The change in volumetric water content determined from selected MOG surveys reveals a more complex evolution of wetting and drying fronts within the sandstone (fig. 7). The impact of the high net rainfall during March 1999 can be seen clearly at a region of high positive water storage change that advances to a maximum depth of 7 m by June 1999. Through the summer of 1999 emergence of a drying front can be seen which continues to develop through to winter 1999. The tomograms also show the effect of the impeding layer previously referred to between 6 and 7 m depth, during the drainage period.

The examples shown here demonstrate the potential value of BGPR for monitoring recharge processes. Our results indicate that, at least for the sandstone site reported here, we are able to resolve changes of less than one percent absolute moisture content. The method allows greater assessment of spatial variability of recharge dynamics than conventional localized measurement approaches (TDR, neutron probe, and so on). When used in profile (ZOP) mode, the method permits an integrated measure of changes in moisture content between two boreholes and, as such, uses a measurement support volume potentially more appropriate for modeling unsaturated zone processes.

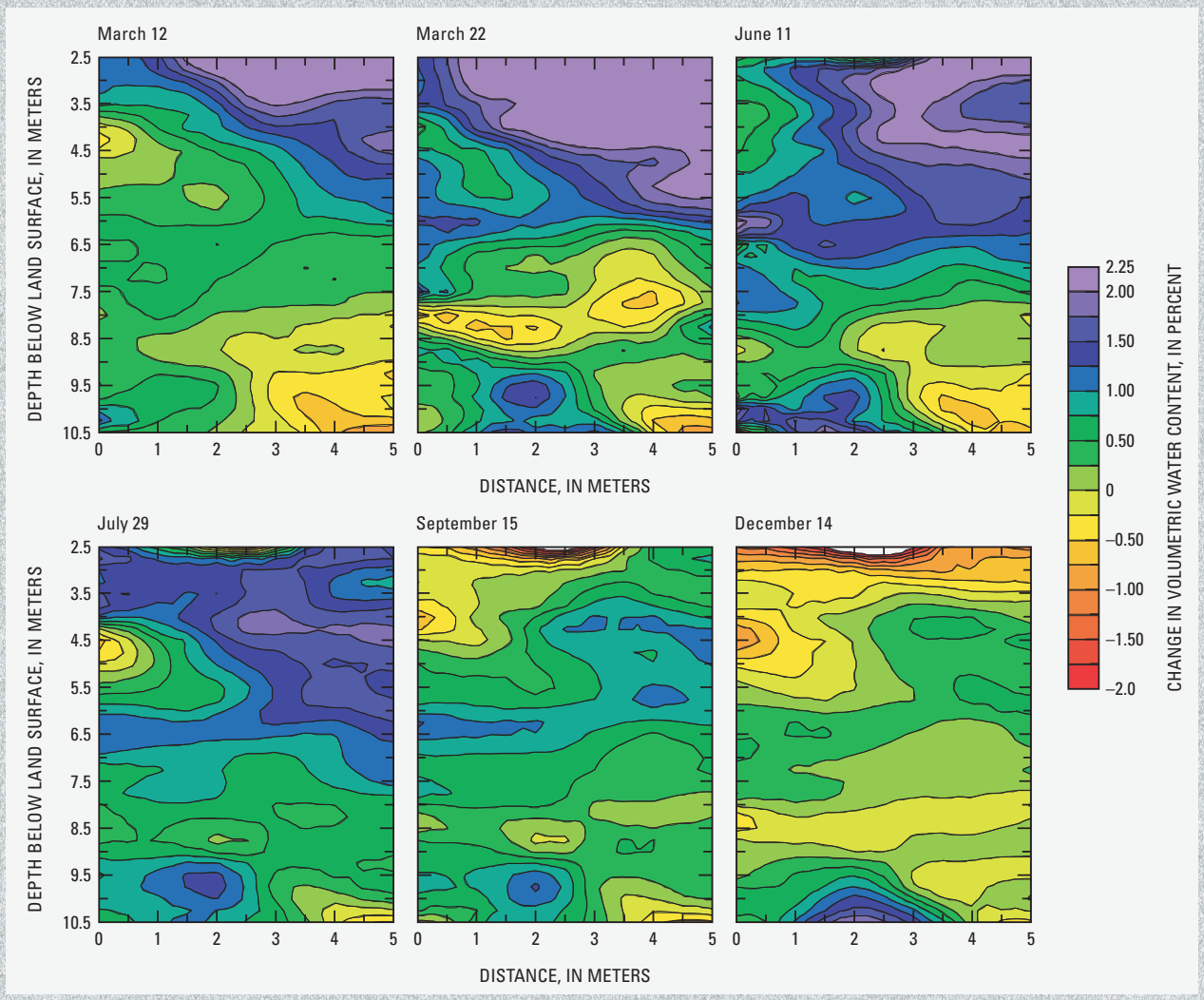

Figure 7. Change in volumetric water content using multiple offset gather (MOG) borehole ground penetrating radar (BGPR) surveys. All differences are relative to February 1, 1999.

on the electrical conductivities of the constituents of the medium. This dependence is described as

$$\sigma_b = \sigma_w \varphi^m S^n + \sigma_s \ , \qquad (2)$$

where

σ_b = the bulk electrical conductivity (1/ohm-L),

σ_w = the pore water electrical conductivity (1/ohm-L),

φ = the porosity (volume of pores per bulk volume),

S = the water saturation (volume of water per volume of pores), and

m, n = empirical fitting parameters (Archie, 1942).

The final term, σ_s (1/ohm-L), has been added to describe the contribution of the electrical conductivity of the soil solids to the bulk electrical conductivity (for example, Patnode and Wyllie, 1950; Waxman and Smits, 1968). The dependence of the bulk electrical conductivity on several properties limits the uniqueness of the interpretation of any one property (water content, for example) from the measured bulk electrical conductivity. However, for many recharge studies, the water quality does not vary enough with time or space to give rise to changes in the pore water electrical conductivity that are large enough to affect interpretations of the water content distribution. In the absence of clay-rich soils, the porosity and the electrical conductivity of the soil solids are nearly constant throughout the unsaturated zone, as well. In most cases, the porosity and electrical conductivity of the soil solids are constant in time. This offers the possibility of location-specific calibration or the use of measured bulk electrical conductivity changes to infer temporal changes in the water content distribution.

The electromagnetic geophysical methods that currently show the most promise for application to recharge monitoring are time domain reflectometry (TDR), time domain transmission (TDT), ground penetrating radar (GPR), capacitance probes, electrical resistance probes, electrical resistance tomography (ERT), electromagnetic induction (EMI), time domain electromagnetics (TEM), self potential or streaming potential (SP), controlled source audio magnetotellurics (CSAMT), and nuclear magnetic resonance (NMR). TDR, TDR, capacitance probes, and GPR are used primarily to measure dielectric permittivity, as discussed above. ERT, EMI, TEM, and CSAMT are used primarily to measure the electrical conductivity distribution of the subsurface. These methods can be divided into direct and inductive methods on the basis of how electrical energy is applied to the ground and how the electrical response of the subsurface is measured. Directly coupled methods require that electrodes be inserted into the ground to apply electrical current and to measure voltage. Inductively coupled methods typically use coils to apply electrical current and to measure voltage, thereby eliminating the need to insert electrodes into the ground. (CSAMT is a hybrid method in which a directly coupled source and both directly and inductively coupled receivers are used.) Electromagnetic methods for measuring the electrical conductivity distribution can be separated further into time domain methods, which measure the electrical conductivity over many frequencies simultaneously, and frequency domain methods, which measure over singles frequencies. TEM is an example of a time domain method, while ERT, EMI, and CSAMT are frequency domain methods. Telford and others (1990) and Rubin and Hubbard (2005) provide reviews of electromagnetic methods.

The design of direct current (or low frequency) EM methods allows for great flexibility in sampled volume, measurement sensitivity, and distribution of measurement sensitivity within the sampled volume. Typically, each measurement is made with four electrodes. Two electrodes are inserted into the ground and used to inject current. The remaining two electrodes are inserted into the ground and used to measure an electrical potential. SP methods are an intriguing variation of direct current electrical conductivity methods in which current is generated naturally due to the flow of water in the subsurface. This method offers the ability to identify regions in the subsurface through which water is flowing. With further development, SP methods combined with other methods may be able to quantify water flux. ER and SP methods use similar instruments and survey designs, so they will be discussed together. The size of the sample volume and the measurement sensitivity within the sample volume of these instruments are controlled by the separations of the electrodes; generally, larger separations lead to larger sample volumes. Further refinement of the sensitivity distribution can be achieved by the choice of array type (the relative positions of the four electrodes). Point scale measurements of the bulk electrical conductivity can be made by using closely spaced electrodes either at the ground surface or within boreholes. The simultaneous inversion of multiple measurements made at the ground surface, in boreholes, or some combination of both, leads to a two- or three-dimensional image of the subsurface bulk electrical conductivity distribution. This is known as electrical resistance tomography (ERT). Modern advances in ERT instrumentation allow for automated selection of electrode sets to conduct many measurements with different combinations of stationary electrodes. This ability makes ERT particularly useful both for structural mapping and for time-lapse monitoring. Because of the sensitivity of the bulk electrical conductivity to properties of both the medium (porosity, solid electrical conductivity) and the fluid (water saturation, pore water electrical conductivity), ERT is less useful for stand-alone structural mapping than seismic methods. However, when used in conjunction with other methods (seismics, for example), ERT can improve structural mapping and can be used for water content mapping and monitoring. Based on these qualities of ERT, together with the ability of ERT to construct multidimensional images from static instruments, it is likely that ERT will be applied more routinely for monitoring changes in water

content throughout the unsaturated zone both for constraining detailed hydrologic models and for direct interpretation of the water fluxes during transient infiltration. ERT has been applied widely in hydrologic studies and many examples of its successful use have been published. The great flexibility of the ERT method to allow for novel applications is demonstrated through the steel-casing resistivity technology (SCRT) variation of the mise-a-la-masse method described by Telford and others (1990, p. 523) in the case study "Temporal monitoring of infiltration by using a hybrid electrical method."

As with the directly coupled low frequency EM methods, there is also a wide variety of designs of inductively coupled electrical conductivity measurement devices. Typically, these instruments are comprised of two coils. One coil applies a time-varying EM field. The second coil measures secondary currents that are induced in conductive bodies in the subsurface. Frequency domain methods measure the applied and induced signals simultaneously while the signal is applied; the induced field is determined by nulling or accounting for the primary field. Time-domain methods measure the time rate of decay of the induced currents after the source current has been turned off. The size of the sample volume and the measurement sensitivity within the sample volume are controlled by the separation of the coils and the frequency of the applied signal. Generally, larger separations and lower frequencies lead to larger sample volumes and lower resolution within the sample volume. Inductively coupled EM methods range from very small scale (hand held metal detectors and down-hole EM tools, for example) to very large scale (TEM, for example) with an instrument available for almost every intermediate scale of measurement. EM induction methods can also be used to profile through a nonmetallic borehole, providing very high resolution of the electrical conductivity profile. Callegary and others (2007) analyze spatial resolution and exploration depth of low-induction-number frequency-domain electromagnetic induction methods.

Inductive EM techniques are most likely to contribute to recharge monitoring either through definition of geologic structure (especially airborne methods and borehole logging) and through time-lapse monitoring at smaller scales or at single locations. Two examples are provided to demonstrate the use of frequency domain methods. "Use of electromagnetic logs to monitor downward movement of focused infiltration" describes the quantitative use of borehole EM for monitoring infiltration. Depth profiling with surface-based frequency domain methods requires the use of different frequencies and different coil separations, limiting the practically achievable temporal and spatial resolution of the electrical conductivity profile. Time domain methods measure over a wide range of frequencies in a short time, allowing for efficient depth profiling. However, because these methods typically require the use of relatively large antennae loops, they are difficult to deploy quickly at many surface locations, limiting spatial coverage. The ability of time domain electromagnetic methods to make rapid, nondestructive measurements of electrical conductivity suggests that these methods could contribute to monitoring transient infiltration and to calibrating numerical models describing water flow throughout the unsaturated zone. However, quantitative application of these methods for recharge monitoring will require improved understanding of the spatial resolution of TEM methods to subsurface water content distributions. Therefore, borehole logging remains the most useful approach to depth profiling for hydrologic investigations. "Electromagnetic induction as a reconnaissance tool to map recharge" examines the use of surface-based EM to map likely areas of recharge. This case study is of particular interest because EM mapping is often included in hydrogeologic investigations because the lack of direct contact of the instrument with the ground allows for rapid mapping of lateral changes in hydrogeologic structure over large areas.

Proton Precession

Protons of hydrogen atoms in water molecules have a magnetic moment that aligns with an external magnetic field. Typically, this magnetic moment is aligned with the local magnetic field of the earth. When another magnetic field is applied, the axes of the spinning protons are deflected to align with the total field. When the applied field is removed, the protons realign with the local magnetic field of the earth. As the protons realign, they generate a relaxation magnetic field. Nuclear magnetic resonance (NMR) methods measure this relaxation magnetic field in response to a magnetic field due to an alternating current in a loop placed on the ground surface. The instrument response is a time-varying, time-decaying voltage measured with either the same loop or a secondary loop. The initial amplitude and rate of decay of the measured voltage is related to the volumetric water content of the subsurface. The water-content profile can be inferred based on measurements made with a range of excitation intensities. In addition, the decay time can be related to the mean pore size, giving an indication of the hydraulic conductivity (Yaramanci and others, 1999). As with most surface-based geophysical methods, the resolution and accuracy of the method decrease with depth. Currently, 100–150 m depth can be investigated with a resolution of a few decimeters at shallow depths and a few meters at greater depths. The accuracy achievable for water content is roughly a few percent, depending on depth. NMR is a promising new method for rapid profiling to great depths, but the method is currently in too early a stage of development to present a case study for recharge monitoring.

Mass Change

The gravitational attraction at a point on the surface of the Earth depends primarily on the density distribution of the materials in the subsurface. Gravity methods have long made use of spatial changes in the subsurface density distribution to define geologic structure. However, given that water is less dense that geologic materials and that the shape of the water table typically changes gradually with lateral distance (unless

Temporal Monitoring of Focused Infiltration Using a Hybrid Electrical Method

By James B. Fink and Marc T. Levitt

A performance evaluation test was performed at the Hanford Nuclear Reservation in Benton County, eastern Washington State to meet U.S. Environmental Protection Agency and American Society of Testing and Materials protocols for statistically determining the effectiveness of electrical geophysical methods for monitoring leaking underground storage tanks using measurements made exclusively exterior to the tank. Although the controlled leak sources were released at points, the results can be extended to electrical geophysical methods for monitoring infiltration beneath planar sources, such as recharge impoundments, ephemeral streambeds, or basin floors under field conditions. The location of the test at the Hanford facility was of particular interest for recharge investigations because of its thick unsaturated zone and desert conditions, making it a useful model for much of the western U.S. As part of this investigation, a new application, called steel casing resistivity technology (SCRT), was evaluated.

The target of the investigation was a mock-tank cold test facility in the 200 East area of Hanford (NRC, 2001). The mock tank is a two-thirds-scale mock-up of a million-gallon (3,800 cubic meters), single-shell-tank (SST) such as those buried in several tank farms at Hanford. The 15-m diameter mock-tank was partially buried to better simulate tank-farm conditions with the bottom of the tank 1.2 m below ground surface and the top of the tank 3.0 m above the ground surface. Figure 8 shows a plan view of the mock tank and related infrastructure. Fourteen injection points were in the base of the mock-tank to simulate point-source leaks beneath SSTs.

The mock tank is placed in the Hanford formation, a permeable, unconsolidated sand and gravel sequence ranging in thickness from 60 to 100 m. The formation is characterized by little or no clast cementation and few fine-grained horizons. Gravel content is commonly more than 40 percent. Depth to water beneath the mock tank is approximately 60 m. The Hanford formation typically has a volumetric water content of 0.06 m^3/m^3. The saturated volumetric water content ranges from 0.12 to 0.38 m^3/m^3. The saturated hydraulic conductivity ranges from 4×10^{-6} to 2×10^{-4} m/s.

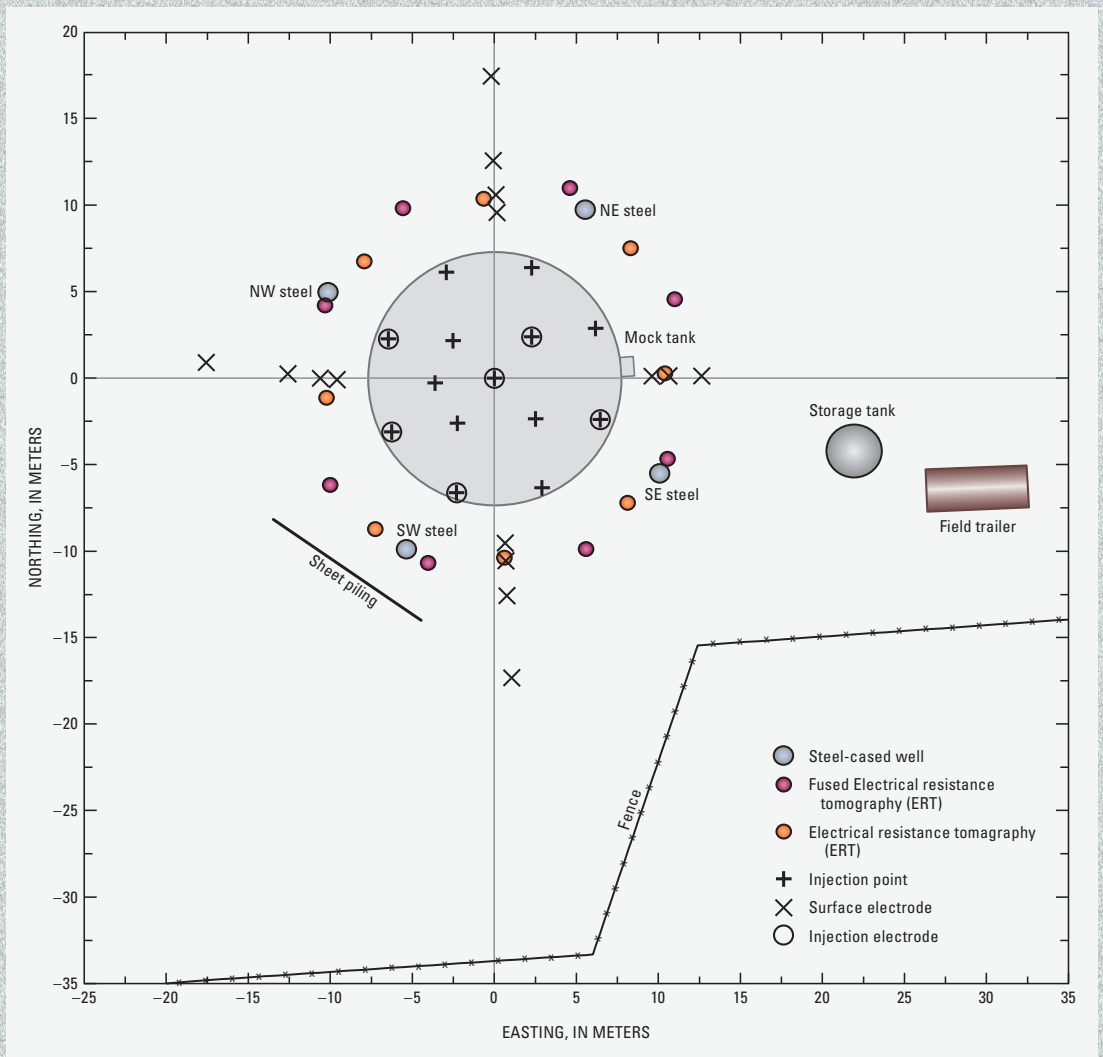

Figure 8. Plan view of the mock tank and test-related infrastructure at the Hanford site.

Generally, the Hanford formation allows rapid vertical infiltration. The Hanford formation is underlain by a Pliocene–Pleistocene unit, which constitutes an impermeable clay-and-caliche-rich zone up to 8-m thick and variably present throughout the facility. This confining unit is either absent beneath the mock tank facility or sufficiently deep to have no effect on infiltration within the depth of this investigation.

The solution used for the test was 36 percent by weight sodium thiosulfate pentahydrate ($Na_2S_2O_3$–$5H_2O$). This solution was selected to simulate the specific gravity, concentration, relative viscosity, and electrical conductivity of typical tank waste. A total volume of about 51 cubic meters (m^3) was released in 14 leak events of approximately 4.6 m^3 each. Test leak rates were 0 (no-leak), 7.6, 38, and 76 liters per hour (2, 10, and 20 gallons per hour). Specific leak timing was unknown to monitoring personnel.

Sixteen vertical electrode arrays had been placed uniformly around the mock tank by direct push technology. Each array was located approximately three meters away from the edge of the mock tank. Each array was made up of eight stainless steel screen electrodes approximately ten centimeters long and spaced equally from a few centimeters to ten meters below surface. In addition to the point electrode arrays, four steel casings were installed to simulate drywells surrounding the tanks within the tank farms. One casing was placed in each quadrant around the tank. Each casing was about three meters from the tank and extended to a depth of about ten meters. A steel sheet piling about five meters tall by ten meters wide was placed to the southwest of the mock tank to represent the effects of an adjacent tank. The sheet piling was electrically connected to the mock tank for the majority of the testing period. It was disconnected as an additional complicating factor during a brief portion of the test.

The SCRT measurements were collected continuously throughout the 110-day test except for a two-hour period each day when ERT data were acquired. Each SCRT sweep required approximately 15 minutes. Approximately 3.8 million data points were acquired during the test. The SCRT surveys made use of the four steel dry-well casings and the eight electrically shorted ERT arrays that were intended to approximate drywell casings. In addition, the steel mock tank, the injected solution, surface electrodes and other electrically grounded infrastructure were used to inject current and to detect potential distributions. This use of the tank and the leaked solution is an important difference between conventional ERT methods and the SCRT approach. This direct connection to the leaking solution allowed SCRT to acquire mise-a-la-masse type data by energizing the leaking solution. The reciprocal arrangement of receiving on the tank while energizing a dry well, for example, performed equally well. All data acquisition activities were controlled remotely through a virtual private network that was accessible via the Internet. All instruments were kept in a climate-controlled, temporary enclosure on-site at the mock tank and powered from the regional electrical grid.

The SCRT results include measurements with many combinations of electrodes and electrode types. For ease of visualization, the SCRT time series for one dry-well sensor is shown in figure 9 for a portion of the test. The abscissa is time in decimal days. The ordinate of the SCRT time series is normalized transfer resistance; that is, the normalized intensity of the electric field measured using a four-electrode array. The leak events are indicated by increasing portions of the cumulative infiltration-volume curve. The leaks and intervening non-leak periods are readily seen as sudden changes in the SCRT time series at both the onset and the cessation of each leak. Such well-defined offsets in the time series could offer accurate, long-term, quantitative monitoring of the timing of leak activity. After compensation for cultural distortions of the local electric field, the change in transfer resistance with time during leak periods is highly correlated with the leak rate. The time series collected at other locations show similar patterns through time, but different amplitudes reflecting the length of the electrode, distance from the leak, and location within the background electric field. Such techniques provide possibilities for long-term, semi-automated monitoring of ground-water recharge from ephemeral stream infiltration.

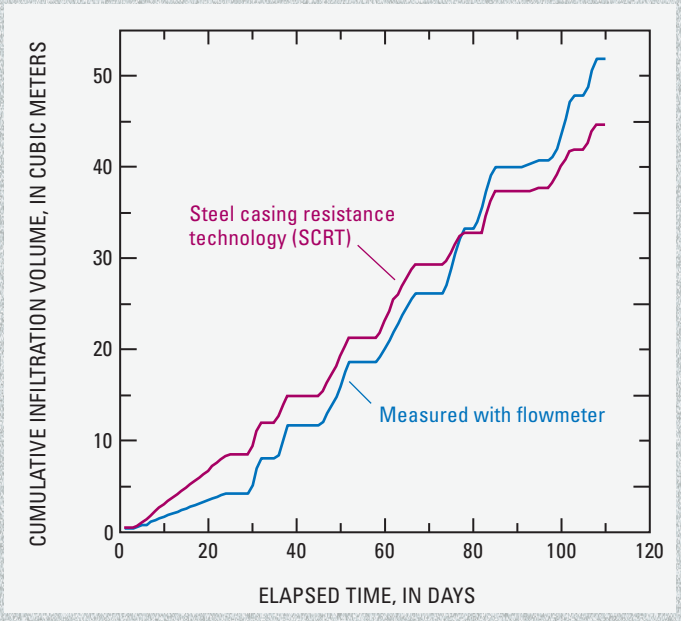

Figure 9. Measured and steel casing resistance technology (SCRT) derived infiltration volume during the entire leak test.

Use of Electromagnetic Logs to Monitor Downward Movement of Focused Infiltration

By John A. Izbicki and Steven M. Crawford

An experiment was conducted to determine if water infiltrated from a 0.4-hectare artificial recharge pond could recharge the water table about 122 m below land surface. The facility was located along Oro Grande Wash in the western Mojave Desert, near Victorville, Calif. (fig. 10). About 580,000 m^3 of water was infiltrated during three periods from October 1 to December 19, 2002; February 10 to March 24, 2003; and May 10 to September 31, 2003. The pond was allowed to dry between infiltration periods and accumulated fines were removed before more water was infiltrated.

The downward movement of water in the unsaturated zone beneath the pond was monitored at an instrumented borehole adjacent to the pond by using a variety of techniques. The U.S. Geological Survey installed the borehole in January 2001. Air, rather than water, was used to drill the borehole and remove drill cuttings. Steel casing stabilized the borehole during drilling and instrument installation. The cuttings from the hole were logged at 0.3-m intervals. On the basis of those logs, the 0.22-m diameter borehole was instrumented with three tensiometers connected to land surface with 0.025-m diameter PVC pipe, eight heat-dissipation probes, five suction-cup lysimeters, and a 0.05-m diameter PVC well screened across the water table. The well also served as an access tube for repeated logging with geophysical tools. Each instrument was packed in suitable material to allow communication with the formation (combinations of 60-mesh sand and diatomaceous earth) and isolated vertically with low-permeability bentonite grout to prevent flow of water within the borehole during the experiment. The grout was installed dry, and hydrated in the borehole within several weeks of installation. The steel casing used to stabilize the borehole was removed as the instruments and backfill material were installed.

The tensiometers and heat-dissipation probes installed within the borehole recorded changes in matric potential at 4-hour intervals during the recharge experiment. The tensiometers recorded both matric potential and head (positive pressures). In addition to changes in moisture content, the tensiometers also were sensitive to changes in air pressure and compression of the unsaturated material beneath the pond from the weight of the infiltrated water. The heat-dissipation probes measured only matric potential and were not sensitive to changes in air pressure or compressional forces. Both the tensiometers and heat-dissipation probes responded to the rapid downward movement of a small amount of water in advance of the main wetting front.

The position of the wetting front also was measured intermittently during the experiment with an electromagnetic induction (EMI) geophysical tool. In this case, an EMI tool was chosen rather than a neutron probe because of the likelihood that the hydrated bentonite grout used to seal the borehole would lead to an unacceptably small sensitivity of the neutron probe to the surrounding medium. The EMI tool has a larger sample volume, making it sensitive to changes in the moisture content of the native material beyond the grout.

Selected EMI logs collected between November 11, 2002, and May 6, 2003, show the downward movement of water in the upper 75 m of the borehole (the lower 47 m are not shown; fig. 11). Increased water content as the wetting front progressed downward was recorded as increased electrical conductivity on the EMI log. The downward rate of movement of the wetting front ranged from 0.75 to 0.06 m/d (fig. 12). The position of the wetting front measured with the EM logs and other instruments within the borehole show good agreement throughout the experiment. The downward rate of movement, initially as high as 1 m/d, decreased through time to a relatively constant rate of about 0.08 m/d (fig. 12). Assuming no impermeable units were encountered, the wetting front was estimated to reach the water table underlying the pond by late February 2005 (fig. 12). The downward rate of movement of the wetting front decreased rapidly at the beginning of the experiment as the wetting front spread laterally in the subsurface. The downward rate of movement of the wetting front decreased further between December 22, 2002, and May 6, 2003, when water was not being continuously infiltrated from the pond.

Decreased water content, recorded as decreased electrical conductivity on the EMI logs (fig. 11), also was measured at certain depths within the unsaturated zone during the recharge experiment. The largest decreases occurred after water accumulated on top of coarse-grained gravel layers. Saturated conditions developed on top of these layers until the pressure exceeded the entry pressure of the underlying coarser-grained deposits. Once the entry pressure was exceeded the water drained rapidly to greater depths. Smaller decreases in resistivity were associated with redistribution of previously infiltrated water to greater depths when no water was being infiltrated at the ground surface.

The arrival of the wetting front estimated from heat-dissipation probe data appears to lag the arrival estimated on the basis of tensiometer and EM log data (fig. 12). This probably results from the placement of the instruments within the borehole. For example, several heat-dissipation probes were placed beneath clay layers thought to impede the downward movement of water.

Borehole logging instruments allow more flexibility in a monitoring program than buried instruments. For example, in this study, the EM data could have been collected at any time to determine the position of the wetting front. This would

not possible be with the instruments that were installed at a fixed depth, which require that the depth of the wetting front be inferred between measurement points. The EM logs also yielded information throughout the entire thickness of the unsaturated zone and were sensitive to the dynamic movement of water within the subsurface in both fine-grained and coarse-grained units. The EM logs were not sensitive to confounding influences from air-pressure changes or compression of unsaturated material as the water from the pond moved downward. As a result, borehole EM data were useful for monitoring wetting front movement and for predicting the arrival of the infiltrated water at the water table, especially when used together with traditional unsaturated-zone monitoring techniques.

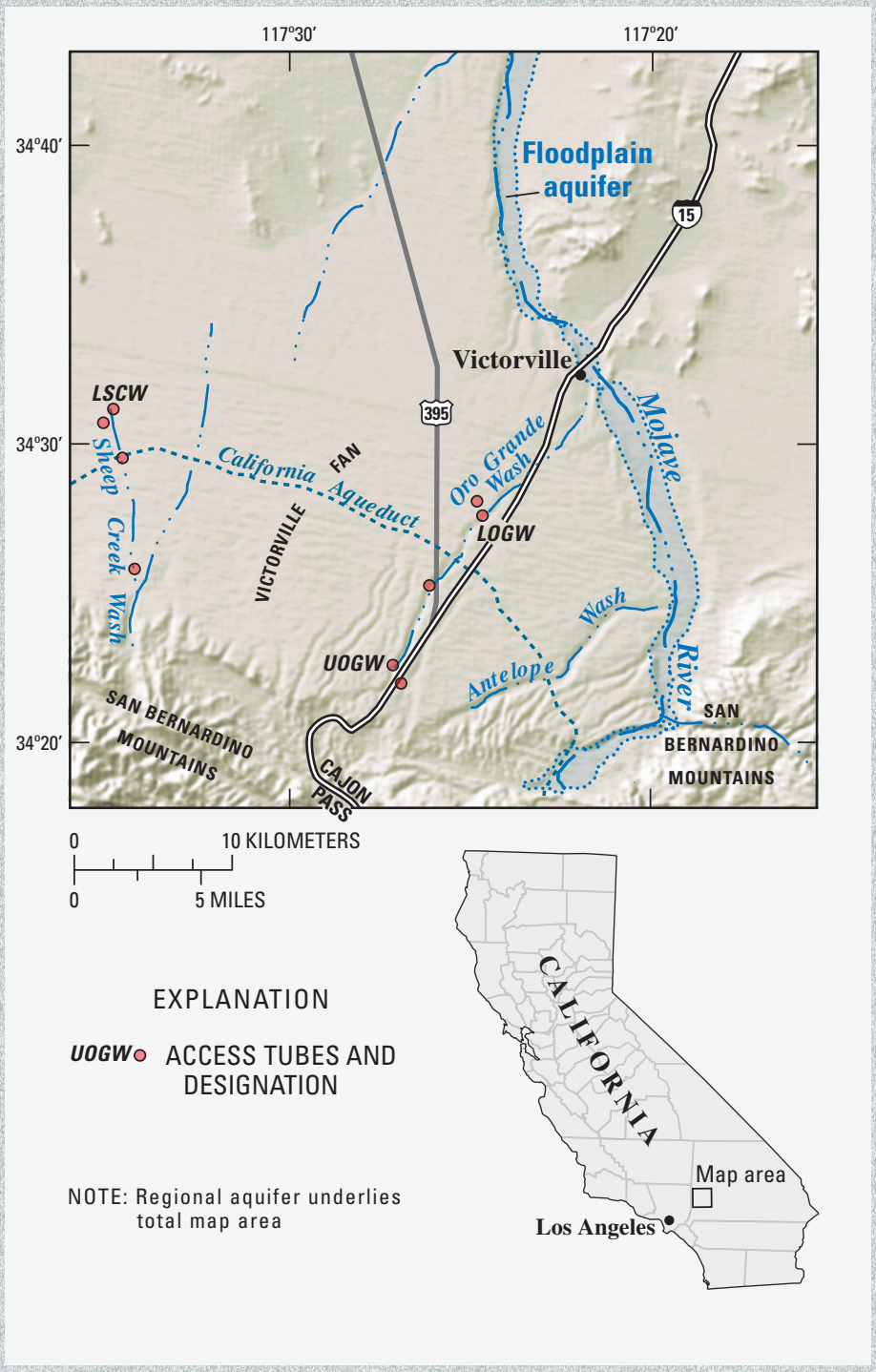

Figure 10. Location of artificial recharge pond along Oro Grande Wash, western Mojave Desert near Victorville, Calif.

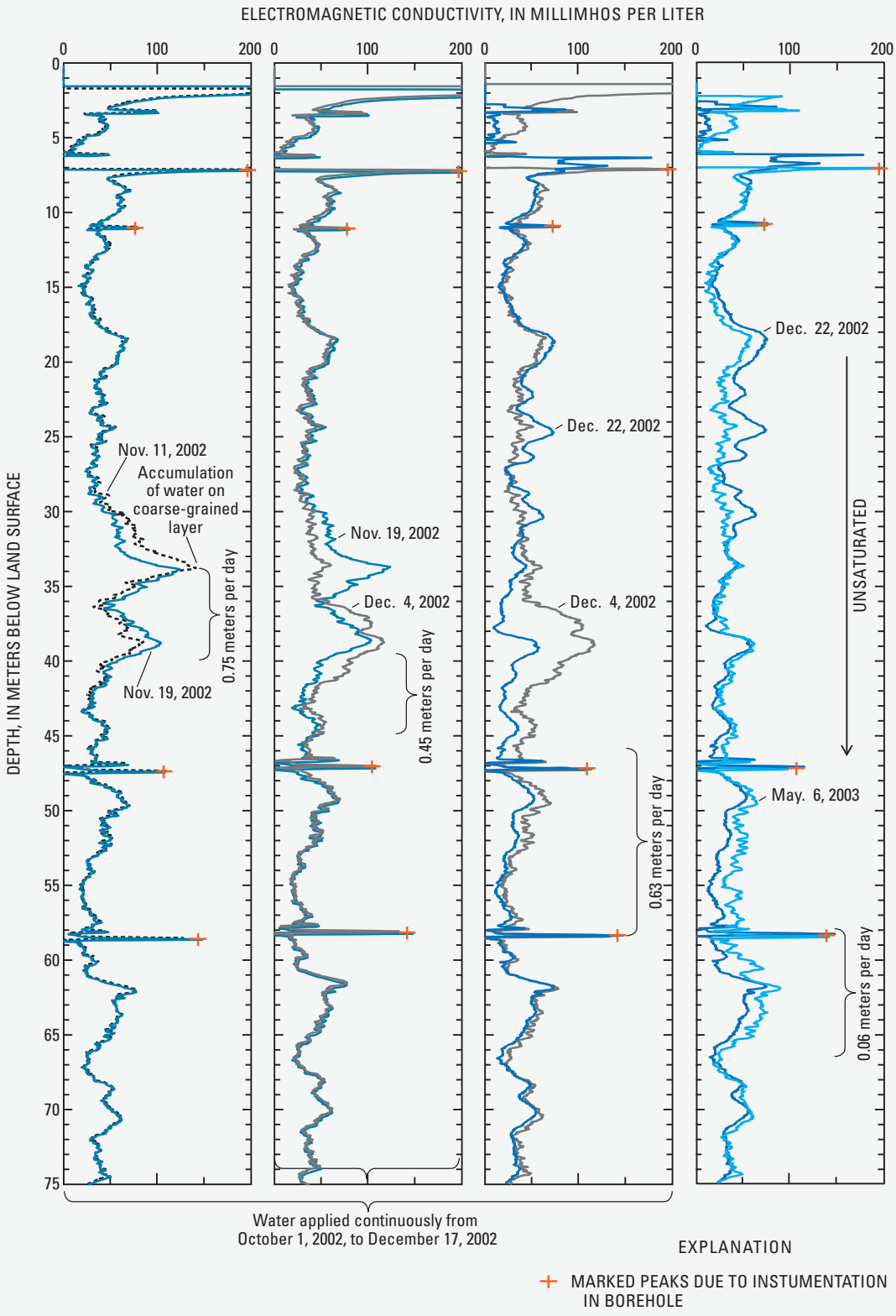

Figure 11. Selected electromagnetic logs measured from a plastic access tube emplaced within an instrumented borehole next to an artificial recharge pond near Oro Grande Wash, western Mojave Desert (near Victorville, Calif.) November 11, 2002, to May 6, 2003.

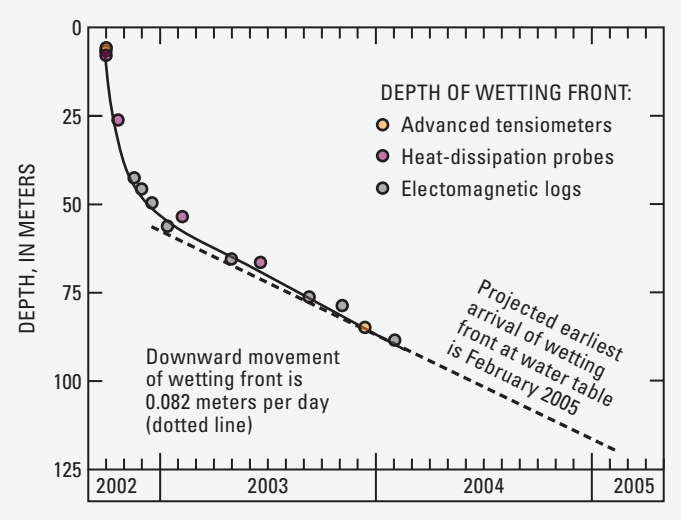

Figure 12. Downward movement of wetting front at an artificial recharge pond near Oro Grande Wash, western Mojave Desert near Victorville, Calif.

Electromagnetic Induction as a Reconnaissance Tool to Map Recharge

By Bridget R. Scanlon

This study was conducted to evaluate the potential of surface-based electromagnetic (EM) induction as a reconnaissance tool to map recharge areas at a site 120 km southeast of El Paso, Texas, in the Chihuahuan Desert (fig. 13; Scanlon and others, 1999). Because EM induction measures the apparent electrical conductivity (EC_a), which varies with clay content, water content, and salinity, it may be able to map recharge indirectly through relationships between recharge and one of these parameters. For example, Cook and Kilty (1992) showed a correlation between recharge and EC_a that was controlled by clay content. Other studies have shown a correlation between high chloride concentrations in pore water with high evaporative concentration in areas of low recharge (Scanlon, 1991; Phillips, 1994; Tyler and others, 1996). Despite the promise of EM induction methods for identifying areas of relatively high recharge, the possibility of conflicting multiple influences on the EM response must be considered for each site.

To evaluate the potential of EM induction for mapping recharge, we first need to determine what parameter exerts a controlling influence on the EM response for a given site. Then we need to assess the hydrologic significance of that parameter relative to recharge. In this study, surface-based EM transects were conducted with EM31 and EM38 meters (Geonics Inc., Mississauga, Canada) from a playa to an interplaya setting and across a fissure (fig. 13). The playa is characterized by lacustrine clay sediments whereas the adjacent interplaya is a sand-dune setting. Previous studies in the High Plains have shown that playas focus recharge (Wood and Sanford, 1995; Scanlon and Goldsmith, 1997). The fissure (640-m long) consists of an alignment of discontinuous surface collapse structures underlain by a fracture. Water ponds occasionally on this structure, possibly inducing focused recharge. In addition to the EM transects, boreholes were drilled and sampled for clay, water, and chloride contents.

The playa has higher EC_a values than the interplaya sand sheet setting due to 50 percent higher water content and 60 percent higher clay content (figs. 14 and 15A). Higher water contents in the playa sediments could reflect higher recharge through the playa or may simply be related to higher clay content within the playa. In this case, there is a high correlation coefficient (r) between the water and clay contents in samples collected in a profile adjacent to the playa (GL 4, $r^2 = 0.97$, fig. 15B). This indicates that the variability in water content can be explained entirely by variations in water storage associated with differing clay contents and is not related to recharge. Therefore, mapping EC_a with surface EM in this region would not be an effective approach to mapping recharge.

The EC_a was higher in the fissure relative to the adjacent sediments in several transects (fig. 16). The fissure sediments are characterized by lower weighted average chloride content, higher water content, and higher clay content than the adjacent sediments.

The higher water content and lower chloride content indicate the presence of focused flow beneath the fissure. The increased water content and increased clay content tend to increase EC_a, while the decreased chloride concentration tends to decrease EC_a. Increased clay contents are generally associated with lower recharge. Decreased chloride concentration suggests increased recharge. As discussed above, increased water content can indicate higher recharge or higher clay content. In this case, higher water contents in the fissure reflect higher recharge as shown by lower weighted average clay contents in profiles beneath the fissure relative to those adjacent to the fissure (Scanlon and others, 1999). In addition, considering all paired profiles (fissure versus nonfissure) with similar clay contents, there are higher water contents beneath fissures than adjacent to the fissures. Therefore, the high EC_a values in the fissure are primarily due to increased water content that reflects higher recharge in the fissure, and not simply variations in clay content. The EC_a value is not well correlated with the chloride content because water contents in areas of high chloride are too low for electrolytic conduction.

The results of this study indicate mixed utility of EM induction for mapping recharge. Areas where EC_a is controlled by clay content may be hydrologically significant if clay content controls infiltration and recharge (Cook and Kilty, 1992). However, in this study variations in clay content do not play a significant role in controlling recharge. Correlations between EC_a and water content are difficult to interpret—in many cases they simply reflect variations in clay content because clay and water contents are codependent, such as in the playa-interplaya setting. Higher water contents in the fissure were related to higher recharge. Differences in chloride content are extremely valuable in delineating water flux in unsaturated systems because chloride is readily leached in zones of high recharge and accumulates in areas of low recharge. In fact, chloride is a much more accurate indicator of high recharge than water content because of the complexities of clay-water content codependence. Unfortunately, high water flux is associated with high water content, which contributes to high EC_a, while low chloride content leads to low EC_a. Therefore, the effects of water content and chloride content counter each other, potentially limiting the effectiveness of monitoring of recharge with EM methods. As a result of the competing influences of salinity, water content, and clay content on the response EM instruments, the utility of EM methods for recharge monitoring must be assessed on a site by site basis.

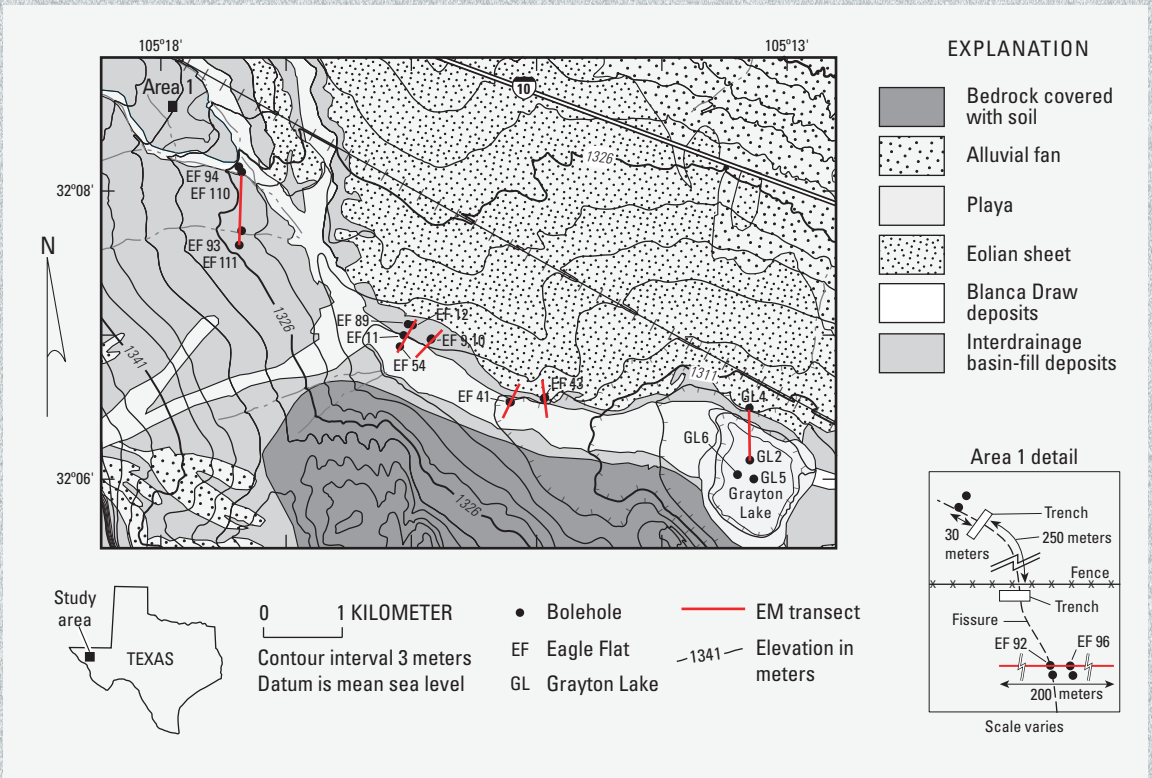

Figure 13. Location of electromagnetic (EM) induction transects and sampled boreholes relative to surface geomorphic settings in Eagle Flat Basin. Adapted from Scanlon and others (1999).

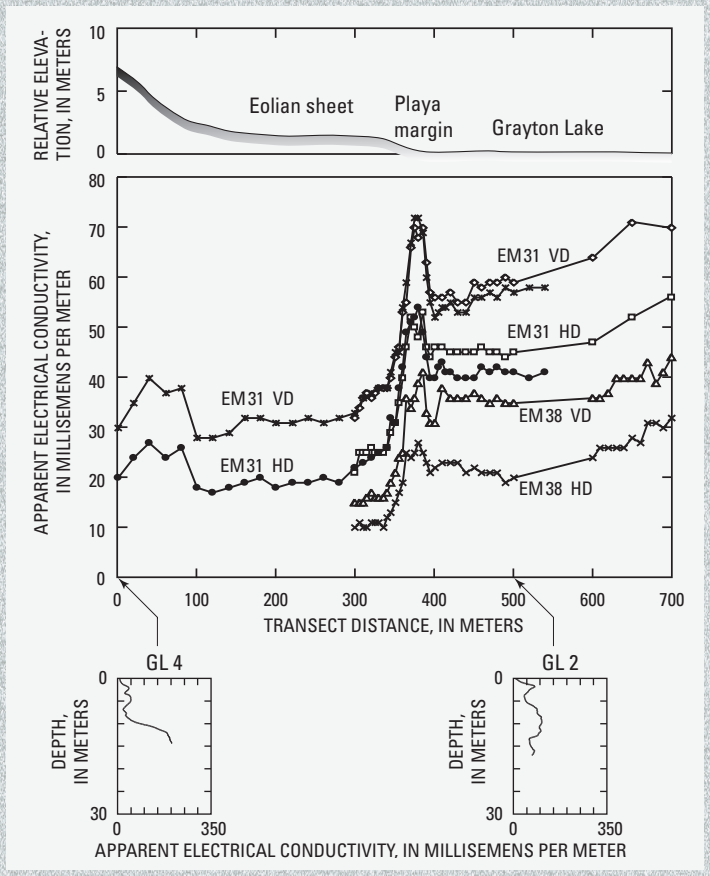

Figure 14. Variations in apparent electrical conductivity (EC_a) along a horizontal transect from the sand sheet to the playa measured with model EM31 and EM38 conductivity meters, and in a vertical profile in boreholes GL4 and GL2 measured with a model EM39 meter. Horizontal-transect EC_a was determined using vertical and horizontal dipole configurations (VD and HD). Adapted from Scanlon and others (1999). See figure 13 for locations.

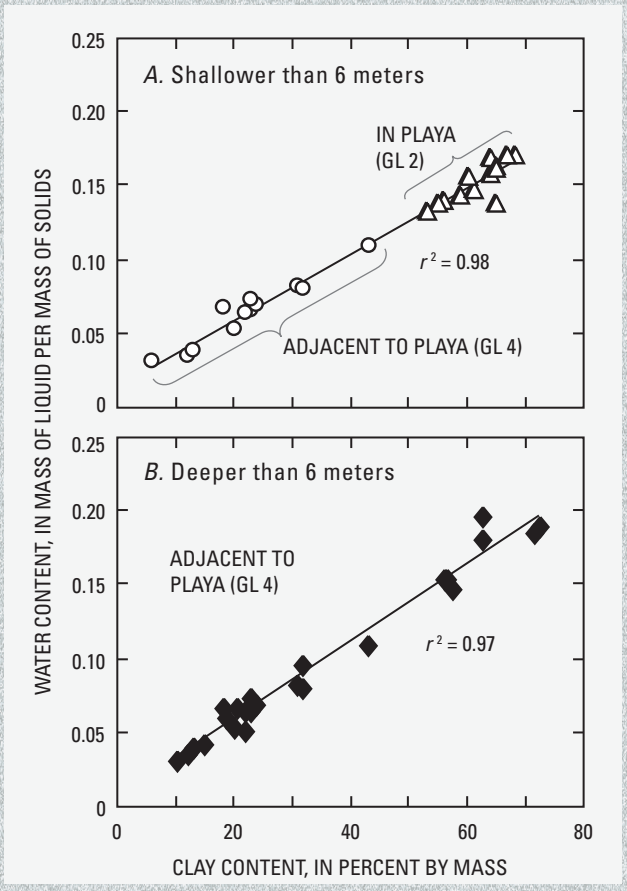

Figure 15. Relationship between water content and clay content: *A*, in the uppermost six meters (holes GL2 and GL4; *B*, deeper than six meters. The square of the correlation coefficient (r^2) indicates the fraction of variation accounted for by each line. Adapted from Scanlon and others (1999). See figure 13 for locations.

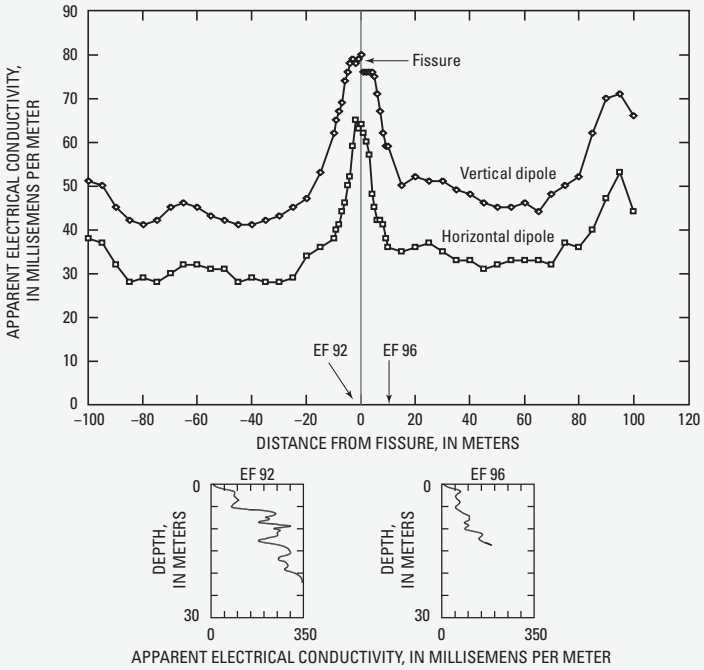

Figure 16. Variations in apparent electrical conductivity across and adjacent to a fissure, measured on land surface with a model EM31 meter in vertical- and horizontal-dipole modes, and down hole with the EM39 meter. Borehole EF92 is in the fissure; EF96 is ten meters away. Adapted from Scanlon and others (1999). See figure 13 for locations.

controlled by geology) gravity monitoring has limited use for subsurface water content mapping.

Recently, however, the value of time-lapse gravity surveys has been recognized for inferring changes in subsurface water content distributions. This use of gravity methods relies on the fact that, in most environments, changes in subsurface mass through time are dominated by changes in water storage. Therefore, after standard corrections are applied for tidal and instrument effects, the change in gravitational attraction at the ground surface can be related to the cumulative change in the water stored in the subsurface. Gravity-based water storage change monitoring has great promise for water balance applications because the method is portable, rapid, and requires far less infrastructure than monitoring wells. However, the method does not provide measurements of the subsurface water distribution. In fact, the method may be susceptible to errors if water accumulates at shallow depths above the water table, due to the inverse dependence of gravitational attraction on the distance to a body. Despite this potential error, gravity-based methods are uniquely capable of providing spatial estimates of water storage change over large areas. As a result, they will likely see expanded use both for direct estimation of water storage change and for calibration of saturated flow models. An example of the direct use of time-lapse gravity for monitoring changes in water storage throughout a basin is provided in "Monitoring temporal changes in water storage with gravity."

Hydrogen Density

One borehole logging technique has shown particular promise for recharge monitoring—neutron logging. Neutron probes emit epithermal neutrons produced from a radioactive source. These neutrons enter the medium surrounding the borehole, where they collide with the constituents of the medium. Because neutrons and hydrogen atoms have similar masses, collisions of epithermal neutrons with hydrogen atoms cause a relatively large loss of energy. Many such collisions "thermalize" (slow) the emitted neutrons. By counting the rate of thermalization of the emitted neutrons, the hydrogen density of the medium can be inferred. In the absence of neutron capturing elements, neutron counts are well correlated with the volumetric water content of the medium in close proximity to the borehole. Neutron probes are unique among water content profiling methods in their ability to measure to great depths. This ability is due to the location of both the neutron source and the detector in the probe body, requiring only a one-way information link with the surface. However, the placement of the radioactive source in the borehole is also a primary limit on the widespread, continuing use of neutron methods due to regulatory and liability considerations. In addition, because neutron methods use a radioactive source, measurements must be made over relatively long times (0.5 – 1 minute per measurement point). This measurement time is fast enough to track slow recharge, but may not be sufficiently rapid to characterize rapid processes near the ground surface. Furthermore, due to neutron loss across the ground surface and to safety

considerations, neutron methods are not typically used at or near the ground surface. Due to their unrivaled ability to profile the water content to great depths in a single borehole, it is likely that neutron probes will remain a standard method for measuring water content profiles to calibrate unsaturated flow models. The case study "Estimating recharge using time-lapse neutron moisture logging" is provided as an example of the unique abilities of neutron probes for episodic recharge monitoring.

Well Logging

Many borehole-logging techniques have been developed for oil and mineral exploration (Labo and Mentemeier, 1987; Kearey and others, 2002). Most of these methods are aimed at defining either geologic structure or fluid distributions, both of which may be adopted for similar uses for recharge monitoring. Borehole logging techniques typically give high-resolution depth-continuous measurements at a limited number of locations. The utility of borehole geophysical methods is commonly increased through simultaneous interpretation of multiple methods. Similarly, borehole methods are useful for constraining the interpretation of surface-based geophysical methods. Borehole geophysical measurements are often conducted in boreholes upon completion. It is likely that this information could be used more routinely and more completely to characterize the spatial structure of the chemical, physical, and hydraulic properties within the unsaturated zone. At a minimum, these data should be used to identify those areas that may impact water flow and solute transport to ensure that more-detailed measurements are made in critical zones. This would represent a first step toward the use of geophysical methods to optimize the design of monitoring networks for recharge monitoring.

Standard texts provide descriptions of the full range of well logging methods (for example, Desbrandes and Brace, 1986; Keys, 1990; Telford and others, 1990). Neutron logging and electromagnetic-induction logging were already discussed in connection with the mapping of fluid distributions. An illustration of the combined use of neutron and electromagnetic-induction logging to define geologic structure appears in the case study "Geophysical well-logging to estimate subsurface physical and hydraulic properties."

Closing Remarks—A Conceptual Framework for Applying Geophysics to Recharge Monitoring

Geophysics has much to offer to the characterization of the rates, timing, and patterns of recharge. Gravity could be used directly by water resource planners to monitor water storage changes in time. Temperature monitoring and self potential methods may allow for direct measurement of water fluxes in the subsurface, offering the possibility to quantify recharge locally. Seismic and well-logging methods can be used to build more accurate representations of subsurface hydrogeologic structure. Borehole ground penetrating radar, neutron probes, and borehole electromagnetic induction, and point methods like TDR and capacitance probes allow for detailed monitoring throughout the unsaturated zone, improving the calibration of unsaturated flow models and thereby advancing our understanding of the linkages between unsaturated zone processes and recharge. Finally, a suite of electromagnetic methods allow for coarse-scale monitoring of unsaturated zone processes throughout a basin, allowing for better identification of critical areas within a basin that require more intensive characterization.

The key to the successful use of geophysics in recharge investigations is the identification of the appropriate geophysical method or methods for specific hydrologic monitoring needs. The choice of monitoring method must begin with the eventual application in mind. That is, what will be the primary use of the geophysical data? Possible uses include definition of the hydrogeologic structure of the subsurface for basin scale saturated flow models or for more localized unsaturated flow models, estimation of recharge for use in saturated flow models, testing of conceptual models of unsaturated flow, and identifying critical areas for traditional hydrologic monitoring efforts. It is critical that hydrologic insight be used to identify these key processes for a particular investigation. Once the eventual uses of the geophysical data are identified, available geophysical methods should be analyzed quantitatively to address two questions. First, is the method likely to have sufficient sensitivity to the key hydrologic parameters of interest to help resolve the hydrologic question? Second, is the method likely to produce data with sufficient spatial and temporal resolution for accurate hydrologic analysis? These questions can only be addressed confidently through the application of geophysical insight, through the direct participation of someone who is familiar with the application of geophysics to hydrologic problems. The optimal use of geophysics in hydrologic studies will likely require the increased use of geophysical forward models to predict instrument response for expected hydrologic conditions. Ideally, these models should be integrated with standard numerical flow models to encourage the routine use of geophysical tools in hydrologic investigations. The case studies presented here have shown just a few examples of the promises and pitfalls of geophysical methods for recharge monitoring. The common lesson is that measurement methods can only be successful if they are applied to appropriate problems. Eventually, all monitoring methods (traditional hydrologic methods, geochemical methods, and geophysical methods) should be considered in a common cost-benefit framework, balancing the capital and labor costs of measurement methods with their likely benefits in terms of reduced uncertainties in hydrologic analyses. This will allow for the design of an optimal mixture of methods to address a given problem within an available budget. This holistic, integrated view of the role of measurement in hydrology provides an effective conceptual framework for applying geophysics to recharge monitoring.

Monitoring Temporal Changes in Water Storage With Gravity

By Donald R. Pool

Gravity methods were used to monitor ground-water storage and estimate magnitudes and distributions of recharge in a 141 km^2 region in the foothills of the Santa Catalina Mountains, Tucson, Ariz., from summer 1999 through winter 2002. Several ephemeral streams discharge from the crystalline rocks, cross the area in incised channels, and discharge to Rillito Creek and other tributary channels (fig. 17). Tertiary sediments of low to moderate permeability have been exposed by incision of the current drainage system. However, narrow stringers of highly

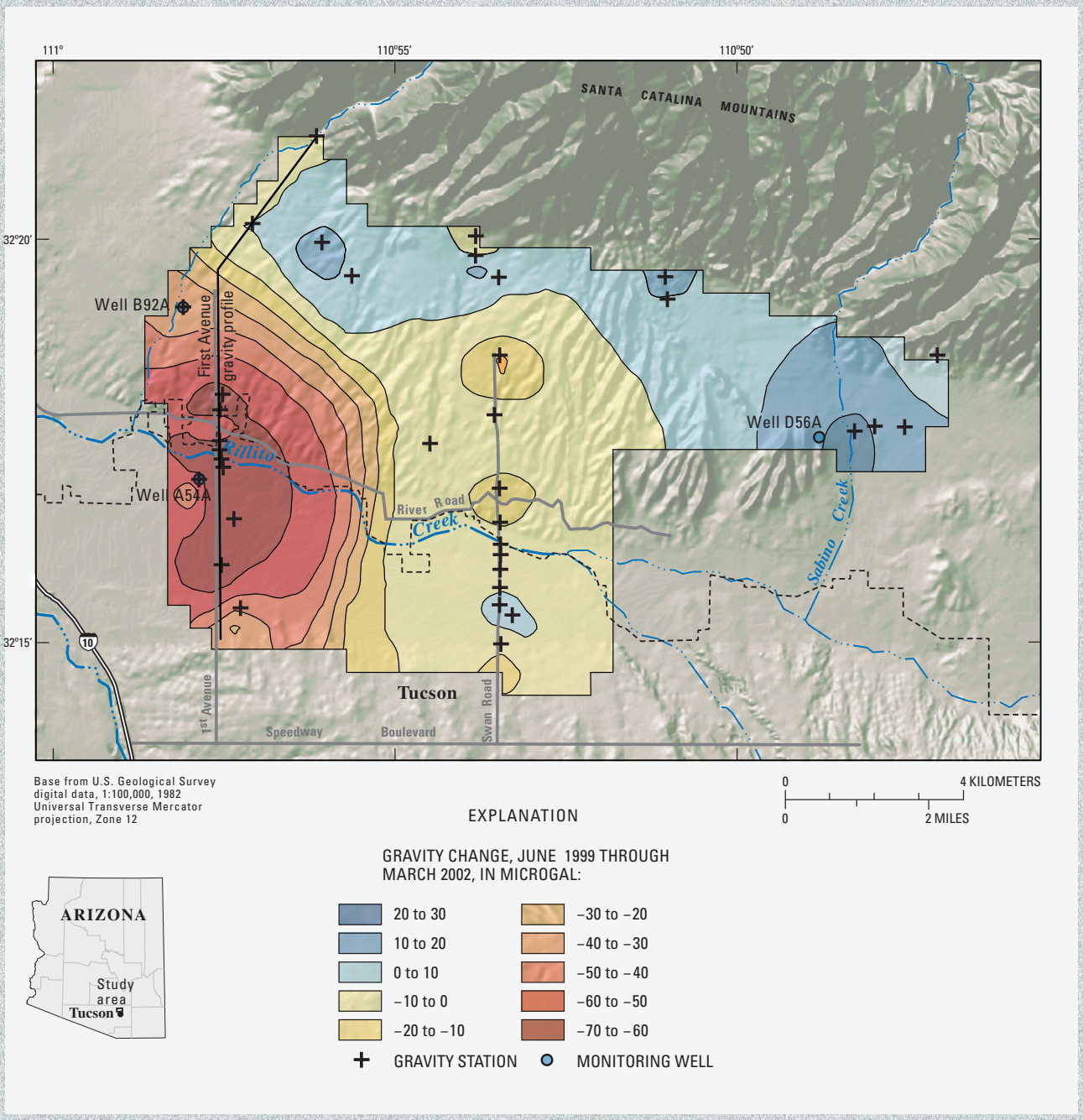

Figure 17. Location of gravity-network stations and changes in gravity, June 1999 through March 2002, near the foothills of the Santa Catalina Mountains, Tucson, Ariz.

permeable alluvium occur along the stream channels and may accept and store significant amounts of streambed infiltration. Ground water is removed from the aquifer through ground-water withdrawals, evapotranspiration, and ground-water flow out of the study area. Ground-water withdrawals and evapotranspiration within the study area are small, however, in comparison to ground-water flow across the area boundary. Ground-water primarily flows toward a major area of ground-water withdrawal south of Rillito Creek and outside of the study area.

The foothills gravity-station network included 23 stations. Two stations were on crystalline rock at the base of the mountains where ground-water storage and gravity change should be minimal. One of the stations on crystalline rocks was also a gravity reference station where the absolute acceleration of gravity was measured six times during the study by the National Geodetic Survey. Gravity at each station was measured relative to the reference station nine times between June 1999 and March 2002. Few wells are available for water level monitoring in the area because few water supply wells have been drilled in the relatively low-permeability saturated-zone materials. Water levels were measured at monitoring wells shown on figure 17.

The general distribution of gravity changes during the study period included an area of decline of up to 60–70 microgal along the lower reaches of Rillito Creek and a swath of increased gravity (up to 10–20 microgal) along the base of the Santa Catalina Mountains (fig. 17). The largest increase in gravity was measured near Sabino Creek, the largest drainage from the mountains. The distribution of gravity change was dominated by declines due to ground-water flow out of the study area and increases due to periodic streamflow infiltration along the major ephemeral channels. Increased storage resulted from precipitation and streamflow infiltration that primarily occurred during two periods, summer of 1999 and July through October of 2000 (fig. 18). Three water-level hydrographs display representative variations in water-level response to infiltration and recharge (fig. 18). Two of the wells, B-92A and A-54A, display water-level declines of 1 to 3.5 m resulting from ground-water withdrawals outside of the study area. High rates of water-level decline along Rillito Creek also resulted from redistribution of recharge that occurred during the winter of 1998. Well D-56A is far from major areas of ground-water withdrawal and displayed slight water-level increases during the period. Gravity change during the period displays a pattern similar to the water levels. Major periods of infiltration and recharge were followed by water-level recovery or significantly reduced rates of water-level decline near major ephemeral streams (wells D-56A and A-54A). Gravity increases also occurred at most stations following major periods of infiltration and recharge.

The distribution of gravity change was monitored in detail along two profiles across Rillito Creek (fig. 17) to assess the redistribution of infiltrated water following major streamflow. Distributions of subsurface storage change in the unsaturated and saturated zones across a profile along First Avenue were simulated with a 2-dimensional gravity model that applies the algorithm of Talwani and others (1959; fig. 19). Constraints on the interval of saturated storage change were available from water levels at several wells. Changes in gravity were defined by surveys on June 25 and August 18, 1999, which included a period of high precipitation and streamflow. Changes along the profile indicate that increases in gravity of 30 to 70 microgal near the stream channel were superimposed on a regional trend of declining gravity (fig. 19). Increases occurred near Rillito Creek and near the mountains. A portion of the gravity change near the stream was attributable to a rise in the water table of a few meters at well North First. The remaining gravity increase was caused by increased storage in the unsaturated zone. The lateral extent of the unsaturated zone storage increase is well constrained by the distribution of gravity stations. The model assumes saturated zone storage change near the Santa Catalina Mountains; however, the vertical distribution of storage change within the saturated and unsaturated zones in the area cannot be separated because no water-level data are available. Gravity decline of less than 10 microgal at most wells distant from the stream channel were simulated adequately by using the measured water-level decline and assuming a specific yield of 0.27. Gravity decline of 10 to 30 microgal at wells A-54A and B-92A, however, were larger than could be explained by the observed water-level change. Significant storage change in the unsaturated zone was therefore required at these wells to simulate the observed gravity change.

The volume of ground-water storage change for the monitored period within the study area was estimated by integration of the linearly interpolated gravity changes across the study area and applying the excess-mass equation (Telford, 1990). Storage change since June 1999 was calculated for gravity surveys done in August 1999, January 2000, June 2000, November 2000, March 2001, and March 2002 (fig. 20). Total ground-water storage for the study area increased more than 25 million cubic meters (Mm^3) following July 1999 and generally decreased thereafter to a total loss of more than 40 Mm^3. Storage changes in the Rillito Creek and foothills subareas displayed somewhat different trends. The foothills subarea comprised most of the increase following July 1999, 20 Mm^3, and displayed continuous declines thereafter. The Rillito Creek subarea displayed a smaller increase following July 1999 and slight increases in storage following October 2000 with declines through the rest of the monitoring period.

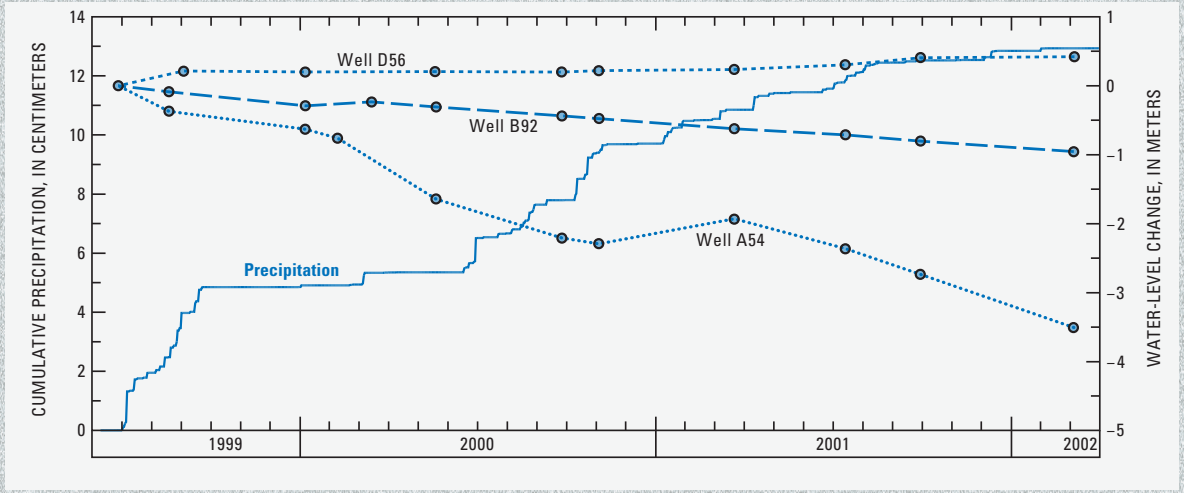

Figure 18. Cumulative precipitation and water levels in selected wells, June 1999 through March 2002, near the foothills of the Santa Catalina Mountains, Tucson, Ariz.

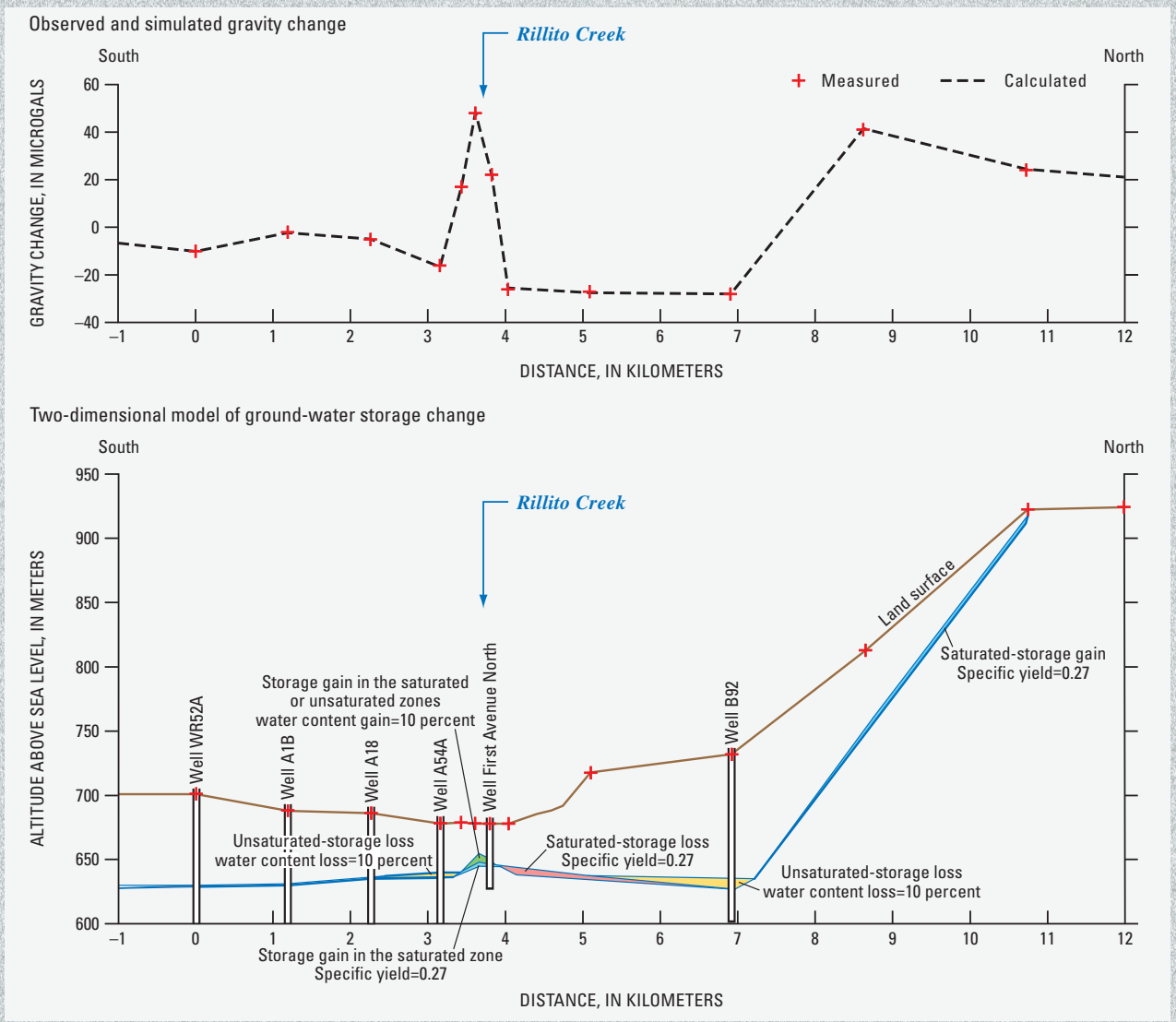

Figure 19. Two-dimensional simulation of ground-water storage change along First Avenue, June 24 to August 17, 1999, near the foothills of the Santa Catalina Mountains, Tucson, Ariz.

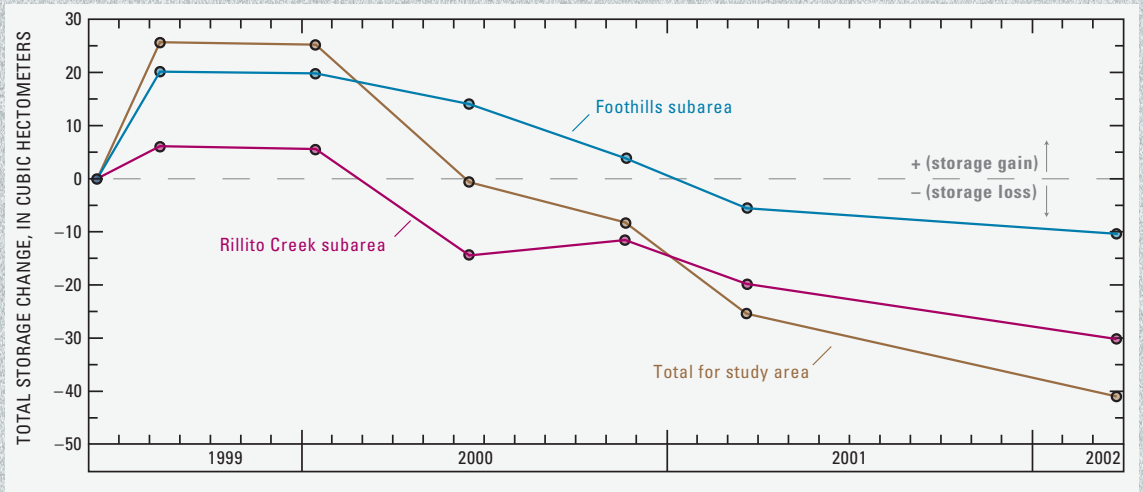

Figure 20. Total storage change in the foothills of the Santa Catalina Mountains, June 1999 through March 2002, Tucson, Ariz. Total for study area is the sum of Rillito Creek and foothills subareas.

Estimating Recharge Using Time-Lapse Neutron Moisture Logging

By Alan L. Flint and Lorraine E. Flint

Spatially distributed recharge from natural precipitation was estimated by measuring soil-water-content profiles at Yucca Mountain, southern Basin and Range, Nevada. Soil-water contents were determined with moisture meters containing an americium-beryllium neutron source (model CPN-503, Campbell Pacific Nuclear, Martinez, Calif.; Flint and others, 2001). Profiles were measured in 100 boreholes for up to ten years by using field- and laboratory-calibrated neutron-moisture meters. The boreholes ranged in depth from approximately 10 meters to 84 meters. Water-content profiles were measured regularly—on a monthly basis and more frequently after major rainfall events (Flint and Flint, 1995). These measurements were used to help develop conceptual models of the mechanisms of recharge in various topographic settings.

One method of interpretation of the water content profiles was to identify the depth of the wetting front as a function of time following a precipitation event. The wetting front depth can be determined by statistical analysis of a time series of water content profiles. Due to the random radioactive decay from the neutron source, the smallest resolvable variation in water content is about 0.01 m^3/m^3 (Hignett and Evett, 2002). The depth below which the measured water content changes with time are less than this threshold can be associated with the depth to which water has infiltrated. Data collected during a ten-year period show that, on the basis of this criterion, infiltration never reached depths greater than five meters in the thick alluvium at the location shown in figure 21.

Examination of a time series of water content profiles provides additional insight into the infiltration, redistribution, and recharge processes. A ten-year series of water content profiles was collected in a site located in a wash with 8 m of alluvium overlying a nonwelded volcanic tuff (fig. 22). The borehole was installed in 1984, several weeks after a major runoff event. Water drained from the alluvium and the underlying tuff during the next several years. Several minor runoff events occurred in the mid 1980s, followed by dry conditions persisting throughout the drought of 1989 and 1990, followed by El Niño period runoff events in 1991 and 1992. Even these large events do not show measurable increases in water content below three meters, indicating that evapotranspiration could easily remove the infiltrated water before it became recharge. In contrast, the 1995 El Niño runoff event caused significant infiltration below the zone of evapotranspiration, eventually resulting in recharge.

The previous analyses use relative measures of water content change to identify the maximum depths of infiltration. These can be achieved without the need for soil-specific calibrations. More-quantitative assessments of infiltration flux require calibration to determine the volumetric water content from neutron counts. As an example, neutron counts, measured in a 79-m borehole drilled through alluvium and several different types of tuffaceous rock, are compared with laboratory-measured water contents from rock cores (fig. 23*A*). A linear correlation between counts and volumetric water content has a square correlation coefficient (r^2) of 0.88, a root-mean-square error of 0.036, and a measurement repeatability of 0.01. The laboratory- and field-measured water content profiles compare well except at the surface (fig. 23*B*). This discrepancy is likely due to the effects of large changes in

water content with depth in this region and uncertainty regarding the averaging of water contents within the vertical sampling interval (approximately 0.5 m; Klenke and Flint, 1991).

The ability to measure changes in volumetric water content with time to great depths allows for the calculation of transient infiltration fluxes directly through measurements of changes in water storage. Based on the time series of water content profiles shown in figure 22, it can be argued that recharge will occur only if infiltration extends below a depth where evapotranspiration can remove all infiltrated water. Flint and Flint (2000) used measured increases and decreases in water content below the zone of evapotranspiration to determine recharge rates in a variety of topographic positions. Specifically, increased water contents below the depth of evapotranspiration were taken to represent potential recharge. Borehole UZ N-15, located in a small channel in a large flat mesa, was drilled in 1992 and flowed once during 1993 and twice during the 1995 El Niño periods (fig. 24*A*). The soil is 0.7 m thick and overlies fractured, welded tuff grading downward to a moderately welded tuff with depth. The soil-tuff interface became saturated allowing water to enter the fractured rock. The water content initially increased following each runoff event, and then drained throughout the profile. Specifically, water moved through fractures in the top 2 m of welded tuff with little imbibition into the matrix. Below 3 m, water was imbibed by the more permeable moderately welded tuff. The average water content between 2 m depth and the soil/bedrock contact increased after each event (fig. 23*B*). There were increases ranging from 150 to more than 300 mm of water in storage from the four infiltration events. Drainage, calculated as the slope of the line between the last El Niño event in 1993 and the first El Niño event in 1995, declined at an average rate of approximately 20 mm/yr (fig. 24*B*).

Under steady-state conditions, infiltration occurs without changes in water storage with time. Assuming a unit gradient condition, the measured water content can be used together with an independent measure of the unsaturated conductivity function (Flint and others, 1999) to calculate the steady-state flux with the Buckingham–Darcy flux law (Jury and others, 1991). This method was employed to develop the first spatially distributed map of net infiltration for Yucca Mountain, NV (Flint and Flint, 1994). More advanced analysis of water content profiles makes use of inverse hydrologic modeling to calibrate infiltration models, which in turn can be used to calculate recharge. Hevesi and others (1994) and Hudson and others (1994) used this approach to calibrate 1-dimensional models at Yucca Mountain. Eventually a series of 1-dimensional models were combined to develop a large-scale rainfall/runoff model by using runoff data and the estimated fluxes in the neutron holes (Flint and others, 1996). The calibrated model results were used to provide the upper boundary conditions for a three-dimensional site scale model of the Yucca Mountain region (Flint and others, 2001; 2002).

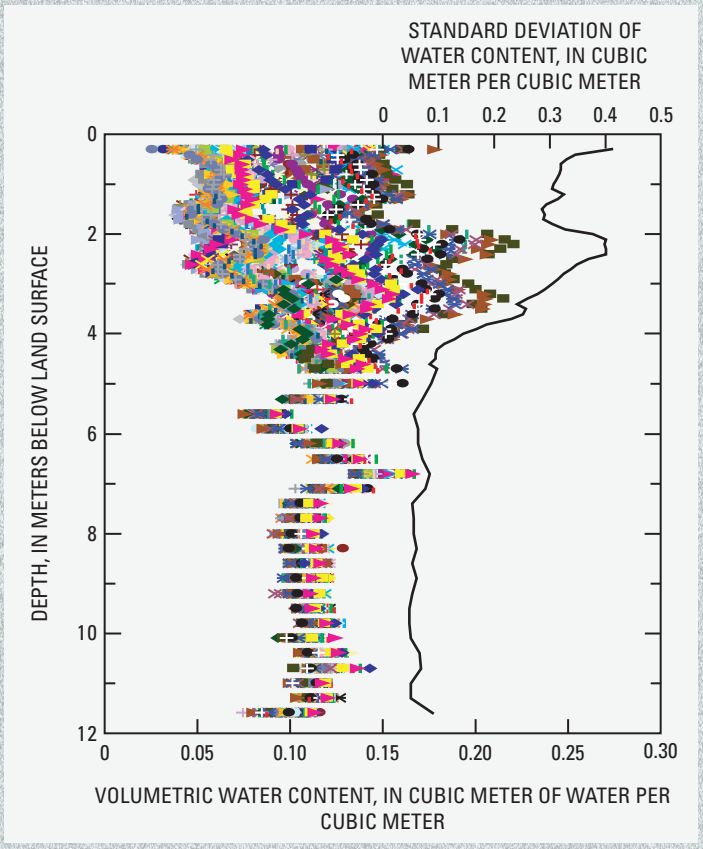

Figure 21. Volumetric water content (points) and standard deviation (curve) with depth at borehole UZN #19 for ten years of sampling during 1984–1995. Each symbol type denotes measurements from a different day.

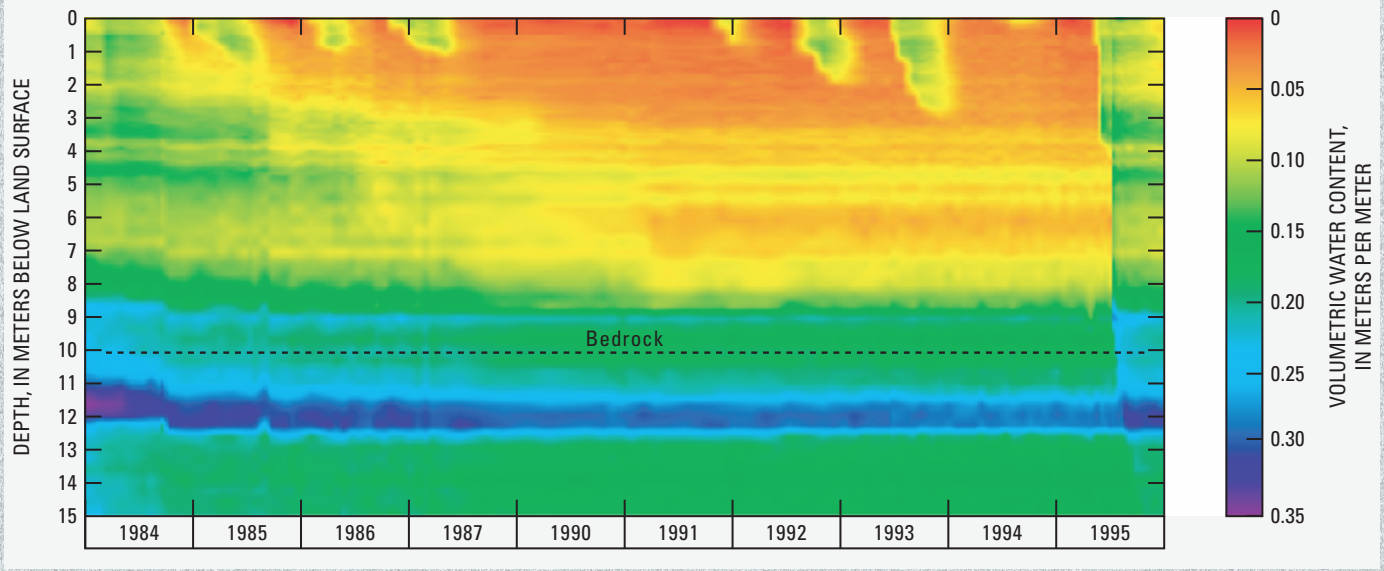

Figure 22. Volumetric water content with depth for ten years at borehole UZN #1.

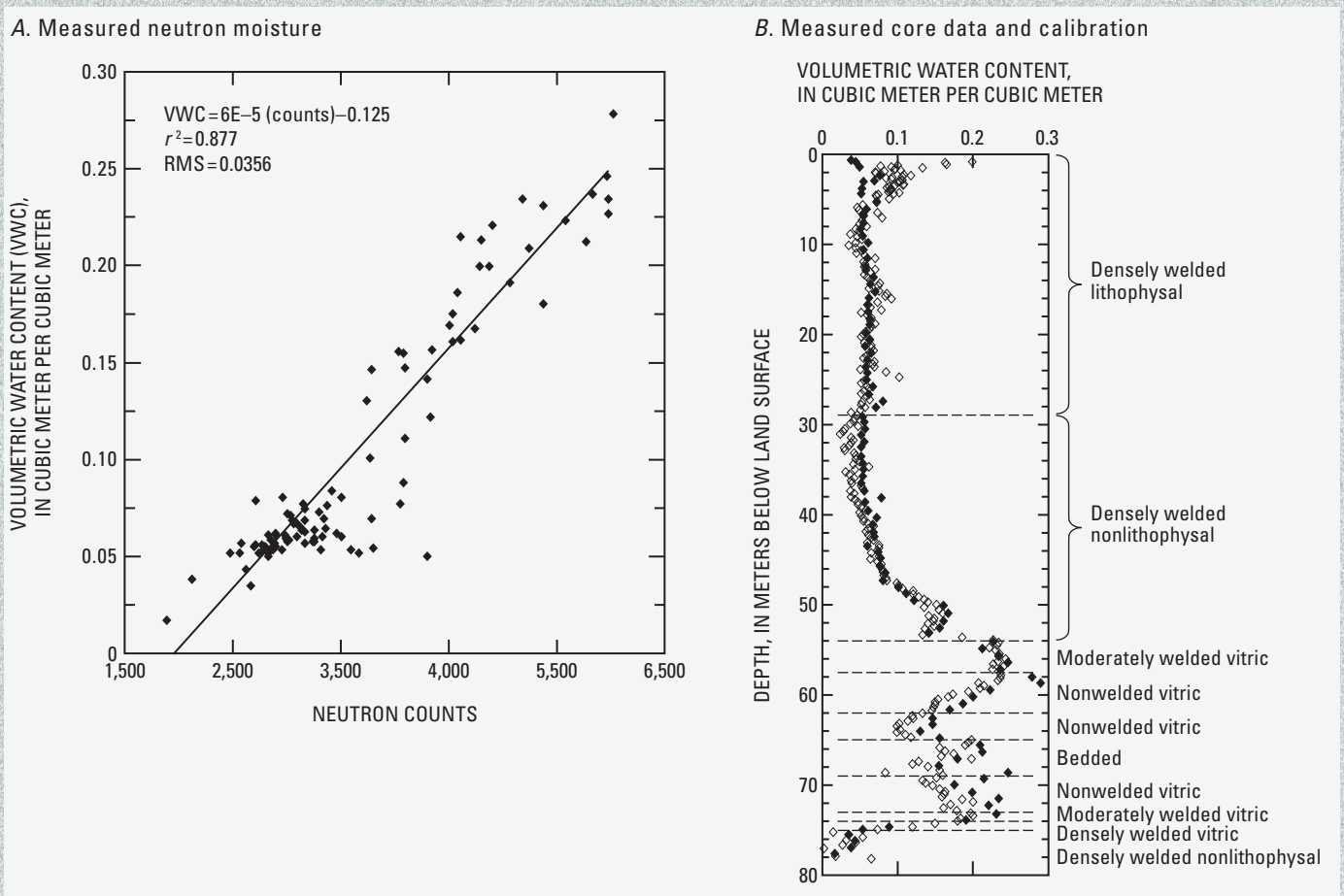

Figure 23. Neutron moisture meter calibration data included: *A,* Measured neutron moisture meter counts versus measured core data, and; *B,* Measured core data for borehole UZ N-55 (solid diamonds) and calibration equation applied to moisture meter logs (open diamonds).

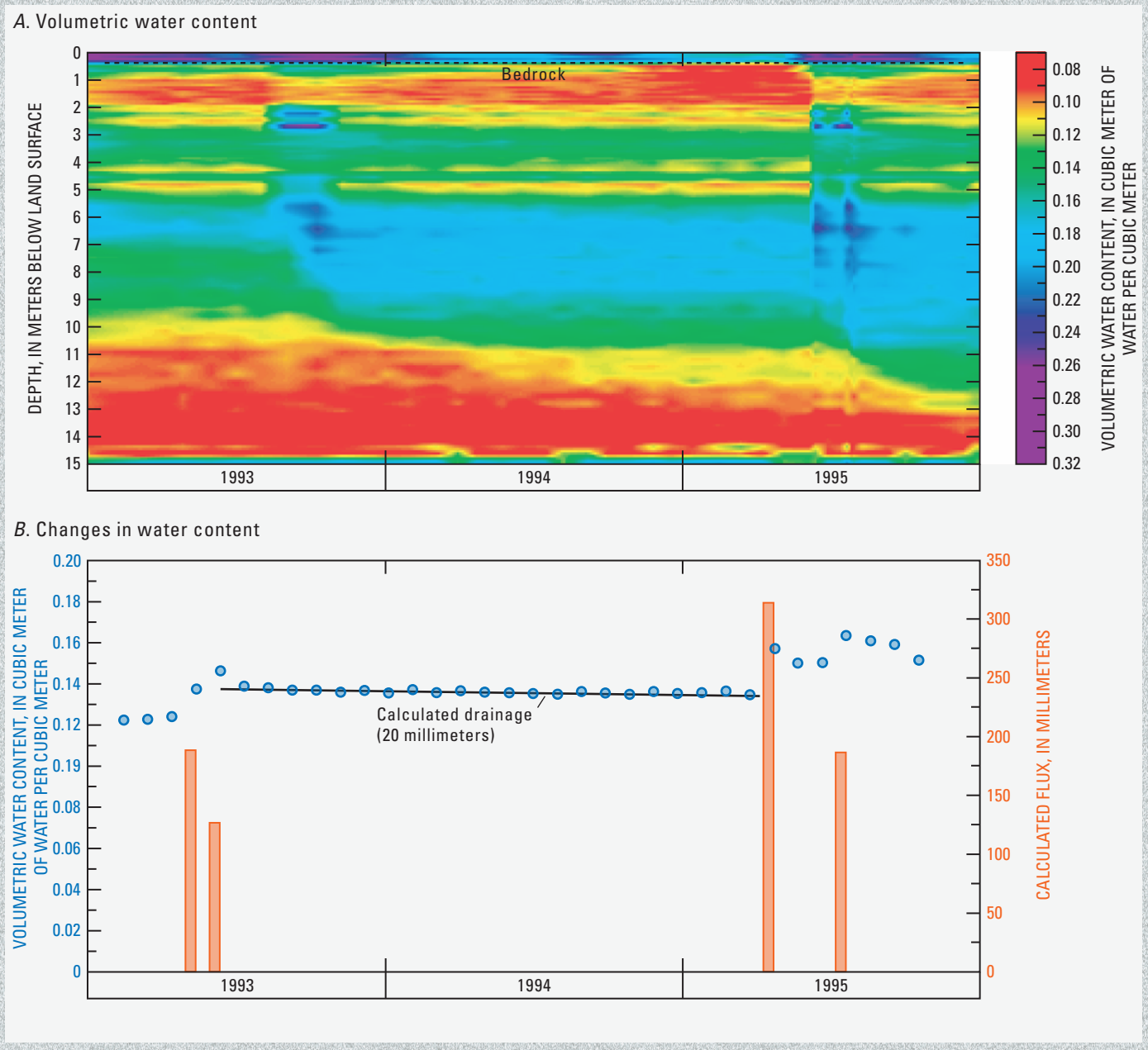

Figure 24. Application of neutron-based water-content measurements to calculate flux at borehole UZ-N15, where 0.8 meters of alluvium overlies fractured bedrock: *A,* Volumetric water content with a depth for three years, and; *B,* Changes in water content below two meters in bedrock, flux calculated from those measurements, and the drainage between rainfall events (calculated from the slope of the line).

Geophysical Well-Logging to Estimate Subsurface Physical and Hydraulic Properties

By James B. Callegary

Geophysical well-log data were collected to identify areas of active recharge and to help quantify recharge in ephemeral channels of the Sierra Vista subwatershed of the Upper San Pedro River Basin, Ariz. (fig. 25). Sixteen boreholes were drilled at 15 sites, twelve in the active portions of ephemeral stream channels and four in inter-basin sites. The boreholes in active channels were distributed among five ephemeral channels, representing the variation of tributary types found in the Sierra Vista subwatershed. All boreholes were lined with unscreened polyvinyl chloride (PVC) casing with a diameter of 0.05 meters. Most of the boreholes were completed above the regional water table. Manual estimation of the grain size distribution of cuttings was conducted in the field for each 0.3-meter depth interval. Gaps in the grain size distribution logs occur where cuttings were not retrieved or were lost. Laboratory estimates of grain size distribution were conducted on cuttings and a subset of retrieved cores in three boreholes.

Electromagnetic induction logging (EMI) was used to distinguish between clay layers and sand/gravel layers. Analyses of drill cuttings showed uniformly low chloride concentrations. Therefore, zones of increased electrical conductivity (EC) can be associated with high volumetric water content or high clay content. High neutron counts are associated with zones of high volumetric water content. As a result, the EMI and neutron results can be used together to distinguish zones of increased water content or clay-rich regions. This can be especially useful for distinguishing between zones with high water content due to high water retention associated with high clay content, and zones with high water content due to subsurface structure, such as capillary barriers.

EMI measurements were collected in all boreholes at a logging rate of 3 meters per minute. Measurements were recorded at 0.01–0.02-m intervals. Neutron soil moisture counts were measured in six boreholes. Counts were measured over a 32-second period at each depth with a 0.25-m measurement interval. Quantitative analysis of volumetric water content requires soil-specific calibration (Hignett and Evett, 2002). No calibration was performed in this investigation. Rather, the neutron responses were used as qualitative indicators of variations in water content with depth.

Data collected at Banning Creek represent the subsurface conditions of an incised, ephemeral stream channel (fig. 26). Incision of the channel near the borehole ranges from 2 to 5 meters. The channel surface is cobbly to sandy. Flows occur only after summer convective or winter synoptic scale storms. The laboratory and field grain size distributions are similar. Both grain size distribution logs show shallow and deep regions with relatively low clay fractions bounding a middle depth interval (7–17 m) that is more clay rich. Both logs also show isolated, thin

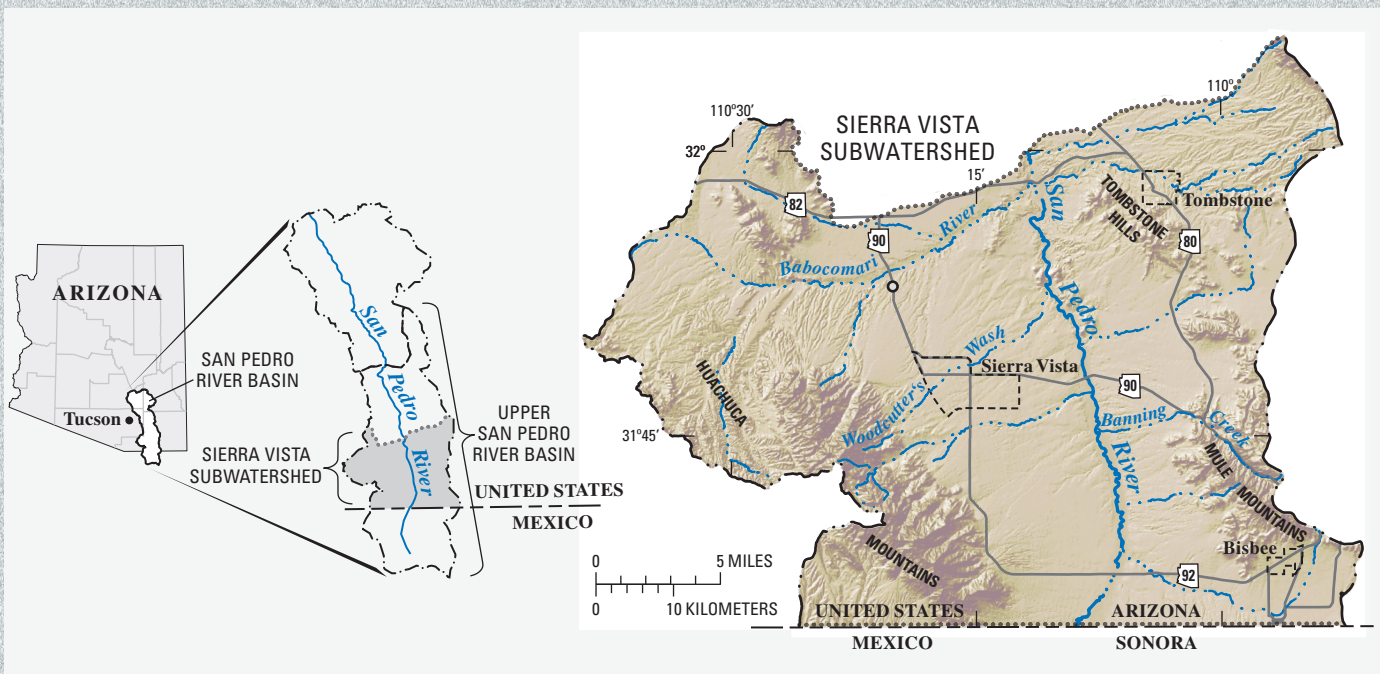

Figure 25. Location of Sierra Vista subwatershed of the Upper San Pedro River Basin, southeastern Ariz.

clay-rich zones in the shallow and deep regions. Laboratory-determined clay content tended to be lower than field estimates for depths greater than seven meters. This situation was reversed for shallower depths, where a different analyst performed the laboratory determinations. The difference may therefore reflect operator bias.

There is also general agreement between the grain size distribution logs and the EMI results. The EC is relatively high in the middle depth region compared with the shallow and deep zones. In addition, clay-rich zones at 3, 19–21, and 25 meters depth are identified. Finally, the EMI results agree with the laboratory results in identify-

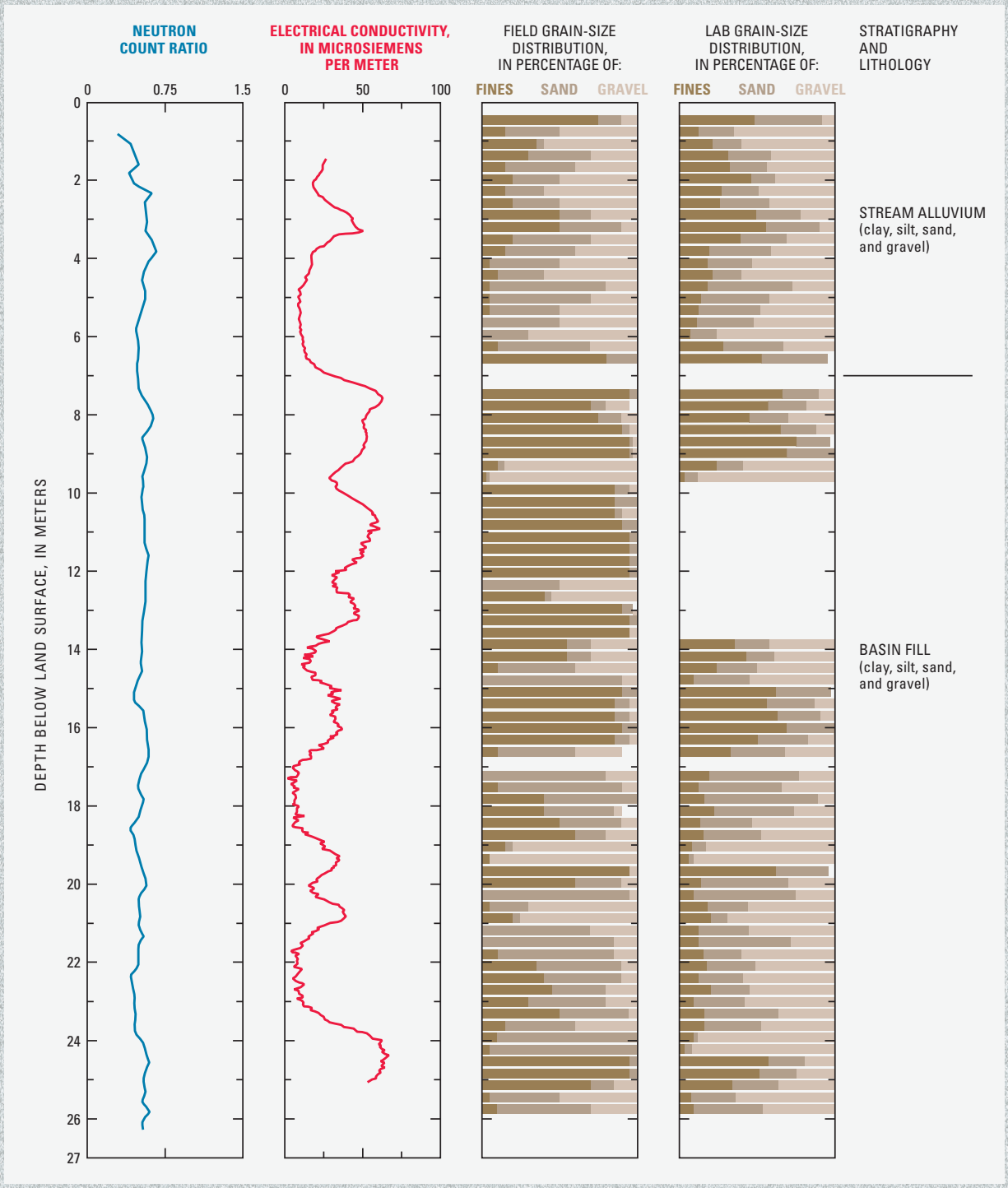

Figure 26. Neutron soil log, electrical conductivity, field and lab grain-size distribution (GSD), stratigraphy and lithology, Banning Creek, Upper San Pedro Basin, southeastern Ariz.

ing relatively low clay contents at 23 meters depth.

All electrical conductivity methods suffer from lack of uniqueness in distinguishing among lithologic, temperature, and pore water salinity. As described above, these confounding factors are accounted for in this study through uniformly low pore water salinity and the combined use of EMI and neutron logs. However, lack of depth resolution remains as a primary limitation on using EMI alone for identifying subsurface structure. This arises due to the relatively large sample volume of the instrument, evident in the EMI response to the 0.3-m thick clay layer located 20 meters below the surface. The EMI response shows a double peak that spans a depth interval of approximately three meters. The double peak is caused by the relatively high sensitivity of the instrument near the transmitting and receiving coils, which are separated by 0.5 meters vertically in the borehole. This instrument response places a limitation on the achievable spatial resolution. The neutron log, as a result of a smaller sample volume, provides higher resolution than the EMI log.

Woodcutter's Wash is also incised (about 6 m) and ephemeral with a sandy channel bottom and outcrops of caliche both up- and downstream of the borehole. Data gathered at Woodcutter's Wash demonstrate the utility of combining EMI and neutron logs (fig. 27). Unlike the Banning Creek logs, the neutron probe counts vary strongly with depth. This is especially apparent at a depth of seven meters, where neutron counts drop significantly while the measured EC remains high. The neutron response indicates that the region has a low volumetric water content. Assuming that pore water electrical conductivity (EC) does not vary significantly with depth, the high EC in this region could indicate that the clay content is higher than the surrounding regions. The elevated clay content would offset the reduction in EC associated with the lower water content. This could be associated with water ponding above the low water content region and the change in lithology below this region. The change in lithology is supported by the laboratory grain size analysis, which indicates that the deepest cuttings (from about 9 m) contain significantly less clay than the material above, possibly indicating the presence of a capillary barrier. However, it is difficult to infer the soil physical property distribution on the basis of one set of cuttings and geophysical logs. Additional laboratory analyses for grain size distribution and water content would result in a better understanding of the spatial variations in these properties. This underscores the fact that geophysical logs are often most useful as a screening tool for identifying regions in which the drill cuttings should be examined closely to interpret subsurface structure.

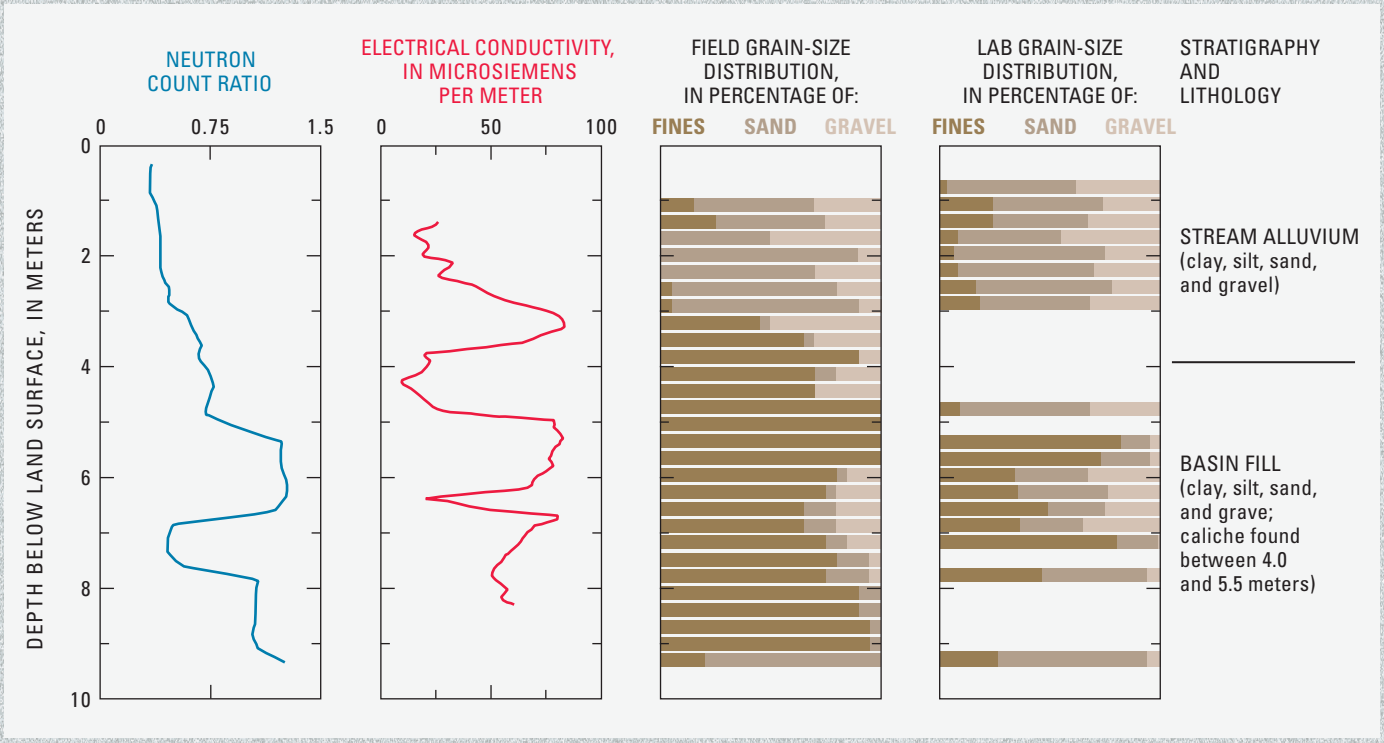

Figure 27. Neutron soil log, electrical conductivity, field and lab grain-size distribution (GSD), stratigraphy and lithology, Woodcutter's Wash, Upper San Pedro Basin, southeastern Ariz.

References Cited

Archie, G.E., 1942, The electrical resistivity log as an aid to determining some reservoir characteristics: Transactions of the American Institute of Mining and Metallurgical Engineers, v. 146, p. 389–409.

Binley, A., Winship, P., Middleton, R., Pokar, M., and West, J., 2001, High resolution characterization of vadose zone dynamics using cross-borehole radar: Water Resources Research, v. 37, no. 11, p. 2639–2652.

Binley, A., Cassiani, G., Middleton, R., and Winship, P., 2002, Vadose zone model parameterisation using cross-borehole radar and resistivity imaging: Journal of Hydrology, v. 267, nos. 3–4, p. 147–159.

Binley, A., Winship, P., West, L.J., Pokar, M., and Middleton, R., 2002, Seasonal variation of moisture content in unsaturated sandstone inferred from borehole radar and resistivity profiles, Journal of Hydrology, v. 267, nos. 3–4, p. 160–172.

Birch, F., 1966, Compressibility, elastic constants, *in* Clark, S.P., ed., Handbook of physical constants: Geological Society of America Memoir 97, p. 97–173.

Blasch, K.W., 2003, Streamflow timing and estimation of infiltration rates in and ephemeral stream channel using variably saturated heat and fluid transport methods: Tucson, University of Arizona, Ph.D. dissertation, 204 p.

Callegary, J.B., Ferré, T.P.A., and Groom, R.W., 2007, Vertical spatial sensitivity and exploration depth of low-induction-number electromagnetic-induction instruments: Vadose Zone Journal, v. 6, no. 1, p. 158–167, doi:10.2136/vzj2006.0120.

Cook, P.G., and Kilty, S., 1992, A helicopter-borne electromagnetic survey to delineate groundwater recharge rates: Water Resources Research, v. 28, p. 2953–2961.

Dane, J.H., and Topp, G.C., eds., 2002, Methods of soil analysis—Part 4, physical methods: Madison, Wisc., Soil Science Society of America, Book Series no. 5, 1692 p.

Desbrandes, R., and Brace, G., 1985, Encyclopedia of well logging: Houston, Gulf Publishing Company, 584 p.

Flint, A.L., and Flint, L.E., 1994, Spatial distribution of potential near surface moisture flux at Yucca Mountain, *in* Fifth International Conference on High Level Radioactive Waste Management, Las Vegas, Nev., May 22– 26, 1994, Proceedings: La Grange Park, Ill., American Nuclear Society, v. 4, p. 2,352–2,358.

Flint, L.E., and Flint, A.L., 1995, Shallow infiltration processes at Yucca Mountain—Neutron logging data 1984–93: U.S. Geological Survey Water-Resources Investigations Report 95–4035, 46 p.

Flint, A.L., and Flint, L.E., 2000, Near surface infiltration monitoring using neutron moisture logging, Yucca Mountain, Nevada, *in* Looney, B. and Falta, R., eds., Vadose zone science and technology solutions: Columbus, Ohio, Battelle Press, p. 457–474.

Flint, A.L., Flint, L.E., Kwicklis, E.M., Bodvarsson, G.S., and Fabryka-Martin, J.T., 2001, Hydrology of Yucca Mountain: Reviews of Geophysics, v. 39, no. 4, p. 447–470.

Flint, A.L., Flint, L.E., Kwicklis, E.M., Fabryka-Martin, J.T., and Bodvarsson, G.S., 2002, Estimating recharge at Yucca Mountain, Nevada, USA, Comparison of methods: Hydrogeology Journal, v. 10, p. 180–204.

Flint, A.L., Hevesi, J.A., and Flint, L.E., 1996, Conceptual and numerical model of infiltration for the Yucca Mountain area, Nevada: Las Vegas, Nev., U.S. Department of Energy, Milestone Report 3GUI623M, 210 p.

Flint, L.E., Hudson, D.B., and Flint, A.L., 1999, Unsaturated hydraulic parameters using indirect and direct methods: *in* van Genuchten, M. Th., Leij, F. J., and Wu, L. eds., Proceedings of the International Workshop for the Characterization and Measurement of the Hydraulic Properties of Unsaturated Porous Media, Riverside, Calif., October 22–24, 1997: Riverside, U.S. Salinity Laboratory, Agricultural Research Service, U.S. Department of Agriculture, and the Department of Environmental Sciences, University of California, p. 293–302.

Geller, J.T., and Myer, L.R., 1995, Ultrasonic imaging of organic liquid contaminants in unconsolidated porous media: Journal of Contaminant Hydrology, v. 19, no. 3, p. 85–104.

Hevesi, J.A., Flint, A.L., and Flint, L.E., 1994, Verification of a 1-dimensional model for predicting shallow infiltration at Yucca Mountain, *in* Fifth International Conference on High Level Radioactive Waste Management, Las Vegas, Nev., May 22– 26, 1994, Proceedings: La Grange Park, Ill., American Nuclear Society, v. 4, p. 2,323–2,332.

Hignett, C. and Evett, S.R., 2002, Neutron thermalization, *in* Dane, J.H., and Topp, G.C., eds., Methods of soil analysis—Part 4, physical methods: Madison, Wis., Soil Science Society of America, Book Series, Number 5, p. 501–521.

Hoffmann, J.P., Ripich, M.A, and Ellett, K.M., 2002, Characteristics of shallow deposits beneath Rillito Creek, Pima County, Arizona: U.S. Geological Survey Water- Resources Investigations Report 01–4257, 51 p.

Hook, W.R., Ferré, T.P.A., and Livingston, N.J., 2004, The effects of salinity on the accuracy and uncertainty of water content measurement: Soil Science Society of America Journal, v. 68, no. 1, p. 47–56.

Hudson, D.B., Flint, A.L. and Guertal, W.R., 1994, Modeling a ponded infiltration experiment at Yucca Mountain, NV, *in* Fifth International Conference on High Level Radioactive Waste Management, Las Vegas, Nev., May 22– 26, 1994, Proceedings: La Grange Park, Ill., American Nuclear Society, v. 4, p. 2,168–2,174.

Huisman, J.A., Hubbard, S.S., Redman, J.D., and Annan, A.P., 2003, Measuring soil water content with ground penetrating radar, a review: Vadose Zone Journal, v. 2, p. 476–491.

Jackson, M.J. and Tweeton, D.R., 1996, 3DTOM, three-dimensional geophysical tomography: U.S. Geological Survey Open-File Report 2000–456, 84 p.

Jury, W.A., Gardner, W.R., and Gardner, W.H., 1991, Soil physics (5th ed.): New York, John Wiley and Sons, 328 p.

Katz, L.T., 1987, Steady state infiltration processes along the Santa Cruz and Rillito rivers: Tucson, University of Arizona, master's thesis, 119 p.

Kearey, P., Brooks, M., and Hill, I., 2002, An introduction to geophysical exploration: Oxford, United Kingdom, Blackwell Science Ltd., 262 p.

Keys, W.S., 1990, Borehole geophysics applied to groundwater investigations: U.S. Geological Survey Techniques of Water-Resources Investigations, book 2, chap. E2, 150 p.

Klenke, J.M., and Flint, A.L., 1991, A collimated neutron tool for soil-water measurements: Soil Science Society of America Journal, v. 55, p. 916–923.

Kohnen, H., 1974, The temperature dependence of seismic waves in ice, Journal of Glaciology, v. 13, no. 6, p. 144–147.

Labo, J.A., and Mentemeier, S.H., 1987, A practical introduction to borehole geophysics: Tulsa, Okla., Society of Exploration Geophysicists, 330 p.

Lucius, J.E., Langer, W.H., and Ellefsen, K.J., 2007, An introduction to using surface geophysics to characterize sand and gravel deposits: U.S. Geological Survey Circular 1310, 33 p.

McKittrick, M.A., 1988, Surficial geologic maps of the Tucson metropolitan area: Arizona Geological Survey Open-File Report 88–18 [12 maps; 6 p. text], scale 1:24,000.

NRC (National Research Council) Committee on the Review of the Hanford Site's Environmental Remediation Science and Technology Plan, 2001, Science and technology for environmental cleanup at Hanford: Washington, D.C., The National Academies Press, 192 p.

Or, D., and Wraith, J.M., 1999, Temperature effects on soil bulk dielectric permittivity measured by time domain reflectometry, a physical model: Water Resources Research, v. 35, no. 2, p. 371–383

Patnode, H.W., and Wyllie, M.R.J., 1950, The electrical resistivity log as an aid to determining some reservoir characteristics: Transactions of the American Institute of Mining and Metallurgical Engineers, v. 189, p. 47–52.

Phillips, F.M., 1994. Environmental tracers for water movement in desert soils of the American Southwest: Soil Science Society of America Journal, v. 58, p. 14–24.

Pokar, M., West, L.J., Winship, P., and Binley, A.M., 2001, Estimating petrophysical data from borehole geophysics, *in* Symposium on the Applications of Geophysics to Engineering and Environmental Problems (SAGEEP2001), Proceedings: Denver, Colo., Environmental and Engineering Geophysical Society (CD-ROM).

Reynolds, J.M., 1997, An introduction to applied and environmental geophysics: New York, John Wiley and Sons, 796 p.

Robinson, D.A., Jones, S.B., Wraith, J.M., Or, D., and Friedman, S.P., 2003, A review of advances in dielectric and electrical conductivity measurement in soils using time domain reflectometry: Vadose Zone Journal, v. 2, p. 444–475.

Rubin, Y., and Hubbard, S.S., eds., 2005, Hydrogeophysics: Dordrecht, Netherlands, Kluwer, Water Science and Technology Library, v. 50, 523 p.

Scanlon, B.R., 1991, Evaluation of moisture flux from chloride data in desert soils: Journal of Hydrology, v. 128, no. 1–4, p. 137–156.

Scanlon, B.R., and Goldsmith, R. S., 1997, Field study of spatial variability in unsaturated flow beneath and adjacent to playas: Water Resources Research, v. 33, p. 2239–2252.

Scanlon, B.R., Paine, J.G., and Goldsmith, R. S., 1999, Evaluation of electromagnetic induction as a reconnaissance technique to characterize unsaturated flow in an arid setting: Ground Water v. 37, p. 296–304.

Telford, W.M., Geldart, L.P., and Sheriff, R.E., 1990, Applied geophysics (2nd ed.): Cambridge, United Kingdom, Cambridge University Press, 770 p.

Topp, G.C., Davis, J.L., and Annan, A.P., 1980, Electromagnetic determination of soil water content—measurement in coaxial transmission lines: Water Resources Research, v. 16, p. 574–582.

Turner, S.F., 1943, Ground-water resources of the Santa Cruz Basin, Arizona: Tucson, Ariz., United States Department of the Interior, Geological Survey [not part of a formal publication series], OCLC no. ocm04835814, 84 p.

Tucson Water, 2000, Annual static water level basic data report, Tucson Basin and Avra Valley, Pima County, Arizona, 1997: City of Tucson Water, Planning, and Engineering Division.

Tyler, S.W., Chapman, J.B., Conrad, S.H., Hammermeister, D.P., Blout, D.O., Miller, J.J., Sully, M.J., and Ginanni, J.M., 1996, Soil-water flux in the southern Great Basin, United States—temporal and spatial variations over the last 120,000 years: Water Resources Research, v. 32, no. 6, p. 1481–1499.

Waxman, M.H. and Smits, L.J.M., 1968, Electrical conductivities in oil-bearing shaly sands: Society of Petroleum Engineers Journal, v. 8., no. 2, p. 107–122.

West, L.J., Handley, K., Huang, Y., and Pokar, M., 2003, Radar frequency dielectric dispersion in sand and sandstone, implications for determination of moisture content and clay content: Water Resources Research, v. 39, no. 2, p. 1-1–1-12, doi:10.1029/2001WR000923.

Wilson, L.G., DeCook, K.J., and Neuman, S.P., 1980, Regional recharge research for southwest alluvial basins (final report): Tucson, Ariz., Water Resources Research Center, Department of Hydrology and Water Resources, University of Arizona, OCLC no. ocm19659149, 408 p.

Wood, W.W., and Sanford, W.E., 1995, Chemical and isotopic methods for quantifying groundwater recharge in a regional, semiarid environment: Ground Water, v. 33, p. 458–468.

Yaramanci, U., Lange, G., and Knödel, K., 1999, Surface NMR within a geophysical study of an aquifer at Haldensleben (Germany): Geophysical prospecting, v. 47, p. 923–943.

Yeh, T.-C. J., and Simunek, J., 2002, Stochastic fusion of information for characterizing and monitoring the vadose zone: Vadose Zone Journal, v. 1, p. 207–221.

ISBN 978-1-4113-2165-6